frontiers | Research Topics

Understanding ocean ridges, a new frontier for science and development

Edited by
Philip Weaver, David Billett, Pei-Yuan Qian and Jozee Sarrazin

Published in
Frontiers in Marine Science

ISSN 1664-8714
ISBN 978-2-8325-2739-9
DOI 10.3389/978-2-8325-2739-9

About Frontiers

Frontiers is more than just an open access publisher of scholarly articles: it is a pioneering approach to the world of academia, radically improving the way scholarly research is managed. The grand vision of Frontiers is a world where all people have an equal opportunity to seek, share and generate knowledge. Frontiers provides immediate and permanent online open access to all its publications, but this alone is not enough to realize our grand goals.

Frontiers journal series

The Frontiers journal series is a multi-tier and interdisciplinary set of open-access, online journals, promising a paradigm shift from the current review, selection and dissemination processes in academic publishing. All Frontiers journals are driven by researchers for researchers; therefore, they constitute a service to the scholarly community. At the same time, the *Frontiers journal series* operates on a revolutionary invention, the tiered publishing system, initially addressing specific communities of scholars, and gradually climbing up to broader public understanding, thus serving the interests of the lay society, too.

Dedication to quality

Each Frontiers article is a landmark of the highest quality, thanks to genuinely collaborative interactions between authors and review editors, who include some of the world's best academicians. Research must be certified by peers before entering a stream of knowledge that may eventually reach the public - and shape society; therefore, Frontiers only applies the most rigorous and unbiased reviews. Frontiers revolutionizes research publishing by freely delivering the most outstanding research, evaluated with no bias from both the academic and social point of view. By applying the most advanced information technologies, Frontiers is catapulting scholarly publishing into a new generation.

What are Frontiers Research Topics?

Frontiers Research Topics are very popular trademarks of the *Frontiers journals series*: they are collections of at least ten articles, all centered on a particular subject. With their unique mix of varied contributions from Original Research to Review Articles, Frontiers Research Topics unify the most influential researchers, the latest key findings and historical advances in a hot research area.

Find out more on how to host your own Frontiers Research Topic or contribute to one as an author by contacting the Frontiers editorial office: frontiersin.org/about/contact

Understanding ocean ridges, a new frontier for science and development

Topic editors

Philip Weaver — Seascape Consultants Ltd, United Kingdom

David Billett — Deep Seas Environmental Solutions Ltd., United Kingdom

Pei-Yuan Qian — Hong Kong University of Science and Technology, Hong Kong, SAR China

Jozee Sarrazin — Institut Français de Recherche pour l'Exploitation de la Mer (IFREMER), France

Citation

Weaver, P., Billett, D., Qian, P.-Y., Sarrazin, J., eds. (2023). *Understanding ocean ridges, a new frontier for science and development*. Lausanne: Frontiers Media SA. doi: 10.3389/978-2-8325-2739-9

Philip Weaver is Managing Director of Seascape Consultants Ltd a company he founded in 2010.

Table of contents

frontiers | Frontiers in Marine Science

TYPE Editorial
PUBLISHED 27 December 2022
DOI 10.3389/fmars.2022.1098359

OPEN ACCESS

EDITED AND REVIEWED BY
Ana Hilário,
University of Aveiro, Portugal

*CORRESPONDENCE
Philip P. E. Weaver
weaverphil0@gmail.com

SPECIALTY SECTION
This article was submitted to Deep-Sea Environments and Ecology, a section of the journal Frontiers in Marine Science

RECEIVED 14 November 2022
ACCEPTED 28 November 2022
PUBLISHED 27 December 2022

CITATION
Weaver PPE, Billett DSM, Qian P-Y and Sarrazin J (2022) Editorial: Understanding ocean ridges, a new frontier for science and development. *Front. Mar. Sci.* 9:1098359. doi: 10.3389/fmars.2022.1098359

Editorial: Understanding ocean ridges, a new frontier for science and development

Philip P. E. Weaver[1]*, David S. M. Billett[2,3], Pei-Yuan Qian[4,5] and Jozée Sarrazin[6]

[1]Seascape Consultants, Romsey, Hampshire, United Kingdom, [2]Deep Seas Environmental Solutions Ltd., Ashurst, United Kingdom, [3]National Oceanography Centre, Southampton, United Kingdom, [4]Southern Marine Science and Engineering Guangdong Laboratory (Guangzhou), Guangzhou, Nansha, China, [5]Department of Ocean Science, Hong Kong University of Science and Technology, Hong Kong, Hong Kong SAR, China, [6]Univ Brest, CNRS, Ifremer, UMR6197 BEEP, Plouzané, France

KEYWORDS

ocean ridge, deep sea mining, polymetallic sulfide, marine ecosystem, marine management

Editorial on the Research Topic
Understanding ocean ridges, a new frontier for science and development

Ocean ridges form where new lithospheric crust is generated by seafloor spreading at tectonic plate boundaries. Some stretch for tens of thousands of kilometres through the oceans, but others can be quite short e.g., in back arc basins. They host a range of habitats including active and inactive hydrothermal vents, peripheral areas, rocky slopes and soft sediments, all connected to the pelagic environment above. Active vents harbour exceptionally productive ecosystems fuelled by chemosynthesis and are colonized by endemic species. Seafloor massive sulfide deposits are formed over long periods of time at hydrothermal vents and may be rich in metals including copper, zinc, lead, gold, and silver. Recent interest by the mining industry in these minerals has stimulated scientific projects to better understand these poorly-known environments, including their biodiversity, functioning and connectivity. New knowledge is needed to inform management plans and ensure the protection of the marine environment.

To date most research on ocean ridges has focussed on active hydrothermal vents and their unique fauna, but mining activities are likely to be directed at inactive and extinct hydrothermal vents. The impacts of mining, in addition to those from deep-water fisheries at some depths, could significantly affect other surrounding seabed and pelagic habitats. There are many scientific knowledge gaps (Amon et al., 2022) including the need to understand the fine-scale distributions of different taxa and their connectivity along and between ridges, as well as the potential impacts of mining activities including those caused by particle load and potential toxicity of mining plumes (Weaver and Billett, 2019). This Research Topic brings together results aimed at filling the most important gaps in our understanding of ocean ridges. Some of the papers are reviews of our knowledge of mid-ocean ridge ecosystems in the Atlantic and Indian Oceans. Others describe new research including on the Juan de Fuca Ridge and East Pacific Rise in the

Pacific Ocean and on the Scotia Ridge in the Southern Ocean. The Research Topic includes results relating to four of the seven contractors to the ISA for polymetallic sulphides (China Ocean Mineral Resources Research and Development Association, The Government of the Republic of Korea, Institut Francais de Recherche pour l'Exploitation de la Mer (Ifremer) and The Government of Poland).

Boschen-Rose and Colaço provide a comprehensive review of fauna at active vent locations and at hydrothermally inactive habitats on the northern Mid-Atlantic Ridge (MAR). A regional biogeographic analysis identified distinct faunal groupings related to depth and the chemical composition of active/inactive chimneys. They describe the biodiversity of communities, and report on ecosystem functioning, connectivity, trophic relationships, temporal variability, ecosystem resilience and recovery. The authors conclude that ecological data need to be collected over a range of time scales from hours to decades at multiple locations to establish robust baseline information that can be used in monitoring studies to distinguish between natural phenomena and impacts from mining. This highlights that deep-sea mining contractors cannot complete environmental studies within a period of two to three years, but require steady, planned and comprehensive data collection over longer timescales.

The unique ecosystems and biodiversity associated with mid-ocean ridge hydrothermal vent systems contrast sharply with surrounding deep-sea habitats and both may be increasingly threatened by anthropogenic activities including mining and climate change. It is thus of utmost importance to be able to evaluate the mechanisms by which these ecosystems function and respond to oceanic, crustal, and anthropogenic forces. Matabos et al. provide an extensive review on the development of deep-sea observatories at hydrothermal vents, examine recent scientific and technological advancements and give recommendations to support future studies. Notably, they evaluate their potential to monitor the long-term dynamics of deep-sea ecosystems through a multidisciplinary approach as well as to define effective environmental monitoring plans including the characterization of biological and environmental baseline states, the evaluation of natural versus anthropogenic changes and the assessment of degradation, resilience and recovery of faunal communities after disturbance. These approaches can represent valuable tools for environmental impact assessment in the context of deep-sea mining. The proposed recommendations include, among other things, the establishment of common global scientific questions and the identification of Essential Ocean Variables (EOVs) specific to Mid-Ocean Ridge systems.

Perez et al. provide a similar review to Boschen-Rose and Colaço but focus on ultra-slow spreading hydrothermal sites on the Western Indian Ocean ridge. Most of the information relates to fauna at active hydrothermal vents. To date, thirteen hydrothermally active locations have been identified on this ridge. Connectivity of fauna appears to be influenced by distance and geomorphological barriers. However, contrasting differences in gene flow have been documented across species. The authors note that a much better understanding of the reproductive biology of species on Indian Ocean ridges is required. Data from a wider variety of benthic size classes, including microbes, meiofauna and fish as well as information on inactive sulfide chimneys and the surrounding seabed should be acquired. As for Boschen-Rose and Colaço a detailed appraisal assessment is made of knowledge gaps and research needs.

Radziejewska et al. review current knowledge of benthic ecosystems within the Polish Exploration Contract Area for polymetallic sulfides on the MAR. The contract was signed with the ISA in 2018 and will run for 15 years in the first instance. This study identified that apart from research at two hydrothermal areas, with markedly different hydrothermal and ecosystem histories, very little is known about the fauna in the wider area. Many knowledge gaps remain. The paper recognises the challenge for contractors in generating environmental baseline studies sufficient to be used in Environmental Impact Assessments. Furthermore, they emphasize the time and investment needed in expertise and best practice sampling technologies to generate suitable data in this challenging environment.

Sarrazin et al. report on a new type of faunal assemblage dominated by gastropods at hydrothermal vent sites between c. 800 and 3500 m on the MAR. Two different gastropod species dominate, between the shallowest Menez Gwen vent field (850m, Lepetodrilus atlanticus) and the deepest Lucky Strike and Snake Pit vent fields (1700 m and 3450 m respectively, Peltospira smaragdina) depending, possibly, on the depth of the locality. The gastropod assemblages occur at sites with environmental characteristics - notably temperature and vent fluid chemistry - mussels in low temperature habitats and 2) shrimps in warmer habitats. The gastropod assemblages appear to play an important role in the functioning and dynamics of MAR hydrothermal vent communities and may even constitute one of the first steps of Atlantic vent ecological succession.

Guéganton et al. provide a detailed study of symbiotic microbial communities in the digestive systems of two common and dominant species of caridean shrimps on the MAR. Using molecular 16S RNA techniques, the authors assessed whether different microbial assemblages occurred in different compartments of the digestive systems of *Rimicaris exoculata* and *Rimicaris chacei*. Different microbial groups dominated in different gut compartments in both species, however, the same microbes occurred in the two shrimp species. In contrast, there were highly significant differences between the two species in the structure of the gut. While the habitats of the adults of the two species are well known, knowledge of the juvenile and larval stages and their associated microorganisms are still required.

Plumes of sediment-laden water with a toxic component will be generated by the mining process on the seafloor and dewatering of ores on the support vessel (Weaver and Billett, 2019). These will spread away from the mine site where they may have negative impacts on both the benthic and pelagic fauna. Morato et al. modelled the potential magnitude and spread of these plumes using three-dimensional hydrodynamic models of the Azores region combined with a theoretical commercial mining operation of polymetallic sulfides to simulate the dispersal of plumes originating from different phases of mining operations and to assess the magnitude of potential impacts. The models showed considerable variability between locations along the ridge axis but predicted impacts at least 10-20 km away from the mine site covering areas up to 150 km^2 and extending more than 800 km into the water column. In some cases the predictions show impacts to areas where cold-water corals are predicted to occur.

The impact of the plumes will depend on their particulate content and their toxicity plus the susceptibility of the organisms impacted. Carrreiro-Silva et al. present results of a controlled aquaria experiment that tested the effects of suspended polymetallic sulfide (PMS) particles generated during simulated mining activities on *Dentomuricea aff. meteor* (low case), an important habitat-forming octocoral in the Azores. Their results show how relatively low concentrations of suspended small PMS particles (2-3 mg/l) can impair the physiology of cold-water octocorals, ultimately resulting in their death within a short period of 2 to 4 weeks. The high sensitivity of corals to PMS particles likely resulted from the combined and potentially synergistic toxicological effect (high copper) with the mechanical effect of the angular shape of PMS particles.

Priede et al. examine the drivers for biomass and biodiversity of the non-chemosynthetic fauna of the MAR which has greater richness than that of the adjacent but deeper abyssal plains even though the primary productivity in surface waters does not differ. Most of the bottom fauna on the ridges is composed of "normal" deep-sea species that are directly or indirectly dependent on fall-out of food material from the surface ocean. Priede et al. estimate the quantity of particulate organic matter reaching the sea floor to be in proportion to surface export production scaled by bathymetry. They estimated that the MAR would receive 1.3 to 3 times the flux received by the adjacent abyssal plains due to its elevated position, and that this accounts for the increased species richness and biomass on the ridge. The ridge also has a variety of habitats from hard rock to soft sediment covered slopes and plains over a wide range of water depths, creating niches for a high diversity of species. The ridge also forms an overlap zone between the faunas of the western and eastern basins allowing counts of species from both.

Little is known about the transport and export of chemoautotrophic produced organic carbon to deep-sea habitats surrounding hydrothermal vents. Roohi et al. examine vent carbon export and its influence on benthic food webs in sediments at the Rainbow vent field located on the MAR at ~2200 m depth. Two sites were considered along the dispersal direction of the Rainbow vent plume: a first near-vent site located in the close vicinity at about ~30-100 m and a second "off-vent" site at 4 km distance to the nearest venting area. At both sites, box corers were used to sample sediments and their fauna while a turbidity sensor was used to identify the presence of the vent plume in the water column. Suspended particulate organic matter was sampled from the plume as well as from surface waters at 75 m depth. Nitrogen and carbon stable isotopic analyses showed that carbon derived from *in situ* chemoautotrophy was the main nutrition source of the "near-vent" infauna while fauna at the "off-vent" site showed a signature more typical for photosynthetic-derived material. The abundance and biomass of the fauna were variable but not different at the two studied sites. This study emphasize the need to take into account the connectivity of vent and non-vent habitats when designing spatial management plans with regard to deep-seabed mining.

Vecchione and Bergstad report on numerous observations of strange linear sets of holes in sediments at a depth of about 2100 m on the MAR. A series of stunning images were captured using a Remotely Operated Vehicle during the Census of Marine Life field project MAR-ECO (2000-2010). The holes extended from less than a metre to many metres. The authors contrast their observations to several other studies which have noted similar marks on deep-sea sediments. While the source of the holes remains unknown, the authors note they bear a strong resemblance to reported ichnofossils and therefore are likely to be a feature of deep-sea sediments for a very long time. The authors also note that the holes introduce local small-scale heterogeneity into the mid-ocean ridge environment which potentially influence the distributions of smaller organisms. This may be important when considering sampling strategies in baseline studies and subsequent monitoring programmes if mining goes ahead.

Woods et al. describe how relict, inactive black-smoker chimneys on the East Pacific Rise can in some cases be colonised by large numbers of suspension-feeding brisingid sea stars at a depth of about 2300 m on the summit of a seamount. A detailed analysis of the spatial distribution of these sea stars demonstrates that they are clustered on the inactive chimneys and are absent from active vents and much less common on other hard substrata in the area. This study demonstrates that inactive chimneys can act as particular habitats for certain species.

Neufeld et al. address the distribution of non-vent fauna living in proximity to hydrothermal vents and which might be impacted by mining activities. Specifically, they studied two localities on the Juan de Fuca Ridge in the north-western Pacific Ocean using a Remotely Operated Vehicle. Fauna studied included megafaunal sponges, antipatharian and alcyonacean corals, actiniarians, ophiuroids, crinoids and

ascidians. Very few corals occurred within 50 m of an active hydrothermal vent, and almost none within 25m. Notable differences in the composition and distribution of corals were also noted between different localities. Slow growing deep-water taxa, such as corals and sponges, will be particularly sensitive to mining impacts, including smothering by sediment plumes and possible toxicity of weathered sulfides.

Lim et al. provided a detailed characterization of geochemistry of surface sediment from Onnuri vent field (OVF) in the middle region of the Central Indian ridge (CIR). Based on their report, OVF is about ~12 km from the ridge axis along the CIR. They found that the OVF sediments were characterized with high concentrations of Fe, Si, Ba, Cu, and Zn, derived from hydrothermal fluid and S and Mg from seawater. However, these sediments did not have depleted C-S isotope compositions and contained abundant hydrothermally precipitated minerals (i.e., Fe–Mn hydroxides, sulfide and sulfate minerals, and opal silica). The occurrence of pure talc and barite indicated strong hydrothermal activity at this site. Furthermore, their sulfur and strontium isotope geochemistry suggested that the seawater was well mixed with high-temperature fluid. They argued that the OVF is a good representative of off-axis, high-temperature vent circulation system and could be the most common type of hydrothermal activity in the CIR. Overall, this study provide some good insights into vent system along mid-ocean ridges.

Namirimu et al. conducted metagenomics analysis of microbial communities of three sediment samples collected from the Invent E and Onnuri vent fields (OVF) and found that microbial communities were similar and dominated by Bacteria. Proteobacteria, Firmicutes, Bacteroidetes and Euryarchaeota. Analysis of KEGG categories indicated that microbial communities have capabilities of conducting aerobic respiration, carbon fixation through the Calvin-Bassham-Benson cycle and the reverse tricarboxylic acid cycle. They also have reductive acetyl-CoA pathway and sulphur and nitrogen metabolic functions. When comparing metagenomics information with those from different ridges in the world oceans, they found that microbial communities differed between highly active and low active vents, which further support the early findings showing the relationship between venting activities and microbial community structures. Overall, this study provided the first hand information on microbial community structure and functions in sediments from two newly discovered vent fields in mid-Indian Ocean ridge area.

Jang et al. assessed the influence of geological and geographic factors on the divergence of symbiotic bacteria of deep-sea hydrothermal vent mussels *Bathymodiolus* from the CIR (slow spreading ridge) and the eastern Pacific Ridges (fast-spreading ridge). They concluded that the differentiation of symbiont populations was the highest between these two geological locations, followed by inter-ridge sites between the East Pacific Rise and the Pacific Antarctic Ridge. A biogeographic physical barrier have played a very important role in population differentiation for both symbionts and their host mussels. Within a single ridge, the degree of differentiation was driven by geological distance in the CIR whereas this factor hardly played any role in the eastern Pacific ridges. The authors argued that different ridge spreading rates are main drivers of spatial and temporal connectivity of vent habitats. However, this observation is not supported by other recent studies on endosymbiont population genetics of deep-sea mussels. Based on analysis of population divergence processes of both symbionts and hosts from three ridge segments of the CIR, the authors argued that historical and physical constraints for habitats and dispersal between vents in the CIR affected dynamics of microbial population divergence.

Pereira et al. evaluated the role of magmatic fluid influx in vent systems of the East Scotia Ridge located in the Scotia Sea. For this, they analysed the chemical and isotopic compositions as well as fluid inclusions from three chimneys and showed that hydrothermal fluids varied over time within the studied basin. They conclude that the observed depletions in some fluid-mobile elements, since the previous fluid sampling 9 years before, was due to leaching. Their results also indicated that high-temperature fluid-rock interactions were key in setting the composition of the fluids. In particular, the cation-to-chloride ratios suggest a common "root zone" for the studied vent sites. The concentrations of dissolved gases provided new insights in the connection between magmatic degassing and its influence on end-member vent fluid composition and results point to a minor influx of magmatic vapour. When comparing the concentrations of conservative elements in the fluids of the different sampling sites, Pereira et al. found different behaviour, reflecting either sub-seafloor mixing between end-member fluid and seawater or the combination of abiotic and biotic reactions. Thermodynamic computations confirm that the East Scotia Ridge system is dominated by sulfide oxidation as a major catabolic pathway, favourable to sustain a robust sub-seafloor biosphere.

Author contributions

All authors listed have made a substantial, direct, and intellectual contribution to the work and approved it for publication.

Funding

PW and DB were financially supported by the Atlantic REMP project, funded by the European Union through service contract

no. EASME/EMFF/2017/1.3.1.1 - SI2.775068. PYQ was supported by Southern Marine Science and Engineering Guangdong Laboratory (Guangzhou) (2021HJ01, SMSEGL20SC01).

Conflict of interest

Author PW was employed by Seascape Consultants Ltd. Author DB was employed by Deep Seas Environmental Solutions Ltd.

The remaining authors declare that the research was conducted in the absence of any commercial or financial relationships that could be construed as a potential conflict of interest.

Publisher's note

All claims expressed in this article are solely those of the authors and do not necessarily represent those of their affiliated organizations, or those of the publisher, the editors and the reviewers. Any product that may be evaluated in this article, or claim that may be made by its manufacturer, is not guaranteed or endorsed by the publisher.

frontiers in Marine Science

SYSTEMATIC REVIEW
published: 20 August 2021
doi: 10.3389/fmars.2021.657358

Northern Mid-Atlantic Ridge Hydrothermal Habitats: A Systematic Review of Knowledge Status for Environmental Management

Rachel E. Boschen-Rose[1*†] *and Ana Colaço*[2,3*]

[1] Seascape Consultants Ltd., Romsey, United Kingdom, [2] Okeanos Research Centre, Universidade dos Açores, Horta, Portugal, [3] IMAR Instituto do Mar, Universidade dos Açores, Horta, Portugal

OPEN ACCESS

Edited by:
David Billett, Deep Seas Environmental Solutions Ltd., United Kingdom

Reviewed by:
Michael Vecchione, National Oceanic and Atmospheric Administration (NOAA), United States
Mustafa Yucel, Middle East Technical University, Turkey
Elva G. Escobar-Briones, National Autonomous University of Mexico, Mexico

***Correspondence:**
Rachel E. Boschen-Rose
reboschen-rose@outlook.com
Ana Colaço
maria.aa.colaco@uac.pt

†Present address:
Rachel E. Boschen-Rose, Ocean and Earth Science, University of Southampton, Southampton, United Kingdom

Specialty section:
This article was submitted to Deep-Sea Environments and Ecology, a section of the journal Frontiers in Marine Science

Received: *22 January 2021*
Accepted: *27 July 2021*
Published: *20 August 2021*

Citation:
Boschen-Rose RE and Colaço A (2021) Northern Mid-Atlantic Ridge Hydrothermal Habitats: A Systematic Review of Knowledge Status for Environmental Management. Front. Mar. Sci. 8:657358. doi: 10.3389/fmars.2021.657358

Highly specialised biota occurring at hydrothermally active vents on the northern Mid-Atlantic Ridge (nMAR: from south of Iceland to the Equator) have been the subject of numerous research projects over the 36-year period since these habitats were first discovered in the region. When hydrothermal activity ceases, biota endemic to hydrothermally active habitats are lost, and a new biota colonise these sites. Little is known about the biota colonising hydrothermally inactive sulphide habitats on the nMAR, although these sites may be the target of deep-sea mining within the next decade. In this review, we seek to clarify the current knowledge of biological communities colonising hydrothermally active habitats and inactive sulphide habitats on the nMAR. To achieve this, we (1) used a systematic review process to update the species list of benthic invertebrates associated with hydrothermally active habitats, (2) conducted a regional biogeographic analysis of hydrothermally active vent fields on the nMAR, (3) undertook a comprehensive literature review to provide a descriptive account of biological communities, and (4) identified key knowledge gaps in the current understanding of nMAR hydrothermally active and inactive ecosystems. Our updated species list increases the number of benthic invertebrates recorded from hydrothermally active habitats on the nMAR to 158 taxa. Our regional biogeographic analysis separates nMAR hydrothermal vent fields into distinct clusters based on depth/latitude and chimney composition. Vent fields close to the Azores (Menez Gwen, Lucky Strike, Rainbow) formed a separate cluster from those at greater depths south of the Azores (Broken Spur, TAG, Snake Pit, Logatchev, and Ashadze-1). Moytirra, located north of the Azores, clustered separately, as did Lost City with its unique carbonate chimneys. We present detailed information on the biological communities at hydrothermally active and inactive habitats in this region, and discuss the information available on the diversity, ecosystem function, trophic relationships, connectivity, temporal variability, and resilience and recovery of these communities. Many knowledge gaps still exist, with detailed information needed on all aspects of the biological communities at hydrothermally active habitats and inactive sulphide habitats on the nMAR to understand and predict impacts from natural and human-induced disturbances in the region.

Keywords: active hydrothermal vent, inactive sulphide habitats, polymetallic sulphide, North Atlantic, deep-sea mining, biodiversity, biogeography, ecology

INTRODUCTION

Hydrothermal habitats[1] form along the mid-ocean ridges and back-arc spreading centres of the global ocean. Where hydrothermal activity is sustained, this can support highly productive biological communities dependent on the chemosynthetic activity of microbes at the base of the food web. Despite the discovery of more than 300 confirmed active vent fields to date (Beaulieu and Szafranski, 2020), the global surface area of hydrothermally active habitats is small, representing <0.00001% of the surface area of the planet (Van Dover et al., 2018). Globally, more than 500 species have been described from hydrothermally active habitats, dominated by benthic invertebrate megafaunal and macrofaunal taxa with some meiofaunal taxa and fishes (Desbruyères et al., 2006). These hydrothermally active habitats and their diverse associated biota are considered to have considerable scientific and societal value (Van Dover et al., 2018).

Hydrothermal activity does not continue at a site indefinitely. Over a timescale of years to centuries, hydrothermal activity wanes and eventually ceases, leaving hydrothermally inactive sulphide sites and fields (Jamieson and Gartman, 2020). Where hydrothermal activity has ceased, the supply of reduced compounds essential to chemosynthesis is removed, and biota endemic to hydrothermally active habitats are subsequently lost. Although little is known about colonisation steps for inactive sulphide substrata, it is presumed that biota endemic to hydrothermally active habitats is gradually replaced by organisms which are not reliant on hydrothermal activity but are able to cope with weathered sulphide substrata.

Hydrothermal activity supports highly specialised biota, which have been the subject of numerous research projects over the 36-year period since the initial discovery of these habitats on the Mid-Atlantic Ridge (MAR) in 1985 (Kong et al., 1985; Rona et al., 1986). Many of the species recorded from hydrothermally active habitats on the northern MAR (nMAR: from south of Iceland to the Equator) are highly adapted and only occur in this region, such as *Bathymodiolus azoricus* and *B. puteoserpentis* mussels, and *Rimicaris exoculata* shrimp. The occurrence of species endemic to the nMAR has led to this region being identified as a separate biogeographic province (Bachraty et al., 2009; Moalic et al., 2012) with some analyses further dividing this region into two provinces (Van Dover et al., 2002). The location of 13 confirmed active vent fields where biological community information is available is provided in **Figure 1**. Where hydrothermal activity has been "inferred" on the nMAR from water column chemistry (Beaulieu and Szafranski, 2020), further visual surveys may confirm the occurrence of additional hydrothermal vent fields with thriving biological communities.

There are few records of hydrothermally inactive sulphide habitats along the nMAR, for example Mag Mell in the Moytirra vent field between the Azores and Iceland (Wheeler et al., 2013); and some chimneys within the Eiffel Tower sulphide complex in the Lucky Strike vent field near the Azores (Cuvelier et al., 2009). Whilst there are additional occurrences of inactive sulphide substrata along the nMAR, such as the Mir and Alvin zones of the TAG vent field (Rona et al., 1993; Krasnov et al., 1995; Lalou et al., 1998) and the Yubileinoe and Surprise vent fields (Bel'tenev et al., 2017), these commonly have little or no record of any associated biological communities. The distribution of hydrothermally inactive sulphide habitats along the MAR has probably been under-reported to date, with more occurrences waiting to be discovered in off-axis locations or along the ridge axis at sites more distant from active venting (Hannington et al., 2011).

Alongside the biological wealth of hydrothermally active habitats and inactive sulphide habitats on the nMAR, there is growing interest in the potential mineral wealth associated with some of these locations. Hydrothermal fluids can contain high concentrations of metal sulphides, and in some locations, these may form polymetallic sulphides (PMS) of sufficient grade and tonnage to be of economic interest. However, there are currently no exploitation (commercial mining) activities occurring on the MAR, and such activities may not be anticipated for several years, given that exploration contracts currently in place on the nMAR beyond national jurisdiction each have at least 6 years remaining (ISA, 2021).

In this paper, we review the available literature for the biological communities of nMAR hydrothermally active habitats and inactive sulphide habitats. In reviewing this information, we have four aims, to: (1) update the species list of benthic invertebrates associated with hydrothermally active habitats; (2) conduct a regional biogeographic analysis of the known hydrothermally active vent fields on the nMAR; (3) provide a multi-disciplinary descriptive account of the biological communities of nMAR hydrothermally active habitats and inactive sulphide habitats; and (4) discuss the results of our review and identify knowledge gaps in the current understanding of nMAR hydrothermally active and inactive ecosystems. By presenting this information, we hope to clarify the knowledge status for nMAR hydrothermal habitats, particularly in the context for environmental management of human activities on the ridge, including future deep-sea mining.

MATERIALS AND METHODS

Species List and Abundance Information for Benthic Invertebrates at Hydrothermally Active Habitats

To generate the updated species list and taxa abundance at the different vent fields, we searched the biological literature for studies that reported biodiversity from the hydrothermal vents on the northern section of the Mid Atlantic Ridge (nMAR: between south of Iceland and north of the Equator, see **Figure 1**). For this systematic review, we followed a PRISMA approach (**Figure 2**; **Supplementary Table 1**). Literature searches were conducted using the ISI Web of Science Database (featuring combinations of the keywords: hydrothermal vents; North Atlantic ridge biodiversity; Moytirra, Menez Gwen, Lucky

[1]For the purpose of this review, "hydrothermal habitats" encompasses (1) "hydrothermally active habitats," where hydrothermal activity is ongoing and provides seafloor habitats, and (2) "inactive sulphide habitats," where hydrothermal activity has ceased leaving behind sulphide substrata.

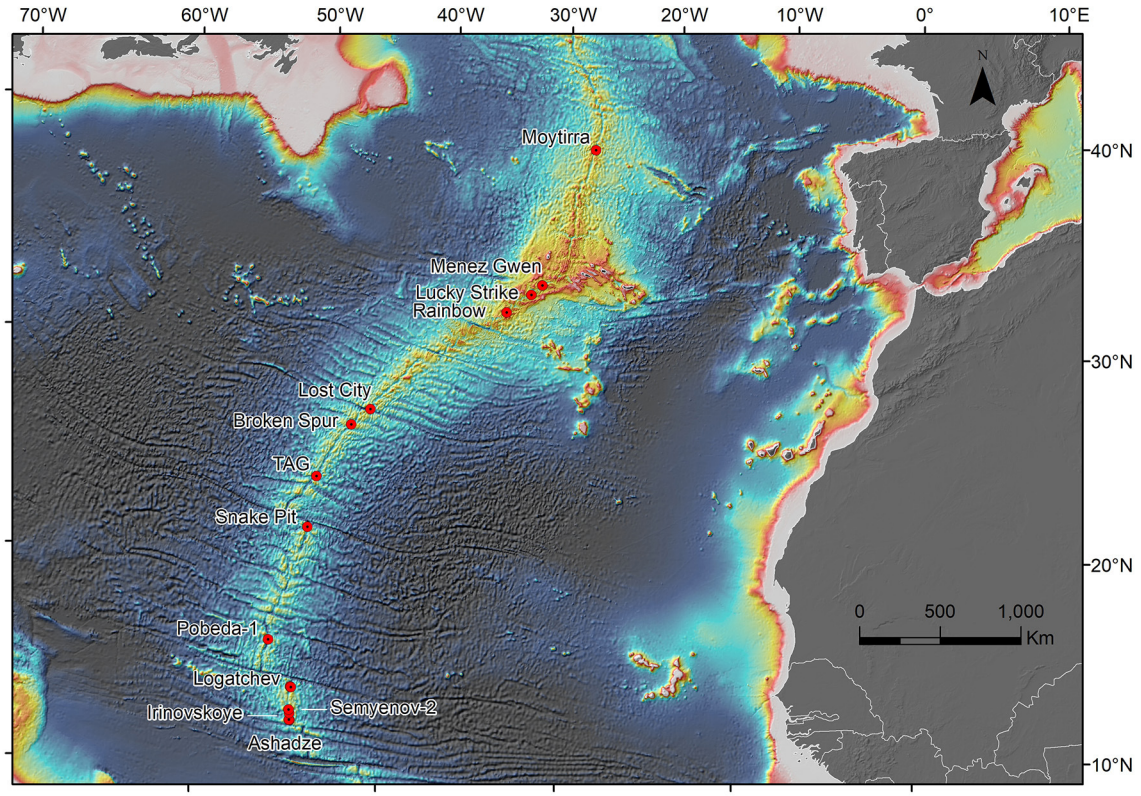

FIGURE 1 | The location of 13 hydrothermally active vent fields on the northern Mid-Atlantic Ridge. Map produced using the ETOPO1 1 Arc-Minute Global Relief Model: Procedures, Data Sources and Analysis. NGDC, NESDIS, NOAA, U.S. Dept. of Commerce, Boulder, CO. Escartin, J., M. Cannat, G. Pouliquen, A. Rabain and J. Lin. 2001. Lourenço, N., J.M. Miranda, J.F. Luis, A. Ribeiro, L.A.Mendes Victor, J. Madeira, and H.D. Needham. 1998.

Strike, Rainbow, Lost City, Broken Spur, Snake Pit, TAG, Logatchev, Pobeda, Irinovskoye, Semyenov, and Ashadze) and by following reference lists in papers. The "Handbook of deep-sea hydrothermal vent fauna" edited by Desbruyères et al. (2006) compiles all the available literature prior to 2006 to create the most comprehensive species list for vent invertebrates recorded from hydrothermally active habitats along the MAR to date. Consequently, we focused our literature compilation on all available literature between 2005 and 2020 (June), including all peer-reviewed studies.

All studies were screened for relevance to by reading the title and abstract; this step identified 32 studies as being relevant to the generation of the updated species list and associated abundance information. Full text was obtained for the 32 studies that were selected by the subject-based screening. The full text of these papers was examined and studies were excluded from our analyses if they presented the results of colonisation studies at hydrothermal vent fields using substrata of non-hydrothermal origin. The decision to exclude these studies was taken to avoid addition of taxa that would not usually be recorded from hydrothermally active habitats. Studies were also excluded if they occurred outside of the geographic scope for the study, or if they did not document additional species or location information when compared to Desbruyères et al. (2006). The taxonomic status of all taxa was checked and updated using the World Register of Marine Species (World Register of Marine Species, 2020). The final taxa list with accompanying abundance information was created using Desbruyères et al. (2006) and a further 12 studies (Stöhr and Segonzac, 2005; Ivanenko et al., 2006, 2012; Zekely et al., 2006a; Fabri et al., 2011; Wheeler et al., 2013; Sarrazin et al., 2015; Tchesunov, 2015; Plum et al., 2017; Yahagi et al., 2019).

The taxonomic and abundance information available for generating the revised species list and abundance dataset is potentially limited by differences in sampling effort amongst sites, and sampling biases introduced by differences in sampling methods or focus on certain taxonomic groups. To account for differences in abundance that may occur because of these potential biases, we restricted our quantitative analyses to the use of presence-absence data. Vent fields where there was insufficient information to provide reliable presence-absence data were excluded from quantitative analyses (see section Regional biogeographic analysis for hydrothermally active vent fields). The potential for these limitations to influence observed trends in diversity along the nMAR was carefully considered in the interpretation of our results (see section Species list for benthic invertebrates at hydrothermally active habitats).

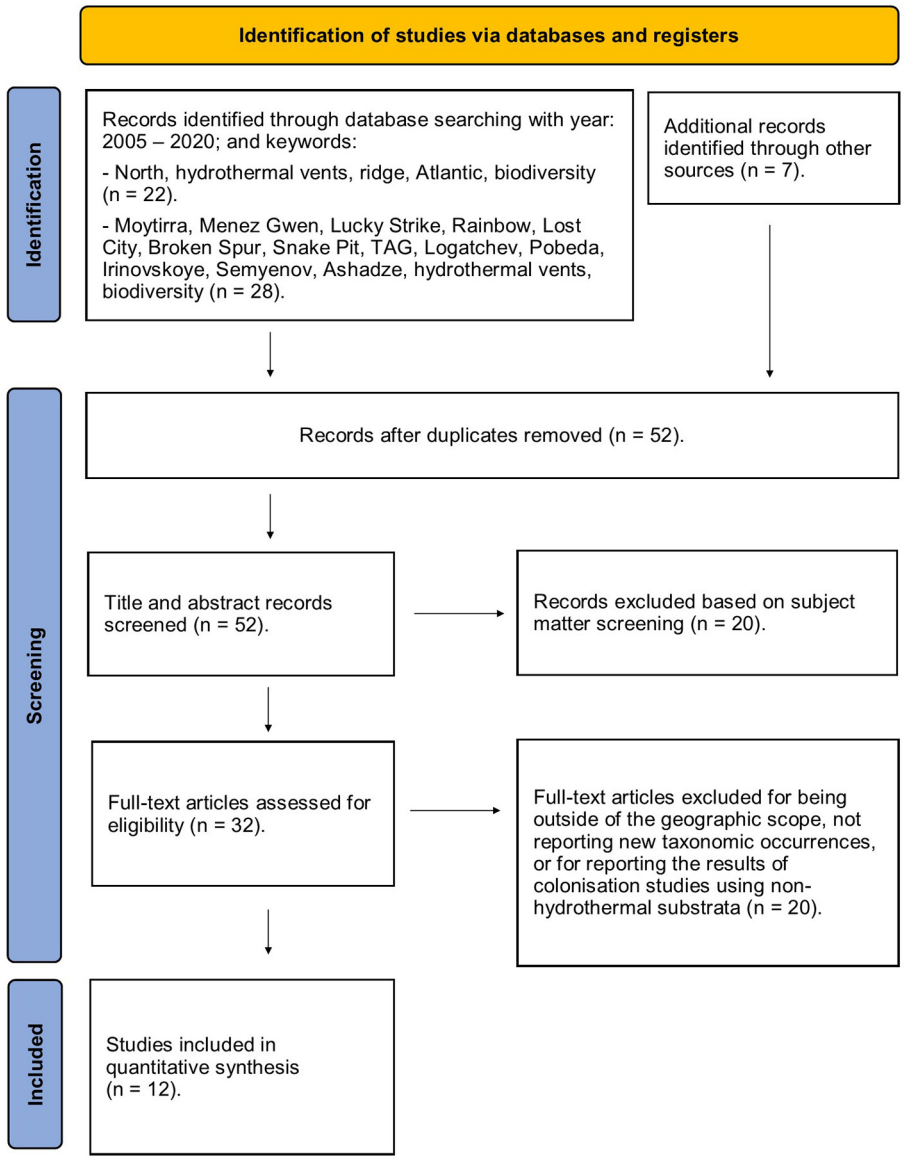

FIGURE 2 | The systematic review protocol to obtain records for quantitative synthesis was conducted according to PRISMA guidelines, adapted from Page et al. (2020). See PRISMA checklist in **Supplementary Table 1**.

Regional Biogeographic Analysis for Hydrothermally Active Vent Fields

Using the updated taxa list and abundance records described in section Species list and abundance information for benthic invertebrates at hydrothermally active habitats (see **Supplementary Table 2**), the biological information recorded from 10 of the 13 nMAR vent fields (Motirra, Menez Gwen, Lucky Strike, Rainbow, Lost City, Broken Spur, Snake Pit, TAG, Logatchev, and Ashadze-1) was used for multivariate analysis. There was insufficient biological information to include three of the vent fields (Pobeda-1, Irinovskoye, and Semyenov-2) in the analysis.

Presence-absence data for taxa recorded from the 10 vent fields were analysed using multivariate routines in the statistical software package PRIMER 7. Hierarchical Cluster Analysis (CLUSTER) was performed on the Bray-Curtis resemblance matrix, with a SIMPROF test (at $p = 0.05$) to determine sample group structure i.e., which vent fields had similar assemblage structure based on the presence-absence of taxa. The Bray-Curtis of a presence-absence matrix is directly equivalent of a Sorensen resemblance matrix (Clarke et al., 2014). In this type of resemblance matrix, joint absences have no effect on similarity amongst samples, instead similarity is determined by the presence of species amongst samples. Inclusion of additional

TABLE 1 | Environmental data for the 10 vent fields on the northern Mid-Atlantic Ridge.

Indicator	Moytirra	Menez Gwen	Lucky Strike	Rainbow	Lost City	Broken Spur	Snake Pit	TAG	Logatchev	Ashadze-1
Location Latitude (decimal degrees)	45.000	37.850	37.283	36.217	30.125	29.170	23.368	26.137	14.752	12.973
Depth (max depth m)	2,085	850	1,700	2,300	850	3,100	3,500	3,670	3,050	4,200
Host rock	Basalt	Basalt	Basalt	Ultramaphic	Ultramaphic	Basalt	Basalt	Basalt	Ultramaphic	Ultramaphic
Tectonic setting	Tectonic	Magmatic	Magmatic	Tectonic	Tectonic	Magmatic	Magmatic	Tectonic	Tectonic	Tectonic
Chimney type	Sulphides	Sulphides	Sulphides	Sulphides	Carbonates	Sulphides	Sulphides	Sulphides	Sulphides	Sulphides

Sources: Ludwig et al. (2006), Marques et al. (2007), Wheeler et al. (2013), German et al. (2016), and Beaulieu and Szafranski (2020).

samples does not affect the similarity amongst existing samples (Clarke et al., 2014). The cluster mode was group average with 9,999 permutations.

Non-metric Multidimensional Scaling (nMDS) plots and CLUSTER diagrams were produced to visualise patterns in the grouping of vent fields. For the nMDS, test parameters included minimum and maximum dimensions of 2 and 3 respectively; 50 restarts; a minimum stress of 0.01; and Kruskal fit scheme 1. To determine the taxa that contributed the most to similarity amongst SIMPROF groups, a SIMPER test was performed on the presence-absence data with a cut-off of 100%. The maximum SIMPER cut-off value of 100% was chosen to fully characterise the similarities amongst vent fields within SIMPROF groups.

To explore the relationship between the SIMPROF groups and potential environmental drivers, a BEST test (BioEnv & Stepwise) was performed using the BioENV setting. The test used 9,999 permutations and Spearman Rank Correlation, performed using the presence-absence Bray Curtis resemblance matrix and a Euclidean environmental data matrix. The environmental data matrix featured eight variables for each vent field (**Table 1**), which were grouped into four indicators: location (latitude); depth (maximum reported depth); host rock (basalt or ultramaphic); tectonic setting (tectonic or magmatic); and chimney type (sulphides or carbonates). These environmental variables were normalised to account for different units (latitude in decimal degrees; depth in metres; host rock, tectonic setting, and chimney type in presence-absence). A PCA plot was produced to illustrate the direction of effect that environmental variables had on the similarities amongst vent fields.

Descriptive Account of Biological Communities

To provide a detailed descriptive account of the biological communities at hydrothermally active habitats and inactive sulphide habitats on the nMAR, we reviewed a wide range of multidisciplinary literature, including biodiversity studies, species descriptions, ecological and geological studies, and studies relating to the function, trophic structure, connectivity, and resilience of these communities. We used more than 100 published literature sources to provide detailed accounts of the regional diversity of biological communities at hydrothermally active and inactive habitats, including microorganisms, benthic invertebrates, and benthic and benthopelagic fishes; ecosystem function; trophic relationships; connectivity; temporal variability; and resilience and recovery.

RESULTS

Species List for Benthic Invertebrates at Hydrothermally Active Habitats

The updated list for benthic invertebrates colonising hydrothermally active habitats on the nMAR features 158 taxa (see **Supplementary Table 2**). These taxa are phyletically diverse, including Foraminifera (1 taxon), Porifera (3 taxa), Cnidaria (15 taxa), Mollusca (25 taxa), Nematoda (30 taxa), Annelida (13 taxa), Arthropoda (64 taxa), Echinodermata (6 taxa), and Chaetognatha (1 taxon). The vent field with the highest taxonomic richness was Lucky Strike, followed by Snake Pit, Menez Gwen, Rainbow, Logatchev, Ashadze-1, Broken Spur, TAG, Lost City, and Moytirra (**Table 2**).

Regional Biogeographic Analysis for Hydrothermally Active Vent Fields

Northern MAR hydrothermal vent fields formed four clusters, according to CLUSTER and SIMPROF analyses and visualised by CLUSTER diagram (**Figure 3A**) and nMDS (**Figure 3B**). Group *c* contained most of the vent fields (Ashadze-1, Logatchev, Snake Pit, Broken Spur, TAG, and Rainbow). Group *d* contained Menez Gwen and Lucky Strike, which occur closer to the Azores. Moytirra and Lost City each formed their own cluster in the analysis.

From the SIMPER test, group *d* had an average similarity of 35.94%. Within group *d*, each of the 23 taxa present at both vent fields contributed equally (4.35%) to the similarity between vent fields (**Supplementary Table 3**), largely due to the use of presence-absence data and the existence of only two vent fields within this group. Group *c* had an average similarity of 43.93%. Within group *c*, only 10 taxa contributed more than 4% to the similarity amongst the six vent fields (**Supplementary Table 4**).

The clustering of nMAR hydrothermal vent fields by taxonomic composition was correlated with environmental variables. The BEST test with variables grouped by indicator determined that the SIMPROF clusters of vent fields had the strongest correlation with a combination of depth and chimney type (Rho $= 0.767$, $p < 0.05$). Inclusion of additional environmental variable groups, such as location, host rock or tectonic setting reduced the strength of correlation between the faunal presence-absence data and the environmental variables. Pearson correlation tests to check for confounding variables indicated that depth and latitude were strongly correlated (−0.69), with depth increasing with decreasing latitude, meaning

TABLE 2 | Number of taxa recorded from each of the 10 vent fields included in the study, from North to South: Moytirra, Menez Gwen, Lucky Strike, Rainbow, Lost City, Broken Spur, TAG, Snake Pit, Logatchev, and Ashadze 1.

Vent field	Moytirra	Menez Gwen	Lucky Strike	Rainbow	Lost City	Broken Spur	Snake Pit	TAG	Logatchev	Ashadze-1
Total number of taxa	9	35	93	31	13	22	44	21	27	24

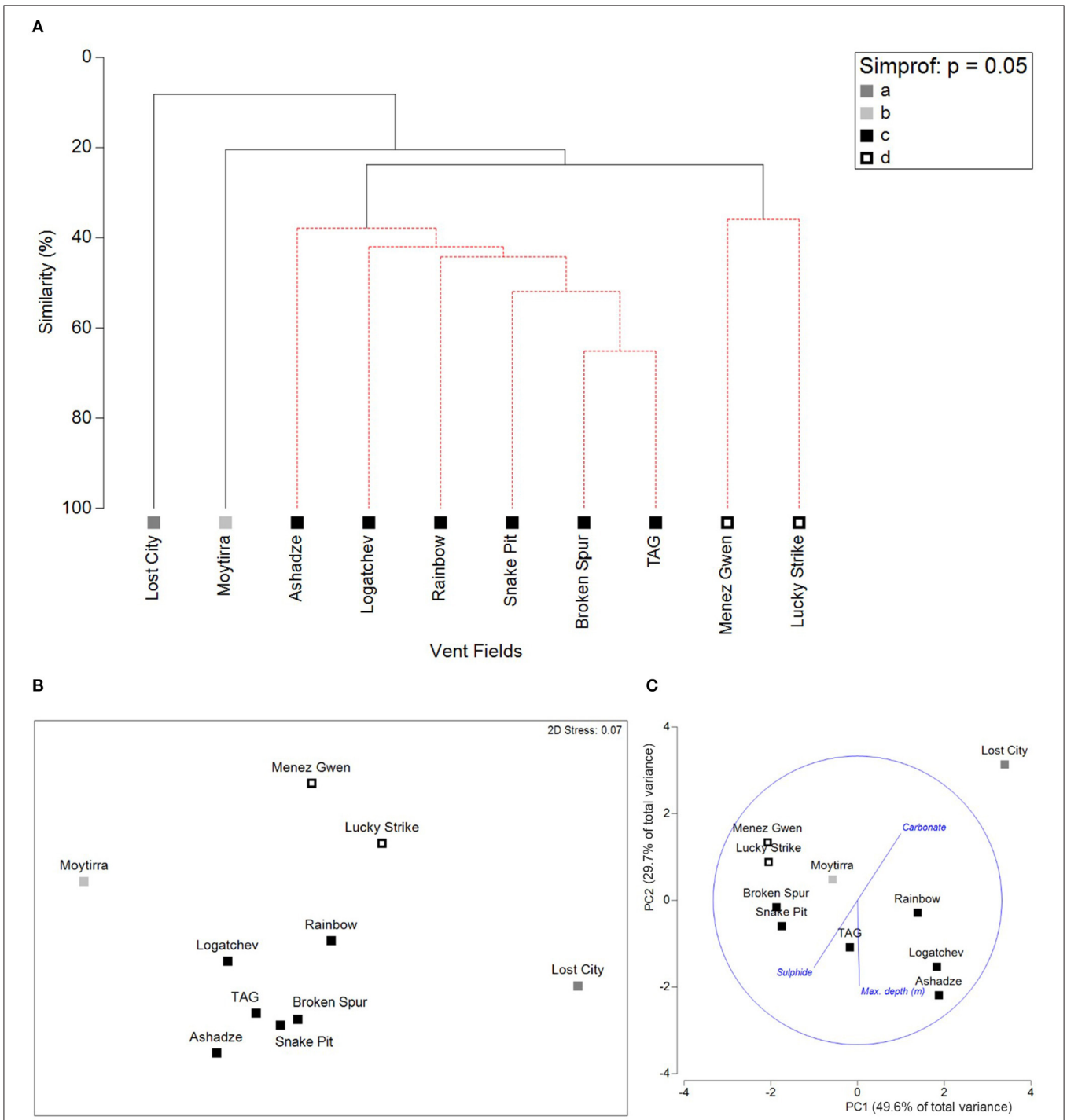

FIGURE 3 | (A) CLUSTER diagram of vent field similarity; **(B)** Non-metric Multidimensional Scaling (nMDS) plot of vent field similarity; **(C)** PCA of environmental variables, vectors displayed are the environmental variables (identified by the BEST test) with the strongest correlation with the presence-absence of taxa at the different vent fields.

that the influence of depth and latitude cannot be distinguished. However, including latitude in the model in addition to depth did not increase the explanatory power of the model. The PCA plot (**Figure 3C**) displays the three individual environmental variable vectors (maximum reported depth, carbonate chimneys, and sulphide chimneys) that contributed to the BEST test result with the strongest correlation with vent field taxa presence-absence data. Principle Component (PC) axes 1 and 2 explain 49.6 and 29.7% of the total variance respectively, explaining 79.3% of the total variance collectively.

Regional Diversity of Biological Communities at Hydrothermally Active Habitats and Hydrothermally Inactive Sulphide Habitats

Microorganisms

The local distribution patterns of methanotrophic and chemoautolithotrophic Archaea and Bacteria on the nMAR is linked to the chemistry of hydrothermal fluids, including the relative abundance of methane and sulphide, and the geological setting, such as basalt or ultramaphic rocks (Perner et al., 2007). On the nMAR, different archaeal and bacterial communities were associated with the different geological settings of ultramaphic-hosted Rainbow and basalt-hosted Lucky Strike vent fields (Flores et al., 2011). Comparisons between three ultramaphic-hosted vent fields (Rainbow, Ashadze-1, and Lost City) identified a diverse archaeal community heterogeneously distributed between the hydrothermal sites and types of samples analysed (seawater, hydrothermal fluid, chimney, and sediment) (Roussel et al., 2011). Of these sites, Lost City hosted a distinct microbial diversity, reflecting the highly alkaline warm fluids unique to this location (Roussel et al., 2011). Microbial mats from basalt-hosted Lucky Strike hydrothermal vent field had low diversity of archaeal genetic sequences, compared to ultramaphic-hosted sites, with just a single archaeal group (Crepeau et al., 2011). Conversely, Lucky Strike microbial mats have a diverse and active chemoautolithotrophic bacterial community, including methanotrophic and thiotrophic symbionts associated with bathymodiolid vent mussels (Crepeau et al., 2011).

Some protist lineages appear to occur in hydrothermal areas in multiple oceans, however some lineages have only been detected in the Atlantic (Lopez-Garcia et al., 2003). Microcoloniser experimental systems deployed on the hydrothermally active Eiffel Tower chimney in Lucky Strike indicated that bodonid and ciliate protists may be pioneers in the colonisation process of bare hydrothermally active substrata (Lopez-Garcia et al., 2003). There are no studies characterising the microbial communities of inactive sulphide habitats on the nMAR.

Benthic Invertebrates

According to the literature reviewed, the relative abundance of different megafaunal taxa varies between nMAR vent fields, with differences in abundance potentially being linked to depth or latitude. Starting at Moytirra the dominant megafaunal species in high temperature fluid areas are *Peltospira* sp. limpets and *Mirocaris* sp. shrimp, whilst bathymodiolid mussels are absent from the vent field (Wheeler et al., 2013). Moving south, as summarised by Rybakova and Galkin (2015), Menez Gwen and Lucky Strike are dominated by the vent shrimp *Mirocaris fortunata* in high temperature (20–40°C) habitats, with the vent mussel *Bathymodiolus azoricus* dominant in lower temperature (2–20°C) habitats. Continuing south and into deeper water, high temperature habitats at Rainbow, Broken Spur, TAG, Snake Pit, and Logatchev are not dominated by *M. fortunata,* as observed for more northerly sites; instead, these vent fields are dominated by the shrimp *Rimicaris exoculata* (Van Dover et al., 1988a; Copley et al., 2007; Rybakova and Galkin, 2015). Low temperature habitats at Rainbow remain dominated by *B. azoricus*, but there is a switch in the dominant mussel species to *Bathymodiolus puteoserpentis* at Broken Spur, through Snake Pit, and Logatchev (Rybakova and Galkin, 2015). Broken Spur represents a hybridisation zone between *B. azoricus* and *B. puteoserpentis*, with both species present and apparently able to interbreed (O'Mullan et al., 2001). The hydrothermal vent fauna of Lost City is sparse, comprising of a few "extremely rare" *B. azoricus* mussels (Kelley and Shank, 2010). Bathymodiolid mussels are absent from TAG vent field, with low temperature habitats dominated by the sea anemone *Maractis rimicarivora*, and on hydrothermal sediments, the chaetopterid polychaete *Phyllochaetopterus polus* (Galkin and Moskalev, 1990; Van Dover, 1995; Morineaux et al., 2010; Fabri et al., 2011). Moving to the most southern vent field on the nMAR, Ashadze-1, bathymodiolid mussels are also absent and the hydrothermally active hard substrata are dominated by *M. rimicarivora* (Fabri et al., 2011). Vent shrimp are also present at Ashadze-1, with *M. fortunata* having the highest abundance (Fabri et al., 2011). Illustrative examples of the biological communities at nMAR hydrothermally active habitats are provided in **Figure 4**.

From the quantitative studies conducted on meiofauna at hydrothermally active habitats on the nMAR, meiofaunal diversity appears to be low, with 15 meiofauna species found associated with *B. puteoserpentis* mussel beds at Snake Pit (Zekely et al., 2006a) and 25 meiofaunal taxa identified during a 2-year colonisation experiment on *B. azoricus* mussel beds at Lucky Strike (Cuvelier et al., 2014). At Snake Pit, metazoan meiofauna consisted of seven nematode species (63% of sampled individuals), six copepod species (35% of sampled individuals), one ostracod species, and one mite species (Zekely et al., 2006a). Meiofaunal taxa at Lucky Strike also included nematodes, copepods, and a mite species, with nematodes and copepods being the most and second-most dominant species, respectively (Cuvelier et al., 2014). Tchesunov (2015) determined that nematodes were the most abundant (700 individuals) and diverse (16 morpho-species) at Lucky Strike, whilst Lost City had the lowest abundance (172 individuals) but similar diversity (14 morpho-species) of nematodes. Sites further North at Menez Gwen, and further South at Snake Pit, were characterised by low diversity with high dominance of single species (Zekely et al., 2006b; Tchesunov, 2015).

The most common copepods recorded from hydrothermally active habitats on the nMAR are dirivultid copepods, a family of copepods which occurs almost exclusively at hydrothermal vents (Gollner et al., 2010a). The majority of the 12 dirivultid species

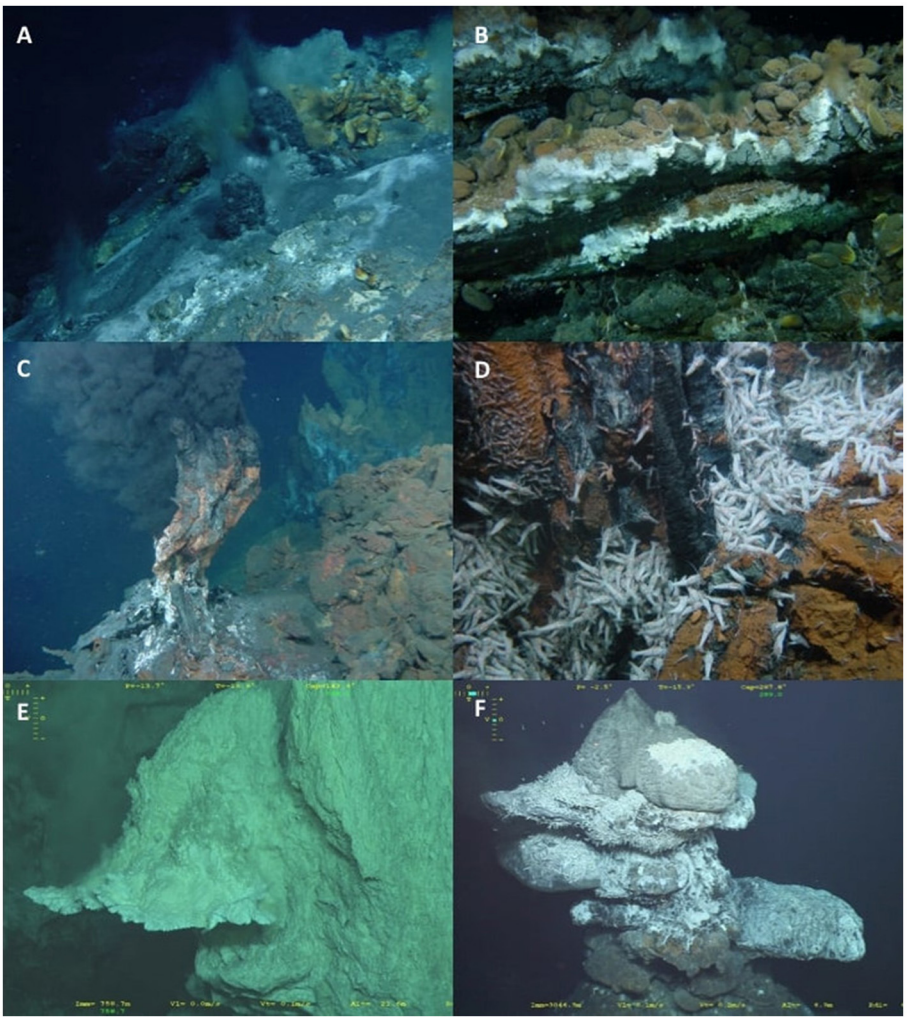

FIGURE 4 | (A) Menez Gwen hydrothermal vent field; **(B)** Lucky Strike hydrothermal vent field with *Bathymodiolus azoricus* mussel beds; **(C,D)** Rainbow vent field with swarms of the vent shrimp *Rimicaris exoculata*; **(E)** Carbonate chimney flange at Lost City vent field; **(F)** Chimney at the Broken Spur vent field with swarms of *R. exoculata*. Images **(A–D)** reproduced with permission: ©SEAHMA – PDCTM/MAR/15281/1999. Images **(E,F)** reproduced with permission: ©Ifremer – Mission Transect (Le Bris, 2018).

recorded from MAR vents only occur along the MAR, although four species have been recorded from at least one Pacific Ocean region (Gollner et al., 2010a). Harpacticoid copepod species have also been recorded from the nMAR, including from *B. azoricus* mussel beds at Lucky Strike (Ivanenko and Defaye, 2004; Ivanenko et al., 2012; Cuvelier et al., 2014) and from Snake Pit and Lucky Strike (Zekely et al., 2006a; Gollner et al., 2010b; Cuvelier et al., 2014).

For most hydrothermally inactive sulphide occurrences reported along the nMAR, there are no descriptions of associated biological communities (Reviewed by Krasnov et al., 1995; Lalou et al., 1998; Gablina et al., 2012; Bel'tenev et al., 2017; Van Dover, 2019; Rona et al., 1993). Small patches of inactive sulphide substratum on the Eiffel Tower edifice, Lucky Strike, were colonised by scavenging bythorgraeid crabs and hydroids, as identified from imagery surveys (Cuvelier et al., 2009). A similar occurrence of mobile scavengers, including bythograeid crabs, was reported from the inactive sulphide edifice Mag Mell in the Moytirra vent field (Wheeler et al., 2013). Preliminary data from biological collections made along the MAR between 12°58′N and 13°31′N using geological sampling gear suggested that fauna is scarce at inactive sulphide habitats (Molodtsova et al., 2014). The benthic invertebrates collected were mostly represented by sessile suspension feeders, such as Porifera (sponges), Alcyonacea (soft corals), Antipatharia (black corals), Hydrozoa (hydroids), Cirripedia (barnacles), and Bryozoa (bryozoans) (Molodtsova et al., 2014). Some of the species collected by Molodtsova et al. (2014), such as the black coral *Alternatipathes alternata*, golden coral *Metallogorgia melanotrichos,* and its associated basket star *Ophiocreas oedipus,* are widely distributed, lower bathyal species. According to Molodtsova et al. (2014), there did not appear to be any benthic invertebrate species endemic to hydrothermally

TABLE 3 | Fish species recorded from hydrothermal vents along the Mid-Atlantic Ridge.

Family	Species name	Common name
Bythitidae	*Cataetyx laticeps*[G]	Bythitid fish
Chimaeridae	*Hydrolagus affinis*[G]	Small-eyed rabbit fish
	Hydrolagus pallidus[G]	Pallid ghost shark
Lotidae	*Gaidropsarus* sp.*	Gadoid fish
Macrouridae	*Coryphaenoides armatus*[G]	Armed grenadier
Moridae	*Lepidion schmidti*[G]	Schmidt's cod
Sebastidae	*Trachyscorpia echinata*[G]	Spiny scorpion fish
Synaphobranchidae	*Ilyophis saldanhai**	Arrow-tooth eel
Zoarcidae	*Pachycara saldanhai**	Eel pout
	*Pachycara thermophilum**	Eel pout

*Species records were taken from Desbruyères et al. (2006). Taxonomic status was updated using the World Register of Marine Species (WoRMS Editorial Board, 2021). *vent species; [G]general deep-sea species.*

inactive sulphide habitats. Preliminary studies from within the Russian Exploration Area along the MAR indicated that seafloor massive sulphide outcrops were characterised by low densities of megafauna, whereas non-hydrothermal rocky habitats were colonised by assemblages of larger suspension feeders, especially at elevated locations (Galkin et al., 2019).

Benthic and Benthopelagic Fishes

There is limited information available on the benthic and benthopelagic fishes at hydrothermally active habitats or inactive sulphide habitats along the nMAR. Ten species of fish were recorded from hydrothermally active habitats in Desbruyères et al. (2006) (**Table 3**). Four of these species were considered endemic to hydrothermally active areas, whilst the remaining six species were known from other habitats in the North Atlantic or from other oceans.

Almost nothing is known about the benthic and benthopelagic fishes occurring at inactive sulphide habitats on the nMAR, with only one record of a *Pachycara* sp. zoarcid fish observed at the hydrothermally inactive chimneys of Mag Mell, an edifice in the Moytirra vent field (Wheeler et al., 2013). These mobile predators were also recorded elsewhere within the vent field and were not considered endemic to inactive sulphide habitats.

Ecosystem Function

Vent fields on the nMAR with different geochemistry host functionally different microbial communities, for example, the absence of methanogens at certain sites (Flores et al., 2011). So far, only the following vent fields have been studied for microbial function - Logatchev, Rainbow, TAG, and Snake Pit. At the Irina II site within Logatchev vent field, two important groups of primary producers, Epsilonproteobacteria and Gammaproteobacteria, were discovered to use different pathways for sulphur oxidation and carbon fixation (Hügler et al., 2010). A range of sulphate-reducing prokaryotes were also identified from the Irina II site, including Deltaproteobacteria, Thermodesulfobacteria, and Archaeoglobales. The latter two prokaryotes are thermophyllic and hyperthermophyllic, respectively and are thought to inhabit the higher temperature environment of the seafloor subsurface, being subsequently carried to the seafloor within vent fluids (Hügler et al., 2010). Chemolithoautotrophic iron oxidising Zetaproteobacteria are thought to play an essential role in the global iron cycle and have been identified from Rainbow, TAG, and Snake Pit vent fields (Scott et al., 2015). Zetaproteobacteria at these sites are rare if an iron source is not readily available, suggesting that this organism is likely locally restricted to iron-rich marine environments but may exhibit wide-scale geographic distribution (Scott et al., 2015). Zetaproteobacteria have also been reported in association with the gill chamber of the hydrothermal vent shrimp *Rimicaris exoculata* from the Rainbow vent field (Zbinden et al., 2004; Jan et al., 2014).

There is no published information available on the ecosystem function of microbial communities colonising hydrothermally inactive sulphide habitats along the nMAR. Other than trophic interactions (see section Trophic Relationships), the functional roles of benthic invertebrates and fishes found at hydrothermally active habitats or inactive sulphide habitats on the nMAR are also unknown.

Trophic Relationships

According to Polar Lipid Fatty Acid (PLFA) profiles, benthic invertebrate species at nMAR hydrothermally active habitats can be divided into two feeding groups: the first group, consisting of mussels, commensal polychaetes, and gastropods, is more dependent on sulphur-oxidising bacteria; the second group, comprising shrimps and crabs, has more anaerobic sulphate-reducing bacteria biomarkers (Colaço et al., 2007). Other benthic invertebrate species fall between the two groups, presenting a mixed feeding strategy that includes feeding on bacteria in addition to other types of food. Of the benthic invertebrates studied, the ampharetid polychaete *Amathys lutzi* had the most diversified bacterial diet, presenting fatty acid biomarkers from both S-oxidising and S-reducing bacteria (Colaço et al., 2007).

The complex trophic linkages between microbial communities and the fauna at nMAR hydrothermally active habitats were initially determined using the isotopic composition of 24 invertebrate taxa, bacterial mats, and filamentous bacteria from seven vent fields (Menez Gwen, Lucky Strike, Rainbow, Broken Spur, TAG, Snake Pit, and Logatchev) (Colaço et al., 2002). As is typical for hydrothermal vent ecosystems, chemolithotrophic bacteria (both symbiotic and free-living) formed the basis of the food web at the nMAR vent fields. These bacteria support primary consumers through symbioses with nMAR benthic invertebrates or through the grazing of free-living bacteria in warmer vent habitats. Well-documented examples of these symbiotic relationships include the nMAR vent mussels *Bathymodiolus puteoserpentis* and *B. azoricus*, which harbour both sulphuroxidising and methane-oxidising bacteria in specialised organs, bacteriocytes, within their gill tissue (Fiala-Médioni et al., 2002; Duperron et al., 2016); and the nMAR vent shrimp *Rimicaris exoculata*, which harbours two different bacterial epibionts on specialised appendages and on the inner surface of its gill chamber (Petersen et al., 2010). *Rimicaris exoculata* also benefits from free-living bacteria, which it grazes

from the warmer vent habitats (Colaço et al., 2002). The most recently proposed symbiosis on the nMAR occurs with a new species of nematode described from Lucky Strike, *Oncholaimus dyvae*, which may harbour symbiotic sulphur-oxidising bacteria (Bellec et al., 2018; Zeppilli et al., 2019).

According to stable isotope ratios, many benthic invertebrates at the Menez Gwen, Lucky Strike, Rainbow, Broken Spur, TAG, Snake Pit, and Logatchev vent fields have mixed feeding strategies (Colaço et al., 2002; De Busserolles et al., 2009; Portail et al., 2018). The initial food web description for nMAR hydrothermally active habitats provided by Colaço et al. (2002) indicates that small invertebrates living within the byssus threads of bathymodiolid mussel colonies feed on bacteria or detritus trapped within the byssus net. The shrimp *Rimicaris chacei* and *Mirocaris fortunata* are mixotrophic, feeding on bacteria, shrimps, and other small invertebrates. Other shrimp species are predatory, such as *Alvinocaris markensis,* which consumes other shrimps. The main predators that are restricted to nMAR hydrothermally active habitats include the gastropod snail *Phymorhynchus* sp., which feeds almost exclusively on the bathymodiolid mussels, and the crab *Segonzacia mesatlantica,* which eats shrimps and small invertebrates. The top predators consist of common bathyal species, such as the crab *Chaceon affinis* and some fishes, which make incursions into nMAR vent fields to feed, particularly at shallower sites where the phase separation of fluids and depletion in metals makes these environments less inhospitable to non-vent predators (Colaço et al., 2002).

Stable isotope ratios have also been measured for the four visually most-dominant species of benthic invertebrates at Ashadze-1 vent field: the gastropod snail *Phymorhynchus moskalevi*, sea anemone *Maractis rimicarivora*, shrimp *Mirocaris fortunata,* and chaetopterid polychaete worm *Phyllochaetopterus polus* (Fabri et al., 2011). All four species were discovered to be heterotrophic, with comparisons between the of $\delta^{13}C$ values from Ashadze-1 and other vent fields along the nMAR suggesting that they have the same food source at all vent sites (Fabri et al., 2011). The generally high $\delta^{15}N$ values for these four species indicated that their nitrogen source came from recycled organic matter, supporting the concept that these species are all secondary consumers in the Ashadze-1 ecosystem (Fabri et al., 2011). Based on the mean $\delta^{34}S$ values for these species, it was considered that the Ashadze-1 food web is based on locally produced organic matter, such as vent sulphides, pore-water sulphides, and thiosulphate (Fabri et al., 2011). The Sulphur isotopic values and high trophic level of the four species investigated were considered evidence for the existence of a chemosynthetic ecosystem at Ashadze-1, despite the visual absence of species known to exhibit chemosynthetic symbiosis during the survey (Fabri et al., 2011).

The food webs of hydrothermal vent fields along the nMAR can also exhibit intra- and inter-field variation. Whilst the dominant basal organic matter sources of food webs at Menez Gwen, Lucky Strike and Rainbow vent fields are similar, there are intra- and inter-field variations in their relative contributions, relating to the availability of reduced compounds to support methanotrophy and chemoautotrophy (Portail et al., 2018). The contribution of photosynthetic-derived organic matter was negligible in all three of these vent fields, irrespective of vent field depth. All the species shared amongst sites exhibited high trophic flexibility, suggesting that differences in the basal organic matter source amongst sites may not be a structuring factor (Portail et al., 2018). Despite variation in environmental conditions and community structure, functional structure was similar across assemblages, and was thought to reflect both the trophic flexibility of vent heterotrophs and the ability of vent fauna to adapt to several geological contexts (Portail et al., 2018).

Smaller scale variation in trophic relationships can also occur at hydrothermally active habitats on the nMAR, as described for the Eiffel Tower edifice within the Lucky Strike vent field (De Busserolles et al., 2009). *Bathymodiolus azoricus* mussel bed communities were sampled from 12 different locations on the Eiffel Tower edifice, with three species (*A. lutzi*, *B. azoricus* and its associated polychaete *Bathynoe seepensis*) exhibiting significant spatial variability in isotopic signatures. Environmental conditions were at least partially responsible for this variability, with vent fluid characteristics thought to be key factors in the variation of local carbon sources, through influences on microbial production (De Busserolles et al., 2009). In support of previous work conducted at Lucky Strike (Colaço et al., 2002, 2007), De Busserolles et al. (2009) also found two apparently independent trophic groups, the symbiont-bearing fauna (*B. azoricus* and associated polychaete *Bathynoe seepensis*), and the heterotrophic fauna (bacterivores, detritivores, scavengers, and predators).

The feeding guilds of meiofaunal taxa collected from Snake Pit were investigated by Zekely et al. (2006a) who determined that primary consumers, mostly deposit feeders, comprised more than 95% of the total meiobenthos at the site, followed by parasitic copepods and mites. All the nematodes and 80% of copepod individuals were primary consumers, with 20% of the copepod community being parasitic. Meiofaunal predators were absent in all samples collected from Snake Pit (Zekely et al., 2006a). Three meiofaunal taxa were also included within the work of Portail et al. (2018), where the isotopic signatures of suspension-feeding ostracods were consistent with bacteriovores or detritivores/scavengers, and the isotopic signatures of deposit-feeding *Aphotopontius* sp. copepods were consistent with bacteriovores or commensals. The deposit feeding *Oncholaimus dyvae* nematodes were either detritivore/scavengers or predators according to their stable isotope signatures (Portail et al., 2018).

The non-vent endemic benthopelagic fauna of the Broken Spur vent field exhibited isotopic signatures closer to the chemosynthetic vent fauna than might be expected (Vereshchaka et al., 2000), which was interpreted to indicate some degree of coupling between benthopelagic shrimp and fish and the chemosynthetic communities more typical of hydrothermally active habitats. The trophic structure of the biota colonising inactive sulphide habitats along the nMAR is unknown, largely because the biota of these habitats has not yet been characterised.

Connectivity

Hydrothermal vents along the nMAR can exist in a steppingstone manner along the ridge, with vent fields separated by distances of a few to hundreds of km distance

(Murton et al., 1994; German et al., 1996; Beaulieu and Szafranski, 2020). The steppingstone model of connectivity has been suggested for *Bathymodiolus* mussels along the MAR, where mussel populations are contemporarily isolated and population connectivity can only be maintained in a stepwise manner (Breusing et al., 2016). It has been further suggested that, despite a long pelagic larval duration for *Bathymodiolus* spp. (Arellano and Young, 2009), the connectivity patterns observed on the MAR would indicate the existence of additional, yet uncharacterised ("phantom"), steppingstones to maintain the isolated populations (Breusing et al., 2017).

Bathymodiolus species on the MAR also exhibit a mid-ocean hybridisation zone, with *B. azoricus* occurring at the shallower (850–2,251 m) northern localities, *B. puteoserpentis* occurring at the deeper (3,080–3,650 m) southern localities (Maas et al., 1999), and both species occurring and hybridising at an intermediate latitude (O'Mullan et al., 2001). Examination of DNA sequences from seven nuclear loci and a mitochondrial locus suggests that these closely related species may have split <1 million years ago (Faure et al., 2009), with the genetically mixed population at intermediate latitudes providing no evidence for hybrid incompatibilities (Breusing et al., 2017).

Other species at hydrothermally active habitats on the nMAR have population connectivity patterns more akin to panmixia, with high rates of gene flow and limited evidence of population genetic structure. The shrimp *R. exoculata* exhibits extraordinarily high rates of gene flow along the MAR (Teixeira et al., 2010), thought to result from the life history traits of this species, including the production of large lecithotrophic eggs and planktotrophic larvae that feed in the photic zone before settling as juveniles (Dixon and Dixon, 1996). *Shinkailepas briandi* limpets are common in several vent fields on the nMAR, including Menez Gwen and Ashadze-1, with this species exhibiting panmixia throughout its geographic and bathymetric distribution (Yahagi et al., 2019). From the retention of eye pigmentation in newly settled *S. briandi* juveniles, along with genetic panmixia, it has been suggested that the hatched larvae of *S. briandi* vertically migrate to the surface waters to take advantage of richer food supplies and stronger currents for dispersal (Yahagi et al., 2019).

Some species on the nMAR are found both at hydrothermally active habitats and at other chemosynthetic habitats in the North Atlantic and further afield. The clam *Abyssogena southwardae* has been recorded from Logatchev on the nMAR, Clueless vent field on the southern MAR (north and south of the Romanche Fracture Zone, respectively), and from cold seep sites on the West Florida Escarpment, the Barbados Accretionary Prism, and the Lobes of the Congo (Krylova et al., 2010; LaBella et al., 2017). The *A. southwardae* populations on the MAR were included within the same lineage as the West Florida Escarpment, Barbados Accretionary Prism, and Lobes of the Congo populations, whilst an additional lineage was restricted to the Lobes of the Congo population (LaBella et al., 2017). Haplotypic evidence suggests that there is no major hydrographic barrier for *A. southwardae* populations north and south of the Romanche Fracture Zone (Van der Heijden et al., 2012; LaBella et al., 2017), with multiple lines of genetic evidence supporting connectivity between the Logatchev, Clueless, and Barbados Accretionary Prism populations of *A. southwardae* (LaBella et al., 2017).

It has been suggested that some nMAR meiofaunal taxa, such as dirivultid copepods, may have high dispersal potential and thus population connectivity (Gollner et al., 2011). Further research confirmed high genetic connectivity of copepods at hydrothermally active habitats and highlighted the high diversity and expansive population growth of this group (Gollner et al., 2016). Connectivity between hydrothermally active habitats for these copepods may be further facilitated using intermediate non-hydrothermal chemosynthetic habitats as steppingstones (Gollner et al., 2016), a concept which has also been proposed for bathymodiolid mussels (Breusing et al., 2016) and the clam *A. southwardae* (LaBella et al., 2017).

Little is known about the population connectivity of symbiotic bacteria at hydrothermally active habitats on the nMAR. The two dominant thiotroph- and methanotroph-related symbionts found in *B. azoricus* and *B. puteoserpentis* mussels collected from vent sites along the MAR shared highly similar or identical 16S rRNA phylotypes (Duperron et al., 2006), suggesting that populations of symbionts may show different connectivity patterns from their invertebrate hosts. Full population genetics studies of nMAR symbionts have not yet been undertaken. There are no studies on the connectivity of biota colonising inactive sulphide habitats along the nMAR.

Temporal Variability

Temporal variability in biological communities at hydrothermally active habitats along the nMAR has been assessed using a variety of methods. These include repeat surveys of the same site over multiple months or years (Copley et al., 2007; Cuvelier et al., 2011b); fixed-term deployment of *in-situ* monitoring equipment, such as the TEMPO module deployed at Lucky Strike (Sarrazin et al., 2014); and long-term monitoring through fixed observatories, such as the EMSO-Azores non-cabled seafloor multidisciplinary observatory, also at Lucky Strike.

Some nMAR microbial communities demonstrate potential for rapid colonisation of new suitable substrata, as observed in the Snake Pit vent field where deployment of an *in-situ* growth chamber (vent cap) resulted in the formation of a white microbial mat following only 5 days of deployment (Reysenbach et al., 2000). This new microbial community contained a mix of hyperthermophiles, moderate thermophiles, and mesophiles, reflecting the gradual reduction in temperature within the chamber (70–20°C) during the 5 days of deployment (Reysenbach et al., 2000). Microbial communities on the nMAR can also respond to episodic events, such as the natural de-gassing events between 2009 and 2010 at the Eiffel Tower site, Lucky Strike, which promoted the development of thermophilic/anaerobic Archaea and Bacteria (Archaeoglobales, Nautiliales, Nitratiruptoraceae) (Rommevaux et al., 2019). The periodicity of natural de-gassing events at Lucky Strike is not known; the frequency of this disturbance and related shift in microbial community is equally unknown. However,

these studies demonstrate that microbial communities at high temperature hydrothermally active habitats on the nMAR can respond (at a community level) to rapid changes in environmental parameters, including episodic events.

Shifts in archaeal and bacterial communities at the nMAR Lost City vent field can occur in response to environmental changes over 1,000-year timescales (Brazelton et al., 2009). Lost City presents a different environment for microbial communities, with its carbonate chimneys forming through highly alkaline vent fluid, in contrast to the acidic vent fluids occurring at all other known vent fields along the MAR. "Rare" members of the Lost City microbial community can become dominant when environmental conditions change, on 1,000-year timescales, with the long history of chimney growth cycles at Lost City resulting in numerous closely related microbial "species," each preadapted to a particular set of reoccurring environmental conditions (Brazelton et al., 2009).

There is evidence from Lucky Strike vent field that relatively diverse assemblages of macrofauna and meiofauna (20 and 25 taxa, respectively) can inhabit newly-available adjacent substrata within a short time (2 years) (Cuvelier et al., 2014). Temporal variation of these groups at shorter or longer time periods is unknown.

The nMAR benthic invertebrate megafauna demonstrates multiple scales of temporal variability, including changes in feeding behaviour corresponding to semi-diurnal tidal cycles (Cuvelier et al., 2017), and seasonality in reproduction for some species (Colaço et al., 2006; Dixon et al., 2006). Different benthic invertebrates may demonstrate different patterns in temporal variation, for example, *B. azoricus* mussels from Menez Gwen vent field demonstrate seasonal patterns in reproduction linked to the timing of the winter-spring phytoplankton bloom (Dixon et al., 2006; Colaço et al., 2009), whereas there was no evidence for seasonal reproduction in *R. exoculata* shrimp from TAG vent field (Copley et al., 2007).

Some nMAR benthic invertebrate communities at hydrothermally active habitats demonstrate considerable stability, over multiple time scales. Daily observations of *B. azoricus* from Lucky Strike during a 48-day period demonstrated the stability of vent mussel assemblages during this time, reflecting the relative stability of environmental conditions (Sarrazin et al., 2014). Although tidal signals could be detected at this site, there was no evidence that the vent mussels, shrimp, crabs, or bucciniform gastropods responded to tidal periodicity. However, polynoid worms did exhibit significant multi-day periodicities, suggesting that the harmonics of tidal cycles may influence their distribution (Cuvelier et al., 2017). Over intermediate time periods at Lucky Strike, only small changes in *B. azoricus* coverage and density were observed, with an 11% increase in mussel densities between 2006 and 2008 (Sarrazin et al., 2014). Stable patterns of the vent shrimp *M. fortunata* and crab *Segonzacia mesatlantica* were also observed at Lucky Strike over a 9-month period (Matabos et al., 2015).

Northern MAR benthic invertebrate communities can also demonstrate stability over multiple years, even decadal periods (Copley et al., 2007; Cuvelier et al., 2011b). Vent shrimp populations at Broken Spur were stable over a 15-month period (Copley et al., 1997), whilst mature vent communities at TAG (Copley et al., 2007) and Lucky Strike (Cuvelier et al., 2011b) demonstrated decadal stability in the abundance of dominant species at the edifice scale. Within the Eiffel Tower edifice at Lucky Strike, significant differences in assemblage coverage and distribution were linked to localised fluctuations in hydrothermal activity (Cuvelier et al., 2011a). Within the Logatchev vent field, significant changes in the population density of predatory gastropods *Phymorchynchus* spp. and the disappearance of a live vesicomyid clam population over a 10-year period were similarly linked to fluctuations in hydrothermal activity (Gebruk et al., 2010).

There is also some evidence for changes in local biological assemblages linked to alterations in the hydrothermal activity of habitats patches on the nMAR. Changes in the coverage of hydrothermally inactive sulphide habitats patches ("Substratum 1a": Cuvelier et al., 2009) on the Eiffel Tower edifice within Lucky Strike over a 14-year period were accompanied by increasing colonisation of these patches by *B. azoricus* mussels, consistent with hydrothermal fluid flux increase (Cuvelier et al., 2011b). There are no studies on the nMAR specifically assessing the temporal variability of biota at inactive sulphide habitats.

Resilience and Recovery

On the nMAR, high-intensity illumination associated with Human-Occupied Vehicles (HOVs) and Remotely Operated Vehicles (ROVs) has been implicated in photoreceptor damage in *Rimicaris exoculata* shrimp that aggregate at high-temperature hydrothermal vents (Van Dover, 2014). The visual pigment (rhodopsin) of the thoracic eyes in adult *R. exoculata* is sensitive to light, with studies demonstrating that it degrades rapidly with light exposure (Johnson et al., 1995; Herring et al., 1999). The thoracic eyes of *R. exoculata* are thought to be an adaptation for detecting the dim light generated by high-temperature venting as a near-field remote-sensing means of avoiding thermal stress and mortality (Van Dover et al., 1989). Behavioural consequences of damage to photoreceptors in vent shrimp are unknown, although there is no evidence for negative impacts on shrimp populations repeatedly exposed to high-intensity illumination (Copley et al., 2007).

Based on physical and genetic studies, the recolonisation of disturbed sites by *Bathymodiolus* mussels (foundation species where they are present on the MAR) is only expected to occur by chance (Breusing et al., 2017), indicating that populations of these species have a low resilience to impact. A recent small scale disturbance experiment assessing recovery after an artificial disturbance inside the Lucky Strike hydrothermal vent field demonstrated that after 2 years there was a major change in faunal composition, only a partial recovery of faunal densities, and that the species composition of the neighbouring faunal assemblages strongly affects the species composition of the recolonising community (Marticorena et al., 2021).

DISCUSSION

Species List for Benthic Invertebrates at Hydrothermally Active Habitats

The global taxa list for hydrothermal vent invertebrates presented by Desbruyères et al. (2006) included 100 benthic invertebrate

taxa sampled from the MAR, representing nearly 20% of the global hydrothermal vent fauna diversity known at that time. Most benthic invertebrate taxa listed by Desbruyères et al. (2006) were megafauna and macrofauna, reflecting that many studies have focused on megafauna, with few studies on macrofauna and even fewer on meiofauna. The megafauna is the only group that can be readily studied through imagery, however abundances of these taxa generated from imagery are often lower compared to abundances generated from physical samples (Cuvelier et al., 2012). Physical samples are needed to fully characterise nMAR communities, especially for macrofaunal taxa such as smaller polychaetes and gastropods, pycnogonids, ostracods, actinids, halacarids, nematodes, copepods, tanaids, and amphipods (Cuvelier et al., 2012).

Further survey and research efforts along the nMAR have discovered new species, including smaller meiofaunal species, which do not feature in the Desbruyères et al. (2006) taxa list. The updated taxa list presented here features 158 taxa and is expected to be refined following ongoing scientific expeditions to the nMAR. The updated list includes a greater number of recorded taxa at nMAR vent fields than was reported previously (Fabri et al., 2011; Sun et al., 2020), reflecting ongoing species discovery in the region. The most northern, shallowest nMAR vent fields (Menez Gwen, Lucky Strike, Rainbow) were reported by Fabri et al. (2011) as having the highest species richness, followed by Snake Pit. This general pattern also occurs in the present analysis, although the deeper Snake Pit vent field is the second most taxonomically diverse, after Lucky Strike, and before Menez Gwen and Rainbow. As in Fabri et al. (2011), the deeper more southerly vent fields (Ashadze-1, Logatchev, TAG, and Broken Spur) all have lower taxonomic diversity than the more northerly, shallower vent fields. Lost City has very low taxonomic diversity in both studies. The vent field with the lowest taxonomic diversity in the present study was Moytirra, which was discovered after Fabri et al. (2011) was published.

It is possible that the apparent trends in diversity may be linked to differences in sampling effort amongst sites. However, given that similar patterns in diversity have been observed in the present study and Fabri et al. (2011), despite the present study having almost twice the number of taxa compared to Fabri et al. (2011) (158 and 88 taxa, respectively), the observed differences in taxonomic diversity may represent true trends in diversity distribution along the nMAR. Further targeted sampling programs across vent fields, using standard methods and spanning whole communities (microbes to megafauna), would be needed to confirm this apparent trend in diversity distribution along the nMAR.

Regional Biogeographic Analysis for Hydrothermally Active Vent Fields

Apart from the earlier work of Desbruyères et al. (2000, 2001), there have been few studies on the regional differences in vent fauna along the nMAR. Global biogeographic analyses have identified the nMAR as a separate biogeographic province (Bachraty et al., 2009; Moalic et al., 2012). Some analyses have further divided this province into two additional provinces, with the boundary between the north and south nMAR provinces occurring just south of the Azores (Van Dover et al., 2002). Various statistical methods have been used in previous studies to compare vent communities between segments on the same ridge (Gebruk et al., 1997; Van Dover et al., 2002; Tsurumi and Tunnicliffe, 2003) however, these studies were rarely able to include presence-absence data for taxa from all vent fields in the region because the available faunal data were insufficient to be used in statistical or biological and ecological studies (Van Dover, 1995; Jollivet, 1996; Gebruk et al., 1997; Tsurumi and Tunnicliffe, 2003).

The analysis in the present study is the first quantitative regional (meso-scale) biogeography analysis to include presence-absence data for taxa at the recently discovered Moytirra vent field (Wheeler et al., 2013) and the unusual geochemical environment occurring at Lost City. These multivariate results suggest that, based on presence-absence data, the regional biogeography of benthic invertebrate vent fauna on the nMAR is structured by depth/latitude and chimney type (sulphide or carbonate), with the shallower vent fields closer to the Azores (Menez Gwen and Lucky Strike) having a different taxonomic composition from those occurring at greater depths further south (Ashadze-1, Logatchev, Snake Pit, Broken Spur, TAG, and Rainbow). These results are similar to those obtained by Van Dover et al. (2002) and Fabri et al. (2011), where vent fields on the nMAR also formed two groups: the shallower vent fields close to the Azores and the deeper vent fields further south. As for these previous studies, our analysis was unable to separate the covarying effects of latitude and depth in influencing regional biogeography. Our results differ from Fabri et al. (2011) in the clustering of Rainbow vent field (2,300 m depth) with the deeper vent fields of Broken Spur, Snake Pit, TAG, Logatchev, and Ashadze-1 (3,050–4,200 m depth), instead of clustering with the shallower Menez Gwen and Lucky Strike vent fields (850–1,700 m depth).

Moytirra falls within a separate cluster, which may result from its higher latitude location, with the Azores potentially acting as a barrier to faunal dispersal for some species. The biological information available for Moytirra is less detailed, with only nine taxa reported from this vent field, which may contribute to it clustering separately. Lost City also forms its own cluster which, according to the environmental analyses results, is probably due to the different geochemical environment, with serpentinisation leading to hydrogen- and methane-rich vent fluids and the precipitation of its unique carbonate chimneys. Future analyses may be able to include biological information from additional nMAR vent fields, such as Pobeda-1, Irinovskoye, and Semyenov-2, when these have been better characterised through further survey efforts.

It is also important to note that in the present analysis, taxonomic similarity is not 100% within the same vent field cluster, i.e., not all taxa occur at each vent field. Vent fields within the same cluster are taxonomically more similar compared to vent fields in other clusters. However, vent fields within each cluster do not have exactly the same taxonomic composition, which is an important consideration for environmental management. Clustering of nMAR vent

fields according to faunal presence-absence data provides useful information on the regional biogeography for these taxa, and in combination with environmental analyses, indicates the environmental variables that may be the cause of these clusters. However, presence-absence data do not offer any information on the dominance of species at different vent fields, only their occurrence at any given location. More detailed quantitative datasets would be needed to compare all vent fields based on their abundance-weighted community structure.

Biological Communities at Hydrothermally Active Habitats and Hydrothermally Inactive Sulphide Habitats and Key Knowledge Gaps

Despite more than three decades of scientific research, our detailed literature review of nMAR biological communities highlights that key knowledge gaps still need to be addressed. The most information is available on the biodiversity and distribution of nMAR hydrothermally active ecosystems, with considerably less known about the temporal variation, connectivity, ecosystem function (including trophic relationships), and resilience and recovery of these ecosystems. Almost nothing is known about the biological communities colonising inactive sulphide habitats on the nMAR. Inactive sulphide habitats are poorly characterised in most oceans (Van Dover, 2019), yet are considered to have specific environmental management needs (Van Dover et al., 2020). Here, we discuss the key knowledge gaps for nMAR hydrothermally active and inactive ecosystems to spur collaborative research in the region, and to support regional-scale environmental management of human activities on the nMAR, including future deep-sea mining.

Biodiversity and Distribution

Existing data on the biodiversity and distributions of biota at hydrothermally active habitats relate mainly to benthic invertebrate megafauna. Considerably less information is available for smaller organisms, such as the macrofauna, meiofauna, and microorganisms at these habitats. Some vent fields, such as Moytirra, have been less studied than other fields, such as Lucky Strike, with the consequence that their biological communities are not as comprehensively characterised. More detailed studies are needed, replicated across all vent fields with standard methods, to determine the regional biodiversity and distributions for the biota. This is particularly the case for smaller organisms not identifiable from imagery. Further visual surveys may confirm the occurrence of additional hydrothermal vent fields supporting biological communities, particularly where hydrothermal activity has been "inferred" on the nMAR from water column chemistry (Beaulieu and Szafranski, 2020). Continued survey and research efforts are also needed to review and update the species list for benthic and benthopelagic fishes occurring at hydrothermally active habitats and inactive sulphide habitats on the nMAR.

Little is known about the biota colonising inactive sulphide habitats on the nMAR. Historically, there are few records of benthic invertebrates colonising nMAR hydrothermally inactive sulphide habitats, although this apparent absence of biological communities may reflect the geological focus of earlier studies and not a true absence of biota at these habitats. Preliminary data from more recent studies suggest that fauna may be scarce at nMAR inactive sulphide habitats (Molodtsova et al., 2014; Galkin et al., 2019), although these results may in part reflect limitations of the sampling gear used. Of the organisms observed, most of the benthic invertebrates were suspension feeders (Molodtsova et al., 2014). Studies in other regions support these findings, for example, some inactive sulphide chimneys in the southwest Pacific were devoid of benthic invertebrate megafauna, although other chimneys supported elevated abundances (Boschen et al., 2016a). Suspension feeders also dominated the invertebrate assemblages occurring at inactive sulphide habitats in the southwest Pacific (Galkin, 1997; Collins et al., 2012; Sen et al., 2014; Boschen et al., 2016a) and Indian Ocean (Gerdes et al., 2019). There is currently no evidence for benthic invertebrate species that are endemic to the weathered sulphide environment on the nMAR. Invertebrate-symbiont associations, similar to those seen at hydrothermally active habitats, have not been reported from inactive sulphide habitats (Van Dover, 2019). Most benthic invertebrates observed at inactive sulphide habitats have also been recorded from non-hydrothermal hard substrata in the region, suggesting a broad regional distribution of taxa occurring at hydrothermally inactive sulphides (reviewed by Van Dover, 2019). Dedicated studies are needed to determine if benthic invertebrate assemblages colonising inactive sulphide habitats on the nMAR occur at other non-hydrothermal habitats in the wider region.

Hydrothermally active habitats on the nMAR support an array of microorganisms, including Archaea, Bacteria, and protozoa, which can occur as free-living on the substrata, within hydrothermal plumes, and in symbiosis with hydrothermal vent fauna (Dick, 2019). Studies on microorganisms colonising hydrothermally active habitats have focussed on free-living and symbiotic chemoautotrophic groups, generally at the site or vent field scale. Comprehensive regional analyses looking at trends in the biodiversity and distribution of microbial communities across all nMAR vent fields have not been reported. Archaea and some Bacteria may be thiotrophic (oxidises Sulphur compounds) or methanotrophic (oxidises methane) and potentially endemic to hydrothermally active habitats (either basalt or ultramaphic rocks) along the nMAR. Other microorganisms, such as protozoa, fungi, and some Bacteria, are heterotrophic (metabolise organic carbon sources) and may occur in other deep-sea habitats along the nMAR. Microscopic eukaryotes are particularly under-studied, although studies from other regions show these can be abundant at hydrothermally active habitats (Van Dover et al., 1988b; Brönnimann et al., 1989). The regional distribution of nMAR symbiotic bacteria is little known. Bacterial symbionts on the MAR do not always share the same regional distribution as their hosts, for example the genealogies of chemoautotrophic and methanotrophic symbionts of *Bathymodiolus* spp. located on the MAR north and south of the Equator were inconsistent, and different from their mussel hosts, indicating disconnected biogeography patterns (Van der Heijden et al., 2012).

TABLE 4 | Types of ecosystem functions as defined by De Groot et al. (2002).

Function type	Definition of function
Regulatory functions	The capacity of natural ecosystems to regulate essential ecological processes and life support systems
Habitat functions	Where natural ecosystems provide refuge and reproductive habitat to wild organisms
Production functions	Photosynthesis, chemosynthesis, and nutrients uptake by autotrophs converts energy, carbon dioxide and nutrients into a wide variety of carbohydrate structures which are then used by secondary producers
Information functions	Natural ecosystems provide an essential 'reference function' and provide important contributions to cultural appreciation of the natural environment

There are no studies characterising the microbial communities of inactive sulphide habitats on the nMAR. The distribution patterns from other oceans (reviewed by Van Dover, 2019) could provide some insight into the nMAR. For example, bacterial density at inactive sulphide habitats along the Juan de Fuca Ridge decreases according to the following mineral sequence: elemental sulphur, chimney sulphide, marcasite, pyrite, sphalerite, chalcopyrite (Edwards et al., 2003). If the same pattern occurs along the nMAR, then this may impact the regional distribution of bacterial communities. It has been suggested that inactive sulphide habitats may host microorganisms not found elsewhere or only detectable in low numbers (Han et al., 2018); others suggest that microbial communities at inactive sulphides may be similar to groups common in other marine sediments (Meier et al., 2019). Dedicated studies are needed to characterise the microbial communities colonising inactive sulphide habitats on the nMAR, and to compare these with microbial communities colonising other habitats in the wider region.

In general, more detailed information is needed on the spatial distribution of species and communities colonising nMAR hydrothermally active habitats and inactive sulphide habitats. To get a complete picture of communities colonising these habitats, biodiversity characterisation needs to span microbes to larger benthic invertebrates and benthopelagic fishes, at suitable spatial scales and resolution. Fully characterising these communities over a wide area of the nMAR would enable quantitative regional biodiversity analyses to be conducted, alongside the identification of ecologically important locations that may require enhanced environmental management measures.

Ecosystem Function, Including Trophic Relationships

Ecosystem function has been defined in multiple ways. For the purpose of this review, ecosystem function was considered to be "the capacity of natural processes and components to provide goods and services that satisfy human needs, either directly or indirectly" (De Groot et al., 2002). Through this definition, ecosystem functions are a subset of ecological processes and ecosystem structures, with each function the result of the natural processes of the ecological system (De Groot et al., 2002). Ecosystem functions in this context include regulatory functions, habitat functions, production functions, and information functions (see **Table 4**). Regulatory and habitat functions are essential to the maintenance of natural processes and components, and to the delivery of production and information functions.

The functions and services provided by the deep-sea environment are habitat or ecosystem dependent (Thurber et al., 2014; Le et al., 2017). In a general sense, deep-sea hydrothermally active habitats and hydrothermally inactive sulphide habitats provide all four of the ecosystem function groups, making particularly important contributions to the regulatory and habitat functions that are essential to maintaining biological communities at hydrothermally active habitats and inactive sulphide habitats (Turner et al., 2019). Hydrothermally active habitats provide key production functions, as these habitats are biologically more productive and generally support greater biomass relative to surrounding non-hydrothermal deep-sea habitats (Levin et al., 2016; Bell et al., 2017; Turner et al., 2019). Other production functions provided by hydrothermally active habitats include enhanced trophic and structural complexity, which provides the setting for complex trophic interactions (Colaço et al., 2007; Portail et al., 2018, Turner et al., 2019). Hydrothermally active habitats also provide regulatory functions through their role in global biogeochemical cycling and elemental transformation of carbon, sulphur, and nitrogen (Lilley et al., 1995; Petersen et al., 2011; Sievert and Vetriani, 2012).

Microorganisms play a particularly important role in both the regulatory and production functions of hydrothermally active habitats. Chemolithoautotrophic microorganisms use the energy released through the oxidation of reduced compounds within hydrothermal fluids for the fixation of inorganic carbon, thus mediating the transfer of energy from the geothermal source to higher trophic levels and so forming the basis of the unique food webs existing in these environments (Hügler et al., 2010). Microorganisms within hydrothermally active habitats perform numerous functions, including sulphur oxidation and sulphate reduction; ammonia and nitrite oxidation; nitrate reduction; hydrogen and methane oxidation; manganese oxidation; and iron II oxidation and reduction (Ding et al., 2017).

The functional roles of free-living microorganisms colonising hydrothermally active habitats have been studied at Logatchev, Rainbow, TAG, and Snake Pit (Hügler et al., 2010; Scott et al., 2015). However, detailed studies at other nMAR vent fields would be needed to fully appreciate microbial contribution to regional ecosystem function. For hydrothermally inactive sulphide habitats on the nMAR, microbial contribution to ecosystem function is not known, but studies from other regions suggests microbial communities can perform a range of functions, as reviewed by Van Dover (2019). For example, Bacteria and Archaea at inactive sulphide habitats have the metabolic potential for nitrogen (nitrogen fixation, ammonia oxidation, denitrification) and methane cycling, in addition to iron and sulphide oxidation (Zhang et al., 2016; Li et al., 2017). Some of the microbes associated with hydrothermally inactive sulphides may also have the potential to enhance bioleaching of potentially toxic metals (iron, copper, zinc) from sulphides and to accelerate galvanic interactions that increase metal dissolution rates (Fallon et al., 2017).

Ecosystem function studies on the nMAR have largely focussed on the trophic relationships at hydrothermally active habitats in the Menez Gwen, Lucky Strike, Rainbow, Broken Spur, TAG, and Snake Pit vent fields (Colaço et al., 2002; De Busserolles et al., 2009; Portail et al., 2018); and separately at Ashadze-1 vent field (Fabri et al., 2011). However, trophic relationships have not been characterised for Moytirra or Lost City vent fields, and there are no analyses assessing trends in trophic relationships across all ten nMAR vent fields. Most studies conducted to date on the trophic relationships of the benthic invertebrates at hydrothermally active habitats have focused on the megafauna or macrofauna, with comparatively few studies addressing the trophic role of meiofauna.

Trophic relationships for the biota colonising hydrothermally inactive sulphide habitats along the nMAR are unknown, largely because these biological communities have not been characterised. Whilst not demonstrated for the nMAR, there is some evidence from other regions that non-vent suspension feeders colonising inactive sulphide habitats may benefit from secondary production at active vents (Erickson et al., 2009). It is not known whether the microbial community colonising inactive sulphide habitats along the nMAR provides an important nutritional source for any benthic invertebrates in these habitats.

Other than trophic relationships, the functional role of benthic invertebrates and fishes found at hydrothermally active habitats or inactive sulphide habitats on the nMAR has not been reported. The global hydrothermal vent functional traits database produced by Chapman et al. (2019) includes species recorded from the nMAR, and should facilitate future functional studies for those taxa included in the database.

Further studies are needed to appreciate the role of different taxa and groups (microbes to benthic invertebrates and benthopelagic fishes) in ecosystem function, where there is functional overlap, and any cases where species have a unique contribution to ecosystem function. This is essential knowledge in the context of predicting disturbance-induced impacts to ecosystem function, and for implementing the ecosystem approach in environmental management.

Connectivity

The most referred to concept of connectivity is population connectivity, which describes how individuals or groups of individuals from the same species can move between populations, and in the case of genetic connectivity, the extent to which they are able to exchange genetic material. The persistence and maintenance of populations distributed amongst patchy hydrothermally active habitats is thus determined by the balance between the loss of individuals and the provision of new recruits to the population, either from the resident population or from neighbouring populations. Excepting the more mobile crabs and fishes, most species at hydrothermally active habitats are sessile as adults and are reliant on larval dispersal to maintain connectivity amongst sites. Local vent communities are linked by pelagic larval dispersal, together forming regional metacommunities nested within biogeographic provinces (Mitarai et al., 2016; Mullineaux et al., 2018). Connectivity patterns are thus influenced by the larval development mode, where larvae travel within the water column, and the local and regional current regime, amongst other factors (Hilário et al., 2015; Boschen et al., 2016b).

Of the models describing connectivity amongst populations, the two most applicable to populations at hydrothermally active habitats are isolation-by-distance and panmixia (Vrijenhoek, 2010; Boschen et al., 2016b), both of which have been demonstrated for benthic invertebrates colonising nMAR hydrothermally active habitats. Connectivity patterns of hydrothermally active habitats on the nMAR can be complicated in space and time, largely because these habitats are spatially fragmented, and can change over time.

Population connectivity has only been determined for a small number of typically abundant benthic invertebrate species at hydrothermally active habitats along the nMAR; there are still many species where connectivity has not been assessed. Most population connectivity studies on the nMAR have focused on megafaunal and macrofaunal taxa, with very few studies assessing the connectivity of meiofaunal taxa. Even for species where some aspects of connectivity are known, there are still multiple knowledge gaps, including population size, reproductive biology, larval duration, and ocean currents (Hilário et al., 2015). Full population genetics studies of nMAR symbionts have not yet been conducted, however studies from other regions suggest that bacterial symbionts can demonstrate different connectivity patterns from their hosts. For example, a study from the East Pacific Rise, Galápagos Rift, and Pacific-Antarctic Ridge demonstrated that northern and southern bacterial symbionts appeared to be completely isolated, despite mussel species hybridising along the Easter Microplate (Ho et al., 2017). It is not known if a similar pattern occurs in bathymodiolid symbionts at hybridisation zones along the MAR, such as Broken Spur vent field.

The connectivity of the biota colonising hydrothermally inactive sulphide habitats on the nMAR is completely unknown, as is the potential for inactive sulphide habitats to support source populations important for regional population connectivity. In other regions, most species observed at inactive sulphides have been recorded from other habitats (reviewed by Van Dover, 2019).

In terms of environmental management for human activities, such as deep-sea mining, understanding connectivity patterns between the proposed mine site and hydrothermally active habitats in the broader region is key to determining the potential impacts of the proposed mining operation and the potential for recovery at that site (Boschen et al., 2016b). For example, locating a mine site at a source population, which provides recruits to other populations in the region as part of a metapopulation framework, could impact neighbouring populations which are reliant on larval supply from the source population (Boschen et al., 2016b; Mullineaux et al., 2018). If the proposed mine site harbours a self-recruiting population, then extirpation of this population could mean that this species is not able to recolonise the site once mining activities have ceased. A detailed review of connectivity in the context of deep-sea mining of PMS deposits, environmental management, and the role of genetic tools, is provided by Boschen et al. (2016b).

Connectivity assessments need to be undertaken for a greater number of species colonising hydrothermally active habitats on the nMAR, spanning the full range of potential life histories. At a regional level, there needs to be detailed information on population source-sink dynamics and self-recruitment to predict impacts from disturbance to populations, and to inform decisions on potential networks of protected areas. It is also important to consider the potential influence of ocean currents on connectivity patterns. A recent study based on biophysical modelling on the nMAR suggested that there are both persistent zones of connectivity and barriers to dispersal along the ridge; knowledge of such locations could be used to inform environmental management decisions for region (Yearsley et al., 2020).

Temporal Variability

Temporal variability can be related to food availability, breeding and reproductive cycles, ontogenetic shifts, or changes in environmental parameters (Colaço et al., 2009; Glover et al., 2010; Cuvelier et al., 2011b). These factors can lead to variability over multiple time scales, including diurnal, monthly, seasonal, inter-annual, or even decadal time scales (Glover et al., 2010). Temporal variation can be particularly complex for biota at hydrothermally active habitats, with multiple scales of both temporal and spatial variability potentially interacting to influence overall productivity of this community (Le Bris et al., 2019). Less predictable episodic events can also result in temporal variability in such communities, such as volcanic eruptions (reviewed by Le Bris et al., 2019). The slow-spreading MAR axis is considered to be a relatively stable environment for hydrothermally active biological communities, predicted to have distantly spaced vent fields with lower frequency of episodic events than fast-spreading locations, such as the East Pacific Rise and Juan de Fuca Ridge (Vrijenhoek, 2010).

Temporal variability in ecological processes has been documented for microbes and benthic invertebrates at hydrothermally active habitats on the nMAR, using a variety of methods and across a range of temporal scales. Studies on the temporal variability of benthic invertebrates at hydrothermally active habitats have to date focused on the megafauna, with little known about the temporal variability of the macrofauna or meiofauna.

Although not demonstrated for hydrothermal vents with sulphide chimneys on the nMAR, studies in other ocean regions suggest that the microbial communities can stabilise over multiple years (Fortunato et al., 2018). It has also been suggested that microbial communities on the MAR in low-temperature fluids (circa 8°C) may exhibit greater short-term variability (minutes to hours) than those at high-temperature habitats, as has been observed at mussel beds in the Clueless vent field (5°S) in response to short-term hydrothermal fluid variability (Perner et al., 2009). If this also occurs at mussel beds on the nMAR, microbial communities in different hydrothermal fluid environments may have different abilities to respond to changes in environmental conditions associated with both natural and human induced disturbance.

There have not been any dedicated studies addressing temporal variation for microbial communities or benthic invertebrates at hydrothermally inactive sulphide habitats on the nMAR. As hydrothermally active areas along the nMAR become inactive, hydrothermal vent endemic biota will be lost, and over time there may be an increase in microbes and benthic invertebrates who can either tolerate or exploit the inactive sulphide habitats. Although this style of succession has been suggested for other ocean regions (Sen et al., 2014), it has yet to be observed for the nMAR. Some hydrothermally inactive habitats, such as relict or extinct sulphide structures, may provide stable habitats for colonisation by benthic invertebrates, as has been observed in other regions (Boschen et al., 2016a; Gerdes et al., 2019).

Characterising temporal variability is particularly important in the context of environmental management, as it would enable impacts from human activities, such as future deep-sea mining, to be assessed against natural temporal variability. Understanding temporal variability is also key to the development of suitable environmental management measures, to ensure that these measures can accommodate natural temporal variability within the region, and that they will remain effective in the context of longer-term environmental variability, such as climate change.

Ecological information for nMAR hydrothermally active habitats and inactive sulphide habitats needs to be collected over a range of time scales (hours, days, week, months, years, decades) at multiple locations to establish a robust regional baseline for temporal variability against which to measure disturbance-induced changes, and to help predict future responses. More long-term data collection stations or observatories are needed on the nMAR to help provide this information.

Resilience and Recovery

Resilience represents a key concept in ecosystem response to disturbance effects. In the context of this review, recoverability, or resilience, refers to persistence of ecosystems in the face of natural or anthropogenic disturbances (Holling, 1973), and can be quantified as the recovery time to the original state after disturbance (Holling, 1996). Resilience can be further defined as the ability of a system to maintain its overall identity i.e., the same function and structure, in the face of internal change and external perturbations (Walker et al., 2004; Cumming et al., 2013).

Disturbances to hydrothermally active ecosystems can be natural or human induced, across different spatial and temporal scales. The temporal scale of natural disturbances to hydrothermally active ecosystems can range from decades to centuries (Van Dover, 2014). Few human induced disturbances have been studied at hydrothermal vent ecosystems, excepting research conducted on the effect of the high-intensity illumination associated with HOVs and ROVs.

Apart from a recent small-scale disturbance experiment conducted in the Lucky Strike vent field (Marticorena et al., 2021), dedicated resilience and recovery studies have not been conducted for the biological communities colonising hydrothermally active habitats or inactive sulphide habitats on the nMAR. The results from the study by Marticorena et al. (2021) demonstrated the complexity of recovery patterns in response to even small-scale disturbances on the nMAR, highlighting the importance of prior information on connectivity

and temporal patterns to fully understand recovery processes after a major disturbance.

Recovery patterns of biological communities colonising hydrothermally active habitats have been assessed in greater detail in the Pacific Ocean. On the East Pacific Rise (EPR), observations on the recovery of biological communities from disturbance due to volcanic activity suggested that most of the diversity and biomass recovered within 5 years (reviewed by Gollner et al., 2017). Recoverability on the EPR varied significantly amongst biological communities from hydrothermally active vents, inactive vents, and within the vent periphery (Gollner et al., 2017). A recent study indicates that faunal succession on the EPR continued a decade after volcanic disturbance, and that there is strong variation amongst and across environmental gradients (Mullineaux et al., 2020). Recovery time on the EPR was considered slower than previously expected, with communities having lower resilience to disturbances, such as deep-sea mining, than initially estimated (Mullineaux et al., 2020). Variable recovery times for hydrothermal vent communities were also predicted in the western Pacific Ocean, based on modelling simulated disturbance for communities in 131 vent fields (Suzuki et al., 2018). The analysis identified substantial differences in recovery time (from <2 years to more than 400 years) due to differences in regional connectivity between known vent fields. In some cases, simultaneous disturbance of a series of vent fields was predicted to delay or wholly prevent recovery (Suzuki et al., 2018).

Predicting the recovery of nMAR hydrothermal vent communities based on the more extensive observations and models from the Pacific Ocean is inherently flawed, given the differences in the frequency of natural disturbance events between these regions and an absence of information on local controls for the nMAR (Mullineaux et al., 2018). There is also limited information on the importance of self-recruitment for populations of nMAR hydrothermal vent fauna. If self-recruitment occurs, a disturbance event at that site could remove or reduce the abundance of eggs and larvae for benthic invertebrate populations, which alongside localised loss or degradation of suitable habitat for colonisation, could severely reduce recovery potential for that population or even result in localised species extinction.

Some of the organisms colonising hydrothermally inactive sulphide habitats may be both sessile and slow growing, such as the hard corals observed on inactive sulphide chimneys along the Kermadec Volcanic Arc in the southwest Pacific, estimated to be at least 160 years old (Boschen et al., 2016a). If the species of black and golden corals recorded from inactive sulphide habitats on the nMAR (Molodtsova et al., 2014) are also slow-growing and long-lived, as has been demonstrated for other species of black corals on the nMAR (Carreiro-Silva et al., 2013), these corals may take decades or centuries to recover from disturbances.

Information is urgently needed on the resilience to disturbance of species and communities colonising hydrothermally active habitats and inactive sulphide habitats on the nMAR. Information is also needed on the biological succession sequence for these habitats following disturbance, and the frequency of natural disturbances on the nMAR. This knowledge is essential for predicting responses to disturbance, assessing environmental impacts, and monitoring recovery from impact. In the absence of natural disturbance events to observe and monitor, controlled disturbance experiments could be used to evaluate biological responses.

DATA AVAILABILITY STATEMENT

The original contributions presented in the study are included in the article/**Supplementary Material**, further inquiries can be directed to the corresponding authors.

AUTHOR CONTRIBUTIONS

RB-R and AC jointly conceived the idea for the manuscript. AC generated the updated taxa list, RB-R conducted the statistical analyses. RB-R and AC jointly reviewed the literature and wrote the manuscript. Both authors contributed to the article and approved the submitted version.

FUNDING

This research was conducted as part of the Atlantic REMP Project (Areas of particular environmental interest in the Atlantic: EASME/EMFF/2017/1.3.1.1 - SI2.775068) funded by the European Commission. AC was also supported through the FunAzores - ACORES 01-0145-FEDER-000123 grant and by FCT and Direção-Geral de Politica do Mar (DGPM) through the project Mining2/2017/005. AC was further supported by Investigadores MarAZ (ACORES-01-0145-FEDER-000140 and by national funds through FCT Foundation for Science and Technology within the scope of UIDB/05634//2020 and UIDP/05634/2020 granted to OKEANOS.

ACKNOWLEDGMENTS

We gratefully acknowledge the support of Prof. Phil Weaver as Project Coordinator for the Atlantic REMP Project, Prof. Nadine Le Bris for allowing us to reproduce the Mission Transect images, Ricardo Medeiros for help with **Figure 1**, and three reviewers for their constructive comments on the manuscript.

SUPPLEMENTARY MATERIAL

The Supplementary Material for this article can be found online at: https://www.frontiersin.org/articles/10.3389/fmars.2021.657358/full#supplementary-material

REFERENCES

Arellano, S. M., and Young, C. M. (2009). Spawning, development, and the duration of larval life in a deep-sea cold-seep mussel. *Biol. Bull.* 216, 149–162. doi: 10.1086/BBLv216n2p149

Bachraty, C., Legendre, P., and Desbruyères, D. (2009). Biogeographic relationships among deep-sea hydrothermal vent faunas at a global scale. *Deep-Sea Res. Part I* 56, 1371–1378. doi: 10.1016/j.dsr.2009.01.009

Beaulieu, S. E., and Szafranski, K. M. (2020). *InterRidge Global Database of Active Submarine Hydrothermal Vent Fields Version 3.4*. PANGEA.

Bell, J. B., Woulds, C., and Oevelen, D. V. (2017). Hydrothermal activity, functional diversity and chemoautotrophy are major drivers of seafloor carbon cycling. *Sci. Rep.* 7:12025. doi: 10.1038/s41598-017-12291-w

Bellec, L., Cambon Bonavita, M. A., Cueff-Gauchard, V., Durand, L., Gayet, N., and Zeppilli, D. (2018). A nematode of the mid-Atlantic ridge hydrothermal vents harbors a possible symbiotic relationship. *Front. Microbiol.* 9:2246. doi: 10.3389/fmicb.2018.02246

Bel'tenev, V. E., Lazareva, L. I., Cherkashev, G. A., Ivanov, V. I., Rozhdestvenskaya, I. I., Kuznetsov, V., et al. (2017). New hydrothermal sulphide fields of the Mid-Atlantic Ridge: Yubileinoe (20°09'N) and Surprise (20°45.4'N). *Dokl. Earth Sci.* 476, 1010–1015. doi: 10.1134/S1028334X17090227

Boschen, R. E., Collins, P. C., Tunnicliffe, V., Carlsson, J., Gardner, J. P. A., Lowe, J., et al. (2016b). A primer for use of genetic tools in selecting and testing the suitability of set-aside sites protected from deep-sea seafloor massive sulfide mining activities. *Ocean Coast. Manag.* 122, 37–48. doi: 10.1016/j.ocecoaman.2016.01.007

Boschen, R. E., Rowden, A. A., Clark, M. R., Pallentin, A., and Gardner, J. P. A. (2016a). Seafloor massive sulfide deposits support unique megafaunal assemblages: implications for seabed mining and conservation. *Mar. Env. Res.* 115, 78–88. doi: 10.1016/j.marenvres.2016.02.005

Brazelton, W. J., Ludwig, K. A., Sogin, M. L., Andreishcheva, E. N., Kelley, D. S., Shen, C.-C., et al. (2009). Archaea and bacteria with surprising microdiversity show shifts in dominance over 1,000-year time scales in hydrothermal chimneys. *Proc. Natl. Acad. Sci. U. S. A.* 107, 1612–1617. doi: 10.1073/pnas.0905369107

Breusing, C., Biastoch, A., Drews, A., Metaxas, A., Jollivet, D., Vrijenhoeck, C., et al. (2016). Biophysical and population genetic models predict the presence of "phantom" stepping stones connecting Mid-Atlantic Ridge vent ecosystems. *Curr. Biol.* 26, 2257–2267. doi: 10.1016/j.cub.2016.06.062

Breusing, C., Vrijenhoek, R. C., and Reusch, T. B. H. (2017). Widespread introgression in deep-sea hydrothermal vent mussels. *BMC Evol. Biol.* 17:13. doi: 10.1186/s12862-016-0862-2

Brönnimann, P., Van Dover, C., and Whittaker, J. E. (1989). Abyssotherma pacifica, n. gen., n. sp., a recent remaneicid (Foraminiferida, Remaneicacea) from the East Pacific Rise. *Micropaleontology* 35, 142–149. doi: 10.2307/1485465

Carreiro-Silva, M., Andrews, A. H., Braga-Henriques, A., Porteiro, F. M., Matos, V., and Santos, R. S. (2013). Variability in growth rates of long-lived black coral *Leiopathes* sp. from the Azores (NE Atlantic). *Mar. Ecol. Prog. Ser.* 473, 189–199. doi: 10.3354/meps10052

Chapman, A.S., Beaulieu, S.E., Colaço, A., Gebruk, A.V., Hilario, A., Kihara, T.C., et al. (2019). sFDvent: a global trait database for deep-sea hydrothermal vent fauna. *Glob. Ecol. Biogeog.* 28, 1538–1551. doi: 10.1111/geb.12975

Clarke, K. R., Gorley, R. N., Somerfield, P. J., and Warwick, R. M. (2014). *Change in Marine Communities: An Approach to Statistical Analysis and Interpretation, 3rd Edn*. Plymouth: PRIMER-E.

Colaço, A., Desbruyères, D., and Dehairs, F. (2002). Nutritional relations of deep-sea hydrothermal fields at the Mid-Atlantic Ridge: a stable isotope approach. *Deep-Sea Res. Part I* 49, 395–412. doi: 10.1016/S0967-0637(01)00060-7

Colaço, A., Desbruyères, D., and Guezennec, J. (2007). The use of polar lipid fatty acids to determine trophic links in chemosynthetic communities. *Mar. Ecol.* 28, 15–24. doi: 10.1111/j.1439-0485.2006.00123.x

Colaço, A., Martins, I., Laranjo, M., Pires, L., Leal, C., Prieto, C., et al. (2006). Annual spawning of the hydrothermal vent mussel, *Bathymodiolus azoricus*, under controlled aquarium conditions at atmospheric pressure. *J. Exp. Mar. Biol. Ecol.* 333, 166–171. doi: 10.1016/j.jembe.2005.12.005

Colaço, A., Prieto, C., Martins, A., Figueiredo, M., Lafon, V., Monteiro, M., et al. (2009). Seasonal variations in lipid composition of the hydrothermal vent mussel *Bathymodiolus azoricus* from the Menez Gwen vent field. *Mar. Environ. Res.* 67, 146–152. doi: 10.1016/j.marenvres.2008.12.004

Collins, P. C., Kennedy, R., and Van Dover, C. L. (2012). A biological survey method applied to seafloor massive sulphides (SMS) with contagiously distributed hydrothermal-vent fauna. *Mar. Ecol. Prog. Ser.* 452, 89–107. doi: 10.3354/meps09646

Copley, J. T. P., Jorgensen, P. B. K., and Sohn, R. A. (2007). Assessment of decadal-scale ecological change at a deep Mid-Atlantic hydrothermal vent and reproductive time-series in the shrimp *Rimicaris exoculata*. *J. Mar. Biolog. Assoc.* 87, 859–867. doi: 10.1017/S0025315407056512

Copley, J. T. P., Tyler, P. A., Murton, B. J., and Van Dover, C. L. (1997). Spatial and interannual variation in the faunal distribution at Broken Spur vent field (29°N, Mid-Atlantic Ridge). *Mar. Biol.* 129, 723–733. doi: 10.1007/s002270050215

Crepeau, V., Bonavita, M.-A. C., Lesongeur, F., Randrianalivelo, H., Sarradin, P.-M., Sarrazin, J., et al. (2011). Diversity and function in microbial mats from the Lucky Strike hydrothermal vent field. *FEMS Microbiol. Ecol.* 76, 524–540. doi: 10.1111/j.1574-6941.2011.01070.x

Cumming, G. S., Olsson, P., Chapin, F. S., and Holling, C. S. (2013). Resilience, experimentation, and scale mismatches in social-ecological landscapes. *Landscape Ecol.* 28, 1139–1150. doi: 10.1007/s10980-012-9725-4

Cuvelier, D., Beesau, J., Ivanenko, V. N., Zeppilli, D., Sarradin, P.-M., and Sarrazin, J. (2014). First insights into macro- and meiofaunal colonisation patterns on paired wood/slate substrata at Atlantic deep-sea hydrothermal vents. *Deep-Sea Res. Part I* 87, 70–81. doi: 10.1016/j.dsr.2014.02.008

Cuvelier, D., de Busserolles, F., Lavaud, R., Floc'h, E., Fabri, M. C., Sarradin, P. M., et al. (2012). Biological data extraction from imagery – How far can we go? A case study from the Mid-Atlantic Ridge. *Mar. Environ. Res.* 82, 15–27. doi: 10.1016/j.marenvres.2012.09.001

Cuvelier, D., Legendre, P., Laes-Huon, A., Sarradin, P. M., and Sarrazin, J. (2017). Biological and environmental rhythms in (dark) deep-sea hydrothermal ecosystems. *Biogeosciences* 14, 2955–2977. doi: 10.5194/bg-14-2955-2017

Cuvelier, D., Sarradin, P.-M., Sarrazin, J., Colaco, A., Copley, J. T., Desbruyères, D., et al. (2011a). Hydrothermal faunal assemblages and habitat characterisation at the Eiffel Tower edifice (Lucky Strike, Mid-Atlantic Ridge). *Mar. Ecol.* 32, 243–255. doi: 10.1111/j.1439-0485.2010.00431.x

Cuvelier, D., Sarrazin, J., Colaço, A., Copley, J., Glover, A., Tyler, P., et al. (2011b). Community dynamics over 14 years at the Eiffel Tower hydrothermal edifice on the Mid-Atlantic Ridge. *Limnol. Oceanogr.* 56, 1624–1640. doi: 10.4319/lo.2011.56.5.1624

Cuvelier, D., Sarrazin, J., Colaco, A., Copley, J. T., Desbruyères, D., Glover, A. G., et al. (2009). Distribution and spatial variation of hydrothermal faunal assemblages at Lucky Strike (Mid-Atlantic Ridge) revealed by high-resolution video image analysis. *Deep-Sea Res. Part I* 56, 2026–2040. doi: 10.1016/j.dsr.2009.06.006

De Busserolles, F., Sarrazin, J., Gauthier, O., Gelinas, Y., Fabri, M. C., Sarradin, P. M., et al. (2009). Are spatial variations in the diets of hydrothermal fauna linked to local environmental conditions? *Deep-Sea Res. Part II* 56, 1649–1664. doi: 10.1016/j.dsr2.2009.05.011

De Groot, R. S., Wilson, M. A., and Bourmans, R. M. J. (2002). A typology for the classification, description and valuation of ecosystem functions, goods and services. *Ecol. Econ.* 41, 393–408. doi: 10.1016/S0921-8009(02)00089-7

Desbruyères, D., Almeida, A., Biscoito, M., Comtet, T., Khripounoff, A., Le Bris, N., et al. (2000). A review of the distribution of hydrothermal vent communities along the northern Mid-Atlantic Ridge: dispersal vs. environmental controls. *Hydrobiologia* 440, 201–216. doi: 10.1023/A:1004175211848

Desbruyères, D., Biscoito, M., Caprais, J.-C., Colaco, A., Comtet, T., Crassous, P., et al. (2001). Variations in deep-sea hydrothermal vent communities on the Mid-Atlantic Ridge near the Azores plateau. *Deep-Sea Res. Part I* 48, 1325–1346. doi: 10.1016/S0967-0637(00)00083-2

Desbruyères, D., Segonzac, M., and Bright, M. (2006). *Handbook of Deep-Sea Hydrothermal Vent Fauna*. Land Oberösterreich, Biologiezentrum der Oberösterreichische Landesmuseen.

Dick, G. J. (2019). The microbiomes of deep-sea hydrothermal vents: distributed globally, shaped locally. *Nat. Rev. Microbiol.* 17, 271–283. doi: 10.1038/s41579-019-0160-2

Ding, J., Zhang, Y., Wang, H., Jian, H., Leng, H., and Xiao, X. (2017). Microbial community structure of deep-sea hydrothermal vents on the ultraslow spreading Southwest Indian Ridge. *Front. Microbiol.* 8:1012. doi: 10.3389/fmicb.2017.01012

Dixon, D. R., and Dixon, L. R. J. (1996). Results of DNA analyses conducted on vent shrimp post larvae collected above the Broken Spur vent field during the CD95 cruise, August 1995. *BRIDGE Newsletter* 11, 9–15.

Dixon, D. R., Lowe, D. M., Miller, P. I., Villemin, G. R., Colaco, A., Serrao-Santos, R., et al. (2006). Evidence of seasonal reproduction in the Atlantic vent mussel *Bathymodiolus azoricus*, and an apparent link with the timing of photosynthetic primary production. *J. Mar. Biolog. Assoc.* 86, 1363–1371. doi: 10.1017/S0025315406014391

Duperron, S., Bergin, C., Zielinski, F., Blazejak, A., Pernthaler, A., McKiness, Z. P., et al. (2006). A dual symbiosis shared by two mussel species, *Bathymodiolus azoricus* and *Bathymodiolus puteoserpentis* (Bivalvia: Mytilidae), from hydrothermal vents along the northern Mid-Atlantic Ridge. *Environ. Microbiol.* 8, 1441–1447. doi: 10.1111/j.1462-2920.2006.01038.x

Duperron, S., Quiles, A., Szafranski, K. M., Leger, N., and Shilito, B. (2016). Estimating symbiont abundances and gill surface areas in specimens of the hydrothermal vent mussel *Bathymodiolus puteoserpentis* maintained in pressure vessels. *Front. Mar. Sci.* 3:16. doi: 10.3389/fmars.2016.00016

Edwards, K. J., McCollom, T. M., Konishi, H., and Buseck, P. R. (2003). Seafloor bioalteration of sulphide minerals: results from in situ incubation studies. *Geochim. Cosmochim.* 67, 2843–2856. doi: 10.1016/S0016-7037(03)00089-9

Erickson, K. L., Macko, S. A., and Van Dover, C. L. (2009). Evidence for a chemoautotrophically based food web at inactive hydrothermal vents (Manus Basin). *Deep-Sea Res. Part II* 56, 1577–1585. doi: 10.1016/j.dsr2.2009.05.002

Fabri, M.-C., Bargain, A., Briand, P., Gebruk, A., Fouquet, Y., Morineaux, M., et al. (2011). The hydrothermal vent community of a new deep-sea field, Ashadze-1, 12°58'N on the Mid-Atlantic Ridge. *J. Mar. Biolog. Assoc.* 91, 1–13. doi: 10.1017/S0025315410000731

Fallon, E. K., Petersen, S., Brooker, R. A., and Scott, T. B. (2017). Oxidative dissolution of hydrothermal mixed-sulphide ore: an assessment of current knowledge in relation to seafloor massive sulphide mining. *Ore Geol. Rev.* 86, 309–337. doi: 10.1016/j.oregeorev.2017.02.028

Faure, B., Jollivet, D., Tanguy, A., Bonhomme, F., and Bierne, N. (2009). Speciation in the deep sea: multi-locus analysis of divergence and gene flow between two hybridizing species of hydrothermal vent mussels. *PLoS ONE* 4:e6485. doi: 10.1371/journal.pone.0006485

Fiala-Médioni, A., McKiness, Z., Dando, P., Boulegue, J., Mariotti, A. A. A. D., Alayse-Danet, A., et al. (2002). Ultrastructural, biochemical, and immunological characterization of two populations of the mytilid mussel *Bathymodiolus azoricus* from the mid-Atlantic ridge: evidence for a dual symbiosis. *Mar. Biol.* 141, 1035–1043. doi: 10.1007/s00227-002-0903-9

Flores, G. E., Campbell, J. H., Kirshtein, J. D., Meneghin, J., Podar, M., Steinberg, J. I., et al. (2011). Microbial community structure of hydrothermal deposits from geochemically different vent fields along the Mid-Atlantic Ridge. *Environ. Microbiol.* 13, 2158–2171. doi: 10.1111/j.1462-2920.2011.02463.x

Fortunato, C. S., Larson, B., Butterfield, A. B., and Huber, J. A. (2018). Spatially distinct, temporally stable microbial populations mediate biogeochemical cycling at and below the seafloor in hydrothermal vent fluids. *Environ. Microbiol.* 20, 769–784. doi: 10.1111/1462-2920.14011

Gablina, I. F., Dobretsova, I. G., Bel'tenev, V. E., Lyutkevich, A. D., Narkenskii, E. V., and Gustaitis, A. N. (2012). Peculiarities of present-day sulfide mineralization at 19°15'N - 20°08'N, Mid Atlantic Ridge. *Dokl. Earth Sci.* 442, 163–167. doi: 10.1134/S1028334X1202002X

Galkin, S. V. (1997). Megafauna associated with hydrothermal vents in the Manus Back-arc Basin (Bismark Sea). *Mar. Geol.* 142, 197–206. doi: 10.1016/S0025-3227(97)00051-0

Galkin, S. V., Molodtsova, T. N., Minin, K. V., and Kobyliansky, S. G. (2019). Ecological studies of the Russian Exploration Area on the Mid-Atlantic Ridge on the 39th cruise of RV Professor Logachev. *Oceanology* 59, 616–617. doi: 10.1134/S0001437019040040

Galkin, S. V., and Moskalev, L. I. (1990). Hydrothermal fauna of the Mid-Atlantic Ridge. *Oceanology* 30, 624–627.

Gebruk, A. V., Fabri, M.-C., Briand, P., and Desbruyères, D. (2010). Community dynamics over a decadal scale at Logatchev, 14°45'N, Mid-Atlantic Ridge. *Cah. Biol. Mar.* 51, 383–388. doi: 10.21411/CBM.A.FB805CDE

Gebruk, A. V., Galkin, S. V., Vereshchaka, A. L., Moskalev, L. I., and Southward, A. J. (1997). Ecology and biogeography of the hydrothermal vent fauna of the Mid-Atlantic Ridge. *Adv. Mar. Biol.* 32, 93–144. doi: 10.1016/S0065-2881(08)60016-4

Gerdes, K. H., Arbizu, P. M., Schwentner, M., Freitag, R., Schwarz-Schampera, U., Brandt, A., et al. (2019). Megabenthic assemblages at the southern Central Indian Ridge–Spatial segregation of inactive hydrothermal vents from active-, periphery-and non-vent sites. *Mar. Environ. Res.* 151:104776. doi: 10.1016/j.marenvres.2019.104776

German, C. R., Parson, L. M., Bougalt, H., Coller, D., Critchley, M., Dapoigny, A., et al. (1996). Hydrothermal exploration near the Azores Triple Junction: tectonic control of venting at slow-spreading ridges? *Earth Planet. Sci. Lett.* 138, 93–104. doi: 10.1016/0012-821X(95)00224-Z

German, C. R., Petersen, S., and Hannington, M. D. (2016). Hydrothermal exploration of mid-ocean ridges: where might the largest sulfide deposits be forming? *Chem. Geol.* 420, 114–126. doi: 10.1016/j.chemgeo.2015.11.006

Glover, A. G., Gooday, A. J., Bailey, D. M., Billett, D. S. M., Chevaldonné, P., Colaço, A., et al. (2010). Temporal change in deep-sea benthic ecosystems: a review of the evidence from recent time-series studies. *Adv. Mar. Biol.* 58, 1–95. doi: 10.1016/B978-0-12-381015-1.00001-0

Gollner, S., Fontaneto, D., and Martinez Arbizu, P. (2011). Molecular taxonomy confirms morphological classification of deep-sea hydrothermal vent copepods (Dirivultidae) and suggests broad physiological tolerance of species and frequent dispersal along ridges. *Mar. Biol.* 158, 221–231. doi: 10.1007/s00227-010-1553-y

Gollner, S., Ivanenko, V. N., Martinez Arbizu, P., and Bright, M. (2010a). Advances in taxonomy, ecology, and biogeography of Dirivultidae (Copepoda) associated with chemosynthetic environments in the deep sea. *PLoS ONE* 5:e9801. doi: 10.1371/journal.pone.0009801

Gollner, S., Kaiser, S., Menzel, L., Jones, D. O. B., Brown, A., Mestre, N. C., et al. (2017). Resilience of benthic deep-sea fauna to mining activities. *Mar. Environ. Res.* 129, 76–101. doi: 10.1016/j.marenvres.2017.04.010

Gollner, S., Reimer, B., Martinez-Arbizu, P., Le Bris, N., and Bright, M. (2010b). Diversity of meiofauna from the 9°50'N East Pacific Rise across a gradient of hydrothermal fluid emissions. *PLoS ONE* 5:e12321. doi: 10.1371/journal.pone.0012321

Gollner, S., Stuckas, H., Kihara, T. C., Laurent, S., Kodami, S., and Arbizu, P. M. (2016). Mitochondrial DNA analyses indicate high diversity, expansive population growth and high genetic connectivity of vent copepods (Dirivultidae) across different oceans. *PLoS ONE* 11:e0163776. doi: 10.1371/journal.pone.0163776

Han, Y., Gonnella, G., Adam, N., Schippers, A., Burkhardt, L., Kurtz, S., et al. (2018). Hydrothermal chimneys host habitat-specific microbial communities: analogues for studying the possible impact of mining seafloor massive sulfide deposits. *Sci. Rep.* 8:10386. doi: 10.1038/s41598-018-28613-5

Hannington, M., Jamieson, J., Monecke, T., Petersen, S., and Beaulieu, S. (2011). The abundance of seafloor massive sulfide deposits. *Geology* 39, 1155–1158. doi: 10.1130/G32468.1

Herring, P. J., Gaten, E., and Shelton, P. M. (1999). Are vent shrimps blinded by science? *Nature* 398, 116–116. doi: 10.1038/18142

Hilário, A., Metaxas, A., Gaudron, S. M., Howell, K. L., Mercier, A., Mestre, N. C., et al. (2015). Estimating dispersal distance in the deep sea: challenges and applications to marine reserves. *Front. Mar. Sci.* 2:6. doi: 10.3389/fmars.2015.00006

Ho, P. T., Park, E., Hong, S. G., Kim, E. H., Kim, K., Jang, S. J., et al. (2017). Geographical structure of endosymbiotic bacteria hosted by *Bathymodiolus* mussels at eastern Pacific hydrothermal vents. *BMC Evol. Biol.* 17:121. doi: 10.1186/s12862-017-0966-3

Holling, C. S. (1973). Resilience and stability of ecological systems. *Ann. Rev. Ecol. Syst*. 4, 1–23. doi: 10.1146/annurev.es.04.110173.000245

Holling, C. S. (1996). "Engineering resilience versus ecological resilience," in *Engineering Within Ecological Constraints*, ed National Academy of Engineering (Washington, DC: National Academies Press), 31–44.

Hügler, M., Gärtner, A., and Imhoff, J. F. (2010). Functional genes as markers for sulfur cycling and CO2 fixation in microbial communities of hydrothermal bents of the Logatchev field. *FEMS Microb. Ecol*. 73, 526–537. doi: 10.1111/j.1574-6941.2010.00919.x

ISA (2021). *Minerals: Polymetallic Sulphides*. Available online at: https://www.isa.org.jm/exploration-contracts/polymetallic-sulphides (accessed January 10, 2021).

Ivanenko, V.N., Martínez Arbizu, P., and Stecher, J. (2006). Copepods of the family Dirivultidae (Siphonostomatoida) from deep-sea hydrothermal vent fields on the Mid-Atlantic Ridge at 14°N and 5°S. Zootaxa 1277, 1–21. doi: 10.11646/zootaxa.1277.1.1

Ivanenko, V. N., Corgosinho, P. H. C., Ferrari, F., Sarradin, P.-M., and Sarrazin, J. (2012). Microhabitat distribution of *Smacigastes micheli* (Copoepoda: harpacticoida: Tegastidae) from deep-sea hydrothermal vents at the Mid-Atlantic Ridge, 37°N (Lucky Strike), with a morphological description of its Nauplius. *Mar. Ecol*. 33, 1–11. doi: 10.1111/j.1439-0485.2011.00484.x

Ivanenko, V. N., and Defaye, D. (2004). A new and primitive genus and species of deep-sea Tegastidae (Crustacea, Copepoda, Harpacticoida) from the Mid-Atlantic Ridge, 37°N (Azores Triple Junction, Lucky Strike). *Cah. Biol. Mar*. 45, 255–268. doi: 10.21411/CBM.A.8BB81F1F

Jamieson, J. W., and Gartman, A. (2020). Defining active, inactive, and extinct seafloor massive sulfide deposits. *Mar. Pol*. 117:103926. doi: 10.1016/j.marpol.2020.103926

Jan, C., Petersen, J. M., Werner, J., Teeling, H., Huang, S., Golyshina, O. V., et al. (2014). The gill chamber epibiosis of deep-sea shrimp *Rimicaris exoculata*: an in-depth metagenomic investigation and discovery of Zetaproteobacteria. *Environ. Microbiol*. 16, 2723–2738. doi: 10.1111/1462-2920.12406

Johnson, M. L., Shelton, P. M., Herring, P. J., and Gardner, S. (1995). Spectral responses from the dorsal organ of a juvenile *Rimicaris exoculata* from the TAG hydrothermal vent. *BRIDGE Newsletter* 8, 38–42.

Jollivet, D. (1996). Specific and genetic diversity at deep-sea hydrothermal vents: an overview. *Biodivers. Conserv*. 5, 1619–1653. doi: 10.1007/BF00052119

Kelley, D. S., and Shank, T. M. (2010). Hydrothermal systems: a decade of discovery in slow spreading environments. *Geophys. Monogr. Ser*. 188, 369–407. doi: 10.1029/2010GM000945

Kong, L., Ryan, W. B. F., Mayer, L., Detrick, R. S., Fox, P. J., and Manchester, K. (1985). Bare-rock drill sites, ODP Legs 106 and 109: evidence for hydrothermal activity at 23° N in the Mid-Atlantic Ridge. *Eos* 66:1106.

Krasnov, S. G., Cherkashev, G. A., Stepanova, T. V., Batuyev, B. N., Krotov, A. G., Malin, B. V., et al. (1995). "Detailed geological studies of hydrothermal fields in the North Atlantic," in *Hydrothermal Vents and Processes*, eds L. M. Parson, C. L. Walker, and D. R. Dixon (London: Geological Society Special Publication 87), 43–64. doi: 10.1144/GSL.SP.1995.087.01.05

Krylova, E. M., Sahling, H., and Janssen, R. (2010). Abyssogena: a new genus of the family Vesicomyidae (Bivalvia) from deep-water vents and seeps. *J. Mollus. Stud*. 76, 107–132. doi: 10.1093/mollus/eyp052

LaBella, A. L., Van Dover, C. L., Jollivet, D., and Cunningham, C. W. (2017). Gene flow between Atlantic and Pacific Ocean basins in three lineages of deep-sea clams (Bivalvia: Vesicomyidae: Pliocardiinae) and subsequent limited gene flow within the Atlantic. *Deep-Sea Res. Part II* 137, 307–317. doi: 10.1016/j.dsr2.2016.08.013

Lalou, C., Reyss, J. L., and Brichet, E. (1998). Age of sub-bottom sulphide samples at the TAG active mound. *Proc. Ocean Drilling Prog. Sci. Results* 158, 111–117. doi: 10.2973/odp.proc.sr.158.214.1998

Le Bris, N. (2018). TRANSECT cruise. RV L'Atalante,

Le Bris, N., Yücel, M., Das, A., Sievert, S. M., LokaBharathi, P., and Girguis, P. R. (2019). Hydrothermal energy transfer and organic carbon production at the deep seafloor. *Front. Mar. Sci*. 5:531. doi: 10.3389/fmars.2018.00531

Le, J. T., Levin, L. A., and Carson, R. T. (2017). Incorporating ecosystem services into environmental management of deep-seabed mining. *Deep-Sea Res. Part II* 137, 486–503. doi: 10.1016/j.dsr2.2016.08.007

Levin, L. A., Baco, A. R., Bowden, D. A., Colaço, A., Cordes, E. E., Cunha, M. R., et al. (2016). Hydrothermal vents and methane seeps: rethinking the sphere of influence. *Front. Mar. Sci*. 3:72. doi: 10.3389/fmars.2016.00072

Li, J., Cui, J., Yang, Q., Cui, G., Wei, B., Wu, Z., et al. (2017). Oxidative weathering and microbial diversity of an inactive seafloor hydrothermal sulfide chimney. *Front. Microbiol*. 8:1378. doi: 10.3389/fmicb.2017.01378

Lilley, M. D., Feely, R. A., and Trefry, J. H. (1995). "Chemical and biochemical transformations in hydrothermal plumes," in *Seafloor Hydrothermal Systems: Physical, Chemical, Biological, and Geological Interactions*, eds S. E. Humphris, R. A. Zierenberg, L. S. Mullineaux, and R. E. Thomson (Washington, DC: American Geophysical Union), 369–391. doi: 10.1029/GM091p0369

Lopez-Garcia, P., Philippe, H., Gail, F., and Moreira, D. (2003). Authochthonous eukaryotic diversity in hydrothermal sediment and experimental microcolonizers at the Mid-Atlantic Ridge. *Proc. Natl. Acad. Sci. U. S. A*. 100, 697–702. doi: 10.1073/pnas.0235779100

Ludwig, K. A., Kelley, D. S., Butterfield, D. A., Nelson, B. K., and Früh-Green, G. (2006). Formation and evolution of carbonate chimneys at the Lost City Hydrothermal Field. *Geochim. Cosmochim. Acta* 70, 3625–3645. doi: 10.1016/j.gca.2006.04.016

Maas, P. A. Y., O'Mullan, G. D., Lutz, R. A., and Vrijenhoek, R. C. (1999). Genetic and morphometric characterization of mussels (Bivalvia: Mytilidae) from Mid-Atlantic hydrothermal vents. *Biol. Bull*. 196, 265–272. doi: 10.2307/1542951

Marques, A. F. A., Barriga, F. J., and Scott, S. D. (2007). Sulfide mineralization in an ultramafic-rock hosted seafloor hydrothermal system: from serpentinization to the formation of Cu–Zn–(Co)-rich massive sulfides. *Mar. Geol*. 245, 20–39. doi: 10.1016/j.margeo.2007.05.007

Marticorena, J., Matabos, M., Ramirez-Llodra, E., Cathalot, C., Laes-Huon, A., Leroux, R., et al. (2021). Recovery of hydrothermal vent communities in response to an induced disturbance at the Lucky Strike vent field (Mid-Atlantic Ridge). *Mar. Env. Res*. 168:105316. doi: 10.1016/j.marenvres.2021.105316

Matabos, M., Cuvelier, D., Brouard, J., Shillito, B., Ravaux, J., Zbinden, M., et al. (2015). Behavioural study of two hydrothermal crustacean decapods: *Mirocaris fortunata* and *Segonzacia mesatlantica*, from the Lucky Strike vent field (Mid Atlantic Ridge). *Deep-Sea Res. Part II* 121, 146–158. doi: 10.1016/j.dsr2.2015.04.008

Meier, D. V., Pjevac, P., Bach, W., Markert, S., Schweder, T., Jamieson, J., et al. (2019). Microbial metal-sulfide oxidation in inactive hydrothermal vent chimneys suggested by metagenomic and metaproteomic analyses. *Environ. Microbiol*. 21, 682–701. doi: 10.1111/1462-2920.14514

Mitarai, S., Watanabe, H., Nakajima, Y., Shchepetkin, A. F., and McWilliams, J. C. (2016). Quantifying dispersal from hydrothermal vent fields in the western Pacific Ocean. *Proc. Natl. Acad. Sci. U. S. A*. 113, 2976–2981. doi: 10.1073/pnas.1518395113

Moalic, Y., Desbruyères, D., Duarte, C. M., Rozenfeld, A., Bachraty, C., and Arnaud-Haond, S. (2012). Biogeography revisited with network theory: Retracing the history of hydrothermal vent communities. *Syst. Biol*. 61, 127–137. doi: 10.1093/sysbio/syr088

Molodtsova, T. N., Galkin, S. V., and Dobretsova, I. (2014). "Preliminary data on fauna of inactive hydrothermal sulfide fields on the Mid Atlantic Ridge at 12°58'-13°31'N," in *World Conference on Marine Biodiversity* (Qingdao).

Morineaux, M., Nishi, E., Ormos, A., and Mouchel, O. (2010). A new species of Phyllochaetopterus (Annelida: Chaetopteridae) from deep-sea hydrothermal Ashadze-1 vent field, Mid-Atlantic Ridge: taxonomical description and partial COI DNA sequence. *Cah. Biol. Mar*. 51, 239–248. doi: 10.21411/CBM.A.42737680

Mullineaux, L. S., Metaxas, A., Beaulieu, S. E., Bright, M., Gollner, S., Grupe, B. M., et al. (2018). Exploring the ecology of deep-sea hydrothermal vents in a metacommunity framework. *Front. Mar. Sci*. 5:49. doi: 10.3389/fmars.2018.00049

Mullineaux, L. S., Mills, S. W., Le Bris, N., Beaulieu, S. E., Sievert, S. M., and Dykman, L. N. (2020). Prolonged recovery time after eruptive disturbance of a deep-sea hydrothermal vent community. *Proc. R. Soc. London B* 287:20202070. doi: 10.1098/rspb.2020.2070

Murton, B. J., Klinkhammer, G., Becker, K., Briais, A., Edge, D., Hayward, N., et al. (1994). Direct evidence for the distribution and occurrence of hydrothermal activity between 27°N – 30°N on the Mid-Atlantic Ridge. *Earth Planet. Sc. Lett*. 125, 119–128. doi: 10.1016/0012-821X(94)90210-0

O'Mullan, G. D., Maas, P. A. Y., Lutz, R. A., and Vrijenhoek, R. C. (2001). A hybrid zone between hydrothermal vent mussels (Bivalvia: Mytilidae) from the Mid-Atlantic Ridge. *Mol. Ecol.* 10, 2819–2831. doi: 10.1046/j.0962-1083.2001.01401.x

Page, M. J., McKenzie, J. E., Bossuyt, P. M., Boutron, I., Hoffmann, T. C., Mulrow, C. D., et al. (2020). The PRISMA 2020 statement: an updated guideline for reporting systematic reviews. *BMJ* 372:n71. doi: 10.1136/bmj.n71

Perner, M., Bach, W., Hentscher, M., Koschinsky, A., Garbe-Schonberg, D., Streit, W. R., et al. (2009). Short-term microbial and physico-chemical variability in low-temperature hydrothermal fluids near 5°S on the Mid-Atlantic Ridge. *Environ. Microbiol.* 11, 2526–2541. doi: 10.1111/j.1462-2920.2009.01978.x

Perner, M., Kuever, J., Seifert, R., Pape, T., Koschinsky, A., Schmidt, K., et al. (2007). The influence of ultramafic rocks on microbial communities at the Logatchev hydrothermal field, located 15°N on the Mid-Atlantic Ridge. *FEMS Microb. Ecol.* 61, 97–109. doi: 10.1111/j.1574-6941.2007.00325.x

Petersen, J. M., Ramette, A., Lott, C., Cambon-Bonavita, M. A., Zbinden, M., and Dubilier, N. (2010). Dual symbiosis of the vent shrimp *Rimicaris exoculata* with filamentous gamma-and epsilonproteobacteria at four Mid-Atlantic Ridge hydrothermal vent fields. *Environ. Microbiol.* 12, 2204–2218. doi: 10.1111/j.1462-2920.2009.02129.x

Petersen, J. M., Zielinski, F. U., Pape, T., Seifert, R., Moraru, C., Amann, R., et al. (2011). Hydrogen is an energy source for hydrothermal vent symbioses. *Nature* 476, 176–180. doi: 10.1038/nature10325

Plum, C., Pradillon, F., Fujiwara, Y., and Sarrazin, J. (2017). Copepod colonization of organic and inorganic substrata at a deep-sea hydrothermal vent site on the Mid-Atlantic Ridge. *Deep-Sea Res. Part II* 137, 335–348. doi: 10.1016/j.dsr2.2016.06.008

Portail, M., Brandily, C., Cathalot, C., Colaço, A., Gelinas, Y., Husson, B., et al. (2018). Food-web complexity across hydrothermal vents on the Azores triple junction. *Deep-Sea Res. Part I* 131, 101–120. doi: 10.1016/j.dsr.2017.11.010

Reysenbach, A.-L., Longnecker, K., and Kirshtein, J. (2000). Novel bacteria and archaeal lineages from an *in-situ* growth chamber deployed at a Mid-Atlantic Ridge hydrothermal vent. *Appl. Environ. Microbiol.* 66, 3798–3806. doi: 10.1128/AEM.66.9.3798-3806.2000

Rommevaux, C., Henri, P., Degboe, J., Chavagnac, V., Lesongeur, F., Godfroy, A., et al. (2019). Prokaryote communities at active chimney and in-site colonization devices after a magmatic degassing event (37°N MAR, EMSO-Azores DeepSea Observatory). *Geochem. Geophy. Geosy.* 20, 3056–3089. doi: 10.1029/2018GC008107

Rona, P. A., Hannington, M. D., Raman, C. V., Thompson, G., Tivey, M. K., Humphris, S. E., et al. (1993). Active and relict sea-floor hydrothermal mineralization at the TAG hydrothermal field, Mid-Atlantic Ridge. *Econ. Geol.* 88, 1989–2017. doi: 10.2113/gsecongeo.88.8.1989

Rona, P. A., Klinkhammer, G., Nelsen, T. A., Trefry, J. H., and Elderfield, H. (1986). Black smokers, massive sulphides and vent biota at the Mid-Atlantic Ridge. *Nature* 321, 33–37. doi: 10.1038/321033a0

Roussel, E. G., Konn, C., Charlou, J.-L., Donval, J.-P., Fouquet, Y., Querellou, J., et al. (2011). Comparison of microbial communities associated with three Atlantic ultramafic hydrothermal systems. *FEMS Microbial. Ecol.* 77, 647–665. doi: 10.1111/j.1574-6941.2011.01161.x

Rybakova, E., and Galkin, S. (2015). Hydrothermal assemblages associated with different foundation species on the East Pacific Rise and Mid-Atlantic Ridge, with a special focus on mytilids. *Mar. Ecol.* 36, 45–61. doi: 10.1111/maec.12262

Sarrazin, J., Cuvelier, D., Peton, L., Legendre, P., and Sarradin, P. M. (2014). High-resolution dynamics of a deep-sea hydrothermal vent mussel assemblage monitored by the EMSO-Azores MoMAR observatory. *Deep-Sea Res. Part I* 90, 62–75. doi: 10.1016/j.dsr.2014.04.004

Sarrazin, J., Legendre, P., De Busserolles, F., Fabri, M. C., Guilini, K., Ivanenko, V. N., et al. (2015). Biodiversity patterns, environmental drivers and indicator species on a high temperature hydrothermal edifice, Mid-Atlantic Ridge. *Deep-Sea Res. Pt II* 121, 177–192. doi: 10.1016/j.dsr2.2015.04.013

Scott, J. J., Breier, J. A., Luther, I. I. I., G. W., and Emerson, D. (2015). Microbial iron mats at the MidAtlantic Ridge and evidence that Zetaproteobacteria may be restricted to iron-oxidizing systems. *PLoS ONE* 10:e0119284. doi: 10.1371/journal.pone.0119284

Sen, A., Podowski, E. L., Becker, E. L., Shearer, E. A., Gartman, A., Yucel, M., et al. (2014). Community succession in hydrothermal vent habitats of the Eastern Lau Spreading Center and Valu Fa Ridge, Tonga. *Limnol. Oceanogr.* 59, 1510–1528. doi: 10.4319/lo.2014.59.5.1510

Sievert, S., and Vetriani, C. (2012). Chemoautotrophy at deep-sea vents: past, present, and future. *Oceanography* 25, 218–233. doi: 10.5670/oceanog.2012.21

Stöhr, S., and Segonzac, M. (2005). Deep-sea ophiuroids (Echinodermata) from reducing and non-reducing environments in the North Atlantic Ocean. *J. Mar. Biol. Assoc. U. K.* 85, 383–402. doi: 10.1017/S0025315405011318h

Sun, J., Zhou, Y., Chen, C., Hang Kwan, Y., Sun, Y., Wang, X., et al. (2020). Nearest vent, dearest friend: biodiversity of Tiancheng vent field reveals cross-ridge similarities in the Indian Ocean. *R. Soc. Open Sci.* 7:200110. doi: 10.1098/rsos.200110

Suzuki, K., Yoshida, K., Watanabe, H., and Yamamoto, H. (2018). Mapping the resilience of chemosynthetic communities in hydrothermal vent fields. *Sci. Rep.* 8, 1–8. doi: 10.1038/s41598-018-27596-7

Tchesunov, A. V. (2015). Free-living nematode species (Nematoda) dwelling in hydrothermal sites of the North Mid-Atlantic Ridge. *Helg. Mar. Res.* 69, 343–384. doi: 10.1007/s10152-015-0443-6

Teixeira, S., Cambon-Bonavita, M. A., Serrao, E. A., Desbruyères, D., and Arnaud-Haond, S. (2010). Recent population expansion and connectivity in the hydrothermal shrimp *Rimicaris exoculata* along the Mid-Atlantic Ridge. *J. Biogeogr.* 38, 564–574. doi: 10.1111/j.1365-2699.2010.02408.x

Thurber, A. R., Sweetman, A. K., Narayanaswamy, B. E., Jones, D. O., Ingels, J., and Hansman, R. L. (2014). Ecosystem function and services provided by the deep sea. *Biogeosciences* 11, 3941–3963. doi: 10.5194/bg-11-3941-2014

Tsurumi, M., and Tunnicliffe, V. (2003). Tubeworm-associated communities at hydrothermal vents on the Juan de Fuca Ridge, Northeast Pacific. *Deep Sea Res. Part I Oceanogr. Res. Pap.* 50, 611–629. doi: 10.1016/S0967-0637(03)00039-6

Turner, P. J., Thaler, A. D., Freitag, A., and Collins, P. C. (2019). Deep-sea hydrothermal vent ecosystem principles: Identification of ecosystem processes, services and communication of value. *Mar. Pol.* 101, 118–124. doi: 10.1016/j.marpol.2019.01.003

Van der Heijden, K., Petersen, J. M., Dubilier, N., and Borowski, C. (2012). Genetic connectivity between North and South Mid-Atlantic Ridge chemosynthetic bivalves and their symbionts. *PLoS ONE* 7:e39994. doi: 10.1371/journal.pone.0039994

Van Dover, C. L. (1995). "Ecology of Mid-Atlantic Ridge hydrothermal vents," in *Hydrothermal Vents and Processes*, eds L. M. Parson, C. L. Walker, and D. R. Dixon (London: Geological Society Special Publication 87), 257–294. doi: 10.1144/GSL.SP.1995.087.01.21

Van Dover, C. L. (2014). Impacts of anthropogenic disturbances at deep-sea hydrothermal vent ecosystems: a review. *Mar. Environ. Res.* 102, 59–72. doi: 10.1016/j.marenvres.2014.03.008

Van Dover, C. L. (2019). Inactive sulphide ecosystems in the deep sea: a review. *Front. Mar. Sci.* 6:461. doi: 10.3389/fmars.2019.00461

Van Dover, C. L., Arnaud-Haond, S., Gianni, M., Helmreich, S., Huber, J. A., Jaeckel, A. L., et al. (2018). Scientific rationale and international obligations for protection of active hydrothermal vent ecosystems from deep-sea mining. *Mar. Pol.* 90, 20–28. doi: 10.1016/j.marpol.2018.01.020

Van Dover, C. L., Berg, C. J., Jr., and Turner, R. D. (1988b). Recruitment of marine invertebrates at deep-sea hydrothermal vents on the East Pacific Rise and Galapagos spreading center. *Deep-Sea Res. Part I* 35, 1833–1849. doi: 10.1016/0198-0149(88)90052-0

Van Dover, C. L., Colaço, A., Collins, P. C., Croot, P., Metaxas, A., Murton, B. J., et al. (2020). Research is needed to inform environmental management of hydrothermally inactive and extinct polymetallic sulfide (PMS) deposits. *Mar. Pol.* 121:104183. doi: 10.1016/j.marpol.2020.104183

Van Dover, C. L., Fry, B., Grassle, J. F., Humphris, S., and Rona, P. A. (1988a). Feeding biology of the shrimp *Rimicaris exoculata* at hydrothermal vents on the Mid-Atlantic Ridge. *Mar. Biol.* 98, 209–216. doi: 10.1007/BF00391196

Van Dover, C. L., German, C. R., Speer, K. G., Parson, L. M., and Vrijenhoek, R. (2002). Evolution and biogeography of deep-sea vent and seep invertebrates. *Science* 295, 1253–1257. doi: 10.1126/science.1067361

Van Dover, C. L., Szuts, E. Z., Chamberlain, S. C., and Cann, J. R. (1989). A novel eye in 'eyeless' shrimp from hydrothermal vents of the Mid-Atlantic Ridge. *Nature* 337, 458–460. doi: 10.1038/337458a0

Vereshchaka, A. L., Vinogradov, G. M., Lein, A. Y., Dalton, S., and Dehairs, F. (2000). Carbon and nitrogen isotopic composition of the fauna

from the Broken Spur hydrothermal vent field. *Mar. Biol.* 136, 11–17. doi: 10.1007/s002270050002

Vrijenhoek, R. C. (2010). Genetic diversity and connectivity of deep-sea hydrothermal vent metapopulations. *Mol. Ecol.* 19, 4391–4111. doi: 10.1111/j.1365-294X.2010.04789.x

Walker, B., Holling, C. S., Carpenter, S. R., and Kinzig, A. (2004). Resilience, adaptability and transformability in social–ecological systems. *Ecol. Soc.* 9:5. doi: 10.5751/ES-00650-090205

Wheeler, A. J., Murton, B., Copley, J. T., Lim, A., Carlsson, J., Collins, P. C., et al. (2013). Moytirra: discovery of the first known deep-sea hydrothermal vent field on the slow-spreading Mid-Atlantic Ridge north of the Azores. *Geochem. Geophy. Geosys.* 14, 4170–4184. doi: 10.1002/ggge.20243

World Register of Marine Species (2020). Available online at: http://www.marinespecies.org at VLIZ (accessed July 22, 2020).

Yahagi, T., Fukumori, H., Warén, A., and Kano, Y. (2019). Population connectivity of hydrothermal vent limpets along the northern Mid-Atlantic Ridge (Gastropoda: Neritimorpha: Phenacolepadidae). *J. Mar. Biolog. Assoc.* 99, 179–185. doi: 10.1017/S0025315417001898

Yearsley, J. M., Salmanidou, D. M., Carlsson, J., Burns, D., and Van Dover, C. L. (2020). Biophysical models of persistent connectivity and barriers on the northern Mid-Atlantic Ridge. *Deep-Sea Res. Part II* 180:104819. doi: 10.1016/j.dsr2.2020.104819

Zbinden, M., Le Bris, N., Gaill, F., and Compere, P. (2004). Distribution of bacteria and associated minerals in the gill chamber of the vent shrimp *Rimicaris exoculata* and related biogeochemical processes. *Mar. Ecol. Prog. Ser.* 284, 237–251. doi: 10.3354/meps284237

Zekely, J., Sørensen, M. V., and Bright, M. (2006b). Three new nematode species (Monhysteridae) from deep-sea hydrothermal vents. *Meiofauna Marina* 15, 25–42. Available online at: https://pfeil-verlag.de/publikationen/meiofauna-marina-band-15/

Zekely, J., Van Dover, C. L., Nemeschkal, H. L., and Bright, M. (2006a). Hydrothermal vent meiobenthos associated with mytilid mussel aggregations from the Mid-Atlantic Ridge and the East Pacific Rise. *Deep-Sea Res. Part I* 53, 1363–1378. doi: 10.1016/j.dsr.2006.05.010

Zeppilli, D., Bellec, L., Cambon-Bonavita, M.-A., Decraemer, W., Fontaneto, D., Fuchs, S., et al. (2019). Ecology and trophic role of *Oncholaimus dyvae* sp. nov. (Nematoda: Oncholaimidae) from the lucky strike hydrothermal vent field (Mid-Atlantic Ridge). *BMC Zool.* 4, 1–15. doi: 10.1186/s40850-019-0044-y

Zhang, X., Fang, J., Bach, W., Edwards, K. J., Orcutt, B. N., and Wang, F. (2016). Nitrogen stimulates the growth of subsurface basalt-associated microorganisms at the western flank of the Mid-Atlantic Ridge. *Front. Microbiol.* 7:633. doi: 10.3389/fmicb.2016.00633

Conflict of Interest: RB-R was employed by the company Seascape Consultants Ltd. during this research.

The remaining author declares that the research was conducted in the absence of any additional commercial or financial relationships that could be construed as a potential conflict of interest.

Publisher's Note: All claims expressed in this article are solely those of the authors and do not necessarily represent those of their affiliated organizations, or those of the publisher, the editors and the reviewers. Any product that may be evaluated in this article, or claim that may be made by its manufacturer, is not guaranteed or endorsed by the publisher.

frontiers in Marine Science

REVIEW
published: 11 October 2021
doi: 10.3389/fmars.2021.744874

Structure and Connectivity of Hydrothermal Vent Communities Along the Mid-Ocean Ridges in the West Indian Ocean: A Review

*Maëva Perez[1,2,3], Jin Sun[4], Qinzeng Xu[5] and Pei-Yuan Qian[1,2]**

[1] Department of Ocean Science and Hong Kong Branch of Southern Marine Science and Engineering Guangdong Laboratory (Guangzhou), The Hong Kong University of Science and Technology, Kowloon, Hong Kong SAR, China, [2] Southern Marine Science and Engineering Guangdong Laboratory, Guangzhou, China, [3] Département des Sciences Biologiques, Université de Montréal, Montreal, QC, Canada, [4] Institute of Evolution and Marine Biodiversity, Ocean University of China, Qingdao, China, [5] MNR Key Laboratory of Marine Eco-Environmental Science and Technology, First Institute of Oceanography, Ministry of Natural Resources, Qingdao, China

To date, 13 biologically active hydrothermal vent (HTV) fields have been described on the West Indian Ocean ridges. Knowledge of benthic communities of these vent ecosystems serves as scientific bases for assessing the resilience of these ecosystems under the global effort to strike an elegant balance between future deep-sea mining and biodiversity conservation. This review aims to summarize our up-to-date knowledge of the benthic community structure and connectivity of these Indian vents and to identify knowledge gaps and key research questions to be prioritized in order to assess the resilience of these communities. The HTVs in the West Indian Ocean are home to many unique invertebrate species such as the remarkable scaly-foot snail. While distinct in composition, the macrofaunal communities of the Indian HTVs share many characteristics with those of other HTVs, including high endemism, strong zonation at the local scale, and a simple food web structure. Furthermore, Indian vent benthic communities are mosaic compositions of Atlantic, Pacific, and Antarctic HTV fauna possibly owning to multiple waves of past colonization. Phylogeographic studies have shed new light into these migratory routes. Current animal connectivity across vent fields appears to be highly influenced by distance and topological barriers. However, contrasting differences in gene flow have been documented across species. Thus, a better understanding of the reproductive biology of the Indian vent animals and the structure of their population at the local scale is crucial for conservation purposes. In addition, increased effort should be given to characterizing the vents' missing diversity (at both the meio and micro-scale) and elucidating the functional ecology of these vents.

Keywords: conservation, ecology, chemosynthesis, gene-flow, mining, Indian Ocean ridge, biodiversity, knowledge gaps

OPEN ACCESS

Edited by:
Lorenzo Angeletti, Institute of Marine Science, National Research Council (CNR), Italy

Reviewed by:
Americo Montiel, Universidad de Magallanes, Chile
Miguel Angel Ahumada-Sempoal, University of the Sea, Mexico

***Correspondence:**
Pei-Yuan Qian
boqianpy@ust.hk

Specialty section:
This article was submitted to Deep-Sea Environments and Ecology, a section of the journal Frontiers in Marine Science

Received: *21 July 2021*
Accepted: *13 September 2021*
Published: *11 October 2021*

Citation:
Perez M, Sun J, Xu Q and Qian P-Y (2021) Structure and Connectivity of Hydrothermal Vent Communities Along the Mid-Ocean Ridges in the West Indian Ocean: A Review. Front. Mar. Sci. 8:744874. doi: 10.3389/fmars.2021.744874

Abbreviations: HTV, hydrothermal vent; SWIR, Southwest Indian Ridge; CIR, Central Indian Ridge; SEIR, Southeast Indian Ridge; CR, Carlsberg Ridge.

INTRODUCTION

The International Seabed Authority (ISA) has been working with stakeholders and lawmakers to draft regulations governing seabed mining by 2023 (International Seabed Authority, 2018). Given the growing interest in mining polymetallic deposits at hydrothermal vents (HTVs), assessing the vulnerability of their biological communities, which are predicted to hold valuable natural products (Thornburg et al., 2010; Van Dover et al., 2018) and play an important role in carbon cycling (Bell et al., 2017), is an urgent and essential task. Mining operations on vent ecosystems are foreseen to have multiple severe consequences (Reed et al., 2015; Ellis et al., 2017; Gollner et al., 2017; Van Dover et al., 2018; Washburn et al., 2019), but specific guidelines for conservation are hard to formulate because of immense knowledge gaps on the ecology of these ecosystems and in particular their natural resilience and connectivity. HTV communities were initially presumed to be highly resilient because of the great variability and unpredictability of the environmental conditions to which they have adapted (Hessler et al., 1988; Juniper and Tunnicliffe, 1997; Sarrazin et al., 1997), but the discovery of slow-growing species (Urcuyo et al., 2007) and highly stable vent communities (Boschen et al., 2015; Du Preez and Fisher, 2018) has challenged these assumptions and highlighted the need for a global assessment of HTV biodiversity. In a recent study, Gollner et al. (2021) assessed 11 confirmed vent fields on the northern Mid-Atlantic Ridge (MAR) by using a combination of criteria set for "Vulnerable Marine Ecosystems" by FAO and "Ecologically or Biologically Significant Areas" by CBD and "Particularly Sensitive Sea Areas" by IMO, and concluded that 10 of those 11 HTV fields met all the criteria for ecosystems in need of protection.

The spreading ridges of the Indian Ocean and their hydrothermal ecosystems (**Figure 1**) are unique but have less known vent ecosystems than those in the Atlantic and Pacific mid-ocean ridges in terms of their spreading rate (Müller et al., 2008; Beaulieu, 2015), mineral composition (German et al., 2016), and carbon input from the surface (Harms et al., 2021). Indian Ocean spreading ridge vent ecosystems have been hypothesized to serve as a corridor of connectivity between Atlantic and Pacific vent fauna (Ramirez-Llodra et al., 2007; Bachraty et al., 2009; Moalic et al., 2012; Rogers et al., 2012).

The mid-ocean ridges of the Indian Ocean display contrasting spreading rates that range from intermediate (∼80 mm/year) to ultraslow (<20 mm/year). Slower spreading at mid-ocean ridges usually translates to less intense hydrothermal activity (Baker et al., 1996; German and Parson, 1998), but this correlation is not always true at ultraslow spreading ridges (Dick et al., 2003; Snow and Edmonds, 2007; German et al., 2016) as evidenced by the discovery of large active HTV fields (Edmonds et al., 2003; Connelly et al., 2007; Tao et al., 2009; Kinsey and German, 2013). At ultraslow spreading ridges, hydrothermal fluids penetrate deeper in the crust, possibly below the Moho boundary (Tao et al., 2020), and hydrothermal circulation is more stable (Baker et al., 2004). It is estimated, for instance, that hydrothermal activity at the now inactive vent site Mount Jourdanne had lasted for more than 50,000 years. Given these unique characteristics, polymetallic sulfide deposits may be more important (German et al., 2016) and richer in copper and gold (German et al., 2016) at the slower-spreading Indian ridges and are thus of greater interest to mining companies. At the same time, their higher stability and lower nutritional resources may render their HTV communities more vulnerable to environmental disturbances (Fjeldsaå and Lovett, 1997; Du Preez and Fisher, 2018).

In this short review, we summarize the current state of knowledge about the community composition and connectivity of HTVs in the West Indian Ocean ridges, focusing mainly on macrofaunal species. Specifically, we aim to address the following questions: (1) How diverse and variable are the HTV communities, and do diversity and variability impact the resilience of these ecosystems? (2) To what extent are the Indian mid-ocean ridges HTV ecosystems connected, and how do these connectivity patterns vary across species? (3) How unique are the characteristics of community composition and connectivity in the West Indian mid-ocean ridges in comparison to vent systems in the other oceans? and (4) What are the knowledge gaps that need to be filled first in order to assess the sustainability of mining operations?

COMMUNITY STRUCTURE

Diversity and Endemicity

Macrofaunal communities in the Western Indian Ocean HTVs are akin to other deep-sea chemosynthetically based ecosystems with low species richness but high abundance of individuals (Tsurumi, 2003; Dover and Doerries, 2005; Sarrazin et al., 2015) (see **Supplementary Material**). Macrofaunal species richness in the HTVs of the Indian Ocean are in the range of what has been observed elsewhere (see **Supplementary Material**). At the Southwest Indian Ridge (SWIR) and the Central Indian Ridge (CIR), 39 and 37 macrofauna taxa were identified, respectively (Watanabe and Beedessee, 2015; Zhou et al., 2018), whereas between 1 and 116 (21 species on average) were described from other vents worldwide (Bachraty et al., 2009). Dominant macrofaunal species in the Indian Ocean vent ecosystems include the shrimp *Rimicaris kairei*, the mussel *Bathymodiolus marisindicus*, the crab *Austinograea rodriguezensi*, the scaly-foot snail *Chrysomallon squamiferum*, the snails of the genus *Gigantopelta* and *Alvinichoncha,* the stalked barnacle *Neolepas marisindica*, and the polychaetes *Ophryotrocha jiaolongi* (SWIR) and *Branchipolynoe longqiensis*, which are commensal worms in the mantle cavity of *B. marisindicus* (SWIR).

Like elsewhere, macrofaunal vent communities in the Indian Ocean also possess high endemicity (Ramirez-Llodra et al., 2007; Rogers et al., 2012; **Figure 2**). The Indian vent communities are also distinct in composition from other oceans because almost all the dominant taxa above are unique to the Indian vents (Hashimoto et al., 2001; Nakamura et al., 2012; Copley et al., 2016; Zhou et al., 2018; Kim et al., 2020). With the restricted distribution of these animals, fragmented habitat, and uncertainties about their demographic fluctuations, the proposed idea was to first place these species preemptively in the IUCN Red List of threatened species (Sigwart J. D. et al., 2019). These

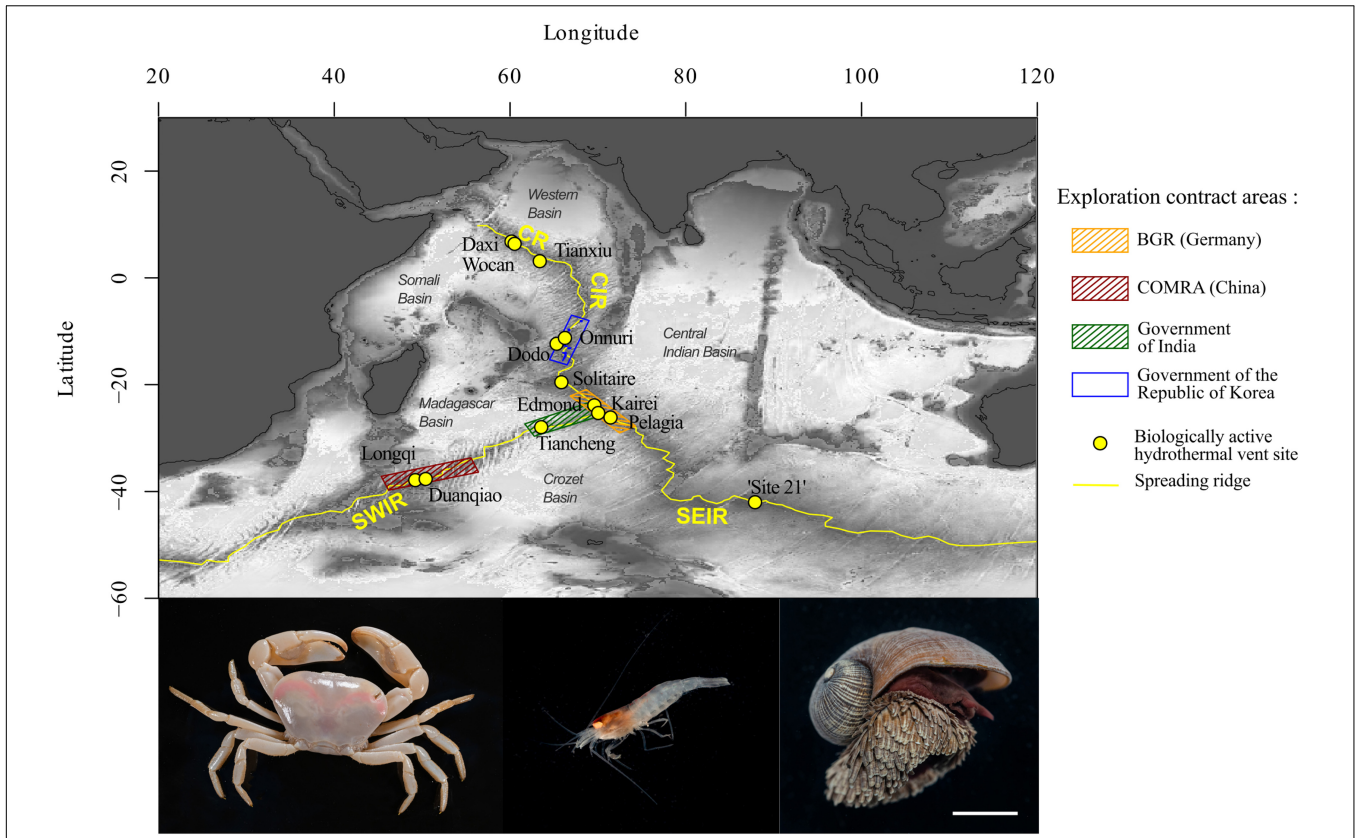

FIGURE 1 | Biologically active hydrothermal vents of the Indian mid-ocean ridges. The Indian Ocean counts eight topological ridges, including four that are active plate boundary rift zones. In recent years, exploration campaigns by the Federal Institute for Geosciences and Natural Resources of Germany (BGR), COMRA (China), the Government of India, and the Government of the Republic of Korea (6 areas within the blue rectangle), who were awarded exploration permits by the ISA between 2011 and 2016 (Minerals: Polymetallic Sulfides | International Seabed Authority), resulted in the discovery of additional vent fields on the CIR, CR, SWIR, and SEIR. At the time of writing this review, 13 active hydrothermal vent fields with associated macrofaunal communities have been described in the Indian mid-ocean ridge. Some of the endemic taxa of the Indian ridges are shown. **Bottom-left:** *Austinograea rodriguezensis,* **bottom-middle:** *Mirocaris indica,* **bottom-right:** *Chrysomallon squamiferum*. Scale bar = 2 cm. Bathymetric data from NOAA, exploration contract areas from https://www.isa.org.jm/exploration-contracts/polymetallic-sulfides. Photos courtesy of Dr. Jin Sun.

criteria permitted the addition of the scaly-foot snail to that list in 2019 (Sigwart J. et al., 2019). Furthermore, a similar degree of variation in community composition exists within the Indian biogeographic province itself (**Figure 2**). For instance, roughly a quarter of the macrofaunal vent species found on the SWIR were not found in other vent fields in the Indian Ocean (Zhou et al., 2018), and major differences in species richness and abundance can be observed between sites located even on the same spreading ridge (see section "Community Differences Across Vent Fields").

Spatial Zonation at the Local Scale

Strong spatial zonation on the scale of a few meters, similar to the situations described for the Juan de Fuca Ridge and East Pacific Rise (EPR) vents (Shank et al., 1998; Sarrazin et al., 1999), was observed in the HTVs of the Indian Ocean (Nakamura et al., 2012; Watanabe and Beedessee, 2015; Copley et al., 2016; Zhou et al., 2018). Invertebrates with strong nutritional reliance on chemosymbionts (e.g., shrimps and mussels) and to a lesser extent various grazers and omnivorous taxa (e.g., crabs and polychaetes) were the dominant macrofauna in high-sulfide environments, whereas suspension feeders such as Actinians cnidarians were found on the periphery of these assemblages (Watanabe and Beedessee, 2015). Studies from other vents suggest that physicochemical parameters (notably temperature and hydrogen sulfide concentration) significantly affect species distribution (Sarrazin et al., 1999; Le Bris et al., 2005; Podowski et al., 2010), but in all studies, the examined environmental parameters could explain only a small percentage of the differences among the various community patches. Other factors such as species interactions (Micheli et al., 2002) and colonization history (Le Bris et al., 2006) are also known to contribute to the communities' composition. For instance, the early colonizers often alter the physicochemical parameters of their surrounding environment and facilitate (or inhibit) colonization by other species (Mullineaux et al., 2003; Pradillon et al., 2009; Govenar, 2010). In the Indian HTVs, neither the small-scale abiotic environments nor the species interactions have been sufficiently characterized for determining their roles in the composition and distribution of species assemblages. Furthermore, models of niche partition from better-studied vent

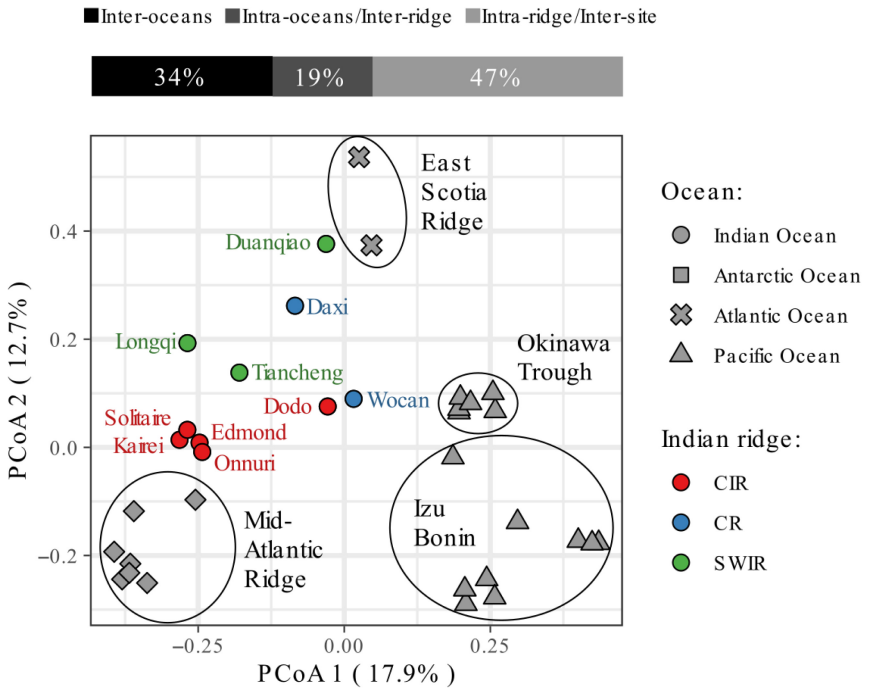

FIGURE 2 | Partition of the variance in community composition (genus level) across hydrothermal vents in the Indian, Antarctic, Atlantic, and West Pacific oceans. The Principal Coordinate Analysis (PcoA) plot is based on the Jaccard distance between vent sites. The presence/absence of taxa was compiled from Wang et al. (2021); Nakajima et al. (2014), Sun et al. (2020), and Kim et al. (2020), building upon Copley et al. (2016) and is provided as **Supplementary Material** with additional β-diversity indices. All hierarchical levels (inter-ocean and inter-ridge) significantly contribute to the observed differences in community composition at the genus level (db-RDA *p*-value = 0.001). ANOSIM analyses also support the ocean- and ridge-level groupings of vent communities (significance = 1e-04) with dissimilarities across mid-ocean ridges higher than across oceans (ANOSIM statistic $R = 0.8$ and 0.59, respectively). Within the Indian Ocean, ridge-level groups are statistically significant but less supported (ANOSIM significance = 0.0245). Note that the species lists for CR vents are likely incomplete due to lower sampling effort.

fields cannot be directly applied to the Indian HTV because of the different chemical composition of their hydrothermal fluids (Kumagai et al., 2008; Wang et al., 2017) and because of the different species composition of their communities.

Local-Scale Temporal Succession

Macrofaunal communities at vents typically shift overtime in response to changes in hydrothermal output and biologically driven changes in environmental conditions. Analysis on the temporal community succession in the Indian Ocean HTVs has always been hindered by the lack of continuous observations and a small number of available reports. Such succession was observed at Longqi with varying degrees throughout the site (Zhou et al., 2018). After revisiting the same black smoker at Longqi, Zhou et al. (2018) found that in the span of 3 years, its venting output had diminished considerably while at the same time, the diversity of its macrofaunal communities had increased and "peripheral" species commonly found at other diffuse vents (e.g., *Neolepas* sp., *B. marisindicus*) had been recruited. In contrast, the authors noticed the community assemblages in the areas of the vent field with more diffuse flow had been highly stable. In these environments, most taxa found in 2011 were found again in 2014/2015, and the pattern of their spatial zonation was conserved. This intra-site variation in community stability was also observed on the Juan de Fuca Ridge, where the communities living on the active sulfide chimneys shifted rapidly on the order of months to a few years (Sarrazin et al., 1997), whereas the communities on basalts away from the sulfide edifices were estimated to be at least 30 years old (Urcuyo et al., 2007).

Food Webs

Few studies have investigated food web structures of macrofaunal communities in the Indian vents and reported that these communities possessed 2–4 trophic levels (Van Dover et al., 2001; Copley et al., 2016; Reid et al., 2020). These short trophic chains are typical of other vent communities [e.g., in the EPR (Gaudron et al., 2012; Reid et al., 2013), Juan de Fuca Ridge (Bergquist et al., 2007; Sweetman et al., 2013; Lelièvre et al., 2017), and MAR (Vereshchaka et al., 2000)].

The dominant macrofaunal species are typically symbiotic primary consumers. Unique stable isotope signatures and additional evidence from *in situ* hybridization and hologenomic analyses revealed that these dominant taxa rely heavily or exclusively on chemosymbionts for food, including *C. squamiferum* (Van Dover, 2002; Goffredi et al., 2004; Nakagawa et al., 2014; Chen et al., 2015b; Reid et al., 2020), *Gigantopelta aegis* (Copley et al., 2016; Lan et al., 2021), *Alviniconcha marissindica* (Miyazaki et al., 2020; Yang Y. et al., 2020), *R. kairei* (Zbinden et al., 2008; Petersen et al., 2010;

Guri et al., 2012; Jiang et al., 2020), and *B. marisindicus* (Yamanaka et al., 2003; McKiness and Cavanaugh, 2005; Copley et al., 2016). With the exception of *C. squamiferum* and *G. aegis*, symbiosis was known for congeneric species of these taxa in other oceans (Belkin et al., 1986; Stein et al., 1988; Endow and Ohta, 1989; Nelson et al., 1995; Rieley et al., 1999; Won et al., 2003). Carbon and nitrogen stable isotope analyses suggest most of the other species are omnivorous, possibly feeding on bacterial mats, mucus biofilms, and/or animal tissues (Van Dover, 2002). In the CIR, the highest trophic levels are composed of the polynoids *Branchinotogluma*, nemertean worms, and anemones for which direct predation on shrimp was captured on video surveys (Van Dover, 2002).

This first sketch of the food webs of the Indian vent ecosystems appears to reflect a resilient trophic structure with a few dominant symbiotic species and many opportunistic primary or secondary consumers. However, trophic ecology for most of the Indian vent ecosystems remains unknown. First, the primary producers have not sufficiently been identified to provide an accurate estimation of the diversity of food sources. Next, observations on animal behavior are too insufficient to infer trophic interactions with confidence. Third, the communities at the meio- and microscale, where many trophic interactions are expected to happen (Schmid-Araya and Schmid, 2000; Zekely et al., 2006; Nomaki et al., 2008, 2019; Ptatscheck et al., 2020), remain virtually undescribed. Only one study characterizing the Indian vent meiofaunal communities has been published to date (Kang and Kim, 2021). Last but not least, how these structures vary in time and space is unclear. Furthermore, ontogenic shifts in diet were observed in vent arthropods both in the Indian Ocean and elsewhere (Van Dover, 2002; Methou et al., 2020), and the microbial diet of several species varies across sites (Reid et al., 2020; Ma and Wang, 2021). However, the implications of these changes in food source on the ecology and adaptability of vent animals are still obscure.

Active vs. Inactive Sites

Mining plans for polymetallic sulfides suggest that activities be focused on inactive chimneys and vent fields to avoid technical issues posed by hot and reduced hydrothermal fluids, and to mitigate the impact on vent fauna; inactive sites do not have the lush vent communities typically found at active sites. Yet, the idea that inactive sites are of lesser or no biological interest has been challenged by the discovery of unique slow-growing communities in the West Pacific (Boschen et al., 2015; Du Preez and Fisher, 2018). A call has been made for a better understanding of the ecosystem functions and services of hydrothermally inactive sites (Van Dover et al., 2020). Active and inactive chimneys represent vastly different ecosystems, and inactive chimneys are neither lifeless nor akin to other diffuse flow ecosystems as initially hypothesized (Van Dover, 2019). At the Longqi site, the biodiversity in the diffuse-flow environments was lost at the inactive chimneys, which were occupied exclusively by the polychaete *Amphisamytha* sp. (Zhou et al., 2018). On the CIR, Gerdes et al. (2019) characterized five discrete types of faunal assemblages across the active and inactive vent fields of Edmond and Gauss, respectively, and found that assemblages in inactive vents were distinct from those of active vents, those at the periphery of active vents, and typical non-vent assemblages. The effect of substrate composition on the community structure was significant but could explain only a small percentage of the variation (12.5%) observed across the different communities. Another study that surveyed the microbial diversity on active and inactive vent chimneys at the Kairei and Pelagia vent fields revealed the inactive chimneys are home to rare and unique microbes (Han et al., 2018). Overall, these studies support the idea that inactive chimneys and inactive vent fields in the Indian Ocean hold important biological resources and stress that they should be better studied to assess their role in the ecosystem function of HTVs (Van Dover et al., 2020).

Community Differences Across Vent Fields

An important first step to characterize the ecological niche of vent species in the Indian Ocean is to assess the natural variability of HTV communities. Corroborating the variation in community composition with environmental parameters can provide important information on the physicochemical factors that affect species distribution and thus their resilience. On a larger scale, differences in community structure are also a first line of evidence for biological barriers to connectivity.

The vent field ecosystems on Carlsberg Ridge (CR) and the Southeast Indian Ridge (SEIR) have not been sufficiently investigated to assess intra-ridge variation but even if sampling was sparse, multiple HTVs have been characterized within each of the CIR and SWIR (**Figures 3**, **4**). On each of the SWIR and CIR, the community composition of the macrofauna and microbiota differs across vent sites and these variations correlate with distance. *R. kairei* shrimps, for instance, form dense swarms at Edmond and Kairei (near the Rodrigues Triple Junction) but are more sparse in the northernmost vents of Dodo and Solitaire (Beedessee et al., 2013). Whether the

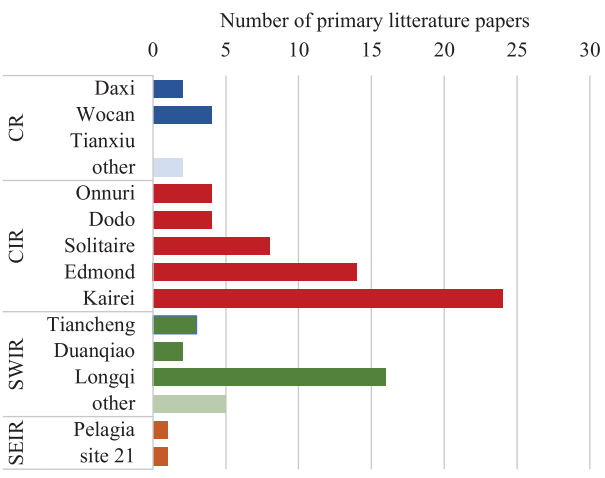

FIGURE 3 | Biological study bias across HTV fields of the Indian mid-ocean ridges. Based on 50 studies cited in this review (full list available as **Supplementary Material**).

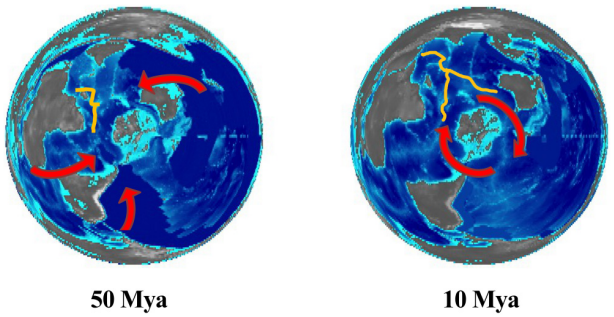

FIGURE 4 | Possible migration routes for vent species into the Indian Ocean. Paleo-digital elevation models from Scotese and Wright (2018) viewed from the South Pole. The Indian spreading ridges are sketched in yellow.

underlying attributes of the shifts in community structure are local differences in environmental conditions or patterns of population connectivity is still unclear. For example, the stalked barnacle (Watanabe et al., 2018) possesses distinct morphotypes along the CIR, but whether these morphological variations are the results of phenotypic plasticity or genetic differentiation between populations is unknown. The stalked barnacle did not appear to be genetically different across vent fields, but their phylogenetic relationship was assessed only by using the mitochondrial COI gene, which is not good enough to discriminate closely related populations (Paz-Vinas et al., 2021).

The strongest contrasts in community composition were detected across the mid-ocean ridges. The first vent macrofauna described from CR was characterized by a high abundance of the polychetes *Hesiolyra heteropoda* and *Paralvinella mira* (Han et al., 2021) and dense swarms of *R. kairei*. CR communities showed the highest similarity to the CIR (Wang et al., 2021) but did not include other common species found at the CIR and SWIR, such as *C. squamiferum*, *A. marisindica*, and *B. marisindicus*. Disparate species are also found across the CIR and SWIR. Taxa present only at the SWIR include *Gigantopelta aegis*, *Ophryotrocha* n. sp. "F-038/1b," *Phymorhynchus* n. sp. "SWIR," and *Lepetodrilus* n. sp. "SWIR" (Copley et al., 2016), whereas *Alviniconcha marisindica* is a common species at both the CIR and CR but absent at the SWIR (Copley et al., 2016; Zhou et al., 2018). Across the CIR and SWIR, the abundance of *R. kairei* is much lower (or even found as solitaire individuals) at the SWIR than at the CIR (Copley et al., 2016; Zhou et al., 2018). Such strong contrasts in community composition were also observed across the disjunct spreading ridges of the eastern Pacific (Tunnicliffe, 1988; Van Dover et al., 1990), indicating that the topological discontinuities along the Indian spreading ridges likely act as strong barriers to dispersal for many species.

CONNECTIVITY

Indian Mid-Ocean Ridges Communities as Melting Pots of Atlantic and Pacific Vent Species

One long-held hypothesis is that the Indian ridges act as a corridor of population connectivity between the Atlantic and Western Pacific vents (German et al., 1998). This idea was brought up by early surveys of global vent biodiversity on the basis of the presence/absence of vent macrofauna, which classified the Indian vents into a distinct biogeographic province with strong connection to both the Atlantic and West Pacific provinces (Ramirez-Llodra et al., 2007; Moalic et al., 2012; **Figure 2**). Many studies investigating the biogeography of macrofaunal taxa at the species level also highlighted the evolutionary connection between the Atlantic, Pacific, and Indian oceans (Hashimoto et al., 2001; McKiness and Cavanaugh, 2005; Ramirez-Llodra et al., 2007; Miyazaki et al., 2010; Rogers et al., 2012; Borda et al., 2013; Roterman et al., 2013; Breusing et al., 2015, 2020; Chen et al., 2015b; Johnson et al., 2015; Copley et al., 2016; Watanabe et al., 2018; Zhou et al., 2018; Lee et al., 2019; Jang et al., 2020; Han et al., 2021). However, an important detail to recognize is that these biogeographical inferences are at a high taxonomic level (i.e., comparing closely related species) rather than the population level and thus may be indicative of past migration but may not necessarily be the current existing connection. For this reason, a potentially safer approach is to describe the Indian Ocean HTVs as a mosaic of colonizers from the Atlantic and Western Pacific oceans rather than as a corridor between them until more solid evidence on corridor theory becomes available.

Recent studies have shed new light into the dispersal route of some of the Indian vent taxa (**Figure 4**). One possible dispersal route was through the deep water passage between the Eurasian and Australian plates present in the Eocene (50–30 Mya). Vent endemics, which are most closely related to congeners from the West Pacific Ocean (e.g., *Alviniconcha*, *Paralvinella*), tend to be prevalent in the northernmost Indian hydrothermal fields (McKiness and Cavanaugh, 2005; Miyazaki et al., 2010; Borda et al., 2013; Breusing et al., 2015, 2020; Johnson et al., 2015; Zhou et al., 2018; Lee et al., 2019; Jang et al., 2020; Han et al., 2021). Molecular clocks calibrated on fossil records corroborate this hypothesis for *Alviniconcha* (Breusing et al., 2020). *A. marisindica* and *A. boucheti* appear to have speciated about 38 Mya (Breusing et al., 2020). HTVs generated from hot-spot volcanism during the northward migration of the Indian plate during the Eocene possibly served as a stepping stones for this species and others to reach the nascent mid-ocean spreading ridge that includes current CR and CIR. Species that are able to colonize other chemosynthetic environments such as cold seeps may have been able to use a variety of migration routes and maintain high connectivity across the Pacific and Indian oceans for extended periods (Breusing et al., 2015).

A more recent colonization event appears to have brought species from the East Pacific and Atlantic oceans into the SWIR through the Southern Ocean superconvergence. With the increasing intensity of the Antarctic Circumpolar Current during the middle Miocene (∼13.0 Mya), species in the Southern Ocean may have been isolated from the MAR and EPR and pushed eastward. This dispersal route is supported by fossil records and phylogeography of several taxa from SWIR that are closely related to those from East Scotia Ridge in the southern Atlantic Ocean, including *Kiwa* spp. (Roterman et al., 2013), *G. aegis* (Chen et al., 2015b), the polychaetes *Polinoidae* and *Hesiolyra* cf. *bergi* (Copley et al., 2016; Wang et al., 2020), and *Neolepas marisindica*

(Rogers et al., 2012; Watanabe et al., 2018). Interestingly, these taxa are most abundant at the easternmost SWIR sites (Longqi and Duanqiao) (Zhou et al., 2018), suggesting a higher historical connectivity within ridges along the Southern Ocean.

Current Patterns of Connectivity Within and Across Indian Mid-Ocean Ridges

Modern vent species have multiple interconnected sub-populations (Vrijenhoek, 1997). The population structure and migrant flux of each species are closely linked to the persistence of these metapopulations and are therefore of great interest for conservation. When vent populations are structured according to the stepping stone model (Kimura and Weiss, 1964), they are well connected to their close neighbors, leading to a pattern of genetic variation with distance. In this scenario, the destruction of a habitat can lead to interruptions in the gene flow and isolate populations, thus making them more vulnerable to extinction. However, under the island model of population structure, species have high dispersal capabilities and are not affected by distance, but differences in habitat quality may result in patches of "source" populations that produce many dispersing migrants and "sink" populations sustained by constant import of new recruits (Vrijenhoek, 1997). In this scenario, extinction of source populations would negatively impact the sink sites.

The current patterns of connectivity of five macrofaunal taxa (*B. marisindicus*, *A. marisindica*, *C. squamiferum*, *A. rodriguezensis*, and *R. kairei*) for the Indian Ocean HTVs were evaluated using population genetics. High connectivity among the vent fields within the CIR was found (Nakamura et al., 2012; Beedessee et al., 2013; Chen et al., 2015a; Watanabe et al., 2018; Breusing et al., 2020) although these studies could provide only a coarse resolution of the population structures because few vent fields were surveyed (a maximum of four), a relatively small number of individuals (less than 50) were sampled within each site, and only one or few conserved genetic markers were used. Nevertheless, the estimated gene flow appeared to be from the southern (Kairei and Edmond) to northern sites, (Solitaire), suggesting that the southern vent fields serve as sources of dispersing migrants (Beedessee et al., 2013; Chen et al., 2015a).

Across the CIR and SWIR, a striking pattern of genetic isolation was observed (Chen et al., 2015a; Sun et al., 2020) and the topography of the Rodrigues Triple Junction was hypothesized as a strong dispersal barrier between the spreading ridges (Chen et al., 2015a). However, populations sampled from a venting site on the SWIR near the triple junction displayed strong gene flow with the CIR vents located at the triple junction, supporting a stepping stone model for larval dispersal and also indicating that transform faults on the SWIR itself are the strongest barriers to connectivity between SWIR and CIR (Sun et al., 2020).

Variation Across Species

Vent connectivity of macrofaunal species is a process influenced by the interactions of oceanic currents and larval biology (Adams et al., 2012). The dispersal of larvae is strongly affected by their vertical position in the water column because hydrothermal activity and ridge topography lead to a layering of currents with contrasting speed and direction. For instance, the Endeavor segment of the Juan de Fuca Ridge is characterized by deep valleys that trap buoyant hydrothermal water and the southward outflow of this water mass forces an northward inflow of near-bottom cold water (Thomson et al., 2003). Hence, swimming larvae may be able to reach shallower, stronger currents and thus disperse further, while the dispersal of the others will be dictated by their buoyancy (Adams et al., 2012; Yahagi et al., 2017).

In the Indian Ocean, different HTV taxonomic groups with different larval characteristics displayed different dispersal patterns on the basis of genetic data. At the CIR, some crustacean populations appear to reproduce periodically as multimodal distributions of sizes (an indication of multiple animal cohorts) were observed for *A. rodriguezensis* and *R. kairei* at some sites (Beedessee et al., 2013). Furthermore, *A. rodriguezensis*, unlike other species such as the scaly-foot snail or *Alvinichoncha* sp., disperses preferentially in a southward direction and its source population seems to be in the Solitaire vent field rather than Edmond or Kairei (Beedessee et al., 2013). It is possible that the crab larvae are active swimmers and use currents in the upper water column to disperse further and across topological discontinuities. On the MAR, the population structure of the shrimp *Rimicaris exoculata* also suggests widespread connectivity (Teixeira et al., 2012). In contrast, the genetic structure of the scaly-foot snail populations indicates that this species can be widely discovered across the whole Indian Ocean Ridge, suggesting a stronger dispersal ability. However, its dispersal may be strongly affected by topographical barriers such as transform faults. This hypothesis is supported by the fact that the scaly-foot snail has negatively buoyant eggs (Beedessee et al., 2013; Sun et al., 2020). Moving forward, more information on the reproductive and larval biology and life history of vent specie coupled with better models of deep-sea flow dynamics (Giangrande et al., 2017) is crucial to assess the decadal-scale patterns of population connectivity of vent species in the Indian Ocean.

PERSPECTIVE: KNOWLEDGE GAPS TO PRIORITIZE FOR ASSESSING THE RESILIENCE OF INDIAN VENT COMMUNITIES

Since the first discovery of a biologically active HTV in the West Indian Ocean in 2000, 13 biologically active vent fields have been discovered and a few more have been inferred through the detection of hydrothermal plumes. Among the four active spreading ridges of the Indian Ocean, CR and the SEIR have just been explored recently (**Figure 3**). In the recent years, the ISA has granted exploration permits to governmental and semi-private entities for exploring HTV fields in the Indian Ocean. Contractors are requested to collect and submit environmental and biodiversity baseline information to the ISA (International Seabed Authority, 2021), which encourages more field surveys to be conducted in the Indian Ocean HTVs and will help fill the gaps in our understanding of connectivity and biodiversity of the areas of concerns. On the basis of all the publicly available information,

we identified several knowledge gaps critical for assessing the resilience of Indian HTV biological communities.

What Is the Vent Biodiversity at Meso- and Microscales?

Compared with macrofaunal communities, much less focus has been given to meiofauna and microbiotas even though they are recognized as key players for ecosystem function (Finlay et al., 1997; Schratzberger and Ingels, 2018). Only a handful of studies have examined the biodiversity of Indian HTV microorganisms in various microhabitats. These genetic surveys revealed that microbial vent communities are distinct from those of the Atlantic or Pacific vents (Ding et al., 2017; Li et al., 2020; Yang Z. et al., 2020), are highly specialized to their local environment, and may hold great biological novelty. In the SWIR, the microbial community structures on active chimneys (Ding et al., 2017) and vent sediments (Xu et al., 2018; Yang Z. et al., 2020) vary within a single vent field or a single chimney structure according to the temperature and chemical composition of the substrates. On the CIR, active and inactive vent chimneys at the Kairei and Pelagia HTV fields are home to distinct microbes, many of which are rare and expected to hold unique biological innovations (Han et al., 2018; Van Dover, 2019). Metagenome barcoding and eDNA appear to be useful proxies for further assessing biodiversity at the meio- and microscales. Meta-transcriptomic data at various size fractions would provide additional information about cross-scale biological interactions, which are key to assessing ecosystem function.

What Drives the Variance in Community Composition?

Vents on the Indian mid-ocean ridges are similar to other vent systems in that their communities are characterized by high endemicity and spatial variance of their composition. To date, only a small fraction of the variation in community composition can somewhat be explained by abiotic physio-chemical factors (Sarrazin et al., 1999, 2015), but the physical environment has not been well studied at small scales (e.g., within the range of the faunal succession). The influence of life history traits (reproduction, larval development, larval dispersal, settlement process, and so on) on species dispersal, gene flows, population genetics, and evolutionary process remains unknown for most taxa (see more discussion below). Furthermore, the impact of temporal and spatial population dynamics of individual vent species and the role of species interactions (competition, mutualism, etc.) in structuring vent macrofaunal community and biogeographical patterns have hardly been tested in the Indian Ocean. Biological adaptation to environmental variables and the resilience and constraints of vent communities in response to natural environmental disturbances are also fundamental information for a better understanding of what drives the variance in community structures of the vent ecosystems. With the rapid development of deep-sea capacity, time series assessment by autonomous underwater observatories will be able to collect biological and environmental data at fine scales in the near future.

How Diverse and Variable Are Community Functional Traits?

The biological characteristics of species such as size, mobility, trophic mode, and body structure robustness are more ecologically informative than taxonomic rank alone (Faith, 2015; Gross et al., 2017; Biggs et al., 2020; de Bello et al., 2021). Thus, functional traits approaches are valuable to assess the resilience and recoverability of vent communities to various natural or anthropogenic disturbances. For instance, Boschen-Rose et al. (2021) used trait-based analyses to estimate the sensitivity of macrofaunal assemblages from the Kermadec volcanic arc to different types of mining impacts (such as sediment plume and seafloor disturbance by mining equipment) and produced local maps of vulnerable communities. Dykman et al. (2021) highlighted the need for trait-based impact assessments by showing that communities' functional diversity (a proxy for ecosystem stability and resilience) recovered more slowly than species diversity following an eruption in the EPR.

Such a trait-based perspective should be applied in the Indian Ocean. In fact, the current global database for functional diversity at vents (Chapman et al., 2019) already includes a fair number of taxa from the Indian Ocean HTVs. Still, to gain important insights into the ecosystem functions and resilience of Indian vents, the functional trait repertoire needs to be substantially expanded to represent a comprehensive collection of Indian vent animals and include better estimates of the variability associated with each of their trait. Functional traits related to species morphologic or behavioral phenotypes are context dependent and their variation can affect our predictions of ecosystem function (Cassidy et al., 2020). Hence, more research needs to be conducted to gather baseline information on the biology of Indian vent macrofauna, and communities need to be surveyed further to provide reliable estimates for the spatial and temporal variance of their traits.

How Do the Life History Traits of Foundation Species Affect Connectivity and Community Structure?

Vent connectivity has so far mostly been inferred from genetic data, which gives a rough picture of the general trend in gene flow over thousands of years (Lowe and Allendorf, 2010). This resolution may not be relevant for conservation purposes as impact assessments aim to determine the ability of an ecosystem to recover perturbation on much shorter time scales (i.e., years or decades). Hence, we need to know more about larval biology and colonization process especially for foundation species such as *B. marisindicus*. To assess demographic connectivity, we need more information of larval dispersal, colonization processes, and deep oceanic current patterns and variability. Better models of deep-sea currents would also allow us to make predictions as to the consequences of climate change. Dominant macrofaunal species of the Indian ridge HTVs rely on chemoautotrophic symbionts for their survival, and in many instances, these symbionts have a strong degree of specificity to their host and are acquired from the environment. Thus, these microbial species are keystone to the whole community. More focus should

be placed on better understanding their biology, distribution, and connectivity.

How Many HTV Fields Are in the Indian Mid-Ocean Ridges?

Last but not least, one obvious gap to our understanding of vent population connectivity in the Indian Ocean spans from the fact that we do not know how many HTV fields are present, and for the vent fields that we do know (including both active and inactive fields), we have yet to acquire fine-resolution topographic and bathymetric maps. Given this sporadic sampling and the lack of sufficient information on near-bottom current, near-field, and far-field flow dynamic, estimating regional connectivity between vents is highly challenging. The seemingly high gene flow observed for vent species across long distances and topographic discontinuities remains highly intriguing. One likely explanation is the presence of smaller and more diffuse HTV in between the known vent fields, which are predicted by geological modeling (Hashimoto et al., 2001; Beaulieu et al., 2015; Baker et al., 2016) but have yet to be discovered. Large-scale surveys of the seafloor enabled through additional ISA mineral exploration contracts could help fill these gaps if the mapping data were made publicly available.

AUTHOR CONTRIBUTIONS

P-YQ conceptualized the project. MP prepared the initial draft and figures. JS and QX provided inputs to the initial manuscript. All the authors revised the manuscript.

FUNDING

This study was supported by the China Ocean Mineral Resource Research and Development Association (DY135-E2-1-03), the Guangdong Major Project of Basic and Applied Basic Research (2019B030302004-04), the Southern Marine Science and Engineering Guangdong Laboratory (Guangzhou) (GML2019ZD0409), and the Hong Kong Branch of South Marine Science and Engineering Guangdong Laboratory (SMSEGL20Sc01). Additional support was provided to MP by the Quebec Centre for Biodiversity Science (QCBS) and the "Fonds Québécois de la Recherche sur la Nature et les Technologies" (FRQNT) international internship grant.

ACKNOWLEDGMENTS

In preparation for this review, the authors used relevant information from the "Data Report: compilation of scientific information on the HTV fields along the mid-ocean ridge in the west Indian Ocean," which was prepared by a group of Chinese marine scientists supported by China Ocean Mineral Resource Research and Development Association and distributed to all the participants of the "ISA workshop on marine science research in the Area: establishing collaborative platform to enhance biodiversity knowledge for environmental management in mid-ocean ridge ecosystem focusing on the Indian Ocean," which was held online from December 15–17, 2020. In particular, the authors would like to thank Chengjun Sun, Li Li, and Lingyun Qu from the First Institute of Oceanography, Ministry of Natural Resource, and Yadong Zhou and Xiqiu Han from the Second Institute of Oceanography, Ministry of Natural Resource. who contributed to the preparation of that data report.

SUPPLEMENTARY MATERIAL

The Supplementary Material for this article can be found online at: https://www.frontiersin.org/articles/10.3389/fmars.2021.744874/full#supplementary-material

REFERENCES

Adams, D., Arellano, S., and Govenar, B. (2012). Larval dispersal: vent life in the water column. *oceanog* 25, 256–268. doi: 10.5670/oceanog.2012.24

Bachraty, C., Legendre, P., and Desbruyères, D. (2009). Biogeographic relationships among deep-sea hydrothermal vent faunas at global scale. *Deep Sea Res. Part I Oceanogr. Res. Papers* 56, 1371–1378. doi: 10.1016/j.dsr.2009.01.009

Baker, E. T., Chen, Y. J., and Phipps Morgan, J. (1996). The relationship between near-axis hydrothermal cooling and the spreading rate of mid-ocean ridges. *Earth Planet. Sci. Lett.* 142, 137–145. doi: 10.1016/0012-821X(96)00097-0

Baker, E. T., Edmonds, H. N., Michael, P. J., Bach, W., Dick, H. J. B., Snow, J. E., et al. (2004). Hydrothermal venting in magma deserts: The ultraslow-spreading Gakkel and Southwest Indian Ridges. *Geochem. Geophys. Geosyst.* 5:2004GC000712. doi: 10.1029/2004GC000712

Baker, E. T., Resing, J. A., Haymon, R. M., Tunnicliffe, V., Lavelle, J. W., Martinez, F., et al. (2016). How many vent fields? New estimates of vent field populations on ocean ridges from precise mapping of hydrothermal discharge locations. *Earth Planet. Sci. Lett.* 449, 186–196. doi: 10.1016/j.epsl.2016.05.031

Beaulieu, S. E. (2015). *InterRidge global database of active submarine hydrothermal vent fields: prepared for InterRidge, Version 3.4*. Available online at: http://vents-data.interridge.org (accessed March 6, 2018)

Beaulieu, S. E., Baker, E. T., and German, C. R. (2015). Where are the undiscovered hydrothermal vents on oceanic spreading ridges? *Deep Sea Res. Part II Top. Stud. Oceanogr.* 121, 202–212. doi: 10.1016/j.dsr2.2015.05.001

Beedessee, G., Watanabe, H., Ogura, T., Nemoto, S., Yahagi, T., Nakagawa, S., et al. (2013). High connectivity of animal populations in deep-sea hydrothermal vent fields in the Central Indian Ridge relevant to its geological setting. *PLoS One* 8:e81570. doi: 10.1371/journal.pone.0081570

Belkin, S., Nelson, D. C., and Jannasch, H. W. (1986). Symbiotic assimilation of CO_2 in two hydrothermal vent animals, the mussel *Bathymodiolus thermophilus* and the tube worm *Riftia pachyptila*. *Biol. Bull.* 170, 110–121. doi: 10.2307/1541384

Bell, J. B., Woulds, C., Oevelen, D., and van. (2017). Hydrothermal activity, functional diversity and chemoautotrophy are major drivers of seafloor carbon cycling. *Sci. Rep.* 7:12025. doi: 10.1038/s41598-017-12291-w

Bergquist, D., Eckner, J., Urcuyo, I., Cordes, E., Hourdez, S., Macko, S., et al. (2007). Using stable isotopes and quantitative community characteristics to determine a local hydrothermal vent food web. *Mar. Ecol. Prog. Ser.* 330, 49–65. doi: 10.3354/meps330049

Biggs, C. R., Yeager, L. A., Bolser, D. G., Bonsell, C., Dichiera, A. M., Hou, Z., et al. (2020). Does functional redundancy affect ecological stability and resilience? A review and meta-analysis. *Ecosphere* 11:e03184. doi: 10.1002/ecs2.3184

Borda, E., Kudenov, J. D., Chevaldonné, P., Blake, J. A., Desbruyères, D., Fabri, M.-C., et al. (2013). Cryptic species of *Archinome* (Annelida: Amphinomida) from vents and seeps. *Proce. R. Soc. B Biol. Sci.* 280:20131876. doi: 10.1098/rspb.2013.1876

Boschen, R. E., Rowden, A. A., Clark, M. R., Barton, S. J., Pallentin, A., and Gardner, J. P. A. (2015). Megabenthic assemblage structure on three New Zealand seamounts: implications for seafloor massive sulfide mining. *Mar. Ecol. Prog. Ser.* 523, 1–14. doi: 10.3354/meps11239

Boschen-Rose, R. E., Clark, M. R., Rowden, A. A., and Gardner, J. P. A. (2021). Assessing the ecological risk to deep-sea megafaunal assemblages from seafloor massive sulfide mining using a functional traits sensitivity approach. *Ocean Coastal Manage.* 210:105656. doi: 10.1016/j.ocecoaman.2021.105656

Breusing, C., Johnson, S. B., Tunnicliffe, V., and Vrijenhoek, R. C. (2015). Population structure and connectivity in Indo-Pacific deep-sea mussels of the *Bathymodiolus septemdierum* complex. *Conserv. Genet.* 16, 1415–1430. doi: 10.1007/s10592-015-0750-0

Breusing, C., Johnson, S. B., Tunnicliffe, V., Clague, D. A., Vrijenhoek, R. C., and Beinart, R. A. (2020). Allopatric and sympatric drivers of speciation in Alviniconcha hydrothermal vent snails. *Mol. Biol. Evolut.* 37, 3469–3484. doi: 10.1093/molbev/msaa177

Cassidy, C., Grange, L. J., Garcia, C., Bolam, S. G., and Godbold, J. A. (2020). Species interactions and environmental context affect intraspecific behavioural trait variation and ecosystem function. *Proc. R. Soc. B Biol. Sci.* 287:20192143. doi: 10.1098/rspb.2019.2143

Chapman, A. S. A., Beaulieu, S. E., Colaço, A., Gebruk, A. V., Hilario, A., Kihara, T. C., et al. (2019). sFDvent: A global trait database for deep-sea hydrothermal-vent fauna. *Glob. Ecol. Biogeogr.* 28, 1538–1551. doi: 10.1111/geb.12975

Chen, C., Linse, K., Roterman, C. N., Copley, J. T., and Rogers, A. D. (2015b). A new genus of large hydrothermal vent-endemic gastropod (Neomphalina: Peltospiridae). *Zool. J. Linnean Soc.* 175, 319–335. doi: 10.1111/zoj.12279

Chen, C., Copley, J. T., Linse, K., and Rogers, A. D. (2015a). Low connectivity between 'scaly-foot gastropod' (Mollusca: Peltospiridae) populations at hydrothermal vents on the Southwest Indian Ridge and the Central Indian Ridge. *Org. Divers. Evol.* 15, 663–670. doi: 10.1007/s13127-015-0224-8

Connelly, D. P., German, C. R., Asada, M., Okino, K., Egorov, A., Naganuma, T., et al. (2007). Hydrothermal activity on the ultra-slow spreading southern Knipovich Ridge. *Geochem. Geophys. Geosyst.* 8:2007GC001652. doi: 10.1029/2007GC001652

Copley, J. T., Marsh, L., Glover, A. G., Hühnerbach, V., Nye, V. E., Reid, W. D. K., et al. (2016). Ecology and biogeography of megafauna and macrofauna at the first known deep-sea hydrothermal vents on the ultraslow-spreading Southwest Indian Ridge. *Sci. Rep.* 6:39158. doi: 10.1038/srep39158

de Bello, F., Lavorel, S., Hallett, L. M., Valencia, E., Garnier, E., Roscher, C., et al. (2021). Functional trait effects on ecosystem stability: assembling the jigsaw puzzle. *Trends Ecol. Evolut.* 2021:001. doi: 10.1016/j.tree.2021.05.001

Dick, H. J. B., Lin, J., and Schouten, H. (2003). An ultraslow-spreading class of ocean ridge. *Nature* 426, 405–412. doi: 10.1038/nature02128

Ding, J., Zhang, Y., Wang, H., Jian, H., Leng, H., and Xiao, X. (2017). Microbial community structure of deep-sea hydrothermal vents on the ultraslow spreading Southwest Indian Ridge. *Front. Microbiol.* 8:01012. doi: 10.3389/fmicb.2017.01012

Dover, C. L. V., and Doerries, M. B. (2005). Community structure in mussel beds at Logatchev hydrothermal vents and a comparison of macrofaunal species richness on slow- and fast-spreading mid-ocean ridges. *Mar. Ecol.* 26, 110–120. doi: 10.1111/j.1439-0485.2005.00047.x

Du Preez, C., and Fisher, C. R. (2018). Long-term stability of back-arc basin hydrothermal vents. *Front. Mar. Sci.* 5:00054. doi: 10.3389/fmars.2018.00054

Dykman, L. N., Beaulieu, S. E., Mills, S. W., Solow, A. R., and Mullineaux, L. S. (2021). Functional traits provide new insight into recovery and succession at deep-sea hydrothermal vents. *Ecology* 2021:e03418. doi: 10.1002/ecy.3418

Edmonds, H. N., Michael, P. J., Baker, E. T., Connelly, D. P., Snow, J. E., Langmuir, C. H., et al. (2003). Discovery of abundant hydrothermal venting on the ultraslow-spreading Gakkel ridge in the Arctic Ocean. *Nature* 421, 252–256. doi: 10.1038/nature01351

Ellis, J. I., Clark, M. R., Rouse, H. L., and Lamarche, G. (2017). Environmental management frameworks for offshore mining: the New Zealand approach. *Mar. Policy* 84, 178–192. doi: 10.1016/j.marpol.2017.07.004

Endow, K., and Ohta, S. (1989). The symbiotic relationship between bacteria and a mesogastropod snail, *Alviniconcha hessleri*, collected from hydrothermal vents of the Mariana Back-Arc Basin. *Bull. Jap. Soc. Microb. Ecol.* 3, 73–82. doi: 10.1264/microbes1986.3.73

Faith, D. P. (2015). The unimodal relationship between species' functional traits and habitat gradients provides a family of indices supporting the conservation of functional trait diversity. *Plant Ecol.* 216, 725–740. doi: 10.1007/s11258-015-0454-z

Finlay, B. J., Maberly, S. C., and Cooper, J. I. (1997). Microbial diversity and ecosystem function. *Oikos* 80, 209–213. doi: 10.2307/3546587

Fjeldsaå, J., and Lovett, J. C. (1997). Biodiversity and environmental stability. *Biodivers. Conservat.* 6, 315–323. doi: 10.1023/A:1018304522320

Gaudron, S. M., Lefebvre, S., Nunes Jorge, A., Gaill, F., and Pradillon, F. (2012). Spatial and temporal variations in food web structure from newly-opened habitat at hydrothermal vents. *Mar. Environ. Res.* 77, 129–140. doi: 10.1016/j.marenvres.2012.03.005

Gerdes, K. H., Martínez Arbizu, P., Schwentner, M., Freitag, R., Schwarz-Schampera, U., Brandt, A., et al. (2019). Megabenthic assemblages at the southern Central Indian Ridge – Spatial segregation of inactive hydrothermal vents from active-, periphery- and non-vent sites. *Mar. Environ. Res.* 151:104776. doi: 10.1016/j.marenvres.2019.104776

German, C. R., and Parson, L. M. (1998). Distributions of hydrothermal activity along the Mid-Atlantic Ridge: interplay of magmatic and tectonic controls. *Earth Planet. Sci. Lett.* 160, 327–341. doi: 10.1016/S0012-821X(98)00093-4

German, C. R., Baker, E. T., Mevel, C., Tamaki, K., and the Fuji Science Team. (1998). Hydrothermal activity along the southwest Indian ridge. *Nature* 395, 490–493. doi: 10.1038/26730

German, C. R., Petersen, S., and Hannington, M. D. (2016). Hydrothermal exploration of mid-ocean ridges: Where might the largest sulfide deposits be forming? *Chem. Geol.* 420, 114–126. doi: 10.1016/j.chemgeo.2015.11.006

Giangrande, A., Gambi, M. C., and Gravina, M. F. (2017). Paradigm shifts in community ecology: Open versus closed units, challenges and limits of connectivity studies. *Mar. Ecol.* 38:e12480. doi: 10.1111/maec.12480

Goffredi, S. K., Warén, A., Orphan, V. J., Dover, C. L. V., and Vrijenhoek, R. C. (2004). Novel forms of structural integration between microbes and a hydrothermal vent gastropod from the Indian Ocean. *Appl. Environ. Microbiol.* 70, 3082–3090. doi: 10.1128/AEM.70.5.3082-3090.2004

Gollner, S., Colaço, A., Gebruk, A., Halpin, P. N., Higgs, N., Menini, E., et al. (2021). Application of scientific criteria for identifying hydrothermal ecosystems in need of protection. *Mar. Policy* 132:104641. doi: 10.1016/j.marpol.2021.104641

Gollner, S., Kaiser, S., Menzel, L., Jones, D. O. B., Brown, A., Mestre, N. C., et al. (2017). Resilience of benthic deep-sea fauna to mining activities. *Mar. Environ. Res.* 129, 76–101. doi: 10.1016/j.marenvres.2017.04.010

Govenar, B. (2010). "Shaping vent and seep communities: Habitat provision and modification by foundation species," in *The Vent and Seep Biota: Aspects from Microbes to Ecosystems* Topics in Geobiology, ed. S. Kiel (Dordrecht: Springer Netherlands), 403–432. doi: 10.1007/978-90-481-9572-5_13

Gross, N., Bagousse-Pinguet, Y. L., Liancourt, P., Berdugo, M., Gotelli, N. J., and Maestre, F. T. (2017). Functional trait diversity maximizes ecosystem multifunctionality. *Nat. Ecol. Evol.* 1, 1–9. doi: 10.1038/s41559-017-0132

Guri, M., Durand, L., Cueff-Gauchard, V., Zbinden, M., Crassous, P., Shillito, B., et al. (2012). Acquisition of epibiotic bacteria along the life cycle of the hydrothermal shrimp *Rimicaris exoculata*. *ISME J.* 6, 597–609. doi: 10.1038/ismej.2011.133

Han, Y., Gonnella, G., Adam, N., Schippers, A., Burkhardt, L., Kurtz, S., et al. (2018). Hydrothermal chimneys host habitat-specific microbial communities: analogues for studying the possible impact of mining seafloor massive sulfide deposits. *Sci. Rep.* 8:10386. doi: 10.1038/s41598-018-28613-5

Han, Y., Zhang, D., Wang, C., and Zhou, Y. (2021). Out of the Pacific: a new alvinellid worm (Annelida: Terebellida) from the northern Indian Ocean hydrothermal vents. *Front. Mar. Sci.* 8:669918. doi: 10.3389/fmars.2021.669918

Harms, N. C., Lahajnar, N., Gaye, B., Rixen, T., Schwarz-Schampera, U., and Emeis, K.-C. (2021). Sediment trap-derived particulate matter fluxes in the oligotrophic subtropical gyre of the South Indian Ocean. *Deep Sea Res. Part II Top. Stud. Oceanogr.* 2021:104924. doi: 10.1016/j.dsr2.2020.104924

Hashimoto, J., Ohta, S., Gamo, T., Chiba, H., Yamaguchi, T., Tsuchida, S., et al. (2001). First hydrothermal vent communities from the Indian Ocean discovered. *Jzoo* 18, 717–721. doi: 10.2108/zsj.18.717

Hessler, R. R., Smithey, W. M., Boudrias, M. A., Keller, C. H., Lutz, R. A., and Childress, J. J. (1988). Temporal change in megafauna at the Rose Garden hydrothermal vent (Galapagos Rift; eastern tropical Pacific). *Deep Sea Res. Part A Oceanogr. Res. Papers* 35, 1681–1709. doi: 10.1016/0198-0149(88)90044-1

International Seabed Authority (2018). *ISBA/24/A/4: Consideration, with a view to adoption, of the draft strategic plan of the International Seabed Authority for the period 2019–2023*. Kingston: International Seabed Authority.

International Seabed Authority (2021). *Minerals: Polymetallic Sulphides*. Available online at: https://www.isa.org.jm/exploration-contracts/polymetallic-sulphides (accessed March 25, 2021)

Jang, S.-J., Ho, P.-T., Jun, S.-Y., Kim, D., and Won, Y.-J. (2020). A newly discovered *Gigantidas* bivalve mussel from the Onnuri Vent Field in the northern Central Indian Ridge. *Deep Sea Res. Part I Oceanogr. Res. Papers* 161:103299. doi: 10.1016/j.dsr.2020.103299

Jiang, L., Liu, X., Dong, C., Huang, Z., Cambon-Bonavita, M.-A., Alain, K., et al. (2020). "*Candidatus* Desulfobulbus rimicarensis," an uncultivated deltaproteobacterial epibiont from the deep-sea hydrothermal vent shrimp *Rimicaris exoculata*. *Appl. Environ. Microbiol.* 86, 2549–2519. doi: 10.1128/AEM.02549-19

Johnson, S. B., Warén, A., Tunnicliffe, V., Dover, C. V., Wheat, C. G., Schultz, T. F., et al. (2015). Molecular taxonomy and naming of five cryptic species of *Alviniconcha* snails (Gastropoda: Abyssochrysoidea) from hydrothermal vents. *Systemat. Biodivers.* 13, 278–295. doi: 10.1080/14772000.2014.970673

Juniper, S. K., and Tunnicliffe, V. (1997). Crustal accretion and the hot vent ecosystem. *Philosop. Transact. R. Soc. London A Mathemat. Phys. Engine. Sci.* 355, 459–474. doi: 10.1098/rsta.1997.0017

Kang, T., and Kim, D. (2021). Meiofauna and nematode community composition in a hydrothermal vent and deep-sea sediments in the Central Indian Ridge. *Mar. Pollut. Bull.* 170:112616. doi: 10.1016/j.marpolbul.2021.112616

Kim, J., Son, S.-K., Kim, D., Pak, S.-J., Yu, O. H., Walker, S. L., et al. (2020). Discovery of active hydrothermal vent fields along the central Indian Ridge, 8–12°S. *Geochem. Geophys. Geosyst.* 21:e2020GC009058. doi: 10.1029/2020GC009058

Kimura, M., and Weiss, G. H. (1964). The stepping stone model of population structure and the decrease of genetic correlation with distance. *Genetics* 49, 561–576.

Kinsey, J. C., and German, C. R. (2013). Sustained volcanically-hosted venting at ultraslow ridges: Piccard Hydrothermal Field, Mid-Cayman Rise. *Earth Planet. Sci. Lett.* 380, 162–168. doi: 10.1016/j.epsl.2013.08.001

Kumagai, H., Nakamura, K., Toki, T., Morishita, T., Okino, K., Ishibashi, J.-I., et al. (2008). Geological background of the Kairei and Edmond hydrothermal fields along the Central Indian Ridge: Implications of their vent fluids' distinct chemistry. *Geofluids* 8, 239–251. doi: 10.1111/j.1468-8123.2008.00223.x

Lan, Y., Sun, J., Chen, C., Sun, Y., Zhou, Y., Yang, Y., et al. (2021). Hologenome analysis reveals dual symbiosis in the deep-sea hydrothermal vent snail *Gigantopelta aegis*. *Nat. Commun.* 12:1165. doi: 10.1038/s41467-021-21450-7

Le Bris, N., Govenar, B., Le Gall, C., and Fisher, C. R. (2006). Variability of physico-chemical conditions in 9°50'N EPR diffuse flow vent habitats. *Mar. Chem.* 98, 167–182. doi: 10.1016/j.marchem.2005.08.008

Le Bris, N., Zbinden, M., and Gaill, F. (2005). Processes controlling the physico-chemical micro-environments associated with Pompeii worms. *Deep Sea Res. Part I Oceanogr. Res. Pap.* 52, 1071–1083. doi: 10.1016/j.dsr.2005.01.003

Lee, W.-K., Ju, S.-J., Hou, B. K., and Kim, S.-J. (2019). DNA barcoding for the hydrothermal vent crab *Austinograea* species (Crustacea: Bythograeidae) from the North Fiji Basin, Southwestern Pacific Ocean. *Anim. Systemat. Evolut. Divers.* 35, 30–32. doi: 10.5635/ASED.2019.35.1.004

Lelièvre, Y., Sarrazin, J., Marticorena, J., Schaal, G., Day, T., Legendre, P., et al. (2017). Biodiversity and trophic ecology of hydrothermal vent fauna associated with tubeworm assemblages on the Juan de Fuca Ridge. *Biogeosci. Discuss* 2017, 1–34. doi: 10.5194/bg-2017-411

Li, J., Yang, J., Sun, M., Su, L., Wang, H., Gao, J., et al. (2020). Distribution and succession of microbial communities along the dispersal pathway of hydrothermal plumes on the Southwest Indian Ridge. *Front. Mar. Sci.* 7:581381. doi: 10.3389/fmars.2020.581381

Lowe, W. H., and Allendorf, F. W. (2010). What can genetics tell us about population connectivity? *Mol. Ecol.* 19, 3038–3051. doi: 10.1111/j.1365-294X.2010.04688.x

Ma, L., and Wang, W.-X. (2021). Zinc source differentiation in hydrothermal vent mollusks: Insight from Zn isotope ratios. *Sci. Total Environ.* 773:145653. doi: 10.1016/j.scitotenv.2021.145653

McKiness, Z. P., and Cavanaugh, C. M. (2005). The ubiquitous mussel: *Bathymodiolus* aff. *brevior* symbiosis at the Central Indian Ridge hydrothermal vents. *Mar. Ecol. Prog. Ser.* 295, 183–190. doi: 10.3354/meps295183

Methou, P., Michel, L. N., Segonzac, M., Cambon-Bonavita, M.-A., and Pradillon, F. (2020). Integrative taxonomy revisits the ontogeny and trophic niches of *Rimicaris* vent shrimps. *R. Soc. Open Sci.* 7:200837. doi: 10.1098/rsos.200837

Micheli, F., Peterson, C. H., Mullineaux, L. S., Fisher, C. R., Mills, S. W., Sancho, G., et al. (2002). Predation structures communities at deep-sea hydrothermal vents. *Ecol. Monogr.* 72, 365–382.

Miyazaki, J., Ikuta, T., Watsuji, T., Abe, M., Yamamoto, M., Nakagawa, S., et al. (2020). Dual energy metabolism of the *Campylobacterota* endosymbiont in the chemosynthetic snail *Alviniconcha marisindica*. *ISME J.* 14, 1273–1289. doi: 10.1038/s41396-020-0605-7

Miyazaki, J.-I., Martins, L., de, O., Fujita, Y., Matsumoto, H., and Fujiwara, Y. (2010). Evolutionary process of deep-sea Bathymodiolus mussels. *PLoS One* 5:e10363. doi: 10.1371/journal.pone.0010363

Moalic, Y., Desbruyères, D., Duarte, C. M., Rozenfeld, A. F., Bachraty, C., and Arnaud-Haond, S. (2012). Biogeography revisited with network theory: retracing the history of hydrothermal vent communities. *Systemat. Biol.* 61, 127–127. doi: 10.1093/sysbio/syr088

Müller, R. D., Sdrolias, M., Gaina, C., and Roest, W. R. (2008). Age, spreading rates, and spreading asymmetry of the world's ocean crust. *Geochem. Geophys. Geosyst.* 9:2007GC001743. doi: 10.1029/2007GC001743

Mullineaux, L. S., Peterson, C. H., Micheli, F., and Mills, S. W. (2003). Successional mechanism varies along a gradient in hydrothermal fluid flux at deep-sea vents. *Ecol. Monogr.* 73, 523–542. doi: 10.1890/02-0674

Nakagawa, S., Shimamura, S., Takaki, Y., Suzuki, Y., Murakami, S., Watanabe, T., et al. (2014). Allying with armored snails: the complete genome of gammaproteobacterial endosymbiont. *ISME J.* 8, 40–51. doi: 10.1038/ismej.2013.131

Nakajima, R., Yamakita, T., Watanabe, H., Fujikura, K., Tanaka, K., Yamamoto, H., et al. (2014). Species richness and community structure of benthic macrofauna and megafauna in the deep-sea chemosynthetic ecosystems around the Japanese archipelago: an attempt to identify priority areas for conservation. *Divers. Distribut.* 20, 1160–1172. doi: 10.1111/ddi.12204

Nakamura, K., Watanabe, H., Miyazaki, J., Takai, K., Kawagucci, S., Noguchi, T., et al. (2012). Discovery of new hydrothermal activity and chemosynthetic fauna on the Central Indian Ridge at 18°–20°S. *PLoS One* 7:e32965. doi: 10.1371/journal.pone.0032965

Nelson, D. C., Hagen, K. D., and Edwards, D. B. (1995). The gill symbiont of the hydrothermal vent mussel *Bathymodiolus thermophilus* is a psychrophilic, chemoautotrophic, sulfur bacterium. *Mar. Biol.* 121, 487–495. doi: 10.1007/BF00349457

Nomaki, H., Ogawa, N. O., Ohkouchi, N., Suga, H., Toyofuku, T., Shimanaga, M., et al. (2008). Benthic foraminifera as trophic links between phytodetritus and benthic metazoans: carbon and nitrogen isotopic evidence. *Mar. Ecol. Prog. Ser.* 357, 153–164. doi: 10.3354/meps07309

Nomaki, H., Uejima, Y., Ogawa, N., Yamane, M., Watanabe, H., Senokuchi, R., et al. (2019). Nutritional sources of meio- and macrofauna at hydrothermal vents and adjacent areas: natural-abundance radiocarbon and stable isotope analyses. *Mar. Ecol. Prog. Ser.* 622, 49–65. doi: 10.3354/meps13053

Paz-Vinas, I., Jensen, E. L., Bertola, L. D., Breed, M. F., Hand, B. K., Hunter, M. E., et al. (2021). Macrogenetic studies must not ignore limitations of genetic markers and scale. *Ecol. Lett.* 2021:13732. doi: 10.1111/ele.13732

Petersen, J. M., Ramette, A., Lott, C., Cambon-Bonavita, M., Zbinden, M., and Dubilier, N. (2010). Dual symbiosis of the vent shrimp *Rimicaris exoculata* with filamentous gamma-and epsilonproteobacteria at four Mid-Atlantic Ridge hydrothermal vent fields. *Environment. Microbiol.* 12, 2204–2218. doi: 10.1111/j.1462-2920.2009.02129.x

Podowski, E., Ma, S., Luther, G., Wardrop, D., and Fisher, C. (2010). Biotic and abiotic factors affecting distributions of megafauna in diffuse flow on andesite and basalt along the Eastern Lau Spreading Center, Tonga. *Mar. Ecol. Prog. Ser.* 418, 25–45. doi: 10.3354/meps08797

Pradillon, F., Zbinden, M., Le Bris, N., Hourdez, S., Barnay, A.-S., and Gaill, F. (2009). Development of assemblages associated with alvinellid colonies on the

walls of high-temperature vents at the East Pacific Rise. *Deep Sea Res. Part II Top. Stud. Oceanogr.* 56, 1622–1631. doi: 10.1016/j.dsr2.2009.05.009

Ptatscheck, C., Brüchner-Hüttemann, H., Kreuzinger-Janik, B., Weber, S., and Traunspurger, W. (2020). Are meiofauna a standard meal for macroinvertebrates and juvenile fish? *Hydrobiologia* 847, 2755–2778. doi: 10.1007/s10750-020-04189-y

Ramirez-Llodra, E., Shank, T. M., and German, C. M. (2007). Biodiversity and biogeography of hydrothermal vent species: thirty years of discovery and investigations. *Oceanography* 20, 30–41. doi: 10.5670/oceanog.2007.78

Reed, D. C., Breier, J. A., Jiang, H., Anantharaman, K., Klausmeier, C. A., Toner, B. M., et al. (2015). Predicting the response of the deep-ocean microbiome to geochemical perturbations by hydrothermal vents. *ISME J.* 9, 1857–1869. doi: 10.1038/ismej.2015.4

Reid, W. D. K., Sweeting, C. J., Wigham, B. D., Zwirglmaier, K., Hawkes, J. A., McGill, R. A. R., et al. (2013). Spatial differences in East Scotia Ridge hydrothermal vent food webs: Influences of chemistry, microbiology and predation on trophodynamics. *PLoS One* 8:e65553. doi: 10.1371/journal.pone.0065553

Reid, W. D. K., Wigham, B. D., Marsh, L., Weston, J. N. J., Zhu, Y., and Copley, J. T. (2020). Trophodynamics at the Longqi hydrothermal vent field and comparison with the East Scotia and Central Indian Ridges. *Mar. Biol.* 167:141. doi: 10.1007/s00227-020-03755-1

Rieley, G., Dover, C. L. V., Hedrick, D. B., and Eglinton, G. (1999). Trophic ecology of *Rimicaris exoculata*?: a combined lipid abundance/stable isotope approach. *Mar. Biol.* 133, 495–499. doi: 10.1007/s002270050489

Rogers, A. D., Tyler, P. A., Connelly, D. P., Copley, J. T., James, R., Larter, R. D., et al. (2012). The Discovery of new deep-sea hydrothermal vent communities in the Southern Ocean and implications for biogeography. *PLoS Biol.* 10:e1001234. doi: 10.1371/journal.pbio.1001234

Roterman, C. N., Copley, J. T., Linse, K. T., Tyler, P. A., and Rogers, A. D. (2013). The biogeography of the yeti crabs (Kiwaidae) with notes on the phylogeny of the Chirostyloidea (Decapoda: Anomura). *Proc. R. Soc. B Biol. Sci.* 280:20130718. doi: 10.1098/rspb.2013.0718

Sarrazin, J., Juniper, S. K., Massoth, G., and Legendre, P. (1999). Physical and chemical factors influencing species distributions on hydrothermal sulfide edifices of the Juan de Fuca Ridge, northeast Pacific. *Mar. Ecol. Prog. Ser.* 190, 89–112.

Sarrazin, J., Legendre, P., de Busserolles, F., Fabri, M.-C., Guilini, K., Ivanenko, V. N., et al. (2015). Biodiversity patterns, environmental drivers and indicator species on a high-temperature hydrothermal edifice, Mid-Atlantic Ridge. *Deep Sea Res. Part II Top. Stud. Oceanogr.* 121, 177–192. doi: 10.1016/j.dsr2.2015.04.013

Sarrazin, J., Robigou, V., Juniper, S., and Delaney, J. (1997). Biological and geological dynamics over four years on a high-temperature sulfide structure at the Juan de Fuca Ridge hydrothermal observatory. *Mar. Ecol. Prog. Ser.* 153, 5–24.

Schmid-Araya, J. M., and Schmid, P. E. (2000). Trophic relationships: integrating meiofauna into a realistic benthic food web. *Freshw. Biol.* 44, 149–163. doi: 10.1046/j.1365-2427.2000.00594.x

Schratzberger, M., and Ingels, J. (2018). Meiofauna matters: The roles of meiofauna in benthic ecosystems. *J. Exp. Mar. Biol. Ecol.* 502, 12–25. doi: 10.1016/j.jembe.2017.01.007

Scotese, C. R., and Wright, N. (2018). *PALEOMAP paleodigital elevation models (PaleoDEMS) for the Phanerozoic*. Available online at: *https://www.earthbyte.org/paleodem-resource-scotese-and-wright-2018* (accessed August 19, 2018)

Shank, T. M., Fornari, D. J., Von Damm, K. L., Lilley, M. D., Haymon, R. M., and Lutz, R. A. (1998). Temporal and spatial patterns of biological community development at nascent deep-sea hydrothermal vents (9°50'N, East Pacific Rise). *Deep Sea Res. Part II Top. Stud. Oceanogr.* 45, 465–515. doi: 10.1016/S0967-0645(97)00089-1

Sigwart, J. D., Chen, C., Thomas, E. A., Allcock, A. L., Böhm, M., and Seddon, M. (2019). Red Listing can protect deep-sea biodiversity. *Nat. Ecol. Evolut.* 3, 1134–1134. doi: 10.1038/s41559-019-0930-2

Sigwart, J., Chen, C., and Elin, T. (2019). *IUCN Red List of Threatened Species: Chrysomallon squamiferum. IUCN Red List of Threatened Species*. Gland: IUCN.

Snow, J. E., and Edmonds, H. N. (2007). Ultraslow-spreading ridges rapid paradigm changes. *Oceanography* 20, 90–101. doi: 10.5670/oceanog.2007.83

Stein, J. L., Cary, S. C., Hessler, R. R., Vetter, R. D., Felbeck, H., Ohta, S., et al. (1988). Chemoautotrophic symbiosis in a hydrothermal vent gastropod. *Biol. Bull.* 174, 373–378. doi: 10.2307/1541963

Sun, J., Zhou, Y., Chen, C., Kwan, Y. H., Sun, Y., Wang, X., et al. (2020). Nearest vent, dearest friend: biodiversity of Tiancheng vent field reveals cross-ridge similarities in the Indian Ocean. *R. Soc. Open Sci.* 7:200110. doi: 10.1098/rsos.200110

Sweetman, A., Levin, L., Rapp, H., and Schander, C. (2013). Faunal trophic structure at hydrothermal vents on the southern Mohn's Ridge, Arctic Ocean. *Mar. Ecol. Prog. Ser.* 473, 115–131. doi: 10.3354/meps10050

Tao, C., Seyfried, W. E., Lowell, R. P., Liu, Y., Liang, J., Guo, Z., et al. (2020). Deep high-temperature hydrothermal circulation in a detachment faulting system on the ultra-slow spreading ridge. *Nat. Commun.* 11:1300. doi: 10.1038/s41467-020-15062-w

Tao, C., Wu, G., Ni, J., Zhao, H., Su, X., Zhou, N., et al. (2009). New hydrothermal fields found along the SWIR during the Legs 5-7 of the Chinese DY115-20 Expedition. *AGU Fall Meeting Abstracts* 21, 21A–1150A.

Teixeira, S., Serrão, E. A., and Arnaud-Haond, S. (2012). Panmixia in a fragmented and unstable environment: The hydrothermal shrimp *Rimicaris exoculata* disperses extensively along the Mid-Atlantic Ridge. *PLoS One* 7:e38521. doi: 10.1371/journal.pone.0038521

Thomson, R. E., Mihály, S. F., Rabinovich, A. B., McDuff, R. E., Veirs, S. R., and Stahr, F. R. (2003). Constrained circulation at Endeavour ridge facilitates colonization by vent larvae. *Nature* 424, 545–549. doi: 10.1038/nature01824

Thornburg, C. C., Zabriskie, T. M., and McPhail, K. L. (2010). Deep-sea hydrothermal vents: Potential hot spots for natural products discovery? *J. Nat. Prod.* 73, 489–499. doi: 10.1021/np900662k

Tsurumi, M. (2003). Diversity at hydrothermal vents. *Glob. Ecol. Biogeogr.* 12, 181–190. doi: 10.1046/j.1466-822X.2003.00016.x

Tunnicliffe, V. (1988). Biogeography and evolution of hydrothermal-vent fauna in the eastern Pacific Ocean. *Proc. R. Soc. London B Biol. Sci.* 233, 347–366. doi: 10.1098/rspb.1988.0025

Urcuyo, I. A., Bergquist, D. C., MacDonald, I. R., VanHorn, M., and Fisher, C. R. (2007). Growth and longevity of the tubeworm *Ridgeia piscesae* in the variable diffuse flow habitats of the Juan de Fuca Ridge. *Mar. Ecol. Prog. Ser.* 344, 143–157.

Van Dover, C. L. (2002). Trophic relationships among invertebrates at the Kairei hydrothermal vent field (Central Indian Ridge). *Mar. Biol.* 141, 761–772. doi: 10.1007/s00227-002-0865-y

Van Dover, C. L. (2019). Inactive sulfide ecosystems in the deep sea: A review. *Front. Mar. Sci.* 6:00461. doi: 10.3389/fmars.2019.00461

Van Dover, C. L., Arnaud-Haond, S., Gianni, M., Helmreich, S., Huber, J. A., Jaeckel, A. L., et al. (2018). Scientific rationale and international obligations for protection of active hydrothermal vent ecosystems from deep-sea mining. *Mar. Policy* 90, 20–28. doi: 10.1016/j.marpol.2018.01.020

Van Dover, C. L., Colaço, A., Collins, P. C., Croot, P., Metaxas, A., Murton, B. J., et al. (2020). Research is needed to inform environmental management of hydrothermally inactive and extinct polymetallic sulfide (PMS) deposits. *Mar. Policy* 121:104183. doi: 10.1016/j.marpol.2020.104183

Van Dover, C. L., Grassle, J. F., and Boudrias, M. (1990). Hydrothermal vent fauna of Escanaba Trough (Gorda Ridge). *SpringerLink* 1990, 285–287. doi: 10.1007/978-1-4612-3258-2_21

Van Dover, C. L., Humphris, S. E., Fornari, D., Cavanaugh, C. M., Collier, R., Goffredi, S. K., et al. (2001). Biogeography and ecological setting of Indian Ocean hydrothermal vents. *Science* 294, 818–823. doi: 10.1126/science.1064574

Vereshchaka, A. L., Vinogradov, G. M., Lein, A. Yu, Dalton, S., and Dehairs, F. (2000). Carbon and nitrogen isotopic composition of the fauna from the Broken Spur hydrothermal vent field. *Mar. Biol.* 136, 11–17. doi: 10.1007/s002270050002

Vrijenhoek, R. C. (1997). Gene flow and genetic diversity in naturally fragmented metapopulations of deep-sea hydrothermal vent animals. *J. Hered.* 88, 285–293. doi: 10.1093/oxfordjournals.jhered.a023106

Wang, Y., Han, X., Petersen, S., Frische, M., Qiu, Z., Li, H., et al. (2017). Mineralogy and trace element geochemistry of sulfide minerals from the Wocan Hydrothermal Field on the slow-spreading Carlsberg Ridge, Indian Ocean. *Ore Geol. Rev.* 84, 1–19. doi: 10.1016/j.oregeorev.2016.12.020

Wang, Y., Han, X., Zhou, Y., Qiu, Z., Yu, X., Petersen, S., et al. (2021). The Daxi Vent Field: An active mafic-hosted hydrothermal system at a non-transform offset on the slow-spreading Carlsberg Ridge, 6°48'N. *Ore Geol. Rev.* 129:103888. doi: 10.1016/j.oregeorev.2020.103888

Wang, Z., Xu, T., Zhang, Y., Zhou, Y., Liu, Z., Chen, C., et al. (2020). Molecular phylogenetic and morphological analyses of the 'monospecific' *Hesiolyra* (Annelida: Hesionidae) reveal two new species. *Deep Sea Res. Part I Oceanogr. Res. Papers* 166:103401. doi: 10.1016/j.dsr.2020.103401

Washburn, T. W., Turner, P. J., Durden, J. M., Jones, D. O. B., Weaver, P., and Van Dover, C. L. (2019). Ecological risk assessment for deep-sea mining. *Ocean Coastal Manage.* 176, 24–39. doi: 10.1016/j.ocecoaman.2019.04.014

Watanabe, H. K., Chen, C., Marie, D. P., Takai, K., Fujikura, K., and Chan, B. K. K. (2018). Phylogeography of hydrothermal vent stalked barnacles: a new species fills a gap in the Indian Ocean 'dispersal corridor' hypothesis. *R. Soc. Open Sci.* 5:172408. doi: 10.1098/rsos.172408

Watanabe, H., and Beedessee, G. (2015). ""Vent fauna on the Central Indian Ridge,"," in *Subseafloor Biosphere Linked to Hydrothermal Systems: TAIGA Concept*, eds J. Ishibashi, K. Okino, and M. Sunamura (Tokyo: Springer Japan), 205–212. doi: 10.1007/978-4-431-54865-2_16

Won, Y.-J., Hallam, S. J., O'Mullan, G. D., Pan, I. L., Buck, K. R., and Vrijenhoek, R. C. (2003). Environmental acquisition of thiotrophic endosymbionts by deep-sea mussels of the genus *Bathymodiolus*. *Appl. Environ. Microbiol.* 69, 6785–6792. doi: 10.1128/AEM.69.11.6785-6792.2003

Xu, W., Gong, L., Pang, K.-L., and Luo, Z.-H. (2018). Fungal diversity in deep-sea sediments of a hydrothermal vent system in the Southwest Indian Ridge. *Deep Sea Res. Part I Oceanogr. Res. Papers* 131, 16–26. doi: 10.1016/j.dsr.2017.11.001

Yahagi, T., Watanabe, H., Shigeaki, K., and Yasunori, K. (2017). Do larvae from deep-sea hydrothermal vents disperse in surface waters? *Ecology* 98, 1524–1534. doi: 10.1002/ecy.1800

Yamanaka, T., Mizota, C., Fujiwara, Y., Chiba, H., Hashimoto, J., Gamo, T., et al. (2003). Sulphur-isotopic composition of the deep-sea mussel *Bathymodiolus marisindicus* from currently active hydrothermal vents in the Indian Ocean. *J. Mar. Biol. Associat. U K* 83, 841–848. doi: 10.1017/S0025315403007872h

Yang, Y., Sun, J., Chen, C., Zhou, Y., Lan, Y., Dover, C. L. V., et al. (2020). Tripartite holobiont system in a vent snail broadens the concept of chemosymbiosis. *bioRxiv* [Preprint]:295170. doi: 10.1101/2020.09.13.295170

Yang, Z., Xiao, X., and Zhang, Y. (2020). Microbial diversity of sediments from an inactive hydrothermal vent field, Southwest Indian Ridge. *Mar. Life Sci. Technol.* 2, 73–86. doi: 10.1007/s42995-019-00007-0

Zbinden, M., Shillito, B., Le Bris, N., de Montlaur, C. D. V., Roussel, E., Guyot, F., et al. (2008). New insigths on the metabolic diversity among the epibiotic microbial communitiy of the hydrothermal shrimp *Rimicaris exoculata*. *J. Exp. Mar. Biol. Ecol.* 359, 131–140. doi: 10.1016/j.jembe.2008.03.009

Zekely, J., Van Dover, C. L., Nemeschkal, H. L., and Bright, M. (2006). Hydrothermal vent meiobenthos associated with mytilid mussel aggregations from the Mid-Atlantic Ridge and the East Pacific Rise. *Deep Sea Res. Part I Oceanogr. Res. Papers* 53, 1363–1378. doi: 10.1016/j.dsr.2006.05.010

Zhou, Y., Zhang, D., Zhang, R., Liu, Z., Tao, C., Lu, B., et al. (2018). Characterization of vent fauna at three hydrothermal vent fields on the Southwest Indian Ridge: Implications for biogeography and interannual dynamics on ultraslow-spreading ridges. *Deep Sea Res. Part I Oceanogr. Res. Pap.* 137, 1–12. doi: 10.1016/j.dsr.2018.05.001

Conflict of Interest: The authors declare that the research was conducted in the absence of any commercial or financial relationships that could be construed as a potential conflict of interest.

Publisher's Note: All claims expressed in this article are solely those of the authors and do not necessarily represent those of their affiliated organizations, or those of the publisher, the editors and the reviewers. Any product that may be evaluated in this article, or claim that may be made by its manufacturer, is not guaranteed or endorsed by the publisher.

frontiers in Marine Science

BRIEF RESEARCH REPORT
published: 31 January 2022
doi: 10.3389/fmars.2022.812915

Numerous Sublinear Sets of Holes in Sediment on the Northern Mid-Atlantic Ridge Point to Knowledge Gaps in Understanding Mid-Ocean Ridge Ecosystems

Michael Vecchione[1]* *and Odd Aksel Bergstad*[2†]

[1] National Marine Fisheries Service (NMFS) National Systematics Laboratory, National Museum of Natural History, Washington, DC, United States, [2] Institute of Marine Research, Bergen, Norway

OPEN ACCESS

Edited by:
David Billett,
Deep Seas Environmental Solutions Ltd., United Kingdom

Reviewed by:
Alfred Uchman,
Jagiellonian University, Poland
Rachel Przeslawski,
Aquatic Ecosystems Unit, New South Wales Department of Primary Industries, Australia
Brian James Bett,
National Oceanography Centre, United Kingdom

***Correspondence:**
Michael Vecchione
vecchiom@si.edu

†Present address:
Odd Aksel Bergstad,
Nedre Brattbakken 19, Kristiansand, Norway

Specialty section:
This article was submitted to Deep-Sea Environments and Ecology, a section of the journal Frontiers in Marine Science

Received: 10 November 2021
Accepted: 06 January 2022
Published: 31 January 2022

Citation:
Vecchione M and Bergstad OA (2022) Numerous Sublinear Sets of Holes in Sediment on the Northern Mid-Atlantic Ridge Point to Knowledge Gaps in Understanding Mid-Ocean Ridge Ecosystems. Front. Mar. Sci. 9:812915. doi: 10.3389/fmars.2022.812915

On 13 July 2004, during an expedition exploring biodiversity along the northern Mid-Atlantic Ridge, an ROV dive recorded videos of numerous sublinear sets of holes in sediment at ca. 2,082 m depth. The location was north of the Azores. Each set appeared track-like. Lengths of individual series ranged from < 1 m to many meters. Each was straight or gently curved. Some series intersected or crossed. Close examination of the holes showed them to be elongate, with the long axis parallel to the axis of the series. The holes were ca. 6 × 1.5 cm, with distance between holes similar to hole length. The holes that appeared to be most recently formed were each surrounded by raised sediment. Holes that appeared older were partly filled with sediment and the raised surrounding sediment was less obvious. Overall, these lebensspuren created small-scale heterogeneity in the local soft-bottom benthic ecosystem. The source of the holes or how they were constructed is unknown, but the raised sediment may indicate excavation by an infaunal organism or digging and removal by e.g., a feeding appendage of a large epifaunal animal. None of our closeups showed any sign of living organisms inhabiting the holes. Whether the holes were connected beneath the sediment surface was not visible. The traces observed are reminiscent of ichnofossils reported from deep marine facies. We hope that future studies of the lebensspuren we report here will resolve the mystery of what created them.

Keywords: lebensspuren, ichnofossils, ROV, Azores, MAR-ECO

INTRODUCTION

"Lebensspuren" is a term used in early reports of photography of the deep-sea bottom (Ewing and Davis, 1967; Heezen and Hollister, 1971). It translates as "life traces" and refers to patterns in surface sediments resulting from bioturbation. The study of these extant life traces (neoichnology) is a modern equivalent of paleoichnology, which is generally concerned with fossilized tracks, trails, burrows, borings, or other trace fossils (ichnofossils) and integrates paleontology, sedimentology, and biology. Understanding the distribution and diversity of lebensspuren is ecologically important because these traces introduce a variety of small-scale heterogeneity in surface sediments and affect

the accumulation of pelagic detritus at the sediment-water interface. Furthermore, lebensspuren are often the only indication in visual surveys of the presence of infaunal or mobile animals capable of avoiding camera platforms.

The decade-long Census of Marine Life (CoML) was a global program to increase knowledge of marine biodiversity (McIntyre, 2010). One field project within CoML, entitled Patterns and Processes of the Ecosystem of the Northern mid-Atlantic (MAR-ECO), focused on the Mid-Atlantic Ridge between Iceland and the Azores (Bergstad et al., 2008; Vecchione et al., 2010) using a broad suite of methods (Wenneck et al., 2008). Although often thought of as primarily hard substrate, the Mid-Atlantic Ridge is largely covered with sediment (Niedzielski et al., 2013; Priede et al., 2013a). At one of the sediment-covered MAR-ECO locations, we encountered numerous widespread lebensspuren in a pattern that seemed reminiscent of tracks from an unknown animal. We describe here those traces in the sediment and consider their similarity to ichnofossils.

METHODS

The flagship expedition for the MAR-ECO project was conducted on the R/V *G.O. Sars* during June-July 2004. Among the methods employed was a series of dives with two remotely operated vehicles (ROVs). These dives observed and recorded standard-definition video of benthic epifauna and substrata at 22 locations between the Azores Archipelago and the Charlie-Gibbs Fracture Zone, with bottom depths surveyed between 900 and 3,500 m.

The ROVs were equipped with four parallel lasers for measurement. However, laser measurement was problematic on the dive described below because two of the lasers were not functioning. The remaining two were from different pairs (i.e., opposite corners of the square pattern) and therefore illuminated different distances from the ROV, resulting in a parallax problem. We therefore used objects of known size (shells of the pteropod *Clio recurva*, maximum reported length ca. 3 cm) near the holes to estimate the size of the holes. Distances from previously published locations were calculated using the NOAA Latitude/Longitude Distance Calculator.[1]

RESULTS

On 13 July 2004, ROV *Bathysaurus* was used to explore benthic habitats centered around 2,082 m depth in the vicinity of 42° 56′ N 028° 36′ W (**Figure 1**). Video was recorded throughout the dive (**Figure 2**). During a period of > 1 h the ROV traversed areas where surface sediments were perforated by many sublinear series of holes. Bottom depths of these observations were 2,074–2,097 m and the near-bottom temperature was 3.6°C.

Lengths of individual series ranged from < 1 m (**Figure 2C**) to many meters (**Figure 2A**). Each series was nearly straight (**Figure 2C**) or gently curved (**Figure 2B**). Some series intersected or crossed. Close examination of the individual holes showed them to be elongate, with the long axis parallel to the axis of the series. Based on comparison with nearby shells of *Clio recurva*, the holes were ca. 6 × 1.5 cm, with distance between holes similar to hole length. The shape of the holes varied from narrow and acute (**Figure 2H**) to a more

[1]https://www.nhc.noaa.gov/gccalc.shtml

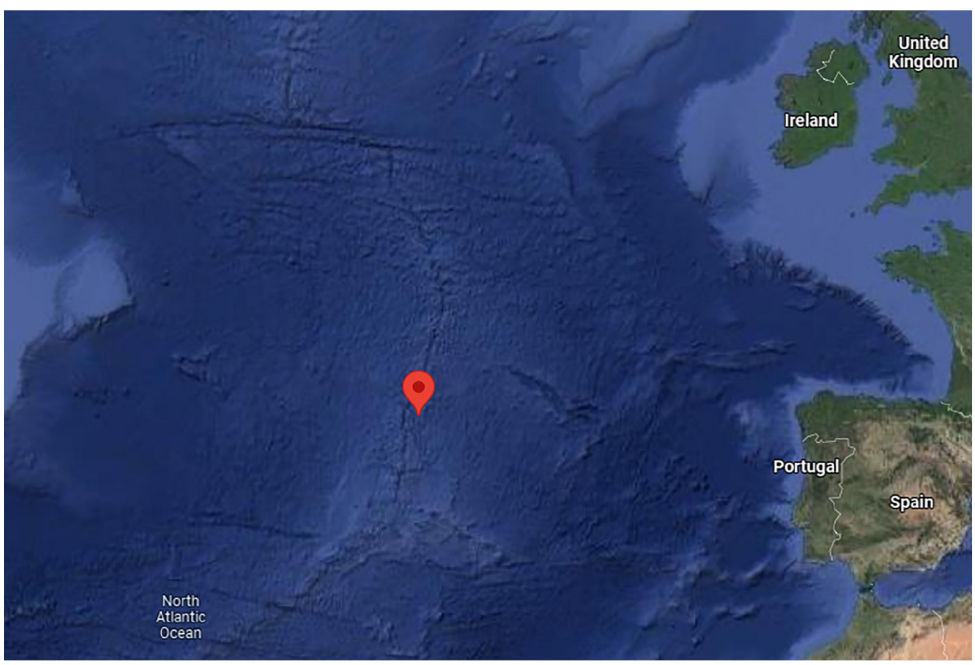

FIGURE 1 | Google Maps representation of the dive location (42° 56′ N 028° 36′ W), on the Mid-Atlantic Ridge north of the Azores Archipelago.

rounded appearance (**Figure 2G**). The holes that appeared to be most recently formed were each surrounded by raised sediment (**Figures 2C,F**). Holes that appeared older were partly filled with sediment and the raised surrounding sediment was less obvious (**Figure 2E**). In areas where the seafloor was covered by extensive phytodetritus, the holes were often filled with phytodetritus (**Figure 2C**). None of our closeups showed any sign of living organisms inhabiting the holes (**Figures 2G,H**). Nor could we detect subsurface connections between adjacent holes.

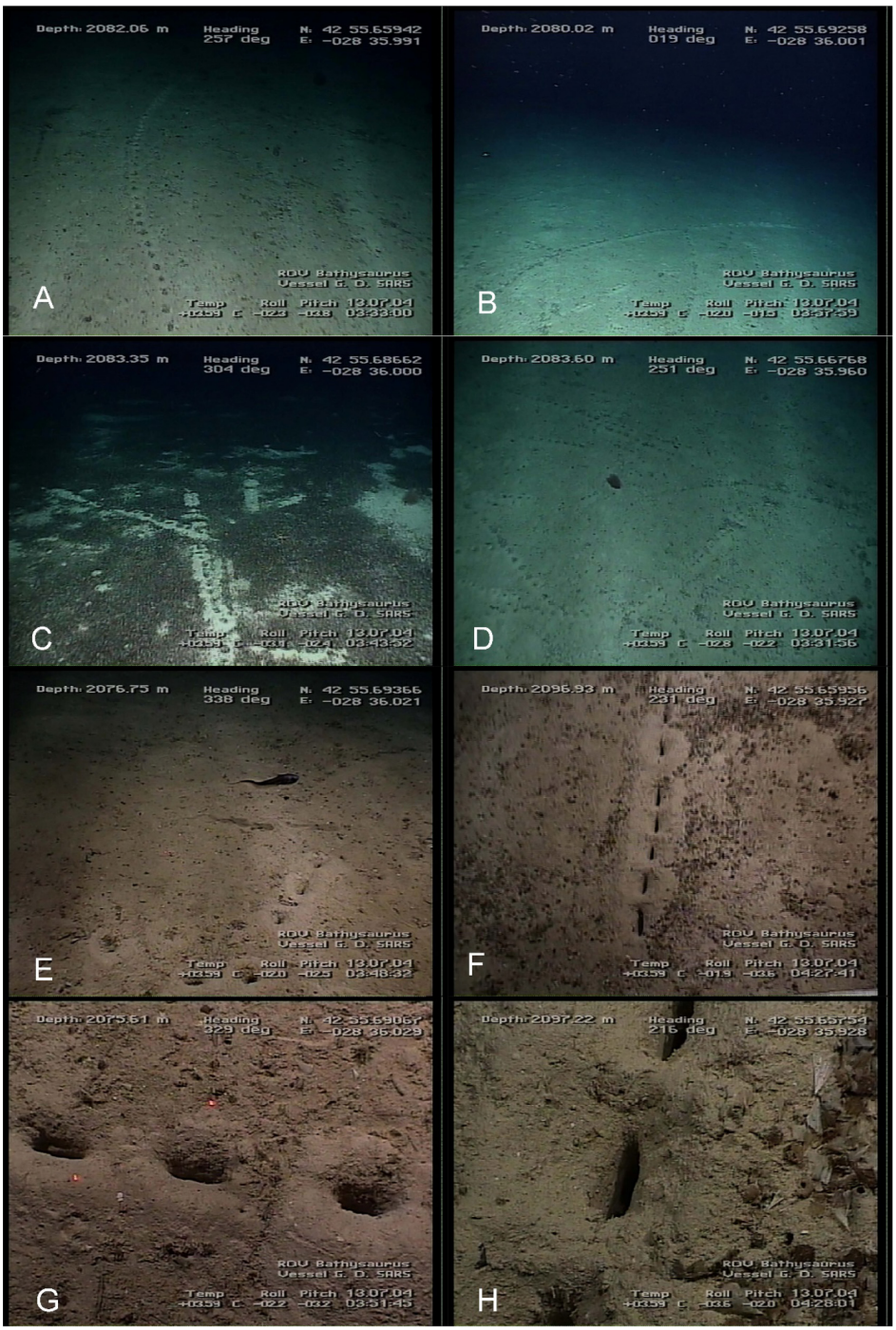

FIGURE 2 | Screen grabs from standard-definition video recorded *in situ* by remotely operated vehicle. **(A)** Single long series, gently curving; **(B)** multiple intersecting series; **(C)** multiple short series in an area heavily covered with phytodetritus; **(D)** an area with many series of varying lengths; **(E)** moderate closeup of rounded holes; **(F)** moderate closeup of narrow holes; **(G)** maximum closeup of rounded holes; **(H)** maximum closeup of narrow holes.

DISCUSSION

When we first encountered these formations, we referred to them as track-like (Vecchione et al., 2010). We speculated that they may have been caused by a large benthic crustacean, such as the blind lobster (*Acanthacaris caeca*). However, there is no evidence to support that speculation.

Bell et al. (2013), following Przeslawski et al. (2012), quantified many types of lebensspuren at four locations in the vicinity of the Charlie-Gibbs Fracture Zone explored by the ECOMAR project (Priede et al., 2013b), all far north of the location we describe here. Our rounded-hole morphotype is similar to a type they termed "pogo stick tracks" of indeterminate origin, but the latter appeared to have even more rounded holes, grading to circular. The latter was found only at their SouthEast station (SE; 49° 02′ N, 027° 41′ W), with very low occurrence there. They also mentioned a type termed "Indeterminate perforated trail" encountered in low numbers at their NorthWest station (NW; 53° 59′ N, 036° 07′ W). Whereas their SE station is closest to our location (682 km), the NW station is farthest from it (1,345 km). The linear series of holes we report here may be related to either of these rare categories in Bell et al. (2013) study, but in contrast to their rarity at the locations farther north, our series comprise the dominant small-scale structure in surface sediments of the area on which we report. South of our location, Heezen and Hollister (1971) observed "crater rows" at three sites, 1,471–1,723 m water depth, around the Azores.

The raised sediment may possibly have been pushed aside by insertion of e.g., a feeding appendage of a large epifaunal animal but it may alternatively indicate excavation by infauna. Therefore, it is not clear whether these should be considered crawling, feeding, or residence structures (three of the five categories considered by Bell et al., 2013). The traces we observed are reminiscent of ichnofossils, such as *Paleomeandron*, reported from deep marine facies (Buatois et al., 2001), although the latter is smaller and is interpreted as a system of burrows having vertical shafts, which appear at the sediment surface as a series of paired holes. This interpretation of surface elements of such "graphoglyptid" trace fossils as a horizontal subsurface tunnel (Seilacher, 1977; Fan et al., 2018) connected upward to the surface of the sediment would not be visible in our videos. However, the paired series of holes characteristic of *Paleomeadron* appear more complex than the observed burrows reported here. Other trace fossils that might be analogs include *Treptichnus pedum* or *Hormosiroidea canadensis*, as illustrated by Laing (2018) with possible explanations by Crimes and Anderson (1985) for how such traces may have been produced. But *T. pedum* is even smaller than *Paleomeandron* and occurs in Lower Paleozoic shallow marine deposits. Other *Treptichnus* are mostly continental traces. *Hormosiroidea canadensis* was included in *Saerichnites* in Uchman (1995), a fact overlooked in the Ph.D. thesis by Laing (2018).

Perforation of the sediment by numerous holes would affect the vertical distribution in nearby sediment of oxygenated pore water, in turn affecting habitat suitability for infauna. Additionally, the local aggregation of sediment backfilling old holes and the very local accumulation of phytodetritus within the holes would change small-scale availability of food for epifaunal grazers and surface-deposit feeding infauna.

We think our current state of knowledge about these lebenspurren is similar to early studies of extant lebensspuren identified as *Paleodictyon* based on resemblance to other ichnofossils. Those geometric traces are widespread in deep-sea sediments (Durden et al., 2017). Subsequent investigation has inferred the inhabitants of such geometric traces may be a compressed form of a hexactinellid sponge adapted to sedimentary substrate (Rona et al., 2009) but this inference is not considered to be confidently resolved (Durden et al., 2017). Our goal here is not to inventory known ichnofossils and identify our traces as the same as, or related to, the most similar fossil. We simply want to point out that the fossil record includes traces in deep-marine facies that are similar to these locally abundant traces in the deep-sea sediment of the Mid-Atlantic Ridge. Although we don't know what caused them, similar processes have likely been going on in deep sedimented areas for a very long time. We hope that future studies of the unknown lebensspuren we report here will resolve the mystery of what created them and their roles in mid-ocean ridge ecosystems.

DATA AVAILABILITY STATEMENT

Publicly available datasets were analyzed in this study. These data can be found here: original videos on which this contribution are based are available from the Institute of Marine Research, Norway.

AUTHOR CONTRIBUTIONS

OB planned and arranged ROV dives. MV drafted manuscript which OB revised. Both authors participated equally in conducting and interpreting observations.

ACKNOWLEDGMENTS

We appreciate comments by AU and two other reviewers. Their comments on the ichnofossil literature were particularly helpful. The MAR-ECO project was an element of the Census of Marine Life and supported by the A.P. Sloan Foundation, New York, in the period 2003–2010.

REFERENCES

Bell, J. B., Jones, D. O. B., and Alt, C. H. S. (2013). Lebensspuren of the bathyal Mid-Atlantic Ridge. *Deep Sea Res. 2 Top. Stud. Oceanogr.* 98, 341–351. doi: 10.1016/j.dsr2.2012.09.004

Bergstad, O. A., Falkenhaug, T., Asthorsson, O., Byrkjedal, I., Gebruk, A. V., Piatkowski, U., et al. (2008). Towards improved understanding of the diversity and abundance patterns of the mid-ocean ridge macro- and megafauna. *Deep Sea Res. 2 Top. Stud. Oceanogr.* 55, 1–5. doi: 10.1016/j.dsr2.2007.10.001

Buatois, L. A., Mangano, M. G., and Sylvester, Z. (2001). A diverse deep-marine ichnofauna from the Eocene Tarcau sandstone of the eastern Carpathians, Romania. *Ichnos* 8, 28–62. doi: 10.1080/10420940109380172

Crimes, T. P., and Anderson, M. M. (1985). Trace fossils from Late Precambrian-Early Cambrian strata of southeastern Newfoundland (Canada): temporal and environmental implications. *J. Paleontol.* 59, 310–343.

Durden, J. M., Simon-Lledo, E., Gooday, A. J., and Jones, D. O. B. (2017). Abundance and morphology of *Paleodictyon nodosum*, observed at the Clarion-Clipperton Zone. *Mar. Biodiv.* 47, 265–269. doi: 10.1007/s12526-017-0636-0

Ewing, M., and Davis, R. A. (1967). "Lebensspuren photographed on the ocean floor," in *Deep-sea Photography*, ed. J. B. Hersey (Baltimore: The John Hopkins Press), 259–294.

Fan, R.-Y., Gong, Y.-M., and Uchman, A. (2018). Topological analysis of graphoglyptid trace fossils, a study of macrobenthic solitary and collective animal behaviors in the deep-sea environment. *Paleobiology* 44, 1–20. doi: 10.1017/pab.2018.1

Heezen, B. C., and Hollister, C. D. (1971). *The Face of the Deep*. New York: Oxford University Press.

Laing, B. A. (2018). *Redefining the Treptichnus pedum Zone at the Global Boundary Stratotype Section and Point (GSSP): A Critical Reassessment of the Ediacaran-Cambrian Boundary*. Ph.D. thesis. Saskatoon: University of Saskatchewan.

McIntyre, A. D. (ed.) (2010). *Life in the World's Oceans*. Hoboken: Blackwell Publishing Ltd.

Niedzielski, T., Høines, Å, Shields, M. A., Linley, T., and Priede, I. G. (2013). A multi-scale investigation into seafloor topography of the northern Mid-Atlantic Ridge based on geographic information system analysis. *Deep Sea Res. 2 Top. Stud. Oceanogr.* 98, 231–243. doi: 10.1016/j.dsr2.2013.10.006

Priede, I. G., Bergstad, O. A., Miller, P. I., Vecchione, M., Gebruk, A., Falkenhaug, T., et al. (2013a). Does presence of a mid-ocean ridge enhance biomass and biodiversity? *PLoS One* 8:e61550. doi: 10.1371/journal.pone.0061550

Priede, I. G., Billett, D. S. M., Brierley, A. S., Hoetzel, A. R., Inall, M., Miller, P. I., et al. (2013b). The ecosystem of the Mid-Atlantic Ridge at the sub-polar front and Charlie–Gibbs Fracture Zone; ECO-MAR project strategy and description of the sampling programme 2007–2010. *Deep Sea Res. 2 Top. Stud. Oceanogr.* 98, 220–230. doi: 10.1016/j.dsr2.2013.06.012

Przeslawski, R., Dundas, K., Radke, L., and Anderson, T. J. (2012). Deep-sea Lebensspuren of the Australian continental margins. *Deep Sea Res. I.* 65, 26–35. doi: 10.1016/j.dsr.2012.03.006

Rona, P. A., Seilacher, A., de Vargas, C., Gooday, A. J., Bernhard, J. M., Bowser, S., et al. (2009). *Paleodictyon nodosum*: a living fossil on the deep-sea floor. *Deep Sea Res. 2 Top. Stud. Oceanogr.* 56, 1700–1712. doi: 10.1016/j.dsr2.2009.05.015

Seilacher, A. (1977). Evolution of trace fossil communities. *Dev. Palaeontol. Stratigr.* 5, 359–376. doi: 10.1016/S0920-5446(08)70331-5

Uchman, A. (1995). Taxonomy and palaeoecology of flysch trace fossils: the Marnoso-arenacea formation and associated facies (Miocene, Northern Apennines, Italy). *Beringeria* 15, 3–115.

Vecchione, M., Bergstad, O. A., Byrkjedal, I., Falkenhaug, T., Gebruk, A. V., Godø, O. R., et al. (2010). "Biodiversity patterns and processes on the mid-Atlantic Ridge," in *Life in the World's Oceans*, ed. A. D. McIntyre (Hoboken: Blackwell Publishing Ltd), 103–121. doi: 10.1002/9781444325508.ch6

Wenneck, T. L., Falkenhaug, T., and Bergstad, O. A. (2008). Strategies, methods, and technologies adopted on the R.V. G.O. Sars MAR-ECO expedition to the Mid-Atlantic Ridge in 2004. *Deep Sea Res. 2 Top. Stud. Oceanogr.* 55, 6–28. doi: 10.1016/j.dsr2.2007.09.017

Conflict of Interest: The authors declare that the research was conducted in the absence of any commercial or financial relationships that could be construed as a potential conflict of interest.

frontiers in Marine Science

ORIGINAL RESEARCH
published: 11 February 2022
doi: 10.3389/fmars.2022.810949

Characterization of Geochemistry in Hydrothermal Sediments From the Newly Discovered Onnuri Vent Field in the Middle Region of the Central Indian Ridge

Dhongil Lim[1,2], Jihun Kim[1,2], Wonnyon Kim[1], Jonguk Kim[1], Dongsung Kim[1], Le Zhang[3], Kyungun Kwack[1] and Zhaokai Xu[4,5,6]**

[1] Korea Institute of Ocean Science & Technology, Busan, South Korea, [2] Department of Ocean Science, KIOST School, University of Science & Technology, Daejeon, South Korea, [3] State Key Laboratory of Isotope Geochemistry, Guangzhou Institute of Geochemistry, Chinese Academy of Sciences, Guangzhou, China, [4] CAS Key Laboratory of Marine Geology and Environment, Institute of Oceanology, Chinese Academy of Sciences, Qingdao, China, [5] Center for Ocean Mega-Science, Chinese Academy of Sciences, Qingdao, China, [6] CAS Center for Excellence in Quaternary Science and Global Change, Xi'an, China

OPEN ACCESS

Edited by:
Pei-Yuan Qian,
Hong Kong University of Science and Technology, Hong Kong SAR, China

Reviewed by:
Rebecca Zitoun,
Royal Netherlands Institute for Sea Research (NIOZ), Netherlands
Pavlos Megalovasilis,
University of Patras, Greece

***Correspondence:**
Dhongil Lim
oceanlim@kiost.ac.kr
Zhaokai Xu
zhaokaixu@qdio.ac.cn

Specialty section:
This article was submitted to Deep-Sea Environments and Ecology, a section of the journal Frontiers in Marine Science

Received: 08 November 2021
Accepted: 11 January 2022
Published: 11 February 2022

Citation:
Lim D, Kim J, Kim W, Kim J, Kim D, Zhang L, Kwack K and Xu Z (2022) Characterization of Geochemistry in Hydrothermal Sediments From the Newly Discovered Onnuri Vent Field in the Middle Region of the Central Indian Ridge. Front. Mar. Sci. 9:810949. doi: 10.3389/fmars.2022.810949

The recently discovered Onnuri hydrothermal vent field (OVF) is a typical off-axis ultramafic-hosted vent system, located on the summit of the dome-like ocean core complex (OCC) at a distance of ~12 km from the ridge axis along the middle region of the Central Indian Ridge (CIR). The plume chemistry with high methane anomaly was consistent with the precursor of hydrothermal activity; however, the fundamental characteristic of the OVF system, such as the hydrothermal circulation process and source of heat, remains poorly understood. Here, we focus on the geochemical features of surface sediments and minerals collected at and around the OVF region in order to better understand this venting system. The results reveal that the OVF sediments are typified by remarkably high concentrations of Fe, Si, Ba, Cu, and Zn, derived from hydrothermal fluid and S and Mg from seawater; depleted C-S isotope compositions; and abundant hydrothermally precipitated minerals (i.e., Fe–Mn hydroxides, sulfide and sulfate minerals, and opal silica). Notably, the occurrence of pure talc and barite bears witness to strong hydrothermal activity in the OVF, and their sulfur and strontium isotope geochemistry agree with extensive mixing of the unmodified seawater with high-temperature fluid derived from the gabbroic rock within the ultramafic-dominated ridge segment. The findings reveal that the OVF is a representative example of an off-axis, high-temperature hydrothermal circulation system, possibly driven by the exothermic serpentinization of exposed peridotites. Given the widespread distribution of OCC with detachment faults, furthermore, the OVF may be the most common type of hydrothermal activity in the CIR, although the paucity of data precludes generalizing this result. This study provides important information contributing to our understanding of the ultramafic-hosted hydrothermal vent system with a non-magmatic heat source along mid-ocean ridges.

Keywords: hydrothermal sediments, talc and barite, geochemistry, serpentinization, Central Indian ridges

INTRODUCTION

Because of the importance of the hydrothermal vent system in ocean chemistry, earth dynamics, and biological communities, as well as the increasing interest in massive metal deposits, the exploration of mid-ocean ridges has recently increased dramatically, revealing considerable diversity in hydrothermal systems. Hundreds of hydrothermal vents (more than 500 sites), including hydrothermal sulfide deposits, have been discovered and investigated, mainly in the Pacific and Atlantic Oceans (Hannington et al., 2011; Beaulieu et al., 2013, 2015; German and Seyfried, 2014). In the Indian Ocean ridges that are up to approximately 18,000 km in length (28% of the global total), however, only a few hydrothermal vent sites (i.e., the Dodo, Solitaire, Edmond, Kairei, and Longqi vent fields) have been visually confirmed (e.g., Nakamura et al., 2012 and reference therein; Tao et al., 2012). In the Indian Ocean ridges with various speeding rates (<12–60 mm/yr in full spreading rate), the hydrothermal vent systems are expected to vary in accordance with diverse geological and tectonic features (German et al., 1998; Wang et al., 2011; Beaulieu et al., 2015); however, these ridges remain underexplored relative to the Pacific and Atlantic ridges, and thus available data regarding their hydrothermal vents is still very limited. In this respect, recent systematic ridge expeditions at the Central and Southwest Indian regions and their results have been receiving scientific attention (e.g., Son et al., 2014; Park et al., 2017; Suo et al., 2017; Liao et al., 2018a,b, 2019; Zhou et al., 2018; Choi et al., 2021).

Systematic deep-sea exploration recently uncovered four new active hydrothermal vent fields in the middle region of the Central Indian Ridge (CIR) between 8 and 14°S, where ridge morphology and tectonic structure (e.g., detachment faults and ocean core complexes, OCCs) control increased plume incidence at ridge flank and rift wall locations (Kim et al., 2020). These hydrothermal vent fields, located more than 800 km north of previously known vent fields (i.e., the Dodo and Solitaire fields, Nakamura and Takai, 2015) are characterized by particle-poor, diffuse venting with abundant vent fauna and sulfide deposition. Notably, these new hydrothermal vents show diverse venting styles and plume compositions, attributed to distinctive hydrothermal fluid formation conditions and transport pathways in the slow- to ultraslow-rate spreading ridge setting (Son et al., 2014; Kim et al., 2020). In particular, the Onnuri hydrothermal vent field (OVF) site, located on the summit of OCC at a water depth of ∼2,000 m in Segment 3 (**Figures 1A–C**), is attracting considerable scientific attention because of its isolated location, diffuse venting style, methane-rich plume composition, ultramafic-hosted system, and community of hydrothermal vent fauna. Specifically, water column plumes from this vent site are characterized by negative oxidation-reduction potential anomalies, high dissolved methane (CH_4) concentrations, and low dissolved metal concentrations (Kim et al., 2020). Interestingly, the preliminary observation and plume chemistry suggest that the OVF may be a low-temperature hydrothermal vent, probably supported by the exothermic serpentinization process (Kim et al., 2020). This venting system is thus quite different from the well-known basaltic-hosted venting systems of high-temperature and metal-rich black smoker, driven by magmatic activity in the CIR (e.g., Dodo and Edmond sites, Tivey, 2007; Nakamura and Takai, 2015). However, solid evidence for the serpentinization reaction (e.g., heat source) and the fluid temperature of the OVF is still lacking.

Recently, hydrothermal sediments and minerals have received increasing attention because their geochemical signatures can provide useful information for grasping the character of the associated hydrothermal system, such as the composition, source, and temperature of the fluid, the source of heat, and the process of seawater/fluid interaction (e.g., Cave et al., 2002; D'Orazio et al., 2004; Dias and Barriga, 2006; Dekov et al., 2011; Eickmann et al., 2014; Liao et al., 2019; Zhang et al., 2020). In particular, sulfur and strontium isotopic compositions of hydrothermal minerals – barite and talc – strongly depend on the fluid from which they precipitate and are therefore ideal for tracing the nature of fluid/rock interaction and estimating the formation temperatures of the minerals (e.g., Paytan et al., 1993; Melekestseva et al., 2014; Zhang et al., 2020). In the ultramafic-hosted OVF with a low magma supply, the hydrothermal process and fluid composition are expected to result in different geochemical compositions of sediments compared to those of magma-driven, basalt-hosted hydrothermal vent fields. However, geochemical and mineralogical investigations of the ultramafic-hosted vent sediments are relatively poor.

In this study, we present geochemical (elemental and isotopic compositions) and mineralogical features of hydrothermal sediments (conceivably containing distinct hydrothermal components), collected in and around the OVF in the middle region of the CIR. Of particular interest in this study is the occurrence of peculiar hydrothermal minerals (i.e., hydrothermal talc and barite) and their geochemical and isotopic compositions, providing deeper insights into nature of this hydrothermal vent system. The implications of this study, including new geochemical-mineralogical data regarding the hydrothermal deposits in the CIR, include the ability of the OVF to contribute valuable information for better understanding of hydrothermal vent systems in the Indian Ocean.

STUDY AREA

The middle region of CIR (8–18°S; approximately 700 km of ridge length) is typical of slow-spreading ridges (34–45 mm/yr in full spreading rate, Park et al., 2017), with axial valleys of 500–1000 m relief and spreading segments connected by transform faults and non-transform offsets (Son et al., 2014). OCCs exposed by detachment faults are common features in this area and may lead to extensive hydrothermal circulation at off-axis sites; notably, these faults may be the primary path for hydrothermal fluids that ascend in off-axis regions (Boschi et al., 2008; Park et al., 2017). The OVF with abundant vent fauna located on the summit of dome-like OCC (11°24.9′S, 66°25.4′E; a water depth of ∼2,000 m) at a distance of approximately 12 km from the axial neo-volcanic zone.

The OVF's general characteristics (e.g., bathymetry, geological settings, basement rock compositions, plume chemistry, and

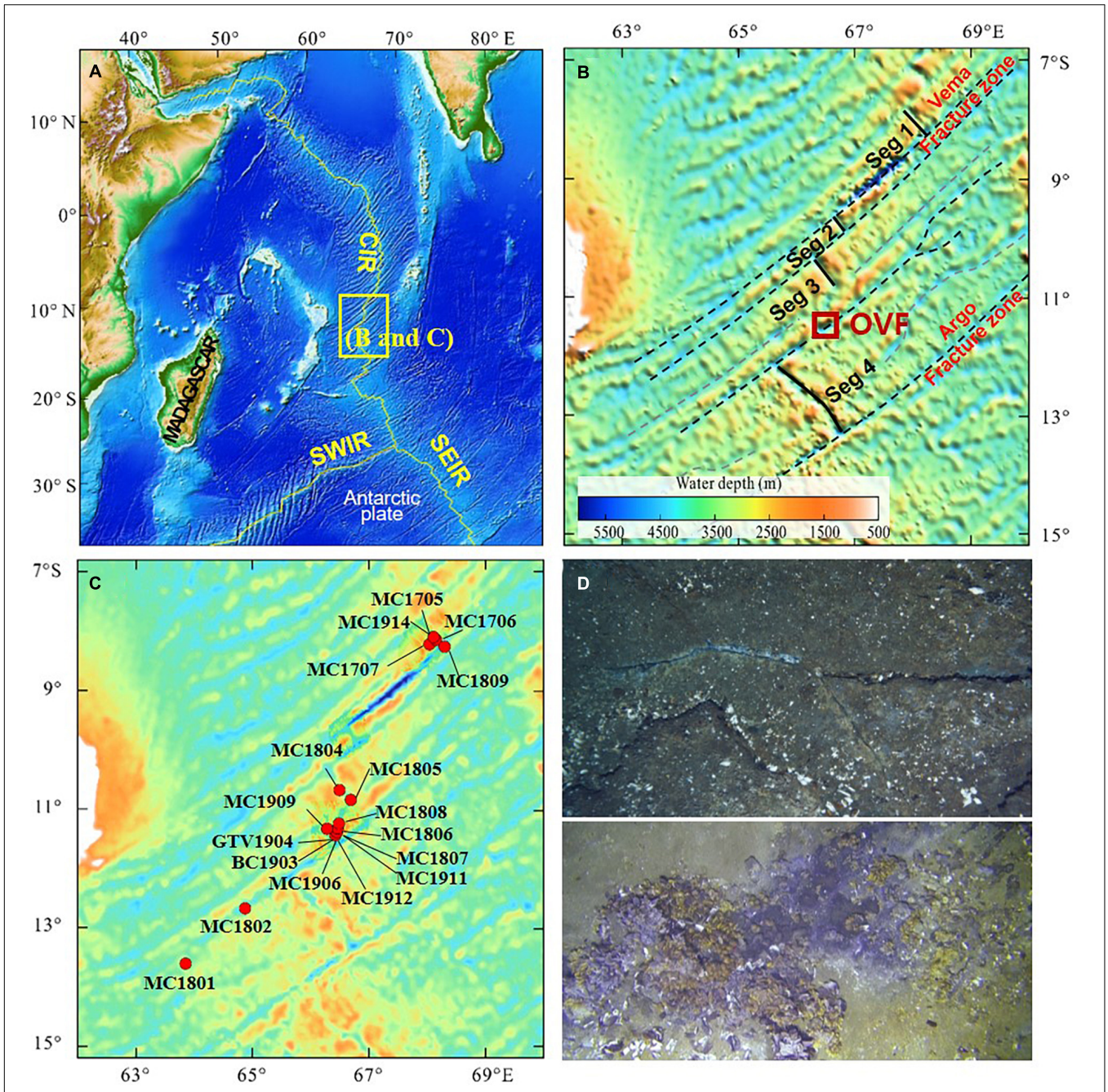

FIGURE 1 | (A) Map showing the Indian Ocean ridges and **(B)** the location of the Onnuri hydrothermal vent field (red square) and **(C)** sampling sites. **(D)** Photographs showing zonation of the active OVF (Widths of photographs are ~6 m, Kim et al., 2020). Note the fissures filled with vent fauna indicating possible diffuse flow and the clusters of various living vent fauna. CIR, Central Indian ridge, SWIR and SEIR, Southwestern and Southeastern Indian ridge; OVF, Onnuri hydrothermal vent field.

fauna diversity) were outlined by Kim et al. (2020). In brief, hydrothermal fluid in the OVF typically effuses from the fissures of basement rock, and no typical chimney structure is observed (**Figure 1D**). Around the OVF, small chimney fragments, altered rocks, and Fe-oxide crust are widely distributed in an area approximately 100–150 m in diameter. Numerous hydrothermal animals (21 macrofaunal taxa) have been observed on and around the diffuse vent, with a distribution range of approximately 100 m in diameter from the vent; these animals include mussels, gastropods, crabs, shrimps, barnacles, and anemones. Rock samples dredged at the OVF have indicated that the basement rock of the vent field consists primarily of altered gabbroic and ultramafic (i.e., serpentinized-peridotite) sequences. Furthermore, breccia-type sulfides collected by rock dredges have displayed thin greenish layers of copper (Cu)-bearing secondary minerals. The plume over the OVF site is

particle-poor (e.g., max. ΔNTU = 0.002 in particle anomaly), although it is characterized by a substantial oxidation-reduction potential anomaly (ΔE = −20 mV at approximately 100 m above the bottom), with a corresponding increase in the total dissolved iron (Fe, 191 nM in maximum value), manganese (Mn, 1.5 nM in maximum value) and methane (CH_4, 52.5 nM in maximum value). The average dissolved Fe/Mn and CH_4/Mn ratios were 5.6 and 36.2, respectively, which are within the typical range of the mid-ocean ridge hydrothermal system (Kim et al., 2020 and reference therein).

MATERIALS AND METHODS

A total of 18 surface sediments were collected in and around the OVF using TV-grab and multiple box-core samplers on the cruises of R/V ISABU between 2017 and 2019 (**Figure 1C**). Angular, dark glossy volcaniclastic particles (pyroclastic shards, Lim et al., 2020, 2021) abundantly observed in some surface sediments were also collected for geochemical compositions. For geochemical compositions, sediment and volcaniclastic particle samples were freeze-dried and then ground using an agate mortar. The total nitrogen (TN), carbon (TC), and sulfur (TS) contents of these sediments were measured using an elemental analyzer (FLASH 2000, Thermo Fisher Scientific, Waltham, MA, United States), and the total inorganic carbon (TIC) content was measured using a CO_2 coulometer (model CM5014: UIC, Joliet, IL, United States) in the geochemistry laboratory of Library for Marine Samples (LIMS), Korea Institute of Ocean Science & Technology (KIOST). The analytical accuracy and precision of these elements were within 5%, based on an analysis of standard reference materials [L-cysteine for TN and TC analysis, BBOT for TS analysis, and pure calcium carbonate ($CaCO_3$) with 12.00 C% for TIC analysis] and replicated samples. TIC content was converted to $CaCO_3$ content as a weight percentage using a multiplication factor of 8.333, and total organic carbon (TOC) content was calculated from the difference between the TC and TIC contents.

For the concentration of 17 elements (SiO_2, Al_2O_3, Fe_2O_3, MgO, CaO, Na_2O, K_2O, TiO_2, MnO, Ba, Co, Cr, Cu, Ni, Pb, Sn, and Zn), each powered sediment sample was fused with lithium metaborate ($LiBO_2$) flux and the molten beads were then poured into a volume of dilute nitric acid and stirred until dissolved (Lim et al., 2015). The resultant solutions were then analyzed using a combination of a Thermo ICAP 6500 radial inductively coupled plasma optical emission spectroscopy (ICP-OES) and Thermo Elemental X Series II ICP mass spectrometry (ICP-MS). Calibration for both instruments was achieved via matrix matched calibration standards produced from combinations of ICP-grade single element standards. The accuracy of the analytical method was monitored by repeated analysis of standard reference materials (ACE, OU6 and SBC-1, n = 5, respectively), together with a batch of sediment samples. The results showed that relative deviations between measured and certificated values were less than 5–10% in most elements (**Supplementary Table 1**). To gain detailed information about the origin and mode of occurrence of the elements in these surface sediments, we analyzed the concentrations of the acid leachable fraction (hereafter the labile phase) of each sample, including the water-soluble, exchangeable, and acid-soluble phases (Cronan and Hodkinson, 1997; Song and Choi, 2009; Mascarenhas-Pereira and Nath, 2010). For element composition of the labile fraction, bulk sediment samples were leached with 1N hydrochloric acid (HCl) for 24 h at room temperature (Yang et al., 2004; Song and Choi, 2009), and then the supernatant (solution) was analyzed for the leached concentrations of 17 elements using ICP-OES and ICP-MS at Korea Basic Science Institute, Korea. Here, the elemental concentration of the residual fraction was defined as the difference between the total and labile fractions of bulk sediments.

The stable carbon isotope ($\delta^{13}C$) of organic matter and sulfur isotope ($\delta^{34}S$) of bulk sediments and hydrothermal minerals were measured using an Elemental Analyzer-Isotope Ratio Mass Spectrometer (EA-IRMS, Elementar GmbH, Langenselbold, Hesse, Germany), hosted at the LIMS, KIOST. Isotopic compositions were reported relative to conventional reference materials; Vienna Peedee Belemnite (VPDB) for carbon and Vienna Canyon Diablo Troilite (VCDT) for sulfur. The measured $\delta^{13}C$ for the carbonate-removed sediments were calibrated using international reference materials; IAEA-600, USGS40, USGS43, and IAEA-CH-6. For $\delta^{34}S$ composition, untreated samples were combusted with vanadium pentoxide (V_2O_5) and the measured $\delta^{34}S$ was calculated using international reference materials; IAEA-S1, IAEA-S2, and IAEA-SO6. All sediment samples, together with standard materials, were analyzed in duplicate or triplicate. Measurement reproducibility as determined from replicate analysis was less than approximately ± 0.04‰ for $\delta^{13}C$ and ± 0.3‰ for $\delta^{34}S$ (**Supplementary Table 1**).

For identifying hydrothermal minerals (i.e., barite and talc) found in surface sediments, the X-ray diffraction (XRD) data were collected with a Bruker D8 Advance A25 diffractometer using graphite-monochromatised CuKα radiation at Gyungsang National University, Korea; the mineral grains were collected from some surface sediments under the microscope and were then powdered for subsequent analysis. The samples were measured from 4° to 70° (2θ) at an interval of 0.02° step size with 0.2 s of time scan under the conditions of 40 kV/40 mA of accelerating voltage and CuKα (1.5418 Å) radiation. Their morphologies and chemical compositions were taken using a JEOL JSM 7600F field emission scanning electron microscope (SEM) equipped with an energy dispersive x-ray spectrometer (EDS) at the LIMS, KIOST. The analyses were performed under the conditions of an acceleration voltage of 10–20 kV and a beam diameter of 3 μm.

Strontium ($^{86}Sr/^{87}Sr$) isotope compositions of the barite grain samples (n = 12) were analyzed using a Neptune Plus multi-collector ICP-MS (MC-ICP-MS, Thermo Fisher Scientific, Waltham, MA, United States), coupled with a RESOlution M-50 193 nm laser ablation system (Resonetics, Nashua, NH, United States), hosted at the State Key Laboratory of Isotope Geochemistry, Guangzhou Institute of Geochemistry, Chinese Academy of Sciences (GIG, CAS). The interferences of ^{84}Kr and ^{86}Kr on ^{84}Sr and ^{86}Sr were corrected by subtracting gas blank from the raw time-resolved signal intensities. ^{85}Rb

was used to correct the interference of ^{87}Rb on ^{87}Sr with a natural $^{85}Rb/^{87}Rb = 2.593$ (Catanzaro et al., 1969). The mass bias of $^{87}Sr/^{86}Sr$ was normalized to $^{86}Sr/^{88}Sr = 0.1194$ with an exponential law. The detailed data reduction procedure is reported in Zhang et al. (2018). Ten analyses of NKT-1G (a basaltic glass) during the course of this measurement yielded a weighted mean of $^{87}Sr/^{86}Sr = 0.70355 \pm 0.00009$ (2SD), which is consistent within error of the value reported in Elburg et al. (2005). Fifteen analyses of an in-house plagioclase glass (PZHPL) yielded a weighted mean of $^{87}Sr/^{86}Sr = 0.70435 \pm 0.00010$ (2 SD), agreeing within error with the result measured by solution method (Zhang et al., 2019).

In this study, multivariate statistical approaches were applied to clarify the distribution of geochemical components and to better define the significant relationships between them. Statistical analyses were performed using Excel-XLSTAT (Version 2009.1.01).

RESULTS

Most surface sediments are composed of yellowish, foraminiferal nanofossiliferous ooze, frequently including angular, dark glossy volcaniclastic particles, except for the sediment samples proximal to the hydrothermal edifices of the OVF with low $CaCO_3$ contents. The analytical results for the geochemical compositions of all sediments samples and their statistic summary are given in **Table 1** and **Supplementary Table 2**, respectively. The geochemical compositions of the sediments vary considerably depending on the sample site. TN, TOC, and TS contents range from 236 to 735 μg/g (average: 433 μg/g), 1,947–5,941 μg/g (average: 3,967 μg/g), and 1,110–19,177 μg/g (average: 3,652 μg/g), respectively. The $CaCO_3$ contents are generally between 50 and 84%, excluding some samples with low contents (<10%) and agree with the total concentration of CaO, suggesting that the calcium in the sediments is derived largely from biogenic components (i.e., foraminiferal tests). Carbon and sulfur isotope compositions also exhibit a wide range; $\delta^{13}C$ of organic matter and $\delta^{34}S$ of bulk sediments ranged from –25.20 to –19.77‰ (average –21.35‰) and +13.57 to +22.27‰ (average: +19.52‰), respectively.

In total concentration, CaO (average: 30.65%, range: 0.25–48.16%) and SiO_2 (average: 23.33%, range: 4.84–68.81%) are the most abundant elements, followed by MgO, Fe_2O_3, Na_2O, and Al_2O_3 with average values of 6.76% (range: 0.55–25.45%), 3.28% (range: 0.73–13.50%), 2.87% (range: 0.90–4.27%), and 2.22% (range: 0.65–7.50%), respectively. The concentrations of MnO, K_2O, and TiO_2 are generally low, ranging from 0.03 to 2.77% (average: 0.26%), 0.09 to 0.40% (average: 0.23%), and 0.00 to 0.36% (average: 0.10%), respectively. Of the trace elements, the concentrations of Ba (average: 6,026 μg/g, range: 466–41,101 μg/g) and Cu (average: 437 μg/g, range: 37–3,545 μg/g)

TABLE 1 | Descriptive statistics of elemental compositions for surface sediments of the study area.

	OVF sediments (*n* = 18)								OVF volcaniclastic grains (*n* = 6)				*MORB	*Basalt (*n* = 26)
	Total fraction				1 N leachable fraction									
Elements	**Average**	***SD***	**Min**	**Max**	**Average**	***SD***	**Min**	**Max**	**Average**	***SD***	**Min**	**Max**	**Average**	**Average**
TN (μg/g)	433	146	236	735	–	–	–	–	–	–	–	–	–	–
TOC (μg/g)	3967	1020	1947	5941	–	–	–	–	–	–	–	–	–	–
TS (μg/g)	3652	4675	1110	19177	–	–	–	–	–	–	–	–	–	–
$CaCO_3$ (%)	51.1	29.4	0.1	83.6	–	–	–	–	–	–	–	–	–	–
Al_2O_3 (%)	2.22	2.27	0.65	7.50	0.81	0.72	0.15	2.37	15.91	0.55	15.39	16.62	14.95	16.16
CaO (%)	30.65	16.63	0.25	48.16	29.94	16.74	0.22	47.97	11.41	0.15	11.24	11.67	11.39	–
Fe_2O_3 (%)	3.28	2.94	0.73	13.50	1.82	2.37	0.36	10.92	9.80	0.36	9.35	10.16	11.30	11.10
K_2O (%)	0.23	0.09	0.09	0.40	0.18	0.07	0.05	0.30	0.16	0.02	0.13	0.17	0.14	0.14
MgO (%)	6.76	8.18	0.55	25.45	1.47	0.87	0.47	2.79	7.64	0.14	7.53	7.86	7.69	8.38
MnO (%)	0.26	0.63	0.03	2.77	0.13	0.21	0.01	0.97	0.17	0.02	0.16	0.21	0.18	0.16
Na_2O (%)	2.87	0.89	0.90	4.27	2.71	0.83	0.81	4.23	2.60	0.04	2.57	2.66	2.76	2.39
SiO_2 (%)	23.33	19.20	4.84	68.81	1.69	1.00	0.72	5.07	49.39	0.37	48.93	49.92	50.41	48.95
TiO_2 (%)	0.10	0.11	0.00	0.36	0.02	0.03	0.00	0.09	1.39	0.03	1.35	1.43	1.68	1.10
Ba (μg/g)	6206	11577	466	41101	614	1288	21	5408	17	3	12	20	23	–
Co (μg/g)	15	11	4	44	9	8	1	29	43	3	41	49	43	49
Cr (μg/g)	81	118	2	444	17	21	0	78	409	121	300	627	251	230
Cu (μg/g)	437	879	37	3545	278	591	4	2292	67	4	61	72	75	93
Ni (μg/g)	60	71	7	225	26	28	0	95	124	17	115	158	97	143
Pb (μg/g)	42.5	87.8	1.7	334.2	31.9	65.6	1.5	230.7	2.8	2.1	1.0	6.9	0.5	2.0
Sn (μg/g)	4.09	8.80	0.16	34.91	2.20	4.88	0.00	19.48	1.07	0.15	0.89	1.30	0.79	–
Zn (μg/g)	74	109	16	478	43	68	12	311	84	6	77	91	87	95

**Data from MORB and basalt are from Gale et al. (2013) and Liao et al. (2019) respectively.*

are highest, followed by Cr, Zn, Ni, and Pb, with averages of 81 μg/g (range: 2–444 μg/g), 74 μg/g (range: 16–478 μg/g), 60 μg/g (range: 7–225 μg/g), and 43 μg/g (range: 2–334 μg/g), respectively. Co and Sn are less than 45 and 35 μg/g in maximum concentrations, respectively (**Table 1**). The relative proportion of the labile phase (1M HCl leachable fraction) compared with the total concentration was as high as 70% in average values for Ca, K, Mn, Na, and Pb, followed by Co, Cu, Fe, Mg, and Zn; the average ranges were 50–70%. In contrast, Ba, Cr, Si, and Ti were lower than 30% on average, suggesting that they mainly exist in acid-insoluble fractions (e.g., silicate and/or sulfate minerals).

Pure sand-sized volcaniclastic particles from some sediments are clearly distinguished from bulk sediments with respect to their elemental composition (**Table 1**). SiO_2, Al_2O_3, and CaO are the most abundant elements, with averages of 49.39% (range: 48.93–49.92%), 15.91% (range: 15.39–16.62%), and 11.41% (range: 11.24–11.67%), respectively, followed by Fe_2O_3 (average: 9.80%, range: 9.35–10.16%), MgO (average: 7.64%, range: 7.53–7.86%), Na_2O (average: 2.60%, range: 2.57–2.66%), TiO_2 (average: 1.39%, range: 1.35–1.43%), MnO (average: 0.17%, range: 0.16–0.21%), and K_2O (average: 0.16%, range: 0.13–0.17%). Among the trace elements, the average concentrations of Cr, Ni, and Zn reached 409 μg/g (range: 300–627 μg/g), 124 μg/g (range: 115–158 μg/g), and 84 μg/g (range: 77–91 μg/g), respectively. Other elements, including Co and Cu, were as low as 40–70 μg/g; Ba, Pb, and Sn were less than 20 μg/g. Characteristically, Al, Co, Cr, Fe, and Ti concentrations were much higher than those of the surface sediments of the OVF; however, Ba, Cu, K, Mn, Pb, and Sn concentrations were lower (**Table 1**).

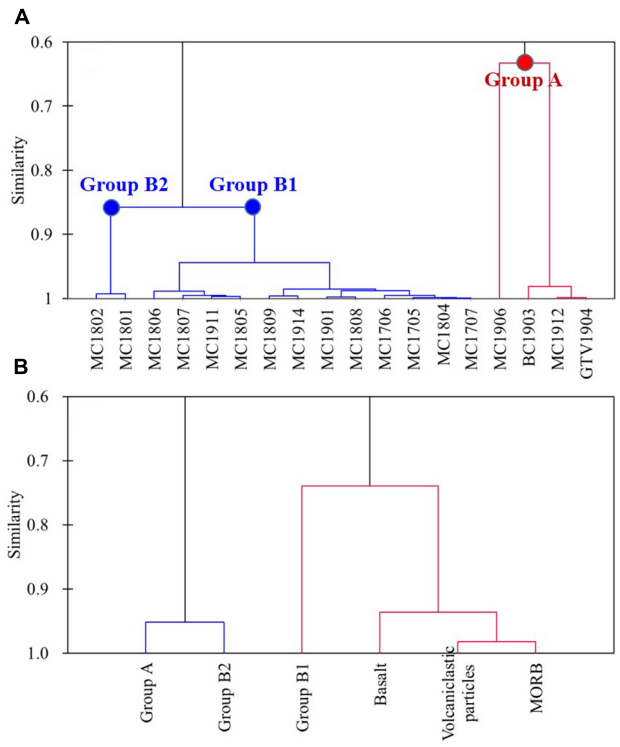

FIGURE 2 | Dendrograms showing the results of agglomerative hierarchical clustering for **(A)** the sediment sampling stations and **(B)** the sediment groups of the study area and end-members (volcaniclastic particles, basalt, and MORB) using the Pearson's correlation coefficient method. MORB, mid-ocean ridge basalt.

DISCUSSION

Geochemical Characteristics of Mid-Ocean Ridge Sediments

The agglomerative hierarchical clustering (AHC) analysis grouped the surface sediments into three clusters (A, B1, and B2) on the basis of compositional similarity between the samples (**Figure 2A**). The sediments of group A, corresponding to the hydrothermal edifice of the OVF, were characterized by the highest concentrations of Fe, Mg, Mn, Si, Ba, Cu, Sn, Pb, and Zn (**Table 2**). Group B1, comprising of sediment samples around and distant from the OVF, had significantly higher in Al, K, Na, Ti, Cr, Co, and Ni concentrations. Another distal sediment group located far from the OVF (group B2) had the highest concentrations of Ca but the lowest concentrations of most other elements, possibly due to the carbonate dilution effect.

Identification of the hydrothermal components and their quantitative contributions in mid-ocean ridge sediments can be estimated using various elemental discrimination diagrams. For example, element ratios such as Al/(Al + Fe + Mn) and (Fe + Mn)/Ti have been successfully used as indicators

TABLE 2 | Average concentrations of elements for each sediment group of the study area, MORB, and basalt.

Elements	This study				*MORB	*Basalt
	Group A	Group B1	Group B2	Volcaniclastic particles		
Al_2O_3 (%)	1.19	2.80	0.78	15.91	14.95	16.16
CaO (%)	3.70	36.92	46.86	11.41	11.35	–
Fe_2O_3 (%)	5.63	2.89	0.97	9.80	11.30	11.10
K_2O (%)	0.14	0.26	0.22	0.16	0.14	0.14
MgO (%)	20.37	3.24	0.65	7.64	7.69	8.38
MnO (%)	0.72	0.13	0.13	0.17	0.17	0.16
Na_2O (%)	1.65	3.33	2.52	2.60	2.76	2.39
SiO_2 (%)	54.36	15.85	6.19	49.39	50.41	48.95
TiO_2 (%)	0.02	0.13	0.03	1.39	1.54	1.10
Ba (μg/g)	24590	947	987	17	23	–
Co (μg/g)	11	17	8	43	43	49
Cr (μg/g)	28	111	4	409	251	230
Cu (μg/g)	1566	124	57	67	75	93
Ni (μg/g)	25	79	15	124	97	143
Pb (μg/g)	170.4	5.8	6.5	2.8	0.5	2.0
Sn (μg/g)	17.06	0.41	0.21	1.07	0.79	–
Zn (μg/g)	212	38	19	84	87	95

Data from MORB and basalt are from Gale et al. (2013) and Liao et al. (2019), respectively.

of hydrothermal sedimentation (e.g., Marchig et al., 1982; Boström, 1983; Chen et al., 2004; Dias and Barriga, 2006; Slack et al., 2009; He et al., 2016; Liao et al., 2018b). The metalliferous index, calculated as Al/(Al + Fe + Mn), is helpful for distinguishing hydrothermal components in various sediments; for instance, the ratio decreases with increasing hydrothermal input. Generally, pelagic deep-sea sediments have a metalliferous index of >0.4, but metal-enriched sediments are less than 0.4 in this index (Boström, 1973, 1983). As shown in **Figure 3A**, all studied sediment samples plotted on the mixing line of the hydrothermal sediments (e.g., modern metalliferous sediments) and non-hydrothermal components (e.g., modern pelagic sediment, MORB, and upper continental crust)—the decreasing Fe/Ti ratio and increasing Al/(Al + Fe + Mn) ratio indicate that most sediments of the study area are mixtures of hydrothermal-pelagic-volcanic components (e.g., Dias and Barriga, 2006; Liao et al., 2018b). The sediments of group A are within a typical metalliferous hydrothermal domain [Al/(Al + Fe + Mn) ratio of <0.2] (**Figure 3A**); the high hydrothermal affinity in these OVF sediments is also evident in the Al–Fe–Mn ternary plot (**Figure 3B**). In addition, the Si/Al ratio is much higher in the sediments of group A (Si/Al of 27–70), compared with other groups that exhibited Si/Al ratios of 4–10, further supporting that these sediments are products of intense hydrothermal sedimentation from the OVF (Dias and Barriga, 2006). Meanwhile, the sediments of group B have a wide range of Al/(Al + Fe + Mn) ratios from ∼0.2 to 0.6, depending on the relative influence of the hydrothermal plume components. Hydrothermal sediments from the Rodrigues Triple Junction of CIR with the ratio of ∼0.25 are geochemically most similar to some sediments of group B with relatively strong hydrothermal influence (**Figures 3A,B**). In group B1, characteristically, some sediments (samples MC1706, MC1809, MC1705, and MC1914, **Figure 1C**) have much higher ratios of Al/(Al + Fe + Mn) (>0.4), which are close to the values of MORB as well as volcaniclastic particles. This result is also supported by the Al–Fe–Mn ternary plot (**Figure 3B**), suggesting that these sediments are predominantly composed of non-hydrothermal components (especially volcanic debris). Subsequently, the sediments of group A represent pronounced hydrothermal components of the OVF, while the group B1 sediments are mixtures of hydrothermal sediments and volcanic materials. Considering the low TOC, TS, and high $CaCO_3$ contents, the sediments of group B2 are primarily composed of typical calcareous pelagic sediments, including some hydrothermal components (Liao et al., 2019). The AHC analysis for average elemental concentrations of each sediment group and non-hydrothermal end-members (i.e., volcaniclastic particles, MORB, and upper continental crust) also supports this conclusion (**Figure 2B**). Besides, the overall elemental compositions of these volcaniclastic particles are similar to those of MORB and basalts. Therefore, the elemental composition of volcaniclastic particles collected from the studied samples is considered as end-member component of the ridge volcanism, which is representative of the MORB composition in the CIR. Here, we have established a set of element indicators for hydrothermal or volcanic sedimentation, including discrimination diagrams, which can be employed to more accurately estimate the source of elements, and thus to better understand the characteristic of hydrothermal vent fluid, especially in the ancient deep-sea ridge deposits.

Controlling Factors of Elemental Compositions

Principal component analysis in this study revealed three key components that explained 87% of the total variance (**Table 3**).

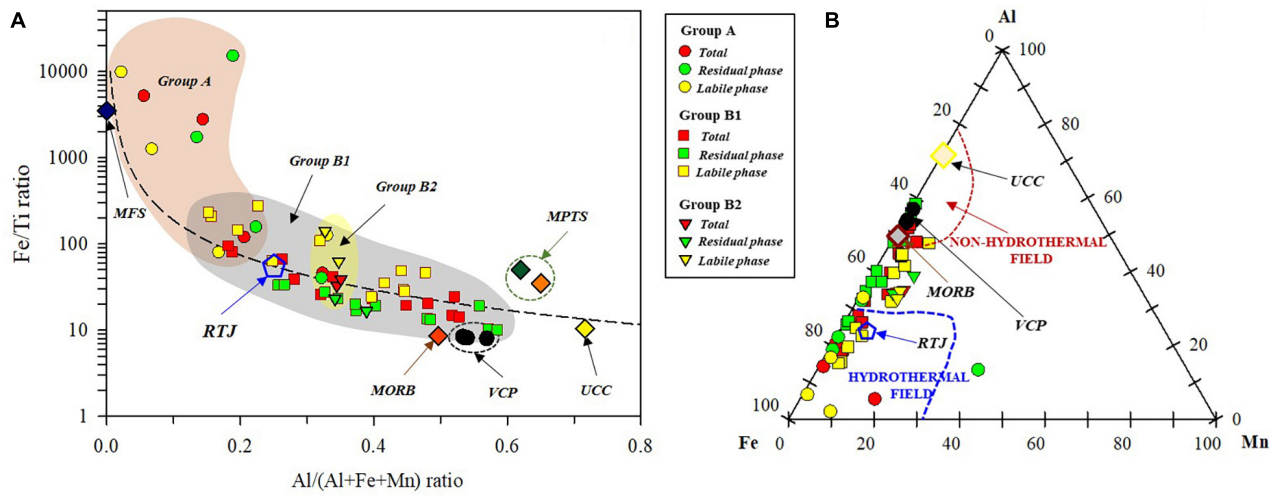

FIGURE 3 | (A) Al/(Al + Fe + Mn) vs. Fe/Ti discrimination diagram of mixing hydrothermal metalliferous sediments with deep-sea sediments (after Marchig et al., 1982; Boström, 1983). Curved line represents ideal mixing between Al-free hydrothermal sediment (MFS) and modern pelagic or terrigenous sediments (MPTS). **(B)** Ternary Fe–Mn–Al diagram indicating the hydrothermal affinity of the OVF sediments (after Adachi et al., 1986). RTJ, Average value of core top sediments from the Rodrigues Triple Junction (RTJ), Central Indian Ocean (Kuhn et al., 2000); UCC, upper continental crust (Taylor and McLennan, 1985); MORB, mid-ocean ridge basalt (Gale et al., 2013); VCP, volcaniclastic particles (this study).

TABLE 3 | Results of principal component analysis for the sediment dataset and percentage of variance explained for the individual factor loadings (>0.5 value).

	Factor 1	Factor 2	Factor 3
Eigenvalue	9.8	5.4	3.2
Variability (%)	35	25	28
TN (μg/g)	0.65	–0.06	0.61
TOC (μg/g)	0.05	0.12	0.71
TS (μg/g)	0.96	–0.20	–0.04
$CaCO_3$ (%)	–0.82	–0.29	–0.46
Al_2O_3 (%)	–0.01	0.95	–0.05
CaO (%)	–0.84	–0.22	–0.47
Fe_2O_3 (%)	0.14	0.35	0.90
K_2O (%)	–0.52	0.54	–0.03
MgO (%)	0.91	0.05	0.39
MnO (%)	–0.03	–0.03	0.94
Na_2O (%)	–0.73	0.45	–0.13
SiO_2 (%)	0.85	0.16	0.32
TiO_2 (%)	–0.09	0.90	–0.15
Ba (μg/g)	0.96	–0.22	0.09
Cr (μg/g)	0.04	0.92	–0.06
Cu (μg/g)	0.29	–0.13	0.93
Ni (μg/g)	–0.04	0.88	0.04
Zn (μg/g)	0.32	–0.02	0.94
Co (μg/g)	–0.08	0.94	0.25
Pb (μg/g)	0.43	–0.19	0.87
Sn (μg/g)	0.94	–0.16	0.07

Factor 1 (35% of the total variance) was highlighted by high positive loadings for TS, Si, Mg, Ba, and Sn, which are largely enriched in the sediments of group A (i.e., the OVF hydrothermal sediments). The high concentrations of SiO_2 (45–68%) and MgO (14–25%), as well as the good affinity (r^2 = 0.80) between these elements, imply the presence of hydrothermal phyllosilicate minerals (e.g., talc and serpentine). Indeed, the presence of talc {$[Mg_3Si_4O_{10}(OH)_2]$, 63.5% SiO_2, 31.7% MgO, and 4.8% H_2O} in the OVF deposits was confirmed by XRD and SEM analyses (**Figures 4A–F**, **5A**). Bulk XRD analyses of the massive, globular, and white-colored aggregates (up to 5 mm in size, **Figures 4A–C**) separated from the group A sediments showed peaks at approximately 9.6 Å (for the 001 plane) and 4.7 Å, confirming talc as the dominant phase (**Figure 5A**). SEM observations also revealed that these minerals are characterized by predominant platy and flaky texture, resulting in the formation of boxwork- or honeycomb-like structures (**Figures 4D,E**). SEM-EDS microanalysis of two talc granules (n = 33 points) yielded the following average composition results (**Figure 4F**): 53.6 ± 4.4% (39.0–58.6%) of Si, 33.2 ± 3.7% (24.9–38.2%) of Mg, 9.7 ± 6.7% (3.3–34.2%) of Fe, 2.3 ± 0.5% (1.1– 3.4%) of Al, 0.7 ± 1.4% (0.0–3.9%) of Cu, and 0.5 ± 0.4% (0.2–2.2%) of Ca. Si and Mg contents at >85% and the high Si/Mg molar ratio (average: 1.41, range: 1.24–1.72)—which is close to or slightly higher than that of pure magnesian talc (1.33)—demonstrated that the talc invariably has an almost pure end-member composition. The slightly higher Si/Mg ratios may be associated with the amorphous silica (>95% in SiO_2, opal-A) frequently observed inside talc (**Supplementary Figures 1A–C**). Accordingly, the abundant occurrence of talc is reflected in the whole sediment geochemistry by the high concentrations of Si and Mg.

Another remarkable feature of Factor 1 is the presence of significant correlations among TS, Ba, and Sn, suggesting that they are mainly derived from hydrothermal barites ($BaSO_4$, **Figures 4G–L**, **5B**); the importance of this mineral is discussed in section "Hydrothermal Barite." This preliminary result demonstrated that hydrothermal minerals have a substantial effect on these elemental concentrations and spatial distributions. Notably, $CaCO_3$, Ca, K, and Na with high negative loadings may be highly dependent on the amounts of the biogenic components and/or seawaters included in the sediments (**Table 3**). The labile phase of these elements comprises more than 90% of the total concentration and is uniform across all sediments without spatial distribution trend.

Factor 2 (25% of the total variance) exhibited significant positive component loadings for Al, Co, Cr, K, Ni, and Ti (**Table 3**), as well as good correlations among them (**Supplementary Figure 2**). Their concentrations were significantly higher in the sediments of group B1 (**Table 2**), including volcaniclastic particles commonly dispersed in mid-ocean ridge sediments. As discussed above, these particles from the study area are characterized by significantly higher Al, Cr, Ni, and Ti concentrations, as well as lower K concentrations, compared with the surrounding sediments. On the basis of K_2O/TiO_2 ratio (average: 0.11), the volcaniclastic particles from the study area may correspond to the transitional MORB (Marty and Zimmermann, 1999). Therefore, the elemental components of Factor 2 may result from a contribution of volcanic materials (e.g., pyroclastic shard particles) from the ridge volcanism around the OVF (Kuhn et al., 2000; Lim et al., 2020, 2021; Chen et al., 2021).

Factor 3 (28% of the total variance) showed positive loadings for TN, TOC, Fe, Mn, Cu, Pb, and Zn; their concentrations are highest in group A (**Tables 2**, **3**). Considering the excellent covariation among them (**Supplementary Figure 2**) and the increased enrichment of the elements in the sediments of group A proximal to the vent field, hydrothermal-derived materials (e.g., Fe–Mn oxyhydroxides and/or sulfides associated with organic matter) may be the primary controlling factor in the concentrations of these elements and their spatial distributions (Chen et al., 2021). However, biogenic and volcanic influences on these elements are generally minor. In conclusion, the OVF hydrothermal sediments (group A) are characterized by high concentrations of TS, Si, Mg, and Ba derived from talc and barite minerals, as well as Fe, Mn, and some trace elements from the Fe–Mn oxides and/or sulfides; but, Al, K, Na, Ti, Co, Ni, and Cr are likely from ridge volcanisms.

Stable Carbon and Sulfur Isotopes

The $\delta^{13}C$ and $\delta^{34}S$ values of the surface sediments in the study area show a distinct difference between the sediment groups (**Figure 6**). The $\delta^{13}C$ in the hydrothermal sediments of group A (–25.20 to –22.47‰) exhibit lighter isotope values, compared with the sediments of group B (–21.29 to –19.77‰), within the range of marine plankton (–22 to –20‰, Imbus et al., 1992;

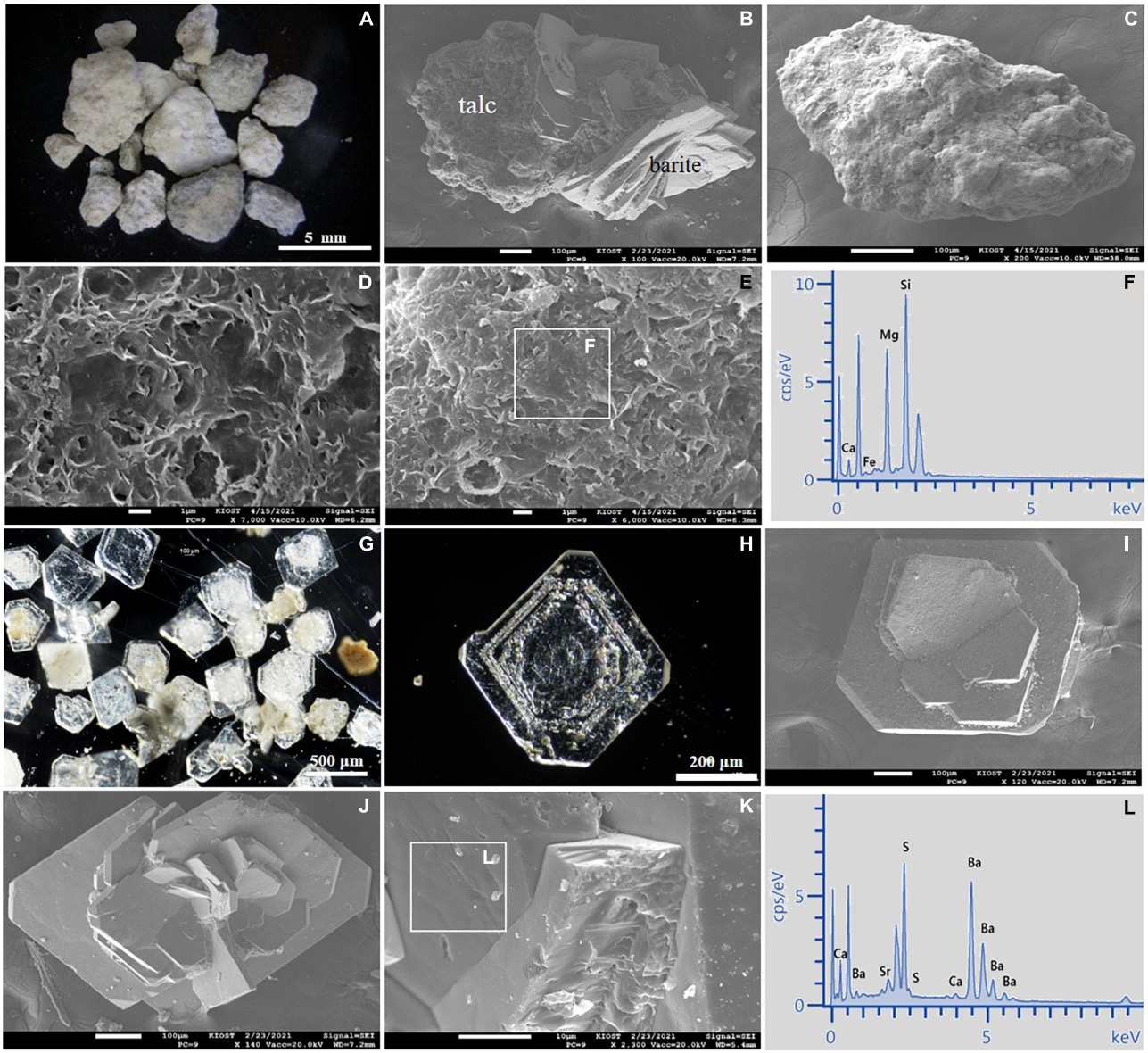

FIGURE 4 | (A) Microscopic photograph and **(B–E)** SEM-BSI images of talc samples from the OVF surface sediments (BC1903 and GTV1904). **(G,H)** Microscopic photographs and **(I–K)** SEM-BSI images of barite samples from the OVF surface sediment (GTV1904). **(F,L)** EDS analysis of talc and barite sample, respectively.

Walinsky et al., 2009). The $\delta^{13}C$ values of hydrothermal vent fluid for CH_4 at the East Pacific Rise and the southern Juan de Fuca ridge ranged from −20.8 to −15.0‰ and −50.8 to −43.2‰ at the Guaymas Basin (Shanks et al., 1995 and reference therein). In contrast, the $\delta^{13}C$ values of the hydrothermal vent fluid for CO_2 are mostly higher than approximately −10‰ (Shanks et al., 1995 and references therein; Shanks, 2001). Thus, the lower $\delta^{13}C$ value in the hydrothermal sediments—particularly compared with the value in marine plankton—suggests some contributions of organic carbon from the benthic fauna that depend on methane-oxidizing (methanotrophic) metabolism (Kennicutt et al., 1992). This interpretation is also confirmed by the sulfur isotopic composition and a close linkage ($r^2 = 0.78$) between the $\delta^{13}C$ and $\delta^{34}S$ values (**Figure 6**).

In the sediments of group B with a comparatively low S/C ratio (<0.5), the $\delta^{34}S$ value ranged from +19 to +23‰ (average: +21.03‰), corresponding to the values of present-day seawater (+21.0 ± 0.2‰, Rees et al., 1978) and marine phytoplankton (+ 15 to +20‰, Shanks et al., 1995), which assimilate sulfate; however, the $\delta^{34}S$ value of the group B sediments is much higher than that of bacteriogenic pyrite (approximately −15‰, Krouse, 1980; Kaplan, 1983). Assimilatory reduction occurs in autotrophic organisms where sulfur is incorporated in proteins, particularly as S^{2-} in amino-acids, the bonding of the produced

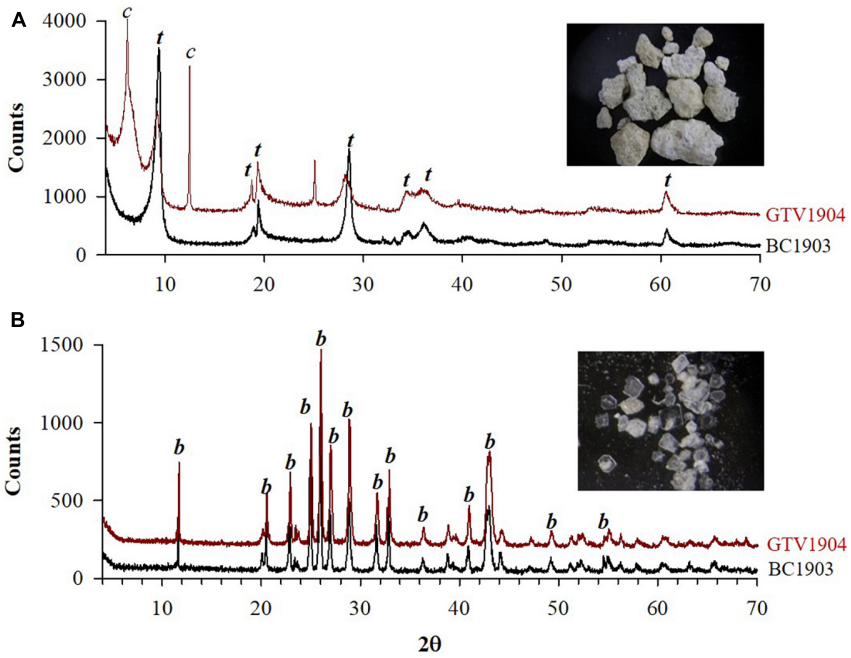

FIGURE 5 | X-ray diffraction spectra of **(A)** talc and **(B)** barite grain samples from the OVF surface sediments. t, talc peaks; c, chlorite peaks; b, barite peaks.

sulfur is similar to the dissolved sulfate ion, and fractionations are small (+0.5 to −4.5‰, Kaplan, 1983). Considering that the $\delta^{34}S$ value of organic sulfur in extant marine organisms incorporated by assimilatory processes is generally depleted by 0–5‰ relative to the ocean (Paytan and Gray, 2012), most sulfur in the sediments of group B appears to exist as organosulfur compounds by the biological assimilation of seawater sulfate (Oduro et al., 2012).

Importantly, the $\delta^{34}S$ values (+13 to +15‰) of the hydrothermal sediments (group A) of the OVF are significantly depleted, compared with the group B sediments. The $\delta^{34}S$ values of group A are much higher than those of basaltic oceanic crust (−1 to +1‰, Shanks et al., 1995), but are similar to or slightly higher than the upper limit value of the compositional range (−7.0 to +13.8‰, mostly −0.8 to +10.2‰) of primary sulfides from modern mid-ocean ridge hydrothermal fields (Melekestseva et al., 2014 and references therein; Fan et al., 2021 and references therein). In the study area, moreover, $\delta^{34}S$ values decrease as TS contents increase ($r^2 = 0.5$). In hydrothermal vent areas of mid-ocean ridges, most sulfur occurs predominantly as sulfide minerals, which often formed as the result of biogenic processes, and to a lesser extent, as organically bound sulfur. The biogenic processes are dominated by reduction during early diagenesis of seawater sulfate to form sulfides (e.g., pyrite) by sulfur-reducing bacteria, resulting in substantial isotopic fractionation, which ranges from 15 to 60‰ (average: 40‰, Shanks et al., 1995; Peters et al., 2011), leading to negative $\delta^{34}S$ values (e.g., Alt and Shanks, 2011). In most sediment-starved mid-ocean ridges, moreover, hydrothermal sulfides with basaltic sulfur as the principal source have $\delta^{34}S$ values from 0 to +7‰ (Herzig et al., 1998; Shanks, 2001). Thus, the lighter sulfur isotopic composition in the sediments of group A with high TS contents indicates a sulfur contribution from hydrothermal sulfides with the relatively low $\delta^{34}S$ value that is closely linked to bacterial sulfate reduction of seawater and/or thermochemical sulfate reduction. A comparatively very high sulfur/carbon ratio (1–6) in this group further supports the contribution of hydrothermal sulfide (Imbus et al., 1992). The relatively low $\delta^{34}S$ value in the sediments of group A, accordingly, reflects the mixed contribution of isotopically depleted sulfides (e.g., bacteriogenic pyrite) and enriched marine biomass (e.g.,

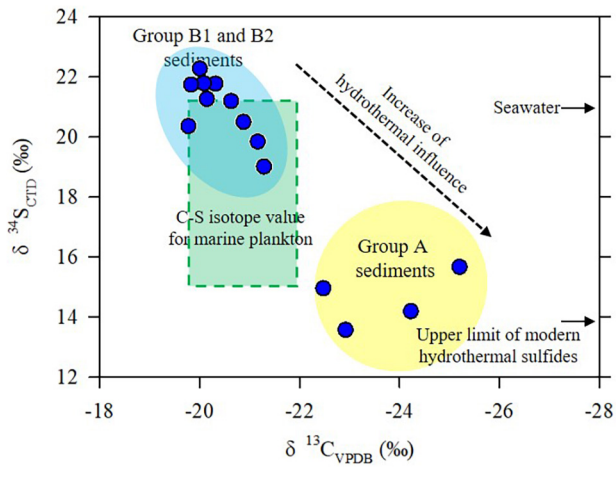

FIGURE 6 | Stable carbon ($\delta^{13}C$) and sulfur ($\delta^{34}S$) isotopic compositions of the bulk surface sediment samples from the OVF.

organosulfur compounds). Considering the abundant occurrence of barite with $\delta^{34}S$ similar to seawater (details provided in section "Hydrothermal Barite"), the sulfate mineral may act in the direction of increasing $\delta^{34}S$ value. Our finding reveals that paired carbon-sulfur isotopic compositions along with the elemental signature are useful precursors for better recognition of hydrothermal input in deep-sea sediments; the hydrothermal sediments are characterized by much lighter values in all stable isotopes, compared with the surrounding deep-sea sediments and seawater.

Hydrothermal Barite

Barite with a transparent, tubular form and a high degree of crystallinity was abundantly present in some hydrothermal sediments of group A (**Figures 4G,H**, **5B**). In hydrothermal environments, in general, pure barite is formed by the mixture of vent fluid and seawater (Paytan et al., 2002; Eickmann et al., 2014; Jamieson et al., 2016; Zhang et al., 2020), and its isotope compositions cannot fractionate during and after crystallization (Paytan et al., 1993). Thus, the occurrence of barite in the surface sediments represents direct evidence of the OVF hydrothermal activity; furthermore, its chemical-isotopic compositions provide insights for better characterizing this hydrothermal system. To our knowledge, there have been no reports of barite in the Indian ridge hydrothermal fields. SEM observation has shown that barites occur in a typical rosette morphology consisting of tabular or plate crystals with mainly hexagonal forms, with sizes varying from approximately 100–500 μm (**Figures 4I–K**). EDS microanalysis to achieve chemical characterization of barite (n = 22 points in two representative barite grains) has shown average contents of 76.5 ± 3.0% (72.6–80.8%) for Ba, 19.0 ± 2.8% (15.0–22.3%) for S, and 4.1 ± 1.0% (2.3–5.2%) for Sr (**Figure 4L**). More than 90% of barite consists of Ba and S, and the Ba/S molar ratio of the samples (average: 1.07, range: 0.83–1.30) is close to that of pure barite.

Eickmann et al. (2014) proposed a scheme for differentiating the various mechanisms of barite precipitation based on sulfur and strontium isotope compositions, and we added our results to their dataset (**Figure 7**). The $\delta^{34}S$ values of the OVF barite samples ranged from +21.2 to +23.0‰ (average + 22.3 ± 0.5‰, n = 20 barite samples), which are comparable with, but slightly higher than, $\delta^{34}S$ value of present-day seawater (+21.0 ± 0.2‰, Rees et al., 1978). However, these values are much lower than those of diagenetic barites (+24 to +59‰, Paytan et al., 2002), although they are more radiogenic than hydrothermal fluid (approximately 0‰) (**Figure 7**). In principle, the $\delta^{34}S$ value (e.g., +16.1 to +16.7‰, Herzig et al., 1998) of barite associated with the sulfides should be significantly lighter than that of seawater. As presented above, the $\delta^{34}S$ values of barite are higher than those of group A hydrothermal sediments containing some sulfide minerals, but are similar to those of the group B sediments (average: +21.0 ± 0.9‰) that are related with the organosulfur compounds by the biological assimilation of seawater sulfate. There is increasing evidence that barite precipitation induced by hydrothermal activity yields $\delta^{34}S$ values that are similar to or slightly lower than the value of seawater sulfate (Paytan et al., 2002; De Ronde et al., 2003; Eickmann et al., 2014); however, barite that precipitates from fluids modified by microbial sulfate reduction exhibits higher $\delta^{34}S$ values than the value of seawater sulfate (Wortmann et al., 2007; Feng and Roberts, 2011; Griffith and Paytan, 2012). Therefore, the results indicate that barite precipitation in the OVF may result from the hydrothermal reduction of seawater sulfate accompanied by the isotopic enrichment of the residual sulfate (Shanks et al., 1995) and/or involvement of weak biogenic processes in barite formation (Paytan et al., 2002).

To identify the origin of Ba in barite and to further confirm a hydrothermal contribution, the Sr isotopic ($^{87}Sr/^{86}Sr$) composition in barite grains was examined. The $^{87}Sr/^{86}Sr$ values of barites ranged from 0.70569 to 0.70753 (average: 0.70641 ± 0.00067), although most barite samples were within the range of 0.70606–0.70753. This range is slightly lower than the value of seawater (0.70917, Butterfield et al., 2001) and surface sediments from the CIR (average: 0.70944, range: 0.70810–0.71027, Anand et al., 2019), but is considerably higher than the ranges of CIR and Southwest Indian Ridge basalts (average: 0.70285 ± 0.00029 and 0.70494 ± 0.00037, respectively, Michard and Albarède, 1986) and volcanic glass samples (0.70297, Price et al., 1986). As presented in **Figure 7**, the $^{87}Sr/^{86}Sr$ values of the OVF barites overlap with those of other hydrothermal barites that have distinctive Sr isotope values that are much less radiogenic than seawater (Eickmann et al., 2014). In general, the Sr isotope compositions of barites from sediment-free hydrothermal fields are between those of basement rocks and seawater. In contrast, barites from the thick sediment-covered hydrothermal field have an unusually higher $^{87}Sr/^{86}Sr$ value (0.71284–0.71749, Zhang et al., 2020) than seawater and associated basement rock, indicating interactions between hydrothermal fluid and local sediments. Therefore, the strontium isotope composition of barites from the sediment-free OVF hydrothermal field, which lies between the compositions of seawater and MORB or peridotite (**Figure 7**), reflects the sufficient fluid/seawater interaction in this region.

Based on simple mixing calculation using the Sr contents and isotopic values of end-members (seawater, gabbro, and barite), the relative contributions of hydrothermal fluid and seawater in the mixing fluid were estimated by applying a simple two-component mixing model as follows (Kuhn et al., 2003; Zhang et al., 2020):

$$\begin{aligned} HF(\%) = 100 \times Sr_{SW}((^{86}Sr/^{87}Sr)_{SW} - (^{86}Sr/^{87}Sr)_{BA})/ \\ (Sr_{SW}((^{86}Sr/^{87}Sr)_{SW} - (^{86}Sr/^{87}Sr)_{BA}) + \\ Sr_{HF}((^{86}Sr/^{87}Sr)_{BA} - (^{86}Sr/^{87}Sr)_{HF})) \end{aligned}$$

where HF (%) is the proportion of hydrothermal fluid, and Sr_{SW} and Sr_{HF} are Sr concentrations of seawater (89.9 μmol kg^{-1}; Gallant and Von Damm, 2006) and hydrothermal fluid, respectively. The $(^{86}Sr/^{87}Sr)_{SW}$, $(^{86}Sr/^{87}Sr)_{BA}$, and $(^{86}Sr/^{87}Sr)_{HF}$ are Sr isotope ratios for seawater (0.70917), barite, and hydrothermal fluid, respectively. For Sr concentration and isotopic ratio of hydrothermal fluid, values of the ultramafic-hosted Kairei hydrothermal fluid (75.3 μmol kg^{-1}, Gallant and Von Damm, 2006) and the gabbro from the CIR (0.70287,

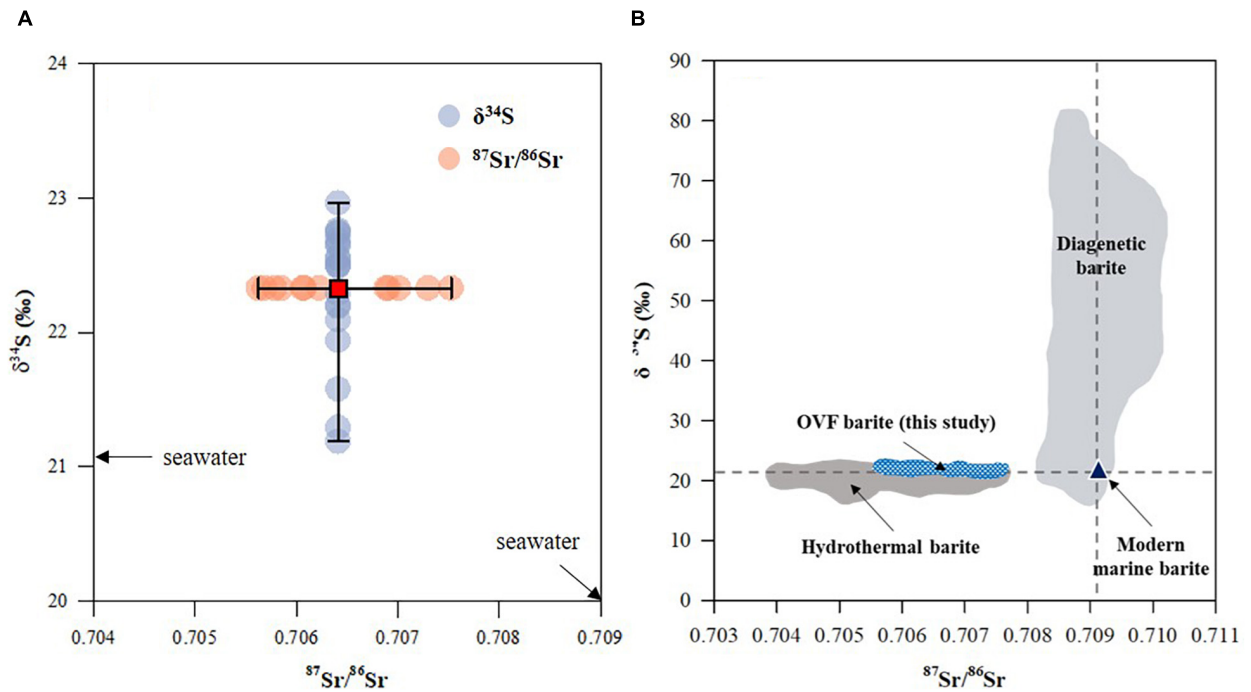

FIGURE 7 | (A) Strontium ($^{87}Sr/^{86}Sr$) and sulfur ($\delta^{34}S$) isotopic compositions of the OVF barite samples. **(B)** Plot of Sr and S isotope values for discriminating the origin of barite (after Eickmann et al., 2014). Note that the OVF barite samples plotted in the field of known hydrothermal barite and were clearly distinctive from the diagenetic barite.

Ray et al., 2011) near the study area, respectively, were used. The results showed that the average contribution of hydrothermal fluid is estimated to be approximately 50% (range: 30–60%), even though there are uncertainties in values of hydrothermal fluid, implying that the physiochemical condition of mixing fluid changes considerably during the mineralization process. From such isotopic signatures, we concluded that the OVF hydrothermal barite was a primary precipitate from Ba-rich hydrothermal fluid mixed with seawater, which contrasts to marine barite precipitated in the water column and diagenetic barite precipitated at the oxic-anoxic boundary within sediments in association with sulfate-reducing conditions.

Characteristics of Onnuri Vent Field Hydrothermal System

The off-axis, ultramafic-hosted OVF has been primarily considered to be a low-temperature diffuse venting system (Kim et al., 2020). However, our results, together with plume chemistry data, suggest that the OVF has the characteristic of a high-temperature venting system with a weak or no magmatic heat source. Hydrothermal vent fluids associated with serpentinization of upper mantle peridotite are typically characterized by unusually high concentrations of abiogenic H_2 and CH_4, a high CH_4/Mn ratio, and much lower dissolved silicate concentrations, compare with basalt-hosted hydrothermal system (Donval et al., 1997; Kelley et al., 2001; Charlou et al., 2002 and references therein). In particular, the serpentinization reaction, especially at OCCs distant from the ridge axis, is capable of driving non-volcanic hydrothermal circulation (e.g., Rona et al., 1987; Grácia et al., 2000; Lowell and Rona, 2002; Kelley et al., 2005; Dias and Barriga, 2006; Hodgkinson et al., 2015). It is likely to occur in the OVF hydrothermal system hosted by serpentinized-peridotites and gabbros exposed by detachment faults; manifestation of such extensive reaction in this vent field can be inferred from the high CH_4 enrichment, high CH_4/Mn ratio, and negligible dissolved metal concentration in the vent plume (Kim et al., 2020). This nature of OVF system is better characterized by the massive occurrence and geochemistry of typical talc and barite minerals from hydrothermal sediments.

Considering the predominant occurrence of fragile talc granules with pure end-composition and boxwork-like microstructure, as well as other results (i.e., minor occurrence of sulfide minerals, absence of magnesite, and absence of sediment cover), the talc presumably precipitates directly from Si-rich hydrothermal fluids that seep out directly from the serpentinized-peridotites/gabbro reaction zone, rather than originating from the hydrothermal alteration of ultramafic rocks including the serpentinite (D'Orazio et al., 2004; Dias and Barriga, 2006; Hodgkinson et al., 2015). This prediction is further supported by the $^{87}Sr/^{86}Sr$ ratios (0.706156–0.707549, n = 6, Lim et al. unpublished data) for the talc samples form the OVF, which are similar to (but slightly less than) the ratio of present-day seawater (0.70917) and the Von Damm

Vent Field talc samples (0.706313–0.709168, Hodgkinson et al., 2015) that precipitated directly as a result of mixing between vent fluid and seawater. This implies that a substantial component of seawater was mixed with the vent fluids during the talc precipitation. Moreover, a manifestation of such direct precipitation of talc from the fluids mixed with seawater at the vent may be inferred from the presence of amorphous silica (**Supplementary Figures 1C,D**); for instance, Hodgkinson et al. (2015) proposed the possibility of instantaneous precipitation of talc and silica as the primary phases in mixing the hot (∼215°C) vent fluid with cold seawater in the Von Damm Vent Field. At the OVF, the low metal content of the fluid may only result in accessory amounts of metal sulfides, possibly allowing talc to become the dominant phase. In many respects (e.g., geological conditions conducive to serpentinization, CH_4-rich fluid composition, and talc-dominated mineral deposits), the OVF system is comparable with the Von Damm, Lost City, St. Paul F.Z., and Saldanha hydrothermal vent fields, which are representative hydrothermal systems driven by the serpentinization reaction (Kelley et al., 2001, 2005; D'Orazio et al., 2004; Dias and Barriga, 2006; Hodgkinson et al., 2015). Accordingly, the precipitation of talc mineral is linked to the activity of the serpentinite/gabbro-hosted hydrothermal system, indicating that talc-dominated vent deposits may be considered an indicator of active off-axis hydrothermal fields, possibly sustained by serpentinization in the slow- and ultra-slow spreading CIR ridges where the basaltic magma flux is weakest.

Although the high CH_4 concentration suggests that serpentinization of the ultramafic rocks comprising the OVF basement has influenced fluid composition, the precipitation of barite indicates that the OVF hydrothermal fluids were likely influenced by interaction with mafic rocks (e.g., gabbro). Overall the ultramafic-hosted hydrothermal systems appear to be generally poor in Ba and barite because the Ba released from the hydrothermal leaching of ultramafic rocks is considerably limited, thereby resulting in precipitation of barite-free mineral assemblages (Noguchi et al., 2011; Melekestseva et al., 2014). This was also corroborated in seawater/peridotite thermodynamic reaction model and experimental studies, demonstrating that the ultramafic-hosted hydrothermal system cannot produce significant barite precipitates (Melekestseva et al., 2014 and references therein). Therefore, a mafic origin for the OVF barite appears most likely and is consistent with the presence of gabbroic rocks that were commonly dredged in and around the vent site. As discussed above, such evidence also exists for the talc formation, which is closely linked to interactions with Si-rich hydrothermal fluids, representing mafic components derived from interactions with gabbroic rocks within a peridotite-dominated ridge segment.

Accumulated evidence from several hydrothermal deposits, including the Grimsey and Guaymas Vent Fields, has revealed that the estimated temperature of talc formation in the hydrothermal environments is typically within the range of 250–370°C (Koski et al., 1985; D'Orazio et al., 2004 and references therein; Boschi et al., 2008; Dekov et al., 2008 and references therein). Considering these previous results, the talc-dominated OVF may be a comparatively high-temperature hydrothermal system; this is also roughly consistent with the barite precipitation condition (approximately 240°C at maximum temperature, Melekestseva et al., 2014). This is supported, to some extent, by the abundant occurrence of breccia-type sulfides with Cu-bearing secondary minerals in the OVF, indicative of episodically higher vent temperatures (e.g., >200°C, Kim et al., 2020). In fact, this speculation is confirmed by the temperature (160–250°C, Lim et al. unpublished data) measured in the subsurface sediment layer (5 cm in sediment depth) of the OVF region using ROV. This high temperature of the OVF vent fluid is approximately equal to the temperature of heat released from the exothermic serpentinization reaction (150–250 °C, Batch et al., 2002; Alt et al., 2007; Boschi et al., 2008). However, the low fluid temperature at the escape orifices (∼4–12°C, Lim et al., unpublished data) is probably a consequence of cooling effects during conductive circulation and seawater interactions in the diffuse vent system; in general, many hydrothermal fields include both high-temperature vents in the center and low-temperature vents near the perimeter (e.g., Dias and Barriga, 2006; Chen et al., 2018 and reference therein). Subsequently, the occurrence of barite and talc minerals in the hydrothermal sediments support that the OVF is a high temperature hydrothermal circulation system driven by serpentinization. Furthermore, this conclusion suggests that the serpentinization process can heat up circulating water to >200°C, even though some authors argued that this process does not produce enough heat to explain peridotite-hosted hydrothermal systems (e.g., Batch et al., 2002; Lowell and Rona, 2002; Allen and Seyfried, 2003).

CONCLUSION

Considering the presence of serpentinized-peridotite, a strong methane anomaly, an apparent lack of a magmatic heat source, and the predominant occurrence of talc and barite, we conclude that the serpentinization of exposed mantle rocks along the detachment faults likely plays a key role in the OVF hydrothermal circulation. Unlike the early study that described the OVF as a low-temperature hydrothermal venting system, our results reveal that the studied diffuse vent is the high-temperature system of >200°C. Considering the widespread occurrence of OCCs in the CIR, the OVF may be a representative off-axis peridotite-hosted hydrothermal system in the CIR, characterized by talc-dominated mineralization. Our study yields important geochemical data regarding hydrothermal sediments and minerals that provide a unique perspective on the ultramafic-hosted hydrothermal system in an off-axis OCC setting with a non-magmatic heat source, which was previously poorly investigated in the CIR.

DATA AVAILABILITY STATEMENT

The original contributions presented in the study are included in the article/**Supplementary Material**, further inquiries can be directed to the corresponding author/s.

AUTHOR CONTRIBUTIONS

DL and JoK contributed to conception and design of the study and wrote the first draft of the manuscript. LZ, KK, and JiK performed the analyses and organized the data. All authors contributed to manuscript revision, read, and approved the submitted version.

FUNDING

This work was supported by the Ministry of Oceans and Fisheries, South Korea, as part of the project titled 'Understanding the deep-sea biosphere on seafloor hydrothermal vents in the Indian Ridge' (Grant Number 20170411), the National Research Foundation of Korea (NRF) grant (2021R1A2C1014443) funded by the Ministry of Science and ICT of Korea government and the Strategic Priority Research Program of the Chinese Academy of Sciences (XDB42000000 and XDB40010100).

ACKNOWLEDGMENTS

We sincerely thank scientists and crews of the RV/LISABU for their support during the sampling and data collection. We would also like to appreciate the reviewers whose comments allowed us to greatly improve this manuscript.

SUPPLEMENTARY MATERIAL

The Supplementary Material for this article can be found online at: https://www.frontiersin.org/articles/10.3389/fmars.2022.810949/full#supplementary-material

REFERENCES

Adachi, M., Yamamoto, K., and Sugisaki, R. (1986). Hydrothermal cherts and associated silicious rocks from northern Pacific: their geological significance as indication of ocean ridge activity. *Sed. Geol.* 47, 125–148. doi: 10.1016/0037-0738(86)90075-8

Allen, D. E., and Seyfried, W. E. Jr. (2003). Compositional controls on vent fluids from ultramafic-hosted hydrothermal systems at mid-ocean ridges: an experimental study at 400°C, 500 bars. *Geochim. Cosmochim. Acta* 67, 1531–1542. doi: 10.1016/S0016-7037(02)01173-0

Alt, J. C., and Shanks, W. C. (2011). Microbial sulfate reduction and the sulfur budget for a complete section of altered oceanic basalts, IODP Hole 1256D (eastern Pacific). *Earth Planet. Sci. Lett.* 310, 73–83. doi: 10.1016/j.epsl.2011.07.027

Alt, J. C., Shanks, W. C., Bach, W., Paulick, H., Garrido, C. J., and Beaudoin, G. (2007). Hydrothermal alteration and microbial sulfate reduction in peridotite and gabbro exposed by detachment faulting at the Mid-Atlantic Ridge, 15°20′N (ODP Leg 209): A sulfur and oxygen isotope study. *Geochem. Geophys. Geosyst.* 8:Q08002. doi: 10.1029/2007GC001617

Anand, S. S., Rahaman, W., Lathika, N., Thamban, M., Patil, S., and Mohan, R. (2019). Trace Elements and Sr, Nd Isotope Compositions of Surface Sediments in the Indian Ocean: An Evaluation of Sources and Processes for Sediment Transport and Dispersal. *Geochem. Geophys. Geosyst.* 20, 3090–3112. doi: 10.1029/2019GC008332

Batch, W., Garrido, C. J., Paulick, H., Harvey, J., and Rosner, M. (2002). Seawater-peridotite interactions: First insights from ODP Leg 209, MAR 15°N. *Geochem. Geophys. Geosyst.* 5:Q09F26. doi: 10.1029/2004GC000744

Beaulieu, S., Baker, E. T., and German, C. R. (2015). Where are the undiscovered hydrothermal vents on oceanic spreading ridges? *Deep Sea Res. Part II* 121, 202–212. doi: 10.1016/j.dsr2.2015.05.001

Beaulieu, S., Baker, E. T., German, C. R., and Maffei, A. (2013). An authoritative global database for active submarine hydrothermal vent fields. *Geochem. Geophys. Geosyst.* 14, 4892–4905. doi: 10.1002/2013GC004998

Boschi, C., Dini, A., Früh-Green, G. L., and Kelley, D. S. (2008). Isotopic and element exchange during serpentinization and metasomatism at the Atlantis Massif (MAR 30°N): Insights from B and Sr isotope data. *Geochim. Cosmochim. Acta* 72, 1801–1823. doi: 10.1016/j.gca.2008.01.013

Boström, K. (1973). The origin and fate of ferromanganoan active ridge sediments. *Stockh. Contrib. Geol.* 27, 149–243.

Boström, K. (1983). "Genesis of Ferromanganese Deposits—Diagnostic Criteria for Recent and Old Deposits," in *Hydrothermal Processes at Seafloor Spreading Centers*, ed. P. A. Rona (Berlin: Springer), 473–489. doi: 10.1007/978-1-4899-0402-7_20

Butterfield, D. A., Nelson, B. K., Wheat, C. G., Mottl, M., and Roe, K. (2001). Evidence for basaltic Sr in mid ocean ridge flank hydrothermal systems and implications for the global oceanic Sr isotope balance. *Geochim. Cosmochim. Acta* 65, 4141–4153. doi: 10.1016/S0016-7037(01)00712-8

Catanzaro, E. J., Murphy, T. J., Garner, E. L., and Shields, W. R. (1969). Absolute isotopic abundance ratio and atomic weight of terrestrial rubidium. *J. Res. Natl. Bur. Stand. A* 73, 511–516. doi: 10.6028/jres.073A.041

Cave, R. R., German, C. R., Thomson, J., and Nesbitt, R. W. (2002). Fluxes to sediments underlying the Rainbow hydrothermal plume at 36°14′N on the Mid-Atlantic Ridge. *Geochim. Cosmochim. Acta* 66, 1905–1923. doi: 10.1016/S0016-7037(02)00823-2

Charlou, J. L., Donval, J. P., Fouquet, Y., Jean-Baptiste, P., and Holm, N. (2002). Geochemistry of high H_2 and CH_4 vent fluids issuing from ultramafic rocks at the Rainbow hydrothermal field (36°14′N, MAR). *Mar. Geol.* 191, 345–359. doi: 10.1016/S0009-2541(02)00134-1

Chen, J. F., Sun, S. L., Liu, W. H., and Zheng, J. J. (2004). Geochemical characteristics of organic matter-rich strata of lower Cambrian in Tarim Basin and its origin. *Sci. China Ser. D Earth Sci.* 47, 125–132. doi: 10.1360/04zd0031

Chen, J., Tao, C., Liang, J., Liao, S., Dong, C., Li, H., et al. (2018). Newly discovered hydrothermal fields along the ultraslow spreading Southwest Indian Ridge around 63°E. *Acta Oceanol. Sin.* 37, 61–67. doi: 10.1007/s13131-018-1333-y

Chen, X., Sun, X., Wu, Z., Wang, Y., Lin, X., and Chen, H. (2021). Mineralogy and geochemistry of deep-sea sediments from the ultraslow-spreading Southwest Indian Ridge: Implications for hydrothermal input and igneous host rock. *Minerals* 11:138. doi: 10.3390/min11020138

Choi, S. K., Park, S. J., Kim, J., Park, J.-W., and Son, S.-K. (2021). Gold and tin mineralisation in the ultramafic-hosted Cheoeum vent field, Central Indian Ridge. *Miner. Deposita* 56, 885–906. doi: 10.1007/s00126-020-01012-5

Cronan, D. S., and Hodkinson, R. A. (1997). Geochemistry of hydrothermal sediments from ODP Sites 834 and 835 in the Lau Basin, southwest Pacific. *Mar. Geol.* 141, 237–268. doi: 10.1016/S0025-3227(97)00071-6

D'Orazio, M., Boschi, C., and Brunelli, D. (2004). Talc-rich hydrothermal rocks from the St. Paul and Conrad fracture zones in the Atlantic Ocean. *Eur. J. Mineral.* 16, 73–83. doi: 10.1127/0935-1221/2004/0016-0073

De Ronde, C. E. J., Faure, K., Bray, C. J., Chappell, D. A., and Wright, I. C. (2003). Hydrothermal fluids associated with seafloor mineralization at two southern Kermadec arc volcanoes, offshore New Zealand. *Miner. Deposita* 38, 217–233. doi: 10.1007/s00126-002-0305-4

Dekov, V., Boycheva, T., Halenius, U., Billstrom, K., Kamenov, G. D., Shanks, W. C., et al. (2011). Mineralogical and geochemical evidence for hydrothermal activity at the west wall of 12°50'N complex (Mid-Atlantic ridge): a new ultramafic-hosted seafloor hydrothermal deposit? *Mar. Geol.* 283, 90–102.

Dekov, V. M., Cuadros, J., Shanks, W. C., and Koski, R. A. (2008). Deposition of talc—kerolite–smectite — smectite at seafloor hydrothermal vent fields: Evidence from mineralogical, geochemical and oxygen isotope studies. *Chem. Geol.* 247, 171–194. doi: 10.1016/j.chemgeo.2007.10.022

Dias, A. A., and Barriga, F. J. A. S. (2006). Mineralogy and geochemistry of hydrothermal sediments from the serpentinite-hosted Saldanha hydrothermal field (36°34′N; 33°26′W) at MAR. *Mar. Geol.* 225, 157–175. doi: 10.1016/j.margeo.2005.07.013

Donval, J. P., Charlou, J. L., Douville, E., Knoery, J., Fouquet, Y., Poncevera, E., et al. (1997). High H_2 and CH_4 content in hydrothermal fluids from Rainbow site newly sampled at 36°14′N on the AMAR segment, Mid-Atlantic Ridge (diving FLORES cruise, July 1997): Comparison with other MAR sites. *EOS Trans. Am. Geophys. Union* 78:V51.

Eickmann, B., Thorseth, I. H., Peters, M., Strauss, H., Brocker, M., and Pedersen, R. B. (2014). Barite in hydrothermal environments as a recorder of subseafloor processes: A multiple isotope study from the Loki's Castle vent field. *Geobiology* 12, 308–321. doi: 10.1111/gbi.12086

Elburg, M., Vroon, P., Wagt, B. V. D., and Tchalikian, A. (2005). Sr and Pb isotopic composition of five USGS glasses (BHVO-2G, BIR-1G, BCR-2G, TB-1G, NKT-1G). *Chem. Geol.* 223, 196–207. doi: 10.1016/j.chemgeo.2005.07.001

Fan, L., Wang, G., Holzheid, A., Zoheir, B., and Shi, X. (2021). Sulfur and copper isotopic composition of seafloor massive sulfides and fluid evolution in the 26°S hydrothermal field, Southern Mid-Atlantic Ridge. *Mar. Geol.* 435:106436. doi: 10.1016/j.margeo.2021.106436

Feng, D., and Roberts, H. (2011). Geochemical characteristics of the barite deposits at cold seeps from the northern Gulf of Mexico. *Earth Planet. Sci. Lett.* 309, 89–99. doi: 10.1016/j.epsl.2011.06.017

Gale, A., Dalton, C. A., Langmuir, C. H., Su, Y., and Schilling, J.-G. (2013). The mean composition of ocean ridge basalt. *Geochem. Geophys. Geosyst.* 14, 489–518. doi: 10.1029/2012GC004334

Gallant, R. M., and Von Damm, K. L. (2006). Geochemical controls on hydrothermal fluids from the Kairei and Edmond Vent Fields, 23°–25°S, Central Indian Ridge. *Geochem. Geophys. Geosyst.* 7:Q06018. doi: 10.1029/2005GC001067

German, C. R., and Seyfried, W. E. Jr (2014). "Hydrothermal processes," in *Treatise on Geochemistry*, Vol. 8, eds H. D. Holland and K. K. Turekian (Oxford: Elsevier), 191–233. doi: 10.1016/B978-0-08-095975-7.00607-0

German, C. R., Baker, E. T., Mevel, C., Tamaki, K., and the Fuji Scientific Team. (1998). Hydrothermal activity along the Southwest Indian Ridge. *Nature* 395, 490–493. doi: 10.1038/26730

Grácia, E., Charlou, J. L., Radford-Knoery, J., and Parson, M. (2000). Non-transform offsets along the Mid-Atlantic Ridge south of the Azores (38°N–34°N): Ultramafic exposures and hosting of hydrothermal vents, Earth Planet. *Sci. Lett.* 177, 89–103. doi: 10.1016/S0012-821X(00)00034-0

Griffith, E. M., and Paytan, A. (2012). Barite in the ocean–occurrence, geochemistry and palaeoceanographic applications. *Sedimentology* 59, 1817–1835. doi: 10.1111/j.1365-3091.2012.01327.x

Hannington, M., Jamieson, J., Monecke, T., Petersen, S., and Beaulieu, S. (2011). The abundance of seafloor massive sulfide deposits. *Geology* 39, 1155–1158. doi: 10.1130/G32468.1

He, C., Ji, L., Wu, Y., Su, A., and Zhnag, M. (2016). Characteristics of hydrothermal sedimentation process in the Yanchang Formation, south Ordos Basin, China: Evidence from element geochemistry. *Sediment. Geol.* 345, 33–41. doi: 10.1016/j.sedgeo.2016.09.001

Herzig, P. M., Hannington, M. D., and Arribas, A. Jr. (1998). Sulfur isotopic composition of hydrothermal precipitates from the Lau back-arc: implications for magmatic contributions to sea-floor hydrothermal systems. *Miner. Deposita* 33, 226–237. doi: 10.1007/s001260050143

Hodgkinson, M. R. S., Webber, A. P., Roberts, S., Mills, R. A., Connelly, D. P., and Murton, B. J. (2015). Talc-dominated seafloor deposits reveal a new class of hydrothermal system. *Nat. Commun.* 6:10150. doi: 10.1038/ncomms10150

Imbus, S. W., Macko, S. A., Elmore, R. D., and Engel, M. H. (1992). Stable isotope (C, S, N) and molecular studies on the Precambrian Nonesuch Shale (Wisconsin-Michigan, U.S.A.): Evidence for differential preservation rates, depositional environment and hydrothermal influence. *Chem. Geol.* 101, 255–281. doi: 10.1016/0009-2541(92)90007-R

Jamieson, J. W., Hannington, M. D., Tivey, M. K., Hansteen, T., Williamson, N. M. B., Stewart, M., et al. (2016). Precipitation and growth of barite within hydrothermal vent deposits from the endeavour segment, Juan de Fuca Ridge. *Geochim. Cosmochim. Acta* 173, 64–85. doi: 10.1016/j.gca.2015.10.021

Kaplan, I. R. (1983). "Stable isotopes of sulfur, nitrogen and deuterium in recent marine environments," in *Stable Isotopes in Sedimentary Geology*, ed. M. A. Arthur (Oklahoma, OK: SEPM Society for Sedimentary Geology), 1–108.

Kelley, D. S., Karson, J. A., Blackman, D. K., Fruh-Green, G. L., Butterfield, D. A., Lilley, M. D., et al. (2001). An off-axis hydrothermal vent field near the Mid-Atlantic Ridge at 30°N. *Nature* 412, 145–149. doi: 10.1038/35084000

Kelley, D. S., Karson, J. A., Fruh-Green, G. L., Yoerger, D., Shank, T. M., Butterfield, D. A., et al. (2005). A serpentinite-hosted ecosystem: The Lost City Hydrothermal Field. *Science* 307, 1428–1434. doi: 10.1126/science.1102556

Kennicutt, M. C., Burke, R. A., Macdonald, I. R., Brooks, J. M., Denoux, G. J., and Macko, S. A. (1992). Stable isotope partitioning in seep and vent organisms–chemical and ecological significance. *Chem. Geol.* 101, 293–310. doi: 10.1016/0009-2541(92)90009-T

Kim, J., Son, S. -K., Kim, D., Pak, S. J., Yu, O. H., Walker, S. L., et al. (2020). Discovery of active hydrothermal vent fields along the Central Indian Ridge, 8–12°S. *Geochem. Geophys. Geosyst.* 21:e2020GC009058. doi: 10.1029/2020GC009058

Koski, R. A., Lonsdale, P. F., Shanks, W. C., Berndt, M. E., and Howe, S. S. (1985). Mineralogy and geochemistry of a sediment-hosted hydrothermal sulfide deposit from the Southern Trough of Guaymas Basin, Gulf of California. *J. Geophys. Res.* 90, 6695–6707. doi: 10.1029/JB090iB08p06695

Krouse, H. R. (1980). "Sulphur isotopes in our environment," in *Handbook of Environmental Isotope Geochemistry*, eds P. Fritz and J. C. Fontes (Amsterdam: Elsevier), 435–471. doi: 10.1016/B978-0-444-41780-0.50017-1

Kuhn, T., Burger, H., Castradori, D., and Halbach, P. (2000). Volcanic and hydrothermal history of ridge segments near the Rodrigues Triple Junction (Central Indian Ocean) deduced from sediment geochemistry. *Mar. Geol.* 169, 391–409. doi: 10.1016/S0025-3227(00)00080-3

Kuhn, T., Herzig, P. M., Hannington, M. D., Garbe-Schönberg, D., and Stoffers, P. (2003). Origin of fluids and anhydrite precipitation in the sediment-hosted Grimsey hydrothermal field north of Iceland. *Chem. Geol.* 202, 5–21. doi: 10.1016/S0009-2541(03)00207-9

Liao, S., Tao, C., Dias, A. A., Su, X., Yang, Z., Ni, J., et al. (2019). Surface sediment composition and distribution of hydrothermal derived elements at the Duanqiao-1 hydrothermal field, Southwest Indian Ridge. *Mar. Geol.* 416, 105975. doi: 10.1016/j.margeo.2019.105975

Liao, S., Tao, C., Li, H., Barriga, F. J. A. S., Liang, J., Yang, W., et al. (2018a). Bulk geochemistry, sulfur isotope characteristics of the Yuhuang-1 hydrothermal field on the ultraslow-spreading Southwest Indian Ridge. *Ore Geol. Rev.* 96, 13–27. doi: 10.1016/j.oregeorev.2018.04.007

Liao, S., Tao, C., Li, H., Zhang, G., Liang, J., Yang, W., et al. (2018b). Surface sediment geochemistry and hydrothermal activity indicators in the Dragon Horn area on the Southwest Indian Ridge. *Mar. Geol.* 398, 22–34. doi: 10.1016/j.margeo.2017.12.005

Lim, D. I., Xu, Z., Choi, J., Li, T., and Kim, S. (2015). Holocene changes in detrital sediment supply to the eastern part of the central Yellow Sea and their forcing mechanisms. *J. Asian Ear. Sci.* 105, 18–31. doi: 10.1016/j.jseaes.2015.03.032

Lim, D., Kim, H., Kim, J., Jeong, D., and Kim, D. (2020). Mercury proxy for hydrothermal and submarine volcanic activities in the sediment cores of Central Indian Ridge. *Mar. Pollut. Bull.* 159:111513. doi: 10.1016/j.marpolbul.2020.111513

Lim, D., Kim, J., Kim, J., Kim, D., Jeong, D., Kim, H., et al. (2021). Enhancement of volcanic eruption in mid-ocean ridge system during the last deglaciation: new sedimentary evidence in the Central Indian Ridge. *Mar. Geol.* 440:106574. doi: 10.1016/j.margeo.2021.106574

Lowell, R. P., and Rona, P. A. (2002). Seafloor hydrothermal systems driven by the serpentinization of peridotite. *Geophys. Res. Lett.* 29:1531. doi: 10.1029/2001GL014411

Marchig, V., Gundlach, H., Möller, P., and Schley, F. (1982). Some geochemical indicators for discrimination between diagenetic and hydrothermal metalliferous sediments. *Mar. Geol.* 50, 241–256. doi: 10.1016/0025-3227(82)90141-4

Marty, B., and Zimmermann, L. (1999). Volatiles (He, C, N, Ar) in mid-ocean ridge basalts: assesment of shallow-level fractionation and characterization of source composition. *Geochim. Cosmochim. Acta* 63, 3619–3633. doi: 10.1016/S0016-7037(99)00169-6

Mascarenhas-Pereira, M. B. L., and Nath, B. N. (2010). Selective leaching studies of sediments from a seamount flank in the Central Indian basin: resolving

hydrothermal, volcanogenic and terrigenous components using major, trace and rare-earth elements. *Mar. Chem.* 121, 49–66. doi: 10.1016/j.marchem.2010.03.004

Melekestseva, I. Y., Tret'yakov, G. A., Nimis, P., Yuminov, A. M., Maslennikov, V. V., Maslennikova, S. P., et al. (2014). Barite-rich massive sulfides from the Semenov-1 hydrothermal field (Mid-Atlantic Ridge, 13°30.87′ N): Evidence for phase separation and magmatic input. *Mar. Geol.* 349, 37–54. doi: 10.1016/j.margeo.2013.12.013

Michard, A., and Albarède, F. (1986). The REE content of some hydrothermal fluids. *Chem. Geol.* 55, 51–60. doi: 10.1016/0009-2541(86)90127-0

Nakamura, K., and Takai, K. (2015). "Indian Ocean Hydrothermal Systems: Seafloor Hydrothermal Activities, Physical and Chemical Characteristics of Hydrothermal Fluids, and Vent-Associated Biological Communities," in *Subseafloor biosphere linked to hydrothermal systems*, eds J. Ishibashi, et al. (Berlin: Springer), 147–162. doi: 10.1007/978-4-431-54865-2_12

Nakamura, K., Watanebe, H., Miyazaki, J., Takai, K., Kawagucci, S., Noguchi, T., et al. (2012). Discovery of new hydrothermal activity and chemosynthetic fauna on the Central Indian Ridge at 18°–20°S. *PLoS One* 7:e32965. doi: 10.1371/journal.pone.0032965

Noguchi, T., Shinjo, R., Ito, M., Takada, J., and Oomori, T. (2011). Barite geochemistry from hydrothermal chimneys of the Okinawa Trough: Insight into chimney formation and fluid/sediment interaction. *J. Miner. Petrol. Sci.* 106, 26–35. doi: 10.2465/jmps.090825

Oduro, H., Von Alstyne, K. L., and Farquhar, J. (2012). Sulfur isotope variability of oceanic DMSP generation and its contributions to marine biogenic sulfur emissions. *Proc. Natl. Acad. Sci.* 109, 9012–9016. doi: 10.1073/pnas.1117691109

Park, S. J., Moon, J. W., Kim, J., Chandler, M. T., Kim, H. S., Son, J., et al. (2017). Widespread tectonic extension at the Central Indian Ridge between 8°S and 18°S. *Gondwana Res.* 45, 163–179. doi: 10.1016/j.gr.2016.12.015

Paytan, A., and Gray, E. T. (2012). "Sulfur Isotope Stratigraphy," in *The Geologic Time Scale*, eds F. M. Gradstein, J. G. Ogg, M. Schmitz, and G. Ogg (Berlin: Elsevier), 167–179. doi: 10.1016/B978-0-444-59425-9.00009-3

Paytan, A., Kastner, M., Martin, E. E., Macdougal, J. D., and Herbert, T. (1993). Marine barite as a monitor of seawater strontium isotope composition. *Nature* 366, 445–449. doi: 10.1038/366445a0

Paytan, A., Mearon, S., Cobb, K., and Kastner, M. (2002). Origin of marine barite deposits: Sr and S isotope characterization. *Geology* 30, 747–750. doi: 10.1130/0091-7613(2002)030<0747:OOMBDS>2.0.CO;2

Peters, M., Strauss, H., Petersen, S., Kummer, N.-A., and Thomazo, C. (2011). Hydrothermalism in the Tyrrhenian Sea: Inorganic and microbial sulfur cycling as revealed by geochemical and multiple sulfur isotope data. *Chem. Geol.* 280, 217–231. doi: 10.1016/j.chemgeo.2010.11.011

Price, R. C., Kennedy, A. K., Riggs-Sneeringer, M., and Frey, F. A. (1986). Geochemistry of basalts from the Indian Ocean triple junction: implications for the generation and evolution of Indian Ocean ridge basalts. *Ear. Planet. Sci. Lett.* 78, 379–396. doi: 10.1016/0012-821X(86)90005-1

Ray, D., Misra, S., Banerjee, R., and Weis, D. (2011). Geochemical implications of gabbro from the slow-spreading Northern Central Indian Ocean Ridge, Indian Ocean. *Geol. Mag.* 148, 404–422. doi: 10.1017/S001675681000083X

Rees, C. E., Jenkins, W. J., and Monster, J. (1978). The sulphur isotope geochemistry of ocean water sulphate. *Geochim. Cosmochim. Acta* 42, 377–382. doi: 10.1016/0016-7037(78)90268-5

Rona, P. A., Widenfalk, L., and Bostrom, K. (1987). Serpentinized ultramafics and hydrothermal activity at the Mid –Atlantic Ridge crest near 15°N. *J. Geophys. Res.* 92, 1417–1427. doi: 10.1029/JB092iB02p01417

Shanks, W. C. (2001). "Stable isotopes in seafloor hydrothermal systems: vent fluids, hydrothermal deposits, hydrothermal alteration, and microbial processes," in *Stable Isotope Geochemistry*, eds J. W. Valley and D. R. Cole (Washington D.C: Mineralogical Society of America), 469–517. doi: 10.1515/9781501508745-011

Shanks, W. C., Bohlke, J. K., and Seal, R. R. (1995). "Stable Isotopes in Mid-Ocean Ridge Hydrothermal Systems: Interactions between Fluids, Minerals, and Organisms," in *Seafloor Hydrothermal Systems: Physical, Chemical, Biological, and Geological Interactions*, eds S. E. Humphris, R. A. Zierenberg, L. S. Mullineaux, and R. E. Thomson (Washington, DC: American Geophysical Union), 194–221. doi: 10.1029/GM091p0194

Slack, J. F., Grenne, T., and Bekker, A. (2009). Seafl oor-hydrothermal Si-Fe-Mn exhalites in the Pecos greenstone belt, New Mexico, and the redox state of ca. 1720 Ma deep seawater. *Geospere* 5, 302–314. doi: 10.1130/GES00220.1

Son, J., Pak, S. J., Kim, J., Baker, E. T., You, O. R., Son, S. K., et al. (2014). Tectonic and magmatic control of hydrothermal activity along the slow-spreading Central Indian Ridge, 8°S–17°S. *Geochem. Geophys. Geosyst.* 15, 2011–2020. doi: 10.1002/2013GC005206

Song, Y. H., and Choi, M. S. (2009). REE geochemistry of fine-grained sediments from major rivers around the Yellow sea. *Chem. Geol.* 266, 328–342. doi: 10.1016/j.chemgeo.2009.06.019

Suo, Y., Li, S., Li, X., Zhang, Z., and Ding, D. (2017). The potential hydrothermal systems unexplored in the Southwest Indian Ocean. *Mar. Geophys. Res.* 38, 61–70. doi: 10.1007/s11001-016-9300-5

Tao, C., Lin, J., Guo, S., Chen, Y. J., Wu, G., Han, X., et al. (2012). First active hydrothermal vents on an ultraslow-spreading center: Southwest Indian Ridge. *Geology* 40, 47–50. doi: 10.1130/G32389.1

Taylor, S. R., and McLennan, S. M. (1985). *The Continental Crust: its Composition and Evolution*. New York, NY: Oxford University Press.

Tivey, M. K. (2007). Generation of seafloor hydrothermal vent fluids and associated mineral deposits. *Oceanography* 20, 50–65. doi: 10.5670/oceanog.2007.80

Walinsky, S. E., Prahl, F. G., Mix, A. C., Finney, B. P., Jaeger, J. M., and Rosen, G. P. (2009). Distribution and composition of organic matter in surface sediments of coastal Southeast Alaska. *Cont. Shelf Res.* 29, 1565–1579. doi: 10.1016/j.csr.2009.04.006

Wang, T., Chen, Y. J., and Tao, C. (2011). Revisit the K-segment of the Southeast Indian Ridge for new evidence of hydrothermal plumes. *Chin. Sci. Bull.* 56, 3605–3609. doi: 10.1007/s11434-011-4723-5

Wortmann, U. G., Chernyavsky, B. M., Bernasconi, S. M., Brunner, B., Böttcher, M. E., and Swart, P. K. (2007). Oxygen isotope biogeochemistry of pore water sulfate in the deep biosphere: dominance of isotope exchange reactions with ambient water during microbial sulfate reduction (ODP Site 1130). *Geochim. Cosmochim. Acta* 71, 4221–4232. doi: 10.1016/j.gca.2007.06.033

Yang, S. Y., Lim, D. I., Jung, H. S., and Oh, B. C. (2004). Geochemical composition and provenance discrimination of coastal sediments around Cheju Island in the southeastern Yellow Sea. *Mar. Geol.* 206, 41–53. doi: 10.1016/j.margeo.2004.01.005

Zhang, L., Ren, Z.-Y., Handler, M. R., Wu, Y.-D., Zhang, L., Qian, S.-P., et al. (2019). The origins of high-Ti and low-Ti magmas in large igneous provinces, insights from melt inclusion trace elements and Sr-Pb isotopes in the Emeishan large Igneous Province. *Lithos* 344-345, 122–133. doi: 10.1016/j.lithos.2019.06.014

Zhang, L., Ren, Z.-Y., Wu, Y.-D., and Li, N. (2018). Strontium isotope measurement of basaltic glasses by laser ablation multiple collector inductively coupled plasma mass spectrometry based on a linear relationship between analytical bias and Rb/Sr ratios. *Rapid Commun. Mass Spectrom.* 32, 105–112. doi: 10.1002/rcm.8011

Zhang, X., Zhai, S. K., and Yu, Z. H. (2020). Strontium Isotope Compositions of Hydrothermal Barite from the Yonaguni IV: Insight into Fluid/Sediment Interaction and Barite Crystallization Condition. *J. Ocean Univ. China* 19, 377–385. doi: 10.1007/s11802-020-4021-4

Zhou, Y., Zhang, D., Zhang, R., Liu, Z., Tao, C., Lu, B., et al. (2018). Characterization of vent fauna at three hydrothermal vent fields on the Southwest Indian Ridge: Implications for biography and interannual dynamics on ultraslow-spreading ridges. *Deep-Sea Res. Part I* 137, 1–12.

Conflict of Interest: The authors declare that the research was conducted in the absence of any commercial or financial relationships that could be construed as a potential conflict of interest.

Publisher's Note: All claims expressed in this article are solely those of the authors and do not necessarily represent those of their affiliated organizations, or those of the publisher, the editors and the reviewers. Any product that may be evaluated in this article, or claim that may be made by its manufacturer, is not guaranteed or endorsed by the publisher.

frontiers in Marine Science

ORIGINAL RESEARCH
published: 17 February 2022
doi: 10.3389/fmars.2022.774628

Making Use of Relicts: Brisingid Seastars Aggregate on Hydrothermally Inactive Sulfide Chimneys Near Black Smokers

*Daniel Woods[1], Michael J. Cheadle[2], Barbara E. John[2], Christopher R. German[3] and Cindy L. Van Dover[1]**

[1] Division of Marine Science and Conservation, Nicholas School of the Environment, Duke University, Beaufort, NC, United States, [2] Department of Geology and Geophysics, University of Wyoming, Laramie, WY, United States, [3] Department of Geology and Geophysics, Woods Hole Oceanographic Institution, Woods Hole, MA, United States

OPEN ACCESS

Edited by:
Philip Weaver, Seascape Consultants Ltd., United Kingdom

Reviewed by:
Helena Passeri Lavrado, Federal University of Rio de Janeiro, Brazil
Rachel Elizabeth Boschen-Rose, Marine Scotland, United Kingdom
Marie-Anne Cambon, Institut Français de Recherche pour l'Exploitation de la Mer (IFREMER), France

***Correspondence:**
Cindy L. Van Dover
clv3@duke.edu

Specialty section:
This article was submitted to Deep-Sea Environments and Ecology, a section of the journal Frontiers in Marine Science

Received: *12 September 2021*
Accepted: *25 January 2022*
Published: *17 February 2022*

Citation:
Woods D, Cheadle MJ, John BE, German CR and Van Dover CL (2022) Making Use of Relicts: Brisingid Seastars Aggregate on Hydrothermally Inactive Sulfide Chimneys Near Black Smokers. Front. Mar. Sci. 9:774628. doi: 10.3389/fmars.2022.774628

When hydrothermal activity ceases at black-smoker chimneys on mid-ocean ridges, populations of associated invertebrates hosting chemoautotrophic endosymbionts decline and then disappear, but the chimneys can persist on the seabed as relicts. Suspension-feeding brisingid seastars colonize hydrothermally inactive (relict) chimneys on the East Pacific Rise (EPR), though their distribution relative to available hard substrata and proximity to hydrothermal activity is poorly documented. In this study, brisingid abundance on sulfide and basalt substrata was assessed along an ∼3,700 m ROV *Jason II* transect at the summit of Pito Seamount (SE Pacific; ∼2,275 m). Brisingids were non-randomly distributed, with highest densities (up to ∼300 m^{-2}) on relict sulfides chimneys near active black smokers. Brisingids were relatively uncommon on basalt substrata, and absent on black smokers. We infer that both relict sulfide structures and proximity to black smokers play key roles in the maintenance of dense brisingid populations on Pito Seamount and in similar environments on the EPR. Our observations suggest that experimental introduction of "artificial" relict chimneys providing microtopographic relief could test whether such an approach might mitigate potential impacts of mineral extraction on populations of suspension-feeding invertebrates.

Keywords: brisingid seastar, East Pacific Rise (EPR), hydrothermal vent, Pito Seamount, *Nautile Hydrothermal Field*, deep-sea mining (DSM), black smoker, hydrothermally inactive sulfide

INTRODUCTION

High-temperature hydrothermal activity (black smokers) in the deep sea typically forms meters- to 10 s-of-meters-high, 3-dimensional structures (chimneys) composed of precipitated sulfide minerals rich in copper, iron, zinc, and other metals (Petersen et al., 2016). Chemosynthetic primary productivity is intense at black smokers (Van Dover, 2000) and is exported beyond the immediate community of endemic invertebrate and fish taxa associated with venting fluids (Levin et al., 2016). Indeed, 10–33% of the particulate organic carbon reaching the entire deep ocean floor worldwide may be stimulated by activity at hydrothermal vents (German et al., 2015).

Black smokers ultimately wane and expire as conduits are clogged through mineralization, as flow is redirected due to tectonic activity, and as volcanic eruptions repave the ocean floor (Fustec et al., 2013; Van Dover, 2019; Jamieson and Gartman, 2020). Relict, hydrothermally inactive sulfide structures may remain as chimneys and mounds, or collapse into blocks and rubble. Where high-temperature hydrothermal activity persists for long periods (thousands of years or more; Lalou et al., 1985, 1995), polymetallic sulfides may accumulate as deposits of sufficient size and mineral quality to be of interest to an emergent deep-sea mining industry (Hoagland et al., 2010; Hannington et al., 2011; Cherkashov, 2017). Long-duration hydrothermal activity and large accumulations of mineral precipitates at relatively low spatial frequencies are known from intermediate-, slow-, and ultraslow- spreading mid-ocean ridges (Rona et al., 1993; Halbach et al., 1998; Karson et al., 2015), as well as off-axis sites on the fast-spreading East Pacific Rise (EPR) (Hekinian and Fouquet, 1985; Fouquet et al., 1996). On the EPR itself, the spatial frequency of vent fields with high-temperature (∼350°C) black smokers is relatively high, on the order of ∼4 fields per 100 km (Chen et al., 2021), and the duration of venting activity is short (decadal scale or less; Lalou and Brichet, 1982; Karson et al., 2015).

Because of the relatively short life cycle for black smokers on the EPR, sulfide accumulations are small (<3,000 tons for a given vent field; Hannington et al., 2011). Further, accumulations of mineral precipitates along the EPR are composed primarily of iron sulfides with little to no economic value at present (Petersen et al., 2016). To date, no contracts for polymetallic sulfide mineral exploration along fast-spreading mid-ocean ridges of the seabed beyond national jurisdictions in the eastern Pacific (i.e., along the EPR, Galapagos Spreading Center, Pacific-Antarctic Ridge) have been awarded by the International Seabed Authority. Nevertheless, study of the biology of hydrothermally inactive sulfide accumulations in this region adds to our understanding of the role of seabed sulfide occurrences as habitat and may inform environmental management of future seabed mining in this area.

The fauna associated with relict sulfide accumulations is in general poorly known (reviewed in Van Dover, 2019; Van Dover et al., 2020). Small macrofaunal and meiofaunal organisms such as nematodes, gastropods, copepods, and amphipods occur in association with inactive sulfides on the EPR (Gollner et al., 2020). Suspension-feeding brisingid seastars have also been reported on relict sulfide structures on the EPR (Desbruyeres et al., 2006) and elsewhere from peripheral zones of active vent fields (Kim and Hammerstrom, 2012). Deep-sea seastars in the family Brisingidae are common benthic organisms found worldwide (Emson and Young, 1994), often associated with hard substrata such as drop stones (Lacharité and Metaxas, 2017), corals (Mah, 2016), or manmade objects (Mordecai et al., 2011; Edwards et al., 2016). Brisingids rely on deep-ocean currents for delivery of prey (e.g., copepods and other small planktonic organisms) that is captured by raptorial pedicellariae and transferred to the mouth (Emson and Young, 1994; Howell et al., 2003; Gale et al., 2013). Brisingid seastars on relict sulfide structures are not endemic to active hydrothermal vents or other deep-sea chemosynthetic ecosystems (Mah et al., 2015), but likely benefit from primary productivity associated with chemosynthetic production (Carney, 2010; Levin et al., 2016).

To increase our understanding of the distribution of brisingid seastars in the vicinity of deep-sea hydrothermal vents and the potential importance of relict sulfides as habitat, we undertook a census of brisingid distributions relative to substratum type along a geological transect at Pito Seamount (2,240–2,325 m; Naar et al., 2004; Cheadle et al., 2017), which lies at the northern tip of the propagating EPR axis on the eastern side of the Easter Microplate (**Figure 1**). Hydrothermal activity was first discovered on Pito Seamount in 1993 by scientists in the submersible *Nautile* (Naar et al., 2004). In 2017, more than 50 black smokers and relict sulfide chimneys comprising the *Nautile Hydrothermal Field* were detected using high-resolution mapping with the Autonomous Underwater Vehicle (AUV) *Sentry*. Black smoker and relict sulfide chimney targets were further explored using the Remotely Operated Vehicle (ROV) *Jason II* during the 2017 geological expedition.

Here we provide a descriptive account of brisingid distributions, using tests of *a posteriori* hypotheses to assess whether brisingid seastars (i) aggregate on relict sulfides, especially sulfide chimneys with microscale relief (∼0.5–15 m), (ii) are relatively uncommon on basalt substrata, (iii) are absent on black smokers, and (iv) are scarce in the nearby Pito Deep, where hydrothermal activity is absent (51 km northwest of Pito Seamount, **Figure 1**).

MATERIALS AND METHODS

Mapping

R/V Atlantis Cruise AT37-08 was devoted to mapping and understanding volcanic processes in Pito Deep and rifting of Pito Seamount [PaleoMagnetism and Gabbro Cruise (PMaG); M Cheadle, Chief Scientist]. The cruise included a 1-dive subcomponent to assess the extent of the hydrothermal field reported by Naar et al. (2004) on Pito Seamount. AUV *Sentry* Dive 427 (6 February 2017) mapped the summit of Pito Seamount (0.5–1 m resolution) using a Reson 7125 multibeam sonar system at a nominal altitude of 80 m above the seafloor, with 85 m line spacing to ensure > 100% overlapping multibeam coverage between adjacent survey lines. The multibeam coverage angle was reduced to 70° from the standard 120° to accommodate the increased altitude and reduced track-line spacing. Fledermaus 7.7.4 was used to render 3-D perspectives of the terrain. Multibeam data was used to identify sulfide targets on the seafloor.

Image Collection, Archive, and Analysis

Time-stamped and georeferenced (latitude, longitude, depth) images were captured during ROV *Jason II* Dive 961 at the *Nautile Hydrothermal Field* on Pito Seamount (23.3275°S, 111.635°W; 10 February 2017) during the PMaG Cruise to document the terrain and geological sampling efforts. During this dive transect, most of the sulfide features identified during the multibeam mapping effort were visited. SciCam images (frame

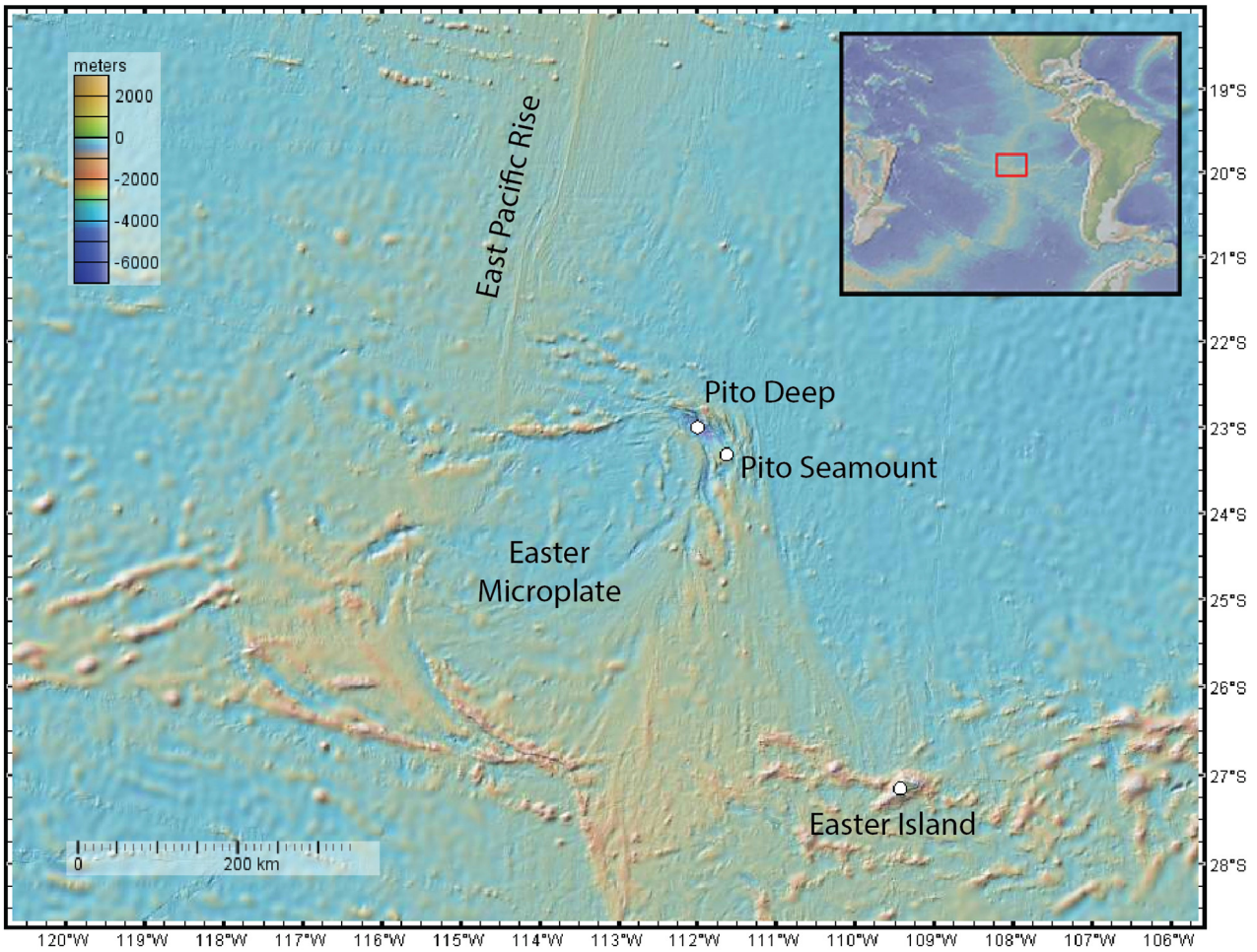

FIGURE 1 | Study locations: Pito Seamount, Pito Deep. GeoMapApp (www.geomapapp.org).

grabs) were automatically collected every 30 s, augmented by manual image captures at the discretion of scientists on watch at the time. Due to the nature of the geological exploration, vehicle speed, heading, and altitude were variable, as was stand-off distance from vertical surfaces. The frequency of image collection was also variable, increasing in the vicinity of black smokers and hydrothermally inactive sulfides occurrences and when geological samples were collected. Thumbnail images from the SciCam are available on the Jason Virtual Van System[1] under "2017: at37–08"; images and metadata are archived at the Woods Hole Oceanographic Institution. There are evident limitations to the dataset obtained in this study, including an inability (i) to assess total abundance of brisingids on any given vertical surface, since only one face of a structure was in the field of view on the transect, (ii) to reliably measure brisingid densities, since stand-off distances from vertical surfaces were variable and not measured, or (iii) to capture a quantitative estimate of sampling effort for each substratum type. Nevertheless, we could reliably quantify the abundance of brisingid seastars in each photo and the nature of the substratum on which each brisingid was located. Duplicate counting of individuals was avoided by attention to overlapping fields of view between images. Because lighting, water clarity, and scale varied among photos and likely contributed to color variation in the images, no quantitative data was collected on the relative abundance of two different color morphs (orange and white) of Pito Seamount brisingids.

The substratum was broadly classified as basalt or sulfide. Following Karson et al. (2015), basalt substrata were further classified as hackly, rubble, edge (e.g., scarp edge), pillow, sheet, ropey, and lobate (**Figure 2**). Hydrothermally inactive (relict) sulfide substrata (i.e., visually devoid of shimmering water or other indication of fluid flux) were further classified as chimney, boulder, ledge, and debris (**Figure 3**). Locations of black smokers observed along the Dive 961 transect were also recorded (**Table 1**).

To supplement observations of brisingid distributions on the Pito Seamount transect, Virtual Van SciCam thumbnail images from ROV *Jason II* Dives 953 through 960 from the walls of nearby Pito Deep (max depth of 5,260 m; PMaG cruise; 22.97°S, 111.95°W; **Figure 1**) were reviewed. Pito Deep provides

[1]http://4dgeo.whoi.edu/jason

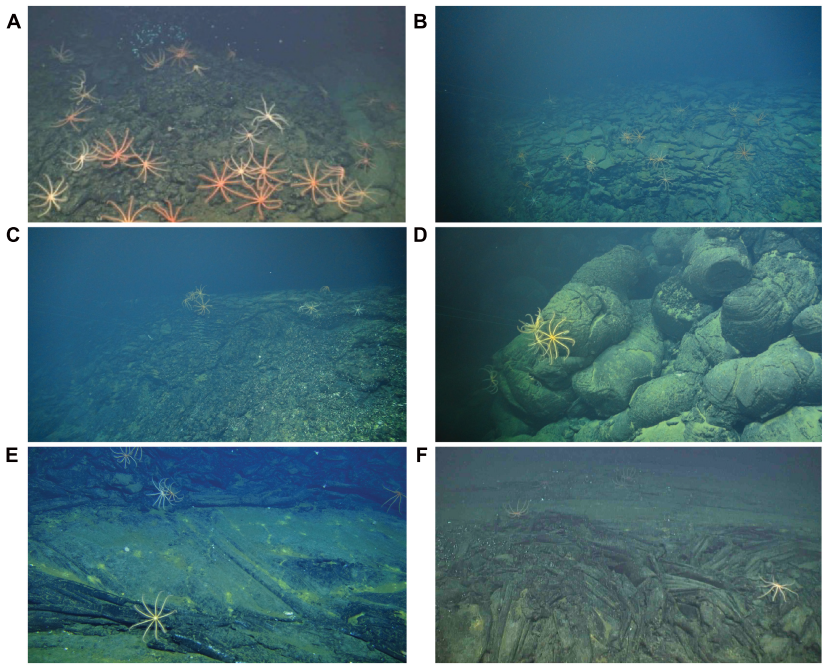

FIGURE 2 | Examples of basalt substrata hosting brisingids at Pito Seamount: **(A)** hackly and sheet; **(B)** edge and rubble; **(C)** lobate and edge; **(D)** pillow; **(E)** sheet; **(F)** ropey and sheet.

a cross section through rifted crust of the EPR, is dominated by hard rock substrata, and is devoid of hydrothermal activity and sulfide features.

Data Analysis

Brisingid data analyses and visualizations were undertaken using R (R Core Team, 2020) and ggplot2 (Wickham, 2016). To test for significant differences among brisingid median abundances and substratum types, a Kruskal-Wallis rank sum test followed by a Dunn *post-hoc* test was undertaken using "rcompanion" (Mangiafico, 2016).

RESULTS

Pito Seamount: Transect Effort and Brisingid Seastar Distributions

At Pito Seamount, the seabed was visible in 2,773 photos collected during a 15.6-h, non-linear transect that covered ∼3,700 m. Depth varied by < 100 m, from 2,240 to 2,325 m. Seven black smoker complexes (**Figure 4**) plus ∼57 discrete hydrothermally inactive, relict sulfide chimneys (ranging in height from 0.15 to ∼15 m) were visited during the transect. About a third of the photos (963) included black smokers, another third (886) were of basalt substrata, and the remainder (924) were of hydrothermally inactive sulfides (**Table 2**). Distributions of substratum types among photos, while indicative, are not quantitative measures of sampling effort given the limitations of the survey strategy as described in section "Materials and Methods."

Of the photos collected, 301 (∼10%; excluding overlapping images) included one or more 9-armed, orange or white/cream-colored (**Figure 2A**) brisingid seastars (**Supplementary Table 1**). The total number of brisingids recorded was 4,005 individuals. Apart from an occasional gorgonian whip coral (n = ∼11 total), two seastars (2 different species), and invertebrate taxa associated with black smoker complexes, other benthic megafauna were inconspicuous along the transect.

Brisingid seastars were observed at intervals along the entire ROV *Jason II* Dive 961 transect, occurring occasionally as solitary individuals and most often in aggregations (**Figures 2**, **3**). Most brisingids (∼90%) occurred on relict sulfide substrata (**Table 2** and **Figure 5**). Highest abundances of brisingids on relict sulfide substrata were observed near the *Sniper, Sentry,* and *ABE* black smokers and on relict sulfide chimneys 120 m to the NE of the *Jason* and *Medea* vents (**Figure 6**). Highest abundances of brisingids on basalt were observed near the *Jason* and *Medea* black smokers (**Figure 6**). There was a single example of brisingids on hydrothermally inactive chimneys within just a few to tens of centimeters of a black smoker at *Scotty's Castle* (**Figure 3E**). Eight relict sulfide chimneys (of 57; < 15%) were devoid of brisingids. Two chimney-scale structures were also devoid of brisingids, but the photos were not of sufficient quality to distinguish whether the substratum was basalt or sulfide. In addition, one basalt pillar was observed, also devoid of brisingid seastars.

Median brisingid abundances were greatest on sulfide substrata classified as relict sulfide chimneys (**Table 2** and **Figure 7**; see also **Supplementary Figure 1**). Relict sulfide

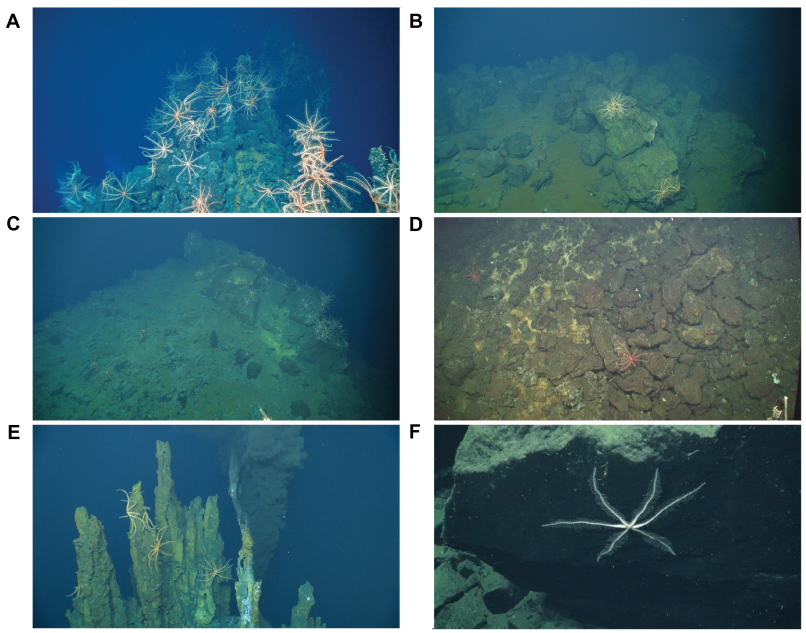

FIGURE 3 | Examples of hydrothermally inactive (relict) sulfide substrata at Pito Seamount: **(A)** chimney; **(B)** boulders; **(C)** ledge; **(D)** debris; **(E)** example of brisingids on relict chimneys close to *Scotty's Castle* black smoker; **(F)** six-armed brisingid on olivine gabbro talus at 5,200 m in Pito Deep.

TABLE 1 | Pito Seamount black smoker coordinates, depth, maximum temperature, and ROV *Jason II* event number.

Black smokers	Latitude S (decimal degree)	Longitude W (decimal degree)	Depth (m)	Measured T_{max}°C	ROV *Jason II* event number
Jason	23.3412278	111.6399361	2,319	370.68	20,769
Medea	23.3414611	111.6397111	2,311	368	21,176
ABE	23.334875	111.6392417	2,267	>279*	22,241
Sentry	23.3348778	111.6393694	2,270	>263*	22,341
Sniper	23.3342917	111.6398028	2,272	>286*	22,533
Scotty's castle	23.3301472	111.6416722	2,252	344	23,043
Magnificent village	23.3299972	111.6421417	2,254	338.85	23,141

**Measured temperatures are inferred to reflect entrainment of seawater during measurement; end-member fluids for these black smokers are inferred to be above 300°C, given the presence of metal precipitates ("smoke") in the fluids.*

chimneys were also the substratum type that had the greatest variability in brisingid abundance per photo and the greatest number of outlier abundances in boxplots (i.e., lying more than 1.5× the length of the box from either end). One image included nearly 200 brisingids (estimated maximum density on the order of 300 individuals per m^2). Brisingids were scarce on low-relief basalt substrata (**Figure 7**) and absent on black-smoker chimneys. Brisingid abundances for the sulfide substratum type "chimney" and the basalt substratum type "hackly" differed significantly from those of all other basalt and sulfide substratum types [Kruskal-Wallis rank sum test; chi-squared (H) = 45.1, d.f. = 10, $p < 0.001$, followed by a Dunn test ($p < 0.001$); **Figure 7**].

Pito Deep: Transect Effort and Brisingid Seastar Distributions

During nine ROV *Jason II* dives in the Pito Deep locale, 20,544 images were collected during a total of 362 h, covering ∼22 km along the seafloor (transects not illustrated). Solitary brisingid seastars were observed in 21 of these photos (0.001%), from depths of 3,680 to 5,260 m (**Supplementary Table 2**). Pito Deep brisingids were 6-armed (**Figure 3F**), distinct from those of Pito Seamount, and inferred here to be a different species.

DISCUSSION

Despite decades of scientific study on the EPR, surprisingly little is known about the distribution of benthic invertebrates (abundance, composition, functional traits, etc.) relative to black smokers and relict sulfide occurrences. This study is, to our knowledge, the only mapping of non-vent-endemic invertebrate distributions relative to substratum types in an EPR-like setting. Analytical limitations encountered during the opportunistic study described here (e.g., challenges in quantifying sampling effort) point to the need of "fit-for-purpose" surveys and attention to sampling design.

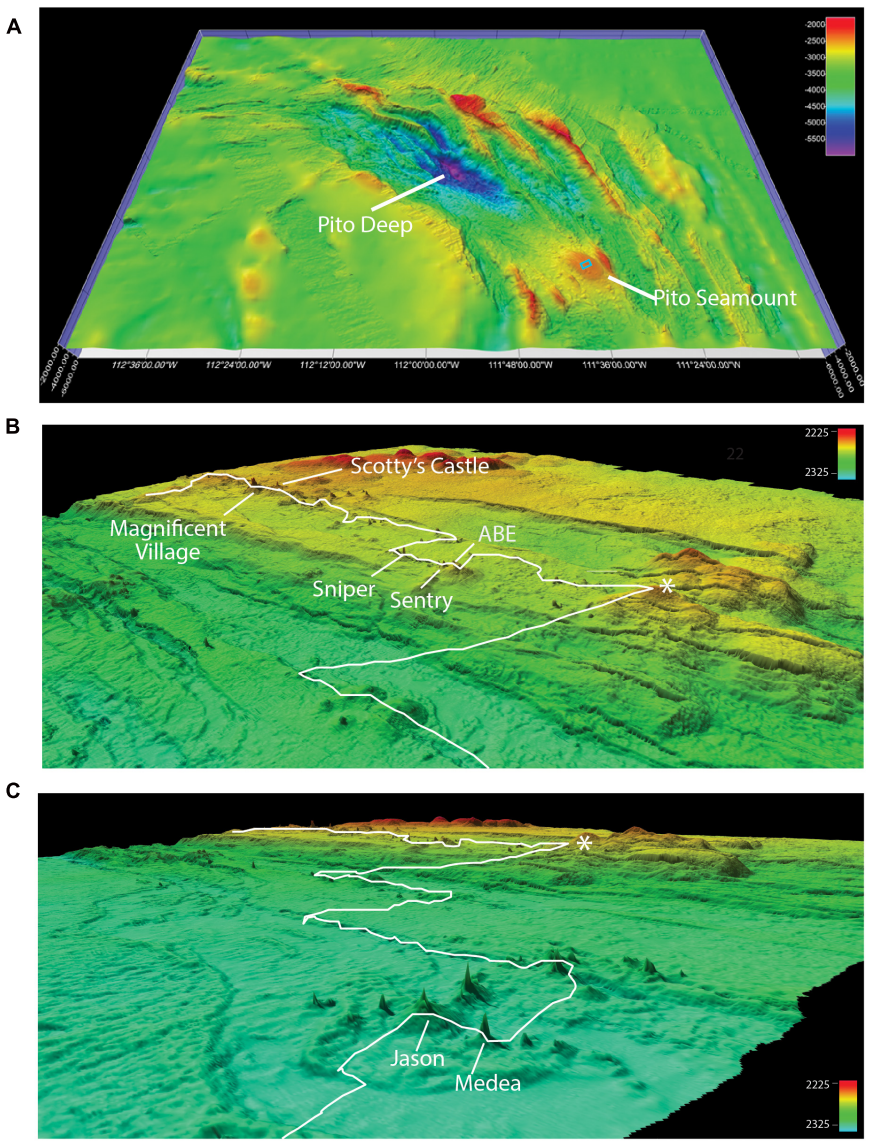

FIGURE 4 | Geomorphological context of the ROV *Jason II* Dive 961 transect. **(A)** Ship multibeam bathymetry (60-m resolution) from R/V *Atlantis* cruise 11–33 (2005) infilled with satellite-derived bathymetry to show the location of Pito Seamount and the study area detailed in **(B,C)** (blue rectangle) relative to Pito Deep. **(B,C)** Overlapping Fledermaus-rendered perspectives, Pito Seamount study site. Approximate location of ROV *Jason II* Dive 961 transect (white line) is overlain on high-resolution bathymetry (0.5–1 m resolution) collected during AUV Sentry Dive 427 at the summit of Pito Seamount. Asterisks in B and C mark the same geographical locale. Active hydrothermal vents visited during the transect are labeled (see also **Table 1**). All images produced in Fledermaus v 7.7.4.

Less surprising is the finding that relict sulfides in the *Nautile Hydrothermal Field* were not colonized by large, long-lived (decades and more) corals and sponges. This contrasts with observations of relict sulfides covered by relatively dense and/or distinct assemblages of attached and sessile invertebrates, including those reported from Manus Basin back arc spreading centers (Erickson et al., 2009), New Zealand Seamounts (Boschen et al., 2015, 2016), and the Central Indian Ridge (Gerdes et al., 2019). While we do not know the age of the relict sulfides observed in this study, they may be too young (decadal or less) to have accumulated long-lived taxa, but other explanations can be imagined. Alternative (and non-exclusive) explanations for the absence of large, attached organisms include differences in predominant sulfide mineralogies and substratum instability or other geochemical conditions that render the substratum unsuitable for establishment and persistence of coral, sponge, or other attached, long-lived taxa.

Suspension-feeding brisingid seastars on Pito Seamount were the visually dominant organisms on hydrothermally inactive sulfide substrata in this study. They were most abundant on relict sulfide chimneys elevated above the seafloor by 10 s of cm to ∼15 meters or more and within meters to 100's of meters of black smokers. Of the basalt substrata, the frequency of occurrence of brisingids was slightly elevated on hackly basalt adjacent

TABLE 2 | Pito Seamount.

Substratum type	Estimated relief	Total number of photos*	Photos with brisingids	Total brisingid abundance	Brisingid relative abundance (%)	Median brisingid abundance per photo	Mean brisingid abundance per photo
Basalt							
Hackly	5–10 cm	277	38	226	5.6	2.5	6
Pillow	20–30 cm	220	9	30	0.7	2	3.3
Lobate	20–25 cm	120	6	16	0.4	2.5	2.7
Sheet	0–2 cm	121	9	32	0.8	2	3.6
Ropey	10–20 cm	53	2	8	0.2	4	4
Rubble	5–10 cm	46	8	32	0.8	2	4
Edge	na	49	10	78	1.9	6.5	7.8
Total		886	82	422	10	2.5	5.2
Sulfide (relict)							
Chimney	0.5–15 m	531	126	2,628	65.6	10	20.9
Debris	15–30 cm	255	50	422	10.5	3	8.4
Boulder	10–50 cm	128	41	514	12.8	7	12.5
Ledge	na	10	2	19	0.5	9.5	9.5
Total		924	219	3,583	90	8	16.4
Black smoker		963	0	0	0	0	0
SUMS		2,773		4,005			

*Substratum types, estimated relief, number of photos with each substratum type, brisingid abundances by substratum type, summary statistics (see also **Figures 5**, **7**); na, not applicable.*

**The total number of photos for each substratum type is an indicative rather than quantitative measure of sampling effort, given the limitations of the survey strategy as described in section "Materials and Methods."*

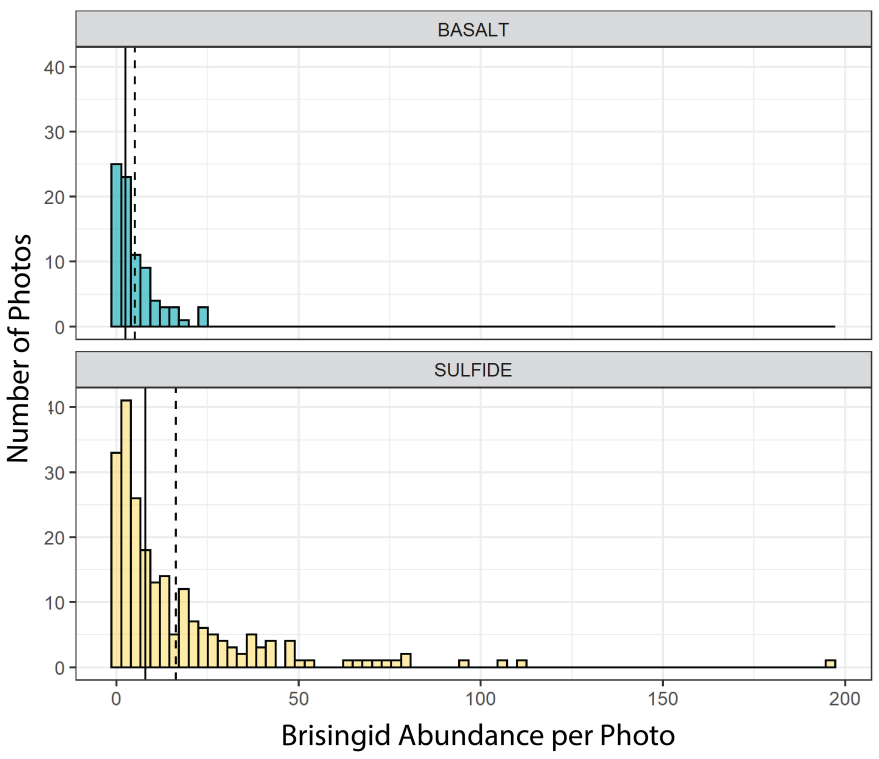

FIGURE 5 | Frequency distributions of brisingid abundances per photo on basalt and hydrothermally inactive sulfide substrata. Solid lines: median; dashed lines: mean.

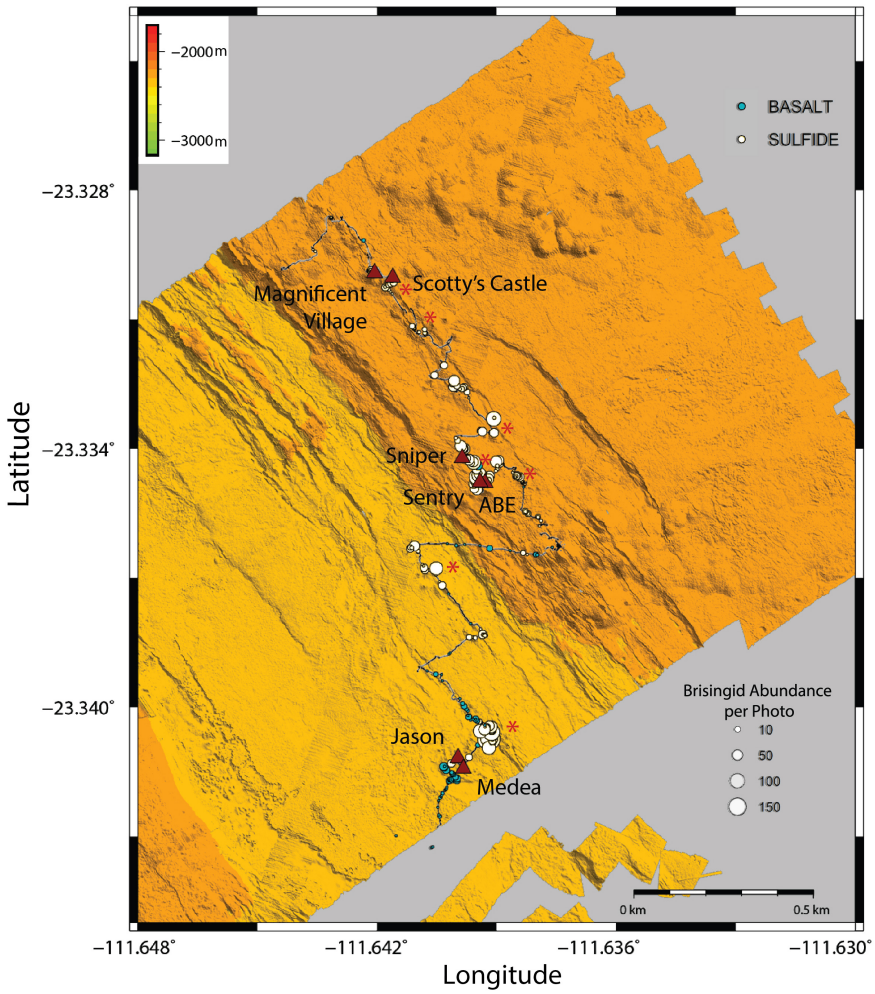

FIGURE 6 | ROV *Jason II* Dive 961 navigation track overlain with brisingid abundance (per photo) bubble plots for basalt and hydrothermally inactive sulfide substrata. Labeled triangles indicate locations of active black smokers; asterisks indicate aggregations of relict sulfide chimneys.

to black smokers. Anecdotally, relief alone is not sufficient to attract brisingids, given their absence on a meters-tall basalt pillar captured in the photos. The absence of brisingids on black smokers at Pito Seamount suggests that hydrothermal fluids emanating from sulfide surfaces create a thermally and/or chemically noxious habitat for this taxon. Brisingid seastars (likely a different species from those on Pito Seamount) were scarce in Pito Deep, where there was no hydrothermal activity and where food delivery may be diminished due to the greater depth. Future assessments of controls on brisingid distributions would benefit from surveys of basalt substrata at Pito Seamount (i.e., conspecifics at similar depths) but further removed from hydrothermal activity.

Aggregations of brisingids on hydrothermally relict chimneys some distance (up to 300 m) away from black smokers suggests that additional factors other than proximity to hydrothermal activity may contribute to their observed distribution. These include (i) microtopographically modified currents that deliver enhanced particulate organic material (POM) from chemosynthetic activity within the hydrothermal field and from surface-derived photosynthetic activity to suspension feeders on relict sulfide chimneys (Tunnicliffe et al., 1986; Erickson et al., 2009; Washburn et al., 2019); (ii) diffuse low-temperature and low-toxicity fluid flux that may persist in what might visually appear to be "relict" sulfide chimneys and that supports primary production by free-living microorganisms, which in turn serves as food for brisingids (Van Dover, 2019); (iii) autotrophic production based on oxidation of sulfide minerals (rather than dissolved sulfide or other reduced compounds in hydrothermal fluids) that serves as a food source for brisingid seastars occupying relict chimneys (Kato et al., 2010; Li et al., 2017); and (iv) microbes associated with undetected areas of diffuse, low-temperature flow through faults and cracks in the basalt that contribute to chemoautotrophic food resources for brisingids.

Currents that deliver suspended particles are known to be modified in areas of microtopographic (meters) relief, with acceleration zones over and between structures and eddy dissipation in the wake of structures (Hench and Rosman, 2013).

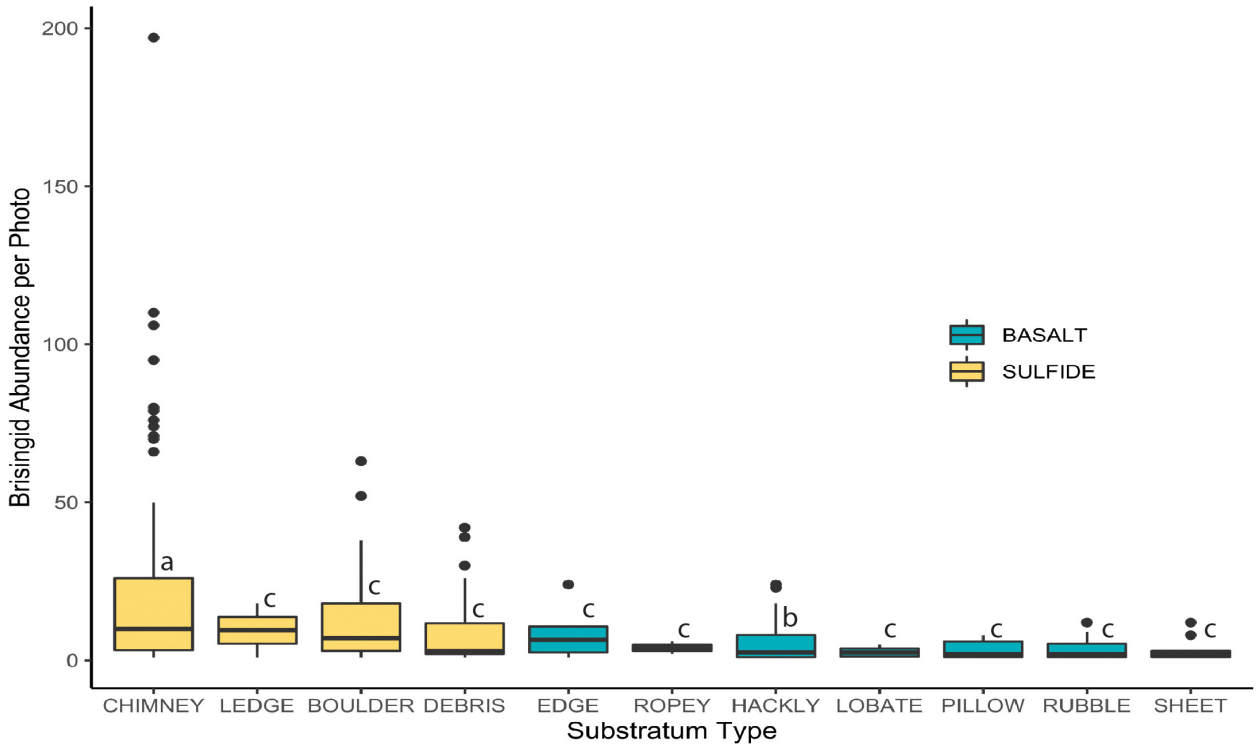

FIGURE 7 | Brisingid abundance per photo on sulfide and basalt, ordered by median values. Horizontal line: median; filled area: 25th through 75th percentiles; whiskers: maximum and minimum values; symbols: outliers (i.e., more than 1.5 × the length of the box from either end). Letters indicate significant differences ($p \leq 0.001$).

The observed higher abundances and densities of brisingids on relict chimneys proximal to black smokers is consistent with the hypothesis that brisingids benefit from such modified currents and from enhanced delivery of organic material produced at and exported from nearby areas of hydrothermal activity. Stable isotope analyses of suspension-feeding invertebrates in areas peripheral to active vents in Manus Basin (Erickson et al., 2009) provide indirect support of this food-enrichment and delivery hypothesis. However, where gradual mineralization leads to clogging and cessation of high-temperature fluid flux in a black smoker chimney, diffuse flow may continue to be emitted. Without sensitive temperature or fluid flux measures, we cannot state with certainty that relict sulfide chimneys on Pito Seamount lacked a diffuse flow component of hydrothermal activity, below what would be apparent from shimmer in the real-time video as our imagery was collected. Nor can we be certain there were no areas of diffuse flow through fissures or cracks in basalt outside the field of view of the ROV cameras. We also can offer no evidence that the sulfide substratum itself is essential to maintaining dense aggregations of brisingids, although chemoautotrophic microbial production based on oxidation of sulfide minerals of relict sulfide chimneys is well documented (Van Dover, 2019; Orcutt et al., 2020; Van Dover et al., 2020). The abundance and activity of microbial communities at relict sulfides may even be comparable to or greater than that of microbial communities on black smoker chimneys (Edwards et al., 2003; Kato et al., 2010; Li et al., 2017), but whether these microbes are available to suspension feeders remains to be determined.

A nutritional connection between brisingid abundance and chemosynthetic productivity exported from active hydrothermal vents on Pito Seamount and elsewhere on the EPR thus remains conjectural in the absence of direct evidence. Future studies may gather systematic data to refine the spatial "sphere of influence" (Levin et al., 2016) of hydrothermal activity and brisingid distributions. Such efforts might include undertaking more detailed characterization of the hydrothermal status of "relict" chimneys and using a combination of abundance data and stable isotope compositions of megafaunal tissues along transects approaching zones of hydrothermal activity to estimate the relative importance of photosynthetically and chemosynthetically derived organic material.

Reproductive benefits of aggregative behaviors may also underlie brisingid distributions near hydrothermal vents. While brisingids are sedentary, they are capable of some movement over the substratum. One species was observed to shift position by ∼1 cm in 10 min, presumably in response to shifting currents (Edwards et al., 2016). The extent to which dense aggregations of brisingids contribute to reproductive success of the species is unknown, but high densities may be important in the maintenance of local populations. Where eggs and sperm of a species are broadcast into the water column, as indicated

for brisingid seastars, aggregation of adults that exploit enriched sources of food could mitigate reproductive Allee effects, where fertilization success is limited among more solitary individuals (Gascoigne and Lipcius, 2004).

While it seems unlikely that relict sulfide occurrences such as those observed at Pito Seamount will be the target of deep-sea mining activities, they do appear to be an important habitat for brisingid seastars. If conservation measures should be merited to conserve biodiversity in this region, area-based management interventions could be used to protect representative aggregations of brisingids (Boschen et al., 2016; Van Dover, 2019; Boschen-Rose et al., 2021). While it can be challenging to suggest effective mitigation or restoration actions in the deep sea (Van Dover et al., 2014; Da Ros et al., 2019), this study suggests that construction of "artificial" microtopographic features within 10–100's of meters of hydrothermal activity might passively attract mobile taxa and/or new recruits, or might be repopulated through transplant of individuals from sites targeted for disturbance. Such an approach might be considered for aggregated taxa associated with relict sulfides elsewhere, as, for example, corals and urchins found on hydrothermally inactive sulfide occurrences associated with New Zealand seamounts (Boschen et al., 2015, 2016). Further research would be merited, however, to determine the design and efficacy of such artificial structures as mitigation interventions in any given region.

CONCLUSION

Suspension-feeding brisingid seastars were the visually dominant megafaunal invertebrate observed along the ROV *Jason II* Dive 961 transect at Pito Seamount and were most abundant on microtopographic relief provided by relict sulfide chimneys near black smokers. The sphere of influence of vent productivity on brisingid abundance may extend > 300 m from black smokers. Together, relict sulfide chimneys and proximity to black smokers likely play key roles in the maintenance of brisingid population density on Pito Seamount, though there may be other contributing factors. Experimental introduction of "artificial" microtopographic relief could test whether such an approach might mitigate potential impacts of mineral extraction on populations of suspension-feeding invertebrates.

DATA AVAILABILITY STATEMENT

The original contributions presented in the study are included in the article/**Supplementary Material**, further inquiries can be directed to the corresponding author/s.

AUTHOR CONTRIBUTIONS

DW: image analysis, statistics, visualizations, and writing (original draft, review, and edit). MC, BJ, and CG: resources and writing (visualization, review, and edit). CV: conceptualization, funding acquisition, supervision, methodology, statistics, visualization, and writing (original draft, review, and edit). All authors contributed to the article and approved the submitted version.

FUNDING

This project was partially supported by the Global Ocean Biodiversity Initiative through the International Climate Initiative (IKI; grant no. 16_IV_049_Global_A_Global Ocean Biodiversity Initiative GOBI). The Federal Ministry for the Environment, Nature Conservation, and Nuclear Safety (BMU) supports IKI on the basis of a decision adopted by the German Bundestag. DW was supported by Duke University funds to CV. CG's participation was funded through WHOI's Deep Ocean Exploration Institute. The AT37-08 cruise was funded by NSF OCE-1459462 (MC and BJ) and OCE-1459387 (J Gee, Scripps Institution of Oceanography).

ACKNOWLEDGMENTS

We thank the Captain and crew of the R/V Atlantis, the ROV Jason II and AUV Sentry teams, as well as Jeff Gee (Scripps Institution of Oceanography) and the Pito Deep 2017 Scientific Party for their efforts collecting images used in this study. We also value the preliminary work of students in the 2018 Deep-Sea Science and Environmental Management course at Duke University: A. Alberini, K. Johnson-Sapp, S. Poulin, K. Kochvar, E. Olszewski, L. Breitkreutz, E. Darnell, and N. Jacobson. The manuscript benefitted from reviewers' constructive comments.

SUPPLEMENTARY MATERIAL

The Supplementary Material for this article can be found online at: https://www.frontiersin.org/articles/10.3389/fmars.2022.774628/full#supplementary-material

Supplementary Figure 1 | Frequency distributions of brisingid abundances per photo on basalt and sulfide substrata.

Supplementary Table 1 | Brisingid abundances and substratum types, Pito Seamount.

Supplementary Table 2 | Brisingid abundances, Pito Deep.

REFERENCES

Boschen, R. E., Rowden, A. A., Clark, M. R., Pallentin, A., and Gardner, J. P. A. (2016). Seafloor massive sulfide deposits support unique megafaunal assemblages: implications for seabed mining and conservation. *Mar. Environ. Res.* 115, 78–88. doi: 10.1016/j.marenvres.2016.02.005

Boschen, R., Rowden, A., Clark, M., Barton, S., Pallentin, A., and Gardner, J. (2015). Megabenthic assemblage structure on three New Zealand seamounts: implications for seafloor massive sulfide mining. *Mar. Ecol. Prog. Ser.* 523, 1–14. doi: 10.3354/meps11239

Boschen-Rose, R. E., Clark, M. R., Rowden, A. A., and Gardner, J. P. A. (2021). Assessing the ecological risk to deep-sea megafaunal assemblages from seafloor

massive sulfide mining using a functional traits sensitivity approach. *Ocean Coast. Manag.* 210:105656. doi: 10.1016/j.ocecoaman.2021.105656

Carney, R. S. (2010). Stable isotope trophic patterns in echinoderm megafauna in close proximity to and remote from Gulf of Mexico lower slope hydrocarbon seeps. *Deep Sea Res. Part II Top. Stud. Oceanogr.* 57, 1965–1971. doi: 10.1016/j.dsr2.2010.09.027

Cheadle, M., John, B., German, C., Gee, J., Coogan, L., Gillis, K., et al. (2017). Pito Seamount revisited: the discovery and mapping of new black smoker vents. *AGU Fall Meet. Abstr.* 2017, 51D–0388D.

Chen, S., Tao, C., and German, C. R. (2021). Abundance of low-temperature axial venting at the equatorial East Pacific Rise. *Deep. Res. Part I Oceanogr. Res. Pap.* 167:103426. doi: 10.1016/j.dsr.2020.103426

Cherkashov, G. (2017). "Seafloor massive sulfide deposits: distribution and prospecting," in *Deep-Sea Mining*, ed. R. Sharma (Berlin: Springer International Publishing), 143–164. doi: 10.1007/978-3-319-52557-0

Da Ros, Z., Dell'Anno, A., Morato, T., Sweetman, A. K., Carreiro-Silva, M., Smith, C. J., et al. (2019). The deep sea: the new frontier for ecological restoration. *Mar. Policy* 108:103642. doi: 10.1016/j.marpol.2019.103642

Desbruyeres, D., Segonzac, M., and Bright, M. (2006). Handbook of deep-sea hydrothermal vent fauna. *Denisia* 18, 1–434.

Edwards, K. J., Bach, W., and Rogers, D. R. (2003). Geomicrobiology of the ocean crust: a role for chemoautotrophic Fe-bacteria. *Biol. Bull.* 204, 180–185. doi: 10.2307/1543555

Edwards, M. H., Fornari, D. J., Rognstad, M. R., Kelley, C. D., Mah, C. L., Davis, L. K., et al. (2016). Time-lapse camera studies of sea-disposed chemical munitions in Hawaii. *Deep. Res. Part II Top. Stud. Oceanogr.* 128, 25–33. doi: 10.1016/j.dsr2.2015.03.003

Emson, R. H., and Young, C. M. (1994). Feeding mechanism of the brisingid starfish *Novodinia antillensis*. *Mar. Biol.* 118, 433–442. doi: 10.1007/BF00350300

Erickson, K. L., Macko, S. A., and Van Dover, C. L. (2009). Evidence for a chemoautotrophically based food web at inactive hydrothermal vents (Manus Basin). *Deep Sea Res. Part II Top. Stud. Oceanogr.* 56, 1577–1585. doi: 10.1016/j.dsr2.2009.05.002

Fouquet, Y., Knott, R., Cambon, P., Fallick, A., Rickard, D., and Desbruyeres, D. (1996). Formation of large sulfide mineral deposits along fast spreading ridges. Example from off-axial deposits at 12°43'N on the East Pacific Rise. *Earth Planet. Sci. Lett.* 144, 147–162. doi: 10.1016/0012-821x(96)00142-2

Fustec, A., Desbruyères, D., Juniper, S. K., Fustec, A., and Desbruyeres, D. (2013). Deep-sea hydrothermal vent communities at 13°N on the East Pacific Rise: microdistribution and temporal variations. *Biol. Oceanogr.* 4, 121–164. doi: 10.1080/01965581.1987.10749487

Gale, K. S. P., Hamel, J. F., and Mercier, A. (2013). Trophic ecology of deep-sea Asteroidea (Echinodermata) from eastern Canada. *Deep. Res. Part I Oceanogr. Res. Pap.* 80, 25–36. doi: 10.1016/j.dsr.2013.05.016

Gascoigne, J., and Lipcius, R. N. (2004). Allee effects in marine systems. *Mar. Ecol. Prog. Ser.* 269, 49–59. doi: 10.3354/meps269049

Gerdes, K. H., Martínez Arbizu, P., Schwentner, M., Freitag, R., Schwarz-Schampera, U., Brandt, A., et al. (2019). Megabenthic assemblages at the southern Central Indian Ridge – Spatial segregation of inactive hydrothermal vents from active-, periphery- and non-vent sites. *Mar. Environ. Res.* 151:104776. doi: 10.1016/j.marenvres.2019.104776

German, C. R., Legendre, L. L., Sander, S. G., Niquil, N., Luther, G. W., Bharati, L., et al. (2015). Hydrothermal Fe cycling and deep ocean organic carbon scavenging: model-based evidence for significant POC supply to seafloor sediments. *Earth Planet. Sci. Lett.* 419, 143–153. doi: 10.1016/j.epsl.2015.03.012

Gollner, S., Govenar, B., Arbizu, P. M., Mullineaux, L. S., Mills, S., Bris, N. L., et al. (2020). Animal community dynamics at senescent and active vents at the 9° N East Pacific Rise after a volcanic eruption. *Front. Mar. Sci.* 6:832. doi: 10.3389/fmars.2019.00832

Halbach, P., Blum, N., Münch, U., Plüger, W., Garbe-Schönberg, D., and Zimmer, M. (1998). Formation and decay of a modern massive sulfide deposit in the Indian Ocean. *Miner. Depos.* 33, 302–309. doi: 10.1007/s001260050149

Hannington, M., Jamieson, J., Monecke, T., Petersen, S., and Beaulieu, S. (2011). The abundance of seafloor massive sulfide deposits. *Geology* 39, 1155–1158. doi: 10.1130/G32468.1

Hekinian, R., and Fouquet, Y. (1985). Volcanism and metallogenesis of axial and off-axial structures on the East Pacific Rise near 13N. *Econ. Geol.* 80, 221–249.

Hench, J. L., and Rosman, J. H. (2013). Observations of spatial flow patterns at the coral colony scale on a shallow reef flat. *J. Geophys. Res. Ocean.* 118, 1142–1156. doi: 10.1002/jgrc.20105

Hoagland, P., Beaulieu, S., Tivey, M. A., Eggert, R. G., German, C., Glowka, L., et al. (2010). Deep-sea mining of seafloor massive sulfides. *Mar. Policy* 34, 728–732. doi: 10.1016/j.marpol.2009.12.001

Howell, K., Pond, D., Billett, D., and Tyler, P. (2003). Feeding ecology of deep-sea seastars (*Echinodermata*: *Asteroidea*): a fatty-acid biomarker approach. *Mar. Ecol. Prog. Ser.* 255, 193–206. doi: 10.3354/meps255193

Jamieson, J., and Gartman, A. (2020). Defining active, inactive, and extinct seafloor massive sulfide deposits. *Mar. Policy* 117:103926. doi: 10.1016/j.marpol.2020.103926

Karson, J., Kelly, D., Fornari, D., Perfit, M., and Shank, T. (2015). *Discovering the Deep: A Photographic Atlas of the Seafloor and Ocean Crust*. Cambridge: Cambridge University Press.

Kato, S., Takano, Y., Kakegawa, T., Oba, H., Inoue, K., Kobayashi, C., et al. (2010). Biogeography and biodiversity in sulfide structures of active and inactive vents at deep-sea hydrothermal fields of the Southern Mariana Trough. *Appl. Environ. Microbiol.* 76, 2968–2979. doi: 10.1128/AEM.00478-10

Kim, S., and Hammerstrom, K. (2012). Hydrothermal vent community zonation along environmental gradients at the Lau back-arc spreading center. *Deep. Res. Part I Oceanogr. Res. Pap.* 62, 10–19. doi: 10.1016/j.dsr.2011.12.010

Lacharité, M., and Metaxas, A. (2017). Hard substrate in the deep ocean: how sediment features influence epibenthic megafauna on the eastern Canadian margin. *Deep. Res. Part I Oceanogr. Res. Pap.* 126, 50–61. doi: 10.1016/j.dsr.2017.05.013

Lalou, C., and Brichet, E. (1982). Ages and implications of East Pacific Rise sulphide deposits at 21 °N. *Nature* 300, 169–171. doi: 10.1038/300169a0

Lalou, C., Brichet, E., and Hekinian, R. (1985). Age dating of sulfide deposits from axial and off-axial structures on the East Pacific Rise near 12°50'N. *Earth Planet. Sci. Lett.* 75, 59–71. doi: 10.1016/0012-821X(85)90050-0

Lalou, C., Reyss, J.-L., Brichet, E., Rona, P. A., and Thompson, G. (1995). Hydrothermal activity on a 10ˆ5-year scale at a slow-spreading ridge, TAG hydrothermal field, Mid-Atlantic Ridge 26oN. *J. Geophys. Res.* 100, 17855–17862.

Levin, L. A., Baco, A. R., Bowden, D. A., Colaco, A., Cordes, E. E., Cunha, M. R., et al. (2016). Hydrothermal vents and methane seeps: rethinking the sphere of influence. *Front. Mar. Sci.* 3:72. doi: 10.3389/fmars.2016.00072

Li, J., Cui, J., Yang, Q., Cui, G., Wei, B., Wu, Z., et al. (2017). Oxidative weathering and microbial diversity of an inactive seafloor hydrothermal sulfide chimney. *Front. Microbiol.* 8:1378. doi: 10.3389/fmicb.2017.01378

Mah, C. L. (2016). A new species of Brisingenes from the Hawaii undersea military munitions assessment area with an overview of Hawaiian brisingid in situ video observations and functional morphology of subambulacral spines (*Forcipulatacea*; *Asteroidea*). *Deep. Res. Part II Top. Stud. Oceanogr.* 128, 43–52. doi: 10.1016/j.dsr2.2014.06.003

Mah, C., Linse, K., Copley, J., Marsh, L., Rogers, A., Clague, D., et al. (2015). Description of a new family, new genus, and two new species of deep-sea Forcipulatacea (Asteroidea), including the first known sea star from hydrothermal vent habitats. *Zool. J. Linn. Soc.* 174, 93–113. doi: 10.1111/zoj.12229

Mangiafico, S. (2016). *Summary and Analysis of Extension Program Evaluation in R, Version 1.18.8*.

Mordecai, G., Tyler, P. A., Masson, D. G., and Huvenne, V. A. I. (2011). Litter in submarine canyons off the west coast of Portugal. *Deep. Res. Part II Top. Stud. Oceanogr.* 58, 2489–2496. doi: 10.1016/j.dsr2.2011.08.009

Naar, D., Hekinian, R., Segonzac, M., Francheteau, J., and The Pito Dive Team. (2004). "Vigorous venting and biology at Pito Seamount, Easter Microplate," in *Mid-Ocean Ridges: Hydrothermal Interactions Between the Lithosphere and Ocean*, eds C. German, J. Lin, and L. M. Parson (Washington, DC: American Geophysical Union), 305–318. doi: 10.1029/148gm13

Orcutt, B. N., Bradley, J. A., Brazelton, W. J., Estes, E. R., Goordial, J. M., Huber, J. A., et al. (2020). Impacts of deep-sea mining on microbial ecosystem services. *Limnol. Oceanogr.* 65, 1489–1510. doi: 10.1101/463992

Petersen, S., Krätschell, A., Augustin, N., Jamieson, J., Hein, J. R., and Hannington, M. D. (2016). News from the seabed – Geological characteristics and resource potential of deep-sea mineral resources. *Mar. Policy* 70, 175–187. doi: 10.1016/j.marpol.2016.03.012

R Core Team (2020). *R: A Language and Environment for Statistical Computing*. Vienna: R Core Team.

Rona, P., Hannington, M. D., Tivey, K., and Lalou, C. (1993). Active and relict seafloor hydrothermal mineralization at the TAG hydrothermal field, Mid-Atlantic Ridge. *Econ. Geol.* 88, 1989–2017.

Tunnicliffe, V., Botros, M., De Burgh, M. E., Dinet, A., Johnson, H. P., Juniper, S. K., et al. (1986). Hydrothermal vents of explorer ridge, northeast Pacific. *Deep Sea Res. Part A Oceanogr. Res. Pap.* 33, 401–412. doi: 10.1016/0198-0149(86)90100-7

Van Dover, C. L. (2000). *The Ecology of Deep-Sea Hydrothermal Vents*. Princeton, NJ: Princeton University Press, doi: 10.2307/177518

Van Dover, C. L. (2019). Inactive sulfide ecosystems in the deep sea: a review. *Front. Mar. Sci.* 6:461. doi: 10.3389/fmars.2019.00461

Van Dover, C. L., Aronson, J., Pendleton, L., Smith, S., Arnaud-Haond, S., Moreno-Mateos, D., et al. (2014). Ecological restoration in the deep sea: desiderata. *Mar. Policy* 44, 98–106. doi: 10.1016/j.marpol.2013.07.006

Van Dover, C. L., Colaço, A., Collins, P. C., Croot, P., Metaxas, A., Murton, B. J., et al. (2020). Research is needed to inform environmental management of hydrothermally inactive and extinct polymetallic sulfide (PMS) deposits. *Mar. Policy* 121:104183. doi: 10.1016/j.marpol.2020.104183

Washburn, T. W., Turner, P. J., Durden, J. M., Jones, D. O. B., Weaver, P., and Van Dover, C. L. (2019). Ecological risk assessment for deep-sea mining. *Ocean Coast. Manag.* 176, 24–39. doi: 10.1016/j.ocecoaman.2019.04.014

Wickham, H. (2016). *ggplot2: Elegant Graphics for Data Analysis*. New York, NY: Springer-Verlag.

Conflict of Interest: The authors declare that the research was conducted in the absence of any commercial or financial relationships that could be construed as a potential conflict of interest.

The reviewer RB-R declared a past co-authorship with one of the authors CV to the handling editor.

Publisher's Note: All claims expressed in this article are solely those of the authors and do not necessarily represent those of their affiliated organizations, or those of the publisher, the editors and the reviewers. Any product that may be evaluated in this article, or claim that may be made by its manufacturer, is not guaranteed or endorsed by the publisher.

frontiers in Marine Science

ORIGINAL RESEARCH
published: 17 February 2022
doi: 10.3389/fmars.2022.784807

Microbial Community Structure and Functional Potential of Deep-Sea Sediments on Low Activity Hydrothermal Area in the Central Indian Ridge

*Teddy Namirimu[1,2], Yun Jae Kim[1,2], Mi-Jeong Park[1,2], Dhongil Lim[2,3], Jung-Hyun Lee[1,2] and Kae Kyoung Kwon[1,2]**

[1] Marine Biotechnology Research Center, Korea Institute of Ocean Science and Technology, Busan, South Korea, [2] Major of Ocean Science, University of Science and Technology, Daejeon, South Korea, [3] Library of Marine Samples, Korea Institute of Ocean Science and Technology, Busan, South Korea

Little is known about the community structure and metabolic potential of microbial communities in hydrothermal fields in the Central Indian Ridge (CIR). In this study, a metagenomic sequencing approach was conducted to explore the microbial diversity in three sediment samples collected during the 2019 expedition from two recently discovered hydrothermal vent fields; Invent E and Onnuri Vent Field (OVF). Analysis of unassembled metagenomic reads using the Metagenomic analysis server (MG-RAST) revealed that microbial communities of the two sampling sites were very similar, showing the dominance of Bacteria over Archaea. *Proteobacteria*, *Firmicutes, Bacteroidetes*, as well as *Euryarchaeota* were dominant in all samples. Functional annotation based on KEGG categories shows that the microbial populations in these vent fields possess metabolic capabilities for aerobic respiration, carbon fixation through the Calvin–Bassham–Benson (CBB) cycle, the reverse tricarboxylic acid (rTCA) cycle, and reductive acetyl-CoA pathway as well as sulfur and nitrogen metabolisms. Comparative metagenome analysis with different datasets obtained from different ocean ridges showed that microbial communities at low activity or hydrothermally influenced area differ from highly active hydrothermal communities. This study provides insights into the genetic diversity and functional capability of the microbial communities of slow to intermediate spreading hydrothermal systems.

Keywords: slow to intermediate spreading, hydrothermal vent, microbial community, metagenome, Central Indian Ridge (CIR)

OPEN ACCESS

Edited by:
Pei-Yuan Qian, Hong Kong University of Science and Technology, Hong Kong SAR, China

Reviewed by:
Man Kit Cheung, The Chinese University of Hong Kong, China
Zongze Shao, Third Institute of Oceanography, China

***Correspondence:**
Kae Kyoung Kwon
kkkwon@kiost.ac.kr

Specialty section:
This article was submitted to Deep-Sea Environments and Ecology, a section of the journal Frontiers in Marine Science

Received: *28 September 2021*
Accepted: *17 January 2022*
Published: *17 February 2022*

Citation:
Namirimu T, Kim YJ, Park M-J, Lim D, Lee J-H and Kwon KK (2022) Microbial Community Structure and Functional Potential of Deep-Sea Sediments on Low Activity Hydrothermal Area in the Central Indian Ridge. Front. Mar. Sci. 9:784807. doi: 10.3389/fmars.2022.784807

INTRODUCTION

Deep-sea hydrothermal vents contain extreme thermal and chemical gradients, yet they harbor the most unique and diverse habitats for various microorganisms (Zeng et al., 2021). As seawater percolates into the ocean crust, volcanic water-rock reactions lead to hot, reduced metal-rich hydrothermal fluids venting from the seafloor. Biomass production in vent ecosystems is mainly fueled by oxidation of reduced compounds in hydrothermal fluids to fix carbon primarily by chemolithoautotrophic microorganisms (Fisher et al., 2007; Nakagawa and Takai, 2008) and consequently, they provide a source of nutrition for the higher organisms. In addition, many

microbial populations play a crucial role in the global biogeochemical cycling of methane, nitrogen, sulfur, and carbon in these unique ecosystems (Zeng et al., 2021).

The discovery of deep hydrothermal vent fields in the 1970s (Francheteau et al., 1979) has attracted great attention to scientists with over 700 vent fields discovered and investigated along mid-ocean ridges, volcanic arcs, and tectonic settings (Dick, 2019; Beaulieu and Szafrański, 2020). However, until recently, majority of the hydrothermal system discoveries and investigation have exclusively focused on the Pacific and Atlantic Oceans (Nakamura and Takai, 2015), thus, the Indian Ocean hydrothermal systems remain understudied. To date a limited number of hydrothermal fields have been identified in the Indian Ocean including the MESO Mineral Zone (Halbach et al., 1998), Kairei (Gamo et al., 2001), Edmond (Van Dover et al., 2001), Solitaire, Dodo (Nakamura et al., 2012), and Onnuri fields (Kim et al., 2020) in the Central Indian Ridge (CIR), Daxi and Wocan fields in the Carlsberg Ridge (Wang et al., 2017, 2020), Mount Jourdanne (Münch et al., 2001), Yuhuang-1 (Liao et al., 2018), Longqi (Tao et al., 2012), Duanqiao (Yang et al., 2017), and Tiancheng (Zhou et al., 2018) in the South West Indian Ridge (SWIR), and Pelagia vent field (Han et al., 2018) in the South East Indian Ridge (SEIR).

Despite their inaccessible locations, recent advances in sampling equipment and NGS approaches have revealed that the geochemical and biological communities of the Indian Ocean hydrothermal vent systems are quite diverse (Cao et al., 2014; Ding et al., 2017; Yang et al., 2020). Using an integrated approach, the predominance of formate- and CO-utilizing bacteria among others was observed in the serpentinite-hosted Old City hydrothermal field in SWIR (Lecoeuvre et al., 2021). A previous 16S rRNA analysis of microbial communities at a black smoker in Dodo field showed that it is dominated by *Bacteria* with dominance of *Gammaproteobacteria*, *Alphaproteobacteria*, and *Bacteroidetes* (Kawagucci et al., 2016). In the high-temperature Edmond sulfide chimney, representative taxa included *Epsilonproteobacteria* and *Aquificales* as well as archaeal genera *Aciduliprofundus* and *Thermococcus* (Hoek et al., 2003) whereas H_2-enriched fluids from Kairei field were dominated by (hyper)thermophilic hydrogenotrophic methanogens (Takai et al., 2004). These chemolithotrophic microbial communities involved in hydrogenotrophic, thiotrophic, and methanotrophic metabolisms have been reported to mediate biogeochemical processes in deep-sea hydrothermal systems (Nakamura and Takai, 2014).

Previous studies in the CIR listed above have solely relied on 16S rRNA gene libraries, however, 16S rRNA gene surveys offer limited information on understanding biological patterns of microbial communities within an environment. In this study, we describe the microbial structure and functional diversity in hydrothermally influenced sediments from the newly discovered vent fields in the CIR. This is the first study using metagenomic approach, to report in detail the metabolic potential of microbial communities from hydrothermal vent fields in the CIR. Comparative metagenomic analysis of hydrothermally influenced and hydrothermal samples from different locations and/or with different geochemistry would give us a better understanding of the metabolic potential of microbial communities inhabiting slow to intermediate spreading hydrothermal systems in the Indian Ocean.

MATERIALS AND METHODS

Study Site and Sample Collection

The Onnuri vent field (OVF) (Kim et al., 2020) is an ultramafic-hosted active vent located more than ∼800 km north of previously known active vent fields (i.e., Dodo and Solitaire fields) (Son et al., 2014). It is located about 11 km off axis, 1,990–2,170 m deep, characterized with small chimneys, and low-temperature clear fluid effusing from rock fissures supporting a wide range of vent fauna. The OVF vent fluids are enriched in CH_4 (52.5 nM max) and low metal concentrations (Kim et al., 2020). In contrast, segment 1 (Invent B) appears to be a magmatic basaltic-hosted system with several inactive vent chimneys structures. Diffuse venting was observed characterized with high temperature, high concentration of Fe (366 nM max), Mn (46 nM max), and dissolved methane (13.0 nM max) (Kim et al., 2020). Invent E sediments geochemical compositions included Fe_2O_3 (45.6%), MnO (7.8%), CaO (1.4%), TN (313 μg/g), TOC (1865 μg/g), and TS (1374 μg/g) in total concentration (**Table 1** and **Supplementary Table 1**). These unique venting styles and different geological properties of the newly identified vent fields provide an interesting opportunity to understand the microbial community structure and metabolic potentials of hydrothermal vents in slow to intermediate spreading ridges.

Deep-sea sediments were obtained from three different vent fields along the CIR during the deep-sea expedition aboard *R/V* ISABU of Korea Institute of Ocean Science and Technology (KIOST) in June 2019. Sediment samples were collected using either a TV-grab (GTV), multiple corer (MC) and/or box corer (BC). Eight sediment samples BC1902, BC1903, GTV1904, GTV1907, GTV1906, MC1906, and MC1912 were collected around Onnuri Vent Field (OVF), a newly identified and the sixth hydrothermal vent system discovered in the Central Indian Ridge (Kim et al., 2020). Two other sediment samples GTV1902 and GTV1908 were collected from Invent E and Invent B fields respectively, currently inferred hydrothermal vent fields in the CIR (**Figure 1**). In case of OVF samples were retrieved from the venting areas (∼100–150 m diameter), however, samples from Invents B and E were obtained from areas that did not show signature of plume. Once on board, samples were subsampled, preserved at −80°C until further use.

Amplicon Sequencing and Analysis

DNA in duplicate was extracted from each of the sediments using the FastDNA^{TM} SPIN Kit for soil (MP Biomedicals, LLC, Solon, OH, United States) following the manufacturer's instructions. Microbial communities were characterized by sequencing the 16S rRNA gene using prokaryotic universal primers 314F (5′-CCTACGGGRBGCASCAG-3′)/805R (5′-GACTACNVGGGTATCTAAT-3′) which target the V3-V4 regions (Takahashi et al., 2014). The concentration of the amplicons was quantified using NanoDrop^{TM} 2000

TABLE 1 | Sampling information, physico-chemical characteristics of samples, and summary statistics of the three metagenomes studied obtained from MG-RAST.

Hydrothermal Vent	GTV1902 (Invent E)	GTV1904 (OVF)	GTV1906 (OVF)
Description	CH_4, H_2, metal-rich, coarse sands	CH_4, H_2, metal-poor, volcaniclastic grains	CH_4, H_2, metal-poor, volcaniclastic grains
Latitude	12.371062′S	11.248869′S	11.24962′S
Longitude	66.076′E	66.254197′E	66.253989′E
Depth (m)	3027.7	2014.5	2023.2
TN (μg/g)	313	625	338
TS (μg/g)	1374	19177	7998
TOC (μg/g)	1865	3166	783
TIC (μg/g)	910	156	94
$CaCO_3$	0.76	0.13	0.08
Total no. of bases	3,540,030,759	3,048,036,623	4,266,969,176
Number of reads after QC	17,533,939	15,395,496	16,971,386
Mean sequence length (bp)	170 ± 44	167 ± 43	154 ± 24
Mean GC%	57 ± 11	52 ± 12	55 ± 12
No. of predicted proteins	6,305,326	6,081,369	5,459,878
Unknown function	10,101,194	8,363,064	10,586,291
Bacteria (>60% ident) [%]	85.57	97.16	93.79
Archaea (>60% ident) [%]	13.28	1.72	4.83
Eukaryota (>60% ident) [%]	1.12	1.07	1.33
Viruses (>60% ident) [%]	0.03	0.04	0.04

spectrophotometer and visualized by gel electrophoresis. The purified PCR products were pooled at equimolar concentrations and paired-end sequenced using Illumina Miseq platform at Chunlab, Inc., South Korea. 16S rRNA gene reads were processed using *Mothur* version 1.41.0 (Schloss et al., 2009), and operational taxonomic units (OTUs) at 97% similarity were classified using the SILVA v128 database (Quast et al., 2013). Sequence data were normalized by randomly sub-sampling all datasets to the lowest sample size. Statistical analyses were carried out in R version 4.1.0 (R Core Team, 2021). Diversity analyses (alpha and beta diversity) were calculated using the packages *phyloseq* (McMurdie and Holmes, 2013) and *microeco* (Liu et al., 2021). Visualization was performed using the *ggplot2* package (Wickham et al., 2016).

Metagenome DNA Extraction and Sequencing

Based on the amplicon preliminary results, three representative samples (GTV1902, GTV1904, and GTV1906) were selected for shotgun sequencing. GTV1902 presented the most contrasting microbial community from the other studied sediments while GTV1904 and GTV1906 from which high-quality DNA could be obtained were the most diverse representative community among OVF samples. DNA purification from the three sediment samples was carried out using sterilized spatulas, separate pipettes, and reagents to avoid cross contamination. Sediment samples (0.5 g each) were subjected to DNA extraction using the FastDNA^{TM} SPIN Kit for soil (MP Biomedicals, LLC, Solon, OH, United States). Briefly, each sample was transferred into separate lysing matrix E tubes and then used for community DNA extraction. Two to four DNA extractions were pooled into a single sample and further concentrated by ethanol precipitation to obtain sufficient DNA for each sediment sample. DNA quality was verified by agarose gel electrophoresis and quantified using NanoDrop^{TM} 2000 spectrophotometer. Paired-end read sequencing of 2 × 250 bp was performed using Illumina MiSeq platform 2500 at Chunlab, Seoul (South Korea).

Metagenome Analysis, Assembly, and Annotation

Unassembled reads from the three datasets (GTV1902, GTV1904, and GTV1906) were submitted to the MG-RAST webserver version 4.0.3[1] (Meyer et al., 2019) for processing following their standard protocol. Briefly, the mate-pairs were joined and then pre-processed for quality control. Adapter sequences were identified and trimmed using skewer (Jiang et al., 2014). Using duplicate read inferred sequencing error estimation (DRISEE) (Keegan et al., 2012) artificial duplicate reads (ADRs) (Gomez-Alvarez et al., 2009) were analyzed and de-replicated. Host DNA contamination was removed using Bowtie2 (Langmead and Salzberg, 2012). Coding regions within the sequences were predicted using FragGeneScan (Rho et al., 2010) and clustered at 90% homology using CD-HIT (Fu et al., 2012). Sequences similarity searches were then performed using BLAST-like alignment tool (BLAT) (Kent, 2002) against the M5NR non-redundant protein database (Wilke et al., 2012) in MG-RAST version 4.0.3 (Meyer et al., 2019). Taxonomic and functional classification was performed using the RefSeq (O'Leary et al., 2016) and Kyoto Encyclopedia of Genes and Genome (KEGG) Orthology (KO) (Kanehisa et al., 2007) or SEED (Overbeek et al., 2005) databases with default parameters,

[1]http://metagenomics.anl.gov/

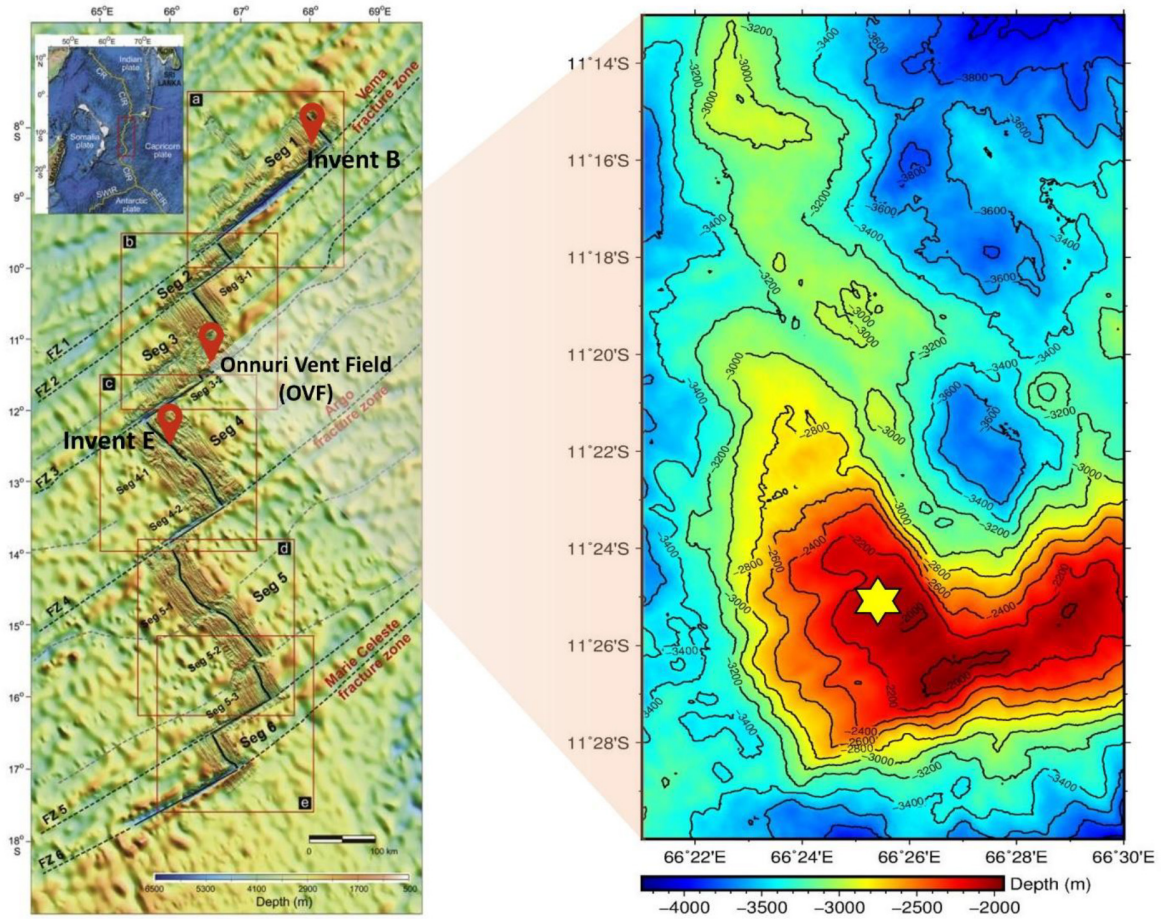

FIGURE 1 | Location of the studied hydrothermal vent fields. Bathymetric map of Invent B, Invent E and Onnuri Vent Field (OVF) located on segment 1, segment 3 and Segment 4 along the Central Indian Ridge [map modified from Pak et al. (2017)]. Sampling site at OVF is noted with yellow star.

respectively. The resulting profiles were downloaded for further analyses in R version 4.1.0 (R Core Team, 2021). The taxonomic composition and relative abundance of the key metabolic genes in the metagenomes were visualized using the package ggplot2 (Wickham et al., 2016).

The raw sequence reads were also assembled *de novo* into contigs using metaSPAdes (v 3.10) (Nurk et al., 2017) implemented in ATLAS (Kieser et al., 2020), using the default parameters for the three metagenomes (GTV1902, GTV1904, and GTV1906). Genome binning was carried out individually for each sample using two binning methods MetaBat v2.12.1 (Kang et al., 2019) and MaxBin v2.2.6 (Wu et al., 2016). The resulting bins were further refined using the DAS Tool (Sieber et al., 2018) into metagenome-assembled genomes (MAGs) and the quality of each MAG was assessed using CheckM (Parks et al., 2015). Open reading frames (ORFs) within MAGs from each sample were predicted using Prodigal v2.6.3 (Hyatt et al., 2010), clustered using mmseqs (Steinegger and Soding, 2017) and the resulting gene catalogs were mapped to the eggNOG catalog v5 (Huerta-Cepas et al., 2019) using eggNOG mapper implemented in ATLAS (Kieser et al., 2020). Taxonomic annotation of the resulting MAGs was inferred using the genome taxonomy database tool kit (GTDB-tk) (Parks et al., 2018).

Phylogenetic Analysis of Dissimilatory Sulfite Reductase Genes

The dissimilatory sulfite reductase (*dsr*) is a key enzyme in both the reduction of sulfate in sulfate-reducing microorganisms or functions in reverse in sulfide-oxidizing microorganism. To distinguish the pathway directionality of dissimilatory sulfate reduction or oxidation, *dsrAB* phylogeny was conducted (Müller et al., 2015). The gene sequences encoding *dsrAB* (KO number K11180, K11181) were retrieved manually from all metagenomic contigs based on KEGG annotations. Reference protein sequences for phylogenetic analyses were obtained by BLAST searches against the NCBI protein database. Using several reference sequences, phylogenetic trees were reconstructed using the maximum-likelihood treeing method with Jones–Taylor–Thornton (JTT) amino acid substitution model (Jones et al., 1992). All processes were conducted by using MEGA ver. 7 (Kumar et al., 2016).

Comparative Metagenomic Analysis

The CIR metagenomic datasets were compared to seven hydrothermal vent metagenomes available within the MG-RAST pipeline. Two datasets from Mid Atlantic Ridge (MAR) were retrieved by searching the MG-RAST database using appropriate keywords (e.g., "hydrothermal vent," "shotgun metagenome," "sediment"). The other five Southwest Indian ridge metagenome datasets were downloaded from the NCBI's SRA, uploaded into MG-RAST server, and processed according to the methods described above. A double hierarchical heatmap was constructed using the RefSeq, SEED, and KEGG profiles of each metagenome to compare the taxonomic and functional diversity in different vent systems. The number of sequence hits in each metagenome was normalized, and their Euclidean distances were calculated and visualized in R using the package *pheatmap* (Kolde, 2019).

Data Availability

The raw reads from this study were deposited to NCBI under the Bio project accession number PRJNA751690 The metagenomic sequencing data are also publicly available from the MG-RAST server version 4.0.3 (see text footnote 1) (Meyer et al., 2008) under the following IDs: mgm4898492.3 for GTV1902, mgm4898484.3 for GTV1904, and mgm4898483.3 for GTV1906.

RESULTS

Physico-Chemical Composition of the Sediments

The geochemical compositions of the sediments were found to vary across sediment samples. TN, TS, and TOC were enriched in GTV1904 (OVF) than in the other two studied sediments, whereas TIC and $CaCO_3$ were found to be higher in GTV1902 (**Table 1**). The detailed geochemical and elemental compositions of the three sediment samples studied are given in **Table 1** and **Supplementary Table 1**, respectively. The concentration of Ba was the highest in GTV1904 and GTV1906, whereas that of Cu was the highest in GTV1902. In addition, sediment GTV1902 from Invent E presented higher concentrations of Fe_2O_3, MnO, CaO, K_2O, Na_2O, V, and Zn than those of sediments from OVF (GTV1904 and GTV1906); however, SiO_2, Sn, and Pb concentrates were lower (**Supplementary Table 1**). These differences in physicochemical compositions may be reflected in the microbial community composition of the three sediment samples.

16S rRNA Sequencing Diversity

Initially, we assessed the microbial community diversity associated with hydrothermally influenced sediments from different vent fields along the CIR by targeting the 16S rRNA gene V3-V4 region. Bacteria were the most diverse across all samples dominated by *Gammaproteobacteria* (26.7% in the Invent B; 40.8%–12.5% in the OVF samples) except GTV1902 (Invent E) where *Thermoplasmata* (18.2%) were the most dominant OTUs observed (**Supplementary Figure 1**). Gammaproteobacterial marine benthic group *JTB255*, the *OM1* clade (*Actinobacteria*), *SAR202* (*Chloroflexi*), and *Epsilonproteobacteria* members *Sulfurovum* and *Sulfurimonas* were some of the abundant OTUs identified (**Supplementary Figure 2**). The NMDS plot showed that sediment from Invent B clustered together with OVF sediments while Invent E sample clustered further apart from the rest of the samples (**Supplementary Figure 3**). Sample GTV1902 had the most contrasting microbial community composition and GTV1904 presented the highest abundance of *Bacteroidetes* while GTV1906 was the most diverse and representative sample among OVF samples. These preliminary findings prompted us to further investigate the microbial communities of GTV1902, GTV1904, and GTV1906 by shotgun metagenome sequencing.

Microbial Community Composition

Shotgun metagenomic sequencing resulted in a total of 65,672,806 raw sequencing reads from the three samples with an average length of 166 bases. Quality processing produced 17,533,939 sequence reads from GTV1902, 15,395,496 for GTV1904, and 16,971,386 from GTV1906. Of the sequence reads that passed QC, 6,305,326 (GTV1902), 6,081,369 (GTV1904), and 5,459,878 (GTV1906) sequences contained predicted proteins with known functions while 10,101,194 (GTV1902), 8,363,064 (GTV1904), and 10,586,291 (GTV1906) sequence contained predicted proteins with unknown functions. The metagenome sequence statistics for the three metagenomes and the publicly available metagenomes used in this study are shown in **Table 1** and **Supplementary Table 2**.

Taxonomic classification of protein-coding genes was assigned using the NCBI RefSeq (O'Leary et al., 2016) protein database as implemented in MG-RAST. Bacterial sequences dominated in all metagenomes with 85.6% (GTV1902), 97.2% (GTV1904), and 93.8% (GTV1906) of the total assigned reads (**Table 1**). GTV1902 metagenome exhibited the highest archaeal representatives accounting for 13.3% of the total hits. Eukaryotic reads were also detected while less than 1% of the reads were assigned to viruses (**Table 1**). Sequences from all datasets were assigned to 28 different bacterial and 5 archaeal phyla.

All three samples shared *Proteobacteria* as the most dominant phylum. GTV1902 was dominated by *Deltaproteobacteria* (12.9%), within those the genus *Geobacter*, was the most abundant taxa (**Supplementary Figure 4**). Bacteria belonging to the phylum *Firmicutes* had the second highest relative abundance (17.6%), followed by *Chloroflexi* (8.7%), *Actinobacteria* (7.5%), and *Bacteroidetes* (4.8%) (**Figure 2A**). Members of the genera *Clostridium* and *Bacillus* were the representatives of the phylum *Firmicutes* while the most abundant *Chloroflexi* genera detected in GTV1902 were *Roseiflexus* and *Dehalococcoides* (**Supplementary Figure 4**). In contrast, the bacterial community in GTV1904 and GTV1906 were mainly composed of *Gammaproteobacteria* (29.6% and 22.3%, respectively; **Figure 2A**). *Thioalkalivibrio*, *Pseudomonas,* and *Nitrosococcus* were the dominant gammaproteobacterial genera found in GTV1904 and GTV1906 metagenomes (**Supplementary Figure 4** and **Supplementary Table 3**). Other dominant bacterial phyla within GTV1904 and GTV1906 included *Bacteroidetes*, *Firmicutes*, *Actinobacteria,* and *Planctomycetes* (**Figure 2A**).

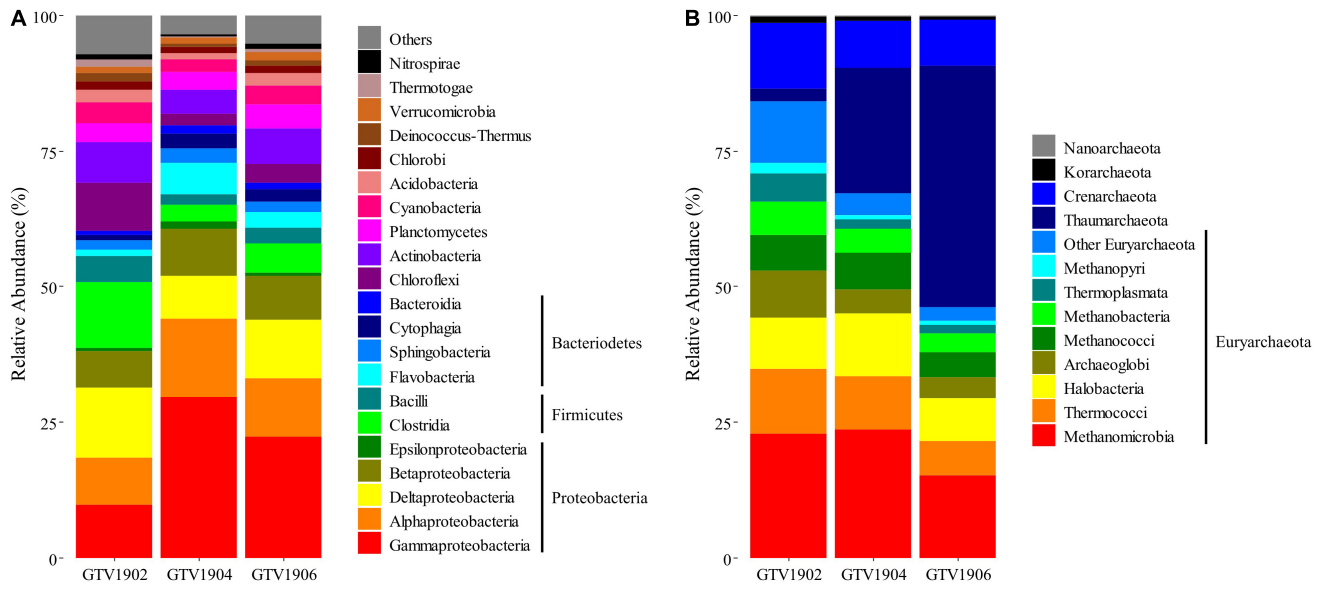

FIGURE 2 | Taxonomic composition and relative abundance of **(A)** Bacteria and **(B)** Archaea in the three different metagenomes based on protein-coding genes using RefSeq database at class level. "Others" represent those accounting for <1% of the total hits in each sample and are shown in gray at the top of each bar.

A detailed taxonomic analysis of the archaeal representatives found in the different metagenomes is shown in **Figure 2B**. While GTV1902 and GTV1904 archaeal community was dominated by *Euryarchaeota*, the archaeal community of GTV1906 was equally dominated by *Euryarchaeota* and *Thaumarchaeota*. *Methanomicrobia* was the most prevalent class in GTV1902 and GTV1904 accounting for 22.9% and 23.7% of the total assigned sequences, respectively. Unclassified (derived from *Thaumarchaeota*) was the most abundant class accounting for 44.4% of the total assigned reads of GTV1906 and followed by *Methanomicrobia* (15.1%). GTV1902 exhibited a predominance of *Aciduliprofundum* while the thaumarchaeotal genera *Nitrosopumilus* dominated the archaeal community in both GTV1904 and GTV1906 (**Supplementary Figure 4** and **Supplementary Table 4**).

Metagenome-Assembled Genomes

The GTV1902 assembly generated 61,732 contigs of sizes from 500 to 105,415 bp with an N50 of 12,795. The GTV1904 assembly generated 57,779 contigs of sizes from 500 to 99,270 base pairs with an N50 of 9,946 while 38,882 contigs of sizes from 500 to 39,457 base pairs with an N50 of 9,769 were retrieved from GTV1906 assembly (**Supplementary Table 5**). Metagenome binning yielded 20 medium- to high-quality MAGs on the established standards (Bowers et al., 2017) including 4 Archaea and 16 Bacteria (**Supplementary Table 6**). Taxonomic annotation based on the GTBD-Tk revealed that the 16 bacterial MAGs could be assigned to 8 phyla including the KSB1 (2 MAGs), *Actinobacteriota* (3), *Bacteroidota* (4), *Chloroflexota* (1), *Gemmatimonadota* (2), *Nitrospirota* (1), *Planctomycetota* (1), and *Proteobacteria* (2). In addition, we assembled four archaeal MAGs, which were affiliated to two phyla: *Thermoplasmatota* (3) and *Asgardarchaeota* (1) (**Supplementary Table 6**). Except for archaeal phylum *Asgardarchaeota*, similar taxa as the MAGs assembled here were observed in the 16S rRNA gene amplicon data.

Functional Composition

To determine the functional potential of the communities across the different metagenomes, we analyzed the relative abundance of key metabolic genes in the three CIR metagenomes. Biomass production in deep-sea hydrothermal vents is fueled by the oxidation of reduced inorganic compounds to fix inorganic carbon, therefore, key metabolic genes for carbon, sulfur, nitrogen, and methane metabolism were analyzed. The overall functional potential was similar across metagenomes with majority of the genes universally present across all samples and a few differences in relative abundances. The relative normalized abundances of the key genes involved in energy generation and biogeochemical cycling based on assembled contigs and unassembled raw reads are shown in **Figure 3** and **Supplementary Figure 5**, respectively.

Carbon Fixation

Genes related to the key enzymes of Calvin–Benson–Bassham (CBB) cycle (*rbcLS* and *prkB*) were found in all metagenomic datasets (**Figure 3** and **Supplementary Table 7**) however they were highly enriched in OVF (GTV1904 and GTV1906). Sequences were most related to gammaproteobacterial *genera Nitrosococcus* and *Allochromatium*, among others were observed (**Supplementary Table 8**). The three key genes of the reductive tricarboxylic acid (rTCA) cycle, ATP citrate lyase (*acly*), 2-oxoglutarate ferredoxin oxidoreductase (*korABCD*), and pyruvate ferredoxin oxidoreductase (*porABCD*) are higher in

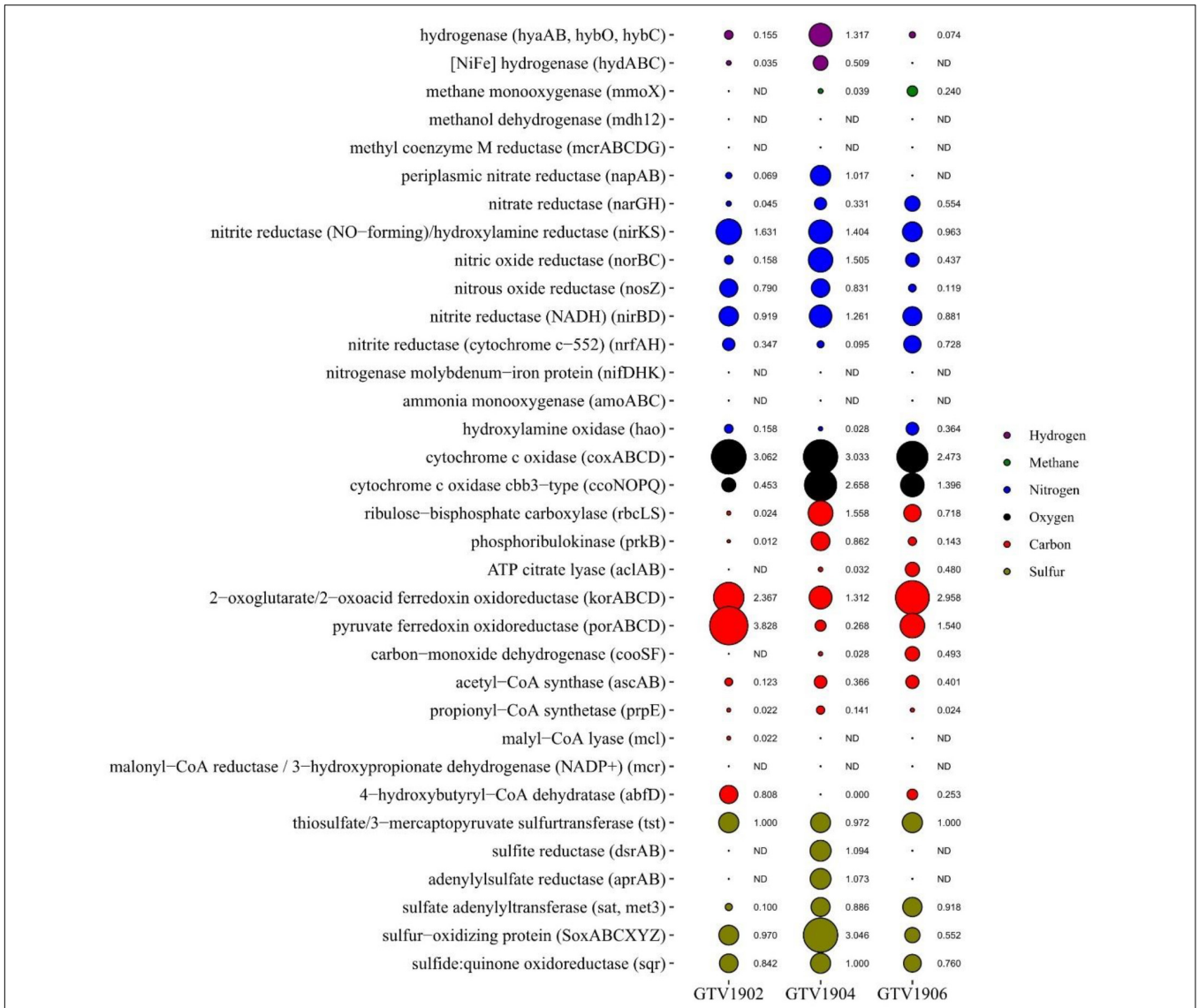

FIGURE 3 | The relative abundance of key metabolic genes involved in energy-yielding processes and carbon fixation pathways in the different metagenome assemblies. Each bubble size represents the relative abundance of specific genes against the total number of KO hits in each assembly.

GTV1902 (Invent E) compared to GTV1904 and GTV1906. However, the marker gene for the complete rTCA cycle ATP citrate lyase (*aclAB*) was not found in GTV1902 (**Figure 3** and **Supplementary Table 7**). The *acly* sequences found in the GTV1906 sites were closely affiliated with *Chlorobi*. In contrast sequences in GTV1904 share high similarities with those from *Epsilonproteobacteria* (**Table 2** and **Supplementary Table 8**). Markers for the Wood-Ljungdhal (WL) (=reductive acetyl-CoA) pathway had a slightly higher abundance in GTV1906 (OVF) metagenome (**Figure 3**). These genes were closely related to *Firmicutes* and *Deltaproteobacteria* groups (**Supplementary Table 8**). The key enzymes for the 3-hydroxypropionate (3-HP) and 3-HP/4-hydroxybutyrate (3-HP/4-HB) cycle, 4-hydroxybutyryl-CoA dehydratase (*abfD*), propionyl-CoA synthetase (*prpE*), and malyl-CoA lyase (*mcl*), were also detected in low abundance, however, malonyl-coA reductase (*mcr*) was missing in all datasets (**Figure 3** and **Supplementary Table 7**).

Sulfur Metabolism

The complete set of genes encoding the enzymes dissimilatory sulfite reductase (*dsrAB*), adenylylsulfate reductase (*aprAB*), and sulfate adenylyltransferase (*sat*) were enriched in GTV1904 (**Figure 3**). Majority of the *dsrAB* sequences in all the metagenomic datasets were taxonomically assigned to *Gamma-* (e.g., *Allochromatium*, *Thioalkalivibrio*, *Alkalilimnicola*), *Alpha-* (e.g., *Rhodomicrobium*, *Magnetospirillum*), *Betaproteobacteria* (e.g., *Thiobacillus*, *Sideroxydans*) as well as *Chlorobi* representatives, with the remainder being closely related to the reductive type of *Deltaproteobacteria*, *Firmicutes*, and *Nitrospirae*

TABLE 2 | Assignment of metabolic roles to major taxonomic groups based on detection of key genes-coding proteins in the metagenomes.

Pathways	GTV 1902	GTV1904	GTV1906
CBB	*Gamma-, Beta-, Alphaproteobacteria, Archaea*	*Gamma-, Beta-, Alphaproteobacteria*	*Gamma-, Beta-, Alphaproteobacteria*
rTCA	*Chlorobi, Nitrospirae*	*Epsilonproteobacteria, Chlorobi, Nitrospirae, Aquificae*	*Chlorobi, Nitrospirae*
WL	*Firmicutes, Deltaproteobacteria, Archaea*	*Deltaproteobacteria, Firmicutes, Archaea*	*Deltaproteobacteria, Firmicutes, Archaea*
3-HP	*Alpha-, Gammaproteobacteria, Actinobacteria*	*Alpha-, Gammaproteobacteria, Actinobacteria*	*Alpha-, Gammaproteobacteria, Actinobacteria*
Sulfate reduction/sulfur oxidation	*Alphaproteobacteria, Firmicutes*	*Gamma-, Beta-, Alphaproteobacteria*	*Gamma-, Alpha-, Betaproteobacteria*
Thiosulfate oxidation	*Beta-, Alpha-, Gammaproteobacteria*	*Gamma-, Alpha-, Betaproteobacteria, Chlorobia*	*Beta-, Alpha-, Gammaproteobacteria, Chlorobia*
Denitrification	*Delta-, Betaproteobacteria, Archaea*	*Gamma-, Beta-, Alpha-, Epsilon-, Deltaproteobacteria*	*Delta-, Gamma-, Beta-, Alphaproteobacteria*
N fixation	*Firmicutes, Deltaproteobacteria, Archaea*	*Deltaproteobacteria, Chlorobi,*	*Cyanobacteria, Archaea, Firmicutes*
Ammonia oxidation	*Delta-, Betaproteobacteria,*	*Delta-, Betaproteobacteria*	*Delta-, Betaproteobacteria*
Methane oxidation	*Alpha-, Gamma-, Betaproteobacteria*	*Gamma-, Alpha-, Betaproteobacteria*	*Alpha-, Gamma-, Betaproteobacteria*
Methanogenesis	*Archaea*		*Archaea*
Hydrogen utilization	*Clostridia, Deltaproteobacteria, Chloroflexi*	*Beta-, Gamma-, Alphaproteobacteria*	*Beta-, Delta-, Gamma-Alphaproteobacteria, Clostridia*
Aerobic respiration	*Beta-, Alpha-, Gammaproteobacteria*	*Beta-, Gamma-, Alphaproteobacteria*	*Beta-, Gammaproteobacteria*

Only taxa with >10% of the total hits are shown.

(**Table 2** and **Supplementary Table 9**). Most *aprAB* (66.2%) hits were affiliated to *Firmicutes* and *Deltaproteobacteria* in GTV1902 metagenome while those from GTV1904 and GTV1906 were largely assigned to *Beta-*, and *Gammaproteobacteria* representing 88.9% and 81.9%, respectively.

Because the same set of genes are involved in both types of dissimilatory sulfur metabolism, the oxidative or reductive directionality of the pathway cannot easily be deduced from taxonomy and the presence of these genes alone. To determine whether the *dsrAB* genes identified were associated with sulfate reduction or sulfur oxidation, we inferred the taxonomy and catalytic type of the *dsrAB* based on their phylogenies. Sequence analysis of the dsrAB proteins assembled from the GTV1904 and GTV1906 metagenomes suggested that were of the oxidative type, which clustered with sulfur-oxidizing bacteria affiliated to *Alpha-* (e.g., *Rhodospirillales*) and *Gammaproteobacteria* such as *Thiogranum*, *Thiotrichaceae, Acidithiobacillales,* and other unclassified hydrothermal environmental sequences (**Supplementary Figures 6**, **7**). Sulfate-reducing bacteria-type *dsrAB* sequences affiliated to *Deltaproteobacteria* (*Desulfobulbaceae*) were also detected. In contrast, the DsrAB protein tree demonstrated that the *dsrAB* genes assembled from GTV1902 were only of the reductive type affiliated with genes from uncultured sulfate-reducing bacterium (**Supplementary Figures 6**, **7**).

Incomplete oxidation of sulfides can produce thiosulfate, which can be oxidized to sulfate through sulfur-oxidizing proteins (soxABXYZ). The key genes involved in sulfur-oxidizing (SOX) system were found in all the metagenomes with a higher relative abundance in GTV1906 whereas thiosulfate sulfurtransferase (*tst*) that oxidize thiosulfate to sulfite (SO_3^{2-}) and sulfide:quinone oxidoreductase encoding gene (*sqr*) for periplasmic sulfide oxidation, similar abundances were identified across all metagenomes. Potential oxidation of reduced sulfur compounds via the SOX system was affiliated to the *Alpha-* and *Gammaproteobacteria* (**Table 2** and **Supplementary Table 9**).

Nitrogen Metabolism

All the genes, including periplasmic nitrate reductase (*napA*), nitrate reductase (*narGH*), nitrite reductase (NO-forming) (*nirKS*), nitric oxide reductase (*norBC*), and nitrous oxide reductase (*nosZ*) encoding for complete denitrification pathway were identified in all three metagenomes, but with divergent abundances, being overrepresented in GTV1904 (**Figure 3**), with most of the sequences assigned to *Gammaproteobacteria* members (**Table 2** and **Supplementary Table 10**). Dissimilatory nitrate reduction to ammonia via nitrite reductases (*nirBD*) were also detected and were found to be closely related to *Beta-* and *Gammaproteobacteria* groups. Nitrogenases (*nifDHK*), genes required for nitrogen fixation and ammonia monooxygenases (*amoABC*), and key enzymes in ammonia oxidation were absent across all samples; however, genes encoding for hydroxylamine oxidase (*hao*) mainly associated with *Deltaproteobacteria* were detected across all metagenomes (**Figure 3** and **Table 1**). Members of the genera *Anaeromyxobacter, Nitrosomonas,* and *Nitrosospira* seemed to be the primary ammonia oxidizers in all metagenomes (**Supplementary Table 10**).

Other Metabolic Pathways

Cytochrome c oxidase and cbb3-type cytochrome c oxidase complexes involved in aerobic respiration were predominately identified in OVF samples GTV1904 and GTV1904 (**Figure 3**). Both cytochrome c oxidase and cbb3-type cytochrome c oxidase genes majorly affiliated to aerobic proteobacterial lineages (**Table 2** and **Supplementary Table 11**). GTV1904 showed a higher abundance of both hydrogenases (*hyaAB*) and [NiFe]-hydrogenases (*hydAB*) with the highest

similarity to *Proteobacteria* and *Firmicutes* (**Table 2** and **Supplementary Table 12**). Genes encoding enzymes involved in methane oxidation (*pmoABC* and *mdh12*) and marker genes for methanogenesis (metyl-CoM reductase; *mcr*) were absent in all metagenomes. However, traces of soluble methane monooxygenase (*mmoX*) were identified in GTV1904 and GTV1906 (**Figure 3** and **Supplementary Table 13**).

Comparative Metagenomic Analysis

To explore the unique features of the CIR metagenomes, we compared our datasets to a collection of selected metagenomes obtained by shotgun sequencing from different ocean ridges (**Supplementary Table 2**). The double hierarchical clustering of the samples and KEGG pathways is shown in **Figure 4**. A cluster analysis of the KEGG level 3 pathways did group the samples into two clusters; the hydrothermally influenced sediments formed one group while the hydrothermal chimney samples clustered together and formed another group. The three CIR metagenomes (GTV1902, GTV1904, and GTV1906) clustered most closely with RB35 sample from MAR, and they formed a group with the sample MG35 from MAR and OCT chimney sample from the SWIR, whereas the rest of the chimney samples from SWIR (ToMo, BaC, PiMo, and Chan) grouped separately. A very similar grouping pattern was observed by clustering of samples based on the SEED subsystems and RefSeq databases (**Supplementary Figures 8**, **9**).

The hydrothermally influenced or low activity field sediment samples (GTV1902, GTV1904, GTV1906, RB35, and MG35) were almost depleted in KEGG level 3 categories, while the chimney samples (ToMo, BaC, PiMo, Chan, and OCT) showed higher abundance in majority of the KEGG categories. Compared to other hydrothermally influenced sediments, GTV1902 and GTV1904 samples were more enriched with enzymes for methane and nitrogen metabolisms respectively. Further comparison of the taxonomic relative abundances of the ten metagenomes against the RefSeq database revealed that GTV1902 had a higher proportion of sequences related with *Euryarchaeota* and *Korarchaeota*, when compared with other metagenomes (**Supplementary Figure 9**).

DISCUSSION

Microbial communities in deep-sea sediments play important roles in biogeochemical processes (Zeng et al., 2021). This study is the first to report the microbial community of deep-sea sediment from recently discovered hydrothermal vents in the CIR using shotgun metagenomic sequencing. To reveal the unique features of the CIR microbial community structures we conducted a comparative study with datasets from different hydrothermal systems, including five chimney metagenomes from Old City in SWIR (Lecoeuvre et al., 2021), and two sediment metagenomes from the Azores in the MAR (Cerqueira et al., 2018).

Microbial Community Composition

Taxonomic analyses revealed that the bacterial community was highly diverse. *Proteobacteria* (especially *Gammaproteobacteria*) was the most dominant followed by *Firmicutes* and *Bacteroidetes*. Although the three metagenomes shared several taxa, they differed with respect to overall phyla abundances (**Figure 2**). Sulfur-oxidizing genera *Thioalkalivibrio*, and ammonia-oxidizing bacteria *Nitrosococcus* were the most abundant genera within the *Gammaproteobacteria*. Previous investigation on the microbial diversity in the Indian Ocean Ridge (IOR) also revealed that *Proteobacteria* were the dominant bacterial phylum, but with contrasting proportions in its classes (Cao et al., 2014; Lecoeuvre et al., 2021). Serpentinite-hosted systems are enriched in hydrogen and methane as a result of seawater-rock reactions (Charlou et al., 2002; Proskurowski et al., 2008). The presence of H_2 and metal oxides (mainly Fe and Mn) as alternative electron acceptors especially at OVF site (Kim et al., 2020) may have contributed to the abundance of *Firmicutes* present in the CIR samples. Among the phylum *Firmicutes* *Clostridium* and *Bacillus* were the predominant genera found in the three metagenomes. Representatives of *Bacillus* are known for their tolerance in extreme environments. Members of the genus *Clostridium* are strict anaerobes that use hydrogen as electron donor to fix CO_2, autotrophically, through the acetyl-CoA pathway. In this study, a higher abundance of *Firmicutes* representatives in the metagenomes capable of H_2-dependent carbon fixation indicates that the microbial communities depend on these hydrogen-utilizing microorganisms for biomass production. The presence of high concentrations of methane and sulfides in the OVF could explain the predominance of methane-oxidizing *Gammaproteobacteria* related to the genus *Methylococcus*. Indeed, several studies have shown that the predominance of *Gammaproteobacteria* is associated with serpentinite-hosted hydrothermal fields (Brazelton et al., 2006; Lecoeuvre et al., 2021). Members of *Chloroflexi*, *Actinobacteria*, and *Planctomycetes* among others which are generally recovered from deep-sea hydrothermal environments (Zeng et al., 2021) were also identified in the CIR metagenomes.

Euryarchaeota, *Thaumarchaeota,* and *Crenarchaeota* were the dominant archaeal phyla identified in the three metagenomes studied. Previous studies have shown that these are known to be the three major archaeal phyla found in deep-sea hydrothermal vents in the chimney fluids from SWIR (Lecoeuvre et al., 2021) as well as in hydrothermal sediments from the MAR (Cerqueira et al., 2018). Similar to a recent metagenomic study in serpentinite-hosted Old City hydrothermal field in SWIR (Lecoeuvre et al., 2021), *Euryarchaeota* was the most frequently observed archaeal phyla in the three metagenomes. Specifically, majority of the *Euryarchaeota* sequences in the GTV1902 were assigned to *Aciduliprofundum* a thermoacidophilic iron and sulfur reducing heterotroph originally isolated from deep-sea hydrothermal vents (Reysenbach et al., 2006). On the other hand, potential methanogenic Archaea (i.e., *Methanosarcina*) were predominant in GTV1904 and GTV1906. The presence of these methanogenic Archaea in methane-rich sediments from OVF suggests that the high concentration of methane at this site may be accumulated as a result of both biotic and abiotic processes.

In addition, although in low abundances *Korarchaeota* and the *Nanoarchaeota* represented by the genera "*Candidatus*

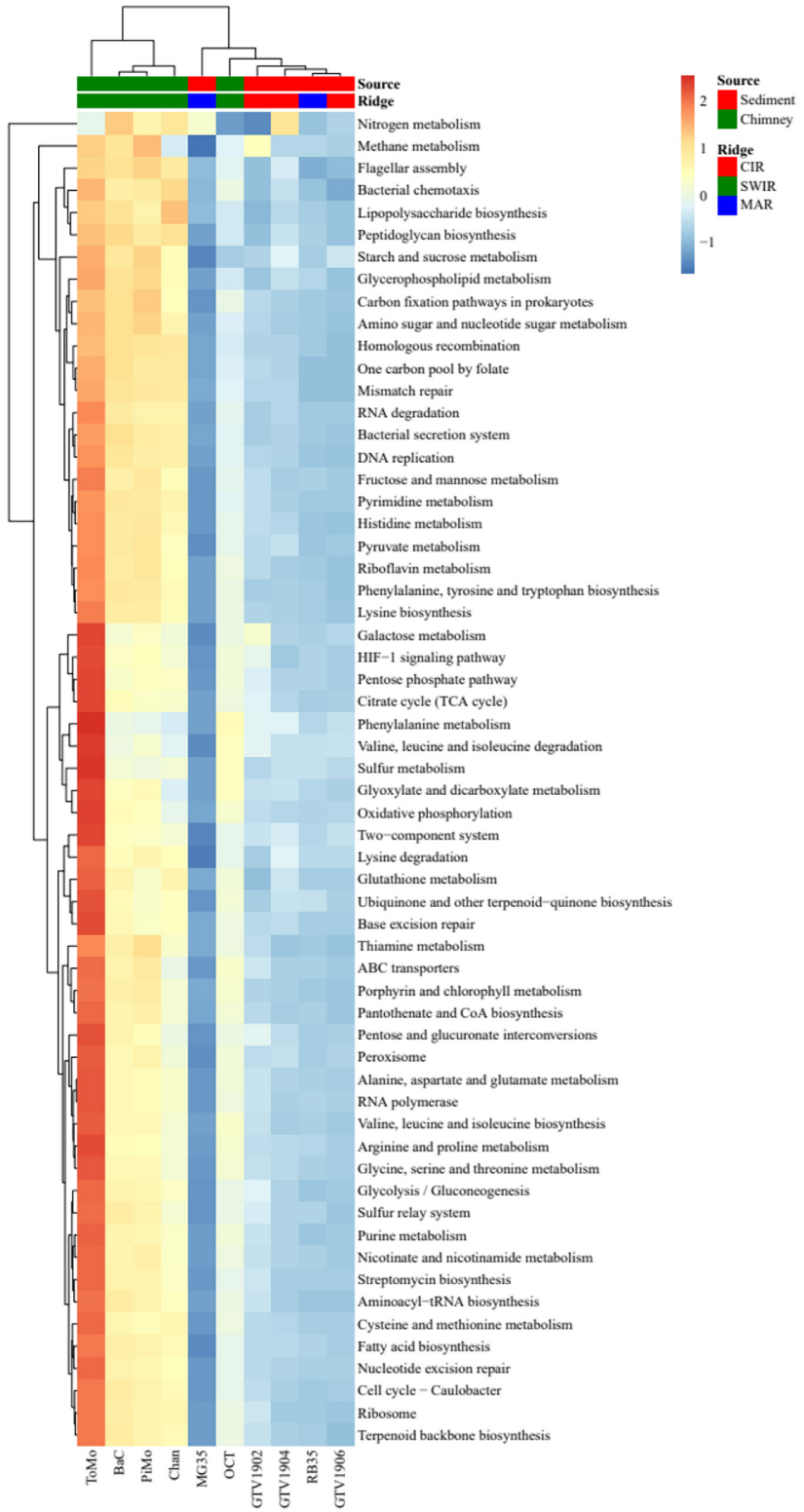

FIGURE 4 | Two-way cluster analysis of samples and level 3 KEGG pathways based on the relative abundances of the KEGG-annotated sequences with hits in each category. The heatmap was clustered based on the Euclidean distance matrix. The shading is proportional to the normalized values calculated based on the functional hits of each category per sample. Only pathways with sum of hits >186,000 across the 10 metagenomes are shown.

Korarchaeum" and *Nanoarchaeum* respectively were also observed in our metagenomes. Several 16S rRNA gene studies have reported *Korarchaeota* to be found in extreme terrestrial and marine environments including hot springs (Barns et al., 1994), coastal thermal areas (Yan et al., 2018), as well as hydrothermal systems (Takai and Sako, 1999; Teske et al., 2002; Schrenk et al., 2003). However, "*Cand.* Korarchaeum" has been reported in terrestrial hot springs (Elkins et al., 2008) and more recently in a shallow hydrothermal vent in Eolian Islands (Gugliandolo and Maugeri, 2019). To the best of our knowledge, this is the first metagenome survey to observe "*Cand.* Korarchaeum" in deep-sea hydrothermal vents. The finding of *Cand.* Korarchaeum in hydrothermally influenced deep-sea sediments in CIR suggests that *Korarchaeum* are globally distributed in extreme environments.

Carbon Metabolism

Carbon fixation by deep-sea hydrothermal vents organisms has been reported to occur through several metabolic pathways such as CBB cycle, rTCA cycle, 3-HP, 3-HP/4-HB, WP pathway, and dicarboxylate/4-HB cycle (Nakagawa and Takai, 2008; Minic and Thongbam, 2011). In this study key genes for CBB cycle were affiliated primarily with sulfur-oxidizing and nitrifying *Gammaproteobacteria* as well as *Euryarchaeota* members (**Supplementary Table 8**) similar to what has been reported from the metagenomic studies in the SWIR (Cao et al., 2014; Lecoeuvre et al., 2021) and other deep-sea vent systems (Elsaied et al., 2007; Nakagawa and Takai, 2008; Cerqueira et al., 2018).

The rTCA cycle in deep-sea hydrothermal systems is preferred by *Epsilonproteobacteria*, *Aquificae,* and *Nitrospirae* (Nakagawa and Takai, 2008; Minic and Thongbam, 2011; Cerqueira et al., 2018; Zeng et al., 2021) which were also observed in our datasets. However, compared to the above-mentioned groups, majority of the *acl* sequences a key enzyme in the rTCA cycle were affiliated to the phylum *Chlorobi* represented by *Chlorobium, Chlorobaculum,* and *Pelodictyon* (**Supplementary Table 8**). The rTCA is ubiquitous among the *Chlorobiaceace* family (Imhoff, 2014; Ward and Shih, 2021) whose members have been identified in deep-sea black smoker along the East Pacific Rise (Beatty et al., 2005). The predominance of *Chlorobi acl* indicates that the rTCA in the metagenomes is supported by geothermal light which provides a selective advantage for phototrophs over chemoautotrophs. Like other studies in deep-sea sediments (Cerqueira et al., 2018), some key enzymes in the 3-HP pathway were missing in our metagenomes suggesting that the 3-HP pathway was not an important carbon fixation pathway in the hydrothermally influenced sediments in OVF and Invent E sites. Therefore, carbon fixation is thought to occur either via CBB, and/or the rTCA in the OVF and Invent E metagenomes.

Sulfur Metabolism

The accumulation of metal oxides and sulfides in OVF (Kim et al., 2020) make OVF site as a great habitant for sulfur-oxidizing microorganisms. Sulfur-oxidation in deep-sea hydrothermal vents occurs via the reverse sulfate reduction and SOX pathways. Majority of the key genes in sulfur cycle observed in the OVF metagenomes were affiliated to families *Ectothiorhodospiraceae* and *Chromatiaceae* within the class *Gammaproteobacteria*. Sulfur-chemolithoautotrophs such as *Thiomicrospira* and *Thioalkalivibrio* and photolithotrophic *Allochromatium* were the dominant sulfur-oxidizing genera which were consistent with the findings from previous studies in other deep-sea vent systems (Nakagawa and Takai, 2008; Yamamoto and Takai, 2011; Cao et al., 2014; Cerqueira et al., 2018).

Taxonomic annotation and analysis of the rTCA pathway revealed several sequence hits related to sulfur-oxidizing *Epsilonproteobacteria* representatives of the genera *Sulfurimonas* and *Sulfurovum* in the OVF sediments. Interestingly, sulfur oxidation via the SOX complex was dominated by the sulfur-oxidizing *Gammaproteobacteria* (e.g., *Thiomicrospira* and *Thioalkalivibrio* genera), although the *Epsilonproteobacteria* are known to use the SOX pathway for oxidation of reduced sulfur compounds in deep-sea environments (Yamamoto and Takai, 2011). This result is consistent with the predominance of *Gammaproteobacteria* and low proportion of *Epsilonproteobacteria* observed in sediments. *Epsilonproteobacteria* are known to dominate less oxygenated/high sulfide hydrothermal fluids and chimneys (Hou et al., 2020) while the *Gammaproteobacteria* require presence of high reduced compounds and oxygen concentrations. The level of hydrothermal activity together with the degree of mixing of diffuse flow fluids with surrounding seawater in OVF possibly favors *Gammaproteobacteria* over *Epsilonproteobacteria.* This indicates that oxidation of reduced sulfur compounds in OVF occurs in multiple niches via both the reverse sulfate reduction and SOX pathway similar to what was observed in hydrothermally influenced Rainbow sediments in the MAR (Cerqueira et al., 2018) and consistent with other hydrothermal systems (Hügler et al., 2010).

The presence of key metabolic genes for sulfur utilization affiliated with *Alphaproteobacteria* and *Bacteroidetes* groups suggests the role of these taxa in the sulfur cycle. Sulfur-oxidizing *Alphaproteobacteria* and *Bacteroidetes* are widely distributed in marine environments including deep-sea hydrothermal vents (Sylvan et al., 2013; Stokke et al., 2015). The sulfur-oxidizing members of the *Rhodobacterales* within *Alphaproteobacteria* are enriched in all samples and these were also observed in Old City hydrothermal vent in SWIR (Lecoeuvre et al., 2021). An amplicon survey in inactive sulfide chimneys in Lau Basin also reports the dominance of sulfur-oxidizing *Alphaproteobacteria* and *Bacteroidetes* linages outside the chimneys (Sylvan et al., 2013).

We observed differences in gene abundances as well as differences in microbial community abundance suggesting that Invent E was distinct from the OVF. OVF sediments (GTV1904 and GTV1906) were dominated by *Gammaproteobacteria* while *Deltaproteobacteria* were predominant in GTV1902. The predominance of *Deltaproteobacteria* and *Firmicutes* in GTV1902 (**Figure 2**) suggests dissimilatory sulfate-reduction dominates in Invent E site. However, it should be noted that dissimilatory sulfite reductase (*dsrAB*) responsible for oxidation

of sulfur to sulfite, adenylylsulfate reductase (*aprAB*) were nearly absent in GTV1902 metagenome. A similar set of *dsr* genes is found in both sulfur-reducing microorganism and sulfur-oxidizing microorganisms (Müller et al., 2015). Recent findings of Thorup et al. (2017), show that *Deltaproteobacteria* possess the capabilities to perform dissimilatory sulfate reduction and oxidation by the same reversible enzymes, *sat*, *apr*, and *dsr*. Based on phylogeny of the *dsrAB* genes assembled from GTV1902, the identified sequences were of the reductive type affiliated with uncultured sulfate-reducing bacterium. This affiliation is strongly suggestive that the *Deltaproteobacteria* identified in GTV1902 perform dissimilatory sulfate reduction. Within OVF, many sulfur-oxidizing bacteria were found, such as *Ectothiorhodospiraceae*, and *Thiotrichaceae* families, but also some sulfate-reducing bacteria such as *Desulfobulbaceae*. Analysis of *dsrAB* genes also indicated that sulfate reduction by *Deltaproteobacteria* appeared to be occurring exclusively in GTV1902 while sulfur oxidation by the *Gammaproteobacteria* was occurring at OVF. This result is also consistent with the finding of higher total sulfur concentrations in OVF (GTV1904 and GTV1906) samples compared to GTV1902 (Invent E) which is most likely controlling the community structure of total bacteria and sulfur-cycling bacteria.

Nitrogen Metabolism

Nitrate and nitrite are important electron acceptors for oxidation of reduced sulfur compounds although they are usually depleted in serpentinite-hosted systems (Nakagawa and Takai, 2008; Zeng et al., 2021). Analysis of key genes involved in the nitrogen cycle identified genes involved in the dissimilatory nitrate reduction, and denitrification, across all three metagenomes which were consistent with the diverse taxonomic abundance of nitrogen metabolizing taxa in the three metagenomes including *Proteobacteria*, *Firmicutes*, *Chlorobi*, *Cyanobacteria,* and Archaea among others. Denitrification pathway was the most prevalent among metagenomes affiliated with primarily the *Delta-* and *Gammaproteobacteria*. Similar observations of denitrification-related taxa have been documented in the SWIR (Cao et al., 2014; Lecoeuvre et al., 2021). These findings indicate that sulfur-oxidation/sulfate reduction coupled with denitrification are important energy-generating pathways fueling the microbial communities at the OVF and Invent E sites. Although marker genes *amoABC* for ammonia oxidation were not detected in three metagenomes, ammonia-oxidizing members in the *Betaproteobacteria* such as *Nitrosomonas* and *Nitrosospira* are potential ammonia oxidizers identified in all three metagenomes consistent with what was reported previously from hydrothermally influenced sediments from Rainbow vent in MAR (Cerqueira et al., 2018) but different from SWIR Old City chimneys where *Thaumarchaeota* was reported to be involved in ammonia oxidation (Lecoeuvre et al., 2021).

Other Metabolic Pathways

Methane concentrations produced by serpentinization reactions in OVF site were recorded up to 52.5 nM (Kim et al., 2020), therefore, methane oxidation is expected in the OVF sediments. The *pmmo* catalyzes the production of methanol, which is further oxidized to formaldehyde by a periplasmic methanol dehydrogenase. However, *pmmo*/*mmo* key enzymes in the methanotrophy are missing in all datasets with a very low abundance of *mmoX* observed exclusively in OVF. Potential methane-oxidizing *Methylococcales* (*Gammaproteobacteria*) which have been reported in several serpentinite-hosted hydrothermal systems including Old City in the SWIR (Brazelton et al., 2006; Cerqueira et al., 2018; Lecoeuvre et al., 2021) were observed in the studied sediments. The presence of methanotrophic *Methylococcus* in our datasets suggests a possibility that methane oxidation exists in OVF sediments although it might not be an important energy-yielding metabolic pathway.

Interestingly, the key genes for methanogenesis were missing in all metagenomes, however methanogenic Archaea dominated by *Methanosarcinales* were observed and being almost exclusive to GTV902 (**Supplementary Table 13**). Previous studies have also reported similar methanogenic Archaea in several deep-sea hydrothermal vents, such as presence of *Methanosarcinales* in Old City in SWIR (Lecoeuvre et al., 2021), Lost City (MAR) chimneys being dominated by *Methanosarcinales* (Brazelton et al., 2006), as well as the predominance of *Methanococcales* in CIR Kairei field (Takai et al., 2004). Although we recognize that no significant conclusions can be made due to lack of replicate samples, we speculate that Invent E site is highly enriched in hydrogen that supports the high abundance of methanogenic Archaea observed in this site. Nevertheless, much work remains to be conducted within each of these vent fields for a clear understanding of the resident microbial communities and their metabolic potentials.

Apart from the metabolic pathways discussed above, the geochemistry of the vents especially OVF offers preferable conditions for aerobic respiration hydrogen metabolism. Although our study didn't focus on these pathways, it was evident through taxonomic characterization which reveals presence of genera such as *Geobacter*, *Thiobacillus*, *Anaeromyxobacter*, *Acidithiobacillus*, *Sideroxydans,* and *Pseudomonas* among others capable of hydrogen utilization and aerobic respiration. Majority of the hydrogenases identified in the OVF site were closely related to *Beta-*, *Gamma-*, and *Alphaproteobacteria* while *Clostridia*, *Deltaproteobacteria,* and *Chloroflexi* dominated in the Invent E site (**Supplementary Table 12**). Chemosynthesis in deep-sea hydrothermal environments may be coupled to both aerobic and anaerobic respiration. Genes encoding cytochrome c oxidase and cbb3-type cytochrome c oxidase involved in aerobic respiration were identified across metagenomes (**Figure 3**) suggesting that chemosynthesis in OVF and Invent E depends on oxygen as a terminal electron acceptor other than nitrate, sulfate, etc. Both cytochrome c oxidase and cbb3-type cytochrome c oxidase genes majorly affiliated to aerobic proteobacterial linages (**Table 2** and **Supplementary Table 11**). Thus, oxygen derived from the constant mixing of diffuse fluids with the surrounding seawater is thought to be a key electron acceptor allowing sulfur-oxidizing *Proteobacteria* to thrive in the OVF and Invent E sites.

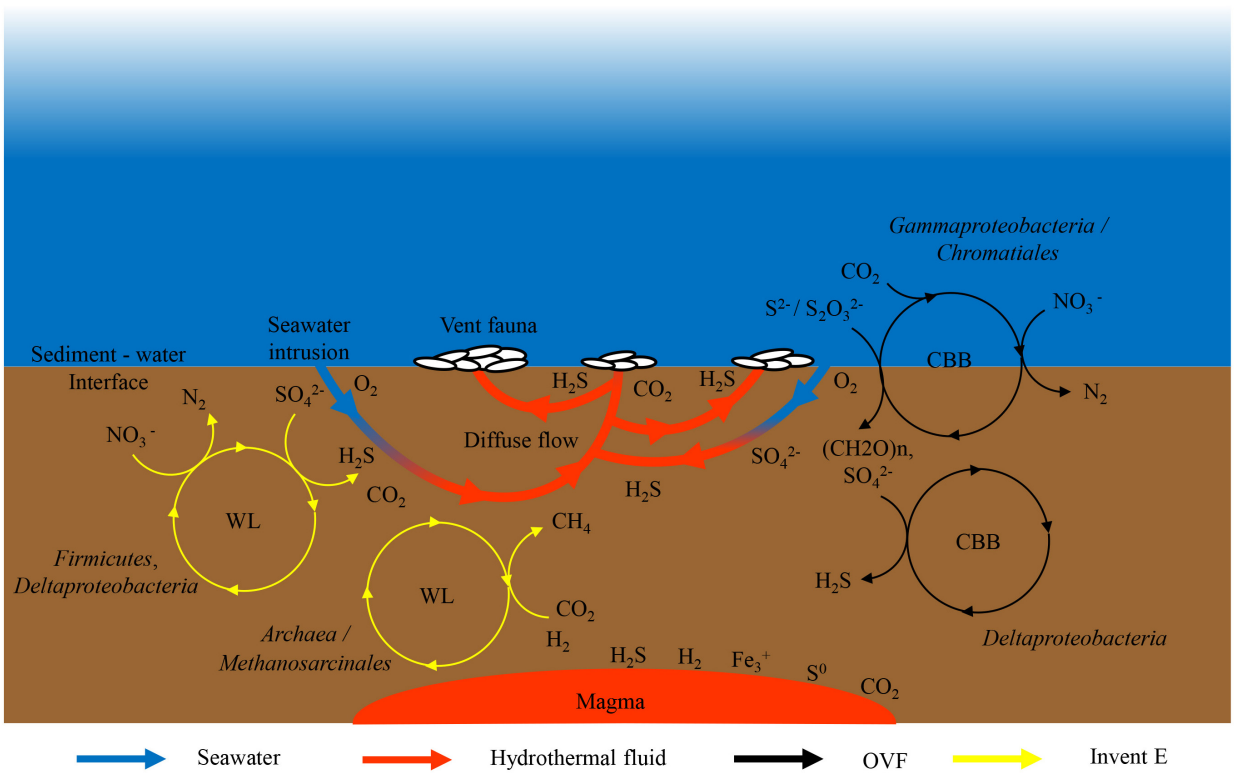

FIGURE 5 | Schematic illustration of key microbial metabolisms of carbon, sulfur, methane, and nitrogen in the diffuse flow hydrothermal vents at OVF and Invent E sites. SO_4^{2-}, sulfate; S^0, sulfur; $S_2O_3^{2-}$, thiosulfate; S_2^-, sulfide; H_2S, hydrogen sulfide; NO_3^-, nitrate; N_2, nitrogen; H_2, hydrogen; CH_4, methane; CO_2, carbon dioxide; O_2, oxygen.

Metagenome Comparison From Other Hydrothermal Systems

Currently, no metagenomes from hydrothermal vent field in the CIR are available for comparison. Within the SWIR, only two metagenome studies have been reported, one from chimney sulfides (Cao et al., 2014) and more recently from Old City hydrothermal system (Lecoeuvre et al., 2021). Unfortunately, only the metagenomes from Old City were used for comparison due to the unavailability of the sequencing data of sulfides metagenomes in NCBI's database. Metagenome comparisons showed that the Old City chimney metagenomes clustered together except sample OCT, which may be attributed to the fact that OCT chimney had a greater influence on seawater intrusions than in other chimney samples (Lecoeuvre et al., 2021). In addition, metagenomes from hydrothermal vent chimneys (ToMo, BaC, PiMo, Chan, and OCT) were enriched in metabolic functions suggesting that hydrothermal microbial communities have evolved extensive metabolisms as an adapting strategy in response to the steep chemical and thermal gradients observed at vent chimneys.

Rainbow metagenome (RB35 collected 100 m from the active vent) did not cluster together with its counterpart Menez Gwen (MG35 collected near the chimney) from the MAR but rather closely clustered next to our metagenomes from the CIR. The difference in the microbial community structure of the two metagenomes from MAR is also consistent with the one that has been reported before (Cerqueira et al., 2018). The physicochemical conditions of the Rainbow vent and OVF are strikingly different (for example, the diffuse flow of OVF is weak with low temperature, metal-poor, and methane-rich (Kim et al., 2020), whereas Rainbow is characterized with very high rates of fluid flow ~360°C and high metal contents (Cerqueira et al., 2018), however the sediment samples studied both represent low hydrothermal activity samples that are continuously exposed to the surrounding sea water as a result these prevailing environmental conditions have a significant influence on the microbial community structure and distribution of functional gene categories. This result indicates the stratification in hydrothermally influenced and hydrothermal microbial communities.

CONCLUSION

In this study, using a metagenomic approach, we report for the first time the microbial ecology of the recently discovered hydrothermal vents (OVF and Invent E) located along the slow-spreading CIR. The microbial community structures and

metabolic properties across metagenomes were largely similar although dominant taxa and functional potential vary between vent fields. The oxidation and reduction of sulfur may be important energy metabolism pathways in the two sampling sites. We illustrated these key metabolic pathways fueling microbial communities at the OVF and Invent E sites (**Figure 5**). The *Gammaproteobacteria* are the major primary producers at OVF site fixing CO_2 via CBB cycle and retrieving energy from oxidation of reduced mineral sulfides through reverse sulfate reduction pathway or SOX complex leading to the oxidation of sulfide to sulfate. *Deltaproteobacteria* lineages known to be involved in sulfate reduction characterized Invent E. We speculate that the *Deltaproteobacteria* and *Firmicutes* utilize the sulfates from the seawater, fixing CO_2 through the WL cycle contributing to the production hydrogen sulfide in the hydrothermal fluids. In addition, hydrogen from serpentinization processes supplies metabolic energy for methanogenic Archaea. Oxygen and nitrates from the surrounding seawater are possible electron acceptors for sulfate-reducing and sulfur-oxidizing bacteria.

Although our study is limited by lack of replicate samples and sufficient environmental data, our results indicate that OVF and Invent E may exhibit diverging geochemistry reflected in the sediment microbial ecology. Autotrophic *Gammaproteobacteria* known to be involved in oxidation of reduced sulfur compounds, using oxygen or nitrate as electron acceptors to fix carbon via CBB characterized OVF. The microbial lineages and functional profiles of sediments from diffuse-flow OVF are similar to hydrothermally influenced sediments from highly active vents. This study provides a baseline of the microbial ecology associated with deep-sea sediments from low activity hydrothermal vents in the CIR. Further sampling and investigations are required to broadly determine the microbial metabolic activities and specific contributions of the above-described metabolic pathways in slow to intermediate spreading hydrothermal systems.

DATA AVAILABILITY STATEMENT

The datasets presented in this study can be found in online repositories. The names of the repository/repositories and accession number(s) can be found below: https://www.ncbi.nlm.nih.gov/, PRJNA751690 and http://metagenomics.anl.gov/, mgm4898492.3, mgm4898484.3, and mgm4898483.3.

AUTHOR CONTRIBUTIONS

TN conducted the experiments and data analyses and prepared the manuscript. YK collected the sediment samples. M-JP assisted in data analyses and graphics. DL contributed metal concentration data. J-HL conceived the study. YK and KK supervised the study. All authors reviewed and approved the final manuscript.

FUNDING

This research was funded by the Ministry of Oceans and Fisheries Republic of Korea, as part of the project titled "Understanding the deep-sea biosphere on seafloor hydrothermal vents in the Indian Ridge" (Grant No. 20170411).

ACKNOWLEDGMENTS

We thank all the crew members and participants on R/V ISABU cruise during the 2019 Indian Ocean Expedition for their assistance in collecting the samples. We would also like to thank Jonguk Kim from Deep-Sea and Seabed Mineral Resources Research Center, KIOST, who provided us with the original map of the study area.

SUPPLEMENTARY MATERIAL

The Supplementary Material for this article can be found online at: https://www.frontiersin.org/articles/10.3389/fmars.2022.784807/full#supplementary-material

REFERENCES

Barns, S. M., Fundyga, R. E., Jeffries, M. W., and Pace, N. R. (1994). Remarkable archaeal diversity detected in a Yellowstone National Park hot spring environment. *Proc. Natl. Acad. Sci. U.S.A.* 91, 1609–1613. doi: 10.1073/pnas.91.5.1609

Beatty, J. T., Overmann, J., Lince, M. T., Manske, A. K., Lang, A. S., Blankenship, R. E., et al. (2005). An obligately photosynthetic bacterial anaerobe from a deep-sea hydrothermal vent. *Proc. Natl. Acad. Sci. U.S.A.* 102, 9306–9310. doi: 10.1073/pnas.0503674102

Beaulieu, S. E., and Szafrański, K. M. (2020). *InterRidge Global Database of Active Submarine Hydrothermal Vent Fields Version 3.4. PANGAEA*. doi: 10.1594/PANGAEA.917894

Bowers, R., Kyrpides, N., Stepanauskas, R., Harmon-Smith, M., Doud, D., Reddy, T. B., et al. (2017). Minimum information about a single amplified genome (MISAG) and a metagenome-assembled genome (MIMAG) of bacteria and archaea. *Nat. Biotechnol.* 35, 725–731. doi: 10.1038/nbt.3893

Brazelton, W. J., Schrenk, M. O., Kelley, D. S., and Baross, J. A. (2006). Methane- and sulfur-metabolizing microbial communities dominate the Lost City hydrothermal field ecosystem. *Appl. Environ. Microbiol.* 72, 6257–6270. doi: 10.1128/AEM.00574-06

Cao, H., Wang, Y., Lee, O. O., Zeng, X., Shao, Z., and Qian, P. Y. (2014). Microbial sulfur cycle in two hydrothermal chimneys on the Southwest Indian Ridge. *mBio* 5:e00980-13. doi: 10.1128/mBio.00980-13

Cerqueira, T., Barroso, C., Froufe, H., Egas, C., and Bettencourt, R. (2018). Metagenomic signatures of microbial Communities in deep-sea hydrothermal sediments of Azores vent fields. *Microb. Ecol.* 76, 387–403. doi: 10.1007/s00248-018-1144-x

Charlou, J., Donval, J., Fouquet, Y., Jean-Baptiste, P., and Holm, N. (2002). Geochemistry of high H2 and CH4 vent fluids issuing from ultramafic rocks at the Rainbow hydrothermal field (36 14' N, MAR). *Chem. Geol.* 191, 345–359. doi: 10.1016/S0009-2541(02)00134-1

Dick, G. J. (2019). The microbiomes of deep-sea hydrothermal vents: distributed globally, shaped locally. *Nat. Rev. Microbiol.* 17, 271–283. doi: 10.1038/s41579-019-0160-2

Ding, J., Zhang, Y., Wang, H., Jian, H., Leng, H., and Xiao, X. (2017). Microbial community structure of deep-sea hydrothermal vents on the ultraslow Spreading Southwest Indian Ridge. *Front. Microbiol.* 8:1012. doi: 10.3389/fmicb.2017.01012

Elkins, J. G., Podar, M., Graham, D. E., Makarova, K. S., Wolf, Y., Randau, L., et al. (2008). A korarchaeal genome reveals insights into the evolution of the Archaea. *Proc. Natl. Acad. Sci. U.S.A.* 105, 8102–8107. doi: 10.1073/pnas.0801980105

Elsaied, H. E., Kimura, H., and Naganuma, T. (2007). Composition of archaeal, bacterial, and eukaryal RuBisCO genotypes in three Western Pacific arc hydrothermal vent systems. *Extremophiles* 11, 191–202. doi: 10.1007/s00792-006-0025-2

Fisher, C. R., Takai, K., and Le Bris, N. (2007). Hydrothermal vent ecosystems. *Oceanography* 20, 14–23. doi: 10.5670/oceanog.2007.75

Francheteau, J., Needham, H., Choukroune, P., Juteau, T., Seguret, M., Ballard, R. D., et al. (1979). Massive deep-sea sulphide ore deposits discovered on the East Pacific Rise. *Nature* 277, 523–528.

Fu, L., Niu, B., Zhu, Z., Wu, S., and Li, W. (2012). CD-HIT: accelerated for clustering the next-generation sequencing data. *Bioinformatics* 28, 3150–3152. doi: 10.1093/bioinformatics/bts565

Gamo, T., Chiba, H., Yamanaka, T., Okudaira, T., Hashimoto, J., Tsuchida, S., et al. (2001). Chemical characteristics of newly discovered black smoker fluids and associated hydrothermal plumes at the Rodriguez Triple Junction, Central Indian Ridge. *Earth Planet. Sci. Lett.* 193, 371–379. doi: 10.1016/S0012-821x(01)00511-8

Gomez-Alvarez, V., Teal, T. K., and Schmidt, T. M. (2009). Systematic artifacts in metagenomes from complex microbial communities. *ISME J.* 3, 1314–1317. doi: 10.1038/ismej.2009.72

Gugliandolo, C., and Maugeri, T. L. (2019). Phylogenetic diversity of Archaea in shallow hydrothermal vents of Eolian Islands, Italy. *Diversity* 11:156. doi: 10.3390/d11090156

Halbach, P., Blum, N., Münch, U., Plüger, W., Garbe-Schönberg, D., and Zimmer, M. (1998). Formation and decay of a modern massive sulfide deposit in the Indian Ocean. *Miner. Deposita* 33, 302–309. doi: 10.1007/s001260050149

Han, Y., Gonnella, G., Adam, N., Schippers, A., Burkhardt, L., Kurtz, S., et al. (2018). Hydrothermal chimneys host habitat-specific microbial communities: analogues for studying the possible impact of mining seafloor massive sulfide deposits. *Sci. Rep.* 8:10386. doi: 10.1038/s41598-018-28613-5

Hoek, J., Banta, A., Hubler, F., and Reysenbach, A. L. (2003). Microbial diversity of a sulphide spire located in the Edmond deep-sea hydrothermal vent field on the Central Indian Ridge. *Geobiology* 1, 119–127. doi: 10.1046/j.1472-4669.2003.00015.x

Hou, J., Sievert, S. M., Wang, Y., Seewald, J. S., Natarajan, V. P., Wang, F., et al. (2020). Microbial succession during the transition from active to inactive stages of deep-sea hydrothermal vent sulfide chimneys. *Microbiome* 8:102. doi: 10.1186/s40168-020-00851-8

Huerta-Cepas, J., Szklarczyk, D., Heller, D., Hernandez-Plaza, A., Forslund, S. K., Cook, H., et al. (2019). eggNOG 5.0: a hierarchical, functionally and phylogenetically annotated orthology resource based on 5090 organisms and 2502 viruses. *Nucleic Acids Res.* 47, D309–D314. doi: 10.1093/nar/gky1085

Hügler, M., Gärtner, A., and Imhoff, J. F. (2010). Functional genes as markers for sulfur cycling and CO2 fixation in microbial communities of hydrothermal vents of the Logatchev field. *FEMS Microbiol.* 73, 526–537. doi: 10.1111/j.1574-6941.2010.00919.x

Hyatt, D., Chen, G. L., Locascio, P. F., Land, M. L., Larimer, F. W., and Hauser, L. J. (2010). Prodigal: prokaryotic gene recognition and translation initiation site identification. *BMC Bioinformatics* 11:119. doi: 10.1186/1471-2105-11-119

Imhoff, J. F. (2014). "The family chlorobiaceae," in *The Prokaryotes*, eds E. Rosenberg, E. F. DeLong, S. Lory, E. Stackebrandt, and F. Thompson (Berlin: Springer Berlin Heidelberg), 501–514. doi: 10.1007/978-3-642-38954-2_142

Jiang, H., Lei, R., Ding, S. W., and Zhu, S. (2014). Skewer: a fast and accurate adapter trimmer for next-generation sequencing paired-end reads. *BMC Bioinformatics* 15:182. doi: 10.1186/1471-2105-15-182

Jones, D. T., Taylor, W. R., and Thornton, J. M. (1992). The rapid generation of mutation data matrices from protein sequences. *Comput. Appl. Biosci.* 8, 275–282. doi: 10.1093/bioinformatics/8.3.275

Kanehisa, M., Araki, M., Goto, S., Hattori, M., Hirakawa, M., Itoh, M., et al. (2007). KEGG for linking genomes to life and the environment. *Nucleic Acids Res.* 36, D480–D484. doi: 10.1093/nar/gkm882

Kang, D. D., Li, F., Kirton, E., Thomas, A., Egan, R., An, H., et al. (2019). MetaBAT 2: an adaptive binning algorithm for robust and efficient genome reconstruction from metagenome assemblies. *PeerJ* 7:e7359. doi: 10.7717/peerj.7359

Kawagucci, S., Miyazaki, J., Noguchi, T., Okamura, K., Shibuya, T., Watsuji, T., et al. (2016). Fluid chemistry in the Solitaire and Dodo hydrothermal fields of the Central Indian Ridge. *Geofluids* 16, 988–1005. doi: 10.1111/gfl.12201

Keegan, K. P., Trimble, W. L., Wilkening, J., Wilke, A., Harrison, T., D'Souza, M., et al. (2012). A platform-independent method for detecting errors in metagenomic sequencing data: DRISEE. *PLoS Comput. Biol.* 8:e1002541. doi: 10.1371/journal.pcbi.1002541

Kent, W. J. (2002). BLAT – the BLAST-like alignment tool. *Genome Res.* 12, 656–664. doi: 10.1101/gr.229202

Kieser, S., Brown, J., Zdobnov, E. M., Trajkovski, M., and McCue, L. A. (2020). ATLAS: a Snakemake workflow for assembly, annotation, and genomic binning of metagenome sequence data. *BMC Bioinformatics* 21:257. doi: 10.1186/s12859-020-03585-4

Kim, J., Son, S. K., Kim, D., Pak, S. J., Yu, O. H., Walker, S. L., et al. (2020). Discovery of active hydrothermal vent fields along the Central Indian Ridge, 8-12 degrees S. *Geochem. Geophys. Geosyst.* 21:e2020GC009058. doi: 10.1029/2020GC009058

Kolde, R. (2019). *pheatmap: Pretty Heatmaps. R Package Version 1.0.12.*

Kumar, S., Stecher, G., and Tamura, K. (2016). MEGA7: molecular evolutionary genetics analysis version 7.0 for bigger datasets. *Mol. Biol. Evol.* 33, 1870–1874. doi: 10.1093/molbev/msw054

Langmead, B., and Salzberg, S. L. (2012). Fast gapped-read alignment with Bowtie 2. *Nat. Methods* 9, 357–359. doi: 10.1038/nmeth.1923

Lecoeuvre, A., Menez, B., Cannat, M., Chavagnac, V., and Gerard, E. (2021). Microbial ecology of the newly discovered serpentinite-hosted Old City hydrothermal field (southwest Indian ridge). *ISME J.* 15, 818–832. doi: 10.1038/s41396-020-00816-7

Liao, S., Tao, C., Li, H., Barriga, F. J. A. S., Liang, J., Yang, W., et al. (2018). Bulk geochemistry, sulfur isotope characteristics of the Yuhuang-1 hydrothermal field on the ultraslow-spreading Southwest Indian Ridge. *Ore Geol. Rev.* 96, 13–27. doi: 10.1016/j.oregeorev.2018.04.007

Liu, C., Cui, Y., Li, X., and Yao, M. (2021). microeco: an R package for data mining in microbial community ecology. *FEMS Microbiol. Ecol.* 97:fiaa255. doi: 10.1093/femsec/fiaa255

McMurdie, P. J., and Holmes, S. (2013). phyloseq: an R Package for reproducible interactive analysis and graphics of microbiome census data. *PLoS One* 8:e61217. doi: 10.1371/journal.pone.0061217

Meyer, F., Bagchi, S., Chaterji, S., Gerlach, W., Grama, A., Harrison, T., et al. (2019). MG-RAST version 4-lessons learned from a decade of low-budget ultra-high-throughput metagenome analysis. *Brief. Bioinform.* 20, 1151–1159. doi: 10.1093/bib/bbx105

Meyer, F., Paarmann, D., D'Souza, M., Olson, R., Glass, E. M., Kubal, M., et al. (2008). The metagenomics RAST server – a public resource for the automatic phylogenetic and functional analysis of metagenomes. *BMC Bioinformatics* 9:386. doi: 10.1186/1471-2105-9-386

Minic, Z., and Thongbam, P. D. (2011). The biological deep sea hydrothermal vent as a model to study carbondioxide capturing enzymes. *Mar. Drugs* 9, 719–738. doi: 10.3390/md9050719

Müller, A. L., Kjeldsen, K. U., Rattei, T., Pester, M., and Loy, A. (2015). Phylogenetic and environmental diversity of DsrAB-type dissimilatory (bi)sulfite reductases. *ISME J.* 9, 1152–1165. doi: 10.1038/ismej.2014.208

Münch, U., Lalou, C., Halbach, P., and Fujimoto, H. (2001). Relict hydrothermal events along the super-slow Southwest Indian spreading ridge near 63° 56' E—mineralogy, chemistry and chronology of sulfide samples. *Chem. Geol.* 177, 341–349. doi: 10.1016/S0009-2541(00)00418-6

Nakagawa, S., and Takai, K. (2008). Deep-sea vent chemoautotrophs: diversity, biochemistry and ecological significance. *FEMS Microbiol. Ecol.* 65, 1–14. doi: 10.1111/j.1574-6941.2008.00502.x

Nakamura, K., and Takai, K. (2014). Theoretical constraints of physical and chemical properties of hydrothermal fluids on variations in chemolithotrophic microbial communities in seafloor hydrothermal systems. *Prog. Earth Planet. Sci.* 1:5. doi: 10.1186/2197-4284-1-5

Nakamura, K., and Takai, K. (2015). "Indian Ocean hydrothermal systems: seafloor hydrothermal activities, physical and chemical characteristics of hydrothermal fluids, and vent-associated biological communities," in *Subseafloor Biosphere Linked to Hydrothermal Systems: TAIGA Concept*, eds J.-I. Ishibashi, K. Okino, and M. Sunamura (Tokyo: Springer Japan), 147–161. doi: 10.1007/978-4-431-54865-2_12

Nakamura, K., Watanabe, H., Miyazaki, J., Takai, K., Kawagucci, S., Noguchi, T., et al. (2012). Discovery of new hydrothermal activity and chemosynthetic fauna on the Central Indian Ridge at 18–20 S. *PLoS One* 7:e32965. doi: 10.1371/journal.pone.0032965

Nurk, S., Meleshko, D., Korobeynikov, A., and Pevzner, P. A. (2017). metaSPAdes: a new versatile metagenomic assembler. *Genome Res.* 27, 824–834. doi: 10.1101/gr.213959.116

O'Leary, N. A., Wright, M. W., Brister, J. R., Ciufo, S., McVeigh, D. H. R., Rajput, B., et al. (2016). Reference sequence (RefSeq) database at NCBI: current status, taxonomic expansion, and functional annotation. *Nucleic Acids Res.* 44, D733–D745. doi: 10.1093/nar/gkv1189

Overbeek, R., Begley, T., Butler, R. M., Choudhuri, J. V., Chuang, H.-Y., Cohoon, M., et al. (2005). The subsystems approach to genome annotation and its use in the project to annotate 1000 genomes. *Nucleic Acids Res.* 33, 5691–5702. doi: 10.1093/nar/gki866

Pak, S. J., Moon, J. W., Kim, J., Chandler, M. T., Kim, H. S., Son, J., et al. (2017). Widespread tectonic extension at the Central Indian Ridge between 8S and 18S. *Gondwana Res.* 45, 163–179. doi: 10.1016/j.gr.2016.12.015

Parks, D. H., Chuvochina, M., Waite, D. W., Rinke, C., Skarshewski, A., Chaumeil, P. A., et al. (2018). A standardized bacterial taxonomy based on genome phylogeny substantially revises the tree of life. *Nat. Biotechnol.* 36, 996–1004. doi: 10.1038/nbt.4229

Parks, D. H., Imelfort, M., Skennerton, C. T., Hugenholtz, P., and Tyson, G. W. (2015). CheckM: assessing the quality of microbial genomes recovered from isolates, single cells, and metagenomes. *Genome Res.* 25, 1043–1055. doi: 10.1101/gr.186072.114

Proskurowski, G., Lilley, M. D., Seewald, J. S., Fruh-Green, G. L., Olson, E. J., Lupton, J. E., et al. (2008). Abiogenic hydrocarbon production at Lost City hydrothermal field. *Science* 319, 604–607. doi: 10.1126/science.1151194

Quast, C., Pruesse, E., Yilmaz, P., Gerken, J., Schweer, T., Yarza, P., et al. (2013). The SILVA ribosomal RNA gene database project: improved data processing and web-based tools. *Nucleic Acids Res.* 41, D590–D596. doi: 10.1093/nar/gks1219

R Core Team (2021). *R: A Language and Environment for Statistical Computing*. Vienna: R Foundation for Statistical Computing.

Reysenbach, A.-L., Liu, Y., Banta, A. B., Beveridge, T. J., Kirshtein, J. D., Schouten, S., et al. (2006). A ubiquitous thermoacidophilic archaeon from deep-sea hydrothermal vents. *Nature* 442, 444–447. doi: 10.1038/nature04921

Rho, M., Tang, H., and Ye, Y. (2010). FragGeneScan: predicting genes in short and error-prone reads. *Nucleic Acids Res.* 38:e191. doi: 10.1093/nar/gkq747

Schloss, P. D., Westcott, S. L., Ryabin, T., Hall, J. R., Hartmann, M., Hollister, E. B., et al. (2009). Introducing mothur: open-source, platform-independent, community-supported software for describing and comparing microbial communities. *Appl. Environ. Microbiol.* 75, 7537–7541. doi: 10.1128/AEM.01541-09

Schrenk, M. O., Kelley, D. S., Delaney, J. R., and Baross, J. A. (2003). Incidence and diversity of microorganisms within the walls of an active deep-sea sulfide chimney. *Appl. Environ. Microbiol.* 69, 3580–3592. doi: 10.1128/Aem.69.6.3580-3592.2003

Sieber, C. M. K., Probst, A. J., Sharrar, A., Thomas, B. C., Hess, M., Tringe, S. G., et al. (2018). Recovery of genomes from metagenomes via a dereplication, aggregation and scoring strategy. *Nat. Microbiol.* 3, 836–843. doi: 10.1038/s41564-018-0171-1

Son, J., Pak, S. J., Kim, J., Baker, E. T., You, O. R., Son, S. K., et al. (2014). Tectonic and magmatic control of hydrothermal activity along the slow-spreading Central Indian Ridge, 8 degrees S-17 degrees S. *Geochem. Geophys. Geosyst.* 15, 2011–2020. doi: 10.1002/2013gc005206

Steinegger, M., and Soding, J. (2017). MMseqs2 enables sensitive protein sequence searching for the analysis of massive data sets. *Nat. Biotechnol.* 35, 1026–1028. doi: 10.1038/nbt.3988

Stokke, R., Dahle, H., Roalkvam, I., Wissuwa, J., Daae, F. L., Tooming-Klunderud, A., et al. (2015). Functional interactions among filamentous Epsilon*proteobacteria* and Bacteroidetes in a deep-sea hydrothermal vent biofilm. *Environ. Microbiol.* 17, 4063–4077. doi: 10.1111/1462-2920.12970

Sylvan, J. B., Sia, T. Y., Haddad, A. G., Briscoe, L. J., Toner, B. M., Girguis, P. R., et al. (2013). Low temperature geomicrobiology follows host rock composition along a geochemical gradient in Lau basin. *Front. Microbiol.* 4:61. doi: 10.3389/fmicb.2013.00061

Takahashi, S., Tomita, J., Nishioka, K., Hisada, T., and Nishijima, M. (2014). Development of a prokaryotic universal primer for simultaneous analysis of Bacteria and Archaea using next-generation sequencing. *PLoS One* 9:e105592. doi: 10.1371/journal.pone.0105592

Takai, K., and Sako, Y. (1999). A molecular view of archaeal diversity in marine and terrestrial hot water environments. *FEMS Microbiol. Ecol.* 28, 177–188. doi: 10.1016/S0168-6496(98)00103-2

Takai, K., Gamo, T., Tsunogai, U., Nakayama, N., Hirayama, H., Nealson, K. H., et al. (2004). Geochemical and microbiological evidence for a hydrogen-based, hyperthermophilic subsurface lithoautotrophic microbial ecosystem (HyperSLiME) beneath an active deep-sea hydrothermal field. *Extremophiles* 8, 269–282. doi: 10.1007/s00792-004-0386-3

Tao, C. H., Lin, J., Guo, S. Q., Chen, Y. J., Wu, G. H., Han, X. Q., et al. (2012). First active hydrothermal vents on an ultraslow-spreading center: Southwest Indian Ridge. *Geology* 40, 47–50. doi: 10.1130/G32389.1

Teske, A., Hinrichs, K. U., Edgcomb, V., de Vera Gomez, A., Kysela, D., Sylva, S. P., et al. (2002). Microbial diversity of hydrothermal sediments in the Guaymas Basin: evidence for anaerobic methanotrophic communities. *Appl. Environ. Microbiol.* 68, 1994–2007. doi: 10.1128/AEM.68.4.1994-2007.2002

Thorup, C., Schramm, A., Findlay, A. J., Finster, K. W., and Schreiber, L. (2017). Disguised as a sulfate reducer: growth of the deltaproteobacterium *Desulfurivibrio alkaliphilus* by sulfide oxidation with nitrate. *mBio* 8:e00671-17. doi: 10.1128/mBio.00671-17

Van Dover, C. L., Humphris, S. E., Fornari, D., Cavanaugh, C. M., Collier, R., Goffredi, S. K., et al. (2001). Biogeography and ecological setting of Indian Ocean hydrothermal vents. *Science* 294, 818–823. doi: 10.1126/science.1064574

Wang, Y., Han, X., Petersen, S., Frische, M., Qiu, Z., Li, H., et al. (2017). Mineralogy and trace element geochemistry of sulfide minerals from the Wocan Hydrothermal Field on the slow-spreading Carlsberg Ridge, Indian Ocean. *Ore Geol. Rev.* 84, 1–19. doi: 10.1016/j.oregeorev.2016.12.020

Wang, Y., Han, X., Zhou, Y., Qiu, Z., Yu, X., Petersen, S., et al. (2020). The Daxi Vent Field: an active mafic-hosted hydrothermal system at a non-transform offset on the slow-spreading Carlsberg Ridge, 6° 48' N. *Ore Geol. Rev.* 129:103888. doi: 10.1016/j.oregeorev.2020.103888

Ward, L. M., and Shih, P. M. (2021). Phototrophy and carbon fixation in Chlorobi postdate the rise of oxygen. *bioRxiv* [preprint]. doi: 10.1101/2021.01.22.427768

Wickham, H., Chang, W., Henry, L., Pedersen, T. L., Takahashi, K., et al. (2016). *ggplot2: Create Elegant Data Visualisations Using the Grammar of Graphics. R Package Version. 3.3.5*.

Wilke, A., Harrison, T., Wilkening, J., Field, D., Glass, E. M., Kyrpides, N., et al. (2012). The M5nr: a novel non-redundant database containing protein sequences and annotations from multiple sources and associated tools. *BMC Bioinformatics* 13:141. doi: 10.1186/1471-2105-13-141

Wu, Y. W., Simmons, B. A., and Singer, S. W. (2016). MaxBin 2.0: an automated binning algorithm to recover genomes from multiple metagenomic datasets. *Bioinformatics* 32, 605–607. doi: 10.1093/bioinformatics/btv638

Yamamoto, M., and Takai, K. (2011). Sulfur metabolisms in Epsilon- and Gamma-*Proteobacteria* in deep-sea hydrothermal fields. *Front. Microbiol.* 2:192. doi: 10.3389/fmicb.2011.00192

Yan, L. J., Yu, D., Hui, N., Naanuri, E., Viggor, S., Gafarov, A., et al. (2018). Distribution of archaeal communities along the coast of the Gulf of Finland and their response to oil contamination. *Front. Microbiol.* 9:15. doi: 10.3389/fmicb.2018.00015

Yang, W., Tao, C., Li, H., Liang, J., Liao, S., Long, J., et al. (2017). 230Th/238 U dating of hydrothermal sulfides from Duanqiao hydrothermal field, Southwest Indian Ridge. *Mar. Geophys. Res* 38, 71–83. doi: 10.1007/s11001-016-9279-y

Yang, Z., Xiao, X., and Zhang, Y. (2020). Microbial diversity of sediments from an inactive hydrothermal vent field, Southwest Indian Ridge. *Mar. Life Sci. Technol.* 2, 73–86. doi: 10.1007/s42995-019-00007-0

Zeng, X., Alain, K., and Shao, Z. (2021). Microorganisms from deep-sea hydrothermal vents. *Mar. Life Sci. Technol.* 3, 204–230. doi: 10.1007/s42995-020-00086-4

Zhou, Y. D., Zhang, D. S., Zhang, R. Y., Liu, Z. S., Tao, C. H., Lu, B., et al. (2018). Characterization of vent fauna at three hydrothermal vent fields on the Southwest Indian Ridge: implications for biogeography and interannual dynamics on ultraslow-spreading ridges. *Deep Sea Res. Part I* 137, 1–12. doi: 10.1016/j.dsr.2018.05.001

Conflict of Interest: The authors declare that the research was conducted in the absence of any commercial or financial relationships that could be construed as a potential conflict of interest.

Publisher's Note: All claims expressed in this article are solely those of the authors and do not necessarily represent those of their affiliated organizations, or those of the publisher, the editors and the reviewers. Any product that may be evaluated in this article, or claim that may be made by its manufacturer, is not guaranteed or endorsed by the publisher.

frontiers | Frontiers in Marine Science

ORIGINAL RESEARCH
published: 05 April 2022
doi: 10.3389/fmars.2022.866654

Drivers of Biomass and Biodiversity of Non-Chemosynthetic Benthic Fauna of the Mid-Atlantic Ridge in the North Atlantic

Imants G. Priede[1], Frank E. Muller-Karger[2], Tomasz Niedzielski[3], Andrey V. Gebruk[4], Daniel O. B. Jones[5] and Ana Colaço[6]*

[1] Oceanlab, Institute of Biological & Environmental Sciences, University of Aberdeen, Aberdeen, United Kingdom, [2] Institute for Marine Remote Sensing, College of Marine Science, University of South Florida, St Petersburg, FL, United States, [3] Department of Geoinformatics and Cartography, Faculty of Earth Sciences and Environmental Management University of Wrocław, Wrocław, Poland, [4] Shirshov Institute of Oceanology, Russian Academy of Sciences, Moscow, Russia, [5] National Oceanography Centre, Southampton, United Kingdom, [6] Instituto de Investigação em Ciências do Mar - Okeanos, Universidade dos Açores, Horta, Portugal

OPEN ACCESS

Edited by:
Philip Weaver, Seascape Consultants Ltd., United Kingdom

Reviewed by:
Teresa Radziejewska, University of Szczecin, Poland
Jose Angel Alvarez Perez, Universidade do Vale do Itajaí, Brazil

***Correspondence:**
Imants G. Priede
i.g.priede@abdn.ac.uk

Specialty section:
This article was submitted to Deep-Sea Environments and Ecology, a section of the journal Frontiers in Marine Science

Received: *31 January 2022*
Accepted: *01 March 2022*
Published: *05 April 2022*

Citation:
Priede IG, Muller-Karger FE, Niedzielski T, Gebruk AV, Jones DOB and Colaço A (2022) Drivers of Biomass and Biodiversity of Non-Chemosynthetic Benthic Fauna of the Mid-Atlantic Ridge in the North Atlantic. Front. Mar. Sci. 9:866654. doi: 10.3389/fmars.2022.866654

We examine the main drivers that may elevate biomass and biodiversity of non-chemosynthetic benthic megafauna of the lower bathyal (800-3500m depth) of the Mid-Atlantic Ridge in the North Atlantic Ocean (MAR). Specifically: 1. Primary production in surface waters (10°-48°N) from remote sensing data 2002-2020 over the MAR was not significantly different from abyssal regions to the east and west. We reject the hypothesis that presence of a mid ocean ridge may enhance surface primary production. 2. The quantity of particulate organic matter reaching the sea floor was estimated as a proportion of surface export production scaled by bathymetry. Flux was 1.3 to 3.0 times greater on the MAR as a function of shorter vertical transport distance from the surface than on adjacent abyssal regions. 3. Depth variation effect on species richness. Demersal fishes living between 41° and 60°N showed a maximum of species richness at 2000 m depth and linear increase in regional (Gamma) diversity of 32 species per 1,000 m elevation of the MAR above the abyss. Elevated topography provides niches for species that cannot otherwise survive. 4. Substrate heterogeneity. The MAR >95% covered with soft sediment with frequent hard rocky patches spaced at a mean nearest neighbour distance of <500 m. Over 90% were <1 km apart. Animals are readily able to disperse between such patches increasing biodiversity through the additive effect of soft and hard substrate fauna on the MAR. 5. Presence of a biogeographic overlap zone. The MAR harbours bathyal species known from Western Atlantic and Eastern Atlantic continental slopes with meridional asymmetry resulting in bias toward predominance of Eastern species. The mix of species contributes to increased diversity to the east of the MAR. Multiple factors support increase in biomass and biodiversity on the MAR. Biological data are almost entirely absent from 12° to 33°N, the part of the MAR

which may be mined for polymetallic sulphide ore deposits. This study enables some predictions of biomass and biodiversity but there is urgent need for intensive biological sampling across the MAR throughout the proposed mining areas south of the Azores.

Keywords: mid-ocean ridge, deep-sea, biodiversity, organic carbon flux, sediment fauna, biogeography, primary production

INTRODUCTION

The global mid ocean ridge system is one of the largest geomorphological features on the planet. It extends over 65,000 km through all the major oceans (Searle, 2013). The elevated seafloor in mid-ocean regions hosts greater biomass and biodiversity than the surrounding abyssal plains located between 3500 - 6500 m depth (UNESCO, 2009; Vecchione et al., 2010). Much attention has been directed to the specialized chemosynthetically sustained communities living on hydrothermal vent systems distributed along the ridge axis (Van Dover, 2000). However, most of the biomass on the ridge system is dependent on the sinking export of particulate organic matter derived from plankton production occurring in the sunlit surface layers of the ocean (Priede et al., 2013a). This photosynthetically dependent fauna comprises representatives of all forms of deep-sea life, including interstitial and burrowing species living in sediments, surface browsers, sessile species attached to hard substrates, and predators on and above the sea floor.

Here we consider the diversity and abundance of sessile and mobile megafauna including demersal fishes living at lower bathyal depths (800-3500 m) as defined by UNESCO (2009). Although the energy source for this fauna is export production from the surface, how this is transformed into biomass and diversity is determined by factors related to the topography of the MAR and processes of colonisation. Patterns of primary production in the surface layers and export of organic carbon to the seafloor can be regarded as fundamental drivers. Elevation of the sea floor, diversity of substrates, hydrography and biographic considerations are additional drivers that support enhanced benthic biomass and biodiversity on the MAR compared with the adjacent abyssal plains. Our study focusses on following main drivers

Primary Production in Surface Waters Over the MAR

Water flow around oceanic islands (Pollard et al., 2007) and seamounts (White et al., 2008) can result in advection of nutrients to surface layers, enhancing primary production and increased export flux to the deep-sea floor. However, White et al. (2008) point out that evidence for enhancement effects over seamounts is highly variable and inconclusive. Furthermore, phytoplankton blooms in the vicinity of islands occur at some distance from the islands themselves as nutrients are carried downstream on prevailing currents (Pollard et al., 2007; Messié et al., 2020). Over the relatively shallow northern Reykjanes segment of the MAR, there is evidence of localised elevated primary production compared with the adjacent Central Irminger Sea and Iceland Basin (Miller et al., 2013; Tilstone et al., 2014). Here we undertake a more extensive evaluation of patterns of primary production and export flux over the MAR between 10° and 48°N.

Export Production Over the MAR

A major pathway for export of primary production from the surface layers to the deep sea is the continuous rain of particulate organic carbon (POC). This flux is attenuated with depth by consumption, respiration, and remineralization in the water column so that typically only 1-5% of export production reaches abyssal depths (Deuser et al., 1990; Lampitt and Antia, 1997; Smith et al., 2009). Muller-Karger et al. (2005) quantified the global POC flux arriving on the sea floor and buried in the sediments by estimating the net primary production (NPP) from remote sensing data and applying a depth-dependent exponential decay model. This analysis showed the importance of shallow ocean margins for carbon sequestration in the context of the global ocean carbon cycle. Here we extend this model to estimate the magnitude and variability of the sinking POC flux on the MAR compared with surrounding abyssal areas. We also examine the potential influence of this deep sea POC flux on benthic biomass.

Depth Variability in the MAR

Deep-sea animals generally have preferred depths resulting in restricted distributions within narrow depth ranges due to hydrostatic pressure tolerance (Macdonald, 2021) and hydrographic conditions, bottom substrate and interspecific competition (Rowe and Menzies, 1969; King et al., 2006). Perez et al. (2020) show that on the São Paulo Ridge in the SW Atlantic topography-related deep-water flow dynamics and interfaces between water masses at different depths are the main drivers of benthic megafauna distribution. Living cold water corals occur within a narrow range seawater density found at particular depths in the NE Atlantic (Dullo et al., 2008) and aggregations of zooplankton and fish tend to occur over abrupt topographies (Genin, 2004). In some cases, there are fundamental physiological depth limitations, for example amongst fishes few sharks can survive at depths greater than 3000 m (Priede et al., 2006; Treberg and Speers-Roesch, 2016). On continental slopes these depth limits result in species turnover, or species replacement along the depth gradient hence increasing Beta diversity (Rex and Etter, 2010). On continental slopes, both invertebrates (Rex and Etter, 2010) and fishes (Priede et al., 2010) show a maximum of species diversity at mid-slope depths. Here we analyse the trends in biodiversity with depth on the Mid-Atlantic Ridge.

Substrate Heterogeneity on the MAR

The MAR is an undersea mountain range, but despite the rugged topography, Niedzielski et al. (2013) found that between 42° and 56°N it is 95% sediment covered with relatively smooth contours including flat terraces. The slow seafloor spreading rate at the MAR (Searle, 2013) has allowed 50-250 m thick sediment to accumulate on the MAR (Straume et al., 2019) at a rate of a few centimetres per year (Restreppo et al., 2020) obscuring most of the underlying hard oceanic crust. Riehl et al. (2020) highlight the importance of relatively rare exposed abyssal rock patches that can support sessile deep-sea fauna such as Bryozoa, Porifera, or Cnidaria. They estimate that fracture zones provide over 260,000 km^2 of hard rock habitat, equivalent to *ca*. 0.5% of area in the deep North Atlantic. Niedzielski et al. (2013) found that 4% of the MAR was exposed hard rock, including vertical cliffs and rocky outcrops, providing a greater area of hard substrate than available on the surrounding abyssal plains. Here we extend this analysis to examine the spatial distribution of rocky patches to evaluate whether colonisation by sessile fauna is enhanced by reduced dispersal distances and hence greater connectivity between suitable habitats.

Biogeographic Overlap Zones in and Around the MAR

Dispersal of benthic species from the continental slope into the open ocean (on island slopes, seamounts, and mid-ocean ridges) may occur in two stages (Mironov, 2014; Mironov et al., 2015): first, dispersal goes along the continental slope, and second, some species with adaptations to the open-ocean environment disperse from the near-continental zone into the open ocean. There are significant differences in the near-continental environment and the environment of the open ocean. For example, in the open ocean there is a decrease in the amount of organic matter, both in the water column and in sediments (Sokolova, 2000) as well as discontinuities in substrate composition at certain slope depths. As a result, the number of bathyal species decreases beyond a maximum diversity depth in the near-continental zone (Rex and Etter, 2010). In the Atlantic Ocean, colonisation occurs from continental slopes in the West and in the East, with biodiversity gradually decreasing towards the open ocean. Where the East and West Atlantic faunas meet on the Mid-Atlantic Ridge there may be an increase in mid-ocean biodiversity. Furthermore, the distance between the MAR and nearest continental slopes may give rise to population isolation and endemism amongst some of the fauna. Here we review the evidence for biogeographic mid-ocean domain effects that may explain biodiversity observed on the MAR. (**Figure 1**).

Scope of this Study

Here we examine patterns of net primary production (NPP) and sinking particulate organic carbon (POC) flux for the part of the MAR between 10° and 48°N using satellite remote sensing. The area to the south was excluded because it is influenced by the North Equatorial Current and a strong ocean colour signal from the Amazon River plume (Muller-Karger et al., 1995). The area north of 48° was excluded because of limitations in the availability of ocean colour satellite data products with seasons (see below). The MAR area to the north has been the subject of extensive previous research (Read et al., 2010; Miller et al., 2013; Tilstone et al., 2014). The part of the MAR between 12°N and 33°N which is being explored for mining of polymetallic sulphides under the auspices of the International Seabed Authority (Billett et al., 2019) is within this area examined using satellite data, but we have limited data on the benthic fauna for this region.

The rest of the analyses in this paper are largely derived from two major studies carried out on the MAR as part of the Census of Marine Life: MAR-ECO and ECOMAR. MAR-ECO sampled the area of the MAR between the Azores and Iceland during expeditions from different nations including a two-month voyage by the Norwegian *RV GO Sars* in 2004 (Bergstad et al., 2008a; Vecchione et al., 2010). ECOMAR contributed to MAR-ECO with voyages by the UK RRS *James Cook* focussing on two transects across the MAR at *ca*. 49°N and 54°N, south and north of the Charlie-Gibbs Fracture Zone respectively during 2007-2010 (Gebruk et al., 2013; Priede et al., 2013b).

The distribution of demersal fish species is analysed in detail because for this component of the bottom fauna there is data available over the greatest depth range (Porteiro et al., 2017). This analysis is combined with a new assessment of the distribution of substrate patches in this area of the MAR from 42° to 56°N. Aspects of the benthic megafauna on different substrates surveyed by MAR-ECO and ECOMAR are discussed with reference to previous publications (Gebruk, 2008; Gebruk et al., 2010; Alt et al., 2013; Bell et al., 2013; Gebruk et al., 2013; Jones et al., 2013; Bell et al., 2016; Alt et al., 2019) but no new analyses are presented.

MATERIALS AND METHODS

Net Primary Production and Particulate Organic Carbon Flux

NPP and POC flux were derived from remote sensing data collected using the NASA Aqua satellite MODIS (Moderate Resolution Imaging Spectro-radiometer) sensor for the North Atlantic between 10° and 48°N. The area to the north of 48°N is not processed by the standard NASA MODIS Ocean colour algorithms during winter months due to low ocean reflectance caused by low sun elevations. Time series of monthly (arithmetic) mean regional NPP observations, in units of ($gC.m^{-2}.day^{-1}$), were extracted from the standard Vertically Generalised Production Model (VGPM) (Behrenfeld and Falkowski, 1997) products distributed by the Ocean Productivity program at Oregon State University (Ocean Productivity, 2022). The monthly mean NPP values were based on near-surface chlorophyll concentration, daytime sea surface temperatures, and cloud-corrected incident daily photosynthetically active radiation (PAR) estimates derived from the MODIS sensor (global grid size of 2,160 x 4,320 pixels: MODIS reprocessing version R2018). In order to use a complete time series of NPP products without breaks in monthly coverage, we used the MODIS VGPM NPP products

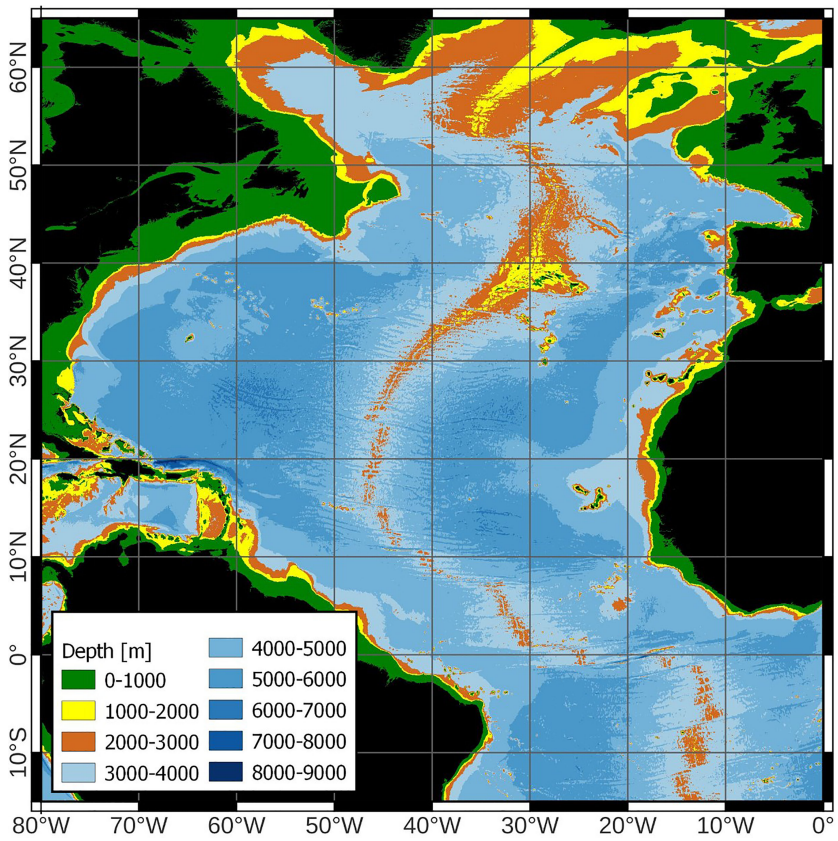

FIGURE 1 | Chart of the North Atlantic Ocean showing the Mid-Atlantic Ridge.

covering 1 August 2002 through 31 July 2020, or 18 complete annual cycles. MODIS suffered a short-lived malfunction that led to a gap in coverage for August and September 2020, and we did not use subsequent observations to avoid incomplete annual cycles in the analyses.

Global POC flux to the ocean bottom, in units of (gC m^{-2} day^{-1}), was estimated following the approach of Muller-Karger et al. (2005). We used an exponential decay function of the monthly mean gridded MODIS NPP datasets to compute global maps of the sinking POC flux using the Pace et al. (1987) model (i.e., flux(Z) = 3.523*NPP*$Z^{-0.734}$), where Z are ocean bottom depths at each cell of the NPP grids. Depths were based on the ETOPO1 global relief model of the Earth's surface. For this study, we excluded all data of the ocean bathymetry shallower than 800 m. Thus, the area examined follows the widely accepted definition of "lower bathyal" 800-3500 m (UNESCO, 2009). For the purposes of this analysis, we did not introduce a lag in the POC flux relative to the NPP observations. The commonly accepted average velocity for bulk POC is of the order of 100 m day^{-1} (Deuser et al., 1990). Since our averaging time step is a month, there is somewhat of a smear in the actual settling of particles to the bottom at depths >2,000 m between months. The analysis also does not account for episodic rapid settling of massive surface blooms (e.g., Conte et al., 1998; Thunell et al., 2007; Lorenzoni et al., 2012).

NPP and POC flux data were extracted from the gridded global fields to construct several summary time series. For example, data for each dataset were extracted in transects and polygons. Polygons were used to derive monthly mean values over the geographic area covered by the polygon. Only POC fluxes in areas deeper than 800 m were included in our analyses, while all pixels with valid data were included in similar transects and polygons for the NPP monthly means.

Three polygons were defined: West, MAR, and East (**Figure 2**) spanning the latitudinal range from 10°N to 48°N. The MAR polygon was defined as the region between smoothed boundaries at 3500 m depth west and east of the ridge, corresponding to lower bathyal with depths shallower than 800 m removed. The West and East polygons represent the abyssal regions of the North Atlantic on either side of the ridge from 3500 m to maximum depth either side of the MAR. To define the polygons, depth measurements were made at 2.5° latitudinal intervals except in regions of complex topography (e.g., at fracture zones) where more frequent points were used. Following preliminary inspection of the data, these polygons were further subdivided into three latitudinal strata, North 48°-40°N, Azores 40°-32.5°N and South 32.5°-10°N. Three transects were also extracted for analysis, specifically two latitudinal transects at 25°N (58.5°W to 32.5° W) and 47°N (40.25° W to

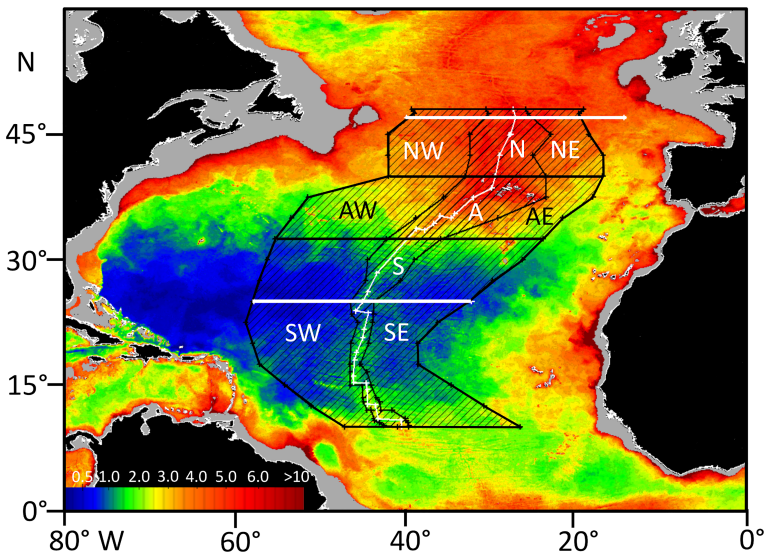

FIGURE 2 | Mean Daily Particulate Organic Carbon Flux (mg C.m^{-2}.day^{-1}) to the sea floor in the North Atlantic calculated for October 2002. The three polygons for remote sensing analysis of net primary production (NPP) and particulate organic carbon flux (POC), West, MAR and East are shown together with three latitudinal strata, North (NW, N, NE) Azores (AW, A, AE) and South (SW, S, SE). The MAR polygon is defined as the area enclosing lower bathyal depths (3500-800 m depth) on either side of the ridge. The West and East polygon outer boundaries correspond to the deepest points either side of the ridge. The thick white lines are latitudinal transects at 25°N and 47°N. The thin white line is the axis of the MAR.

14.34° W), and one transect along the axis of the ridge from 48°N to 10°N.

Demersal Fish Depth Distribution

Data on demersal fish species, including minimum and maximum depths of occurrence on the Mid-Atlantic Ridge between the Azores and Iceland (41°-60°N), were extracted from the compilation by Porteiro et al. (2017) of fishes captured during cruises by the *RV G.O. Sars* and *MS Loran* as part of the MAR-ECO programme in 2004. Designation of demersal species was based on capture in bottom trawls and bottom-set long lines broadly following Bergstad et al. (2008b). All members of the family Alepocephalidae (slickheads) were included plus six species of Platytroctidae (searsids) that were represented in bottom trawls. Platytroctidae are not normally considered demersal but those included here for analysis are considered to be associated with the MAR on the basis of capture in bottom trawls (Porteiro et al., 2017) or designation as benthopelagic in Fishbase (Froese and Pauly, 2021). This gave a total of 100 species (**Table 3**). The maximum depth in Porteiro et al. (2017) is 4300m and in Bergstad et al. (2008b) 3527 m. For species with a known distribution at greater depths, their ranges were extended according to data for the abyssal North Atlantic presented in Priede et al. (2010), and a maximum depth for one species *Porogadus miles* taken from Fishbase (Froese and Pauly, 2021).

Hard Substrate Distribution Analysis

The analysis of Niedzielski et al. (2013) was extended to evaluate the distances between adjacent hard rock patches on the MAR. Steep areas with slope >30° were used as proxies for hard rock patches, since video surveys had shown these to be 66.9% sediment free.

In order to characterise the empirical distribution of nearest distances between steep (>30°) slope patches of sea floor, a geographic information system (GIS) analysis of sea floor topography was carried out. Digital elevation models (DEMs) of parts of the MAR – i.e. bathymetric data sets acquired during cruises of the *RV G.O. Sars* in 2004 (Wenneck et al., 2008) and the *RRS James Cook* in 2007 (Priede et al., 2013b) – were processed in QGIS software v. 3.20.3 Odense. Seven transects, spatially corresponding to transects 1L–7L presented by Niedzielski et al. (2013), were analysed. The data had varying spatial resolutions, ranging between 42 and 59 m for *RV G.O. Sars* (five data sets) and between 99 and 100 m for the *RRS James Cook* (two data sets).

Each of seven DEMs was processed separately. First, slope rasters were computed. Second, they were reclassified into new rasters with two classes: steep slopes (ones corresponded to slope values greater than 30°) and flat terrain or non-steep slopes (zeros corresponded to slope values between 0° and 30°). Third, the reclassified rasters were converted to vector polygons. Fourth, from the newly produced vector data sets, polygons coded as ones (steep slopes) were selected, and therefore vector maps of steep patches were generated. Next, geometries of the resulting vector layers were corrected. Such data became input to the subsequent nearest neighbour analysis.

To compute nearest distances between steep slope patches, geometries of polygons which represented steep slopes were

approximated by centroids. That was conducted in QGIS NNJoin plugin. The same tool was also used to calculate the nearest distance between the joined features – each steep slope vector data set was joined with itself, and the approximation of geometry by centroids was enabled. For each transect, nearest distances were recorded in a newly created field in the attribute table. The data were exported to XLSX format and then saved as TXT files. Since the resolutions of the available bathymetric data sets were dissimilar and fitted two groups – (1) the *RV G.O. Sars* (42, 44, 47, 54 and 59 m) and (2) the *RRS James Cook* (99 and 100 m) – the histograms of nearest distances between steep slope patches were produced jointly for five transects provided by the *RV G.O. Sars* and jointly for two transects provided by the *RRS James Cook*.

RESULTS

Net Primary Production

For the entire area considered in the North Atlantic between 10° and 48°N, there was a strong seasonal cycle of NPP. The peak occurred predominantly in May-June each year in the North (**Figure 3A**), March-April in the Azores (**Figure 3B**), and February-March in the South (**Figure 3C**). There was strong trend of decrease In NPP from North to South, from an overall 18 year mean of 625 mgC.m^{-2}.day^{-1} in the Northern stratum, to 432 mgC.m^{-2}.day^{-1} around the Azores and 227 mgC.m^{-2}.day^{-1} in the South. In the Northern stratum there was no significant difference in NPP between, the West, MAR, and Eastern polygons (**Table 1**). In the Azores stratum there was no significant difference between the West and the MAR polygons but

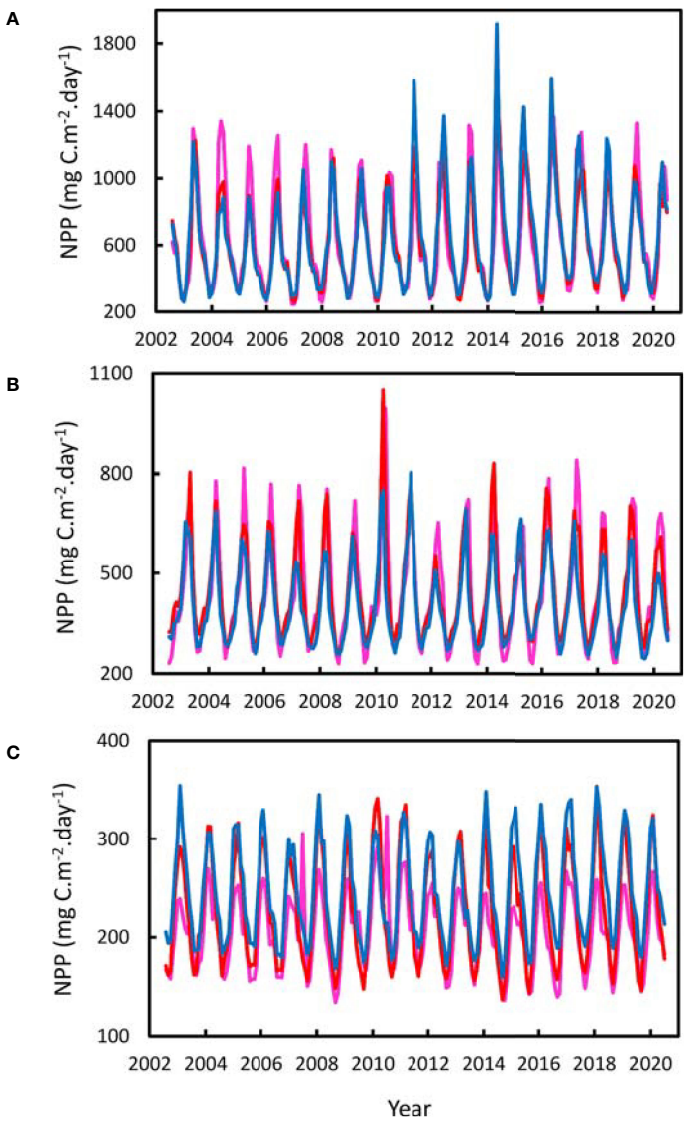

FIGURE 3 | Monthly Net Primary Production (NPP) for the years 2002-2020. **(A)** Northern Stratum 40°-48°N, **(B)** Azores Stratum 32.5°-40°N, **(C)** Southern Stratum 10°-32.5°N. Red line - MAR Polygon, Pink line – West Polygon. Blue line - East Polygon.

TABLE 1 | Comparison of surface net primary production (NPP) mg C.m^{-2}.day^{-1} over the Mid- Atlantic Ridge (MAR) and adjacent abyssal regions West and East during 2002-2020 for the three latitudinal strata shown in **Figure 2**.

Northern Stratum			
	West	**MAR**	**East**
Mean	630.62	613.36	631.46
SD	40.01	53.48	75.92
		P	Significance
ANOVA		0.60	NS
Azores Stratum			
	West	**MAR**	**East**
Mean	442.67	448.30	406.49
SD	23.56	27.58	26.59
		P	Significance
ANOVA		<0.0001	***
Post Hoc West v MAR		0.53	NS
Post Hoc East v MAR		<0.001	**
Post Hoc West v East		<0.0001	***
Southern Stratum			
	West	**MAR**	**East**
Mean	207.65	229.17	245.46
SD	12.55	7.43	7.88
		P	Significance
ANOVA		<0.0001	***
Post Hoc West v MAR		<0.0001	***
Post Hoc East v MAR		<0.0001	***
Post Hoc West v East		<0.0001	***

*Results of Analysis of Variance and posthoc t-tests with Bonferroni correction are given. *** highly significant P <0.0001, ** significant P <0.001, NS, not significant.*

NPP in the East was significantly (9%) lower. In the south there was a small but highly significant trend of increase in NPP from a mean of 208 mgC.m^{-2}.day^{-1} in the west to 245 mgC.m^{-2}.day^{-1} in the east. Inspection of the NPP data for the transect at 25°N confirms this pattern of increase towards the east (**Figure 4**). There was no evidence of elevated NPP over the axis of the ridge in either of the transects at 25° and 47°N.

In the transect at 47°N, there was a peak in average NPP (**Figure 4A**) around 350 km east of the ridge summit. This is associated with high values of NPP in the east from 2011 onwards (**Figure 3A**), the location of which was highly variable and could not be regarded as a consistent phenomenon associated with the topography of the MAR. We found no evidence of elevated NPP over the axis of the MAR.

Particulate Organic Carbon Flux

The POC flux to the bottom of the North Atlantic between 10° and 48°N showed an annual cycle and decrease from North to South reflecting the temporal and latitudinal trends in NPP (**Figure 5**). In the Northern and Azores strata there was no significant difference between POC flux to the west and east of the MAR (**Table 2**). In the southern stratum the POC flux was significantly higher in the East than in the West. At all latitudes the POC flux was significantly higher over the MAR than in the abyssal regions to the west and east. In the Northern stratum the mean POC flux was 31% higher, 65% higher in the Azores stratum and 32% in the south. In the abyssal regions, east and west of the ridge, an average of 0.75% of surface production was predicted to be deposited on the seafloor. On the MAR itself this amounted to an overall average 0.92-1.1% of NPP.

On the transect across the MAR at 25°N, the predicted POC flux on the summit was 2.73 mgC.m^{-2}.day^{-1} compared with minimum values of 0.86 mgC.m^{-2}.day^{-1} to the west and 1.23 mgC.m^{-2}.day^{-1} to the east (**Figure 4B**). At 47°N, the summit flux was 9.78 mgC.m^{-2}.day^{-1} compared with minimum values of 4.39 mgC.m^{-2}.day^{-1} to the west and 4.68 mgC.m^{-2}.day^{-1} to the east. The predicted POC flux strongly follows the bathymetry, resulting in peak values over the MAR summits up to 2-3 times higher than on abyssal slopes on either side of the ridge.

Examining the trend in POC flux from north to south along the axis of the ridge (**Figure 6**), there was a decrease from values of 6-13 mgC.m^{-2}.day^{-1} north of the Azores to a minimum of less than 2 mgC.m^{-2}.day^{-1} around 25°N (also evident in **Figures 2**, **5**). In the Northern stratum, there is a strong seasonal cycle in POC flux with up to 13-fold change between winter and summer, whereas in the southern stratum the seasonal cycle was attenuated to a 1.5-2.3-fold amplitude.

Demersal Fish Depth Distribution

Figure 7 and **Table 3** show the depth ranges of species ranked in order of minimum depth of occurrence. The first eight species with minimum depths between the sea surface and 450 m were all benthopelagic species caught in pelagic net tows over the MAR as well as by bottom long-lines and trawls on the MAR

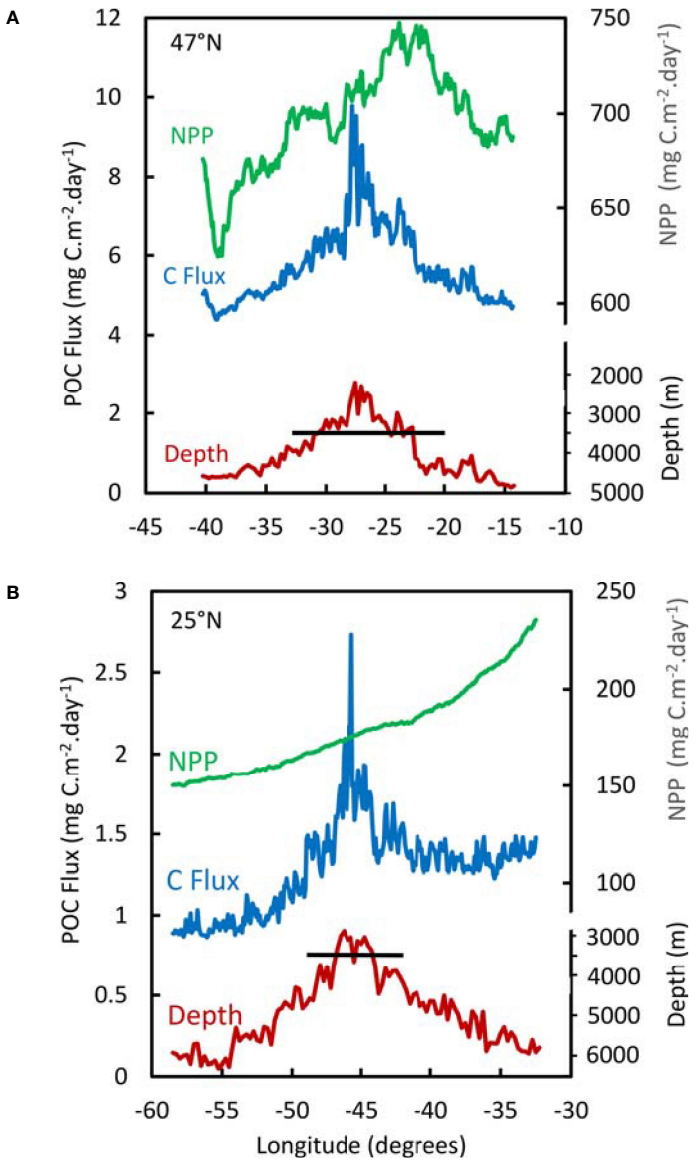

FIGURE 4 | Mean NPP and POC Flux during the years 2002-2020 along transects across the MAR at 47°N **(A)** and 25°N **(B)**. The horizontal black line indicates 3500 m depth, the boundary of the lower bathyal zone.

itself. These included five Platytroctids, one Alepocephalid (*Xenodermichthys copei*), one macrourid (*Coryphaenoides rupestris*) and the wolffish (*Anarhichas denticulatus*). Of the shallowest twenty species associated with summits of the MAR, the majority, 18 were benthopelagic. Furthermore, benthopelagic species were found at all depths comprising 35% of species ranked >20. Overall, 47% of species were benthopelagic.

Demersal species richness shows a peak of over 50 species present at 2000 m (**Figure 8A**). Examining this in cumulative form (**Figure 8B**) the total number of species increases with height of the ridge. Fitting a linear relationship from 1000 to 4000 m depth predicts, 2.5 species were present at 4000m, 35 species up to 3000m, 67 species up to 2000 m and 99 species up to 1000 m.

Twenty species of Chondrichthyes were caught including Chimaeras, Sharks, and Rays distributed from the ridge summit down to a maximum bottom depth of 3366 m, where the Leafscale gulper shark (*Centrophorus squamosus*) and Pale ray (*Bathyraja pallida*) were recorded. Twenty-one families of teleosts were recorded, the most speciose being: Macrouridae (18 species), Alepocephalidae (17 species), Moridae (7 species), Ophidiidae (6 species) and Platytroctidae (6 species).

Hard Substrate Distribution Analysis

The bathymetric surveys comprised a series of transects across the summit of the MAR at latitudes from 41.5°N to 56°N

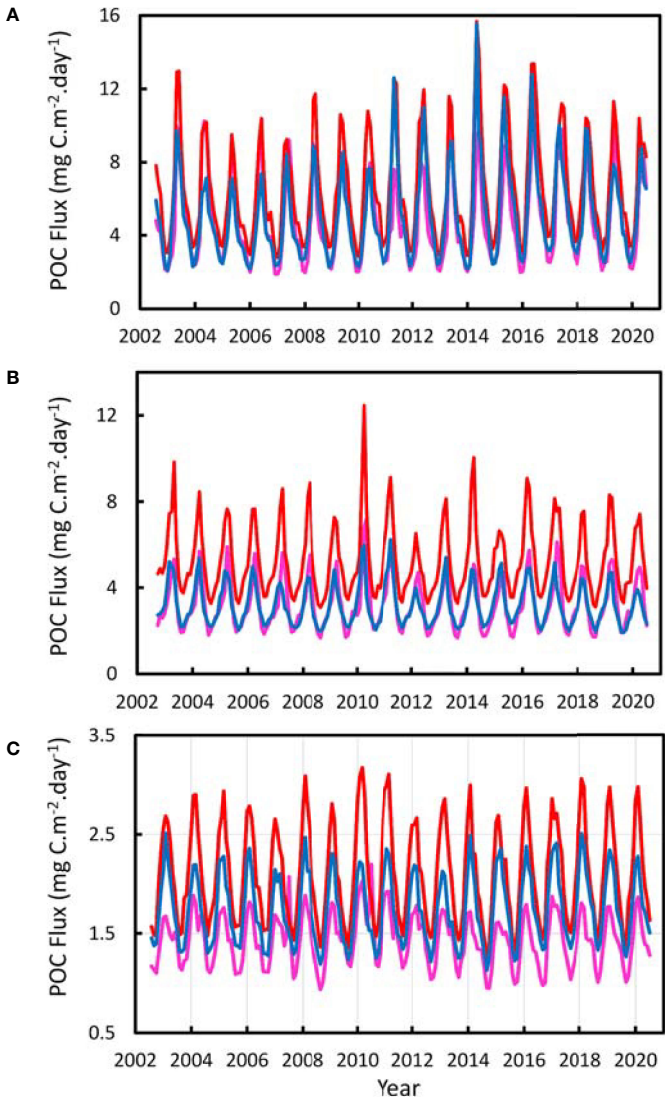

FIGURE 5 | Monthly Particulate Organic Carbon Flux (POC Flux) reaching the sea floor for the years 2002-2020. **(A)** Northern Stratum 40°-48°N, **(B)** Azores Stratum 32.5°-40°N, **(C)** Southern Stratum 10°-32.5°N. Red line - MAR Polygon, Pink line – West Polygon. Blue line - East Polygon.

withinthe region between the Azores and the Reykjanes Ridge (Niedzielski et al., 2013). Within this area, 11,237 discrete patches of steep terrain with slope > 30° were identified which corresponds to 0.91 steep patches km^{-2} over an estimated total survey area of 10,268 km^2. Niedzielski et al. (2013) estimate that within each patch, an average of 67% of the area would be exposed hard rock. The mean nearest neighbour distance between patches was 409 m (SD 454 m) for the RRS *James Cook* data, and 199 m (SD 268 m) for the *RV GO Sars* data (**Figure 9**). The medians were 266 and 127 m respectively, and the most isolated patch in the combined data set was 10,595 m from its nearest neighbour. The overwhelming majority of nearest neighbour distances were less than 1,000 m; 91.9% and 98.7% for the *RRS James Cook* and *RV GO Sars* data respectively.

DISCUSSION

Net Primary Production and Particulate Organic Carbon Flux Over the MAR

The mean net primary production (NPP) on the MAR (3,500 -800 m depth) was not significantly different from that in adjacent waters over the abyssal regions (>3500 m depth) either side of the ridge. Therefore, the hypothesis that the presence of the ridge directly enhances surface productivity is rejected. In the NE Atlantic, significant spring enhancement of primary production has been observed over the Gorringe seamount, where the summit is in the photic zone, about 30 m below the surface (Oliveira et al., 2016). In a global analysis, based on remote sensing over seamounts, Leitner et al. (2020) found evidence of long-term decadal time-scale persistent surface chlorophyll enhancement in

TABLE 2 | Comparison of particulate organic carbon flux (POC Flux) mgC.m^{-2}.day^{-1} over the Mid- Atlantic Ridge (MAR) and adjacent abyssal regions West and East during 2002-2020 for the three latitudinal strata shown in **Figure 2**.

Northern Stratum			
	West	**MAR**	**East**
Mean	4.85	6.49	5.08
SD	0.31	0.57	0.62
		P	Significance
ANOVA		<0.0001	***
Post Hoc West v MAR		<0.0001	***
Post Hoc East v MAR		<0.0001	***
Post Hoc West v East		0.18	NS
Azores Stratum			
	West	**MAR**	**East**
Mean	3.23	5.30	3.20
SD	0.17	0.32	0.21
		P	Significance
ANOVA		<0.0001	***
Post Hoc West v MAR		<0.0001	***
Post Hoc East v MAR		<0.0001	***
Post Hoc West v East		0.62	NS
Southern Stratum			
	West	**MAR**	**East**
Mean	1.45	2.11	1.75
SD	0.08	0.07	0.05
		P	Significance
ANOVA		<0.0001	***
Post Hoc West v MAR		<0.0001	***
Post Hoc East v MAR		<0.0001	***
Post Hoc West v East		<0.0001	***

*Results of Analysis of Variance and posthoc t-tests with Bonferroni correction are given. *** highly significant P <0.0001, NS, not significant.*

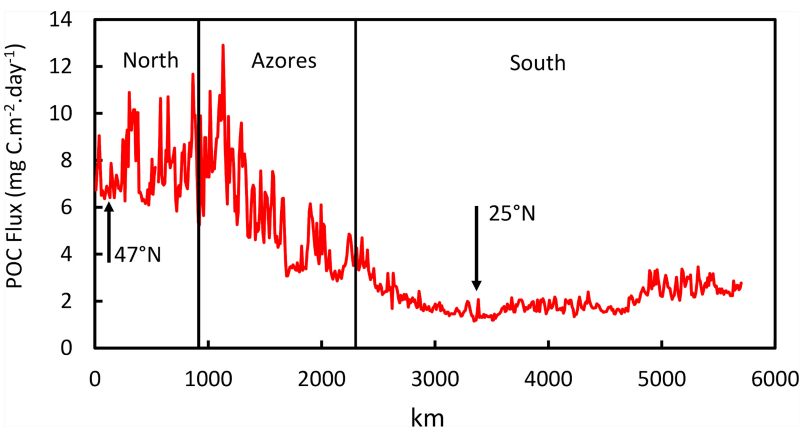

FIGURE 6 | Mean POC Flux during the years 2002-2020 along the axis of the MAR from 48°N (0 km) to 10°N across the three latitudinal strata, North, Azores and South. Arrows at 47°N and 25°N are locations of transects in shown in **Figure 4**.

27% of summits ≤100 m below the surface and 6% of summits ≤1000 m depth. Our results show that such seamount-induced chlorophyll enhancement (SICE) does not generally occur over the MAR, most of which is too deep to produce any observable effect at the surface.

The predicted particulate organic carbon flux arriving on the seafloor was 31-65% higher on the MAR lower bathyal than in the adjacent abyssal regions to the east and west. Peak values on the summits averaged 2-3 times higher the flux observed in the abyss. This increase in POC flux is explained by elevation of the

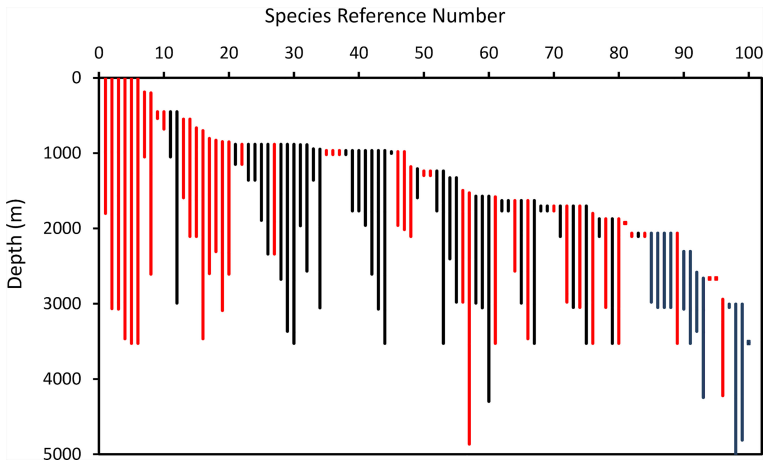

FIGURE 7 | Depth ranges of 100 species of demersal (black) and benthopelagic (red) fishes on the North Mid- Atlantic Ridge, ranked in order of minimum depth of occurrence. (The key to species is in **Table 3**).

sea floor of the MAR and the shorter vertical distance over which POC flux is attenuated with depth. Increased supply of organic carbon is likely to support higher biomass and abundance of benthic fauna.

After initial colonisation of a hypothetical new segment of ridge, there is probably a positive feedback effect further increasing biomass through active biological processes. For example, near the summits most of the demersal fishes present are bentho-pelagic species (**Figure 7**) which actively forage in the water column over the ridge capturing prey in the mesopelagic and surface layers, thus actively transporting additional organic matter to the MAR. Many invertebrates including sessile fauna such as corals as well as mobile species capture planktonic and nektonic prey from the waters surrounding the MAR. These active processes may be particularly enhanced by the vast pelagic biomass of the deep-scattering layers impinging on MAR particularly during their diurnal descent to their maximum depth (Genin et al., 1994; Fock et al., 2002).

There is a trend of decrease in POC flux from North to South (**Figures 2, 4–6**). According to the Longhurst (1998) biogeographic representation of the ocean our Northern stratum (40°-48°N) intersects the North Atlantic Drift Province (NADR), which is the region of greatest seasonal oscillation in NPP in the world's ocean. The Azores stratum (40°-32.5°N) is within the North Atlantic Subtropical Gyre Province (NAST). The southern stratum (32.5°-10°N) is in the Trade Wind Biome of the North Atlantic Tropical Gyral Province (NATR) which has the lowest NPP in the North Atlantic (Longhurst, 1998). The part of the MAR being explored for mining of polymetallic sulphides (12°N - 33°N) is within the southern stratum and experiences relatively low organic carbon input compared to areas North of the Azores.

Biodiversity - Depth Relationships

Analysis of demersal fish with depth (**Figure 8**) shows a maximum of species-richness at around 2,000 m, followed by a decline towards abyssal depths. This is similar to patterns described for a variety of taxa on continental slopes including gastropods, polychaetes, bivalves, cumaceans, invertebrate megafauna and fish (Rex, 1981). A maximum of species richness at mid-slope depths is a widespread phenomenon (Gage and Tyler, 1991). For demersal fishes in the NE Atlantic on the slopes of the Porcupine Seabight, Priede et al. (2010) found a species richness maximum at around 1,500 m depth. The diversity maximum on the MAR is at greater depth than on the slopes, possibly reflecting absence of habitat at shallow depths on the MAR.

The total number of demersal fish species present across the MAR in the North Atlantic (100 species) is close to that observed in the Porcupine Seabight (108). However, the present dataset for the MAR spans a wide latitudinal range (41°-60°N) with some species only occurring in part of the survey area. For example, *Macrourus berglax* is mainly a northern species, whereas *Histiobranchus bathybius* only occurs south of 52°N.

Bergstad et al, (2008b) suggested that some species may be exclusively observed either on the Western or Eastern slope of the ridge. Biodiversity in our analysis is however greater than would be expected based on previous observations at any given location along the MAR. The fish fauna of the MAR are relatively less well studied than those on continental slopes (Porteiro et al., 2017), so the species inventory may not be complete. Haedrich and Merrett (1988) list a total of 338 deep demersal fish species in the North Atlantic, although this includes species living at shallower depths than available on the MAR. In an analysis of a subset of the present data, Bergstad et al. (2008b) found a general decrease in abundance, biomass, and species number with depth. They also documented a change in dominant species with depth. Their cluster analysis revealed six species groups segregated by depth and latitude but with no clear zonation by depth.

Figure 8B shows that there is an increase in total number of species with increase in height of the MAR above the abyssal

TABLE 3 | Demersal and Benthopelagic Fishes of the Mid Atlantic Ridge (41°-60°N) ranked in order of minimum depth of occurrence.

Ref	Family	Species name	Depths (m)			
			Min	Max	Max^{x}	
1	Platytroctidae	*Holtbyrnia macrops* Maul, 1957	0	1800		†‡
2	Platytroctidae	*Searsia koefoedi* Parr, 1937	0	3065		†‡
3	Platytroctidae	*Normichthys operosus* Parr, 1951	0	3071		†‡
4	Alepocephalidae	*Xenodermichthys copei* (Gill, 1884)	0	3465		†‡
5	Macrouridae	*Coryphaenoides rupestris* Gunnerus, 1765	0	3527		†‡
6	Platytroctidae	*Holtbyrnia anomala* Krefft, 1980	0	3527		†‡
7	Anarhichadidae	*Anarhichas denticulatus* Krøyer, 1845	188	1050		†‡
8	Platytroctidae	*Maulisia argipalla* Matsui and Rosenblatt, 1979	200	2607		†‡
9	Phycidae	*Phycis blennoides* (Brünnich, 1768)	450	540		‡
10	Sebastidae	*Sebastes norvegicus* (Ascanius, 1772)	450	680		‡
11	Lotidae	*Brosme brosme* (Ascanius, 1772)	450	1050		
12	Etmopteridae	*Etmopterus princeps* Collett, 1904	450	2992		
13	Moridae	*Lepidion eques* (Günther, 1887)	549	1592		‡
14	Macrouridae	*Macrourus berglax* Lacepède, 1801	549	2106		‡
15	Moridae	*Halargyreus johnsonii* Günther, 1862	665	2107		†
16	Platytroctidae	*Maulisia microlepis* Sazonov and Golovan, 1976	702	3465		†
17	Alepocephalidae	*Bajacalifornia megalops* (Lütken, 1898)	805	2600		†‡
18	Macrouridae	*Bathygadus melanobranchus* Vaillant, 1888	829	2308		†
19	Moridae	*Antimora rostrata* (Günther, 1878)	848	3090		‡
20	Alepocephalidae	*Photostylus pycnopterus* Beebe, 1933	850	2607		†‡
21	Centrophoridae	*Centroscymnus owstonii* Garman, 1906	883	1149		
22	Moridae	*Mora moro* (Risso, 1810)	883	1149		‡
23	Centrophoridae	*Deania calcea* (Lowe, 1839)	883	1358		
24	Pseudotriakidae	*Pseudotriakis microdon* de Brito Capello, 1868	883	1358		
25	Centrophoridae	*Centroselachus crepidater* (Barbosa du Bocage and de Brito Capello, 1864)	883	1892		
26	Centrophoridae	*Centroscymnus coelolepis* Barbosa du Bocage and de Brito Capello, 1864	883	2340		
27	Moridae	*Lepidion guentheri* (Giglioli, 1880)	883	2340		‡
28	Chimaeridae	*Hydrolagus pallidus* Hardy and Stehmann, 1990	883	2675		
29	Centrophoridae	*Centrophorus squamosus* (Bonnaterre, 1788)	883	3366		
30	Synaphobranchidae	*Histiobranchus bathybius* (Günther, 1877)	883	3527		
31	Synaphobranchidae	*Synaphobranchus kaupii* Johnson, 1862	888	1964		
32	Rajidae	*Amblyraja jenseni* (Bigelow and Schroeder, 1950)	888	2567		
33	Pentanchidae	*Galeus murinus* (Collett, 1904)	944	1358		
34	Chimaeridae	*Hydrolagus affinis* (de Brito Capello, 1868)	948	3055		
35	Trichiuridae	*Aphanopus carbo* Lowe, 1839	966	1019		‡
36	Trachichthyidae	*Hoplostethus atlanticus* Collett, 1889	966	1019		‡
37	Oreosomatidae	*Neocyttus helgae* (Holt and Byrne, 1908)	966	1019		†
38	Rajidae	*Rajella bigelowi* (Stehmann, 1978)	966	1019		
39	Macrouridae	*Coelorinchus labiatus* (Köhler, 1896)	966	1767		
40	Notacanthidae	*Notacanthus bonaparte* Risso, 1840	966	1767		
41	Pentanchidae	*Apristurus manis* (Springer, 1979)	966	1959		
42	Notacanthidae	*Notacanthus chemnitzii* Bloch, 1788	966	2607		
43	Alepocephalidae	*Alepocephalus agassizii* Goode and Bean, 1883	966	3071		
44	Notacanthidae	*Polyacanthonotus rissoanus* (De Filippi and Verany, 1857)	966	3527		
45	Moridae	*Guttigadus latifrons* (Holt and Byrne, 1908)	981	1003		
46	Halosauridae	*Aldrovandia phalacra* (Vaillant, 1888)	981	1959		‡
47	Liparidae	*Psednos groenlandicus* Chernova, 2001	981	2015		†
48	Alepocephalidae	*Rouleina attrita* (Vaillant, 1888)	1180	2107		†‡
49	Pentanchidae	*Apristurus microps* (Gilchrist, 1922)	1208	1592		
50	Macrouridae	*Nezumia sclerorhynchus* (Valenciennes, 1838)	1237	1296		‡
51	Macrouridae	*Trachyrincus murrayi* Günther, 1887	1237	1297		‡
52	Ipnopidae	*Bathypterois dubius* Vaillant, 1888	1237	1767		
53	Bathysauridae	*Bathysaurus ferox* Günther, 1878	1237	3527		
54	Moridae	*Lepidion schmidti* Svetovidov, 1936	1327	2404		
55	Alepocephalidae	*Alepocephalus australis* Barnard, 1923	1327	2979		
56	Alepocephalidae	*Bathytroctes microlepis* Günther, 1878	1496	2979		†‡
57	Macrouridae	*Coryphaenoides armatus* (Hector, 1875)	1528	4300	4865	‡
58	Somniosidae	*Somniosus microcephalus* (Bloch and Schneider, 1801)	1572	2992		
59	Arhynchobatidae	*Bathyraja richardsoni* (Garrick, 1961)	1572	3055		
60	Ophidiidae	*Spectrunculus grandis* (Günther, 1877)	1572	3366	4298	
61	Macrouridae	*Coryphaenoides mediterraneus* (Giglioli, 1893)	1580	3527		‡

(Continued)

TABLE 3 | Continued

Ref	Family	Species name	Depths (m)			
			Min	Max	Max^{x}	
62	Ipnopidae	*Bathypterois phenax* Parr, 1928	1630	1767		
63	Bythitidae	*Cataetyx laticeps* Koefoed, 1927	1630	1767		
64	Alepocephalidae	*Narcetes stomias* (Gilbert, 1890)	1630	2567		‡
65	Macrouridae	*Coryphaenoides guentheri* (Vaillant, 1888)	1630	2992		
66	Macrouridae	*Coryphaenoides brevibarbis* (Goode and Bean, 1896)	1630	3465		‡
67	Halosauridae	*Halosauropsis macrochir* (Günther, 1878)	1630	3527		
68	Macrouridae	*Bathygadus favosus* Goode and Bean, 1886	1702	1767		
69	Alepocephalidae	*Conocara macropterum* (Vaillant, 1888)	1702	1767		‡
70	Macrouridae	*Sphagemacrurus hirundo* (Collett, 1896)	1702	1767		
71	Pentanchidae	*Apristurus profundorum* (Goode and Bean, 1896)	1702	2107		
72	Synaphobranchidae	*Ilyophis brunneus* Gilbert, 1891	1702	2979		‡
73	Aphyonidae	*Aphyonus gelatinosus* Günther, 1878	1702	3050		
74	Alepocephalidae	*Conocara murrayi* (Koefoed, 1927)	1702	3050		‡
75	Macrouridae	*Coryphaenoides leptolepis* Günther, 1877	1702	3527		
76	Alepocephalidae	*Bathytroctes macrolepis* Günther, 1887	1800	3527		‡
77	Liparidae	*Paraliparis nigellus* Chernova and Møller, 2008	1872	2107		
78	Alepocephalidae	*Narcetes erimelas* Alcock, 1890	1872	3050		‡
79	Macrouridae	*Coryphaenoides carapinus* Goode and Bean, 1883	1872	3527		
80	Alepocephalidae	*Rinoctes nasutus* (Koefoed, 1927)	1872	3527		‡
81	Chimaeridae	*Chimaera monstrosa* Linnaeus, 1758	1929	1929		
82	Alepocephalidae	*Leptoderma macrophthalmum* Byrkjedal et al., 2011	2063	2107		‡
83	Ophidiidae	*Penopus microphthalmus* (Vaillant, 1888)	2063	2107		
84	Macrouridae	*Squalogadus modificatus* Gilbert and Hubbs, 1916	2063	2107		‡
85	Stephanoberycidae	*Acanthochaenus luetkenii* Gill, 1884	2063	2979		‡
86	Alepocephalidae	*Alepocephalus productus* Gill, 1883	2063	3050		
87	Ipnopidae	*Bathypterois grallator* (Goode and Bean, 1886)	2063	3050		
88	Macrouridae	*Paracetonurus flagellicauda* (Koefoed, 1927)	2063	3050		
89	Notacanthidae	*Polyacanthonotus challengeri* (Vaillant, 1888)	2063	3527		‡
90	Rhinochimaeridae	*Harriotta haeckeli* Karrer, 1972	2306	3071		
91	Ophidiidae	*Spectrunculus crassus* (Vaillant, 1888)	2306	3527		
92	Arhynchobatidae	*Bathyraja pallida* (Forster, 1967)	2582	3366		
93	Platytroctidae	*Bathysaurus mollis* Günther, 1878	2660	2670		
94	Ophidiidae	*Lamprogrammus niger* Alcock, 1891	2660	2670		‡
95	Alepocephalidae	*Talismania mekistonema* Sulak, 1975	2660	2670		‡
96	Alepocephalidae	*Bathytroctes michaelsarsi* Koefoed, 1927	2941	2955	4222	‡
97	Macrouridae	*Asthenomacrurus victoris* Sazonov and Shchherbachev, 1982	3005	3050		
98	Ophidiidae	*Porogadus miles* Goode and Bean, 1885	3005	3050	5050*	
99	Ophidiidae	*Holcomycteronus squamosus* (Roule, 1916)	3005	3527	4812	
100	Macrouridae	*Coryphaenoides profundicolus* (Nybelin, 1957)	3505	3527	4865	

*Minimum and maximum depth data from Porteiro et al. (2017). Max^{x}: additional data from Priede et al. (2010). *data from Fishbase (Froese and Pauly, 2021), † also captured in pelagic trawl (Porteiro et al., 2017), ‡ benthopelagic according to Fishbase (Froese and Pauly, 2021).*

plains. The slope of the linear regression corresponds to an increase in total species of 32 species per 1000 m. On the Porcupine abyssal plain to the east of the MAR, Priede et al. (2010) recorded 10 demersal fish species at depths >4500 m. By providing depth niches for different species, the bathymetry of the MAR has a major effect on mid ocean deep-sea fish biodiversity.

Substrate Heterogeneity

Distances Between Rocky Substrate Patches

In a previous study, Niedzielski et al. (2013) showed that over 95% of the MAR between 41.5°N and 56°N is covered in sediment. This provides habitat for burrowing species, interstitial infauna, and browsing megafauna. Flat plains filled with soft sediment comprised 38% of the area surveyed, arranged in a series of terraces on either side of the axis of the ridge. This new analysis shows that although hard substrate occupies less than 5% of the MAR area, the distance between neighbouring patches is typically less than 500 m and over 90% of patches are less than 1 km away from their nearest neighbour (**Figure 9**). We conclude that for successful dispersal of fauna between patches of suitable habitat the animals need to be able to move, or broadcast eggs or larvae to be carried over distances of 200 to 1,000 m.

The difference in spatial resolution between the *RRS James Cook* (*ca*. 100 m) and *RV GO Sars* (*ca*, 50 m) is a complicating factor that cannot be resolved without new data. Nevertheless, it is evident that hard substrate patches are relatively close to one another on the MAR. Furthermore, within each steep slope pixel there are likely to be multiple patches of hard substrate areas, including isolated single rocks, exposed summits or near-vertical cliff faces.

We assume that transport by bottom currents is an important mechanism for dispersal of hard substrate fauna. Priede et al. (2013a) measured tidal currents up to 0.05 m.s^{-1} with long-term

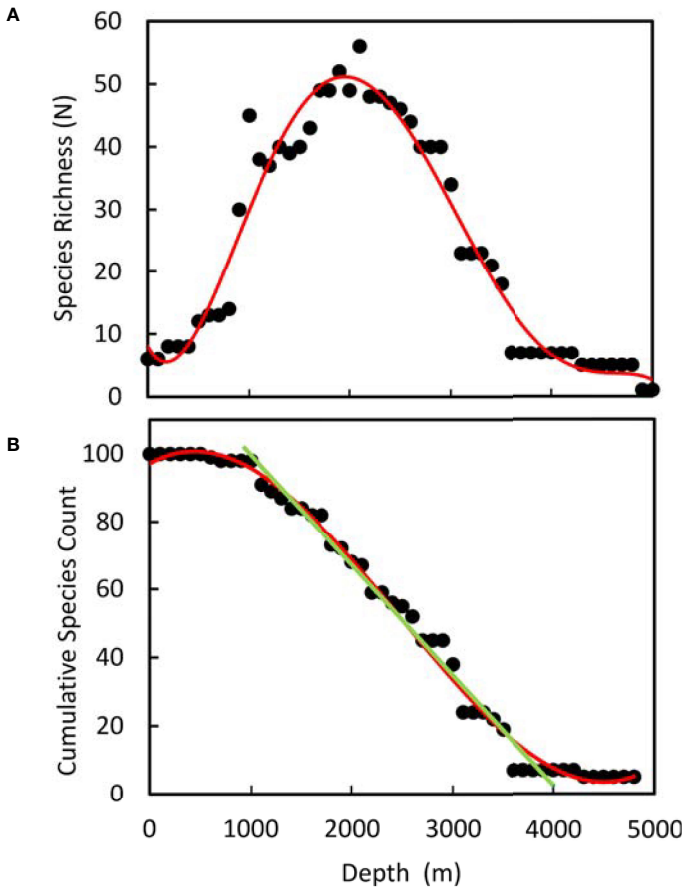

FIGURE 8 | Species richness on the Mid-Atlantic Ridge (41°-60°N) derived from the depth range data in **Figure 6** and **Table 3** assuming species occurrence is continuous between maximum and minimum observed depth. **(A)** Total species per 100m depth stratum. Red line - fitted polynomial. **(B)** Cumulative species count from maximum to minimum depth, Red line- fitted polynomial. Green line: Linear relationship 1000 - 4000m depth: y = -0.0323x + 131.69 R^2 = 0.984.

currents up to 0.025 $m.s^{-1}$ on the flanks of the ridge. Dale and Inall (2015) showed that topography has an important influence, and recorded above-bottom tidal flows of up to 0.1 $m.s^{-1}$. A transport speed of 0.05 $m.s^{-1}$ or 180 $m.h^{-1}$ is sufficient to allow movement between most patches of hard substrate within one tidal cycle. Long term residual flow of 0.02 $m.s^{-1}$ would result in transport over a distance of 1.73 $km.day^{-1}$.

Riehl et al. (2020) emphasise the importance of fracture zones in providing rare patches of rocky substrate at abyssal depths. In the North Atlantic there are approximately 65 fracture zones between the equator and 60°N (Müller and Roest, 1992). This would give an average distance between fracture zones of 135 km; it is evident that on the MAR, distances between rocky patches are shorter, and hence connectivity much enhanced compared with the abyss.

Connectivity Processes

In the previous section we show that to ensure effective connectivity of populations across the MAR hard substrate fauna need to be able to disperse over distances of 200-1000m. Connectivity of benthic species is the result of larval dispersal, settlement and recruitment leading to recruitment into the adult population (Metaxas and Saunders, 2009). This depends on hydrographic conditions and the presence of suitable habitat for the larvae, including the type of bottom substrate (hard or soft), within a viable distance given motility and directionality of the organisms and currents.

A major factor is the duration of the larvae development either as planktonic larvae (*i.e.* Planktonic Larval Duration-PLD) or on the substrate if it is a crawler; and the ability to survive until the next suitable habitat (travel distance). Planula larvae of the octocoral *Drifa glomerulata*, for example, are demersal and actively probe the substratum immediately upon release whereas other species drift between the water column and seabed usually settling after 1-30 days (Sun et al., 2010). The few studies that exist show that species with a 24 h pelagic larval phase can disperse around one kilometre, and species with a longer pelagic phase can travel hundreds of kilometres (Shanks, 2009).

The distance that the larvae can travel is also dependent on whether the larva is planktotrophic; able to feed in the water column enabling longer travel distance, or lecithotrophic,

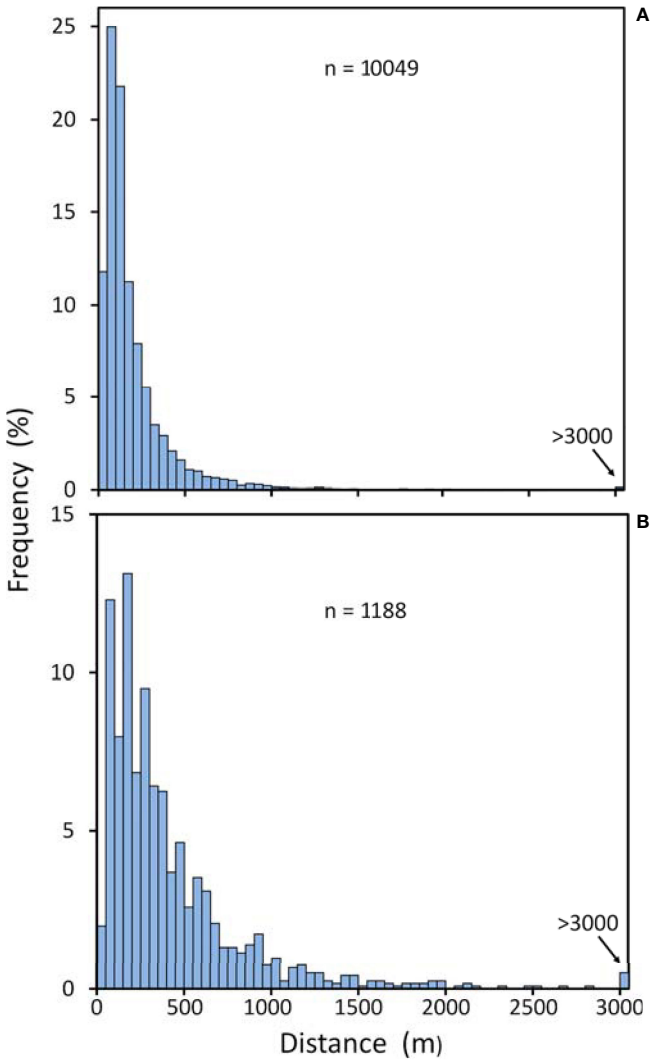

FIGURE 9 | Nearest neighbour distances between centroids of steep slope (>30°) patches from transects across at the MAR at 41.5°N to 56°N. **(A)** Data from the *RV GO Sars* (42-59m resolution). **(B)** Data from the *RRS James Cook* (99-100m resolution).

dependent entirely on food reserves (e.g. in the yolk sac) in which case travelling distances may be shorter (Danovaro et al., 2014). Little is known about the larval biology of deep-sea benthic species such as octocorals. Knowledge is limited to some brooding species, with very short PLD (Sun et al., 2010) while others are broadcast-spawners that have different larval characteristics and dispersal capabilities (Rakka et al., 2021). Some authors showed that for sponges a short PLD is an advantage (surviving better, growing faster and with a more regular shape), confirming the hypothesis that long-lived larvae bring fewer reserves to the post-settlement period (Maldonado and Young, 1999). A review by Young (2003) showed that pelagic lecithotrophy, rather than brooding, is the main reproductive mode in the deep sea.

The results presented here (**Figure 9**) show that the distance between centroids of hard substrate patches is generally less than 1km. Dispersal over such distances is readily achieved by larvae of many deep-sea species and suggests a high degree of connectivity between patches of suitable habitat for sessile benthic species. The rugged topography of MAR can create areas of strong turbulent near-bed currents (Dale and Inall, 2015). Such flows may enhance food supply and provide favourable conditions for the settlement of suspension-feeding fauna, such as cold-water corals and sponges (Mortensen et al., 2008). Larval rearing experiments showed that without aeration, larvae of octocorals have a strong negative buoyancy, remaining at the bottom (Rakka et al., 2021), showing the importance of seabed currents for larval dispersal.

Most of the hard substrate species on the MAR are indicators of vulnerable marine ecosystems, which are characterised as long living, low fecundity and slow growing (ICES, 2020). Short distances between neighbouring hard substrate patches favour

connectivity. However, dispersal over larger distances to seamounts or the ocean margin (**Figure 1**) depend on mesoscale phenomena, such as eddies or benthic storms (Vic et al., 2018). The close spacing between hard substrate patches enables them to be used as stepping-stones for faunal dispersal over long distances as hypothesised for the chains of seamounts (Miller and Gunasekera, 2017)

Hard Substrate Megafauna of the MAR

Hard substratum on the Mid-Atlantic Ridge takes many forms from exposed rocks on otherwise fine sediment areas to extensive vertical walls of basalt on the ridge scarps (**Figure 10**). Organisms have been observed living attached to and in association with all these forms of hard substratum (Bell et al., 2016; Alt et al., 2019). Indeed, even small boulders can support extensive communities of large megafauna, such as stalked crinoids and sponges (Craig et al., 2011). Despite these occurrences, hard substratum is generally absent from flat areas and relatively rare (1.6% of area) in gently sloping areas in the vicinity of the Charlie-Gibbs Fracture Zone (Alt et al., 2019) and likely elsewhere (Niedzielski et al., 2013). These sedimented plains with low slopes make up most of the MAR area (flat: 37.7% and gentle slopes: 56.7%; Niedzielski et al., 2013). Even the limited additional heterogeneity offered in the sloping sites may contribute to the enhanced species richness found in the majority of these areas (Alt et al., 2019) for there are many species that live attached to hard substratum. Even the limited additional heterogeneity offered in the sloping sites may contribute to the enhanced species richness found in the majority of these areas (Alt et al., 2019) for there are many species that live attached to hard substratum. While there is a rapid decrease in the density of deepwater corals with depth below about 1,300 m in the MAR (Mortensen et al., 2008), many of the distinctive and large taxa living on hard substrata are observed across multiple surveys at similar depth bands (Morris et al., 2012; Gebruk and Krylova, 2013; Bell et al., 2016). This suggests that at least some species have widespread distributions across patches of suitable habitat within particular depth horizons. In the ECOMAR video surveys at 2500 m depth, Linley et al. (2013) found no consistent relationship between fish distribution and seafloor slopes with different substrates but around the Azores, Parra et al. (2017) report a general preference for mixed sediments, sandy and rocky areas, with low fish numbers on muddy areas.

Soft Sediment Megafauna

In the ECOMAR study areas (49°N & 54°N), soft sediments in flat and gentle (<30°) slopes were predominantly clay to coarse sand with fine silt (1-10 μm) (Alt et al., 2019). At 49°N, south of the Charlie-Gibbs Fracture Zone, accumulations of pteropod shells were common. The seafloor was disturbed in most areas by the traces of megafauna (Lebensspuren), which covered between around 5 and 10% of the seabed area (Bell et al., 2013). These Lebensspuren consisted of mounds, burrows, tracks, faecal casts, body impressions and depressions caused by animal activity (Bell et al., 2013). The proportions of these types were variable between areas. A total of 58 distinct Lebensspuren types could be differentiated (Bell et al., 2013).

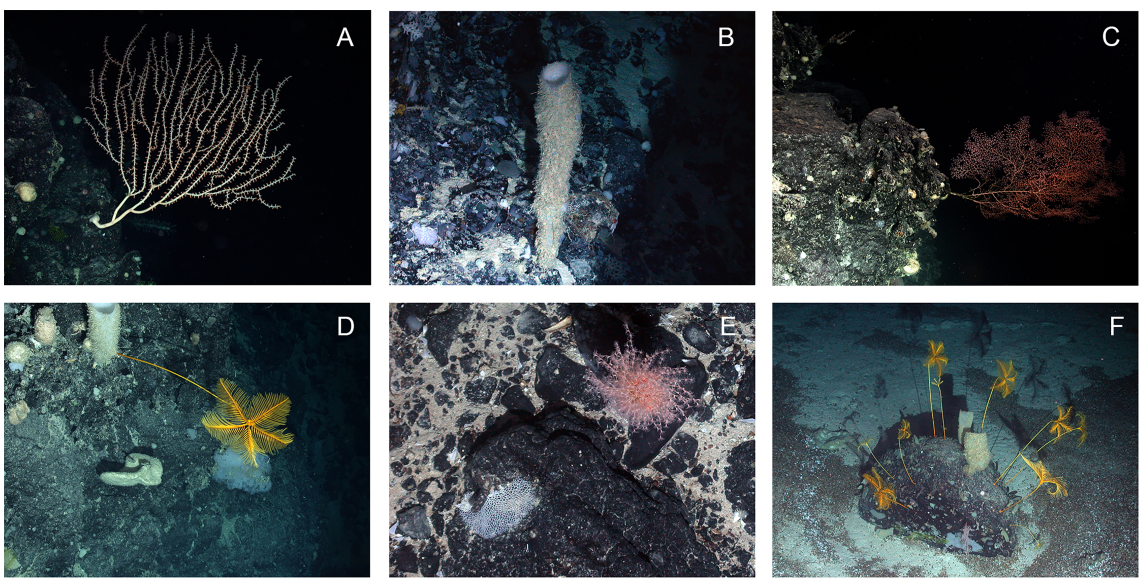

FIGURE 10 | Examples of species associated with rocky substratum on the northern Mid-Atlantic Ridge. Dive number indicated with D in caption. **(A)** Isididae sp. on steep rock wall D173; **(B)** Sponge on rock wall D159; **(C)** *Chrysogorgia* sp. on steep rock wall D173; **(D)** *Anachalypsicrinus nefertiti* on rocky wall D173; **(E)** Unknown octocoral on rock in mixed substratum area D178; **(F)** soft sediment with pteropod thanatocoenoses and boulder with multiple crinoids (*Anachalypsicrinus nefertiti*) and sponges D178. Images collected on two dives during ECOMAR cruise JC048: Dive 173 (station 40, ECOMAR SW Site, Date 21 June 2010, 48° 44.118 N 28° 39.335 W, 2623-2428 m depth) and Dive 178 (station 53, ECOMAR SE Site, Date 27 June 2010, 49° 1.439 N 27° 41.264, 2442-2630 m depth).

The faunal communities inhabiting soft sediments on the Mid-Atlantic Ridge, at least in the ECOMAR and MARECO areas, were dominated by echinoderms. Holothurians were the most abundant of these and include at least 55 species (Gebruk, 2008; Rogacheva et al., 2013). Sponges and cnidarians were also abundant (Gebruk et al., 2010; Alt et al., 2019). There was some spatial heterogeneity in the available species-level data from benthic trawl surveys of the MAR. However, it is difficult to separate ecological differences in the limited amounts of semi-quantitative trawl data. In the case of the trawl surveys of the MARECO area (41.5°N to 56°N) (Gebruk et al., 2010) and the smaller ECOMAR area around the Charlie Gibbs Fracture Zone (Alt et al., 2013), there were a total of 226 species of invertebrates named, with 193 species in the MARECO dataset (Gebruk et al., 2010) and 90 species (excluding unclear identifications) in the ECOMAR dataset (Alt et al., 2013). The two areas had 58 species in common. The best studied and likely most comparable taxon in those datasets, the echinoderms, had a total of 118 named species between the two studies, of which 50 were shared.

Biodiversity and Substrate Heterogeneity

Since hard and soft substrates provide habitat for distinctive assemblages of species it is reasonable to assume that a heterogeneous environment with both kinds of substrate should have higher biodiversity through an additive effect. There are differences between studies in the habitat that contributes most to the biodiversity of the region. Studies of the megafauna (**Figure 11**) of the Charlie-Gibbs fracture zone between 1700 – 4500 m depth using the submersibles *Mir-1* and *Mir-2* (Felley et al., 2008; Gebruk and Krylova, 2013) observed more morphospecies (29) associated with rocks than with soft sediment (16). In contrast, in the ECOMAR study areas at *ca.* 2500 m depth on the flanks of the MAR (49°N and 54°N), the steeper rocky areas appear to have a generally lower density and lower species richness in the same surface area of flat and gently sloping sediment (Bell et al., 2016 and Alt et al., 2019), with most faunal groups having at least an order of magnitude lower density in rocky areas. However, not all taxa followed this trend, with both sponges and cnidarians being particularly abundant on rocky areas (Bell et al., 2016) and occurring at densities of similar orders of magnitude to the flatter sediment-covered areas. Rocky areas in all studies had distinct morphospecies, for example at the ECOMAR sites 15 morphospecies were observed in rocky areas (Bell et al., 2016) that were not seen in flatter areas (Alt et al., 2019). Some motile species usually associated with soft sediments, such as holothurians (Rogacheva et al., 2013) and enteropneusts (Jones et al., 2013) were seen in rocky areas. The differences between these results are likely related to faunal variation associated with depth, as even in the Mir datasets (Gebruk and Krylova, 2013) the *ca.* 2500 m depth band had particularly high richness of sediment-associated fauna.

One reason for higher species diversity on rocks may be the association between species: some species provide a substrate to others, for example comatulid crinoids and ophiuroids settle on gorgonian corals (Gebruk and Krylova, 2013). In a region of the MAR between the southern part of the Reykjanes Ridge and the Azores (~45°N), 10 times more corals were found on rocky areas than sediment-covered areas (Morris et al., 2012) and areas with corals hosted 1.6 times more megafaunal taxa than areas without corals (Mortensen et al., 2008).

Biogeographic Patterns

In the North Atlantic, the MAR accounts for 46% of the lower bathyal at depths from 800 to 3500 m (Niedzielski et al., 2013). The ridge provides habitat for bathyal species that also occur on

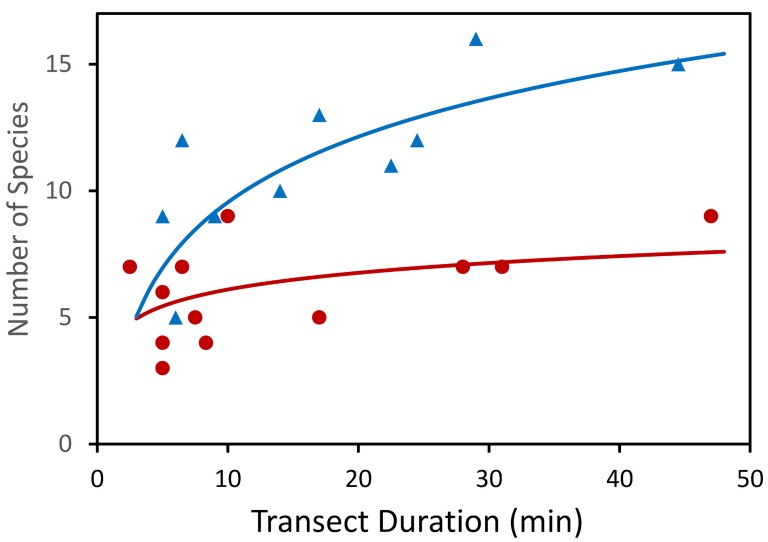

FIGURE 11 | Number of species observed during video transects across hard and soft substrates of the Charlie Gibbs Fracture Zone. Circles dark red – soft sediment. Triangles blue – hard rock. (After Gebruk and Krylova, 2013).

Western Atlantic and Eastern Atlantic continental slopes. For fish and invertebrates, there is some prevalence of Eastern Atlantic species on the MAR (Mironov, 2006; Priede et al., 2013a).

The overall pattern of distribution of bathyal species in the open Atlantic Ocean is complicated. There are no commonly accepted schemes of regionalization of the bathyal in the Atlantic (see Dinter, 2001). Few existing schemes are based on differing approaches and therefore are not comparable. Moreover, approaches to zonation are not always clearly explained. The variety of approaches in marine biogeography was examined and structured by Mironov (2013), who distinguished three main biogeographic frameworks differing in the subject of study and methods. The first approach deals with species ranges - "faunistic" (or "biotic") approach after Mironov. The second is the "biocenotic" approach, it deals with communities (or biocenoces). The third is designated as "landscape" and considers environmental parameters. In the faunistic approach, the main criterion of a biogeographic boundary is a zone of crowding of species range boundaries. In the biocenotic approach, the criterion of a boundary is the difference between local biotas commonly revealed using cluster analysis (based on such parameters as species abundance, biomass and diversity). In the landscape approach, boundaries usually correspond to pronounced gradients of physical-chemical parameters.

Proposed schemes of zonation differ significantly. Based on environmental parameters, Watling et al. (2013) distinguished a single unit "North Atlantic Province" at depths 800-3500 m south of the sub-Polar front in the North Atlantic. Regionalization of the Atlantic bathyal based on the distribution of species is more complicated (Briggs, 1974; Mironov, 1994; Zezina, 1997; Dinter, 2001; Watling et al., 2013).

Mironov (1994) suggested a scheme of faunistic regionalization of sublittoral and bathyal of the ocean based on the distribution of echinoid species and the scheme of Briggs (1974) (**Figure 12A**). A notable feature in the scheme of Mironov is the "meridional asymmetry" in the distribution of species across the open ocean in the east-west direction. Thus, in the Atlantic Ocean, the West Atlantic species are distributed in the open oceanic regions more widely than the East Atlantic species (Mironov, 1989; Mironov, 2006). Some of the West Atlantic species' ranges extend eastward up to the seamounts and islands of the Eastern Atlantic, whereas the East Atlantic ranges extend westward only up to the Mid-Atlantic Ridge. Using data on distribution of cnidaria (corals) Watling and Lapointe (2022) propose division of the North Atlantic lower bathyal biogeographic province into eastern and western units. However, these east-west patterns in the North Atlantic are true only for latitudes north of ~30°N. To the south the ridge in the Atlantic goes deeper with little space for species living at depths shallower than 2000 m (**Figure 1**). South of 30°N the meridional asymmetry between areas to the west and to the east of the MAR in the North Atlantic is more pronounced: the limit of distribution of western and eastern species shifts closer to the African coast and goes by the Cabo Verde Islands (**Figure 12B**). In the scheme of pelagic provinces (Spalding et al., 2012), there is

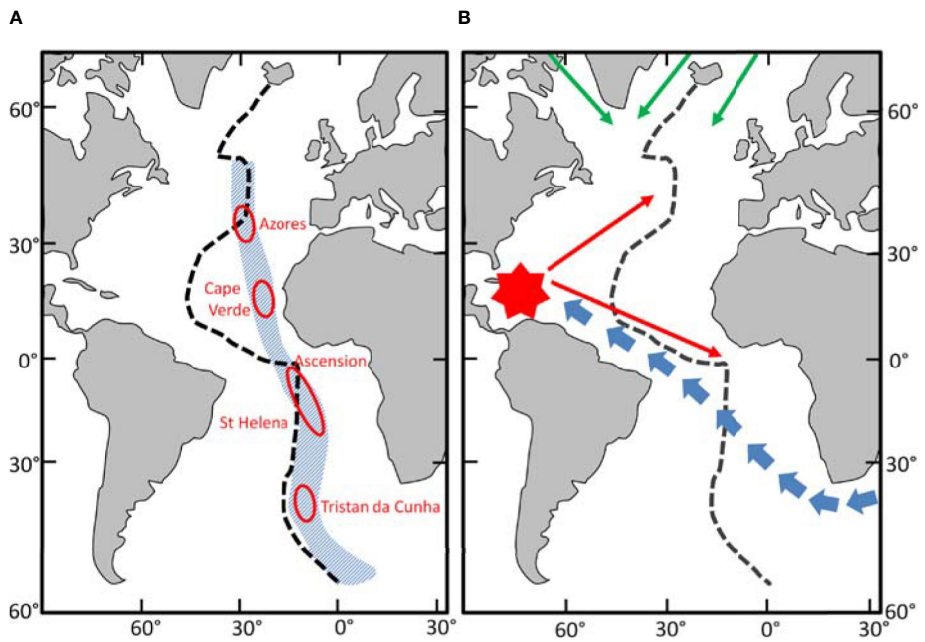

FIGURE 12 | Biogeography of the Atlantic Ocean. Dashed line Mid-Atlantic Ridge. **(A)** The faunistic boundary where East & West Atlantic species meet (Blue shaded area). Red Ovoids – Exotic regions. (After Mironov, 1994). **(B)** Pattern of late Cenozoic (from 10 MYA) colonisation of the Atlantic Ocean bathyal and sublittoral. Blue arrows –from Indo-West Pacific centre of re-distribution. Red symbol – West Atlantic centre of re-distribution. Green arrows – from the North Pacific *via* the Arctic Ocean (After Mironov, 2006).

also asymmetry in the North Atlantic with the border between the North Central Atlantic and Canary Current provinces stretching from Canary Islands to south off Cabo Verde.

According to Mironov and Krylova (2006), the effect of meridional asymmetry is a result of marine fauna distribution from "centres of redistribution". The concept of a "centre of redistribution" is a development of the formerly more widely used Darwinian concept of "centre of origin" of fauna (Croizat et al., 1974). To become a centre of redistribution, an area passes stages of fauna accumulation, speciation, and dispersal. In the post-Tethys history, there were three main centres of redistribution of the sublittoral and bathyal faunas: the Indo-Malayan, the North-West Pacific, and the West Atlantic (Mironov, 2006; Mironov and Krylova, 2006). The higher the species richness in the "centre of redistribution", the further stretch the ranges of species dispersing from this centre into the adjacent ocean. The West Atlantic fauna is only slightly richer than that of the East Atlantic (however, in some taxa the difference is rather strong - see Zezina, 1997), therefore the meridional asymmetry in the North Atlantic is less pronounced than in the Pacific where the West Pacific fauna successfully disperses far into the ocean across the East Pacific barrier.

CONCLUSIONS

Multiple factors influence biomass and biodiversity on the Mid-Atlantic Ridge. Our results show that there is no enhancement of NPP over the ridge region compared with adjacent deeper areas of the Atlantic Ocean. However, on average, POC flux arriving on the ridge is estimated to be 31-65% higher than in adjacent regions and up to three times greater on the summits. Generally, deep-sea standing stocks of macrofauna are strongly correlated with POC flux (Smith et al., 1997; Rex and Etter, 2010) so high biomass can be expected over the MAR. The relationship between biomass and productivity is not simple or the same everywhere. Leduc et al. (2012) found a unimodal relationship with a biodiversity peak at intermediate biomass of deep-ocean nematodes. Elevation of the mid-ocean floor provides niches for a wide variety of demersal fishes culminating in a regional or gamma biodiversity more than 10 times higher than on an equivalent area of abyssal sea floor. Other benthic taxa are probably similarly affected. Substrate heterogeneity on the MAR is increased by the presence of hard rocky patches. Although these represent a small percentage of sea floor area, they are frequent, with an average spacing of <500 m conducive to dispersal of specialist hard substrate fauna hence increasing biodiversity (Zeppilli et al., 2016). Biogeographically the MAR is located at the interface between Eastern and Western Atlantic biota further increasing biodiversity.

Currently much interest in the environment of the MAR is concerned with the potential impacts of deep-sea mining of polymetallic sulphide ore deposits that occur on the axis of the ridge associated with active and extinct hydrothermal vent sites (Washburn et al., 2019). Contract areas for development of mining on the MAR are concentrated within the latitudinal range 12° to 33°N. All the biological information on the MAR analysed in this paper is from the MAR-ECO and ECOMAR projects that sampled between 41 and 60°N. From the general principles reviewed in this study it is possible to predict that, in view of the low productivity of surface waters south of the Azores, low POC flux and greater depth, the biomass is likely to be at least an order of magnitude lower in the mining contract areas than reported for the MAR-ECO areas in Priede et al. (2013a). Inspection of the Ocean Biodiversity Information System (OBIS, 2022) reveals a severe lack of data for the MAR south of 33°N. There may also be different species present compared to the more northerly areas including species new to science in the mining contract areas. To a large extent the ecology of the deep part of the MAR south of the Azores is unknown and there is an urgent need for studies across the ridge in this region at all depths from the summits to the abyssal areas on either side.

DATA AVAILABILITY STATEMENT

Publicly available datasets were analyzed in this study. This data can be found here: Ocean Productivity (2022) http://sites.science.oregonstate.edu/ocean.productivity/ Porteiro et al. (2017) Fishes of the Northern Mid-Atlantic Ridge collected during the MAR-ECO cruise in June-July 2004: an annotated checklist. Arquipelago. Life and Marine Sciences. Supplement 10: iii +125 pp.

AUTHOR CONTRIBUTIONS

IP Led the writing process and analysed demersal fish biodiversity, FM-K analysed net primary production and POC fluxes, TN analysed substrate patch distributions, AG, DJ, and AC contributed review material. All authors participated in writing and editing the text and approved the final, submitted manuscript.

FUNDING

IGP was financially supported by the Atlantic REMP project, funded by the European Union through service contract no.EASME/EMFF/2017/1.3.1.1 - SI2.775068. FMK was supported by NASA, United States (grant numbers NNX14AP62A and 80NSSC20K0017); NSF, United States (grant numbers 1762493 and 1728913); NOAA, United States Integrated Ocean Observing System (grant numbers NA19NOS0120199 and NA16NOS0120018), DJ received support from NERC through National Capability funding to NOC as part of the Climate Linked Atlantic Section Science (CLASS) programme, grant number NE/R015953/1. DJ received funding from UK Natural Environment Research Council through the Seabed Mining And Resilience To EXperimental impact (SMARTEX) project (Grant Reference NE/T003537/1). AC received support from the Operational Program AZORES 2020, through the Fund 01-0145-FEDER-000140 "MarAZ

Researchers: Consolidate a body of researchers in Marine Sciences in the Azores" of the European Union. AC also acknowledges funds through the FCT – Foundation for Science and Technology, I.P., under the project OKEANOS UIDB/05634/2020 and UIDP/05634/2020.

ACKNOWLEDGMENTS

Thanks to Claudia H. S. Alt and James B. Bell for providing the original datasets behind their papers on the ECOMAR area for comparative analysis.

REFERENCES

Alcock, A. W. (1890). Natural History Notes From H. M. Indian Marine Survey Steamer `Investigator,' Commander R. F. Hoskyn, R. N., Commanding. – No. 18. On the Bathybial Fishes of the Arabian Sea, Obtained During the Season 1889-1890. *Ann. Mag. Nat. Hist. (Series 6)* 6 (34), 295–311.

Alcock, A. W. (1891). Class Pisces. In: II.–Natural History Notes From H. M. Indian Marine Survey Steamer `Investigator,' Commander R. F. Hoskyn, R. N., Commanding.–Series II., No. 1. On the Results of Deep-Sea Dredging During the Season 1890-91. *Ann. Mag. Nat. Hist. (Series 6).* 8 (43/44), 119–138.

Alt, C. H. S., Kremenetskaia, A., Gebruk, A. V., Gooday, A. J., and Jones, D. O. B. (2019). Bathyal Benthic Megafauna From the Mid-Atlantic Ridge in the Region of the Charlie-Gibbs Fracture Zone Based on Remotely Operated Vehicle Observations. *Deep-sea. Res. Pt. I.* 145, 1–12. doi: 10.1016/j.dsr.2018.12.006

Alt, C. H. S., Rogacheva, A., Boorman, B., Alan Hughes, J., Billett, D. S. M., Gooday, A. J., et al. (2013). Trawled Megafaunal Invertebrate Assemblages From Bathyal Depth of the Mid-Atlantic Ridge (48°–54°N). *Deep-sea. Res. Pt. II.* 98B, 326–340. doi: 10.1016/j.dsr2.2013.02.003

Ascanius, P. (1772). *Icones Rerum Naturalium, Ou Figures Enluminées D'histoire Naturelle Du Nord*. Pt. 2, 8 (Copenhagen), pp., Pls. 11–20.

Barbosa du Bocage, J. V., and de Brito Capello, F. (1864). Sur Quelques Espèces Inédites De Squalidae De La Tribu Acanthiana, Gray, Qui Fréquentent Les Côtes Du Portugal. *Proc. Zool. Soc. Lond.* 1864, 260–263.

Barnard, K. H. (1923). Diagnoses of New Species of Marine Fishes From South African Waters. *Ann. S. Afr. Mus.* 13, 439–445.

Beebe, W. (1933). Deep-Sea Isospondylous Fishes. Two New Genera and Four New Species. *Zoologica* 13 (8), 159–167.

Behrenfeld, M. J., and Falkowski, P. G. (1997). Photosynthetic Rates Derived From Satellite-Based Chlorophyll Concentration. *Limnol. Oceanogr.* 42, I–20. doi: 10.4319/lo.1997.42.1.0001

Bell, J. B., Alt, C. H. S., and Jones, D. O. B. (2016). Benthic Megafauna on Steep Slopes at the Northern Mid-Atlantic Ridge. *Mar. Ecol.* 37, 1290–1302. doi: 10.1111/maec.12319

Bell, J. B., Jones, D. O. B., and Alt, C. H. S. (2013). Lebensspuren of the Bathyal Mid-Atlantic Ridge. *Deep-Sea. Res. Pt. II.* 98B, 341–351. doi: 10.1016/j.dsr2.2012.09.004

Bergstad, O. A., Falkenhaug, T., Astthorsson, O. S., Byrkjedal, I., Gebruk, A. V., Piatkowski, U., et al. (2008a). Towards Improved Understanding of the Diversity and Abundance Patterns of the Mid-Ocean Ridge Macro- and Megafauna. *Deep-Sea. Res.Pt.II* 55, 1–5. doi: 10.1016/j.dsr2.2007.10.001

Bergstad, O. A., Menezes, G., and Høines, Å. S. (2008b). Demersal Fish on a Mid-Ocean Ridge: Distribution Patterns and Structuring Factors. *Deep-Sea. Res.Pt.II* 55, 185–202. doi: 10.1016/j.dsr2.2007.09.005

Bigelow, H. B., and Schroeder, W. C. (1950). New and Little Known Cartilaginous Fishes From the Atlantic. *Bull. Mus. Comp. Zool.* 103 (7), 385–408.

Billett, D. S. M., Jones, D. O. B., and Weaver, P. P. E. (2019). "Improving Environmental Management Practices in Deep-Sea Mining," in *Environmental Issues of Deep-Sea*. Ed. R. Sharma (Switzerland AG: Springer Nature), pp 403–pp 446. doi: 10.1007/978-3-030-12696-4_15

Bloch, M. E. (1788). Ueber Zwey Merkwürdige Fischarten. *Abhandlungen Der Böhmischen Gesellschaft der Wissenschaften*, 3, 278–282.

Bloch, M. E., and Schneider, J. G. (1801). *M. E. Blochii, Systema Ichthyologiae Iconibus Cx Ilustratum. Post Obitum Auctoris Opus Inchoatum Absolvit, Correxit, Interpolavit Jo. Gottlob Schneider, Saxo. Berolini. Sumtibus Auctoris Impressum Et Bibliopolio Sanderiano Commissum*. i–lx + 1-584, Pls. 1-110.

Bonnaterre, J. P. (1788). *Tableau Encyclopédique Et Methodique Des Trois Règnes De La Nature* (Paris: Ichthyologie. Panckoucke), i–lvi + 1-215, Pls. A-B + 1-100.

Briggs, J. C. (1974). *Marine Zoogeography* (New York: McGraw Hill Book Co), 475 p.

Brünnich, M. T. (1768). *Ichthyologia Massiliensis, Sistens Piscium Descriptiones Eorumque Apud Incolas Nomina. Accedunt Spolia Maris Adriatici. Hafniae Et Lipsiae. Ichthyologia Massiliensis, Sistens Piscium Descriptiones Eorumque Apud Incolas Nomina.* I-Xvi + 1-110.

Byrkjedal, I., Poulsen, J. Y., and Galbraith, J. (2011). *Leptoderma Macrophthalmum* N.Sp., a New Species of Smooth-Head (Otocephala: Alepocephalidae) From the Mid Atlantic Ridge. *Zootaxa* 2876, 49–56.

Chernova, N. V. (2001). A Review of the Genus *Psednos* (Pisces, Liparidae) With Description of Ten New Species From the North Atlantic and Southwestern Indian Ocean. *Bull. Mus. Comp. Zool.* 155 (10), 477–507.

Chernova, N. V., and Møller, P. R. (2008). A New Snailfish, *Paraliparis Nigellus* Sp. Nov. (Scorpaeniformes, Liparidae), From the Northern Mid-Atlantic Ridge – With Notes on Occurrence of Psednos in the Area. *Mar. Biol. Res.* 4, 368–375.

Collett, R. (1889). Diagnoses De Poissons Nouveaux Provenant Des Campagnes De "L'Hirondelle." III.– Description D'une Espèce Nouvelle Du Genre *Hoplostethus*. *Bull. Soc Zool. Fr.* 14, 306.

Collett, R. (1896). *Poissons Provenant Des Campagnes Du Yacht "L'Hirondelle" (1885-1888). Résultats Des Campagnes Scientifiques Accomplies Sur Son Yacht Par Albert I, Prince Souverain De Monaco. Résultats Des Campagnes Scientifiques Du Prince De Monaco. Fasc*. 10: i–viii + 1-198, Pls. 1-6.

Collett, R. (1904). Diagnoses of Four Hitherto Undescribed Fishes From the Depths South of the Faroe Islands. *Forh. Vidensk.-Selsk. Kristiania.* 9, 1–7.

Conte, M. H., Weber, J. C., and Ralph, N. (1998). Episodic Particle flux in the Deep Sargasso Sea:an Organic Geochemical Assessment. *Deep-Sea. Res. I.* 45, 1819–1841. doi: 10.1016/S0967-0637(98)00046-6

Craig, J., Jamieson, A. J., Bagley, P. M., and Priede, I. G. (2011). Naturally Occurring Bioluminescence on the Deep-Sea Floor. *J. Mar. Syst.* 88 (4), 563–567. doi: 10.1016/j.jmarsys.2011.07.006

Croizat, L., Nelson, G., and Rosen, D. E. (1974). Centers of Origin and Related Concepts. *Syst. Zool.* 23, 265–287. doi: 10.2307/2412139

Dale, A. C., and Inall, M. E. (2015). Tidal Mixing Processes Amid Small-Scale, Deep-Ocean Topography. *Geophys. Res. Lett.* 42, 484–491. doi: 10.1002/2014GL062755

Danovaro, R., Snelgrove, P. V. R., and Tyler, P. (2014). Challenging the Paradigms of Deep-Sea Ecology. *Trends Ecol. Evol.* 29, 464–475. doi: 10.1016/j.tree.2014.06.002

de Brito Capello, F. (1868). Descripção De Dois Peixes Novos Provenientes Dos Mares De Portugal. *Jornal do Sciências Mathemáticas Phys. e Naturaes Lisboa* 1 (4), 314–317, Pl. 5.

De Filippi, F., and Verany, J. B. (1857). Sopra Alcuni Pesci Nuovi O Poco Noti Del Mediterraneo. *Memorie Accad. Sci. Torino (Ser. 2)* 18, 187–199.

Deuser, W. G., Muller-Karger, F. E., Evans, R. H., Brown, O. B., Esaias, W. E., and Feldman, G. C. (1990). Surface-Ocean Color and Deep-Ocean Carbon Flux: How Close a Connection? *Deep-Sea. Res.* 37, 1331–1343. doi: 10.1016/0198-0149(90)90046-X

Dinter, W. P. (2001). *Biogeography of the OSPAR Maritime Area* (Bonn: Federal Agency for Nature Conservation), 167 p.

Dullo, W., Flogell, S., and Ruggerberg, A. (2008). Cold-Water Coral Growth in Relation to the Hydrography of the Celtic and Nordic European Continental Margin. *Mar. Ecol. Prog. Ser.* 371, 165–176. doi: 10.3354/meps07623

Felley, J. D., Vecchione, M., and Wilson, R. R. (2008). Small-Scale Distribution of Deep-Sea Demersal Nekton and Other Megafauna in the Charlie-Gibbs Fracture Zone of the Mid-Atlantic Ridge. *Deep-Sea. Res.Pt.II* 55, 153–160. doi: 10.1016/j.dsr2.2007.09.021

Fock, H., Matthiessen, B., Zidowitz, H., and von Westernhagen, H. (2002). Diel and Habitat- Dependent Resource Utilisation by Deep Sea Fishes at the Great Meteor Seamount: Niche Overlap and Support for the Sound Scattering Layer Interception Hypothesis. *Mar. Ecol.-Prog. Ser.* 244, 219–233. doi: 10.3354/meps244219

Forster, G. R. (1967). A New Deep-Sea Ray From the Bay of Biscay. *J. Mar. Biol. Assoc. U.K.* 47 (2), 281–286.

Froese, R., and Pauly, D. (Eds.) (2021). *FishBase* (World Wide Web electronic publication). Available at: www.fishbase.org. version (08/2021).

Gage, J. D., and Tyler, P. (1991). *Deep-Sea Biology: A Natural History of Organisms at the Deep-Sea Floor* (Cambridge, England: Cambridge University Press).

Garman, S. (1906). New Plagiostomia. *Bull. Mus. Comp. Zool.* 46 (11), 203–208.

Garrick, J. A. F. (1961). Studies on New Zealand Elasmobranchii. Part XIII–A New Species of Raja From 1,300 Fathoms. *Trans. R. Soc New Z.* 88 (4), 743–748.

Gebruk, A. V. (2008). Holothurians (Holothuroidea, Echinodermata) of the Northern Mid-Atlantic Ridge Collected by the G.O.Sars MAR-ECO Expedition With Descriptions of Four New Species. *Mar. Biol. Res.* 4, 48–60. doi: 10.1080/17451000701842898

Gebruk, A., Budaeva, N. E., and King, N. (2010). Bathyal Benthic Fauna of the Mid-Atlantic Ridge Between the Azores and the Reykjanes Ridge. *J. Mar. Biol. Assoc. UK.* 90, 1–14. doi: 10.1017/S0025315409991111

Gebruk, A. V., and Krylova, E. M. (2013). Megafauna of the Charlie–Gibbs Fracture Zone (Northern Mid-Atlantic Ridge) Based on Video Observations. *J. Mar. Biol. Assoc. UK.* 93 (5), 1143–1150. doi: 10.1017/S0025315412001890

Gebruk, A. V., Priede, I. G., Fenchel, T., and Uiblein, F. (2013). Benthos of the Sub-Polar Front Area on the Mid- Atlantic Ridge: Results of the ECOMAR Project. *Mar. Biol. Res.* 9, 443–446. doi: 10.1080/17451000.2012.749999

Genin, A. (2004). Bio-Physical Coupling in the Formation of Zooplankton and Fish Aggregations Over Abrupt Topographies. *J. Mar. Syst.* 50, 3– 20. doi: 10.1016/j.jmarsys.2003.10.008

Genin, A., Greene, C., Haury, L., Wiebe, P., Gal, G., Kaartvedt, S., et al. (1994). Zooplankton Patch Dynamics: Daily Gap Formation Over Abrupt Topography. *Deep-Sea. Res. Pt. I.* 41, 941–951. doi: 10.1016/0967-0637(94)90085-X

Giglioli, E. H. (1880). On *Haloporphyrus Lepidion* (Risso). *Nat. (London)* 21 (531), 202.

Giglioli, E. H. (1893). Di Una Nuova Specie Di Macruride Appartenente Alla Fauna Abissale Del Mediterraneo. *Zool. Anz.* 16 (428), 343–345.

Gilbert, C. H. (1890). A Preliminary Report on the Fishes Collected by the Steamer Albatross on the Pacific Coast of North America During the Year 1889, With Descriptions of Twelve New Genera and Ninety-Two New Species. *Proc. U. S. Natl. Mus.* 13 (797), 49–126.

Gilbert, C. H. (1891). Descriptions of Apodal Fishes From the Tropical Pacific. In: Scientific Results of Explorations by the U. S. Fish Commission Steamer Albatross. *Proc. U. S. Natl. Mus.* 14 (856), 347–352.

Gilbert, C. H., and Hubbs, C. L. (1916). Report on the Japanese Macrouroid Fishes Collected by the United States Fisheries Steamer "Albatross" in 1906, With a Synopsis of the Genera. *Proc. U. S. Natl. Mus* 51 (2149), 135–214.

Gilchrist, J. D. F. (1922). Deep-Sea Fishes Procured by the S.S. "Pickle" (Part I). *Report Fisheries and Marine Biological Survey, Union of South Africa*, 2. 41–79.

Gill, T. N. (1883). Diagnosis of New Genera and Species of Deep-Sea Fish-Like Vertebrates. *Proc. U. S. Natl. Mus.* 6 (380), 253–260.

Gill, T. N. (1884). Three New Families of Fishes Added to the Deep-Sea Fauna in a Year. *Am. Nat.* 18 (4), 433.

Goode, G. B., and Bean, T. H. (1883). Reports on the Results of Dredging Under the Supervision of Alexander Agassiz, on the East Coast of the United States, During the Summer of 1880, by the U. S. Coast Survey Steamer "Blake," Commander J. R. Bartlett, U. S. N., Commanding. *Bull. Mus. Comp. Zool.* 10 (5), 183–226.

Goode, G. B., and Bean, T. H. (1885). Descriptions of New Fishes Obtained by the United States Fish Commission Mainly From Deep Water Off the Atlantic and Gulf Coasts. *Proc. U. S. Natl. Mus.* 8 (543), 589–605.

Goode, G. B., and Bean, T. H. (1886). Reports on the Results of Dredging ... In the Gulf of Mexico (1877-78) and in the Caribbean Se-80), by the U.S. Coast Survey Steamer "Blake," ... XXVIII.–Description of Thirteen Species and Two Genera of Fishes From the "Blake" Collection. *Bull. Mus. Comp. Zool.* 12 (5), 153–170.

Goode, G. B., and Bean, T. H. (1896). Oceanic Ichthyology, a Treatise on the Deep-Sea and Pelagic Fishes of the World, Based Chiefly Upon the Collections Made by the Steamers Blake, Albatross, and Fish Hawk in the Northwestern Atlantic, With an Atlas Containing 417 Figures. *Special Bulletin U. S. National Museum* No. 2: Text: I-Xxxv + 1-26 + 1-553, Atlas: I-Xxiii, 1-26, 123 Pls.

Gunnerus, J. E. (1765). Efterretning Om Berglaxen, En Rar Norsk Fisk, Som Kunde Kaldes: *Coryphaenoides Rupestris. Der Trondhiemske Selskabs Skrifter*, 3, 50–58.

Günther, A. (1862). *Catalogue of the Fishes in the British Museum. Catalogue of the Acanthopterygii, Pharyngognathi and Anacanthini in the Collection of the British Museum* v. 4 (London: British Museum), i–xxi + 1-534.

Günther, A. (1877). Preliminary Notes on New Fishes Collected in Japan During the Expedition of H. M. S. `Challenger.' *Ann. Mag. Nat. Hist. (Series 4)* 20 (119), 433–446.

Günther, A. (1878). Preliminary Notices of Deep-Sea Fishes Collected During the Voyage of H. M. S. `Challenger'. *Ann. Mag. Nat. Hist. (Series 5)* 2, 17–28.

Günther, A. (1887). Report on the Deep-Sea Fishes Collected by H. M. S. Challenger During the Years 1873-76. *Report on the Scientific Results of the Voyage of Voyage H. M. S. Challenger* 22 (pt 57), i–lxv + 1-268, Pls. 1-66.

Haedrich, R. L., and Merrett, N. R. (1988). Summary Atlas of Deep-Living Fishes in the North Atlantic. *J. Nat. Hist.* 22, 1325–1362. doi: 10.1080/00222938800770811

Hardy, G. S., and Stehmann, M. F. W. (1990). A New Deep-Water Ghost Shark, *Hydrolagus pallidus* N. Sp. (Holocephali, Chimaeridae), From the Eastern North Atlantic, and Redescription of *Hydrolagus Affinis* (De Brito Capello, 1867). *Archiv für Fischereiwissenschaft* 40 (3), 229–248.

Hector, J. (1875). Descriptions of Five New Species of Fishes Obtained in the New-Zealand Seas by H. M. S -"Challenger" Expedition, July 1874. *Ann. Mag. Nat. Hist. (Series 4)* 15 (85), 78–82.

Holt, E. W. L., and Byrne, L. W. (1908). New Deep-Sea Fishes From the South-West Coast of Ireland. *Ann. Mag. Nat. Hist. (Series* 8) 1 (1), 86–95.

ICES. (2020). ICES/NAFO Joint Working Group on Deep-Water Ecology (WGDEC). *ICES. Sci. Rep.* 2:62, 171. doi: 10.17895/ices.pub.6095

Johnson, J. Y. (1862). Descriptions of Some New Genera and Species of Fishes Obtained at Madeira. *Proc. Zool. Soc. Lond.* 1862 (pt 2), 167–180.

Jones, D. O. B., Alt, C. H. S., Priede, I. G., Reid, W. D. K., Wigham, B. D., Billett, D. S. M., et al. (2013). Deep-Sea Surface-Dwelling Enteropneusts From the Mid-Atlantic Ridge: Their Ecology, Distribution and Mode of Life. *Deep-Sea. Res.Pt.II* 98B, 374–387. doi: 10.1016/j.dsr2.2013.05.009

Karrer, C. (1972). *Die Gattung Harriotta Goode and Bean, 1895(Chrondrichthyes, Chimaeriformes, Rhinochimaeridae). Mit Beschreibung Einer Neuen Art Aus Dem Nordatlantik* v. 48 (Mitteilungen aus dem Zoologischen Museum in Berlin), 203–221.

King, N., Bagley, P. M., and Priede, I. G. (2006). Depth Zonation and Latitudinal Distribution of Deep Sea Scavenging Demersal Fishes of the Mid-Atlantic Ridge, 42°-53°N. *Marine. Ecol. Prog. Ser.* 319, 263–274. doi: 10.3354/MEPS319263

Koefoed, E. (1927). Fishes From the Sea-Bottom. Scientific Results of the Michael Sars North Atlantic Deep-Sea Expedition 1910 4(1),1–148.

Köhler, R. (1896). *Résultats Scientifiques De La Campagne Du "Caudan" Dans Le Golfe De Gascogne – Aout-Septembre*. 1895 – *Poissons. Ann. Univ. Lyon* 26,475–526.

Krefft, G. (1980). A New Species of Holtbyrnia Parr (Searsiidae, Salmoniformes) From the Northern Atlantic Ocean. *Archiv für Fischereiwissenschaft* 31 (2), 53–62.

Krøyer, H. N. (1845). Preliminary Report. Overs. *Kongel. Danske Vidensk. Selsk. Forh. Medlemmers Arbeider (Kjøbenhavn)*, 1844(8), 139–141.

Lacepède, B. G. E. (1801). *Histoire Naturelle Des Poissons* v. 3 (Plassan, Paris), i–lxvi + 1-558, Pls. 1-34.

Lampitt, R. S., and Antia, A. N. (1997). Particle Flux in Deep Seas: Regional Characteristics and Temporal Variability. *Deep-Sea. Res. Pt. I.* 44, 1377–1403. doi: 10.1016/S0967-0637(97)00020-4

Leduc, D., Rowden, A. A., Bowden, D. A., Probert, P. K., Pilditch, C. A., and Nodder, S. D. (2012). Unimodal Relationship Between Biomass and Species Richness of Deep-Sea Nematodes: Implications for the Link Between Productivity and Diversity. *Mar. Ecol.-Prog. Ser.* 454, 53. doi: 10.3354/meps09609

Leitner, A. B., Neuheimer, A. B., and Drazen, J. C. (2020). Evidence for Long-Term Seamount-Induced Chlorophyll Enhancements. *Sci. Rep.* 10, 12729. doi: 10.1038/s41598-020-69564-0

Linley, T. D., Alt, C. H. S., Jones, D. O. B., and Priede, I. G. (2013). Bathyal Demersal Fishes of the Charlie-Gibbs Fracture Zone Region (49°–54°N) of the Mid-Atlantic Ridge: III. Results From Remotely Operated Vehicle (ROV) Video Transects. *Deep-Sea. Res.Pt.II* 98B, 407–411. doi: 10.1016/j.dsr2.2013.08.013

Linnaeus, C. (1758). *Systema Naturae, Ed. X. (Systema Naturae Per Regna Tria Naturae, Secundum Classes, Ordines, Genera, Species, Cum Characteribus, Differentiis, Synonymis, Locis. Tomus I. Editio Decima, Reformata.) Holmiae*, v. 1. i–ii + 1-824.

Longhurst, A. (1998). *Ecological Geography of the Sea* (San Diego CA: Academic Press).

Lorenzoni, L., Benitez-Nelson, C. R., Thunell, R. C., Hollander, D., Varela, R., Astor, Y., et al. (2012). Potential Role of Event-Driven Sediment Transport on Sediment Accumulation in the Cariaco Basin, Venezuela. *Mar. Geol.* 307-310, 105–110. doi: 10.1016/j.margeo.2011.12.009

Lowe, R. T. (1839). A Supplement to a Synopsis of the Fishes of Madeira. *Proc. Zool. Soc. Lond.* 1839 (pt 7), 76–92.

Lütken, C. F. (1898). *The Ichthyological Results. Danish Ingolf Expedition, II. Copenhagen*, 215-254. Pls. 1–Pls. 4.

Macdonald, A. (2021). *Life at High Pressure: In the Deep Sea and Other Environments* (Heidelberg: Springer), 470pp, ISBN: .

Maldonado, M., and Young, C. M. (1999). Effects of the Duration of Larval Life on Postlarval Stages of the Demosponge *Sigmadocia Caerulea*. *J. Exp. Mar. Biol. Ecol.* 232, 9 –21. doi: 10.1016/S0022-0981(98)00076-8

Matsui, T., and Rosenblatt, R. H. (1979). Two New Searsid Fishes of the Genera Maulisia and *Searsia* (Pisces: Salmoniformes). *Bull. Mar. Sci.* 29 (1), 62–78.

Maul, G. E. (1957). Further Additions to the Previously Revised Family Searsidae. *Bol. Mus. Munic. Funcha.* 10, 5–21.

Messié, M., Petrenko, A., Doglioli, A. M., Aldebert, C., Martinez, E., Koenig, G., et al. (2020). The Delayed Island Mass Effect: How Islands can Remotely Trigger Blooms in the Oligotrophic Ocean. *Geophys. Res. Lett.* 47, e2019GL085282. doi: 10.1029/2019GL085282

Metaxas, A., and Saunders, M. (2009). Quantifying the "Bio-" Components in Biophysical Models of Larval Transport in Marine Benthic Invertebrates: Advances and Pitfalls. *Biol. Bull.* 216, 257–272. doi: 10.1086/BBLv216n3p257

Miller, K., and Gunasekera, R. A. (2017). Comparison of Genetic Connectivity in Two Deep Sea Corals to Examine Whether Seamounts are Isolated Islands or Stepping Stones for Dispersal. *Sci. Rep.* 7, 46103. doi: 10.1038/srep46103

Miller, P. I., Read, J. F., and Dale, A. C. (2013). Thermal Front Variability Along the North Atlantic Current Observed Using Satellite Microwave and Infrared Data. *Deep-Sea. Res.Pt.II* 98, 244–256. doi: 10.1016/j.dsr2.2013.08.014

Mironov, A. N. (1989). Meridional Asymmetry and Marginal Effect in Distribution of Sea Urchins in Open Ocean Regions. *Okeanologiya* 29 (5), 845–854.

Mironov, A. N. (1994). *Bottom Faunistic Complexes 0f Oceanic Islands and Seamounts. Transactions of the P.P. Shirshov Institute of Oceanology* Vol. 129 (In Russian: Trudy Instituta Okeanologii), 7–16. English summary.

Mironov, A. N. (2006). Centers of Marine Fauna Redistribution. *Entomol. Rev.* 86 (1), S32–S34. doi: 10.1134/S0013873806100034

Mironov, A. N. (2013). Biotic Complexes of the Arctic Ocean. *Invertebrate. Zool.* 10 (1), 3–48. doi: 10.15298/invertzool.10.1.02

Mironov, A. N. (2014). "The Influence of Redistribution Biota Centers on the Bottom Fauna in the Central Oceanic Regions," in *The World Ocean.Vol. II.Physics, Chemistry and Biology of the Ocean*. Eds. L. I. Lobkovsky and R. I. Nigmatulin (Moscow: Scientific World), 264–280. (In Russian).

Mironov, A. N., and Krylova, E. M. (2006). "Origin of the Fauna of the Meteor Seamounts, North-Eastern Atlantic," in *Biogeography of the North Atlantic Seamounts*. Eds. A. N. Mironov, A. V. Gebruk and A. J. S. Southward (Moscow: KMK Sci. Press), 22–57.

Mironov, A. N., Minin, K. V., and Dilman, A. B. (2015). Abyssal Echinoid and Asteroid Fauna of the North Pacific. *Deep-Sea. Res.Pt.II* 111, 357–375. doi: 10.1016/j.dsr2.2014.08.006

Morris, K., Tyler, P. A., Murton, B., and Rogers, A. D. (2012). Lower Bathyal and Abyssal Distribution of Coral in the Axial Volcanic Ridge of the Mid-Atlantic Ridge at 45°N. *Deep-Sea. Res. Pt. I.* 62, 32–39. doi: 10.1016/j.dsr.2011.11.009

Mortensen, P. B., Buhl-Mortensen, L., Gebruk, A. V., and Krylova, E. M. (2008). Occurrence of Deepwater Corals on the Mid-Atlantic Ridge Based on MAR-ECO Data. *Deep-sea. Res.Pt.II* 55, 142 – 152. doi: 10.1016/j.dsr2.2007.09.018

Muller-Karger, F. E., Richardson, P. L., and McGillicuddy, D. (1995). On the Offshore Dispersal of the Amazon's Plume in the North Atlantic. *Deep-Sea. Res. Pt. I.* 42, 2127–2137. doi: 10.1016/0967-0637(95)00085-2

Muller-Karger, F. E., Varela, R., Thunell, R., Luerssen, R., Hu, C., and Walsh, J. J. (2005). The Importance of Continental Margins in the Global Carbon Cycle, Geophys. *Res. Lett.* 32, L01602. doi: 10.1029/2004GL021346

Müller, R. D., and Roest, W. R. (1992). Fracture Zones in the North Atlantic From Combined Geosat and Seasat Data. *J. Geophys. Res.* 97 (B3), 3337–3350. doi: 10.1029/91JB02605

Niedzielski, T., Høines, Å., Shields, M. A., Linley, T., and Priede, I. G. (2013). A Multi-Scale Investigation Into Sea Floor Topography of the Northern Mid-Atlantic Ridge Based on Geographic Information System Analysis. *Deep-Sea. Res.Pt.II* 98B, 231–243. doi: 10.1016/j.dsr2.2013.10.006

Nybelin, O. (1957). Deep-Sea Bottom Fishes. *Reports of the Swedish Deep-Sea Expedition 1947-1948*, v. 2 (Zool.) (fasc. 3) (art. 20), 247–345, Pls. 1-7.

OBIS. (2022). *Ocean Biodiversity Information System* (Intergovernmental Oceanographic Commission of UNESCO). Available at: www.obis.org (Accessed January 11, 2022).

Ocean Productivity (2022). Available at: http://sites.science.oregonstate.edu/ocean.productivity/ (Accessed January 11, 2022).

Oliveira, A. P., Coutinho, T. P., Cabeçadas, G., Brogueira, M. J., Coca, J., Ramos, M., et al. (2016). Primary Production Enhancement in a Shallow Seamount (Gorringe — Northeast Atlantic). *J. Mar. Syst.* 164, 13–29. doi: 10.1016/j.jmarsys.2016.07.012

Pace, M., Knauer, G., Karl, D., and Martin, J. (1987). Primary Production, New Production and Vertical Flux in the Eastern Pacific Ocean. *Nature* 325, 803–804. doi: 10.1038/325803a0

Parr, A. E. (1928). *Deepsea Fishes of the Order Iniomi From the Waters Around the Bahama and Bermuda Islands. With Annotated Keys to the Sudididae, Myctophidae, Scopelarchidae, Evermannellidae, Omosudidae, Cetomimidae and Rondeletidae of the World. (Scientific Results of the Third Oceanographic Expedition of the "Pawnee" 1927.)* Vol. 3 (Bulletin of the Bingham Oceanographic Collection Yale University), 1–193.

Parr, A. E. (1937). *Concluding Report on Fishes. With Species Index for Articles 1-7 (Fishes of the Third Oceanographic Expedition of the "Pawnee")* Vol. 3 (Bulletin of the Bingham Oceanographic Collection Yale University), 1–79.

Parr, A. E. (1951). Preliminary Revision of the Alepocephalidae, With the Introduction of a New Family, Searsidae. *Am. Mus. Novit.* 1531, 1–21.

Parra, H. E., Pham, C. K., Menezes, G. M., Rosa, A., Tempera, F., and Morato, T. (2017). Predictive Modeling of Deep-Sea Fish Distribution in the Azores. *Deep-Sea. Res. II.* 145, 49–60. doi: 10.1016/j.dsr2.2016.01.004

Perez, J. A. A., Gavazzoni, L., de Souza, L. H. P., Sumida, P. Y. G., and Kitazato, H. (2020). Deep-Sea Habitats and Megafauna on the Slopes of the São Paulo Ridge, SW Atlantic. *Front. Mar. Sci.* 7. doi: 10.3389/fmars.2020.572166

Pollard, R., Sanders, R., Lucas, M., and Statham, P. (2007). The Crozet Natural Iron Bloom and Export Experiment (CROZEX). *Deep-Sea. Res.Pt.II* 54, 1905–1914. doi: 10.1016/j.dsr2.2007.07.023

Porteiro, F. M., Sutton, T. T., Byrkjedal, I., Orlov, A. M., Heino, M., and Menezes G. and Bergstad, O. A. (2017). Fishes of the Northern Mid-Atlantic Ridge Collected During the MAR-ECO Cruise in June-July 2004: An Annotated Checklist. *Arquipelago Life Marine. Sci.* Supplement 10, iii +125.

Priede, I. G., Bergstad, O. A., Miller, P. I., Vecchione, M., Gebruk, A., Falkenhaug, T., et al. (2013a). Does Presence of a Mid Ocean Ridge Enhance Biomass and Biodiversity? *PloS One* 8 (5), e61550. doi: 10.1371/journal.pone.0061550

Priede, I. G., Billett, D. S. M., Brierley, A. S., Hoelzel, A. R., Inall, M., Miller, P. I., et al. (2013b). The Ecosystem of the Mid-Atlantic Ridge at the Sub-Polar Front and Charlie Gibbs Fracture Zone; ECO-MAR Project Strategy and Description of the Sampling Program 2007–2010. *Deep-Sea. Res.Pt.II* 98B, 220–230. doi: 10.1016/j.dsr2.2013.06.012

Priede, I. G., Froese, R., Bailey, D. M., Bergstad, O. A., Collins, M. A., Dyb, J. E., et al. (2006). The Absence of Sharks From Abyssal Regions of the World's Oceans. *Proc. R. Soc B.* 273, 1435–1441. doi: 10.1098/rspb.2005.3461

Priede, I. G., Godbold, J. A., King, N. J., Collins, M. A., Bailey, D. M., and Gordon, J. D. M. (2010). Deep-Sea Demersal Fish Species Richness in the Porcupine Seabight, NE Atlantic Ocean: Global and Regional Patterns. *Mar. Ecol.* 31, 247–260. doi: 10.1111/j.1439-0485.2009.00330.x

Rakka, M., Godinho, A., Orejas, C., and Carreiro-Silva, M. (2021). Embryo and Larval Biology of the Deep-Sea Octocoral *Dentomuricea* Aff. Meteor Under Different Temperature Regimes. *PeerJ* 9, e11604. doi: 10.7717/peerj.11604

Read, J. F., Pollard, R. T., Miller, P. I., and Dale, A. C. (2010). Circulation and Variability of the North Atlantic Current in the Vicinity of the Mid-Atlantic Ridge. *Deep-Sea. Res. Pt. I.* 57, 307–318. doi: 10.1016/j.dsr.2009.11.010

Restreppo, G. A., Wood, W. T., and Phrampus, B. J. (2020). Oceanic Sediment Accumulation Rates Predicted via Machine Learning Algorithm: Towards Sediment Characterization on a Global Scale. *Geo-Mar. Lett.* 40, 755–763. doi: 10.1007/s00367-020-00669-1

Rex, M. A. (1981). Community Structure in the Deep-Sea Benthos. *Annu. Rev. Ecol. Evol. Syst.* 12, 331–353. doi: 10.1146/annurev.es.12.110181.001555

Rex, M. A., and Etter, R. (2010). *Deep-Sea Biodiversity: Pattern and Scale* (Cambridge MA: Harvard University Press), 354.

Riehl, T., Wölfl, A.-C., Augustin, N., Devey, C. W., and Brandt, A. (2020). Discovery of Widely Available Abyssal Rock Patches Reveals Overlooked Habitat Type and Prompts Rethinking Deep-Sea Biodiversity. *Proc. Natl. Acad. Sci. U. S. A* 117 (27), 15450–15459. doi: 10.1073/pnas.1920706117

Risso, A. (1810). *Ichthyologie De Nice, Ou Histoire Naturelle Des Poissons Du Département Des Alpes Maritimes* (Paris: F. Schoell), i–xxxvi + 1-388, Pls. 1-11.

Risso, A. (1840). Observations Sur Quelques Poissons De La Mer De Nice. *Archiv für Naturgeschichte* 6 (pt. 1), 376–393, Pl. 10.

Roule, L. (1916). Notice Préliminaire Sur Quelques Espèces Nouvelles Ou Rares Des Poissons Provenant Des Croisières De S. A. S. Le Prince De Monaco. *Bull. Inst. océanogr. (Monaco)* 320, 1–32.

Rogacheva, A., Gebruk, A., and Alt, C. H. S. (2013). Holothuroidea of the Charlie Gibbs Fracture Zone Area, Northern Mid-Atlantic Ridge. *Mar. Biol. Res.* 9 (5-6), 587–623. doi: 10.1080/17451000.2012.750428

Rowe, G. T., and Menzies, R. J. (1969). Zonation of Large Benthic Invertebrates in the Deep-Sea Off the Carolinas. *Deep-Sea. Res.* 16, 531–537. doi: 10.1016/0011-7471(69)90041-2

Sazonov, Y., and Golovan, G. A. (1976). New Species of Fishes of the Family Searsiidae (Salmoniformes, Alepocephaloidei) From the Eastern Atlantic Ocean. *Tr. Inst. Okeanol. im. P. P. Shirshova Akad. Nauk SSSR* 104, 7–12.

Sazonov, Y., and Shcherbachev, Y. (1982). A Preliminary Review of Grenadiers Related to the Genus *Cetonurus* Günther (Gadiformes, Macrouridae). Description of New Taxa Related to the Genera *Cetonurus* Günther and *Kumba* Marshall. *Voprosy Ikhtiologii* 22 (5), 707–721.

Searle, R. (2013). *Mid-Ocean Ridges* (Cambridge, England: Cambridge University Press). 978-1-107-01752-8.

Shanks, A. L. (2009). Pelagic Larval Duration and Dispersal Distance Revisited. *Biol. Bull.* 216 (3), 373–385. doi: 10.1086/BBLv216n3p373

Smith, C. R., Berelson, W., DeMaster, D. J., Dobbs, F. C., Hammond, D., Hoover, D. J., et al. (1997). Latitudinal Variations in Benthic Processes in the Abyssal Equatorial Pacific: Control by Biogenic Particle Flux. *Deep-Sea. Res.Pt.II* 44, 2295–2317. doi: 10.1016/S0967-0645(97)00022-2

Smith, K., Ruhl, H. A., Bett, B. J., Billett, D. S. M., Lampitt, R. S., and Kaufmann, R. S. (2009). Climate, Carbon Cycling, and Deep-Ocean Ecosystems. *Proc. Natl. Acad. Sci. U.S.A* 106, 19211–19218. doi: 10.1073/pnas.0908322106

Sokolova, M. N. (2000). *Feeding and Trophic Structure of the Deep-Sea Macrobenthos* (Washington D.C: Smithsonian Institution Libraries).

Spalding, M. D., Agostini, V. A., Rice, J., and Grant, S. M. (2012). Pelagic Provinces of the World: A Biogeographic Classification of the World's Surface Pelagic Waters. *Ocean. Coast. Manage.* 60, 19–30. doi: 10.1016/j.ocecoaman.2011.12.016

Springer, S. (1979). A Revision of the Catsharks, Family Scyliorhinidae. *NOAA (National Oceanic and Atmospheric Administration) Technical Report NMFS (National Marine Fisheries Service) Circular*, 422, 1–152.

Stehmann, M. F. W. (1978). *Raja "Bathyphila"*, Eine Doppelart Des Subgenus Rajella: Wiederbeschreibung Von *R. Bathyphila* Holt & Byrne, 1908 Und *Raja Bigelowi* Spec. Nov. (Pisces, Rajiformes, Rajidae). *Archiv für Fischereiwissenschaft* 29 (1/2), 23–58.

Straume, E. O., Gaina, C., Medvedev, S., Hochmuth, K., Gohl, K., Whittaker, J. M., et al. (2019). GlobSed: Updated Total Sediment Thickness in the World's Oceans. *Geochem. Geophys. Geosystems.* 20, 1756–1772. doi: 10.1029/2018GC008115

Sulak, K. J. (1975). Biological Results of the University of Miami Deep-Sea Expeditions. 111. *Talismania Mekistonema*, a New Atlantic Species of the Family Alepocephalidae (Pisces: Salmoniformes). *Bull. Mar. Sci.* 25 (1), 88–93.

Sun, Z., Hamel, J. F., and Mercier, A. (2010). Planulation Periodicity, Settlement Preferences and Growth of Two Deep-Sea Octocorals From the Northwest Atlantic. *Mar. Ecol.-Prog. Ser.* 410, 71–87. doi: 10.3354/meps08637

Svetovidov, A. N. (1936). *Lepidion Schmidti*, Eine Neue Fischart. *Zool. Anz.* 113, 266–269.

Thunell, R. C., Benitez-Nelson, C. R., Varela, R., Astor, Y., and Muller-Karger, F. E. (2007). Particulate Organic Carbon Fluxes Along Upwelling-Dominated Continental Margins: Rates and Mechanisms. *Global Biogeochem. Cycles.* 21, GB1022. doi: 10.1029/2006GB002793

Tilstone, G. H., Miller, P. I., Brewin, R. J. W., and Priede, I. G. (2014). Enhancement of Primary Production in the North Atlantic Outside of the Spring Bloom, Identified by Remote Sensing of Ocean Colour and Temperature. *Remote Sens. Environ.* 148, 77–86. doi: 10.1016/j.rse.2013.04.021

Treberg, J. R., and Speers-Roesch, B. (2016). Does the Physiology of Chondrichthyan Fishes Constrain Their Distribution in the Deep Sea? *J. Exp. Biol.* 219, 615–625. doi: 10.1242/jeb.128108

UNESCO (2009). *Global Open Oceans and Deep-Sea Bed (GOODS)—Biogeographic Classification* (Paris: UNESCO-IOC (IOC Technical Series, 84).

Vaillant, L. L. (1888). *Expéditions Scientifiques Du "Travailleur" Et Du "Talisman" Pendant Les Années 1880, 1881, 1882, 1883 Poissons*. Paris. 1-406, Pls. 1–28.

Valenciennes, A. (1838). "Ichthyologie Des Îles Canaries, Ou Histoire Naturelle Des Poissons Rapportés Par Webb & Berthelot," in *Histoire Naturelle Des Îles Canaries*, vol. 2. Eds. P. B. Webb and S. Berthelot (Paris), 1835–1850.

Van Dover, C. L. (2000). *The Ecology of Deep-Sea Hydrothermal Vents* (Princeton New Jersey USA: Princeton University Press), 424pp.

Vecchione, M., Bergstad, O. A., Byrkjedal, I., Falkenhaug, T., Gebruk, A. V., Godø, O. R., et al. (2010). "Biodiversity Patterns and Processes on the Mid-Atlantic Ridge," in *Life in the World's Oceans: Diversity, Distribution, and Abundance*. Ed. A. D. McIntyre (Oxford: Blackwell), 103–121.

Vic, C., Gula, J., Roullet, G., and Pradillon, F. (2018). Dispersion of Deep-Sea Hydrothermal Vent Effluents and Larvae by Submesoscale and Tidal Currents. *Deep-Sea. Res. Pt. I.* 133, 1–18. doi: 10.1016/j.dsr.2018.01.001

Washburn, T. W., Turner, P. J., Durden, J. M., Jones, D. O. B., Weaver, P., and Van Dover, C. L. (2019). Ecological Risk Assessment for Deep-Sea Mining. *Ocean. Coast. Manag.* 176, 24–39. doi: 10.1016/j.ocecoaman.2019.04.014

Watling, L., Guinotte, J., Clark, M. R., and Smith, C. R. (2013). A Proposed Biogeography of the Deep Ocean Floor. *Prog. Oceanogr.* 111, 91–112. doi: 10.1016/j.pocean.2012.11.003

Watling, L., and Lapointe, A. (2022). Global Biogeography of the Lower Bathyal (700–3000 M) as Determined From the Distributions of Cnidarian Anthozoans. *Deep-Sea. Res. Part I.* 181, 103703. doi: 10.1016/j.dsr.2022.103703

Wenneck, T., Falkenhaug, T., and Bergstad, O. A. (2008). Strategies, Methods, and Technologies Adopted on the R.V. G.O. Sars MAR-ECO Expedition to the Mid-Atlantic Ridge in 2004. *Deep-Sea. Res. II.* 55, 6–28. doi: 10.1016/j.dsr2.2007.09.017

White, M., Bashmachnikov, I., Aristegui, J., and Martins, A. M. (2008). "Physical Processes and Seamount Productivity," in *Seamounts: Ecology, Fisheries and Conservation*. Ed. T. J. Pitcher, T. Morato, P. J. B. Hart, M. R. Clark, N. Haggan and R. S. Santos (Oxford: Blackwell), 65–84. doi: 10.1002/9780470691953.ch4

Young, C. M. (2003). "Reproduction, Development and Life-History Traits," in *Ecosystems of the Deep Oceans, Vol. 28. Of Ecosystems of the World*. Ed. P. A. Tyler (Amsterdam: Elsevier), 381–426.

Zeppilli, D., Pusceddu, A., Trincardi, F., and Danovaro, R. (2016). Seafloor Heterogeneity Influences the Biodiversity–Ecosystem Functioning Relationships in the Deep Sea. *Sci. Rep.* 6, 26352. doi: 10.1038/srep26352

Zezina, O. N. (1997). Biogeography of the Bathyal Zone. *Adv. Mar. Biol.* 32, 390–428. doi: 10.1016/S0065-2881(08)60020-6

Conflict of Interest: The authors declare that the research was conducted in the absence of any commercial or financial relationships that could be construed as a potential conflict of interest.

frontiers | Frontiers in Marine Science

REVIEW
published: 13 May 2022
doi: 10.3389/fmars.2022.866422

Integrating Multidisciplinary Observations in Vent Environments (IMOVE): Decadal Progress in Deep-Sea Observatories at Hydrothermal Vents

Marjolaine Matabos[1†], Thibaut Barreyre[2*†], S. Kim Juniper[3], Mathilde Cannat[4], Deborah Kelley[5], Joan M. Alfaro-Lucas[6], Valérie Chavagnac[7], Ana Colaço[8], Javier Escartin[9], Elva Escobar[10], Daniel Fornari[11], Jörg Hasenclever[12], Julie A. Huber[13], Agathe Laës-Huon[1], Nadine Lantéri[1], Lisa Ann Levin[14], Steve Mihaly[3], Eric Mittelstaedt[15], Florence Pradillon[1], Pierre-Marie Sarradin[1], Jozée Sarrazin[1], Beatrice Tomasi[16,17], Ramasamy Venkatesan[18] and Clément Vic[19] on behalf of IMOVE InterRidge working group*

[1] Ifremer, Département REM, Plouzané, France, [2] Department of Earth Science and Centre for Deep Sea Research, University of Bergen, Bergen, Norway, [3] Ocean Networks Canada, University of Victoria, Victoria, BC, Canada, [4] Equipe de Géosciences Marines, Université de Paris, Institut de Physique du Globe de Paris, UMR CNRS, Paris, France, [5] School of Oceanography, University of Washington, Seattle, WA, United States, [6] Department of Marine Zoology, Senckenberg Research Institute and Natural History Museum, Frankfurt am Main, Germany, [7] Géosciences Environnement Toulouse CNRS UMR IRD/UPS/CNES, Université de Toulouse, Toulouse, France, [8] Instituto de Investigação em Ciências do Mar - Okeanos, Universidade dos Açores, Horta, Portugal, [9] Laboratoire de Géologie, CNRS, UMR, École Normale Supérieure, PSL University, Paris, France, [10] Universidad Nacional Autónoma de México, Instituto de Ciencias del Mar y Limnología, Ciudad Universitaria Mexico City, Mexico, [11] Geology and Geophysics Department, Woods Hole Oceanographic Institution, Woods Hole, MA, United States, [12] Institute of Geophysics, Center for Earth System Research and Sustainability, Hamburg University, Hamburg, Germany, [13] Marine Chemistry and Geochemistry, Woods Hole Oceanographic Institution, Woods Hole, MA, United States, [14] Center for Marine Biodiversity and Conservation, Scripps Institution of Oceanography, UC San Diego, La Jolla, CA, United States, [15] Department of Earth and Spatial Sciences, University of Idaho, Moscow, ID, United States, [16] L@BISEN, ISEN Yncréa Ouest, Brest, France, [17] Norwegian Research Center, NORCE, Bergen, Norway, [18] Ocean Observation Systems, National Institute of Ocean Technology, Chennai, India, [19] Univ. Brest, CNRS, IRD, Ifremer, Laboratoire d'Océanographie Physique et Spatiale, Plouzané, France

OPEN ACCESS

Edited by:
Jacopo Aguzzi,
Spanish National Research Council (CSIC), Spain

Reviewed by:
Karthik Anantharaman,
University of Wisconsin-Madison, United States
Daniel Mihai Toma,
Universitat Politecnica de Catalunya, Spain

***Correspondence:**
Marjolaine Matabos
marjolaine.matabos@ifremer.fr
Thibaut Barreyre
thibaut.barreyre@uib.no

[†]These authors have contributed equally to this work and share first authorship

Specialty section:
This article was submitted to Deep-Sea Environments and Ecology, a section of the journal Frontiers in Marine Science

Received: 31 January 2022
Accepted: 11 April 2022
Published: 13 May 2022

Citation:
Matabos M, Barreyre T, Juniper SK, Cannat M, Kelley D, Alfaro-Lucas JM, Chavagnac V, Colaço A, Escartin J, Escobar E, Fornari D, Hasenclever J, Huber JA, Laës-Huon A, Lantéri N, Levin LA, Mihaly S, Mittelstaedt E, Pradillon F, Sarradin P-M, Sarrazin J, Tomasi B, Venkatesan R and Vic C (2022) Integrating Multidisciplinary Observations in Vent Environments (IMOVE): Decadal Progress in Deep-Sea Observatories at Hydrothermal Vents. Front. Mar. Sci. 9:866422. doi: 10.3389/fmars.2022.866422

The unique ecosystems and biodiversity associated with mid-ocean ridge (MOR) hydrothermal vent systems contrast sharply with surrounding deep-sea habitats, however both may be increasingly threatened by anthropogenic activity (e.g., mining activities at massive sulphide deposits). Climate change can alter the deep-sea through increased bottom temperatures, loss of oxygen, and modifications to deep water circulation. Despite the potential of these profound impacts, the mechanisms enabling these systems and their ecosystems to persist, function and respond to oceanic, crustal, and anthropogenic forces remain poorly understood. This is due primarily to technological challenges and difficulties in accessing, observing and monitoring the deep-sea. In this context, the development of deep-sea observatories in the 2000s focused on understanding the coupling between sub-surface flow and oceanic and crustal conditions, and how they influence biological processes. Deep-sea observatories provide long-term, multidisciplinary time-series data comprising repeated observations

and sampling at temporal resolutions from seconds to decades, through a combination of cabled, wireless, remotely controlled, and autonomous measurement systems. The three existing vent observatories are located on the Juan de Fuca and Mid-Atlantic Ridges (Ocean Observing Initiative, Ocean Networks Canada and the European Multidisciplinary Seafloor and water column Observatory). These observatories promote stewardship by defining effective environmental monitoring including characterizing biological and environmental baseline states, discriminating changes from natural variations versus those from anthropogenic activities, and assessing degradation, resilience and recovery after disturbance. This highlights the potential of observatories as valuable tools for environmental impact assessment (EIA) in the context of climate change and other anthropogenic activities, primarily ocean mining. This paper provides a synthesis on scientific advancements enabled by the three observatories this last decade, and recommendations to support future studies through international collaboration and coordination. The proposed recommendations include: i) establishing common global scientific questions and identification of Essential Ocean Variables (EOVs) specific to MORs, ii) guidance towards the effective use of observatories to support and inform policies that can impact society, iii) strategies for observatory infrastructure development that will help standardize sensors, data formats and capabilities, and iv) future technology needs and common sampling approaches to answer today's most urgent and timely questions.

Keywords: essential ocean variables (EOVs), essential biological variables (EBVs), mid-ocean ridge (MOR), sensors, seabed platforms, vent fluid dynamics, vent communities dynamics

INTRODUCTION

Over the past ~70 years, since the revolution in Earth and Ocean sciences precipitated by the confirmation of seafloor spreading and plate tectonics, the technological challenges, limited access, and high costs associated with deep-sea studies led to significant gaps in understanding spatial and temporal changes associated with chemical, biological and physical phenomena in the deep ocean. This has been especially true of seasonal processes that occur over a wide range of spatial and temporal scales throughout the global oceans (e.g., Glover et al., 2010). To date, deep-sea time-series investigations have documented notable environmental and biological variations from seconds to decades in a wide range of ecosystems from bathyal and abyssal zones (e.g., Hartman et al., 2012; Barreyre et al., 2014b; Cuvelier et al., 2014b; Doya et al., 2014; Matabos et al., 2014; Sarrazin et al., 2014; Cuvelier et al., 2017; Lelièvre et al., 2017; Taylor et al., 2017; Chavagnac et al., 2018a; Taylor et al., 2018; Durden et al., 2020). Increasing societal interest in deep-ocean resources has been accompanied by a growing recognition of the urgent need for a comprehensive assessment of the status and health of deep-sea ecosystems (Rogers et al., 2015; Franke et al., 2020). Robust environmental and biological baselines as well as understanding of their natural dynamics are key to assessing and predicting the impacts and responses of interconnected ecosystems to large-scale disturbances caused by natural processes (e.g., earthquakes and volcanic eruptions), and anthropogenic activities (e.g., ocean acidification and warming and their climate and environmental impacts) (e.g., Ramirez-Llodra et al., 2010; Danovaro et al., 2017b; Danovaro et al., 2020). Multi-decadal and multidisciplinary time-series studies at variable spatial scales are essential for discriminating between human-induced impacts, and long-term natural periodic and episodic variability, and inform our assessment of the environmental drivers and their biological consequences.

The need for long-term, time-series measurements of key ocean variables with a specific focus on the deep-sea (Thiel et al., 1994), has been identified as a critical topic since the 1990s (National Research Council, 2000), and has led to the development of seafloor-water column observatories. The Committee on Seafloor Observatories, bringing together scientists from all fields of Ocean and Earth sciences, gathered in 2000 to provide a vision for a global Seafloor Observatory Network including the risks and benefits of ocean observation platforms (National Research Council, 2000). They defined "seafloor observatories" as an autonomous "system of instruments, sensors, and command modules connected either acoustically or *via* a seafloor junction box to a surface buoy or a fiber optic cable to land". This comprehensive report highlighted scientific questions that observatories could specifically address. Observatories were foreseen as requiring a major investment of resources over many decades. In the following two decades, a number of observatories have developed around the world, with instruments distributed from seafloor to the water column (e.g., Kelley et al., 2014; Smith et al., 2018; Dañobeitia et al., 2020). More recently an observatory was defined as an "integrated

observing, monitoring, and experimenting infrastructure which aims to collect high-resolution data in a restricted geographical region" (Crise et al., 2018). One of the first areas of interest for observatories has been highly-dynamic mid-ocean ridges and back-arc spreading centres, where seafloor volcanism and tectonic activity predominate.

Mid-Ocean Ridge (MOR) and back-arc spreading systems host unique ecosystems and biodiversity (Tunnicliffe, 1991; Ramirez-Llodra et al., 2010; Mullineaux et al., 2018; Chapman et al., 2019). Hydrothermal circulation within these environments is responsible for significant transfer of heat and chemical constituents between the oceanic lithosphere and the overlying hydrosphere, thus controlling the thermo-mechanical state of the crust, its formation and deformation, rock alteration, and influencing element balances in the ocean. (e.g., Boyd and Ellwood, 2010; Fitzsimmons et al., 2014). Hydrothermal circulation also supports high-biomass chemosynthesis-based ecosystems that sharply contrast with surrounding deep-sea habitats (e.g., Kelley et al., 2005; Lutz et al., 2008; Nees et al., 2008; Dick, 2019). Hydrothermal vents sustain dense populations of endemic faunal species that rely on microbial dark CO_2 fixation (Tunnicliffe, 1991; Tunnicliffe et al., 2003) that is coupled to the oxidation of reducing elements (e.g., HS^-, H_2, CH_4, etc.) in discharging hydrothermal fluids (Le Bris et al., 2019). Its footprint impacts neighbouring water and seafloor and marine ecosystems (Levin et al., 2016). Vent fauna communities are influenced by local population's demography and connected by dispersing planktonic larvae, which impact the dynamics of the vent metacommunity at a regional scale (Mullineaux et al., 2018). Challenging physico-chemical conditions at seafloor vents constrain faunal diversity (Tunnicliffe, 1991), whereas highly diverse prokaryotes exploit a broad range of habitats (Dick, 2019). These ecosystems broaden our understanding of the potential origins of life on Earth (Martin et al., 2008; Barge et al., 2019) and of the possibilities for life on other worlds (e.g., Hand and German, 2018). Furthermore, adaptations of vent fauna and microorganisms to extreme conditions have been a source of inspiration for biotechnology, but also in Design and Art (reviewed in Van Dover, 2014). Growing interests in the mining of polymetallic sulphide deposits raise concerns about the potential impacts of mineral extraction on these unique ecosystems, stressing the need for research to inform environmental policy and management strategies (Boschen et al., 2013; Van Dover, 2019; Orcutt et al., 2020; Smith et al., 2020; Van Dover et al., 2020). Climate change is also expected to affect the deep sea through increased bottom temperatures, loss of oxygen in certain areas of the ocean, and modifications to deep water circulation (Levin and Le Bris, 2015; Sweetman et al., 2017; Galaasen et al., 2020; Levin et al., 2020). Understanding how these changes will affect ecosystem integrity and function requires detailed baseline knowledge of natural processes, with an understanding of the mechanisms involved.

Questions remain regarding the evolution of biological communities through time including non-directional change (i.e., change in species compositions, symbiosis, and abundances due to immigration, extinction, competition, predation), as well as on directional change (i.e., succession after natural and/or anthropogenic disturbance). Those processes can only be addressed with robust baseline knowledge provided by time series observations. Since the discovery of low-hydrothermal vents in 1977 (Ballard and Van Andel, 1977; Corliss et al., 1979), only a few areas have been repeatedly visited (Glover et al., 2010; Fornari et al., 2012). Long-term time-series acquired at these sites, including 9°N or 13°N along the East Pacific Rise, allowed significant advances in our understanding of community dynamics and successional processes (e.g., Sarrazin et al., 1997; Shank et al., 1998; Marcus et al., 2009; Cuvelier et al., 2011; Du Preez and Fisher, 2018; Mullineaux et al., 2020). However understanding episodic and periodic hydrothermal and sub-seafloor processes that operate over time scales of seconds to years (e.g., Tivey et al., 2002; Scheirer et al., 2006; Barreyre et al., 2014b; Barreyre et al., 2022), and the associated faunal and microbial responses require continuous or at least annual *in situ* monitoring and observations (e.g., Huber et al., 2003).

Cabled and autonomous deep-sea observatories can provide long-term time-series collection of multi-disciplinary data (e.g., geological, physical, chemical, biological) at high temporal resolution and over years to decades. Repeated submersible visits to study sites, combined with observatory maintenance, have documented submarine volcanic eruptions and associated changes to hydrothermal vent fields (e.g., Chadwick et al., 2012; Fornari et al., 2012; Chadwick et al., 2013; Nooner and Chadwick, 2016; Wilcock et al., 2016; Chadwick et al., 2022; Barreyre et al., 2022), changes in community structure and activity (Shank et al., 1998; Fortunato et al., 2018; Rommevaux et al., 2019) as well as interactions with other nearby chemosynthetic and peripheral surrounding ecosystems (Levin et al., 2016). Together, these data contribute to answering a number of questions across various disciplines from geophysics to microbiology:

- How are hydrothermal heat, mass and chemical fluxes to the ocean impacted by seismicity, volcanic activity and ground deformation at a diverging plate boundary?
- Does tectonic setting impact the long-term stability or temporal variability of these systems?
- How do steep axial valley topography and hydrothermal buoyancy flux affect the dynamics of water masses, and how do local dynamics impact the dispersion of hydrothermal effluents?
- How do species compositions differ between habitats, geological settings, and ridges?
- How do pioneering species colonise new sites and which processes are involved?
- What are the impacts of telluric, climatic, and anthropogenic changes on deep seafloor ecosystems and hydrothermal communities?

There are currently three observatory installations at hydrothermally active MOR systems. Plans for a fourth at the Mohn Ridge (EMSO-Mohn), north of Jan Mayen, are ongoing (https://emso.eu/observatories-node/nordic-seas/). In concert,

these observatories provide Ocean and Earth scientists, engineers, educators, policy makers, and the public opportunities to deepen multidisciplinary understanding of myriad processes operating at MOR environments and utilization and advancement of deep-sea technology. The InterRidge Working Group on Integrating Multidisciplinary Observations in Vent Environments (IMOVE; https://www.interridge.org/working-group/wg_imove/) was created to advance and coordinate the integration of observatory research at deep-sea vent fields. InterRidge (IR - www.interridge.org) is an international non-profit organization created in 1992 that brings together ca. 1600 scientists from 20 nations involved in MOR research. IR aims to (i) facilitate interdisciplinary, international collaboration; (ii) coordinate scientific exchange - including information, technology and facilities; (iii) encourage the protection and environmental management of ridge environments; and (iv) promote communication between scientists and members of the society through coordinated outreach efforts. InterRidge Working Groups (WGs) are formed to support the implementation of these objectives in priority areas. The IMOVE WG was formed to advance multi-disciplinary research within and across the three MOR observatories.

A large volume of temporally- and spatially-variable multidisciplinary data has been collected at the three presently active MOR vent observatories (**Figure 1**), requiring considerable support from funding agencies. One of the goals of the IMOVE WG is to advance the integration of data from different disciplines into quantitative, cross-disciplinary models relevant to hydrothermal processes on the global MOR system. Coordinating the efforts of the scientific communities working at MOR observatories has the potential to produce transformative research outcomes and major knowledge advancements. The IMOVE WG held two international workshops (2019 and 2020) to set the stage for such a global effort. The results of these workshops, including recommendations for future MOR observatory science, are presented in this paper (IMOVE, working group, 2019).

CURRENT OBSERVATORIES AT MID-OCEAN RIDGES

The three currently operating MOR ocean observatories are the Azores component of the European Multidisciplinary Seafloor and water column Observatory (EMSO), the Endeavour node of Ocean Networks Canada (ONC) and the Axial Seamount array of Ocean Observatory Initiative (OOI) (**Figure 1**, **Box 1**). EMSO-Azores, part of the EMSO European Research Infrastructure Consortium (ERIC), is located on the slow-spreading Mid-Atlantic Ridge (MAR), at the summit of a magmatically robust central volcano hosting the Lucky Strike hydrothermal field (Blandin et al., 2010; Colaço et al., 2011; Cannat et al., 2016) (**Figure 2**). The two other observatories include submarine high power and bandwidth cables spanning the intermediate-spreading Juan de Fuca Ridge (JdFR) in the NE Pacific. ONC-Endeavour, located on the intensely hydrothermally-active Endeavour Segment, is significantly influenced by seismicity, extensional tectonics and faulting and is operated by ONC (Kelley et al., 2012; Kelley et al., 2014) (**Figure 3**). OOI-Axial Seamount, located on the magmatically robust and volcanically active Axial volcano is operated by the University of Washington for the US OOI (Kelley et al., 2014; Delaney et al., 2016), as part of the OOI Regional Cable Array (RCA, **Figure 4**). All three observatories support research aimed at understanding second, to daily, to multidecadal geophysical and geochemical processes occurring at these submarine volcanoes and their vent systems, and, in turn, how these processes affect the water column and

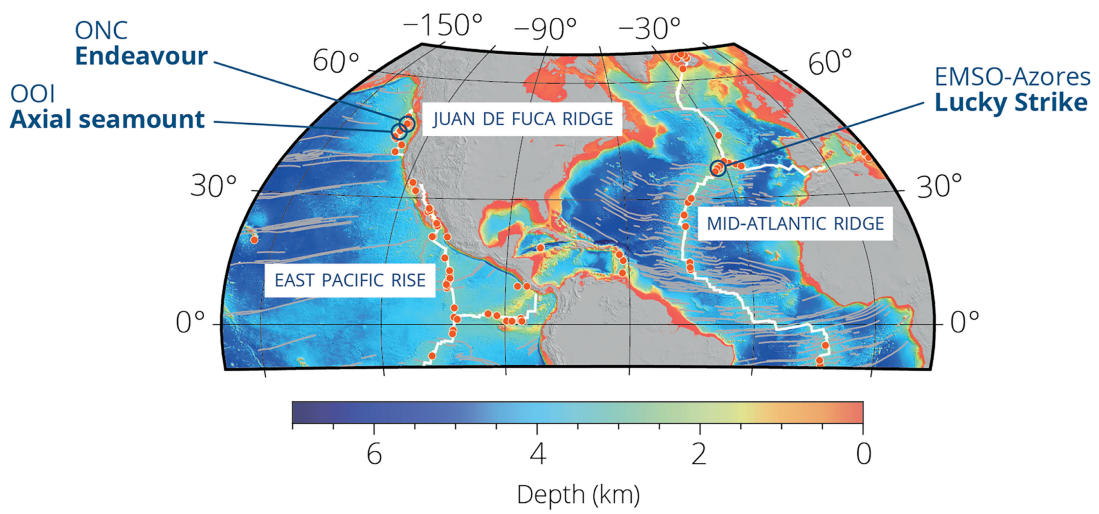

FIGURE 1 | Location of the three currently operating seafloor and water column mid-ocean ridges ocean observatories in the Pacific and Atlantic oceans. Orange dots represent active known vent fields.

BOX 1 – Observatories at Mid Ocean Ridges and Vents

Currently three observatories operate at vents on the Mid-Atlantic and Juan de Fuca Ridges including EMSO-Azores, part of the European Multidisciplinary Seafloor and water column Observatory Research Infrastructure (EMSO-ERIC), the Endeavour node of the Ocean Networks Canada NEPTUNE observatory (ONC) and the Axial Seamount component of the Ocean Observatories Initiative Regional Cabled Array (OOI-RCA). They provide real-time to nearly real-time open access data, tools for data visualization and download and resources for training and outreach.

EMSO-Azores

EMSO-ERIC website: http://emso.eu/

EMSO-Azores: https://www.emso-fr.org/EMSO-Azores

Data download: https://www.emso-fr.org/EMSO-Azores/Data-download

Data visualization tool: http://www.emso-fr.org/charts/azores/

Infrastructure design: https://www.emso-fr.org/EMSO-Azores/Infrastructure-2021-2022

Maintenance cruises: https://campagnes.flotteoceanographique.fr/series/130/

ONC-Endeavour

Ocean Networks Canada website https://www.oceannetworks.ca/

Data download: https://data.oceannetworks.ca/DataSearch

Data visualization: https://data.oceannetworks.ca/home?TREETYPE=1&LOCATION=11&TIMECONFIG=0

Infrastructure: https://www.oceannetworks.ca/observatories/pacific/endeavour

Regional Cabled Array – Axial Seamount

OOI website: https://oceanobservatories.org/

University of Washington Educational Site: https://interactiveoceans.washington.edu/

Data access and visualization: https://dataexplorer.oceanobservatories.org/

Axial seamount

Live video stream https://oceanobservatories.org/streaming-underwater-video/

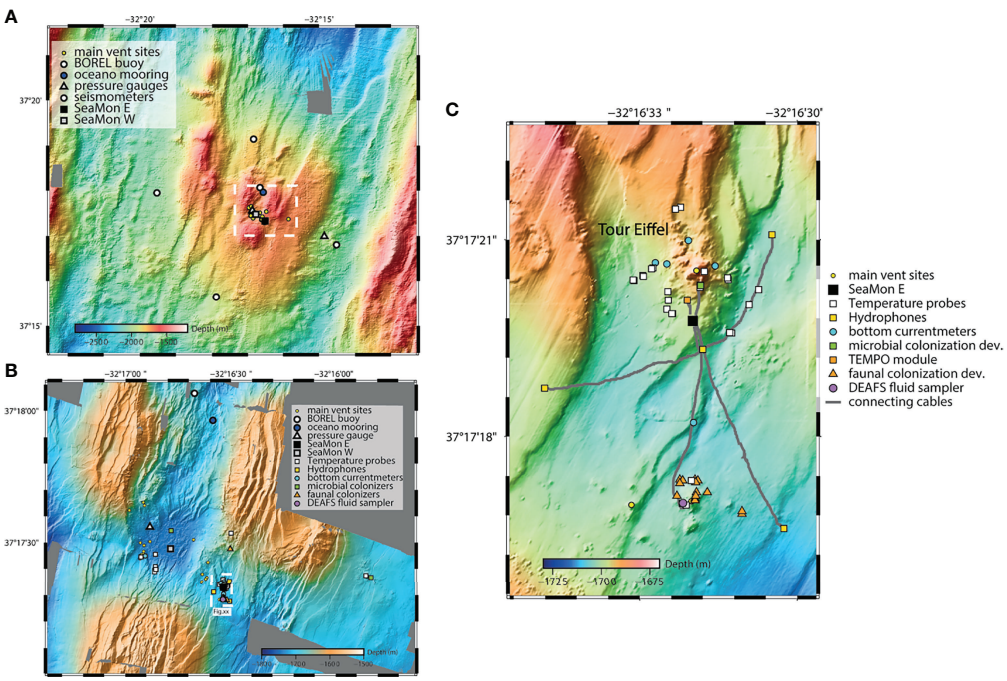

FIGURE 2 | The EMSO-Azores observatory displaying instruments location. **(A)** Segment of the Mid-Atlantic Ridge showing the location of the Lucky Strike vent field. **(B)** The Lucky Strike vent field showing the location of the EMSO-Azores observatory (area represented by the white dashed box in **A**). **(C)** Detail of the instrumentation at Tour Eiffel (area represented by the white dashed box in **B**).

drive biological responses in time and space, below, at, and above the seafloor. The multidisciplinary observatories host sensors to characterize crustal dynamics, hydrothermal circulation, fluid dynamics and composition both below and above ground, and biological activity.

The EMSO-Azores Observatory, Lucky Strike Vent Field, Mid-Atlantic Ridge

EMSO-Azores sits atop an active volcano close to the Azores Triple Junction on the northern part of the Mid-Atlantic Ridge (MAR). The volcano hosts Lucky Strike, one of the largest active

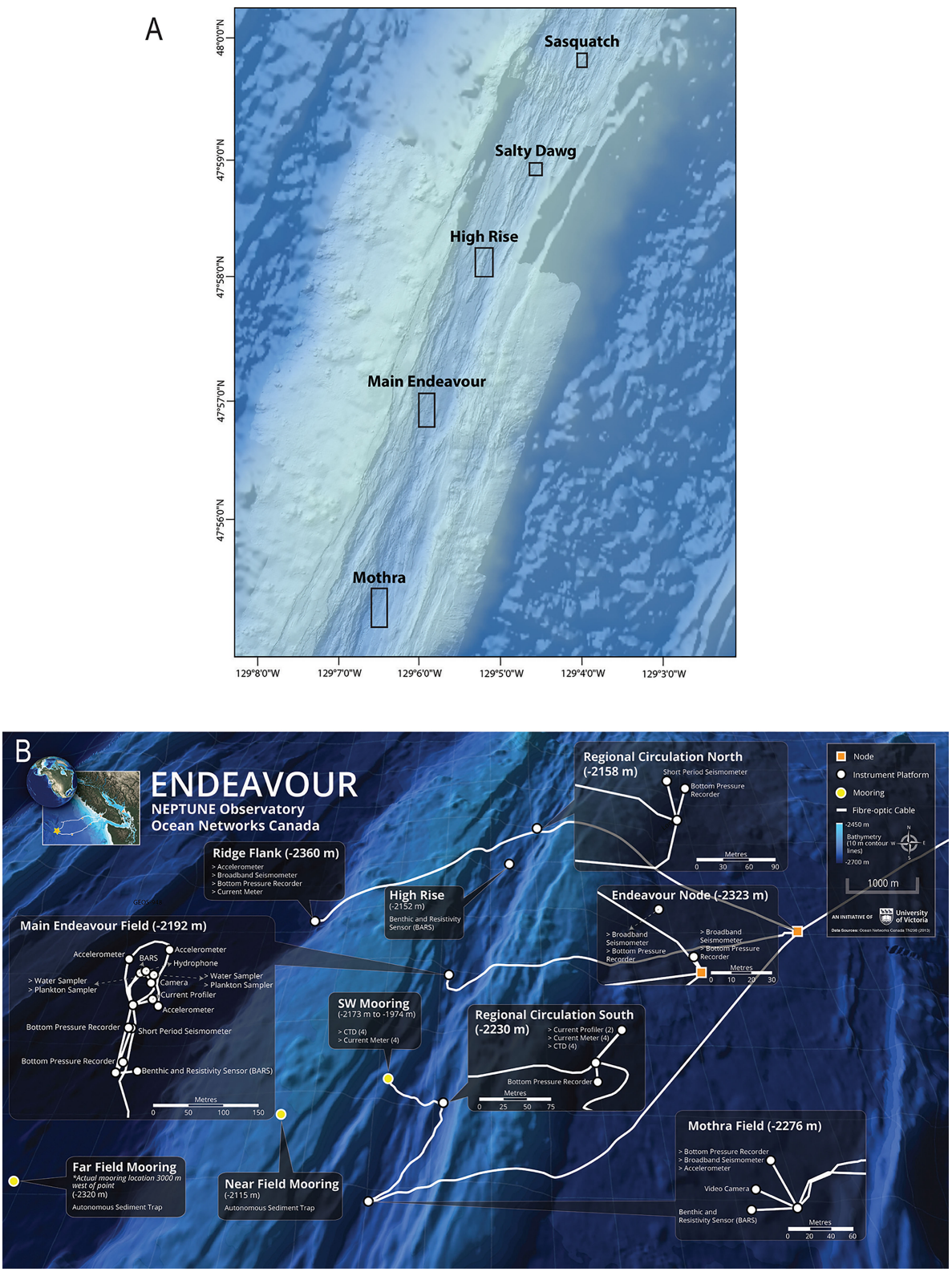

FIGURE 3 | The Ocean Networks Canada on the Endeavour segment of the Juan de Fuca Ridge. **(A)** Regional bathymetry showing the main hydrothermal vent fields. **(B)** Details of the instruments location at the Endeavour node.

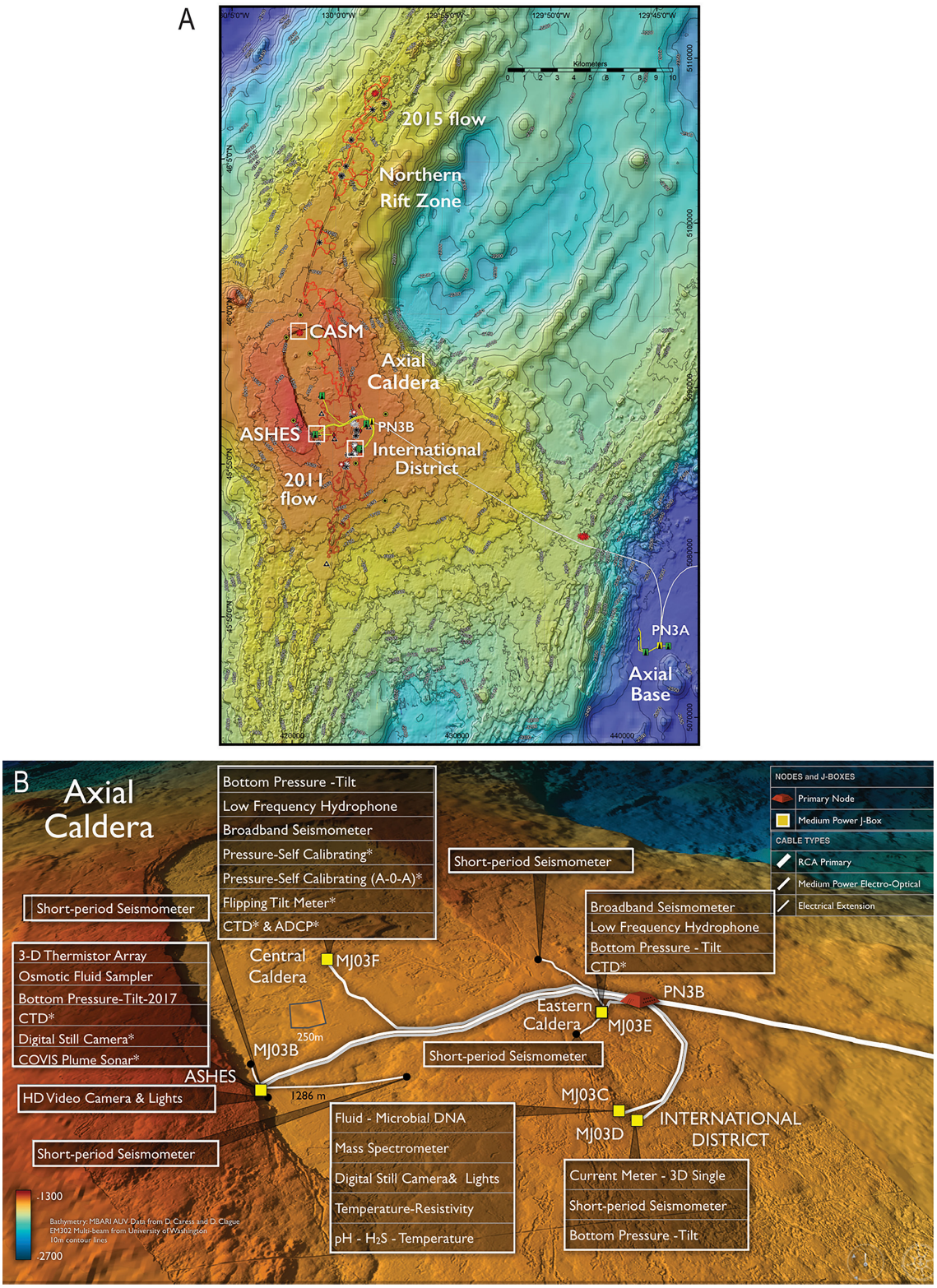

FIGURE 4 | The Ocean Observatory Initiative Axial Seamount array on the Juan de Fuca Ridge. **(A)** Regional bathymetry showing the main hydrothermal vent fields. **(B)** Details of the instruments locations within the axial caldera. * indicate instruments funded outside of OOI.

ridge-related hydrothermal vent fields (~1 km^2, Langmuir et al., 1997; Barreyre et al., 2012; Beaulieu and Szafranski, 2020). This basalt-hosted field, situated at an average water depth of 1700 m, contains over twenty active hydrothermal edifices distributed around a fossilized lava lake (Ondréas et al., 2009; Barreyre et al., 2012), and overlying a magma chamber at ~3 km depth below seafloor (Singh et al., 2006). Part of the venting area is included in a Marine Protected Area (MPA) in the Portuguese Exclusive Economic Zone (EEZ) (Menini and Van Dover, 2019). Planning for this observatory began in October 1998 at an Interridge workshop dedicated to the long-term Monitoring of the Mid-Atlantic Ridge (MoMAR). A series of follow-up MoMAR workshops (Santos et al., 2002; Barriga et al., 2005) established scientific objectives, technical goals, and experimental designs. These plans served as a basis for the implementation of the observatory, funded for the most part by the French ministry of research with support over the years of several EC research grants. The autonomous observing system EMSO-Azores, first deployed in 2010 (Cannat et al., 2011; Colaço et al., 2011; Legrand et al., 2019), comprises two Sea Monitoring Nodes (SeaMoN) that provide local electrical power (28V), sensor control, and data archiving, and limited satellite data transmission to shore *via* an acoustic connection to a surface buoy (**Figure 2**). It supports research focused on understanding hydrothermal circulation above the magmatic chamber to the seafloor, and its influence on deep-sea ecosystem functioning and water column processes in the context of a magmatically robust slow-spreading ridge environment. This multidisciplinary array has evolved over its, now, 11 years of continuous recording and the following description concerns its present-day configuration.

The first node, SeaMoN west, is deployed at a former lava lake that formed within a series of rifted volcanic cones at the summit of the central volcano (e.g., Ondréas et al., 2009; Escartín et al., 2014). This node measures seafloor seismic activity, vertical seafloor motion, and is presently also equipped with the multisensor platform EGIM (EMSO Generic Instrumentation Module) that comprises a turbidimeter, a CTD, an ADCP, one hydrophone, an Oxygen optode, and a pressure gauge (Lantéri et al., 2022). The SeaMoN East node is deployed at the base of the Tour Eiffel active hydrothermal edifice and is dedicated to physical, chemical and ecological studies. An High-Definition (HD) video camera module (Sarrazin et al., 2007), chemical sensor (Laës-Huon et al., 2020), and thermistor string, support studies of the dynamics of mussel assemblages and their environment. Biological and chemical properties of high-temperature fluids are monitored with the microbial colonization module CISICS (Connected *In Situ* Instrumented Colonizing System), and the *in situ* automated sampling of high-temperature hydrothermal fluid device DEAFS (DEep sea Autonomous Fluid Sampler). The two nodes are acoustically linked to a surface relay instrumented buoy, ensuring satellite communication to the land base station in Brest, France. Data are archived, published with a DOI, and available on the EMSO-Azores web page (**Box 1**).

In addition to these nodes, the observatory setup comprises several sets of autonomous instruments, with data recovered during yearly maintenance cruises. The autonomous instruments deployed at Lucky Strike include 4 short-period Ocean Bottom Seismometers (OBS), 2 pressure gauges, a physical oceanography mooring, a seabed array of four cabled hydrophones that supports microseismicity and marine sound studies at the Tour Eiffel site, a vast array of temperature probes distributed in hot and diffuse vents through the hydrothermal field, several bottom current meters and over 20 autonomous faunal colonization devices. A complementary ship-based field program is implemented during the cruises and contributes to increasing the set of accessible parameters and their temporal and spatial coverage (e.g., fluid and rock sampling, ecological studies, surveys of active and inactive areas, *in situ* experimentations and repeated high-resolution mapping and 3D imaging of the venting areas). The EMSO-Azores observatory is maintained annually during the MoMARsat cruises (Cannat and Sarradin, 2010). All seafloor system components are recovered, serviced onboard and redeployed by either the Remote Operated Vehicle (ROV) Victor 6000 or the Human Occupied Vehicle (HOV) Nautile. Each dataset is linked to the relevant cruises, which are listed in the data DOI, and each cruise DOI includes a list of the available data with their DOIs (**Box 1**).

ONC-Endeavour

The hydrothermally active Endeavour Segment, located on the northern part of the intermediate-spreading Juan de Fuca Ridge, is 10 km long, with a 1 km wide axial valley that has rift walls reaching 200 m. Endeavour Segment hosts five major hydrothermal vent fields (Kelley et al., 2012; Kelley et al., 2014) that are underlain by magma lenses at depths of ~2-3 km (e.g., Van Ark et al., 2007) with microseismic activity linked to hydrothermal circulation between the magma lens and the seafloor (e.g., Toomey et al., 2009; Hooft et al., 2010). The Endeavour Hydrothermal Vents (EHV) became Canada's first MPA, following an act of parliament in 2003. Ocean Networks Canada has been operating real-time observing systems there since September 2010.

The scientific goals of the Endeavour observatory were established during a series of workshops, following which researchers developed a multi-disciplinary community experiment proposal that competed for instrumentation funds with other community experiment proposals during the design and instrumentation phase of the ONC NEPTUNE (NorthEast Pacific Time-series Undersea Networked Experiments) network. The observatory design had to be compliant with the MPA Management Plan, which allowed for two of the vent fields, Mothra and Main Endeavour Field (MEF), to be cabled with scientific instrumentation and experiments. A third vent field, High Rise, was to be left in its natural state, and monitored through ROV visits and occasional deployments of autonomous instruments. The Endeavour Node is sited 5 km east of the axial valley on a relatively flat seafloor. Three fibre optic extension cables provide power and two-way data communications to seafloor junction boxes located in the Mothra and Main Endeavour vent fields, and at a site north of the High Rise field (**Figure 3**). The junction boxes provide power and communication to sensors and instruments on seafloor

platforms and water column moorings. The Main Endeavour Field instrumentation was initially concentrated on a nearly 50 m-across, actively venting sulphide edifice named Grotto (Kelley et al., 2014; Juniper et al., 2019). A seismometer array, designed to precisely locate shallow micro-seismic events in the hydrothermal up-flow zone below the seafloor, supports study of their links to vent fluid discharge. On Grotto, several different temperature sensor technologies monitor hydrothermal discharge at vents that vary from a >335°C black smoker vent to diffuse warm flows. Two camera modules look out onto a tubeworm assemblage and new sulphide worm habitat, and three monitoring systems provide data on chemical properties of the vent environment. Outside of the vent fields, two pairs of water column moorings (RCM), one pair between High Rise and Salty Dawg, the other between Mothra and MEF, monitor water column properties and currents to constrain buoyancy-driven flow in the axial valley (**Figure 3**). A Junction Box (JB) placed near the northern RCM pair supports a broadband seismometer and bottom pressure recorder on the western flank of the Endeavour segment, about two kilometers west of the MEF, on the Pacific Plate.

A near-tripling of ONC's observing system at the Endeavour hydrothermal vents is nearing completion. This expansion will enhance the simultaneous, real-time monitoring in the Mothra and Main Endeavor vent fields (**Figure 3**), with new sensors (including additional cameras and instruments for *in situ* hydrothermal fluid chemistry), and the completion of the larger scale seismometer network around the segment with deployments at the Endeavour node on the JdF plate. The extension of the observing system to the Mothra vent field provides biologists with new settings to test hypotheses about the coupling of vent communities to habitat dynamics. Expansion of the observing system began in 2016 with the installation of extension optical cables to connect the Endeavour node to the Mothra vent field and a site north of the High Rise field. Installation of new sensors and camera systems began in 2019 and are scheduled for completion in 2022. All data are available for download and visualization through an online query interface linked to the data archive and GIS database (**Box 1**).

During the deployment of the 840 km backbone NEPTUNE cable, a spur cable (with a cable termination assembly) was extended to the Middle Valley hydrothermal area, to the north of the Endeavour Segment (**Figure 3**). This installation could support future development of a node and instruments to contrast the hydrothermal activity at the sedimented Middle Valley, with the sediment-starved spreading centre at Endeavour. This would also support extension of the network onto the Pacific Plate to the west, and the Sovanco Fracture Zone to the northeast.

Ocean Observatories Initiative (OOI): Regional Cabled Array on Axial Seamount

Axial Seamount is the largest and most magmatically active volcano along the JdFR (Kelley et al., 2014; Kelley et al., 2016; Smith et al., 2018). It is also the best imaged submarine volcano worldwide, with multiple 3D seismic surveys delineating two magma chambers and a series of stacked feeder sills (West et al., 2001; Arnulf et al., 2014; Arnulf et al., 2018; Carbotte et al., 2020). Repeated high resolution (1 m) bathymetric surveys acquired with deep-sea autonomous vehicles of the caldera and surrounding walls have allowed documentation of the volcanic and hydrothermal geomorphology, and the extent and volume of different volcanic eruptions and of vertical seafloor displacements (e.g., Caress et al., 2012; Clague et al., 2017).

The OOI marine infrastructure was designed and built to meet science requirements developed through community workshops, which identified broad-ranging critical ocean science questions requiring comprehensive and sustained (up to ~25 years) ocean observing infrastructure, enabling examination of processes at multiple spatial (ocean basin to tidal basin) and temporal (short-term, stochastic events and large-scale decadal cycles) scales. The Axial observatory is part of the RCA (**Box 1**; **Figure 4**). A 525 km-long, high power (10 kV) and bandwidth (10 gb/s) submarine fiber optic cable provides power and two-way communication from Pacific City, Oregon, to the volcano. In 2014, the RCA observatory was installed at the base and within the caldera of Axial Seamount. Axial Caldera currently hosts a diverse array of 23 core seafloor instruments (**Figure 4**). In 2016, following commissioning of the RCA, NSF opened the door to Principal Investigators (PI) to add infrastructure onto the RCA through funding outside of OOI. Within Axial Caldera, nine PI instruments are now on the cable and there are three uncabled instruments. Twenty additional cabled and uncabled instruments are funded for installation in the caldera and on its walls. Infrastructure located in Axial Caldera is focused at four sites: The ASHES and International District Hydrothermal Fields, and the Central Caldera and Eastern Caldera sites focused on geophysical investigations (**Figure 4**).

The geophysical instruments positioned within the caldera that monitor seismic and volcanic activity – including explosive events (Wilcock et al., 2016; Caplan-Auerbach et al., 2017; Chadwick et al., 2022) – include five short-period seismometers, in addition to two pairs of broadband seismometers and low-frequency hydrophones. Four bottom pressure-tilt instruments situated in the Central and Eastern Caldera regions, and the ASHES and International District vent fields, monitor, in real time, changes in seafloor elevation/tilt associated with the inflation/deflation of the magma chamber and are being used for forecast future volcanic eruptions (**Box 1**). Also distributed within the caldera are three CTDs (Central Caldera, Eastern Caldera, and ASHES) to monitor hydrothermal fluid interactions with crustal and seafloor processes (e.g., diking-eruptive events).

At the ASHES vent field (**Figure 4**), a 3D-thermistor array and a collocated osmotic-based fluid sampler provide temperature distribution in a diffuse flow site along with physical samples for shore-based chemical analysis of emanating fluids. A HD video camera focused on the 4 m tall actively venting 'Mushroom' edifice provides real-time streaming imagery every 3 hrs covering the entire edifice to monitor changes in chimney development and biological communities colonizing the edifice and surrounding seafloor (**Box 1**). The site also hosts a COVIS multibeam sonar system focused on the 4 m

tall edifice Inferno and surrounding diffuse flow sites, and thermistor arrays within diffuse flow.

At the International District vent field (**Figure 4**), an instrument suite is used for real-time monitoring of temperatures and fluid chemistry of hydrothermal vents and collecting fluids and DNA for later shore-based chemical analyses (Kelley et al., 2014). A high-temperature, resistivity, and redox potential probe (TRHPH/BARS) is installed in the Escargot hydrothermal chimney to examine boiling processes. A high-temperature probe (THSPH) that measures H_2, H_2S, and pH is installed in the Diva hydrothermal chimney. Instruments positioned at the Tiny Towers site include a mass spectrometer to measure dissolved gases in the venting fluids, coupled microbial DNA (PPS) and hydrothermal fluid (RAS) samplers with temperature co-registered vent fluid temperature. These instruments' intakes are collocated in a 'vent cap' positioned atop emanating diffuse flow thereby providing real-time monitoring of dissolved gas concentrations in hydrothermal fluids while simultaneously allowing for collection of microbial DNA and fluids for post-recovery metagenomic and chemical analyses. A digital still camera at this site allows monitoring of the hydrothermal activity, changes in biological communities, and condition of the previous instrument installations. A 3D single point current meter provides real-time monitoring of currents near the seafloor. A second nearby bare-rock site, includes a short-period seismometer, current meter, and bottom pressure tilt instrument. This site is the focus of an International Ocean Discovery Program proposal to include an array of holes with cabled CORKED observatories to examine the deep biosphere, crustal hydrogeology, and magma injection and crustal deformation (Huber et al., 2021).

The Central Caldera site has become a key site for testing of geodetic instruments to examine seafloor deformation with follow-on applications to monitoring the Cascadia Subduction Zone. Here, the co-registration of two different kinds of self-calibrating pressure sensors and a "flipping" tilt meter along-side Core OOI instrumentation allows cross referencing of these new technologies. Also hosted at this site is a newly developed ADCP to image the entire ~ 1500 m of water column. Finally, two state-of-the-art instrumented cabled profiling moorings at the base of the seamount provide environmental measurements from ~ 2600 m to 125 m to 5 m beneath the ocean's surface. In concert, the two moorings host a diverse suite of 24 instruments, provide insight into internal waves and may capture the formation-evolution of the next megaplume (Kelley et al., 2016; Devine et al., 2020).

TEN YEARS OF OBSERVATORY RESEARCH AT VENTS

Understanding the functioning and dynamics of vent ecosystems requires resolving the range of scales at which processes operate. The three seafloor observatories have supported a decade of multidisciplinary research at hydrothermal environments hosted in a basaltic upper crust, and overlying magma chambers at varying depths. The data and follow-on research have enabled significant advancements in our understanding of processes occurring at multiple scales from the sub-seafloor to the water column. These magmatic sites are visited every year as part of the maintenance cruises allowing for systematic surveys and sampling and integration of the different scales of biological and environmental data. The following section summarizes results obtained using seafloor observatories during the last 10 years, based on both time-series analyses and modeling.

Crustal Processes

While MOR's represent the world's largest hydrothermal-volcanic system, we still lack an in-depth understanding of the complex interplay of magmatic, tectonic, and hydrothermal processes that take place along the ~65,000 km of ridge axis. Comprehensive databases acquired in recent decades show that hydrothermal fluids expelled at vents along magmatically robust sections of a MOR have a large spatial and temporal variability in exit fluid velocity, temperature, and chlorinity (e.g., Scheirer et al., 2006; Larson et al., 2007; Sohn, 2007; Sarrazin et al., 2009; Barreyre et al., 2014b; Germanovich et al., 2015; Xu et al., 2017). Monitoring seafloor deformation and seismic activity at active volcanoes provided insights into magma movement at depth (Chadwick et al., 2016; Nooner and Chadwick, 2016; Wilcock et al., 2016) and into the location and time-evolution of the domain of hydrothermal heat extraction (Tolstoy et al., 2006; Crawford et al., 2013; Wilcock et al., 2016). The RCA infrastructure, online for the Axial 2015 eruption, captured the first real-time cabled observatory data of the timing, location, dynamics and volume of eruption-related magma movements, eruptive explosions and fissuring, and egress of fluids out of the subseafloor (Chadwick et al., 2016; Wilcock et al., 2016; Caplan-Auerbach et al., 2017; Spietz et al., 2018). Additionally, an eruption response has been observed in high-temperature vents at Axial instrumented with data logging temperature probes. After the 2011 eruption, temperatures in some high-temperature vents adjacent to the eruptive area dropped to just over 100°C, perhaps as a consequence of rapid recharge of cold seawater that replenished warm fluids injected into the caldera and formation of spectacular snow blowers from which issued microbes and microbial material flowing from the subseafloor (Kelley et al., 2014).

Being on a slow spreading ridge, the Lucky Strike volcano has a significantly lower melt flux than the JdF ridge vent areas, resulting in less frequent eruptions (Rubin et al., 2012). Monitoring full cycles of volcanic activity at a slow spreading ridge is beyond human time scales. Indications for recent magmatic activity at the Lucky Strike volcano include an earthquake swarm interpreted as due to a dike injection in 2001 (Dziak et al., 2004), and increased CO2 content in the vent fluids in 2008 (Pester et al., 2012) and 2010 (Chavagnac et al., 2015; Rommevaux et al., 2019).

One of the most critical crustal accretion variables, and one that is commonly poorly constrained, is indeed permeability, as it is a major control on fluid flow below the seafloor. The use of the natural forcing from ocean tides to constrain crustal dynamics and permeability structure of MOR hydrothermal fields brought new insights in the study of hydrothermal circulation processes

and fluxes in the oceanic crust (e.g., Crone and Wilcock, 2005; Barreyre et al., 2018). Using a time series of fluid temperature data, differences in phase lags between tides and the thermal response of exit fluids were shown to correspond to variations in the shallow crustal permeability structure and therefore in mass and heat fluxes (Barreyre et al., 2018). Similar approaches also showed a strong control of shallow spatial variations in permeability on diffuse exit fluids at the ASHES vent field and Lucky Strike (e.g., Mittelstaedt et al., 2016). Recent studies have investigated the feasibility of using models of the poroelastic response to tidal loading manifested in exit-fluid velocity and temperature records to obtain shallow crustal permeability constraints below MOR vent fields (e.g., Jupp and Schultz, 2004; Crone and Wilcock, 2005; Barreyre et al., 2014a; Barreyre and Sohn, 2016; Barreyre et al., 2018). High-resolution seismic studies provide additional constraints into possible subseafloor heterogeneities and related fluid paths between the axial magma chamber and the seafloor (e.g., Marjanović et al., 2019).

While these data sets pertaining to seismic and fluid flow studies provide valuable constraints for coupled geodynamic-hydrothermal models (e.g., Theissen-Krah et al., 2016), these snapshots of the "current state" at a specific location are difficult to interpret in the context of a dynamically evolving hydrothermal and magmatic system. At the same time, numerical models have evolved in recent years and can now handle more realistic thermodynamic fluid properties and two-phase flow phenomena (Coumou et al., 2009; Lewis and Lowell, 2009; Afanasyev et al., 2018; Vehling et al., 2021). An outstanding strength of numerical forward models is their ability to establish process-based causal links between different observations and data sets, including spatial and temporal dependencies. Time series data sets from recurring expeditions to the same geographical location or, ideally, permanent installations, are extremely valuable and enable the stringent design and calibration of models and facilitate non-ambiguous interpretation of transient model results. The combination of state-of-the-art numerical modeling techniques and data from (nearly) continuous monitoring will enhance our understanding of processes and mechanisms taking place at inaccessible locations inside the Earth.

Interface and Biological Response

Integrated studies at the interface of the subseafloor and the water column have contributed to a better understanding of links between geological, geochemical and biological processes. At the Lucky Strike seafloor, the hydrothermal fluid fluxes of 14 monitored vents (Leleu, 2017) have immediate impact on trace element dispersion within the hydrosphere and microbial development. For example, high fluid CO_2 contents, induced by replenishment of the magmatic chamber at depth stimulate the thriving of thermophilic and anaerobic Archaea and Bacteria (Archaeoplobales, Nautiliales and Nitratiruptoraceae) (Rommevaux et al., 2019). In addition, the progressive mixing of end-member hydrothermal fluid and surrounding seawater leads to the formation of hydrothermally-derived minerals, in particular sulfate-bearing minerals (anhydrite and barite) which control dissolved rare earth element fluxes and the Nd isotope signature of the hydrothermal plume (Chavagnac et al., 2018b). At Axial Seamount, the past three eruptions provide some insights into subseafloor hydrothermal processes because these eruptions have significantly affected crustal hydrology, fluid geochemistry, and microbial communities. This is exemplified by the development of low-temperature, diffuse snowblower vents formed within ~50 m of eruptive fissures by subsurface circulation of warm, volatile-rich fluids, which results in microbial growth and discharge, indicating a near-instantaneous increase in heat and mass fluxes, followed by exponential decay (Cann et al., 1997; Butterfield et al., 2004; Chadwick et al., 2013; Meyer et al., 2013; Nooner and Chadwick, 2016). Diffuse vent fluids at Axial are hotspots of primary production in the deep ocean, while also providing access points to infer microbial and geochemical processes in the subseafloor (e.g., Butterfield et al., 2004; Huber et al., 2007; Fortunato and Huber, 2016; Olins et al., 2017; Fortunato et al., 2018). Time-series microbial and geochemical studies of these fluids at Axial began in 1998, shortly after the volcano erupted. These multi-year studies at Axial showed that individual vent sites maintained microbial communities and specific populations, with spatially distinct communities and activities mediated by both endemic and unique groups at each site (Opatkiewicz et al., 2009; Fortunato et al., 2018). Such results, combined with cultivation experiments and modeling efforts, suggest that the type and quantity of subseafloor microbes beneath particular vents is controlled by a combination of geochemistry and local geology at individual sites, leading to spatially and temporally stable fluid paths that allow for the persistence of distinct subseafloor microbial communities (Opatkiewicz et al., 2009; Fortunato et al., 2018; Stewart et al., 2019).

In the mixing zone, recurrent *in situ* sampling with filtration and analysis during maintenance cruises allowed the investigation of the dissolved and particulate partitioning of metals in the early buoyant plume (4–150°C) of smokers at Lucky Strike (Cotte et al., 2020). Noted spatial variability of the chemical composition (Fe and Cu) of the buoyant plume throughout the vent field was limited in the warmest part of the plume. Even though metal partitioning was strongly affected by different precipitation and oxidation processes, hydrothermal iron was almost completely preserved (> 90%) in the dissolved fraction along the mixing gradient (Laës-Huon et al., 2016; Waeles et al., 2017; Cotte et al., 2018). A long-term *in situ* study of reactive iron (CHEMINI) in a diffuse vent at the base of the Tour Eiffel active edifice showed that reactive iron stabilization over time prevented precipitation and could enhance iron availability to the local biological community structure (Laës-Huon et al., 2016). These studies highlight that metal stabilization processes allow the local export of hydrothermally sourced iron and copper into the deep ocean.

Observatory studies of biological responses to habitat variability combine sensor data on habitat conditions with imagery that documents species presence/absence and behaviour. The few long-term studies at the assemblage-scale have shown faunal communities to be relatively stable in relation to baseline environmental variability (Sarrazin et al., 2014; Van Audenhaege et al. 2022). At the organism-scale, analyses of

imagery have highlighted species behavioral responses that correlate with tides and surface storms, both on the MAR and the JdFR (Cuvelier et al., 2014b; Lee et al., 2015; Cuvelier et al., 2017; Lelièvre et al., 2017; Mat et al., 2020). Deep current inversions in response to tides affect the mixing of hydrothermal fluid inputs with surrounding seawater, thus modifying local environmental conditions in vent habitats. Symbiotic vent mussels at Lucky Strike open and close, and tubeworms from MEF extract and retract, following the tidal cycle, probably in response to their physiological/endosymbiont needs (Cuvelier et al., 2014b; Mat et al., 2020). On the JdFR, non-symbiotic species also appear to respond to environmental variability by adjusting their position and behaviour, possibly as a trade-off between resource availability/predation and physiological tolerance (Lelièvre et al., 2017). Daily recording of video imagery has also proved to be a good tool for characterizing the behaviour and interactions of species that could not otherwise be reared in aquaria under controlled conditions (Matabos et al., 2015; Van Audenhaege et al. 2022). It remains a challenge to relate micro environmental changes to life history strategies and physiological tolerances. Combining imagery with multi-variable sensor data should improve our ability to relate recruitment to local environmental cues and broader oceanographic drivers, and consequently better understand regional reproductive patterns.

Maintenance cruises offer opportunities to sample and describe natural communities (e.g., Sarrazin et al., 2015; Husson et al., 2017; Lelièvre et al., 2018; Sarrazin et al., 2020) and perform manipulative and colonizing experiments over time. Extensive experiments conducted during maintenance cruises (e.g., Cannat and Sarradin, 2010) have produced key insights into the biodiversity, functional diversity, and ecology of MAR hydrothermal communities. These include (re-) colonization processes and relationships between vent and cognate communities along a vent gradient and on different types of substrata (Cuvelier et al., 2014a; Zeppilli et al., 2015; Plum et al., 2016; Baldrighi et al., 2018; Alfaro-Lucas et al., 2020; Cowart et al., 2020; Marticorena et al., 2021). Biological samples have contributed to increasing basic knowledge of species biology (Husson et al., 2017; Marticorena et al., 2020), trophic interactions (Lelièvre et al., 2018; Portail et al., 2018; Zeppilli et al., 2019), biological rhythms (Mat et al., 2020) and physiology (Husson et al., 2018), leading to a growing understand of vent faunal functional traits (Chapman et al., 2019; Alfaro-Lucas et al., 2020; Murdock et al., 2021). Post-eruption succession patterns have been studied at Axial, particularly following the 1998 eruption, from repeated visits both pre-eruption as well as 7-, 18-, 30-, and 42-months post-eruption (Marcus et al., 2009).

Water Column: Deep Circulation, Fluid Dispersal and Connectivity

The ocean dynamics above MOR systems and specifically around vents are complex. Broadly, they feature three families of processes with their own phenomenology and impacts. First, the interaction of oscillating tidal currents with the rough seafloor topography generates internal waves at tidal frequencies called internal tides. These waves are unstable and eventually break close to their generation sites, provoking irreversible vertical mixing (St. Laurent and Garrett, 2002; Vic et al., 2018a). Although the astronomical (tidal) forcing is now easily predicted and appears to be remarkably in-phase with the local tidal energy density over ridges (Vic et al., 2021), the spatio-temporal variability of mixing remains poorly quantified, due to sparse data. Studies conducted these last decades highlighted key processes associated with internal tides, including their interactions with seafloor topography and background currents, leading to dynamical modifications of the mean state of the deep ocean (Thomson et al., 1990; Thomson et al., 2003; Lahaye et al., 2019; Lahaye et al., 2020).

Second, low-frequency currents drag on the valley walls and destabilise, generating small-scale swirling structures called submesoscale coherent vortices (SCVs, Vic et al., 2018b). SCVs can feature lifespans of many months and travel thousands of kilometres [recent survey in McCoy et al. (2020)]. Thus, they are effective at trapping and spreading deep-ocean material to the ocean interior (e.g., Bower et al., 2013; Vic et al., 2018b). Observations of SCVs are very sparse in general and even more specifically at depths of MOR.

Third, hydrothermal venting introduces a heat flux that generates mixing of vent fluids with ambient waters near the seabed. In addition, hydrothermal plumes that form over the vent field contain chemical constituents, larvae and microbes. These plumes have buoyant and neutrally-buoyant components. Buoyant plumes rise into the water column, entraining surrounding seawater, until they achieve neutral buoyancy through dilution and cooling. Near the bottom, this upward buoyancy flux drives an inflow towards the vent field and is effective in the retention of plankton (Thomson et al., 2003). Hydrothermal plumes can also carry plankton up into the ambient oceanic currents to be dispersed in along the axis, or off-axis to possibly a less hospitable deep-sea environment. In contrast, organisms with the ability to swim vertically or alter their density can utilise these dynamics and larvae have been shown to actively alter their positions to stay near their preferred environment (Mullineaux et al., 2013). The influence of hydrothermal venting on the chemistry of the deep-sea near the Endeavour segment has been investigated by Coogan et al. (2017). Using tow-yo hydrocasts, sediment traps and push cores they revealed that the plume heat and particulate anomalies indicate a half contribution from the particle-poor diffuse flow and half from (particle rich) high-temperature venting. Coogan et al. (2017) also found that less than 2% of all measured elements accumulate on the seafloor within 1.5 km of the individual vent fields. This implies that most of the chemical flux is transported significant distances away. The variability of plume position at higher frequencies is regulated by the local oscillatory currents in the inertial, tidal and weather bands (Xu and Di Iorio, 2012) and the periodicity of the immediate fallout from the plume, in addition to the direct effects of the local currents, appears to have an effect on the benthic ecology

(Lelièvre et al., 2017). Above the neutrally buoyant plume, towed nets along with acoustical methods identified a deep scattering layer associated with the aggregation of zooplankton (e.g., Burd and Thomson, 2012). This deep scattering layer has been shown to have a complex seasonal and higher frequency (20-40d) variability likely due to a combination of both ontogenetic migration and dynamic advective processes (Burd and Thomson, 2019). In the rift valley of the northern MAR, the compilation of different *in situ* data acquired by CTD-LADCP casts and mooring deployments during repeated visits (Lahaye et al., 2019), combined with modeling studies (Vic et al., 2018b) has revealed consistent north-eastward along-valley currents below 2000 m at sub-inertial time scales. Current variability, dominated by slow time scales (weeks), favors the northward dispersion of tracers. Over the Endeavour segment of the JdFR, data from current meters and tracking of the neutrally buoyant plume, indicate that the long-term mean current tends to the southwest (Thomson et al., 2003; Coogan et al., 2017), with observations suggesting it has been steady for decades.

Integrating ecological/biogeochemical/physical data with modeling approaches can help address dispersion and connectivity questions (e.g., owen and Sponaugle, 2009; Artigue et al., 2021). In coastal studies, sub-kilometer-grid, primitive-equation models have been used to perform Lagrangian dispersion since the 2000's ('reef-scale' models; Werner et al., 2007). No such method has been used in deep-ocean studies until recently. Mesoscale-resolving models (Young et al., 2012; Breusing et al., 2016) and submesoscale-permitting models (Bracco et al., 2016; Cardona et al., 2016; Mitarai et al., 2016; Vic et al., 2018b) have been employed to study connectivity between benthic communities at depths below 1000 m, resulting in improved realism of flow-topography interactions in many ways (Bracco et al., 2016; Vic et al., 2018b). Notably, tidal currents, hitherto absent from high-resolution regional models, are found to increase the vertical spreading of particles and help them cross topographic barriers (Vic et al., 2018b).

TOWARDS A COORDINATED UNDERSTANDING OF MID-OCEAN RIDGES (MOR) HYDROTHERMAL VENTS AND THEIR ECOSYSTEMS

The IMOVE working group seeks to refine common process-oriented research questions that can be addressed with data in hand, and identifying what is needed to address questions raised by today's societal challenges, in order to help and foster interoperability across vent observatory platforms. The locations of the three observatories permits the study of hydrothermal processes in contrasting environments and settings. Each is representative of different dynamics of seafloor spreading and volcanism, from slow (MAR) to intermediate (JdFR) spreading rates, and the relative importance of tectonic (Endeavour) and volcanic (Lucky Strike, Axial Volcano) processes. They also provide contrasting examples of hydrothermal plume behaviour: with episodic megaplume generation during eruptions at Axial volcano, (e.g., Palmer and Ernst, 1998; Baker et al., 2019) a continuously present intense plume generated by multiple hydrothermal vents along the axis of the Endeavour segment (Thomson et al., 2003; Kelley et al., 2012), whereas megaplume events were yet never detected at Lucky Strike. Early international workshops in the 90s and 2000s (National Research Council, 2000) set the scene for a globally-coordinated design of seafloor observatories. Following this collaborative effort, programmatic and funding realities have resulted in each observatory having its own infrastructure design, research goals, and specific scientific questions (Barnes and Tunnicliffe, 2008; Favali and Beranzoli, 2009; Cannat et al., 2011). Since their deployment, large volumes of data have been acquired from all three current observatories, creating opportunities for studies that extend across locations. The first workshop (IMOVE, working group, 2019) defined priority themes and vent processes, establishing a basis for setting common scientific questions. This framework was then used to structure the science-based workshop at which participants developed a set of scientific questions and related societal challenges. This provided a basis for further exploiting existing data, and for identifying EOVs and Essential Biodiversity Variables (EBVs) that need to be measured to improve our understanding of hydrothermal processes (see next Section).

Processes of particular interest include fluid flow geometry, fluxes (heat, mass, chemical), their variability (i.e. periodic and episodic) and how they partition, local oceanographic currents and associated biological responses (**Figure 5**). These processes can be divided in three domains: the subseafloor, the interface at the ocean floor, and the water column. In the subseafloor, ground deformation, heat transfer, fluid-rock interactions affect fluid flow geometry, fluid composition and crustal stress and permeability, fluid residence times and recharge, and microbial community composition. At the seafloor interface, where the fluid meets the cold background seawater, thermo-chemical exchanges and mixing impact fluid flow characteristics, microbial and vent species distributions and biomass, and energy flow (e.g., carbon flux) (Le Bris et al., 2019). Finally, in the water column, oceanographic forcing, including currents, tides and their interactions with the local topography, drives plume dispersal, hydrothermal fluxes and exports to the ocean, faunal distribution, behaviour and larval dispersal, and influences species connectivity (**Table 1** and **Figure 5**). The multidisciplinary approach enabled by observatories through the concomitant acquisition of environmental and biological variables provides a unique opportunity to integrate this wide range of processes and assess mechanisms driving vent ecosystem function and temporal trajectories. Four key, integrative questions emerged from the two IMOVE workshops:

- How does hydrothermal circulation and associated heat and matter fluxes respond to crustal and oceanographic forces at varying temporal scales?
- How does the interaction between hydrothermal circulation and shallow mixing with seawater control fluid chemistry, flux and temperature in the mixing zone where microbial communities and vent fauna develop?

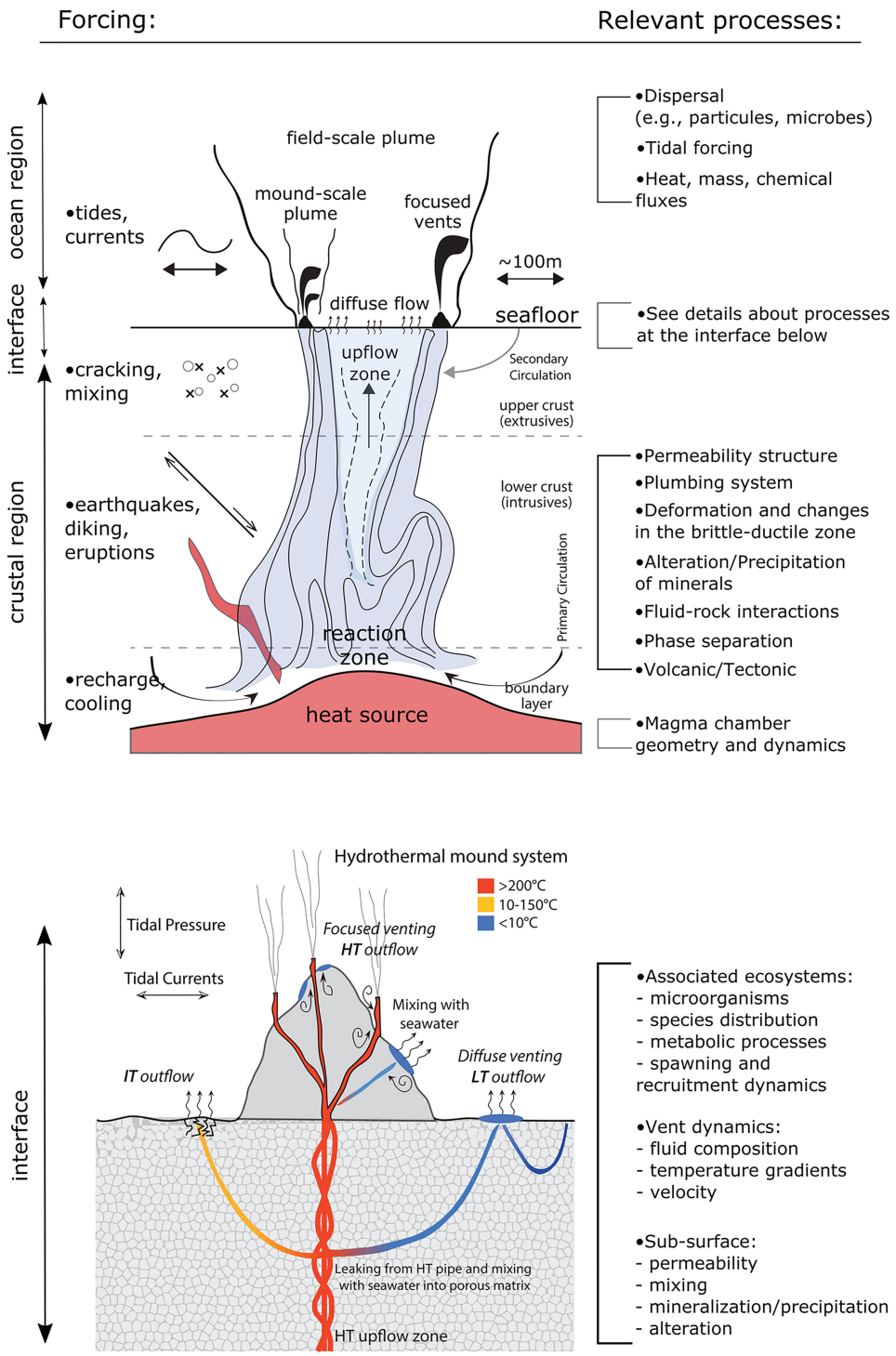

FIGURE 5 | Top Conceptual model of a hydrothermal plumbing system at depth, with the upwelling of a single plume above the magmatic heat source that is focused along high-permeability zones associated with main faults and fractures networks. Bottom Close-up of a hydrothermal mound edifice. High-temperature (HT) outflow is directly fed by the high-temperature up-flow zone (here represented as an anastomosing, interconnected series of conduits), intermediate-temperature (IT) outflow is fed from leakage from the HT pipe and mixed with cold water into the porous matrix [i.e., hypothesis (1)] and low-temperature (LT) outflow is fed from either hypothesis (1) or conductively heated bottom water drawn into the seafloor as part of a secondary circulation system [i.e., hypothesis (2)]. Modified from Barreyre et al. (2014b).

TABLE 1 | Themes and processes to be considered at vents as defined during the first workshop and that can be addressed through observatories and their associated maintenance cruises.

Discipline	Processes
Biology	Connectivity between vents, mounds, ridges, peripheral zones
	Role of ocean circulation on larval dispersal
	Recruitment dynamics
	Energy flow and fluxes
Chemistry	Chemical signatures: time-scale, stability, low- and high-temperature
	Phase separation
	Dynamic coupling of diffuse/focused venting
	Magmatic chamber replenishment
	Mixing
	Mineral precipitation, chemical speciation, chemical fluxes
Geophysics	Seafloor dynamics: compliance and ground deformation
	Plumbing system and fluid flow geometry over a range of substrata
	Subsurface characterization
	Crustal geothermal processes, permeability and stress states
	Forcing of sub-seafloor processes on seafloor systems (volcanic, tectonic, alteration and precipitation of minerals)
Oceanography	Plume characterization and dispersal
	Kinetic energy dissipation and turbulent mixing
	Carbon cycle
	Geochemical and thermal fluxes impacts on ocean
	Forcing of ocean dynamics on seafloor systems

- How do the hydrothermal biological communities respond to changes in environmental conditions?
- How do vent fluxes, productivity, and communities influence the surrounding deep-sea ecosystems and vice versa?

This fundamental knowledge is prerequisite to evaluating faunal responses to anthropogenic disturbances, elaborating conservation strategies, and addressing the societal challenges that mid-ocean ridge systems are increasingly facing.

Anthropogenic Challenges and the Scientific Questions to Address

The three main current or foreseeable anthropogenic challenges to deep-sea vent environments are climate change, pollution (e.g., microplastics, persistent organic pollutants) and deep-sea mining. Fisheries are not discussed since most MOR vents are at (currently) non-fishable depths and do not host significant standing stocks of fish. Observatories contribute to enhancing our fundamental knowledge of ecosystem function, and yearly visits on site offer opportunities for seafloor experiments (Alfaro-Lucas et al., 2020; Marticorena et al., 2021) and collection of biological samples to increase our knowledge of species biology and ecology (e.g., Husson et al., 2017; Lelièvre et al., 2018; Murdock et al., 2021). Directly assessing the potential impacts of deep-sea mining will require similar experimental and sampling approaches. Regular sampling is also needed to characterize the abundance and composition of microplastics in these environments and understand how local and regional hydrography impacts their distribution. Standardized protocols should be defined and shared in order to ensure cross-comparison between observatories and the detection of long-term trends. Future research will also contribute to a new, more environmentally responsible relationship between terrestrial society and the deep sea, in the form of regulations, best practices, environmental ethic, and societal awareness. Section on *Observatories and New Societal Approaches to Deep-sea Environments* discusses these new research avenues and how they can benefit from observatory infrastructure and associated maintenance cruises.

ESSENTIAL VARIABLES AND COMMON BEST PRACTICES FOR MID-OCEAN RIDGES (MOR) VENT OBSERVATORIES

The first workshop (IMOVE, working group, 2019) identified all variables currently measured or acquired by the different existing sensors at each established observatory. Each variable was then translated into an observable belonging to a biological, geophysical or geochemical domain (**Table 2**). As an example, a video camera (the sensor) allows counting the visible species (variable) to measure species distribution and abundance (observable) in the biology (domain) (**Table 2**). The final table revealed a number of commonalities among the three observatories highlighting the potential for defining common measurable characteristics. Based on this table and the list of common scientific questions, discussions during the second workshop resulted in a list of EOVs to be monitored across the different observatories. Some of the variables measured are mature EOVs, especially the ones related to physics and geochemistry. The biological related EOVs are not yet mature, most of the seabed ones are still at the merging phase, and the specificity of the different environments, require standardization and calibration (e.g., EOVs body size, or biomass or % cover, which are based on imagery, need a standardization towards automation, and calibration of surface observable, calibration size, weight, etc.). This list was built in light of work previously

TABLE 2 | List of variables currently measured at the three vent observatory platforms and the corresponding observables.

Domain	Observable	Variable	Instrument/Sensor	Observatory
Biology	Species abundance	Visible species	Video camera	OOI – ONC – EMSO
Biology	Species behaviour	Animal activity	Video camera	OOI – ONC – EMSO
Biology	Microbial colonization	Fluid samples	CISICS	EMSO
Biology	Microbial community composition	Fluid samples	PPS	OOI – ONC
Chemistry	Salinity	Conductivity	CTD	OOI – ONC – EMSO
Chemistry	Chlorinity	Resistivity	BARS/TRHPH	OOI – ONC – EMSO
Chemistry	pH, Eh (redox potential), H_2S	Redox potential (V)	THSPH/TRHPH	OOI – ONC
Chemistry	Oxygen concentration	Optic (phosphorescence quenching)	Optode	OOI – ONC – EMSO
Chemistry	Turbidity	Optical backscatter	Turbidity meter/Nephelometer	OOI – ONC – EMSO
Chemistry	Vent fluid chemistry	Iron concentration	CHEMINI	ONC – EMSO
Chemistry	Vent fluid chemistry	Fluid samples	RAS	OOI – ONC
Chemistry	Vent fluid chemistry	Fluid samples	DEAFS	EMSO
Chemistry	Diffuse vent chemistry	Fluid samples	OSMOI	OOI
Flow	Velocity, Flux	Particle displacement	Video camera (imagery/pixels)	OOI – ONC – EMSO
Physics	Seismicity	Seafloor acceleration	Seismometer	OOI – ONC – EMSO
Physics	Seismicity	Seafloor tilt	Tilt meter	OOI – ONC
Physics	Currents	Water movement	Current meter	OOI – ONC – EMSO
Physics	Currents	Particle displacement	ADCP	OOI – ONC – EMSO
Physics	Currents	Particle displacement	ADCP profiler	OOI – ONC – EMSO
Physics	Flux	Forward scattering	Acoustic scintillation	OOI – ONC
Physics & biology	Ocean soundscape	Passive acoustics	Hydrophone	OOI – ONC – EMSO
Physics	Deformation	Pressure	Bottom Pressure Tilt meter	OOI
Physics	Pressure	Pressure	Pressure gauge	OOI – ONC – EMSO
Physics	Seawater temperature	Temperature	CTD	OOI – ONC EMSO
Physics	High and low temperature	Temperature	Autonomous temperature sensors	OOI – ONC – EMSO
Physics	Diffuse vent temperature	Temperature	RAS	OOI – ONC – EMSO
Physics	Diffuse vent temperature	Temperature	TMPSF	OOI
Physics	High temperature	Temperature	BARS/TRHPH	OOI – ONC – EMSO

conducted by international networks including The Group on Earth Observations Biodiversity Observation Network (GEO BON; Pereira et al., 2013) and the Deep Ocean Observing Strategy (DOOS; Levin et al., 2019). A number of EOVs recommended by GOOS and DOOS were considered as observables to measure at vents in the context of seafloor observatories and associated maintenance cruises. **Table 3** reports these variables that can be measured and provides new ones to be considered when conducting observations at vents. **Box 2** summarizes recommendations issued during the second workshop.

The DOOS demonstration projects in the Azores and NE Pacific offer opportunities to feature hydrothermal vents within the concept of integrated observing (Levin et al., 2019). The linkage of multiple platforms and sensors operation both inside (observatories, repeat visits) and outside but proximate to the vents in these regions (e.g., Argo floats, Ocean Sites moorings, GoSHIP tracks, Ocean exploration activities, gliders), can contribute to a powerful multidimensional understanding in space and time of the external forces affecting vent communities and the influence of these ecosystems on surrounding environments.

Monitoring Long-Term Changes in the Context of Climate Change

By enabling sub-daily to multidecadal monitoring, seafloor observatories harbor a great potential to assess long-term changes in the context of climate change. The deep-sea is expected to lose oxygen, increase in temperature and change in pH (Levin and Le Bris, 2015; Sweetman et al., 2017; Levin et al., 2020). One big common question that the scientific community can tackle using an integrated approach is the impact of water column and subseafloor processes on global climate, not only through the emission of gases like CH_4 and CO_2, which in general are negligible, but also as organic carbon producers, CO_2 consumers, and O_2 consumption (Le Bris et al., 2019).

Processes identified during the first workshop that should be considered when addressing climate change are the carbon cycle and geochemical and thermal fluxes impacts on the ocean (**Table 1**). The next paragraphs summarse the recommendations issued during the second workshop.

In an environment characterized by high environmental heterogeneity over limited spatial scales, it appears essential to monitor background seawater characteristics. Although basic, this type of data is not routinely acquired today at all sites. EMSO developed, in the framework of the European Commission H2020 EMSODev project (Grant Agreement 676555), the EGIM, designed to continuously measure long-term series of key variables (Lantéri et al., 2022). EGIM is originally equipped with a CTD, ADCP, oxygen sensor, pressure temperature, turbidity meter and hydrophone to measure conductivity, precise pressure, dissolved O_2, turbidity, passive acoustics, and ocean currents but can host additional sensors. The module has been successfully deployed on a number of EMSO-ERIC observatories and can actively contribute to the international effort undertaken by the Global Ocean Observing System on Essential Ocean Variables (Levin et al., 2019; Sloyan et al., 2019).

TABLE 3 | Global Ocean Observing System (GOOS) Essential Ocean Variable (EOVs), additional EOVs proposed by the Deep Ocean Observing Strategy (DOOS) and new observables specific to ridges proposed by the InterRidge Integrated Multidisciplinary Observations at Vent Environments that can be measured by seafloor vent observatories, their associated surface buoys and/or during annual maintenance cruises (modified from Levin et al., 2019).

	Water column (Physics*)	Subsurface	Interface fluxes (Biogeochemistry*)	Interface Biological Responses (Biology and Ecosystems*)
GOOS EOVs	Sea state Ocean surface stress Sea surface height Sea surface temperature Sea Surface currents Sea Surface salinity Subsurface salinity		Oxygen Nutrients Inorganic carbon Particulate matter Transient tracer Nitrous oxide Stable carbon isotopes Dissolved organic Carbon	Fish abundance and distribution Hard coral cover and composition Ocean sound Microbe biomass and diversity Benthic invertebrate abundance and distribution
DOOS EOVs	Ocean turbulence	Ocean bottom Pressure	Seafloor fluxes	Body size
			Seafloor labile organic matter Seafloor fluid and gas effluxes (focus on methane) Litter including microplastics	Seafloor sponge habitat cover Connectivity of species
IMOVEs suggested observables	Ocean bottom temperature	Seafloor deformation	Heat and fluid fluxes and velocity	Engineer species cover
	Ocean bottom salinity Ocean bottom oxygen concentration Bottom currents	Seismicity Subsurface fluid flow Fluid chemical composition	Chlorinity Fluid chemical composition	Vent species behavior Pelagic species presence

BOX 2 – List of main recommendations from workshop 2

1. Climate change
   - Deploy an European Generic Instrument Module -EGIM- (Lantéri et al., 2022), or equivalent, to monitor key regional water mass characteristics at each site
   - Sample bottom and full water column seawater to conduct ground truthing chemical measurements and enable sensor calibration
   - Install cabled, instrumented profiling moorings for full water column measurements
2. Subsurface processes
   - Conduct 2D/3D seismic surveys to image subsurface features that include magma-mush zones, sills, and faults
   - Install arrays of broadband and short-period seismometers, low frequency hydrophones, and bottom pressure tilt instruments to monitor magma movement, seafloor deformation
   - Install temperature -chemical sensors in vents to inform fluid-rock reactions in the subsurface that are vent fluid sources
   - Utilize IODP capabilities for installation of cabled and uncabled CORKed Observatories that allow downhole measurements, sampling (fluid-biological), and cross hole hydrogeological experiments
3. Interface and biological response
   - Compile a list of recommended standardized protocols provided by experts to be applied during maintenance including sampling (i.e. microplastics, eDNA), video acquisition (fluid flux estimation)
   - Conduct seafloor routine transects with ROVs and AUV's to map megafauna abundance, geological and chemical features and litter distribution using common protocol acquisition and logging terminology (see "Biological Responses to Hydrothermal Forcing")
   - Consistently record vertical video transects during ascent and descent of submersibles
   - Quantify the magnitude and distribution of heat, chemical and biological fluxes
4. Water column: deep circulation, megaplume formation, fluid dispersal and connectivity
   - Deploy an array of full water column profiling moorings equipped with a diverse suite of instruments at distances of 500 m to 1 km to mimic the scales resolved by numerical models.
   - Conduct standardized routine vertical transect with CTD measurements and discrete fluid sampling

A first recommendation is thus to deploy an EGIM-like module at each observatory site, away from vent influence. This will require the definition of standardized instruments and calibration protocols and the development of new sensors, in particular for long-term pH measurements.

By measuring water mass circulation, dissolved oxygen concentrations, temperature, POC fluxes and chemical and heat exchanges, the vent observatory community can contribute to address some of the key questions raised by DOOS (Levin et al., 2019). However, because yearly maintenance involves recovery and redeployment of platforms, change in sensors and their potential location, some common good practices must be adopted to help make sense of data acquired, and are supported by existing Best Practices guides (Coppola et al., 2016). Groundtruthing measurements and sampling should be performed whenever possible and at every maintenance cruise. This includes oxygen calibration with Winkler measurements, characterizing seawater particulate load by sampling bottom water, *in situ* temperature

measurements using high resolution, reliable and properly calibrated temperature sensors.

The nature of the coupling of water column processes to benthic processes is critical to understanding the ocean's carbon cycle and its link to climate change and biodiversity (Cathalot et al., 2021 and reference therein). Long term observations of benthic-pelagic coupling can address vent stimulation of photosynthetic productivity or dark carbon fixation, influences on microbes, pelagic larvae and adults of vent and non-vent species, and alteration of food supply for mixotrophic vent species (Levin et al., 2016). These have relevance for the biological pump and opportunities for carbon sequestration. Newly developed seafloor rovers such as RB-II or other benthic crawlers that have potential to track carbon inputs, remineralisation rates and oxygen levels can associate with cabled observatories to obtain power and transmit data in association with other observatory monitoring (Smith et al., 2021).

Crustal and Sub-Surface Processes

During the first IMOVE workshop, several processes were identified as important when addressing subsurface processes: seafloor dynamics including compliance and ground deformation, plumbing system and fluid flow geometry, subsurface characterization, crustal geothermal signature, subseafloor microbial communities, and forcing of sub-seafloor processes on seafloor systems (**Figure 5** and **Table 1**). Similarly, the first workshop identified several processes as important when addressing fluid fluxes and heat exchanges at the interface: forcing of sub-seafloor processes on seafloor systems, chemical signature, dynamic coupling of diffuse/focused venting, crustal plumbing system and fluid flow geometry, phase separation, and sub-surface and post-exit fluid mixing (**Figure 5** and **Table 1**).

During the workshop, several approaches were proposed to better constrain models of fluid circulation and characterize fluid flux dynamics on a local scale. Repeat mapping of smoker vents at certain sites (e.g., Barreyre et al., 2012; Girard et al., 2020) can help better characterize the long-term changes and stability of vent circulation in different ridge settings. Such repeat mapping could occur during maintenance cruises by a submersible or by future drones linked to connected or autonomous benthic docking stations allowing power recharge and data transfer (see section on *Ocean Sensing Technology and Future Directions*). Taking this standardized approach to fluid flow characterization will foster comparison among different ridge systems and help better understand how temporal and spatial changes in the distribution of hydrothermal venting impacts ecosystem stability and species' adaptation to their environment (e.g., reproductive biology, growth, mobility). A benefit of the above approach is the ease with which it could be extended to other systems where repeated visits allow for temporal monitoring (e.g., East Pacific Rise, Lau Basin, Guaymas Basin).

As part of repeated monitoring efforts, the use of non-invasive video sequence analyses could be key for volume, heat, and chemical flux estimations at smoker vents. Using pixel-based correlation methods (Particle Image Velocimetry or Diffuse Fluid Velocimetry; Crone et al., 2010; Mittelstaedt et al., 2010; Mittelstaedt et al., 2012; Escartín et al., 2015; Puzenat et al., 2021), the flow of high-temperature and low-temperature fluids can be estimated with reasonable accuracy and in relatively short image capture sequences. To allow uniform, inter-comparable results using these techniques requires a common protocol with guidelines for image acquisition (camera distance; use of chessboard for image calibration; Escartin et al., 2013; minimum image resolution and frame rate guidelines), the implementation of a user-friendly computer program to process images as part of routine maintenance visits to vent sites, and sufficiently stable imaging platforms to avoid image motion related to currents and/or vehicle motions. To constrain heat and chemical fluxes, the above techniques for estimating flow rates should be coupled with simultaneous exit-temperature and near-simultaneous fluid sampling data.

Biological Responses to Hydrothermal Forcing

Processes identified during the first workshop that should be considered when addressing biological responses at the interface are: chemical signature, dynamic coupling of diffuse/focused venting, mixing, recruitment dynamics, energy flow and fluxes (**Figure 5** and **Table 2**).

A number of common variables were identified as potential ridge EBVs and were discussed in relation to the work already done by Significant Ecological Components (SECs, DFO, 2006), DOOS (Levin et al., 2019) and GEO BON (Pereira et al., 2013). Variables that can contribute to the ones already defined or proposed by GOOS and DOOS respectively, are presented in **Table 3**, and new ones are proposed in the context of ridge monitoring. Repeated visits and cameras deployed on the seafloor provide information on species presence/absence, faunal abundance in relation to oceanographic variables. However, because it is not possible to generalize fixed-point observations to regional scale, routine transects should be conducted during cruises when possible to extend the spatial extent of observations. Protocols should be standardized and shared to enable large-scale comparisons and should include the use of a common real-time dive logging strategies and terminology (i.e. annotation of fauna, geological or chemical features, litter) (Schoening et al., 2020). Alternatively, this acquisition could be achieved by resident drones or AUVs in parallel with chemical and geological features mapping (see section on *Ocean Sensing Technology and Future Directions*). Time-series observations should focus on species and habitats that are indicators of change (e.g., Sarrazin et al., 2015). Deep pelagic ecosystems represent more than 90% of the biosphere but remain the most unexplored and least understood environment (Webb et al., 2010). Maintenance cruises can contribute to enhancing our knowledge of this ecosystem by routinely recording vertical video transect during the ascent and descent of submersibles, coupled with CTD measurements and discrete water samples.

Video imagery collected during observatory maintenance activities is a potentially important and currently undervalued source of information on the spatial distribution and biomass of visible vent and non-vent organisms and on seasonal and inter-annual variability in species abundances and diversity. A structured approach to real-time and post-cruise annotations of

video records can greatly increase their usefulness for extraction of biodiversity information. The value of these annotations can be further enhanced by the standardization of vocabularies and their alignment with recognized terms used by international organizations such as the World Registry of Marine Species (WoRMS). Ocean Networks Canada has recently collaborated with WoRMS and the US National Oceanic and Atmospheric Administration (NOAA) Office of Ocean Exploration & Research (OER) to develop a standardized video annotation system. The SeaTube interface allows users at sea or *via* telepresence to annotate live video streams, and permits post cruise annotation of ROV video recordings. Annotations may be entered as free-format text or structured annotations adhering to custom or standard taxonomies (such as WoRMS, CMECS, etc.). Ancillary data from both ROV and ship mounted sensors are also displayed in conjunction with the video, all synchronised with the video timestamp (**Figure 6**). Live links to the WoRMS database while annotating allows for near-real-time validation of species identifications against known geographic distributions, and the flagging of potential new occurrences or identification errors.

Finally, maintenance cruises represent unique opportunities for repeated sampling and have enabled a better characterization of the geological, geochemical and biological settings of vent ecosystems (see section 2). These cruises should be further used to collect opportunistic samples following standardized protocols to monitor microplastics distribution, environmental DNA (eDNA), or other EOVs and pollutants but also to characterize ecosystem function and services (Danovaro et al., 2020). One solution to optimize the acquisition and processing of samples is to involve and offer access to cruises for external researchers which will contribute to fostering a mutualisation of the infrastructures. Such an effort is currently under development within the EMSO-Eric through the establishment of access services including the Transnational Access (TNA) to EMSO ERIC observatories (https://emso.eu/transnational-access/).

Water Column: Deep Circulation, Fluid Dispersal and Connectivity

Processes identified during the first workshop that should be considered when addressing fluid dispersal and connectivity are: plume characterization and dispersal, turbulent mixing and energy dissipation, forcing of ocean dynamics on seafloor systems, connectivity between vents, seafloor topography, mounds, ridges, and role of ocean circulation on larval and free-living microorganisms dispersal (**Table 2**).

One of the next challenges needed to be addressed in deep-ocean modeling with likely implications for Lagrangian spreading is the representation of the thermal plume dynamics. Due to the lack of sustained measurements in the deep ocean, spatial scale coverage, assessing the realism of numerical models remains arduous. Another challenge is to understand if the mesoscale processes are periodic, or asynchronous, having implications on the connectivity of species, and consequently succession patterns and community resilience. Numerical models of the deep-ocean circulation are now routinely reaching submesoscale-resolving and internal wave-resolving resolutions (dx<1 km). Although the phenomenology of resolved processes is widening, uncovering smaller eddies and turbulent processes, we lack a trustworthy 3-D *in situ* picture to assess the models' performances. A rather low-cost solution to address this limitation would be to deploy an array of moorings equipped with deep T-S sensors and current-meters and distant by ca. 1 km to mimic the scales resolved by numerical models. This would allow the measurement of the gradients of the essential properties of oceanic flows, i.e., velocity and density, and a direct comparison with modeled data.

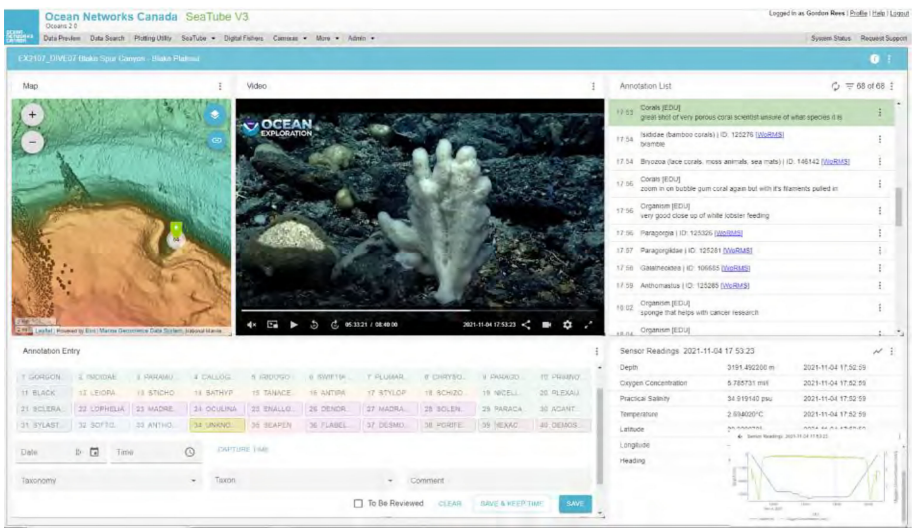

FIGURE 6 | Example of video annotation interface for SeaTube 3.0 showing location of ROV on seafloor bathymetry, a deep-sea coral of interest, and the user-designated annotation options available for identifying the coral. Sensor data from the ROV are also linked to the annotation. Screen capture courtesy of NOAA Office of Ocean Exploration and Research.

The routine acquisition of EOVs currently not measured on autonomous observing systems requires the development of new technologies and sensors, more particularly for biological and biogeochemical variables that currently require *in situ* sampling. The collection of samples calls for dedicated time during the yearly maintenance cruises which are already demanding in terms of human and operational resources. The group agreed on the need to reduce and optimize maintenance cruises and several solutions made possible by the current technological developments emerged (see section on *Ocean Sensing Technology and Future Directions*).

OCEAN SENSING TECHNOLOGY AND FUTURE DIRECTIONS

R&D activities on ocean observing sensors is expected to reach USD 128.56 billion by 2025, registering a CAGR of 8.86%, during the period of 2020-2025 (van den Burg et al., 2021). The global underwater drone market integrating these sensors is projected to reach USD 7391 million by 2027, registering a CAGR (i.e. Compounded Annual Growth Rate) of 11.7% (van den Burg et al., 2021). The reason for this growth is the need for precise, reliable, and pervasive sensing technology to measure and follow multiscale spatio-temporal dynamics of ocean physical, geochemical, and biological processes. This technology aims to explore and quantify the role of the ocean and seafloor processes in climate change, in provisioning of rare minerals and unexplored biological resources, and availability of biomass. The future directions on ocean sensors development are within the design of i) novel sensing technology, such as underwater mass spectrometer, eDNA collectors and *in situ* sequencing, ii) energy efficient and/or resilient solutions to minimise battery consumption and/or harvest ocean energy, iii) use of Artificial Intelligence (AI) to reduce energy/data storage by "pre-filtering" data or allow adaptive sampling, and iv) new networking architectures that integrate the sensor networks at the surface, e.g., as described in Aguzzi et al. (2019) and Mariani et al. (2021) with the underwater sensor networks.

Sensing and Monitoring Platforms

Platforms that integrate ocean sensors and operate over a long time at sea can be fixed, e.g., surface buoys, moorings and landers, or mobile such as Argo floats, crawlers, surface vehicles, gliders and Autonomous Underwater Vehicles (AUV) (Aguzzi et al., 2019; Rountree et al., 2020). These platforms can be cabled with power and data transmission ensured from the shore - but unchangeable location strongly constrains the cable route and price -, or wireless with battery and data storage capabilities dimensioned according to the duration of the foreseen deployment on board the seabed station (Matabos et al., 2016). The future directions on platforms' development need to address a number of limitations highlighted through the experience acquired over a decade of operation (also see Rountree et al., 2020): i) The operational cost is high, partly because underwater vehicles are required for maintenance operation to place the sensor with precision and perform underwater connection; ii) the time between the maintenance operations is limited due to requirement for sensor calibration and, in case of wireless system, for energy pack and data storage replacement; iii) the spatial coverage is limited to the close surrounding of the seabed station; iv) new regulation will urge for new deployment processes with low environmental footprint; v) a larger number and variety of sensors are fundamental for multidisciplinary approaches and the amount of energy and volume of data storage needed keeps increasing.

These limitations call for technological and operational breakthrough, and the future trends in fixed-point long-term observation are central to developments going on in the field (**Figure 7**). First, decreasing operational cost requires combining

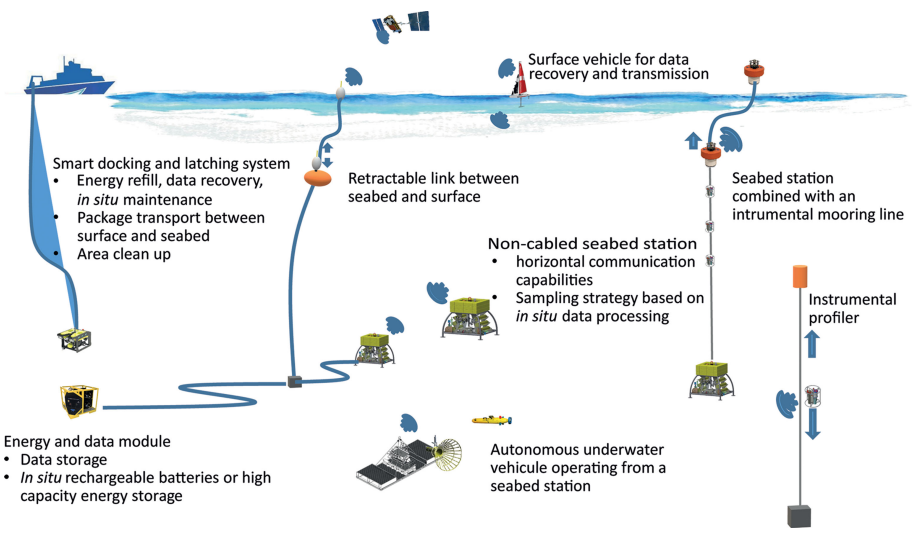

FIGURE 7 | Illustration of future technological and operational breakthroughs to reduce deployment and maintenance cost and reduce environmental footprint.

various efforts to reduce the time and means required for maintenance operation at sea. In terms of means, this can be achieved by improving the global robustness of the system to insure the endurance to meteorological and other heavy environmental conditions. Surface buoys relaying the information to the shore, sensitive to storms, can be replaced by autonomous surface vehicle patrolling to recover the data weather permitting. The development of submarine tools specialized and optimized for deployment and recovery of systems could carry out the maintenance from a small ship instead of large multipurpose ROVs. Wireless contacts to recharge batteries and recover data would avoid plugging connectors underwater and can reduce the number of packages to be recovered onboard for refurbishing and contribute to reducing time at sea (Aguzzi et al., 2019). Increasing the intervals between maintenance requires technological developments at the platform and sensor level. For a wireless autonomous system, the amount of energy and data storage volume available are fundamental parameters to determine maintenance frequency considering the growing ambition of observatories (more sensors, better images definitions, etc.). Spare energy and data storage require establishing strategies to collect the data (e.g., optimize multidisciplinary integration and reinforce collaborative strategies), reduce the duration of measurements, and/or trigger measurements on predictable (foreseeable) events detected using sensors with low power needs or using *in situ* decisions based on IA algorithms for pattern recognition (Aguzzi et al., 2022). An alternative is to harvest energy in small yet decisive quantities from heat exchange occurring at mid-ocean ridges. Technologies are progressing quickly and high capacity energy and data storage are expected in the coming years. As an example, optical fibre cable, supporting fast data transmission, can also power over a few kilometres from the central station low consumption sensors (Matsuura, 2021). This technology by reducing the cable cost also contributes to extending the observations spatial coverage.

Extended spatial coverage is a challenge for ocean observation. Fixed observatories, in particular, give a very partial view of the seafloor generally limited to a few meters around the central place (Rountree et al., 2020). There are already a few examples of static or moving devices expanding the scope around the central station, for instance the 100 m thermistance chain deployed on EMSO Azores or the Internet Operated Deep-Sea Crawler Wally (Chatzievangelou et al., 2020) at ONC. Developments are on the way to deep-sea autonomous mobile vehicles operating from a seabed station with large excursion capacities and wireless docking stations to refill batteries and download data (e.g., Costanzi et al., 2020). However with the technologies presently available to store the energy, the feasibility of a vehicle operating around a non-cabled observatory is not conceivable and will be first limited to cabled observatories. Things are however changing very quickly in this field. Fuel cells tomorrow, or quantum batteries in the future, could drastically increase the amount of energy available.

Finally, environmental footprint concerns appeared some 10 years ago and the number of marine protected areas has increased since then. Research activities and observations are a source of disturbance to marine ecosystems (Juniper et al., 2019) and constitute an additional constraint when designing observation systems and operation scenarios.

Internet of Things (IoT)

These platforms can communicate at the surface through IoT protocols, as described in Mariani et al. (2021) or underwater through underwater acoustic, optical, and/or magnetic inductive modems. Acoustic waves propagate over long ranges (orders of km) but can transfer limited data rate (some kpbs) optical modem can reach a few tens of meters with data rates of up to 500 kbps and finally magnetic inductive modems can support contactless data transfer (very short range few cm). Even though the internet of underwater things (Jahanbakht et al., 2021) is a concept introduced a decade ago, and underwater sensor networks have been studied for two decades (Heidemann et al., 2012), it is only recently that *in situ* underwater networks have been deployed for scientific and industrial use cases (Qiu et al., 2019). Examples of services enabled by this technology are:

(1) Real-time data transfer to a node connected to the end user through IT infrastructure.
(2) Machine-to-machine communication to remotely operate instrumentation, e.g., in hazardous conditions.
(3) Extended spatial coverage data acquisition through resident autonomous drones.
(4) On-demand data offloading of standalone sensors.

The challenges of underwater acoustic communication relate to the impact of environmental factors on acoustic waves propagation in shallow and deep water (Tomasi et al., 2010; Tomasi et al., 2011). In deep waters, variations in sound speed alter the direction of propagation of acoustic waves (i.e., sound refraction). This causes shadow zones and reflected echoes from seabed also affects communication.

The future directions on underwater networks development are within the design of novel networking solutions where both stationary and mobile nodes can connect and coordinate towards a common mission defined by the end user and provide an underwater positioning system. One shift of paradigm that could be enabled by this development is going from ocean observatories to *in situ* ocean laboratories and virtual laboratories.

Geochemical Sensors

Along with the evolution of the platforms, a larger number and variety of sensors are expected to complement data acquisition. The sensor required for ocean measurements has undergone various phases of technological advancements to meet requirements of robustness, reliability and low maintenance in harsh environments. Some examples of the last technology available to measure chemical properties are based on optical measurement. Optical sensors provide conventional measurements by providing highly stable values for long term applications. As an example, the ECO (Environment Characterization Optics-SBE) technology is used for measuring various parameters such as turbidity, fluorescence, Colored Dissolved Organic Matter (CDOM), Photosynthetically Active Radiation or chlorophyll. For pH, usage

of glass electrode-based measurement often poses challenges at remote locations in the ocean and are prone to drift with errors. The recent advancement in pH measurement is by using the state-of-the- art ion-sensitive electronic devices such as ion-sensitive field effect transistors [ISFET type sensor, SeaFET - Seabird Electronics (SBE)] that uses advanced transistor-based technology. The MBARI Submersible Ultraviolet Nitrate Analyzer (SUNA) and In Situ Ultraviolet Spectrophotometer (ISUS) provide a highly stable measurement of nitrate over a wide range of environmental conditions although their sensitivity and accuracy are poorer than those of wet chemical analyzers in conditions of high turbidity and high CDOM (Daniel et al., 2020). These sensors use technology based on the absorption characteristics of nitrate in the UV light spectrum. *In situ* pCO_2 values of seawater are measured using 4 broad approaches such as gas based, electrochemical, wet-chemical or fluorescent. The partial pressure of carbon dioxide in surface ocean waters is a key parameter used to study ocean CO_2 absorption, acidification, primary productivity, carbon cycle, source, and sinks of CO_2, and biogeochemistry. Finally, better understanding metals transfer from the hydrothermal sources to the open ocean column needs the development of sensors capable of measuring trace metal micronutrients at levels found in the open ocean. There is a clear gap in the development of more sensitive techniques for trace metal analysis and the sensor support infrastructure needs to be redesigned to fully access their dynamic distribution and impact on ocean productivity (Grand et al., 2019).

Biological Sensors

One example of technological development in the last decade that includes these three technological developments is represented by high-throughput sequencing solutions that are increasingly used in ecology and environmental management studies. eDNA studies are also applied in the deep ocean (Laroche et al., 2020). The available technology requires *a priori* knowledge of deep-sea taxonomy, meaning that a large effort of species barcoding is needed (Cowart et al., 2020). However, in well-known areas observatory site time series where fluid/DNA samplers exist and are coupled to fluid-temperature samplers, we can track changes in microbial communities over time and in response to perturbation events (e.g., Huber et al., 2003; Fortunato et al., 2018). Because lifeforms in the ocean contain or leave behind a biomolecular trace that can be analyzed directly from a seawater sample, 4D seascapes could be a possibility with the development of multi-omic biodiversity sensing capabilities by integrating probes or sensors to existing observing systems (Stefanni et al., 2022). These latter offer the opportunity to integrate additional concomitant biological, biogeochemical and physical parameters to take in consideration the influence of habitat heterogeneity, fluid and larvae dispersion, as well as regional and local oceanography.

If eDNA and other high-throughput sequencing technologies hold great promise to uncover the multiple facets of deep-sea biodiversity, understanding fundamental processes involved in population's persistence and resilience still requires observations of the organisms themselves, throughout their life cycle, particularly at early life-stages. The development of biophysical modeling to predict connectivity patterns simulating larval trajectories requires *in situ* observations for model validation and biological parametrization. Taking advantage of the infrastructure of established observatories, where combinations of existing plankton collection tools could be integrated, would most effectively foster rapid advancement in deep-sea larval biology. For example, large volume plankton samplers such as the SyPRID currently deployed on the Woods Hole Oceanographic Institution Sentry AUV (Billings et al., 2017) could be further developed and miniaturized for integration with other platforms, such as small mobile long-range vehicle docking on a seabed station, which could greatly expand the spatial coverage of deep-sea plankton observations. Development of imaging, automated taxonomic identification through machine learning algorithms, and adaptive sampling can also accelerate deep-sea larval research. Recent technological advancements in *in situ* plankton imaging such as the Underwater Vision Profiler (UVP, Picheral et al., 2010) or holographic cameras (e.g., LISST-Holo2, Sequoia, Lombard et al., 2019) are currently being further developed for deployment on diverse deep-sea observing platforms (e.g., Picheral et al., 2021). New imaging techniques are currently under development to document spawning or larval settlement events in conjunction with multi-parameter sensors to identify environmental cues or oceanographic patterns driving life cycles in the deep sea. Machine-learning can allow for rapid identification of high-volume image samples, as well as enable the collection of higher-resolution samples following detection of an anomaly (adaptive sampling). While such technological innovation could greatly accelerate our knowledge on deep-sea benthic and planktonic communities, most deep-sea species are still undescribed in their adult form, and this is only amplified for their larval forms. Therefore, their identification from images still requires the collection of physical specimens for morphological or genetic analyses, which will feed biodiversity baseline databases and provide training sets for machine learning (e.g., Stefanni et al., 2022).

OBSERVATORIES AND NEW SOCIETAL APPROACHES TO DEEP-SEA ENVIRONMENTS

Seafloor observatories are a natural platform for collaboration within the ocean science and technology sectors and offer unique opportunity for demonstrations to the public and policy makers about oceanic and ocean floor processes that can stimulate society's interest in the marine realm and impacts that society is having on oceanic processes. Looking to the future, seafloor observatories have an important role to play in understanding and mitigating the effects of climate change and resource exploitation on deep-sea ecosystems.

A Tool to Inform Environmental Managers and Policy Makers

Because observatories constitute technological development platforms, they can support the design, testing and implementation of environmental monitoring strategies and evolve with new emergent technologies and the innovation of instrumentation for sustained, systematic data acquisition (e.g.,

Danovaro et al., 2017a). The Endeavour nodes of ONC and EMSO-Azores are both located within an MPA. Together, these seafloor infrastructures constitute an essential tool to inform MPA management and efficiency for the benefits of the local governments but also of international instances such as the International Seafloor Authority (ISA) which is currently developing the standards and guidelines of the international mining code. As an example, ONC has developed SeaTube (**Box 1**), a software system for assembling ROV dive navigation logs and video records, including real-time annotations, into an online archive and a GIS database. The database can be queried to generate maps for researchers and MPA managers that illustrate the spatial distribution of seafloor features of interest. Juniper et al. (2019) provide examples of how this geodatabase can be used to analyse the distribution of species of interest, debris, and human pressures resulting from research activity. All observatory sensor data and ROV expedition video and navigation records from the Endeavour Hydrothermal Vent MPA are archived and made publicly available by ONC (**Box 1**). The combined data archive therefore has the potential to support adaptation of the EHV MPA management plan and conservation objectives to a growing understanding of natural rates and scales of environmental and ecosystem change, and the spatial distribution of research activity.

To standardize and implement these conservation objectives at a larger scale, regular workshops should be organized with various stakeholders, including the ISA, State environmental ministries, Non-Governmental Organisations (NGOs), Business/Industry, Science Networks and the civil society to identify their respective needs and work towards the co-design, co-development and co-delivery of commonly defined monitoring approaches and tools. Sustained funding together with governance are required to guarantee future long-term systematic observations.

Outreach and Education

Real-time data available on-line and the associated data archives are an under-tapped resource for educational purposes and for general public communication. Hydrothermal systems are dynamic, and the different links between physical and biological processes could be included in education curricula, at all levels. The associated annual cruises also provide unprecedented opportunities to develop outreach and educational projects. The colossal imagery archive of hydrothermal systems can be exploited and showcased to attract the general public's interest towards these systems in particular, and oceanography and deep-sea research in general, while increasing the awareness regarding the unknown and endangered ecosystem that the deep ocean still has to reveal fully both to science and society. In the context of increased anthropogenic activities, it is of utmost importance to engage with the next generation and inform the society about our research, especially since they occur in inaccessible areas.

For the last 10 years, various original actions have been proposed in all three observatories to make the science, the people and life onboard accessible to the public. Primary outreach activities are related to maintenance expeditions at sea at all three MOBs (**Box 3**). At Ocean Networks Canada, live-streaming video with commentary by shipboard personnel allows members of the public to follow ROV dives and on-deck action on the research vessel. The audience for these live streams has been greatly augmented in recent years through a partnership with the Ocean Exploration Trust (OET). ONC has frequently chartered the Exploration Vessel Nautilus with Hercules ROV to perform maintenance activity at the Endeavour observatory. OET has a large global audience for their Nautilus Live program and Education and Outreach staff on the vessel are experienced in interpreting science for the public, providing live commentary during dives and fielding questions from the online audience. OET's Science Communication Fellowship and Science and Engineering Internship Program allows educators and students to join the outreach staff at sea.

A well-established University of Washington experiential at-sea learning program 'VISIONS' supports outreach at the Axial Seamount component of OOI's RCA. Since 2010, over 160 undergraduate and graduate students have participated in this uniquely interdisciplinary, hands-on at-sea program that provides training in research and engagement related to many important oceanographic processes operating within the Northeast Pacific ocean and on the seafloor. The oceanographic expeditions are an important component of the National Science Foundations' OOI RCA operations and maintenance cruises using the global class research ships the R/V Thompson (University of Washington, UW), the R/V Revelle (Scripps Institution of Oceanography, SIO), and the R/V Atlantis (Woods Hole Oceanographic Institution, WHOI). All cruises utilize state-of-the-art underwater robotic vehicles (ROV) that allow students to directly witness some of the most extreme

BOX 3 – Outreach activities and materiel related to observatories

EMSO-Azores

Educational resources for the public and researchers:www.deepseaspy.com (see educational resources tab)
Artistic creations: https://www.teatrpiba.bzh/en/
3D immersive visit: https://www.youtube.com/watch?v=hNK1MERlzaY

Endeavour component of ONC

Training and outreach resources: https://www.oceannetworks.ca/learning
Sight and sounds: https://www.oceannetworks.ca/sights-sounds

Regional Cabled Array – Axial Seamount

Educational website https://interactiveoceans.washington.edu/
UW Regional Cabled Array educational Data Portal https://app.interactiveoceans.washington.edu/
Blog to chronicle eruption forecasts at Axial Seamount https://www.pmel.noaa.gov/eoi/axial_blog.html

environments on Earth. On all annual expeditions, similar to ONC, live video is continuously streamed from the ship and from the ROV's to viewers around the globe. In addition, the UW RCA team has developed the interactiveoceans website (**Box 3**) that provides rich and diverse content about the RCA sites, technologies, expeditions and educational components of the RCA.

In addition to live interactions during cruises, other original actions have been developed including, among others, participative science and art & science projects. AbyssBox, the first permanent public exhibition of live deep-sea hydrothermal fauna maintained at *in situ* pressure (170 bars, Shillito et al., 2015), is a first step towards maintaining a variety of deep-sea fauna year-round, serving both scientific and public purposes. The Deep Sea Spy (DSS) project (**Box 3**), developed by Ifremer allows society to be involved in the research process by contributing to the annotation of deep-sea hydrothermal vent imagery acquired by seafloor observatories. To date, over 1300 citizens annotated almost 50,000 images through the DSS platform building a reference database for machine algorithms developments. This alternative approach to the study of ecosystems, by increasing public engagement, also provides scientific transparency which can improve the credibility and relevance of the research process. The SPLUJ and DONVOR (**Box 3**), two radiophonic theatre plays, co-created in 2018 by Ifremer scientists and the professional theatre company Teatr PIBA, invite the public to explore the unknown and the imaginary by "doing" and "living" in a complete sensitive immersion. This artistic approach helped take up the challenge to reach "different" public: those who are not naturally attracted to science or those living far from the ocean. To date, over 22 000 spectators have assisted to one of the plays and over 50 representations are expected in 2022. Finally, the visit of the Tour Eiffel edifice in an immersive environment using virtual goggles provides a unique way to experience and comprehend an otherwise inaccessible environment (**Box 3**). This innovative way of accessing the deep ocean significantly increases the outreach potential to raise ocean awareness in the general public. It is essential to develop a wide range of outreach material exploring all five senses to reach the widest range of people. Collaboration with artists, writers and musicians, whose multifaceted visions allow us to explore the unknown in original and diverse fashions, can help meet this objective.

The DSS project supported the development of educational resources for kids from 3 to 11 years old (**Box 3**), promoting the use of the annotation online platform as a tool in school programs. Similar resources, based on the use of data, can support programs for students in middle school and high-school in several languages. Immersive environments offered by virtual goggles, such as the one developed with the active edifice Tour Eiffel, can allow « field work » in remote environments, including exploration, observation and annotation and harbor valuable application in training by bringing students on a «field trip». More should be achieved with kids and young people in Least Developed Countries (LDCs) and Small Island Developing States (SIDs), more particularly those in the Pacific and the Caribbean Sea that are increasingly concerned with future deep-seabed mining.

While some of these projects result from individual/few scientist initiatives, an important step could be achieved by hiring communication specialists dedicated to each observatory, especially to cope with the numerous media available (e.g., Youtube, Instagram, Twitter). For example, in the EMSO-ERIC European infrastructure, a communication service group exists but is composed of overloaded scientists/engineers and has no targeted budget. At ONC, a communications team supports outreach activities during expeditions that use the Nautilus, and ensures at-sea outreach activities during maintenance expeditions that use other vessels and ROVs.

CONCLUSIONS

The InterRidge IMOVE workgroup aimed to internationally coordinate and optimize ridge seafloor infrastructures in terms of technology, scientific questions through a multinational and multi-collaborative endeavor. However, given the variability of hydrothermal systems, particularly at slow-spreading ridges, it is also clear that this limited number of sites, focused in magmatic ridge systems, do not cover key hydrothermal systems such as those that are hosted in peridotite, or displaying only low-temperature hydrothermal outflow and temporal studies at these distinct systems are required.

This review offers an overarching umbrella that can help community-based experiments to react to specific events, and help in designing, as well as coordinating observatory maintenance and complementary samples during cruises. The paper presents the state of the art in terms of results and advances enabled by these observation systems, as well as data, tools and the infrastructure available to address scientific, technological, educational and societal issues. Data acquired the last 10 years enabled great advancement in our understanding of ridges, and more particularly vent ecosystems dynamics. The next step will be to integrate across disciplines to better constrain the overall ecosystem functioning, from geological processes to biological communities' distribution and responses. This can be achieved by a joint effort in defining common variables, sensors and protocols for complementary systematic samples and data acquisition. Science service groups, such as the ones proposed through the EMSO network can help propagate ocean good practices guidelines of surveying ecosystems from the seafloor to the water column and create a global capacity development initiative that includes data management and accessibility. A wealth of data is being acquired through a number of observing programs and observatories in coastal and global oceans. An effort should be made to link the data to surrounding observations (e.g., Argo, deep Argo, GoSHIP, OceanSITES, OTN) in order to reach an integrated and multidisciplinary understanding of ecosystems functioning at the regional scale. More particularly, the DOOS proposed region-specific

interdisciplinary projects to demonstrate the feasibility of sustained deep-ocean observing. Two of the three proposed locations include the Azores Archipelago and the Northeast Pacific from the Cascadian Margin to the Juan de Fuca Ridge. The implementation of such projects provides the opportunity to develop a community-based approach for large-scale interdisciplinary studies, placing the ridge environment and its influence at the heart of the global ocean.

Our ten years' experience also proved that observatories constitute great means to involve and inform the society about the importance of the deep sea and the challenges we are facing to maintain a healthy ocean and the ecosystem services it provides. However, more should be done to expand our capacity building endeavor and widen the public to be reached. The scientific community needs to imagine new ways to exchange outreach, arts & science experiences across observatories by building dedicated communication plans. The complexity of marine ecosystems in relation to climate change and other anthropogenic impacts confronts us with the need to interact with many scientific disciplines. Researchers from fields in Social and Human Sciences need to be involved to conduct science in the context of sustainability and socio-ecosystems and help develop regulations. They can help in new ways to engage public and policy makers/public administration and advise environmental scientists in the development and management of multi and transdisciplinary studies in order to optimize the societal scope, including the traditional knowledge holders where feasible, and impact of deep-sea research projects in accordance with today's society mandates.

AUTHOR CONTRIBUTIONS

MM and TB led the working group, conceived the review and wrote the first draft of the manuscript. All authors contributed the manuscript ideas and text. All authors read and approved the final manuscript.

FUNDING

The first workshop in Bergen was additionally funded by the K.G. Jebsen Centre for Deep Sea Research and the University of Bergen. The second workshop was supported by ISblue project, Interdisciplinary graduate school for the blue planet (ANR-17-EURE-0015) and co-funded by a grant from the French government under the program "Investissements d'Avenir". Additional funding was provided by Ifremer, and the département du Finistère. The operation and maintenance of the EMSO-Azores observatory is funded by the by the EMSO-FR Research Infrastructure (MESR), which is managed by an Ifremer-CNRS collaboration. The operation and maintenance of the Endeavour observatory is funded by the Canada Foundation for Innovation's Major Science Infrastructure program and the Department of Fisheries and Oceans (Canada). The operation and maintenance of the Axial Seamount observatory is funded by the National Science Foundation as part of the Ocean Observatories Initiative Regional Cabled Array. MM, JS and PMS acknowledge funding from the EU Horizon 2020 iAtlantic project (Grant Agreement No. 818123). AC was supported by the Operational Program AZORES 2020, through the Fund 01-0145-FEDER-1279 000140 "MarAZ Researchers: Consolidate a body of researchers in Marine Sciences in the Azores" of the European Union. She was also supported by FCT – Foundation for Science and Technology, I.P., under the project UIDB/05634/2020 and UIDP/05634/2020 and through the Regional Government of the Azores through the initiative to support the Research Centers of the University of the Azores and through the project M1.1.A/REEQ.CIENTÍFICO UI&D/2021/010.

ACKNOWLEDGMENTS

The authors acknowledge the support of the InterRidge office in Paris, Nadine Lebris, Jérôme Dyment and Kamil Szafrański. Thanks to Jina Mousseau (ONC) for creating **Figure 3**. We thank the captains and crews of the research vessels that enabled infrastructure maintenance: RV Pourquoi Pas?, RV L'Atalante, RV Thalassa, CCGS John P. Tully, RV Thomas G Thompson, EV Nautilus. We are also grateful to the pilots of the submersible Nautile, Victor6000, ROPOS, Hercules, Argus, Odysseus. The work reviewed in this paper would have not been possible without the help of all mechanical, electric and computer engineers and technicians from Ifremer (RDT and RIC), ONC and OOI. The working group was supported by InterRidge (2017-2020). Other participants in IMOVE Working Group: Lise Artigue, Loïc Van Audenhaege, Valérie Ballu, Catherine Borremans, Greace Crystle, Cécile Cathalot, Jerome Dyment, Aida Farough, Anne Godfroy, Sabine Gollner, Zhikui Guo, Orest Kawka, Noé Lahaye, Marie Eide Lien, Anna Lim, Jean-Arthur Olive, Giuliana Panieri, Rolf Birger Pedersen, Eoghan Reeves, Celine Rommevaux, Guillaume Roullet, Lars Rüpke, Ben Snook, Adam Soule, Kamil Szafranski, Julie Tourolle, Benjamin Wheeler. Finally the group would like to thank two reviewers K. Anantharaman and D. M. Toma and Editor Jacopo Aguzzi for their comments.

REFERENCES

Afanasyev, A., Blundy, J., Melnik, O., and Sparks, S. (2018). Formation of Magmatic Brine Lenses *via* Focussed Fluid-Flow Beneath Volcanoes. *Earth Planet. Sci. Lett.* 486, 119–128. doi: 10.1016/j.epsl.2018.01.013

Aguzzi, J., Chatzievangelou, D., Marini, S., Fanelli, E., Danovaro, R., Flögel, S., et al. (2019). New High-Tech Interactive and Flexible Networks for the Future Monitoring of Deep-Sea Ecosystems. *Environ. Sci. Technol.* 53, 6616–6631. doi: 10.1021/acs.est.9b00409

Aguzzi, J., Flögel, S., Marini, S., Thomsen, L., Ibiez, J., Weiss, P., et al. (2022). Developing Technological Synergies Between Deep-Sea and Space Research. *Elementa Sci. Anthropocene* 10, 1–9. doi: 10.1525/elementa.2021.00064

Alfaro-Lucas, J. M., Pradillon, F., Zeppilli, D., Michel, L. N., Martinez-Arbizu, P., Tanaka, H., et al. (2020). High Environmental Stress and Productivity Increase

Functional Diversity Along a Deep-Sea Hydrothermal Vent Gradient. *Ecology* 101, 1–13. doi: 10.1002/ecy.3144

Arnulf, A. F., Harding, A. J., Kent, G. M., Carbotte, S. M., Canales, J. P., and Nedimović, M. R. (2014). Anatomy of an active submarine volcano. *Geology* 42, 655–658. doi: 10.1130/G35629.1

Arnulf, A. F., Harding, A. J., Kent, G. M., and Wilcock, W. S. D. (2018). Structure, Seismicity, and Accretionary Processes at the Hot Spot-Influenced Axial Seamount on the Juan de Fuca Ridge. *J. Geophys. Res. Solid Earth* 123, 4618–4646. doi: 10.1029/2017JB015131

Artigue, L., Wyatt, N. J., Lacan, F., Mahaffey, C., and Lohan, M. C. (2021). The Importance of Water Mass Transport and Dissolved-Particle Interactions on the Aluminum Cycle in the Subtropical North Atlantic. *Global Biogeochem. Cycles* 35, e2020GB006569. doi: 10.1029/2020GB006569

Baker, E. T., Walker, S. L., Chadwick, W. W., Butterfield, D. A., Buck, N. J., and Resing, J. A. (2019). Posteruption Enhancement of Hydrothermal Activity: A 33-Year, Multieruption Time Series at Axial Seamount (Juan de Fuca Ridge). *Geochem. Geophys. Geosystems* 20, 814–828. doi: 10.1029/2018GC007802

Baldrighi, E., Zeppilli, D., Crespin, R., Chauvaud, P., Pradillon, F., and Sarrazin, J. (2018). Colonization of Synthetic Sponges at the Deep-Sea Lucky Strike Hydrothermal Vent Field (Mid-Atlantic Ridge): A First Insight. *Mar. Biodivers.* 48, 89–103. doi: 10.1007/s12526-017-0811-3

Ballard, R. D., and Van Andel, T. H. (1977). Project FAMOUS: Operational Techniques and American Submersible Operations. *GSA Bull.* 88, 495–506. doi: 10.1130/0016-7606(1977)88<495:PFOTAA>2.0.CO;2

Barge, L. M., Flores, E., Baum, M. M., Velde, D. G. V., and Russell, M. J. (2019). Redox and pH Gradients Drive Amino Acid Synthesis in Iron Oxyhydroxide Mineral Systems. *Proc. Natl. Acad. Sci. U. S. A.* 116, 4828–4833. doi: 10.1073/pnas.1812098116

Barnes, C. R., and Tunnicliffe, V. (2008). "Building the World's First Multi-Node Cabled Ocean Observatories (NEPTUNE Canada and VENUS, Canada): Science, Realities, Challenges and Opportunities," in *OCEANS 2008 - MTS/IEEE Kobe Techno-Ocean*. 1–8 (IEEE). doi: 10.1109/OCEANSKOBE.2008.4531076

Barreyre, T., Escartin, J., Sohn, R., and Cannat, M. (2014a). Permeability of the Lucky Strike Deep-Sea Hydrothermal System: Constraints From the Poroelastic Response to Ocean Tidal Loading. Earth Planet. *Sci. Lett.* 408, 146–154. doi: 10.1016/j.epsl.2014.09.049

Barreyre, T., Escartín, J., Garcia, R., Cannat, M., Mittelstaedt, E., and Prados, R. (2012). Structure, Temporal Evolution, and Heat Flux Estimates From the Lucky Strike Deep-Sea Hydrothermal Field Derived From Seafloor Image Mosaics. Geochemistry, Geophys. *Geosystems* 13, 4Q04007. doi: 10.1029/2011GC003990

Barreyre, T., Escartín, J., Sohn, R. A., Cannat, M., Ballu, V., and Crawford, W. C. (2014b). Temporal Variability and Tidal Modulation of Hydrothermal Exit-Fluid Temperatures at the Lucky Strike Deep-Sea Vent Field, Mid-Atlantic Ridge. *J. Geophys. Res. Solid Earth.* 119(4), 2543–2566. doi: 10.1002/2013JB010478

Barreyre, T., Olive, J. A., Crone, T. J., and Sohn, R. A. (2018). Depth-Dependent Permeability and Heat Output at Basalt-Hosted Hydrothermal Systems Across Mid-Ocean Ridge Spreading Rates. *Geochem. Geophys. Geosystems* 19, 1259–1281. doi: 10.1002/2017GC007152

Barreyre, T., Parnell-Turner, R., Wu, J. N., and Fornari, D. J. (2022). Tracking Crustal Permeability and Hydrothermal Response During Seafloor Eruptions at the East Pacific Rise, 9° 50'n. *Geophys. Res. Lett.* 49 (3), e2021GL095459. doi: 10.1029/2021GL095459

Barreyre, T., and Sohn, R. A. (2016). Poroelastic Response of Mid-Ocean Ridge Hydrothermal Systems to Ocean Tidal Loading: Implications for Shallow Permeability Structure. *Geophys. Res. Lett.* 43, 1660–1668. doi: 10.1002/2015GL066479

Barriga, F. J. A. S., Colaço, A., Escartín, J., Hooft, E., Humphris, S. E., Le Bris, N., et al. (2005). *Long-Term Monitoring of the Mid-Atlantic Ridge: Proceedings of the III MOMAR Workshop*. Lisbon (Portugal) 63, 7–9.

Beaulieu, S. E., and Szafranski, K. M. (2020). InterRidge Global Database of Active Submarine Hydrothermal Vent Fields Version 3.4. *PANGAEA*. doi: 10.1594/PANGAEA.917894

Billings, A., Kaiser, C., Young, C. M., Hiebert, L. S., Cole, E., Wagner, J. K. S., et al. (2017). SyPRID Sampler: A Large-Volume, High-Resolution, Autonomous, Deep-Ocean Precision Plankton Sampling System. *Deep Sea Res. Part II Top. Stud. Oceanogr.* 137, 297–306. doi: 10.1016/j.dsr2.2016.05.007

Blandin, J., Colaço, A., Legrand, J., Cannat, M., Sarradin, P., and Sarrazin, J. (2010). The MoMAR-D Project: A Challenge to Monitor in Real Time the Lucky Strike Hydrothermal Vent Field. *ICES J. Mar. Sci.* 68, 416–424. doi: 10.1093/icesjms/fsq075

Boschen, R. E., Rowden, A. A., Clark, M. R., and Gardner, J. P. A. (2013). Mining of Deep-Sea Seafloor Massive Sulfides: A Review of the Deposits, Their Benthic Communities, Impacts From Mining, Regulatory Frameworks and Management Strategies. *Ocean Coast. Manage.* 84, 54–67. doi: 10.1016/j.ocecoaman.2013.07.005

Bower, D. J., Gurnis, M., and Seton, M. (2013). Lower Mantle Structure From Paleogeographically Constrained Dynamic Earth Models. *Geochem. Geophys. Geosystems* 14, 44–63. doi: 10.1029/2012GC004267

Boyd, P. W., and Ellwood, M. J. (2010). The Biogeochemical Cycle of Iron in the Ocean. *Nat. Geosci.* 3, 675–682. doi: 10.1038/ngeo964

Bracco, A., Choi, J., Joshi, K., Luo, H., and McWilliams, J. C. (2016). Submesoscale Currents in the Northern Gulf of Mexico: Deep Phenomena and Dispersion Over the Continental Slope. *Ocean Model.* 101, 43–58. doi: 10.1016/j.ocemod.2016.03.002

Breusing, C., Biastoch, A., Drews, A., Metaxas, A., Jollivet, D., Vrijenhoek, R. C., et al. (2016). Biophysical and Population Genetic Models Predict the Presence of "Phantom" Stepping Stones Connecting Mid-Atlantic Ridge Vent Ecosystems. *Curr. Biol.* 26, 2257–2267. doi: 10.1016/j.cub.2016.06.062

Burd, B. J., and Thomson, R. E. (2012). Estimating Zooplankton Biomass Distribution in the Water Column Near the Endeavour Segment of Juan De Fuca Ridge Using Acoustic Backscatter and Concurrently Towed Nets. *Oceanography* 25, 269–276. doi: 10.5670/oceanog.2012.25

Burd, B. J., and Thomson, R. E. (2019). Seasonal Patterns in Deep Acoustic Backscatter Layers Near Vent Plumes in the Northeastern Pacific Ocean. *FACETS* 4, 183–209. doi: 10.1139/facets-2018-0027

Butterfield, D. A., Roe, K. K., Lilley, M. D., Huber, J. A., Baross, J. A., Embley, R. W., et al. (2004). "Mixing, Reaction and Microbial Activity in the Sub-Seafloor Revealed by Temporal and Spatial Variation in Diffuse Flow Vents at Axial Volcano," in *Subseafloor Biosph. Mid-Ocean Ridges*. eds Wilcock, W. S., Delong, E. F., Kelley, D. S., Baross, J. A., and Craig, S. (Geophysical Monograph Series) 144, 269–289. doi: 10.1029/144GM17

Cannat, M., and Sarradin, P. (2010). *MOMARSAT: MONITORING THE MID ATLANTIC RIDGE*. doi: 10.18142/130

Cannat, M., Sarradin, P., Blandin, J., Ballu, V., Barreyre, T., Chavagnac, V., et al. (2016). EMSO-Azores : Monitoring Seafloor and Water Column Processes at the Mid-Atlantic Ridge. *Fix03 - Proj. Newsl. Serv. Act. Spec.* 3, 11. https://archimer.ifremer.fr/doc/00353/46444/46194.pdf.

Cannat, M., Sarradin, P., Blandin, J., Escartín, J., Party, M. D. S., Aron, M., et al (2011). MoMar-Demo at Lucky Strike. A Near-Real Time Multidisciplinary Observatory of Hydrothermal Processes and Ecosystems at the Mid-Atlantic Ridge. *AGU Fall Meeting Abstracts* 2011, OS22A–05.

Cann, J. R., Elderfield, H., Laughton, A., Butterfield, D. A., Jonasson, I. R., Massoth, G. J., et al. (1997). Seafloor Eruptions and Evolution of Hydrothermal Fluid Chemistry. *Philos. Trans. R. Soc Lond. Ser. A Math. Phys. Eng. Sci.* 355, 369–386. doi: 10.1098/rsta.1997.0013

Caplan-Auerbach, J., Dziak, R. P., Haxel, J., Bohnenstiehl, D. R., and Garcia, C. (2017). Explosive Processes During the 2015 Eruption of Axial Seamount, as Recorded by Seafloor Hydrophones. *Geochem. Geophys. Geosystems* 18, 1761–1774. doi: 10.1002/2016GC006734

Carbotte, S. M., Arnulf, A., Spiegelman, M., Lee, M., Harding, A., Kent, G., et al. (2020). Stacked Sills Forming a Deep Melt-Mush Feeder Conduit Beneath Axial Seamount. *Geology* 48, 693–697. doi: 10.1130/G47223.1

Cardona, Y., Ruiz-Ramos, D. V., Baums, I. B., and Bracco, A. (2016). Potential Connectivity of Coldwater Black Coral Communities in the Northern Gulf of Mexico. *PloS One* 11. doi: 10.1371/journal.pone.0156257

Caress, D. W., Clague, D. A., Paduan, J. B., Martin, J. F., Dreyer, B. M., Chadwick, W. W., et al. (2012). Repeat Bathymetric Surveys at 1-Metre Resolution of Lava Flows Erupted at Axial Seamount in April 2011. *Nat. Geosci.* 5, 483–488. doi: 10.1038/ngeo1496

Cathalot, C., Roussel, E. G., Perhirin, A., Creff, V., Donval, J. P., Guyader, V., et al. (2021). Hydrothermal Plumes as Hotspots for Deep-Ocean Heterotrophic Microbial Biomass Production. *Nat. Commun.* 12, 4–13. doi: 10.1038/s41467-021-26877-6

Chadwick, W. W., Clague, D. A., Embley, R. W., Perfit, M. R., Butterfield, D. A., Caress, D. W., et al. (2013). The 1998 Eruption of Axial Seamount: New Insights on Submarine Lava Flow Emplacement From High-Resolution Mapping. *Geochem. Geophys. Geosystems* 14, 3939–3968. doi: 10.1002/ggge.20202

Chadwick, W. W., Nooner, S. L., Butterfield, D. A., and Lilley, M. D. (2012). Seafloor Deformation and Forecasts of the April 2011 Eruption at Axial Seamount. *Nat. Geosci.* 5, 474–477. doi: 10.1038/ngeo1464

Chadwick, W. W., Paduan, J. B., Clague, D. A., Dreyer, B. M., Merle, S. G., Bobbitt, A. M., et al. (2016). Voluminous Eruption From a Zoned Magma Body After an Increase in Supply Rate at Axial Seamount. *Geophys. Res. Lett.* 43, 12,12–63,70. doi: 10.1002/2016GL071327

Chadwick, W. W., Wilcock, W. S. D., Nooner, S. L., Beeson, J. W., Sawyer, A. M., and Lau, T.-K. (2022). Geodetic Monitoring at Axial Seamount Since Its 2015 Eruption Reveals a Waning Magma Supply and Tightly Linked Rates of Deformation and Seismicity. *Geochem. Geophys. Geosystems* 23, e2021GC010153. doi: 10.1029/2021GC010153

Chapman, A. S. A., Beaulieu, S. E., Colaço, A., Gebruk, A. V., Hilario, A., Kihara, T. C., et al. (2019). sFDvent: A Global Trait Database for Deep-Sea Hydrothermal-Vent Fauna. *Glob. Ecol. Biogeogr.* 28, 1538–1551. doi: 10.1111/geb.12975

Chatzievangelou, D., Aguzzi, J., Ogston, A., Suárez, A., and Thomsen, L. (2020). Visual Monitoring of Key Deep-Sea Megafauna With an Internet Operated Crawler as a Tool for Ecological Status Assessment. *Prog. Oceanogr.* 184, 102321. doi: 10.1016/j.pocean.2020.102321

Chavagnac, V., Leleu, T., Boulart, C., Barreyre, T., Castillo, A., Menjot, L., et al. (2015). "Deep-Sea Observatory EMSO-Azores (Lucky Strike, 37°17'N MAR): Impact of Fluid Circulation Pathway on Chemical Hydrothermal Fluxes," in *AGU Fall Meeting Abstracts, OS42A-07*.

Chavagnac, V., Leleu, T., Fontaine, F. J., Cannat, M., Ceuleneer, G., and Castillo, A. (2018a). Spatial Variations in Vent Chemistry at the Lucky Strike Hydrothermal Field, Mid-Atlantic Ridge (37°N): Updates for Subseafloor Flow Geometry From the Newly Discovered Capelinhos Vent. *Geochem. Geophys. Geosystems* 19, 4444–4458. doi: 10.1029/2018GC007765

Chavagnac, V., Saleban Ali, H., Jeandel, C., Leleu, T., Destrigneville, C., Castillo, A., et al. (2018b). Sulfate Minerals Control Dissolved Rare Earth Element Flux and Nd Isotope Signature of Buoyant Hydrothermal Plume (EMSO-Azores, 37°N Mid-Atlantic Ridge). *Chem. Geol.* 499, 111–125. doi: 10.1016/j.chemgeo.2018.09.021

Clague, D., Paduan, J., Caress, D., Chadwick, W. W., Le Saout, M., Dreyer, B., et al. (2017). High-Resolution AUV Mapping and Targeted ROV Observations of Three Historical Lava Flows at Axial Seamount. *Oceanography* 30, 82–89. doi: 10.5670/oceanog.2017.426

Colaço, A., Blandin, J., Cannat, M., Carval, T., Chavagnac, V., Connelly, D. P., et al. (2011). MoMAR-D: A Technological Challenge to Monitor the Dynamics of the Lucky Strike Vent Ecosystem. *ICES J. Mar. Sci. J. du Cons.* 68, 416–424. doi: 10.1093/icesjms/fsq075

Coogan, L. A., Attar, A., Mihaly, S. F., Jeffries, M., and Pope, M. (2017). Near-Vent Chemical Processes in a Hydrothermal Plume: Insights From an Integrated Study of the Endeavour Segment. *Geochem. Geophys. Geosystems* 18, 1641–1660. doi: 10.1002/2016GC006747

Coppola, L., Ntoumas, M., Bozzano, R., Bensi, M., Hartman, S. E., Charcos Llorens, M., et al. (2016). *Handbook of Best Practices for Open Ocean Fixed Observatories* (European Commission, FixO3 project, FP7 Programme 2007-2013 under grant agreement n° 312463). doi: 10.25607/OBP-1488.

Corliss, J. B., Dymond, J., Gordon, L. I., Edmond, J. M., Von Herzen, R. P., Ballard, R. D., et al. (1979). Submarine Thermal Springs on the Galapagos Rift. *Science (80-)* 203, 1073–1083. doi: 10.1126/science.203.4385.1073

Costanzi, R., Fenucci, D., Manzari, V., Micheli, M., Morlando, L., Terracciano, D., et al. (2020). Interoperability Among Unmanned Maritime Vehicles: Review and First In-Field Experimentation. *Front. Robot. AI* 7. doi: 10.3389/frobt.2020.00091

Cotte, L., Chavagnac, V., Pelleter, E., Laës-Huon, A., Cathalot, C., Dulaquais, G., et al. (2020). Metal Partitioning After *in Situ* Filtration at Deep-Sea Vents of the Lucky Strike Hydrothermal Field (EMSO-Azores, Mid-Atlantic Ridge, 37 Degrees N). *Deep Sea Res. Part I Oceanogr. Res. Pap.* 157, 103204. doi: 10.1016/j.dsr.2019.103204

Cotte, L., Omanović, D., Waeles, M., Laës, A., Cathalot, C., Sarradin, P., et al. (2018). On the Nature of Dissolved Copper Ligands in the Early Buoyant Plume of Hydrothermal Vents. *Environ. Chem.* 15, 58–73. doi: 10.1071/EN17150

Coumou, D., Driesner, T., Weis, P., and Heinrich, C. (2009). Phase Separation, Brine Formation, and Salinity Variation at Black Smoker Hydrothermal Systems. *J. Geophys. Res.* 114, B03212. doi: 10.1029/2008JB005764

Cowart, D. A., Matabos, M., Brandt, M. I., Marticorena, J., and Sarrazin, J. (2020). Exploring Environmental DNA (eDNA) to Assess Biodiversity of Hard Substratum Faunal Communities on the Lucky Strike Vent Field (Mid-Atlantic Ridge) and Investigate Recolonization Dynamics After an Induced Disturbance. *Front. Mar. Sci.* 6. doi: 10.3389/fmars.2019.00783

Crawford, W. C., Rai, A., Singh, S. C., Cannat, M., Escartín, J., Wang, H., et al. (2013). Hydrothermal Seismicity Beneath the Summit of Lucky Strike Volcano, Mid-Atlantic Ridge. *Earth Planet. Sci. Lett.* 373, 118–128. doi: 10.1016/j.epsl.2013.04.028

Crise, A., d'Alcalà, M. R., Mariani, P., Petihakis, G., Robidart, J., Iudicone, D., et al. (2018). A Conceptual Framework for Developing the Next Generation of Marine OBservatories (MOBs) for Science and Society. *Front. Mar. Sci.* 5. doi: 10.3389/fmars.2018.00318

Crone, T. J., and Wilcock, W. S. D. (2005). Modeling the Effects of Tidal Loading on Mid-Ocean Ridge Hydrothermal Systems. *Geochem. Geophys. Geosystems* 6, Q07001. doi: 10.1029/2004GC000905

Crone, T. J., Wilcock, W. S. D., and McDuff, R. E. (2010). Flow Rate Perturbations in a Black Smoker Hydrothermal Vent in Response to a Mid-Ocean Ridge Earthquake Swarm. *Geochem. Geophys. Geosystems* 11, 1–13. doi: 10.1029/2009GC002926

Cuvelier, D., Beesau, J., Ivanenko, V. N., Zeppilli, D., Sarradin, P., and Sarrazin, J. (2014a). First Insights Into Macro-and Meiofaunal Colonisation Patterns on Paired Wood/Slate Substrata at Atlantic Deep-Sea Hydrothermal Vents. *Deep Sea Res. Part I Oceanogr. Res. Pap.* 87, 70–81. doi: 10.1016/j.dsr.2014.02.008

Cuvelier, D., Legendre, P., Laës-Huon, A., Sarradin, P., and Sarrazin, J. (2017). Biological and Environmental Rhythms in (Dark) Deep-Sea Hydrothermal Ecosystems. *Biogeosciences* 14, 2955–2977. doi: 10.5194/bg-14-2955-2017

Cuvelier, D., Legendre, P., Laes, A., Sarradin, P., and Sarrazin, J. (2014b). Rhythms and Community Dynamics of a Hydrothermal Tubeworm Assemblage at Main Endeavour Field–A Multidisciplinary Deep-Sea Observatory Approach. *PloS One* 9, e96924. doi: 10.1371/journal.pone.0096924

Cuvelier, D., Sarrazin, J., Colaço, A., Copley, J. T. P., Glover, A. G., Tyler, P. A., et al. (2011). Community Dynamics Over 14 Years at the Eiffel Tower Hydrothermal Edifice on the Mid-Atlantic Ridge. *Limnol. Oceanogr.* 56, 1624–1640. doi: 10.4319/lo.2011.56.5.1624

Daniel, A., Laës-Huon, A., Barus, C., Beaton, A. D., Blandfort, D., Guigues, N., et al. (2020). Toward a Harmonization for Using *in Situ* Nutrient Sensors in the Marine Environment. *Front. Mar. Sci.* 6. doi: 10.3389/fmars.2019.00773

Dañobeitia, J. J., Pouliquen, S., Johannessen, T., Basset, A., Cannat, M., Gerrit Pfeil, B., et al. (2020). Toward a Comprehensive and Integrated Strategy of the European Marine Research Infrastructures for Ocean Observations. *Front. Mar. Sci.* 7. doi: 10.3389/fmars.2020.00180

Danovaro, R., Aguzzi, J., Fanelli, E., Billet, D., Gjerde, K., Jamieson, A., et al. (2017a). A New International Ecosystem-Based Strategy for the Global Deep Ocean. *Science* 355, 452–454. doi: 10.1126/science.aah7178

Danovaro, R., Corinaldesi, C., Dell'Anno, A., and Snelgrove, P. V. R. (2017b). The Deep-Sea Under Global Change. *Curr. Biol.* 27(11), R461–R465. doi: 10.1016/j.cub.2017.02.046

Danovaro, R., Fanelli, E., Aguzzi, J., Billett, D., Carugati, L., Corinaldesi, C., et al. (2020). Ecological Variables for Developing a Global Deep-Ocean Monitoring and Conservation Strategy. *Nat. Ecol. Evol.* 4, 181–192. doi: 10.1038/s41559-019-1091-z

Delaney, J. R., Kelley, D. S., Marburg, A., Stoermer, M., Hadaway, H., Juniper, S. K., et al. (2016). "Axial Seamount - Wired and Restless: A Cabled Submarine Network Enables Real-Time, Tracking of a Mid-Ocean Ridge Eruption and Live Video of an Active Hydrothermal System Juan De Fuca Ridge, NE Pacific," in *OCEANS 2016 MTS/IEEE Monterey*. 1–8. doi: 10.1109/OCEANS.2016.7761484

Devine, B. M., Baker, K. D., Edinger, E. N., and Fisher, J. A. D. (2020). Habitat Associations and Assemblage Structure of Demersal Deep-Sea Fishes on the Eastern Flemish Cap and Orphan Seamount. *Deep. Res. Part I Oceanogr. Res. Pap.* 157, 103210. doi: 10.1016/j.dsr.2019.103210

DFO (2006). "Identification of Ecologically Significant Species and Community Properties," in *DFO Can. Sci. Advis. Sec. Sci. Advis. Rep. 2006/04*.

Dick, G. J. (2019). The Microbiomes of Deep-Sea Hydrothermal Vents: Distributed Globally, Shaped Locally. *Nat. Rev. Microbiol.* 17, 271–283. doi: 10.1038/s41579-019-0160-2

Doya, C., Aguzzi, J., Pardo, M., Matabos, M., Company, J. B., Costa, C., et al. (2014). Diel Behavioral Rhythms in Sablefish (Anoplopoma Fimbria) and

Other Benthic Species, as Recorded by the Deep-Sea Cabled Observatories in Barkley Canyon (NEPTUNE-Canada). *J. Mar. Syst.* 130, 69–78. doi: 10.1016/j.jmarsys.2013.04.003

Du Preez, C., and Fisher, C. R. (2018). Long-Term Stability of Back-Arc Basin Hydrothermal Vents. *Front. Mar. Sci.* 5. doi: 10.3389/fmars.2018.00054

Durden, J. M., Bett, B. J., Huffard, C. L., Pebody, C., Ruhl, H. A., and Smith, K. L. (2020). Response of Deep-Sea Deposit-Feeders to Detrital Inputs: A Comparison of Two Abyssal Time-Series Sites. *Deep. Res. Part II Top. Stud. Oceanogr.* 173, 104677. doi: 10.1016/j.dsr2.2019.104677

Dziak, R. P., Smith, D. K., Bohnenstiehl, D. W. R., Fox, C. G., Desbruyeres, D., Matsumoto, H., et al. (2004). Evidence of a Recent Magma Dike Intrusion at the Slow Spreading Lucky Strike Segment, Mid-Atlantic Ridge. *J. Geophys. Res. Solid Earth* 109, 1–15. doi: 10.1029/2004JB003141

Escartin, J., Garcia, R., Barreyre, T., Cannat, M., Gracias, N., Shihavuddin, A., et al. (2013). "Optical Methods to Monitor Temporal Changes at the Seafloor: The Lucky Strike Deep-Sea Hydrothermal Vent Field (Mid-Atlantic Ridge)," in *2013 IEEE International Underwater Technology Symposium (UT 2013)*. 1–6 (Tokyo, France: IEEE). doi: 10.1109/UT.2013.6519838

Escartín, J., Barreyre, T., Cannat, M., Garcia, R., Gracias, N., Deschamps, A., et al. (2015). Hydrothermal Activity Along the Slow-Spreading Lucky Strike Ridge Segment (Mid-Atlantic Ridge): Distribution, Heatflux, and Geological Controls. *Earth Planet. Sci. Lett.* 431, 173–185. doi: 10.1016/j.epsl.2015.09.025

Escartín, J., Soule, S. A., Cannat, M., Fornari, D. J., Düsünür, D., and Garcia, R. (2014). Lucky Strike Seamount: Implications for the Emplacement and Rifting of Segment-Centered Volcanoes at Slow Spreading Mid-Ocean Ridges. *Geochem. Geophys. Geosystems* 15, 4157–4179. doi: 10.1002/2014GC005477

Favali, P., and Beranzoli, L. (2009). EMSO: European Multidisciplinary Seafloor Observatory. *Nucl. Instrum. Methods Phys. Res. Sect. A Accel. Spectrometers Detect. Assoc. Equip.* 602, 21–27. doi: 10.1016/j.nima.2008.12.214

Fitzsimmons, J., Boyle, E. A., and Jenkins, W. J. (2014). Distal Transport of Dissolved Hydrothermal Iron in the Deep South Pacific Ocean. *Proc. Natl. Acad. Sci.* 111, 16654 16661. doi: 10.1073/pnas.1418778111

Fornari, D. J., Von Damm, K. L., Bryce, J. G., Cowen, J. P., Ferrini, V., Fundis, A., et al. (2012). The East Pacific Rise Between 9°N and 10°N: Twenty-Five Years of Integrated, Multidisciplinary Oceanic Spreading Center Studies. *Oceanography* 25, 18–43. doi: 10.5670/oceanog.2012.02

Fortunato, C. S., and Huber, J. A. (2016). Coupled RNA-SIP and Metatranscriptomics of Active Chemolithoautotrophic Communities at a Deep-Sea Hydrothermal Vent. *ISME J.* 10, 1925–1938. doi: 10.1038/ismej.2015.258

Fortunato, C. S., Larson, B., Butterfield, D. A., and Huber, J. A. (2018). Spatially Distinct, Temporally Stable Microbial Populations Mediate Biogeochemical Cycling at and Below the Seafloor in Hydrothermal Vent Fluids. *Environ. Microbiol.* 20, 769–784. doi: 10.1111/1462-2920.14011

Franke, A., Blenckner, T., Duarte, C. M., Ott, K., Fleming, L. E., Antia, A., et al. (2020). Operationalizing Ocean Health: Toward Integrated Research on Ocean Health and Recovery to Achieve Ocean Sustainability. *One Earth* 2, 557–565. doi: 10.1016/j.oneear.2020.05.013

Galaasen, E. V., Ninnemann, U. S., Kessler, A., Irvalı, N., Rosenthal, Y., Tjiputra, J., et al. (2020). Interglacial Instability of North Atlantic Deep Water Ventilation. *Science* 367, 1485–1489. doi: 10.1126/science.aay6381

Germanovich, L. N., Hurt, R. S., Smith, J. E., Genc, G., and Lowell, R. P. (2015). Journal of Geophysical Research : Solid Earth Hydrothermal Environments. *J. Geophys. Res. Solid Earth* 120, 8031–8055. doi: 10.1002/2015JB012245.Received

Girard, F., Sarrazin, J., Arnaubec, A., Cannat, M., Sarradin, P., Wheeler, B., et al. (2020). Currents and Topography Drive Assemblage Distribution on an Active Hydrothermal Edifice. *Prog. Oceanogr.* 187. doi: 10.1016/j.pocean.2020.102397

Glover, A. G., Gooday, A. J., Bailey, D., Billet, D. S. M., Chevaldonné, P., Colaço, A., et al. (2010). Temporal Change in Deep-Sea Benthic Ecosystems: A Review of the Evidence From Recent Time-Series Studies. *Adv. Mar. Biol.* 58, 1–95. doi: 10.1016/B978-0-12-381015-1.00001-0

Grand, M. M., Laës-Huon, A., Fietz, S., Resing, J. A., Obata, H., Luther, G. W. III, et al. (2019). Developing Autonomous Observing Systems for Micronutrient Trace Metals. *Front. Mar. Sci.* 6, 35. doi: 10.3389/fmars.2019.00035

Hand, K. P., and German, C. R. (2018). Exploring Ocean Worlds on Earth and Beyond. *Nat. Geosci.* 11, 2–4. doi: 10.1038/s41561-017-0045-9

Hartman, S. E., Lampitt, R. S., Larkin, K. E., Pagnani, M., Campbell, J., Gkritzalis, T., et al. (2012). The Porcupine Abyssal Plain Fixed-Point Sustained Observatory (PAP-SO): Variations and Trends From the Northeast Atlantic Fixed-Point Time-Series. *ICES J. Mar. Sci.* 69, 776–783. doi: 10.1093/icesjms/fss077

Heidemann, J., Stojanovic, M., and Zorzi, M. (2012). Underwater Sensor Networks: Applications, Advances and Challenges. *Philos. Trans. R. Soc A* 370, 158–175. doi: 10.1098/rsta.2011.0214

Hooft, E. E. E., Patel, H., Wilcock, W., Becker, K., Butterfield, D., Davis, E., et al. (2010). A Seismic Swarm and Regional Hydrothermal and Hydrologic Perturbations: The Northern Endeavour Segment, February 2005. *Geochem. Geophys. Geosystems* 11, Q12015. doi: 10.1029/2010GC003264

Huber, J. A., Butterfield, D. A., and Baross, J. A. (2003). Bacterial Diversity in a Subseafloor Habitat Following a Deep-Sea Volcanic Eruption. *FEMS Microbiol. Ecol.* 43, 393–409. doi: 10.1016/S0168-6496(02)00451-8

Huber, J. A., Crone, T. J., and Soule, D. (2021). *Integrating the Regional Cabled Array With Ocean Drilling to Facilitate Observatory-Based Subseafloor Science at Axial Seamount. Ocean Observatories Initiative Facility Board, Ocean Observatories Initiative (OOI) Science Plan: Exciting Science Opportunities Using OOI Data*. doi: 10.23860/ooi-science-plan-2021-01

Huber, J. A., David, B. M. W., Morrison, H. G., Huse, S. M., Neal, P. R., Butterfield, D. A., et al. (2007). Microbial Population Structures in the Deep Marine Biosphere. *Science (80-.).* 318 (5847), 97–100. doi: 10.1126/science.1146689

Husson, B., Sarradin, P., Zeppilli, D., and Sarrazin, J. (2017). Picturing Thermal Niches and Biomass of Hydrothermal Vent Species. *Deep. Res. Part II Top. Stud. Oceanogr.* 137, 6–25. doi: 10.1016/j.dsr2.2016.05.028

Husson, B., Sarrazin, J., van Oevelen, D., Sarradin, P., Soetaert, K., and Menesguen, A. (2018). Modelling the Interactions of the Hydrothermal Mussel Bathymodiolus Azoricus With Vent Fluid. *Ecol. Modell.* 377, 35–50. doi: 10.1016/j.ecolmodel.2018.03.007

IMOVE, working group (2019) *IMOVE - Integrating Multidisciplinary Observations in Vent Environments. An InterRidge Working Group. Workshop, Feb. 6-8, Bergen, Norway*. Available at: https://archimer.ifremer.fr/doc/00623/73522/.

Jahanbakht, M., Xiang, W., Hanzo, L., and Azghadi, M. R. (2021). Internet of Underwater Things and Big Marine Data Analytics—A Comprehensive Survey. *IEEE Commun. Surv. Tutor.* 23, 904–956. doi: 10.1109/COMST.2021.3053118

Juniper, S. K., Thornborough, K., Douglas, K., and Hillier, J. (2019). Remote Monitoring of a Deep-Sea Marine Protected Area: The Endeavour Hydrothermal Vents. *Aquat. Conserv. Mar. Freshw. Ecosyst.* 29, 1–19. doi: 10.1002/aqc.3020

Jupp, T. E., and Schultz, A. (2004). Physical Balances in Subseafloor Hydrothermal Convection Cells. *J. Geophys. Res. Solid Earth* 109, 1–12. doi: 10.1029/2003JB002697

Kelley, D. S., Carbotte, S. M., Caress, D. W., Clague, D. A., Delaney, J. R., Gill, J. B., et al. (2012). Endeavour Segment of the Juan De Fuca Ridge: One of the Most Remarkable Places on Earth. *Oceanography* 25, 44–61. doi: 10.5670/oceanog.2012.03

Kelley, D. S., Delaney, J. R., and Juniper, S. K. (2014). Establishing a New Era of Submarine Volcanic Observatories: Cabling Axial Seamount and the Endeavour Segment of the Juan De Fuca Ridge. *Mar. Geol.* 352, 426–450. doi: 10.1016/j.margeo.2014.03.010

Kelley, D. S., Delaney, J. R., and Team, C. A. (2016). "NSF's Cabled Array: A Wired Tectonic Plate and Overlying Ocean," in *Ocean. 2016 MTS/IEEE Monterey, OCE 2016*. doi: 10.1109/OCEANS.2016.7761398

Kelley, D. S., Karson, J. A., Früh-Green Gretchen, L., Yoerger, D. R., Shank, T. M., Butterfield, D. A., et al. (2005). A Serpentinite-Hosted Ecosystem: The Lost City Hydrothermal Field. *Science (80-.).* 307 (5714), 1428–1434. doi: 10.1126/science.1102556

Laës-Huon, A., Davy, R., Thomas, L., Legrand, J., Le Piver, D., Rousseaux, P., et al. (2020). CHEMINI: Chemical Miniaturised Analyser for in situ Monitoring of Macronutrients and Bioactive Metals in Marine Waters. *Ocean Science meeting AGU* (San Diego), 16-02 / 21-02 2020.

Laës-Huon, A., Cathalot, C., Legrand, J., Tanguy, V., and Sarradin, P. (2016). Long-Term *In Situ* Survey of Reactive Iron Concentrations at the EMSO-Azores Observatory. *IEEE J. Ocean. Eng.* 41, 744–752. doi: 10.1109/JOE.2016.2552779

Lahaye, N., Gula, J., and Roullet, G. (2020). Internal Tide Cycle and Topographic Scattering Over the North Mid-Atlantic Ridge. *J. Geophys. Res. Ocean.* 125, 1–21. doi: 10.1029/2020jc016376

Lahaye, N., Gula, J., Thurnherr, A. M., Reverdin, G., Bouruet-Aubertot, P., and Roullet, G. (2019). Deep Currents in the Rift Valley of the North Mid-Atlantic Ridge. *Front. Mar. Sci.* 6. doi: 10.3389/fmars.2019.00597

Langmuir, C. H., Humphris, S. E., Fornari, D. J., Van Dover, C. L., Von Damm, K., Tivey, M. K., et al. (1997). Hydrothermal Vents Near a Mantle Hot Spot: The Lucky Strike Vent Field at 37°N on the Mid-Atlantic Ridge. *Earth Planet. Sci. Lett.* 148, 69–91. doi: 10.1016/S0012-821X(97)00027-7

Lantéri, N., Ruhl, H. A., Gates, A., Martínez, E., del Rio Fernandez, J., Aguzzi, J., et al. (2022). The EMSO Generic Instrument Module (EGIM): Standardized and Interoperable Instrumentation for Ocean Observation. *Front. Mar. Sci.*, 9. doi: 10.3389/fmars.2022.801033

Laroche, O., Kersten, O., Smith, C. R., and Goetze, E. (2020). From Sea Surface to Seafloor: A Benthic Allochthonous eDNA Survey for the Abyssal Ocean. *Front. Mar. Sci.* 7. doi: 10.3389/fmars.2020.00682

Larson, B. I., Olson, E. J., and Lilley, M. D. (2007). *In Situ* Measurement of Dissolved Chloride in High Temperature Hydrothermal Fluids. *Geochim. Cosmochim. Acta* 71, 2510–2523. doi: 10.1016/j.gca.2007.02.013

Le Bris, N., Yücel, M., Das, A., Sievert, S. M., LokaBharathi, P. P., and Girguis, P. R. (2019). Hydrothermal Energy Transfer and Organic Carbon Production at the Deep Seafloor. *Front. Mar. Sci.* 5. doi: 10.3389/fmars.2018.00531

Lee, R. W., Robert, K., Matabos, M., Bates, A. E., and Juniper, S. K. (2015). Temporal and Spatial Variation in Temperature Experienced by Macrofauna at Main Endeavour Hydrothermal Vent Field. *Deep. Res. Part I Oceanogr. Res. Pap.* 106, 154–166. doi: 10.1016/j.dsr.2015.10.004

Legrand, J., Sarradin, P., and Cannat, M. (2019). EMSO Azores Deep-Sea Observatory: 9 Years of Operations. *EGU General Assembly 2019* (Vienna) https://archimer.ifremer.fr/doc/00489/60087/.

Leleu, T. (2017). Variabilité Spatio-Temporelle De La Composition Des Fluides Hydrothermaux (Observatoire Fond De Mer EMSO-Açores, Lucky Strike): Traçage De La Circulation Hydrothermale Et Quantification Des Flux Chimiques Associées / Spatial and Temporal Variability of the Composition of Hydrothermal Fluids (Deep Sea Observatory EMSO-Azores, Lucky Strike): Tracing the Hydrothermal Pathway and Quantification of the Associated Chemical Fluxes. PhD Thesis (Université De Toulouse). Available at: https://archimer.ifremer.fr/doc/00692/80380/.

Lelièvre, Y., Legendre, P., Matabos, M., Mihaly, S., Lee, R. W., Sarradin, P., et al. (2017). Astronomical and Atmospheric Impacts on Deep-Sea Hydrothermal Vent Invertebrates. *Proc. R. Soc Lond. B Biol. Sci.* 284, 20162123. doi: 10.1098/rspb.2016.2123

Lelièvre, Y., Sarrazin, J., Marticorena, J., Schaal, G., Day, T., Legendre, P., et al. (2018). Biodiversity and Trophic Ecology of Hydrothermal Vent Fauna Associated With Tubeworm Assemblages on the Juan De Fuca Ridge. *Biogeosciences* 15, 2629–2647. doi: 10.5194/bg-15-2629-2018

Levin, L. A., Baco, A. R., Bowden, D. A., Colaço, A., Cordes, E. E., Cunha, M. R., et al. (2016). Hydrothermal Vents and Methane Seeps: Rethinking the Sphere of Influence. *Front. Mar. Sci.* 3, 766–768. doi: 10.3389/fmars.2016.00072

Levin, L. A., Bett, B. J., Gates, A. R., Heimbach, P., Howe, B. M., Janssen, F., et al. (2019). Global Observing Needs in the Deep Ocean. *Front. Mar. Sci.* 6. doi: 10.3389/fmars.2019.00241

Levin, L. A., and Le Bris, N. (2015). The Deep Ocean Under Climate Change. *Science (80-.)* 350, 766–768. doi: 10.1126/science.aad0126

Levin, L. A., Wei, C. L., Dunn, D. C., Amon, D. J., Ashford, O. S., Cheung, W. W. L., et al. (2020). Climate Change Considerations are Fundamental to Management of Deep-Sea Resource Extraction. *Glob. Change Biol.* 26, 4664–4678. doi: 10.1111/gcb.15223

Lewis, K., and Lowell, R. P. (2009). Numerical Modeling of Two-Phase Flow in the NaCl-H2O System: Introduction of a Numerical Method and Benchmarking. *J. Geophys. Res.* 114, B05202. doi: 10.1029/2008JB006029

Lombard, F., Boss, E., Waite, A., Uitz, H. M., Stemmann, J., Sosik, J., et al (2019). Globally Consistent Quantitative Observations of Planktonic Ecosystems. *Front. Mar. Sci.* 6. doi: 10.3389/fmars.2019.00196

Lutz, R. A., Shank, T. M., Luther, G. W., Vetriani, C., Tolstoy, M., Nuzzio, D. B., et al. (2008). Interrelationships Between Vent Fluid Chemistry, Temperature, Seismic Activity, and Biological Community Structure at a Mussel-Dominated, Deep-Sea Hydrothermal Vent Along the East Pacific Rise. *J. Shellfish Res.* 27, 177–190. doi: 10.2983/0730-8000(2008)27[177:IBVFCT]2.0.CO;2

Marcus, J., Tunnicliffe, V., and Butterfield, D. A. (2009). Post-Eruption Succession of Macrofaunal Communities at Diffuse Flow Hydrothermal Vents on Axial Volcano, Juan De Fuca Ridge, Northeast Pacific. *Deep Sea Res. Part II Top. Stud. Oceanogr.* 56, 1586–1598. doi: 10.1016/j.dsr2.2009.05.004

Mariani, P., Bachmayer, R., Kosta, S., Pietrosemoli, E., Ardelan, M. V., Connelly, D. P., et al. (2021). Collaborative Automation and IoT Technologies for Coastal Ocean Observing Systems. *Front. Mar. Sci.* 8. doi: 10.3389/fmars.2021.647368

Marjanović, M., Barreyre, T., Fontaine, F. J., and Escartín, J. (2019). Investigating Fine-Scale Permeability Structure and Its Control on Hydrothermal Activity Along a Fast-Spreading Ridge (the East Pacific Rise, 9°43′–53′N) Using Seismic Velocity, Poroelastic Response, and Numerical Modeling. *Geophys. Res. Lett.* 46, 11799–11810. doi: 10.1029/2019GL084040

Marticorena, J., Matabos, M., Ramirez-Llodra, E., Cathalot, C., Laës-Huon, A., Leroux, R., et al. (2021). Recovery of Hydrothermal Vent Communities in Response to an Induced Disturbance at the Lucky Strike Vent Field (Mid-Atlantic Ridge). *Mar. Environ. Res.* 168, 105316. doi: 10.1016/j.marenvres.2021.105316

Marticorena, J., Matabos, M., Ramirez-Llodra, E., and Sarrazin, J. (2020). Contrasting Reproductive Biology of Two Hydrothermal Gastropods From the Mid – Atlantic Ridge : Implications for Resilience of Vent Communities. *Mar. Biol.* 167, 1–19. doi: 10.1007/s00227-020-03721-x

Martin, W., Baross, J., Kelley, D. S., and Russell, M. (2008). Hydrothermal Vents and the Origin of Life. *Nat. Rev. Micro.* 6 (11), 805–814. doi: 10.1038/nrmicro1991

Matabos, M., Best, M., Blandin, J., Hoeberechts, M., Juniper, S. K., Pirenne, B., et al. (2016). "Seafloor Observatories," in *Biological Sampling in the Deep Sea*. Eds. M. R. Clark, M. Consalvey and A. A. Rowden (Blackwell, Chichester, UK: Wiley), 306–337. doi: 10.1002/9781118332535.ch14

Matabos, M., Bui, A. O. V., Mihaly, S., Aguzzi, J., Juniper, S. K., and Ajayamohan, R. S. (2014). High-Frequency Study of Epibenthic Megafaunal Community Dynamics in Barkley Canyon: A Multi-Disciplinary Approach Using the NEPTUNE Canada Network. *J. Mar. Syst.* 130, 56–68. doi: 10.1016/j.jmarsys.2013.05.002

Matabos, M., Cuvelier, D., Brouard, J., Shillito, B., Ravaux, J., Zbinden, M., et al. (2015). Behavioural Study of Two Hydrothermal Crustacean Decapods: Mirocaris Fortunata and Segonzacia Mesatlantica, From the Lucky Strike Vent Field (Mid-Atlantic Ridge). *Deep Sea Res. Part II Top. Stud. Oceanogr.* 121, 146–158. doi: 10.1016/j.dsr2.2015.04.008

Mat, A. M., Sarrazin, J., Markov, G. V., Apremont, V., Dubreuil, C., Eché, C., et al. (2020). Biological Rhythms in the Deep-Sea Hydrothermal Mussel Bathymodiolus Azoricus. *Nat. Commun.* 11, 1–12. doi: 10.1038/s41467-020-17284-4

Matsuura, M. (2021). Recent Advancement in Power-Over-Fiber Technologies. *Photonics* 8, 335. doi: 10.3390/photonics8080335

McCoy, D., Bianchi, D., and Stewart, A. L. (2020). Global Observations of Submesoscale Coherent Vortices in the Ocean. *Prog. Oceanogr.* 189, 102452. doi: 10.1016/j.pocean.2020.102452

Menini, E., and Van Dover, C. L. (2019). An Atlas of Protected Hydrothermal Vents. *Mar. Policy* 108, 103654. doi: 10.1016/j.marpol.2019.103654

Meyer, J., Akerman, N., Proskurowski, G., and Huber, J. (2013). Microbiological Characterization of Post-Eruption "Snowblower" Vents at Axial Seamount, Juan De Fuca Ridge. *Front. Microbiol.* 4. doi: 10.3389/fmicb.2013.00153

Mitarai, S., Watanabe, H., Nakajima, Y., Shchepetkin, A. F., and McWilliams, J. C. (2016). Quantifying Dispersal From Hydrothermal Vent Fields in the Western Pacific Ocean. *Proc. Natl. Acad. Sci. U. S. A.* 113, 2976–2981. doi: 10.1073/pnas.1518395113

Mittelstaedt, E., Davaille, A., Van Keken, P. E., Gracias, N., and Escartin, J. (2010). A Noninvasive Method for Measuring the Velocity of Diffuse Hydrothermal Flow by Tracking Moving Refractive Index Anomalies. *Geochem. Geophys. Geosystems* 11, Q10005. doi: 10.1029/2010GC003227

Mittelstaedt, E., Escartín, J., Gracias, N., Olive, J. A., Barreyre, T., Davaille, A., et al. (2012). Quantifying Diffuse and Discrete Venting at the Tour Eiffel Vent Site, Lucky Strike Hydrothermal Field. *Geochem. Geophys. Geosystems* 13, Q04008. doi: 10.1029/2011GC003991

Mittelstaedt, E., Fornari, D. J., Crone, T. J., Kinsey, J., Kelley, D. S., and Elend, M. (2016). Diffuse Venting at the ASHES Hydrothermal Field: Heat Flux and Tidally Modulated Flow Variability Derived From *in Situ* Time-Series Measurements. *Geochem. Geophys. Geosystems* 17, 1435–1453. doi: 10.1002/2015GC006144

Mullineaux, L. S., McGillicuddy, D. J., Mills, S. W., Kosnyrev, V. K., Thurnherr, A. M., Ledwell, J. R., et al. (2013). Active Positioning of Vent Larvae at a Mid-Ocean Ridge. *Deep Sea Res. Part II Top. Stud. Oceanogr.* 92, 46–57. doi: 10.1016/j.dsr2.2013.03.032

Mullineaux, L. S., Metaxas, A., Beaulieu, S. E., Bright, M., Gollner, S., Grupe, B. M., et al. (2018). Exploring the Ecology of Deep-Sea Hydrothermal Vents in a Metacommunity Framework. *Front. Mar. Sci.* 5. doi: 10.3389/fmars.2018.00049

Mullineaux, L. S., Mills, S. W., Le Bris, N., Beaulieu, S. E., Sievert, S. M., and Dykman, L. N. (2020). Prolonged Recovery Time After Eruptive Disturbance of a Deep-Sea Hydrothermal Vent Community. *Proc. R. Soc B.* 287, 20202070. doi: 10.1098/rspb.2020.2070

Murdock, S., Tunnicliffe, V., Boschen-Rose, R. E., and Juniper, S. K. (2021). Emergent "Core Communities" of Microbes, Meiofauna and Macrofauna at Hydrothermal Vents. *ISME Commun.* 1, 27. doi: 10.1038/s43705-021-00031-1

National Research Council (2000). *Illuminating the Hidden Planet: The Future of Seafloor Observatory Science* (Washington, DC, USA: National Academy Press). doi: 10.17226/9920

Nees, H. A., Moore, T. S., Mullaugh, K. M., Holyoke, R. R., Janzen, C. P., Ma, S., et al. (2008). Hydrothermal Vent Mussel Habitat Chemistry, Pre- and Post-Eruption at 9°50′North on the East Pacific Rise. *J. Shellfish Res.* 27, 169–175. doi: 10.2983/0730-8000(2008)27[169:HVMHCP]2.0.CO;2

Nooner, S. L., and Chadwick, W. W. (2016). Inflation-Predictable Behavior and Co-Eruption Deformation at Axial Seamount. *Science (80-.).* 354 (6318), 1399–1403. doi: 10.1126/science.aah4666

Olins, H. C., Rogers, D. R., Preston, C., Ussler, W., Pargett, D., Jensen, S., et al. (2017). Co-Registered Geochemistry and Metatranscriptomics Reveal Unexpected Distributions of Microbial Activity Within a Hydrothermal Vent Field. *Front. Microbiol.* 8. doi: 10.3389/fmicb.2017.01042

Ondréas, H., Cannat, M., Fouquet, Y., Normand, A., Sarradin, P., and Sarrazin, J. (2009). Recent Volcanic Events and the Distribution of Hydrothermal Venting at the Lucky Strike Hydrothermal Field, Mid-Atlantic Ridge. *Geochem. Geophys. Geosystems* 10, Q02006. doi: 10.1029/2008GC002171

Opatkiewicz, A. D., Butterfield, D. A., and Baross, J. A. (2009). Individual Hydrothermal Vents at Axial Seamount Harbor Distinct Subseafloor Microbial Communities. *FEMS Microbiol. Ecol.* 70, 413–424. doi: 10.1111/j.1574-6941.2009.00747.x

Orcutt, B. N., Bradley, J. A., Brazelton, W. J., Estes, E. R., Goordial, J. M., Huber, J. A., et al. (2020). Impacts of Deep-Sea Mining on Microbial Ecosystem Services. *Limnol. Oceanogr.* 65, 1489–1510. doi: 10.1002/lno.11403

Palmer, M. R., and Ernst, G. G. J. (1998). Generation of Hydrothermal Megaplumes by Cooling of Pillow Basalts at Mid-Ocean Ridges. *Nature* 393, 643–647. doi: 10.1038/31397%0A

Pereira, H. M., Ferrier, S., Walters, M., Geller, G. N., Jongman, R. H. G., Scholes, R. J., et al. (2013). Essential Biodiversity Variables. *Science (80-.).* 339 (6117), 277–278. doi: 10.1126/science.1229931

Pester, N. J., Reeves, E. P., Rough, M. E., Ding, K., Seewald, J. S., and Seyfried, W. E. (2012). Subseafloor Phase Equilibria in High-Temperature Hydrothermal Fluids of the Lucky Strike Seamount (Mid-Atlantic Ridge, 37°17'n). *Geochm. Cosmochim. Acta* 90, 303–322. doi: 10.1016/j.gca.2012.05.018

Picheral, M., Catalano, C., Brousseau, D., Claustre, H., Coppola, L., Leymarie, E., et al. (2021). The Underwater Vision Profiler 6: An Imaging Sensor of Particle Size Spectra and Plankton, for Autonomous and Cabled Platforms. *Limnol. Oceanogr. Methods* 20, 115–129. doi: 10.1002/lom3.10475 Association for the Sciences of Limnology and Oceanography.

Picheral, M., Guidi, L., Stemmann, L., Karl, D. M., Iddaoud, G., and Gorsky, G. (2010). The Underwater Vision Profiler 5: An Advanced Instrument for High Spatial Resolution Studies of Particle Size Spectra and Zooplankton. *Limnol. Oceanogr. Methods* 8, 462–473. doi: 10.4319/lom.2010.8.462

Plum, C., Pradillon, F., Fujiwara, Y., and Sarrazin, J. (2016). Copepod Colonization of Organic and Inorganic Substrata at a Deep-Sea Hydrothermal Vent Site on the Mid-Atlantic Ridge. Deep Sea Res. Part II Top. *Stud. Oceanogr.* 137, 335–348. doi: 10.1016/j.dsr2.2016.06.008

Portail, M., Brandily, C., Cathalot, C., Colaço, A., Gélinas, Y., Husson, B., et al. (2018). Food-Web Complexity Across Hydrothermal Vents on the Azores Triple Junction. *Deep. Res. Part I Oceanogr. Res. Pap.* 131, 101–120. doi: 10.1016/j.dsr.2017.11.010

Puzenat, V., Escartín, J., Martelat, J. E., Barreyre, T., Bauer, S. L. M., Nomikou, P., et al. (2021). Shallow-Water Hydrothermalism at Milos (Greece): Nature, Distribution, Heat Fluxes and Impact on Ecosystems. *Mar. Geol.* 438, 106521. doi: 10.1016/j.margeo.2021.106521

Qiu, T., Zhao, Z., Zhang, T., Chen, C., and Chen, C. L. P. (2019). Underwater Internet of Things in Smart Ocean: System Architecture and Open Issues. *IEEE Trans. Ind. Inf.* 16, 4297–4307. doi: 10.1109/TII.2019.2946618

Ramirez-Llodra, E., Brandt, A., Danovaro, R., De Mol, B., Escobar, E. G., German, C. R., et al. (2010). Deep, Diverse and Definitely Different: Unique Attributes of the World's Largest Ecosystem. *Biogeosciences* 7, 2851–2899. doi: 10.5194/bg-7-2851-2010

Rogers, A., Brierley, A., Croot, P., Cunha, M., Danovaro, R., Devey, C., et al. (2015). "Delving Deeper: Critical Challenges for 21st Century Deep-Sea Research," in *Position Paper 22 of the European Marine Board*. Eds. K. E. Larkin, K. Donaldson and N. McDonough(Ostend, Belgium: Position Paper 22 of the European Marine Board), 224 . doi: 10.13140/RG.2.1.4077.0009

Rommevaux, C., Henri, P., Degboe, J., Chavagnac, V., Lesongeur, F., Godfroy, A., et al. (2019). Prokaryote Communities at Active Chimney and *In Situ* Colonization Devices After a Magmatic Degassing Event (37°N MAR, EMSO-Azores Deep-Sea Observatory). *Geochem. Geophys. Geosystems* 20, 3065–3089. doi: 10.1029/2018GC008107

Rountree, R. A., Aguzzi, J., Marini, S., Fanelli, E., DE LEO, F. C., Del Rio, J., et al. (2020). "Towards an Optimal Design for Ecosystem-Level Ocean Observatories," in *Oceanography and Marine Biology* 58, 79–105. doi: 10.1201/9780429351495-2

Rubin, K. H., Soule, S. A., Chadwick, W. W., Fornari, D. J., Clague, D. A., Embley, R. W., et al. (2012). Volcanic Eruptions in the Deep Sea. *Oceanography* 25, 143–157. doi: 10.5670/oceanog.2012.12

Santos, R. S., Escartín, J., Colaço, A., and Adamczewska, (2002). *Towards Planning of Seafloor Observatory Programs for the MAR Region: Proceedings of the II MoMAR Workshop*. (Azores, Portugal), 14–17 (Suppl. 3), 64.

Sarrazin, J., Blandin, J., Delauney, L., Dentrecolas, S., Dorval, P., Dupont, J., et al. (2007). "TEMPO: A New Ecological Module for Studying Deep-Sea Community Dynamics at Hydrothermal Vents," in *OCEANS 2007-Europe*. 1–4 (Ieee). doi: 10.1109/OCEANSE.2007.4302310

Sarrazin, J., Cuvelier, D., Peton, L., Legendre, P., and Sarradin, P. (2014). High-Resolution Dynamics of a Deep-Sea Hydrothermal Mussel Assemblage Monitored by the EMSO-Açores MoMAR Observatory. *Deep Sea Res. Part I Oceanogr. Res. Pap.* 90, 62–75. doi: 10.1016/j.dsr.2014.04.004

Sarrazin, J., Legendre, P., de Busserolles, F., Fabri, M.-C., Guilini, K., Ivanenko, V. N., et al. (2015). Biodiversity Patterns, Environmental Drivers and Indicator Species on a High-Temperature Hydrothermal Edifice, Mid-Atlantic Ridge. *Deep Sea Res. Part II Top. Stud. Oceanogr.* 121, 177–192. doi: 10.1016/j.dsr2.2015.04.013

Sarrazin, J., Portail, M., Legrand, E., Cathalot, C., Laes, A., Lahaye, N., et al. (2020). Endogenous Versus Exogenous Factors: What Matters for Vent Mussel Communities? *Deep. Res. Part I Oceanogr. Res. Pap.* 160, 103260. doi: 10.1016/j.dsr.2020.103260

Sarrazin, J., Robigou, V., Juniper, S. K., and Delaney, J. R. (1997). Biological and Geological Dynamics Over Four Years on a High-Temperature Sulfide Structure at the Juan De Fuca Ridge Hydrothermal Observatory. *Mar. Ecol. Prog. Ser.* 153, 5–24. doi: 10.3354/meps153005

Sarrazin, J., Rodier, P., Tivey, M. K., Singh, H., Schultz, A., and Sarradin, P. (2009). A Dual Sensor Device to Estimate Fluid Flow Velocity at Diffuse Hydrothermal Vents. *Deep. Res. Part I Oceanogr. Res. Pap.* 56, 2065–2074. doi: 10.1016/j.dsr.2009.06.008

Scheirer, D. S., Shank, T. M., and Fornari, D. J. (2006). Temperature Variations at Diffuse and Focused Flow Hydrothermal Vent Sites Along the Northern East Pacific Rise. *Geochem. Geophys. Geosystems* 7, Q03002. doi: 10.1029/2005GC001094

Schoening, T., Purser, A., Langenkämper, D., Suck, I., Taylor, J., Cuvelier, D., et al. (2020). Megafauna Community Assessment of Polymetallic-Nodule Fields With Cameras: Platform and Methodology Comparison. *Biogeosciences* 17, 3115–3133. doi: 10.5194/bg-17-3115-2020

Shank, T. M., Fornari, D. J., Von Damm, K. L., Lilley, M. D., Haymon, R. M., and Lutz, R. A. (1998). Temporal and Spatial Patterns of Biological Community Development at Nascent Deep-Sea Hydrothermal Vents (9°50'n, East Pacific Rise). *Deep. Res. Part II Top. Stud. Oceanogr.* 45, 465–515. doi: 10.1016/S0967-0645(97)00089-1

Shillito, B., Ravaux, J., Sarrazin, J., Zbinden, M., Sarradin, P., and Barthelemy, D. (2015). Long-Term Maintenance and Public Exhibition of Deep-Sea

Hydrothermal Fauna: The AbyssBox Project. *Deep. Res. Part II Top. Stud. Oceanogr.* 121, 137–145. doi: 10.1016/j.dsr2.2015.05.002

Singh, S. C., Crawford, W. C., Carton, H., Seher, T., Combier, V., Cannat, M., et al. (2006). Discovery of a Magma Chamber and Faults Beneath a Mid-Atlantic Ridge Hydrothermal Field. *Nature* 442, 1029–1032. doi: 10.1038/nature05105

Sloyan, B. M., Wilkin, J., Hill, K. L., Chidichimo, M. P., Cronin, M. F., Johannessen, J. A., et al. (2019). Evolving the Global Ocean Observing System for Research and Application Services Through International Coordinatio. *Front. Mar. Sci.* 6. doi: 10.3389/fmars.2019.00449

Smith, L. M., Barth, J. A., Kelley, D. S., Plueddemann, A., Rodero, I., Ulses, G. A., et al. (2018). The Ocean Observatories Initiative. *Oceanography* 31, 16–35. doi: 10.5670/oceanog.2018.105

Smith, K. L., Sherman, A. D., McGill, P. R., Henthorn, R. G., Ferreira, J., Connolly, T. P., et al. (2021). Abyssal Benthic Rover, an Autonomous Vehicle for Long-Term Monitoring of Deep-Ocean Processes. *Sci. Robot.* 6, eabl4925. doi: 10.1126/scirobotics.abl4925

Smith, C. R., Tunnicliffe, V., Colaço, A., Drazen, J. C., Gollner, S., Levin, L. A., et al. (2020). Deep-Sea Misconceptions Cause Underestimation of Seabed-Mining Impacts. *Trends Ecol. Evol.* 35, 853–857. doi: 10.1016/j.tree.2020.07.002

Sohn, R. A. (2007). Stochastic Analysis of Exit Fluid Temperature Records From the Active TAG Hydrothermal Mound (Mid-Atlantic Ridge, 26°N): 1. Modes of Variability and Implications for Subsurface Flow. *J. Geophys. Res.* 112, B07101. doi: 10.1029/2006JB004435

Spietz, R. L., Butterfield, D. A., Buck, N. J., Larson, B. I., Chadwick, W. W., Walker, S. L., et al. (2018). Deep-Sea Volcanic Eruptions Create Unique Chemical and Biological Linkages Between the Subsurface Lithosphere and the Oceanic Hydrosphere. *Oceanography* 31, 128–135. doi: 10.5670/oceanog.2018.120

Stefanni, S., Mirimin, L., Stanković, D., Chatzievangelou, D., Bongiorni, L., Marini, S., et al. (2022). Framing Cutting-Edge Integrative Taxonomy in Deep-Sea Biodiversity Monitoring *via* eDNA and Optoacoustic Augmented Observatories. *Front. Mar. Sci.* 8, 1914. doi: 10.3389/fmars.2021.797140

Stewart, L. C., Algar, C. K., Fortunato, C. S., Larson, B. I., Vallino, J. J., Huber, J. A., et al. (2019). Fluid Geochemistry, Local Hydrology, and Metabolic Activity Define Methanogen Community Size and Composition in Deep-Sea Hydrothermal Vents. *ISME J.* 13, 1711–1721. doi: 10.1038/s41396-019-0382-3

St. Laurent, L., and Garrett, C. (2002). The Role of Internal Tides in Mixing the Deep Ocean. *J. Phys. Oceanogr.* 32, 2882–2899. doi: 10.1175/1520-0485(2002)032<2882:TROITI>2.0.CO;2

Sweetman, A. K., Thurber, A. R., Smith, C. R., Levin, L. A., Mora, C., Wei, C.-L., et al. (2017). Major Impacts of Climate Change on Deep-Sea Benthic Ecosystems. *Elem. Sci. Anth.* 5, 4. doi: 10.1525/elementa.203

Taylor, J., Krumpen, T., Soltwedel, T., Gutt, J., and Bergmann, M. (2017). Dynamic Benthic Megafaunal Communities: Assessing Temporal Variations in Structure, Composition and Diversity at the Arctic Deep-Sea Observatory HAUSGARTEN Between 2004 and 2015. *Deep. Res. Part I Oceanogr. Res. Pap.* 122, 81–94. doi: 10.1016/j.dsr.2017.02.008

Taylor, J., Staufenbiel, B., Soltwedel, T., and Bergmann, M. (2018). Temporal Trends in the Biomass of Three Epibenthic Invertebrates From the Deep-Sea Observatory HAUSGARTEN (Fram Strait, Arctic Ocean). *Mar. Ecol. Prog. Ser.* 602, 15–29. doi: 10.3354/meps12654

Theissen-Krah, S., Rüpke, L. H., and Hasenclever, J. (2016). Modes of Crustal Accretion and Their Implications for Hydrothermal Circulation. *Geophys. Res. Lett.* 43, 1124–1131. doi: 10.1002/2015GL067335

Thiel, H., Kirstein, K. O., Luth, C., Luth, U., Luther, G. W., Meyer-Reil, L. A., et al. (1994). Scientific Requirements for an Abyssal Benthic Laboratory. *J. Mar. Syst.* 4, 421–439. doi: 10.1016/0924-7963(94)90019-1

Thomson, R. E., Mlhály, S. F., Rabinovich, A. B., McDuff, R. E., Veirs, S. R., and Stahr, F. R. (2003). Constrained Circulation at Endeavour Ridge Facilitates Colonization by Vent Larvae. *Nature* 424, 545–549. doi: 10.1038/nature01824

Thomson, R. E., Roth, S. E., and Dymond, J. (1990). Near-Inertial Motions Over a Mid-Ocean Ridge: Effects of Topography and Hydrothermal Plumes. *J. Geophys. Res.* 95, 7261–7278. doi: 10.1029/JC095iC05p07261

Tivey, M. K., Bradley, A. M., Joyce, T. M., and Kadko, D. (2002). Insights Into Tide-Related Variability at Seafloor Hydrothermal Vents From Time-Series Temperature Measurements. *Earth Planet. Sci. Lett.* 202, 693–707. doi: 10.1016/S0012-821X(02)00801-4

Tolstoy, M., Cowen, J. P., Baker, E. T., Fornari, D. J., Rubin, K. H., Shank, T. M., et al. (2006). A Sea-Floor Spreading Event Captured by Seismometers. *Science (80-.).* 314 (5807), 1920–1922. doi: 10.1126/science.1133950

Tomasi, B., Preisig, J., Deane, G. B., and Zorzi, M. (2011). "A Study on the Wide-Sense Stationarity of the Underwater Acoustic Channel for Non-Coherent Communication Systems," in *17th European Wireless 2011 - Sustainable Wireless Technologies*: Vienna. 1–6.

Tomasi, B., Zappa, G., McCoy, K., Casari, P., and Zorzi, M. (2010). "Experimental Study of the Space-Time Properties of Acoustic Channels for Underwater Communications," in *Ocean. IEEE Sydney, Ocean. 2010*. doi: 10.1109/OCEANSSYD.2010.5603667

Toomey, D. R., Jousselin, D., Dunn, R. A., Wilcock, W. S. D., and Detrick, R. S. (2009). Toomey Et Al. Reply. *Nature* 458, E12–E13. doi: 10.1038/nature07888

Tunnicliffe, V. (1991). The Biology of Hydrothermal Vents - Ecology and Evolution. *Oceanogr. Mar. Biol.* 29, 319–407.

Tunnicliffe, V., Juniper, S. K., and Sibuet, M. (2003). "Reducing Environments of the Deep-Sea Floor," in *Ecosystems of the World: The Deep Sea. Chapter 4* (Amsterdam, Netherlands: Elsevier Press), 81–110.

Van Ark, E., Detrick, R., Canales, J. P., Carbotte, S. M., Harding, A., Kent, G., et al. (2007). Seismic Structure of the Endeavour Segment, Juan De Fuca Ridge: Correlations With Seismicity and Hydrothermal Activity. *J. Geophys. Res.* 112, B02401. doi: 10.1029/2005JB004210

Van Audenhaege, L., Matabos, M., Brind'Amour, A., Drugmand, J., Laës-Huon, A., Sarradin, P. -M., et al. (2022). Long-Term Monitoring Reveals Unprecedented Stability of a Vent Mussel Assemblage on the Mid-Atlantic Ridge. *Prog. Oceano.* 204. doi: 10.1016/j.pocean.2022.102791

van den Burg, S., Visscher, M., Sonneveld, A., Berges, B., Jansen, L., Sharp, F., et al. (2021). Uptake of New Technology for Ocean Observation. *Eur. Marit. Fish. Fund. Publications Office*, 2021. doi: 10.2926/37198

Van Dover, C. L. (2014). Impacts of Anthropogenic Disturbances at Deep-Sea Hydrothermal Vent Ecosystems: A Review. *Mar. Environ. Res.* 102, 59–72. doi: 10.1016/j.marenvres.2014.03.008

Van Dover, C. L. (2019). Inactive Sulfide Ecosystems in the Deep Sea: A Review. *Front. Mar. Sci.* 6. doi: 10.3389/fmars.2019.00461

Van Dover, C. L., Colaço, A., Collins, P. C., Croot, P., Metaxas, A., Murton, B. J., et al. (2020). Research is Needed to Inform Environmental Management of Hydrothermally Inactive and Extinct Polymetallic Sulfide (PMS) Deposits. *Mar. Policy* 121, 104183. doi: 10.1016/j.marpol.2020.104183

Vehling, F., Hasenclever, J., and Rüpke, L. (2021). Brine Formation and Mobilization in Submarine Hydrothermal Systems: Insights From a Novel Multiphase Hydrothermal Flow Model in the System H2O–NaCl. *Transp. Porous Media* 136, 65–102. doi: 10.1007/s11242-020-01499-6

Vic, C., Ferron, B., Thierry, V., Mercier, H., and Lherminier, P. (2021). Tidal and Near-Inertial Internal Waves Over the Reykjanes Ridge. *J. Phys. Oceanogr.* 51, 419–437. doi: 10.1175/jpo-d-20-0097.1

Vic, C., Garabato, A. C. N., Green, J. A. M., Spingys, C., Forryan, A., Zhao, Z., et al. (2018a). The Lifecycle of Semidiurnal Internal Tides Over the Northern Mid-Atlantic Ridge. *J. Phys. Oceanogr.* 48, 61–80. doi: 10.1175/JPO-D-17-0121.1

Vic, C., Gula, J., Roullet, G., and Pradillon, F. (2018b). Dispersion of Deep-Sea Hydrothermal Vent Effluents and Larvae by Submesoscale and Tidal Currents. *Deep. Res. Part I Oceanogr. Res. Pap.* 133, 1–18. doi: 10.1016/j.dsr.2018.01.001

Waeles, M., Cotte, L., Pernet-Coudrier, B., Chavagnac, V., Cathalot, C., Leleu, T., et al. (2017). On the Early Fate of Hydrothermal Iron at Deep-Sea Vents: A Reassessment After *in Situ* Filtration. *Geophys. Res. Lett.* 44, 4233–4240. doi: 10.1002/2017GL073315

Webb, T. J., Vanden Berghe, E., and O'Dor, R. (2010). Biodiversity's Big Wet Secret: The Global Distribution of Marine Biological Records Reveals Chronic Under-Exploration of the Deep Pelagic Ocean. *PloS One* 5, e10223. doi: 10.1371/journal.pone.0010223

Werner, F. E., Cowen, R. K., and Paris, C. B. (2007). Coupled Biological and Physical Models: Present Capabilities and Necessary Developments for Future Studies of Population Connectivity. *Oceanography* 20, 54–69. doi: 10.5670/oceanog.2007.29

West, M., Menke, W., Tolstoy, M., Webb, S., and Sohn, R. (2001). Magma Storage Beneath Axial Volcano on the Juan De Fuca Mid-Ocean Ridge. *Nature* 413, 833–836. doi: 10.1038/35101581

Wilcock, W. S. D., Tolstoy, M., Waldhauser, F., Garcia, C., Tan Yen, J., Bohnenstiehl, D. R., et al. (2016). Seismic Constraints on Caldera Dynamics From the 2015 Axial Seamount Eruption. *Science* 354 (6318), 1395–1399. doi: 10.1126/science.aah5563

Xu, G., and Di Iorio, D. (2012). Deep Sea Hydrothermal Plumes and Their Interaction With Oscillatory Flows. *Geochem. Geophys. Geosystems* 13, 1–18. doi: 10.1029/2012GC004188

Xu, G., Larson, B. I., Bemis, K. G., and Lilley, M. D. (2017). A Preliminary 1-D Model Investigation of Tidal Variations of Temperature and Chlorinity at the Grotto Mound, Endeavour Segment, Juan De Fuca Ridge. *Geochem. Geophys. Geosystems* 18 (1), 75–92. doi: 10.1002/2016GC006537

Young, C. M., He, R., Emlet, R. B., Li, Y., Qian, H., Arellano, S. M., et al. (2012). Dispersal of Deep-Sea Larvae From the Intra-American Seas: Simulations of Trajectories Using Ocean Models. *Integr. Comp. Biol.* 52, 483–496. doi: 10.1093/icb/ics090

Zeppilli, D., Bellec, L., Cambon-Bonavita, M.-A., Decraemer, W., Fontaneto, D., Fuchs, S., et al. (2019). Ecology and Trophic Role of Oncholaimus Dyvae Sp. Nov. (Nematoda: Oncholaimidae) From the Lucky Strike Hydrothermal Vent Field (Mid-Atlantic Ridge). *BMC Zool.* 4, 6. doi: 10.1186/s40850-019-0044-y

Zeppilli, D., Vanreusel, A., Pradillon, F., Fuchs, S., Mandon, P., James, T., et al. (2015). Rapid Colonisation by Nematodes on Organic and Inorganic Substrata Deployed at the Deep-Sea Lucky Strike Hydrothermal Vent Field (Mid-Atlantic Ridge). *Mar. Biodivers.* 45, 489–504. doi: 10.1007/s12526-015-0348-2

Conflict of Interest: The authors declare that the research was conducted in the absence of any commercial or financial relationships that could be construed as a potential conflict of interest.

frontiers | Frontiers in Marine Science

ORIGINAL RESEARCH
published: 27 May 2022
doi: 10.3389/fmars.2022.849976

Non-Vent Megafaunal Communities on the Endeavour and Middle Valley Segments of the Juan de Fuca Ridge, Northeast Pacific Ocean

Monika Neufeld[1]*, *Anna Metaxas*[1] and *John W. Jamieson*[2]

[1] Department of Oceanography, Dalhousie University, Halifax, NS, Canada, [2] Department of Earth Sciences, Memorial University of Newfoundland, St. John's, NL, Canada

There has been increasing interest in mining polymetallic sulfide deposits at deep-sea inactive hydrothermal vents, leading to the development of regulations to minimize risk to the marine environment. While an extensive body of literature exists on the ecological communities at active vents, fauna at inactive hydrothermal vents and the vent periphery are poorly described and their vulnerability to disturbance is unknown. We examined patterns in abundance of non-vent epibenthic megafauna on two segments of the Juan de Fuca Ridge, Northeast Pacific Ocean. Video footage was collected by the remotely operated vehicle ROPOS during four dives at the Endeavour Segment and two dives at Middle Valley in August 2016. At the Endeavour Segment, the substrate is characterized predominantly by basalt and edifices of hydrothermal sulfide that range in hydrothermal activity from inactive to vigorous, high-temperature venting. In contrast, Middle Valley is heavily sedimented and most hydrothermal activity is low-temperature diffuse flow. While inactive substrates at both sites harboured slow-growing sessile fauna, the dominant members of the community differed between sites. At Endeavour, the most abundant morphotaxa included rossellid vase sponges, alcyonacean corals, and crinoids. Estimated richness and total abundance of morphotaxa was higher on hard substrates than sedimented substrates and highest on inactive chimneys. At Middle Valley, the most abundant morphotaxa included antipatharian corals, anemones, and ascidians. Species richness was higher on inactive chimneys and mixed substrates than sediment. The abundance of some megafauna varied with proximity to active vents. At Endeavour, deep-water corals were nearly absent within 25 m of active chimneys and very few occurred between 26 and 50 m from active chimneys. Rossellid vase sponges were in low abundance within 25 m of active chimneys but were more abundant than corals at 26-50 m from active chimneys. This project contributes baseline data on megafaunal assemblages on inactive hydrothermal vents and can provide the basis for more focused research on the structure and function of inactive vent ecosystems.

Keywords: deep-sea fauna, Juan de Fuca Ridge, polymetallic sulfide deposits, deep-sea mining, non-vent fauna, deep-water corals, vasiform sponges, inactive hydrothermal vents

OPEN ACCESS

Edited by:
David Billett,
Deep Seas Environmental Solutions Ltd., United Kingdom

Reviewed by:
Klaas Gerdes,
INES - Integrated Environmental Solutions, Germany
Tina Molodtsova,
P.P. Shirshov Institute of Oceanology (RAS), Russia

***Correspondence:**
Monika Neufeld
Monika.Neufeld@dal.ca

Specialty section:
This article was submitted to Deep-Sea Environments and Ecology, a section of the journal Frontiers in Marine Science

Received: *06 January 2022*
Accepted: *27 April 2022*
Published: *27 May 2022*

Citation:
Neufeld M, Metaxas A and Jamieson JW (2022) Non-Vent Megafaunal Communities on the Endeavour and Middle Valley Segments of the Juan de Fuca Ridge, Northeast Pacific Ocean. Front. Mar. Sci. 9:849976. doi: 10.3389/fmars.2022.849976

INTRODUCTION

At deep-sea hydrothermal vents, hot, metal-rich, fluid is discharged into the ocean from beneath the seafloor. Upon mixing with ambient seawater, sulfide and sulfate minerals precipitate out of the hydrothermal fluid and accumulate on the seabed (Haymon, 1983). Hydrothermal vents occur along seafloor tectonic boundaries such as mid-ocean ridges, volcanic arcs, and back arc basins, where shallow magmatic heat sources drive convective circulation of seawater through oceanic crust (Hannington et al., 2005). These polymetallic sulfide-rich deposits accumulate over the lifetime of the active vent, forming chimney structures that can be 10s of meters tall and mounds with diameters of up to several hundred meters (Hannington et al., 2010). Vents typically cluster to form vent fields consisting of several chimneys and/or mounds spread over 1,000s of square meters. Vents, and vent fields, have a finite lifetime that, depending on the tectonic setting, can be up to hundreds of thousands of years, but will eventually become inactive (Cherkashov et al., 2017; Jamieson and Gartman, 2020). However, even within an active vent field, the locations of venting can change over time, and active vent fields typically contain a mixture of active and inactive chimneys and/or mounds. Once vent chimneys become inactive, they can persist as upright structures, but will weather over time and collapse into sulfide rubble or boulders on the seafloor.

Active hydrothermal vents support highly productive and dense communities of endemic species that rely on symbiotic chemoautotrophic microbes and fluid flow (Tunnicliffe et al., 1998; Van Dover, 2000). Community succession and dynamics on active hydrothermal vents is primarily driven by changes in fluid flow and temperature (Sarrazin et al., 1997; Marcus et al., 2009; Sen et al., 2014). When fluid flow wanes and eventually ceases, many vent-endemic species, particularly those with symbiont requirements, such as tubeworms can no longer survive, and non-vent fauna can colonize the deposits and nearby area. The high temperature, low oxygen, high sulfide and high metal fluid conditions at active hydrothermal vents are thought to be toxic to non-vent taxa which will not colonize a vent site until fluid flow has subsided (Van Dover, 2000).

The sphere of influence of the hydrothermal conditions beyond their immediate area of occurrence is currently poorly understood (Levin et al., 2016). 'Peripheral' areas to hydrothermal vents fall outside the direct impact of active hydrothermal fluid and are thought to be a transition zone between the active environments and the rest of the deep sea (Arquit, 1990; Sen et al., 2016). Closer to active vents, faunal communities comprise both vent associated and non-vent fauna, but non-vent taxa dominate at increasing distances (Arquit, 1990). Non-vent communities in the peripheral zone are higher in biomass and density than the surrounding deep sea, likely benefitting from increased primary productivity closer to vents (Arquit, 1990; Galkin, 1997). Non-vent fauna include species that are found on substrates throughout the deep sea and utilize nutritional resources derived from the photosynthetic food chain.

While an extensive body of literature exists on the ecological communities associated with active vents (ex. Tunnicliffe, 1991; Tunnicliffe et al., 1998; Van Dover, 2000; Mullineaux et al., 2018; Dasgupta et al., 2021), fauna at inactive hydrothermal vents are poorly described (Van Dover et al., 2020). Generally, inactive vents support communities of non-vent 'background fauna' that occur on hard substrates throughout the deep sea (Galkin, 1997; Erickson et al., 2009; Collins et al., 2012; Sen et al., 2014; Boschen et al., 2015; Boschen et al., 2016; Gerdes et al., 2019; Van Dover, 2019), but it is possible that inactive vents harbor unique species assemblages adapted to the conditions of weathering sulfide minerals (Van Dover, 2011; Van Dover et al., 2020). In the western South Pacific, these non-vent faunal communities associated with inactive vents include large gorgonian corals, actiniarian anemones, hydroids, brisingid sea stars, carnivorous sponges, and stalked barnacles (Galkin, 1997; Erickson et al., 2009; Collins et al., 2012). In addition to these taxa, assemblages in the South Pacific and Indian Oceans also include comatulid crinoids, hexactinellid sponges, ascidians, and brachiopods (Boschen et al., 2015; Boschen et al., 2016; Gerdes et al., 2019). These assemblages on inactive deposits are unique compared to assemblages on both active vents (Boschen et al., 2015; Boschen et al., 2016) and adjacent hard substrates (Gerdes et al., 2019). Large corals, possibly up to 200 years old, are a dominant member of inactive vent communities (Boschen et al., 2016), and aggregate on the tallest and most exposed surfaces of inactive chimneys (Galkin, 1997). While some inactive chimneys are densely populated, others are barren, indicating that colonization may be impacted by factors such as the proximity to active vents or ocean currents (Boschen et al., 2016).

In the Northeast Pacific, faunal communities on the vent periphery closely resemble typical benthic non-vent fauna in the surrounding area. On Cobb Seamount, away from active hydrothermal vents, deep-sea (up to 1150 m) fauna included actiniarian anemones, Alcyonacea and Antipatharia corals, holothurians, crabs, and glass sponges (Rossellidae) (Du Preez et al., 2016). On the periphery of active vents on the Juan de Fuca Ridge, sponges, crabs, sea stars, and holothurians were common (Arquit, 1990; Milligan and Tunnicliffe, 1994). On the Cleft segment, the most abundant groups included alcyonacean corals and sea pens, crinoids, and holothurians (Milligan and Tunnicliffe, 1994). On the vent periphery on Gorda Ridge in the Northeast Pacific, filter feeders such as crinoids and deep-water corals dominated hard substrate, while deposit feeders and scavengers such as asteroids and holothurians were more abundant on sediment (Carey et al., 1990).

There is increasing interest in mining polymetallic sulfide deposits that form at hydrothermal vent fields due to their potential high concentrations of metals such as copper, zinc, gold and silver (Petersen et al., 2016). Hydrothermally active polymetallic sulfide deposits are detected by chemical and physical anomalies in the seawater caused by the plumes of black smokers. However, active deposits are considered ecologically vulnerable and their protection from mining activities has been proposed (Van Dover et al., 2018). Hydrothermally inactive sulfide deposits may provide an

alternative target for mining, but they are much more difficult to locate as they do not have an associated hydrothermal plume. In addition to the impacts on communities inhabiting inactive deposits themselves, inactive deposits and active vents often cluster together (Clague et al., 2020), thus mining inactive deposits could still harm nearby active vent ecosystems (Jamieson and Gartman, 2020).

No commercial mining is currently being undertaken in the deep sea, but Japan conducted a testing of mining equipment on an inactive hydrothermal mound off the coast of Okinawa in 2017 (Okamoto et al., 2018). Before commercial mining starts, there is a critical need for baseline ecological studies on inactive vents to fully understand how faunal communities will be impacted by mining sulfide deposits on the seafloor (Van Dover et al., 2020). Further, better data are required to inform a mining code that is currently in development by the International Seabed Authority (ISA) (Earth Negotiations Bulletin, 2020).

The Endeavour and Middle Valley segments form part of the Juan de Fuca Ridge, which is spreading at an intermediate full rate of 6 cm yr^{-1} (full rate; Riddihough, 1984). The segments host two geologically distinct hydrothermal systems, with differences in associated substrate and style of venting. The Endeavour vent field has five main hydrothermally active vent clusters, spaced ~2 km apart along the unsedimented basaltic floor of a 0.5 -1 km wide axial valley (Kelley et al., 2012). A wide range of hydrothermal venting conditions occur within this vent field, from tall (> 20 m), high-temperature active chimneys to areas of low-temperature diffuse flow. Abundant (> 500) inactive chimneys and mounds occur between the active vent clusters, indicating a dynamic evolution of hydrothermal venting over the ~6,000 years of recorded hydrothermal activity along the axial valley (Jamieson et al., 2013; Clague et al., 2020). The vent field, located in Canada's exclusive economic zone, is a designated Marine Protected Area (MPA). The Middle Valley vent field is located 60 km northeast of Endeavour. A key difference between Middle Valley and Endeavour is the nearly 500 m of continental-derived turbidite sediments that have accumulated along Middle Valley, compared to the exposed basalt at Endeavour (Delaney et al., 1992; Juniper et al., 1992). There are two known locations of active venting at Middle Valley: Area of Active Venting (AAV) and Bent Hill (Ames et al., 1993). Unlike Endeavour, there is no evidence for abundant past (i.e. now inactive) venting outside of the active venting areas. Hydrothermal activity is primarily characterized by low-temperature diffuse flow, although there are a few focused, higher-temperature active chimneys in the area.

In this study, we quantified the type, abundance, and distribution of non-vent epibenthic megafaunal assemblages at the Endeavour and Middle Valley vent fields using data collected by the remotely operated vehicle ROPOS in August 2016. We described the distribution of select taxa relative to active venting using patterns in faunal abundance along transects that extended from active chimneys to inactive sulfide deposits and peripheral hard substrate. We expected that non-vent taxa would include deep-water corals, crinoids, sponges, and anemones at both Endeavour and Middle Valley, but also expected differences in the specific composition and abundance of these faunal communities between the two locations because of the differences in substrate and style of venting. Additionally, we predicted that the abundance of non-vent fauna would increase with distance from active hydrothermal flow. This study will contribute to a better understanding of the ecology at inactive vent sites on two types of hydrothermal systems, ultimately supporting the development of conservation and resource management plans for polymetallic sulfide deposits.

MATERIALS AND METHODS

Data Collection

Video footage was collected with the remotely operated vehicle (ROV) ROPOS aboard the CCGS John P. Tully during four dives at the Endeavour segment (R1938, R1939, R1940 and R1941) and two dives at Middle Valley (R1942 and R1943), between 7 and 13 August 2016 (**Figure 1**). At Endeavour, dives R1938 and R1941 traversed along the axial valley floor near the active Sasquatch and High Rise vent clusters, while dives R1939 and R1940 started at the valley floor near Main Endeavour, and traversed up the eastern and western axial valley walls, respectively. At Middle Valley, dives R1942 and R1943 traversed Bent Hill and the Dead Dog vent field (located in the AAV), respectively. Individual dive tracks ranged in length between 2814 and 4646 m at the Endeavour vent field, and between 3180 and 3751 m at Middle Valley (**Table 1**).

ROPOS is equipped with two HD (1,920 × 1,080 pixels) video cameras: a forward-facing Insite Pacific Zeus-Plus with pan, tilt, and zoom capabilities and a downward-facing Insite Pacific Mini-Zeus with tilt only. Both cameras were equipped with a set of parallel scaling lasers that were spaced 10 cm apart into the field of view. Metadata associated with the dives included date, time, geographical coordinates, depth, heading, and altitude from the seafloor of ROPOS. An IXSEA GAPS ultra-short baseline system, combined with a Sonardyne SYRINX Doppler velocity log and an IXSEA OCTANS III survey-grade gyrocompass using the Canadian Scientific Submersible Facility's LOKI Kalman filter were used for vehicle positioning at the seafloor, providing absolute positioning at better than 5-m accuracy.

Imagery Analysis

Two different analytical approaches were used to estimate the abundance of non-vent morphotaxa (typical vent taxa were excluded from the analysis). The occurrence of large-sized megafauna of relatively low abundance, such as deep-water alcyonacean and black corals and rossellid vase sponges (Rossellidae), were recorded using the forward-facing Zeus video. The video was annotated during playback using the Ocean Floor Observation Protocol software (OFOP 3.3.8c, Huetten and Greinert, 2008; Scientific Abyss Mapping Services, 2009). OFOP synchronizes the video file with the location data recorded during the dive, georeferencing all observations along

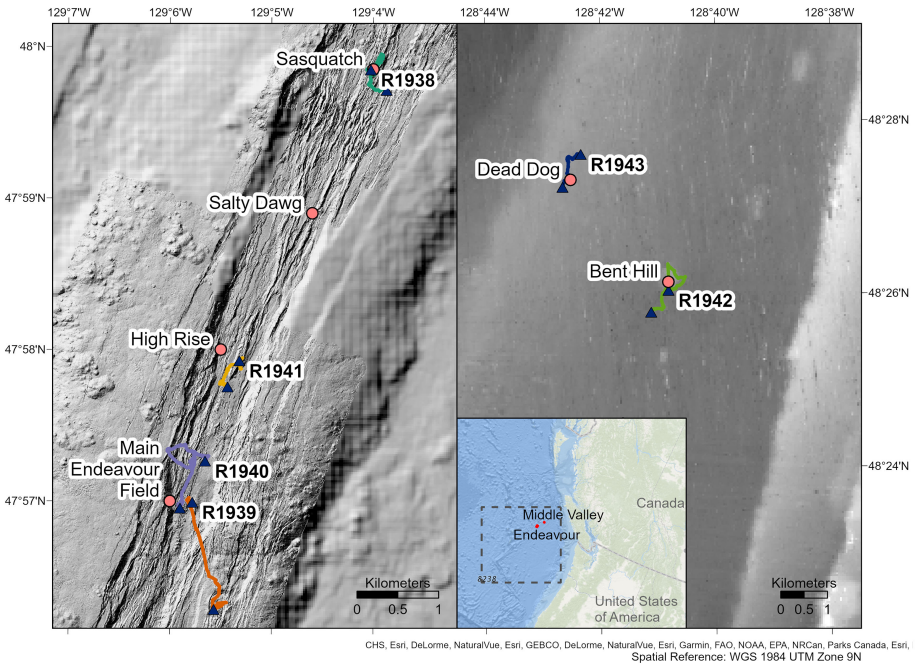

FIGURE 1 | Track lines of dives R1938-R1943 conducted by the remotely operated vehicle ROPOS on the Endeavour (left) and Middle Valley (right) segments of the Juan de Fuca Ridge. Triangles represent the start and end points of dives. Known vent fields are shown. The general location of the Juan de Fuca Ridge (dashed box) and position of Endeavour and Middle Valley are shown in the inset map. Maps created in ArcGIS Pro, bathymetry and vent locations provided by ONC, MBARI, and the University of Washington.

the dive track. During playback, all visible megafauna greater than ~ 5 cm in the largest dimension (identified to the highest taxonomic resolution) were annotated, along with the substrate type to which they were attached and the location of every active and inactive chimney over the entire dive track. We ensured that duplicate recordings of the same individuals were avoided.

For all other morphotaxa, abundance was measured using images that were extracted from the downward-facing Mini Zeus video at approximately 20-m intervals using the OFOP software (**Supplementary Figure 1**). Suitable images were selected based on several criteria: (1) the area of the image did not exceed 20 m^2; (2) the substrate was perpendicular to the camera angle (± ~ 10˚); (3) the scaling lasers were visible and on the same plane as the substrate; and (4) the seafloor was clearly visible. Images were cropped to include only the extent of seafloor that was visible as a single horizontal plane and to exclude any areas obstructed by fish, the ROPOS vehicle, lens distortions, or suspended sediment. Cropped images were not included in the analysis if the area after cropping was < 1 m^2. If an image was deemed unsuitable, the next available image was used. If the

TABLE 1 | Characteristics of dives performed by the remotely operated vehicle ROPOS at the Endeavour vent field (R1938-R1941) and Middle Valley (R1942 and R1943) on the Juan de Fuca Ridge.

Dive	Date	Start		End		Total track length			Mean depth
	(yyyy-mm-dd)	Latitude	Longitude	Latitude	Longitude	Time (hours)	Length (m)	Length with visible seafloor (m)	[m; range]
R1938	2016-08-07	47.9975	-129.0671	47.9953	-129.0645	7.08	4,282	3,769	2149 [2104-2169]
R1939	2016-08-09	47.9499	-129.0963	47.9381	-129.0928	8.50	3,189	2,704	2178 [2110-2214]
R1940	2016-08-10	47.9545	-129.0942	47.9493	-129.0983	8.67	4,646	3,913	2166 [2066-2201]
R1941	2016-08-11	47.9626	-129.0906	47.9655	-129.0886	8.63	2,814	2,651	2181 [2135-2189]
R1942	2016-08-12	48.4299	-128.6853	48.4341	-128.6803	7.33	3,751	3,647	2432 [2390-2450]
R1943	2016-08-13	48.4603	-128.7056	48.4540	-128.7109	7.27	3,180	3,148	2408 [2394-2416]

Coordinates are given in decimal degrees.

distance between suitable images exceeded ~ 50 m, images were captured manually in OFOP to maintain the ~ 20-m spacing where possible. However, there were large segments of the dives where there were no suitable images because the ROV was travelling too far above the seafloor. To capture data from the vertical walls of inactive chimneys, images were extracted in a similar fashion but from the forward-facing Zeus footage because it was perpendicular to the substrate. All suitable images were imported into ImageJ, an image processing and analysis software, and the 2D area of the image was calculated using the scaling lasers. All visible megafauna > 2 cm were enumerated and identified to the highest taxonomic resolution. Additionally, the substrate in each image was classified by measuring the percent cover of each of 4 substrate types (basalt, hydrothermally derived, sediment, and actively venting) and their combinations if more than one type was present in an image. A substrate was classified as actively venting if live tubeworms or microbial matting were present in the image. If a substrate accounted for > 75% of the total image area, it was classified as the dominant type. If multiple substrate types were present, each accounting for > 25% of the image area, the image was classified as a mixed substrate type.

Data Analysis

All records of deep-water corals and rossellid vase sponges (Rossellidae) from the forward-facing video extracted from OFOP were loaded into the mapping software ArcGIS Pro, where the data were plotted along the dive tracks and summed over a 10 x 10 m square grid superimposed onto the dive track. For the dives at Endeavour only, the distance from each coral and vase sponge record to the nearest active vent was measured in ArcGIS Pro to determine the influence of active hydrothermal fluid flow on the abundance of these groups. To do this, the georeferenced positions of all known active vents and their areal extent within the Endeavour segment (Jamieson et al., 2014; Clague et al., 2020; this study) were combined into a single polygon layer in ArcGIS Pro. The polygons represent the extent of the sulfide edifices (i.e. the physical vent structures) and we assumed that fluid discharge would occur primarily within the polygon boundaries. It is possible that active venting occurs in areas outside the polygons, but we assumed it to be insignificant compared to the venting inside the polygon. For each of the active vents recorded in this study, we applied a 10-m buffer as an estimate of the extent of fluid flow at each chimney (Kelly et al., 2007). Areal extent was used to account for the presence of multiple chimneys at a single vent (e.g., Big Bad Ben) and positional error of the navigation system (5 m, Auger - CSSF personal communication). The distance from each coral or sponge record to the edge of the nearest vent polygon was measured. This analysis was not done for Middle Valley because, while there were a few focused chimneys (8 total), most hydrothermal activity was characterized as diffuse flow that spanned a large area with no distinct point source. For all dives at Endeavour, total abundance of morphotaxa was calculated for each substrate type.

The abundance data from the image capture analysis was used to construct individual-based rarefaction curves for each dive and each substrate type at Endeavour and at Middle Valley. We combined images from all dives on each segment, assuming a similar species pool within each location, to maximize the number of individuals recorded on each substrate type. The richness of morphotaxa was compared between dives and substrate types using a common number of individuals sampled (Hurlbert, 1971). Analyses were conducted in RStudio using the iNEXT software package (Chao et al., 2014; Hsieh et al., 2016).

RESULTS

In total, 101 morphotaxa from 8 different phyla were identified at Endeavour and Middle Valley (**Supplementary Table 1**). At Endeavour, the most abundant morphotaxa were demosponges, comatulid crinoids, rossellid vase sponges, alcyonacean corals, and holothurians (Family Laetmogonidae). At Middle Valley, the most abundant morphotaxa were black corals, holothurians (Family Psychropotidae), anemones, ascidians, and stalked barnacles.

Substrate

At Endeavour, the most common substrate type was basalt, often as lobate basalt or sheet flows. This segment of the ridge is not heavily sedimented, resulting in mostly exposed hard substrate. Inactive sulfide deposits occurred as large upright chimneys and talus (**Figure 2**). Chimneys were defined as active if there was visible fluid flow in the video footage, or if there were vent obligate species present. There were 3 active chimneys recorded on dive R1938, 9 on dive R1939, 9 on dive R1940, and 4 on dive R1941. In contrast, Middle Valley was characterized primarily by thick sediment and diffuse hydrothermal flow was present over large areas without an identifiable point source. The few active chimneys (2 on dive R1942, 6 on dive R1943) that were present were much smaller than the large edifices on the Endeavour segment. Small patches of hydrothermal material were dispersed across the sedimented seafloor.

Large Mega-Epifauna

At Endeavour, 814 deep-water corals were recorded, mostly in the Order Alcyonacea (86.7% Alcyonacea, 11.7% Antipatharia). The most represented groups included Alcyoniidae (37%), Primnoidae (21%), and various small antipatharian corals (Antipatharia spp., 21%, likely Schizopathidae) on dive R1938; Plexauridae (60%) and Primnoidae (15%) on dive R1939; and Plexauridae (64%) and Alcyoniidae (32%) on dive R1940. No corals were recorded on dive R1941. Corals were always observed attached to hard substrate (basalt and inactive hydrothermal deposits) and were often seen on elevated and more exposed surfaces of basalt ridges and inactive chimneys.

Overall, the abundance of deep-water corals was highest on the walls of inactive chimneys and basalt ridges, and at distances > 50 m from active chimneys (**Figures 3**, **4**). Corals were nearly absent within 25 m of active chimneys and sparse at 26-50 m despite the availability of hard substrate, except on dives R1938 and R1939 where a few soft corals (Alcyoniidae spp.) were recorded (**Figure 4**). On dive R1939, many corals were clustered on inactive sulfide deposits and chimneys at the

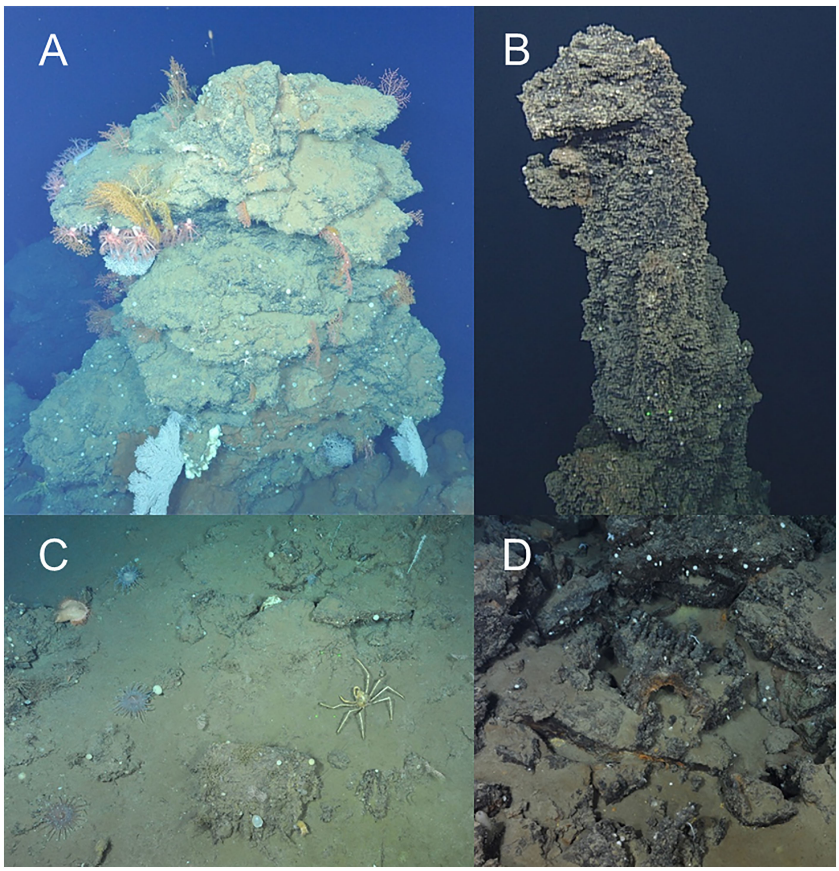

FIGURE 2 | Photographs of inactive sulfide deposits at Endeavour and Middle Valley captured by ROPOS in August 2016. **(A)** An inactive chimney (dive R1939) populated with corals (Alcyoniidae spp., Plexauridae spp., Primnoidae sp. 1 and Primnoidae sp. 3), sponges (Demospongiae sp. 1 and white encrusting), and a holothurian (*Pannychia moseleyi*); **(B)** 'Big Bad Ben', the > 30-m tall inactive chimney (dive R1938); **(C)** Sedimented sulfide rubble (dive R1943) colonized by jewelled and fly trap anemones (*Corallimorphus* sp. 1 and *Actinoscyphia aurelia*), stalked barnacles (Scalpellidae sp. 1), bamboo coral (*Lepidisis* sp. 1), schizopathid corals (*Umbellapathes* sp. 1), ascidians, and an oregoniid (*Macroregonia* sp. 1) crab; **(D)** Sulfide rubble with fragments of a toppled chimney (dive R1938).

south end of the dive (at the farthest distances from active chimneys and from the ridge axis) and on a basalt ridge located 201-300 m from active chimneys. The highest abundances of corals on dives R1938 and R1940 also correspond with the locations of inactive chimneys and basalt ridges.

There did not appear to be a difference in the occurrence of deep-water corals between basalt and hydrothermally derived substrate (**Figure 5**). A greater number of corals were recorded on basalt than on hydrothermally derived substrate on dive R1938 while the opposite was the case on dive R1940. There was no difference between the two on dive R1939.

At Endeavour, rossellid vase sponges (Rossellidae) were the other numerically dominant large mega-epifaunal morphotaxon and were present almost everywhere on the dive tracks except directly on active chimneys (**Figure 6**). In all dives, they occurred in low abundance within 25 m of active chimneys but were more abundant than corals at 26-50 m from active chimneys (**Figure 4**). Very few rossellid vase sponges occurred on heavily sedimented regions of the dives at Endeavour. Unlike deep-water corals, there tended to be more records of rossellid vase sponges on basalt than hydrothermally derived substrate for all dives (**Figure 5**).

At Middle Valley, 798 large deep-water corals were recorded, mostly from Antipatharia (94.9% Antipatharia, 5.1% Alcyonacea). Schizopathidae corals, specifically *Umbellapathes* sp. 1 were the most dominant group (92%) on both dives. These corals clustered on or around hard substrate (**Supplementary Figures 2, 3**), but also occurred in areas characterized as sediment. In sedimented areas, it is likely they were attached to smaller rocks or pieces of chimney debris that were buried. There did not seem to be a relationship between coral abundance and proximity to fluid flow since corals were recorded both near and far from active chimneys and diffuse flow. Very few rossellid vase sponges were recorded on dive R1942 (**Supplementary Figure 2**) and they were absent from dive R1943.

Small Mega-Epifauna

At Endeavour, small white demosponges (Demospongiae sp. 1) and brittle stars (Ophiuroidea spp.) were common (occurred in

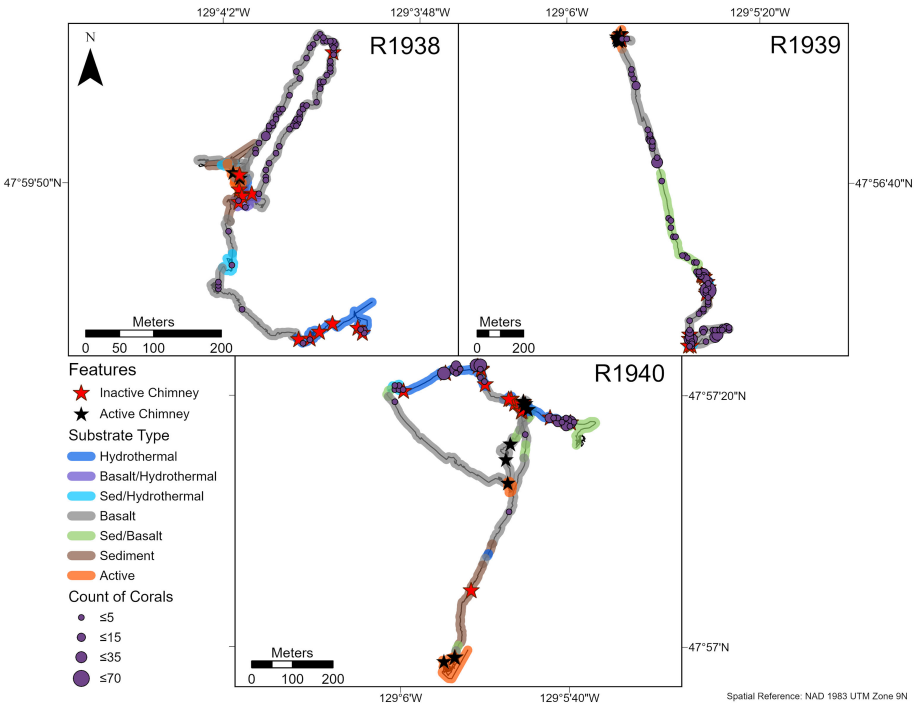

FIGURE 3 | Abundance and distribution of deep-water corals (see Results for dominant morphotaxa) on dives R1938-R1940 at the Endeavour segment, Juan de Fuca Ridge in August 2016. Inactive and active chimney locations and broad scale substrate classifications are also plotted onto the track. "Hydrothermal" substrate refers to inactive substrate that is hydrothermally derived. Counts were summed over a 10 x 10 m tessellation in ArcGIS Pro.

≥ 25% of captured images) on all dives (**Supplementary Figure 4**). Comatulid crinoids (Comatulida sp. 1) were common on dives R1938 and R1939, but not on dives R1940 and R1941. The greatest abundances of these groups were found at distances > 100 m from active chimneys on dives R1938 (**Figure 7**) and R1940 (**Figure 8**). Common morphotaxa were either absent or occurred in low abundance around active chimneys (**Supplementary Figures 5, 6**). On dive R1940, the small white demosponges were often absent or at low densities on highly sedimented substrate.

Total abundance of non-vent megafauna varied among the seven recorded substrate types (**Figure 9**). At Endeavour, the highest total abundance was on inactive chimneys, but was much more variable than on any other substrate type. The lowest total abundance was measured on sedimented substrates. For some substrate types, we were only able to capture a single image, making those estimates unreliable (**Figure 9**).

At Middle Valley, brittle stars (Ophiuroidea spp.) were the only morphotaxon commonly observed (occurred in ≥ 25% of captured images) on both dives; however, small white demosponges (Demospongiae sp. 1), a schizopathid coral (*Umbellapathes* sp.1), and jewelled anemones (*Corallimorphus* sp. 1) were also common on dive R1943 (**Supplementary Figure 7**). All four faunal groups were observed on both sediment and sulfide substrate types (**Supplementary Figures 8, 9**). On dive R1943, the highest abundance of brittle stars, demosponges, and *Umbellapathes* corals occurred on hard sulfide substrate, while the lowest abundances over areas of sediment or directly on diffuse flow.

Richness

The individual-based rarefaction curves did not reach an asymptote for any of the dives at Endeavour or Middle Valley (**Figure 10**). At Endeavour, for a common sample size of 246 individuals, there was no significant difference in expected richness among dives R1938, R1939, and R1940, but the expected richness for dive R1941 was significantly lower. At Middle Valley, for a common sample size of 413 individuals, the estimated richness of morphotaxa was significantly higher on dive R1943 than R1942.

Individual-based rarefaction curves also did not reach an asymptote for any of the substrate types at Endeavour or Middle Valley (**Figure 11**; **Supplementary Figures 10, 11**). At Endeavour, for a common sample size of 69 individuals, the expected richness of 'inactive chimney' was significantly greater than both 'basalt' and 'hydrothermal', which in turn were not significantly different from one another, but were significantly greater than 'sediment/basalt' and 'sediment'. The expected richness of 'sediment/hydrothermal' was significantly higher than "sediment" but was not significantly different from the other substrate types. At Middle Valley, for a common sample size of 32 individuals, the expected richness of 'inactive chimney' and 'sediment/hydrothermal' were significantly higher than 'sediment' but were not significantly different from each other.

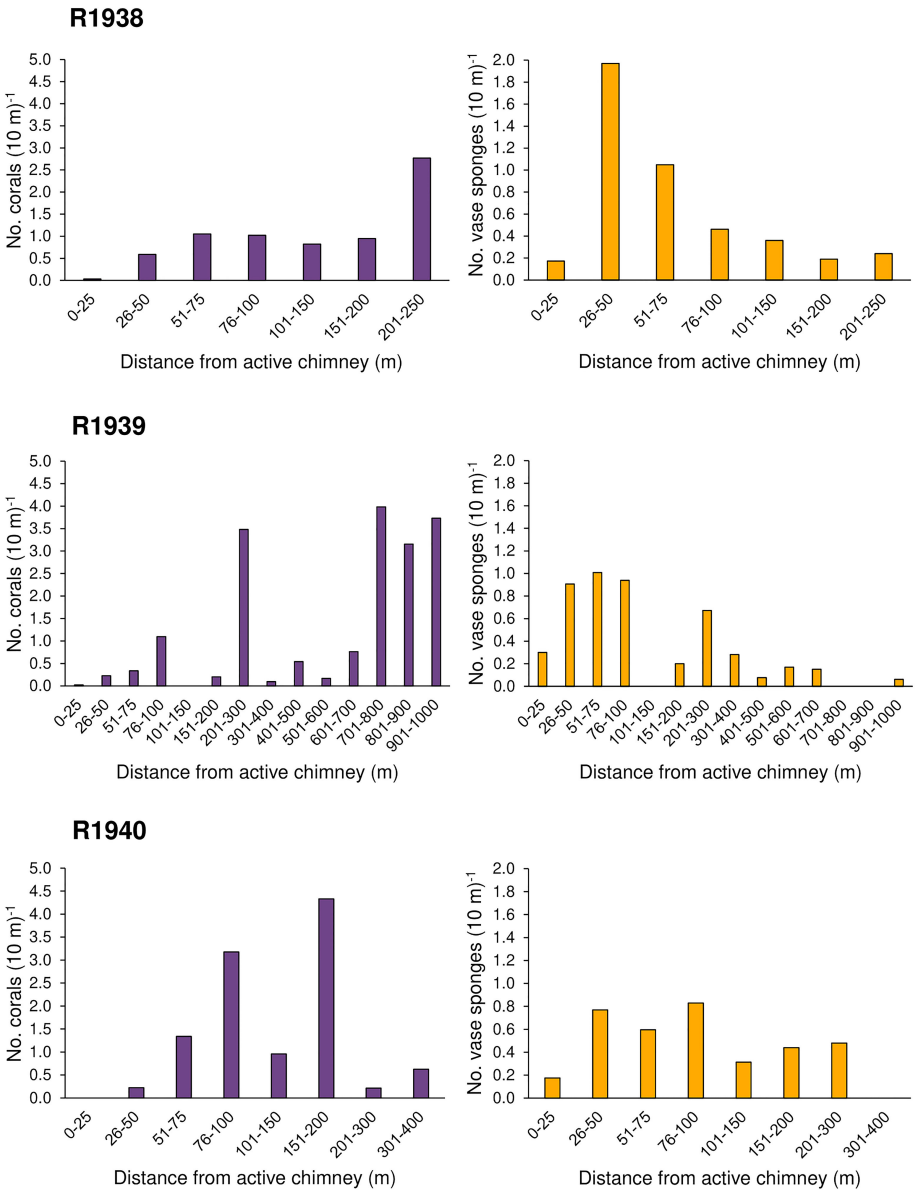

FIGURE 4 | Number of deep-water corals and rossellid vase sponges (Rossellidae) (per 10 m of dive track) occurring within distance categories from active hydrothermal chimneys for each of 3 dives at the Endeavour segment of the Juan de Fuca Ridge, in August 2016. Dive R1941 was not included as no deep-water corals and only three rossellid vase sponges were recorded. Distance to the closest active feature was calculated in ArcGIS Pro (see Methods).

The expected richness of 'hydrothermal' was significantly lower than 'sediment/hydrothermal' but was not different from the other substrate types.

DISCUSSION

Our study characterized non-vent faunal communities on two distinct hydrothermal systems on the Juan de Fuca Ridge. Overall, inactive vents harboured slow growing sessile mega-epifauna, but abundance varied widely among sites. Faunal assemblages at Endeavour were dominated by alcyonacean corals, stalked and comatulid crinoids, sponges, and holothurians. This pattern was very similar to that on the Cleft segment of the Juan de Fuca Ridge, where the most abundant non-vent taxa were alcyonacean corals and sea pens, stalked and comatulid crinoids, and holothurians (Milligan and Tunnicliffe, 1994). The Cleft segment is located further south on the Juan de Fuca Ridge and is also characterized by basalt lava flows (Milligan and Tunnicliffe, 1994). At Middle Valley, which is heavily sedimented, black corals, anemones, holothurians and ascidians were abundant. This community was different from

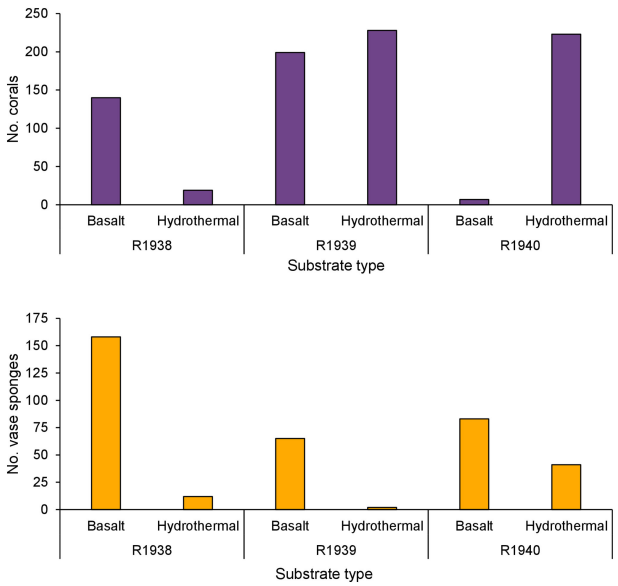

FIGURE 5 | The occurrence of deep-water corals and rossellid vase sponges on basalt and hydrothermally derived substrate on dives R1938, R1939, and R1940. Dive R1941 was not included as no deep-water corals and only three vase sponges were recorded. Dives were conducted by remotely operated vehicle ROPOS at the Endeavour segment of the Juan de Fuca Ridge, NE Pacific, in August 2016.

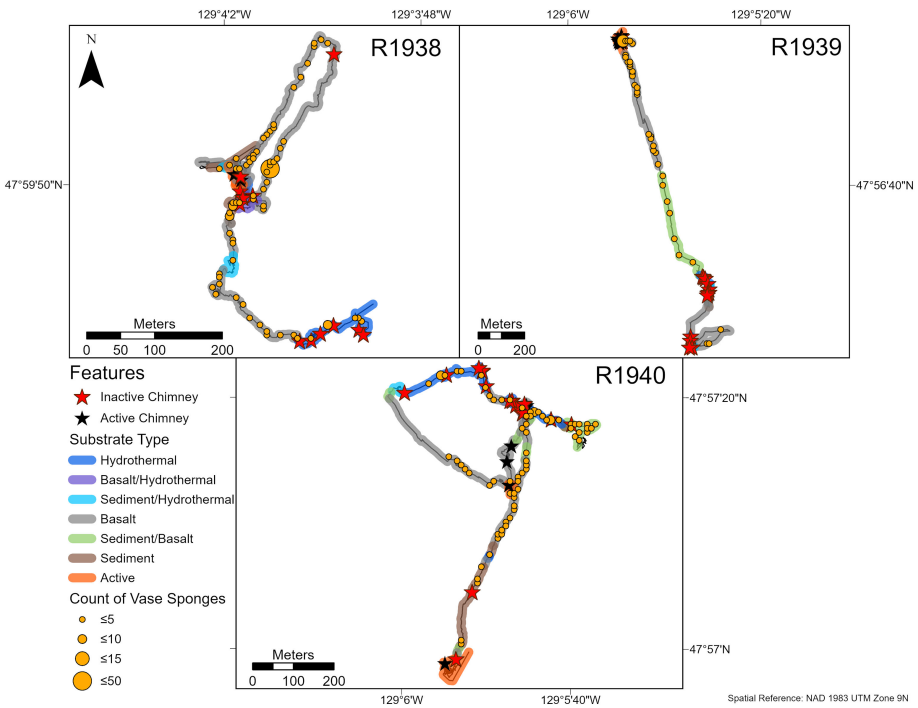

FIGURE 6 | Abundance and distribution of rossellid vase sponges (Rossellidae) on dives R1938-R1940 at the Endeavour segment, Juan de Fuca Ridge in August 2016. Inactive and active chimney locations and broad scale substrate classifications are also plotted onto the track. "Hydrothermal" substrate refers to inactive substrate that is hydrothermally derived. Counts were summed over a 10 x 10 m tessellation in ArcGIS Pro.

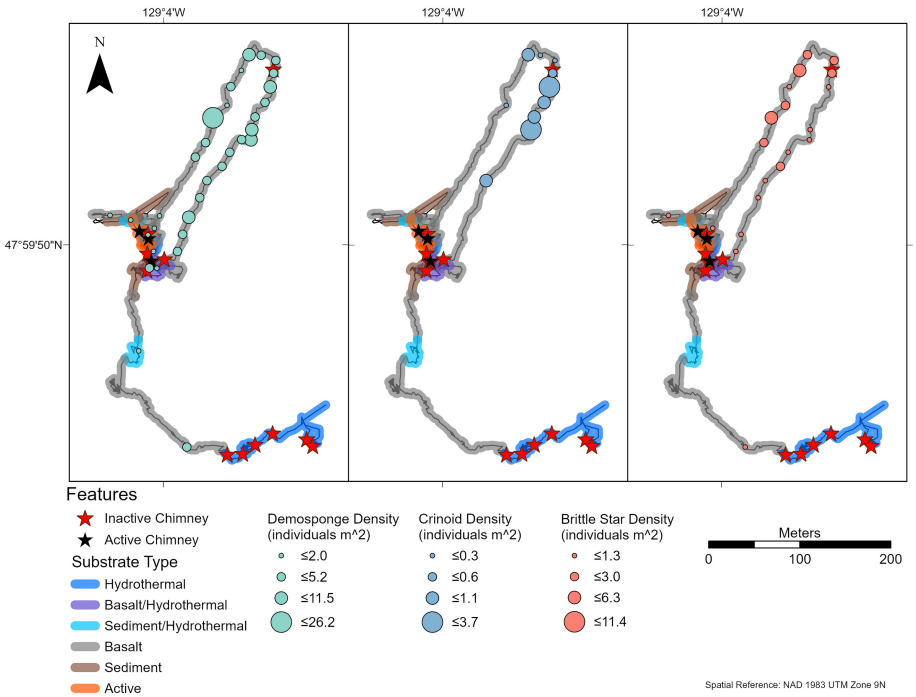

FIGURE 7 | Density of brittle stars (Ophiuroidea spp.), comatulid crinoids (Comatulida sp. 1), and demosponges (Demospongiae sp. 1) on dive R1938, at the Endeavour Segment of the Juan de Fuca Ridge sampled in August 2016. Each symbol indicates density in an image captured at that location. These three morphotaxa were identified as the numerically dominant faunal groups (present in ≥ 25% of images) (n = 20, 10, 33 for Ophiuroidea spp., Comatulida sp. 1, and Demospongiae sp.1, respectively). "Hydrothermal" substrate refers to inactive substrate that is hydrothermally derived.

that observed in the heavily sedimented environment of Mohn's Treasure mound on Mohn's Ridge, where echinoderms and sponges were the most common morphotaxa, and fields of stalked crinoids were observed in the sediment (Ramirez-Llodra et al., 2020). However, similar to Mohn's Treasure, small patches or outcrops of hard substrate were dominated by suspension feeding taxa, while the sediment was typically inhabited by more mobile fauna such as echinoderms.

Deep-water coral communities were recorded at both Endeavour and Middle Valley, but there were notable differences in the composition and their distribution on the substrate. At Endeavour, alcyonacean corals dominated, and they aggregated on elevated and exposed hard surfaces, such as walls of basalt ridges and chimneys. Similarly, in the Southwest Pacific, non-vent suspension feeders, including large gorgonian corals, were more abundant at elevated surfaces of inactive chimneys (Galkin, 1997). The presence of corals on chimneys and vertical walls is likely related to nutrition since elevated substrates provide access to faster water flow, and, therefore, increased food supply (Genin et al., 1986; Levin et al., 2016). At Middle Valley, black corals (Antipatharia) of the genus *Umbellapathes* were the most abundant taxon on both sedimented and exposed substrates. *Umbellapathes* attach to hard substrate by a basal plate at the bottom of a long and thin upright stalk (Opresko and Wagner, 2020). This stalk can extend more than 50 cm from the seafloor before branching. It is possible that the tall and flexible structure of these corals is better adapted to areas of high sedimentation, such as Middle Valley, and allows the corals to occur on both exposed and buried hydrothermal substrates. *Umbellapathes* was not recorded at Endeavour, and none of the most abundant groups of alcyonacean corals at Endeavour were recorded at Middle Valley. In fact, only a few alcyonacean corals were recorded at Middle Valley, and most were unbranched Isididae which also have a tall structure. The morphology and distribution of these corals suggests that the differences in community composition of deep-water corals at Endeavour and Middle Valley were influenced by available substrate and level of sedimentation.

At Endeavour, the abundance of soft corals was low at distances < 50 m from active chimneys. Active hydrothermal vents can be inhospitable for non-vent taxa because of the composition of the hydrothermal fluid (Corliss et al., 1979) and frequent physical disturbance (Grigg, 1997). At Endeavour, hydrothermal plumes extend roughly 150-300 m above active vent sites and chemical anomalies have been detected as much as 5 km away from central vent sites (Thomson et al., 1992). It is likely that corals colonize areas at distances from vents that maximize increased availability of vent-derived nutrients (Erickson et al., 2009) but also minimize exposure to toxic chemicals (Grigg, 1997; Sen et al., 2016). Interestingly, the greatest number of corals at Endeavour were recorded on and around inactive chimneys (on dive R1939) that were located

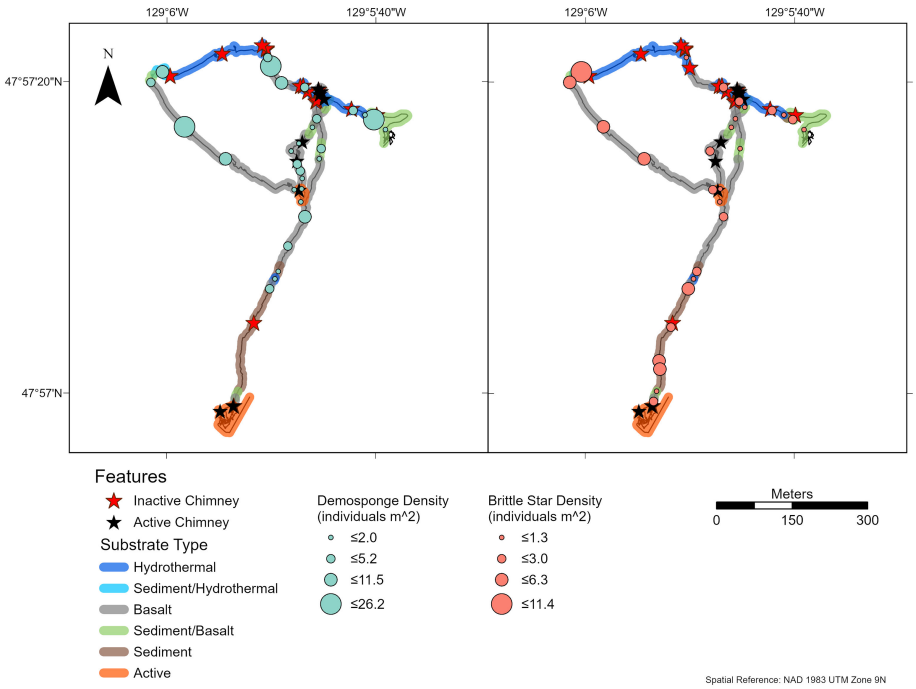

FIGURE 8 | Density of brittle stars (Ophiuroidea spp.) and demosponges (Demospongiae sp. 1) on dive R1940, at the Endeavour Segment of the Juan de Fuca Ridge sampled in August 2016. Each symbol indicates density in an image captured at that location. These two morphotaxa were identified as the numerically dominant faunal groups (present in ≥ 25% of images) (n = 28, 29 for Ophiuroidea spp. and Demospongiae sp.1, respectively). "Hydrothermal" substrate refers to inactive substrate that is hydrothermally derived.

furthest from the ridge axis. Radioisotope dating of inactive vents at Endeavour has shown that, in general, the oldest vents occur on the axial valley walls or outside the axial valley (Jamieson et al., 2013). Older chimneys that are further away from the ridge axis, and have been inactive for a longer period, provide a stable environment for slow growing deep-water corals (Andrews et al., 2001; Roark et al., 2009; Sherwood and Edinger, 2009). Therefore, the particularly dense assemblage of corals found on dive R1939 could be related to the age of the sulfide deposit and the distance from active fluid flow. Since there was no notable difference in the total number of corals between basalt and hydrothermally derived hard substrates, the observed patterns were not related to the geological composition of the substrate but rather to the topography and distance from vent activity.

Rossellid vase sponges at Endeavour occurred mostly on hard substrates (basalt and sulfide). Although their abundance was

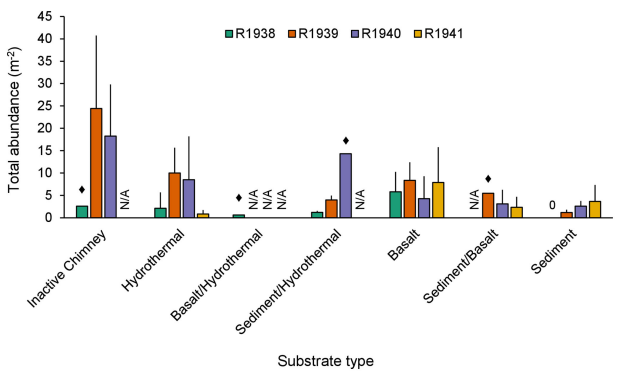

FIGURE 9 | Average total abundance (+SD) of all non-vent morphotaxa on each substrate type for dives R1938, R1939, R1940, and R1941 at the Endeavour segment of the Juan de Fuca Ridge. Abundances were averaged across image captures of the same substrate type. ♦: n=1. "N/A": indicates absence of that substrate type from the particular dive; 0 indicates true absence. "Hydrothermal" substrate refers to inactive substrate that is hydrothermally derived.

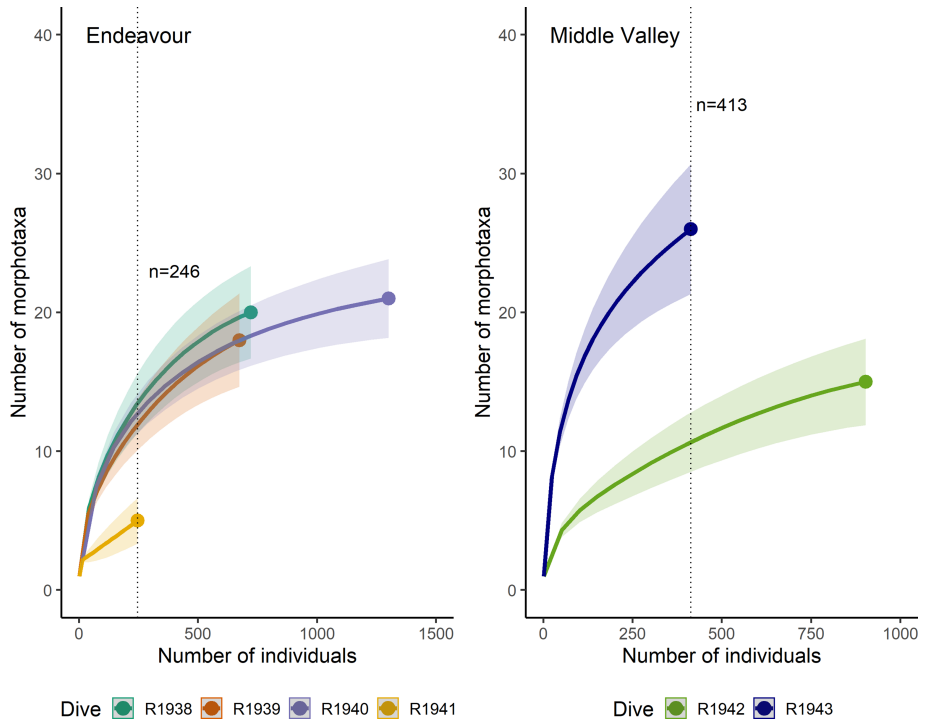

FIGURE 10 | Individual-based rarefaction curves for the dives at Endeavour (R1938-R1941) and Middle Valley (R1942 and R1943). The dotted vertical line indicates the minimum number of individuals sampled across all dives at each site.

also low within 25 m of active chimneys, sponges were more abundant than corals at distances of 26-50 m from active chimneys. Due to the difficulty in identifying species of morphotaxa from imagery, it is possible that more than one species is represented within this morphotaxon. However, their proximity to active vents suggests this morphotaxon overall is more tolerant of toxic chemicals than corals and may be utilizing particulate organic carbon and microbes in the water column, which have increased concentrations near hydrothermal vents (Enright et al., 1981; Galkin, 1997). Other glass sponges rely on fluid flow (Erickson et al., 2009), possibly even housing endosymbiotic bacteria to derive chemosynthetic energy (Georgieva et al., 2020). The sponges that may house these bacteria typically occur within 20 m of vents (Georgieva et al., 2020); however, in our study, rossellid vase sponges occurred at all distances to active venting, suggesting that they are not likely to be reliant on fluid flow but benefitting from elevated nutrients and the hard substrate.

The most common small mega-epifauna were brittle stars, demosponges, and crinoids at Endeavour and brittle stars, *Umbellapathes* corals, demosponges, and jewelled anemones at Middle Valley. The absence of crinoids at Middle Valley may be attributed to the lack of exposed and elevated hard substratum (Boschen et al., 2015; Ramirez-Llodra et al., 2020). Generally, brittle stars, demosponges, and crinoids seemed to be more abundant further away from active venting. At Endeavour, the absence of fauna from available hard substrate near active chimneys indicated that these groups were not limited by available substrate, but rather avoided fluid discharge.

Richness of morphotaxa at Endeavour was comparable across three of the dives (R1938-R1940), which were of similar length and in regions of the ridge with similar hydrothermal conditions and substrate. Dive R1941, however, mainly sampled three large active chimneys and a few short (< 250 m) segments of inactive substrate, resulting in a lower number of suitable images, and significantly lower estimated richness. Although the total track length for this dive was 2651 m, visible inactive substrate was only surveyed along 923 m of the total length, and only to a maximum of 86 m away from vent activity. At Middle Valley, richness differed significantly between the two dives. Dive R1942 traversed the Bent Hill vent field which was largely characterized by sediment, while dive R1943 traversed the Dead Dog vent field and surveyed sediment, inactive hydrothermal deposits and chimneys. Sampling more substrate types each with different associated faunal assemblages, resulted in a higher estimated richness on dive R1943 than R1942.

Among all substrate types at Endeavour, faunal communities on inactive chimneys had the greatest estimated richness and total abundance. However, the greatest variation in total abundance was also measured on inactive chimneys. Similarly to the South Pacific (Boschen et al., 2016), not all inactive chimneys in our study were colonized by fauna; some hosted dense communities while others were devoid of megafauna. This variation, even between chimneys at similar distances from active vents, suggests that factors such as

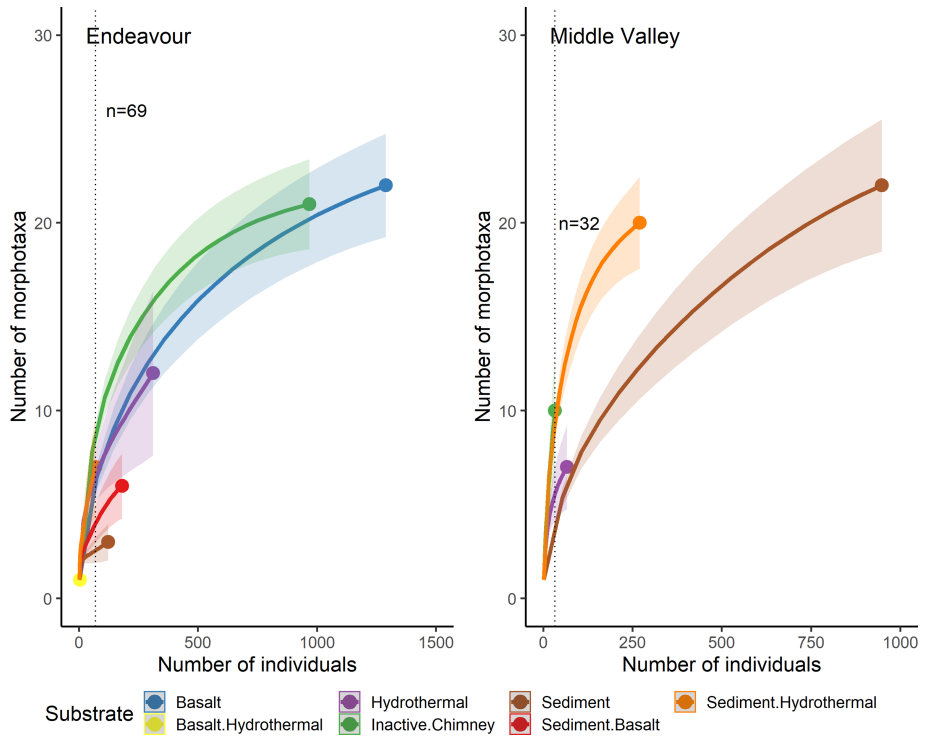

FIGURE 11 | Individual-based rarefaction curves for each substrate type, pooled across all dives sampled at Endeavour (R1938, R1939, R1940 and R1941) and Middle Valley (R1942 and R1943) on the Juan de Fuca Ridge, NE Pacific. "Hydrothermal" substrate refers to inactive substrate that is hydrothermally derived. The substrate 'basalt/hydrothermal' was omitted from the rarefaction analysis because only 3 individuals of a single morphotaxon were recorded.

local currents, and the chemical and microbial composition of the chimneys could be influencing colonization (Boschen et al., 2016). Communities on basalt and hydrothermal substrates had the next highest richness and total abundance, exceeding that of sedimented substrate types. This may be due to the life history traits of the non-vent assemblages at Endeavour, which are largely composed of sessile and sedentary suspension feeders that attach to hard substrates. It is important to note that the difference in richness between substrates was recorded at a small common sample size which was constrained by the sampling effort on sedimented substrates. A similar comparison at 1000 individuals indicates no difference in richness between basalt and inactive chimney substrates.

At Middle Valley, the mixed sediment/hydrothermal substrate type exhibited higher estimated richness than either sediment or hydrothermal alone. This is probably because fauna associated with both substrate types were present. A similar trend was observed at a highly sedimented area of the Arctic Mid-Ocean Ridge, where higher richness was found in areas with mixed substrate (Ramirez-Llodra et al., 2020). Inactive chimneys exhibited a higher estimated richness than sediment, indicating that fauna also utilize elevated and exposed substrate at Middle Valley.

Our study was opportunistic and thus based on a non-systematic layout of transects on each dive. The ROV stopped to sample frequently, flew over the same area multiple times resulting in duplicate footage, and often flew too far above the seafloor to obtain suitable imagery, making large portions of the dive track unusable for this study. Often, the scaling lasers were turned off or moved out of the field of view, providing no size reference for analysis. Additionally, the quality of imagery from the downward-looking camera was variable because of frequent changes in altitude above the seafloor, speed and direction of flight of the ROV, and unsuitable camera angles. This resulted in a non-uniform distribution of suitable images along the dive tracks, likely misrepresenting the number and distribution of morphotaxa on each dive and under sampling small and rare species, as also evidenced by the rarefaction curves. To better understand the distribution of non-vent fauna at inactive vents, studies should follow a well-designed and systematic sampling regime that prioritizes image quality throughout the dive by maintaining a constant altitude above the seafloor, speed, and camera/laser angle.

The increasing interest in mining polymetallic sulfide deposits at deep-sea hydrothermal vents necessitates the development of environmental regulations to minimize risk to the marine environment. Mining operations will have substantial direct and indirect impacts on both the targeted vents and the vent periphery. Our study demonstrates that inactive hydrothermal vents at Endeavour and Middle Valley support non-vent assemblages that are dominated by suspension feeding taxa such as corals, crinoids, and rossellid vase sponges. These

taxa are fragile and sensitive to indirect plume impacts from deep sea mining (Boschen-Rose et al., 2021). Deep-water corals and sponges are considered particularly vulnerable to mining impacts because they are long-lived and slow growing, and their recovery potential is uncertain (Clark et al., 2016). To ultimately assess the vulnerability of inactive vent ecosystems to mining operations and develop sustainable management plans, it is critical to gain a basic understanding of the structure and ecology of the communities that inhabit them and the surrounding area.

DATA AVAILABILITY STATEMENT

The raw data supporting the conclusions of this article will be made available by the authors, without undue reservation.

AUTHOR CONTRIBUTIONS

AM conceptualized this study. MN and AM designed the protocol for data analysis. MN conducted the analysis of the video and data and prepared the manuscript. JJ participated on the research cruise and co-directed the ROV dives, contributed the video and supported data analysis. All authors contributed to the article and approved the submitted version.

FUNDING

This project was supported by Natural Sciences and Engineering Research Council of Canada (NSERC) Discovery Grants to AM [RGPIN-2016-04878] and undergraduate summer research awards (Nancy Witherspoon Memorial Summer Research Award, Rob Stewart Undergraduate Summer Research Award in Marine Conservation) to MN. The 2016 research cruise to Endeavour and Middle Valley aboard the CCGS John P. Tully was co-led by researchers at Fisheries and Oceans Canada and the University of Victoria, with Memorial University of Newfoundland as a contributing partner. The cruise was funded in part by the NSERC Canadian Healthy Oceans Network and its Partners: Department of Fisheries and Oceans Canada and INREST (representing the Port of Sept-Îles and City of Sept-Îles) [NETGP 468437 – 14]. JJ acknowledges funding support from the Canada Research Chairs Program [950 - 233103] for the ROV dives and participation on the cruise.

ACKNOWLEDGMENTS

We thank the ROV ROPOS pilots and technical team, and crew of the CCGS John P. Tully for their critical contribution to the collection of the video data for this project. We thank Janelle Curtis (Fisheries and Oceans Canada), and Kim Juniper and Verena Tunnicliffe (University of Victoria) for their contribution to conceptualization of the 2016 research cruise, as well as cruise organization and logistics. We thank Ben Grupe for his expert role as Chief Scientist during the cruise. We would like to thank Cherisse Du Preez and Merlin Best (DFO – British Columbia) for offering their expertise and resources on the identification of deep-sea taxa; Adrienne Schumlich, Sean Mullan and Fabio De Leo (Ocean Networks Canada) for providing access to bathymetry data and main vent field locations used in figures; and Sarah de Mendonça, Kate Arpin, and Graeme Guy for offering their advice and assistance throughout the project.

SUPPLEMENTARY MATERIAL

The Supplementary Material for this article can be found online at: https://www.frontiersin.org/articles/10.3389/fmars.2022.849976/full#supplementary-material

REFERENCES

Ames, D. E., Franklin, J. M., and Hannington, M. D. (1993). Mineralogy and Geochemistry of Active and Inactive Chimneys and Massive Sulfide, Middle Valley, Northern Juan De Fuca Ridge: An Evolving Hydrothermal System. *Can. Mineral* 31:4, 997–1024.

Andrews, A. H., Cordes, E. E., Mahoney, M. M., Munk, K., Coale, K. H., Cailliet, G. M., et al. (2001). Age, Growth and Radiometric Age Validation of a Deep-Sea, Habitat-Forming Gorgonian (Primnoa Resedaeformis) From the Gulf of Alaska. *Hydrobiologia* 471, 101–110. doi: 10.1023/A:1016501320206

Arquit, A. M. (1990). Geological and Hydrothermal Controls on the Distribution of Megafauna in Ashes Vent Field, Juan De Fuca Ridge. *J. Geophys. Res. – Sol Ea* 95:B8, 12947–12960. doi: 10.1029/JB095iB08p12947

Boschen-Rose, R. E., Clark, M. R., Rowden, A. A., and Gardner, J. P. A. (2021). Assessing the Ecological Risk to Deep-Sea Megafaunal Assemblages From Seafloor Massive Sulfide Mining Using a Functional Traits Sensitivity Approach. *Ocean Coast Manage.* 210. doi: 10.1016/j.ocecoaman.2021.105656

Boschen, R. E., Rowden, A. A., Clark, M. R., Barton, S. J., Pallentin, A., and Gardner, J. P. A. (2015). Megabenthic Assemblage Structure on Three New Zealand Seamounts: Implications for Seafloor Massive Sulfide Mining. *Mar. Ecol. Prog. Ser.* 523, 1–14. doi: 10.3354/meps11239

Boschen, R. E., Rowden, A. A., Clark, M. R., Pallentin, A., and Gardner, J. P. A. (2016). Seafloor Massive Sulfide Deposits Support Unique Megafaunal Assemblages: Implications for Seabed Mining and Conservation. *Mar. Environ. Res.* 115, 78–88. doi: 10.1016/j.marenvres.2016.02.005

Carey, A. G., Stein, D. L., and Rona, P. L. (1990). Benthos of the Gorda Ridge Axial Valley (NE Pacific Ocean): Taxonomic Composition and Trends in Distribution. *Prog. Oceanog* 24, 47–57. doi: 10.1016/0079-6611(90)90018-W

Chao, A., Gotelli, N. J., Hsieh, T. C., Sander, E. L., Ma, K. H., Colwell, R. K., et al. (2014). Rarefaction and Extrapolation With Hill Numbers: A Framework for Sampling and Estimation in Species Diversity Studies. *Ecol. Monogr.* 84, 45–67. doi: 10.1890/13-0133.1

Cherkashov, G., Kuznetsov, V., Kuksa, K., Tabuns, E., Maksimov, M., and Bel'tenev, V. (2017). Sulfide Geochronology Along the Northern Equatorial Mid-Atlantic Ridge. *Ore Geol. Rev.* 87, 147–154. doi: 10.1016/j.oregeorev.2016.10.015

Clague, D. A., Martin, J. F., Paduan, J. B., Butterfield, D. A., Jamieson, J. W., Le Saout, M., et al. (2020). Hydrothermal Chimney Distribution on the Endeavour Segment, Juan De Fuca Ridge. *Geochem Geophys. Geosyst* 21, 6. doi: 10.1029/2020GC008917

Clark, M. R., Althaus, F., Schlacher, T. A., Williams, A., Bowden, D. A., and Rowden, A. A. (2016). The Impacts of Deep-Sea Fisheries on Benthic Communities: A Review. *ICES J. Mar. Sci.* 73, i51–i69. doi: 10.1093/icesjms/fsv123

Collins, P. C., Kennedy, R., and Van Dover, C. L. (2012). A Biological Survey Method Applied to Seafloor Massive Sulphides (SMS) With Contagiously

Distributed Hydrothermal-Vent Fauna. *Mar. Ecol. Prog. Ser.* 452, 89–107. doi: 10.3354/MEPS09646

Corliss, J. B., Dymond, J., Gordon, L. I., Edmond, J. M., von Herzen, R. P., Ballard, R. D., et al. (1979). Submarine Thermal Springs on the Galápagos Rift. *Science* 203:4385, 1073–1083. doi: 10.1126/science.203.4385.1073

Dasgupta, S., Peng, X., and Ta, K. (2021). Interaction Between Microbes, Minerals, and Fluids in Deep-Sea Hydrothermal Systems. *Minerals* 11, 1–15. doi: 10.3390/min11121324

Delaney, J. R., Robigou, V., Mcduff, R. E., and Tivey, M. K. (1992). Geology of a Vigorous Hydrothermal System on the Endeavour Segment, Juan De Fuca Ridge. *J. Geophys. Res.* 97:B13, 19663–19682. doi: 10.1029/92jb00174

Du Preez, C., Curtis, J. M. R., and Clarke, M. E. (2016). The Structure and Distribution of Benthic Communities on a Shallow Seamount (Cobb Seamount, Northeast Pacific Ocean). *PloS One* 11 (10), e0165513. doi: 10.1371/journal.pone.0165513

Earth Negotiations Bulletin (2020) *Summary of the Twenty-sixth Annual Session of the International Seabed Authority (First Part): 17-21 February 2020*. Available at: https://enb.iisd.org/events/1st-part-26th-annual-session-international-seabed-authority-isa/summary-report-17-21 (Accessed October 3, 2021).

Enright, J. T., Newman, W. A., Hessler, R. R., and McGowan, J. A. (1981). Deep-Ocean Hydrothermal Vent Communities. *Nature* 289, 219–221. doi: 10.1038/289219a0

Erickson, K. L., Macko, S. A., and Van Dover, C. L. (2009). Evidence for a Chemoautotrophically Based Food Web at Inactive Hydrothermal Vents (Manus Basin). *Deep-Sea Res. II* 56, 1577–1585. doi: 10.1016/j.dsr2.2009.05.002

Galkin, S. V. (1997). Megafauna Associated With Hydrothermal Vents in the Manus Back-Arc Basin (Bismarck Sea). *Mar. Geol.* 142, 197–206. doi: 10.1016/S0025-3227(97)00051-0

Genin, A., Dayton, P. K., Lonsdale, P. F., and Spiess, F. N. (1986). Corals on Seamount Peaks Provide Evidence of Current Acceleration Over Deep-Sea Topography. *Nature* 322, 59–61. doi: 10.1038/322059a0

Georgieva, M. N., Taboada, S., Riesgo, A., Diez-Vives, C., De Leo, F. C., Jeffreys, R. M., et al. (2020). Evidence of Vent-Adaptation in Sponges Living at the Periphery of Hydrothermal Vent Environments: Ecological and Evolutionary Implications. *Front. Microbiol.* 11. doi: 10.3389/fmicb.2020.01636

Gerdes, K. H., Martinez Arbizu, P., Schwentner, M., Freitag, R., Schwarz-Schampera, U., Brandt, A., et al. (2019). Megabenthic Assemblages at the Southern Central Indian Ridge – Spatial Segregation of Inactive Hydrothermal Vents From Active-, Periphery- and Non-Vent Sites. *Mar. Environ. Res.* 151, 1–11. doi: 10.1016/j.marenvres.2019.104776

Grigg, R. W. (1997). Benthic Communities on Lo'ihi Submarine Volcano Reflect High-Disturbance Environment. *Pac Sci.* 51, 209–220.

Hannington, M., De Ronde, C., and Petersen, S. (2005). "Sea-Floor Tectonics and Submarine Hydrothermal Systems" in *One Hundredth Anniversary Volume*. Eds. J. Hedenquist, J. Thompson, R. Goldfarb and J. Richards (Littleton, CO, USA: Society of Economic Geologists), 111–141. doi: 10.5382/AV100.06

Hannington, M. D., Jamieson, J., Monecke, T., and Petersen, S. (2010). ""Modern Seafloor Massive Sulfides and Base Metal Resources: Toward an Estimate of Global Seafloor Massive Sulfide Potential"," in *The Challenge of Finding New Mineral Resources: Global Metallogeny, Innovative Exploration, and New Discoveries*. Eds. R. Goldfarb, E. Marsh and T. Monecke (Littleton, CO USA: Society of Economic Geologists), 317–338. doi: 10.5382/SP.15.2.001

Haymon, R. M. (1983). Growth History of Black Smoker Hydrothermal Chimneys. *Nature* 301, 695–698. doi: 10.1038/301695a0

Hsieh, T. C., Ma, K. H., and Chao, A. (2016). iNEXT: An R Package for Interpolation and Extrapolation of Species Diversity (Hill Numbers). *Methods Ecol. Evol.* 7:12, 1451–1456. doi: 10.1111/2041-210X.12613

Huetten, E., and Greinert, J. (2008). Software Controlled Guidance, Recording and Post-Processing of Seafloor Observations by ROV and Other Towed Devices: The Software Package OFOP. *Geophys. Res. Abstr* 10, EGU2008–A-03088.

Hurlbert, S. H. (1971). The Nonconcept of Species Diversity: A Critique and Alternative Parameters. *Ecology* 52, 577–586. doi: 10.2307/1934145

Jamieson, J. W., Clague, D. A., and Hannington, M. D. (2014). Hydrothermal Sulfide Accumulation Along the Endeavour Segment, Juan De Fuca Ridge. *Earth Planet Sc Lett.* 395, 136–148. doi: 10.1016/j.epsl.2014.03.035

Jamieson, J. W., and Gartman, A. (2020). Defining Active, Inactive, and Extinct Seafloor Massive Sulfide Deposits. *Mar. Policy* 117. doi: 10.1016/j.marpol.2020.103926

Jamieson, J. W., Hannington, M. D., Clague, D. A., Kelley, D. S., Delaney, J. R., Holden, J. F., et al. (2013). Sulfide Geochronology Along the Endeavour Segment of the Juan De Fuca Ridge, Geochem. *Geophys. Geosyst* 14, 2084–2099. doi: 10.1002/ggge.20133

Juniper, S. K., Tunnicliffe, V., and Southward, C. (1992). Hydrothermal Vents in Turbidite Sediments on a Northeast Pacific Spreading Centre: Organisms and Substratum at an Ocean Drilling Site. *Can. J. Zool.* 70, 1792–1809. doi: 10.1139/z92-247

Kelley, D. S., Carbotte, S. M., Caress, D. W., Clague, D. A., Delaney, J. R., Gill, J. B., et al. (2012). Endeavour Segment of the Juan De Fuca Ridge: One of the Most Remarkable Places on Earth. *Oceanography* 25:1, 44–61. doi: 10.5670/oceanog.2012.03

Kelly, N., Metaxas, A., and Butterfield, D. (2007). Spatial and Temporal Patterns of Colonization by Deep-Sea Hydrothermal Vent Invertebrates on the Juan De Fuca Ridge, NE Pacific. *Aquat Biol.* 1, 1–16. doi: 10.3354/ab00001

Levin, L. A., Baco, A. R., Bowden, D. A., Colaco, A., Cordes, E. E., Cunha, M. R., et al. (2016). Hydrothermal Vents and Methane Seeps: Rethinking the Sphere of Influence. *Front. Mar. Sci.* 3. doi: 10.3389/fmars.2016.00072

Marcus, J., Tunnicliffe, V., and Butterfield, D. A. (2009). Posteruption Succession of Macrofaunal Communities at Diffuse Flow Hydrothermal Vents on Axial Volcano, Juan De Fuca Ridge, Northeast Pacific. *Deep-Sea Res. Part II* 56, 1586–1598. doi: 10.1016/j.dsr2.2009.05.004

Milligan, B. N., and Tunnicliffe, V. (1994). Vent and Nonvent Faunas of Cleft Segment, Juan De Fuca Ridge, and Their Relations to Lava Age. *J. Geophys. Res.* 99:B3, 4777–4786. doi: 10.1029/93JB03210

Mullineaux, L. S., Metaxas, A., Beaulieu, S. E., Bright, M., Gollner, S., Grupe, B. M., et al. (2018). Exploring the Ecology of Deep-Sea Hydrothermal Vents in a Metacommunity Framework. *Front. Mar. Sci.* 5. doi: 10.3389/fmars.2018.00049

Okamoto, N., Shiokawa, S., Kawano, S., Sakurai, H., Yamaji, N., and Kurihara, M. (2018). Current Status of Japan's Activities for Deep-Sea Commercial Mining Campaign. In *2018 OCEANS - MTS/IEEE Kobe Techno-Oceans (OTO), 2018*. 1–7. doi: 10.1109/OCEANSKOBE.2018.8559373

Opresko, D. M., and Wagner, D. (2020). New Species of Black Corals (Cnidaria: Anthozoa: Antipatharia) From Deepsea Seamounts and Ridges in the North Pacific. *Zootaxa* 4868:4, 543–559. doi: 10.11646/zootaxa.4868.4.5

Petersen, S., Krätschell, A., Augustin, N., Jamieson, J., Hein, J. R., and Hannington, M. D. (2016). News From the Seabed – Geological Characteristics and Resource Potential of Deep-Sea Mineral Resources. *Mar. Policy* 70, 175–187. doi: 10.1016/j.marpol.2016.03.012

Ramirez-Llodra, E., Hilario, A., Paulsen, E., Costa, C. V., Bakken, T., Johnsen, G., et al. (2020). Benthic Communities on the Mohn's Treasure Mound: Implications for Management of Seabed Mining in the Arctic Mid-Ocean Ridge. *Front. Mar. Sci.* 7. doi: 10.3389/fmars.2020.00490

Riddihough, R. (1984). Recent Movements of the Juan-de-Fuca Plate System. *J. Geo- Phys. Res.* 89:B8, 6980–6994. doi: 10.1029/JB089iB08p06980

Roark, E. B., Guilderson, T. P., Dunbar, R. B., Fallon, S. J., and Mucciarone, D. A. (2009). Extreme Longevity in Proteinaceous Deep-Sea Corals. *Proc. Natl. Acad. Sci. U.S.A.* 106:13, 5204–5208. doi: 10.1073/pnas.0810875106

Sarrazin, J., Robigou, V., Juniper, S. K., and Delaney, J. R. (1997). Biological and Geological Dynamics Over Four Years on a High-Temperature Sulfide Structure at the Juan De Fuca Ridge Hydrothermal Observatory. *Mar. Ecol. Prog. Ser.* 153, 5–24. doi: 10.3354/meps153005

Scientific Abyss Mapping Services. (2009) *Ofop Documentation: Version 3.2.0k*. Available at: http://www.ofop-by-sams.eu/ (Accessed November 7, 2017).

Sen, A., Kim, S., Miller, A. J., Hovey, K. J., Hourdez, S., and Luther Iii, G. W. (2016). Peripheral Communities of the Eastern Lau Spreading Center and Valu Fa Ridge: Community Composition, Temporal Change and Comparison to Near-Vent Communities. *Mar. Ecol.* 37, 3. doi: 10.1111/maec.12313

Sen, A., Podowski, E. L., Becker, E. L., Shearer, E. A., Gartman, A., and Yücel, M. (2014). Community Succession in Hydrothermal Vent Habitats of the Eastern Lau Spreading Center and Valu Fa Ridge, Tonga. *Limnol. Oceanogr.* 59:5, 1510–1528. doi: 10.4319/lo.2014.59.5.1510

Sherwood, O. A., and Edinger, E. N. (2009). Ages and Growth Rates of Some Deep-Sea Gorgonian and Antipatharian Corals of Newfoundloand and Labrador. *Can. J. Fish Aquat Sci.* 66, 142–152. doi: 10.1139/F08-195

Thomson, R. E., Delaney, J. R., McDuff, R. E., Janecky, D. R., and McClain, J. S. (1992). Physical Characteristics of the Endeavour Ridge Hydrothermal Plume

During July 1988. *Earth Planet Sci. Lett.* 111:1, 141–154. doi: 10.1016/0012-821X(92)90175-U

Tunnicliffe, V. (1991). The Biology of Hydrothermal Vents: Ecology and Evolution. *Oceanogr Mar. Biol. Annu. Rev.* 29, 319–407.

Tunnicliffe, V., McArthur, A. G., and McHugh, D. (1998). A Biogeographical Perspective of the Deep-Sea Hydrothermal Vent Fauna. *Adv. Mar. Biol.* 34, 353–442. doi: 10.1016/S0065-2881(08)60213-8

Van Dover, C. L. (2000). *The Ecology of Deep-Sea Hydrothermal Vents* (Princeton, NJ, USA: Princeton University Press).

Van Dover, C. L. (2011). Mining Seafloor Massive Sulphides and Biodiversity: What Is at Risk? *ICES J. Mar. Sci.* 68:2, 341–348. doi: 10.1093/icesjms/fsq086

Van Dover, C. L. (2019). Inactive Sulfide Ecosystems in the Deep Sea: A Review. *Front. Mar. Sci.* 6. doi: 10.3389/fmars.2019.00461

Van Dover, C. L., Arnaud-Haond, S., Gianni, M., Helmreich, S., Huber, J. A., Jaeckel, A. L., et al. (2018). Scientific Rationale and International Obligations for Protection of Active Hydrothermal Vent Ecosystems From Deep-Sea Mining. *Mar. Policy* 90, 20–28. doi: 10.1016/j.marpol.2018.01.020

Van Dover, C. L., Colaço, A., Collins, P. C., Croot, P., Metaxas, A., Murton, B. J., et al. (2020). Research Is Needed to Inform Environmental Management of Hydrothermally Inactive and Extinct Polymetallic Sulfide (PMS) Deposits. *Mar. Policy* 121, 1–7. doi: 10.1016/j.marpol.2020.104183

Conflict of Interest: The authors declare that the research was conducted in the absence of any commercial or financial relationships that could be construed as a potential conflict of interest.

Publisher's Note: All claims expressed in this article are solely those of the authors and do not necessarily represent those of their affiliated organizations, or those of the publisher, the editors and the reviewers. Any product that may be evaluated in this article, or claim that may be made by its manufacturer, is not guaranteed or endorsed by the publisher.

frontiers | Frontiers in Marine Science

ORIGINAL RESEARCH
published: 13 June 2022
doi: 10.3389/fmars.2022.732740

Influence of Chemoautotrophic Organic Carbon on Sediment and Its Infauna in the Vicinity of the Rainbow Vent Field

Reyhaneh Roohi[1], Ragna Hoogenboom[1], Ronald Van Bommel[2], Marcel T. J. Van Der Meer[2], Furu Mienis[1] and Sabine Gollner[1]*

[1] Department of Ocean Systems, Royal Netherlands Institute for Sea Research (NIOZ), Texel, Netherlands,
[2] Department of Marine Microbiology and Biogeochemistry, Royal Netherlands Institute for Sea Research (NIOZ), Texel, Netherlands

Hydrothermal vents have been recognised as isolated islands of productivity in the deep sea, but very little is known about the transport and export of chemoautotrophic produced organic carbon to vent surrounding habitats. Here, we investigate vent carbon export and its influence on benthic food webs in sediments at the Rainbow (RB) vent field at the Mid Atlantic Ridge in ~2200 m water depth. Two sites were considered along the dispersal direction of the RB vent plume for sample collection: the close vicinity at about ~30-100 m ("near-vent"); and at 4 km distance ("off-vent") to the nearest venting area. At both sites, box corers were used to sample sediments and their fauna. A turbidity sensor mounted on a CTD/Rosette provided data on the presence of a vent fluid plume in the water column. Niskin bottles were used to sample suspended particulate organic matter (SPOM) from the plume, as well as from surface waters at 75 m depth. SPOM, sediments and fauna were analysed for nitrogen and carbon stable isotopes. Carbon derived from *in situ* chemoautotrophy, characterised by depleted $\delta^{13}C$, was taken up by infauna close to the venting area as the main nutrition source, while fauna at the off-vent site showed less depleted $\delta^{13}C$ with a signature more typical for photosynthetic- derived material. Nematodes were the most abundant faunal taxon. Their abundance and biomass were variable and not different at the two studied sites. *In situ* derived organic matter was traced back in the food web in the close vicinity of the venting area. The connectivity of vent and non-vent habitats should be taken appropriately into account when designing future spatial management plans with regard to deep-seabed mining at hydrothermal vents.

Keywords: hydrothermal vent, deep-sea sediment, plume, connectivity, trophic interaction, isotopes, fauna, organic carbon

OPEN ACCESS

Edited by:
Jozee Sarrazin, Institut Français de Recherche pour l'Exploitation de la Mer (IFREMER), France

Reviewed by:
Travis William Washburn, Geological Survey of Japan (AIST), Japan
Xikun Song, Xiamen University, China

****Correspondence:***
Reyhaneh Roohi
reyhane.roohi@gmail.com

Specialty section:
This article was submitted to Deep-Sea Environments and Ecology, a section of the journal Frontiers in Marine Science

Received: *29 June 2021*
Accepted: *13 May 2022*
Published: *13 June 2022*

Citation:
Roohi R, Hoogenboom R, Van Bommel R, Van Der Meer MTJ, Mienis F and Gollner S (2022) Influence of Chemoautotrophic Organic Carbon on Sediment and Its Infauna in the Vicinity of the Rainbow Vent Field. Front. Mar. Sci. 9:732740. doi: 10.3389/fmars.2022.732740

1 INTRODUCTION

It has only recently been recognized that deep-sea vents are not isolated ecosystems, but also influence the surrounding areas (Levin et al., 2016). Deep-sea vent plumes transport vent larvae (Adams et al., 2012; Kim et al., 2015) and export nutrients and trace metals to the vent surroundings, influencing the microbial community composition in the water column

(Haalboom et al., 2020). Faunal communities on hard substrates in the vent surroundings harbor a mix of typical "vent" meiofaunal species (e.g. Dirivultid copepods) and of species/genera known from coastal areas and deep-sea sediments (Gollner et al., 2010; Gollner et al., 2015; Gollner et al., 2020), and show increased functional diversity (Alfaro-Lucas et al., 2020). Benthic species composition in sediments surroundings Rainbow is different compared to control deep-sea sediments and highly influenced by the vent plume's fall out (Klunder et al., 2020). Nematode community composition in sediments in the surroundings of Snake Pit and TAG vent fields on the Mid-Atlantic Ridge is hypothesized to be influenced by geochemical setting and food availability (Spedicato et al., 2020). A study in the northern West-Pacific, suggested that the effect of *in situ* derived organic matter as a food source near vents may be limited to at most several 100 m away from the venting area (Nomaki et al., 2019). Overall, very little is known about the role of vent *in situ* derived organic matter on food web and community composition in the vent surroundings.

The importance of understanding the interactions of vents with their surroundings is growing, as the potential for disturbances in the form of deep-seabed mining rises. Hydrothermal vent ecosystems are typically rich in seafloor massive sulfides and there is globally a growing interest to mine these minerals in the future (Dover, 2011; Boschen et al., 2013; Dover et al., 2018). Some countries have already tested mining or plan mining-tests in their national waters (Collins et al., 2013; Boschen et al., 2015), and to date, 7 exploration contracts for seafloor massive sulfide mining have been issued by the International Seabed Authority (ISA) in areas beyond national jurisdiction (www.isa.org.jm). Mining will have impacts on the environment, including for example removal of habitat or the creation of sediment plumes (Gollner et al., 2017). The ISA is currently working on the development of Regional Environmental Management Plans, which shall include mitigation actions, such as areas to be protected from seabed mining (ISA, 2019). Understanding the extent of vent influence and ecological connectivity to the surrounding environment are needed to ensure proper mitigation actions for human disturbances, and to border marine protected areas in the deep sea.

One form of determining the geographical size or "footprint" of an ecosystem includes the detection of trophic links within and between ecosystems. Food web studies can use stable isotopes of carbon and nitrogen to detect the sources of the production, and define the trophic level, by comparing the ratio of the heavier to lighter isotopes (Griffin and Valiela, 2001; Govenar, 2012). Analyzing nitrogen and carbon stable isotopes allows the establishment of trophic interactions between species (Pinnegar and Polunin, 2000). At hydrothermal vents, there are different potential food sources with different $\delta^{13}C$ ratios including (1) photosynthetically derived organic matter from the sea surface (-24‰ to -22‰), (2) chemo-autotrophs that fix carbon through sulfide oxidation based on Calvin-Benson-Bassham (CBB) cycle (-36‰ to -30‰), (3) chemo-autotrophs that fix carbon through sulfide oxidation based on reductive tricarboxylic acid (rTCA) cycle (-15‰ to -10‰) and (4) methanotrophs (-19 ± 3.5‰ at Rainbow (RB) vent) (Portail et al., 2018 and references therein). Therefore, the $\delta^{13}C$ signature can be used to identify which organic carbon sources (chemo- or photosynthetic) fauna in the vent surrounding rely on.

The RB vent produces one of the most persistent and strongest plumes on the Mid-Atlantic Ridge (MAR, German et al., 1996; Thurnherr and Richards, 2001), making it a good location to explore the extent of *in situ* produced organic matter export to vent surroundings. The RB vent field (36°149N, 33° 549W, ~2250 m depth) was discovered in 1996 on the Azores triple junction (ATJ) along the MAR (German et al., 1996) (**Figure 1A**). It is located at a slow-spreading ridge with a spreading rate of approximately 21.5 mm yr^{-1} (Andreani et al., 2014). At least ten black smokers eject the plume that is rising up to 200 m above the vent field and is dispersed predominantly to the north and east of the source with an average current speed of 5-6 cms^{-1} (Thurnherr and Richards, 2001; Thurnherr et al., 2002; Edmonds and German, 2004). The vent fluid dispersal is controlled by the variation of vent emission and deep-sea current direction which is following the contours of the rift valley and can be detected up to 50 km away from the vent site (Khripounoff et al., 2001; Edmonds and German, 2004; Haalboom et al., 2020). The plume is enriched in trace metals in which the composition changes as it is aged and dispersed, it has very low concentrations of organic carbon and is characterized by the presence of chemoautotrophic microbial communities (Khripounoff et al., 2001; Edmonds and German, 2004; Haalboom et al., 2020).

The fauna living on/very close to black smokers at the RB vent field is relatively well known and characterized by small mussel beds and shrimp swarms, with associated species such as *Amathys lutzi* or spionid polychaetes (Desbruyères et al., 2000; Desbruyères et al., 2001; Portail et al., 2018). Portail et al. (2018) studied the food web complexity at the RB vent. However, there is no knowledge of food webs in vent surrounding areas, and very limited knowledge on the taxonomic composition of sediment infauna, with metabarcoding revealing that their composition is influenced by the RB vent plume's fall out (Klunder et al., 2020). Here, we investigate the ecological "footprint" of the RB vent field, i.e., the export of *in situ* produced organic carbon and its importance as a potential food source for faunal communities living in the sediments in the vent surrounding areas. Along the dispersal direction of the plume, water column and sediment samples were collected at two sites: near-vent (~30-100 m distance from RB black smokers) and off-vent (4 km away from RB). We analysed the organic matter content, carbon and nitrogen stable isotopes of suspended particulate organic matter (SPOM) in the water column, and of sediments and fauna living in the sediments. In addition, we analysed faunal abundance and biomass of nematodes, the dominant taxon in the sediments.

2 MATERIAL AND METHODS

2.1 Sampling

The sampling sites were chosen based on preliminary studies of plume dispersal by Haalboom et al. (2020), and based on exact

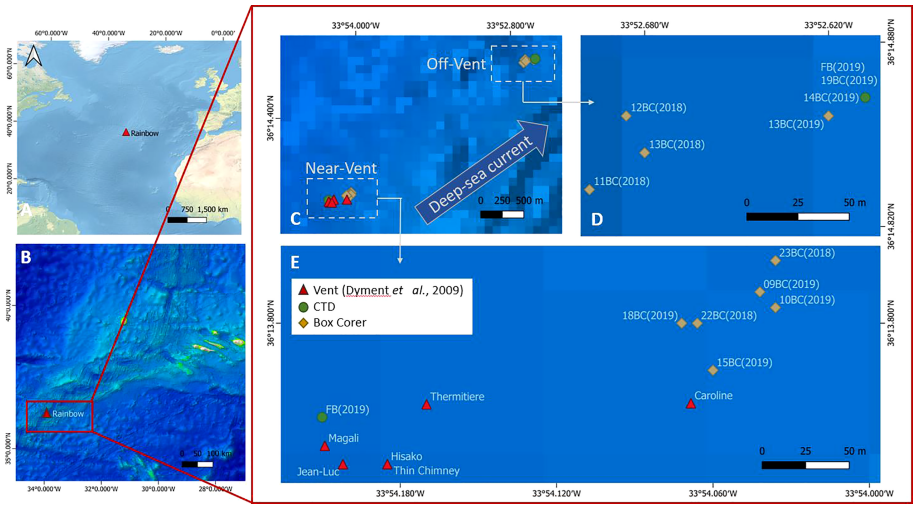

FIGURE 1 | **(A)** The Mid-Atlantic Ridge and Rainbow vent field location, **(B)** Location of the Rainbow vent field on the Azores triple junction, **(C–E)** Locations of active black smokers (red triangles), and of sedimented near-vent and off-vent sites. Samples were taken at both sites. Sediment samples were taken with a video-guided box corer (yellow square), and water samples were taken by a CTD (green circles) during the RV Pelagia expeditions in 2018 (64PE441) and 2019 (64PE454). Red triangles: black smoker structures (coordinates and names as given in Dyment et al., 2009); yellow squares: Box Corer (BC) samples; green circles: CTD (FB) in which FB near-vent comprises samples 1,4,7,10 and 13 and FB off-vent samples 16,19,22,25and 28. Map with QGIS 3.18.

coordinates of RB vent smokers by Dyment et al. (2009). Samples were obtained during two research expeditions with RV Pelagia during cruise 64PE441 (16th to 25th of June 2018) and 64PE454 (24th of June to 4th of July 2019). Sediment cores and water samples were collected at two sites downstream of the plume: very close to the vent at approximately 30-100 m distance from the nearest black smoker (near-vent) and at ~4 km distance from the vent (off-vent) (**Figures 1B–E** and **Table S1**). A NIOZ-designed video-guided stainless steel cylindrical box corer (inner diameter 50 cm and 55 cm height), a trip valve sealing the box, was used to obtain quantitative sediment samples. The camera was used to avoid sampling hard substrates. In practice, the box corer was (1) lowered towards the bottom until the bottom became visible, (2) the ship with the box corer was moved into position, (3) the box corer was lifted several meters upwards to gain enough speed, (4) the box corer was deployed, resulting in ~30 cm deep penetration into the sediment with ~10-20 cm of overlying bottom water in the box corer. After the box corer was on deck, it was inspected for sampling success (i.e. enough overlying bottom-water; no leaking due to underlying rocks in sediments that had caused deformation of the box corer or incomplete closure). Only successfully retrieved box corers were subsampled with push cores. For all meiofaunal analyses, push cores with a ~5 cm diameter (area of 19.63 cm^2) were used. For higher taxon diversity and nematode biomass analyses, the top 10 cm of each push core was fixed in a 4% buffered formaldehyde solution. For faunal stable isotope analyses, the top 10 cm of the push cores were frozen at -20°C, but only the top 5 cm have been analysed. One retrieved box corer (23BC) contained only a 7 cm thick sediment layer due to the hard substrate below. In addition to 5 cm diameter push cores, plastic syringes with 3 cm diameter (area of 7.07 cm^2) were pushed into the sediment and frozen at -20°C for bulk sediment stable isotope analyses back in the lab.

Water samples were collected with a CTD/Rosette, at the same locations as the sediment samples. 12-liter Niskin bottles were closed at approximately 2000 m water depth, with 4 samples collected at different depths in the maximum deep-water turbidity layer, indicative for the presence of the hydrothermal plume. In addition, one sample was collected in the chlorophyll maximum layer at 75 m water depth (**Figure 2**). For SPOM analyses, 2x10 L of water from each water depth were filtered over pre-weighed and pre-combusted GFF filters on board, rinsed with a minimum amount of MilliQ water to remove salt, and stored at -20°C (**Table S1**).

2.2 TOC, $\delta^{13}C$ and $\delta^{15}N$ Analyses of Water and Sediment Samples

The SPOM filters were decalcified before C and N stable isotope analyses. In total 10 SPOM filters were analysed; 5 from near-vent and 5 from off-vent. One sample (FB10) from the near-vent plume did not have enough material to measure the N stable isotope signature, even though the complete filter was analysed. The filters were moistened with some drops of double-distilled water (bidest) and were placed in a chamber filled with HCl gas overnight, followed by drying in an oven at 60°C. Each SPOM filter was manually folded and compacted in a tin capsule. The C and N isotope ratios for SPOM filters were measured in a single analytical run, and certified isotope standards acetanilide (0.3-0.6 mg), casein (0.2-0.5 mg) and urea (0.3-0.8 mg) were used as reference standards.

A total of 7 sediment cores, 4 from near-vent and 3 from off-vent, were analysed at 1 cm intervals until 5 cm core depth

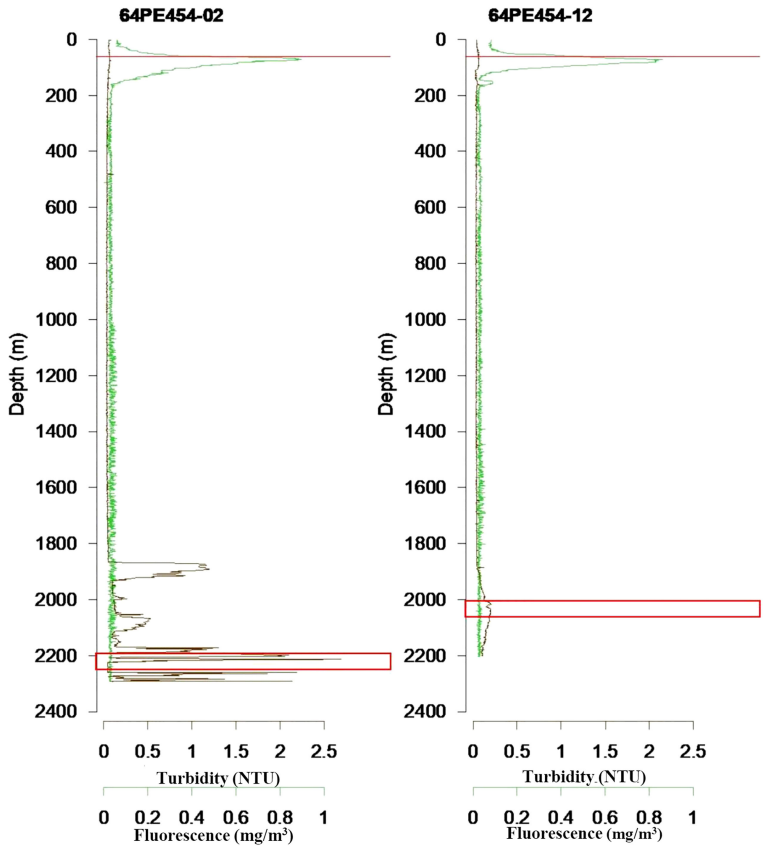

FIGURE 2 | Turbidity and fluorescence profiles in near-vent site (64PE545-02) and off-vent site (64PE545-12) water column. The maximum turbidity in deep water represents the vent plume. The sampling depths are marked with a red line at 75 m water depth, and red squares around 2000 m water depth.

(**Table S1**). The sediment samples were freeze-dried and ground to a fine and homogeneous powder. This powder was used for $\delta^{15}N$ and $\delta^{13}C$ analyses. For $\delta^{13}C$ analyses, the powder was decalcified to remove inorganic carbon. Sediments were decalcified in Borosilicate glass culture tubes with 2M HCL added in drops until no reaction (bubbling) was visible. The tubes with sediments were shaken for 500 minutes in a table shaker and were afterward centrifuged at 2000 RPM for 5 minutes. After centrifugation, to remove acid from the decalcified samples, the liquid above the sediment was carefully removed with a pipet, and 1 ml doubly distilled water (Bidest) was added to the sediments in the tubes and vortexed until the sediments were resuspended and mixed well with water; followed by adding approximately 10 ml Bidest water to fill up the tube. The centrifugation and removing liquid process were repeated until the pH of the remaining liquid above the sediment in tubes was higher than 5, after which the decalcified samples were freeze-dried. All sediment samples were weighed precisely in tin capsules to carry out stable isotope analysis (SIA). The capsules were crimped and manually compacted to minimize internal air space. Great care was made to avoid any contamination with solvents, fingers and dust. Certified standards comprised 0.05-0.12 mg Benzoic acid and Acetanilide to measure $\delta^{13}C$, and Acetanilide (0.5-0.8 mg), Casein (0.3-0.8 mg) and Urea (0.3-0.8 mg) to measure $\delta^{15}N$.

All values for stable isotope analyses are expressed in δ (‰) notation with respect to the PeeDee Belemnite ($\delta^{13}C$), and Air ($\delta^{15}N$) because of the constant average abundance of ^{15}N (Kendall and Caldwell, 1998), in which $\delta^{H}X = [(R_{SAMPLE}/R_{STANDARD} - 1)] \times 10^{3}$, where R is $^{13}C/^{12}C$ or $^{15}N/^{14}N$ (Fry, 2006). The stable isotope composition ($\delta^{13}C$ and $\delta^{15}N$) of all samples was measured using a Flash 2000 (Organic Elemental Analyzer) MAS 200 autosampler that was connected *via* CONFIO IV to DELTA V ADVANTAGE (isotope ratio mass spectrometer (IRMS)) and ISODAT 3.0 Gas Ratio MS Software was used. The total organic carbon (TOC) was measured along with carbon and nitrogen stable isotope ratios and the TOC (%) calculation was based on the MS-signal. To test the relationships of TOC, $\delta^{13}C$ and $\delta^{15}N$, biplots of linear regression were created and the Pearson's correlation coefficient r and p-values calculated.

2.3 Stable Isotope Analyses of Meiofauna

We used 4 box cores (12 push cores) from near-vent and 3 box cores (9 push cores) from off-vent to measure stable C and N isotope values of meiofauna (**Table S2**). For meiofauna

extraction, sediment samples were unthawed and rinsed with 32 µm-filtered tap water through 1 mm and 32 µm mesh sieves. The remaining sediments on the 32 µm sieve were put into centrifugation tubes. For centrifugation of sediments, colloidal silica polymer was used as the flotation medium (H.C. Stark, Levasil 200/40%, q = 1.17) and kaolin was used to hold back the heavier particles during decantation (Holme and McIntyre, 1971). Each sample was centrifuged 3 times for 6 minutes at 3500 rpm. The flotation medium with animals was passed through a 32 µm sieve, rinsed with Milli-Q water, and meiofauna transferred into petri dishes. A stereomicroscope was used to identify meiofauna to higher taxonomic levels (i.e. nematodes, copepods, polychaetes) based on Higgins and Thiel (1988) and Giere (2009). For reliable detection of C and N compositions, the minimum required weight for meiofauna is 0.1 mg (Portail et al., 2018) which is estimated around 300 copepods or nematodes (Lebreton et al., 2012). Meiofaunal individuals were hand-picked under a stereomicroscope and pooled per higher taxon directly into a tin capsule. The total number of individuals per taxon extracted from near-vent was 502 nematodes, 121 copepods, 12 polychaetes and 711 nematodes and 80 copepods for off-vent. No polychaetes were found at this site. Although meiofauna was completely sampled from the sediment samples, there was not enough material to reliably measure $\delta^{15}N$ values of meiofauna and for the off-vent site, not even enough for a $\delta^{13}C$ value for copepods. Tin capsules with animals were freeze-dried, weighed and measured on the Flash 2000 (Organic Elemental Analyzer; see above). Certified isotope standards acetanilide (0.01-0.1 mg), casein (0.015-0.12 mg) and urea (0.03-0.3 mg) were used as the reference standards for $\delta^{13}C$.

2.4 Abundance and Biomass Analyses of Nematodes

In addition to the higher meiofaunal taxa counts obtained whilst picking fauna for stable isotopes analyses (from 21 push cores; see *Meiofauna Abundance, Biomass and Isotope Values*), we analyzed higher meiofaunal taxa, and nematode biomass from additional 9 push cores (**Table S2**). In total, 30 push cores (from 12 box corers) were compared for meiofaunal abundance, 16 push cores from near-vent and 14 push cores from off-vent. Biomass data were based on 4 push cores from near-vent and 5 push cores from off-vent (see **Table S2**).

Biomass was only calculated using non-damaged individuals (81% of specimens near-vent and 79% of specimens off-vent) as required in the formula described by Andrassy (1956). The statistical analysis is based on standardized data for a 10 cm^2 area. The difference in the abundance and biomass of meiofauna near-vent and off-vent was analyzed by applying Welch's t-test (unequal variances t-test).

To extract meiofauna used for biomass analyses from the sediments, formaldehyde from sediment samples was removed, and sediments were centrifuged as described in 3.3. to extract fauna. A stereomicroscope was used to count and identify meiofauna to higher taxonomic levels (i.e. nematodes, copepods, polychaetes) based on Higgins and Thiel (1988) and Giere (2009). Nematodes were mounted on glass slides, by placing them first into a solution of water/ethanol/glycerol (61/35/4) followed by evaporation for 2 days in a 40°C oven. Afterwards, nematodes were placed into a drop of glycerin on a glass slide, covered with a glass slip and sealed with lacquer (Higgins and Thiel, 1988). The biomass of nematodes was calculated by measuring individual's dimensions and according to WW (µg) = $(L \times W^2)/Cf$ (Andrassy, 1956), where L (µm) is the nematode's length, W (µm) is its width at the widest point and Cf is 1.6×10^6 as the conversion factor.

3 RESULTS

3.1 $\delta^{13}C$ and $\delta^{15}N$ of SPOM

The $\delta^{13}C$ signature of SPOM collected in the plume was depleted and similar at the near-vent (-26.33 ± 1.12‰) and off-vent (-26.22 ± 0.31‰). $\delta^{13}C$ signatures of SPOM from surface water samples (75 m water depth) at near-vent and off-vent were -23.14‰ and -22.60‰, respectively (**Table 1** and **Figure 6**). Samples from the near-vent had a lower $\delta^{15}N$ value (average 2.4‰), compared to the off-vent sample (average 6‰).

TABLE 1 | The $\delta^{13}C$ and $\delta^{15}N$ of SPOM filters within the plume close to Rainbow vent (near-vent; between 2190 and 2291 m depth) and at 4 km distance to the vent (off-vent; between 1933 and 2202 m depth).

Site	Filter Name	Water Depth (m)	Volume (ml)	Turbidity (NTU)	$\delta^{13}C$ (‰)	$\delta^{15}N$ (‰)
Near-Vent	FB1	2291	4000	5.72	-26.23	2.49
	FB4	2285	4750	9.76	-27.59	2.87
	FB7	2260	4250	2.00	-25.20	4.86
	FB10	2190	8500	0.40	-27.39	NA
	FB13	75	8500	0.05	-23.14	-0.23
Off-Vent	FB16	2202	8175	0.08	-25.83	7.05
	FB19	2140	8000	0.12	-26.44	4.82
	FB22	2051	8500	0.20	-26.48	5.61
	FB25	1933	8050	0.09	-26.13	6.36
	FB28	75	9050	0.05	-22.60	3.67

In addition, $\delta^{13}C$ ratio of SPOM filters was analysed from surface water samples at 75 m depth. Site, sample name (filter number), sampling depth, volume of the filtered water, turbidity at the location, and delta values of carbon and nitrogen stable isotopes are given.
NA, Not Available.

3.2 TOC, $\delta^{13}C$ and $\delta^{15}N$ in Sediment Samples

Surface sediment TOC concentrations of near-vent sediment samples (0.50% ± 0.16) were ~2.5 times higher than off-vent samples (0.16% ± 0.03). **Figure 3** shows the vertical profile of TOC, $\delta^{13}C$ and $\delta^{15}N$ based on the mean and two standard deviations. Near-vent, the top 2 cm had an average TOC content of 0.50%, which was decreasing to 0.26% in 2 to 5 cm depth. Off-vent, no variation in TOC (average 0.16%) was observed with depth. The average $\delta^{13}C$ value in the first cm in near-vent sediments (-24.6‰) was lower than for the first cm in off-vent sediments (-21.1‰). $\delta^{13}C$ values in near-vent sediments increased with depth (-20.8‰ at 5 cm depth), but remained rather similar off-vent (-20.4‰ at 5 cm depth). A similar trend was observed for $\delta^{15}N$ with values increasing with depth from 4 to 5.4 ‰ near-vent and rather similar $\delta^{15}N$ values from 6.1 to 6.3‰ off-vent. In the sediment samples at the near-vent site, C and N isotopes showed a heterogeneous pattern: the $\delta^{13}C$ varied between -26.7‰ to -20.2‰, and $\delta^{15}N$ from 3.2‰ to 5.9‰, while there was little variation in the sediments from off-vent, for both $\delta^{13}C$ value (-21.7‰ to -19.6‰) and $\delta^{15}N$ (5.6‰ to 6.7‰) (**Figures 3B, C**, **4**). However, a significant correlation was found between $\delta^{13}C$ and TOC ($r^2 = 0.84$, $p<0.001$), $\delta^{15}N$ and *TOC* ($r^2 = 0.84$, $p<0.001$) *when considering all sediment samples* (**Figure 5**).

3.3 Meiofauna Abundance, Biomass and Isotope Values

Meiofaunal abundance was similar near-vent (mean 35.69 ± 28.78 per 10 cm^2) and off-vent (mean 33.20 ± 16.20 per 10 cm^2) (p-value: 0.86). Nematodes dominated the communities with 13 to 83 ind. 10 cm^{-2} near-vent and with 14 to 51 ind. 10 cm^{-2} off-vent. Mean individual nematode biomass was very variable and no statistic difference was detected between "near-vent" (0.50 ± 3.93 µg) and off-vent (0.93 ± 4.35 µg) ($p = 0.72$) (**Table 2**). Mean biomass per 10 cm-2 was also variable (30.68 ± 25.81µg near-vent; 20.05 ± 16.31 µg off-vent; $p = 0.22$). The second most abundant taxon were copepods with <1 to 8 ind. 10 cm^{-2} near-vent, and 1 to 7 ind. 10 cm^{-2} off-vent. Polychaetes, the only macrofaunal taxon observed, were only detected near-vent (**Table 3**).

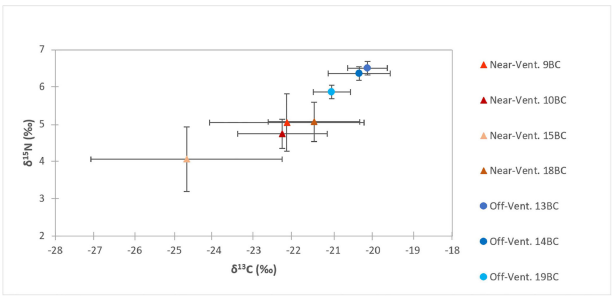

FIGURE 4 | Carbon ($\delta^{13}C$) and nitrogen ($\delta^{15}N$) signatures (mean ± SD) in the first 5 cm of sediments at "near-vent"(~30-100 m distance to RB vent; red triangles) and "off-vent" (~4 km distance to RB vent, blue circles).

Comparing the $\delta^{13}C$ values of nematodes living in the near-vent (-28‰) and the off-vent (-22‰) sediments, depleted values were found in near-vent sites (**Figure 6**). Near the vent, different $\delta^{13}C$ values were detected for nematodes (-28.2‰), copepods (-26.1‰) and polychaetes (-24.9‰). The $\delta^{13}C$ values of meiofauna measured in our study and other studies are provided in **Table 4**.

4 DISCUSSION

4.1 Vent Fluid Associated Organic Carbon Input to the Surrounding Sediments

The hydrothermal plume supplies a potential carbon source in addition to the photosynthetically derived organic matter in the vicinity of the RB vent, which is supported by depleted stable carbon isotope values of SPOM collected within the plume and in the surface sediments near the vent. Plumes are typically rich in free-living sulfur oxidizing and methanotrophic microbes and represent biogeochemical hotspots for carbon fixation in the dark ocean (Mattes et al., 2013). Concentrations of dissolved and particulate organic carbon are elevated in buoyant plume samples (Bennett et al., 2011), and the primary carbon production (chemosynthetic organic carbon) in hydrothermal plumes has been estimated to be at least 2.0 mg C l^{-1} at EPR 21° N

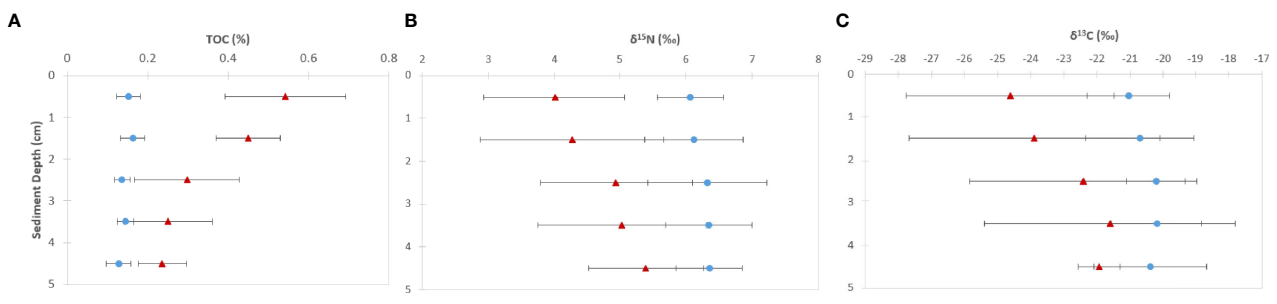

FIGURE 3 | Vertical profiles of **(A)** total organic carbon (TOC) concentration, **(B)** $\delta^{15}N$ and **(C)** $\delta^{13}C$ (mean ± 2SD) of sediment samples (1 cm slices) from surface up to 5 cm core depth in sediments "near-vent" (~30-100 m distance to RB vent, red triangles) and "off-vent" (~4 km distance to RB vent; blue circles).

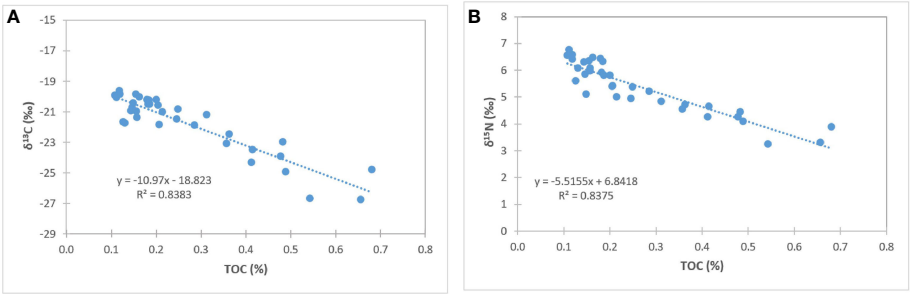

FIGURE 5 | Correlation of $\delta^{13}C$ and TOC **(A)**, and $\delta^{15}N$ and TOC **(B)** concentrations in sediments near-vent and off-vent.

vent fluid (McCollom, 2000). The high fluid fluxes and higher concentration of chemoautotrophic microbes within the plume in the direct vicinity of the vent and to a limited extent also further away may thus provide chemosynthetic TOC to the vent surrounding pelagic environment (Portail et al., 2018; Haalboom et al., 2020).

Total organic carbon in surface sediments was higher near-vent (0.49% ± 0.16) than off-vent (0.15% ± 0.03), suggesting that plume fall out and impact is higher in near-vent areas. Our results are in accordance with findings at vents near Japan located in the Izu-Ogasawara Arc of the western North Pacific, where TOC in sediments at the direct base of the chimney was higher compared to sediments further away from the vent (Nomaki et al., 2019). The reduction of TOC with distance to the RB vent may be closely linked to the observed reduction of plume intensity with distance as shown by a decrease in turbidity with increasing distance to the vent plume source, the chimneys (Haalboom et al., 2020) (**Figure 2**).

Near-vent, $\delta^{13}C$ sediment values were very variable and more depleted (~-25‰) at the sediment surface (0-1 cm) and less depleted at 5 cm sediment depth (~-21‰), showing prominent input of chemosynthetically derived organic carbon from the plume (~26‰) to the surface sediments. The heterogeneity in $\delta^{13}C$ values between samples may be related to vent plume dynamics which are variable in space and time (Haalboom et al., 2020). The high correlation of $\delta^{13}C$ and relative TOC content in sediments (see **Figure 5**) suggests the input of fresh *in situ* derived organic carbon to the sediments near-vent and degradation with depth.

Off-vent, $\delta^{13}C$ sediment values were ~21‰ at the surface and ~-20‰ at 5 cm core depth, pointing to a dominant input of photosynthetically derived OC from the surface ocean (~-22 to -23‰). The discrepancy between $\delta^{13}C$ from surface waters and deep-sea sediments may be explained by a higher proportion of fresh, non-degraded algae, in the surface-waters. While sinking to 2000 m water depth, this algal material is reworked and mixed at the seabed with other carbon pools, which causes a positive shift in carbon isotopes. For instance, algal material being consumed by higher trophic levels would result in an increase of ~0.5 to 1‰ per trophic level (DeNiro and Epstein, 1981; Gearing, 1991).

The $\delta^{13}C$ values and TOC percentage in sediments reflect a mixture of different carbon sources for consumer communities, including fresh chemosynthetically-derived OC and photosynthetically derived OC from the surface ocean. Our data indicate that there is approximately 0.15% TOC in the open ocean sediment with a carbon isotope value of roughly -20.5‰ which represents photosynthetically derived OC. Close to the venting area, in addition to the photosynthetically derived carbon source, fresh *in situ* chemosynthetically derived OC is present, which is reflected by higher TOC and more depleted $\delta^{13}C$ values. Fauna close to vents uses this fresh organic matter as a food source. The contribution of chemosynthetic organic matter decreases with both sediment depth and distance from the vent (**Figures 3**, **4**).

4.2 Chemosynthetic-Derived Organic Carbon as a Food Source for Fauna in Sediments

The $\delta^{13}C$ values of fauna near-vent ranged from ~-25 to -28‰ and were similar to SPOM within the vent plume (-26‰; this study), suggesting selective feeding of (fresh) *in situ* derived organic carbon by near-vent fauna. The variability in stable isotope values may mirror the multiple chemosynthetic pathways of carbon production, such as methanotrophy versus autotrophy based on CBB or rTCA cycles according to the varying concentrations of reduced compounds (e.g. CH_4, H_2S) at vent systems (Portail et al., 2018), as well as differences in the relative contribution of photosynthetic and chemosynthetic material at different sampling locations. The isotopic signatures from vent copepods (-26‰ to -29‰) from Portail's study were very similar to the isotopic signatures from copepods in this study living near-vent (-26‰), while the vent nematode signatures (-22‰ to -25‰) were less depleted than our near-vent nematodes (-28‰) (see **Table 4**).

The distinct $\delta^{13}C$ values of meiofauna near-vent (nematodes, copepods and polychaetes) suggest that these taxa may have different feeding strategies these groups may harbour several different species with different feeding strategies as well and/or ecological niches and rely on different food sources. Copepods and nematodes in sediments near-vent may selectively feed on chemosynthetic-derived organic carbon, similar to what was

TABLE 2 | Biomass of nematodes.

	Near-Vent (n= 417 ind.)	Off-Vent (n= 152 ind.)
Mean biomass of each individual (µg)	0.50 ± 3.93	0.93 ± 4.35
Mean length of each individual (µm)	713.95 ± 375.01	784.53 ± 759.20
Mean width of each individual (µm)	21.46 ± 9.91	25.77 ± 18.51

Mean and standard deviations of biomass, length and width of each individual, are provided for near-vent and off-vent.

TABLE 3 | Density of meiofauna from sediment samples.

Site	Year	Sample	SS	Total Area (cm^2)	Nematode density ($10\ cm^{-2}$)	Copepod density ($10\ cm^{-2}$)	Polychaete density ($10\ cm^{-2}$)	Faunal density ($10\ cm^{-2}$)
Near-Vent	2018	22BC	a+b+c	58.89	82.53	7.98	0	90.51
	2018	23BC	a	19.63	15.28	0.51	0	15.79
	2019	9BC	a+b+c	58.89	13.08	6.45	1.02	20.55
	2019	10BC	a+b+c	58.89	13.92	6.28	0.68	20.88
	2019	15BC	a+b+c	58.89	20.38	0.85	0.17	21.40
	2019	18BC	a+b+c	58.89	37.87	6.96	0.17	45.00
Mean					**30.51**	**4.84**	**0.34**	**35.69**
STD					**27.11**	**3.28**	**0.42**	**28.78**
Off-Vent	2018	11BC	a+b+c	58.89	20.55	4.58	0	25.13
	2018	12BC	a	19.63	23.94	1.02	0	24.96
	2018	13BC	a	19.63	13.75	1.02	0	14.77
	2019	13BC	a+b+c	58.89	50.94	2.72	0	53.66
	2019	14BC	a+b+c	58.89	45.68	7.30	0	52.98
	2019	19BC	a+b+c	58.89	24.11	3.57	0	27.68
Mean					**29.83**	**3.37**	**0**	**33.20**
STD					**14.89**	**2.39**	**0**	**16.20**

Site, year of sampling, name of sample (box corer), subsample (SS), total area of samples, mean density of nematode, copepod,polychaete individuals and total faunal density per 10 cm^2 are given.

observed for copepods in chimney-based sediments at vents near Japan (Nomaki et al., 2019). Less depleted polychaete $\delta^{13}C$ signatures may point to a more mixed diet (photo- and chemosynthetically derived OC), a trophic increase, or a feeding niche in deeper sediment layers. However, Nomaki et al. (2019) detected no depletion in nematodes near-vent, indicating that only copepods may selectively feed on organic matter produced through chemoautotrophy at the studied vent near Japan. In the RB sediments, nematodes showed high depletion and thus ingestion of *in situ* produced organic carbon.

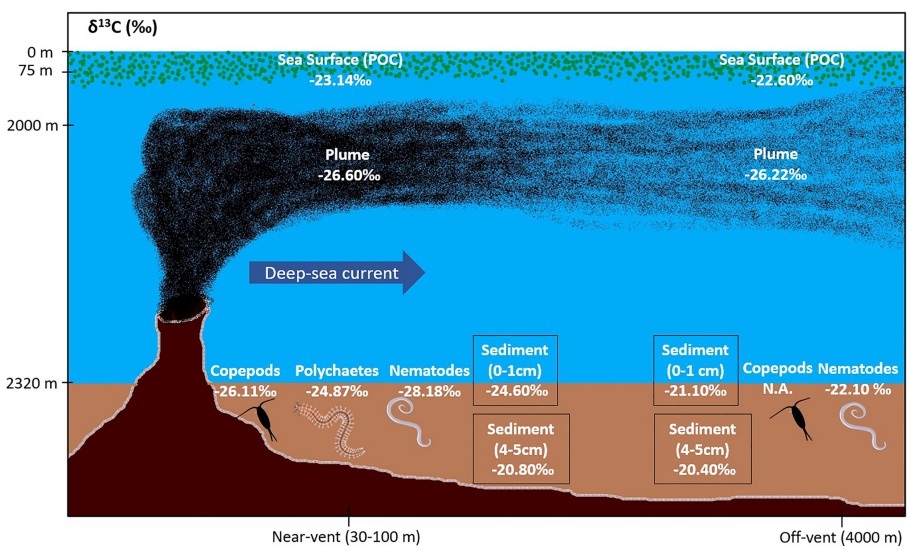

FIGURE 6 | Schematic illustration showing mean $\delta^{13}C$ of sea surface waters, vent plume, sediments and sediment infauna "near-vent" (~30-100 m distance to RB vent; illustrated by black smoker) and "off-vent" (~4 km distance to RB vent). Main plume direction was directly towards the selected off-vent site. Illustration not to scale. POC (Particulate Organic Carbon).

TABLE 4 | $\delta^{13}C$ values of meiofauna from near-vent and off-vent measured in this study in comparison with other studies at and around the Rainbow vent field (MAR).

Location	At Vent			Near-vent			Off-vent	
Distance to vent (m)	0	0	0	185 to 370	< 50	30 to 100	13000	4000
Reference	Nomaki et al.	Alfaro-Lucas et al.	Portail et al.	Nomaki et al.	Alfaro-Lucas et al.	this study	Nomaki et al.	This study
Nematode	-26.61‰ & -23.24‰	-22.73‰	-25.30‰ to -22.80‰	-24.30‰	-23.30‰	-28.18‰	-23.40‰	-22.10‰
Copepod	-21.17‰ to -9.44‰	-34.57‰	-29.30‰ to -26.40‰	-21.30‰	-23.10‰	-26.11‰	-21.60‰	NA
Polychaete	-26.41‰ to -8.23‰	-31.47‰ to -21.69‰	-2.20‰ to -14.70‰	-20.50‰ & -20.10‰	-31.86‰ to -23.55‰	-24.87‰	NA	NA

NA, Not Available.

The $\delta^{13}C$ values of fauna off-vent were relatively similar to SPOM from the sea surface waters, suggesting that off-vent nematodes may feed on phytodetritus (**Figure 6**). Our findings are similar to the study of Nomaki et al. (2019), showing that fauna outside of the caldera and at caldera non-vent sites was less depleted in $\delta^{13}C$ relative to fauna at the base of the chimney (**Table 4**). A similar trend of decreasing depletion with distance from the active vents, although at a smaller scale (from at vent to 90 m to vent) was also observed for copepods at Lucky Strike (Alfaro-Lucas et al., 2020) (**Table 4**). Data thus suggest that the effect of *in situ* derived organic matter uptake by fauna may be limited to at most several 100 m (Nomaki et al., 2019). However, to precise the extent of influence of organic matter of chemosynthetic origin, future studies at RB vent field should consider samples between 100 and 4000 m distance from the vent.

4.3 Faunal Abundance and Biomass

The additional *in situ* derived food source (chemosynthetic OM) at near-vent did not result in enhanced overall abundance or biomass of nematodes, as similar abundance and biomass were observed near-vent and off-vent. Vanreusel et al. (2010) reviewed biomass data from nematodes living in chemosynthetic environments and showed that vent nematodes can be larger in comparison to reference sediments as an adaptation to low oxygen conditions (Vanreusel et al., 2010). In this study, nematodes' biomass (off-vent: 20.05 µgC 10 cm^{-2}, near-vent: 30.68 µg C 10 cm^{-2}) ranged in between the biomass of nematodes from two abyssal sites in the NE Atlantic in which one is oligotroph (EUMELI, 8.52 µgC 10 cm^{-2}) and the other characterized by a high input of organic matter (Porcupine Abyssal Plain, 54.16 µgC10 cm^{-2}) (Vanreusel et al., 1995). Future studies should incorporate the abundance and biomass of all fauna in order to better understand the full impact of enhanced productivity on sediment communities near vents.

5 CONCLUSION

Our study shows that active vents are not isolated systems, but that *in situ* chemosynthetic-derived organic matter is traced back in the food web in near-vent areas. The degree of connection of active vent ecosystems to their non-vent surroundings may depend on the direction, composition and volume of the vent plume. Future studies may explore in greater detail the change of food web and community structures along vent plume gradients and geographical distance to the active vent. Determining the true footprint of active vent systems is necessary in order to be able to determine the geographical size of any future area-based management tool.

DATA AVAILABILITY STATEMENT

The original contributions presented in the study are included in the article/**Supplementary Material**. Further inquiries can be directed to the corresponding author.

AUTHOR CONTRIBUTIONS

RR performed the stable isotope analyses, counted and identified animals, analyzed the data, and wrote the manuscript. RH analyzed nematode biomass. RB performed isotope analyses. MvM and FM advised on isotope and data analyses. SG designed the project, collected samples, and helped with data analyses. MvM, FM, and SG contributed to the writing and discussion. All authors contributed to the article and approved the submitted version.

FUNDING

We acknowledge the funding of the Netherlands Organisation for Scientific Research NWO and Royal Netherlands Institute for Sea Research NIOZ in organizing the Netherlands Initiative Changing Oceans NICO expedition in 2018. The study was supported by the following funds: "Erasmus+ Traineeship scholarship program of the University of Milan-Bicocca (to RR)", the Innovational Research Incentives Scheme of the Netherlands Organisation for Scientific Research (NWO) under grant agreement nos. 016.161.360 (to FM), the UU-NIOZ student work experience (to SG and Mei Nelissen), and the UU-NIOZ project "Protecting deep

seabed hydrothermal vent fields through area-based management tools".

ACKNOWLEDGMENTS

We thank the captain and crew of RV Pelagia for their great support during expeditions. We further thank Rianna Vlierboom, Eva Paulus, and Mei Nelissen for support during research expeditions, for sorting fauna and preparing slides for nematode analyses. We thank the reviewers and the editor for their very valuable comments to improve the quality of this manuscript.

SUPPLEMENTARY MATERIAL

The Supplementary Material for this article can be found online at: https://www.frontiersin.org/articles/10.3389/fmars.2022.732740/full#supplementary-material

REFERENCES

Adams, D. K., Arellano, S. M., and Govenar, B. (2012). Larval Dispersal, Vent Life in the Water Column. *Oceanography* 25 (1), 255–685. doi: 10.5670/oceanog.2012.24

Alfaro-Lucas, J. M., Pradillon, F., Zeppilli, D., Michel, L. N., Martinez-Arbizu, P., Tanaka, H., et al (2020). High Environmental Stress and Productivity Increase Functional Diversity Along a Deep-Sea Hydrothermal Vent Gradient. *Ecology* 101 (11), 1–13. doi: 10.1002/ecy.3144

Andrassy, I. (1956). Die Rauminhalts-Und Gewichtsbestimmung Der Fadenwürmer (Nematoden)". *Acta Zool. Hung.* 2.1, 1–5.

Andreani, M., Ildefonse, B., Godard, M., and Escartin, J. (2014). Tectonic Structure, Lithology, and Hydrothermal Signature of the Rainbow Massif (Mid-Atlantic Ridge 36°14′N). *Geochem. Geophysi. Geosyst.* 15 (9), 3543–3571. doi: 10.1002/2014GC005269.Received

Bennett, S. A., Statham, P. J., Green, D. R.H., Le, N., Mcdermott, J. M., Prado, F., et al (2011). Deep-Sea Research I Dissolved and Particulate Organic Carbon in Hydrothermal Plumes From the East Pacific Rise , 9 1 50 0 NB. *Deep Sea Res. Part I* 58 (9), 922–315. doi: 10.1016/j.dsr.2011.06.010

Boschen, R. E., Rowden, A. A., Clark, M. R., Barton, S. J., Pallentin, A., and Gardner, J. P. A. (2015). Megabenthic Assemblage Structure on Three New Zealand Seamounts: Implications for Seafloor Massive Sulfide Mining. *Mar. Ecol. Prog. Ser.* 523, 1–14. doi: 10.3354/meps11239

Boschen, R. E., Rowden, A. A., Clark, M. R., and Gardner, J. P. A. (2013). Mining of Deep-Sea Seafloor Massive Sulfides: A Review of the Deposits, Their Benthic Communities, Impacts From Mining, Regulatory Frameworks and Management Strategies. *Ocean Coast. Manag.* 84, 54–67. doi: 10.1016/j.ocecoaman.2013.07.005

Collins, P. C., Croot, P., Carlsson, J., Colaço, A., Grehan, A., Hyeong, K., et al. (2013). A Primer for the Environmental Impact Assessment of Mining at Seafloor Massive Sulfide Deposits. *Mar. Policy* 42, 198–209. doi: 10.1016/j.marpol.2013.01.020

DeNiro, M. J., and Epstein, S. (1981). Influence of Diet on the Distribution of Nitrogen Isotopes in Animals. *Geochim. Cosmochim. Acta* 45 (3), 341–351. doi: 10.1016/0016-7037(81)90244-1

Desbruyères, D., Caprais, M. B. J., Colaçoc, A., Comtetd, T., Crassous, P., Fouquet, Y., et al (2001). Variations in Deep-Sea Hydrothermal Vent Communities on the Mid-Atlantic Ridge Near the Azores Plateau. *Dev. Hydrobiol.* 48, 1325–1346. doi: 10.1016/S0967-0637(00)00083-2

Desbruyères, D., Sarradin, P. M., and Segonzac, M. (2000). A Review of the Distribution of Hydrothermal Vent Communities Along the Northern Mid-Atlantic Ridge : Dispersal *vs* . Environmental Controls 201–216. doi: 10.1007/978-94-017-1982-7_19

Dover, C. L. V. (2011). Mining Seafloor Massive Sulphides and Biodiversity: What Is at Risk? *ICES J. Mar. Sci.* 68 (2), 341–348. doi: 10.1093/icesjms/fsq086

Dover, C.L.V., Arnaud-Haond, S., Gianni, M., Helmreich, S., Huber, J. A., Jaeckel, A. L., et al (2018). Scientific Rationale and International Obligations for Protection of Active Hydrothermal Vent Ecosystems From Deep-Sea Mining. *Mar. Policy* 90, 20–28. doi: 10.1016/j.marpol.2018.01.020

Dyment, J., Bissessur, D., Bucas, K., Cueff-Gauchard, V., Durand, L., Fouquet, Y., et al (2009). Detailed Investigation of Hydrothermal Site Rainbow, Mid-Atlantic Ridge, 36°13n: Cruise MoMARDream. *InterRidge News* 19, 22–24.

Edmonds, H. N., and German, C. G. (2004). Particle Geochemistry in the Rainbow Hydrothermal Plume, Mid-Atlantic Ridge. *Geochim. Cosmochim. Acta* 68 (4), 759–25. doi: 10.1016/S0016-7037(03)00498-8

Fry, B. (2006). *Stable Isotope Ecology* (New York, NY: Springer).

Gearing, J. N. (1991). "The Study of Diet and Trophic Relationships Through Natural Abundance 13c." in *Carbon Isotope Techniques*, vol. 201.

German, C. R., Klinkhammer, G. P., and Rudnicki, M. D. (1996). The Rainbow Hydrothermal Plume, 36°15′N, MAR. *Geophys. Res. Lett.* 23 (21), 2979–2982. doi: 10.1029/96GL02883

Giere, O. (2009). The Biotope: Factors and Study Methods," in *Meiobenthology* Springer, Berlin, Heidelberg. doi: 10.1007/978-3-540-68661-3_2

Gollner, S., Govenar, B., Arbizu, P. M., Mills, S., Le Bris, N., Weinbauer, M., et al (2015). Differences in Recovery Between Deep-Sea Hydrothermal Vent and Vent-Proximate Communities After a Volcanic Eruption. *Deep Sea Res. Part I Oceanogr. Res. Pap.* 106, 167–182. doi: 10.1016/j.dsr.2015.10.008

Gollner, S., Govenar, B., Arbizu, P. M., Mullineaux, L. S., Mills, S., Le Bris, N., et al (2020). Animal Community Dynamics at Senescent and Active Vents at the 9° N East Pacific Rise After a Volcanic Eruption. *Front. Mar. Sci.* 6. doi: 10.3389/fmars.2019.00832

Gollner, S., Kaiser, S., Menzel, L., Jones, D. O. B., Brown, A., Mestre, N. C., et al (2017). Resilience of Benthic Deep-Sea Fauna to Mining Activities. *Mar. Environ. Res.* 129, 76–101. doi: 10.1016/j.marenvres.2017.04.010

Gollner, S., Riemer, B., Martínez Arbizu, P., le Bris, N., and Bright, M. (2010). Diversity of Meiofauna From the 9°50′N East Pacific Rise Across a Gradient of Hydrothermal Fluid Emissions. *PloS One* 5 (8), e12321. doi: 10.1371/journal.pone.0012321

Govenar, B. (2012). Energy Transfer Through Food Webs at Hydrothermal Vents Linking the Lithosphere to the Biosphere. *Oceanography* 25 (1), 246–255. doi: 10.5670/oceanog.2012.23

Griffin, M. P. A., and Valiela, I. (2001). Δ15n Isotope Studies of Life History and Trophic Position of Fundulus Heteroclitus and Menidia Menidia. *Mar. Ecol. Prog. Ser.* 214, 299–305. doi: 10.3354/meps214299

Haalboom, S., Price, D. M., Mienis, F., Bleijswijk, J. D.L.V., De Stigter, H. C., Witte, H. J., et al (2020). Patterns of (Trace) Metals and Microorganisms in the Rainbow Hydrothermal Vent Plume at the Mid-Atlantic Ridge. *Biogeosciences* 17 (9), 2499–25195. doi: 10.5194/bg-17-2499-2020

Higgins, R. P., and Thiel, H. (1988). *Introduction to the study of meiofauna.* (Smithsonian Institution Press).

Holme, N. A., and McIntyre, A. D. (1971). *Methods for the Study of Marine Benthos*. Blackwell Scientific Publications.

ISA (2019) *"Guidance to Facilitate the Development of Regional Environmental Management Plans (REMPs)"*. Available at: https://www.isa.org.jm/files/files/documents/remp_guidance_.pdf.

Kendall, C., and Caldwell, E. A. (1998). Fundamentals of Isotope Geochemistry. In Isotope tracers in catchment hydrology (pp. 51-86). Elsevier. doi: 10.1016/B978-0-444-81546-0.50009-4

Khripounoff, A., Vangriesheim, A., Crassous, P., Crassous, P., Segonzac, M., Colaço, A., et al (2001). Particle Flux in the Rainbow Hydrothermal Vent Field (Mid-Atlantic Ridge): Dynamics, Mineral and Biological Composition. *J. Mar. Res.* 59 (4), 633–656. doi: 10.1357/002224001762842217

Kim, S. S. L., Mullineaux, L. S., and Helfrich, K. R. (1994). Larval Dispersal *via* Entrainment Into Hydrothermal Plumes Larval Dispersal *via* Entrainment Into Hydrothermal Vent Plumes. *J. Geophysical Res.: Oceans* 99 (C6), pp.12655–12665. doi: 10.1029/94JC00644

Klunder, L., de Stigter, H., Lavaleye, M. S. S., van Bleijswijk, J. D. L., van der Veer, H. W., Reichart, G. J., et al (2020). A Molecular Approach to Explore the Background Benthic Fauna Around a Hydrothermal Vent and Their Larvae: Implications for Future Mining of Deep-Sea SMS Deposits. *Front. Mar. Sci.* 7. doi: 10.3389/fmars.2020.00134

Lebreton, B., Richard, P., Galois, R., Radenac, G., Brahmia, A., Colli, G., et al (2012). Food Sources Used by Sediment Meiofauna in an Intertidal Zostera Noltii Seagrass Bed: A Seasonal Stable Isotope Study. *Mar. Biol.* 159 (7), 1537–05. doi: 10.1007/s00227-012-1940-7

Levin, L. A., Baco, A. R., Bowden, D. A., Colaco, A., Cordes, E. E., Cunha, M. R., et al (2016). Hydrothermal Vents and Methane Seeps: Rethinking the Sphere of Influence. *Front. Mar. Sci.* 3. doi: 10.3389/fmars.2016.00072

Mattes, T. E., Nunn, B. L., Marshall, K. T., Proskurowski, G., Kelley, D. S., Kawka, O. E., et al (2013). Sulfur Oxidizers Dominate Carbon Fixation at a Biogeochemical Hot Spot in the Dark Ocean. *ISME J.* 7 (12) 2349–2360. doi: 10.1038/ismej.2013.113

McCollom, T. M. (2000). Geochemical Constraints on Primary Productivity in Submarine Hydrothermal Vent Plumes. *Deep Sea Res. Part I Oceanogr. Res. Pap.* 47 (1), 85–101. doi: 10.1016/S0967-0637(99)00048-5

Nomaki, H., Uejima, Y., Ogawa, N. O., Yamane, M., Watanabe, H. K., Senokuchi, R., et al (2019). Nutritional Sources of Meio- And Macrofauna at Hydrothermal Vents and Adjacent Areas: Natural-Abundance Radiocarbon and Stable Isotope Analyses. *Mar. Ecol. Prog. Ser.* 622, 49–65. doi: 10.3354/meps13053

Pinnegar, J. K., and Polunin, N. V. C. (2000). Contributions of Stable-Isotope Data to Elucidating Food Webs of Mediterranean Rocky Littoral Fishes. *Oecologia* 122 (3), 399–4095. doi: 10.1007/s004420050046

Portail, M., Brandily, C., Cathalot, C., Colaço, A., Gélinas, Y., Husson, B., et al (2018). Food-Web Complexity Across Hydrothermal Vents on the Azores Triple Junction. *Deep Sea Res. Part I Oceanogr. Res. Pap.* 131, 101–120. doi: 10.1016/j.dsr.2017.11.010

Spedicato, A., Sánchez, N., Pastor, L., Menot, L., and Zeppilli, D. (2020). Meiofauna Community in Soft Sediments at TAG and Snake Pit Hydrothermal Vent Fields. *Front. Mar. Sci.* 7. doi: 10.3389/fmars.2020.00200

Thurnherr, A. M., and Richards, K. J. (2001). Hydrography and High-Temperature Heat Flux of the Rainbow Hydrothermal Site (36°14′N, Mid-Atlantic Ridge). *J. Geophys. Res. Oceans* 106 (C5), 9411–9426. doi: 10.1029/2000jc900164

Thurnherr, A. M., Richards, K. J., German, C. R., Lane-Serff, G. F., and Speer, K. G. (2002). Flow and Mixing in the Rift Valley of the Mid-Atlantic Ridge 1763–1778. doi: 10.1175/1520-0485(2002)032%3C1763:FAMITR%3E2.0.CO;2

Vanreusel, A., De Groote, A., Gollner, S., and Bright, M. (2010). Ecology and Biogeography of Free-Living Nematodes Associated With Chemosynthetic Environments in the Deep Sea : A Review. *PLoS One* 5 (8), e12449. doi: 10.1371/journal.pone.0012449

Vanreusel, A., Vincx, M., Bett, B. J., and Rice, A. L. (1995). Nematode Biomass Spectra at Two Abyssal Sites in the NE Atlantic With a Contrasting Food Supply. *Int. Rev. Ges. Hydrobiol. Hydrogr.* 80 (2), 287–965. doi: 10.1002/iroh.19950800215

Conflict of Interest: The authors declare that the research was conducted in the absence of any commercial or financial relationships that could be construed as a potential conflict of interest.

Publisher's Note: All claims expressed in this article are solely those of the authors and do not necessarily represent those of their affiliated organizations, or those of the publisher, the editors and the reviewers. Any product that may be evaluated in this article, or claim that may be made by its manufacturer, is not guaranteed or endorsed by the publisher.

frontiers | Frontiers in Marine Science

ORIGINAL RESEARCH
published: 15 June 2022
doi: 10.3389/fmars.2022.765648

Geochemistry of Hydrothermal Fluids From the E2-Segment of the East Scotia Ridge: Magmatic Input, Reaction Zone Processes, Fluid Mixing Regimes and Bioenergetic Landscapes

Samuel I. Pereira[1,2,3], Alexander Diehl[1,2], Jill M. McDermott[4], Thomas Pape[1,2], Lukas Klose[5], Harald Strauss[6], Gerhard Bohrmann[1,2] and Wolfgang Bach[1,2]*

[1] Faculty of Geosciences, University of Bremen, Bremen, Germany, [2] MARUM-Center for Marine Environmental Sciences, Bremen, Germany, [3] Department of Earth Sciences & Centre for Deep Sea Research, University of Bergen, Bergen, Norway, [4] Department of Earth and Environmental Sciences, Lehigh University, Bethlehem, PA, United States, [5] Department of Physics and Earth Sciences, Jacobs University, Bremen, Germany, [6] Department of Geology and Palaeontology, University of Münster, Münster, Germany

OPEN ACCESS

Edited by:
Jozee Sarrazin, Institut Français de Recherche pour l'Exploitation de la Mer (IFREMER), France

Reviewed by:
Domenico Borello, Sapienza University of Rome, Italy
Mustafa Yucel, Middle East Technical University, Turkey

***Correspondence:**
Samuel I. Pereira
Samuel.Pereira@uib.no

Specialty section:
This article was submitted to Deep-Sea Environments and Ecology, a section of the journal Frontiers in Marine Science

Received: *27 August 2021*
Accepted: *13 April 2022*
Published: *15 June 2022*

Citation:
Pereira SI, Diehl A, McDermott JM, Pape T, Klose L, Strauss H, Bohrmann G and Bach W (2022) Geochemistry of Hydrothermal Fluids From the E2-Segment of the East Scotia Ridge: Magmatic Input, Reaction Zone Processes, Fluid Mixing Regimes and Bioenergetic Landscapes. Front. Mar. Sci. 9:765648. doi: 10.3389/fmars.2022.765648

The compositions of hydrothermal fluids in back-arc basins (BABs) can be affected by the influx of magmatic fluids into systems that are dominated by reactions between basement rocks and seawater-derived fluids. The East Scotia Ridge (ESR) in the Scotia Sea hosts such hydrothermal systems where the role of magmatic fluid influx has not yet been addressed. During expedition PS119 in 2019, three chimneys were sampled from the E2 segment. These samples were analysed for their chemical and isotopic composition along with fluid inclusions in corresponding precipitates. Our data provide evidence for the temporal evolution of hydrothermal fluids in this remote back-arc system. Salinity variations in anhydrite-hosted fluid inclusions indicate that phase separation takes place in the subseafloor. Moderate-temperature (<53°C) fluids from the newly discovered E2-West hydrothermal vent field and high-temperature (>320°C) fluids from the E2-South area were sampled. Depletions in fluid-mobile elements, ΣREE and low $\delta^{18}O_{H2O}$ show that the basement in this root zone has been leached since the previous sampling in 2010. The results indicate that high-temperature fluid-rock interactions are key in setting the composition of the fluids with cation-to-chloride ratios suggesting a common root zone for both vent sites. The concentrations of dissolved gases provide new insights in the connection between magmatic degassing and its influence on endmember vent fluid composition. Specifically, stable isotope (O, H) data and elevated CO_2 concentrations point to a minor influx of magmatic vapour. Stable sulphur isotopes provide no evidence for SO_2 disproportionation suggesting a H_2O-CO_2 dominated nature of these vapours. The concentrations of conservative elements in the E2-W fluid reflects subseafloor mixing between E2-S endmember fluid and seawater. In contrast, non-conservative behaviour,

and depletion of Fe, H_2, and H_2S point to a combination of sub-surface abiotic and biotic reactions affecting these fluids. Similarly, E2-W fluids show evidence for H_2S and CH_4 being metabolized in the subseafloor. Thermodynamic computations confirm that the E2 system is dominated by sulphide oxidation as a major catabolic pathway. Our results indicate that the conditions at E2 are favourable to hosting a robust subseafloor biosphere.

Keywords: hydrothermal vents, East Scotia Ridge, back-arc basin, conductive cooling, magmatic water, bioenergetics, Southern Ocean

INTRODUCTION

Back-arc basin (BAB) hydrothermal systems emit fluids with compositions that can be distinct from their mid-oceanic ridge (MOR) counterparts. Besides being affected by fluid-rock interactions and phase separation, they are often influenced by the addition of gases and volatile elements from magmatic fluid influx (e.g., De Ronde and Jambor, 1995; Ishibashi and Urabe, 1995; Yang and Scott, 2006; Reeves et al., 2011; Seewald et al., 2015; Seewald et al., 2019). Magma degassing typically adds H_2O and CO_2 to the circulating seawater-derived fluids (e.g., Lupton et al., 2006; Reeves et al., 2011), but may also deliver acid-sulphate components such as SO_2, HCl and HF (Butterfield et al., 2011; Seewald et al., 2015; Seewald et al., 2019). This addition of magmatic components can influence fluid-rock interactions and also have an effect on dissolved metal concentrations (Reeves et al., 2011; Seewald et al., 2015; Seewald et al., 2019).

The majority of BAB hydrothermal systems are situated in the western Pacific, e.g., Manus Basin, Okinawa Trough, Lau Basin (Takai et al., 2008; Mottl et al., 2011; Reeves et al., 2011; Seewald et al., 2015; Seewald et al., 2019). The East Scotia Ridge (ESR) in the Southern Ocean is the only known BAB to host active hydrothermal systems outside the Pacific (Diehl and Bach, 2020b; Diehl and Bach, 2021). Located in an area where the Atlantic, Pacific and Indian oceans merge, hydrothermal vent sites of the ESR may be important biogeographic stepping stones for vent fauna (Rogers et al., 2012; Herrera et al., 2015). Like in other hydrothermal areas in the deep sea, the foundation of life around the ESR vents are chemosynthetic microorganisms that metabolize reduced gases and metals dissolved in the vent fluids (Rogers et al., 2012; Linse et al., 2019). Establishing the most important catabolic energy sources brought into these ecosystems by hydrothermal venting is hence vital. Existing vent fluid data for the E2-segment of the ESR system (James et al., 2014) shows that the composition of the fluids venting in 2010 were affected by fluid-rock interactions, phase separation and conductive cooling prior to venting at the seafloor, but the contents of dissolved gases (CO_2, H_2 and CH_4) were not determined in previous studies (Cole et al., 2014; James et al., 2014).

During the *RV Polarstern* expedition PS119 (Bohrmann, 2019) a total of three chimneys were sampled from the known E2-South (E2-S) vent site (James et al., 2014) and a newly discovered vent site (E2-West) to the northwest. The use of gas-tight fluid samplers facilitated measuring the contents of dissolved gases, which is critical for constraining magmatic degassing (e.g., Reeves et al., 2011), and *in situ* pH, vital for examining fluid-rock reactions (e.g., McDermott et al., 2018). Dissolved gases are also a key source of energy for catabolic reactions that control chemolithoautotrophic biomass production in these ecosystems (e.g., McCollom and Shock, 1997; Amend et al., 2011; Dahle et al., 2015; Dahle et al., 2018).

The goal of this study is to provide constraints on gas concentrations, as they hold clues about magma-hydrothermal interactions and are important for the bioenergetic landscape of the vent system. Also, the first re-sampling of the vents at E2-S since 2010 (Cole et al., 2014; James et al., 2014), allowed us to determine if vent fluid composition had changed between then and 2019.

GEOLOGICAL SETTING

The East Scotia Ridge (ESR) is a back-arc spreading centre hosted in the Scotia Sea at the northernmost edge of the Southern Ocean (**Figure 1**). The spreading activity is a result of the subduction of the South American plate under the Sandwich plate (German et al., 2000). The ESR is spreading at a rate of 62-70 mm/yr and separates the Scotia plate from the Sandwich plate (Livermore et al., 1997; Larter et al., 2003). The spreading centre can be broadly divided into sub segments E1 to E9 from north to south, respectively (Livermore et al., 1997). The central part of the ESR has a distinct axial valley graben, and features rocks with a composition similar to mid-oceanic ridge basalts (MORBs, Fretzdorff et al., 2002; Leat et al., 2004). The northern and southern parts of the ESR have axial volcanic ridges (AVRs), that likely reflect a higher magma budget and may relate to mantle inflow into the back-arc due to a roll-back induced corner flow of mantle material around the subducting slab (Livermore et al., 1997; Leat et al., 2000; Bruguier and Livermore, 2001). Seismic reflectors at the E2 segment show evidence for the presence of an axial magma chamber at ca. 3 km below seafloor (Livermore et al., 1997) and corroborate enhanced magma supply rates and high crustal heat flux. Indeed, hydrothermal activity was found at the E2 segment with hydrothermal vent sites hosted on one such axial volcanic ridge (German et al., 2000; James et al., 2014). The basement is primarily composed of basaltic andesite with increased Pb concentrations compared to MORBs, suggesting an influx of

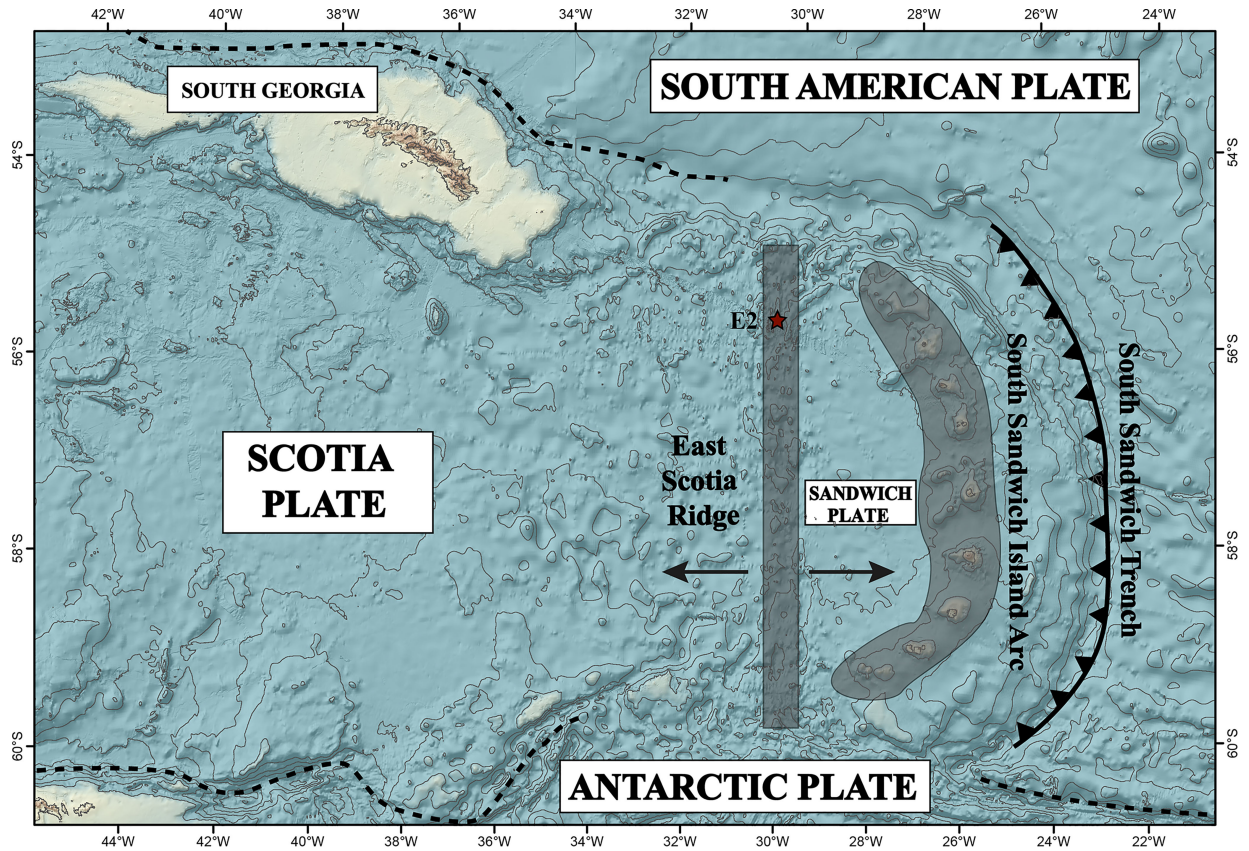

FIGURE 1 | Regional map showing the East Scotia Ridge – back-arc basin (ESR), South Sandwich Island arc (SSIA), associated plate tectonics and the location of E2 hydrothermal vent field (red star) in the Scotia Sea. Adapted after Leat et al. (2016).

slab-derived components (Leat et al., 2000; Fretzdorff et al., 2002; Leat et al., 2004).

The E2-S hydrothermal vent field was discovered in 2009 (Rogers et al., 2012) and low (<20°C) and high (>310°C) temperature fluids were first sampled in 2010 (James et al., 2014). It is situated between 56°05.2' to 56°05.4'S and 30°19.0' to 30°19.35'W in 2600 m water depth between two N-S-striking AVRs exposing pillow lavas of basaltic andesite composition. Two vent sites were sampled in 2010: (1) Dog's Head, a small cluster of ~12-m tall chimneys venting black-smoker type fluids with temperatures as high as 351°C, and (2) Sepia, which is 75 m southwest of Dog's Head, and had fluids (up to 353°C) venting from a 11-m tall bulbous chimney with several flanges, underneath which hot (311°C) fluids pooled (James et al., 2014).

MATERIALS AND METHODS

High and low-temperature hydrothermal fluid samples were collected during expedition PS119 with *RV Polarstern* in April-May 2019. We found hydrothermal activity to the northwest of the sites visited by James et al. (2014). We hence distinguish between E2-S vent area (which includes the Dog's Head and Iced Bun sites) and E2-W ('Alexander von Humboldt' hydrothermal vent field) which is a newly discovered site (**Figure 2**).

The Iced Bun site had not been sampled previously and was actively venting black smoker-type fluid (T_{max} = 320°C, **Figure 3A**). It is in the southern part of the E2-S vent area (56°05.30'S and 30°19.12'W) at a water depth of 2700 m, 20 m west of the Sepia sites and ca. 60 m southeast of the Dog's Head site, both of which were sampled by James et al. (2014). Dog's Head in the northern part of the E2-S vent area (56°05.28'S and 30°19.14'W) is a small cluster of chimneys with several orifices emitting black smoker-type fluid (**Figure 3B**). We recorded a maximum temperature (T_{max}) of 344°C which was lower than the T_{max} of 351°C measured in 2010 (James et al., 2014).

E2-W is situated between 56°04.57' to 56°04.63'S and 30° 19.42' to 30°19.33'W (ca. 1.2 km north-northwest of the E2-S system) at a water depth of 2500 m and covers an area of ca. 1600 m^2 (**Figure 2**). The entire area was venting diffuse fluids evident from shimmering water and distributions of Hoff crabs (Bohrmann, 2019). No venting of high temperature fluids was observed during the dives. In the sampled area, 30 – 50°C warm fluids were diffusely venting out of a prominent broken pillow tube structures (**Figure 3C**, Bohrmann, 2019). This structure was yellowish in colour and at places extensively covered by

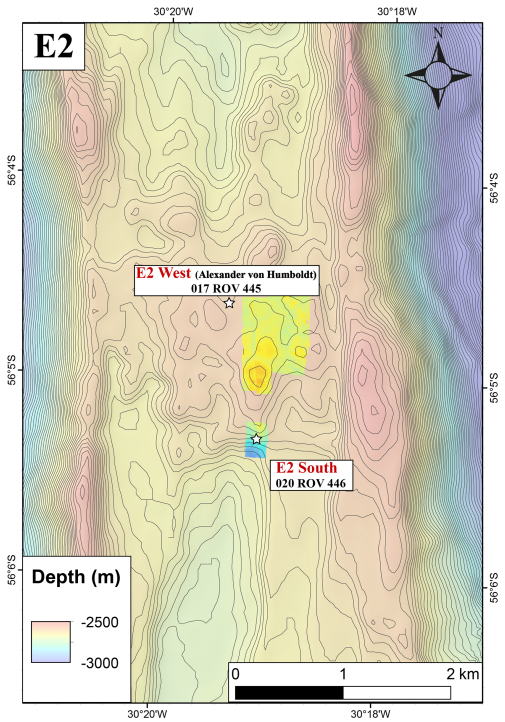

FIGURE 2 | Ship based bathymetry of E2-Segment of the ESR along with the indicated two sites E2-West and E2-South.

microbial mats (**Figure 3D**). A fluid sample at E2-W was collected after a flocculent mat and the pale-yellow precipitates surrounding the orifice were removed by the submersible arm.

Sample Collection and Preparation

Fluids were recovered using 150ml titanium isobaric gas tight (IGT) samplers (Seewald et al., 2002) operated with the Remotely Operated Vehicle (ROV) *MARUM-Quest4000m*. Two fluid samples were collected at the orifices of Dog's Head and Iced Bun at the E2-S segment and one sample was recovered at the newly discovered site called 'E2-West' (Bohrmann, 2019, **Table 1**). The fluids were sampled after breaking off the tip of the chimney structure to allow for better flow of fluid. The temperature of the fluids collected with IGTs were monitored in real-time using a thermocouple attached to the IGT or with the ROV's temperature sensor immediately after fluid sampling. After recovery of the ROV, the IGTs were processed onboard to obtain the fluid as soon as possible (within 12 hours of sampling). The samples were extracted from the IGTs using a HPLC pump and analysed for concentrations of dissolved gases (H_2, CH_4 and H_2S) and $pH_{(25°C)}$.

Filtered (0.45 µm) fluid aliquots for major and trace elemental analysis were collected in acid-cleansed high density-polyethylene (HDPE) Nalgene™ bottles and acidified using 200 µL of concentrated sub-boiled HNO_3. Filtered and unacidified aliquots were collected for anion analysis and for stable hydrogen (δD_{H2O}) and oxygen ($\delta^{18}O_{H2O}$) water isotope analysis in sealed glass ampoules. To determine the total dissolved inorganic carbon (ΣCO_2, abbreviated as CO_2 hereafter), fluid aliquots were injected from gas-tight syringes into pre-weighed He-filled and subsequently evacuated glass serum vials to prevent atmospheric CO_2 contamination. The serum vials were stored upside down to seal the septa and prevent diffuse gas loss. For determination of $\delta^{13}C$ and δD in CH_4 and $\delta^{13}C_{CO2}$, 12-15 ml of gas at standard pressure (STP) were injected into 20 ml glass serum vials containing concentrated NaCl solution. Atmospheric contact of the sample gas was prevented.

Analytical Methods: Fluid Chemistry

Concentrations of H_2 and CH_4 were determined onboard using a 7820A Agilent gas chromatograph (GC). A syringe headspace extraction was done first and the H_2 and CH_4 in the headspace gas was measured using different detectors (Reeves et al., 2011). H_2 was quantified using a thermal conductivity detector (TCD), while CH_4 was determined using a flame ionization detector (FID). The GC was equipped with a Molsieve 60/80 column (Sigma-Aldrich, St Louis, MO) and was operated with N_2 as a carrier gas at 90°C. The analytical uncertainties (2s) are considered as ±5% for H_2 and CH_4. pH (at 25°C and 1 atm) was measured potentiometrically using a 'seven2go' pH electrode (Mettler Toledo, USA) instantly after the fluid was removed from the gas-tight syringe to minimize the effect of degassing. The electrode was calibrated daily using a 4-point calibration with reference solutions of pH 2, 4, 7 and 11. The uncertainty for pH values can be considered within ±0.1 unit.

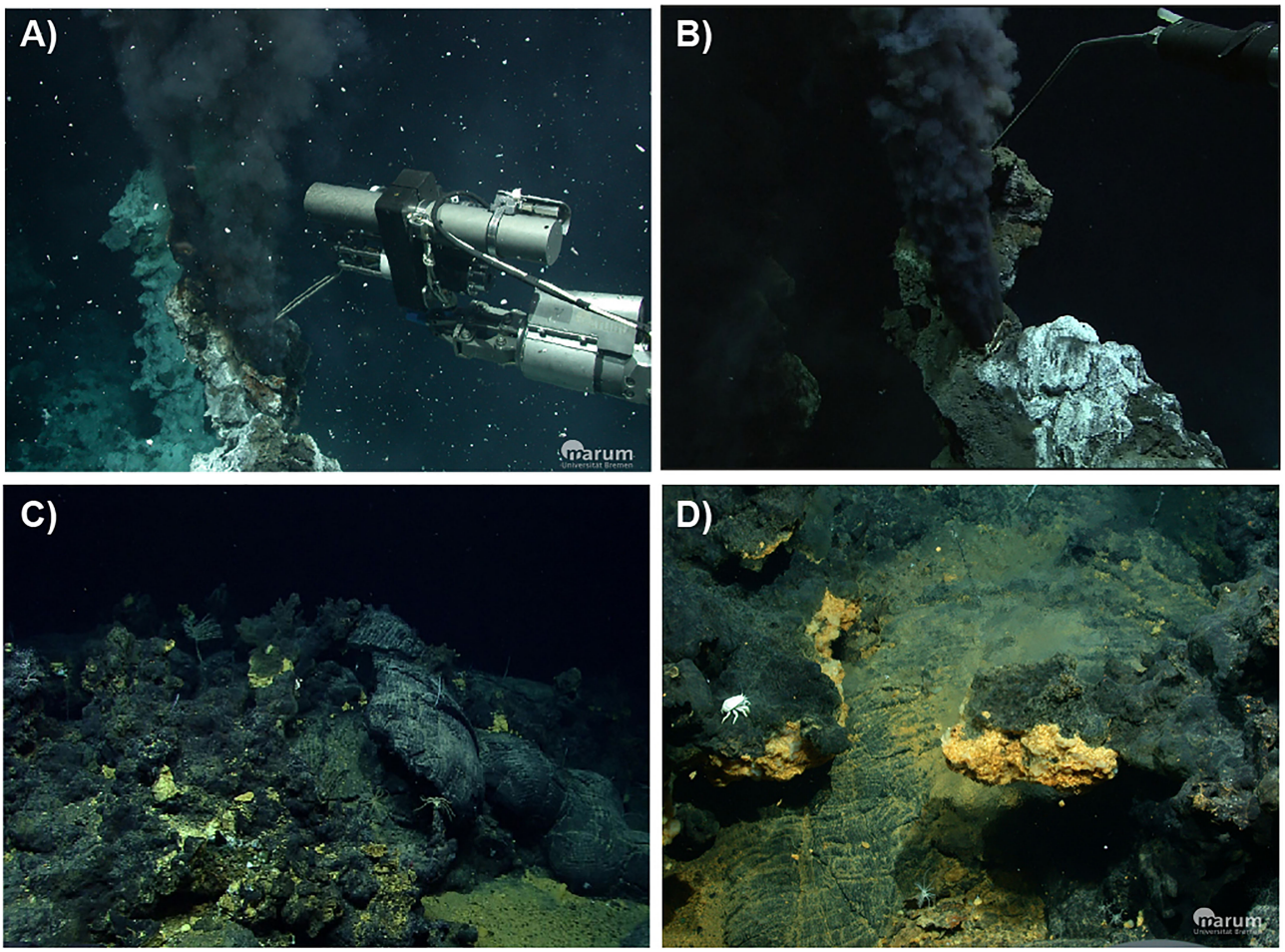

FIGURE 3 | Images of hydrothermal orifices at E2: **(A)** Iced Bun chimney; **(B)** Dog's Head Chimney; **(C)** Diffuse flows escaping from pillow basalts at E2-W **(D)** E2-W tube structure.

Concentrations of major and minor elements were determined using inductively coupled plasma optical emission spectroscopy (ICP-OES, Varian Vista Pro, radial plasma observation) and ion chromatography (IC, Metrohm CompactIC) with a 'METROSEP A Supp 5-150/4.0' column at MARUM, University of Bremen. Trace elements including rare earth elements (REEs), were determined using inductively coupled plasma mass spectroscopy (ICP-MS, Perkin Elmer NexION) at Jacobs University, Bremen. The REEs were determined following a matrix separation and a pre-enrichment method (Schmidt et al., 2010). An ion-exchange column (Sep-Pak C18 cartridge^{TM}) was used for the matrix separation. The accuracy of major and minor elements was monitored using IAPSO standard seawater (supplied by Ocean Scientific International Ltd., UK). The quality of the trace element concentration measurements was monitored using the certified reference material NASS-7 (seawater) from the National Research Council of Canada. The analytical uncertainties (2s) are ±2% for dissolved Na, Si, Mg, Cl, Br and SO_4, ±5% for dissolved Ca, F, Li, Sr, Ba, Al, Fe, Mn and K, ±8% for dissolved B, Rb, Cs and <±10% for REEs.

Total dissolved sulphide (ΣH_2S, hereafter abbreviated as H_2S) was determined gravimetrically at the Faculty of Geosciences, University of Bremen, following shipboard precipitation as Ag_2S in a 5 wt.% $AgNO_3$ solution (prepared on a daily basis) in a method adapted from Seewald et al. (2015). The estimated working range for the gravimetric method is >1mM. Low H_2S concentrations (0.2µM to 1mM) were determined photometrically using the methylene blue method by Cline (1969). CO_2 concentrations were determined onshore after the fluid samples were acidified with 25 wt.% phosphoric acid into the aliquots directing the headspace gas directly into the GC (Thermo Scientific Trace GC Ultra), which was equipped with a Haysep 80/100 column (Sigma-Aldrich, St Louis, MO) and was operated with He as a carrier gas at 50°C. This method was adapted after Reeves et al. (2011). The analytical uncertainties (2s) are considered as ±10% for CO_2 and ±15% for H_2S relative to measured values.

Stable oxygen and hydrogen isotope compositions of vent fluid H_2O were analysed using cavity ring-down spectrometry (CRDS, Picarro L-2130i) at MARUM. The measurement

TABLE 1 | Measured concentrations and isotopic composition of aqueous species from the fluids recovered at E2-South and E2-West hydrothermal vent fields. Lowest Mg fluids sampled in 2010 were added for comparison.

Edifice	Sample	T_{max} [°C] (in situ)	pH_{MIN} (25°C)	pH (in situ)	Mg mM	Na_{Meas} mM	Na_{CB} mM	K mM	Li µM	Rb µM	Cs nM	Ca mM	Sr µM	Ba µM	B µM	Cl mM	Br µM
LOQ		–	–	–	–	–	–	–	7.2	0.003	1.94	–	–	0.04	9.25	–	–
BSW	CTD10-01	0.5	7.7	7.9	51.6	460	463	10.0	25.1	1.26	2.0	9.56	82.6	0.29	399	540	820
E2-West																	
Flange	445-17ROV 03F	53	6.7	6.6	42.6	446	468	13.4	78.4	6.8	63.5	13.2	85.0	1.26	410	543	823
E2- South																	
Iced Bun	446-20ROV 07F	320	3.3	4.8	4.45	412	410	33.0	500	51.0	492	29.9	94.4	37.5	574	515	810
Dog's Head	446-20ROV 10F	344	3.2	5.3	10.5	402	407	28.9	383	42.1	373	23.3	80.5	13.7	480	501	767
E2-South[a]																	
Dog's Head[a]	JC42-132-Y1-07	351	3.1	nd	1.05	434	nd	39.8	614	nd	609	30.8	106	23.6	548	528	837
Sepia[a]	JC42-135-Y2-04	353	3.1	nd	2.04	430	nd	38.1	603	nd	590	31.8	105	15.2	537	528	848
Sepia Flange[a]	JC42-132-B1-02	313	2.9	nd	4.15	420	nd	35.8	557	nd	561	28.9	95.9	19.9	555	521	837

Edifice	Sample	F µM	Si mM	SO_4 mM	Fe µM	Mn µM	Al µM	H_2 µM	H_2S mM	$\delta^{34}S_{H2S}$ ‰	CH_4 µM	$\delta^{13}C_{CH4}$ ‰	$\delta^{2}H_{CH4}$ ‰	CO_2 mm	$\delta^{13}C_{CO2}$ ‰	$\delta^{18}O$ ‰	δD ‰
LOQ		–	–	–	0.9	–	1.85	–	0.0002	–	–	–	–	–	–	–	–
BSW	CTD10-01	72.5	0.104	28.0	0.0	0.0	0.0	0.0	0.0	–	0.0	–	–	2.3[c]	0.3[b]	0[a]	-0.1[a]
E2-West																	
Flange	445-17ROV 03F	61.2	2.12	25.4	12.1	61.8	bdl	0.66	bdl	nd	1.59	bdl	bdl	3.40	-10.8	-0.3	-2.3
E2- South																	
Iced Bun	446-20ROV 07F	47.5	15.0	2.56	570	1301	8.67	59.5	3.3	4.0	48.9	-7.6	-99.9	8.10	-3.7	0.6	-1.2
Dog's Head	446-20ROV 10F	59.4	14.1	6.12	856	1450	8.04	36.0	4.0	6.7	25.6	-7.0	-98.7	10.4	-4.4	0.3	-1.6
E2-South[a]																	
Dog's Head[a]	JC42-132-Y1-07	42.8	17.2	3.7	1387	2075	nd	nd	6.9	nd	nd	nd	nd	nd	nd	1.2	1.8
Sepia[a]	JC42-135-Y2-04	38.8	21.2	1.9	1003	2034	nd	nd	6.8	nd	nd	nd	nd	nd	nd	0.9	-0.2
Sepia Flange[a]	JC42-132-B1-02	40.2	4.06	3.6	748	2095	nd	nd	6.5	nd	nd	nd	nd	nd	nd	0.9	-0.6

mM, mmol/L fluid; µM, µmol/L fluid; nM, nmol/L fluid; mm, mmol/Kg fluid; nd, not determined; bdl, below detection limits; LOQ, Limit of quantification; T_{MAX}, maximum temperature measured; BSW, Bottom seawater; Na_{Meas}, Na measured; Na_{CB}, Na charge balanced (see text).

pH_{MIN} = lowest pH measured at 25°C; pH (in situ) = pH at measured temperature and 250 bar.

a, Data from James et al. (2014); b, data from Craig (1970); c, data from Reeves et al. (2011).

consisted of nine injections of 7 µL each and the result is an average of the last three injections out of nine. The isotope ratios were normalized to VSMOW seawater material. For water isotopes the analytical uncertainties are ∼0.09‰ and ∼0.25‰ for $\delta^{18}O_{H2O}$ and δD_{H2O}, respectively.

Stable carbon and hydrogen isotope ratios ($^{13}C/^{12}C$ and $^{2}H/^{1}H$) of CH_4 and CO_2 were determined using GC-isotope ratio mass spectrometry (GC-IRMS) at MARUM as detailed in Pape et al. (2020a). CH_4 and CO_2 were separated by gas chromatography. Subsequently, CH_4 was either combusted (1,030°C) or pyrolyzed (1,440°C) to generate CO_2 or H_2, respectively. CO_2 or H_2 were then transferred to the IRMS for analysis of $^{13}C/^{12}C$ or $^{2}H/^{1}H$. All gas samples were injected at room temperature by manual syringe injection. Reported isotope ratios are arithmetic means of at least triplicate measurements and are given in the δ-notation relative to Vienna Pee Dee Belemnite (VPDB) and Vienna Standard Mean Ocean Water (VSMOW; for carbon and hydrogen, respectively). Reproducibility was proved using commercial CH_4 and CO_2 standards (Isometric Instruments, Canada; Air Liquide GmbH, Germany). Standard deviations of triplicate stable isotope measurements were <0.5‰ ($\delta^{13}C_{CH4}$). Because CH_4 concentrations were below the calibrated range of the GC-IRMS at the MARUM, samples were re-analysed for $\delta^{13}C_{CH4}$ by GC–IRMS at GEO-data Gesellschaft für Logging-Service mbH, Germany (see Pape et al., 2020b).

Sulphur isotopes ($\delta^{34}S_{H2S}$) were measured using an EA-IRMS (elemental analyser isotope ratio mass spectrometry) using a Flash EA isolink interfaced to a ThermoFisher Scientific Data V Advantage mass spectrometer. Analysis was conducted at the Institute of Geology and Palaeontology at the University of Münster. Results are reported in the δ-notation relative to Vienna Canon Diablo Troilite (VCDT). Reproducibility of the measurement was determined by replicate measurements and was better than ±0.3‰. Analytical performance was monitored using international reference materials IAEA S1, S2, S3 and NBS 127 as well as lab internal standards.

Analytical Methods: Fluid Inclusions

Microthermometry was carried out on anhydrite-hosted fluid inclusions from a chimney sample at the vent orifice of Dog's Head. A Linkam heating/freezing stage in combination with a LNP2 flow regulator and a Zeiss Axioskop was used to observe phase transitions in two-phase liquid-vapour fluid inclusions. The temperature of the heating/freezing stage was calibrated using FLINC® synthetic fluid inclusions hosted in quartz. Phase transitions in the H_2O system (freezing point: 0.0°C, critical temperature: 374.1°C) were used to calibrate the temperature sensor of the Linkam stage. The calibration procedure yielded temperatures of -0.1°C and 373.4°C for the freezing point and critical temperature, respectively. These values agree with the range of 15 long term control measurements of 0.04 ±0.07°C and 373.6 ±0.75 °C and show that the temperature sensor provided accurate and precise temperatures. Both accuracy and precision are within ±0.1°C at temperatures around the freezing point of pure H_2O and are better than ±1°C in the high-temperature regime (>>100°C).

Calculation of Endmember Composition

Sampled hydrothermal vent fluids inadvertently contain a fraction of seawater that was entrained naturally in the subseafloor immediately prior to sampling or accidently during sampling, due to the dead volume of the inlet snorkel. This typically results in a two-component mixture of seawater and hydrothermal fluid. We have used the Mg concentrations in the vent fluid samples at E2-S and E2-W to calculate the chemical composition of hydrothermal endmember solution for all elements by extrapolating to zero Mg.

Endmember temperatures were calculated using isenthalpic-isobaric mixing, by considering a temperature and salinity-dependent heat capacity of the fluid. This dependence of salinity and temperature was calculated using the scheme by Driesner (2007), which calculates the thermodynamic data of H_2O-NaCl fluids using thermodynamic data of pure water (Haar et al., 1985).

Salinities and Entrapment Temperatures (T_e) in Fluid Inclusions

Fluid inclusions in hydrothermal precipitates can be used for tracing salinity and temperature in hydrothermal fluids. When crystals grow from hydrothermal solutions, they tend to incorporate microscopic volumes of the hydrothermal fluid, called fluid inclusions. The study of phase-transitions in these inclusions allows for the reconstruction of physio-chemical conditions in active and fossil hydrothermal systems (Peter and Scott, 1988; Xu, 2000; Baker and Lang, 2001; Bieseler et al., 2018; Diehl et al., 2020a). Measurements of ice-melting temperatures (T_m) and homogenization temperatures (T_{hom}) in two-phased fluid inclusions enable the calculation of salinities and entrapment temperatures (T_e) (Vityk et al., 1994). Both measurements represent the properties of the hydrothermal fluid during crystal growth if the inclusions have not changed in composition or volume since they were incorporated (Roedder, 1984; Bodnar, 2003) they provide key information on temperature and salinity of hydrothermal fluids during crystal growth. Fluid inclusions in anhydrite are known to re-equilibrate easily and may increase in volume (stretching) during the microthermometric measurement itself. We used the procedure proposed by Vanko and Bach (2005) to avoid inclusions being affected by stretching.

Using thermodynamic relationships in the H_2O-NaCl system, salinities were calculated from ice-melting temperatures (T_m) while entrapment temperatures (T_e) were calculated from the homogenization temperatures (T_{hom}) and salinities using empirical relationships (Vityk et al., 1994; Atkinson, 2002). The uncertainties in the determination of these two parameters is based on the uncertainty of the temperature determination during the microthermometric work. The accuracy and precision are ±0.1°C and ±1°C for the freezing point and the homogenization temperature (T_{hom}) determinations, respectively, and result in maximum uncertainties of <±0.2 wt.% NaCl eq. and <±2°C for entrapment temperatures (T_e). The pressure correction for entrapment at seafloor conditions (250 bar) corresponds to a 15-17°C adjustment.

Thermodynamic Modelling

The use of IGTs facilitated the measurement of concentrations of gases dissolved in the fluids, and hence the reconstruction of *in-situ* pH and redox, which are key parameters controlling speciation of elements and solubility of minerals in the hydrothermal fluids prior to venting. The H_2 and H_2S concentration data were plotted in activity-activity plots, constructed using the R based software package CHNOSZ (Dick, 2019). We assumed unity activity coefficients for both gases.

Sub-surface processes in hydrothermal systems can be examined using thermodynamic reaction-path models. Reaction-path models were constructed using the Geochemists Workbench™ (GWB) software package and a tailor-made 400 bar database assembled by SUPCRT92 (Johnson et al., 1992). For these models, measured bottom seawater (BSW) was heated to hydrothermal temperatures while allowing minerals to precipitate. Using the REACT module of GWB, the heated fluid was then allowed to react with the host rock till the fluid became rock-buffered i.e., attained quartz saturation. Host rock data for samples taken in close vicinity to the vent sites (Sample ID: WX.30, 29, 28, 27, 2 & 1) were utilized from Leat et al. (2000). All major elements were considered for the reaction path models (except P). Ba, Cu and Zn concentrations were formally recalculated and added to the system as barite, chalcopyrite, and sphalerite.

Catabolic energy landscape computations were carried out as described in Amend et al. (2011). The REACT module of GWB was used along with a 250 bar database assembled using SUPCRT92 (Johnson et al., 1992) to simulate mixing of cold BSW with hot hydrothermal fluid represented by the Iced Bun site endmember composition. Minerals were not allowed to precipitate during mixing and redox reactions were also suppressed. Acid-base reactions were allowed to equilibrate. For this model 8 catabolic reactions were considered (**Table 2**). Five of the reactions represented aerobic respirations using different inorganic electron donors and three denoted anaerobic respiration.

Values of Gibbs energy (ΔG_r) for catabolic reactions were computed using the relation:

$$\Delta_r G = \Delta_r G^o + RT \ lnQ_r$$

where $\Delta_r G^o$ denotes the standard Gibbs energy of reaction, R and T represent the gas constant and temperature in Kelvin, respectively, and Q_r stands for the activity product of reaction r, which is evaluated with the relation.

$$Q_r = \prod a_i^{v_{i,r}}$$

where a_i denotes the activity of species i raised to the stoichiometric reaction coefficient $v_{i,r}$. The B-dot equation was used to calculate activity coefficients needed to convert species concentrations to activities. The Q-term accounts for the chemical composition of the mixed hydrothermal fluid, it also accounts for intracellular concentrations for building blocks of cells. Values of $\Delta_r G^o$ were calculated at 250 bar and the temperatures of interest with the computer code SUPCRT92 (Johnson et al., 1992), which relies on the relation of

$$\Delta_r G^o = \sum v_{i,r} \Delta_a G_i^o$$

where $\Delta_a G_i^o$ represents the apparent standard Gibbs energy of formation of the i^{th} species in reaction r.

For catabolic reactions the amount of energy available was then calculated as a function of either temperature or mixing ratios. This was done by multiplying the calculated Gibbs energy for the reaction at each temperature with the concentrations of reactants (in the mixed fluid). The stoichiometry of the reaction and the reactant present in limiting supply were taken into account and then multiplied with the amount of mixed fluid at that specific temperature (McCollom, 2007; Amend et al., 2011).

TABLE 2 | Inorganic redox reactions.

Aerobic sulphide oxidation (ASO)	$H_2S + 2O_2 \rightarrow SO_4^{2-} + 2H^+$ (1)
Aerobic methane oxidation (AMO)	$CH_4 + 2O_2 \rightarrow CO_2 + 2H_2O$ (2)
Aerobic iron oxidation (AFeO)	$4Fe^{2+} + O_2 + 10H_2O \rightarrow 4Fe(OH)_3 + 8H^+$ (3)
Aerobic manganese oxidation (AMnO)	$6Mn^{2+} + O_2 + 10H_2O \rightarrow 6MnO_2 + 20H^+$ (4)
Aerobic hydrogen oxidation (AHO)	$2H_2 + O_2 \rightarrow 2H_2O$ (5)
Hydrogenotrophic sulphate reduction	$4H_2 + SO_4^{2-} + 2H^+ \rightarrow H_2S + 4H_2O$ (6)
Hydrogenotrophic methanogenesis	$4H_2 + CO_2 \rightarrow CH_4 + 2H_2O$ (7)
Anaerobic oxidation of methane (AOM)	$CH_4 + SO_4^{2-} + 2H^+ \rightarrow CO_2 + H_2S + 2H_2O$ (8)

All compounds represent aqueous species. $Fe(OH)_3$ represents ferrihydrite.

RESULTS

Temperature, pH, and Mg Contents

Focused venting of black smoker-type fluids at Dog's Head and Iced Bun in the E2-S area took place at maximum temperatures of 344°C and 320°C, respectively (**Table 1**). The fluids have a measured $pH_{(25°C,\ 1bar)}$ of 3.3 at Iced Bun and 3.2 at Dog's Head. Calculated $pH_{(in\text{-}situ)}$ values for these fluids were 4.8 for Iced Bun and 5.3 for Dog's Head (**Table 1**). Isenthalpic-isobaric mixing models indicate endmember temperatures of 386°C and 342°C for Dog's Head and Iced Bun, respectively (**Supplementary Figure 1**). These temperatures are accurate if all the Mg measured was contributed from entrainment of ambient seawater upon sampling.

The fluid at E2-W was characterized by a maximum measured temperature of 53°C (**Table 1**) and a relatively high Mg concentration (42.6 mM). An isenthalpic-isobaric mixing model indicates an endmember temperature of 273°C (**Supplementary Figure 1**). The fluid had a $pH_{(25°C)}$ of 6.7 and a $pH_{(in\text{-}situ)}$ of 6.6 (**Table 1**).

Dissolved Gases

The dissolved gases investigated in the fluids at E2-S (H_2, H_2S, CO_2 and CH_4) show variable concentrations and isotopic compositions (**Table 1**). The fluids at Dog's Head and Iced Bun have endmember H_2 concentration of 45.2 and 65.1 μM, respectively (**Figure 4A**). Endmember concentrations of CO_2 are 8.65 and 12.5 mM, respectively. CH_4 concentrations are 32.0 μM

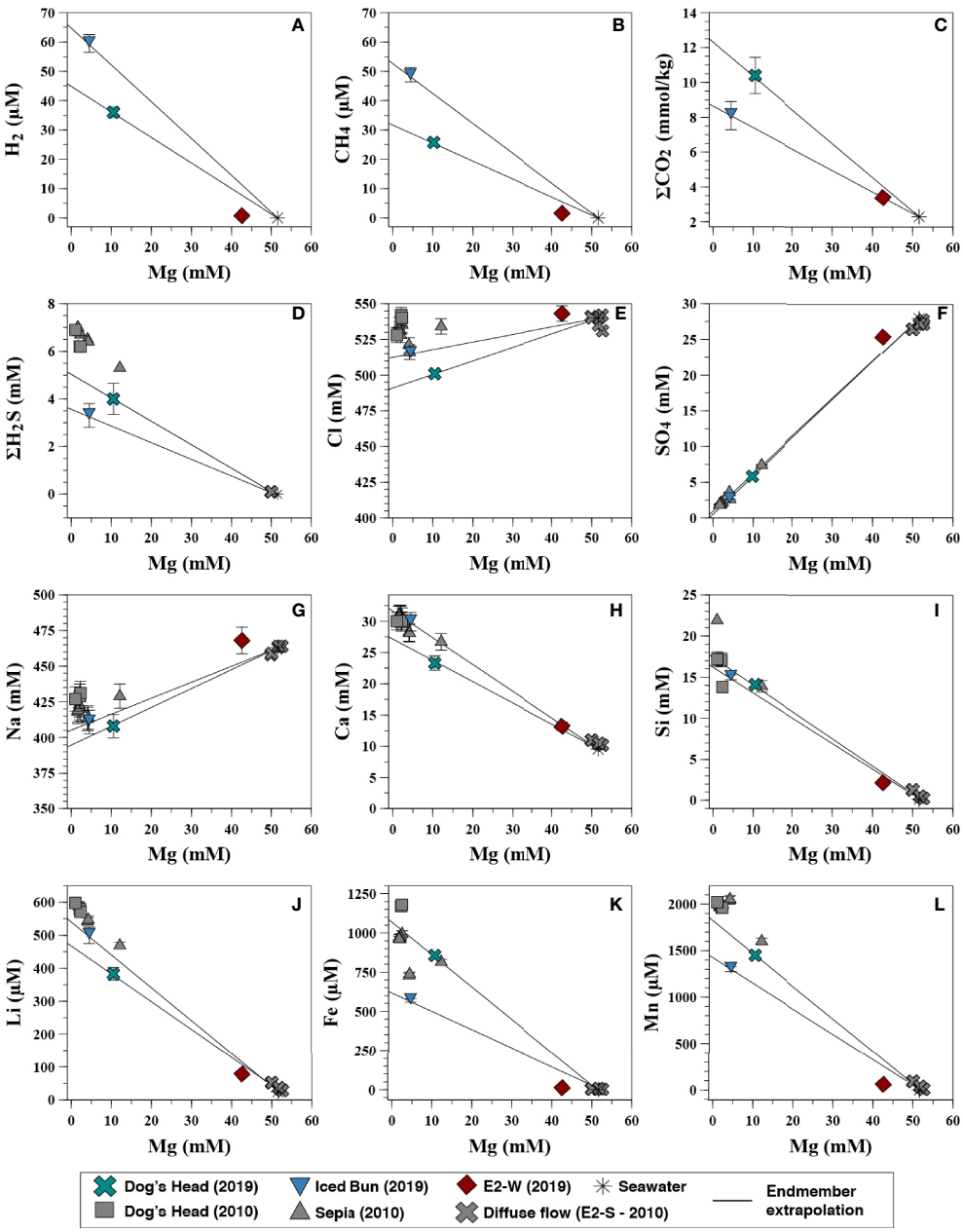

FIGURE 4 | Concentrations of dissolved volatiles, major and minor elements in the fluids recovered from E2 in 2019 (coloured) v/s Mg concentrations of the hydrothermal fluids. Concentrations of fluids sampled in 2010 by James et al. (2014) (Grey) are shown for comparison. The solid lines indicate linear regression to endmember composition. The analytical error bars are shown or are smaller than the symbols. **(A)** H_2 vs Mg, **(B)** CH_4 vs Mg, **(C)** CO_2 vs Mg, **(D)** H_2S vs Mg, **(E)** Cl vs Mg, **(F)** SO_4 vs Mg, **(G)** Na vs Mg, **(H)** Ca vs Mg, **(I)** Si vs Mg, **(J)** Li vs Mg, **(K)** Fe vs Mg, **(L)** Mn vs Mg.

at Dog's Head and 53.5 µM at Iced Bun (**Figures 4B, C**). The endmember fluids at E2-S have $\delta^{13}C_{CO2}$ values of -4.1 and -5.6‰ (**Table 3A**) and $\delta^{13}C_{CH4}$ values of -7.0 and -7.6‰. H_2S concentrations in the endmember fluids are 3.3 and 4.0 mM (**Figure 4D**) and $\delta^{34}S_{H2S}$ values are between +4.0 and +6.7‰.

The endmember concentrations for H_2 and CH_4 at E2-W were 3.75 and 9.03 µM, respectively (**Figures 4A, B**). The H_2S concentration in this fluid was below the detection limit (<0.2 µM). The CO_2 endmember concentration is 8.55 mM (**Figure 4C**). These concentrations of dissolved gases at E2-W are lower than that at E2-S. The $\delta^{13}C_{CO2}$ value of -10.8‰ is lower than for the fluid at E2-S. Endmember values were not calculated for $\delta^{13}C_{CO2}$ due to processes affecting the CO_2 concentrations of the fluid in the mixing zone (cf. Formation of fluid at E2-West).

Other Dissolved Species

The high-temperature fluid feeding E2-S is depleted in Cl by ∼9% relative to seawater with the lowest Cl endmember measuring 491 mM (**Figure 4E**). Sulphate is depleted in the Iced Bun and Dog's Head fluids with endmember concentration of ≤1 mM (**Figure 4F**). The Na_{CB} (Na calculated based on charge balance of the endmember) endmember concentration is depleted by ∼10% relative to seawater (**Figure 4G**). Endmember Ca concentrations in the fluids are 31.8 and 26.8 mM (**Figure 4H**). Endmember Br and F is depleted relative to seawater with 809 – 754 µM and 47.5 - 59.4 µM, respectively (**Table 3A**). Endmember Sr concentrations show both, depletion and enrichment relative to seawater at Dog's Head and Iced Bun, respectively (**Table 3A**). The endmember concentrations of alkali metals K, Li, Rb and Cs (33.7 – 35.1 mM, 383 – 545 µM, 52.6 – 55.7µM, 468 – 538 nM) are higher than those of seawater (**Table 3A**).

Fluids sampled at E2-W have seawater-like concentrations of Na, Cl and Br. Endmember concentrations of K, Ca and Li are 29.3 mM, 30.2 mM and 328 µM, respectively, and are like endmember E2-S concentrations. However, SO_4, F and Si have endmember concentrations of 13 mM, 8.36 µM and 11.5 mM, respectively. These concentrations are markedly different from the endmember concentrations of the E2-S fluids.

The K/Cl, Sr/Cl, Li/Cl, Cs/Cl, Rb/Cl and Br/Cl are elevated in the fluids venting at E2-S and E2-W, except for Br/Cl at E2-W, which is seawater-like (**Table 4**). F/Cl ratios in all fluids are lower than in seawater. The E2-S element-to-Cl ratios measured in this study show deviations to those reported by James et al. (2014) (**Table 4**). Dog's Head fluids have lower Ca/Cl, K/Cl, Sr/Cl, Li/Cl, Cs/Cl and Br/Cl ratios than those sampled in 2010, whereas Na_{CB}/Cl ratios are slightly higher compared to the 2010 ratios.

E2-S endmember fluids are characterized by concentrations of Fe and Mn of 624 – 1074 µM and 1424 – 1821 µM, respectively. The metal concentrations in the endmember fluids from E2-S are lower than in the endmembers calculated from the 2010 samples (**Figures 4K, L**). E2-W has an endmember Fe and Mn concentrations of 69.0 and 351 µM (**Table 3A**; **Figures 4K, L**).

The total endmember REE (ΣREE) concentrations in the fluids from E2-S are 27 nmol/kg and 29 nmol/kg at Iced Bun and Dog's Head, respectively (**Table 3B**). Chondrite-normalized REE_N distribution pattern shows the characteristic light REE (La-Nd) enrichment and a positive Eu anomaly (Douville et al., 1999; Douville et al., 2002; Craddock et al., 2010, **Figure 5**).

Stable Oxygen and Hydrogen Isotopes

The $\delta^{18}O_{H2O}$ endmember value of +0.4 and +0.6‰ for fluids from E2-S are ^{18}O-enriched compared to the endmember ratio for the fluid sample at E2-W (-1.7‰, **Table 3A**). The δD_{H2O} values for all fluids are lower than seawater, with the lowest values in the fluid at E2-W (-2.3‰). The endmember δD_{H2O} and $\delta^{18}O_{H2O}$ values recorded in this study are lower than those of the fluids sampled in 2010 (**Table 3A**).

Fluid Inclusions

Microthermometry of 26 fluid inclusions was conducted in anhydrite precipitates from a chimney sample of Dog's Head (**Supplementary Table 1**). Two fluid inclusion types were identified during the investigation: Inclusion *Type I* is single phased and was not analysed. Inclusion *Type II* contains two-phases, with vapour-liquid inclusions and can be subdivided into *Type IIa* (<50 vol.% vapour) and *Type IIb* (≥50 vol.% vapour). *Type IIa* is the dominant inclusion type with 22 out of 26 measured inclusions. The remaining of 4 inclusions is classified as *Type IIb*. All *Type II* inclusions exclusively homogenize into the liquid phase suggesting a similar origin. T_m (ice-melting temperature) in individual inclusions ranged from -1.6 to -2.1°C. The corresponding calculated salinities range between 2.7 wt.% NaCl eq. (minimum) and 3.6 wt.% NaCl eq. (maximum). The average T_m of -1.8°C corresponds to a mean salinity of 3.1 wt.% NaCl eq., just slightly below seawater, for all inclusions. Calculated salinities (mean) for different inclusion types (*Type IIa* and *Type IIb*) are 3.1 and 3.2 wt.% NaCl eq. According to measured salinities, the inclusions can be grouped into two populations (**Supplementary Figure 3A**): 9 inclusions were determined to contain fluids with salinities significantly below seawater (<3.0 wt.% NaCl eq.) and 22 inclusions contained fluids with near-seawater salinities (3.0-3.6).

T_{hom} were determined between 211°C and 316°C (**Supplementary Figures 3B, C**). The calculated T_e range between 226-333°C with 9 of 22 T_e determinations above 300°C. The highest T_e was determined as 333°C, just 11°C lower than the measured temperature of 344°C during fluid sampling. Both these temperatures are significantly below the boiling temperature of 386°C at seafloor pressure.

DISCUSSION

The high-temperature fluids at E2-S have low Mg and SO_4 concentrations typical for black smoker type vent fluids. They are enriched in dissolved gases (CO_2, H_2, CH_4 and H_2S) and are depleted in Cl relative to seawater values. The fluids are enriched in alkalis, alkaline earth and transition metals as a result of high-temperature fluid-rock interactions in the sub-surface. Furthermore, the fluids have high Na/Cl and low Ca/Cl ratios and lower concentrations of Li, Rb, and REEs than the fluids sampled in 2010 (Cole et al., 2014; James et al., 2014). The low-temperature fluid sampled at E2-W have lower concentrations of dissolved gases, alkalis, alkaline earth, and transition metals than the fluid at E2-S. The high Mg and SO_4 contents of E2-W fluid indicates sub-surface mixing with entrained seawater.

In the following discussion we present evidence for the temporal variation of the E2 vent field, provide evidence for a single sourced fluid feeding the E2 system and imply the depth of the root zone as well as phase separation processes. We discuss the origin of dissolved gases at E2 by magmatic degassing and constrain sinks for the gases both in terms of abiotic and biotic processes taking place in the sub-surface. Important catabolic

TABLE 3A | Endmember concentrations and isotopic compositions of aqueous species from fluids recovered from E2-South and E2-West hydrothermal vent fields.

Edifice	T_{max} [°C]	T_{calc} (C)	pH_{MIN} (25°C)	Na_{Meas} mM	Na_{CB} mM	K mM	Li µM	Rb µM	Cs nM	Ca mM	Sr µM	Cl mM	Br µM	F µM	Si mM	SO_4 mM	Fe µM	Mn µM	Al µM	H_2 µM	H_2S mM	CH_4 µM	CO_2 mm	$\delta^{13}C_{CO2}$ ‰	$\delta^{18}O$ ‰	δD ‰
BSW	0.5	–	7.7	460	463	10.0	25.1	1.26	2.0	9.56	82.6	540	820	72.5	0	28	0	0	0	0	0	0	2.3[c]	0.3[b]	0.0[a]	-0.1[a]
E2-West																										
Flange	53	273	6.7	nd	nd	29.3	328	32.5	351	30.2	96.1	nd	nd	8.36	11.5	13	69.0	351	–	3.75	0	9.03	8.55	nd	-1.7	-12.5
E2- South																										
Iced Bun	320	342	3.3	406	418	35.1	545	55.7	538	31.8	95.5	513	809	47.5	16.4	0	624	1424	9.50	65.1	3.61	53.5	8.65	-4.1	0.6	-1.2
Dog's Head	344	386	3.2	394	413	33.7	474	52.6	468	26.8	79.9	491	754	59.4	17.2	1	1074	1821	10.1	45.2	5.02	32.07	12.5	-5.6	0.4	-2.0
E2-South[a]																										
Dog's Head[a]	351	nd	3.0	435	nd	40.3	618	nd	618	31.5	105	536	842	39.1	17.7	0	1315	2106	nd	nd	6.7	nd	nd	nd	1.1	1.5
Sepia[a]	353	nd	3.1	426	nd	39.1	623	nd	623	32.5	105	532	838	38.4	22.6	0	1038	2116	nd	nd	7.6	nd	nd	nd	1.1	1.4
Sepia Flange[a]	313	nd	2.9	416	nd	38.0	604	nd	604	30.5	96.1	517	838	39.8	22.6	0	816	2280	nd	nd	7.1	nd	nd	nd	1.0	-0.8

TABLE 3B | Rare-earth element concentrations of the fluids from E2-S and E2-W hydrothermal vent fields.

Edifice	T_{max} [°C] (In situ)	Mg mM	La nM	Ce nM	Pr nM	Nd nM	Sm nM	Eu nM	Gd nM	Tb nM	Dy nM	Ho nM	Er nM	Tm nM	Yb nM	Lu nM	ΣREE nM
LOQ	-	-	0.0035	0.0013	0.0004	0.0036	0.0050	0.0002	0.0005	0.0004	0.0007	0.0005	0.0004	0.0001	0.0003	0.0002	-
BSW*100[d]	0	54.3	4.2	0.62	0.63	2.7	0.5	0.12	0.68	0.1	0.77	0.21	0.72	0.1	0.7	0.14	–
E2-West																	
Flange	53	42.6	bdl	bdl	bdl	bdl	0.68	0.41	bdl	bdl	bdl	bdl	0.05	nd	0.04	bdl	1.2
E2- South																	
Iced Bun	320	4.45	7.05	9.56	1.07	3.99	0.87	1.46	0.67	0.1	0.41	0.09	0.24	nd	0.2	0.03	26
		E.M	7.71	10.46	1.17	4.36	0.95	1.60	0.73	0.11	0.45	0.10	0.26	nd	0.22	0.03	27
Dog's Head	344	10.5	5.71	9.22	0.88	2.89	0.63	2.39	0.57	0.07	0.33	0.05	0.14	nd	0.10	0.01	23
		E.M	7.16	11.57	1.10	3.62	0.78	3.00	0.71	0.09	0.41	0.07	0.18	nd	0.12	0.02	29
E2-South[d]																	
Dog's Head[d]	351	1.02	6.28	11.6	1.36	5.26	1.06	1.27	1.61	0.19	0.56	0.09	0.21	0.02	0.13	0.01	30
	323	2.11	8.67	16	2	8.12	1.8	2.29	1.8	0.2	0.95	0.15	0.32	0.03	0.17	0.02	42
	323	2.28	8.06	17.4	2.2	9.14	2.06	1.88	1.9	0.23	1.1	0.17	0.37	0.03	0.19	0.02	45
		E.M	7.92	15.5	1.9	7.75	1.7	1.87	1.61	0.19	0.9	0.14	0.31	0.03	0.17	0.02	40
Sepia[d]	347	1.61	6.58	11.9	1.34	5.1	0.97	1.21	0.98	0.11	0.53	0.08	0.2	0.02	0.11	0.015	29
		E.M	6.8	12.2	1.38	5.25	1.01	1.25	0.98	0.11	0.55	0.09	0.2	0.02	0.12	0.01	30

mM, mmol/L fluid; µM, µmol/L fluid; nM, nmol/L fluid; mm, mmol/Kg fluid; nd, not determined; bdl, below detection limits; LOQ, Limit of quantification; T_{MAX}, maximum temperature measured; BSW, Bottom seawater; Na_{Meas}, Na measured; Na_{CB}, Na charge balanced (see text).

pH_{MIN} = lowest pH measured at 25°C and 1 atm; pH (in situ) = pH at measured temperature and 400 bar.

a, Data from James et al. (2014); b, data from Craig (1970); c, data from Reeves et al. (2011); d, data from Cole et al. (2014).

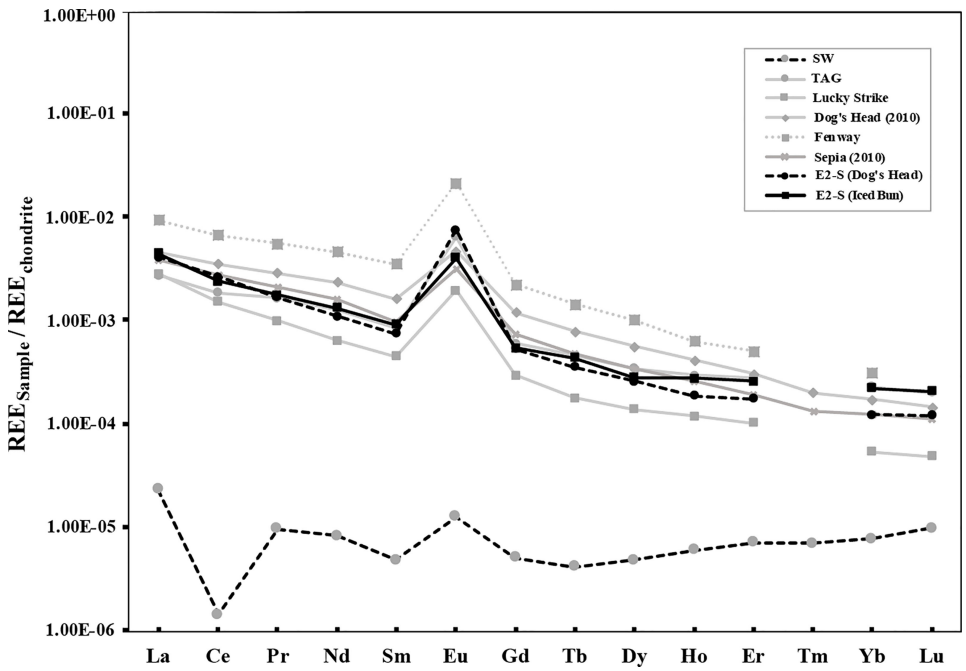

FIGURE 5 | Chondrite normalized REE pattern for endmember fluids from East Scotia ridge (Dog's Head and Iced Bun) compared with endmember fluids from other mid-oceanic ridge systems and back-arc basins that show similar patterns. The data represented here is from Douville et al. (1999) (TAG and Lucky Strike), Cole et al. (2014) (Dog's Head, Sepia), Craddock et al. (2010) (Fenway). The seawater (SW) values are taken from Cole et al. (2014).

reactions responsible for supporting the chemosynthetic ecosystem at E2 are also discussed.

Fluid Mineral Equilibria

Chloride is the dominant anion in hydrothermal fluids, it ranges in concentration due to phase separation and plays a key role in complexing dissolved metals. Hydrothermal vent fluids commonly show a tight correlation between the concentrations of cations and chloride. Metal concentrations in vent fluids can therefore be normalized to Cl for a comparison of fluids affected by different degrees of phase separation. It is known that partitioning of cations in the low-salinity fluid and the brine phase is not uniform during supercritical phase separation. Thus Cl normalization allows a better understanding of the dissolved species (**Table 4**, Berndt and Seyfried, 1990; Foustoukos and Seyfried, 2007a). Na/Cl and Ca/Cl ratios at E2-S are in the range for unsedimented mafic-hosted hydrothermal systems (Gallant and Von Damm, 2006; McDermott et al., 2018; Diehl and Bach, 2020b; Diehl and Bach, 2021). E2-W has a seawater like Na/Cl and Ca/Cl ratios, which are a result of excessive mixing of hydrothermal fluid with seawater. Theoretical studies and laboratory experiments have shown that thermodynamic equilibrium between plagioclase and epidote solid solutions in basalt hosted hydrothermal systems control the Na and Ca concentrations of the fluids (Berndt et al., 1989; Seyfried et al., 1991; Berndt and Seyfried, 1993; Seyfried and Ding, 1995). Higher temperature conditions favour the stability of anorthite, clinozoisite of the plagioclase and epidote solid solutions respectively, due to the following reactions:

$$\underset{\text{Albite}}{2\,NaAlSi_3O_{8(s)}} = \underset{\text{Anorthite}}{CaAl_2Si_2O_{8(s)}} + 2Na^+ + 4SiO_{2(aq)} \quad (9)$$

$$Ca^{2+} + \underset{\text{Anorthite}}{3\,CaAl_2Si_2O_{8(s)}} + 2H_2O_{(l)} = \underset{\text{Clinozoisite}}{2\,Ca_2Al_3Si_3O_{12}(OH)_{(s)}} + 2H^+ \quad (10)$$

These reactions result in Ca fixation and decrease in Ca/Cl ratios in hydrothermal systems. The Na/Cl ratios are lower and the Ca/Cl ratios are higher than seawater, indicating that albitization and Ca-release occur in the root zone of E2-S. However, in 2019 the fluids at Dog's Head had higher Na/Cl and lower Ca/Cl ratios than in 2010 (**Table 4**). This may indicate a subtle switch to less albitization and more Ca fixation. Likewise, the Li/Cl and Cs/Cl ratios were noticeably lower in 2019 than in 2010. These ratios are proxies for water/rock mass ratios (w/r). Field and experimental data have shown that alkalis are highly fluid mobile and get leached from basalt during fluid-rock interactions at high temperatures (Mottl and Holland, 1978; Seyfried et al., 1984; Von Damm et al., 1985a; Von Damm, 1990). The high mobility results in higher concentrations of dissolved alkalis in the fluids that have interacted with large masses of rock (**Table 3A**). Assuming that Li, Rb and Cs are fully leached from the rocks in the root zone w/r ratios can be calculated (e.g., Von Damm et al., 1985a). The glassy lava from the E2 segment contains ca. 0.15 ppm of Cs, ca. 8 ppm of Rb (Leat et al., 2000). Basaltic andesites commonly contain ca. 8 ppm of Li (Ryan and Langmuir, 1987). Using endmember compositions for

TABLE 4 | Molar element/Cl ratios for fluids from ESR. E2-West ratios are calculated from measured concentrations, while E2-S are calculated from EM values.

Edifice	Na_{CB}/Cl	Ca/Cl	K/Cl	Sr/Cl x10^{-3}	Li/Cl x10^{-3}	Rb/Cl x 10^{-3}	Cs/Cl x10^{-3}	Br/Cl x10^{-3}	F/Cl x10^{-3}	Fe/Cl x10^{-3}	Mn/Cl x10^{-3}	Fe/Mn	Sr/Cl x10^{-3}
BSW	0.86	0.02	0.02	0.15	0.05	0.002	0.004	1.52	0.13	0.00	0.00	–	8.64
E2- West													
Flange	0.86	0.02	0.03	0.16	0.14	0.01	0.12	1.52	0.11	0.02	0.11	0.20	6.44
E2- South													
Iced Bun	0.82	0.06	0.07	0.19	1.06	0.11	1.05	1.58	0.09	1.22	2.78	0.44	3.00
Dog's Head	0.84	0.05	0.07	0.16	0.97	0.11	0.95	1.54	0.11	2.19	3.71	0.59	2.98
E2- South[a]													
Dog's Head[a]	0.80	0.06	0.07	0.19	1.12	nd	1.13	1.57	0.07	2.40	3.80	0.62	3.33
Sepia[a]	0.79	0.06	0.07	0.19	1.14	nd	1.12	1.58	0.07	1.90	3.90	0.49	3.24
Sepia Flange[a]	0.79	0.06	0.07	0.18	1.14	nd	1.15	1.62	0.08	1.50	4.30	0.36	3.14

BSW, bottom seawater; Na_{CB}, Na charge balanced (see text).
a = Data from James et al. (2014).

Li, Rb and Cs at E2-S and assuming 100% extraction of the elements the w/r ratios were ca. 2 for Cs and ca. 2 for Rb at both Iced Bun and Dog's head. The w/r ratios of ca. 2 for Iced Bun and ca. 3 for Dog's Head were calculated using Li. Moreover, the ratios in this study are higher compared to that calculated in 2010 (ca. 1.9) because of lower alkali abundances in these fluids.

Dog's Head and Iced Bun have very similar vent fluid compositions in terms of Na/Cl, K/Cl, Br/Cl, Si and predicted w/r ratios, indicating that the high-temperature fluids venting at E2-S are fed by a common root zone. Likewise, back in 2010, Dog's Head and Sepia had identical Na/Cl, K/Cl, Ca/Cl, Li/Cl and Cs/Cl which also points to a single sourced fluid at E2-S. We next discuss how the composition of the Dog's Head fluids has evolved between 2010 and 2019 and how this variation may indicate changes in the common root zone of the E2-S vents.

Temporal Variability of the E2 Vent Field

Continuous alteration of fresh rock over time can result in the loss of elements from the rock, thereby reducing the amount of fresh rock available for w/r interactions (high Na/Cl ratios). This results in higher w/r ratios and decrease in concentration of mobile elements. Higher Na/Cl ratios coupled with higher w/r ratios in 2019 as compared to 2010 provide evidence that the root zone at E2-S has undergone effective alteration over the duration of the past 9 years. Furthermore, the fluids sampled in 2019 have low δD_{H2O} and $\delta^{18}O_{H2O}$ compared to the fluids sampled in 2010 (**Table 3A**). While the low δD_{H2O} at E2 may be related to magmatic water input, the low $\delta^{18}O_{H2O}$ cannot be explained by this process (cf. Magmatic water input). The fluid sampled at Dog's Head in 2010 had an endmember $\delta^{18}O_{H2O}$ value of 1.1‰ while the fluid from 2019 has a lower value of 0.4‰. Hydrothermal alteration of the igneous crust by circulating seawater-derived fluids at high temperature will have the $\delta^{18}O_{H2O}$ values of the altered rocks decrease with time (Shanks, 2001 and references therein). The lower $\delta^{18}O_{H2O}$ values of the 2019 vent fluid may indicate that the rocks in the root zone are more altered, which is consistent with the higher w/r ratios derived from the decreased concentration of fluid mobile elements (Rb, Li).

Experimental work has shown that REE concentrations are also affected by the intensity of hydrothermal alteration: the REE concentrations decrease and the positive Eu anomaly becomes more pronounced as the extent of hydrothermal alteration of mafic rocks increase (Beermann et al., 2017). REE_{CN} (chondrite normalised) pattern observed in the fluids from E2-S are typical for mature mafic hosted hydrothermal systems (**Figure 5**). ΣREE measured in this study is lower than 2010 (Cole et al., 2014). This decrease in total REE content would be consistent with an increased extent of rock alteration in the root zone. However, REE solubility in hydrothermal fluids is also controlled by temperature, pH and redox conditions during high-temperature fluid-rock interactions (Craddock et al., 2010). A lower temperature in the root zone could therefore also explain the observed drop in ΣREE.

Our fluid inclusion study provides insights into the temporal evolution of salinity and phase separation processes taking place at E2. The fluid inclusion data at E2-S show that the fluids salinity was either slightly lower than or close to that of seawater (**Supplementary Figure 3C**). Although the time of entrapment of these inclusions was not determined, the low salinity in most of the inclusions in the young top of the chimney sample provide evidence for low Cl venting fluid at E2 during the past years. In addition to the low Cl concentrations measured in the fluids in 2019 and 2010, the fluid inclusion salinities indicate that phase separation has been affecting fluid compositions at E2-S for a prolonged period, despite the apparent changes in the extent of alteration in the root zone.

In summary, the root zone of E2-S may have changed slightly towards a more altered basement and slightly lower temperatures, but it appears that the process of phase separation (supercritical) taking place at E2 is constant and has not changed significantly.

Depth of the Root Zone

The concentration of dissolved Si in hydrothermal vent fluids can be used to estimate the depth (pressure) and temperature in the hydrothermal root zone (Bischoff and Rosenbauer, 1985; Von Damm et al., 1991; Foustoukos and Seyfried, 2007c). This thermobarometer is calibrated for quartz which is commonly present in hydrothermally altered mafic rocks. Since quartz solubility is a function of temperature and pressure, either one can be estimated if the other one is known. Using this relation,

sub-surface conditions of fluid-quartz equilibration at E2-S was calculated (**Figure 6**). With the calculated endmember Si concentrations and the measured temperature at E2-S, the equilibrium pressure was calculated at ∼300 bar and ∼500 bar at Dog's Head and Iced Bun, respectively. Silica concentrations at Dog's Head in this study is slightly lower than in 2010. Silica concentration in the Sepia fluids was high (22.3 mM, James et al., 2014), corresponding to unreasonably high 800-900 bar pressure. James et al. (2014) argued that the root zone temperatures at 'Sepia' were probably higher than the measured 353°C and that cooling (but no quartz precipitation) in the upflow zone gave rise to the high apparent pressures. The low pressures (300- 350 bar in 2019) obtained for Dog's Head may indicate that quartz did precipitate. At Iced Bun, the estimated depth of quartz equilibria is 500 bar. It is highly unlikely that the depth of the hydrothermal root zone for vent orifices that are in such proximity [ca. 60 m of each other, Tyler, (2012)] have such a huge variability. More plausibly, the estimated pressures are an artefact of conductive cooling (James et al., 2014). When conductive cooling takes place, silica precipitation may or may not take place. The shallow pressures obtained for Dog's Head indicate some quartz precipitation in the upflow zone. In contrast, the high silica concentrations in the Sepia vent fluids in 2010 (James et al., 2014) indicate that quartz did not precipitate upon cooling. The effect of conductive cooling and quartz precipitation kinetics on the Si concentrations of the fluids makes it difficult to obtain a realistic depth of the reaction zone from quartz equilibrium pressures at E2-S.

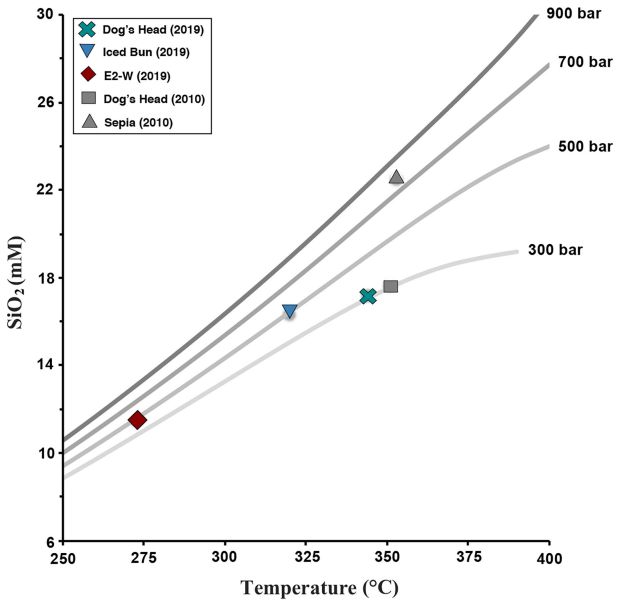

FIGURE 6 | Endmember aqueous SiO_2 concentrations plotted against Tmax of the vent fluids at E2-S and zero Mg extrapolated temperature for E2-W. The colored symbols represent the samples analysed in this study compared with the samples measured in 2010 (grey). The quartz saturation curves were taken from Foustoukos and Seyfried (2007c) and are represented as a function of pressure from 300 to 900 bar and temperatures.

Phase Separation

The high-temperature fluids venting at E2-S have a Cl concentration that is significantly lower than that of seawater. The lowest endmember concentration was 491 mM (**Figure 4E**). No major Cl sink is known to exist in mafic-hosted hydrothermal systems and therefore Cl depletions observed in such systems are typically attributed to phase separation (Von Damm, 1990; Von Damm, 1995; Foustoukos and Seyfried, 2007b). Seafloor pressure of ∼260 bar places the two-phase boundary at 386°C (**Supplementary Figure 2**; Driesner and Heinrich 2007), while the critical point of seawater is 407°C at 298 bars (Bischoff, 1991). Our investigation shows that the observed variability in salinities and temperatures in hydrothermal fluid samples and fluid inclusions cannot be produced by subcritical phase separation (**Supplementary Figure 3**). The Cl concentrations lower than seawater in the hydrothermal fluids at E2-S are therefore likely a result of phase separation at supercritical conditions. Subcritically phase separated fluids would produce mixing lines with considerably lower Cl concentrations when mixing with cold seawater. The temperature-salinity plane observed for fluid samples and inclusion data is characteristic for fluids produced by phase separation at pressures of at least over 300 bar. Elevated Br/Cl ratios at E2-S relative to seawater corroborate the idea of phase separation under supercritical conditions (cf. McDermott et al., 2018). Laboratory experiments have shown that Br partitions preferentially into the low salinity phase under supercritical conditions, resulting in increased Br/Cl ratios (Berndt and Seyfried, 1990; Foustoukos and Seyfried, 2007a). Using the Cl normalized partition coefficients and the following formula:

$$D_{\frac{Br}{Cl}} = \frac{\left(\frac{M_{Br}}{M_{Cl}}\right)_v}{\left(\frac{M_{Br}}{M_{Cl}}\right)_b} \quad (11)$$

where $(\frac{M_{br}}{M_{Cl}})_v$ and $(\frac{M_{br}}{M_{Cl}})_b$ represents the molal concentration of Br/Cl in the low salinity and high salinity phase, respectively (Berndt and Seyfried, 1990; Foustoukos and Seyfried, 2007a). It is known that vapour-brine partition coefficients for Br increases with decreasing fluid density and can be related with the following expression:

$$log\ D_{Br/Cl} = -13.04 - 54.95\ (log\rho_w) - 76.93\ (log\rho_w)^2 - 36.09(\log \rho_w)^3 \quad (12)$$

where p_w = *density of pure seawater* (Foustoukos and Seyfried, 2007a).

Endmember Br/Cl ratios at E2-S are 1.54 and 1.58 (**Table 4**), which are higher relative to seawater value of 1.52. These Br/Cl ratios give values of $D_{Br/Cl}$ of 1.01 and 1.04. Values of D >1 is known to be a result from the formation of a low salinity phase (Foustoukos and Seyfried, 2007a). Moreover, the calculated D values correspond to densities of ∼0.25 g/ml for the fluid at E2-S. This fluid density allows us to confine the conditions of phase separation to a pressure and temperature range of 320 to 390 bar and 420 to 450°C. The Cl-depleted nature of the fluids from E2-S

represents a supercritical phase separated fluid owing to their depleted Cl concentrations relative to seawater and density constraints (Bischoff and Pitzer, 1989; Bischoff, 1991). The cooler temperatures of 320 to 344°C measured at seafloor conditions suggest that the fluids have been undergoing conductive cooling prior to venting.

Phase separation is known to affect the concentrations of dissolved gases in hydrothermal fluids. Cl-depleted fluids have a higher concentration of dissolved gases relative to conjugate brine phases. This is also true for the fluids at E2-S. Fluids with low concentration of Cl show the highest concentration of CO_2 and H_2S (**Figures 4C–E**), while concentrations of dissolved H_2 and CH_4 do not show similar trends. CH_4 abundances likely represent a CH_4-Cl rich fluid (brine phase) mixing with the vapour rich fluid at E2-S.

Sub-Surface Processes and Consequences for Concentrations of Dissolved Metals and Gases

The pH of the fluid and metal-chloro complexes (under the effect of pressure and temperature) play a key role for the concentrations of dissolved metals in hydrothermal fluids. The temperatures required to have high concentrations of metals stable in seawater-like solutions decrease in the order Cu>Fe>Zn>Mn (Seewald and Seyfried, 1990). It is therefore expected that a cooled hydrothermal fluid will lose Cu and Fe by mineral precipitation faster than Zn and Mn. The fluids at E2-S have a relatively high endmember Mn concentration but low Fe concentrations (**Table 3A**). The low Fe/Mn ratios at E2-S (0.20 to 0.59) may represent the loss of Fe relative to Mn because of extensive conductive cooling of the fluid. To test this hypothesis, we applied the Fe/Mn geothermometer by Pester et al. (2012), derived from an empirical relation between the Fe/Mn ratios of hydrothermal fluids and temperature. The calculated temperatures (e.g., 305°C for Dog's Head) are lower than the measured temperatures (here: 344°C). The same applies for the Dog's Head fluids analysed in 2010 (**Table 3A**), which give Fe/Mn temperatures of 308°C (at measured 351°C). Sepia and Sepia Flange show even lower Fe/Mn ratios indicative of even more cooling-related Fe-precipitation there. These overall low Fe/Mn ratios are a clear indication that the fluids venting at E2-S undergo extensive cooling and pyrite precipitation prior to venting at the seafloor (**Figure 8**). The 40°C cooling of Sepia Flange relative to Sepia vent (James et al., 2014) come with a drop in Fe concentrations of >200 μM. The associated changes in H_2S concentrations (drop by 500 μM) and pH (drop from 3.1 to 2.9) are consistent with the idea of pyrite precipitation.

The low concentrations of dissolved H_2 in the fluids at E2-S (<1 mM) are typical for unsedimented mafic hosted hydrothermal systems (e.g., Welhan and Craig, 1983; Merlivat et al., 1987; Evans et al., 1988; Proskurowski et al., 2008; Diehl and Bach, 2020b; Diehl and Bach, 2021). Dissolved H_2 in hydrothermal fluids are known to be controlled as a result of fluid-mineral equilibria and phase separation processes, where H_2 abundances are buffered as a result of equilibration of Fe-bearing sulphide, oxides and aluminosilicate minerals (Seyfried and Ding, 1995; Seyfried et al., 2003). Phase separation can also affect the concentration of dissolved gases such as H_2. Cl-depleted vapour phases are usually associated with high concentration of dissolved gases. However, phase separation alone at E2-S is likely unable to explain the concentration of H_2 in these fluids.

High-temperature fluid-rock interaction in the sub-surface root zone results in buffering the H_2 concentration of these fluids. Experimental basalt alteration studies have shown that pyrite-pyrrhotite-magnetite (PPM) and hematite-magnetite (HM) assemblages are predicted to exist in the range of redox conditions for natural hydrothermal systems (Seewald and Seyfried, 1990; Seyfried et al., 1991; Seyfried and Ding, 1995). The stability of these buffers can be predicted using thermodynamic data at various sets of temperature and pressure conditions. The known endmember H_2 concentrations for the fluids at Iced Bun and Dog's Head, predict H_2 concentrations that are consistent with the HM buffer at temperatures of ∼358 and ∼340°C at 300 bar (**Figure 7**). The higher degree of conductive cooling at Iced Bun relative to Dog's Head results in the offset of the data from the predicted HM buffer. The measured concentrations of H_2 at Iced Bun correspond to an equilibrium fluid temperature of ∼358°C (**Figure 7**), while the fluid at Dog's Head is predicted to have a temperature of ∼340°C. The fluid temperature predicted at Dog's Head are close to the measured temperatures of 344°C. The higher temperature predicted for fluids emitting at Iced Bun could be a result of addition of H_2 from rapid pyrite precipitation after equilibration with the HM buffer, during fluid upflow. However, we cannot rule out the fact that the fluid venting at Iced Bun underwent a higher degree of conductive cooling compared to Dog's Head, and therefore the H_2 concentrations could also be the result of higher equilibration temperatures (>320°C).

Endmember concentrations of dissolved H_2S of 3.61 and 5.02 mM in the fluids emitted at E2-S are within the known range of basalt-hosted hydrothermal systems (Diehl and Bach, 2020b; Diehl and Bach, 2021). $\delta^{34}S_{H2S}$ values of fluids from E2-S range from +4.0 to +6.7‰. Such $\delta^{34}S_{H2S}$ values have been previously reported from the Lau Basin (McDermott et al., 2015a). The H_2S in unsedimented basalt hosted hydrothermal systems can be either a result of mantle derived sulphide present in rocks in the form of pyrite and pyrrhotite with $\delta^{34}S_{H2S}$ values of +0.1 ±0.5‰ (Sakai et al., 1984) and/or reduced seawater SO_4, with a $\delta^{34}S_{H2S}$ value of +21.0 ±0.2 ‰ (Rees et al., 1978). At E2-S the $\delta^{34}S_{H2S}$ values are a result of mantle derived sulphur that varies from 81 and 69% relative to seawater derived sulphur of about 19 and 31% in these fluids.

Conductive cooling of fluids during ascend to the seafloor can result in pyrite precipitation, which can in turn affect the concentration of H_2, H_2S and Fe in the fluid (McDermott et al., 2018). Pyrite precipitation produces H_2 and acidity, while consuming dissolved Fe and H_2S:

$$Fe^{2+} + 2H_2S_{(aq)} = FeS_{2(s)} + 2H^+ + H_{2(aq)} \quad (13)$$

Indeed, the fluid venting at Iced Bun appears to be affected by pyrite precipitation as its fluid is characterized by low

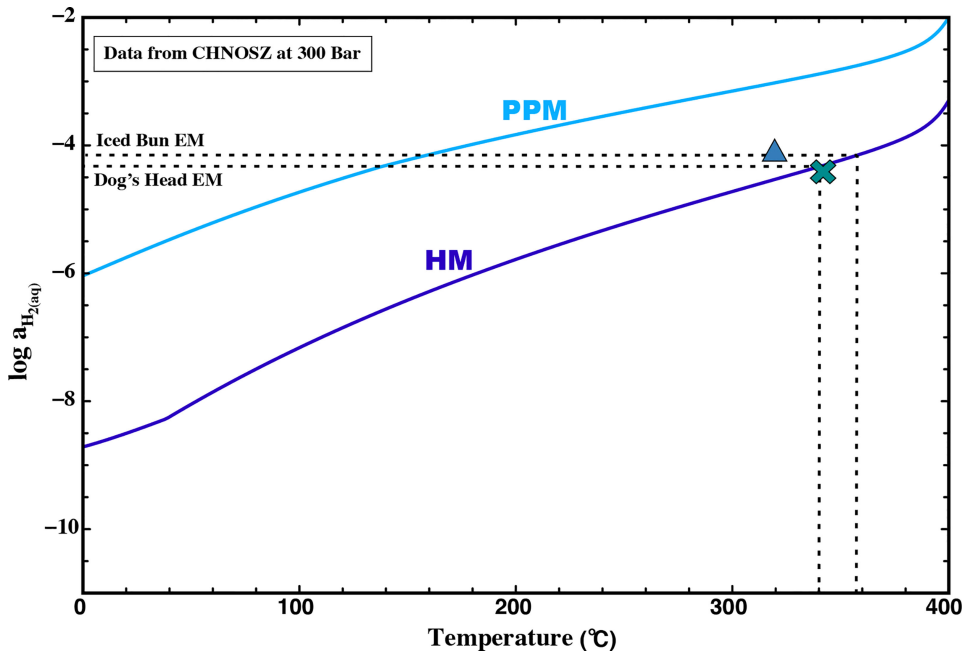

FIGURE 7 | Activity diagram showing aqueous H_2 abundances in equilibrium with pyrite-pyrrhotite-magnetite (PPM, blue line) and heamatite-magnetite (HM, purple line) at 300 bar and corresponding temperatures. The lines were drawn using thermodynamic data from CHNOSZ and references therein (Dick, 2019). Endmember H_2 concentrations and T_{max} for E2 is shown as Dog's Head (cross) and Iced Bun (triangle). The dashed line indicates endmember H_2 extrapolated to its associated temperature as a function of the HM buffer.

concentrations of Fe and H_2S, a higher concentration of H_2, and lower pH $_{(in\text{-}situ)}$ relative to Dog's Head (**Table 1**, **3A**). Fluid venting at Dog's Head could also be affected by pyrite precipitation in the subsurface (low Fe/Mn ratios), but it appears that the pyrite precipitation at Iced Bun is more pronounced than at Dog's Head. Activity-activity diagrams for H_2S and H_2 indicate that Dog's Head and Iced Bun plot near the hematite-magnetite-pyrite invariant point in the Fe-S-O-H system (**Figure 8**). Deviations from the invariant point can be accounted for by the facts that (1) the natural system is compositionally more complex than the Fe-O-H-S system for which the diagram is representative of and (2) there is considerable uncertainties in concentration-activity relations (Scheuermann et al., 2019). H_2S concentrations at E2-S may also have been influenced by phase separation, because Dog's Head fluid (low Cl) have higher concentration of H_2S than the high-Cl fluids venting at Iced Bun (**Table 3A**). As shown, the dissolved H_2 and H_2S concentrations at E2-S are mainly a result of fluid-mineral equilibria, but phase separation and cooling-induced pyrite precipitation are additional influences.

Dissolved Carbon Species

Elevated concentrations of dissolved CO_2 relative to seawater in BAB-hosted hydrothermal systems result from magmatic degassing (Takai et al., 2008; Reeves et al., 2011; Seewald et al., 2015; Seewald et al., 2019). However, a small fraction of CO_2 in the fluids could also result from leaching of CO_2 trapped in rocks as inclusions. Basaltic glasses from the ESR have a CO_2 concentration of <200 ppm (Mattey et al., 1984). Assuming a w/r of 2 (calculated for E2-S in this study), complete leaching of CO_2 from the rocks would contribute a CO_2 concentration of no more than 4 mmol/kg CO_2. Therefore, the higher abundances of dissolved CO_2 (**Figure 4C**) at E2-S are primarily a result of magmatic degassing with a minor possible contribution of CO_2 leached from basalts.

The carbon isotopic signatures of fluids from E2-S reveal endmember $\delta^{13}C_{CO2}$ values of -4.1 and -5.6‰, which are within the known range of BAB hosted hydrothermal system (Reeves et al., 2011; Seewald et al., 2015; Diehl and Bach, 2020b; Diehl and Bach, 2021). In contrast, basaltic glass at ESR has more negative $\delta^{13}C_{CO2}$ values of -15.0 to -19.9‰ (Mattey et al., 1984). Degassed CO_2 from basaltic melts at MOR have more positive $\delta^{13}C_{CO2}$ values, such as those at Lucky Strike hydrothermal system (-3.9 to -5.6‰) that are interpreted to reflect replenishing of the magmatic reservoir (Javoy et al., 1978; Mattey, 1991; Pester et al., 2012; Holloway and Blank, 1994). The high abundance and ^{13}C-enriched nature of CO_2 in the fluids at E2-S relative to the basaltic glass at ESR are likely a result of degassing from a magma reservoir that has undergone replenishment.

The endmember CH_4 concentrations (25.6 and 48.9 μM) are low relative to other BAB-hosted hydrothermal systems (Reeves et al., 2011; Seewald et al., 2015; Seewald et al., 2019). A variety of processes can contribute towards the CH_4 concentrations in hydrothermal systems that can range from abiotic sources, microbial activity and thermogenesis of sediments and/or organic matter (Von Damm et al., 1985b; Welhan, 1988;

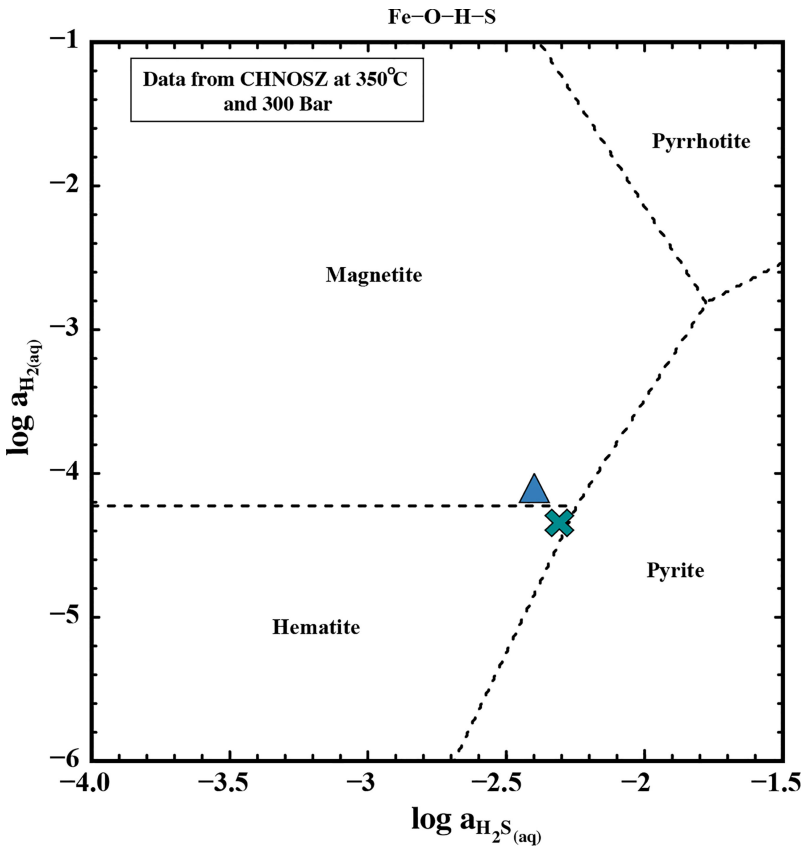

FIGURE 8 | Activity diagram showing the phase relations in a Fe-O-H-S system at 350°C and 300 bar. The data to plot the mineral fields were acquired using CHNOSZ (Dick, 2019). The blue triangle represents endmember data from the fluid at Iced Bun and the green cross represents endmember data from Dog's Head.

Seewald and Seyfried, 1990; Seewald et al., 1994; Von Damm et al., 2005; Cruse and Seewald, 2006; Proskurowski et al., 2008; McDermott et al., 2018; Fiebig et al., 2019). Low concentrations of CH_4 at E2-S coupled to a relatively ^{13}C-enriched $\delta^{13}C_{CH4}$ isotopic composition of -7.0 and -7.6‰ rule out the influences of sediment thermogenesis and microbial derived CH_4 which would be expected to impart more ^{13}C-depleted signatures. Such ^{13}C-enriched $\delta^{13}C_{CH4}$ in combination with ^{2}H-enriched δD_{CH4} values (here: -98.7 and -99.9‰) have previously been associated to a 'potentially abiotic source' of origin (Kelley, 1996; Kelley and Früh-Green, 1999; Wang et al., 2018; McDermott et al., 2018; Klein et al., 2019). However, recent studies indicate that similar values can also be produced as a result of thermogenesis of seawater derived DOM – 'volcanic thermogenesis' (Fiebig et al., 2019; Reeves and Fiebig, 2020). As a result, the CH_4 abundances at E2-S could be a combination of volcanic thermogenesis with a possible contribution from an abiotic source.

An inverse relationship in CO_2 and CH_4 concentrations is observed in the fluids at E2-S such that high concentrations of CO_2 are matched with low CH_4 abundances. High CO_2 abundances are found in the most Cl-depleted fluid, while CH_4 concentrations are highest in the fluid containing with Cl concentrations. This relationship could result from mixing of CH_4- and Cl-bearing hydrothermal fluids and a CO_2-enriched and Cl-poor magmatic vapour in the sub-surface of the E2-S vent site.

Magmatic Water Input

Stable oxygen and hydrogen isotopes in water in hydrothermal systems are mainly affected by three factors: i) interaction between the hydrothermal fluid and the host rock and/or sediments in the sub-surface, ii) phase separation and/or iii) contribution of mantle derived magmatic water. Hydration reactions between the hydrothermal fluids and the oceanic igneous crust yields increasing δD_{H2O} and $\delta^{18}O_{H2O}$ values with decreasing w/r ratios (**Supplementary Figure 4**, Bowers and Taylor, 1985; Bowers, 1989; Shanks et al., 1995; Shanks, 2001). The δD_{H2O} values in fluids from E2-S are depleted in ^{2}H relative to seawater (-2.0 to -1.2‰; **Supplementary Figure 4**). These low δD_{H2O} values are an indication that factors other than w/r interactions affect the H isotopic composition of these fluids.

Experimental work has shown that phase separation can affect the H and O isotope ratios of hydrothermal fluids (Horita et al., 1995; Berndt et al., 1996; Shmulovich et al., 1999; Foustoukos and Seyfried, 2007b). Vapours are slightly elevated in δD_{H2O} values

relative to the brine phase (Von Damm et al., 2003). Oxygen isotopes show the opposite fractionation direction: brines have higher $\delta^{18}O_{H2O}$ values than vapours (Berndt et al., 1996; Foustoukos and Seyfried, 2007b). The low chlorinity fluids analysed in this study show low δD_{H2O} and high $\delta^{18}O_{H2O}$ values (0.4 to 0.6‰), which is opposite of what would be expected for a vapour phase produced by phase separation. An influence of sediments on the fluid chemistry can also explain low δD_{H2O} combined with high $\delta^{18}O_{H2O}$ values (Baumberger et al., 2016; Toki et al., 2016). No sediment was observed at E2-S, and therefore sediment-fluid interactions are likely not responsible for the observed δD_{H2O} and $\delta^{18}O_{H2O}$ data.

The negative δD_{H2O} (-2.0 to -1.2‰) and positive $\delta^{18}O_{H2O}$ values (+0.4 to +0.6‰) in the E2-S hydrothermal vent fluids may indicate that a small fraction of the venting H_2O is derived from magmatic degassing. A constricted range of δD_{H2O} (-65.0 ± 20‰) and $\delta^{18}O_{H2O}$ (+6 ± 1‰, Taylor, 1979; Ohmoto, 1986) has been estimated to be of mantle derived magmatic water. Whereas water resulting from subduction related volcanic vapours (SRVV) have δD_{H2O} values ranging from -10 to -30‰ and $\delta^{18}O_{H2O}$ of +6 to +10‰ (Giggenbach, 1992; Hedenquist and Lowenstern, 1994). Fractionation related to degassing and slab-derived input of water can result in an increase in δD_{H2O} of magmatic waters at convergent margins (Taylor, 1986; Giggenbach, 1992; Hedenquist and Lowenstern, 1994; Taylor, 1997). Linear extrapolation of the fluids at E2-S indicate a possible small input of SRVV component into the fluids (**Figure 9**). Such an SRVV component input has been previously suggested to affect the PACMANUS hydrothermal vent fluids, Manus spreading centre, Papua New Guinea (Reeves et al., 2011), which show CO_2, $\delta^{13}C_{CO2}$, δD_{H2O} and $\delta^{18}O_{H2O}$ characteristics similar to those found at E2-S. The most plausible explanation for the δD_{H2O} and $\delta^{18}O_{H2O}$ data of the fluids venting at E2-S is that seawater-derived hydrothermal fluids underwent extensive water/rock interactions and mixing with small fractions of magmatic water vapour with a SRVV isotopic signature. Moreover, it appears that the fluid in 2010 did not have any involvement of an SRVV component as no highly negative δD_{H2O} values were reported (**Table 3A**). These variations seen at E2 in 2019 further provide a temporal evolution into the ESR systems.

Formation of Fluid at E2-W: Influence of Abiotic and Biotic Processes

The fluids diffusively venting at E2-W are low in temperature (53°C) relative to those emitted at E2-S (320°C, 344°C). Such diffuse low- to moderate-temperature fluids can be a result of either subseafloor mixing of high-temperature fluid with entrained seawater or they can represent conductively heated seawater (Cooper et al., 2000; McDermott et al., 2015b). The Mg depletion (42.6 mM) and K enrichment (13.4 mM) relative to seawater are a clear indication that the fluid at E2-W is a result of a high-temperature fluid that has undergone mixing with seawater prior to venting.

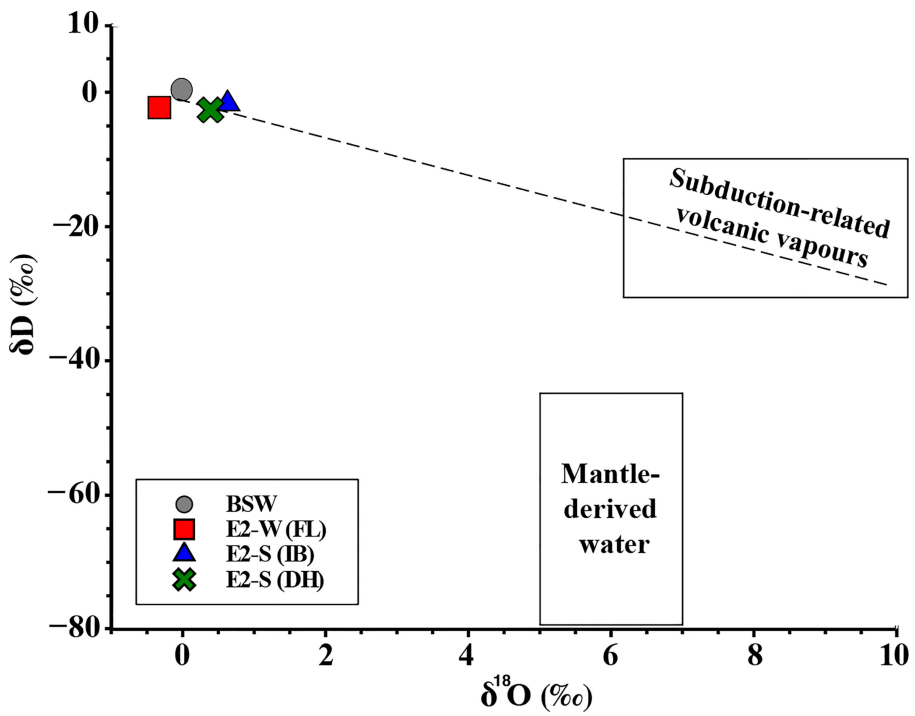

FIGURE 9 | Endmember water isotopic composition for E2-S and measured values for E2-W fluids. The dashed line is the least square regression line for the E2-S fluids and BSW. Data for subduction related volcanic vapours and mantle derived water were taken from Taylor, (1979; Ohmoto (1986) and Giggenbach (1992); Hedenquist and Lowenstern (1994), respectively.

The E2-W hydrothermal system is located about ca. 1.25 km north of the E2-S system. and the two vents investigated at E2-S, Dog's Head and Iced Bun, are fed by a single source fluid. E2-W is proximal enough to E2-S to be fed by fluids from the same root zone. To investigate the plausibility of the idea that a single deeply sourced fluid supplies all the E2 systems sampled in this study, an average composition of the endmember fluid (EF) for E2-S was computed and mixed with seawater (SW) until the Mg measured for the fluid at E2-W, was met (**Supplementary Table 2**). The Mg concentrations of the E2-W fluid reveal an EF: SW mixing ratio of 1:5. Enrichments and depletions of dissolved species in this hypothetical E2-W fluid ($E2\text{-}W_{calc}$) were then compared with the measured E2-W fluid (**Supplementary Table 2**). The excellent correspondence of calculated and measured data indicate that the E2-W fluid could indeed result from mixing of E2-S hydrothermal fluid with seawater. Na, Cl, Br, K, Ca and CO_2 values estimated are either within the analytical errors of the measurements (K, Ca and CO_2) or have seawater-like concentrations (Na, Cl and Br) indicating the fluid may derive from mixing between seawater and the common source fluid that feeds the E2-S vent sites.

Whereas most elements in the fluid at E2-W fit the conservative mixing model, enrichments (SO_4 and Sr) and depletions (H_2, CH_4, H_2S, Si and Fe) relative to the $E2\text{-}W_{calc}$ are observed. Si in hydrothermal systems is believed to behave conservatively and has been extensively used to constrain sub-surface conditions in these systems (Von Damm et al., 1991; Reeves et al., 2011; McDermott et al., 2018). However, depletions in Si relative to calculated $E2\text{-}W_{calc}$ observed is likely a result of sub-surface precipitation of silica. Janecky and Seyfried (1984) have shown that removal of silica through precipitation is only possible with the fluids that have undergone extensive cooling, which is also likely the case for the fluid at E2-W. Reaction path models further indicate this loss of Si in the modelled fluid because of quartz precipitation (**Supplementary Figure 5**).

The fluids at E2-W are enriched in SO_4 (by 2.27 mM) and Sr (by 1.98 μM) relative to the conservative mixing line. Sr in hydrothermal systems is known to substitute Ca in anhydrite precipitation (Kuhn et al., 2003). Therefore, the observed enrichments in Sr and SO_4 can be directly attributed to sub-seafloor dissolution of anhydrite. Endmember extrapolation of SO_4 at E2-W reveals a concentration of 13 mM. These strong SO_4 excesses have commonly been interpreted as evidence of anhydrite dissolution (e.g., Reeves et al., 2011).

Aerobic sulphide oxidation (equation 1) is another possible source of excess sulphate. Indeed, thermodynamic computations indicate that the major source of catabolic energy in the E2-W subseafloor is aerobic sulphide oxidation (**Figure 10**). Furthermore, non-sedimented hydrothermal systems are known to host a variety of sulphide oxidizing microorganisms (Dahle et al., 2015; Dahle et al., 2018). Microbial sulphide oxidation could also further help explain the depletion of H_2S in the fluid (<0.2 μM, below limit of quantification) compared to the calculated 0.81 mM abundance that would be expected if conservative mixing were occurring. However, even if 0.8 mM of H_2S were oxidized to sulphate, the sulphate enrichments of 2.27 mM cannot be fully explained by this process. Moreover, abiotic precipitation of pyrite is another possible sink for H_2S. Indeed, depletion of H_2S is matched by a loss of >90% of the dissolved Fe, which could point to pyrite precipitation. While Fe is likely only affected by abiotic reactions, SO_4 and H_2S concentrations at E2-W could be a result of both biotic as well as abiotic reactions taking place in the sub-surface. We suggest that most of the sulphate excess is due to anhydrite dissolution, whereas H_2S is lost as consequence of pyrite precipitation as well as aerobic sulphide oxidation.

A strong depletion of H_2 relative to the conservative mixing line is also observed in the fluids at E2-W (**Supplementary Table 2**). H_2 in mixing zones in hydrothermal systems can be consumed by the reduction of CO_2 to formic species (McDermott et al., 2015b). If CH_4 was a metabolic product of CO_2 reduction, CH_4 concentrations in the fluids should be higher than predicted from conservative mixing. This is not the case, as the fluid at E2-W is depleted in CH_4 relative to the mixing line by 5.27 μM (**Supplementary Table 2**). Such a depletion of CH_4 at E2-W is likely the result of aerobic oxidation of CH_4 (**Figure 10**). CO_2 and H_2 concentrations of the fluids are inconclusive in this regard, as a H_2 consumption of 8 μM would deplete CO_2 only by 2 μM, which is small relative to the 300 μM mismatch between measured and calculated composition (**Supplementary Table 2**). Moreover, CO_2 could be produced by oxidation of CH_4 by microorganisms. $\delta^{13}C_{CO2}$ at E2-W is -10.8‰ and is more ^{13}C-depleted than the measured $\delta^{13}CO_2$ values at E2-S of -3.7‰ and -4.4‰. If the CO_2 at E2-S is a result of magmatic degassing and the entire E2 system is fed by a common root zone, then a range of $\delta_{13}C_{CO2}$ between -4.4‰ to 0.3‰ would be predicted at E2-W if it simply reflects mixing between the E2-S endmember and seawater. The far more ^{13}C-depleted values of $\delta^{13}C_{CO2}$ at E2-W suggest an additional, non-magmatic source of CO_2 in the vent fluids. Such more negative values of $\delta^{13}C_{CO2}$ relative to the high-temperature fluid have been previously observed at EPR and have been attributed to methanotrophy (Proskurowski et al., 2008). The idea that methane oxidation may contribute to the dissolved CO_2 pool is further supported by catabolic landscape models, which indicate that this aerobic methane oxidation is indeed exergonic at E2-W (**Figure 10**). It is likely that the $\delta^{13}C_{CO2}$ at E2-W represents a combination of the endmember fluid mixed with seawater with contributions from microbial metabolism.

Implications for Surface and Sub-Surface Ecology at E2

A more general assessment of the catabolic energy landscape at E2 is warranted as endmember fluids at E2-S are enriched in H_2S, CH_4, CO_2, H_2, Fe and Mn relative to seawater. The enrichments of these components are a result of high-temperature fluid-rock interaction and magmatic degassing taking place in the sub-surface. A combination of these processes creates an energy gradient representing an appropriate environment for life in the deep-sea at E2 to thrive on.

Just like we established for the E2-W site, this reduced fluid can mix with the oxic seawater entrained in the subseafloor and create an energy rich environment for catabolic reactions to take place (**Figure 10A**, McCollom and Shock, 1997; Amend et al., 2011).

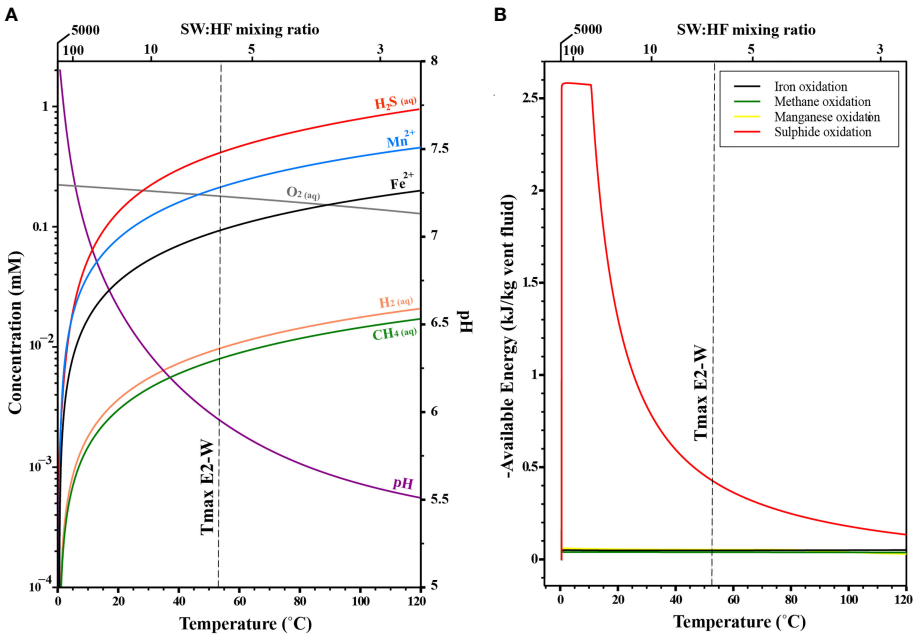

FIGURE 10 | Thermodynamic models for chemical gradient and associated energy landscape at E2. **(A)** Modelled concentration of various species as a function of temperature and mixing ratios. **(B)** Modelled energy available for the various reactions as a function of temperature and mixing ratios.

These reactions (**Table 2**) help support a chemosynthetic ecosystem at E2. The catabolic energy computations we conducted indicate that aerobic sulphide oxidation (ASO) is clearly the dominant energy source at both low and high temperatures (**Figure 10B**). Between 120 and 60°C (i.e., at low SW: HF mixing ratios) ASO has an energy yield between -0.2 and -0.4 kJ/kg of vent fluid. At temperatures <60°C (i.e., high SW: HF mixing ratios), the models predict a higher energy yield as high as -2.6 kJ/kg of vent fluid.

Aerobic methane oxidation (AMO) is the next most abundant energy source predicted at E2 (**Figure 10B**). At high temperatures (120 to 60°C), AMeO has an energy yield of ~ -0.03 kJ/kg of vent fluid, and the energy yield may approach -0.8 kJ/kg for vent fluid at lower temperature. Aerobic iron oxidation (AFeO) and aerobic manganese oxidation (AMnO) account for the lowest energy availability at E2.

The modelling results presented are valid for conservative mixing of hydrothermal fluids with seawater. Conductive cooling, mixing with entrained seawater and related abiotic processes at E2 can greatly affect the composition of the hydrothermal fluids. Studies have shown that abiotic reactions can indeed reduce the energy available for catabolic reactions (McDermott et al., 2020).

The effect of mixing on the energy availability is evident at E2-W, where the fluids have been extensively mixed with BSW prior to venting and have a SW: HF mixing ratio of 5:1. Although the H_2S in the fluid was below <0.8 mM, large microbial mats were observed that covered the flange. In contrast, such features were not evident in the E2-S system. Thermodynamic models predict that these H_2S-depleted and O_2-enriched fluid-seawater mixtures coincide with peak energy availabity to chemosynthetic microbial communities (**Figures 10A, B**).

ASO and AMO are the dominant energy source for all the E2 vents. Large areas of the E2-S have been known to be inhabited by biota that are dependent on mainly ASO for their metabolic pathways (Rogers et al., 2012). The temperature range, extensive mixing with BSW, fluid chemistry and predicted thermodynamic modelling indicate that the conditions at E2-W are suitable to host a robust sub-surface biosphere.

SUMMARY

The chemical and isotopic compositions of hydrothermal fluids from the E2 segment of the ESR are useful guides to subseafloor processes of phase separation, water-rock reactions, and mixing with entrained seawater, followed by pyrite precipitation. Depletion in Cl in the high-temperature fluid at E2-S is attributed to phase separation. Low Fe/Mn ratios and pyrite precipitation indicate that the fluids have undergone excessive conductive cooling in the sub-seafloor prior to venting. The H_2 concentration in the fluids at E2-S are likely a result of equilibration with the hematite-magnetite buffer. The H_2S concentrations in the fluid represents mantle derived sulphur contribution that varies from 81 and 69% relative to seawater derived sulphur of about 19 and 31% in these fluids. CH_4 formation in the fluid can be either from a volcanic thermogenesis of seawater-sourced DOM and/or leaching of abiotic CH_4 from fluid inclusions. The high CO_2 abundances and $\delta^{13}C_{CO2}$ and δD_{H2O} values are evidence that the fluid at E2-S is affected by magmatic components.

The lower temperatures and higher water-rock ratios, along with lower REE, higher Na/Cl and lower Ca/Cl, Li/Cl and Cs/Cl ratios in this study compared to the fluids sampled in 2010

indicate that the root zone has undergone changes towards a slightly more altered basement over the past 9 years. The enriched dissolved gases present in the circulating fluid are a result of combination of fluid-rock interactions and magmatic degassing taking place in the sub-surface. Our data hence indicates progressive alteration of basement in the root zone along with evidence for magmatic degassing taking place at E2. Moreover, mixing of magmatic vapour and elevated $\delta^{13}C_{CO2}$ could reflect replenishing of the magma chamber at E2.

The mixed fluid at E2-W and E2-S appear to originate from a single source fluid at depth (>300 bar). The fluid at E2-W shows enrichments in Sr and SO_4 that can be attributed to anhydrite dissolution. However, aerobic sulphide oxidation could be an additional source for SO_4 and a sink for H_2S. Depletion of H_2S and Fe observed in the fluid at E2-W is a result of pyrite precipitation taking place in the sub-surface. Depleted Si relative to the conservative mixing models reflect loss of Si due to precipitation of amorphous silica. CH_4 depletions in the fluid are likely a result of aerobic methane oxidation. H_2 depletions in the fluid can be either a result of microbial respiration in the sub-seafloor (aerobic hydrogen oxidation) or by reactions involving O_2 and NO_3^- in the mixing zones. Geochemical reaction path models for E2 indicate that mixing of hydrothermal fluids with entrained seawater can support subseafloor microbial life, with aerobic oxidation of sulphide and methane being potent catabolic energy sources.

Our study provides novel insights into the temporal evolution of the E2-S hydrothermal system that may expand our understanding of hydrothermal systems hosted in BABs. Bioenergetics calculations indicate that H_2S is the main provider of catabolic energy followed by CH_4, Fe and H_2. Our findings at E2-W further suggest that these energy sources may indeed be utilized by subseafloor microbial communities.

DATA AVAILABILITY STATEMENT

The original contributions presented in the study are included in the article/**Supplementary Material**. Further inquiries can be directed to the corresponding author.

AUTHOR CONTRIBUTIONS

SP and AD collected the samples during the cruise in 2019. GB led the expedition. JM provided the samplers. WB, AD, and SP designed research. SP, AD, TP, LK, and HS analysed the samples. SP, AD, and WB wrote the paper, but all authors contributed to writing. All authors contributed to the article and approved the submitted version.

FUNDING

The expedition was funded by German Federal Ministry of Education and Research (grant number 03G0880A) and by the German Research Foundation (Deutsche Forschungsgemeinschaft, DFG) within the Cluster of Excellence (EXC-2077, project number 390741603 "The Ocean Floor –Earth's Uncharted Interface") at MARUM – Center for Marine and Environmental Sciences, University of Bremen. This work was further supported by the Trond Mohn Foundation and University of Bergen through Centre for Deep Sea research (grant #TMS2020TMT13).

ACKNOWLEDGMENTS

We would like to thank the captain and the crew of RV *Polarstern* and the ROV team of *MARUM-Quest4000m* for their support in collection of the samples during PS119. Janice Malnati (Faculty of Geoscience, Bremen) is thanked for her assistance with CH_4 and CO_2 isotope analysis. Miriam Römer and Paul Wintersteller are thanked for the bathymetric maps. The study was undertaken under permit RAP 2018/064 issued by the South Georgia and South Sandwich Government.

SUPPLEMENTARY MATERIAL

The Supplementary Material for this article can be found online at: https://www.frontiersin.org/articles/10.3389/fmars.2022.765648/full#supplementary-material

REFERENCES

Amend, J. P., McCollom, T. M., Hentscher, M., and Bach, W. (2011). Catabolic and Anabolic Energy for Chemolithoautotrophs in Deep-Sea Hydrothermal Systems Hosted in Different Rock Types. *Geochim. Cosmochim. Acta* 75 (19), 5736–5748. doi: 10.1016/j.gca.2011.07.041

Atkinson, A. B. Jr (2002). A Model for the PTX Properties of H_2O-NaCl (Doctoral dissertation, Virginia Tech). *MSc. Thesis. Virgin. Tech*, 133pp

Baker, T., and Lang, J. R. (2001). Fluid Inclusion Characteristics of Intrusion-Related Gold Mineralization, Tombstone-Tungsten Magmatic Belt, Yukon Territory, Canada. *Mineral. Deposit.* 36 (6), 563–582. doi: 10.1007/s001260100189

Baumberger, T., Früh-Green, G. L., Thorseth, I. H., Lilley, M. D., Hamelin, C., Bernasconi, S. M., et al. (2016). Fluid Composition of the Sediment-Influenced Loki's Castle Vent Field at the Ultra-Slow Spreading Arctic Mid-Ocean Ridge. *Geochim. Cosmochim. Acta* 187, 156–178. doi: 10.1016/j.gca.2016.05.017

Beermann, O., Garbe-Schönberg, D., Bach, W., and Holzheid, A. (2017). Time-Resolved Interaction of Seawater With Gabbro: An Experimental Study of Rare-Earth Element Behavior Up to 475 °C, 100 Mpa. *Geochim. Cosmochim. Acta* 197, 167–192. doi: 10.1016/j.gca.2016.10.016

Berndt, M. E., Seal, R. R., Shanks, W. C., and Seyfried, W. E. (1996). Hydrogen Isotope Systematics of Phase Separation in Submarine Hydrothermal Systems: Experimental Calibration and Theoretical Models. *Geochim. Cosmochim. Acta* 60 (9), 1595–1604. doi: 10.1016/0016-7037(96)00033-6

Berndt, M. E., and Seyfried, W. E. (1990). Boron, Bromine, and Other Trace Elements as Clues to the Fate of Chlorine in Mid-Ocean Ridge Vent Fluids. *Geochim. Cosmochim. Acta* 54 (8), 2235–2245. doi: 10.1016/0016-7037(90)90048-P

Berndt, M. E., and Seyfried, W. E. (1993). Calcium and Sodium Exchange During Hydrothermal Alteration of Calcic Plagioclase at 400°C and 400 Bars. *Geochim. Cosmochim. Acta* 57 (18), 4445–4451. doi: 10.1016/0016-7037(93)90494-H

Berndt, M. E., Seyfried, W. E., and Janecky, D. R. (1989). Plagioclase and Epidote Buffering of Cation Ratios in Mid-Ocean Ridge Hydrothermal Fluids:

Experimental Results in and Near the Supercritical Region. *Geochim. Cosmochim. Acta* 53 (9), 2283–2300. doi: 10.1016/0016-7037(89)90351-7

Bieseler, B., Diehl, A., Jöns, N., Lucassen, F., and Bach, W. (2018). Constraints on Cooling of the Lower Ocean Crust From Epidote Veins in the Wadi Gideah Section, Oman Ophiolite. *Geochem. Geophys. Geosyst.* 19 (11), 4195–4217. doi: 10.1029/2018GC007679

Bischoff, J. L. (1991). Densities of Liquids and Vapors in Boiling NaCl-H_2O Solutions: A Pvtx Summary From 300° to 500°C. *Am. J. Sci.* 291(4), pp.309–338. doi: 10.2475/ajs.291.4.309

Bischoff, J. L., and Pitzer, K. S. (1989). Liquid-Vapor Relations for the System NaCl-H_2O: Summary of the P-T- X Surface From 300° to 500°C. *Am. J. Sci.*289 (3), pp.217–248. doi: 10.2475/ajs.289.3.217

Bischoff, J. L., and Rosenbauer, R. J. (1985). An Empirical Equation of State for Hydrothermal Seawater (3.2 Percent Nacl). *Am. J. Sci.* 285 (8), 725–763. doi: 10.2475/ajs.285.8.725

Bodnar, R. J., Samson, I., Anderson, A., and Marshall, D. (2003). Reequilibration of Fluid Inclusions." Fluid Inclusions: Analysis and Interpretation. 32, 213–230

Bohrmann, G. (2019). The Expedition PS119 of the Research Vessel POLARSTERN to the Eastern Scotia in 2019. *Reports on Polar and Marine Research*, Alfred-Wegener-Institut, Helmholtz-Zentrum für Polar- und Meeresforschung, Bremerhaven, Germany, 736. doi: 10.2312/BzPM_0736_2019

Bowers, T. S. (1989). Stable Isotope Signatures of Water-Rock Interaction in Mid-Ocean Ridge Hydrothermal Systems: Sulfur, Oxygen, and Hydrogen. *J. Geophys. Res.* 94 (B5), 5775–5786. doi: 10.1029/JB094iB05p05775

Bowers, T. S., and Taylor, H. P. (1985). An Integrated Chemical and Stable-Isotope Model of the Origin of Midocean Ridge Hot Spring Systems. *J. Geophys. Res: Solid Earth* 90(B14),pp.12583–12606. doi: 10.1029/jb090ib14p12583

Bruguier, N. J., and Livermore, R. A. (2001). Enhanced Magma Supply at the Southern East Scotia Ridge: Evidence for Mantle Flow Around the Subducting Slab? *Earth Planet. Sci. Lett.* 191 (1–2), 129–144. doi: 10.1016/S0012-821X(01)00408-3

Butterfield, D. A., Nakamura, K. I., Takano, B., Lilley, M. D., Lupton, J. E., Resing, J. A., et al. (2011). High SO_2 Flux, Sulfur Accumulation, and Gas Fractionation at an Erupting Submarine Volcano. *Geology* 39 (9), 803–806. doi: 10.1130/G31901.1

Cline, J. D. (1969). Spectrophotometric Determination of Hydrogen Sulfide in Natural Waters. *Limnol. Oceanog.* 14 (3), 454–458. doi: 10.4319/lo.1969.14.3.0454

Cole, C. S., James, R. H., Connelly, D. P., and Hathorne, E. C. (2014). Rare Earth Elements as Indicators of Hydrothermal Processes Within the East Scotia Subduction Zone System. *Geochim. Cosmochim. Acta* 140, 20–38. doi: 10.1016/j.gca.2014.05.018

Cooper, M. J., Elderfield, H., and Schultz, A. (2000). Diffuse Hydrothermal Fluids From Lucky Strike Hydrothermal Vent Field: Evidence for a Shallow Conductively Heated System. *J. Geophys. Res.: Solid. Earth* 105 (B8), 19369–19375. doi: 10.1029/2000jb900138

Craddock, P. R., Bach, W., Seewald, J. S., Rouxel, O. J., Reeves, E., and Tivey, M. K. (2010). Rare Earth Element Abundances in Hydrothermal Fluids From the Manus Basin, Papua New Guinea: Indicators of Sub-Seafloor Hydrothermal Processes in Back-Arc Basins. *Geochim. Cosmochim. Acta* 74 (19), 5494–5513. doi: 10.1016/j.gca.2010.07.003

Craig, H. (1970). Abyssal Carbon 13 in the South Pacific. *J. Geophys. Res.* 75 (3), 691–695. doi: 10.1029/jc075i003p00691

Cruse, A. M., and Seewald, J. S. (2006). Geochemistry of Low-Molecular Weight Hydrocarbons in Hydrothermal Fluids From Middle Valley, Northern Juan De Fuca Ridge. *Geochim. Cosmochim. Acta* 70 (8), 2073–2092. doi: 10.1016/j.gca.2006.01.015

Dahle, H., Økland, I., Thorseth, I. H., Pederesen, R. B., and Steen, I. H. (2015). Energy Landscapes Shape Microbial Communities in Hydrothermal Systems on the Arctic Mid-Ocean Ridge. *ISME. J.* 9 (7), 1593–1606. doi: 10.1038/ismej.2014.247

Dahle, H., Le Moine Bauer, S, Baumberger, T., Stokke, R., Pedersen, R. B., Thorseth, I. H., et al. (2018). Energy Landscapes in Hydrothermal Chimneys Shape Distributions of Primary Producers. *Front. Microbiol.* 9. doi: 10.3389/fmicb.2018.01570

De Ronde, C. E., and Jambor, J. L. (1995). Fluid Chemistry and Isotopic Characteristics of Seafloor Hydrothermal Systems and Associated Vms Deposits: Potential for Magmatic Contributions. *Magma. Fluid. Ore. Deposit.* 23 (1), 479–509.

Dick, J. M. (2019). Chnosz: Thermodynamic Calculations and Diagrams for Geochemistry. *Front. Earth Sci.* 7, 150. doi: 10.3389/feart.2019.00180

Diehl, A., and Bach, W. (2020b). MARHYS (Marine HYdrothermal Solutions) Database: A Global Compilation of Marine Hydrothermal Vent Fluid, End Member and Seawater Compositions. *Geochem. Geophys. Geosyst.* 21(12), p.e2020GC009385. doi: 10.1029/2020GC009385

Diehl, A., and Bach, W. (2021). *Marhys Database 2.0. Pangaea*. doi 10.1594/PANGAEA.935649.

Diehl, A., De Ronde, C. E. J., and Bach, W. (2020a). Subcritical phase separation and occurrence of deep-seated brines at the NW Caldera vent field, Brothers volcano: evidence from fluid inclusions in Hydrothermal Precipitates. *Geofluids*. doi: 10.1155/2020/8868259

Douville, E., Bienvenu, P., Charlou, J. P., Donval, J. P., Fouquet, Y., Appriou, P., et al. (1999). Yttrium and Rare Earth Elements in Fluids From Various Deep-Sea Hydrothermal Systems - Evidence for Heat Extraction From Magma Chambers or Cracking Fronts? *Geochim. Cosmochim. Acta* 63 (5), 627–643. doi: 10.1016/S0016-7037(99)00024-1

Douville, E., Charlou, J. L., Oelkers, E. H., Bienvenu, P., Jove Colon, C. F., Donval, J. P., et al. (2002). The Rainbow Vent Fluids (36°14′N, MAR): The Influence of Ultramafic Rocks and Phase Separation on Trace Metal Content in Mid-Atlantic Ridge Hydrothermal Fluids. *Chem. Geolog.* 184 (1–2), 37–48. doi: 10.1016/S0009-2541(01)00351-5

Driesner, T. (2007). The System H_2O-NaCl. Part II: Correlations for Molar Volume, Enthalpy, and Isobaric Heat Capacity From 0 to 1000°C, 1 to 5000 Bar, and 0 to 1 Xnacl. *Geochim. Cosmochim. Acta* 71 (20), 4902–4919. doi: 10.1016/j.gca.2007.05.026

Driesner, T., and Heinrich, C. A. (2007). The System H_2O-NaCl. Part I: Correlation Formulae for Phase Relations in Temperature-Pressure-Composition Space From 0 to 1000 °C, 0 to 5000 Bar, and 0 to 1 XNaCl. *Geochim. Cosmochim. Acta* 71 (20), 4880–4901. doi: 10.1016/j.gca.2006.01.033

Evans, W. C., White, L. D., and Rapp, J. B. (1988). Geochemistry of Some Gases in Hydrothermal Fluids From the Southern Juan De Fuca Ridge. *J. Geophys. Res* 93(B12), pp.15305–15313. doi: 10.1029/jb093ib12p15305

Fiebig, J., Stefánsson, A., Ricci, A., Tassi, F., Viveiros, F., Silva, C., et al. (2019). Abiogenesis Not Required to Explain the Origin of Volcanic-Hydrothermal Hydrocarbons. *Geochem. Perspect. Lett.* 11, 23–27. doi: 10.7185/geochemlet.1920

Foustoukos, D. I., and Seyfried, W. E. (2007a). Trace Element Partitioning Between Vapor, Brine and Halite Under Extreme Phase Separation Conditions. *Geochim. Cosmochim. Acta* 71 (8), 2056–2071. doi: 10.1016/j.gca.2007.01.024

Foustoukos, D. I., and Seyfried, W. E. (2007b). Fluid Phase Separation Processes in Submarine Hydrothermal Systems. *Rev. Mineral. Geochem.* 65, 213–239. doi: 10.2138/rmg.2007.65.7

Foustoukos, D. I., and Seyfried, W. E. (2007c). Quartz Solubility in the Two-Phase and Critical Region of the NaCl-KCl-H_2O System: Implications for Submarine Hydrothermal Vent Systems at 9°50′N East Pacific Rise. *Geochim. Cosmochim. Acta* 71 (1), 186–201. doi: 10.1016/j.gca.2006.08.038

Fretzdorff, S., Livermore, R. A., Devey, C. W., Leat, P. T., and Stoffers, P. (2002). Petrogenesis of the Back-Arc East Scotia Ridge, South Atlantic Ocean. *J. Petrolog.* 43 (8), 1435–1467. doi: 10.1093/petrology/43.8.1435

Gallant, R. M., and Von Damm, K. L. (2006). Geochemical Controls on Hydrothermal Fluids From the Kairei and Edmond Vent Fields, 23°-25°S, Central Indian Ridge. *Geochem. Geophys. Geosyst.* 7 (6), 1–24. doi: 10.1029/2005GC001067

German, C. R., Livermore, R. A., Baker, E. T., Bruguier, N. I., Connelly, D. P., Cunningham, A. P., et al. (2000). Hydrothermal Activity on the East Scotia Ridge: An Isolated High-Latitude Back-Ark Spreading Centre. *Earth Planet. Sci. Lett.*, 184(1) 241–250. doi: 10.1016/S0012-821X(00)00319-8

Giggenbach, W. F. (1992). Isotopic Shifts in Waters From Geothermal and Volcanic Systems Along Convergent Plate Boundaries and Their Origin. *Earth Planet. Sci. Lett.* 113 (4), 495–510. doi: 10.1016/0012-821X(92)90127-H

Haar, L. (1984). NBS/NRC Steam Tables. CRC Press

Haar, V. L., Gallagher, J. S., and Kell, G. S. (1985). NBS/NRC Steam Tables. *Chem. Ing. Tech.* 57, 812–812. doi: 10.1002/cite.330570931

Hedenquist, J. W., and Lowenstern, J. B. (1994). The Role of Magmas in the Formation of Hydrothermal Ore Deposits. *Nature* 370 (August), 519–527. doi: 10.1038/370519a0

Herrera, S., Watanabe, H., and Shank, T. M. (2015). Evolutionary and Biogeographical Patterns of Barnacles From Deep-Sea Hydrothermal Vents. *Mol. Ecol.* 24 (3), 673–689. doi: 10.1111/mec.13054

Holloway, J. R., and Blank, J. G. (1994). "Application of Experimental Results to C-O-H Species in Natural Melts," in *Rev. Mineral Geochem*. 30 (1), 187–230

Horita, J., Cole, D. R., and Wesolowski, D. J. (1995). The Activity-Composition Relationship of Oxygen and Hydrogen Isotopes in Aqueous Salt Solutions: Iii. Vapor-Liquid Water Equilibration of NaCl Solutions to 350°C. *Geochim. Cosmochim. Acta* 59 (6), 1139–1151. doi: 10.1016/0016-7037(95)00031-T

Ishibashi, J., and Urabe, T. (1995). Hydrothermal Activity Related to Arc-Backarc Magmatism in the Western Pacific. In: Backarc Basins. Boston, MA: Springer, 451–495. doi: 10.1007/978-1-4615-1843-3_13

James, R. H., Green, D. R. H., Stock, M. J., Alker, B. J., Banerjee, N. R., Cole, C., et al. (2014). Composition of Hydrothermal Fluids and Mineralogy of Associated Chimney Material on the East Scotia Ridge Back-Arc Spreading Centre. *Geochim. Cosmochim. Acta* 139, 47–71. doi: 10.1016/j.gca.2014.04.024

Janecky, D. R., and Seyfried, W. E. (1984). Formation of Massive Sulfide Deposits on Oceanic Ridge Crests: Incremental Reaction Models for Mixing Between Hydrothermal Solutions and Seawater. *Geochim. Cosmochim. Acta* 48 (12), 2723–2738. doi: 10.1016/0016-7037(84)90319-3

Javoy, M., Pineau, F., and Iiyama, I. (1978). Experimental Determination of the Isotopic Fractionation Between Gaseous CO_2 and Carbon Dissolved in Tholeiitic Magma. *Contrib. Mineral. Petrol.* 67 (1), 35–39. doi: 10.1007/BF00371631

Johnson, J. W., Oelkers, E. H., and Helgeson, H. C. (1992). Supcrt92: A Software Package for Calculating the Standard Molal Thermodynamic Properties of Minerals, Gases, Aqueous Species, and Reactions From 1 to 5000 Bar and 0 to 1000°C. *Comput. Geosci.* Vol. 18 (7), pp.899–947. doi: 10.1016/0098-3004(92)90029-Q

Kelley, D. S. (1996). Methane-Rich Fluids in the Oceanic Crust. *J. Geophys. Res. B.: Solid. Earth* 101 (2), 2943–2962. doi: 10.1029/95JB02252

Kelley, D. S., and Früh-Green, G. L. (1999). Abiogenic Methane in Deep-Seated Mid-Ocean Ridge Environments: Insights From Stable Isotope Analyses. *J. Geophys. Res.: Solid. Earth* 104 (B5), 10439–10460. doi: 10.1029/1999jb900058

Klein, F., Grozeva, N. G., and Seewald, J. S. (2019). Abiotic Methane Synthesis and Serpentinization in Olivine-Hosted Fluid Inclusions. *Proc. Natl. Acad. Sci. Unite. States America* 116 (36), 17666–17672. doi: 10.1073/pnas.1907871116

Kuhn, T., Herzig, P. M., Hannington, M. D., Garbe-Schönberg, D., and Stoffers, P. (2003). Origin of Fluids and Anhydrite Precipitation in the Sediment-Hosted Grimsey Hydrothermal Field North of Iceland. *Chem. Geolog.* 202 (1–2), 5–21. doi: 10.1016/S0009-2541(03)00207-9

Larter, R. D., Vanneste, L. E., Morris, P., and Smythe, D. K. (2003). Structure and Tectonic Evolution of the South Sandwich Arc. *Geolog. Soc. Special. Publ.* 219 (1), 255–284. doi: 10.1144/GSL.SP.2003.219.01.13

Leat, P. T., Fretwell, P. T., Tate, A. J., Larter, R. D., Martin, T. J., Smellie, J. L, et al (2016). Bathymetry and Geological Setting of the South Sandwich Islands Volcanic Arc.. *Antarct. Sci* 28 (4), 293–303

Leat, P. T., Livermore, R. A., Millar, I. L., and Pearce, J. A. (2000). Magma Supply in Back-Arc Spreading. *J. Petrolog.* 41 (6), 845–866. doi: 10.1093/petrology/41.6.845

Leat, P. T., Pearce, J. A., Barker, P. F., Millar, I. L., Barry, T. L., and Larter, R. D. (2004). Magma Genesis and Mantle Flow at a Subducting Slab Edge : The South Sandwich Arc-Basin System. *Earth Planet. Sci. Lett.* 227, 17–35. doi: 10.1016/j.epsl.2004.08.016

Linse, K., Copley, J. T., Connelly, D. P., Larter, R. D., Pearce, D. A., Polunin, N. V. C., et al. (2019). Fauna of the Kemp Caldera and Its Upper Bathyal Hydrothermal Vents (South Sandwich Arc, Antarctica). *R. Soc. Open Sci.* 6, (11). doi: 10.1098/rsos.191501

Livermore, R., Cunningham, A., Vanneste, L., and Larter, R. (1997). Subduction Influence on Magma Supply at the East Scotia Ridge. *Earth Planet. Sci. Lett.* 150 (3–4), 261–275. doi: 10.1016/s0012-821x(97)00074-5

Lupton, J., Butterfield, D., Lilley, M., Evans, L., Nakamura, K. I., Chadwick, W., et al. (2006). Submarine Venting of Liquid Carbon Dioxide on a Mariana Arc Volcano. *Geochem. Geophys. Geosyst.* 7, (8). doi: 10.1029/2005GC001152

Mattey, D. P. (1991). Carbon Dioxide Solubility and Carbon Isotope Fractionation in Basaltic Melt. *Geochim. Cosmochim. Acta* 55 (11), 3467–3473. doi: 10.1016/0016-7037(91)90508-3

Mattey, D. P., Carr, R. H., Wright, I. P., and Pillinger, C. T. (1984). Carbon Isotopes in Submarine Basalts. *Earth Planet. Sci. Lett.* 70 (2), 196–206. doi: 10.1016/0012-821X(84)90005-0

McCollom, T. M. (2007). Geochemical Constraints on Sources of Metabolic Energy for Chemolithoautotrophy in Ultramafic-Hosted Deep-Sea Hydrothermal Systems. *Astrobiology* 7 (6), 933–950. doi: 10.1089/ast.2006.0119

McCollom, T. M., and Shock, E. L. (1997). Geochemical Constraints on Chemolithoautotrophic Metabolism by Microorganisms in Seafloor Hydrothermal Systems. *Geochim. Cosmochim. Acta* 61 (20), 4375–4391. doi: 10.1016/S0016-7037(97)00241-X

McDermott, J. M., Ono, S., Tivey, M. K., Seewald, J. S., Shanks, W. C., and Solow, A. R. (2015a). Identification of Sulfur Sources and Isotopic Equilibria in Submarine Hot-Springs Using Multiple Sulfur Isotopes. *Geochim. Cosmochim. Acta* 160, 169–187. doi: 10.1016/j.gca.2015.02.016

McDermott, J. M., Seewald, J. S., German, C. R., and Sylva, S. P. (2015b). Pathways for Abiotic Organic Synthesis at Submarine Hydrothermal Fields. *Proc. Natl. Acad. Sci. Unite. States America* 112 (25), 7668–7672. doi: 10.1073/pnas.1506295112

McDermott, J. M., Sylva, S. P., Ono, S., German, C. R., and Seewald, J. S. (2018). Geochemistry of Fluids From Earth's Deepest Ridge-Crest Hot-Springs: Piccard Hydrothermal Field, Mid-Cayman Rise. *Geochim. Cosmochim. Acta* 228, 95–118. doi: 10.1016/j.gca.2018.01.021

McDermott, J. M., Sylva, S. P., Ono, S., German, C. R., and Seewald, J. S. (2020). Abiotic Redox Reactions in Hydrothermal Mixing Zones: Decreased Energy Availability for the Subsurface Biosphere. *Proc. Natl. Acad. Sci.*, 117 (34), 20453–20461. doi: 10.1073/pnas.2003108117

Merlivat, L., Pineau, F., and Javoy, M. (1987). Hydrothermal Vent Waters at 13°N on the East Pacific Rise: Isotopic Composition and Gas Concentration. *Earth Planet. Sci. Lett.* 84 (1), 100–108. doi: 10.1016/0012-821X(87)90180-4

Mottl, M. J., and Holland, H. D. (1978). Chemical Exchange During Hydrothermal Alteration of Basalt by Seawater-I. Experimental Results for Major and Minor Components of Seawater. *Geochim. Cosmochim. Acta* 42 (8), 1103–1115. doi: 10.1016/0016-7037(78)90107-2

Mottl, M. J., Seewald, J. S., Wheat, C. G., Tivey, M. K., Michael, P. J., Proskurowski, G., et al. (2011). Chemistry of Hot Springs Along the Eastern Lau Spreading Center. *Geochim. Cosmochim. Acta* 75 (4), 1013–1038. doi: 10.1016/j.gca.2010.12.008

Ohmoto, H. (1986). "Stable Isotope Geochemistry of Ore Deposits." in Stable Isotopes in High Temperature Geological Processes De Gruyter. 491–560. doi: 10.1515/9781501508936-019

Pape, T., Bünz, S., Hong, W. L., Torres, M. E., Riedel, M., Panieri, G., et al. (2020a). Origin and Transformation of Light Hydrocarbons Ascending at an Active Pockmark on Vestnesa Ridge, Arctic Ocean. *J. Geophys. Res.: Solid. Earth* 125, (1). doi: 10.1029/2018JB016679

Pape, T., Haeckel, M., Riedel, M., Kölling, M., Schmidt, M., Wallmann, K., et al. (2020b). Formation Pathways of Light Hydrocarbons in Deep Sediments of the Danube Deep-Sea Fan, Western Black Sea. *Mar. Petrol. Geolog.* 122, 104627. doi: 10.1016/j.marpetgeo.2020.104627

Pester, N. J., Reeves, E. P., Rough, M. E., Ding, K., Seewald, J. S., and Seyfried, W. E. (2012). Subseafloor Phase Equilibria in High-Temperature Hydrothermal Fluids of the Lucky Strike Seamount (Mid-Atlantic Ridge, 37°17'n). *Geochim. Cosmochim. Acta* 90, 303–322. doi: 10.1016/j.gca.2012.05.018

Peter, J.M., and Scott, S. D. (1988). Mineralogy, Composition, and Fluid Inclusion Microthermometry of Sea-Floor Hydrothermal Deposits in the Southern Trough of Guaymas Basin, Gulf of California. *Can. Mineral.* 26(3)567–587

Proskurowski, G., Lilley, M. D., and Olson, E. J. (2008). Stable Isotopic Evidence in Support of Active Microbial Methane Cycling in Low-Temperature Diffuse Flow Vents at 9°50′N East Pacific Rise. *Geochim. Cosmochim. Acta* 72 (8), 2005–2023. doi: 10.1016/j.gca.2008.01.025

Rees, C. E., Jenkins, W. J., and Monster, J. (1978). The Sulphur Isotopic Composition. *Geochim. Cosmochim. Acta* 42 (65), 377–381. doi: 10.1016/0016-7037(78)90268-5

Reeves, E. P., and Fiebig, J. (2020). Abiotic Synthesis of Methane and Organic Compounds in Earth's Lithosphere. *Elements: An Int. Magaz of Mineral., Geochem., and Petrol.*. 16(1), pp.25–31.doi: 10.2138/gselements.16.1.25

Reeves, E. P., Seewald, J. S., Saccocia, P., Bach, W., Craddock, P., Shanks, W. C., et al. (2011). Geochemistry of Hydrothermal Fluids From the PACMANUS, Northeast Pual and Vienna Woods Hydrothermal Fields, Manus Basin, Papua New Guinea. *Geochim. Cosmochim. Acta* 75 (4), 1088–1123. doi: 10.1016/j.gca.2010.11.008

Roedder, E. (1984). *"Introduction to Fluid Inclusions." Reviews in Mineralogy, Volume 12: Fluid Inclusions* (Mineralogical Society of America).

Rogers, A. D., Tyler, P. A., Connelly, D. P., Copley, J. T., James, R., Larter, R. D., et al. (2012). The Discovery of New Deep-Sea Hydrothermal Vent Communities in the Southern Ocean and Implications for Biogeography. *PloS Biol.* 10 (1),e1001234. doi: 10.1371/journal.pbio.1001234

Ryan, J. G., and Langmuir, C. H. (1987). The Systematics of Lithium Abundances in Young Volcanic Rocks. *Geochim. Cosmochim. Acta* 51 (6), 1727–1741. doi: 10.1016/0016-7037(87)90351-6

Sakai, H., Des Marais, D. J., Ueda, A., and Moore, J. G. (1984). Concentrations and Isotope Ratios of Carbon, Nitrogen and Sulfur in Ocean-Floor Basalts. *Geochim. Cosmochim. Acta* 48 (12), 2433–2441. doi: 10.1016/0016-7037(84)90295-3

Scheuermann, P. P., Tutolo, B. M., and Seyfried, W. E. (2019). Anhydrite Solubility in Low-Density Hydrothermal Fluids: Experimental Measurements and Thermodynamic Calculations. *Chem. Geolog.* 524 (June), 184–195. doi: 10.1016/j.chemgeo.2019.06.018

Schmidt, K., Garbe-Schönberg, D., Bau, M., and Koschinsky, A. (2010). Rare Earth Element Distribution in <400°C Hot Hydrothermal Fluids From 5°S, MAR: The Role of Anhydrite in Controlling Highly Variable Distribution Patterns. *Geochim. Cosmochim. Acta* 74 (14), 4058–4077. doi: 10.1016/j.gca.2010.04.007

Seewald, J. S., Doherty, K. W., Hammar, T. R., and Liberatore, S. P. (2002). Instruments and Methods A New Gas-Tight Isobaric Sampler for Hydrothermal Fluids. *Deep-Sea. Res. I.* 49, 189–196. doi: 10.1016/S0967-0637(01)00046-2

Seewald, J. S., Reeves, E. P., Bach, W., Saccocia, P. J., Craddock, P. R., Shanks, W. C., et al. (2015). Submarine Venting of Magmatic Volatiles in the Eastern Manus Basin, Papua New Guinea. *Geochim. Cosmochim. Acta* 163, 178–199. doi: 10.1016/j.gca.2015.04.023

Seewald, J. S., Reeves, E. P., Bach, W., Saccocia, P. J., Craddock, P. R., Walsh, W., et al. (2019). Geochemistry of Hot-Springs at the SuSu Knolls Hydrothermal Field, Eastern Manus Basin: Advanced Argillic Alteration and Vent Fluid Acidity. *Geochim. Cosmochim. Acta* 255, 25–48. doi: 10.1016/j.gca.2019.03.034

Seewald, J. S., and Seyfried, W. E. (1990). The Effect of Temperature on Metal Mobility in Subseafloor Hydrothermal Systems: Constraints From Basalt Alteration Experiments. *Earth Planet. Sci. Lett.* 101 (2–4), 388–403. doi: 10.1016/0012-821X(90)90168-W

Seewald, J. S., Seyfried, W. E., and Shanks, W. C. (1994). Variations in the Chemical and Stable Isotope Composition of Carbon and Sulfur Species During Organic-Rich Sediment Alteration: An Experimental and Theoretical Study of Hydrothermal Activity at Guaymas Basin, Gulf of California. *Geochim. Cosmochim. Acta* 58 (22), 5065–5082. doi: 10.1016/0016-7037(94)90232-1

Seyfried, W. E., and Ding, K. (1995). "Phase Equilibria in Subseafloor Hydrothermal Systems: A Review of the Role of Redox, Temperature, PH and Dissolved Cl on the Chemistry of Hot Spring Fluids at Mid-Ocean Ridges," in *Geophy. Monogr. Ser.* 248–272. doi: 10.1029/GM091p0248.

Seyfried, W. E., Ding, K., and Berndt, M. E. (1991). Phase Equilibria Constraints on the Chemistry of Hot Spring Fluids at Mid-Ocean Ridges. *Geochim. Cosmochim. Acta* 55 (12), 3559–3580. doi: 10.1016/0016-7037(91)90056-B

Seyfried, W. E., Janecky, D. R., and Mottl, M. J. (1984). Alteration of the Oceanic Crust: Implications for Geochemical Cycles of Lithium and Boron. *Geochim. Cosmochim. Acta* 48 (3), 557–569. doi: 10.1016/0016-7037(84)90284-9

Seyfried, W. E., Seewald, J. S., Berndt, M. E., Ding, K., and Foustoukos, D. I. (2003). Chemistry of Hydrothermal Vent Fluids From the Main Endeavour Field, Northern Juan De Fuca Ridge: Geochemical Controls in the Aftermath of June 1999 Seismic Events. *J. Geophys. Res.: Solid. Earth* 108 (B9), 1–23. doi: 10.1029/2002jb001957

Shanks, W. C. (2001). Stable Isotopes in Seafloor Hydrothermal Systems. *Rev. Mineral. Geochem.* 43, 469–526. doi: 10.2138/gsrmg.43.1.469

Shanks, W. C., Böhlke, J. K., and Seal, R. R. (1995). Stable Isotopes in Mid-Ocean Ridge Hydrothermal Systems: Interactions between Fluids, Minerals, and Organisms. *Geophys. Monogr. Ser.* 91), 194–221. doi: 10.1029/GM091p0194

Shmulovich, K. I., Landwehr, D., Simon, K., and Heinrich, W. (1999). Stable Isotope Fractionation between Liquid and Vapour in Water-Salt Systems up to 600°C. *Chem. Geolog.* 157 (3–4), 343–354. doi: 10.1016/S0009-2541(98)00202-2

Takai, K., Nunoura, T., Ishibashi, J. I., Lupton, J., Suzuki, R., Hamasaki, H., et al. (2008). Variability in the Microbial Communities and Hydrothermal Fluid Chemistry at the Newly Discovered Mariner Hydrothermal Field, Southern Lau Basin. *J. Geophys. Res.: Biogeosci.* 113 (G2). doi: 10.1029/2007JG000636

Taylor, B. (1979). Bismarck Sea: Evolution of a Back-Arc Basin. *Geology* 7 (4), 171–174. doi: 10.1130/0091-7613(1979)7<171:BSEOAB>2.0.CO;2

Taylor, B. E. (1986). "Magmatic Volatiles: Isotopic Variation of C, H, and S.", in *Stable Isotopes in High Temperature Geological Processes*. 16 (1), 185–225

Taylor, H. (1997). "Oxygen and Hydrogen Isotope Relationships in Hydrothermal Mineral Deposits.", in *Geochemistry of Hydrothermal Ore Deposits*.229–302

Toki, T., Itoh, M., Iwata, D., Ohshima, S., Shinjo, R., Ishibashi, J. I., et al. (2016). Geochemical Characteristics of Hydrothermal Fluids at Hatoma Knoll in the Southern Okinawa Trough. *Geochem. J.* 50 (6), 493–525. doi: 10.2343/geochemj.2.0449

Tyler, P. A. (2012). RRS James Cook cruise JC80, 2nd Dec-30 Dec 2012. The East Scotia Ridge and Kemp Seamount Caldera, Cruise 4 of the NERC Consortium Grant 'Chemosynthetically driven ecosystems in the Southern Ocean. *Ecology and Biogeography' (ChEsSo)* (Southampton, UK: National Oceanography Centre Southampton).

Vanko, D. A., and Bach, W. (2005). Heating and Freezing Experiments on Aqueous Fluid Inclusions in Anhydrite: Recognition and Effects of Stretching and the Low-Temperature Formation of Gypsum. *Chem. Geolog.* 223 (1–3), 35–45. doi: 10.1016/j.chemgeo.2004.11.021

Vityk, M. O., Bodnar, R. J., and Schmidt, C. S. (1994). Fluid Inclusions as Tectonothermobarometers: Relation between Pressure-Temperature History and Reequilibration Morphology during Crustal Thickening. *Geology* 22 (8), 731–734. doi: 10.1130/0091-7613(1994)022<0731:FIATRB>2.3.CO;2

Von Damm, K. L., Bischoff, J. L., and Rosenbauer, R. J. (1991). Quartz Solubility in Hydrothermal Seawater: An Experimental Study and Equation Describing Quartz Solubility for up to 0.5 M NaCl Solutions. *Am. J. Sci* 291(10), pp.977–1007.. doi: 10.2475/ajs.291.10.977

Von Damm, K. L. (1990). Seafloor Hydrothermal Activity: Black Smoker Chemistry and Chimneys. *Annu. Rev. Earth Planet. Sci.* 18, 173–204. doi: 10.1146/annurev.ea.18.050190.001133

Von Damm, K. L. (1995) Controls on the Chemistry and Temporal Variability of Seafloor Hydrothermal Fluids. *Seafloor Hydrothermal Systems: Physical, Chemical, Biological, and Geological Interactions* 91, 222–247.

Von Damm, K. L., Edmond, J. M., Grant, B., Measures, C. I., Walden, B., and Weiss, R. F. (1985a). Chemistry of Submarine Hydrothermal Solutions at 21 ° N, East Pacific Rise. *Geochim. Cosmochim. Acta* 49 (11), 2197–2220. doi: 10.1016/0016-7037(85)90222-4

Von Damm, K. L., Edmond, J. M., Measures, C. I., and Grant, B. (1985b). Chemistry of Submarine Hydrothermal Solutions at Guaymas Basin, Gulf of California. *Geochim. Cosmochim. Acta* 49 (11), 2221–2237. doi: 10.1016/0016-7037(85)90223-6

Von Damm, K. L., Lilley, M. D., Shanks Iii, W. C., Brockington, M., Bray, A. M., O'Grady, K. M., et al. (2003). Extraordinary Phase Separation and Segregation in Vent Fluids from the Southern East Pacific Rise. *Earth Planet. Sci. Lett.* 206 (3–4), 365–378. doi: 10.1016/S0012-821X(02)01081-6

Von Damm, K. L., Parker, C. M., Zierenberg, R. A., Lilley, M. D., Olson, E. J., Clague, D. A., et al. (2005). The Escanaba Trough, Gorda Ridge Hydrothermal System: Temporal Stability and Subseafloor Complexity. *Geochim. Cosmochim. Acta* 69 (21), 4971–4984. doi: 10.1016/j.gca.2005.04.018

Wang, D. T., Reeves, E. P., McDermott, J. M., Seewald, J. S., and Ono, S. (2018). Clumped Isotopologue Constraints on the Origin of Methane at Seafloor Hot Springs. *Geochim. Cosmochim. Acta* 223, 141–158. doi: 10.1016/j.gca.2017.11.030

Welhan, J. A. (1988). Origins of Methane in Hydrothermal Systems. *Chem. Geolog.* 71 (1–3), 183–198. doi: 10.1016/0009-2541(88)90114-3

Welhan, J. A., and Craig, H. (1983). "Methane, Hydrogen and Helium in Hydrothermal Fluids at 21°N on the East Pacific Rise.", in *Hydrothermal Processes at Seafloor Spreading Centers*. Boston, MA: Springer). 391–409. doi: 10.1007/978-1-4899-0402-7_17.

Xu, G. (2000). Fluid Inclusions with NaCl-$CaCl_2$-H_2O Composition from the Cloncurry Hydrothermal System, NW Queensland, Australia. *Lithos* 53 (1), 21–35. doi: 10.1016/S0024-4937(00)00008-6

Yang, K., and Scott, S. D. (2006). Magmatic Fluids as a Source of Metals in Arc/Back-Arc Hydrothermal Systems: Evidence from Melt Inclusions and Vesicles. *Back. Arc. Spread. Syst.: Geolog. Biologic. Chem. Phys. Interact. Geophys.* 1), 163–184.

Conflict of Interest: The authors declare that the research was conducted in the absence of any commercial or financial relationships that could be construed as a potential conflict of interest.

Publisher's Note: All claims expressed in this article are solely those of the authors and do not necessarily represent those of their affiliated organizations, or those of the publisher, the editors and the reviewers. Any product that may be evaluated in

this article, or claim that may be made by its manufacturer, is not guaranteed or endorsed by the publisher.

frontiers | Frontiers in Marine Science

ORIGINAL RESEARCH
published: 20 June 2022
doi: 10.3389/fmars.2022.903748

Anatomy and Symbiosis of the Digestive System of the Vent Shrimp *Rimicaris Exoculata* and *Rimicaris Chacei* Revealed Through Imaging Approaches

Marion Guéganton, Ouafae Rouxel, Lucile Durand, Valérie Cueff-Gauchard, Nicolas Gayet, Florence Pradillon and Marie-Anne Cambon-Bonavita *

Univ Brest, Ifremer, CNRS, Unité Biologie des Environnements Extrêmes marins Profonds, F-29280, Plouzané, France

OPEN ACCESS

Edited by:
Pei-Yuan Qian, Hong Kong University of Science and Technology, Hong Kong, SAR China

Reviewed by:
Maeva Perez, Université de Montréal, Montreal
Suzanne Dufour, Memorial University of Newfoundland, Canada

***Correspondence:**
Marie-Anne Cambon-Bonavita
Marie.Anne.Cambon@ifremer.fr

Specialty section:
This article was submitted to Deep-Sea Environments and Ecology, a section of the journal Frontiers in Marine Science

Received: *24 March 2022*
Accepted: *23 May 2022*
Published: *20 June 2022*

Citation:
Guéganton M, Rouxel O, Durand L, Cueff-Gauchard V, Gayet N, Pradillon F and Cambon-Bonavita M-A (2022) Anatomy and Symbiosis of the Digestive System of the Vent Shrimp Rimicaris Exoculata and Rimicaris Chacei Revealed Through Imaging Approaches. Front. Mar. Sci. 9:903748. doi: 10.3389/fmars.2022.903748

The shrimp *Rimicaris exoculata* and *Rimicaris chacei* are visually dominant fauna co-occurring at deep-sea hydrothermal sites of the Mid-Atlantic Ridge (MAR). Their co-existence was related to contrasted life-history traits, including differences in their diet and reliance on chemoautotrophic symbionts at the adult stage. Both species of shrimp are colonized by diversified chemosynthetic symbiotic microbial communities in their cephalothoracic cavity. Symbiotic association with bacteria was also evidenced in their digestive system, and the major lineages were identified through sequencing (with Mycoplasmatales in the foregut and Deferribacteres in the midgut) but their precise distribution within each host species was not assessed. For the first time, we used Fluorescence *in situ* Hybridization (FISH) to visualize these lineages and describe their association with digestive structures of their host. The aim of the study was to identify possible differences between host species that could be related to their different life-history traits. For this purpose, we developed new specific FISH probes targeting Deferribacteres and Mycoplasmatales lineages identified in the digestive system of these shrimp. Our FISH results showed a partitioning of the bacterial lineages according to the digestive organ corroborating sequencing data, and highlighted their association with specific anatomical structures. Despite morphological differences between the foreguts of *R. exoculata* and *R. chacei* that could be related to the adult diet, our FISH results showed overall similar distribution of digestive symbionts for the two host species. However, a more comprehensive study is needed with specimens at different life or molt stages to reveal potential host specific patterns. Such comparisons are now possible thanks to our newly designed FISH probes. The tools used in our study are valuable for tracking symbiont lineages in the environment, allowing a better understanding of their relationship with their host along its life cycle, including their acquisition mechanisms.

Keywords: *Rimicaris*, digestive-symbiosis, Deferribacteres, Mycoplasmatales, microscopy, FISH-probes, foregut, midgut

INTRODUCTION

Living communities thriving at deep-sea hydrothermal vents are fueled by chemosynthesis performed by microorganisms that are either free-living or forming associations with protists or metazoan hosts (Kouris et al., 2007; Dubilier et al., 2008; Sogin et al., 2021). These associations are called holobionts (Zilber-Rosenberg and Rosenberg, 2008) and dominate vent biomass near fluid exits, such as *Rimicaris* caridean shrimp along the Mid-Atlantic Ridge (MAR).

Rimicaris exoculata and *Rimicaris chacei* (Williams and Rona, 1986) co-occur at the active vents of many MAR sites (Zbinden and Cambon Bonavita, 2020) (**Figure 1A**). *R. exoculata* live in dense aggregations near the emitted fluids, and are therefore exposed to high temperatures and high concentrations of toxic compounds such as heavy metals or minerals (Schmidt et al., 2008a; Schmidt et al., 2008b) (**Figure 1B**). Juveniles of *R. exoculata* also occur within these aggregations or adjacent to them (Hernández-Ávila et al., 2021; Methou et al., 2022). *R. chacei* shrimp live nearby *R. exoculata* aggregations, sometimes observed hiding in crevices under rocks, or behind mussels (Methou et al., 2022). They can occasionally form small aggregations. However, *R. chacei* adults are much less abundant than R. *exoculata* adults, while numerous juveniles of *R. chacei* live in nurseries at TAG and Snake Pit (Methou et al., 2020; Hernández-Ávila et al., 2021) suggesting that the relatively low adult number results from a population collapse during the recruitment process of this species (Methou et al., 2022). Such a drop in abundance between life stages does not seem to exist for *R. exoculata*, and raises questions on the possible underlying mechanisms. The acquisition of symbiotic communities throughout each species's recruitment process may play a major role in holobiont fitness (Methou et al., 2022).

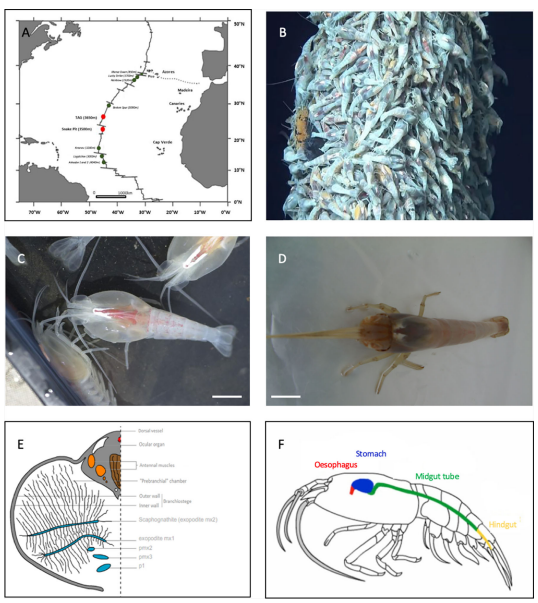

FIGURE 1 | Study models. **(A)** Two main study sites on the MAR: TAG and Snake Pit. **(B)** *Rimicaris exoculata* aggregations on a hydrothermal vent at the TAG site (Nautile-BICOSE2, 2018). **(C)** Adult *Rimicaris exoculata*. **(D)** Adult *Rimicaris chacei*. **(E)** Transversal section of half of the cephalothoracic cavity of *R. exoculata* (adapted from Segonzac et al., 1993). **(F)** Digestive system of *Rimicaris* spp. (adapted from Durand et al., 2009).

In adulthood, *R. exoculata* stands out from other vent shrimp through its enlarged cephalothoracic cavity (**Figure 1C**), enclosing hypertrophied mouthparts (scaphognathites and exopodites) (Van Dover et al., 1988; Segonzac et al., 1993; Komaï and Segonzac, 2008) (**Figures 1C, E**). In contrast, *R. chacei* have a narrower cephalothoracic cavity with the first two pairs of chelipeds remaining visible and functional (Casanova et al., 1993; Segonzac et al., 1993) as well as less hypertrophied mouthparts than *R. exoculata* (Apremont et al., 2018) (**Figure 1D**). These morphological differences may be related to the level of development of the symbiotic bacterial communities, where more abundant communities are observed along with hypertrophied head organs of *R. exoculata* (Segonzac et al., 1993). This cephalothoracic community is dominated by Campylobacteria and Gammaproteobacteria together with other lineages (between 10-30% depending on specimens) (for review see Zbinden and Cambon, 2020).

These microbial mats are cleared, together with the minerals and the cuticle at each molt event (every 10 days for *R. exoculata* – Corbari et al., 2008). In *R. exoculata*, these symbiotic communities play a major trophic role through direct transcuticular transfer of chemosynthetic organic matter to their host (Ponsard et al., 2013). However, chelipeds of *R. chacei* are functional which, together with isotopic data, suggest a mixotrophic regime based on bacteriotrophy, scavenging and symbiosis (Casanova et al., 1993; Apremont et al., 2018).

Rimicaris shrimp also host microbial communities in their digestive system, but the lack of detailed anatomical knowledge prevents a good understanding of the morphological and functional relationships between microbes and their host. The description of the digestive system anatomy has to be better documented. As in other decapods (Vogt, 2021), the digestive system of *R. exoculata* and *R. chacei* comprises three regions: the foregut, the midgut and the hindgut (**Figure 1F**). In farmed shrimp (such as *Penaeus monodon* or*Macrobrachium carcinus*), the foregut is a complex organ because of its numerous internal features allowing crushing and filtration of digested particles (Ceccaldi, 1989; Lima et al., 2016; Štrus et al., 2019). The foregut comprises the œsophagus and the stomach, while the hindgut is the terminal excretion zone located at the end of the abdomen (Vogt, 2021). These two regions have an ectodermic origin and are lined by a cuticle, which is exuviated during the molt. The third region linking the two others is the midgut, comprising the hepatopancreas and the midgut tube (Vogt, 2021). Contrary to the hindgut or the foregut, the midgut is devoid of a cuticle due to its endodermic origin, and therefore does not molt.

The digestive system of *R. exoculata* seems modified in comparison to other crustaceans (Ceccaldi, 1989; Komai and Segonzac, 2008; Lima et al., 2016). The foregut and hindgut are reduced (the stomach being a single and rather small cavity),

while the midgut tube is long (Segonzac et al., 1993; Komaï and Segonzac, 2008; Durand et al., 2009) (**Figure 1F**). In contrast, the stomach of *R. chacei* is larger and looks similar to that of other caridean shrimp (Segonzac et al., 1993; Komai and Segonzac, 2008; Apremont et al., 2018). This is in agreement with a mixotrophic diet involving both symbiosis and scavenging (Casanova et al., 1993; Segonzac et al., 1993; Gebruk et al., 1997; Gebruk et al., 2000; Apremont et al., 2018; Methou et al., 2020). The alimentary bolus of *R. exoculata*, *i.e.* particles ingested by the mouth, passing through the foregut and midgut tube and expulsed by the hindgut as feces after digestion processes, is mainly composed of minerals: iron sulphides and oxides, phosphate and calcium sulphate at different stages of oxidation, as well as some cuticle debris from molts (Segonzac et al., 1993). The alimentary bolus of *R. chacei* seems to differ: in addition to minerals and cuticle debris, organic waste and debris can be found (Casanova et al., 1993; Apremont et al., 2018).

Using 16S rDNA approaches (PCR-cloning), two microbial communities were identified in the digestive system of both shrimp species (**Figure 1F**) (Durand et al., 2009; Durand et al., 2015; Apremont et al., 2018). The foregut community is mainly composed of Mycoplasmatales (Firmicutes-Bacilli) while Deferribacteres are housed in the midgut tube. Fluorescent *in situ* Hybridization (FISH), Scanning Electron Microscopy (SEM) and Transmission Electron Microscopy (TEM) approaches have been used to observe the symbiont lineages. In the midgut tube, long thin "spaghetti-like" bacterial cells inserted between the microvilli of epithelial cells were observed but could not be affiliated to any bacterial lineages identified through sequencing as only the universal bacterial probe Eub338 gave a positive FISH signal (Durand et al., 2009; Durand et al., 2015; Apremont et al., 2018). Morphologically, they do not resemble described Deferribacteres species, which are usually small curved rods (Garrity et al., 2001). The closest relative of Deferribacteres lineage from the midgut tube of *Rimicaris* spp. is *Mucispirillum schaedleri*, isolated from rodent digestive mucus layer (Robertson et al., 2005). The location of the Mycoplasmatales is still unclear. Mycoplasmatales are heterotrophic wall-less bacterial cells usually having a reduced genome (Tully et al., 1993). The closest relatives of *Rimicaris* spp. Mycoplasmatales were identified in the hepatopancreas of the terrestrial isopod *Porcellio scaber*, appearing mostly as amorphous coccoid cells (Wang et al., 2004). In *R. exoculata*, the different microbial lineages retrieved in the digestive system seem to be resident symbionts still present after 72 hours of fasting, which empties the digestive system (Durand et al., 2009). However, microbial communities in the foregut must be cleared out regularly due to molt, contrary to those in the midgut tube. Inter-molt and inter-generation transmission of lineages affiliated to Mycoplasmatales and Deferribacteres remain enigmatic, as are their potential roles. Only one Mycoplasmatales affiliated OTU, but no Deferribacteres (Hügler et al., 2010; Flores et al., 2011; Durand et al., 2015; Cowart et al., 2017) was identified from the shrimp's environment. The level of similarity between Deferribacteres 16S rDNA gene sequences, regardless of sampling site, is higher than 99%, suggesting a single phylotype, which suggests a vertical transmission (Durand et al., 2015). However, this lineage was not found in microbial communities associated with broods (Guri et al., 2012; Cowart et al., 2017; Methou et al., 2019), which would then rather indicate horizontal transmission.

The key questions related with the acquisition of symbionts at the juvenile stage and after each molt (transmission mode, key moments of acquisition, symbiotic evolution, relation between symbiosis and recruitment…), as well as the overall functioning of the digestive system and symbiont niche distribution in *Rimicaris* spp. are debated. To study acquisition and to infer their potential roles in the overall functioning of holobionts, it is first necessary to decipher symbiont niche distribution in the digestive system of adult shrimp. For this purpose, we first described *Rimicaris* spp. foregut anatomy through binocular microscopy and Scanning Electronic Microscopy (SEM). Then, we used fluorescent *in situ* hybridization (FISH) approaches with newly designed molecular probes targeting specific rRNA sequences of these digestive symbiotic lineages. These approaches allow both unaltered symbiotic cell visualization (morphology and localization on host organ/cells) and phylogenetic identification (Amann et al., 1990; Amann et al., 2001). To date, *in situ* observations of Deferribacteres and Mycoplasmatales lineages in *Rimicaris* spp. tissues have failed, as no specific molecular probe except the universal Eub338 bacterial probe has ever given a positive signal (Durand et al., 2009; Durand et al., 2015).

The combination of FISH approaches with SEM imaging of the digestive structures of both shrimp species was then used to answer the following questions: 1) What is the distribution and abundance of digestive symbiotic lineages in each *Rimicaris* species? 2) Is each symbiont lineage associated with a specific digestive structure in each host, possibly reflecting organ partitioning? 3) Can symbiont distribution and abundance in their respective host be related to specific ecological traits of the holobionts (e.g. nutrition type)?

MATERIALS AND METHODS

Sampling and Specimen Processing on Board

Samples were collected at two vent fields along the MAR: TAG (26°8 "N-44°50 "W, 3650 m depth) and Snake Pit (23°22 "N; 44° 57"W, 3460 m depth) during the BICOSE2 cruise (26 January to 10 March 2018, DOI http://dx.doi.org/10.17600/18000004). The specimens were caught in shrimp aggregations using the suction sampler of the HOV (Human Operated Vehicle) Nautile operated from the R/V *Pourquoi pas*?

Once on board, shrimp were dissected under sterile conditions to recover different anatomical parts: the branchiostegites (LB) and the scaphognathites (Sc) in the cephalothoracic cavity, and the digestive system comprising the foregut and the midgut tube. The different organs were

immediately fixed for FISH studies in a 3% formalin seawater solution for 3 hours to keep cell integrity. Samples were then rinsed three times with a phosphate buffered saline solution (PBS) and stored in a PBS/Ethanol (1:1) solution at -20°C (Durand et al., 2009). Some digestive tissues were fixed in a 2.5% glutaraldehyde solution (16 hours at 4°C), and then rinsed and stored at 4°C in a buffered solution containing a biocide to avoid bacterial development [filtrated seawater with 0,44 g/L of NaN_3 at pH 7.4] until use for scanning electron microscopy (SEM) observations. In addition, whole shrimp specimens were frozen at -80°C for later dissections at the laboratory (**Table 1**).

In Silico Design and Validation of New FISH Specific Probes

The FISH method is based on the use of specific molecular probes linked to a fluorescent dye, which are complementary to a region of the 16S or 23S rRNA target molecule, directly inside the native ribosomes of fixed microbial cells. We developed new probes that specifically target Mycoplasmatales symbiont lineages and the single Deferribacteres *Rimicaris* symbiont lineage found in *Rimicaris* (Durand et al., 2009; Durand et al., 2015). These probes were first designed *in silico*, based on the *Rimicaris* symbiont 16S rDNA sequences, obtained by PCR cloning approaches (Durand et al., 2009; Durand et al., 2015; Apremont et al., 2018). These sequences were aligned with the MUSCLE (MUltiple Sequence Comparison by Log- Expectation) algorithm (Edgar, 2004) in Geneious software v9 (Kearse et al., 2012). This software can be used to highlight homology and evolutionary relationships between sequences and thus, to select rRNA molecule regions specific to the digestive symbiont lineages. Literature data (Behrens et al., 2003) were used to select 16S rRNA molecule regions known to be accessible for probe hybridization. First, the 2D conformation of the rRNA was used to select potential zones for probe hybridization and to assess the potential for co-hybridization between two probes. The potential accessible regions are chosen to avoid 3D *in situ* conformations of the rRNA molecule or regions showing interactions with ribosomal proteins. Then, the physical properties of the designed probes were estimated to avoid hairpin structure formation, cross-hybridization, self-dimer formation, and to check their melting temperatures (T_M), using the Geneious Primer Design tool and the Oligo Calc software (Kibbe, 2007). Finally, the complementarity of these designed probes with rRNA gene sequences of non-targeted microorganisms was evaluated more broadly using BLAST (Altschul et al., 1990) with the Silva138 database (test probes v3.0).

Sample Preparation for Fluorescence *In Situ* Hybridization Procedures

Tissue sections were prepared by embedding dissected organs (foregut, midgut tube and scaphognathites) in polyethylene glycol distearate-1-hexadecanol (9: 1) resin (Sigma, St., Louis, MO) after progressive dehydration and immersion series (PBS – ethanol series at ambient temperature and ethanol – resin series at 40°C) (Duperron et al., 2007). After resin polymerization, blocks containing organs were stored at -20°C until trimming. Depending on the sample, 8-10 µm transversal tissue sections were obtained with a RM 2255 microtome (Leica Biosystems, Nussloch, Germany) and placed on slides (Menzel-Gläser Superfrost® Plus, USA). Before hybridization, resin was removed with ethanol (3x5min in 96% ethanol) and tissues were rehydrated (5 min in 70% ethanol).

Determination of Optimal Hybridization Conditions for New FISH Probes

After *in silico* validation, optimal probe hybridization conditions were determined using host tissues known to harbour (e.g. digestive) or lack (e.g. scaphognathites) these target symbiont lineages (**Table 1**). GAM42a targeting Gammaproteobacteria (Manz et al., 1992) and Epsy549 targeting Campylobacteria (Lin et al., 2006) were used as positive controls on scaphognathites (**Table 2**). The universal probe Eub338-I targeting most Eubacteria (Amann et al., 1990) was used as a general positive co-hybridization control (**Table 2**). All probes were synthesized by Eurofins Genomics (Ebersberg, Germany) and were labelled with either Cyanine 3 or Cyanine 5 dyes (**Table 2**).

Appropriate stringency conditions were determined using various combinations of 1) formamide concentrations in the hybridization buffer and 2) hybridization and washing temperatures, both of which act to denature, without altering, the ribosome structure, enabling effective probe hybridization. Sections were immersed in reaction mix containing probes (each at 0.5µM final concentration) in a hybridization buffer [0.9M NaCl, 0.02M Tris-HCl [pH 7.5], 0.01% [w/v] sodium dodecyl sulphate (SDS), 20%, 30%, 35%, 40%, 45% or 50% deionized formamide (**Table 3**)], and incubated for 3 hours at 46°C or 48°C (**Table 3**). Sections were briefly pre-rinsed and then were washed for 15 min or 30 min, at a slightly higher temperature (48°C or 50°C) than the hybridization temperature applied (**Table 3**), in a washing buffer adapted to the formamide concentrations [0.215M, 0.102M, 0.07M, 0.046M, 0.03M or 0.018M NaCl respectively for 20%, 30%, 35%, 40%, 45% or 50% formamide, 0.02M Tris-HCl [pH 7.5], 0.005M EDTA [pH 8] and 0.01% [w/v]

TABLE 1 | Samples selected for the different approaches: SEM, FISH and dissection under binocular microscope.

Vent fields	*Foregut*	*Midgut tube*	*Scaphognathites*
TAG	8 *R. exoculata* → FISH 1 *R. chacei* → FISH 2 *R. exoculata* and 1 *R. chacei* → anatomy	3 *R. exoculata* → FISH 1 *R. chacei* → FISH	1 *R. exoculata* → FISH
Snake Pit	10 *R. exoculata* → FISH 1 *R. chacei* → FISH 2 *R. exoculata* → SEM	2 *R. exoculata* → FISH 1 *R. chacei* → FISH	

TABLE 2 | Probes used for this study.

Phylotype	Probe	Sequence (5'-3')	Fluorochrome	Location (rRNA)	% Formamide	% Optimal Formamide	References
Gammaproteobacteria	GAM42a	GCCTTCCCACATCGTTT	Cy3/Cy5 (family cyanine)	1027 (23S)	20-30-40-50	30	(Manz et al., 1992).
Campylobacteria	Epsy549	CAGTGATTCCGAGTAACG	Cy5	549 (16S)	20-30-40-50	30	(Lin et al., 2006)
Eubacteria	Eub338	GCTGCCTCCCGTAGGAGT	Cy3/y5	338 (16S)	10-20-30-40	30	(Amann et al., 1990)
Deferribacteres	Def1229	GCCCTCTGTATAGTCCATTG	Cy3/Cy5	1229 (16S)	20-30-40-50	30	This study
Mycoplasmatales	Myco378-1	GTGGAAAATTCCCTACTGCTG	Cy3	378 (16S)	35-40-45-50	45	This study
Mycoplasmatales	Myco378-2	GTGAAAAATTCCCTACTGCTG	Cy3	378 (16S)	35-40-45-50	45	This study
Mycoplasmatales	Myco378-3	GCGAAAAATTCCCTACTGCTG	Cy3	378 (16S)	35-40-45-50	45	This study

TABLE 3 | Conditions used in stringency tests performed for probe validation.

Conditions/Samples	*Adultscaphognathites*	*AdultMidgut tubes*	*Adultscaphognathites*	*Adultforeguts*
Formamide in hybridization buffer (%)	20% - 30% - 40% - 50%	20% - 30% - 40% - 50%	35% - 40% - 45% - 50%	35% - 45%
Hybridization temperature (°C)	46°C	46°C	46°C and 48°C	46°C
Washing temperature (°C)	48°C	48°C	48°C and 50°C	48°C
Washing time (min)	15 min	15 min	15 min and 30 min	30 min
Probes	Def1229	Def1229	Myco378-1	Myco378-1
			Myco378-2	Myco378-2
			Myco378-3	Myco378-3

SDS]. Then, they were briefly rinsed twice with distilled water, once at washing temperature then at room temperature. Finally, sections were mounted on slides with SlowFade™ Gold antifade reagent with DAPI (Invitrogen). Observations on hybridized tissues were made using a Zeiss Imager.Z2 microscope equipped with the Apotome.2® sliding module and Colibri.7 light technology (Zeiss, Oberkochen, Germany). The micrographs were analyzed using the Zen software (Zeiss). Differential Interference contrast (DIC) was used to better visualize the host tissues.

Scanning Electron Microscopy

Samples fixed in glutaraldehyde were first dehydrated in ethanol series (10% to 100% in 8 steps). Dehydrated samples were placed in a perforated box, critical-point dried (Leica EM CPD300), affixed to a stub using carbon glue and then coated by gold-sputtering (60% gold/40% Palladium, Quorum Technologies SC7640). SEM observations were performed using a Quanta 200 MK microscope (FEI, Hillsboro, OR) and images were taken with the SCANDIUM acquisition program (Soft Imaging System, Munster, Germany).

RESULTS

Probe Specificity and Optimal Hybridization

Three probes targeting Mycoplasmatales lineages of the two *Rimicaris* species and one probe targeting the Deferribacteres lineage were designed. To ensure their specificity, stringency tests (variation of the formamide percentage in the hybridization buffer, variation of hybridization and washing temperatures) were performed on specific organs: foreguts, midgut tube and scaphognathites of *R. exoculata* adults. Scaphognathites were used as a control for non-specific hybridization, as Deferribacteres or Mycoplasmatales were never detected on these structures using DNA sequencing approaches.

According to these tests, one specific probe covering the diversity of Mycoplasmatales lineages was retained: Myco378-1 (5'GTGGAAAATTCCCTACTGCTG'3) (see **Supplementary Material**; **Supplementary Figures 1**, **2**). The optimal conditions to ensure its best specificity are: hybridization at 46°C for 3 hours with a buffer hybridization containing 45% formamide, washing at 48°C for 30 minutes (see **Supplementary Material**; **Supplementary Table 1**). The probe Def1229 (5'GCCCTCTGTATAGTCCATTG'3) targeting Deferribacteres (see **Supplementary Material**; **Supplementary Figures 3–6**) optimal conditions of use are: hybridization at 46° C for 3 hours with a buffer hybridization containing 30% formamide, washing at 48°C for 15 minutes (see **Supplementary Material**; **Supplementary Table 2**).

Description of Foregut Structure

In *R. exoculata* and *R. chacei*, the stomach is surrounded with the hepatopancreas that appears as an amorphous and oily gland, cream/orange in colour. In our observations, the digestive system differed in size between our two species. In *R. exoculata*, the midgut tube was very long, while the foregut was small and quite flexible. The œsophagus was very short. The stomach appeared as a single cavity that could be mostly black-colored when containing minerals. In contrast, *R. chacei* adults had a more rigid and voluminous foregut, closer to that of other shrimp

(Vogt, 2021), appearing mostly brown in colour. The midgut tube of *R. chacei* was also relatively shorter than that of *R. exoculata*. To date, the foregut of these two species have only been partially described (Segonzac et al., 1993; Apremont et al., 2018), and a more detailed analysis is required prior to characterizing niche colonization by microorganisms. Due to sample limitation, a complete description is given for *R. exoculata* adults only (**Figure 2**), done by comparison with recent descriptions in the caridean shrimp *Macrobrachium carnicus* and other crustaceans (Lima et al., 2016; Vogt, 2021):

A) Global structure (**Figure 2A**): The foregut is located dorsally in the cephalothorax (**Figure 1F**). Like that of *M. carcinus* (Lima et al., 2016), the overall structure seems reduced to a single cavity (**Figure 2B**). The dorsal side presents a bulge, while the ventral side is convex lengthwise. The anterior part of the stomach is connected to the œsophagus. Posteriorly, the stomach connects to the midgut tube, which dips ventrally slightly before rising to reach the dorsal side of the abdomen. The foregut is sometimes difficult to locate because of its small size and concealment in the glandular mass of the hepatopancreas. The hepatopancreas is connected to the stomach ventrally, surrounding the posterior-ventral part of the stomach and ascending towards its dorsal side.

B) Oesophagus (**Figure 2A**): This structure is located anteriorly of the stomach. It is a short, curved and overall narrow structure, which dips slightly from the anterior part of the stomach to the shrimp's mouth (**Figures 2C, D**). The œsophagus is lined with a thin cuticle and is surrounded with muscles. The internal cuticle of the ventral side is covered with numerous long, thin setae (here called "needles").

C) Internal structure (**Figure 2A**): The stomach is composed of two chambers - appearing mostly like those of the shrimp *M. carcinus* - called the "cardiac sac or chamber", and the "pyloric chamber" (**Figures 2C–F**). The cardiac chamber is the larger of the two. It extends laterally towards the posterior part of the stomach and covers the entire pyloric chamber. The latter, which is much less voluminous and hardly visible, is located behind the cardiac floor of the cardiac chamber, in the curved ventral zone of the stomach.

D) Cardiac chamber (**Figure 2A**): This is a "simple" structure of the stomach of *R. exoculata*, which actually comprises most its volume (**Figure 2B**). Its walls are made of striated muscles lined with a cuticle appearing thinner than usually observed in other shrimp. This cuticle is covered with spicules and long thin setae (**Figures 2G, H**). This chamber contains the shrimp's alimentary bolus consisting of food items coming directly from the œsophagus (**Figure 2C**). The cardiac chamber contracts and relaxes thanks to its numerous individual muscles that allow movements of the gastric mill and press plates of the pyloric chamber (Vogt, 2021).

E) Cardiac floor (**Figure 2A**): The cardiac floor is the ventral part of the cardiac chamber. It is easily recognizable because of its "bulbous" shape when viewed dorsally (**Figure 2F**). This floor is made of a combination of ossicles and setae, which give it a curved and thick shape, forming the cardiac floor sieve. The different structures that form the cardiac floor (according to the nomenclature of Lima et al., 2016) are the following (**Figure 3**) (starting from the outermost to the innermost part of the structure).

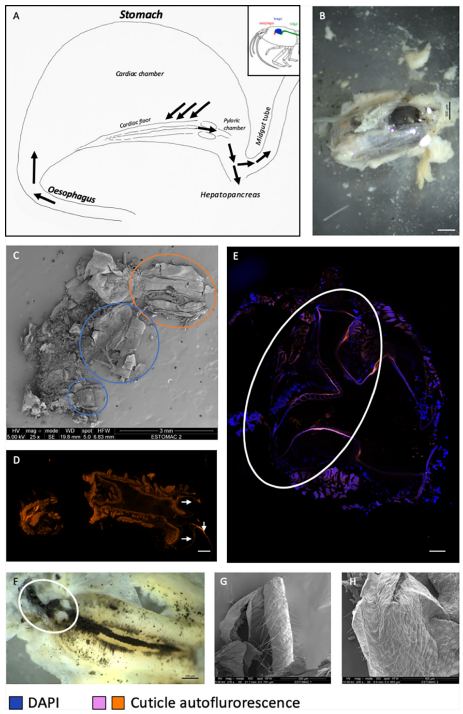

FIGURE 2 | General anatomy of the foregut of a *R. exoculata* adult. **(A)** Drawing of the general shape of a foregut of *R. exoculata* adult (see **Figure 1F**). The black arrows indicate the path of the ingested materials through the stomach. **(B)** Stomach (black colored) dissected from the cephalothorax surrounded by hepatopancreas (white colored) of *R. exoculata* (binocular microscope, scale bar = 500 µm). **(C)** Opened critical-point dried foregut revealing its content (SEM, scale bar = 3 mm). The orange circle shows the œsophagus and the blue circles show the cardiac floor sieve, which is broken in two parts. **(D)** Photography of the transversal section of an œsophagus observed by autofluorescence in orange with 548 wavelength (image mosaic from 5734 x 11264 µm sections, scale bar = 20 µm). The white arrows show the ossicles where setae are located. **(E)** Transversal section of the pyloric chamber observed by autofluorescence in pink with 548 wavelength, image mosaic from 7577 x 7577 µm sections, blue DAPI staining showing host cell nucleus (image mosaic from DIC, Apotome®, scale bar = 20 µm). The circle encloses the different plates and setae – view in transverse section- present in the pyloric chamber. **(F)** Cardiac floor sieve, with the different setae and minerals (binocular microscope, scale bar = 200 µm). The circle corresponds to the probable reduced pyloric chamber. **(G, H)** Inner part of the cardiac chamber showing thin and long setae (SEM). Scale bar = 300 µm **(E)**; Scale bar = 400 µm **(F)**.

A pair of posterior cardiac plates (**Figures 3A, B**). On these two plates, long setae are visible. These are simple, thick setae, but not dense (**Figures 3A–C**). Along the central edge of these two plates, numerous serrulate setae (**Figures 3A, B**) form a thick barrier (called sieve) between the internal structure of the cardiac floor and the two plates. These setae are thick, curved and are themselves covered with small, thin setae (**Figure 3D**). By comparison, these serrulate setae are reminiscent of the setae of

the scaphognathites and exopodites of *R. exoculata* (**Figure 3D**). These setae cover the paired inferior lateral ossicles (**Figures 3A, E**) identified as the cardio-pyloric valve (Lima et al., 2016), and may have a role in filtering and transporting resources to the midgut (hepatopancreas and midgut tube).

-The unpaired anterior ossicle (of the cardio-pyloric valve (Lima et al., 2016)) is located between the pair of inferior lateral ossicles, and is visible between the serrulate setae of the posterior cardiac plates. This structure is a thin triangular calcified plate, covered with simple setae (**Figures 3A, E, F**). These setae are very thin and much shorter than those found on posterior cardiac plates. They are covered with the minerals and materials contained in the shrimp's alimentary bolus, suggesting a role in filtration, which sometimes makes them difficult to distinguish (**Figure 3F**).

-In the center of the anterior ossicle, a longitudinal groove is visible (**Figures 3A, E**). This is the cardiac floor crest, in which the residues of the alimentary bolus accumulate. The residues are brought to the pyloric chamber through this groove. The various and numerous setae allow the passage of nutrient and mineral residues to the pyloric chamber and then to the midgut (hepatopancreas and midgut tube).

F) Pyloric chamber (**Figure 2A**; **Supplementary Figure 7**): This structure is considerably reduced and hardly visible in the stomach of adult *R. exoculata*. It is a very small chamber that connects the cardiac floor to the midgut tube and is probably also connected to the hepatopancreas (**Figures 2A, E, F**), but this last connection was not properly observed here due to sample limitation. By analogy to what is described for omnivorous shrimp, and according to anatomical similarities, the cardiac floor sieve separates the cardiac sac and the pyloric chamber. The cuticle of the pyloric chamber appears to be very curved and covered with dense setae that are folded on themselves (**Figure 2E**; **Supplementary Figure 7**). These setae are probably involved in filtration activity (see Štrus et al., 2019).

The structure of the foregut of *R. exoculata* strongly resembles that of *M. carcinus* shrimp (Lima et al., 2016) but is much smaller. In comparison, the foregut of the single available *R. chacei* specimen observed under the binocular microscope is larger than that of *R. exoculata*, with a more developed pyloric chamber, but full description is needed with new specimens.

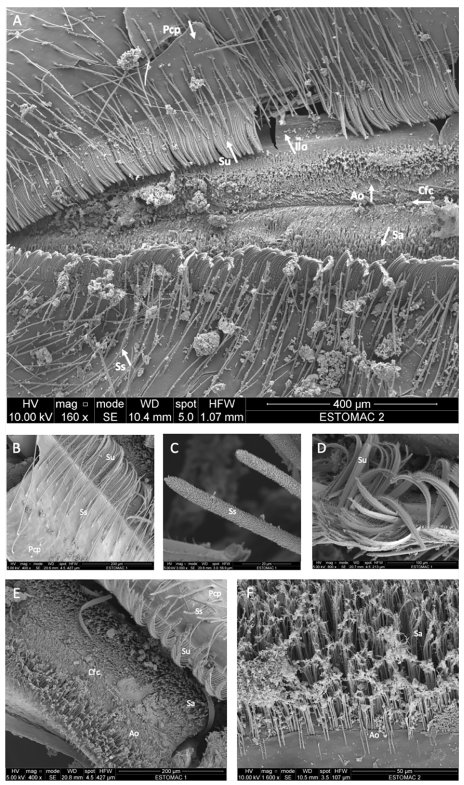

FIGURE 3 | Structure of the cardiac floor of a *R. exoculata* adult observed with scanning electon microscopy. **(A)** Dorsal view of the cardiac floor sieve showing the different ossicles and setae (scale bar = 400 µm). **(B)** The posterior cardiac plate with simple and serrulate setae (scale bar = 200 µm). **(C)** Simple setae of the posterior cardiac plate (scale bar = 20 µm). **(D)** Serrulate setae of the posterior cardiac plate (scale bar = 100 µm). **(E)** Closer view of the anterior ossicle with its setae, minerals along the surface and the cardiac floor crest on the center (scale bar = 200 µm). **(F)** The different setae of the anterior ossicle (scale bar = 50 µm). Pcp, Posterior cardiac plate; Ss, Simple setae; Su, Serrulate setae; Ilo, Inferior lateral ossicle; Ao, Anterior ossicle; Sa, Setae of the anterior ossicle with minerals; Cfc, cardiac floor crest.

Distribution of Mycoplasmatales and Deferribacteres in the Digestive Tract of *Rimicaris spp*.

Mycoplasmatales in the Foregut of *R. Exoculata* and *R. Chacei*

Mycoplasmatales are wall-less bacterial cells with a wide morphological spectrum (from rod to coccoid) (Tully et al., 1993; Wang et al., 2004) that make their visual identification challenging. The use of the Myco378-1 probe revealed for the first time their morphology in both *Rimicaris* spp. with FISH approaches (**Figures 4A–F**). To improve symbiont description in terms of both morphology and distribution on host tissues, many foregut sections were examined from the œsophagus to the posterior end. Depending on the foregut sample, section location in the organ, fixation quality (directly on board or fixed at the laboratory after freezing), or molt stage (cuticle being more or less present and thick), the Mycoplasmatales were not always clearly observable (**Figure 4C**).

For both holobionts, Mycoplasmatales were observed as rod-shaped cells. Many divided rod-cells were observed, suggesting cell division and therefore an active community (**Figure 4D**). In the different specimens available (two *R. chacei* and eighteen *R. exoculata*), symbionts were observed in several areas of the foregut. First, many Mycoplasmatales were found in the œsophagus (**Figures 4A, B**) where symbiont accumulated as thick mats along the thin setae. The same rod morphologies were observed in the pyloric chamber in dense colonies for both *Rimicaris* spp. (**Figures 4C, E, F**). Notably, Mycoplasmatales colonies were much denser in the two *R. chacei* specimens, mostly on setae in the pyloric chamber (**Figures 4E, F**). In contrast, no Mycoplasmatales was observed in the alimentary

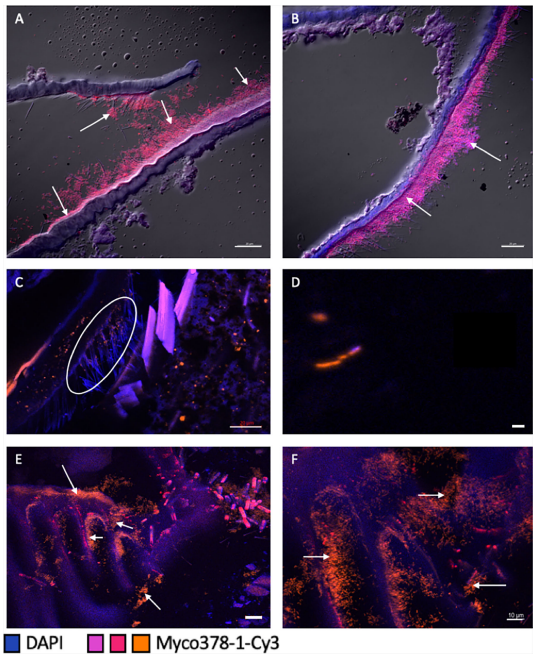

FIGURE 4 | Presence of Mycoplasmatales in the foregut of *R. exoculata* and *R. chacei* adults. **(A–D)** represent sections through the foregut [œsophagus for **(A, B)**, pyloric chamber for **(C, D)**] of a *R. exoculata* adult hybridized with Myco378-1-Cy3 (pink in **(A, B)** or orange in **(C, D)**. Tissue cell nuclei are labeled with DAPI (blue). Formamide concentration in hybridization buffer was 45% **(A–D)**. Images **(A–D)** were taken with Apotome®, and DIC for **(A, B)**. The white circle **(C)** highlights the Mycoplasmatales hidden by the setae. **(E, F)** represent sections through the foregut (pyloric chamber) of a *R. chacei* adult hybridized with Myco378-1-Cy3 (orange). Tissue cell nuclei are labeled with DAPI (blue). White arrows are targeting some Mycoplasmatales observed on the different structures. Formamide concentration in hybridization buffer was 45%. Pictures **(E, F)** were taken with Apotome®. Scale bars = 20 µm **(A–C, E)**; Scale bar = 1 µm **(D)**; Scale bar = 10 µm **(F)**.

bolus, nor along the walls of the cardiac sac (**Figures 4C, E, F**). Furthermore, none was evidenced at the entrance to the midgut tube. Only one adult *R. exoculata* empty foregut (*i.e.* without minerals) could be observed. In this specimen, Mycoplasmatales were visible on the setae of the pyloric chamber and in in the lumen of the stomach (probably detached from their original place). Myco378-1 gave no positive signal on any of the midgut tube sections of adult *R. exoculata*. No fluorescence hybridization signal was observed on "spaghetti-like" filaments or in the alimentary bolus (**Supplementary Table 2**).

Deferribacteres in the Midgut Tube of *R. Exoculata* and *R. Chacei*

Based on previous DNA sequencing data, Deferribacteres were expected to be localized in the midgut tube of *R. exoculata* and *R. chacei* (Durand et al., 2009; Durand et al., 2015; Apremont et al., 2018). FISH observations of the midgut tube sections using the specific probe Def1229 allowed us to validate the presence of these bacteria and to identify them clearly. Labeled bacteria appeared with the same morphology as previously observed with FISH using the general Eub338 probe (Durand et al., 2009) (**Figure 5A**), confirmed by the use of slides from Durand et al., 2015. *Rimicaris* spp. Deferribacteres are long and thin single cells, inserted between the microvilli of the midgut tube epithelial cells. They are visible in the lumen of the midgut tube, located between the intestinal epithelium and the peritrophic membrane, called the ectoperitrophic space (**Figures 5A–C**). The Deferribacteres are present all along the midgut tube (**Figures 5A–C**). In most observations, the bacteria were so long that they curled up on themselves, forming massive clusters on the epithelium of the midgut tube (**Figures 5B, C**).

FISH observations revealed no Deferribacteres in the alimentary bolus, which was rich in minerals and fragments of cuticle - probably from an ingested molt. In fact, the only bacteria

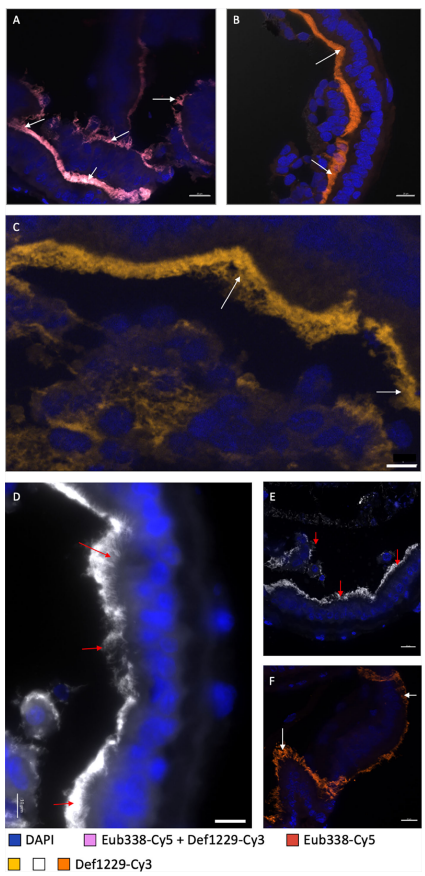

FIGURE 5 | Observation of Deferribacteres in different midgut tube sections of a *R. exoculata* and a *R. chacei* adults. **(A–C)** represent sections through the midgut tube of *R. exoculata* adult hybridized with Eub338-Cy5 (red)/ Def1229-Cy3 (white) **(A)** where double hybridization appeared in pink, or with Def1229-Cy3 (orange in **(B)** and yellow-brown in **(C)**. Tissue cell nuclei are labeled with DAPI (blue). Formamide concentration in hybridization buffer was 30%. Pictures in **(A–C)** were taken with Apotome®, and with Z-stack and DIC for B only. **(D–F)** represent sections through the midgut tube of *R. chacei* adult hybridized with Def1229-Cy3 (white in **(D, E)** and orange in **(F)**. Tissue cell nuclei are labeled with DAPI (blue). Formamide concentration in hybridization buffer was 30%. White and red arrows are targeting some Deferribacteres observed on different part of the midgut tube. Pictures **(E, F)** were taken with Apotome®. Scale bars **(A–C, E, F)** = 20 µm; Scale bar **(D)** = 10 µm.

(few rods and coccoids) visible in the alimentary bolus hybridized only with Epsy549 and GAM42a probes. Upon dissection, the midgut tube appeared more or less transparent (i.e. more or less empty). FISH observations confirmed that when the alimentary bolus was absent (transparent midgut tube), Deferribacteres were still observable while rods and coccoids from the alimentary bolus were not. No Deferribacteres signal was ever revealed on the scaphognathites nor in the foregut sections, suggesting restriction to the midgut tube.

R. chacei midgut tube sections from two specimens were also hybridized with the Def1229 probe and results were comparable to that of *R. exoculata* (**Figures 5D–F**). As for *R. exoculata*, the foregut was devoid of Deferribacteres, contrasting with the midgut tube (**Figures 5D–F**). Campylobacteria and Gammaproteobacteria cells were present only in the alimentary bolus of the midgut tube, showing coccoid and bacilli shapes. Minerals were less abundant in the alimentary bolus of both *R. chacei* specimens. The bolus was filled with cuticle fragments, more common than in *R. exoculata*. Of note, the Deferribacteres seemed longer on both *R. chacei* specimens, compared to *R. exoculata* ones.

To sum up, according to our observations on *Rimicaris* spp. adult specimens, Deferribacteres symbionts are long single-cell filaments. They are located in the ectoperitrophic space of the midgut tube, inserted between host epithelial cell microvilli, and are not washed out with the alimentary bolus (**Figure 6**).

DISCUSSION

Foregut Functioning and Symbiosis

In omnivorous shrimp, the foregut is composed of two chambers, covered with teeth, setae and spicules allowing food processing and filtration of nutriments. The alimentary bolus contained in the cardiac chamber is directed towards the pyloric chamber by means of setose lateral ridges and lateral valves preventing regurgitation. After passing through sieves, the smallest particles within the alimentary bolus (less than 1µm) enter the hepatopancreas (a major digestive and storage gland in crustaceans) and larger ones are directed to the midgut tube, embedded in the peritrophic membrane. Thus, the stomach triturates food and acts as a filter, while the hepatopancreas and midgut tube are involved in nutrient absorption and digestion (Pattarayingsakul et al., 2019; Štrus et al., 2019). Our anatomical study of the stomach of *Rimicaris* spp. also revealed complex filtering structures. In *R. exoculata*, the very small size of the foregut and its thin cuticle reinforce the idea of a weak mechanical action (Segonzac et al., 1993; Durand et al., 2009), reminiscent of that described for the shrimp *Macrobrachium carcinus* (Lima et al., 2016). In *M. carcinus*, the pyloric and cardiac chambers form what appears to be a single cavity (Lima et al., 2016), with almost no grinding appendages – no teeth in the œsophagus, nor in the cardiac chamber, as in other crustaceans (Vogt, 2021). In this species, food trituration by the gastric mill is possible thanks to the large quantity of sand ingested by the shrimp (Lima et al., 2016). By analogy, in *R. exoculata*, ingested minerals may play the role of the grinding appendages, which are absent in this species (lacking teeth) and the alimentary bolus would then be directed toward the midgut through the pyloric sieve. In *R. chacei*, the foregut is almost twice as large as that of *R. exoculata*, with a thicker cuticle. This, together with the presence of functional chelipeds (Casanova et al., 1993), numerous pieces of cuticle and organic material in the digestive tract, strengthen the mixotrophic diet hypothesis (Apremont et al., 2018; Methou et al., 2020), with a more important foregut mechanical digestive activity.

Despite these anatomical differences, both species exhibit similar bacterial colonization of their foregut, including the œsophagus and stomach, with a higher density of bacteria observed in the two *R. chacei* specimens. Mycoplasmatales colonize specific areas inside the foregut of both *Rimicaris* spp. We observed them in dense clusters on the setae at the entrance of the foregut (œsophagus) or on setae of the pyloric chamber for *R. exoculata*, and in high density close to the junction with the midgut tube for *R. chacei*. Mycoplasmatales were sometimes difficult to observe in the pyloric chamber of *R. exoculata*. It can be hypothesized that they were hidden by the cuticle and setae that occupy most of the space in the pyloric chamber

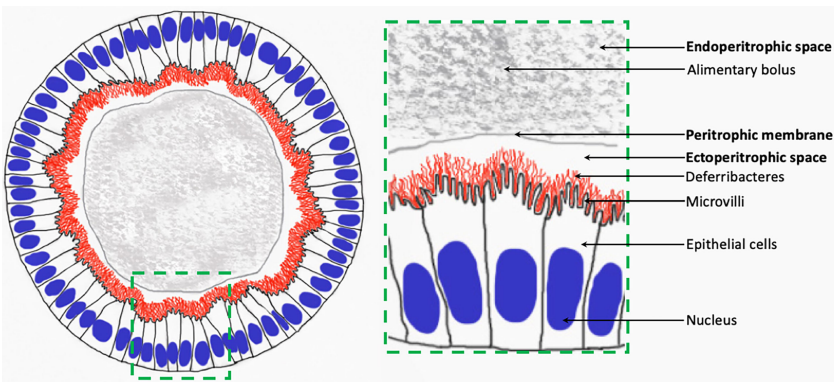

FIGURE 6 | Schematic view of Deferribacteres in adult *Rimicaris* spp. midgut tube.

(**Figure 4C**), or that signal observation may have been impaired due to ingested minerals. However, the morphology of the foregut filtering structures probably depends on the molt cycle stage and the host species (denser and thicker in the mixotrophic *R. chacei*). In the same way, the symbiont colonization may be subjected to molt events and the associated loss of cuticle, including setae. Generally, Mycoplasmatales seemed to colonize preferentially areas with dense setae, which is reminiscent of bacterial colonization in the cephalothorax. However, additional observations on a higher number of specimens would be required to better understand the distribution of Mycoplasmatales within the *Rimicaris* foregut, and identify common patterns or variations related to life stage, molt stage, nutritional status or host species.

Being present in high abundance across all specimens, Mycoplasmatales may play an essential role in the digestion processes of *Rimicaris* spp. Where associated with thin setae in the anterior-most end of the foregut (œsophagus), they may be involved in processing minerals, food items or fragments of pieces. They are also observed on setae forming sieves of the pyloric chamber through which crushed food passes. Their role may then be comparable to that of the Bg1 and Bg2 Mycoplasmatales relatives found in the foregut of the marine isopods *Bathynomus* sp. (Wang et al., 2016). These lineages are close to *'Candidatus* Hepatoplasma crinochetorum' found in the hepatopancreas of terrestrial isopods (Wang et al., 2004; Wang et al., 2007). In the case of *Bathynomus* sp., Bg1 and Bg2 Mycoplasmatales are found in the foregut, and enhance host development in nutrient-poor environments (Wang et al., 2016). In the same way, in terrestrial isopods, Mycoplasmatales are involved in food digestion through complementation of the host's diet, which is based on leaves (Wang et al., 2004; Wang et al., 2007). In terrestrial isopods, digestion occurs in the hepatopancreas, after ingested material is crushed in the foregut, and the midgut tube is almost absent. This differs from marine isopods and was proposed to be an adaptation to terrestrial conditions (Wang et al., 2004). Mycoplasmatales may play the same role in the hepatopancreas of terrestrial isopods and in the foregut of marine crustaceans. In deep-sea hydrothermal environments, most nutrition, but not all, is fueled by symbiotic chemosynthesis. This may also lead to unbalanced diet, with regards to nutrients required to support chitin synthesis for example, as hydrothermal shrimp have a very short molt cycle duration compared to coastal shrimp (10 days for *R. exoculata* against 21 days fort *Penaeus japonicus* and 41 to 98 days for *Macrobrachium rosenbergii*) (Corbari et al., 2008). We can hypothesize that Mycoplasmatales help the host degrade chitin within the cuticle, as described for *Porcellio scaber* (Bouchon et al., 2016). This hypothesis is supported by the occurrence of genes coding for enzymes involved in chitin metabolism in the metagenomes of the Mycoplasmatales symbionts (Aubé, Cambon-Bonavita et al., submitted). Overall, these observations suggest that the Mycoplasmatales colonization is directed toward specific location on specific structures, probably related to their role and function. Neither the host nor the organ (hepatopancreas *vs* foregut) would have an impact on their colonization capacity.

Rimicaris spp. Midgut Tube Houses a Tight and Specific Symbiosis

Unaffiliated single-cell bacteria were previously observed using Transmission Electron Microscopy (TEM) and revealed by FISH with the universal probe Eub338 in the midgut tube of *R. exoculata* adults (Durand et al., 2009; Durand et al., 2015). These preliminary tests confirmed the presence of bacteria in the midgut tube, but did not allow their identification. The present study documents for the first time the main lineage of the midgut tube bacterial community with a specific probe targeting Deferribacteres in both *R. exoculata and R. chacei* (**Figure 5**). Deferribacteres colonize the full length of the midgut tube, even in specimens subjected to prolonged fasting [(Durand et al., 2009); courtesy of Durand slides]. The microorganisms are inserted between the microvilli of midgut tube epithelium cells and are thus separated from the alimentary bolus by the peritrophic membrane. Then, Deferribacteres may not participate in the digestive processes of the shrimp (Durand et al., 2009; Apremont et al., 2018; Zbinden and Cambon Bonavita, 2020), contrasting with gut symbionts known in other crustaceans (Martin et al., 2020). Unlike in the foregut or cephalothoracic cavity, there is no exuviation in the midgut tube, (Štrus et al., 2019). Thus, it is not subject to bacterial turnover with (re)colonization at each molt every 10 days (Corbari et al., 2008). The colonization of the midgut tube by Deferribacteres appears to be a relatively long-term association within the shrimp's life cycle. Sequencing data obtained after a 72-hour fast in adults (Durand et al., 2009) as well as our FISH observations on full or empty midgut tubes confirmed this. Indeed, regardless of the nutritional state of the host, Deferribacteres were attached to the microvilli of the epithelium cell and can be described as resident, rather than transient, in nature.

Filamentous bacteria are usually composed of several subunits resulting from cell division, as observed for Campylobacteria or Gammaproteobacteria lineages in the cephalothoracic cavity of *Rimicaris* shrimp. TEM observations showed a different morphology for Deferribacteres observed in the midgut tube of both hosts (Durand et al., 2009; Apremont et al., 2018). These microorganisms do not undergo cell division, although they appear highly active according to FISH results. As the FISH procedure is based on probe hybridization of rRNA molecules located in the ribosomes, inactive or poorly active cells are expected to have a lower ribosome content and so, would give weak or even no signal, which is not the case here. The morphology of Deferribacteres in the midgut tube of our shrimp is reminiscent of that in bacteria experiencing stress, such as pressure or antibiotic inhibitors (Spratt, 1975; Welch et al., 1993). Indeed, a metagenomic study (Aubé, Cambon-Bonavita et al., submitted) showed that Deferribacteres have the genetic machinery for cell division, which is somehow inhibited. Such inhibition could result from a significant control of the host. Control of symbiont cell division by the host has already been suggested for the symbiont *Vesicomyosocius okutanii* of *Calyptogena* clams (Kuwahara et al., 2007; Duperron, 2017). Our FISH results in co-hybridization with Def1229 and Eub338 probes showed that this community is almost

exclusively composed of Deferribacteres. This further suggests a control by the host, and/or tight recognition mechanisms preventing colonization by other lineages. In the same way, *Vibrio fischeri* is the only symbiont able to colonize the host thanks to complex recognition mechanisms (McFall-Ngai, 2014; Duperron, 2017).

Our FISH observations showed differences between Deferribacteres in our two host species: they appear as relatively longer cells in the two observed *R. chacei* specimens. However, since a low number of individuals were examined here, the variation in Deferribacteres cell length may not be attributable to the host species only, but perhaps also to intraspecific variability related to the host life stage. Additional observations including a larger number of specimens are necessary to evaluate the respective influence of host diet (mixotrophic in *R. chacei* vs symbiotrophic in *R. exoculata*), life stage, molt stage, individual nutritional status, etc … on the Deferribacteres lineages within the midgut tube.

According to our observations, Deferribacteres cells are in direct contact with their host, located in the ectoperitrophic space (**Figure 6**). This contradicts previous reports on shrimp and crustaceans more generally (Martin et al., 2020; Vogt, 2021). In *Artemia salina*, *Daphnia magna*, *Gammarus* spp., *Homarus americanus*, *Tigriopus californicus* and *Sicyonia ingentis*, microorganisms are in the midgut tube and hindgut, located inside the alimentary bolus within the endoperitrophic space. The peritrophic membrane that separates the endoperitrophic space and the ectoperitrophic space usually protects the epithelium against pathogens and more generally prevents any bacterial colonization (Martin et al., 2020). For the six above-mentioned species, microorganisms are ingested during feeding and evacuated with the feces, and are not considered essential for host nutrition and digestion (Martin et al., 2020). Our results show that Deferribacteres are located within the ectoperitrophic space, which is then not "sterile", contrasting with observations made in many other crustaceans (Martin et al., 2020). This exceptional localization strengthens the hypothesis that the Deferribacteres play a specific role in both *Rimicaris* holobiont.

The role of Deferribacteres in the midgut tube remains enigmatic; metagenomics study recently suggested that this lineage would be involved in host nutrition and defense (genes coding for fumarate reductase, genes required for biotin and riboflavin biosynthesis, immunity systems, Aubé, Cambon-Bonavita et al., submitted). Their high abundance in both *Rimicaris* spp. may provide protection against proliferation of deleterious bacteria. This is the case of Deferribacteres found in mammals, particularly in rodents (Lee, 1985). In rats and mice, Deferribacteres relatives (*Mucispirillum schaedleri* (Robertson et al., 2005)) are located in the mucus layer covering and protecting the gastrointestinal epithelial cells (Lee, 1980). This mucus harbors other spiral bacteria belonging to the genus *Helicobacter* and *Campylobacter* (Lee et al., 1968; Davis et al., 1972), as well as *Salmonella enterica serovar Typhimurium* causing non-typhoidal colitis in hosts (Herp et al., 2019). There, Deferribacteres play a key protective role in the symbiosis of the digestive system as they outcompete pathogenic *Salmonella* spp. (Herp et al., 2019). Similarly, in *Rimicaris* shrimp, Deferribacteres may act as a barrier against deleterious microorganisms and play two roles: protection of the host through competitive interactions with other bacteria, and host nutrition. They may also play a role in detoxification of minerals contained in the alimentary bolus. In fact, Deferribacteres are usually described as involved in the use of minerals such as iron, similarly to bacteria of the cephalothoracic cavity that may be involved in mineral detoxification (for review see Zbinden and Cambon Bonavita, 2020).

A Complex Symbiosis Linked to the Diet of Both *Rimicaris spp*.

Similarly to the cephalothoracic cavity of the two *Rimicaris* spp., their digestive system differs in morphology. Our detailed observations confirm that the foregut of *Rimicaris* spp. is a filtering structure as in other shrimp. The œsophagus is reduced to a simple structure with filtering elements. The stomach is deprived of a grinding appendage but exhibits many setae and a sieve to filter nutrients and minerals. This stomach is highly reduced in *R. exoculata* but not the midgut tube. In contrast, the digestive system of the few *R. chacei* observed (FISH, binocular microscope) showed significant morphological differences: the stomach is much more voluminous compared to that of *R. exoculata*, with a thicker cuticle, and a larger pyloric chamber. We hypothesize that the comparably more developed internal structure with grinding appendages and free mandibles facilitate food uptake and digestion in this species. Digestive system size and structure may therefore be related to diet, which is predominantly chemosynthetic in *R. exoculata* and mixotrophic in *R. chacei*. To draw stronger conclusions with regards to anatomical adaptation to nutritional mode in these shrimp, further observations of *R. chacei* specimens are required, across life stages and molt cycles.

The digestive symbioses of both *Rimicaris* spp. share similarities with other species such as mammals for the midgut tube and other terrestrial, freshwater or marine crustaceans for the foregut. These symbioses may allow the host to adapt to hostile and nutrient-poor or unbalanced environments, and in return allow the symbionts to find shelter and colonize favorable niches. Hydrothermal shrimp show commonalities with isopods in the functioning of their foregut and with mice for the midgut tube functioning. This suggests a somewhat "universal" evolution of digestive symbiosis. The specific location of the various microorganisms in the digestive system allows us to propose hypothesis about their role and function. The Deferribacteres could be mainly protective for the host, while the Mycoplasmatales may support host development. Their function has yet to be further studied through metagenomics and *in vivo* studies.

Knowledge gaps persist regarding the transmission of Deferribacteres and Mycoplasmatales lineages along *Rimicaris* life cycle and molt events. Because the foregut is covered with cuticle, which is lost during exuviation, the hypothesis of horizontal transmission is often proposed for Mycoplasmatales. On the contrary, the control of Deferribacteres cell division and

colonization by the host, together with the quasi absence of their free-living relatives in water surrounding shrimp (Hügler et al., 2010; Flores et al., 2011; Durand et al., 2015; Cowart et al., 2017) suggests specific symbiont recognition and potential vertical transmission. However, no symbiont was observed on the envelope of brooded eggs (Methou et al., 2019), raising questions about potential mechanisms allowing such vertical transmission for Deferribacteres. Another mode of transmission may be proposed, as for terrestrial isopods, where juveniles eat the feces of the adults when ingesting food on litter (Wang et al., 2007). This may be the case for the *R. exoculata* where juveniles are recruited close to adult aggregations (Methou et al., 2022). In *R. chacei*, however, juveniles are mainly recruited in isolated patches, with few or no adults (Methou et al., 2022). In theory, recruitment away from adults could hinder the acquisition of digestive symbionts, leading to lower holobiont fitness, and may be a partial explanation of the observed population collapse of *R. chacei*. Still, more studies are required especially on juveniles to establish whether symbionts are acquired during recruitment. Understanding the mode of acquisition of these symbionts (horizontal, vertical and/or mixed transmission) would help to understand the development of both hosts and their relation to their symbionts. The study of juveniles and larvae (Guéganton et al., in prep) is essential to better understand symbiont transmission, localization and functions in these shrimp.

DATA AVAILABILITY STATEMENT

The original contributions presented in the study are included in the article/**Supplementary Material**. Further inquiries can be directed to the corresponding author.

AUTHOR CONTRIBUTIONS

MG contributed to data acquisition and analysis, wrote the first draft of the manuscript, review and editing of this manuscript. LD and VC-G contributed for methodology for biology work. OR and LD contributed for FISH microscopy data acquisition and review of this manuscript. NG contributed for electron microscopy data acquisition. FP and M-AC-B contributed to the conception and the design of this study, review and editing of the manuscript, and the supervision of the project. All authors contributed to the article and approved the submitted version.

FUNDING

Funding was provided by Ifremer REMIMA program, and Ifremer and Région Bretagne doctoral grant.

ACKNOWLEDGMENTS

We thank cruise chief scientist of BICOSE2 2018 cruise (M-AC-B) and the captain and crew of R/V *Pourquoi pas?* and Nautile for logistic assistance in collecting samples.

SUPPLEMENTARY MATERIAL

The Supplementary Material for this article can be found online at: https://www.frontiersin.org/articles/10.3389/fmars.2022.903748/full#supplementary-material

REFERENCES

Altschul, S. F., Gish, W., Miller, W., Myers, E. W., and Lipman, D. J. (1990). Basic Local Alignment Search Tool. *J. Mol. Biol.* 215, 403–410. doi: 10.1016/S0022-2836(05)80360-2

Amann, R. I., Binder, B. J., Olson, R. J., Chisholm, S. W., Devereux, R., and Stahl, D. A. (1990). Combination of 16s Ribosomal-Rna-Targeted Oligonucleotide Probes With Flow-Cytometry for Analyzing Mixed Microbial-Populations. *Appl. Environ. Microbiol.* 56, 1919–1925. doi: 10.1128/aem.56.6.1919-1925.1990

Amann, R., Fuchs, B., and Behrens, S. (2001). The Identification of Microorganisms by Fluorescence *in Situ* Hybridisation. *Curr. Opin. Biotechnol.* 12, 231–236. doi: 10.1016/S0958-1669(00)00204-4

Apremont, V., Cambon-Bonavita, M.-A., Cueff-Gauchard, V., François, D., Pradillon, F., Corbari, L., et al. (2018). Gill Chamber and Gut Microbial Communities of the Hydrothermal Shrimp *Rimicaris Chacei* Williams and Rona 1986: A Possible Symbiosis. *PloS One* 13, e0206084. doi: 10.1371/journal.pone.0206084

Aubé, J., Cambon-Bonavita, M.-A., Velo-Suárez, L., Cueff-Gauchard, V., Lesongeur, F., Guéganton, M., et al. A Novel and Dual Digestive Symbiosis Scales Up the Nutrition and Immune System of the Holobiont *Rimicaris Exoculata*. *Submitted to Microbiome*. doi: 10.21203/rs.3.rs-1584541/v1

Behrens, S., Fuchs, B. M., Mueller, F., and Amann, R. (2003). Is the *In Situ* Accessibility of the 16S rRNA of *Escherichia Coli* for Cy3-Labeled Oligonucleotide Probes Predicted by a Three-Dimensional Structure Model of the 30S Ribosomal Subunit? *Appl. Environ. Microbiol.* 69, 4935–4941. doi: 10.1128/AEM.69.8.4935-4941.2003

Behrens, S., Rühland, C., Inácio, J., Huber, H., Fonseca, Á., Spencer-Martins, I., et al. (2003). *In Situ* Accessibility of Small-Subunit rRNA of Members of the Domains *Bacteria*, *Archea*, and *Eucarya* to Cy3-Labeled Oligonucleotide Probes. *Appl. Environ. Microbiol.* 69, 1748–1758. doi: 10.1128/AEM.69.3.1748–1758.2003

Bouchon, D., Zimmer, M., and Dittmer, J. (2016). The Terrestrial Isopod Microbiome: An All-In-One Toolbox for Animal–Microbe Interactions of Ecological Relevance. *Front. Microbiol.* 7. doi: 10.3389/fmicb.2016.01472

Casanova, B., Brunet, M., and Segonzac, M. (1993). Impact of Bacterial Epibiosis on Functional Morphology of Shrimp Associated With the Mid-Atlantic Hydrothermal Conditions. *Cahiers Biologie Mar.* 34, 573–588. doi: 10.21411/CBM.A.E587F68C

Ceccaldi, H. (1989). "Anatomy and Physiology of Digestive Tract of Crustaceans Decapods Reared in Aquaculture," in *Advances in Tropical Aquaculture*, vol. 9. (Tahiti, French Polynesia: Actes de colloques Ifremer), 243–259. Available at: https://archimer.ifremer.fr/doc/00000/1486/.

Corbari, L., Zbinden, M., Cambon-Bonavita, M.-A., Gaill, F., and Compere, P. (2008). Bacterial Symbionts and Mineral Deposits in the Branchial Chamber of the Hydrothermal Vent Shrimp *Rimicaris Exoculata*: Relationship to Moult Cycle. *Aquat. Biol.* 1, 225–238. doi: 10.3354/ab00024

Cowart, D. A., Durand, L., Cambon-Bonavita, M. A., and Arnaud-Haond, S. (2017). Investigation of Bacterial Communities Within the Digestive Organs of the Hydrothermal Vent Shrimp *Rimicaris Exoculata* Provide Insights Into Holobiont Geographic Clustering. *PloS One* 12, 1–22. doi: 10.1371/journal.pone.0172543

Davis, C. P., Mulcahy, D., Takeuchi, A., and Savage, D. C. (1972). Location and Description of Spiral-Shaped Microorganisms in the Normal Rat Cecum. *Infect. Immunity* 2 (6), 184–192. doi: 10.1128/iai.6.2.184-192.1972

Dubilier, N., Bergin, C., and Lott, C. (2008). Symbiotic Diversity in Marine Animals: The Art of Harnessing Chemosynthesis. *Nat. Rev. Microbiol.* 6, 725–740. doi: 10.1038/nrmicro1992

Duperron, S. (2017). Les Symbioses Microbiennes, Associations Au Cœur Du Vivant. *ISTE editions*. 134.

Duperron, S., Sibuet, M., MacGregor, B. J., Kuypers, M. M. M., Fisher, C. R., and Dubilier, N. (2007). Diversity, Relative Abundance and Metabolic Potential of Bacterial Endosymbionts in Three *Bathymodiolus* Mussel Species From Cold Seeps in the Gulf of Mexico. *Environ. Microbiol.* 9, 1423–1438. doi: 10.1111/j.1462-2920.2007.01259.x

Durand, L., Roumagnac, M., Cueff-Gauchard, V., Jan, C., Guri, M., Tessier, C., et al. (2015). Biogeographical Distribution of *Rimicaris Exoculata* Resident Gut Epibiont Communities Along the Mid-Atlantic Ridge Hydrothermal Vent Sites. *FEMS Microbiol. Ecol.* 91, 1–15. doi: 10.1093/femsec/fiv101

Durand, L., Zbinden, M., Cueff-Gauchard, V., Duperron, S., Roussel, E. G., Shillito, B., et al. (2009). Microbial Diversity Associated With the Hydrothermal Shrimp *Rimicaris Exoculata* Gut and Occurrence of a Resident Microbial Community. *FEMS Microbiol. Ecol.* 71, 291–303. doi: 10.1111/j.1574-6941.2009.00806.x

Edgar, R. C. (2004). MUSCLE: Multiple Sequence Alignment With High Accuracy and High Throughput. *Nucleic Acids Res.* 32, 1792–1797. doi: 10.1093/nar/gkh340

Flores, G. E., Campbell, J. H., Kirshtein, J. D., Meneghin, J., Podar, M., Steinberg, J. I., et al. (2011). Microbial Community Structure of Hydrothermal Deposits From Geochemically Different Vent Fields Along the Mid-Atlantic Ridge. *Environ. Microbiol.* 13, 2158–2171. doi: 10.1111/j.1462-2920.2011.02463.x

Garrity, G. M., Holt, J. M., Huber, H., Karl, O. S., Greene, A. C., Patel, B. K. C., et al. (2001). Pylum BIX. *Deferribacteres Phy. Nov. Bergey's Manual® Systematic Bacteriol.* 1, 465–471. doi: 10.1007/978-0-387-21609-6_26

Gebruk, A. V., Chevaldonne, P., Shank, T., Lutz, R. A., and Vrijenhoek, R. C. (2000). Deep-Sea Hydrothermal Vent Communities of the Logatchev Area (14 Degrees 45'n, Mid-Atlantic Ridge): Diverse Biotopes and High Biomass. *J. Mar. Biol. Assoc. United Kingdom* 80, 383–393. doi: 10.1017/S0025315499002088

Gebruk, A. V., Galkin, S. V., Vereshchaka, A. L., Moskalev, L. I., and Southward, A. J. (1997). Ecology and Biogeography of the Hydrothermal Vent Fauna of the Mid-Atlantic Ridge. *Adv. Mar. Biol.* 32, 93–144. doi: 10.1016/S0065-2881(08)60016-4

Guri, M., Durand, L., Cueff-Gauchard, V., Zbinden, M., Crassous, P., Shillito, B., et al. (2012). Acquisition of Epibiotic Bacteria Along the Life Cycle of the Hydrothermal Shrimp *Rimicaris Exoculata*. *ISME J.* 6, 597–609. doi: 10.1038/ismej.2011.133

Hernández-Ávila, I., Cambon-Bonavita, M.-A., Sarrazin, J., and Pradillon, F. (2021). Population Structure and Reproduction of the Alvinocaridid Shrimp *Rimicaris Exoculata* on the Mid-Atlantic Ridge: Variations Between Habitats and Vent Fields. *bioRxiv* 06.27, 450066. doi: 10.1101/2021.06.27.450066

Herp, S., Brugiroux, S., Garzetti, D., Ring, D., Jochum, L. M., Beutler, M., et al. (2019). *Mucispirillum Schaedleri* Antagonizes *Salmonella* Virulence to Protect Mice Against Colitis. *Cell Host Microbe* 25, 681–694.e8. doi: 10.1016/j.chom.2019.03.004

Hügler, M., Gärtner, A., and Imhoff, J. F. (2010). Functional Genes as Markers for Sulfur Cycling and CO2 Fixation in Microbial Communities of Hydrothermal Vents of the Logatchev Field. *FEMS Microbiol. Ecol.* 73, 526–537. doi: 10.1111/j.1574-6941.2010.00919.x

Kearse, M., Moir, R., Wilson, A., Stones-Havas, S., Cheung, M., Sturrock, S., et al. (2012). Geneious Basic: An Integrated and Extendable Desktop Software Platform for the Organization and Analysis of Sequence Data. *Bioinformatics* 28, 1647–1649. doi: 10.1093/bioinformatics/bts199

Kibbe, W. A. (2007). OligoCalc: An Online Oligonucleotide Properties Calculator. *Nucleic Acids Res.* 35, W43–W46. doi: 10.1093/nar/gkm234

Komai, T., and Segonzac, M. (2008). Taxonomic Review of the Hydrothermal Vent Shrimp Genera *Rimicaris* Williams & Rona and *Chorocaris* Martin & Hessler (Crustacea: Decapoda: Caridea: Alvinocarididae). *J. Shellfish Res.* 27, 21–41. doi: 10.2983/0730-8000(2008)27[21:trothv]2.0.co;2

Kouris, A., Juniper, S. K., Frébourg, G., and Gail, F. (2007). Protozoan-Bacterial Symbiosis in a Deep-Sea Hydrothermal Vent Folliculinid Ciliate (*Folliculinopsis* Sp.) From the Juan De Fuca Ridge. *Mar. Ecol.* 28, 63–71. doi: 10.1111/j.1439-0485.2006.00118.x

Kuwahara, H., Yoshida, T., Takaki, Y., Shimamura, S., Nishi, S., Harada, M., et al. (2007). Reduced Genome of the Thioautotrophic Intracellular Symbiont in Deep-Sea Clam, *Calyptogena Okutanii*. *Curr. Biol.* 17, 881–886. doi: 10.1016/j.cub.2007.04.039

Lee, A. (1980). "Normal Flora of Animal Intestinal Surfaces," in *Adsorption of Microorganisms to Surfaces* (New York: Wiley), 145–173.

Lee, A. (1985). "Neglected Niches," in *Advances in Microbial Ecology: Volume 8 Advances in Microbial Ecology*. Ed. K. C. Marshall (Boston, MA: Springer US), 115–162. doi: 10.1007/978-1-4615-9412-3_3

Lee, A., Gordon, J., and Dubos, R. (1968). Enumeration of the Oxygen Sensitive Bacteria Usually Present in the Intestine of Healthy Mice. *Nature* 220, 1137–1139. doi: 10.1038/2201137a0

Lima, J.de F., Garcia, J.da S., and Tavares, M. (2016). Foregut Morphology of *Macrobrachium Carcinus* (Crustacea, Decapoda, Palaemonidae). *Acta Amaz.* 46, 209–218. doi: 10.1590/1809-4392201501214

Lin, X. J., Wakeham, S. G., Putnam, I. F., Astor, Y. M., Scranton, M. I., Chistoserdov, A. Y., et al. (2006). Comparison of Vertical Distributions of Prokaryotic Assemblages in the Anoxic Cariaco Basin and Black Sea by Use of Fluorescence *in Situ* Hybridization. *Appl. And Environ. Microbiol.* 72, 2679–2690. doi: 10.1128/aem.72.4.2679-2690.2006

Manz, W., Amann, R., Ludwig, W., Wagner, M., and Schleifer, K. H. (1992). Phylogenetic Oligodeoxynucleotide Probes for the Major Subclasses of Proteobacteria - Problems and Solutions. *Systematic Appl. Microbiol.* 15, 593–600. doi: 10.1016/S0723-2020(11)80121-9

Martin, G. G., Natha, Z., Henderson, N., Bang, S., Hendry, H., and Loera, Y. (2020). Absence of a Microbiome in the Midgut Trunk of Six Representative Crustacea. *J. Crustacean Biol.* 40, 122–130. doi: 10.1093/jcbiol/ruz087

McFall-Ngai, M. J. (2014). The Importance of Microbes in Animal Development: Lessons From the Squid-*Vibrio* Symbiosis. *Annu. Rev. Microbiol.* 68, 177–184. doi: 10.1146/annurev-micro-091313-103654

Methou, P., Hernández-Ávila, I., Aube, J., Cueff-Gauchard, V., Gayet, N., Amand, L., et al. (2019). Is It First the Egg or the Shrimp? – Diversity and Variation in Microbial Communities Colonizing Broods of the Vent Shrimp *Rimicaris Exoculata* During Embryonic Development. *Front. In Microbiol.* 10. doi: 10.3389/fmicb.2019.00808

Methou, P., Hernández-Ávila, I., Cathalot, C., Cambon-Bonavita, M.-A., and Pradillon, F. (2022). Population Structure and Environmental Niches of *Rimicaris* Shrimp From the Mid-Atlantic Ridge. *Mar. Ecol. Prog. Ser.* 684, 1–20. doi: 10.3354/meps13986

Methou, P., Michel, L., Segonzac, M., Cambon-Bonavita, M.-A., and Pradillon, F. (2020). Integrative Taxonomy Revisits the Ontogeny and Trophic Niches of *Rimicaris* Vent Shrimp. *R. Soc. Open Sci.* 7. doi: 10.1098/rsos.200837

Pattarayingsakul, W., Pudgerd, A., Munkongwongsiri, N., Vanichviriyakit, R., Chaijarasphong, T., Thitamadee, S., et al. (2019). The Gastric Sieve of Penaeid Shrimp Species Is a Sub-Micron Nutrient Filter. *J. Exp. Biol.* 222, jeb.199638. doi: 10.1242/jeb.199638

Ponsard, J., Cambon-Bonavita, M.-A., Zbinden, M., Lepoint, G., Joassin, A., Corbari, L., et al. (2013). Inorganic Carbon Fixation by Chemosynthetic Ectosymbionts and Nutritional Transfers to the Hydrothermal Vent Host-Shrimp *Rimicaris Exoculata*. *ISME J.* 7, 96–109. doi: 10.1038/ismej.2012.87

Robertson, B. R., O' Rourke, J. L., Neilan, B. A., Vandamme, P., On, S. L. W., Fox, J. G., et al. (2005). *Mucispirillum Schaedleri* Gen. Nov., Sp. Nov., a Spiral-Shaped Bacterium Colonizing the Mucus Layer of the Gastrointestinal Tract of Laboratory Rodents. *Int. J. Systematic Evolutionary Microbiol.* 55, 1199–1204. doi: 10.1099/ijs.0.63472-0

Schmidt, C., Le Bris, N., and Gaill, F. (2008a). Interactions of Deep-Sea Vent Invertebrates With Their Environment: The Case of *Rimicaris Exoculata*. *J. Shellfish Res.* 27, 79–90. doi: 10.2983/0730-8000(2008)27[79:IODVIW]2.0.CO;2

Schmidt, C., Vuillemin, R., Le Gall, C., Gaill, F., and Le Bris, N. (2008b). Geochemical Energy Sources for Microbial Primary Production in the Environment of Hydrothermal Vent Shrimp. *Mar. Chem.* 108, 18–31. doi: 10.1016/j.marchem.2007.09.009

Segonzac, M., de Saint Laurent, M., and Casanova, B. (1993). L'énigme Du Comportement Trophique Des Crevettes Alvinocarididae Des Sites Hydrothermaux De La Dorsale Médio-Atlantique. *Cahiers Biologie Mar.* 34, 535–571. doi: 10.21411/CBM.A.B3683E29

Sogin, E. M., Kleiner, M., Borowski, C., Gruber-Vodicka, H. R., and Dubilier, N. (2021). Life in the Dark: Phylogenetic and Physiological Diversity of Chemosynthetic Symbioses. *Annu. Rev. Microbiol.* 75, 695–718. doi: 10.1146/annurev-micro-051021-123130

Spratt, B. G. (1975). Distinct Penicillin Binding Proteins Involved in the Division, Elongation, and Shape of *Escherichia Coli* K12. *Proc. Nat. Acad. Sci. U.S.A.* 72, 2999–3003. doi: 10.1073/pnas.72.8.2999

Štrus, J., Žnidaršič, N., Mrak, P., Bogataj, U., and Vogt, G. (2019). Structure, Function and Development of the Digestive System in Malacostracan Crustaceans and Adaptation to Different Lifestyles. *Cell Tissue Res.* 377, 415–443. doi: 10.1007/s00441-019-03056-0

Tully, J. G., Bove, J. M., Laigret, F., and Whitcomb, R. F. (1993). Revised Taxonomy of the Class *Mollicutes*: Proposed Elevation of a Monophyletic Cluster of Arthropod-Associated Mollicutes to Ordinal Rank (*Entomoplasmatales* Ord. Nov.), With Provision for Familial Rank To Separate Species With Nonhelical Morphology (*Entomoplasmataceace* Fam. Nov.) From Helical Species (*Spiroplasmataceae*), and Emended Descriptions of the Order *Mycoplasmatales*, Family *Mycoplasmataceae*. *Int. J. Systematic Bacteriol.* 43, 378–385. doi: 10.1099/00207713-43-2-378

Van Dover, C. L., Fry, B., Grassle, J. F., Humphris, S., and Rona, P. A. (1988). Feeding Biology of the Shrimp *Rimicaris Exoculata* at Hydrothermal Vents on the Mid-Atlantic Ridge. *Mar. Biol.* 98, 209–216. doi: 10.1007/BF00391196

Vogt, G. (2021). Synthesis of Digestive Enzymes, Food Processing, and Nutrient Absorption in Decapod Crustaceans: A Comparison to the Mammalian Model of Digestion. *Zoology* 147, 125945. doi: 10.1016/j.zool.2021.125945

Wang, Y., Brune, A., and Zimmer, M. (2007). Bacterial Symbionts in the Hepatopancreas of Isopods: Diversity and Environmental Transmission. *FEMS Microbiol. Ecol.* 61, 141–152. doi: 10.1111/j.1574-6941.2007.00329.x

Wang, Y., Huang, J.-M., Wang, S.-L., Gao, Z.-M., Zhang, A.-Q., Danchin, A., et al. (2016). Genomic Characterization of Symbiotic Mycoplasmas From the Stomach of Deep-Sea Isopod Bathynomus Sp. *Environ. Microbiol.* 18, 2646–2659. doi: 10.1111/1462-2920.13411

Wang, Y., Stingl, U., Anton-Erxleben, F., Geisler, S., Brune, A., and Zimmer, M. (2004). "*Candidatus* Hepatoplasma Crinochetorum", A New, Stalk-Forming Lineage of Mollicutes Colonizing the Midgut Glands of a Terrestrial Isopod. *Appl. Environ. Microbiol.* 70, 6166–6172. doi: 10.1128/AEM.70.10.6166-6172.2004

Welch, T. J., Farewell, A., Neidhardt, F. C., and Bartlett, D. H. (1993). Stress Response of *Escherichia Coli* to Elevated Hydrostatic Pressure. *J. Bacteriol.* 175, 7170–7177. doi: 10.1128/jb.175.22.7170-7177.1993

Williams, A. B., and Rona, P. A. (1986). Two New Caridean Shrimp (Bresiliidae) From a Hydrothermal Field on the Mid-Atlantic Ridge. *J. Crustacean Biol.* 6, 446–462. doi: 10.1163/193724086X00299

Zbinden, M., and Cambon Bonavita, M.-A. (2020). *Rimicaris Exoculata*: Biology and Ecology of a Shrimp From Deep-Sea Hydrothermal Vents Associated With Ectosymbiotic Bacteria. *Mar. Ecology-Progress Ser.* 652, 187–222. doi: 10.3354/meps13467

Zilber-Rosenberg, I., and Rosenberg, E. (2008). Role of Microorganisms in the Evolution of Animals and Plants: The Hologenome Theory of Evolution. *FEMS Microbiol. Rev.* 32, 723–735. doi: 10.1111/j.1574-6976.2008.00123.x

Conflict of Interest: The authors declare that the research was conducted in the absence of any commercial or financial relationships that could be construed as a potential conflict of interest.

frontiers | Frontiers in Marine Science

ORIGINAL RESEARCH
published: 20 July 2022
doi: 10.3389/fmars.2022.910940

Modelling the Dispersion of Seafloor Massive Sulphide Mining Plumes in the Mid Atlantic Ridge Around the Azores

Telmo Morato [1,2†], Manuela Juliano [1,3†], Christopher K. Pham [1,2], Marina Carreiro-Silva [1,2], Inês Martins [1,2] and Ana Colaço [1,2]*

[1]Institute of Marine Sciences - Okeanos, University of the Azores, Horta, Portugal, [2]Instituto do Mar - IMAR, University of the Azores, Horta, Portugal, [3]Marine Environment and Technology Laboratory - Laboratório do Ambiente Marinho e Tecnologia University of Azores, Praia da Vitória, Portugal

OPEN ACCESS

Edited by:
Philip Weaver, Seascape Consultants Ltd., United Kingdom

Reviewed by:
Andrew C. Dale, Scottish Association For Marine Science, United Kingdom
Travis William Washburn, Geological Survey of Japan (AIST), Japan

***Correspondence:**
Telmo Morato
t.morato@gmail.com

†These authors have contributed equally to this work

Specialty section:
This article was submitted to Deep-Sea Environments and Ecology, a section of the journal Frontiers in Marine Science

Received: *01 April 2022*
Accepted: *13 June 2022*
Published: *20 July 2022*

Citation:
Morato T, Juliano M, Pham CK, Carreiro-Silva M, Martins I and Colaço A (2022) Modelling the Dispersion of Seafloor Massive Sulphide Mining Plumes in the Mid Atlantic Ridge Around the Azores. Front. Mar. Sci. 9:910940. doi: 10.3389/fmars.2022.910940

It is increasingly recognised that deep-sea mining of seafloor massive sulphides (SMS) could become an important source of mineral resources. These operations will remove the targeted substrate and produce potentially toxic plumes from in situ seabed excavation and from the return water pumped back down to the seafloor. However, the spatial extent of the impact of deep-sea mining is still uncertain because few field experiments and models of plume dispersion have been conducted. In this study, we used three-dimensional hydrodynamic models of the Azores region together with a theoretical commercial mining operation of polymetallic SMS to simulate the potential dispersal of plumes originating from different phases of mining operations, and to assess the magnitude of potential impacts. Although the model simulations presented here were subject to many caveats, they did reveal some important patterns. The model projected marked differences among sites making generalisations about plume-dispersal patterns in mid-ocean ridges difficult. Nevertheless, the models predicted large horizontal and vertical plume-dispersals above the thresholds adopted. Persistent plumes (temporal frequency >50%, i.e., 6 months out of 12 months) were projected to disperse an average linear distance of 10 to 20 km, cover an area of 17 to 150 km2, and extend more than 800 m in the water column. In fact, the model projected that plumes may disperse beyond the licensed mining areas, reach the flanks and summits of nearby topographic features, and extend into the bathypelagic, mesopelagic, and epipelagic environments. Modelled plume-dispersal overlaps with the predicted distribution of cold-water corals and with existing fishing activities. These potential impacts would be of particular concern in regions such as the Azores, where local populations are highly dependent on the sea for their livelihoods. The findings of this study are an important initial step towards understanding the nature and magnitude of deep-sea mining impacts in space and time.

Keywords: deep-sea, mining, sediment plumes, spatial extent of impacts, hydrodynamic model, MOHID, Mid Atlantic Ridge

1 INTRODUCTION

Recognition that deep-sea seafloor massive sulphides (SMS) mining could become an important source of minerals has become increasingly prevalent (Petersen et al., 2016; Sharma, 2017), as large concentrations of copper, zinc, silver, and gold have been discovered in deep-sea hydrothermal vent deposits in many areas of the world's oceans (Herzig et al., 2002; Hannington et al., 2011; Murton et al., 2019). Not surprisingly, the International Seabed Authority (ISA) has awarded several contracts for polymetallic sulphide exploration in the Mid-Atlantic Ridge (MAR) south of the Azores to Russia, France, and Poland, and in the Mid- and Southwest- Indian Ridges to China, the Republic of Korea, Germany, and India (ISA, 2021).

Although commercial mining of seafloor massive sulphides has not yet occurred, it will likely happen in the future, as the first pilot mining tests have successfully delivered large quantities of ore to the production vessel (Okamoto et al., 2018; Okamoto et al., 2019). These operations will remove the targeted substrate and associated organisms and will produce potentially toxic plumes from *in situ* seabed excavation and from the return water pumped back down close to the seafloor (Coffey Natural Systems, 2008; Boschen et al., 2013; Hauton et al., 2017; Weaver & Billett, 2019; Muñoz-Royo et al., 2021). These impacts will most likely affect local biodiversity, species abundance and ecosystem services, as well as the marine food webs and ecosystem functioning in both benthic and pelagic ecosystems (Boschen et al., 2016; Le et al., 2017; Van Dover et al., 2017; Drazen et al., 2020; Boschen-Rose et al., 2021). It is, therefore, widely recognised that the mining of polymetallic sulphides at active and inactive vent sites can impact the marine environment and human activities even far away from the actual mining site (Levin et al., 2016; Niner et al., 2018; Sharma, 2019; Van Dover, 2019; van der Grient & Drazen, 2021).

The spatial extent of deep-sea mining impacts from water and sediment plumes is, however, still uncertain as few field experiments and models of plume-dispersal have been conducted so far (Jones et al., 2017). In fact, studies on plume-dispersal resulting from the mining of seafloor massive sulphides are particularly limited, being those produced for the Solwara 1 the only ones currently found in the literature (ASA, 2008a; ASA, 2008b). The existing studies, which mostly addressed short term impacts, show very contrasting estimates of plume-dispersal ranging from very few to hundreds of square kilometres depending on the type of resources or threshold used (e.g., Jankowski and Zielke, 2001; Thiel and Tiefsee-Umweltschutz, 2001; Spearman et al., 2020; Muñoz-Royo et al., 2021). Similarly, sediment accumulation on the seafloor has been projected to range from less than one or few millimetres (Thiel and Tiefsee-Umweltschutz, 2001; Gillard et al., 2019; Purkiani et al., 2021) to several centimetres (Aleynik et al., 2017) depending on particle size and distance from the source. A recent expert survey suggested that the footprint of return plumes could reach hundreds of square kilometres in polymetallic nodule fields, tens of square kilometres in cobalt-rich crusts on seamounts, and only a few square kilometres in seafloor massive sulphide vents (Washburn et al., 2019). These discrepancies indicate that further studies are needed to forecast the long-term dispersal and impacts of mining plumes on benthic and pelagic ecosystems, which is of paramount importance to inform environmental management of polymetallic sulphide deposits (Van Dover, 2011; Wedding et al., 2015; Smith et al., 2020; Van Dover et al., 2020; Amon et al., 2022).

Several hydrothermal vents associated with polymetallic sulphide deposits have been identified along the northern Mid-Atlantic Ridge (MAR) (Cherkashov et al., 2010; Hannington et al., 2011; Wheeler et al., 2013; Cherkashov, 2017; Boschen-Rose and Colaço, 2021). The MAR in the Azores region, including both its Exclusive Economic Zone (EEZ) and extended continental shelf, host several active and inactive hydrothermal vents that might represent potential sources of polymetallic sulphide deposits. These vents make the Portuguese EEZ the only EEZ of an EU Member State with sufficient mineral reserves for deep-sea mining in European waters (ECORYS, 2014). The seafloor surrounding Lucky Strike and Rainbow hydrothermal fields are examples of areas with interest for deep-sea mining exploration, but many other locations may also be of interest (ISA, 2002; Marques & Scott, 2011). In this study, we used three dimensional (3-D) hydrodynamic models of the Azores region along with a theoretical commercial mining operation of polymetallic seafloor massive sulphides (Coffey Natural Systems, 2008; Ortega and Boomsma, 2014) to simulate the potential dispersal of plumes originating from the different phases of the mining operations, and to assess the scale of potential impacts. Additionally, we evaluated how the theoretical commercial mining operation could interact with local biodiversity and existing fishing activities.

2 METHODS

2.1 Study Area

Several active deep-water hydrothermal vent fields have been discovered in the northern portion of the slow-spreading MAR. Five of them are located south of the Azores (Beaulieu et al., 2013; Beaulieu and Szafranski, 2020), relatively close to each other and to the Azores islands. These are the Menez-Gwen (at 850m depth) including Bubbylon, Lucky Strike (1,700m) including Ewan, Menez Hom (1,800m), Saldanha (2,200m), and Rainbow (2,400m). The Moytirra hydrothermal vent area was recently discovered north of the Azores (2,900m) at about 45.5°N (Wheeler et al., 2013). The detection of several hydrothermal plume signals on the northern Mid-Atlantic Ridge indicates that more active fields may occur in the region (Hydes et al., 1986; German et al., 1996; Aballéa et al., 1998; Chin et al., 1998; Beaulieu et al., 2015), as recently demonstrated for fast- and intermediate-rate spreading ridges (Baker et al., 2016).

Between 2006 and 2008, the mineral exploration company Nautilus Minerals Inc. approached the Regional Government

TABLE 1 | Areas originally submitted to the Government of the Azores by Nautilus Minerals Inc. for deep-sea SMS mining exploration in the Azores region.

Area name	Total area (km²)	Depth range in m (average depth)	Location in EEZ
Cavala	1,608	267-2,271 (1402)	Inside
Lucky Strike Hole	1,543	626-3,533 (2357)	Inside
Menez Hom	1,564	1,429-3,091 (2484)	Inside
Famous	1,515	1,343-3,245 (2435)	Inside
Saldanha	1,544	1,259-3,261 (2258)	72% inside
Rainbow	1,498	1,213 3,323 (2477)	Outside

With the exception of Cavala seamount, five out of the six proposed areas were published in the official National (Aviso n.° 13357-13360/2012 and 13446/2012) and Regional (Aviso n.° 85/2012-89/2012) journals in 2012.

of the Azores, intending to explore mineral resources in the deep sea inside the Portuguese EEZ around the Azores and the adjacent Extended Continental Shelf claim. Nautilus submitted the first proposal for exploration rights in several areas in the Azores region totalling 9,272 km² (from North to South): Patorra (locally known as Cavala seamount), Moreto (known as Lucky Strike Hole, south of the Menez Gwen hydrothermal vent field and West of Monte Alto and Voador seamounts), Arinto (known as Menez Hom, south of Lucky Strike area, between Sarda and Farpas seamounts), Famous (in the Famous hydrothermal vent field), Saldanha (in the Saldanha hydrothermal vent), and Verdelho (known as the Rainbow hydrothermal vent fields) (**Table 1** and **Figure 1**). With the exception of the Cavala seamount, five out of the six proposed areas were published in the National (Aviso n.° 13357-13360/2012 and 13446/2012) and Regional (Aviso n.° 85-89/2012) official governmental journals in 2012. In the same year, legislation for mineral exploration and exploitation in the Azores and legislation granting access and equitable distribution of scientific results (following the Nagoya Protocol) were created by Regional Government of the Azores. A dispute with the Portuguese government has ruled this legislation unconstitutional (ECORYS, 2014) and has put things on hold. Nautilus Minerals went bankrupt in 2019, and the company's assets were received by Deep Sea Mining Finance Ltd[1]. In this study, we simulated the potential dispersal of SMS mining plumes in all study areas with special emphasis on two case study areas: Cavala and Lucky Strike Hole.

2.2 3D Hydrodynamic Modelling Using MOHID

We used the 3-D hydrodynamic modelling system MOHID[2] water, developed by the Marine and Environmental Technology Research Center at Instituto Superior Técnico, University of Lisbon (Mateus and Neves, 2013), to simulate the dispersal of water and sediment plumes originated from deep-sea mining operations. MOHID water is a three-dimensional water modelling system composed of several modules structured hierarchically (e.g., 3-D baroclinic hydrodynamic module, 1-D turbulence module, an eulerian transport module, 0-D water quality module, lagrangian transport module, oil dispersion module, jet model, a cohesive sediment transport module, and at the surface and the seabed boundary conditions modules). This modelling tool has been extensively used to simulate complex vertical and horizontal ocean circulation patterns and velocity fields, sediments and microplastic transport, seaweed and plume dispersion, primary and secondary production and nutrient cycling, oil spills, and others (e.g., Juliano et al., 2012; Ballent et al., 2013; Marín et al., 2013; Duarte et al., 2014; Plecha et al., 2014; Sousa et al., 2014; Garbossa et al., 2021). MOHID water has been successfully used to model the oceanography of a deep-sea coral reef area off Scotland (Navas et al., 2014).

The MOHID Eulerian model computes the hydrodynamic (velocity, free-surface level temperature and salinity) fields in a fixed grid. It solves Navier-Stokes equations assuming hydrostatic equilibrium and the Boussinesq approximation. The model uses a finite volume approach, with generic vertical discretisation allowing simultaneous implementation of different types of vertical coordinates. The coupled MOHID turbulence module applies the General Ocean Turbulence Model (GOTM[3]). The hydrodynamic model was forced by tide, atmospheric and open boundary conditions. The MOHID lagrangian transport module tracks the trajectories of selected water masses or particles and was used to simulate the movement of the plume generated by deep-sea mining activities using the transport fields calculated with the Eulerian hydrodynamic model. The dispersion was computed using the results from the turbulence model. The coupled MOHIDJET module was used to simulate the initial near field dilution and dispersion of outfalls jets composed of plumes and particles generated by deep-sea mining activities at the discharge point.

2.3 Implementation of the 3D Hydrodynamic Modelling Approach

The hydrodynamic model was implemented using a downscaling domain approach of increasing horizontal resolution (**Supplementary Figure 1**). Domain 1 represents the larger domain in the Azores region with a spatial resolution of 6x6 km (31.0-43.0°N, 21.8-38.9°W), with an area of approximately 2,160,000 km². Domain 2 is the first nested grid corresponding to the MAR (34.7-40.2°N, 36.0-29.2°W), also with a spatial resolution of 6x6km and covering approximately 375,000 km².

[1]https://en.wikipedia.org/wiki/Nautilus_Minerals.
[2]http://www.mohid.com/.
[3]http://www.gotm.net/.

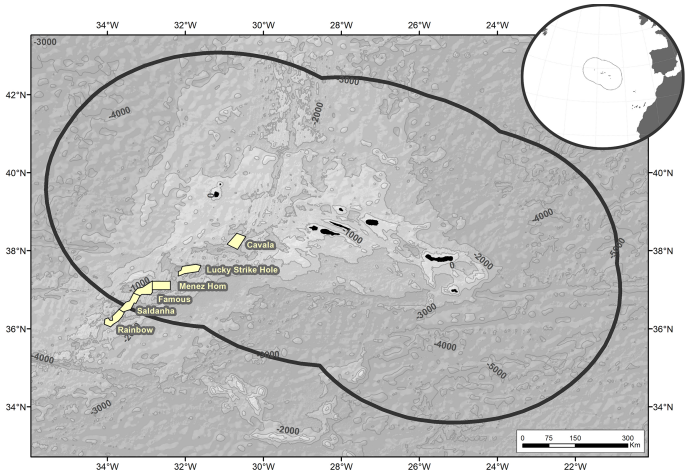

FIGURE 1 | Location of the areas originally submitted to the Government of the Azores by Nautilus Minerals Inc. for deep-sea SMS mining exploration in the Azores region. With the exception of Cavala seamount, five out of the six proposed areas were published in the National (Aviso n.° 13357-13360/2012 and 13446/2012) and Regional (Aviso n.° 85-89/2012) official governmental journals in 2012

Domain 3 is composed of two nested grids of 1.2x1.2 km (37.0-38.9°N, 30.1-32.7°W and 35.7-37.7°N, 31.9-34.5°W), representing the areas of potential deep-sea mining activities in the MAR, and covering approximately 50,000 km^2 each. The time steps considered were 120 seconds for domains 1 and 2, and 60 seconds for domain 3. Bathymetry grids were generated using the Global Bathymetry and Elevation Data at 30 Arc Seconds Resolution (SRTM30_PLUS; Becker et al., 2009) and the European Marine Observation and Data Network (EMODNet) Digital Terrain Model[4]. The bathymetry data were interpolated to the different domain resolutions.

The open boundary tidal forcing for the hydrodynamic model was obtained from the finite element global tides atlas FES2012[5] and applied to domain 1 to generate a 2-D barotropic model. Atmospheric boundary conditions were obtained from the Global Forecast System (GFS[6]), while the Open Boundary Conditions (OBC) were provided by the Mercator Ocean (PSY2V4, Drillet et al., 2005). Domains 2 and 3 are fully 3-D baroclinic circulation models with a z-level vertical discretisation with 50 vertical layers, of which 43 in Cartesian coordinates and the top 7 in sigma coordinates, with a resolution of <1 m near the surface and about 150m at 1,000m depth. We have produced data from 12 months run in hindcast mode using 2011 as the reference year.

The model configuration, the selected parameters and validation results are detailed in Riflet et al. (2008). Validation was done by comparing the outputs of the MOHID hydrodynamic model with temperature and salinity data obtained from remote sensing and *in situ* from ARGO floats[7]. The ARGO data were collected and made freely available by the International Argo Project and the national programs that contribute to it[8]. The vertical thermohaline structure in domain 2 produced by the hydrodynamic model showed Pearson correlations coefficients greater than 0.95, with a large majority being 0.99, when compared to the ARGO float data (**Supplementary Figures 2**, **3**). The outputs of the hydrodynamic model (horizontal and vertical components of the velocity, sea level, temperature, salinity, and density fields) were used to feed the MOHID lagrangian module coupled with MOHIDJET to simulate the plume-dispersal processes in offline mode.

2.4 Plume Dispersal Modelling

Nautilus Minerals developed the "world-first" project for mining high-grade polymetallic Seafloor Massive Sulphide (SMS) in the deep sea, at approximately 1,600m depth off Papua New Guinea (Solwara 1). Nautilus produced a detailed project report on the *modus operandi* of the expected operations for mining SMS deposits (Coffey Natural Systems, 2008). The IHC Merwede worked together with the EU FP7 MIDAS project and developed mining scenarios for SMS deposits in the Mid-Atlantic Ridge, with the main goal of assessing the scale of potential environmental impacts (Ortega and Boomsma, 2014). Although mining in Solwara 1 by Nautilus Minerals is no longer expected, the present study was based on the scenarios and operations developed in these two reports, adapted to our potential mining sites.

Pre-mining operations were expected to occur in the Solwara 1 project in Papua New Guinea, since the exploitation area was covered by a layer of sediment and rock that was expected to be removed prior to mining (ASA, 2008a). This operation would move 130,000 tonnes of unconsolidated sediment and 115,000 tonnes of rock (ASA, 2008a), creating sediment plumes that may spread out considerably. Contrary to Solwara 1 no major

[4]http://www.emodnet-bathymetry.eu/.
[5]http://www.legos.obs-mip.fr/recherches/equipes/ecola/projets/.
[6]https://www.ncdc.noaa.gov/data-access/model-data/modeldatasets/global-forcast-system-gfs.
[7]http://www.argo.ucsd.edu.
[8]http://www.argo.ucsd.edu, http://argo.jcommops.org.

pre-mining operations are expected to occur in the Azores potential mining sites, and no estimates of the amount of sediment to be moved are available. In this study, we modelled the dispersal of the sediment plumes generated during the *in situ* mining operations and the plumes generated during the dewatering process.

2.4.1 Modelling *In Situ* Excavation Sediment Plume

In situ mining operations may generate sediment plumes in different ways (ASA, 2008b). When the seafloor mining tool (SMT) lands or crawls on the seafloor, sediments may be re-suspended and dispersed by local currents. Additionally, during mining operations, portions of the cut ore may escape from the SMT and cause cutting spills that will partially be re-suspended and therefore cause additional sediment plumes. Here, we used the scenarios developed by Ortega and Boomsma (2014) that considered that 25% of the cut materials would not be picked up by the SMT from the seafloor (i.e., cutting spill). Of these solids, 30% may be re-suspended by local and induced currents during the excavation process at the seabed (i.e., resuspension spill). It should be noted that the Coffey Natural Systems (2008) report assumed the mining tools were developed in a way that all fine materials with the potential of forming plumes would be collected by the system and pumped to the surface. However, since this is very unlikely, we based our simulations on Ortega and Boomsma (2014).

The plume created *in situ* during the excavation process was modelled adopting the Ortega and Boomsma (2014) parameters adjusted to local conditions. In these simulations, we have assumed a production of solids of 0.03 $m^3 \cdot s^{-1}$, a resuspension spill of 7.5% of the cut materials, and an average solids density of 3,780 $kg \cdot m^{-3}$. It was further assumed that the crawler at 0.05 $m \cdot s^{-1}$ would produce an initial plume of 2 m in height and 5 m in width at a flow rate of 0.5 $m^3 \cdot s^{-1}$. Therefore, the concentration of suspended solids was assumed to be 17,010 $mg \cdot L^{-1}$. The particle size distribution was estimated by Ortega and Boomsma (2014) in hyperbaric cutting experiments with different types of rocks (**Supplementary Table 1**). The hindered settling velocities of these particles were calculated using Zhiyao et al. (2008) equation, provided in the "Settling Velocity 2.1: Rapid Computer Calculations of the Sedimentation Velocity and the Hindered Settling Rate of Spherical and Natural Sediment Particles" produced by Janwillem Rouweler. The final settling velocities for the different particle sizes were calculated assuming an average particle density of 3,780 $kg \cdot m^{-3}$ (Ortega and Boomsma, 2014) and the local water density from MOHID (**Supplementary Table 1**). The *in situ* sediment plume was modelled assuming a continuous and stationary emission, using the MOHID lagrangian module, coupled to the MOHID water transport and water properties fields. The simulation model was run for 12 months starting on the 1st of January 2011.

2.4.2 Modelling the Dewatering Plume

Based on the Nautilus mining operations plan (Coffey Natural Systems, 2008), the ore extracted at the seafloor by the SMT will be pumped to the surface *via* a riser and lifting system as a slurry, i.e., a semi-liquid mixture of particles and bottom water. On board the mining support vessel, the material will be dewatered and the return water pumped back down to the sea with fine suspended solids smaller than 8 μm in diameter. During the dewatering process, plumes will be formed close to the seafloor, containing contaminated water enriched in toxic metals and fine sediments. Because the contaminated water and sediments have different dispersal patterns, we have modelled them separately as the return water discharge plume and the return sediment discharge plume. We adapted the Nautilus mining operations plan to our potential mining sites.

2.4.2.1 Modelling the Return Water Discharge Plume

The return water discharge plume was modelled based on the Nautilus mining operations plan and parameters (ASA, 2008b) adjusted to local conditions. In the simulations, the return water was released at 30m above the seabed at a rate of 0.253 $m^3 \cdot s^{-1}$ from two U-shaped 170mm diameter pipes that will discharge the water vertically upwards. It was assumed that the return water is composed of 83.3% seafloor water and 16.7% of surface water, representing a starting concentration after pre-dilution of 833,333,333 PPB (parts per billion).

The temperature of the return water discharge was estimated using the Law of Conservation of Energy, assuming that the final temperature of the mixture (i.e., 83.3% surface water and 16.7% of seafloor water) depends on the masses of the two amounts of water and their initial temperatures. The discharge temperature was calculated using the water density and temperature estimated by MOHID for each discharge location, assuming a 1°C increase and decrease during the transport of bottom water to the surface and the return back to the bed, respectively (**Supplementary Table 2**). Discharge temperature was kept constant throughout the simulations assuming a control temperature as the annual minimum temperature of each location (T_1). Three scenarios were used in Cavala seamount and Lucky Strike Hole to analyse the sensitivity of the model projections to different discharge temperatures. Additionally to T_1, we used a higher temperature considering the annual maximum temperature of each location (T_2) and an extremely low temperature assuming the ambient temperature of the local conditions at the seabed (T_{amb}). The Salinity of discharge was calculated assuming the MOHID salinity of 83.3% surface water and 16.7% of seafloor water.

The return water discharge plume was modelled using the MOHID lagrangian module, MOHID water transport and water properties fields, and MOHIDJET module in the near field. It was further assumed that the return water would become too diluted and non-toxic after 10 days from discharge and therefore not modelled from this point onwards. The starting date for the simulations was 1st of January 2011.

2.4.2.2 Modelling Return Sediments Discharge Plume

The return sediments discharge plume was modelled using MOHID Water hydrodynamic module with turbulence and MOHID's Lagrangian module coupled with MOHIDJET for the near field, following Nautilus mining operations plan and adopted

parameters (ASA, 2008b). In our study, the return sediments discharge contained a concentration of suspended solids smaller than 8 μm in diameter at a concentration of approximately 6,000 $mg{\cdot}L^{-1}$. For all study areas, we used an average particle diameter of 4 μm, while for Cavala seamount and Lucky Strike Hole we also used an average diameter of 8 μm to test the sensitivity of the model to particle size. The hindered settling velocities of particles at high concentrations were calculated using Zhiyao et al. (2008) equation. The final settling velocities were calculated assuming an average particle density of 3,780 $kg{\cdot}m^{-3}$ (Ortega and Boomsma, 2014) and the local water density from MOHID are shown in **Supplementary Table 3**. For Cavala seamount and Lucky Strike Hole, an alternative scenario using an average particle density of 3,300 $kg{\cdot}m^{-3}$ was used to test the sensitivity of the outputs to particle density (ASA, 2008b). Simulations were run for 12 months. Temperature and salinity of discharge were calculated as described for the return water discharge plume.

2.4.3 Thresholds

Most of the deep seafloor away from the continental margins, with few exceptions, are known to have low concentrations of suspended solids (<0.01 $mg{\cdot}L^{-1}$), indicating low levels of resuspension and advection of sediments (Gardner et al., 2018). In the Azores region along the MAR, Gardner et al. (2018) estimated that the seafloor away from the influence of hydrothermal vent plumes may average between 0.01 and 0.025 $mg{\cdot}L^{-1}$ of suspended solids concentrations. In the Rainbow hydrothermal vent, the typical background of deep water not affected by the vent plume has an average total suspended solids concentration of 0.04 $mg{\cdot}L^{-1}$, while the maximum turbidity in the core of the 100-m-thick plume was 0.09 $mg{\cdot}L^{-1}$ (Haalboom et al., 2020).

The Coffey Natural Systems (2008) report, the Australian and New Zealand Environment and Conservation Council (ANZECC) and the Management Council of Australia and New Zealand (ARMCANZ) set a target for total suspended solids of 1.2 $mg{\cdot}L^{-1}$, which is one order of magnitude greater than the concentrations of solids in the Rainbow natural hydrothermal vent plume and thirty times higher than the background concentrations mentioned above. The Coffey Natural Systems (2008) set a 5,000-fold dilution as the threshold for meeting the guidelines for all contaminants in the return water discharged plume into the environment. In this study, we, therefore, adopted a concentration of solids in the return sediment discharge plume and in the *in situ* excavation sediment plume of 1.2 $mg{\cdot}L^{-1}$ and a 5,000 fold dilution of the return water discharge plume as the main thresholds for analysing the model projections.

2.5 Data Analyses

The results of the models were analysed in different ways. The concentration of solids and of the discharge water in each horizontal 2-dimensional space cell was calculated as the maximum concentration in the 50 vertical layers of each 2-dimensional cell, for each output time step (3 hours), averaged over all time steps during each trimester and during a 12-months simulation. We also estimated the proportion of simulated time (temporal frequency) that a specific 2-dimensional space contained plume concentrations higher than the adopted thresholds (1.2 $mg{\cdot}L^{-1}$ and 5,000-fold). For this, the maximum plume concentration in each cell and time step was compared to a threshold. Those cells whose temporal frequency above the thresholds was greater than 50%, i.e., 6 months out of 12 months, were considered as cells with persistent plumes. In addition to the thresholds and targets, we also analysed the results for Cavala seamount and Lucky Strike Hole against other thresholds: 5 $mg{\cdot}L^{-1}$, 10 $mg{\cdot}L^{-1}$ and 25 $mg{\cdot}L^{-1}$ for sediments and 1,000-, 600-, 300- and 200-fold dilution for discharge water. Seasonal variations in the plumes dispersal were analysed for Cavala seamount and Lucky Strike Hole by computing the probability of concentration above thresholds for four periods of three months (January-March, April-June, July-September, and October-December). In these scenarios, the model run duration was approximately 90 days. In addition, the vertical footprint of the plumes was assessed by computing plume concentration along meridional and zonal vertical cross-sections along the simulation period. The sediment thickness of the settled sediments from the *in situ* excavation and return sediment discharge were also estimated. Model outputs are available for download at https://doi.org/10.1594/PANGAEA.945244 (Morato et al., 2022).

The sensitivity of the plume-dispersal model projections to different input parameters was tested with Fuzzy Kappa statistic for assessing the similarity of numerical maps. In general terms, the fuzzy numerical map statistic goes beyond a traditional cell-by-cell comparison and takes the neighbouring cells into account to compensate for spatial offsets in correlation analyses through fuzziness of location (Hagen, 2003; Hagen, 2006). We adopted an exponential distance decay membership function considering a neighbourhood radius of 4 cells and a halving distance of 2 cells. These geometric input parameters are adequate for compensating spatial offset errors without exaggerating fuzziness (Negreiros et al., 2021). Cells with plume-dispersal projections of 0 were set to "no data" to prevent overestimating the fuzzy similarity statistics and their dependence on the map size. The similarity of each cell between model projection maps is expressed on a scale between 0 and 1. The resulting fuzzy similarity map was then used to calculate the average similarity over the whole map. All map comparisons were computed in the Map Comparison Kit (Visser and De Nijs, 2006), version 3.2.3.

3 RESULTS

3.1 *In Situ* Mining Excavation Sediment Plume

The 2-dimensional dispersal of the *in situ* excavation sediment plume was projected to vary considerably between sites (**Figure 2**), attaining maximum values in the northern sites of Lucky Strike Hole and Cavala seamounts (27 and 26 $mg{\cdot}L^{-1}$, respectively). In most cases, the excavation plume concentrations above the 1.2 $mg{\cdot}L^{-1}$ threshold were projected

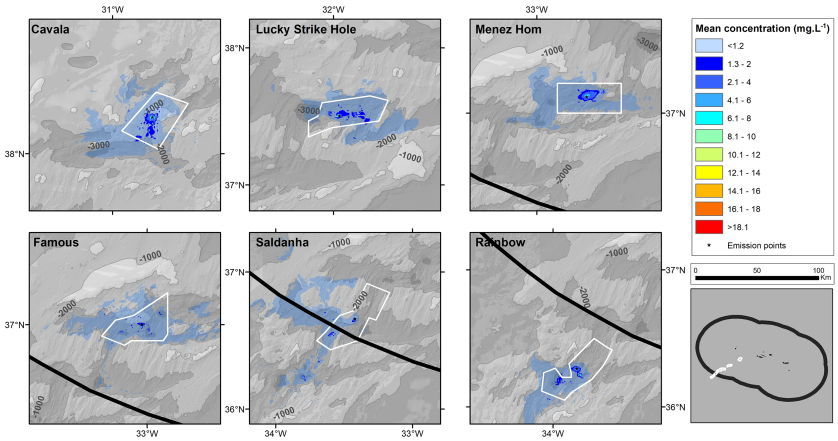

FIGURE 2 | Concentration of sediments produced during the *in situ* excavation sediment plume calculated as the maximum concentration in the 50 vertical layers of each 2-dimensional cell, for each output time step (3 hours), averaged over all time steps during a 12-months simulation. Sediments were composed of six classes of different particle diameter (0-10 µm, 10-50 µm, 50-100 µm, 100-200 µm, 200-2,000 µm, and >2,000 µm), an average particle density of 3,780 kg·m^{-3}, and resultant settling velocities ranging from 75.1 cm·s^{-1} to 0.002 cm·s^{-1}.

to be retained within the exploration areas, but large footprints below this threshold were projected well outside all areas. The horizontal footprint of persistent excavation sediment plumes (temporal frequency greater than 50%, i.e., 6 months out of 12 months) above the 1.2 mg·L^{-1} threshold was projected to average 60 km^2 and to disperse for about 19 km in linear distance (**Figure 3** and **Table 2**). The largest persistent horizontal extents were projected for Lucky Strike Hole, Cavala, and Menez Hom sites, ranging from 73 to 101 km^2, but higher dispersal distances were projected for Lucky Strike Hole and Saldanha (28 and 24 km, respectively). The dispersal of the *in situ* excavation sediment plume, regardless of the temporal frequencies, can be very high, ranging from thousands (1.2 and 5 mg·L^{-1}) to hundreds of squared kilometres (10 mg·L^{-1}) (**Supplementary Table 4**). It should be noted that all concentrations and temporal frequencies were calculated for each 2-dimensional cell, therefore not showing where in the water column the plume is being dispersed.

The vertical footprint of the excavation plume of sediment was projected to extend to much shallower depths than that of the emission point in all studied sites, averaging 800m of vertical thickness at concentrations above the 1.2 mg·L^{-1} threshold (**Figure 4**; **Supplementary Figure 4**). The *in situ* excavation sediment plumes were projected to spread along the flanks and summits of nearby topographic features (**Supplementary Figure 4**).

The cumulative bottom thickness of settled sediments produced from the *in situ* excavation plume was estimated to be from 159 to 402 mm in close vicinity (i.e., one cell) to the emission point (**Figure 5**). It should be noted that the emission point was stationary during this modelling exercise and that the deposited sediment will be distributed throughout the

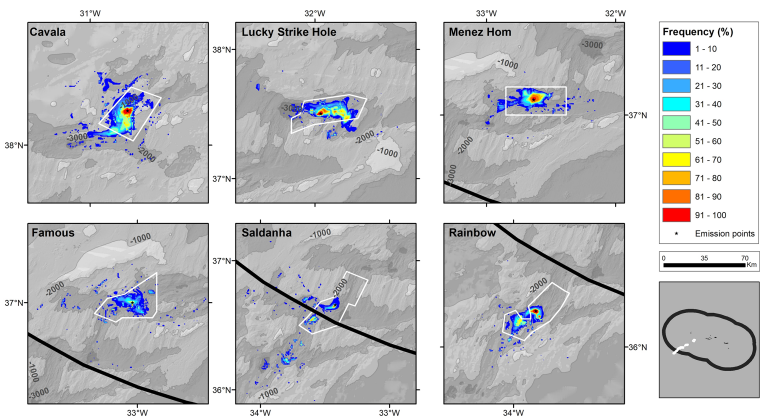

FIGURE 3 | Proportion of simulated time (temporal frequency) that a specific a 2-dimensional space cell, in six study areas, contained *in situ* excavation sediment plume above a 1.2 mg·L^{-1} concentration threshold, during a 12-months simulation, assuming six classes of particle diameter (0-10 µm, 10-50 µm, 50-100 µm, 100-200 µm, 200-2,000 µm, and >2,000 µm), an average particle density of 3,780 kg·m^{-3}, and resultant settling velocities ranging from 75.1 cm·s^{-1} to 0.002 cm·s^{-1}.

TABLE 2 | Projected dispersal in 2-dimensional space of the *in situ* excavation plumes of sediments exceeding 1.2 mg·L^{-1} concentration in area (km^2) and maximum linear distance (km) in relation to the estimated temporal frequency, i.e. the proportion of simulated days that a specific 2-dimensional space contained plumes above the adopted concentration threshold.

	Area (km^2)				Max distance (km)			
	Temporal frequency of concentrations above 1.2 mg·L^{-1}							
	All	**≥25%**	**≥50%**	**≥75%**	**All**	**≥25%**	**≥50%**	**≥75%**
Cavala	10,760	261	94	37	>135	36	22	9
Lucky Strike Hole	4,836	202	101	28	70	29	28	14
Menez Hom	20,981	147	73	36	61	20	13	8
Famous	26,656	76	14	4	105	21	4	3
Saldanha	8,496	61	20	6	98	61	24	4
Rainbow	3,050	112	55	21	64	35	21	9
Average	*12,463*	*143*	*60*	*22*	*89*	*34*	*19*	*8*

Temporal frequencies are 3 months (25%), 6 months (50%), and 9 months (75%).

excavation area during commercial mining operations. In all other cells, including in many close topographic features, the thickness of the settled sediments was predicted to be small, averaging in sites from 0.06 to 0.24 mm (**Figure 5**).

3.2 Dewatering Plume

3.2.1 Return Water Discharge Plume

The simulations of the expected footprint, in 2-dimensional space cells, of the return water discharge projected a large dispersal potential in all studied sites throughout the study period (**Figure 6**). The model simulations projected extensive areas with return water plume at higher concentrations than the accepted dilution threshold (5,000-fold) in many sites spreading beyond the proposed mining areas (**Figure 6**). Higher concentrations of return water plumes, averaged over a one-year period, were projected in Cavala seamount (average dilution= 971-fold), followed by Menez Hom (average dilution= 4,607 fold) and Rainbow site (average dilution= 5,160 fold). Additionally, our model projected high temporal frequencies of return water plumes concentrations greater than the 5,000-fold threshold in large areas of all study sites (**Figure 7**). Higher temporal frequencies were estimated to be attained close to the simulated release points but extending beyond the Rainbow mining area.

The model also projected some differences among the study sites on the patterns of the return water discharge plume dispersal and frequencies above thresholds, probably due to localised current patterns associated with the local topography (**Figures 6**, **7**). For example, the return water plume in Cavala seamount was projected to spread on a latitudinal and longitudinal gradient along the MAR axis, while in the Saldanha and Famous sites were projected to spread mostly on a longitudinal gradient across the main MAR axis. In Menez Hom and Lucky Strike sites, return water plume dispersion was projected to be somehow retained within the main MAR axis.

The models projected large 2-dimensional footprints of the return water discharge plume at larger concentrations than the 5,000-fold dilution threshold, averaging among sites 568 km^2 and 37.3 km of maximum linear distance (**Table 3**). Footprints of the discharge water concentrations five and seventeen times greater than the threshold (i.e., dilutions of 1,000 and 300-fold) averaged among sites 237 km^2 and 72

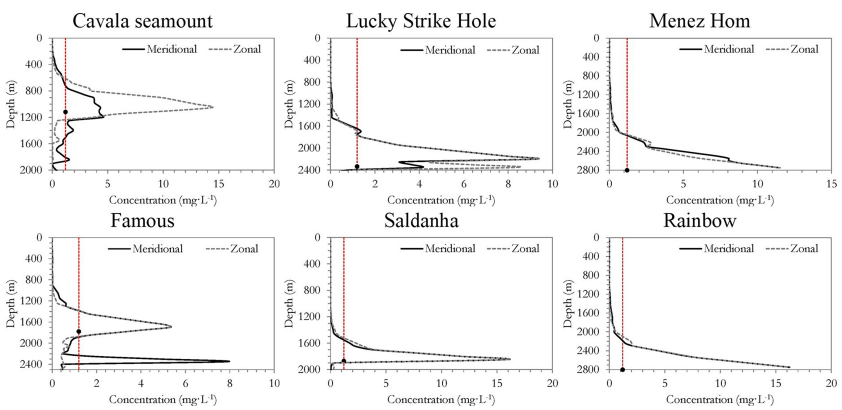

FIGURE 4 | Vertical distribution of the concentration of sediments produced during the *in situ* excavation sediment plume (in mg·L^{-1}) calculated as the maximum concentration in the 50 vertical layers of each 2-dimensional cell, averaged over a 12-months simulation period. Red line shows the 1.2 mg·L^{-1} concentration threshold and the black dot represents the depth of the stationary emission.

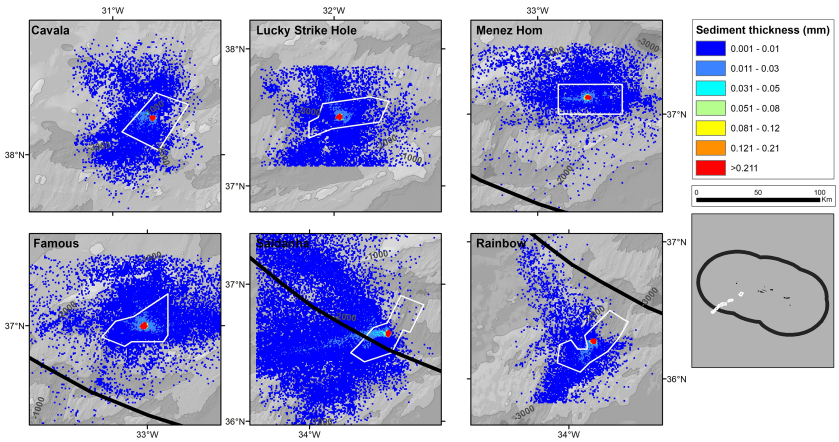

FIGURE 5 | Bottom thickness of settled sediments produced during the *in situ* excavation sediment plume assuming six classes of particle diameter (0-10 μm, 10-50 μm, 50-100 μm, 100-200 μm, 200-2,000 μm, and >2,000 μm), an average particle density of 3,780 kg·m^{-3}, and resultant settling velocities ranging from 75.1 cm·s^{-1} to 0.002 cm·s^{-1}. Duration of the simulation is one year.

km^2 (**Supplementary Table 5**). However, the footprint of persistent plumes with larger concentrations than the 5,000-fold threshold, was projected to be much smaller, averaging 36.5 km^2 and 9.5 km of maximum linear distance (**Table 3** and **Supplementary Table 5**). The model projected some differences among sites, with Saldanha, Rainbow, and Lucky Strike Hole projected to have the largest persistent horizontal footprint, ranging from 10.6 to 11.8 km.

The vertical footprint of the return water discharge plume at concentrations greater than the 5,000-fold dilution threshold showed similar patterns compared to the *in situ* excavation sediment plumes (see 3.1), extending to much shallower depths in all studied sites (**Figure 8**). In general, the model projected a vertical footprint greater than 600 m in the water column. In many study sites (e.g., Cavala, Lucky Strike Hole or Menez Hom), the meridional and zonal cross-sections showed that the plumes of the return water may get trapped on or spread along the flanks and summits of close topographic features (**Supplementary Figure 5**).

The sensitivity of the return water plume-dispersal model projections to the input parameters in Cavala and Lucky Strike Hole showed some seasonal variations but small differences related to discharge temperatures (**Supplementary Figures 6–9**). The computed fuzzy numerical similarities between seasons ranged from 0.16 (poor) and 0.79 (good) for both plume concentrations and temporal frequencies at higher concentrations than the 5,000-fold dilution threshold (**Supplementary Table 6**), with most differences being measured in cells with low values on the plume-dispersal edges. It is worth noting that in Cavala seamount, the main direction of the predicted return water plume-dispersal

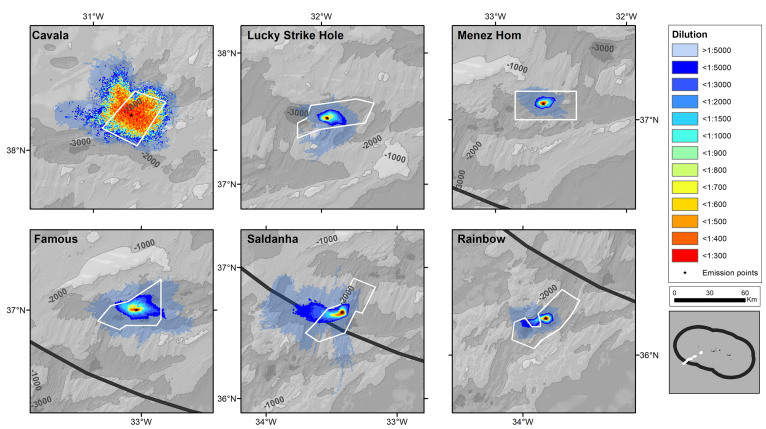

FIGURE 6 | Concentration of return water discharge plume (shown in dilution folds) in six study areas calculated as the maximum concentration in the 50 vertical layers of each 2-dimensional cell, for each output time step (3 hours), averaged over all time steps during a 12-months simulation, and assuming a control temperature as the annual minimum temperature of each location (T_1). Salinity of discharge was calculated assuming the MOHID salinity of 83.3% surface water and 16.7% of seafloor water.

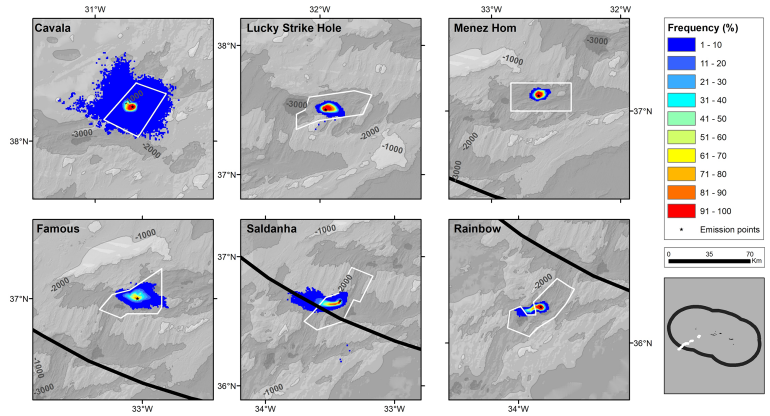

FIGURE 7 | Proportion of simulated time (temporal frequency) that a specific 2-dimensional space, in six study areas, contained return water discharge plume concentrations higher than the adopted thresholds (i.e., 5,000-fold dilution), during a 12-months simulation and assuming a control temperature as the annual minimum temperature of each location (T_1). Salinity of discharge was calculated assuming the MOHID salinity of 83.3% surface water and 16.7% of seafloor water.

varied between seasons and that in both sites slightly higher plume-dispersal were projected in the 4th trimester (October-December). The fuzzy numerical similarities between discharge temperatures ranged from 0.67 (good) and 0.79 (good) (**Supplementary Table 6**), with minor differences projected for both sites (**Supplementary Figures 6–9**). Similar to patterns in the discharge temperature, variations were projected for the temporal frequencies above other concentrations thresholds (**Supplementary Figures 10**, **11**).

3.2.2 Return Sediment Discharge Plume

Similarly to the return water discharge, our simulation projected large 2-dimensional dispersal of the solids in the return sediment discharge plume (**Figure 9**), with higher concentrations, averaged over a one-year period, projected in Cavala seamount, Rainbow, and Menez Hom sites (45, 35 and 34 mg·L^{-1}, respectively). In most sites, return sediment discharge plume concentrations above the accepted threshold of 1.2 mg·L^{-1} were projected to disperse only within the claimed areas. However, in the Rainbow site, we projected plume dispersal outside the claimed area. In all study sites, the model projected persistent sediment solids concentrations of 1.2 mg·L^{-1} (**Figure 10**). The horizontal footprint of persistent return sediment discharge plumes above the 1.2 mg·L^{-1} threshold was projected to average 150 km^2 and 21 km in linear distance (**Table 4**); in some cases, slightly beyond the claimed areas. Menez Hom, Lucky Strike Hole and Rainbow sites were projected to have the largest horizontal footprints (**Table 4**). In three sites, the model projected large areas (>20 km^2) with persistent sediment solids concentrations above 5 mg·L^{-1}; i.e., approx. 125x higher than the background of 0.04 mg·L^{-1} and 4 times higher than the accepted threshold (**Supplementary Table 7**). However, it should be noted that the projected areas impacted by the return sediment discharge plume, regardless of the temporal frequency, can be extremely large (in the order of thousands of squared kilometres) for all concentrations examined (**Table 4** and **Supplementary Table 7**).

TABLE 3 | Projected dispersal in 2-dimensional space of the return water discharge plume in area (km^2) and maximum linear distance (km) in relation to the estimated temporal frequencies, i.e. the proportion of simulated days that a specific 2-dimensional space contained plumes at greater concentrations than the adopted threshold of 5,000-fold dilution.

	Area (km^2)				Max distance (km)			
	Temporal frequency of dilution 5,000 fold							
	All	≥25%	≥50%	≥75%	All	≥25%	≥50%	≥75%
Cavala	2,045	64.3	41.3	28.1	78.5	9.8	8.0	6.8
Lucky Strike Hole	184	71.2	52.7	37.2	22.3	12.3	10.6	8.5
Menez Hom	107	50.4	37.8	24.7	16.2	9.1	8.1	6.0
Famous	459	75.7	22.6	5.2	40.0	14.2	7.0	3.2
Saldanha	459	57.3	27.8	13.9	42.2	15.6	11.8	8.5
Rainbow	151	53.8	36.8	22.9	24.5	14.1	11.6	7.8
Average	*568*	*62.1*	*36.5*	*22.0*	*37.3*	*12.5*	*9.5*	*6.8*

Temporal frequencies are 3 months (25%), 6 months (50%), and 9 months (75%).

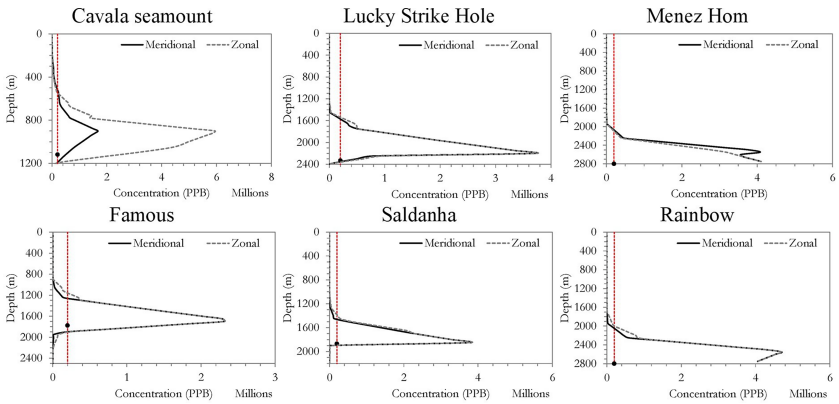

FIGURE 8 | Vertical distribution of the return water discharge plume concentration (in PPB) along meridional and zonal cross sections of the study sites, calculated as the maximum concentration in the 50 vertical layers of each 2-dimensional cell, averaged over a 12-months simulation period. The control temperature was calculated as the annual minimum temperature of each location (T_1). The salinity of discharge was calculated assuming the MOHID salinity of 83.3% surface water and 16.7% of seafloor water. Red line shows the 5,000-fold dilution threshold and the black dot represents the depth of the stationary emission.

The vertical footprint of the return sediment discharge plume showed similar patterns compared to the return water discharge plumes and the *in situ* excavation sediment plumes. It showed an average plume thickness of 800 m in all sites except Saldanha. On average, return sediment discharge plume thickness of 800 m at concentrations above the 1.2 mg·L^{-1} threshold were projected at most studied sites (**Figure 11**; **Supplementary Figure 12**). In many sites (e.g., Cavala, Lucky Strike Hole, Menez Hom, or Rainbow), the meridional and zonal cross-sections showed that the return sediment discharge plumes may get trapped on or spread along the flanks and summits of close topographic features (**Supplementary Figure 12**).

The cumulative bottom thickness of the settled sediment from the sediment discharge was estimated to be very small (averaging in sites from 0.01 to 0.09 mm), with peaks of up to 0.92 mm mostly close to the discharge point (**Figure 12**). However, the estimated footprint varied considerably between sites, with Menez Hom, Famous and Saldanha models showing large areas with settled sediments, reaching many close topographic features (e.g., Sarda seamount, Cavalo and Farpas ridge).

The model projections were not highly affected by the average particle size or particle densities adopted (**Supplementary Figures 13–16**) since the computed fuzzy numerical similarities were greater than 0.76 (good) for the concentration of sediments averaged over time and, in general, greater than 0.50 (fair) for the thickness of settled sediments (**Supplementary Table 8**). Nevertheless, smaller (4 μm) or lighter 4 μm (ρ= 3,300 kg·m^{-3}) particles were projected to settle further away

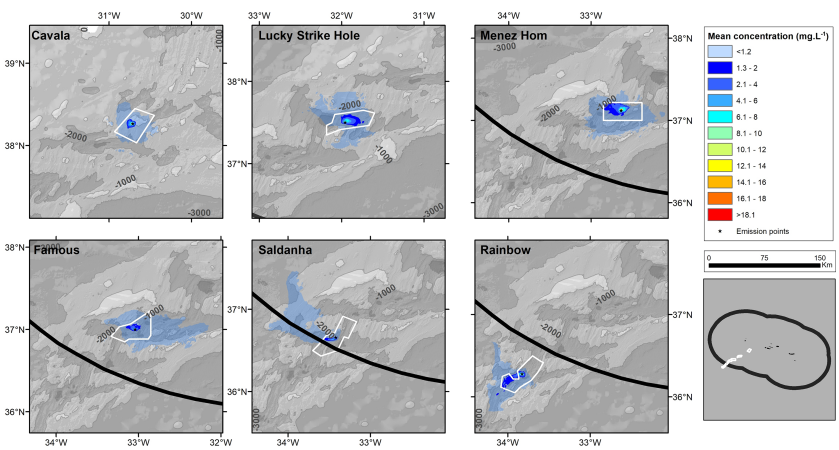

FIGURE 9 | Concentration of sediments in the return sediment discharge plume, calculated as the maximum concentration in the 50 vertical layers of each 2-dimensional cell, for each output time step (3 hours), averaged over all time steps during a 12-months simulation. The average particle diameter was assumed to be 4 μm with an average particle density of 3,780 kg·m^{-3} and a resultant settling velocity of 0.002 cm·s^{-1}.

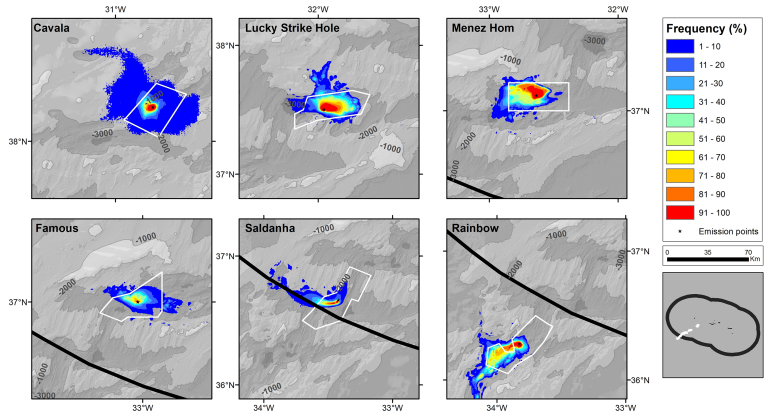

FIGURE 10 | Proportion of simulated time (temporal frequency) that a specific 2-dimensional space cell, in six study areas, contained return sediments discharge plume above a 1.2 mg·L^{-1} concentration threshold, during a 12-months simulation, assuming an average particle diameter of 4 μm, an average particle density of 3,780 kg·m^{-3}, and a resultant settling velocity of 0.002 cm·s^{-1}.

from the emission points. Similar patterns were obtained for the temporal frequencies of all concentration thresholds (**Supplementary Figures 17**, **18**).

3.3 Overlap With Biodiversity and Human Uses

The cumulative plumes projected to be produced during the excavation and the dewatering processes total 2,133 km^2 when all areas are considered simultaneously (**Figure 13**). Of this total, 1,684 km^2 were within the Azores EEZ, representing 0.18% of the total EEZ area. Our model projections indicated that 13% of the sediment plumes produced within the Azores EEZ overlapped with the existing bottom longline fishery, while 10% overlapped with the local pelagic longline and 81% and 83% overlapped with the Portuguese mainland and international pelagic longline fisheries, respectively. In terms of area, the cumulative footprint within the Azores EEZ overlaps with 217 km^2 of the local bottom longline fishing ground (2.6% of the total footprint) and 164 km^2 of the local pelagic longline fishing ground (0.1% of the total footprint) (Morato, unpublished data). In addition, this cumulative footprint overlaps with 1,368 km^2 (0.2% of the total footprint) and 1,395 km^2 (0.9% of the total footprint) of the footprints of the Portuguese mainland and international pelagic longline fleets within the Azores EZZ. The areas of greater overlap were Cavala seamount for the bottom longline fleet and Lucky Strike Hole, Menez Hom, and Famous for the pelagic longline fleet. Finally, the cumulative plumes were projected to overlap 54 km^2 of the predicted suitable habitat for several important habitat-structuring cold-water corals, or 0.5% of the total suitable habitat (Taranto et al., 2020).

4 DISCUSSION

Predicting the dispersion of plumes originating from a future activity is challenging as there are still many uncertainties regarding the mining technologies to be used and the operations to be carried out (Atmanand and Ramadass, 2017; Sharma, 2017; Leng et al., 2021). Therefore, this study should be considered as a first assessment of the potential dispersal of deep-sea mining plumes generated during the exploitation

TABLE 4 | Projected dispersal in 2-dimensional space of the discharge sediment plume exceeding 1.2 mg·L^{-1} concentration in area (km^2) and maximum linear distance (km) in relation to the estimated temporal frequency, i.e. the proportion of simulated days that a specific 2-dimensional space contained plumes above the adopted concentration threshold.

	Area (km^2)				Max distance (km)			
	Temporal frequency of concentrations above 1.2 mg·L^{-1}							
	All	**≥25%**	**≥50%**	**≥75%**	**All**	**≥25%**	**≥50%**	**≥75%**
Cavala	12,098	142	69	38	>125	18	10	8
Lucky Strike Hole	8,734	423	224	113	53	32	22	15
Menez Hom	36,939	475	309	149	55	34	27	21
Famous	36,934	159	50	6	79	20	12	4
Saldanha	26,579	80	37	17	60	18	13	9
Rainbow	13,881	416	209	69	69	48	43	20
Average	*22,527*	*283*	*150*	*65*	*63*	*28*	*21*	*13*

Temporal frequencies are 3 months (25%), 6 months (50%), and 9 months (75%).

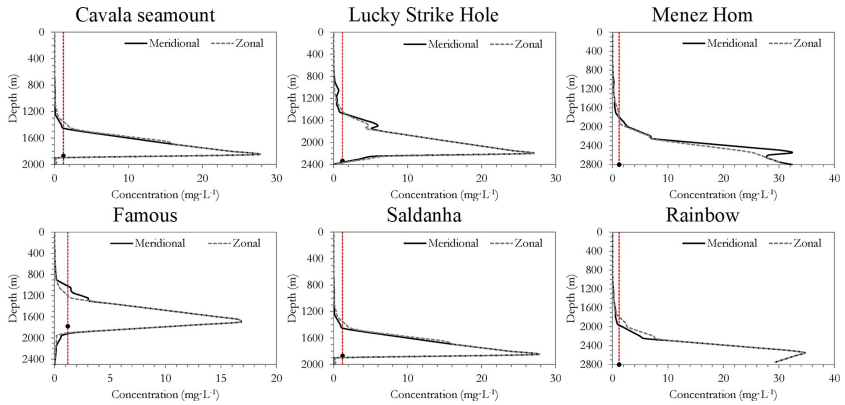

FIGURE 11 | Vertical distribution of the return sediment discharge plume concentration (in mg·L^{-1}) calculated as the maximum concentration in the 50 vertical layers of each 2-dimensional cell, averaged over a 12-months simulation. Red line shows the 1.2 mg·L^{-1} concentration threshold and the black dot represents the depth of the stationary emission.

of SMS deposits in the MAR. Our simulations were based on the Solwara 1 case study as described in Coffey Natural Systems (2008) and on the IHC Merwede mining scenario for SMS deposits in the Mid-Atlantic Ridge (Ortega and Boomsma, 2014) and may not represent the most recent views on SMS mining operations. In addition to the uncertainties associated with the mining operations *per se*, there is also a lack of detailed knowledge about the sediment composition at different sites (e.g., particle sizes, densities and settling velocities), flocculation rates, critical shear stress of erosion, critical shear stress of deposition, and erosion rates, among many others. Another important knowledge gap in our modelling work, relates to the degree of temperature changes during the uplift and subsequent descent of the ore and water, as the reported values varied from 1°C in the Coffey Natural Systems (2008) theoretical scenario to 11°C in a real lifting test (Okamoto et al., 2019). The temperature changes of the discharge water are extremely relevant because temperature oscillation mediates metal toxicity of the SMS mining plumes (Hauton et al., 2017). All these parameters are particularly important to generate realistic model projections and quantify the impacts on the marine environment (e.g., Jankowski and Zielke, 2001; Rolinski et al., 2001; Gillard et al., 2019) but, with few exceptions, in the case of the SMS deposits in the MAR they are mostly unknown. Finally, there are also some obvious uncertainties related to the MOHID hydrodynamic model, mostly considering the complex topography of the deep-sea environment in the Mid-Atlantic Ridge. For example, the resolution of the horizontal (1.2x1.2 km) and vertical (e.g., 150m at 1,000m depth) grids used, although similar to other studies, may not be sufficient to capture the localised mixing in the deep currents triggered mostly by tidal forcing of the mean circulation (Lahaye et al., 2019). Nevertheless, the comparisons made between the MOHID predictions and the remote sensing and *in situ* ARGO floats data suggested a good level of agreement.

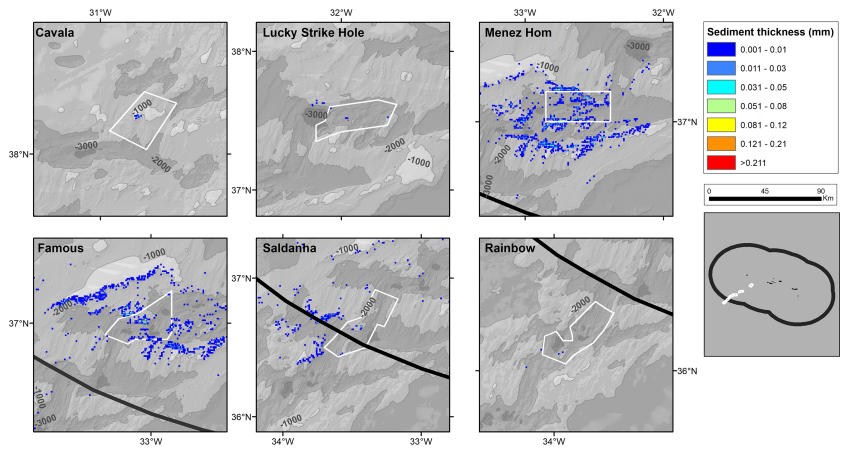

FIGURE 12 | Bottom thickness of settled sediments from the return sediment discharge plume modelled assuming an average particle diameter of 4 μm, an average particle density of 3,780 kg·m^{-3}, and a resultant settling velocity of 0.002 cm·s^{-1}. Duration of the simulation is one year.

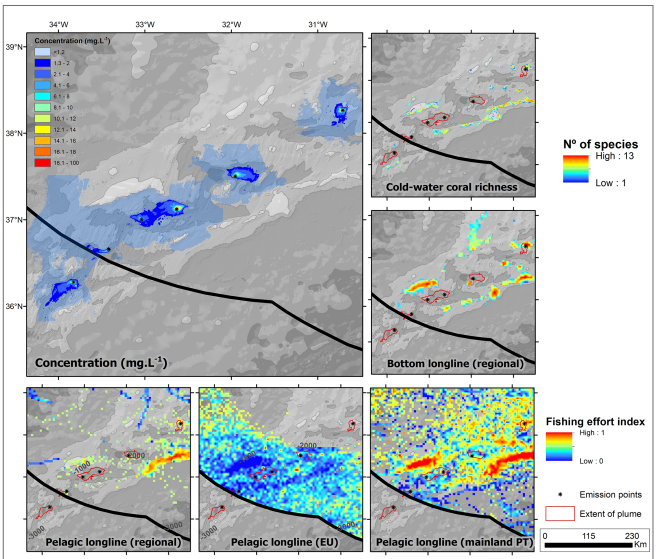

FIGURE 13 | Overlap of the cumulative sediment plumes projected to be produced during the *in situ* excavation and the return sediment discharge process, with the current bottom longline and pelagic longline fishing footprint (Morato, unpublished data) and the predicted suitable habitat for several important habitat-structuring cold-water corals inside the Azores EEZ (Taranto, unpublished data).

Although the model simulations presented here were subject to several caveats, they did reveal some important patterns. The model projected marked differences among sites making generalisations of plume-dispersal patterns in mid-ocean ridges difficult to make. Nevertheless, the model predicted large horizontal plume-dispersal of return water, return sediments, and excavation sediments at concentrations well above the thresholds (1.2 mg·L^{-1} and 5,000-fold dilution) and the typical background of total suspended solids concentration of 0.04 mg·L^{-1} (Haalboom et al., 2020). Although the total footprint of the different plumes varies considerably depending on the adopted thresholds and site, we can make the questionable generalisation that persistent (temporal frequency >50%, i.e., 6 months out 12 months) plumes may disperse, on average, over a linear distance of from 10 to 20 km and cover an area from 17 to 150 km^2. The model predicted that the plumes above concentration thresholds, regardless of the temporal frequencies, could travel for over 100 km and impact more than 10,000 km^2.

In some cases, the plume footprints with higher concentrations than the adopted thresholds were predicted to extend beyond the licensed mining areas, suggesting the need for considering large buffer areas around the licensed areas (Wedding et al., 2013; Dunn et al., 2018). In fact, the model projected that plumes might reach the flanks and summits of close topographic features, potentially impacting the local biodiversity. Additionally, the models also predicted extensive vertical footprints of all plumes modelled, in many instances extending more than 800 m in the water column. If these predictions hold true, it may suggest that bathypelagic, mesopelagic, and epipelagic environments may also be affected by potentially toxic deep-sea mining plumes, corroborating the existing concerns over the impacts of deep-sea mining in oceanic primary productivity, midwater ecosystems and their fisheries (Fuchida et al., 2017; Drazen et al., 2020; van der Grient and Drazen, 2021).

In general, our plume-dispersal predictions extend larger horizontal and vertical distances when compared to previous studies related to seafloor massive sulphides (ASA, 2008b), deep-sea nodule mining on abyssal plains (Muñoz-Royo et al., 2021) and cobalt-rich crusts on seamounts (Spearman et al., 2020). Although we used similar or higher thresholds when compared to these studies, in general, some of the reported differences in plume dispersal estimates are related to the thresholds used in each study (Muñoz-Royo et al., 2021). In our case and similarly to ASA (2008b), we used widely accepted thresholds that, in the case of the sediments, was thirty times higher than the background value for the region (Haalboom et al., 2020). Moreover, these differences may be due in part to the fact that our simulations ran for an entire year, as opposed to field experiments that lasted only a few hours or model runs of a few days (Thiel and Tiefsee-Umweltschutz, 2001; ASA, 2008b; Aleynik et al., 2017; Spearman et al., 2020; Muñoz-Royo et al., 2021). It is also possible that the increased current velocities along the MAR in the Azores region (Lahaye et al., 2019) may increase the horizontal and vertical dispersal of deep-sea mining plumes compared to other locations such as the deep Bismarck Sea (ASA, 2008b) or the abyssal plain hosting nodules fields. On the other hand, sediment plumes consisting of very fine particles and having a lower settling velocity can remain in suspension for a very long time and be carried by local currents for hundreds of kilometres (Rolinski et al., 2001). The same may happen with dissolved metals and other potentially toxic compounds that can potentially harm the marine environment (Holmstrup et al., 2010; Mestre et al., 2014, Mestre et al., 2017; Martins et al., 2017; Martins et al., 2018), although the toxicity of deep-sea mining plumes and their behaviour are not yet understood (Hauton et al., 2017).

The average cumulative sediment thickness projected from both the return sediments (from 0.01 to 0.09 mm·y^{-1}) and excavation sediments (0.06 to 0.24 mm·y^{-1}) plumes are, in general, higher than the range of natural sedimentation. For example, the natural particle flux measured at Lucky Strike and Rainbow hydrothermal vent fields away from the vent influence were estimated as 0.047 mg·cm^2·d^{-1} and 0.013 mg·cm^2·d^{-1}, respectively (Khripounoff et al., 2008), representing an annual deposition of 0.052 mm·y^{-1} and 0.014 mm·y^{-1}, respectively. Other studies have produced estimates ranging from 0.0001 mm·y^{-1} from discharge sediment plumes of nodule mining (Muñoz-Royo et al., 2021) to 0.5-1 mm·10 days^{-1} from *in situ* excavation of nodules (Thiel and Tiefsee-Umweltschutz, 2001; Aleynik et al., 2017).

This study highlights several knowledge gaps and many uncertainties associated with modelling the dispersal of deep-sea mining plumes, but also the potential far-reaching impacts of this activity on the marine environment and existing human activities. Our model projected an overlap of mining plumes with the predicted distribution of cold-water corals. This overlap

may be of conservation concern since seafloor massive sulphide mining plumes were demonstrated to produce high and rapid mortality rates on cold-water corals (Carreiro-Silva et al., this issue). Our model projections also indicated a large overlap between the predicted mining plumes and existing fishing activities. This overlap is of particular concern in regions such as the Azores, where local populations are highly dependent from the sea for their livelihoods (Diogo et al., 2015). Therefore, there is a need to quantify the baseline conditions and the nature and extent of mining impacts in space and time more precisely. This may only be achieved with experiments that are large enough to be representatively and accurately sampled over time (Jones et al., 2017). Future deep-sea mining plume dispersal studies should also consider the potential climate-related changes in the ocean circulation and deep water mass properties (e.g., warming, ocean acidification, and deoxygenation) and the climate-related effects on the dispersal and toxicity of metals associated to polymetallic sulphides (Millero et al., 2009; Levin et al., 2020).

DATA AVAILABILITY STATEMENT

The datasets presented in this study can be found in online repositories. The names of the repository/repositories and accession number(s) can be found below: Model outputs are available for download from PANGAEA at https://doi.org/10.1594/PANGAEA.945244.

AUTHOR CONTRIBUTIONS

TM, MJ, CP, MC-S, and AC contributed to the conception and design of the study. MJ developed the models. TM wrote the first draft of the manuscript. All authors contributed to manuscript revision, read, and approved the submitted version.

FUNDING

The research leading to this work has received funding from the European Union's Seventh Framework Programme under the grant agreement No 603418 (MIDAS), the European Union's Horizon 2020 programme under grant agreements No 678760 (ATLAS) and No 818123 (iAtlantic), by Fundação para a Ciência e a Tecnologia, I.P. (FCT) and Direção-Geral de Política do Mar (DGPM) project Mining2/0005/2017, as well as from the Regional Government of the Azores PO2020 MapGES project (Acores-01-0145-FEDER-000056). This output reflects only the authors' views and the European Union and the Regional Government of the Azores cannot be held responsible for any use that may be made of the information contained therein. TM was also supported by Program Investigador FCT-IP (IF/01194/2013 and IF/01194/2013/CP1199/CT0002). TM and MC-S were also supported by the FCT-IP Program Stimulus of Scientific Employment (CCCIND/03345/2020 and CCCIND/03346/2020, respectively) and the H2020 programme No 689518 (MERCES) and No 818123 (iAtlantic). AC was also supported by the FCT-IP Program Stimulus of Scientific Employment (CEECIND/00101/2021). AC, IM, and CP received support from the Operational Program Azores 2020, through the Fund 01-0145-FEDER-000140 "MarAZ Researchers: Consolidate a body of researchers in Marine Sciences in the Azores" of the European Union. TM, MJ, CP, MC-S, IM, and AC also acknowledge funds through the FCT – Foundation for Science and Technology, I.P., under the project OKEANOS UIDB/05634/2020 and UIDP/05634/2020 and through the FCT Regional Government of the Azores under the project M1.1.A/REEQ.CIENTÍFICO UI&D/2021/010.

ACKNOWLEDGMENT

The authors would like to acknowledge the contributions of many scientists and young researchers that were actively involved in the MIDAS project in the Azores, namely Ricardo Serrão Santos, António Godinho, Daphne Cuvelier, Maria Rakka, Meri Bilan, and Tara Van Belleghem, among many others. We would also like to acknowledge support from Ramiro Neves in the modeling work.

SUPPLEMENTARY MATERIAL

The Supplementary Material for this article can be found online at: https://www.frontiersin.org/articles/10.3389/fmars.2022.910940/full#supplementary-material

REFERENCES

Aballéa, M., Radford-Knoery, J., Appriou, P., Bougault, H., Charlou, J. L., Donval, J. P., et al. (1998). Manganese Distribution in the Water Column Near the Azores Triple Junction Along the Mid-Atlantic Ridge and in the Azores Domain. *Deep sea Res. Part I: oceanographic Res. papers* 45 (8), 1319–1338. doi: 10.1016/S0967-0637(98)80012-5

Aleynik, D., Inall, M. E., Dale, A., and Vink, A. (2017). Impact of Remotely Generated Eddies on Plume Dispersion at Abyssal Mining Sites in the Pacific. *Scientific Reports*, 7 (1), 1-14.

Amon, D. J., Gollner, S., Morato, T., Smith, C. R., Chen, C., Christiansen, S., et al. (2022). Assessment of Scientific Gaps Related to the Effective Environmental Management of Deep-Seabed Mining. *Mar. Policy* 138, 105006. doi: 10.1016/j.marpol.2022.105006

ASA (2008a). "Modelling the Dispersion and Settlement of Sediment Removal Operation Prior to Mining at the Solwara 1 Mining Lease," in *Coffey Natural System 2008. Environmental Impact Statement: Solwara 1 Project, Volume B. Nautilus Minerals Niugini Limited* (Papua New Guinea: Nautilus Minerals Niugini Limited). Available at: https://www.yumpu.com/en/document/read/12085050/appendices-5-13-nautilus-cares-nautilus-minerals. Appendix 11.

ASA (2008b). "Modelling the Dispersion of the Returned Water Discharge Plume From the Solwara 1 Seafloor Mining Project," in *Coffey Natural System 2008. Environmental Impact Statement: Solwara 1 Project, Volume B. Nautilus Minerals Niugini Limited* (Papua New Guinea: Nautilus Minerals Niugini Limited). Available at: https://www.yumpu.com/en/document/read/12085050/appendices-5-13-nautilus-cares-nautilus-minerals. Appendix 12Manus Basin.

Atmanand, M. A. and Ramadass, G. A. (2017). "Concepts of Deep-Sea Mining Technologies," in *Deep-Sea Mining* (Cham: Springer), 305–343.

Baker, E. T., Resing, J. A., Haymon, R. M., Tunnicliffe, V., Lavelle, J. W., Martinez, F., et al. (2016). How Many Vent Fields? New Estimates of Vent

Field Populations on Ocean Ridges From Precise Mapping of Hydrothermal Discharge Locations. *Earth Planetary Sci. Lett.* 449, 186–196. doi: 10.1016/j.epsl.2016.05.031

Ballent, A., Pando, S., Purser, A., Juliano, M. F. and Thomsen, L. (2013). Modelled Transport of Benthic Marine Microplastic Pollution in the Nazaré Canyon. *Biogeosciences* 10 (12), 7957–7970. doi: 10.5194/bg-10-7957-2013

Beaulieu, S. E., Baker, E. T. and German, C. R. (2015). Where are the Undiscovered Hydrothermal Vents on Oceanic Spreading Ridges? *Deep Sea Res. Part II: Topical Stud. Oceanogr.* 121, 202–212. doi: 10.1016/j.dsr2.2015.05.001

Beaulieu, S. E., Baker, E. T., German, C. R. and Maffei, A. (2013). *An Authoritative Global Database for Active Submarine Hydrothermal Vent Fields* (Geophysics, Geosystems, 14(11), pp.4892-4905: Geochemistry).

Beaulieu, S. E. and Szafranski, K. (2020) *InterRidge Global Database of Active Submarine Hydrothermal Vent Fields, Version 3.4. World Wide Web Electronic Publication*. Available at: http://vents-data.interridge.org (Accessed 2021-11-30).

Becker, J. J., Sandwell, D. T., Smith, W. H. F., Braud, J., Binder, P., Depner, J., et al. (2009). Global Bathymetry and Elevation Data at 30 Arc Seconds Resolution: Srtm30_PLUS. *Mar. Geod.* 32 (4), 355–371. doi: 10.1080/01490410903297766

Boschen-Rose, R. E., Clark, M. R., Rowden, A. A. and Gardner, J. P. (2021). Assessing the Ecological Risk to Deep-Sea Megafaunal Assemblages From Seafloor Massive Sulfide Mining Using a Functional Traits Sensitivity Approach. *Ocean Coast. Manage.* 210, 105656. doi: 10.1016/j.ocecoaman.2021.105656

Boschen-Rose, R. E. and Colaço, A. (2021). Northern Mid-Atlantic Ridge Hydrothermal Habitats: A Systematic Review of Knowledge Status for Environmental Management. *Front. Mar. Sci.*, 8, 657358. doi: 10.3389/fmars.2021.657358

Boschen, R. E., Rowden, A. A., Clark, M. R. and Gardner, J. P. A. (2013). Mining of Deep-Sea Seafloor Massive Sulfides: A Review of the Deposits, Their Benthic Communities, Impacts From Mining, Regulatory Frameworks and Management Strategies. *Ocean Coast. Manage.* 84, 54–67. doi: 10.1016/j.ocecoaman.2013.07.005

Boschen, R. E., Rowden, A. A., Clark, M. R., Pallentin, A. and Gardner, J. P. (2016). Seafloor Massive Sulfide Deposits Support Unique Megafaunal Assemblages: Implications for Seabed Mining and Conservation. *Mar. Environ. Res.* 115, 78–88. doi: 10.1016/j.marenvres.2016.02.005

Carreiro-Silva, M., I. Martins, V. Riou, J. Raimundo, M. Caetano, R. Bettencourt, M. et al., Submitted. Mechanical and toxicological effects of deep-sea mining sediment plumes on a habitat-forming cold-water octocoral. *Front. Mar. Sci.* Available at: https://review.frontiersin.org/review/915650/18/137790/

Cherkashov, G. (2017). "Seafloor Massive Sulfide Deposits: Distribution and Prospecting," in *Deep-Sea Mining* (Cham: Springer), 143–164.

Cherkashov, G., Poroshina, I., Stepanova, T., Ivanov, V., Bel'tenev, V., Lazareva, L., et al. (2010). Massive Sulfides From the Northern Equatorial Mid-Atlantic Ridge: New Discoveries and Perspectives. *Mar. Georesources Geotechnology* 28, 222–239. doi: 10.1080/1064119X.2010.483308

Chin, C. S., Klinkhammer, G. P. and Wilson, C. (1998). Detection of Hydrothermal Plumes on the Northern Mid-Atlantic Ridge: Results From Optical Measurements. *Earth planetary Sci. Lett.* 162 (1), 1–13. doi: 10.1016/S0012-821X(98)00141-1

Coffey Natural Systems (2008) Environmental Impact Statement: Solwara1 Project, Volume A. Nautilus Minerals Niugini Limited. Available at: https://www.yumpu.com/en/document/read/38646617/ environmental-impact- statement-nautilus-cares-nautilus-minerals.

Diogo, H., Pereira, J. G., Higgins, R. M., Canha, Â. and Reis, D. (2015). History, Effort Distribution and Landings in an Artisanal Bottom Longline Fishery: An Empirical Study From the North Atlantic Ocean. *Mar. Policy* 51, 75–85. doi: 10.1016/j.marpol.2014.07.022

Drazen, J. C., Smith, C. R., Gjerde, K. M., Haddock, S. H., Carter, G. S., Choy, C. A., et al. (2020). Opinion: Midwater Ecosystems Must be Considered When Evaluating Environmental Risks of Deep-Sea Mining. *Proc. Natl. Acad. Sci.* 117 (30), 17455–17460. doi: 10.1073/pnas.2011914117

Drillet, Y., Bourdalle-Badie, R., Siefridt, L. and Le Provost, C. (2005). Meddies in the Mercator North Atlantic and Mediterranean Sea Eddy-Resolving Model. *J. Geophysical Res.* 110 (C3), C03016. doi: 10.1029/2003JC002170

Duarte, B., Valentim, J. M., Dias, J. M., Silva, H., Marques, J. C. and Cacador, I. (2014). Modelling Sea Level Rise (SLR) Impacts on Salt Marsh Detrital Outwelling C and N Exports From an Estuarine Coastal Lagoon to the Ocean (Ria De Aveiro, Portugal). *Ecol. Model.* 289, 36–44. doi: 10.1016/j.ecolmodel.2014.06.020

Dunn, D. C., Van Dover, C. L., Etter, R. J., Smith, C. R., Levin, L. A., Morato, T., et al. (2018). A Strategy for the Conservation of Biodiversity on Mid-Ocean Ridges From Deep-Sea Mining. *Sci. Adv.* 4 (7), eaar4313. doi: 10.1126/sciadv.aar4313

ECORYS (2014). *Study to Investigate State of Knowledge of Deep Sea Mining. Final Report Under FWC MARE/2012/06 - SC E1/2013/04. ECORYS* (Rotterdam, The Netherlands: Nederland BV), 192 pp.

Fuchida, S., Yokoyama, A., Fukuchi, R., Ishibashi, J. I., Kawagucci, S., Kawachi, M., et al. (2017). Leaching of Metals and Metalloids From Hydrothermal Ore Particulates and Their Effects on Marine Phytoplankton. *ACS omega* 2 (7), 3175–3182. doi: 10.1021/acsomega.7b00081

Garbossa, L. H. P., dos Santos, A. A. and Lapa, K. R. (2021). Seaweed Dispersion Under Different Environmental Scenarios Based on Branches Settling Velocity and Hydrodynamic Lagrangian Model. *Regional Stud. Mar. Sci.* 47, 101909. doi: 10.1016/j.rsma.2021.101909

Gardner, W. D., Richardson, M. J., Mishonov, A. V. and Biscaye, P. E. (2018). Global Comparison of Benthic Nepheloid Layers Based on 52 Years of Nephelometer and Transmissometer Measurements. *Prog. Oceanogr.* 168, 100–111. doi: 10.1016/j.pocean.2018.09.008

German, C. R., Parson, L. M., Bougault, H., Coller, D., Critchley, M., Dapoigny, A., et al. (1996). Hydrothermal Exploration Near the Azores Triple Junction: Tectonic Control of Venting at Slow-Spreading Ridges? *Earth Planetary Sci. Lett.* 138 (1), 93–104. doi: 10.1016/0012-821X(95)00224-Z

Gillard, B., Purkiani, K., Chatzievangelou, D., Vink, A., Iversen, M. H., Thomsen, L., et al. (2019). Physical and Hydrodynamic Properties of Deep Sea Mining-Generated, Abyssal Sediment Plumes in the Clarion Clipperton Fracture Zone (Eastern-Central Pacific). *Elementa: Sci. Anthropocene* 7, 1-14. doi: 10.1525/elementa.343

Haalboom, S., Price, D. M., Mienis, F., Van Bleijswijk, J. D., Stigter, H. C. D., Witte, H. J., et al. (2020). Patterns of (Trace) Metals and Microorganisms in the Rainbow Hydrothermal Vent Plume at the Mid-Atlantic Ridge. *Biogeosciences* 17 (9), 2499–2519. doi: 10.5194/bg-17-2499-2020

Hagen, A. (2003). Fuzzy Set Approach to Assessing Similarity of Categorical Maps. *Int. J. Geographical Inf. Sci.* 17 (3), 235–249. doi: 10.1080/13658810210157822

Hagen, A. (2006). *Comparing Continuous Valued Raster Data: A Cross Disciplinary Literature Scan, Technical Report* (Maastricht: Research Institute for Knowledge Systems (RIKS).

Hannington, M., Jamieson, J., Monecke, T., Petersen, S. and Beaulieu, S. (2011). The Abundance of Seafloor Massive Sulfide Deposits. *Geology* 39, 1155–1158. doi: 10.1130/G32468.1

Hauton, C., Brown, A., Thatje, S., Mestre, N. C., Bebianno, M. J., Martins, I., et al. (2017). Identifying Toxic Impacts of Metals Potentially Released During Deep-Sea Mining—a Synthesis of the Challenges to Quantifying Risk. *Front. Mar. Sci.* 4, 368. doi: 10.3389/fmars.2017.00368

Herzig, P. M., Petersen, S. and Hannington, M. D. (2002). "Polymetallic Massive Sulphide Deposits at the Modern Seafloor and Their Resource Potential," in *Polymetallic Massive Sulphides and Cobalt-Rich Ferromanganese Crusts: Status and Prospects* (Kingston, International Seabed Authority), 7–35.

Holmstrup, M., Bindesbøl, A. M., Oostingh, G. J., Duschl, A., Scheil, V., Köhler, H. R., et al. (2010). Interactions Between Effects of Environmental Chemicals and Natural Stressors: A Review. *Sci. Total Environ.* 408 (18), 3746–3762. doi: 10.1016/j.scitotenv.2009.10.067

Hydes, D. J., Statham, P. J. and Burton, J. D. (1986). A Vertical Profile of Dissolved Trace Metals (Al, Cd, Cu, Mn, Ni) Over the Median Valley of the Mid Atlantic Ridge, 43 N Kingston, Jamaica: Implications for Hydrothermal Activity. *Sci. Total Environ.* 49, 133–145. doi: 10.1016/0048-9697(86)90236-6

ISA (2021). "Polymetallic Sulphides Contractors," in *Minerals: Polymetallic Sulphides*. Available at: https://www.isa.org.jm/exploration-contracts/polymetallic-sulphides.

ISA (2002). Technical Study 2: Polymetallic massive sulphides and cobalt-rich ferromanganese crusts: status and prospects. *Kingston: International Seabed Authority*.

Jankowski, J. A. and Zielke, W. (2001). The Mesoscale Sediment Transport Due to Technical Activities in the Deep Sea. *Deep Sea Res. Part II: Topical Stud. Oceanogr.* 48 (17-18), 3487–3521. doi: 10.1016/S0967-0645(01)00054-6

Jones, D. O., Kaiser, S., Sweetman, A. K., Smith, C. R., Menot, L., Vink, A., et al. (2017). Biological Responses to Disturbance From Simulated Deep-Sea Polymetallic Nodule Mining. *PloS One* 12 (2), e0171750. doi: 10.1371/journal.pone.0171750

Juliano, M., Neves, R., Rodrigues, P. P. G. W., Junior, J. L. and Fernandes, R. (2012). Aplicação Da Plataforma MOHID Para Simulação Computacional De Deriva Oceânica De Petróleo Na Bacia De Campos – Rio De Janeiro. *Boletim do Observatório Ambiental Alberto Ribeiro Lamego* 6 (1), 161–172. doi: 10.5935/2177-4560.20120010

Khripounoff, A., Vangriesheim, A., Crassous, P., Segonzac, M., Lafon, V. and Warén, A. (2008). Temporal Variation of Currents, Particulate Flux and Organism Supply at Two Deep-Sea Hydrothermal Fields of the Azores Triple Junction. *Deep Sea Res. Part I: Oceanographic Res. Papers* 55 (4), 532–551. doi: 10.1016/j.dsr.2008.01.001

Lahaye, N., Gula, J., Thurnherr, A. M., Reverdin, G., Bouruet-Aubertot, P. and Roullet, G. (2019). Deep Currents in the Rift Valley of the North Mid-Atlantic Ridge. *Front. Mar. Sci.* 6, 597. doi: 10.3389/fmars.2019.00597

Le, J. T., Levin, L. A. and Carson, R. T. (2017). Incorporating Ecosystem Services Into Environmental Management of Deep-Seabed Mining. *Deep Sea Res. Part II: Topical Stud. Oceanogr.* 137, 486–503. doi: 10.1016/j.dsr2.2016.08.007

Leng, D., Shao, S., Xie, Y., Wang, H. and Liu, G. (2021). A Brief Review of Recent Progress on Deep Sea Mining Vehicle. *Ocean Eng.*, 228, 108565. doi: 10.1016/j.oceaneng.2020.108565

Levin, L. A., Mengerink, K., Gjerde, K. M., Rowden, A. A., Van Dover, C. L., Clark, M. R., et al. (2016). Defining Serious Harm to the Marine Environment in the Context of Deep-Seabed Mining. *Mar. Pol.* 74, 245–259. doi: 10.1016/j.marpol.2016.09.032

Levin, L. A., Wei, C. L., Dunn, D. C., Amon, D. J., Ashford, O. S., Cheung, W. W., et al. (2020). Climate Change Considerations are Fundamental to Management of Deep-Sea Resource Extraction. *Global Change Biol.* 26 (9), 4664–4678. doi: 10.1111/gcb.15223

Marín, V. H., Tironi, A., Paredes, M. A. and Contreras, M. (2013). Modeling Suspended Solids in a Northern Chilean Patagonia Glacier-Fed Fjord: GLOF Scenarios Under Climate Change Conditions. *Ecol. Model.* 264, 7–16. doi: 10.1016/j.ecolmodel.2012.06.017

Marques, A. F. A. and Scott, S. D. (2011). "Azores Sea: Seafloor Hydrothermal Systems, VMS Deposits and New Exploration Targets," in OCEANS'11 MTS/IEEE KONA. 1–2, IEEE.

Martins, I., Godinho, A., Goulart, J. and Carreiro-Silva, M. (2018). Assessment of Cu Sub-Lethal Toxicity (LC50) in the Cold-Water Gorgonian Dentomuricea Meteor Under a Deep-Sea Mining Activity Scenario. *Environ. pollut.* 240, 903–907. doi: 10.1016/j.envpol.2018.05.040

Martins, I., Goulart, J., Martins, E., Morales-Román, R., Marín, S., Riou, V., et al. (2017). Physiological Impacts of Acute Cu Exposure on Deep-Sea Vent Mussel Bathymodiolus Azoricus Under a Deep-Sea Mining Activity Scenario. *Aquat. Toxicol.* 193, 40–49. doi: 10.1016/j.aquatox.2017.10.004

Mateus, M. and Neves, R. (2013). *Ocean Modelling for Coastal Management - Case Studies With MOHID* (Lilsbon: IST Press), 265 pp.

Mestre, N. C., Rocha, T. L., Canals, M., Cardoso, C., Danovaro, R., Dell'Anno, A.,et al., (2017). Environmental hazard assessment of a marine mine tailings deposit site and potential implications for deep-sea mining. *Environmental Pollution*, 228, 169-178.

Mestre, N. C., Calado, R. and Soares, A. M. (2014). Exploitation of Deep-Sea Resources: The Urgent Need to Understand the Role of High Pressure in the Toxicity of Chemical Pollutants to Deep-Sea Organisms. *Environ. pollut.* 185, 369–371. doi: 10.1016/j.envpol.2013.10.021

Millero, F. J., Woosley, R., DiTrolio, B. and Waters, J. (2009). Effect of Ocean Acidification on the Speciation of Metals in Seawater. *Oceanography* 22 (4), 72–85. doi: 10.5670/oceanog.2009.98

Morato, T., Juliano, M., Pham, C. K., Carreiro-Silva, M., Martins, I. and Colaço, A. (2022). *Model Outputs: Modelling the Dispersion of Seafloor Massive Sulphide Mining Plumes in the Mid Atlantic Ridge Around the Azores* (PANGAEA). doi: 10.1594/PANGAEA.945244

Muñoz-Royo, C., Peacock, T., Alford, M. H., Smith, J. A., Le Boyer, A., Kulkarni, C. S., et al. (2021). Extent of Impact of Deep-Sea Nodule Mining Midwater Plumes is Influenced by Sediment Loading, Turbulence and Thresholds. *Commun. Earth Environ.* 2 (1), 1–16. doi: 10.1038/s43247-021-00213-8

Murton, B. J., Lehrmann, B., Dutrieux, A. M., Martins, S., de la Iglesia, A. G., Stobbs, I. J., et al. (2019). Geological Fate of Seafloor Massive Sulphides at the TAG Hydrothermal Field (Mid-Atlantic Ridge). *Ore Geology Rev.* 107, 903–925. doi: 10.1016/j.oregeorev.2019.03.005

Navas, J. M., Miller, P. L., Henry, L. A., Hennige, S. J. and Roberts, J. M. (2014). Ecohydrodynamics of Cold-Water Coral Reefs: A Case Study of the Mingulay Reef Complex (Western Scotland). *PloS One* 9 (5), e98218. doi: 10.1371/journal.pone.0098218

Negreiros, B., Schwindt, S., Haun, S. and Wieprecht, S. (2021). Fuzzy Map Comparisons Enable Objective Hydro-Morphodynamic Model Validation. *Earth Surface Processes Landforms*. 47, 793–806. doi: 10.1002/esp.5285

Niner, H. J., Ardron, J. A., Escobar, E. G., Gianni, M., Jaeckel, A., Jones, D. O., et al. (2018). Deep-Sea Mining With No Net Loss of Biodiversity—an Impossible Aim. *Front. Mar. Sci.* 5, 53. doi: 10.3389/fmars.2018.00053

Okamoto, N., Shiokawa, S., Kawano, S., Sakurai, H., Yamaji, N. and Kurihara, M. (2018). "Current Status of Japan's Activities for Deep-Sea Commercial Mining Campaign," in *2018 OCEANS-MTS/IEEE Kobe Techno-Oceans (OTO)*, 1–7. IEEE.

Okamoto, N., Shiokawa, S., Kawano, S., Yamaji, N., Sakurai, H. and Kurihara, M. (2019). "World's First Lifting Test for Seafloor Massive Sulphides in the Okinawa Trough in the EEZ of Japan," in *The 29th international ocean and polar engineering conference*. Kobe, Japan OnePetro.

Ortega, A. and Boomsma, W. (2014). *MIDAS: Mining Research Scenarios* (Kinderdijk, Netherlands: Kinderdijk IHC Mining B.V.), 13pp.

Petersen, S., Krätschell, A., Augustin, N., Jamieson, J., Hein, J. R. and Hannington, M. D. (2016). News From the Seabed–Geological Characteristics and Resource Potential of Deep-Sea Mineral Resources. *Mar. Policy* 70, 175–187. doi: 10.1016/j.marpol.2016.03.012

Plecha, S., Picado, A., Chambel-Leitão, P., Dias, J. M. and Vaz, N. (2014). Study of Suspended Sediment Dynamics in a Temperate Coastal Lagoon: Ria De Aveiro (Portugal). *J. Coast. Res.* 70 (sp1), 604–609. doi: 10.2112/SI70-102.1

Purkiani, K., Gillard, B., Paul, A., Haeckel, M., Haalboom, S., Greinert, J., et al. (2021). Numerical Simulation of Deep-Sea Sediment Transport Induced by a Dredge Experiment in the Northeastern Pacific Ocean. *Front. Mar. Sci.*, 8, 719463. doi: 10.3389/fmars.2021.719463

Riflet, G., Juliano, M., Fernandes, L. and Leitão and R. Neves, P. C. (2008). Operational Ocean Forecasting of the Portuguese Waters. *Mercator Ocean Q. Newslett.* 30, 20–32.

Rolinski, S., Segschneider, J. and Sündermann, J. (2001). Long-Term Propagation of Tailings From Deep-Sea Mining Under Variable Conditions by Means of Numerical Simulations. *Deep Sea Res. Part II: Topical Stud. Oceanogr.* 48 (17-18), 3469–3485. doi: 10.1016/S0967-0645(01)00053-4

Sharma, R. (Ed.) (2017). *Deep-Sea Mining: Resource Potential, Technical and Environmental Considerations* (Cham, Switzerland: Springer).

Sharma, R. (Ed.) (2019). *Environmental Issues of Deep-Sea Mining: Impacts, Consequences and Policy Perspectives* (Cham, Switzerland: Springer).

Smith, C. R., Tunnicliffe, V., Colaço, A., Drazen, J. C., Gollner, S., Levin, L. A., et al. (2020). Deep-Sea Misconceptions Cause Underestimation of Seabed-Mining Impacts. *Trends Ecol. Evol.* 35 (10), 853–857. doi: 10.1016/j.tree.2020.07.002

Sousa, M. C., Mendes, R., Alvarez, I., Vaz, N., Gomez-Gesteira, M. and Dias, J. M. (2014). Unusual Circulation Patterns of the Rias Baixas Induced by Minho Freshwater Intrusion (NW of the Iberian Peninsula). *PloS One* 9 (11), e112587. doi: 10.1371/journal.pone.0112587

Spearman, J., Taylor, J., Crossouard, N., Cooper, A., Turnbull, M., Manning, A., et al. (2020). Measurement and Modelling of Deep Sea Sediment Plumes and Implications for Deep Sea Mining. *Sci. Rep.* 10 (1), 1–14. doi: 10.1038/s41598-020-61837-y

Taranto, G. H., González-Irusta, J.-M., Domínguez-Carrió, C., Pham, C. K., Tempera, F., Carreiro-Silva, M., et al., (2020) Habitat suitability and ecoscape predictions for vulnerable and foundation cold-water coral of the Azores (NE Atlantic). University of the Azores, PANGAEA, doi: pangaea.de/10.1594/PANGAEA.921282 (dataset in review)

Thiel, H. and Tiefsee-Umweltschutz, F. (2001). Evaluation of the Environmental Consequences of Polymetallic Nodule Mining Based on the Results of the TUSCH Research Association. *Deep Sea Res. Part II: Topical Stud. Oceanogr.* 48 (17-18), 3433–3452. doi: 10.1016/S0967-0645(01)00051-0

van der Grient, J. M. A. and Drazen, J. C. (2021). Potential Spatial Intersection Between High-Seas Fisheries and Deep-Sea Mining in International Waters. *Mar. Policy* 129, 104564. doi: 10.1016/j.marpol.2021.104564

Van Dover, C. L. (2011). Tighten Regulations on Deep-Sea Mining. *Nature* 470 (7332), 31–33. doi: 10.1038/470031a

Van Dover, C. L. (2019). Inactive Sulfide Ecosystems in the Deep Sea: A Review. *Front. Mar. Sci.* 6, 461. doi: 10.3389/fmars.2019.00461

Van Dover, C. L., Ardron, J. A., Escobar, E., Gianni, M., Gjerde, K. M., Jaeckel, A., et al. (2017). Biodiversity Loss From Deep-Sea Mining. *Nat. Geosci.* 10 (7), 464–465. doi: 10.1038/ngeo2983

Van Dover, C. L., Colaço, A., Collins, P. C., Croot, P., Metaxas, A., Murton, B. J., et al. (2020). Research is Needed to Inform Environmental Management of Hydrothermally Inactive and Extinct Polymetallic Sulfide (PMS) Deposits. *Mar. Policy* 121, 104183. doi: 10.1016/j.marpol.2020.104183

Visser, H. and De Nijs, T. (2006). The Map Comparison Kit. *Environ. Model. Software* 21 (3), 346–358. doi: 10.1016/j.envsoft.2004.11.013

Washburn, T. W., Turner, P. J., Durden, J. M., Jones, D. O., Weaver, P. and Van Dover, C. L. (2019). Ecological Risk Assessment for Deep-Sea Mining. *Ocean Coast. Manage.* 176, 24–39. doi: 10.1016/j.ocecoaman.2019.04.014

Weaver, P. P. E. and Billett, D. (2019). "Environmental Impacts of Nodule, Crust and Sulphide Mining: An Overview," in *Environmental Issues of Deep-Sea Mining*. Ed. Sharma, R. (Cham: Springer), 27–62. doi: 10.1007/978-3-030-12696-4_3

Wedding, L. M., Friedlander, A. M., Kittinger, J. N., Watling, L., Gaines, S. D., Bennett, M., & Smith, C. R. (2013). From principles to practice: a spatial approach to systematic conservation planning in the deep sea. P*roceedings of the Royal Society B: Biological Sciences,* 280 (1773), 20131684.

Wedding, L. M., Reiter, S. M., Smith, C. R., Gjerde, K. M., Kittinger, J. N., Friedlander, A. M., et al. (2015). Managing Mining of the Deep Seabed. *Science* 349 (6244), 144–145. doi: 10.1126/science.aac6647

Wheeler, A. J., Murton, B., Copley, J., Lim, A., Carlsson, J., Collins, P., et al. (2013). Moytirra: Discovery of the First Known Deep-Sea Hydrothermal Vent Field on the Slow-Spreading Mid-Atlantic Ridge North of the Azores. *Geochemistry Geophysics Geosystems* 14 (10), 4170–4184. doi: 10.1002/ggge.20243

Zhiyao, S., Tingting, W., Fumin, X. and Ruijie, L. (2008). A Simple Formula for Predicting Settling Velocity of Sediment Particles. *Water Sci. Eng.* 1 (1), 37–43. doi: 10.1016/S1674-2370(15)30017-X

Conflict of Interest: The authors declare that the research was conducted in the absence of any commercial or financial relationships that could be construed as a potential conflict of interest.

Publisher's Note: All claims expressed in this article are solely those of the authors and do not necessarily represent those of their affiliated organizations, or those of the publisher, the editors and the reviewers. Any product that may be evaluated in this article, or claim that may be made by its manufacturer, is not guaranteed or endorsed by the publisher.

frontiers | Frontiers in Marine Science

ORIGINAL RESEARCH
published: 26 July 2022
doi: 10.3389/fmars.2022.925419

Integrated Study of New Faunal Assemblages Dominated by Gastropods at Three Vent Fields Along the Mid-Atlantic Ridge: Diversity, Structure, Composition and Trophic Interactions

Jozée Sarrazin[1]*, *Cécile Cathalot*[2], *Agathe Laes*[3], *Julien Marticorena*[1], *Loïc N. Michel*[1] *and Marjolaine Matabos*[1]

[1]Univ Brest, Ifremer, CNRS, Unité BEEP, Plouzané, France, [2]Univ Brest, Ifremer, CNRS, Unité GEOCEAN, Plouzané, France, [3]Ifremer, Unité RDT, Plouzané, France

OPEN ACCESS

Edited by:
Elva G. Escobar-Briones, National Autonomous University of Mexico, Mexico

Reviewed by:
Daniel Pech, El Colegio de la Frontera Sur, Mexico
Takuya Yahagi, The University of Tokyo, Japan

***Correspondence:**
Jozée Sarrazin
jozee.sarrazin@ifremer.fr

Specialty section:
This article was submitted to Deep-Sea Environments and Ecology, a section of the journal Frontiers in Marine Science

Received: 21 April 2022
Accepted: 10 June 2022
Published: 26 July 2022

Citation:
Sarrazin J, Cathalot C, Laes A, Marticorena J, Michel LN and Matabos M (2022) Integrated Study of New Faunal Assemblages Dominated by Gastropods at Three Vent Fields Along the Mid-Atlantic Ridge: Diversity, Structure, Composition and Trophic Interactions. Front. Mar. Sci. 9:925419. doi: 10.3389/fmars.2022.925419

To date, two main vent faunal assemblages have been described on active sulfide edifices along the northern Mid-Atlantic Ridge (nMAR): one dominated by bathymodiolin mussels in low temperature areas and the other dominated by alvinocaridid shrimp in warmer habitats. In this study, we describe the ecology of new types of assemblage, dominated by gastropods, that are recurrent in several nMAR vent fields, from ~830 m to 3500 m depth. We assessed and compared the composition, abundance, diversity and trophic niche of these assemblages from three vent fields (Menez Gwen, Lucky Strike and Snake Pit) and characterized their habitats in terms of key environmental conditions. These assemblages, first seen during the Momarsat cruise in 2012 at the Lucky Strike vent field, were investigated during several subsequent cruises. They appear to be widespread along the nMAR, forming two distinct assemblages, one dominated by *Lepetodrilus atlanticus* at the shallowest vent field Menez Gwen, and the other by *Peltospira smaragdina* at the other investigated fields. Our data seem to indicate that these gastropods dominate an intermediate habitat at MAR vents and may play an important ecological role in these communities.

Keywords: gastropod, new assemblage, habitat, environmental conditions, diversity, hydrothermal vent, Mid-Atlantic Ridge

INTRODUCTION

Located on mid-oceanic ridges and back-arc basins, hydrothermal vent communities rely on chemosynthetic processes to sustain dense, but low diversity faunal assemblages (Tunnicliffe, 1991). Since the discovery of vent faunal assemblages in 1977, several studies have focused on the factors driving their spatial distribution in different regions of the world's oceans and at different spatial scales. At the edifice scale, active sulfide structures are colonized by large engineer species that often live in association with symbiotic microorganisms (Govenar, 2012). These foundation species provide substratum, refuge and food to various associated macro- and meiofaunal taxa

(Van Dover, 2002; Van Dover, 2003; Zekely et al., 2006; Govenar and Fisher, 2007; Sarrazin et al., 2015). They form recurrent faunal assemblages that are distributed along a mixing gradient between the cold, oxygenated surrounding seawater and the hot (up to 400°C), often acidic, hydrothermal fluids (e.g. Gebruk et al., 1997; Sarrazin et al., 1997; Sarradin et al., 1999; Marsh et al., 2012; Sen et al., 2013). Over the years, several studies have demonstrated the influence of environmental conditions on species distribution (Sarrazin et al., 1999; Bates et al., 2005; Van Dover and Doerries, 2005; Cuvelier et al., 2009; Cuvelier et al., 2011a; Sen et al., 2013; Husson et al., 2017) and dynamics (Copley et al., 1997; Cuvelier et al., 2011b; Cuvelier et al., 2014; Lelievre et al., 2017) on these large sulfide edifices. The observed mosaics of faunal assemblages are linked to the patchiness of vent emissions (Sarrazin et al., 1997; Sarrazin et al., 1999; Luther et al., 2001; Gollner et al., 2010; Podowski et al., 2010; Marsh et al., 2012; Nye et al., 2013; Sarrazin et al., 2015; Sarrazin et al., 2020). Particularly important in explaining these small-scale patterns are the available concentrations of reduced chemical compounds (e.g. hydrogen sulfide, methane and hydrogen) that are involved in chemosynthetic pathways (Jannasch, 1985; Matabos et al., 2008; Schmidt et al., 2008; Luther et al., 2012) as well as those of metals and oxygen (Desbruyères et al., 2000; Cuvelier et al., 2011a; Martins et al., 2011;). Although vital for the hydrothermal fauna, these chemicals can also have deleterious effects, depending on their concentrations (Martins et al., 2011). Thus, the spatial distribution of vent species results from a trade-off between their tolerance to the environment and their nutritional needs. On top of environmental conditions, biotic factors such as facilitation, predation or competition also interact and modulate the realized niche of these species (e.g. Mullineaux et al., 2003; Sancho et al., 2005; Podowski et al., 2010; Mullineaux et al., 2012).

The northern Mid-Atlantic Ridge (nMAR) harbors 11 known active vent fields between 12°N and 37°N (Beaulieu and Szafranski, 2020; see Gollner et al., 2021 for a map of these fields). Two faunal assemblages appear to be dominant on active edifices at the studied sites: those dominated by the engineer taxon *Bathymodiolus* spp. and those dominated by alvinocaridid shrimp (Desbruyères et al., 2000; Sarrazin et al., 2015; Sarrazin et al., 2020; Hernández-Ávila et al., 2022). In 2012, the discovery of a distinct faunal assemblage, dominated by small (~1 cm) gastropods and not described before, raised our interest. Although these small assemblages were sometimes visually difficult to locate from a submersible, we quickly realized that they were widespread not only at Lucky Strike, but also at many other vent fields of the nMAR (Marcon et al., 2013; Wheeler et al., 2013). Following this discovery, we dedicated dive time during six different cruises to gather biological and environmental data aiming to describe their composition, distribution and ecological role.

The objectives of the present study were to describe and compare the structure of these gastropod assemblages in terms of composition, density and diversity at three vent fields (Menez Gwen, Lucky Strike and Snake Pit) located on the nMAR, to describe their habitats and assess their realized ecological niches using stable isotopes. We address the following questions: Are there differences in faunal community structure between the gastropod assemblages at the three vent fields? What are the environmental conditions characterizing their habitats and are they similar among fields?

MATERIALS AND METHODS

Sampling Sites

Three vent fields, characterized by different geological settings along the nMAR, were investigated for this study: Menez Gwen (MG), Lucky Strike (LS) and Snake Pit (SP) (**Figure 1A**). They differ in depth, fluid chemistry (Charlou et al., 2000), background seawater temperature and composition of faunal assemblages (Charlou et al., 2000; Desbruyères et al., 2001; Sarrazin et al., 2020). MG (37°50′.47″N; 31°33′.37″W, **Figure 1B**) is the shallowest known vent system of the nMAR, with a mean depth of 850 m. The hydrothermally active sites are concentrated on the southern and eastern flanks of this small 15 km diameter volcano (Charlou et al., 2000) and are partly colonized by dense assemblages of *Bathymodiolus azoricus* mussels (Desbruyères et al., 2001; Marcon et al., 2013; Sarrazin et al., 2020). *Mirocaris fortunata* shrimp assemblages are visible close to high-temperature fluids and gastropod patches were previously reported from video observations (Marcon et al., 2013). In contrast to the two other vent fields, environmental conditions at MG include colder end-member fluids (up to 280°C) and higher seawater background temperatures (8.8°C). In addition, the presence of a relatively strong current at a shallow depth near this field – trending southeast to northwest – probably acts as a strong barrier to larval dispersal towards more southern fields (Sarrazin et al., 2020). The 1 km² LS vent field (37°17′.51″N; 32°16′.66″W, **Figure 1C**) has been extensively studied over the past 25 years (Langmuir et al., 1997) and has been host to the EMSO-Azores observatory since 2010 (Cannat et al., 2011). Lying at ca. 1700 m depth, LS is located in the center of three volcanic cones that surround a fossilized lava lake (Ondréas et al., 2009). The magmatic chamber is situated at 3 km below the seafloor, feeding about 20 active sulfide edifices (Singh et al., 2006). *B. azoricus* mussel assemblages largely dominate the biomass of these edifices, but *M. fortunata* assemblages are sparse (Desbruyères et al., 2001; Cuvelier et al., 2009; Cuvelier et al., 2011a; Sarrazin et al., 2015; Husson et al., 2017; Sarrazin et al., 2020). The mussel assemblages preferentially colonize low temperature habitats (4.4 – 6.1°C), whereas those of *M. fortunata* are located in slightly warmer and more variable habitats (5.2 – 9.5°C; Husson et al., 2017). The gastropod assemblages described in this study, present on only a few edifices, have never been described prior to this study. Background temperatures at this field are 4.5°C (Sarrazin et al., 2020). The SP vent field (23°22′.06″N; 44°56′.99″W, **Figure 1D**) is located on the flank of a volcanic cone, 25 km south of the Kane fracture zone (Karson et al., 1987). It harbors several active and inactive sulfide structures that are perched on top of a large talus mound (Fouquet et al., 1993). Dense populations of *Rimicaris exoculata* shrimp colonize the warmest parts of the edifices (Segonzac, 1993; Methou et al., 2019) along with three other species *(Rimicaris chacei, M. fortunata, Alvinocaris markensis*) present in lower abundances. Moreover, a few structures are also colonized by *Bathymodiolus puteoserpentis* mussel assemblages

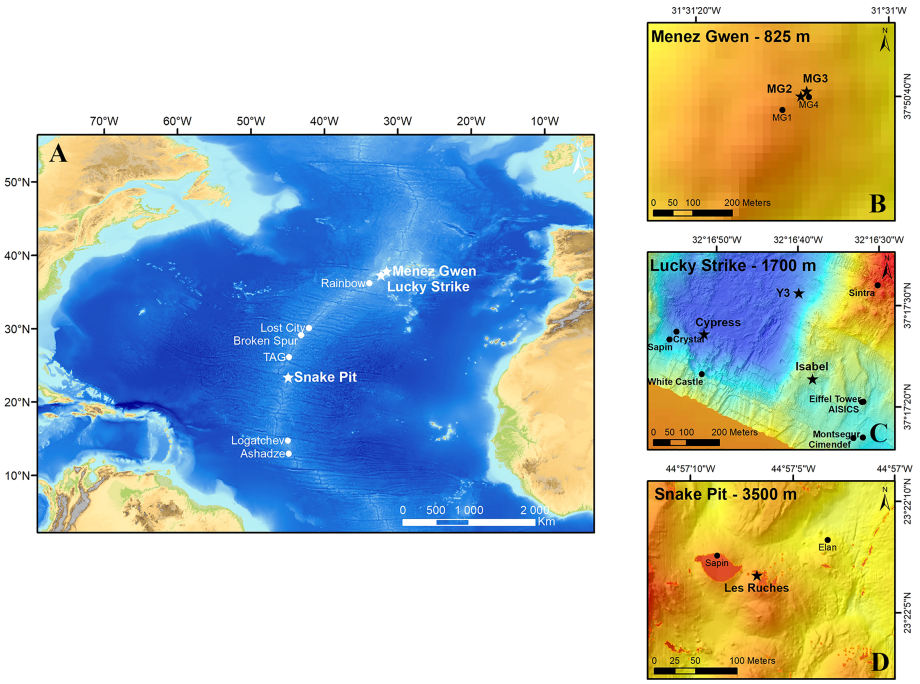

FIGURE 1 | (A) Location of the three vent fields studied along the northern Mid-Atlantic Ridge: Menez Gwen (MG), Lucky Strike (LS) and Snake Pit (SP). **(B-D)**. Locations (stars) of the sampling sites on MG **(B)**, LS **(C)** and SP **(D)**.

(Maas et al., 1999). Background temperatures at this field are 2.6°C (Hernández-Ávila et al., 2022).

Faunal Sampling and Habitat Characterization

Twelve gastropod assemblages were collected during several cruises and using the suction sampler on the ROV *Victor6000* from five sampling locations in the MG (MG3), LS (Y3, Cypress, Isabel) and SP (Les Ruches) vent fields along the nMAR (**Table 1** and **Figures 1**, **2**). The habitat chemistry of these assemblages was characterized prior to faunal sampling using the *in situ* chemical analyzer CHEMINI (Vuillemin et al., 2009), which measures total dissolved sulfide and iron concentrations. In addition, fluid samples within the habitat were collected using the PEPITO water sampler (Sarradin et al., 2009). The availability of these instruments on the submersible depended on the dive/cruise, which explains discrepancies between samples (**Table 1**). The chemical characterization was also carried out on five additional assemblages in which no faunal samples were taken (see **Table 1**) and on the two other dominant assemblages of the nMAR (**Table S1**). In 2014, two thermistor chains were deployed in a gastropod assemblage at the Y3 vent site in LS to capture the longer-term temporal variability of temperature. Each chain was composed of six thermochron i-buttons© enclosed in titanium cases and the thermistors recorded hourly temperature measurements over 5.5 months from 23 July to 31 December 2014, for a total of 3977 data points per probe. The chains were recovered in 2015, but 50% of the thermistors were damaged and could not be read (**Table S2**).

Faunal Sample Processing

For each sample, the total sampled area was estimated from a video capture using a checkerboard (7 mm squares) as a scale, deployed in the camera field of view (**Figure 2**). Surface measurements were performed using Image J© (Schneider et al., 2012). When the checkerboard was not available, scale was assessed from the known size of the submersible suction sampler nozzle, visible on video sequences. Each faunal sample was sieved on 300 µm (macrofauna) and 20 µm (meiofauna) meshes. Individuals in the macrofaunal compartment were sorted, counted and identified to the lowest possible taxonomic level, and those of the meiofauna were identified at higher taxonomic levels.

Stable Isotope Analyses

To characterize their trophic ecology, stable isotope ratios of carbon and nitrogen were analyzed in 61 specimens of four gastropod species (*Lepetodrilus atlanticus, Protolira valvatoides, Divia briandi* and *Peltospira smaragdina*, **Table S3**). After sampling, individuals were either directly frozen, or preserved in ethanol or formalin solutions. Whole individuals were analyzed due to their small body sizes. Gastropods were extracted from their shells, freeze-dried for 24 h and ground to a homogeneous powder using a ball mill. Samples were then sent to the Laboratoire d'analyse en écologie aquatique et en sédimentologie at the Université du Québec à Trois-Rivières (CA) or the Littoral Environnement et Sociétés stable isotope facility at La Rochelle

TABLE 1 | Sampling characteristics and mean environmental conditions in the different gastropod assemblages studied.

Vent field	Site	Sample	Year	Faunal samples	Dive	Depthm	T°C (std)	T°C anomaly	pH	O_2 (std) µM	H_2S (std) µM	Fe (std) µM	CH_4 µM	Mg µM	Mn_d µM	Fe_d µM	Fe_p µM
Menez Gwen	MG3	MG-MG3-13-1	2013	yes	524	827	8.9 (0.3)	0.9	6.55	–	–	–	**40.56**	50.97	0.67	0.85	0.21
		MG-MG3-13-2	2013	no	525	827	8.8 (0.2)	0.8	–	–	**177** (65)	0	–	–	–	–	–
Lucky Strike	Y3	LS-Y3-12-1	2012	yes	504	1730	8.5 (0.6)	3.9	–	–	–	14.6 (0.8)	–	–	–	–	–
		LS-Y3-12-2	2012	no	504	1730	**20.4 (13.5)**	**15.8**	–	–	–	**23.7** (20)	–	–	–	–	–
		LS-Y3-14-1	2014	yes	582	1730	6 (1.2)	1.4	7.15	205.5 (1.2)	28.9 (4.7)	–	4.3	50	2.4	2.2	1.4
		LS-Y3-14-2	2014	yes	582	1730	7.8 (0.6)	3.2	6.7	187.1 (0.6)	72.7 (0.05)	–	6	47.9	**6.8**	11.1	0.5
		LS-Y3-14-3	2014	yes	582	1730	6 (0.9)	1.4	**7.28**	215.0 (1.5)	19.4 (9.2)	–	0.2	49.7	1.9	9.8	**2.9**
		LS-Y3-15-1	2015	yes	600	1730	9.1 (2)	4.5	–	208.1 (1.8)	58.5 (15.8)	–	–	–	–	–	–
		LS-Y3-15-2	2015	yes	600	1730	5.7 (1.1)	1.1	–	–	30.2 (10.5)	–	–	–	–	–	–
		LS-Y3-15-3	2015	yes	600	1730	5.8 (1.8)	1.2	–	–	18.4 (12.9)	–	–	–	–	–	–
	Cypress	LS-Cy-14-1	2014	yes	586	1739	8.5 (0.8)	3.9	6.68	200.5 (1.4)	99.2	4.1 (0.5)	5.6	**51.5**	3.7	3.6	0.6
		LS-Cy-14-2	2014	no	586	1739	9 (1)	4.4	6.49	193.7 (0.5)	72.9 (7.4)	5.6 (0.8)	6.8	50.3	6.4	6.6	0.6
		LS-Cy-14-3	2014	no	586	1739	9.5 (1.7)	4.9	6.46	201.9 (1.0)	68.4 (4.9)	5.8 (0.8)	1.6	49.1	6.4	7.3	1.2
	Isabel	LS-Isa-16	2016	yes	627	1683	–		–	–	–	–	–	–	–	–	–
Snake Pit	Les Ruches	SP-Ru-14-1	2014	no	568	3465	2.6 (0.4)	0	–	243.2 (18.4)	10.7 (2.9)	–	–	–	–	–	–
		SP-Ru-14-2	2014	yes	568	3470	5.2 (2.1)	2.6	–	**296.6 (6.7)**	96.9 (22.7)	–	–	–		13.4	–
		SP-Ru-14-3	2014	yes	568	3465	3.3 (0.65)	0.7	**7.63**	175.6 (12.8)	12.1 (6.6)	–	0.1	41	5.8	**19.4**	–

*T°C: temperature, T°C anomaly: difference between measured temperature and background bottom seawater temperature at the site, O_2: oxygen concentrations, H_2S: in situ hydrogen sulfide concentrations, Fe: in situ dissolved iron concentrations, CH_4: methane concentrations, Mg: magnesium concentrations, Mn: manganese concentrations, Fe_d: total dissolved iron concentrations, Fe_p: total particulate iron concentrations. -: not available. Std: standard deviation. In gray, samples for which there are faunal composition data. In bold, maximum values observed for a variable. Background bottom temperatures are 8.8°C at Menez Gwen (MG), 4.5°C at Lucky Strike (LS) (*Sarrazin et al., 2020*) and 2.6°C at Snake Pit (SP) (Hernández-Ávila et al., 2022).*

Université (FR) for analyses using continuous flow-elemental analysis-isotope ratio mass spectrometry (CF-EA-IRMS). Isotope ratios were expressed using the widespread δ notation (Coplen, 2011) in ‰ and relative to the international references Vienna Pee Dee belemnite (for carbon) and atmospheric air (for nitrogen). Analytical precision based on repeated measurements of the same sample was less than 0.3‰ for both $\delta^{13}C$ and $\delta^{15}N$. Given that chemical preservation can alter stable isotope compositions, correction factors experimentally measured on gastropods (Lau et al., 2012) were applied to ethanol- ($\Delta^{13}C$ = 0.48‰, $\Delta^{15}N$ = 0.47‰) or formalin-preserved ($\Delta^{13}C$ = 1.01‰, $\Delta^{15}N$ = 0.53‰) specimens.

Statistical Analyses

Faunal abundances were converted to densities by dividing the total number of individuals by the estimated surface area, and to relative abundance within each sample (**Table 2**). All analyses were computed using R (R Core Team, 2020). Associated community diversity was assessed using species richness as well as Shannon and Simpson diversity indexes. Species accumulation curves were computed based on the resampling of individuals (rarefaction; Hurlbert, 1971) for each site by combining replicates using Vegan 2.5-6 (Oksanen et al., 2019). A Venn diagram displaying common species among the three vent fields was drawn. A hierarchical clustering of gastropod assemblage samples, based on their species composition, was computed based on Bray-Curtis dissimilarities on square-root transformed data using group average linking. For each environmental variable, mean and standard deviation were calculated when possible (**Table 1**). Correlations between environmental variables were tested using a Pearson correlation coefficient on log-transformed data, and a principal component analysis (PCA) was conducted on the standardized means and standard deviations of temperature and sulfide concentrations to visualize site ordination in a two-dimensional space. Finally, a distance-based redundancy analysis (RDA) was done on Hellinger-transformed abundance data (Legendre and Gallagher, 2001) using temperature and sulfide concentration data only in order to maintain a significant number of samples representative of all sampling locations on the three vent fields. Note that at MG, gastropod assemblages were only collected at the MG3 site where no sulfide data were available. Consequently, and because temperature data were similar, chemical data from the nearby MG2 site were used to characterize environmental conditions of the assemblage from this vent field in the redundancy analysis.

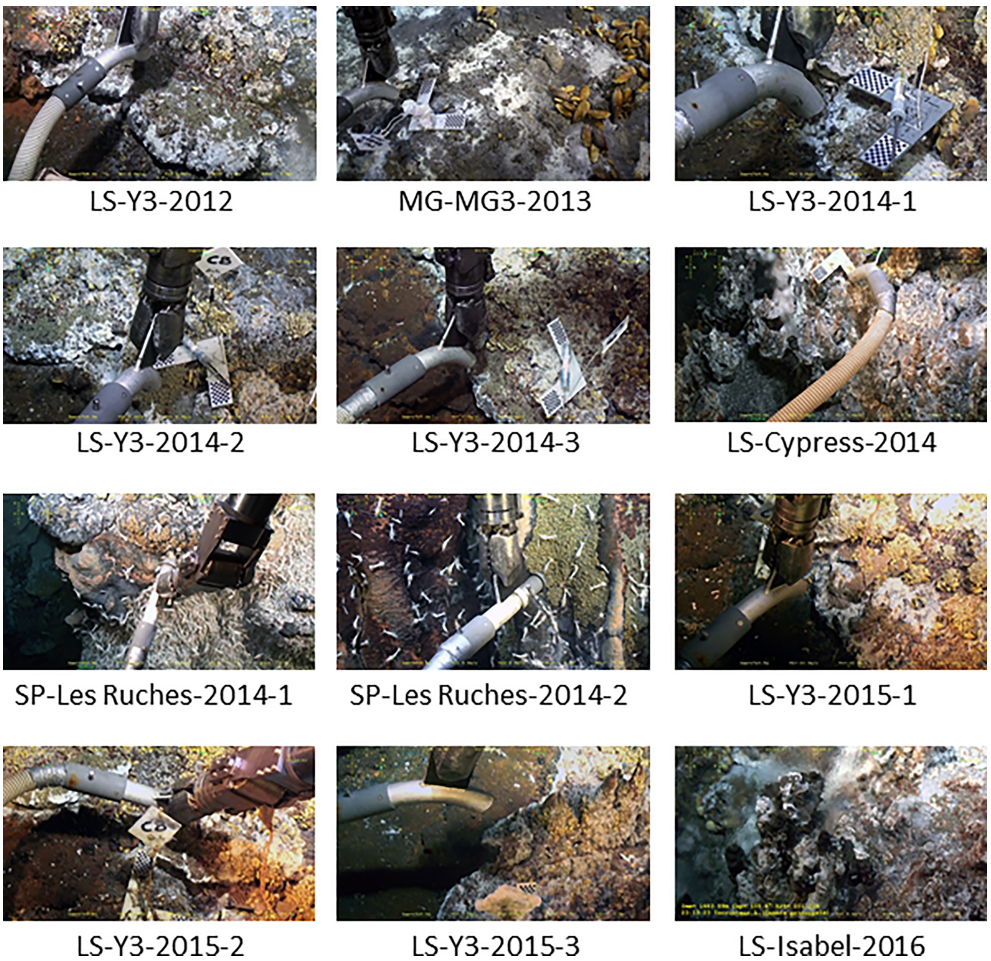

FIGURE 2 | Twelve gastropod assemblages were characterized and sampled during the present study at three vent fields (Menez Gwen, Lucky Strike and Snake Pit) at the northern Mid-Atlantic Ridge. Samples were taken during different cruises in 2012 (Momarsat), 2013 (Biobaz), 2014 (Momarsat for LS, Bicose for SP), 2015 & 2016 (Momarsat). A physico-chemical characterization was carried out on each assemblage prior to faunal sampling. Faunal samples were collected using the ROV suction sampler. A target was placed in the field of the camera and sampling surfaces were estimated from video snapshots using ImageJ software© (see Sarrazin et al., 1997 for protocol).

RESULTS

Community Composition and Diversity

Our results confirm that all samples were dominated by a single species of gastropod that made up 64% to 98% of the total abundance (**Tables 2**, **3**). The species *Peltospira smaragdina* dominated the LS and SP samples, and *Lepetodrilus atlanticus* dominated those from MG (**Figure 3**). The second-most dominant taxa were either alvinocaridid shrimps (in 50% of the samples), copepods (25%) or other vent species (remaining 25%). Nematodes were relatively abundant in only a few samples, particularly on Y3. A few taxa (*Laeviphitus desbruyeresi*, *Branchinotogluma* sp., *Branchipolynoe seepensis*, Cumacea, Isopoda, Ostracoda and Tanaidacea) were only present as singletons or doubletons (**Table 2**). Among the four most abundant gastropod species, *Divia briandi* was the only species present in samples from all three vent fields. For the three others, *L. atlanticus* was only present in the MG samples, *P. smaragdina* was present at the two other fields, but not at MG, and *Protolira valvatoides* was absent from SP samples. The total number of individuals collected were the highest on MG (2 583 individuals) and the smallest on Isabel (LS, 217 individuals; **Table 3**). *P. smaragdina* densities varied from 19 786 ind./m^2 in one sample from Les Ruches to 74 966 ind./m^2 in one sample from Y3. Total faunal densities showed high spatial variability within the same site, being up to three times higher at some sampling sites (e.g. Y3; **Table 3**) and was the highest at MG3, reaching 82 152 ind./m^2 (**Table 3**).

Only two species were shared between the gastropod assemblages of the three vent fields: the shrimp *Mirocaris fortunata* and gastropod *D. briandi* (**Table 2** and **Figure S1**). Each of these taxa was present in all samples but one (**Table 2**). LS and MG gastropod assemblages shared a total of five species, whereas LS and SP shared four species (**Figure S1**). LS samples

TABLE 2 | Raw and relative (in parentheses) abundances of the different macrofaunal (300 µM) and meiofaunal (20 µM) taxa within the 12 sampled gastropod assemblages.

Field/site	Menez Gwen	Lucky Strike									Snake Pit	
Taxonomic groups	MG3-13-1	Y3-12-1	Y3-14-1	Y3-14-2	Y3-14-3	Y3-15-1	Y3-15-2	Y3-15-3	Isa-16	Cy-14-1	Ru-14-2	Ru-14-3
Gastropoda												
Laeviphitus desbruyeresi	0	0	0	1 (0.001)	0	0	0	0	0	0	0	0
Lepetodrilus atlanticus	**2184** (0.85)	0	0	0	0	0	0	0	0	0	0	0
Peltospira smaragdina	0	**899** (0.91)	**533** (0.64)	**962** (0.85)	**931** (0.88)	**482** (0.85)	**389** (0.92)	**332** (0.81)	**195** (0.9)	**584** (0.72)	**647** (0.90)	**1255** (0.98)
Divia briandi	11 (0.004)	2 (0.002)	2 (0.002)	33 (0.03)	18 (0.02)	6 (0.01)	17 (0.04)	28 (0.07)	22 (0.10)	35 (0.04)	7 (0.01)	0
Protolira valvatoides	13 (0.005)	0	24 (0.03)	4 (0.004)	0	0	1 (0.002)	0	0	0	0	0
Bivalvia												
Bathymodiolus azoricus	1 (0.0004)	0	43 (0.05)	65 (0.06)	21 (0.02)	0	2 (0.005)	1 (0.002)	0	29 (0.04)	0	0
Polychaeta												
Amphisamytha lutzi	0	0	0	1 (0.001)	22 (0.02)	0	0	0	0	27 (0.03)	0	0
Branchinotogluma sp.	0	0	0	1 (0.001)	0	0	0	0	0	0	0	0
Branchipolynoe seepensis	0	0	0	2 (0.002)	0	0	0	0	0	0	0	0
Hesiolyra aff. *bergi*	0	9 (0.009)	5 (0.006)	4 (0.004)	2 (0.002)	1 (0.002)	2 (0.005)	1 (0.002)	0	6 (0.007)	0	0
Polychaeta juvenile undet.	0	0	3 (0.004)	0	0	4 (0.007)	2 (0.005)	0	0	0	0	0
Crustacea												
Amphipoda	0	0	1 (0.001)	1 (0.001)	3 (0.003)	0	0	0	0	0	0	0
Copepoda*												
Siphonostomatoida	372 (0.14)	0	0	0	0	0	0	0	0	0	0	0
Dirivultidae												
Copepoda undet.	0	0	113 (0.14)	30 (0.03)	16 (0.02)	14 (0.03)	4 (0.009)	0	0	126 (0.16)	0	0
Cumacea*	0	0	0	0	0	0	2 (0.005)	0	0	0	0	0
Decapoda												
Mirocaris fortunata	1 (0.0004)	75 (0.08)	59 (0.07)	15 (0.01)	31 (0.03)	57 (0.10)	3 (0.007)	45 (0.11)	0	2 (0.002)	15 (0.02)	1 (0.001)
Rimicaris chacei	0	0	0	0	0	1 (0.002)	0	0	0	0	0	3 (0.002)
Rimicaris exoculata	0	0	0	0	0	0	0	0	0	0	49 (0.07)	16 (0.01)
Isopoda- Thylakogaster undet.	0	0	0	0	0	0	0	1 (0.002)	0	0	0	0
Ostracoda*	0	0	2 (0.002)	0	0	0	0	0	0	0	0	0
Tanaidacea	0	0	0	0	0	0	0	1 (0.002)	0	0	0	0
Nematoda*	1 (0.0004)	0	46 (0.06)	13 (0.01)	17 (0.02)	1 (0.002)	0	0	0	1 (0.001)	0	0

Macrofaunal samples were identified to the species level when possible, but meiofaunal samples (indicated by a star) were identified to the higher taxonomic levels (order, family). Highest raw abundances are shown in bold.

harbored the highest number of "exclusive" species (n=12, **Figure S1**). In this vent field, species richness varied from 2 at Isabel to a maximum of 13 at Y3 (**Table 3**). Similar to densities, richness was variable within the same site, varying from 4 to 13 species at Y3. The highest Shannon and Simpson indexes were found on Y3, and the lowest on Les Ruches, despite the high number of organisms collected and large surface area sampled on SP-RU-14-2 (**Table 3**). In fact, the largest sampled surface area at this site corresponds to the lowest densities and diversities (**Table 3**). In LS, Isabel had

TABLE 3 | Global characteristics of the macro- and meiofaunal communities in the 12 faunal samples considered in the present study with the total number of individuals, the surface area sampled, faunal densities, various diversity variables (S: species richness, Shannon, Simpson) and the relative abundance of the dominant species.

Field/site	Sample	Total number of individuals	Surface sampled (cm^2)	Total faunal densities ($ind./m^2$)	S	Shannon	Simpson	Dominant species and relative abundance
Menez Gwen	MG-MG3-13-1	**2583**	0.031 (0.009)	**82 152.14**	7	0.48	0.26	*Lepetodrilus atlanticus* (85%)
Lucky Strike	LS-Y3-12-1	985	0.013 (0.003)	74 965.73	4	0.33	0.16	*Peltospira smaragdina* (91%)
	LS-Y3-14-1	831	0.025 (0.007)	32 739.17	11	1.25	**0.56**	*Peltospira smaragdina* (64%)
	LS-Y3-14-2	1132	0.034 (0.005)	33 407.59	**13**	**0.69**	0.27	*Peltospira smaragdina* (85%)
	LS-Y3-14-3	1061	0.044 (0.005)	24 293.54	9	0.6	0.23	*Peltospira smaragdina* (88%)
	LS-Y3-15-1	566	0.011 (0.001)	52 357.18	8	0.58	0.26	*Peltospira smaragdina* (85%)
	LS-Y3-15-2	422	0.013 (0.001)	31 319.75	9	0.4	0.15	*Peltospira smaragdina* (92%)
	LS-Y3-15-3	409	0.008 (0.002)	51 513.07	7	0.65	0.32	*Peltospira smaragdina* (81%)
	LS-Isa-16	217	–	–	2	0.33	0.18	*Peltospira smaragdina* (90%)
	LS-Cy-14-1	810	0.016 (0.004)	49 312.78	8	0.95	0.45	*Peltospira smaragdina* (72%)
Snake Pit	SP-Ru-14-2	718	0.016 (0.002)	43 703.93	4	0.4	0.18	*Peltospira smaragdina* (90%)
	SP-Ru-14-3	1275	**0.064** (0.021)	19 785.29	4	0.09	0.03	*Peltospira smaragdina* (98%)

Highest values are shown in bold.

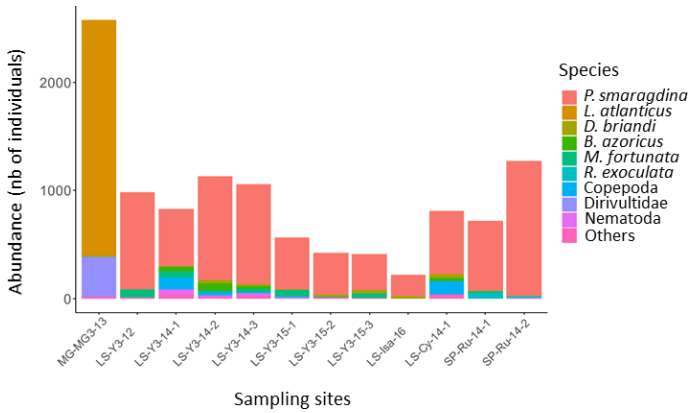

FIGURE 3 | Bar chart of faunal composition (species accounting for >5% of the total relative abundance) in gastropod assemblages collected in three hydrothermal vent fields along the northern Mid-Atlantic Ridge. MG, Menez Gwen; LS, Lucky Strike; SP, Snake Pit. *P. smaragdina: Peltospira smaragdina; L. atlanticus: Lepetodrilus atlanticus; D. briandi: Divia briandi; B. azoricus: Bathymodiolus azoricus; M. fortunata: Mirocaris fortunata; R. exoculata: Rimicaris exoculata.*

a very low species richness and diversity, and gastropod assemblages from Cypress had intermediate diversity values. Overall, Y3 had higher diversity than the two other sites of this field (LS, **Table 3**), but also the highest number of samples (n = 7) compared with Cypress and Isabel, each sampled only once. The rarefaction curves did not reach an asymptote for any of the sampled sites, with the exception of Les Ruches, indicating that the diversity of most sampled sites was not fully characterized (**Figure 4**). Except for Isabel, the gastropod assemblages from LS (Y3 & Cypress) appeared to have higher diversity than that from MG and SP. However, these two fields were only represented by a single sampling site. As expected, results of the hierarchical /clustering showed a clear distinction of the MG gastropod assemblages from those of the two other vent fields (**Figure 5**). Assemblages dominated by *P. smaragdina* did not cluster according to the vent field, but separated samples collected at LS in 2014 from the others. Because the MG gastropod assemblages strongly differ and were dominated by a different species, the two assemblage types will be further characterized independently.

Habitat Characterization

Lepetodrilus azoricus assemblages – These gastropod assemblages at MG were found on a very friable granular substratum, covered by whitish material (probably microbial mats) and surrounded by small shimmering chimneys (<50 cm). Clouds of grayish material formed during sampling and a dark black groove was left afterwards (see **Supplementary Video S1**, https://doi.org/10.24351/88698). These assemblages were surrounded by *B. azoricus* mussel assemblages, a few meters away. The mean temperatures measured in the two sampled assemblages at MG varied from 8.8 to 8.9°C, which is more or less the temperature of bottom seawater. Corresponding habitat conditions are given in **Table 1**. Methane and hydrogen sulfide concentrations were particularly high compared with those at the two other vent sites.

Peltospira smaragdina assemblages – Visually, *P. smaragdina* assemblages from LS were different from one other. At Y3, their habitats resembled those found at MG for *B. azoricus*: very friable substratum, covered with microbial mats near small active chimneys. At this site, the assemblages were not found directly on the edifice, but rather on a large flange lying on the seafloor and covered by a mix of gastropod/mussel assemblages. Individuals

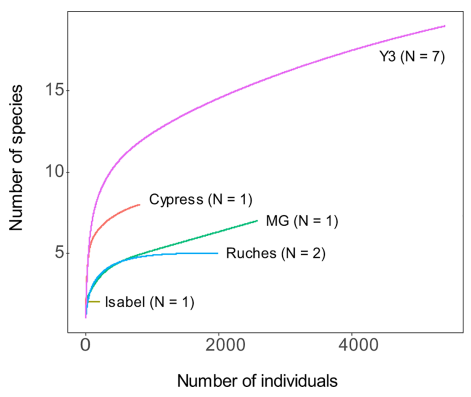

FIGURE 4 | Species accumulation curves based on rarefaction computed for each site among the three hydrothermal vent fields: Menez Gwen (MG3), Lucky Strike (Cypress, Isabel and Y3) and Snake Pit (Les Ruches).

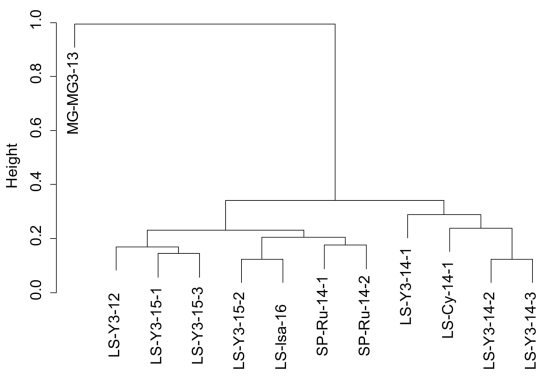

FIGURE 5 | Group average sorting dendrogram based on species composition using the Bray-Curtis similarity among the 12 gastropod samples along the northern Mid-Atlantic Ridge.

were mostly concentrated at the rim of the flange, where there were intense shimmering fluids (see **Supplementary Video S2**, https://doi.org/10.24351/88699). At Isabel and Cypress, *P. smaragdina* assemblages were more similar to those of SP, being found on the edifice walls in areas of intense shimmering. *M. fortunata* shrimps were abundant around them at Isabel. In SP, *P. smaragdina* colonized vertical wall surfaces on tall active edifices. At one sampling site, the gastropods were found on a beehive-like structure, in shimmering fluids and surrounded by *R. exoculata* shrimps (see **Supplementary Video S3**, https://doi.org/10.24351/88700). At the other site, they were in extremely dense patches and covered large areas of the edifice with abundant shimmering fluid (see **Supplementary Video S3**, https://doi.org/10.24351/88700). Overall, the gastropod assemblages in SP were much more visible and extended than those from MG or LS.

The mean temperatures, given by the ROV temperature probe (PT200, frequency: 1 Hz), in the *P. smaragdina* assemblages varied from 5.7°C to 20.4°C in LS and from 2.6°C to 5.2°C in SP (**Table 1**). Given that the bottom temperatures in the two vent fields were quite different, temperature anomaly appears to be a better proxy than mean temperature to assess fluid inputs. These anomalies varied between 0.7°C at Les Ruches (SP) to 15.8°C at Y3 (LS, **Table 1**). At Y3, temperature measured by the i-buttons (4 months of acquisition) directly at the surface of the substrata was three times higher (mean 25.42 ± 2.6°C, n = 6) than that measured by the ROV probe 1-2 cm above the surface (mean 7.83 ± 1.9°C, n=17). High spatial variability in mean temperatures (from 17.25 to 37.34°C) was also observed within the same assemblage between closely spaced i-buttons (**Figure 6** and **Table S2**). Temperatures also varied with time, the highest variation between minimum and maximum values being found on HT2.12 (43.04°C, **Table S2**).

The lowest concentrations of hydrogen sulfide, methane and magnesium concentrations were found at Les Ruches (SP), but pH (ca. 7.63) and dissolved iron concentrations were higher at this site than at the LS sites (**Table 1**). Highest and lowest concentrations of oxygen were measured at Les Ruches (SP). Higher concentrations of hydrogen sulfide, methane and magnesium were found at Cypress (LS, **Table 1**). Y3 harbored both the highest and lowest concentrations of manganese. For total and particulate iron concentrations, only data from LS are available, varying from 4.1 to 23.7 µM (Fe total) and 0.5 to 2.9 µM (particulate Fe; **Table 1**).

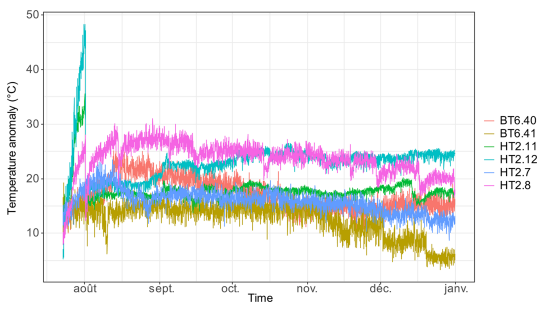

FIGURE 6 | Evolution of temperature anomaly (difference between measured temperature and background bottom seawater temperature at the site) measured with six i-buttons' temperature probes at Y3 (Lucky Strike vent field, Mid-Atlantic Ridge) from 23 July to 31 December 2014. Labels indicate probe name.

The PCA explains 77.6% of the variance in environmental conditions (**Figure 7**). The first axis represents 51.4% of the variance and is associated with average temperature and hydrogen sulfide concentrations as well as with temperature anomaly. The second axis explains 26.2% of the variance and is associated with the standard deviations of temperature and hydrogen sulfide. The PCA does not differentiate the two vent fields, nor the two LS sites or sampling years.

The RDA on environmental conditions was not significant, supporting a certain homogeneity in environmental conditions within the *P. smaragdina* assemblages from the LS and SP vent fields. Mean measured environmental conditions within gastropod assemblages of these two vent fields are presented in **Figure 8**.

Stable Isotope Compositions of Dominant Gastropod Species

$\delta^{13}C$ values of the four species of gastropods were highly variable, ranging from -22.5 to -8.8 ‰ (**Figure 9** and **Table S3**). Regardless of site, $\delta^{13}C$ values were, from the most to the least negative, -18.9 ± 2.0 ‰ for *P. valvatoides*, -14.9 ± 2.4 ‰ for *L. atlanticus*, -13.6 ± 1.9 ‰ for *D. briandi* and -10.8 ± 0.8 ‰ for *P. smaragdina* (mean ± SD in each case). In addition to these general trends, species-specific inter-site variations also seemed to occur (**Figure 9**). $\Delta^{13}C$ of *P. valvatoides* seemed lower at MG than at Y3. *D. briandi* showed comparable $\delta^{13}C$ at MG and Y3 (LS), but less negative values at SP and, to a lesser extent, at Isabel (LS). $\Delta^{13}C$ of *P. smaragdina* were similar at Y3 and Isabel (LS), but seemed slightly less negative at SP. Finally, $\delta^{13}C$ ranges seemed wider at MG than in the two other vent fields. $\Delta^{15}N$ values of the four species of gastropods ranged from 2.4 to 7.7 ‰ (**Figure 9** and **Table S3**). Regardless of site distinction, $\delta^{15}N$ values were, from the lowest to the highest, 5.1 ± 0.9 ‰ for *P. valvatoides*, 5.4 ± 1.5 ‰ for *L. atlanticus*, 6.1 ± 0.6 ‰ for *P. smaragdina* and 6.8 ± 0.6 ‰ for *D. briandi*. Overall, $\delta^{15}N$ seemed to vary less across species and sites than $\delta^{13}C$. Nevertheless, in MG, SP and Isabel, $\delta^{15}N$ seemed to be higher for *D. briandi* than for other species (**Figure 9**). This trend was not observed at Y3.

Environmental Conditions Within the Different Assemblages on the nMAR

In **Table S1**, based on this study and previously published data, we compiled environmental conditions associated with the three assemblages of the nMAR and for each field. The observed patterns differed from one field to the other. In MG, the mean temperatures were similar between the gastropod (*L. atlanticus*) and mussel (*B. azoricus*) assemblages, but the mean hydrogen sulfide concentrations were more than three times higher in the gastropod assemblage. Unfortunately, no data was obtained in the shrimp assemblage in this field. In LS, the *P. smaragdina* assemblage occupied the highest temperatures and sulfide concentrations compared with the mussel (*B. azoricus*) and

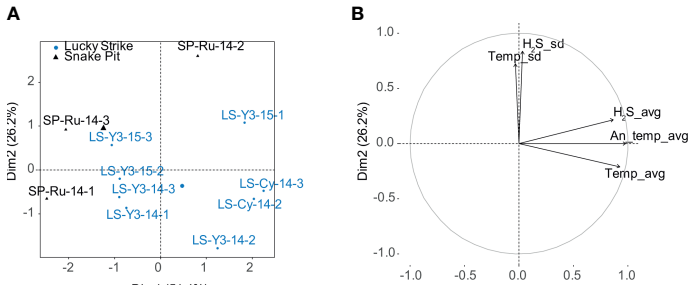

FIGURE 7 | Principal component analysis (PCA) on environmental data measured in gastropod assemblages dominated by *Peltospira smaragdina* at the Lucky Strike and Snake Pit vent fields along the Mid-Atlantic Ridge. **(A)** the distribution of sites in the new space formed by the two first principal components; the big circle and triangle represent the centroid for each vent site. **(B)** the correlation circle shows the contribution of each variable to the explained variance. H_2S_avg & H_2S_sd: average and standard deviation of *in situ* hydrogen sulfide concentrations, Temp-avg: average temperature, An_temp_avg: average temperature anomaly calculated against background seawater temperature and Temp_sd: temperature standard deviation.

shrimp (*Mirocaris fortunata*) assemblages. However, with the exception of Cuvelier et al. (2011a), the conditions reported here for the shrimp assemblage corresponds to those of the warmer mussel habitats (in which shrimp dominated), because a proper characterization of shrimp habitats still needs to be done at this field. Habitat characterization of the three faunal assemblages in SP was done the same year, during the Bicose cruise. Results show that environmental conditions were more differentiated than the two other vent fields: the gastropod (*P. smaragdina*) assemblage occupied intermediate temperature and sulfide concentration habitats (**Table S1**). The mussel (*B. puteoserpentis*) assemblages were characterized by lower concentrations of hydrogen sulfide and the shrimp (*R. exoculata*) colonized the most variable habitats with higher temperatures and sulfide concentrations. In SP, oxygen concentrations were lower in the shrimp (161.1 μM), intermediate in the gastropod (170.6 – 186.4 μM) and higher in the mussel (201.1 – 244.3 μM) assemblages.

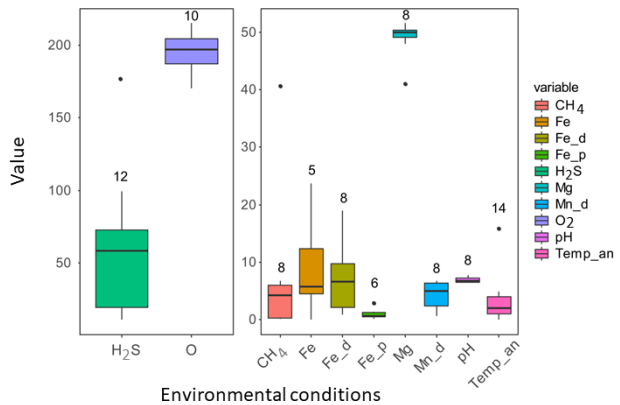

FIGURE 8 | Whisker plots illustrating environmental conditions within assemblages of the gastropod *Peltospira smaragdina* at the Lucky Strike and Snake Pit vent fields along the Mid-Atlantic Ridge. Given that the values were quite high for hydrogen sulfide (H_2S) and oxygen (O_2), we provide two figures. The line corresponds to the median, the box (second and third quantiles) include 50% of the measured data and the upper and lower 25% respectively are represented by vertical lines on each box. Individual dots are outliers. H_2S: *in situ* hydrogen sulfide concentrations, O_2: oxygen concentrations, CH_4: methane concentrations, Fe: *in situ* total iron concentrations, Fe_d: total dissolved iron concentrations, Fe_p: total particulate iron concentrations, Mg: magnesium concentrations, Mn: manganese concentrations, Temp_an: temperature (°C) anomaly calculated against background seawater temperatures. H_2S, O_2, CH_4, Fe, Fe_d, Fe_p, Mg, and Mn_d are in μM. Numbers on graphs represent the number of measurements taken.

DISCUSSION

This study provides the first description of the ecological characteristics of gastropod assemblages that are recurrent in three vent fields – Menez Gwen, Lucky Strike and Snake Pit – along the nMAR, from 830 m to 3500 m depth. Our results confirm that the sampled assemblages were characterized by a strong dominance of a single gastropod species and by distinct environmental conditions compared with the two other dominant assemblages of the MAR, the mussel and shrimp assemblages.

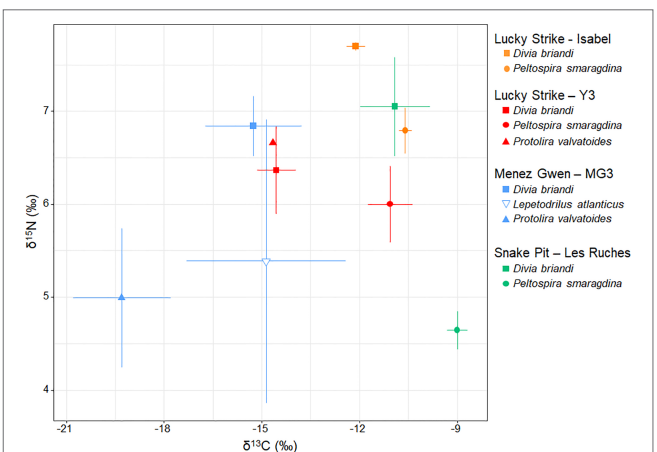

FIGURE 9 | Stable isotope ratios of carbon ($\delta^{13}C$) and nitrogen ($\delta^{15}N$) of the four dominant vent gastropod species from different sites in the three studied vent fields: Menez Gwen (MG3), Lucky Strike (Isabel & Y3) and Snake Pit (Les Ruches) on the northern Mid-Atlantic Ridge. Points are means, error bars are standard deviations.

Furthermore, a retrospective examination of references and imagery from dives in other vent fields revealed evidence for the presence of distinct gastropod assemblages in at least five other MAR vent fields, including Broken Spur, Rainbow (Jollivet, pers. comm.), TAG (pers. obs.), Moytirra (Wheeler et al., 2013; Collins et al., 2020) and Loki's Castle.

Community Structure at the Three Vent Fields

Two distinct gastropod assemblages were characterized, one dominated by *Lepetodrilus atlanticus* (Lepetellida: Lepetodrilidae; (Warén and Bouchet, 2001) at MG and the other dominated by *Peltospira smaragdina* (Neomphalida: Peltospiridae; Warén and Bouchet, 2001) at the LS and SP vent fields. Both genera are endemic to deep-sea chemosynthetic habitats. The former is the most specious with 16 species; however, *Peltospira* has only four described species (WoRMS Editorial Board, 2022). To date, these two species had only been described as associated fauna of *Bathymodiolus* assemblages in the studied vent fields (Sarrazin et al., 2015; Husson et al., 2017; Sarrazin et al., 2020). In the mussel assemblages described in LS, *P. smaragdina* was reported in very low densities and associated with intermediate temperature habitats, and *L. atlanticus* can reach high densities (Husson et al., 2017), particularly in cold microhabitats (Sarrazin et al., 2015; Sarrazin et al., 2020). Here, in contrast, we describe new assemblages dominated and structured by these two small macrofaunal gastropods, *P. smaragdina* and *L. atlanticus*.

These new gastropod assemblages are characterized by low species richness (<13 taxa) and a large proportion (>60%) of singletons or doubletons. They share structural similarities with faunal assemblages from warmer habitats at other vent sites, which are visually dominated by a few species and exhibit low species diversity [e.g. alvinellid assemblages on the EPR (Gollner et al., 2010) and NEPR (Tsurumi and Tunnicliffe, 2003), alvinocaridid assemblages on the MAR (Hernández-Ávila et al., 2022), high-flow siboglinid assemblages on the NEPR (Sarrazin and Juniper, 1999)]. However, the gastropod species of this study differ from the large symbiotic species living in the vent fields of the western Pacific and Indian oceans, because they are much smaller in size (<1 cm compared with 8.5 – 9.5 cm for *Alviniconcha hessleri and Ifremeria nautilei* (Desbruyères et al., 2006). Moreover, contrary to the larger vent gastropods, their association with symbionts has not yet been demonstrated, although suspected for *P. smaragdina* (Collins et al., 2020).

Habitat Characterization

Like faunal composition, environmental conditions were very different at the MG habitats compared with the two other vent fields. The clear separation of MG from other vent fields (i.e. LS & Rainbow) along the MAR was previously reported by Sarrazin et al. (2020) in mussel assemblages, showing both distinct environmental conditions and patterns of abundance and diversity. The mean temperatures (8.8 – 8.9°C) in the MG gastropod assemblages were similar to those reported for bottom temperatures at this field (Sarrazin et al., 2020). At LS, mean temperatures were more variable, probably resulting from the higher number of sampling sites and years compared with MG and SP, but always at least >1°C above ambient temperature (~4.5°C). At SP, the mean temperatures were similar to those reported for bottom water temperatures (~3.6°C), but slightly exceeding them for one sample (+1.6°C). However, these temperatures may not represent those experienced by the gastropods as suggested by the time-series measurements done with the i-button probes at Y3 (LS), which largely exceeded the temperature values measured by the submersible. The videos highlighted the presence of shimmering fluids within the sampled assemblages, suggesting warmer temperatures than those actually measured. Measurements using the submersible probe were performed few centimeters above the gastropod assemblages at three discrete locations and are likely not representative of the temperatures experienced by the organisms over time. Indeed, temperatures can display variations of up to 20°C within a few centimeters in response to turbulence, mixing and biological processes (Le Bris et al., 2005; Lee et al., 2015). Similarly, a recent study showed that temperature values obtained by probes deployed directly on the substratum were significantly higher than those obtained with the submersible sensor few centimeters above the fauna (Marticorena et al., 2021). This difference questions once again the use of single-point temperature measurements to define the niche of vent species. However, submersible measurements can be used to compare different assemblages from different habitats/fields, as it is the case here.

Our results do not show significant differences in environmental conditions between LS and SP habitats, although temperature anomalies were higher in LS and methane concentrations generally lower in SP. Concentrations of hydrogen sulfide were very variable at LS, between edifices and also within the same site, but were within the (large) range found in SP. With these large intra-field variations and without a more substantial (and comparable) number of samples, it remains difficult to further compare gastropod habitats between the two fields. Our comparison of the environmental data from the three key assemblages along the MAR (mussels, gastropods, shrimp) suggests that these small gastropod assemblages occupy an intermediate niche between those of the alvinocaridid shrimp and mussels. This niche separation is visible at SP (dominated by *Rimicaris* species), but additional environmental data in the warmer areas colonized by shrimp assemblages would be necessary in LS (dominated by *Mirocaris fortunata*) to confirm the position of the three assemblage types within the temperature gradient.

The absence of *P. smaragdina* in mussel assemblages in the shallower MG field (Sarrazin et al., 2020) is intriguing and may be linked to bathymetric limits as observed for many deep-sea taxa (McClain and Etter, 2005). Interestingly, *P. smaragdina* assemblages seem increasingly dominant at the deeper vent fields. In fact, their high abundance at the 2095 m Moytirra vent field (Wheeler et al., 2013) and their recent observation at other deeper fields such as Rainbow (2300 m) and Broken Spur (3100 m; Jollivet & Le Bris, comm. pers.) support a possible depth effect on this species' distribution range. Another possibility is that *L. atlanticus* has outcompeted *P. smaragdina* at shallower depths. In fact, the relative dominance of one species can depend

on its abilities to outcompete other species over a given range of environmental conditions as previously shown for *Lepetodrilus elevatus* on the EPR (Matabos et al., 2008). Alternatively, differences in MG abiotic conditions, such as its high sulfide/methane concentrations, may have prevented colonization by *P. smaragdina*. Differences in the concentrations of the reduced chemicals used for chemosynthesis (such as hydrogen sulfide, methane, iron and hydrogen) may also result in distinct patterns of resource availability. In fact, the availability of different chemical elements may have an impact on the composition of microbial communities (De Busserolles et al., 2009). Our results suggest a different basal carbon source (see below) for the two species supporting the existence of resource partitioning, as previously observed at other vents (Levesque et al., 2003; Lelièvre et al., 2018).

Energy Fluxes and Ecological Interactions

Determining trends in stable isotope compositions of consumers in deep-sea hydrothermal vents can be a challenging task, because trophic effects (changes in consumer isotopic compositions due to actual differences in feeding habits) and baseline effects (changes in consumer isotopic compositions due to changes in isotopic compositions of baseline items) are frequently confounded. Variations in environmental conditions are known to influence baseline compositions at multiple scales (De Busserolles et al., 2009; Beinart et al., 2012). Here, the differences between vent fields and/or sites, with consumers from MG being more ^{13}C-depleted compared to those of SP that were generally the most ^{13}C-enriched, are probably largely due to such effects. Nevertheless, other than these baseline shifts, species-specific patterns could be observed.

P. smaragdina had high δ^{13}C values at all sites, ranging from -9.0 to -11.1‰ on average. These values are consistent with reliance on chemosynthetic bacteria favoring the reductive tricarboxylic acid (rTCA) cycle for their metabolism (Hügler and Sievert, 2011). At Les Ruches (SP) and Isabel (LS), *Divia briandi* δ^{13}C values were slightly more negative than those of *P. smaragdina* (-1.5 to -2‰). At Y3 however, the mean difference in carbon isotopic composition between *D. briandi* and *P. smaragdina* was greater (-3.5‰). Although all these values remain in the range of rTCA-fueled microorganisms, the differences suggest that the two species feed on different resources (either different microorganisms or similar microorganisms living in different habitats), and that the degree of ecological divergence between these two species may be site-specific. At MG, both *D. briandi* and *L. atlanticus* had similar average δ^{13}C, whose values (-15.3 and -14.9‰, respectively) were found at the most negative end of the commonly accepted range for rTCA sulfide oxidizers (roughly -10 to -15‰; Hügler and Sievert, 2011). Conversely, at this site, *Protolira valvatoides* had the least negative δ^{13}C (-19.3‰), and was found outside this range. This discrepancy suggests that this species does not depend solely on rTCA sulfide oxidizers for its nutrition. Based on its δ^{13}C, at MG, *P. valvatoides* may combine this resource with sulfide oxidizers that use the Calvin–Benson–Basham (CBB) cycle, methane oxidizers or even photosynthesis-derived organic matter (Portail et al., 2018). Although it has been reported in shrimps, namely *Rimicaris exoculata*, strong reliance on rTCA sulfide oxidizers is not common in fauna from mussel beds of the same sites, which instead seem to feed on microorganisms fueled by the CBB cycle (Portail et al., 2018; Methou et al., 2020). Δ^{15}N values for all species varied from 4.54 to 7.05‰, with few, if any, consistent observed patterns. While these values may indicate minor trophic position differences, they may also indicate differences in the type of inorganic nitrogen used by the producers on which each species relies (nitrate vs. ammonium; Methou et al., 2020).

Overall, from a functional point of view, our results suggest that all gastropods sampled here are grazers/deposit-feeders; however, the interspecific differences in isotope composition point out subtle variations in their feeding habits and/or feeding habitats. Resource partitioning among species of the same group or feeding guild (i.e. grazers using their radula to consume microbial mats) associated with high biomass is common in vent assemblages and highlight the importance of the diversity of free-living microbial communities in structuring vent communities (Lelièvre et al., 2018). Microorganisms represent most of the living organic carbon in the vent environment (Karl, 1995), and free-living microbes, growing on hard surfaces or proliferating in hydrothermal fluids, offer an abundant food source. Nevertheless, other modes of carbon and nutrient acquisition may also be present in the studied gastropods. Recently, Collins et al. (2020) hypothesized that the observed association between *Sulfurimonas* biofilm and *P. smaragdina* at the Moytirra vent field likely represents a holobiontic relationship. These hypotheses still need to be confirmed.

Comparison With Other Vent Gastropod Assemblages

In the present study, in MG, *L. atlanticus* low-diversity assemblages were found in newly formed habitats, characterized by a friable substratum and vigorous venting. *Lepetodrilus* limpets are highly successful at vents, reaching densities of several hundred thousands of individuals at certain sites (Warén et al., 2006). They colonize a large variety of substrata in diffuse-flow emissions areas and usually benefit from the 3D structure formed by engineer species including siboglinid tubeworms (Govenar et al., 2005), mussel shells (Van Dover et al., 2002; Matabos et al., 2011), large symbiotic gastropods (Podowski et al., 2009) and stalked barnacles (Marsh et al., 2012). However, in the MAR mussel assemblages, *Lepetodrilus* densities appear to be lower than those observed in Pacific vents, reaching maximal densities of ~14 000 ind./m^2 on the Eiffel Tower edifice (LS, Sarrazin et al., 2020). At MG gastropod assemblages, *L. atlanticus* reached densities (~69 800 ind./m^2) that are similar to those reported by Marsh et al. (2012) for *Lepetodrilus concentricus* on the East Scotia Ridge (ESR, up to ~57 000 ind./m^2) and higher to those reported by Govenar et al. (2005) on the EPR for the denser *L. elevatus* species (~4 900 ind./m^2). On the northern EPR and Juan de Fuca ridge, lepetodrilids are dominant in zones of intermediate fluid intensity (Sarrazin et al., 1997; Shank et al., 1998; Sarrazin et al., 1999; Bates et al., 2005). Mills et al. (2007) report a distinct distribution between various *Lepetodrilus* species on the EPR. Some such as

L. pustulosus, L. elevatus, L. cristatus are associated with warm areas (up to 20°C, Matabos et al., 2008), whereas others *(L. ovalis*) are associated with the cooler areas (1.8 – 5.9°C), with a niche overlap between the two groups. These examples illustrate the wide range of habitats *Lepetodrilus* species can occupy (Mills et al., 2007). Moreover, they appear to be able to outcompete other species in optimal environmental conditions (Matabos et al., 2008). The abundance and large distribution of this genus may be related, among other factors, to its feeding plasticity and high mobility. In fact, these limpets exhibit various feeding strategies including grazing with their radula, active suspension feeding and even symbiotic relationships (Bates, 2007; Gaudron et al., 2015) and they are able to adjust their position in response to environmental changes (Bates et al., 2005). Their continuous reproduction and planktonic dispersal strategy also make them effective early colonizers (Kelly and Metaxas, 2007; Matabos et al., 2008; Tyler et al., 2008; Bayer et al., 2011; Nakamura et al., 2014) as observed by their rapid colonization after an eruption at the EPR (Bayer et al., 2011).

Peltospira (McLean, 1989) is a genus of small gastropods only found in active deep-sea hydrothermal vents. *P. smaragdina* (Warén and Bouchet, 2001) is the type species for the nMAR where it was originally reported to occur in aggregations of 12 to 50 individuals (Warén and Bouchet, 2001). The three other species of the genus (*P. operculata, P. lamellifera* and *P. delicata*) have been observed at hydrothermal vent sites on the EPR where they occupy high temperature sulfide-rich habitats (Shank et al., 1998; Matabos et al., 2008). On the MAR, *Peltospira* gastropods within mussel assemblages seem to colonize an intermediate niche between the hottest habitats and the milder ones (Husson et al., 2017). Their relative proximity to black smokers and diffusing zones supports this assumption. On the EPR, these three *Peltospira* species are even found in the hottest "alvinellid" zone (Mills et al., 2007). These authors suggest that *Peltospira* species may exploit microhabitats with higher inputs of hydrothermal fluids, even when found within siboglinid or mussel assemblages. This distribution may potentially reflect their needs for higher concentrations of reduced chemicals such as hydrogen sulfide. At the Moytira vent field, *P. smaragdina* gastropods are distributed into discrete grazing zones at far higher concentrations (~50 000 ind./m^2) than previously observed for the species (Collins et al., 2020). Similar to what was observed in our study, these zones were delineated by cracks of white precipitations, allowing the diffusion of vent fluids. These anhydrite-like mineral deposits are known to form at high temperatures (>150°C) supporting their association with warmer areas.

Role of Gastropods in nMAR Communities

A recent study in LS showed the importance of gastropods early in the recolonization processes following a disturbance (Marticorena et al., 2021). They might take advantage of the microbial films forming on "bare" substratum early in the succession process (Sarrazin et al., 1997; Mullineaux et al., 2010; Mullineaux et al., 2012). As the substratum stabilizes and fluid flow diminishes (e.g. see Juan de Fuca Ridge succession model, Sarrazin et al., 2002), gastropods may increase in abundance until they are replaced by large engineer species typical of low temperature habitats such as mussels. In the LS vent field, mussel assemblages are considered as climax communities (Cuvelier et al., 2014). The decadal stability of environmental conditions (at least at LS) and the maturity of sulfide edifices would explain the relative rarity of these early-successional assemblages in the other two deeper vent fields studied (LS & SP). They appear to be more abundant and to colonize larger areas at greater depths, potentially associated with the presence of newly formed substrata. To our knowledge, and after discussion with several colleagues, we can confirm that these gastropod assemblages are present in at least 50% of the known nMAR vent fields (Marcon et al., 2013; Wheeler et al., 2013; Collins et al., 2020). Their recurrence and distribution suggest that they probably play an important role in the functioning and dynamics of vent communities of the MAR and may even constitute one of the first step of Atlantic vent ecological succession.

DATA AVAILABILITY STATEMENT

The datasets and video images presented in this study can be found in online repositories. Metadata from the various cruises are provided here: CAMBON-BONAVITA Marie-Anne (2014) BICOSE cruise, RV Pourquoi pas?, https://doi.org/10.17600/14000100 CANNAT Mathilde, SARRADIN Pierre-Marie (2012) MOMARSAT2012 cruise, RV Thalassa, https://doi.org/10.17600/12040050 CANNAT Mathilde, SARRADIN Pierre-Marie (2016) MOMARSAT2016 cruise, RV L'Atalante, https://doi.org/10.17600/16001200 LALLIER François (2013) BIOBAZ 2013 cruise, RV Pourquoi pas?, https://doi.org/10.17600/13030030 SARRADIN Pierre-Marie, CANNAT Mathilde (2015) MOMARSAT2015 cruise, RV Pourquoi pas?, https://doi.org/10.17600/15000200 SARRADIN Pierre-Marie, CANNAT Mathilde (2014) MOMARSAT2014 cruise, RV Pourquoi pas?, https://doi.org/10.17600/14000300.

AUTHOR CONTRIBUTIONS

JS and MM conceived the ideas and designed the methodology. JS, MM, CC and AL collected the samples on board during oceanographic cruises. JS, CC, AL, JM, LM and MM processed and analyzed the data. MM did the statistical analyses. JS, CC, AL, JM, NM and MM discussed and interpreted the results. JS wrote the first draft of the manuscript and all authors commented on previous versions of the manuscript. All authors read and approved the final manuscript.

FUNDING

This work was supported by the "Laboratoire d'Excellence" LabexMER (ANR-10-LABX-19) and co-funded by a grant from the French government under the "Investissements d'Avenir" program. The project is part of the EMSO-Azores regional node within EMSO-France (http://www.emso-fr.org) and EMSO ERIC Research Infrastructure (http://emso.eu/). The research program was partly funded by an ANR research grant (ANR Lucky Scales ANR-14-CE02-0008-02).

ACKNOWLEDGMENTS

We would like to dedicate this paper to Benoît Pernet-Coudrier, our colleague who passed away in 2016. We thank the captain of the R/Vs *Thalassa*, *L'Atalante* and *Pourquoi pas?* and their crews for their steadfast collaboration in the success of the various cruises. We are particularly grateful to Pierre-Marie Sarradin, Mathilde Cannat, François Lallier and Marie-Anne Cambon, chief scientists of the cruises who greatly supported our sampling program. We are also grateful to the ROV *Victor6000* pilots for their patience and constant support. We warmly thank the LEP technical team for its valuable help both at sea and in the lab. Two master students contributed to sorting the fauna: Roxane Augen-Langonne (M1, 2014) and Bruno Labelle (M2, 2015). PhD student L. Van Audenhaege helped with the video editing. The manuscript was professionally edited by Carolyn Engel-Gautier.

SUPPLEMENTARY MATERIAL

The Supplementary Material for this article can be found online at: https://www.frontiersin.org/articles/10.3389/fmars.2022.925419/full#supplementary-material

REFERENCES

Bates, A. E. (2007). Persistence, Morphology, and Nutritional State of a Gastropod Hosted Bacterial Symbiosis in Different Levels of Hydrothermal Vent Flux. *Mar. Biol.* 152, 557–568. doi: 10.1007/s00227-007-0709-x

Bates, A. E., Tunnicliffe, V. and Lee, R. W. (2005). Role of Thermal Conditions in Habitat Selection by Hydrothermal Vent Gastropods. *Mar. Ecol. Prog. Ser.* 305, 1–15. doi: 10.3354/meps305001

Bayer, S. R., Mullineaux, L. S., Waller, R. G. and Solow, A. R. (2011). Reproductive Traits of Pioneer Gastropod Species Colonizing Deep-Sea Hydrothermal Vents After an Eruption. *Mar. Biol.* 158, 181–192. doi: 10.1007/s00227-010-1550-1

Beaulieu, S. E. and Szafranski, K. M. (2020). *InterRidge Global Database of Active Submarine Hydrothermal Vent Fields Version 3.4*. doi: 10.1594/PANGAEA.917894

Beinart, R. A., Sanders, J. G., Faure, B., Sylva, S. P., Lee, R. W., Becker, E. L., et al. (2012). Evidence for the Role of Endosymbionts in Regional-Scale Habitat Partitioning by Hydrothermal Vent Symbioses. *Proc. Natl. Acad. Sci.* 109 (47), E3241-E3250 doi: 10.1073/pnas.1202690109

Cambon-Bonavita, M.-A. (2014). *BICOSE*, cruise, RV Pourquoi pas? doi: 10.17600/14000100

Cannat, M., Sarradin, P., Blandin, J., Escartın, J. and Colaço, A. (2011). *MoMar-Demo at Lucky Strike. A Near-Real Time Multidisciplinary Observatory of Hydrothermal Processes and Ecosystems at the Mid-Atlantic Ridge* (San Francisco: AGU Fall meeting). Abstract OS22A-05.

Charlou, J., Donval, J., Douville, E., Jean-Baptiste, P., Radford-Knoery, J., Fouquet, Y., et al. (2000). Geochemical Signatures and the Evolution of Menez Gwen (37 50′ N) and Lucky Strike (37 17′ N) Hydrothermal Fluids, South of the Azores Triple Junction on the Mid. *Chem. geology* 171, 49–75. doi: 10.1016/S0009-2541(00)00244-8

Collins, P. C., Hunter, W. R., Carlsson, J. and Carlsson, J. (2020). Fortuitous Insights Into the Ecology of a Recently Charted Deep-Sea Hydrothermal Vent, Using Snails' Feet. *Deep-Sea Res. Part I: Oceanogr. Res. Papers* 163, 103358. doi: 10.1016/j.dsr.2020.103358

Coplen, T. B. (2011). Guidelines and Recommended Terms for Expression of Stable-Isotope-Ratio and Gas-Ratio Measurement Results. *Rapid Commun. Mass Spectrom.* 25, 2538–2560. doi: 10.1002/rcm.5129

Copley, J. T. P., Tyler, P. A., Murton, B. J. and Van Dover, C. L. (1997). Spatial and Inter-Annual Variation in the Faunal Distribution at Broken Spur Vent Field (29°N, Mid-Atlantic Ridge). *Mar. Biol.* 129, 723–733. doi: 10.1007/s002270050215

Cuvelier, D., Legendre, P., Laes, A., Sarradin, P. M. and Sarrazin, J. (2014). Rhythms and Community Dynamics of a Hydrothermal Tubeworm Assemblage at Main Endeavour Field - a Multidisciplinary Deep-Sea Observatory Approach. *PLoS One* 9 (5), e96924. doi: 10.1371/journal.pone.0096924

Cuvelier, D., Sarradin, P., Sarrazin, J., Colaço, A., Copley, J. T. P., Desbruyères, D., et al. (2011a). Hydrothermal Faunal Assemblages and Habitat Characterisation at the Eiffel Tower Edifice (Lucky Strike, Mid-Atlantic Ridge). *Mar. Ecol.* 32, 243–255. doi: 10.1111/j.1439-0485.2010.00431.x

Cuvelier, D., Sarrazin, J., Colaco, A., Copley, J., Desbruyeres, D., Glover, A. G., Tyler P., Santos R.S. (2009). Distribution and Spatial Variation of Hydrothermal Faunal Assemblages at Lucky Strike (Mid-Atlantic Ridge) Revealed by High-Resolution Video Image Analysis. *Deep Sea Res. Part I: Oceanogr. Res. Papers* 56 (11), 2026–2040 doi: 10.1016/j.dsr.2009.06.006

Cuvelier, D., Sarrazin, J., Colaço, A., Copley, J. T., Glover, A. G., Tyler, P. A., et al. (2011b). Community Dynamics Over 14 Years at the Eiffel Tower Hydrothermal Edifice on the Mid-Atlantic Ridge. *Limnology Oceanogr.* 56, 1624–1640. doi: 10.4319/lo.2011.56.5.16241624

De Busserolles, F., Sarrazin, J., Gauthier, O., Gélinas, Y., Fabri, M. C., Sarradin, P. M., et al. (2009). Are Spatial Variations in the Diets of Hydrothermal Fauna Linked to Local Environmental Conditions? *Deep-Sea Res. Part II Topical Stud. Oceanogr.* 56 (19–20), 1649–1664. doi: 10.1016/j.dsr2.2009.05.011

Desbruyères, D., Almeida, A. J., Biscoito, M., Comtet, T., Khripounoff, A., le Bris, N., et al. (2000). A Review of the Distribution of Hydrothermal Vent Communities Along the Northern Mid-Atlantic Ridge: Dispersal vs. Environmental Controls. *Hydrobiologia* 440, 201–216. doi: 10.1023/A:1004175211848

Desbruyères, D., Biscoito, M., Caprais, J.-C., Colaço, A., Comtet, T., Crassous, P., et al. (2001). Variations in Deep-Sea Hydrothermal Vent Communities on the Mid-Atlantic Ridge Near the Azores Plateau. *Deep-Sea Res. Part I: Oceanogr. Res. Papers* 48, 1325–1346. doi: 10.1016/S0967-0637%2800%2900083-2

Desbruyères, D., M. Segonzac and M., Bright (Eds) (2006) *Handbook of Deep-Sea Hydrothermal Vent Fauna*. Linz, Austria: Land Oberösterreich, Biologiezentrum der Oberösterreichische Landesmuseen,

Fouquet, Y., Wafik, A., Cambon, P., Mevel, C., Meyer, G. and Gente, P. (1993). Tectonic Setting and Mineralogical and Geochemical Zonation in the Snake Pit Sulfide Deposit (Mid-Atlantic Ridge at 23°N). *Economic geology* 88, 2018–2036. doi: 10.2113/gsecongeo.88.8.2018

Gaudron, S. M., Marqué, L., Thiébaut, E., Riera, P., Duperron, S. and Zbinden, M. (2015). How are Microbial and Detrital Sources Partitioned Among and Within Gastropods Species at East Pacific Rise Hydrothermal Vents? *Mar. Ecol.* 36, 18–34. doi: 10.1111/maec.12260

Gebruk, A. V., Galkin, S., Vereshchaka, A., Moskalev, L. and Southward, A. J. (1997). Ecology and Biogeography of the Hydrothermal Vent Fauna of the Mid-Atlantic Ridge. *Adv. Mar. Biol.* 32, 93–144. doi: 10.1016/S0065-2881(08)60016-4

Gollner, S., Colaço, A., Gebruk, A., Halpin, P. N., Higgs, N., Menini, E., et al. (2021). Application of Scientific Criteria for Identifying Hydrothermal Ecosystems in Need of Protection. *Mar. Policy* 132, 104641. doi: 10.1016/j.marpol.2021.104641

Gollner, S., Riemer, B., Martínez Arbizu, P., Le Bris, N. and Bright, M. (2010). Diversity of Meiofauna From the 9°50'n East Pacific Rise Across a Gradient of Hydrothermal Fluid Emissions. *PLoS One* 5, e12321. doi: 10.1371/journal.pone.0012321

Govenar, B. (2012). Energy Transfer Through Food Webs at Hydrothermal Vents: Linking the Lithosphere to the Biosphere. *Oceanography* 25, 246–255. doi: 10.5670/oceanog.2012.23

Govenar, B. and Fisher, C. R. (2007). Experimental Evidence of Habitat Provision by Aggregations of *Riftia Pachyptila* at Hydrothermal Vents on the East Pacific Rise. *Mar. Ecol.* 28, 3–14. doi: 10.1111/j.1439-0485.2007.00148.x

Govenar, B., le Bris, N., Gollner, S., Glanville, J., Aperghis, A., Hourdez, S., et al. (2005). Epifaunal Community Structure Associated With *Riftia Pachyptila* Aggregations in Chemically Different Hydrothermal Vent Habitats. *Mar. Ecol. Prog. Ser.* 305, 67–77. doi: 10.3354/meps305067

Hernández-Ávila, I., Cambon-Bonavita, M.-A., Sarrazin, J., and Pradillon, F. (2022). Population Structure and Reproduction of the Alvinocaridid Shrimp Rimicaris Exoculata on the Mid-Atlantic Ridge: Variations between Habitats and Vent Fields. *Deep-Sea Res. I: Oceanogr. Res. Pap.* 186 (103827), 14. doi: 10.1016/j.dsr.2022.103827

Hügler, M. and Sievert, S. M. (2011). Beyond the Calvin Cycle: Autotrophic Carbon Fixation in the Ocean. *Annu. Rev. Mar. Sci.* 3, 261–289. doi: 10.1146/annurev-marine-120709-142712

Hurlbert, S. H. (1971). The Nonconcept of Species Diversity: A Critique and Alternative Parameters. *Ecology* 52, 577–586. doi: 10.2307/1934145

Husson, B., Sarradin, P., Zeppilli, D. and Sarrazin, J. (2017). Picturing Thermal Niches and Biomass of Hydrothermal Vent Species. *Deep-Sea Res. Part II: Topical Stud. Oceanogr.* 137, 6–25. doi: 10.1016/j.dsr2.2016.05.028

Jannasch, H. W. (1985). The Chemosynthetic Support of Life and the Microbial Diversity at Deep-Sea Hydrothermal Vents. *Proc. R. Soc. B: Biol. Sci.* 225, 277–297. doi: 10.1098/rspb.1985.0062

Karl, D. M. (1995). "Ecology of Free-Living, Hydrothermal Vent Microbial Communities," in *The Microbiology of Deep-Sea Hydrothermal Vents*, vol. 1995) . Ed. Karl, D. M. (Boca Raton, FL: CRC Press Inc.), 35–124.

Karson, J. A., Thompson, G., Humphris, S. E., Edmond, J. M., Bryan, W. B., Brown, J. R., et al. (1987). Along-Axis Variations in Seafloor Spreading in the MARK Area. *Nature* 328, 681–685. doi: 10.1038/328681a0

Kelly, N. E. and Metaxas, A. (2007). Influence of Habitat on the Reproductive Biology of the Deep-Sea Hydrothermal Vent Limpet *Lepetodrilus Fucensis* (Vetigastropoda: Mollusca) From the Northeast Pacific. *Mar. Biol.* 151, 649–662. doi: 10.1007/s00227-006-0505-z

Langmuir, C. H., Humphris, S. E., Fornari, D. J., Van Dover, C. L., Von Damm, K., Tivey, M. K., et al. (1997). Hydrothermal Vents Near a Mantle Hot Spot: The Lucky Strike Vent Field at 37°N on the Mid-Atlantic Ridge. *Earth Planetary Sci. Lett.* 148, 69–91. doi: 10.1016/S0012-821X(97)00027-7

Lau, D. C. P., Leung, K. M.Y. and Dudgeon, D. (2012). Preservation Effects on C/N Ratios and Stable Isotope Signatures of Freshwater Fishes and Benthic Macroinvertebrates. *Limnology Oceanogr.: Methods* 10, 75–89. doi: 10.4319/lom.2012.10.75

Le Bris, N., Zbinden, M. and Gaill, F. (2005). Processes Controlling the Physico-Chemical Micro-Environments Associated With Pompeii Worms. *Deep-Sea Res. Part I: Oceanogr. Res. Papers* 52, 1071–1083. doi: 10.1016/j.dsr.2005.01.003

Lee, R. W., Robert, K., Matabos, M., Bates, A. E. and Juniper, S. K. (2015). Temporal and Spatial Variation in Temperature Experienced by Macrofauna at Main Endeavour Hydrothermal Vent Field. *Deep-Sea Res. Part I: Oceanogr. Res. Papers* 106, 154–166. doi: 10.1016/j.dsr.2015.10.004

Legendre, P. and Gallagher, E. (2001). Ecologically Meaningful Transformations for Ordination of Species Data. *Oecologia* 129, 271–280. doi: 10.1007/s004420100716

Lelievre, Y., Legendre, P., Matabos, M., Mihaly, S., Lee, R. W., Sarradin, P.-M., et al. (2017). Astronomical and Atmospheric Impacts on Deep-Sea Hydrothermal Vent Invertebrates. *Proc. Of R. Soc. B-biological Sci.* 284 (1852), 20162123. doi: 10.1098/rspb.2016.2123

Lelièvre, Y., Sarrazin, J., Marticorena, J., Schaal, G., Day, T., Legendre, P., Hourdez S., Matabos M., (2018). Biodiversity and Trophic Ecology of Hydrothermal Vent Fauna Associated With Tubeworm Assemblages on the Juan De Fuca Ridge. *Biogeosciences* 15. 2629–2647 doi: 10.5194/bg-15-2629-2018

Levesque, C., Juniper, S. K. and Marcus, J. (2003). Food Resource Partitioning and Competition Among Alvinellid Polychaetes of Juan De Fuca Ridge Hydrothermal Vents. *Mar. Ecol. Prog. Ser.* 246, 173–182. doi: 10.3354/meps246173

Luther, G. W., Gartman, A., Yücel, M., Madison, A., Moore, T., Nees, H., et al. (2012). Chemistry, Temperature, and Faunal Distributions at Diffuse-Flow Hydrothermal Vents: Comparison of Two Geologically Distinct Ridge Systems. *Oceanography* 25, 234–245. doi: 10.5670/oceanog.2012.22

Luther, G. W., Rozan, T. F., Taillefert, M., Nuzzio, D. B., Di Meo, C., Shank, T. M., et al. (2001). Chemical Speciation Drives Hydrothermal Vent Ecology. *Nature*. 410, 813–816. doi: 10.1038/35071069

Maas, P. A. Y., O'Mullan, G. D., Lutz, R. A. and Vrijenhoek, R. C. (1999). Genetic and Morphometric Characterization of Mussels (Bivalvia: Mytilidae) From Mid-Atlantic Hydrothermal Vents. *Bioogical Bull.* 196, 265–272. doi: 10.2307/1542951

McLean, J.H. (1989). New Archaeogastropod Limpets from Hydrothermal Eents: New Family Peltospiridae, New Superfamily Peltospiracea. *Zool. Scr.* 18 (1), 49-66.

Marcon, Y., Sahling, H., Borowski, C., dos Santos Ferreira, C., Thal, J. and Bohrmann, G. (2013). Megafaunal Distribution and Assessment of Total Methane and Sulfide Consumption by Mussel Beds at Menez Gwen Hydrothermal Vent, Based on Geo-Referenced Photomosaics. *Deep-Sea Res. Part I: Oceanogr. Res. Papers* 75, 93–109. doi: 10.1016/j.dsr.2013.01.008

Marsh, L., Copley, J. T., Huvenne, V. A. I., Linse, K., Reid, W. D. K., Rogers, A. D., et al. (2012). Microdistribution of Faunal Assemblages at Deep-Sea Hydrothermal Vents in the Southern Ocean. *PLoS One* 7, e48348. doi: 10.1371/journal.pone.0048348

Marticorena, J., Matabos, M., Ramirez-Llodra, E., Cathalot, C., Laes-Huon, A., Leroux, R., et al. (2021). Recovery of Hydrothermal Vent Communities in Response to an Induced Disturbance at the Lucky Strike Vent Field (Mid-Atlantic Ridge). *Mar. Environ. Res.* 168 (105316), 14. doi: 10.1016/j.marenvres.2021.105316

Martins, I., Cosson, R. P., Riou, V., Sarradin, P., Sarrazin, J., Santos, R. S., et al. (2011). Relationship Between Metal Levels in the Vent Mussel *Bathymodiolus Azoricus* and Local Microhabitat Chemical Characteristics of Eiffel Tower (Lucky Strike). *Deep-Sea Res. Part I: Oceanogr. Res. Papers* 58, 306–315. doi: 10.1016/j.dsr.2011.01.002

Matabos, M., Le Bris, N., Pendlebury, S. and Thiébaut, E. (2008). Role of Physico-Chemical Environment on Gastropod Assemblages at Hydrothermal Vents on the East Pacific Rise (13 N/EPR). *J. Mar. Biol. Assoc. UK* 88, 995–1008. doi: 10.1017/S002531540800163X

Matabos, M., Plouviez, S., Hourdez, S., Desbruyères, D., Legendre, P., Warén, A., et al. (2011). Faunal Changes and Geographic Crypticism Indicate the Occurrence of a Biogeographic Transition Zone Along the Southern East Pacific Rise. *J. Biogeography* 38, 575–594. doi: 10.1111/j.1365-2699.2010.02418.x

McClain, R. and Etter, R. J. (2005). Mid-Domain Models as Predictors of Species Diversity Patterns: Bathymetric Diversity Gradients in the Deep Sea. *Oikos* 109 (3), 555–566. doi: 10.1111/j.0030-1299.2005.13529.x

Methou, P., Hernández-Ávila, I., Aube, J., Cueff-Gauchard, V., Gayet, N., Amand, L., et al. (2019). Is it First the Egg or the Shrimp? – Diversity and Variation in Microbial Communities Colonizing Broods of the Vent Shrimp *Rimicaris Exoculata* During Embryonic Development. *Front. Microbiol.* 10. doi: 10.3389/fmicb.2019.00808

Methou, P., Michel, L. N., Segonzac, M., Cambon-Bonavita, M.-A. and Pradillon, F. (2020). Integrative Taxonomy Revisits the Ontogeny and Trophic Niches of *Rimicaris* Vent Shrimps. *R. Soc. Open Sci.*, 7 (7), 200837 (13p.). doi: 10.1098/rsos.200837

Mills, S. W., Mullineaux, L. S. and Tyler, P. A. (2007). Habitat Associations in Gastropod Species at East Pacific Rise Hydrothermal Vents (9 Degrees 50'n). *Biol. Bull.* 212, 185–194. doi: 10.2307/25066601

Mullineaux, L. S., Adams, D. K., Mills, S. W. and Beaulieu, S. E. (2010). Larvae From Afar Colonize Deep-Sea Hydrothermal Vents After a Catastrophic Eruption. *Proc. Natl. Acad. Sci.* 107, 7829–7834. doi: 10.1073/pnas.0913187107

Mullineaux, L. S., Le Bris, N., Mills, S. W., Henri, P., Bayer, S. R., Secrist, R. G., et al. (2012). Detecting the Influence of Initial Pioneers on Succession at Deep-Sea Vents. *PLoS One* 7, e50015. doi: 10.1371/journal.pone.0050015

Mullineaux, L. S., Peterson, C. H., Micheli, F. and Mills, S. W. (2003). Successional Mechanisms Varies Along a Gradient in Hydrothermal Fluid Flux at Deep-Sea Vents. *Ecol. Monogr.* 73, 523–542. doi: 10.1890/02-0674

Nakamura, M., Watanabe, H., Sasaki, T., Ishibashi, J.-I., Fujikura, K. and Mitarai, S. (2014). Life History Traits of *Lepetodrilus Nux* in the Okinawa Trough, Based Upon Gametogenesis, Shell Size, and Genetic Variability. *Mar. Ecol. Prog. Ser.* 505, 119–130. doi: 10.3354/meps10779

Nye, V., Copley, J. T. P. and Tyler, P. A. (2013). Spatial Variation in the Population Structure and Reproductive Biology of *Rimicaris Hybisae* (Caridea: Alvinocarididae) at Hydrothermal Vents on the Mid-Cayman Spreading Centre. *PLoS One* 8, e60319. doi: 10.1371/journal.pone.0060319

Oksanen, J., Blanchet, F.G., Kindt, R., Legendre, P., Minchin, P., O'Hara, R.B., et al.(2013). Vegan: Community Ecology Package. in *R Package Version. 2.0-10.* http://CRAN.R-project.org/package=vegan. CRAN.

Ondréas, H., Cannat, M., Fouquet, Y., Normand, A., Sarradin, P.M., Sarrazin, J. (2009). Recent Volcanic Events and the Distribution of Hydrothermal Venting at the Lucky Strike Hydrothermal Field, Mid-Atlantic Ridge. *Geochemistry Geophysics Geosystems* 10 (2), 1-18 . doi: 10.1029/2008GC002171

Podowski E. L., Moore T. S., Zelnio K. A., Luther G. W. and Fisher C. R. (2009) Distribution of Diffuse Flow Megafauna in Two Sites on the Eastern Lau Spreading Center, Tonga. *Deep-Sea Res. I*, 56, 2041-2056. doi: 10.1016/j.dsr.2009.07.002

Podowski, E. L., Ma, S., Luther, G. W., Wardrop, D. and Fisher, C. R. (2010). Biotic and Abiotic Factors Affecting Distributions of Megafauna in Diffuse Flow on Andesite and Basalt Along the Eastern Lau Spreading Center, Tonga. *Mar. Ecol. Prog. Ser.* 418, 25–45. doi: 10.3354/meps08797

Portail, M., Brandily, C., Cathalot, C., Colaço, A., Gélinas, Y., Husson, B., et al. (2018). Food-Web Complexity Across Hydrothermal Vents on the Azores Triple Junction. *Deep Sea Res. Part I: Oceanogr. Res. Papers* 131, 101–120. doi: 10.1016/j.dsr.2017.11.010

R Core Team (2020). *R: A Language and Environment for Statistical Computing* (Vienna, Austria). Available at: http://www.R-project.org/.

Sancho, G., Fisher, C. R., Mills, S. W., Micheli, F., Johnson, G. A., Lenihan, H. S., et al. (2005). Selective Predation by the Zoarcid Fish *Thermarces Cerberus* at Hydrothermal Vents. *Deep Sea Res. Part I: Oceanogr. Res. Papers* 52, 837–844. doi: 10.1016/J.DSR.2004.12.002

Sarradin, P., Caprais, J.-C., Riso, R., Kerouel, R. and Aminot, A. (1999). Chemical Environment of the Hydrothermal Mussel Communities in the Lucky Strike and Menez Gwen Vent Fields, Mid Atlantic Ridge. *Cahiers Biologie Mar.* 40, 93–104.

Sarradin, P., Waeles, M., Bernagout, S., Le Gall, C., Sarrazin, J. and Riso, R. (2009). Speciation of Dissolved Copper Within an Active Hydrothermal Edifice on the Lucky Strike Vent Field (MAR, 37°N). *Sci. Total Environ.* 407, 869–878. doi: 10.1016/j.scitotenv.2008.09.056

Sarrazin, J. and Juniper, S. K. (1999). Biological Characteristics of a Hydrothermal Edifice Mosaic Community. *Mar. Ecol. Prog. Ser.* 185 (1999), 1–19. doi: 10.3354/meps185001

Sarrazin, J., Juniper, S. K., Massoth, G. and Legendre, P. (1999). Physical and Chemical Factors Influencing Species Distributions on Hydrothermal Sulfide Edifices of the Juan De Fuca Ridge, Northeast Pacific. *Mar. Ecol. Prog. Ser.* 190, 89–112. doi: 10.3354/meps185001

Sarrazin, J., Legendre, P., de Busserolles, F., Fabri, M.-C., Guilini, K., Ivanenko, V. N., et al. (2015). Biodiversity Patterns, Environmental Drivers and Indicator Species on a High-Temperature Hydrothermal Edifice, Mid-Atlantic Ridge. *Deep Sea Res. Part II: Topical Stud. Oceanogr.* 121, 177–192. doi: 10.1016/j.dsr2.2015.04.013

Sarrazin, J., Levesque, C., Juniper, S. and Tivey, M. (2002). Mosaic Community Dynamics on Juan De Fuca Ridge Sulphide Edifices: Substratum, Temperature and Implications for Trophic Structure. *Cahiers Biologie Mar.* 43 (3-4), 275–279. https://archimer.ifremer.fr/doc/00000/893/

Sarrazin, J., Portail, M., Legrand, E., Cathalot, C., Laes, A., Lahaye, N., et al. (2020). Endogenous Versus Exogenous Factors: What Matters for Vent Mussel Communities? *Deep-Sea Res. Part I: Oceanogr. Res. Papers* 160, 103260. doi: 10.1016/j.dsr.2020.103260

Sarrazin, J., Robigou, V., Juniper, S. K. and Delaney, J. R. (1997). Biological and Geological Dynamics Over Four Years on a High-Temperature Sulfide Structure at the Juan De Fuca Ridge Hydrothermal Observatory. *Mar. Ecol. Prog. Ser.* 153, 5–24. doi: 10.3354/meps153005

Schmidt, C., le Bris, N. and Gaill, F. (2008). Interactions of Deep-Sea Vent Invertebrates With Their Environment: The Case of *Rimicaris Exoculata*. *J. Shellfish Res.* 27, 79–90. doi: 10.2983/0730-8000(2008)27[79:IODVIW]2.0.CO;2

Schneider, C. A., Rasband, W. S. and Eliceiri, K. W. (2012). NIH Image to ImageJ: 25 Years of Image Analysis. *Nat. Methods*. 9, 671–675. doi: 10.1038/nmeth.2089

Segonzac, M., De Saint-Laurent M., Casanova B. (1993). Enigma of the Trophic Adaptation of the Shrimp Alvinocarididae in Hydrothermal Areas Along the Mid-Atlantic Ridge. *Cah. Biol. Mar.* 34 (4), 535–571.

Sen, A., Becker, E. L., Podowski, E. L., Wickes, L. N., Ma, S., Mullaugh, K. M., et al. (2013). Distribution of Mega Fauna on Sulfide Edifices on the Eastern Lau Spreading Center and Valu Fa Ridge. *Deep Sea Res. Part I: Oceanogr. Res. Papers* 72, 48–60. doi: 10.1016/j.dsr.2012.11.003

Shank, T. M., Fornari, D. J., Von Damm, K. L., Lilley, M. D., Haymon, R. M. and Lutz, R. A. (1998). Temporal and Spatial Patterns of Biological Community Development at Nascent Deep-Sea Hydrothermal Vents (9°50'n, East Pacific Rise). *Deep-Sea Res. Part II: Topical Stud. Oceanogr.* 45, 465–515. doi: 10.1016/S0967-0645(97)00089-1

Singh, S. C., Crawford, W. C., Carton, H., Seher, T., Combier, V., Cannat, M., et al. (2006). Discovery of a Magma Chamber and Faults Beneath a Mid-Atlantic Ridge Hydrothermal Field. *Nature* 442, 1029–1032. doi: 10.1038/nature05105

Tsurumi, M. and Tunnicliffe, V. (2003). Tubeworm-Associated Communities at Hydrothermal Vents on the Juan De Fuca Ridge, Northeast Pacific. *Deep Sea Res. I* 50 (2003), 611–629. doi: 10.1016/S0967-0637(03)00039-6

Tunnicliffe, V. (1991). The Biology of Hydrothermal Vents - Ecology and Evolution. *Oceanogr. Mar. Biol.* 29, 319–407.

Tyler, P. A., Pendlebury, S., Mills, S. W., Mullineaux, L. S., Eckelbarger, K. J., Baker, M. C., et al. (2008). Reproduction of Gastropods From Vents on the East Pacific Rise and the Mid- Atlantic Ridge. *J. Shellfish Res.* 27, 107–118. doi: 10.2983/0730-8000(2008)27[107:ROGFVO]2.0.CO;2

Van Dover, C. L. (2002). Community Structure of Mussel Beds at Deep-Sea Hydrothermal Vents. *Mar. Ecol. Prog. Ser.* 230, 137–158. doi: 10.3354/meps230137

Van Dover, C. L. (2003). Variation in Community Structure Within Hydrothermal Vent Mussel Beds of the East Pacific Rise. *Mar. Ecol. Prog. Ser.* 253, 55–66. doi: 10.3354/meps253055

Van Dover, C. L. and Doerries, M. B. (2005). Community Structure in Mussel Beds at Logatchev Hydrothermal Vents and a Comparison of Macrofaunal Species Richness on Slow- and Fast-Spreading Mid-Ocean Ridges. *Mar. Ecol.* 26 (2), 110–120. doi: 10.1111/j.1439-0485.2005.00047.x

Van Dover, C. L., German, C. R., Speer, K. G., Parson, L. M. and Vrijenhoek, R. C. (2002). Evolution and Biogeography of Deep-Sea Vent and Seep Invertebrates. *Science (New York N.Y.)* 295, 1253–1257. doi: 10.1126/science.1067361

Vuillemin, R., Le Roux, D., Dorval, P., Bucas, K., Laes-Huon, A., Hamon, M., et al. (2009). CHEMINI: A New *in Situ* CHEmical MINIaturized Analyzer. *Deep Sea Res. Part I: Oceanogr. Res. Paper* 56 (8), 1391–1399. doi: 10.1016/j.dsr.2009.02.002

Warén, A. and Bouchet, P. (2001). Gastropoda and Monoplacophora From Hydrothermal Vents and Seeps: New Taxa and Records. *Veliger* 44, 116–231.

Warén, A., Bouchet, P. and von Cosel, R. (2006). "Lepetodrilus McLean 1988, "Dimorphic Limpets," in *Handbook of Deep-Sea Hydrothermal Vent Fauna*. Eds. Desbruyères, D., Segonzac, M. and Bright, M. (Linz: Biologiezentrum der Oberösterreichischen Landesmuseen).

Wheeler, A. J., Murton, B., Copley, J., Lim, A., Carlsson, J., Collins, P. C., et al. (2013). Moytirra: Discovery of the First Known Deep-Sea Hydrothermal Vent Field on the Slow-Spreading Mid-Atlantic Ridge North of the Azores. *Geochemistry Geophysics Geosystems* 14, 4170–4184. doi: 10.1002/ggge.20243

WoRMS Editorial Board (2022). *World Register of Marine Species*. Available at: https://www.marinespecies.org at: (Accessed July 04, 2022).

Zekely, J., Van Dover, C. L., Nemeschkal, H. L. and Bright, M. (2006). Hydrothermal Vent Meiobenthos Associated With Mytilid Mussel Aggregations From the Mid-Atlantic Ridge and the East Pacific Rise. *Deep-Sea Res. Part I: Oceanogr. Res. Papers* 53, 1363–1378. doi: 10.1016/j.dsr.2006.05.01

Conflict of Interest: The authors declare that the research was conducted in the absence of any commercial or financial relationships that could be construed as a potential conflict of interest.

frontiers | Frontiers in Marine Science

TYPE Original Research
PUBLISHED 03 October 2022
DOI 10.3389/fmars.2022.845965

OPEN ACCESS

EDITED BY
Pei-Yuan Qian,
Hong Kong University of Science and Technology, Hong Kong SAR, China

REVIEWED BY
Adam Michael Reitzel,
University of North Carolina at Charlotte, United States
Sébastien Duperron,
Muséum National d'Histoire Naturelle, France

*CORRESPONDENCE
Yong-Jin Won
won@ewha.ac.kr

SPECIALTY SECTION
This article was submitted to Deep-Sea Environments and Ecology, a section of the journal Frontiers in Marine Science

RECEIVED 30 December 2021
ACCEPTED 13 September 2022
PUBLISHED 03 October 2022

CITATION
Jang S-J, Chung Y, Jun S and Won Y-J (2022) Connectivity and divergence of symbiotic bacteria of deep-sea hydrothermal vent mussels in relation to the structure and dynamics of mid-ocean ridges.
Front. Mar. Sci. 9:845965.
doi: 10.3389/fmars.2022.845965

Connectivity and divergence of symbiotic bacteria of deep-sea hydrothermal vent mussels in relation to the structure and dynamics of mid-ocean ridges

Sook-Jin Jang[1], Yujin Chung[2], Siyeong Jun[3] and Yong-Jin Won[3]*

[1]Research Institute of Ecoscience, Ewha Womans University, Seoul, South Korea, [2]Department of Applied Statistics, Kyonggi University, Suwon, South Korea, [3]Division of Ecoscience, Ewha Womans University, Seoul, South Korea

The population divergence process of deep-sea vent invertebrates is driven by both biotic (e.g., dispersal during the larval stage) and abiotic factors such as deep-ocean currents, depth, and the geological setting of vents. However, little is known regarding the divergence of hydrothermal vent microorganisms. Therefore, our study sought to investigate the influence of geological and geographic factors on the divergence of symbiotic bacteria of *Bathymodiolus* vent mussels. The genetic differentiation patterns of symbionts were examined using next-generation sequencing DNA data in two ocean basins with distinct geological features: the slow-spreading Central Indian Ridge (CIR) and the fast- or superfast-spreading eastern Pacific Ridges. Our findings showed that the degree of differentiation of symbiont populations was geographically hierarchical: the highest between ocean basins, followed by inter-ridge sites between the East Pacific Rise and the Pacific Antarctic Ridge. The Easter Microplate intervening these two ridges acted as a biogeographic physical barrier for both symbionts and their host mussels. On a scale of intra-ridge, symbionts showed isolation by distance in the CIR but not in the eastern Pacific ridges. These contrasting genetic patterns relate to different ridge spreading rates determining most of the geological characteristics of mid-ocean ridges that affect the connectivity of vent habitats in space and time. At the intra-ridge geographic scale of the CIR, population divergence processes of both symbionts and hosts from separate three ridge segments were analyzed in detail using a genetic model of isolation with migration (IM). The phylogenetic topology of symbiont populations was congruent with the host populations, indicating the influence of common historical and physical constraints for habitats and dispersal between vents in the Central Indian Ridge. Collectively, our findings provide key insights into the dynamics of microbial population divergence in deep-sea vents.

KEYWORDS

symbiotic bacteria, Bathymodioline mussel, population divergence, seafloor spreading rate, Central Indian Ridge, Eastern Pacific Ocean

Introduction

Studies on macroorganisms suggest that they share phylogeographic patterns with symbiotic microorganisms, although the spatiotemporal scale of these patterns may vary between the two organismic groups. The spatial distribution of microorganisms is mainly constrained by environmental factors, causing niche partitioning and geographical distance between habitats (De Wit and Bouvier, 2006; Hanson et al., 2012; Van Der Gast, 2015). However, the relative magnitude of the two factors remains controversial. Initially, environmental variables were considered the major factors that shape the biogeographical distribution of microorganisms, which supported Bass-Becking's hypothesis: "everything is everywhere, the environment selects" (Finlay and Clarke, 1999). The influence of geographical distance was excluded based on the assumption that microorganisms have unlimited dispersal capability due to their extremely small sizes and massive population sizes. However, a growing body of evidence has suggested that bacterial populations are in fact affected by geographical distance, as demonstrated by studies on the distribution patterns of archaea populations and the phylogeny of hot spring cyanobacteria (Papke et al., 2003; Whitaker et al., 2003). Furthermore, the dispersal of endemic taxa inhabiting isolated habitats appears to be particularly affected by geographic distance (Louca, 2021).

The hydrothermal vent ecosystem is a representative isolated habitat with spatially and temporally discontinuous distribution along the mid-ocean ridge and back-arc basin. Nevertheless, the environmental variations of vent fields are considered important determinants of biogeographical patterns due to the close association between the chemistry of vents and bacterial metabolism. Previous studies have analyzed vent geochemistry and fluid chemistry to characterize their effect on the geographical structure of vent microorganisms by comparing community compositions at various spatial scales (Campbell et al., 2006; Flores et al., 2011; Anderson et al., 2015; Reveillaud et al., 2016; Meier et al., 2017). Interestingly, Huber et al. (2010) proposed that geographic isolation rather than the chemistry of diffuse flow regions affected the biogeographic patterns of *Epsilonproteobacteria* at a large spatial scale (>1,000 km). Likewise, the effect of geographic isolation was observed from the gill-associated symbiotic bacteria of Bathymodioline mussel, *Idas modiolaeformis*, collected from sunken wood and deep in the east Atlantic and Mediterranean (Laming et al., 2015). A comparison among several sites distributed broadly represented that the dissimilarity of bacterial composition was positively correlated with the geographical distance between habitats. The geographic distance was recently proven to be an essential factor for the divergence of the symbiotic bacteria of deep-sea vents: symbionts of northern Mid-Atlantic Ridge (MAR) *Bathymodiolus* mussels (Ücker et al., 2021) and symbionts of scaly-foot vent snails, *Chrysomallon squamiferum*, in the Indian Ocean Ridge (Lan et al., 2022). These few pioneering studies cast research questions about the connectivity and divergence of bacteria of deep-sea hydrothermal vents between mid-ocean ridge systems showing different dynamics of tectonic activities and geological features involving various geographic distance scales, geomorphological structures, and so on.

In the deep-sea hydrothermal vent ecosystem, most invertebrates rely on chemosynthetic bacteria harbored in the specialized organs for the absorption of key nutrients. Therefore, acquiring symbiotic bacteria is directly linked to the survival of host animals. Host animals acquire the bacterial symbiont from the environment (horizontal transmission) or directly from the parent through gametes (vertical transmission) or by a mixed transmission mode of them (leaky vertical transmission). Bathymodioline mussels inhabit deep-sea chemosynthetic environments and harbor sulfur-oxidizing and/or methane-oxidizing bacteria in their gills. The host mussels obtain their symbionts from the environment through horizontal transmission, which has been demonstrated by discrepancies between the phylogenic topology of hosts and symbionts, as well as genome size similarities between symbionts and free-living bacteria (Won et al., 2003; Won et al., 2008; Fontanez and Cavanaugh, 2014; Russell et al., 2020). Fontanez and Cavanaugh (2014) detected strains of symbiotic bacteria in seawater and biofilms, suggesting that the mussel symbionts are acquired from free-living bacterial populations with presumably larger gene pools. Recently, Franke et al. (2021) discovered that the acquisition of symbionts in bathymodioline mussels first occurs during metamorphosis and after settlement. Moreover, the cellular anatomy of *Bathymodiolus septemdierum* demonstrated that there are pathways that connect the internal bacteriocytes to the external environment (Ikuta et al., 2021). Therefore, we hypothesize that population genetic studies of the symbiotic bacteria of mussels, which constitute enriched samples of environmental free-living bacteria, can provide insights into the diverging process of microbial populations in the deep-sea hydrothermal vents.

Bathymodioline mussels inhabiting the central Indian and eastern Pacific Oceans harbor sulfur-oxidizing bacteria, and the symbiont communities of mussels are dominantly composed of a single phylotype (Won et al., 2008; Ho et al., 2017). The two regions have substantially different seafloor spreading rates, with the Central Indian Ridge (CIR) exhibiting slow spreading and the East Pacific Rise (EPR) and Pacific Antarctic Ridge (PAR) of the eastern Pacific Ocean exhibiting fast or ultrafast spreading. The geological characteristics of vents influence genetic diversity in a metapopulational context on a local scale and the geographical connectivity of vent animals on a regional scale (Vrijenhoek, 2010; Mullineaux et al., 2018). In the eastern Pacific Ocean, vent invertebrates exhibit genetically subdivided population structures due to the geographical barrier around

the equator and the Easter Microplate on the southern EPR (Vrijenhoek, 2010). Bathymodioline mussels and their symbiotic bacteria also showed geographically subdivided distributions across the Easter Microplate boundary, suggesting that the physical barrier not only interrupted host dispersal but also affected its symbionts (Johnson et al., 2013; Ho et al., 2017). However, the spatial structure of vent populations along the CIR, particularly between the Onnuri and other vent fields, remains uncharacterized. The Onnuri field, located approximately 780 km north of the Dodo vent field, is the most recently discovered vent field along the CIR (Kim et al., 2020). To date, a total of five vent fields have been found along the CIR: the Kairei and Edmond vent fields near the Rodrigues Triple Junction (Van Dover et al., 2001), the Solitaire and Dodo vent fields in the north (Nakamura et al., 2012), and the Onnuri field in the northernmost region of the CIR (Kim et al., 2020). Previous studies based on mitochondrial genes revealed the high geographical connectivity of invertebrates among the Solitaire, Edmond, and Kairei (Beedessee et al., 2013; Chen et al., 2015; Sun et al., 2020; Zhou et al., 2022). The vent mussels of the Indian Ocean, *Bathymodiolus marisindicus*, exhibited high genetic connectivity within a more geographically extended range than other invertebrates, extending from the Solitaire vent in the CIR to the Longqi vent in the South West Indian Ridge (SWIR) (Sun et al., 2020).

Our study aimed to explore the population divergence of bacteria in a representative hydrothermal vent environment by comparing genetically differentiated patterns of vent bacteria under distinct geological settings: the slow-spreading CIR and the fast-spreading eastern Pacific (EPR and PAR). Most previous studies have compared the composition of taxa based on *16S* rDNA sequences at broad taxonomic levels (e.g., genus or family levels) to detect the biogeographic patterns of microorganisms. However, a finer taxonomic resolution is needed to detect the effect of distance on microbial biogeographic patterns (Hanson et al., 2012). Here, we examined the genetic variation of mussel gill-associated sulfur-oxidizing bacteria belonging to the SUP05 clade based on amplicon sequences obtained by next-generation sequencing (NGS) of multiple protein-coding genes and *16S* rRNA to achieve an acceptable resolution. We compared the genetic differentiation patterns of the symbiotic bacteria in a geographically hierarchical manner from different ocean basins, ridges, and vent fields. Finally, we explored the diverging processes of symbionts and their host mussels among three adjacent ridge segments of the CIR by applying a population divergence genetics model known as the isolation with migration (IM) model to the NGS DNA data of symbiont populations and PCR-sequenced DNA data of host populations.

Materials and methods

Sampling

Bathymodiolus marisindicus mussels were collected from four hydrothermal vent fields on the CIR (Table 1, Figure 1). The mussels were obtained from the Onnuri and the Solitaire vent fields using a video-guided hydraulic grab (Oktopus GmbH, Germany, Dive number: GTV1702, GTV1807, and GTV1809) and from the Edmond and Kairei vent fields using a remotely operated vehicle, Jason I (Dive number: JL301, JL296). All samples were frozen at −80°C on board, transported to the laboratory on dry ice, and stored at −80°C until required for downstream analyses.

Genomic DNA extraction and sequencing

The genomic DNA of the mussels was extracted from each specimen's foot or mantle tissue using the Qiagen DNeasy Tissue kit (Qiagen Inc., Hilden, Germany). One mitochondrial gene (*mtCOI*) and two nuclear genes (*EF1α* and *Col-1*) were amplified using gene-specific primer sets with primer-specific PCR conditions previously designed for bathymodioline mussels (Supplementary Table S1). The PCR was performed in 20 µl volumes including 2 µl of 10× Taq polymerase buffer, 1.5 µl of 2.5 mM stock solution of dNTPs, 1.5 µl of each primer (10 µmol/l), 1 µl of 1 mg/ml bovine serum albumin, 1 µl of extracted DNA (30–150 ng), 0.625 units of IP Taq polymerase (Cosmo Genetech Inc., South Korea), and sterile H_2O to reach the desired volume. The PCR products were purified using the Dr. Prep Kit (Cat. No.

TABLE 1 Sampling localities and sample size.

Location	Lat.	Lon.	Depth (m)	Dive no.[1]	Date	N^H	N^S
Onnuri	11°24.9′S	66°25.4′E	2022	GTV1809	06-2018	24	12
Solitaire	19°33.4′S	65°50.9′E	2634	GTV1807	06-2018	10	6
	19°33.4′S	65°50.9′E	2505	GTV1702	08-2017	10	6
Edmond	23°52.7′S	69°35.8′E	3290–3320	JL301	04-2001	15	12
Kairei	25°19.2′S	70°02.4′E	2415–2460	JL296	04-2001	15	12

[1]GTV, TVgrab; JL, Jason I.
N^H, sample size used for molecular analyses of host species.
N^S, sample size used for molecular analyses of bacterial symbionts.

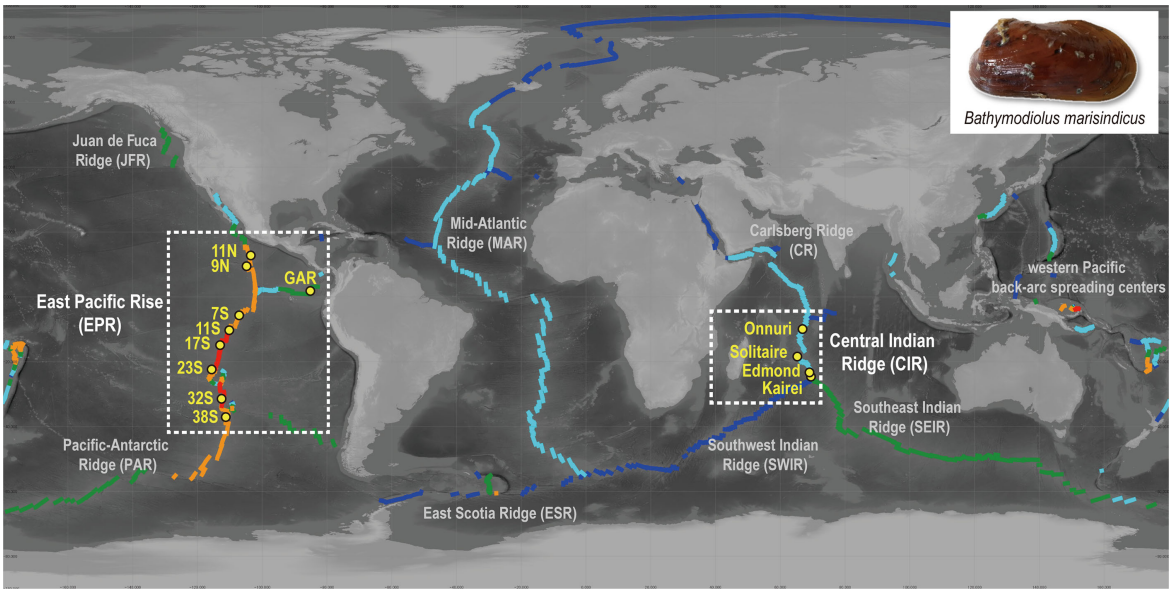

FIGURE 1
Distribution of sampling sites in this study and spreading rate of ridge axes. The colors of the ridge axes represent their spreading rate (Bird, 2003): ultra-slow (dark blue, <20 mm/year), slow (light blue, 20–50 mm/year), intermediate (green, 50–80 mm/year), fast (orange, 30–140 mm/year), and superfast (red, >140 mm/year). Map created with QGIS v. 3.12.3 using bathymetry data from the General Bathymetric Chart of the Oceans (GEBCO).

MK02020, MGmed, South Korea). The DNA sequences were then determined using a Big Dye Terminator V3.1 Cycle Sequencing Kit on an Applied Biosystems 3730xl DNA Analyzer (Applied Biosystems Inc., South Korea). All sequences from the host mussels were deposited in the GenBank database under accession numbers OK509086–OK509159 (*mtCOI*), OK524315–OK524440 (*EF1a*), and OK524441–OK524584 (*Col*).

The genomic DNA of symbiotic bacteria was extracted from the gill tissues of individual mussels using the Qiagen DNeasy Tissue Kit (Qiagen Inc., Hilden, Germany). We targeted single-copy genes including *16S* rRNA and six functional genes with different functional categories used in previous studies on sulfur-oxidizing symbionts of deep-sea mussels of the genus *Bathymodiolus*: sulfur metabolism (*dsrB*), protein folding (*dnaK*), glycolysis (*pfk*, *pgi*, and *pykF*), transcription regulation (*rpoD*) (Fontanez and Cavanaugh, 2014; Ho et al., 2017). Libraries for Illumina-MiSeq sequencing were prepared *via* two-step PCR. First, fragments of seven genes were amplified using specific primer sets with the following conditions (Supplementary Table S2): 95°C for 3 min; 30 cycles at 95°C for 40 s, 50°C–55°C for 30 s, and 72°C for 90 s, and 72°C for 7 min. The *16S* rRNA gene was amplified using a universal prokaryotic primer set targeting the V3 and V4 regions. Functional genes were amplified using a thiotroph-specific primer set designed based on the previously deposited sequences of *B. marisindicus* sulfur-oxidizing endosymbionts and newly generated sequences by PacBio RS II (unpublished data sequenced from gill tissue of specimen "S10" collected at the Solitaire field in 2017). In the second PCR, unique pairs of Illumina Nextera Indices (N7/S5) were attached to the end of the amplified fragments to separate individual hosts. After PCR purification using AMpure XP magnetic beads (Edwards, 2012), the amplicons were pooled at equal quantities (80 ng). Finally, the DNA of the symbiont communities was sequenced on an Illumina MiSeq sequencer (600PE) following a 2 × 300 bp paired-end protocol at the National Instrumentation Center for Environmental Management (NICEM) of Seoul National University (Seoul, Korea). The raw Illumina amplicon data were deposited in the GenBank database under accession number PRJNA769986.

The raw reads of the functional genes were processed using Cutadapt v. 2.3 (Martin, 2011) and the 'DADA2' R package taking into account the DADA2 algorithm designed to detect a fine-scale variation from both 454 and Illumina data with more accuracy (Rosen et al., 2015; Callahan et al., 2016). The paired-end reads were demultiplexed according to gene region, and primer sequences were trimmed using Cutadapt v. 2.3. The DADA2 R package was used for filtering by quality, denoising, merging paired reads, and removing chimeric sequences. These procedures were conducted using the default settings except when removing chimeric sequences to prevent excessive deletion of sequences, in which case the 'minfoldParentOverAbundance (default = 2)' option was modified to 4. Subsequently, the

sequences with <90% similarity with other reads and single reads of each locus were excluded in subsequent analyses.

Raw 454 pyrosequencing data from gill-associated symbionts of bathymodiolin mussels at seven vent fields in the eastern Pacific Ocean were obtained from a previously published study (Ho et al., 2017). Our study analyzed four common loci (*dnaK*, *pgi*, *pykF*, and *rpoD*) used for molecular analyses of symbionts of the CIR. The sequencing data from the CIR and the eastern Pacific symbionts were obtained by two different sequencing techniques (Illumina MiSeq and 454 pyrosequencing platforms, respectively). We used the same pipeline, DADA2, for the NGS data process to minimize the potential bias caused by the usage of different denoising algorithms. The DADA2 pipeline was conducted with the appropriate settings for the pyrosequencing dataset to denoise gap errors in homopolymer sites and restrict the number of insertions that the 454 platform frequently generates (HOMOPOLYMER_GAP_PENALTY = −1, BAND_SIZE = 32). Likewise with the processing of the Illumina dataset, the sequences with <90% similarity and single reads of each locus were excluded in subsequent analyses. The pipelines for the analysis of raw sequence data from Illumina MiSeq and 454 pyrosequencing platforms are schematized in Supplementary Material S1.

Community analyses using the *16S* rRNA gene

The diversity and relative abundance of each bacterial strains in the gill tissue of *B. marisindicus* were characterized by ribotyping of amplicons of the V3–V4 regions of the *16S* rRNA gene. The raw reads were first quality-checked, after which low-quality (<Q25) reads were filtered using Trimmomatic v. 0.32 (Bolger et al., 2014). Afterward, the paired-end sequence data were merged with VSEARCH v. 2.13.4 (Rognes et al., 2016) with the default parameters. Primers were then trimmed with the alignment algorithm of Myers and Miller (1988) at a 0.8 similarity threshold. Non-specific amplicons that do not encode *16S* rRNA were detected using nhmmer 4 in the HMMER software package v. 3.2.1 with hmm profiles. Unique reads were extracted, and redundant reads were clustered with the unique reads using VSEARCH. The EzBioCloud *16S* rRNA database (Yoon et al., 2017) was used for taxonomic assignment followed by more precise pairwise alignment using VSEARCH. The cutoff values of sequence similarity were taken from Yarza et al. (2014). Chimeric reads were filtered based on a <97% similarity threshold *via* reference-based chimeric detection using the UCHIME algorithm (Edgar et al., 2011) and the non-chimeric *16S* rRNA database from EzBioCloud. Finally, operational taxonomic units (OTUs) with single reads were omitted from further analysis. The pipelines for the analysis of the *16S* rRNA raw sequence data are schematized in Supplementary Material S2.

Molecular analyses

Comparison of symbiont populations between the CIR and the eastern Pacific Ocean

The two datasets from the 454 and Illumina MiSeq platforms were normalized by adjusting the number of reads per population for each gene to minimize the bias caused by the large variations in read numbers, in addition to the process of the raw data using the same denoising algorithm, DADA2. The number of sequence reads of each gene from the CIR was normalized by randomly sampling among the processed NGS sequences from Illumina MiSeq and adjusting them to the average number of reads per gene for each population generated by 454 pyrosequencing from the EPR (i.e., the normalized number of sequence reads per gene for population of the CIR symbionts: *dnaK*, 5,213; *pgi*, 4,909; *pykF*, 6,031; *rpoD*, 7,260). The length of fragments for four genes was adjusted to overlapped sites after alignment using the Clustal Omega algorithm on the Geneious Prime 2022.1.1. Subsequently, we compared nucleotide diversity (π) between two datasets to evaluate the effect of different error rates on the level of genetic diversity of symbiont populations. The levels of genetic differentiation among populations were estimated using D_{xy} (Nei, 1987), the average number of pairwise nucleotide differences per site between symbiont populations, to avoid the effect of variation in the genetic diversity of populations (Cruickshank and Hahn, 2014). The D_{xy} of four loci (*dnaK*, *pgi*, *pykF*, and *rpoD*) were estimated according to the Jukes–Cantor substitution model in Arlequin v. 3.5 (Excoffier and Lischer, 2010).

Next, the correlation between genetic differentiation and geographical distances was determined *via* Mantel and Pearson correlation tests using the mean D_{xy} of the four loci according to Legendre and Fortin (2010). Geographic distances were estimated using the latitude/longitude distance calculator on the 'National hurricane center and central pacific hurricane center' website (https://www.nhc.noaa.gov/gccalc.shtml). For the populations in the eastern Pacific Ocean, a partial Mantel test was performed using the open-source software zt (Bonnet and Van De Peer, 2002), which reflected the geographical assignment according to the results of a previous study (Ho et al., 2017) to exclude the effect of physical barriers on gene flow across the Easter Microplates around 25°S: 11N, 9N, 7S, 11S, 17S, 23S, and 32S, 38S. Geographical separation was treated as the third matrix in which a value of zero or one was assigned depending on whether the populations belonged to the same or different clusters, respectively. The Mantel test was carried out using a custom R script for the CIR populations because the sample size was smaller than five, which is the minimum number of samples required by the zt software. The R scripts are included in the Supplementary Data uploaded on Figshare (https://doi.org/10.6084/m9.figshare.17701754.v5). Similarly, the Pearson correlation tests were carried out between populations within the EPR and PAR, respectively, and between populations of the CIR at the intra-ridge level. The correlation tests were conducted on Excel using the

XLSTAT 2022.3. statistical and data analysis solution (Addinsoft, New York, USA).

Comparison of host and symbiont population on the CIR

We next examined the population genetics of the CIR samples, including host and symbiotic bacteria. As indicated in the sequencing section, the fragments of three genes (*mtCOI*, *Col*, and *EF1a*) for the host and seven genes (*16S* rRNA, *dnaK*, *dsrB*, *pfk*, *pgi*, *pykF*, and *rpoD*) for symbiotic bacteria were used. For the *16S* rRNA gene, the reads assigned in the same OTU with ≥97% sequence similarity among the reads belonging to the genus *Candidatus* Thioglobus were used to observe genetic variation at the intraspecific level of bacteria. The reads were extracted using USEARCH v.11 (Edgar, 2010; Edgar, 2013).

For both hosts and symbionts, genetic diversity, analysis of molecular variance (AMOVA), and D_{xy} based on the Jukes–Cantor substitution model were determined using Arlequin v. 3.5 (Excoffier and Lischer, 2010). Median-joining networks of symbionts were generated with CYTOSCAPE v. 3.7.2 (Shannon et al., 2003) based on median-joining network tables (Bandelt et al., 1999) estimated from PopART v. 1.7 (Leigh and Bryant, 2015). To simplify the network, we excluded the private alleles found at only one location. The median-joining networks of hosts were constructed using PopART v. 1.7. The Mantel tests were conducted using the R script, and the Pearson correlation tests were performed using XLSTAT 2022. 3 (Addinsoft, New York, USA).

Neutrality test and estimation of demographic parameters using the IM model

Tajima's *D* (Tajima, 1989) and Fu's *Fs* (Fu, 1997) were estimated using 100 randomly sampled sequences from the dataset pooled from the same vent location regardless of the host. Because the 100 sequences per vent locality was a manageable amount of input data for running the IMa3 computer program when we attempted in this study, we tested the neutrality with those 100 sequences per gene per vent population (Figure 2B). The two neutrality tests assumed non-recombination. Thus, we performed a four-gamete test for each gene in DnaSP v. 5 (Librado and Rozas, 2009) and only the longest non-recombined DNA fragments of each locus were analyzed (*dnaK*, 146 bp; *dsrB*, 161 bp; *pfk*, 128 bp; *pgi*, 134 bp; *pykF*, 94 bp; *rpoD*, 146 bp).

The phylogenetic and demographic history was analyzed using the IMa3 program based on the IM model (Nielsen and Wakeley, 2001; Hey et al., 2018). The IM3 analyses were carried out for only three populations because the computational burden was rapidly increased for four-population analysis when applying our symbiont NGS data. The three vent

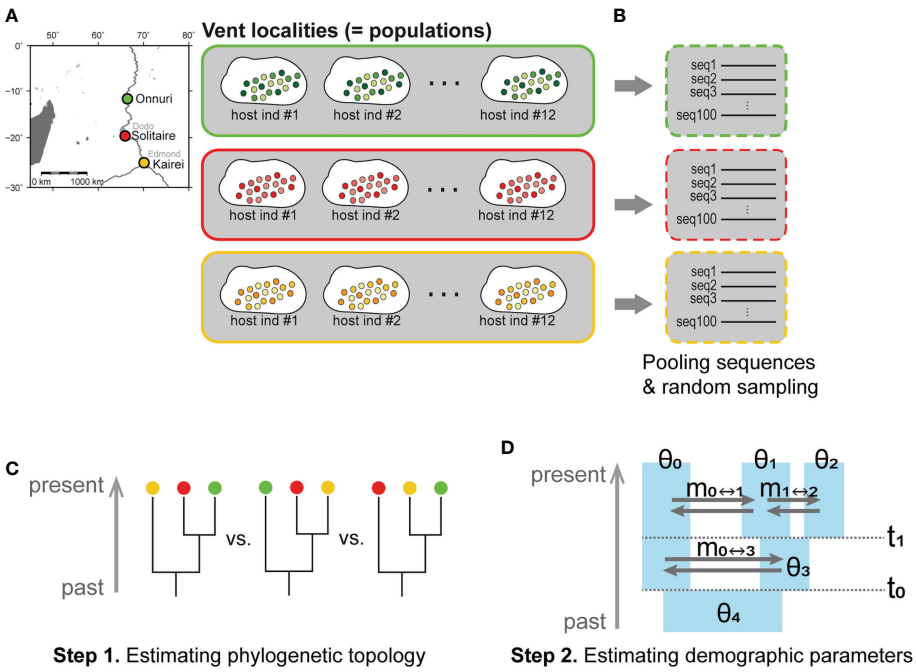

FIGURE 2
Hierarchical level of symbiont populations examined in this study and steps for IMa3 analyses. **(A)** Definition of a population in this study. The sequences from the same vent field were regarded as a population regardless of individual hosts. **(B–D)** Inference about demographic history based on the isolation with migration (IM) model using the IMa3 software: **(B)** Preparation of an input file, **(C)** Step 1. Estimation of phylogenetic topology, **(D)** Step 2. Analysis of demographic parameters scaled by mutation rate (θ, population size; m, migration rate; t, splitting time) (Hey et al., 2018).

localities, Onnuri, Solitaire, and Kairei, were chosen because they represent three adjacent but isolated ridge segments of the CIR north to south (Figure 2A). Because Edmond and Kairei vent fields are located within the same southernmost ridge segment, we chose Kairei because of its slightly higher nucleotide diversity (π) than Edmond (Supplementary Figure S1). As input data for IMa3 running, the same datasets with the neutrality test were used except for the *dsrB* gene (Hey and Wang, 2019). The size of the non-recombination block of *dsrB* for three-population IMa3 was 191 bp, slightly longer than that of the neutrality test (161 bp).

IM analyses were conducted through two steps (Figures 2C, D): 1) inference of phylogeny of three geographic populations, followed by 2) estimation of demographic parameters in step 1. We estimated the marginal posterior probability distribution of phylogenetic tree topologies for three symbiont populations from a Markov chain Montel Carlo (MCMC) simulation. The phylogeny of three symbiont populations with the maximum posterior probability was then chosen. In step 2, we conducted an MCMC simulation to estimate demographic parameters such as population sizes (θ), migration rates (m), and splitting times (t) of symbiont populations based on the estimated phylogeny from step 1. In each step, the Hasegawa–Kishino–Yano (HKY) substitution model was used for symbiont analyses. The inheritance scalar was set as 1.0 for the six symbiont-specific functional genes analyzed herein. The options for the MCMC simulations used for steps 1 and 2 are described in Supplementary Material S3. For each IMa3 analysis, several convergence diagnostics were monitored (Supplementary Material S4).

For the analysis of host mussels, every sequence of three loci obtained from Sanger sequencing (59 for *mtCOI*, 114 for *Col-1*, and 96 for *Ef1a*) was used. Once again, the longest non-recombined fragment of each nuclear gene was used. The IM analyses were performed following the same procedures as for the symbiotic bacteria through steps 1 and 2. The HKY substitution model was used for the symbiotic analyses using an inheritance scalar of 1.0 for two nuclear genes and 0.25 for the *mtCOI* gene. The details for MCMC simulations and convergence diagnostics are described in Supplementary Materials S3 and S4.

The estimated demographic parameters including population sizes, migration rates, and splitting times were converted to each corresponding demographic scale using the geometric mean of ML estimates of relevant mutation rate scalars calculated from a scalar histogram in IMa3 based on previously estimated mutation rates and generation times from previous studies. For symbionts, we used the substitution rate of four functional genes previously estimated by Ho et al. (2017) for synonymous substitutions of *Bathymodiolus* symbiotic bacteria on the EPR: *dnaK* ($1.1–2.33 \times 10^{-8}$ substitution/site/year), *pgi* ($0.99–2.1 \times 10^{-8}$/site/year), *pykF* ($0.43–0.92 \times 10^{-8}$ substitution/site/year), and *rpoD* ($0.63–1.33 \times 10^{-8}$ substitution/site/year). For hosts, we used the substitution rate for *mtCOI* (1.62×10^{-8} substitution/site/year) estimated for bathymodioline mussels based on fossil calibration (Lorion et al., 2013) and a substitution rate of 4.0×10^{-9} substitution/site/year for the two nuclear genes according to the estimate for the *EF1a* gene s brooding starfish belonging to the genus *Leptasterias*, which inhabits the North Pacific (Foltz et al., 2008). The generation time of the host was assumed as 1 year based on a histological study of bathymodioline mussels not only from the Mid-Atlantic Ridge (MAR) and the Gulf of Mexico but also from the South China sea at depths of more than 1,000 m (Colaço et al., 2006; Dixon et al., 2006; Tyler et al., 2007; Zhong et al., 2020). However, the population sizes of symbionts could not be converted to a demographic scale due to a lack of related references for the generation time of symbiotic bacteria.

Results

Composition of the bacterial community in the gill of *B. marisindicus*

A total of 5,776 to 26,558 gill-associated bacterial *16S* rRNA sequence reads were obtained per host mussel from the CIR (Supplementary Table S3). The bacterial reads were identified as Gammaproteobacteria, most of which were classified as sulfur-oxidizing bacteria within the genus *Candidatus* Thioglobus (>80%). Most reads of sulfur-oxidizing bacteria had high sequence similarity (>99%). Next, a small number of reads were identified as bacteria within the genus *Kistimonas* of the family Endozoicomonadaceae regardless of the sampling location (Figure 3, Supplementary Table S3). Likewise, the *Candidatus* Endonucleobacter within the same family Endozoicomonadacea was detected broadly in the Onnuri, Solitaire, and Kairei fields despite the considerably low abundance (<1.28% of reads). Most of the reads were identified as *Candidatus* Endonucleobacter bathymodiolin based on sequence similarity >97%.

Genetic variation of symbiotic bacteria in the CIR and the eastern Pacific Ocean

The number of reads between Illumina and 454 pyrosequencing platforms was considerably different (mean number of reads per gen: Illumina MiSeq data = 94,946–144,842, 454 pyrosequencing = 4,939–7,260; Table 2, Supplementary Table S4). Before the further examination of the genetic divergence of symbiotic bacteria, the nucleotide diversity (π) of each vent locality was measured and compared to each other to check if the different platforms have led to a possible systematic underestimate or overestimate of the population genetic index of D_{xy}. The nucleotide diversities were considerably low in the vents of the

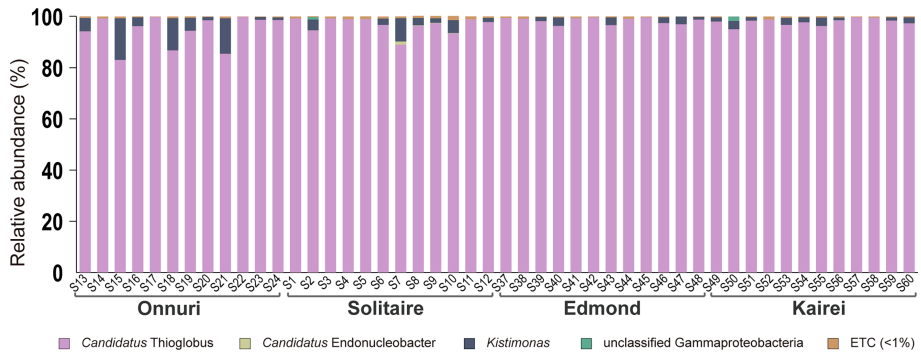

FIGURE 3
Community analyses based on the *16S* rRNA gene of symbiotic bacteria in the gills of *Bathymodiolus marisindicus*. The reads are assigned at the genus level. The taxa with lower abundance <1% commonly in all host mussels were classified into ETC.

eastern Pacific ridges, of which symbiont sequences were generated by 454 pyrosequencing, compared to those from the vents of the CIR of which sequences were generated by Illumina MiSeq (mean nucleotide diversity: eastern Pacific vents = 0.0015–0.0051, central Indian vents = 0.0031–0.0153; Supplementary Figure S1). However, two vent fields, Edmond and Kairei, from the southernmost ridge segment of the CIR were similarly low in nucleotide diversity and equivalent to those of the eastern Pacific vents. In contrast, the symbiont populations in Onnuri and Solitaire vent fields exhibited higher nucleotide diversity than others. The low nucleotide diversity in the eastern Pacific by the 454 pyrosequencing was contrary to the expectation of higher sequencing error rates of this platform. Therefore, the possible introduction of systematic overestimation or underestimation into the present study due to the difference in sequencing platforms was unlikely.

The symbiont populations exhibited a distinct geographical differentiation pattern between the two different ocean basins (Figure 4). The comparison between the CIR and the eastern Pacific Ocean showed the highest range of genetic differentiation D_{xy} (mean = 0.271–0.278; Figure 4; Supplementary Table S5) followed by the estimates between the East Pacific Rise (EPR) including the Galápagos Rift (GAR) and the Pacific Antarctic Ridge (PAR) symbiont populations (mean = 0.019–0.021). The D_{xy} values between CIR symbiont populations ranged from 0.007 to 0.017. Finally, the lowest D_{xy} values between symbiont populations within the same ridges (EPR including GAR, and PAR) in the eastern Pacific Ocean ranged from 0.002 to 0.004. The Mantel test indicated that the mean of genetic differentiation of symbionts in the CIR increased sharply and proportionally with the geographical distance, but this effect was not statistically significant (Mantel's r = 0.912, P = 0.08). However, the Pearson test showed a statistically significant positive correlation between the two variables (Pearson's r = 0.836, P = 0.011). Meanwhile, genetically homogeneous populations were observed in the same ridges in the eastern Pacific Ocean regardless of the geographic distance (partial Mantel's r = 0.13, P = 0.268; Pearson's r = 0.001, P = 0.871).

Population genetic structure of host mussels and symbiotic bacteria on the CIR

Genetic diversity and divergence

Among all genes analyzed for symbiotic bacteria, the *16S* rRNA gene of sulfur-oxidizing symbionts exhibited the lowest genetic diversity regardless of geographic location (H = 0.32–0.36, π = 0.0009–0.001; Table 2). The functional genes of symbionts showed similar genetic diversity values and patterns among all locations, except at the Edmond vent where both genetic and nucleotide diversity were relatively low (H = 0.47–0.64, π = 0.0001–0.0023; Table 2). The Onnuri and Solitaire symbionts had higher genetic diversity despite having fewer reads. A similar pattern of genetic diversity was also observed in the median-joining network (Figure 5A). For most of the six functional genes, the gene pool of the Edmond symbionts consisted of two or three dominant haplotypes with few variants from them. However, the Onnuri and Solitaire symbionts exhibited many haplotypes and different network shapes among different genes. The median-joining networks of symbionts demonstrated the genetic separation of the Onnuri population from the Edmond and Kairei populations (Figure 5A). Very few haplotypes were distributed widely among the four locations. However, the Solitaire symbionts shared haplotypes with all other three populations. The neutrality test of the four symbiont populations could not reject the null hypothesis of equilibrium population size and/or neutrality of markers about selection. After Bonferroni correction, all estimates of Tajima's D and Fu's Fs were statistically non-significant regardless of locations (Supplementary Table S6).

TABLE 2 Genetic diversity indices of symbiont populations on the CIR.

Gene	Diversity[1]	Onnuri	Solitaire	Edmond	Kairei
16S rRNA (427 bp)	n	158,646	186,361	170,900	173,551
	a	2,333	2,515	2,267	2,287
	k	427	427	427	427
	H	0.3562	0.3454	0.3202	0.3339
	π	0.0011	0.0012	0.0009	0.001
dnaK (400 bp)	n	98,875	100,985	186,503	118,923
	a	355	319	13	112
	k	55	58	6	47
	a_p	218	145	0	55
	H	0.95	0.98	0.53	0.95
	π	0.0236	0.02	0.0009	0.0067
dsrB (439 bp)	n	104,806	118,373	168,562	187,628
	a	192	127	10	46
	k	43	46	5	26
	a_p	141	68	0	24
	H	0.97	0.94	0.50	0.62
	π	0.0151	0.0131	0.0004	0.0023
pfk (425 bp)	n	71,113	79,633	124,661	104,378
	a	257	259	8	193
	k	41	56	3	30
	a_p	193	123	0	106
	H	0.97	0.98	0.49	0.98
	π	0.0182	0.0164	0.0023	0.008
pgi (413 bp)	n	111,895	123,482	169,325	137,088
	a	268	289	27	186
	k	47	63	8	47
	a_p	178	159	11	114
	H	0.96	0.96	0.64	0.95
	π	0.0127	0.0096	0.0012	0.0058
pykF (431 bp)	n	81,159	101,642	174,138	174,543
	a	442	269	14	135
	k	51	54	5	41
	a_p	330	122	0	79
	H	0.98	0.98	0.55	0.96
	π	0.0189	0.0192	0.0009	0.0061
rpoD (434 bp)	n	116,394	119,010	160,062	132,425
	a	94	145	4	106
	k	22	32	2	21
	a_p	31	46	0	57
	H	0.92	0.97	0.47	0.96
	π	0.0059	0.0082	0.0001	0.0066

[1] n, number of reads per locus; a, number of alleles; k, number of polymorphic sites; a_p, number of private alleles; H, gene diversity; π, nucleotide diversity.

The genetic variation of the host mussel populations differed depending on the used gene (Table 3). The *mtCOI* gene exhibited the highest genetic diversity, whereas the *EF1a* gene had the lowest (Table 3 and Figure 5B). Contrary to the high variation of genetic diversity among symbiont populations, the host mussels showed a similar level of genetic diversity independent of vent localities. The Onnuri population of mussels exhibited the highest genetic diversity (H = 0.63–0.96, π = 0.0021–0.0087).

The D_{xy} between symbiont populations demonstrated the influence of geographical distance on the genetic differentiation along the CIR (Figure 6A, Supplementary Table S7). As shown in

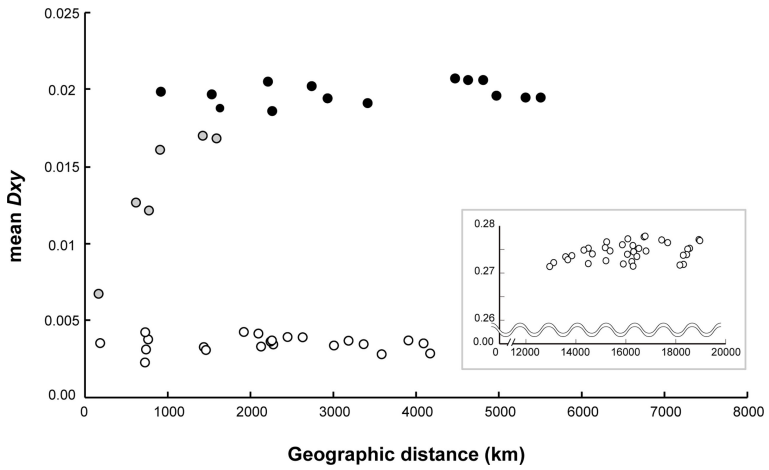

FIGURE 4
Correlation of average population divergence (D_{xy}) with geographic distance between the CIR and the eastern Pacific. The gray circles represent the comparison between vent fields within the CIR, and the white circles represent the comparison between vent fields within each region of the eastern Pacific, the EPR with the GAR, and the PAR. The black circles represent the comparison between the EPR and the PAR in the eastern Pacific. The graph in inset illustrates the comparison between the CIR and the eastern Pacific. This analysis included data collected for 30 years from 1990 at the GAR on the East Pacific Ocean to 2018 at the Onnuri vent field on the Indian Ocean.

Figure 4, which was drawn based on only four functional genes, all of the six functional genes generally exhibited an ascending pattern as the geographic distance between the vents increased. The D_{xy} estimates between the Edmond and Kairei vents on the same ridge segment were the lowest for most genes examined (Supplementary Table S7). The D_{xy} estimates between the Onnuri and the other vent fields were higher regardless of geographic distribution, except for the *pgi* and *rpoD* genes (0.030–0.032 for *dnaK*, 0.019–0.026 for *dsrB*, 0.020–0.023 for *pfk*, and 0.20–0.21 for *pykF*). The Mantel test identified a statistically significant positive correlation between each D_{xy} estimate for *dnaK*, *pfk*, and *rpoD* genes and geographical distance (Mantel's r = 0.93, P = 0.04 for *dnaK*; Mantel's r = 0.927, P = 0.04 for *pfk*; and Mantel's r = 0.723, P = 0.04 for *rpoD*; Supplementary Table S8). In contrast, the Mantel test based on the other three genes showed no statistically significant correlation with geographical distance. The Pearson correlation test exhibited more statistically significant connections. The D_{xy} for four genes, *dnaK*, *dsrB*, *pfk*, and *pykF*, were correlated significantly with geographical distance (Pearson's r = 0.864, P = 0.007 for *dnaK*; Pearson's r = 0.862, P = 0.008 for *dsrB*; Pearson's r = 0.862, P = 0.008 for *pfk*; and Pearson's r = 0.678, P = 0.04 for *pykF*).

For the host mussels, the degree of genetic differentiation was relatively low than symbiont mussels (0.005–0.009 for *mtCOI*, 0.001–0.003 for *Col-1*, and 0.001–0.002 for *EF1a*). The *mtCOI* and *Col-1* genes exhibited a consistently increasing pattern of genetic differentiation among populations with geographical distance (Figure 6B, Supplementary Table S7). According to the Mantel test, only the D_{xy} estimates of the *mtCOI* gene were significantly correlated with geographical distance (Mantel's r = 0.905, P = 0.04), while the Pearson correlation test showed significant correlations between D_{xy} estimates of the *Col-1* gene, as well as *mtCOI*, with geographical distance (Pearson's r = 0.842, P = 0.01 for *Col-1*; Pearson's r = 0.818, P = 0.01 for *mtCOI*; Supplementary Table S8).

For symbiotic bacteria, the AMOVA results for six functional genes revealed the following hierarchical partitioning of genetic variation: among four symbiotic populations (28.64%–50.81%), among host individuals within populations (6.64%–7.88%), and among symbiont strains within individual hosts (42.56%–63.57%) (Supplementary Table S9). On the other hand, AMOVA of the *16S* rRNA gene indicated that most of the genetic variations of the four populations was partitioned among symbiont strains within individuals (99.85%), then among individual hosts within populations (0.11%), and finally among the four populations (0.04%).

Phylogenies and IM model estimates of the CIR mussel hosts and symbionts

For three population analyses on IMa3, we chose one population per ridge segment of the CIR as explained in the *Method* section for representing each three ridge segments from north to south: Onnuri, Solitaire, and Kairei. Finally, Kairei was chosen instead of Edmond based on its slightly higher genetic diversity than Edmond hoping that Kairei represents more general features of the ridge segment than Edmond (Figure 5).

We inferred a population tree topology with the highest posterior probability of symbiotic bacteria and host mussels for the chosen three populations, Onnuri, Solitaire, and Kairei vent fields, on the CIR. The inferred phylogenetic tree topology

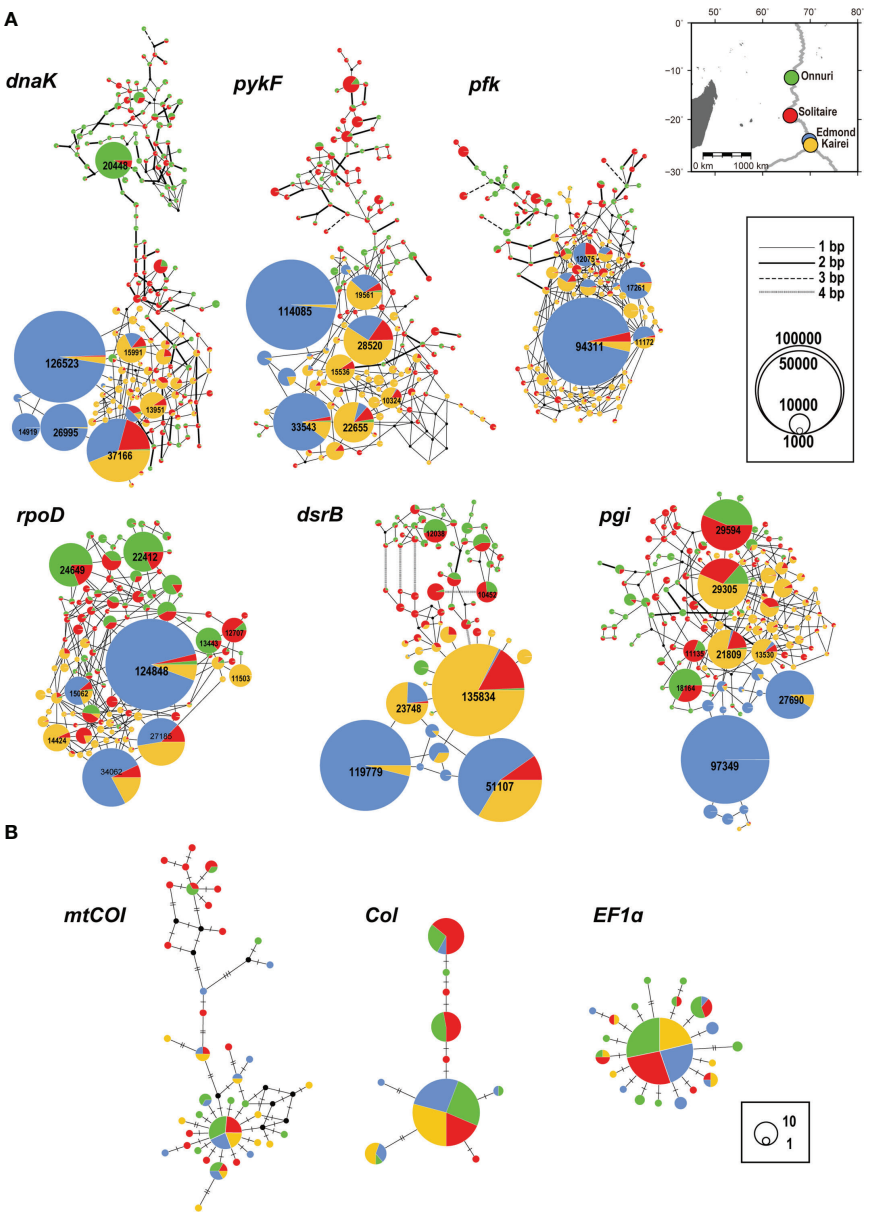

FIGURE 5
Median-joining networks of genes. **(A)** Symbiotic bacteria. **(B)** Host mussels. The colors indicate the geographical locality on the map in **(A)**. The size of the circle represents the abundance of alleles. The black dot represents a hypothetical allele. **(A)** The network was drawn after eliminating private alleles. The number on the circle denotes the abundance of alleles >10,000. The thickness of the edges represents the number of substitutions between alleles. **(B)** The number of hatches denotes the number of substitutions between alleles.

of the host populations was similar to that of the symbiont populations (Table 4, Figure 7): the Onnuri population was identified as a phylogenetically distant group from the Solitaire and Kairei populations. However, the maximum *a posteriori* estimates of two splitting times among three symbiont populations slightly differed from those of the host populations (Figure 7, Supplementary Table S10 and S11). For the symbiotic bacteria, the splitting time between the Onnuri and ancestor populations and between the Solitaire and Kairei populations (t_1) was estimated to be approximately 903 thousand years ago (Kya) (95% highest posterior density (HPD) interval: 702–903 Kya; Supplementary Table S12), which was an older event than the splitting of host populations ($t_{1,\ host}$ = 612 Kya, 95% HPD interval: 37–1,254 Kya; Supplementary Table S12). The splitting time between the Solitaire and Kairei populations (t_0) was estimated to be also older for the symbiotic bacteria (approximately 742 Kya,

TABLE 3 Genetic diversity indices of host populations on the CIR.

Gene	Diversity[1]	Onnuri	Solitaire	Edmond	Kairei
mtCOI (531 bp)	n	24	20	15	15
	a	19	11	10	11
	k	20	15	14	16
	H	0.96	0.87	0.90	0.93
	π	0.0087	0.0052	0.0054	0.0062
Col-1 (539 bp)	n[1]	44	40	30	30
	a	6	6	5	2
	k	5	7	8	2
	H	0.71	0.64	0.41	0.29
	π	0.0031	0.0028	0.0016	0.001
EF1α (461 bp)	n[1]	40	32	30	24
	a	11	7	7	6
	k	12	6	7	5
	H	0.63	0.48	0.55	0.44
	π	0.0021	0.0012	0.0015	0.0011

[1]The abbreviations are the same as those in Table 2.

95% HPD interval: 398–893 Kya) than the host populations (approximately 75 Kya, 95% HPD interval: 13–904 Kya).

The IMa3 analysis resulted in the degree and direction of gene flow among the extant symbiont populations. The bidirectional migration rates between the Onnuri and Solitaire fields were significantly different from zero ($P < 0.01$) according to a likelihood ratio test ($Nm = 0.413$ from the Solitaire to the Onnuri fields; $Nm = 0.696$ from the Onnuri to the Solitaire fields; Supplementary Table S12). On the other hand, the unidirectional migration rate from the Kairei to the Solitaire field ($Nm = 1.00$) was significant according to the likelihood ratio test ($P < 0.001$; Figure 7, Supplementary Table S12). Among host populations, only unidirectional migration was statistically significant from the Onnuri to the Solitaire field ($2Nm = 1.32$, $P < 0.05$; Figure 7, Supplementary Table S12).

For symbionts, the posterior means of population mutation parameters (θ) were commonly estimated close to 0.05 except for the ancestral population between the Solitaire and Kairei populations (approximately 0.027, 95% HPD interval: 0.0034–0.05; Supplementary Table S10). The mean of θ for the Onnuri population was approximately 0.047 (95% HPD interval: 0.041–0.05), which was similar to the mean of the Solitaire population (0.0461, 95% HPD interval: 0.04–0.05) and Kairei population (approximately 0.0465, 95% HPD interval: 0.04–0.05). The mean for the ancestor population of the three populations also exhibited a similar size of approximately 0.045 (95% HPD interval: 0.036–0.05). For the hosts, the posterior means of effective population size (N) of the three populations were estimated to be similarly large (Supplementary Table S12): 809,839 (95% HPD interval: 711,227–862,185) for the Onnuri population; 746,077 (95% HPD interval: 554,231–862,185) for the Solitaire population; and 770,342 (95% HPD interval: 605,125–862,185) for the Kairei population. The estimates of the ancestral populations were smaller, at approximately 505,692 (95% HPD interval: 0–862,185) for the ancestor between the Solitaire and Kairei populations and approximately 540,741 (95% HPD interval: 128,099–862,185) for the ancestor of the three populations.

Discussion

Geographical provincialism of deep-sea hydrothermal vent invertebrate species along the mid-ocean ridge systems is a common biological feature that we have learned since the first discovery of vent and its fauna in 1977 (Corliss et al., 1979; Bachraty et al., 2009; Rogers et al., 2012). Although the past oceanic exploration and comparative biological studies have revealed important regional geophysical and biological factors that lead to the isolation to various extents (Vrijenhoek, 2010), there is a significant knowledge gap about microorganisms in the deep sea. On the other hand, as our knowledge about the abiotic and biotic factors grows, the question of a more quantitative aspect of how long and to what extent specific abiotic barriers affect the connectivity of vent species becomes more interesting. Keeping this context in mind, we attempted to understand the diverging population processes of deep-sea hydrothermal vent animals and their symbiotic bacteria in time and space. To quantify population subdivisions in high resolution, we applied population genetic model-based approaches and comparisons of population DNA sequence data of vent mussels and their symbiotic bacteria from two ocean basins, the Central Indian Ocean and the eastern Pacific Ocean.

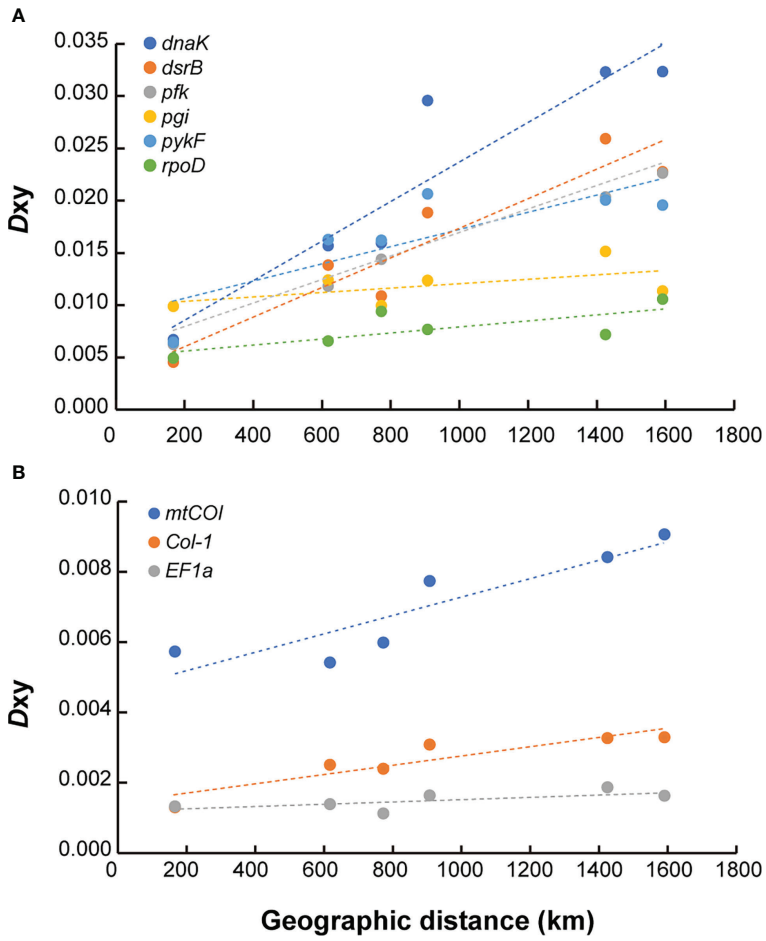

FIGURE 6
Correlation of population divergence (D_{xy}) with geographic distance for functional genes in the CIR. **(A)** Symbiotic bacteria. **(B)** Host mussels. The dashed lines represent the linear regression lines of each locus.

TABLE 4 Estimated phylogenetic topologies of host and symbiotic populations.

Organism	Tree topology[a]	Posterior probability
Symbiontic bacteria	(2,(0,1))	0.0139
	(1,(0,2))	0.0215
	(0,(1,2))	0.9646
Host mussels	(2,(0,1))	0.2682
	(1,(0,2))	0.2372
	(0,(1,2))	0.4945

[a]Different numbers indicate populations separated geographically, 0 = Onnuri, 1 = Solitaire, 2 = Kairei; the tree topologies are shown in Newick tree format, and the numbers of ancestral populations are omitted.

Gill-associated bacteria of *Bathymodiolus marisindicus*

To the best of our knowledge, our study is the first to evaluate the quantitative composition of gill-associated symbiotic bacteria of *B. marisindicus*. Our findings revealed that the mussels harbor symbiotic communities in which sulfur-oxidizing bacteria dominate (minimum >80%) regardless of the geographical distribution along the CIR, which is consistent with previous findings (Won et al., 2008;

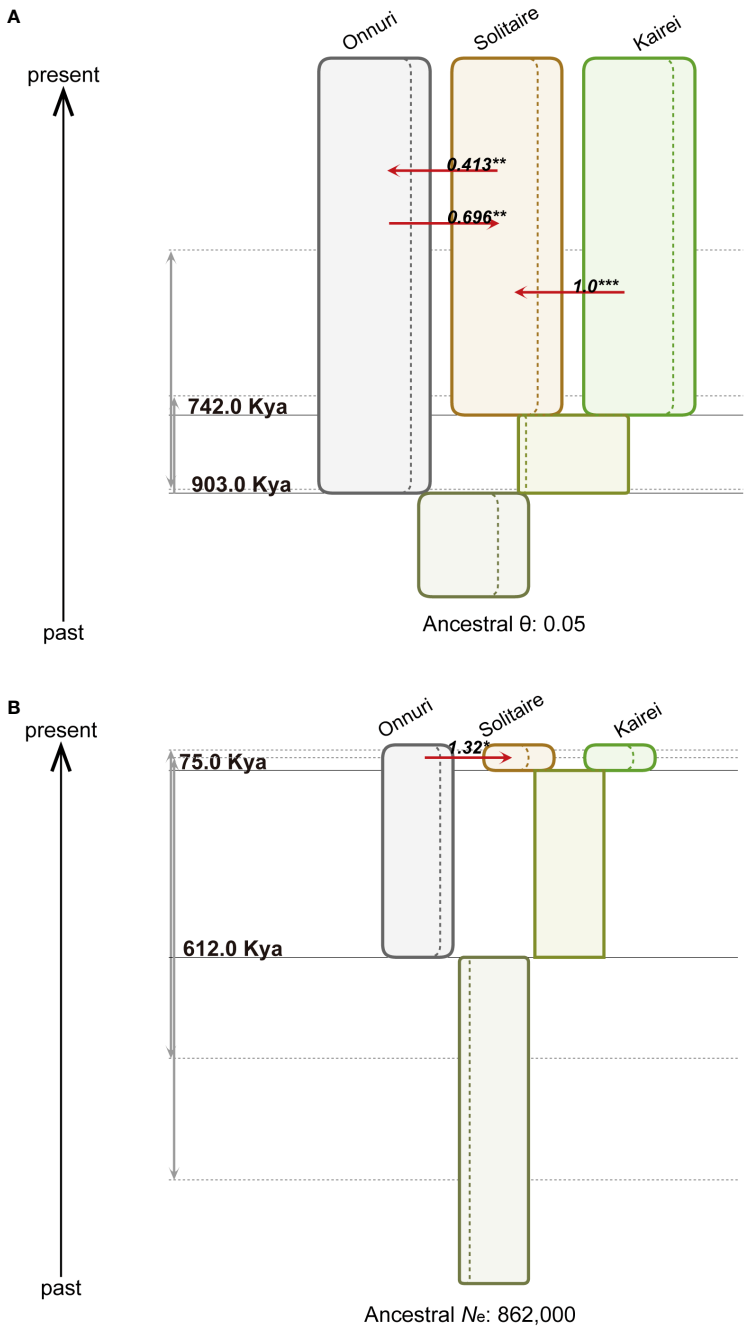

FIGURE 7
Demographic history of populations from three vent localities. The figures represent step 2 in Figure 2D. **(A)** Symbiotic bacteria. The width of the colored boxes is proportional to the maximum a posteriori estimates of the effective population size. The dashed lines within the boxes represent the 95% highest posterior density (HPD) intervals (Supplementary Table S10-12). The red arrow denotes the statistically significant population migration rate per generation (*Nm* for symbiont and *2Nm* for host) using both marginal posterior distribution (* α = 0.05, ** α = 0.01, *** α = 0.001). The gray arrows represent 95% HPD intervals of each splitting time. For the symbiotic bacteria, the effective population size was scaled by mutation rate (θ) due to the uncertainty of the generation time of mussel symbiotic bacteria. **(B)** Host mussels. The figure description is the same as that for **(A)**. The effective population size of hosts (N_e) was estimated assuming a generation time of one year.

Fontanez and Cavanaugh, 2014). On the other hand, from the bacterial community of the gill tissue, we unexpectedly identified several strains belonging to the genus *Kistimonas* of the family Endozoicomonadaceae, typically found in shallow marine invertebrates such as starfish, dead clams, and sandworms (Choi et al., 2010; Lee et al., 2012; Ellis et al., 2019). The genus *Kistimonas* was recently observed in the gills of the deep-sea mussel *Gigantidas haimaensis* (Xu et al., 2019). Recently, other bacterial taxa of the family Endozoicomonadaceae have been identified from various marine mollusks globally (Cano et al., 2020). It suggests that *Kistimonas* sp. is also widely distributed in association with marine invertebrate animals at different ocean depths. Meanwhile, the *Candidatus* Endonucleobacter bathymodioli of the Endozoicomonadaceae is known as parasitic bacteria in nuclei of Bathymodioline mussels (Zielinski et al., 2009). Before our research, the parasites were found in bathymodioline mussels in the Gulf of Mexico, Atlantic, and eastern Pacific oceans (Zielinski et al., 2009). Interestingly, the parasites in that study were not observed in the symbiont-infected cell. Therefore, it is considered that the sulfur-oxidizing bacteria of gill tissue seem to protect the host mussel. This interpretation is supported by the antibacterial activity of mussel gill homogenates and the presence of related genes from gill tissue (Bettencourt et al., 2007). The very low abundance of the *Candidatus* Endonucleobacter bathymodioli compared to the sulfur-oxidizing bacteria is consistent with the expectation according to the hypothesis. Still, the protection mechanism is not known yet.

Nucleotide diversity of symbiont populations measured by the 454 and Illumina platforms

The fact that the two NGS DNA data sets of eastern Pacific and CIR were sequenced by the 454 and Illumina platforms, respectively, might cause a concern of systematic errors in the estimation of D_{xy} between vent localities due to the difference in platforms. Indeed, the two sequencing platforms used in the present study have different sequencing error rates. The Illumina sequencing generates fewer sequencing errors than the 454 platform (Loman et al., 2012). Despite the substantial differences in read length and sequencing process of the two platforms, however, the 454 and Illumina sequencing platforms showed reliable quantitative results about the abundances of genes and genotypes (Luo et al., 2012). The algorithm, DADA2, used for sequencing error correction in this study, was proven for its high performance in identifying more real variants and fewer false-positive sequence variants than other methods (Callahan et al., 2016). The result of nucleotide diversity (π) of symbionts in each vent locality indirectly dispels the concern (Supplementary Figure S1). The nucleotide diversities of the eastern Pacific symbiont populations assessed by the 454 platform were overall lower than those of the CIR that were by the Illumina platform, indicating that the suspected systematic errors cannot have affected our conclusion. In addition, the varying degrees of diversity estimated in the CIR mean that the Illumina platform did not seem to cause a systematic decrease or increase in the variation identification. Therefore, we conclude that the nucleotide diversity of populations and D_{xy} values between them reflect the actual attributes of the mussel symbionts in different mid-ocean ridges.

Influence of geological characteristics on the population divergence of symbionts

The comparison of genetic variation of vent mussel symbionts from the eastern Pacific and CIR allowed us to evaluate various factors influencing the population divergence of symbiotic bacteria. The level of genetic differentiation could be partitioned according to the following geographically hierarchical categories in decreasing order: 1) between oceans, the eastern Pacific, and CIR; 2) inter-ridge site between the EPR and PAR across the well-known physical barrier of Ester Microplate in the eastern Pacific; 3) intra-ridge vent fields in the CIR; and 4) intra-ridge vent fields in the EPR and PAR. These categories involve various geographical, geological, and hydrological features of mid-ocean ridges, such as distances between habitats, depths, ridge-axis offsets, transform faults, ridge spreading rates, microplates, and deep-oceanic currents, and the interaction of these factors.

First, the mussel symbiotic bacteria from the eastern Pacific and the CIR evolved independently for a long time. A phylogenetic tree based on *16S* rRNA gene sequences showed that the two symbionts markedly diverged (Won et al., 2008). Accordingly, the D_{xy} estimates between the oceans are at least 10 times larger than the other subordinate comparisons. Secondly, at the inter-ridge scale of the eastern Pacific, the genetic differentiation was high. The Easter Microplate located at the boundary of the EPR and PAR was observed to impede the dispersal of diverse vent invertebrates and gave rise to a genetic isolation of several vent species (Guinot and Hurtado, 2003; Mateos et al., 2012; Johnson et al., 2013; Jang et al., 2016). The congruent vicariance among different taxonomic groups can be interpreted as a result of the orogeny of the Easter Microplate, 2.5–5.3 million years ago around the boundary of EPR and the PAR (Naar and Hey, 1991). Ho et al. (2017) reported that the EPR and PAR mussel symbionts exhibited complete geographical isolation independent of the hybridization of host species, *B. thermophilus* and *B. antarcticus*. For the first time, these previous studies (Johnson et al., 2013; Ho et al., 2017) indicated that the geomorphological process had driven the population divergence of both host animals and symbiotic bacteria in the eastern Pacific ridges.

Next, the symbionts of intra-ridge on the CIR exhibited a high degree of differentiation with geographical distance in

contrast with the symbiont of intra-ridge sites on the eastern Pacific. In fragmented habitats such as deep-sea hydrothermal vents, the geographical distribution of habitats and life history features of species related to dispersal capability could be the main factors that affect genetic connectivity. This notion suggests that the different geographical distributions of vent habitats must have led to the contrasting genetic differentiation patterns between the eastern Pacific and CIR if we accept that the two symbionts may have similar mobility because they belong to the same taxa, *Candidatus* Thioglobus.

The seafloor spreading rates of ridges are relevant to the geomorphological features, including the distribution pattern of vent habitats along the ridge axes. Contrary to the relatively linear topology of the fast-spreading ridge, disconnection of adjacent ridges by lateral offset frequently occurs, and an extensive depth range often occurs along the slow-spreading ridge. Therefore, the geomorphological feature in the slow-spreading ridge tends to decrease the genetic connectivity of vent organisms and leads to population subdivision and even speciation (Van Dover et al., 2002; Vrijenhoek, 2010). For example, the Blanco Transform Fault (TF) in the Juan de Fuca Ridge, with approximately 450 km offset in the northeast Pacific, contributed to the genetic separation of the vent tubeworm, *Ridgeia piscesae* (Young et al., 2008), and the speciation of vent limpets of the genus *Lepetodrilus* between the northern and southern regions (Johnson et al., 2006). The bathymodioline mussels in the MAR also exhibited a substantial genetic subdivision reaching interspecies levels between the northern and southern MAR across numerous transform faults around the equator, including the largest Romanche TF with an offset of approximately 935-km width and 7-km depth (Van Der Heijden et al., 2012). Likewise, the disconnection of ridge axes by transform faults was observed in the CIR; the Argo and Marie Celeste transform faults between the Onnuri and Solitaire fields offset the ridge by about 100 and 200 km, respectively, and up to 5 km in depth (Pak et al., 2017). The ridge segmentation of the ridge also appears to interrupt the geographical connectivity of symbiotic bacteria along the CIR, especially between the Onnuri and the other fields. The details of population structure of the CIR organisms will be discussed with the genetic variation of host mussels below.

At the intra-ridge scale, the relatively distant vent habitats along the slow-spreading ridge seem to decrease the connectivity of vent organisms. Geological modeling based on the global survey dataset for the past 35 years estimated the frequency of vent field in the fast-spreading EPR up to three- or fourfold higher than the slow-spreading CIR (vent frequency per 100 km = 0.76–1.33 for CIR and 1.79–3.91 for EPR) (Beaulieu et al., 2015). The geological model and the present results predict that isolation by distance (IBD) becomes apparent in a slow-spreading ridge along with ridge-axis offsets by transform faults. For instance, the genetic variation of symbiotic bacteria observed in the slow-spreading MAR supports this hypothesis. The composition of symbiont assemblages of bathymodioline mussel, *I. modiolaeformis*, exhibited a statistically significant correlation with geographic distance (Laming et al., 2015).

A recent study has proved that about 13% of total genetic variation on symbionts of bathymodioline mussels distributed along the northern MAR is determined by geographical distance alone (Ücker et al., 2021). If the factor of geographic distance in that study was combined with other factors of environment and host species, the accountability for the total genetic variation increased by about 45%. Therefore, all findings above indicate that we should consider various factors, including the interaction with the host and natural selection related to the chemical and physical environment, to comprehensively understand the population divergence process of symbiotic bacteria.

Population divergence processes of mussel hosts and their symbionts in the CIR

On a regional scale, the present study examined the genetic diversity and connectivity of the host mussels, *B. marisindicus*, and their symbiotic bacteria along the CIR, including the recently discovered Onnuri field. Hosts' genetic diversity was similar among vent fields and significantly higher at the Onnuri. Similarly, the genetic diversity of symbionts was higher at Onnuri and Solitaire than at Edmond and Kairei. To our interests, a similar pattern of population genetic variation was detected in the symbiotic bacteria of scaly-foot snail, *Chrysomallon squamiferum*, between the Solitaire and Kairei vent fields (Lan et al., 2022). The Edmond mussel symbionts were genetically homogeneous much more than other populations. The genetic diversity of symbionts with the free-living stage is associated with the environmental pool (Ansorge et al., 2019). Frequent habitat turnover by tectonic activity reduces genetic diversity by recurrent bottleneck and founder effect (Wade and Mccauley, 1988; Mccauley, 1991). The loss of genetic diversity of the Edmond mussel symbiont could be attributable to recurrent extinction/recolonization events of bacterial communities or small population size in the first place due to potentially low habitability. In this regard, it is notable that there is circumstantial evidence that the mussel patches in Edmond were very scarce (personal observation during 2001 exploration, which is reported in Van Dover et al., 2001). Additionally, the difference in depths of vent habitats is also a potential factor for the connectivity between vents' low genetic diversity of the Edmond symbionts. Table 1 shows that the depth difference between Edmond and the two nearby adjacent vents, Solitaire and Kairei, ranges from 650 to 800 m. The oceanic currents flowing at different depths may reduce the gene flow between vents with different depths,

increasing geographical isolation by disruption of dispersal (Fujio and Imasato, 1991; Young et al., 2008). The neutrality tests with Tajima's *D* and Fu's *Fs* statistics refute any significant demographic changes in the four symbiont populations in the CIR, which indicates that the symbiont populations from every vent field including Edmond are in selectively neutral and/or in equilibrium of population size (Supplementary Table S6).

The AMOVA results indicated that symbionts were genetically heterogeneous at the intra-host level and homogeneous at the inter-host level within the same vent field regardless of the examined genes (Supplementary Table S9). Wentrup et al. (2014) suggested two hypotheses regarding the source of symbionts during the development of host mussels: 1) continuous acquisition from the environment and 2) self-infection from own older gill tissues. However, these two alternatives may not be mutually exclusive and could be mixed. Several studies supported the self-infection scenario based on the high genetic variation of symbionts at the inter-host level even within the same fields (Ho et al., 2017; Picazo et al., 2019). On the other hand, the homogeneity of symbionts at the inter-host level observed in *B. marisindicus* is similar to the pattern of genetic variation observed from the genomic data of the sulfur-oxidizing symbionts of *Bathymodiolus* mussels in the MAR (Ansorge et al., 2019). These findings suggest that symbiont populations may be intermixed among adjacent host individuals within the same vents by repeated release to and uptake from the environment.

The multi-locus genetic data of symbionts revealed a relatively high level of genetic differentiation among three populations in the Onnuri, Solitaire, and Kairei vent fields (Supplementary Table S7). In contrast, the geographically adjacent Edmond and Kairei symbionts showed relatively low differentiation. The present IM analyses revealed the population divergence order and times from a common ancestral population to the extant three populations representing the three ridge segments of the CIR. To our interest, the population tree topology of symbiotic bacteria was identical to that of the host mussels, although the time depths are different. The northernmost Onnuri mussel populations were phylogenetically distant from the Solitaire and Kairei populations. Meanwhile, the population divergence topologies of host mussel and symbiotic bacteria are consistent with the biogeographic province of vent fauna of the Indian Ocean (Zhou et al., 2022). To our interest, Zhou et al. (2022) reported a summary of faunal similarity in a dendrogram in which a subset of CIR populations reveals an identical tree topology with the present mussel hosts and symbiont populations. Remarkably, the faunal similarity was largely explainable by solely along-ridge distances between vents, about 47.5%. Another relevant finding came out from a phylogeographic study of the scaly-foot snails of the Indian Ocean (Lan et al., 2022), which showed a relatively close relationship between the Solitaire and Kairei symbiont populations compared to the distant populations in the Southwest Indian Ridge (SWIR) and the northernmost Carlsberg ridge. These two studies again emphasizes the strong effect of geographical distance on the divergence of vent invertebrate hosts and their symbiotic bacteria in the Indian Ocean ridges with ultra- to slow-spreading rates. Finally, the consistent pattern of the present study and the previous biogeographic studies altogether indicate the influence of common historical and physical constraints on the population divergence processes of vent invertebrate hosts and their symbionts in the CIR.

According to geochronological analysis, the age of the earliest measurable hydrothermal activity in the Kairei vent field was estimated to be approximately 95 Kya (Wang et al., 2012). From the IM analysis, the host populations of Kairei and Solitaire have undergone the divergence of approximately 75 Kya (95% highest posterior density (HPD) interval: 13–904 Kya). Despite the broad interval of HPD, the highest value is considerably close to the age of the first vent activity measured by isotope, which indicates that the tectonic activity in Kairei may be connected to the divergence of an ancestral mussel population of the Kairei and Solitaire populations. In the present IMa analysis, we could not resolve narrowly how earlier the Onnuri population diverged from the most recent common ancestral population than the subsequent splitting of the Solitaire and Kairei populations. Due to the broad intervals of HPD for the splitting times, the comparison of the divergence between the symbionts and host mussels is difficult. Nevertheless, the coincident pattern of geographical connectivity from the spatially and taxonomically more broad-scaled biogeographic studies suggests that the Onnuri mussel and symbiont populations have diverged substantially from the other populations for a long time.

Overall, both the symbiont and host populations are common in that genetic differentiation increases with geographical distance between habitats along the CIR. The IM analysis provided another insight into migration patterns among populations after divergence of an ancestral population to the descending two populations. We could not detect any significant gene flow between the branches of ancestral populations in both host and symbiont populations. We could only detect significant gene flow in some terminal branches, which implies a sort of secondary contact after divergence in both host and symbiont for a while. The secondary contact after isolation is often observed in deep-sea vent mussels, such as the secondary integration between *B. azoricus* and *B. puteoserpentis* in MAR (Breusing et al., 2017) and between *B. thermophilus* and *B. antarcticus* in the eastern Pacific (Johnson et al., 2013). In the IM analysis of symbionts, the northward gene flow from the southern two symbiont populations is consistent with the direction of the deep oceanic current at an approximately 2,500-m depth, which was estimated based on geostrophic circulation models (Reid, 2003). The northward migration of symbionts from Kairei to Solitaire was the highest (Nm = 1),

indicating that the Kairei population provides genetic variation to Solitaire. The degree of nucleotide diversity at each CIR population agrees well with this convey of genetic variation (Supplement Figure S1), showing a higher level in the receiving populations, Onnuri and Solitaire. On the other hand, the southward gene flow from the Onnuri to Solitaire vents was also detected in the host mussel. It is difficult to interpret this gene flow from Onnuri to Solitaire due to a lack of related environmental information in this area. Considering the daily and seasonal fluctuations of deep oceanic currents, long-distance dispersal of hosts and symbionts may be possible (Murty et al., 2001). Despite the similarities in the phylogenetic tree topologies, the different migration patterns between the hosts and symbionts might be related to different life-history traits and dispersal capabilities of them. The host populations exhibited a higher level of southward gene flow from the Onnuri to Solitaire vents ($2Nm$ >1), which was much more significant than the estimates of the symbiont populations. Bathymodiolin mussels have long-distance dispersal capability due to the long duration of their planktonic larval stage (Lutz et al., 1980; Arellano and Young, 2009; Breusing et al., 2016) and vertical dispersal (Arellano et al., 2014). Therefore, the different patterns and extent of gene flow between the symbionts and hosts indicate that they disperse among vent localities independently.

Conclusion

Our study sought to identify the connection of divergence of microbial populations and geographic features including the distance between vent localities of the ridge system. To this end, we compared orthologous genes of symbiotic bacteria of vent mussels from the central Indian Ocean and the eastern Pacific. Their ridges vary in spreading rates, and as a result, they have a difference in the frequency of active vent habitats for animals and microorganisms. Under this frame of comparison, we could identify several key factors for the divergence of mussel symbionts. First, the degree of differentiation of symbiont populations was hierarchical concerning geographical distance and geophysical barriers for dispersal. At the scale of the ocean basin, the farther geographically, the more differentiated between vent localities. The highest divergence comes first between ocean basins and second between the East Pacific Rise and Pacific Antarctic Ridge. Apart from the distance factor, a substantial geophysical structure such as the Easter Microplates exhibiting a swollen bottom of the sea floor between the EPR and PAR played a long-term barrier to symbionts between the neighboring ridges. The seafloor geological and hydrological features along the ridge axes in the eastern Pacific strongly influenced diverging population processes of both host mussels and their symbiotic bacteria. At the intra-ridge scale, however, contrasting genetic differentiation patterns were observed; the CIR with a slow-spreading rate showed a significant pattern of isolation by distance within 1,600 km, while the eastern Pacific ridges, both EPR and PAR, with superfast- or fast-spreading rates, exhibited an absence of isolation by distance even over 4,000 km. These contrasting patterns result from the denseness of vent habitats, which ultimately relates to the spreading rates of the ridges. Finally, on a more local scale, the application of the population genetic model, isolation with migration, using a large amount of sequence data of symbionts and their host mussels allowed us to unravel their diverging processes in time and space in the CIR. The similar topology of phylogenies between host mussels and symbiotic bacteria among the three representative ridge segments in the CIR also highlights the importance of geological history and habitat configuration along the ridge axis as essential factors for population divergence in both hosts and symbionts. The present study of genetic variation of mussel symbionts at diverse spatial and time scales provides insights into the geographic distribution and genetic divergence processes of microbial populations in deep-sea hydrothermal vents.

Data availability statement

The sequence data presented in the study are deposited in the GenBank repository, accession number OK509086–OK509159; OK524315–OK524584; and PRJNA769986.

Author contributions

S-JJ and Y-JW conceived and designed the study and collected samples. S-JJ conducted the laboratory experiments. S-JJ and SJ analyzed the raw NGS data using the DADA2 pipeline. S-JJ and YC participated in the examination of demographic parameters using the isolation with migration (IM) model. YC wrote the R scripts for MCMC diagnostics to test the statistical convergence of the IMa3 results. S-JJ drafted the manuscript, and Y-JW and YC made substantial improvements. All authors contributed to the article and approved the submitted version.

Funding

This research was part of a project titled 'Understanding the deep-sea biosphere on seafloor hydrothermal vents in the Indian Ridge (No. 20170411)' funded by the Ministry of Oceans and Fisheries, Korea. YC was supported by the National Research Foundation of Korea (NRF) grant funded by the Korean government (MSIT) (No. 2021R1C1C1011250).

Acknowledgments

We thank all the scientists and operation teams who participated in the 2017 and 2018 ISABU cruise to the CIR for their help and assistance on board. We are grateful to Dr. Robert C. Vrijenhoek and Shannon B. Johnson for their help in receiving the specimens of the Edmond and Kairei vents. Lastly, we thank the reviewers for their helpful comments.

Conflict of interest

The authors declare that the research was conducted in the absence of any commercial or financial relationships that could be construed as a potential conflict of interest.

Publisher's note

Supplementary Material

The Supplementary Material for this article can be found online at: https://www.frontiersin.org/articles/10.3389/fmars.2022.845965/full#supplementary-material. All supplementary files in this study are available online at: https://doi.org/10.6084/m9.figshare.17701754

References

Anderson, R. E., Sogin, M. L., and Baross, J. A. (2015). Biogeography and ecology of the rare and abundant microbial lineages in deep-sea hydrothermal vents. *FEMS Microbiol. Ecol.* 91, 1–11. doi: 10.1093/femsec/fiu016

Ansorge, R., Romano, S., Sayavedra, L., Porras, M.Ã.G., Kupczok, A., Tegetmeyer, H. E., et al. (2019). Functional diversity enables multiple symbiont strains to coexist in deep-sea mussels. *Nat. Microbiol.* 4, 2487–2497. doi: 10.1038/s41564-019-0572-9

Arellano, S. M., Van Gaest, A. L., Johnson, S. B., Vrijenhoek, R. C., and Young, C. M. (2014). Larvae from deep-sea methane seeps disperse in surface waters. *Proc. R. Soc. B.: Biol. Sci.* 281, 20133276. doi: 10.1098/rspb.2013.3276

Arellano, S. M., and Young, C. M. (2009). Spawning, development, and the duration of larval life in a deep-sea cold-seep mussel. *Biol. Bull.* 216, 149–162. doi: 10.1086/BBLv216n2p149

Bachraty, C., Legendre, P., and Desbruyeres, D. (2009). Biogeographic relationships among deep-sea hydrothermal vent faunas at global scale. *Deep. Sea. Res. Part I.: Oceanographic. Res. Papers.* 56, 1371–1378. doi: 10.1016/j.dsr.2009.01.009

Bandelt, H.-J., Forster, P., and Röhl, A. (1999). Median-joining networks for inferring intraspecific phylogenies. *Mol. Biol. Evol.* 16, 37–48. doi: 10.1093/oxfordjournals.molbev.a026036

Beaulieu, S. E., Baker, E. T., and German, C. R. (2015). Where are the undiscovered hydrothermal vents on oceanic spreading ridges? *Deep. Sea. Res. Part II.: Topical. Stud. Oceanography.* 121, 202–212. doi: 10.1016/j.dsr2.2015.05.001

Beedessee, G., Watanabe, H., Ogura, T., Nemoto, S., Yahagi, T., Nakagawa, S., et al. (2013). High connectivity of animal populations in deep-sea hydrothermal vent fields in the central Indian ridge relevant to its geological setting. *PloS One* 8, e81570. doi: 10.1371/journal.pone.0081570

Bettencourt, R., Roch, P., Stefanni, S., Rosa, D., Colaço, A., and Santos, R. S. (2007). Deep sea immunity: unveiling immune constituents from the hydrothermal vent mussel *bathymodiolus azoricus*. *Mar. Environ. Res.* 64, 108–127. doi: 10.1016/j.marenvres.2006.12.010

Bird, P. (2003). An updated digital model of plate boundaries. *Geochemistry. Geophysics. Geosystems.* 4, 1027. doi: 10.1029/2001GC000252

Bolger, A. M., Lohse, M., and Usadel, B. (2014). Trimmomatic: a flexible trimmer for illumina sequence data. *Bioinformatics* 30, 2114–2120. doi: 10.1093/bioinformatics/btu170

Bonnet, E., and Van De Peer, Y. (2002). Zt: A sofware tool for simple and partial mantel tests. *J. Stat. software.* 7, 1. doi: 10.18637/jss.v007.i10

Breusing, C., Biastoch, A., Drews, A., Metaxas, A., Jollivet, D., R.,R., et al. (2016). Biophysical and population genetic models predict the presence of "Phantom" stepping stones connecting mid-Atlantic ridge vent ecosystems. *Curr. Biol.* 26, 2257–2267. doi: 10.1016/j.cub.2016.06.062

Breusing, C., Vrijenhoek, R. C., and Reusch, T. B. (2017). Widespread introgression in deep-sea hydrothermal vent mussels. *BMC evolutionary. Biol.* 17, 1–10. doi: 10.1186/s12862-016-0862-2

Callahan, B. J., Mcmurdie, P. J., Rosen, M. J., Han, A. W., Johnson, A. J. A., and Holmes, S. P. (2016). DADA2: high-resolution sample inference from illumina amplicon data. *Nat. Methods* 13, 581. doi: 10.1038/nmeth.3869

Campbell, B. J., Engel, A. S., Porter, M. L., and Takai, K. (2006). The versatile ϵ-proteobacteria: key players in sulphidic habitats. *Nat. Rev. Microbiol.* 4, 458–468. doi: 10.1038/nrmicro1414

Cano, I., Ryder, D., Webb, S. C., Jones, B. J., Brosnahan, C. L., Carrasco, N., et al. (2020). Cosmopolitan distribution of endozoicomonas-like organisms and other intracellular microcolonies of bacteria causing infection in marine mollusks. *Front. Microbiol.* 11, 577481. doi: 10.3389/fmicb.2020.577481

Chen, C., Copley, J. T., Linse, K., and Rogers, A. D. (2015). Low connectivity between 'scaly-foot gastropod'(Mollusca: Peltospiridae) populations at hydrothermal vents on the southwest Indian ridge and the central Indian ridge. *Organisms. Diversity Evol.* 15, 663–670. doi: 10.1007/s13127-015-0224-8

Choi, E. J., Kwon, H. C., Sohn, Y. C., and Yang, H. O. (2010). *Kistimonas asteriae* gen. nov., sp. nov., a gammaproteobacterium isolated from asterias amurensis. *Int. J. systematic. evolutionary. Microbiol.* 60, 938–943. doi: 10.1099/ijs.0.014282-0

Colaço, A., Martins, I., Laranjo, M., Pires, L., Leal, C., Prieto, C., et al. (2006). Annual spawning of the hydrothermal vent mussel, *Bathymodiolus azoricus*, under controlled aquarium, conditions at atmospheric pressure. *J. Exp. Mar. Biol. Ecol.* 333, 166–171. doi: 10.1016/j.jembe.2005.12.005

Corliss, J. B., Dymond, J., Gordon, L. I., Edmond, J. M., Von Herzen, R. P., Ballard, R. D., et al. (1979). Submarine thermal springs on the Galapagos rift. *Science* 203, 1073–1083. doi: 10.1126/science.203.4385.1073

Cruickshank, T. E., and Hahn, M. W. (2014). Reanalysis suggests that genomic islands of speciation are due to reduced diversity, not reduced gene flow. *Mol. Ecol.* 23, 3133–3157. doi: 10.1111/mec.12796

De Wit, R., and Bouvier, T. (2006). 'Everything is everywhere, but, the environment selects'; what did baas becking and beijerinck really say? *Environ. Microbiol.* 8, 755–758. doi: 10.1111/j.1462-2920.2006.01017.x

Dick, G. J. (2019). The microbiomes of deep-sea hydrothermal vents: distributed globally, shaped locally. *Nat. Rev. Microbiol.* 17, 271–283. doi: 10.1038/s41579-019-0160-2

Dixon, D. R., Lowe, D. M., Miller, P. I., Villemin, G. R., Colaço, A., Serrão-Santos, R., et al. (2006). Evidence of seasonal reproduction in the Atlantic vent mussel *Bathymodiolus azoricus*, and an apparent link with the timing of photosynthetic primary production. *J. Mar. Biol. Assoc. United. Kingdom.* 86, 1363–1371. doi: 10.1017/S0025315406014391

Edgar, R. C. (2010). Search and clustering orders of magnitude faster than BLAST. *Bioinformatics* 26, 2460–2461. doi: 10.1093/bioinformatics/btq461

Edgar, R. C. (2013). UPARSE: highly accurate OTU sequences from microbial amplicon reads. *Nat. Methods* 10, 996–998. doi: 10.1038/nmeth.2604

Edgar, R. C., Haas, B. J., Clemente, J. C., Quince, C., and Knight, R. (2011). UCHIME improves sensitivity and speed of chimera detection. *Bioinformatics* 27, 2194–2200. doi: 10.1093/bioinformatics/btr381

Edwards, D. (2012) *PCR purification: AMPure and simple*. Available at: http://www.keatslab.org/blog/pcrpurificationampureandsimple.

Ellis, J. C., Thomas, M. S., Lawson, P. A., Patel, N. B., Faircloth, W., Hayes, S. E., et al. (2019). *Kistimonas alittae* sp. nov., a gammaproteobacterium isolated from the marine annelid alitta succinea. *Int. J. systematic. evolutionary. Microbiol.* 69, 235–240. doi: 10.1099/ijsem.0.003137

Excoffier, L., and Lischer, H. E. L. (2010). Arlequin suite ver 3.5: a new series of programs to perform population genetics analyses under Linux and windows. *Mol. Ecol. Resour.* 10, 564–567. doi: 10.1111/j.1755-0998.2010.02847.x

Finlay, B. J., and Clarke, K. J. (1999). Ubiquitous dispersal of microbial species. *Nature* 400, 828–828. doi: 10.1038/23616

Flores, G. E., Campbell, J. H., Kirshtein, J. D., Meneghin, J., Podar, M., Steinberg, J. I., et al. (2011). Microbial community structure of hydrothermal deposits from geochemically different vent fields along the mid-Atlantic ridge. *Environ. Microbiol.* 13, 2158–2171. doi: 10.1111/j.1462-2920.2011.02463.x

Foltz, D., Nguyen, A., Kiger, J., and Mah, C. L. (2008). Pleistocene speciation of sister taxa in a north pacific clade of brooding sea stars (Leptasterias). *Mar. Biol.* 154, 593–602. doi: 10.1007/s00227-008-0952-9

Fontanez, K. M., and Cavanaugh, C. M. (2014). Evidence for horizontal transmission from multilocus phylogeny of deep-sea mussel (Mytilidae) symbionts. *Environ. Microbiol.* 16, 3608–3621. doi: 10.1111/1462-2920.12379

Franke, M., Geier, B., Hammel, J. U., Dubilier, N., and Leisch, N. (2021). Coming together–symbiont acquisition and early development in deep-sea bathymodioline mussels. *Proc. R. Soc. B.* 288, 20211044. doi: 10.1098/rspb.2021.1044

Fu, Y.-X. (1997). Statistical tests of neutrality of mutations against population growth, hitchhiking and background selection. *Genetics* 147, 915–925. doi: 10.1093/genetics/147.2.915

Fujio, S., and Imasato, N. (1991). Diagnostic calculation for circulation and water mass movement in the deep pacific. *J. Geophysical. Research.: Oceans.* 96, 759–774. doi: 10.1029/90JC02130

Guinot, D., and Hurtado, L. A. (2003). Two new species of hydrothermal vent crabs of the genus *Bythograea* from the southern East pacific rise and from the Galapagos rift (Crustacea decapoda brachyura bythograeidae). *Comptes. Rendus. Biologies.* 326, 423–439. doi: 10.1016/S1631-0691(03)00126-4

Hanson, C. A., Fuhrman, J. A., Horner-Devine, M. C., and Martiny, J. B. (2012). Beyond biogeographic patterns: processes shaping the microbial landscape. *Nat. Rev. Microbiol.* 10, 497–506. doi: 10.1038/nrmicro2795

Hey, J., Chung, Y., Sethuraman, A., Lachance, J., Tishkoff, S., Sousa, V. C., et al. (2018). Phylogeny estimation by integration over isolation with migration models. *Mol. Biol. Evol.* 35, 2805–2818. doi: 10.1093/molbev/msy162

Hey, J., and Wang, K. (2019). The effect of undetected recombination on genealogy sampling and inference under an isolation-with-migration model. *Mol. Ecol. Resour.* 19, 1593–1609. doi: 10.1111/1755-0998.13083

Ho, P.-T., Park, E., Hong, S. G., Kim, E.-H., Kim, K., Jang, S.-J., et al. (2017). Geographical structure of endosymbiotic bacteria hosted by *Bathymodiolus* mussels at eastern pacific hydrothermal vents. *BMC evolutionary. Biol.* 17, 121. doi: 10.1186/s12862-017-0966-3

Huber, J. A., Cantin, H. V., Huse, S. M., Mark Welch, D. B., Sogin, M. L., and Butterfield, D. A. (2010). Isolated communities of epsilonproteobacteria in hydrothermal vent fluids of the Mariana arc seamounts. *FEMS Microbiol. Ecol.* 73, 538–549. doi: 10.1111/j.1574-6941.2010.00910.x

Ikuta, T., Amari, Y., Tame, A., Takaki, Y., Tsuda, M., Iizuka, R., et al. (2021). Inside or out? clonal thiotrophic symbiont populations occupy deep-sea mussel bacteriocytes with pathways connecting to the external environment. *ISME. Commun.* 1, 1–4. doi: 10.1038/s43705-021-00043-x

Jang, S.-J., Park, E., Lee, W.-K., Johnson, S. B., Vrijenhoek, R. C., and Won, Y.-J. (2016). Population subdivision of hydrothermal vent polychaete *Alvinella pompejana* across equatorial and Easter microplate boundaries. *BMC evolutionary. Biol.* 16, 1–15. doi: 10.1186/s12862-016-0807-9

Johnson, S. B., Yong, C. R., Jones, W. J., Warén, A., and Vrijenhoek, R. C. (2006). Migration, isolation, and speciation of hydrothermal vent limpets (Gastropoda; Lepetodrilidae) across the Blanco Transform Fault. *Biol. Bull* 210, 140–157. doi: 10.2307/4134603

Johnson, S. B., Won, Y.-J., Harvey, J. B., and Vrijenhoek, R. C. (2013). A hybrid zone between *Bathymodiolus* mussel lineages from eastern pacific hydrothermal vents. *BMC evolutionary. Biol.* 13, 1–18. doi: 10.1186/1471-2148-13-21

Kim, J., Son, S. K., Kim, D., Pak, S. J., Yu, O. H., Walker, S. L., et al. (2020). Discovery of active hydrothermal vent fields along the central Indian ridge, 8–12°S. *Geochemistry. Geophysics. Geosystems.* 21, e2020GC009058. doi: 10.1029/2020GC009058

Laming, S. R., Szafranski, K. M., Rodrigues, C. F., Gaudron, S. M., Cunha, M. R., Hilário, A., et al. (2015). Fickle or faithful: the roles of host and environmental context in determining symbiont composition in two bathymodioline mussels. *PloS One* 10, e0144307. doi: 10.1371/journal.pone.0144307

Lan, Y., Sun, J., Chen, C., Wang, H., Xiao, Y., Perez, M., et al. (2022). Endosymbiont population genomics sheds light on transmission mode, partner specificity, and stability of the scaly-foot snail holobiont. *ISME. J.*, 16, 2132-2143. doi: 10.1038/s41396-022-01261-4

Lee, J., Shin, N.-R., Lee, H.-W., Roh, S. W., Kim, M.-S., Kim, Y.-O., et al. (2012). *Kistimonas scapharcae* sp. nov., isolated from a dead ark clam (*Scapharca broughtonii*), and emended description of the genus *Kistimonas*. *Int. J. systematic. evolutionary. Microbiol.* 62, 2865–2869. doi: 10.1099/ijs.0.038422-0

Legendre, P., and Fortin, M. J. (2010). Comparison of the mantel test and alternative approaches for detecting complex multivariate relationships in the spatial analysis of genetic data. *Mol. Ecol. Resour.* 10, 831–844. doi: 10.1111/j.1755-0998.2010.02866.x

Leigh, J. W., and Bryant, D. (2015). POPART: full-feature software for haplotype network construction. *Methods Ecol. Evol.* 6, 1110–1116. doi: 10.1111/2041-210X.12410

Librado, P., and Rozas, J. (2009). DnaSP v5: a software for comprehensive analysis of DNA polymorphism data. *Bioinformatics* 25, 1451–1452. doi: 10.1093/bioinformatics/btp187

Loman, N. J., Misra, R. V., Dallman, T. J., Constantinidou, C., Gharbia, S. E., Wain, J., et al. (2012). Performance comparison of benchtop high-throughput sequencing platforms. *Nat. Biotechnol.* 30, 434–439. doi: 10.1038/nbt.2198

Lorion, J., Kiel, S., Faure, B., Kawato, M., Ho, S. Y., Marshall, B., et al. (2013). Adaptive radiation of chemosymbiotic deep-sea mussels. *Proc. R. Soc. B.: Biol. Sci.* 280, 20131243. doi: 10.1098/rspb.2013.1243

Louca, S. (2021). The rates of global bacterial and archaeal dispersal. *ISME. J.*, 16, 159-167. doi: 10.1038/s41396-021-01069-8

Luo, C., Tsementzi, D., Kyrpides, N., Read, T., and Konstantinidis, K. T. (2012). Direct comparisons of illumina vs. Roche 454 sequencing technologies on the same microbial community DNA sample. *PloS One* 7, e30087. doi: 10.1371/journal.pone.0030087

Lutz, R., Jablonski, D., Rhoads, D., and Turner, R. (1980). Larval dispersal of a deep-sea hydrothermal vent bivalve from the Galapagos rift. *Mar. Biol.* 57, 127–133. doi: 10.1007/BF00387378

Martin, M. (2011). Cutadapt removes adapter sequences from high-throughput sequencing reads. *EMBnet. J.* 17, 10–12. doi: 10.14806/ej.17.1.200

Mateos, M., Hurtado, L. A., Santamaria, C. A., Leignel, V., and Guinot, D. (2012). Molecular systematics of the deep-sea hydrothermal vent endemic brachyuran family bythograeidae: a comparison of three Bayesian species tree methods. *PloS One* 7, e32066. doi: 10.1371/journal.pone.0032066

Mccauley, D. E. (1991). Genetic consequences of local population extinction and recolonization. *Trends Ecol. Evol.* 6, 5–8. doi: 10.1016/0169-5347(91)90139-O

Meier, D. V., Pjevac, P., Bach, W., Hourdez, S., Girguis, P. R., Vidoudez, C., et al. (2017). Niche partitioning of diverse sulfur-oxidizing bacteria at hydrothermal vents. *ISME. J.* 11, 1545. doi: 10.1038/ismej.2017.37

Mullineaux, L. S., Metaxas, A., Beaulieu, S. E., Bright, M., Gollner, S., Grupe, B. M., et al. (2018). Exploring the ecology of deep-sea hydrothermal vents in a metacommunity framework. *Front. Mar. Sci.* 5, 49. doi: 10.3389/fmars.2018.00049

Murty, V., Savin, M., Babu, V. R., and Suryanarayana, A. (2001). Seasonal variability in the vertical current structure and kinetic energy in the central Indian ocean basin. *Deep. Sea. Res. Part II.: Topical. Stud. Oceanography.* 48, 3309–3326. doi: 10.1016/S0967-0645(01)00043-1

Myers, E. W., and Miller, W. (1988). Optimal alignments in linear space. *Bioinformatics* 4, 11–17. doi: 10.1093/bioinformatics/4.1.11

Naar, D. F., and Hey, R. (1991). Tectonic evolution of the Easter microplate. *J. Geophysical. Research.: Solid. Earth* 96, 7961–7993. doi: 10.1029/90JB02398

Nakamura, K., Watanabe, H., Miyazaki, J., Takai, K., Kawagucci, S., Noguchi, T., et al. (2012). Discovery of new hydrothermal activity and chemosynthetic fauna on the central Indian ridge at 18–20 s. *PloS One* 7, e32965. doi: 10.1371/journal.pone.0032965

Nei, M. (1987). *Molecular evolutionary genetics*. New York: Columbia University Press.

Nielsen, R., and Wakeley, J. (2001). Distinguishing migration from isolation: a Markov chain Monte Carlo approach. *Genetics* 158, 885–896. doi: 10.1093/genetics/158.2.885

Pak, S.-J., Moon, J.-W., Kim, J., Chandler, M. T., Kim, H.-S., Son, J., et al. (2017). Widespread tectonic extension at the central Indian ridge between 8°S and 18°S. *Gondwana. Res.* 45, 163–179. doi: 10.1016/j.gr.2016.12.015

Papke, R. T., Ramsing, N. B., Bateson, M. M., and Ward, D. M. (2003). Geographical isolation in hot spring cyanobacteria. *Environ. Microbiol.* 5, 650–659. doi: 10.1046/j.1462-2920.2003.00460.x

Picazo, D. R., Dagan, T., Ansorge, R., Petersen, J. M., Dubilier, N., and Kupczok, A. (2019). Horizontally transmitted symbiont populations in deep-sea mussels are genetically isolated. *ISME. J.* 13, 2954–2968. doi: 10.1038/s41396-019-0475-z

Reid, J. L. (2003). On the total geostrophic circulation of the Indian ocean: Flow patterns, tracers, and transports. *Prog. Oceanography.* 56, 137–186. doi: 10.1016/S0079-6611(02)00141-6

Reveillaud, J., Reddington, E., Mcdermott, J., Algar, C., Meyer, J. L., Sylva, S., et al. (2016). Subseafloor microbial communities in hydrogen-rich vent fluids from hydrothermal systems along the mid-Cayman rise. *Environ. Microbiol.* 18, 1970–1987. doi: 10.1111/1462-2920.13173

Rogers, A. D., Tyler, P. A., Connelly, D. P., Copley, J. T., James, R., Larter, R. D., et al. (2012). The discovery of new deep-sea hydrothermal vent communities in the southern ocean and implications for biogeography. *PloS Biol.* 10, e1001234. doi: 10.1371/journal.pbio.1001234

Rognes, T., Flouri, T., Nichols, B., Quince, C., and Mahe, F. (2016). VSEARCH: a versatile open source tool for metagenomics. *PeerJ* 4, e2584. doi: 10.7717/peerj.2584

Rosen, M. J., Davison, M., Bhaya, D., and Fisher, D. S. (2015). Fine-scale diversity and extensive recombination in a quasisexual bacterial population occupying a broad niche. *Science* 348, 1019–1023. doi: 10.1126/science.aaa4456

Russell, S. L., Pepper-Tunick, E., Svedberg, J., Byrne, A., Ruelas Castillo, J., Vollmers, C., et al. (2020). Horizontal transmission and recombination maintain forever young bacterial symbiont genomes. *PloS Genet.* 16, e1008935. doi: 10.1371/journal.pgen.1008935

Shannon, P., Markiel, A., Ozier, O., Baliga, N. S., Wang, J. T., Ramage, D., et al. (2003). Cytoscape: a software environment for integrated models of biomolecular interaction networks. *Genome Res.* 13, 2498–2504. doi: 10.1101/gr.1239303

Sun, J., Zhou, Y., Chen, C., Kwan, Y. H., Sun, Y., Wang, X., et al. (2020). Nearest vent, dearest friend: biodiversity of tiancheng vent field reveals cross-ridge similarities in the Indian ocean. *R. Soc. Open Sci.* 7, 200110. doi: 10.1098/rsos.200110

Tajima, F. (1989). Statistical method for testing the neutral mutation hypothesis by DNA polymorphism. *Genetics* 123, 585–595. doi: 10.1093/genetics/123.3.585

Tyler, P., Young, C. M., Dolan, E., Arellano, S. M., Brooke, S. D., and Baker, M. (2007). Gametogenic periodicity in the chemosynthetic cold-seep mussel "*Bathymodiolus*" *childressi*. *Mar. Biol.* 150, 829–840. doi: 10.1007/s00227-006-0362-9

Ücker, M., Ansorge, R., Sato, Y., Sayavedra, L., Breusing, C., and Dubilier, N. (2021). Deep-sea mussels from a hybrid zone on the mid-Atlantic ridge host genetically indistinguishable symbionts. *ISME. J.* 15, 3076–3083. doi: 10.1038/s41396-021-00927-9

Van Der Gast, C. J. (2015). Microbial biogeography: the end of the ubiquitous dispersal hypothesis? *Environ. Microbiol.* 17, 544–546. doi: 10.1111/1462-2920.12635

Van Der Heijden, K., Petersen, J. M., Dubilier, N., and Borowski, C. (2012). Genetic connectivity between north and south mid-Atlantic ridge chemosynthetic bivalves and their symbionts. *PloS One* 7, e39994. doi: 10.1371/journal.pone.0039994

Van Dover, C. L., German, C., Speer, K. G., Parson, L., and Vrijenhoek, R. (2002). Evolution and biogeography of deep-sea vent and seep invertebrates. *Science* 295, 1253–1257. doi: 10.1126/science.1067361

Van Dover, C. L., Humphris, S. E., Fornari, D., Cavanaugh, C. M., Collier, R., Goffredi, S. K., et al. (2001). Biogeography and ecological setting of Indian ocean hydrothermal vents. *Science* 294, 818–823. doi: 10.1126/science.1064574

Vrijenhoek, R. C. (2010). Genetic diversity and connectivity of deep-sea hydrothermal vent metapopulations. *Mol. Ecol.* 19, 4391–4411. doi: 10.1111/j.1365-294X.2010.04789.x

Wade, M. J., and Mccauley, D. E. (1988). Extinction and recolonization: their effects on the genetic differentiation of local populations. *Evolution* 42, 995–1005. doi: 10.1111/j.1558-5646.1988.tb02518.x

Wang, Y., Han, X., Jin, X., Qiu, Z., Ma, Z., and Yang, H. (2012). Hydrothermal activity events at kairei field, central Indian ridge 25°S. *Resource. Geology.* 62, 208–214. doi: 10.1111/j.1751-3928.2012.00189.x

Wentrup, C., Wendeberg, A., Schimak, M., Borowski, C., and Dubilier, N. (2014). Forever competent: deep-sea bivalves are colonized by their chemosynthetic symbionts throughout their lifetime. *Environ. Microbiol.* 16, 3699–3713. doi: 10.1111/1462-2920.12597

Whitaker, R. J., Grogan, D. W., and Taylor, J. W. (2003). Geographic barriers isolate endemic populations of hyperthermophilic archaea. *Science* 301, 976–978. doi: 10.1126/science.1086909

Won, Y.-J., Hallam, S. J., O'mullan, G. D., Pan, I. L., Buck, K. R., and Vrijenhoek, R. C. (2003). Environmental acquisition of thiotrophic endosymbionts by deep-sea mussels of the genus *Bathymodiolus*. *Appl. Environ. Microbiol.* 69, 6785–6792. doi: 10.1128/AEM.69.11.6785-6792.2003

Won, Y.-J., Jones, W. J., and Vrijenhoek, R. C. (2008). Absence of cospeciation between deep-sea mytilids and their thiotrophic endosymbionts. *J. Shellfish. Res.* 27, 129–138. doi: 10.2983/0730-8000(2008)27[129:AOCBDM]2.0.CO;2

Xu, T., Feng, D., Tao, J., and Qiu, J.-W. (2019). A new species of deep-sea mussel (Bivalvia: Mytilidae: *Gigantidas*) from the south China Sea: morphology, phylogenetic position, and gill-associated microbes. *Deep. Sea. Res. Part I.: Oceanographic. Res. Papers* 146, 79-90. doi: 10.1016/j.dsr.2019.03.001

Yarza, P., Yilmaz, P., Pruesse, E., Glöckner, F. O., Ludwig, W., Schleifer, K.-H., et al. (2014). Uniting the classification of cultured and uncultured bacteria and archaea using 16S rRNA gene sequences. *Nat. Rev. Microbiol.* 12, 635–645. doi: 10.1038/nrmicro3330

Yoon, S.-H., Ha, S.-M., Kwon, S., Lim, J., Kim, Y., Seo, H., et al. (2017). Introducing EzBioCloud: a taxonomically united database of 16S rRNA gene sequences and whole-genome assemblies. *Int. J. systematic. evolutionary. Microbiol.* 67, 1613-1617. doi: 10.1099/ijsem.0.001755

Young, C., Fujio, S., and Vrijenhoek, R. (2008). Directional dispersal between mid-ocean ridges: deep-ocean circulation and gene flow in *Ridgeia piscesae*. *Mol. Ecol.* 17, 1718–1731. doi: 10.1111/j.1365-294X.2008.03609.x

Zhong, Z., Wang, M., Chen, H., Zheng, P., and Li, C. (2020). Gametogenesis and reproductive traits of the cold-seep mussel *Gigantidas platifrons* in the south China Sea. *J. Oceanology. Limnology.* 38, 1304–1318. doi: 10.1007/s00343-020-0027-4

Zhou, Y., Chen, C., Zhang, D., Wang, Y., Watanabe, H. K., Sun, J., et al. (2022). Delineating biogeographic regions in Indian ocean deep-sea vents and implications for conservation. *Diversity Distributions*. doi: 10.1111/ddi.13535

Zielinski, F. U., Pernthaler, A., Duperron, S., Raggi, L., Giere, O., Borowski, C., et al. (2009). Widespread occurrence of an intranuclear bacterial parasite in vent and seep bathymodiolin mussels. *Environ. Microbiol.* 11, 1150–1167. doi: 10.1111/j.1462-2920.2008.01847.x

frontiers | Frontiers in Marine Science

TYPE Original Research
PUBLISHED 11 October 2022
DOI 10.3389/fmars.2022.915650

OPEN ACCESS

EDITED BY
Philip Weaver,
Seascape Consultants Ltd,
United Kingdom

REVIEWED BY
Sandra Brooke,
Florida State University, United States
Antonietta Rosso,
University of Catania, Italy

*CORRESPONDENCE
Marina Carreiro-Silva
marina.pc.silva@uac.pt;
carreirosilvamarina@gmail.com

SPECIALTY SECTION
This article was submitted to Deep-Sea Environments and Ecology, a section of the journal Frontiers in Marine Science

RECEIVED 08 April 2022
ACCEPTED 09 August 2022
PUBLISHED 11 October 2022

CITATION
Carreiro-Silva M, Martins I, Riou V, Raimundo J, Caetano M, Bettencourt R, Rakka M, Cerqueira T, Godinho A, Morato T and Colaço A (2022) Mechanical and toxicological effects of deep-sea mining sediment plumes on a habitat-forming cold-water octocoral.
Front. Mar. Sci. 9:915650.
doi: 10.3389/fmars.2022.915650

Mechanical and toxicological effects of deep-sea mining sediment plumes on a habitat-forming cold-water octocoral

Marina Carreiro-Silva[1,2]*, Inês Martins[1,2], Virginie Riou[1,2], Joana Raimundo[3,4], Miguel Caetano[3,4], Raul Bettencourt[1,2], Maria Rakka[1,2,5], Teresa Cerqueira[1,2], António Godinho[1,2], Telmo Morato[1,2] and Ana Colaço[1,2]

[1]Institute of Marine Sciences - Okeanos, University of the Azores, Horta, Portugal, [2]IMAR - Institute of Marine Research, University of the Azores, Horta, Portugal, [3]IPMA Portuguese Institute of Sea and Atmosphere (Portugal), Algés, Portugal, [4]CIIMAR – Interdisciplinary Centre of Marine and Environmental Research, Matosinhos, Portugal, [5]Oceanography Department, Dalhousie University, Halifax, NS, Canada

Deep-sea mining activities are expected to impact deep-sea biota through the generation of sediment plumes that disperse across vast areas of the ocean. Benthic sessile suspension-feeding fauna, such as cold-water corals, may be particularly susceptible to increased suspended sediments. Here, we exposed the cold-water octocoral, *Dentomuricea* aff. *meteor* to suspended particles generated during potential mining activities in a four weeks experimental study. Corals were exposed to three experimental treatments: (1) control conditions (no added sediments); (2) suspended polymetallic sulphide (PMS) particles; (3) suspended quartz particles. The two particle treatments were designed to distinguish between potential mechanical and toxicological effects of mining particles. PMS particles were obtained by grinding PMS inactive chimney rocks collected at the hydrothermal vent field Lucky Strike. Both particle types were delivered at a concentration of 25 mg L^{-1}, but achieved suspended concentrations were 2-3 mg L^{-1} for the PMS and 15-18 mg L^{-1} for the quartz particles due to the different particle density. Results of the experiment revealed a significant increase in dissolved cobalt, copper and manganese concentrations in the PMS treatment, resulting from the oxidation of sulphides in contact with seawater. Negative effects of PMS exposure included a progressive loss in tissue condition with necrosis and bioaccumulation of copper in coral tissues and skeletons, and death of all coral fragments by the end of the experiment. Physiological changes under PMS exposure, included increased respiration and ammonia excretion rates in corals after 13 days of exposure, indicating physiological stress and potential metabolic exhaustion. Changes in the cellular stress biomarkers and gene expression profiles were more pronounced in corals exposed to quartz particles, suggesting that the mechanical effect of particles although not causing measurable changes in the physiological functions of the coral, can still be detrimental to corals by eliciting cellular stress and immune responses. We hypothesize that the high mortality of corals recorded in the PMS treatment may have resulted from the combined

and potentially synergistic mechanical and toxicological effects of the PMS particles. Given the dispersal potential of mining plumes and the highly sensitive nature of octocorals, marine protected areas, buffer areas or non-mining areas may be necessary to protect deep-sea coral communities.

KEYWORDS

anthropogenic impact, hydrothermal vent, metals, Northeast Atlantic, physiology, sedimentation, Cnidaria

Introduction

Polymetallic Sulphide (PMS) deposits produced at hydrothermal vents in the deep sea are of interest by mining companies as an alternative to terrestrial mineral resources, and to respond to increasing demand for rare minerals for technology (Petersen et al., 2016; Sharma, 2017). However, the potential impacts of mining activities on deep-sea fauna and ecosystems are poorly understood (Van Dover et al., 2017; Van Dover et al., 2020), limiting ecological risk assessments (Durden et al., 2017; Washburn et al., 2019; Smith et al., 2020) and hindering the establishment of management standards and guidelines for deep-sea industries and activities (Wedding et al., 2015; Levin et al., 2016; Jones et al., 2019).

Mining for PMS is expected to impact deep-sea ecosystems in several ways (Gwyther, 2008; Boschen et al., 2013; Van Dover, 2014; Levin et al., 2016; Miller et al., 2018; Weaver and Billet 2019; Christiansen et al., 2020). Physical destruction of the seabed and damage to the habitat and fauna by the mining equipment, along with changes in seafloor topography and geochemical characteristics are expected in the close vicinity of the mining site (Boschen et al., 2013; Miller et al., 2018). In addition, the generation of sediment plumes of fine particulate material by the seabed mining and surface dewatering operations will disperse in the water column and eventually settle on the seafloor, potentially smothering surrounding fauna (Gwyther, 2008; Christiansen et al., 2020; Morato et al., 2022 this issue). These sediment plumes may transport metal complexes trapped in the sediments (e.g., copper, cadmium) that can be released to the water column in concentrations toxic to marine biota (Hauton et al., 2017; Fallon et al., 2019).

Exposure to elevated suspended sediments in the water column can have sublethal and lethal effects on benthic sessile suspension and filter feeding fauna by impairing feeding and respiration (e.g., Erftemeijer et al., 2012; Strachan and Kingston, 2012). The impacts of sediment plumes are of particular concern for cold-water corals that form extensive and highly structured ecosystems in the deep-sea (Roberts et al., 2009). Indeed, recent studies have predicted some degree of overlap between the dispersal of PMS plumes and the distribution of cold-water corals in the Mid Atlantic Ridge and seamounts around the Azores (Morato et al., 2022). In this region, cold-water octocorals are among the most important ecosystem engineers forming dense coral garden communities (Braga-Henriques et al., 2013; Morato et al., 2021). These communities play important ecological roles in carbon and nitrogen cycling (Rakka et al., 2021; Rovelli et al., 2022) and as habitat providers for a variety of invertebrates and commercially important fish species (Pham et al., 2015; Carreiro-Silva et al., 2017; Gomes-Pereira et al., 2017).

Anthropogenic impacts on these ecosystems can be long lasting owing to their slow-growing and long-lived life histories and slow recovery capacity (Roberts et al., 2009; Clark et al., 2019), and thus these ecosystems have been classified as vulnerable marine ecosystems (VMEs) in need of protection (FAO, 2009; OSPAR, 2010). However, the potential impacts of PMS mining plumes on cold-water corals are still poorly understood.

Evidence from tropical environments showed that high sedimentation can cause smothering and burial of coral polyps, resulting in tissue damage, decreased food intake, increased mucus production and polyp movement resulting in increased metabolic costs (Rogers, 1990; Erftemeijer et al., 2012). Prolonged exposure to sedimentation can result in decreased growth rates, reduced reproductive output and increased mortality (Fabricius and Wolanski, 2000; Weber et al., 2006; Jones et al., 2015). The effects of sedimentation on cold-water corals have been investigated for only a few species. Studies on cold-water corals have focused on the impact of natural sediments and drill cuttings originating from hydrocarbon exploration on the scleractinian *Lophelia pertusa* (recently synonymized as *Desmophyllum pertusum*: Addamo et al., 2016), showing little impact on its physiology (Brooke et al., 2009; Larsson and Purser, 2011; Allers et al., 2013; Larsson et al., 2013; Baussant et al., 2018; da Rocha et al., 2021). On the other hand, recent studies on the impacts of excessive sedimentation produced by mine tailing deposition on benthic ecosystems in the Norwegian fjords (Liefmann et al., 2018; Scanes et al., 2018),

suggest that octocorals (*Duva florida, Primnoa resedaeformis*) are more sensitive to suspended sediments than scleractinians. Results of these studies showed tissue damage from the sharp morphology of mine tailings and increased energetic demand likely associated with the active removal of sediments from the polyps. However, there are no studies that have evaluated the impact of PMS on cold-water corals.

Moreover, most of the above studies have focused on physiological impacts on tissue condition and metabolic responses (e.g., respiration, excretion). Nevertheless, cellular changes in protein production and gene expression usually occur before physiological damage is evident (Downs et al., 2005). Therefore, cellular biomarkers can be used as important tools to detect sub-lethal responses to anthropogenic impacts (Downs et al., 2005; Downs et al., 2012). These tools provide a means to evaluate the ability of animals to regulate adaptive responses to stress which ultimately will determine their survival. In corals, changes in gene expression and enzyme activity related to cellular stress, detoxification and oxidative damage have been studied to reveal important physiological pathways to cope with environmental stress and chemical contaminants (e.g., Carreiro-Silva et al., 2014; Marangoni et al., 2017; Fonseca et al., 2019; Servetto et al., 2021). Using these biomarkers is particularly important to identify potential ecotoxicological effects caused by chemicals in the PMS particles that cannot be ascertained at the organism level.

In the present study, we investigated the effects of PMS particles from inactive chimney rocks of the Lucky Strike hydrothermal vent field crushed into fine particles, on the octocoral *Dentomuricea* aff. *meteor*. This species forms extensive coral gardens in the Azores seamounts between 200 and 400 m depth that can be affected by the horizontal and vertical dispersal of mining plumes. The putative mechanical and toxicological effects of PMS particles were evaluated through measurements of the coral physiological responses at the organism (respiration, nutrient excretion), tissue (bioaccumulation of metals, structural integrity) and cell (enzyme activity and gene expression) levels.

Materials and methods

Coral collection and maintenance

Live colonies of *D.* aff. *meteor* were collected at the summit of Condor Seamount (38˚ 08'N, 29˚ 05'W) using the ROV SP at depths between 185-210 m in August 2014, characterized by average bottom temperatures of 15°C and salinity of 36 ppt for this time of the year (Rovelli et al., 2022). Colonies were transferred to the DeepSeaLab aquaria facilities at IMAR/Okeanos in coolers and distributed in two 170 L aquaria in a thermo-regulated room (14 ± 0.7 °C) in darkness, within hours after collection. The aquaria system consisted of a continuous flow-through open system of oligotrophic oceanic seawater pumped from 5 m depth (salinity ca. 36 ppt). Colonies were left to acclimate to atmospheric pressure conditions for two weeks with running natural seawater chilled to match *in situ* temperature and salinity conditions (15 ± 0.9°C, 36 ± 0.1 ppt) using cooling systems connected to temperature controllers. Six colonies were subsequently fragmented into 15 nubbins (i.e., coral fragments with 5-7 cm), mounted on bases made of inert epoxy putty and silicone tubing, and placed in four 25 L aquaria for further two weeks before the experiment. Seawater in each aquarium was continuously renewed (6 times/day at 5 L h^{-1}) and mixed with submersible Iwaki pumps (4.5 W, 280 L h^{-1}). Corals were fed five days a week, once a day, with a mixture of frozen adult *Artemia salina* and nauplii, mysids and microplankton (all from OceanNutrition™), and a food supplement composed of proteins, aminoacids, lipids, vitamins, and oligoelements (Marine Active Supplement, Bentos Nutrition).

Sediment preparation

Hydrothermal polymetallic sulphide. particles representative of plumes produced during the extraction of massive PMS deposits were obtained from an inactive sulphide chimney collected at 1750 m of depth by the ROV VICTOR6000 at the base of the Eiffel Tower structure at the Lucky Strike hydrothermal vent field during the research cruise MoMARSAT-2013 (Blandin et al., 2013) on the RV Pourquoi Pas?. Chimney fragments were ground in a tungsten carbide ring mill pulveriser and subsequently were analysed by laser diffraction (Mastersizer 2000) at the Center of Geology, University of Lisbon - CeGUL, Portugal for particle size analysis. The analysis revealed that 55% of the particles were between 0.5-10 µm in size (23%<2 µm, 32% 2-10 µm), 41% were 10-70 µm and 4% were >70 µm. Energy Dispersive X-Ray Analysis (EDAX) revealed that PMS particles were mainly composed of barite ($BaSO_4$), pyrite (FeS_2), and chalcopyrite ($CuFeS_2$), with a minor composition of sphalerite ((ZnFe)S) (Figure S1). Elemental composition of PMS particles show increased concentrations of manganese (Mn), copper (Cu), nickel (Ni), cobalt (Co), zinc (Zn), arsenic (As), and cadmium (Cd) (Fallon et al., 2019). Polymetallic sulphide particle size matched the range expected by Seafloor Mining Tools excavation and dewatering processes, according to the Nautilus Minerals (80% of 0.5-10 µm and 20% of 10-70 µm) (ASA, 2008).

The quartz particles treatment, was prepared from commercially available silicon dioxide (SiO_2) particles, by mixing 80% of 0.5-10 µm (#S5631, Sigma-Aldrich, Portugal) and 20% of 50-70 µm grain sizes (#274739, Sigma-Aldrich, Portugal). Particles of PMS and quartz were photographed using light and scanning electron microscopy (SEM). For light microscopy, we used a LEICA DM6000 microscope under 400× magnification. For SEM, particles were mounted on aluminum

stubs and sputter-coated with gold. The scanning electron microscope Tescan VEGA3 xmu at 20 keV was used for PMS particles and JEOL JSM-5200LV at 25 keV was used for quartz particles.

Experimental design

Following the acclimation period, coral fragments were exposed to three experimental treatments for a period of 27 days: (1) a control treatment with no sediment addition; (2) suspended PMS particles; (3) suspended quartz particles. The two particles treatments were designed to distinguish between the potential physical and toxicological effects of particle exposure. Coral fragments were distributed in six 10 L aquaria (two aquaria per treatment) so that the same number of fragments of each colony was present in each experimental treatment. Accordingly, 15 coral fragments (five fragments from three different mother colonies) were present in each aquarium at the beginning of the experiment, totaling 30 fragments from six mother colonies in each treatment. Corals were fed once daily, seven days a week, as described in section above. Weekly, the excess food and particles that settled at the bottom of the aquarium were siphoned together with a 25% water replacement for each aquarium before food was added.

A semi-open seawater system was used for the experiment to ensure maximal exposure of the corals to the particle treatment. Thus, 8 hours of running seawater were intercalated with two periods of 4 hours in a closed system. PMS and inert particles were delivered at a concentration of 25 mg L^{-1} to the sediment exposure treatments. This concentration was chosen based on the concentrations used in drill cuttings experiments with the cold-water coral *L. pertusa* (Larsson et al., 2013) to allow for cross studies and particle types comparisons. Particle addition was achieved by adding 250 mg of particles daily in one of the 4-hour closed system period, while the food was added in the other 4 hours closed system period to avoid interference between particles and the added food. Water circulation and particle resuspension were achieved using recirculation pumps (skim350, Eheim), linked to a tubing circuit with outflow holes orientated towards the tank walls.

Monitoring of experimental treatments

The concentration of suspended PMS and quartz particles in each treatment was measured during an exposure period of 4 hours. Suspended particle concentrations were measured one minute after particle addition, and then at intervals of 5, 15, 30 minutes, 1 hour, 2 hours and 4 hours after particle addition in the PMS and quartz particle treatments and in control aquaria with no particle addition. Samples of 0.5 L were collected from each aquarium 1 minute after particle addition with subsequent collection of 1 L seawater at other times. Seawater was filtered onto pre-combusted and pre-weighed 0.45 µm pore size GF/F filters, then washed with Milli-Q water to remove salt and dried at 60°C to constant weight. The concentration of suspended particles in the PMS and quartz particle treatments were estimated by subtracting the weight of filters with suspended particles in the control (no particle addition aquarium) for the weight of filters in the PMS and quartz treatments.

Seawater physical-chemical parameters were measured daily in each aquarium before feeding corals. Seawater salinity was measured with a S30 SevenEasy™ conductivity meter, pH and temperature with a glass electrode (Crison pH 25+), and oxygen with a Fibox4 (PreSens) with a Oxygen Dipping Probe DP-PSt3. Seawater samples (12 mL) for inorganic nutrient analyses were collected on times 0 (immediately before the start of the experiment), and once a week on days 6, 13, 20 and 27 of the experiment, filtered with 0.45 µm filters (Cytiva Whatman™ GD/X Glass Micro Fiber (GMF) syringe filters) and frozen until analyses. Nutrient concentrations (nitrate NO_3^-, ammoniumNH_3 $+NH_4^+$, phosphate PO_4^{3-}) were determined using a colorimetric Autoanalyzer Sanplus with Segmented Flow, applying the methodologies Skalar: M461-318 (EPA 353.2), M155-008R (EPA 350.1) and M503-555R (Standard Method 450-P I).

Analysis of metal contents in seawater and bioaccumulation in corals

Trace elements (Co, Cu, Mn) released from the resuspension of PMS particles to the water column were determined using passive sampling coupled with inductively coupled plasma mass spectrometry (ICPMS). The passive samplers used were from DGT® Research Ltd (Lancaster, UK), with the reference LSNM-NP open-pore Loaded DGT device for metals in solution. DGT sequester dissolved labile metal species, including free ions, inorganic complexes and labile organic complexes (Zhang and Davison, 2000), a proxy for determining the potential biological adverse effects (Montero et al., 2012). DGT-holders were deployed in all aquaria and replaced every week (days 6, 13, 20, 27), which gave an integrated temporal variation of metal released to the water column. DGT samples were processed following the methodology described in Bersuder et al. (2021). Briefly, to minimize contamination, all the materials used were acid cleaned (pro-analysis grade), subsequently rinsed with ultra-pure water, and dried in rooms with environmental conditions limiting sample contamination. Powder-free gloves were also used to minimize contamination. DGT units were removed from holders, opened using a plastic screwdriver, and the resin-gel layer was peeled off retrieved with plastic tweezers. Metals from the gel were back-extracted with a 1 M HNO_3 solution and measured by ICPMS. The final solution was kept refrigerated (4-6 °C) until analysis. Trace elements in the tissues and skeletons of corals in the different treatments (sampled at

days 25-27 for PMS and day 27 for quartz and control treatments) were analyzed after digestion with a mixture of HNO_3 and H_2O_2 to varying temperatures according to the method described by Raimundo et al. (2013). Certified reference material and procedural blanks (coral digestions) were taken through the procedure in the same way as the samples. Metal concentrations in DGT extracts and coral tissues were quantified by a quadrupole ICPMS (Thermo Elemental, X-Series) equipped with a Peltier impact bead spray chamber and a concentric Meinhard nebulizer. Measurements of the stable isotope indium (^{115}In) were used as an online internal standard. The equipment was set up by ensuring low variability of counts (RSD<2%). Typically, 7-point standard calibration curves, including one blank, were used in different dynamic ranges depending on the metal concentration in extracts. Analyzed procedural blanks always accounted for less than 1% of the total element in the samples. The calculation of the DGT concentration was carried out following Zhang and Davison (2000) and using the diffusion coefficients provided by the supplier. The metal concentrations in coral tissues are given in microgram per gram of dry weight tissue (μg g^{-1}; dw).

Tissue integrity and condition

Coral fragments were examined using light microscopy and SEM to observe tissue and polyps' condition and integrity under the different treatments. Light microscopy observations were made using a dissecting microscope Leica MZ 16FA under 30× magnification. For SEM, samples were dried using the critical point drying technique, mounted on stubs and sputter-coated with gold, and examined with a scanning electron microscope JEOL JSM-5200LV at 25 keV.

Respiration and excretion of inorganic nutrients

Integrated measurements of coral respiration and inorganic nutrients release rates were carried out by closed-chamber incubation in cylindrical acrylic chambers (volume 320 mL) on days 0, 13 and 27 of the experiment, except for the PMS particle treatment at day 27, when all corals in this treatment had died. Each coral fragment (N=6 per treatment) was incubated for 7-8 h with 0.2 μm filtered seawater from the respective aquarium and continuously stirred with glass-coated magnetic stirrers. Chambers were placed in a water bath, and temperatures maintained at 15 ± 0.3°C on top of a magnetic stirring plate. Respiration rates were derived from the depletion of dissolved O_2 recorded before closing and immediately after the chamber using a single channel oxygen meter Fibox4 with a PSt3 sensor (PreSens, Germany). These values were adjusted for rates recorded in chambers without corals to account for microbial respiration. Oxygen saturation inside the chambers remained >70%. *Dentomuricea* aff. *meteor* excretion rates of ammonium, during incubations were assessed by calculating the difference between initial and final ammonium concentrations in chambers with and without corals. Nutrient concentrations were determined in 0.2 mL syringe filtered water samples using a colorimetric Autoanalyzer Sanplus with Segmented Flow, applying the described methodologies. Although ammonia (NH_3) and ammonium (NH_4^+) were measured together in our samples, NH_3 was considered as negligible in our conditions (1–2% of total ammonium/ammonia at pH 8.0, for a pKa of 9.68–9.99, Bell et al., 2007). Coral respiration and excretion rates were normalized to the coral skeletal surface area quantified using advanced geometric techniques by approximation of the shape of different sections of the coral fragment to the geometric figure of a cylinder as described by Naumann et al. (2009).

Cellular stress biomarkers

Antioxidant stress related biomarkers in *D.* aff. *meteor* tissues were used to evaluate the degree of cellular stress induced by exposure to PMS and quartz particles. Coral fragments were collected from each treatment at times 0 and 13 days and from the control and quartz treatments also at time 27 days, snap frozen in liquid nitrogen, and stored at -80°C until analysis.

Preparation of tissue extracts for antioxidant enzymes and lipid peroxidation

From each coral fragment from each treatment, tissues were separated from skeletons and homogenized at a 1:3 w/v ratio, in ice-cold Phosphate-buffered Saline solution (PBS pH 7.3: 0.14 M NaCl, 2.7 mM KCl, 8.1 mM Na_2HPO_4, 1.47 mM KH_2PO_4) and 1% (v/v) ProteaseArrest™ (G-Biosciences®), using an Ultra Turrax (Ystral®, D79282) slowly increasing the rotational velocity from 8,000 to 20,000 rpm, during the ~2 min extraction time. The homogenate was centrifuged at 16,000 g for 30 min at 4°C and supernatant fraction was separated into different microtubes and stored at -80 °C for posterior protein quantification and measurements of GST, SOD, CAT and LPO. All enzyme assays were tested with commercial kits obtained from Sigma® and each sample was run in triplicate in a Multiskan™ GO microplate spectrophotometer (Thermo Scientific™).

Determination of antioxidant enzyme activities

Protein quantification For enzyme activity normalization, the total soluble protein content was quantified according to the Bradford method (Bradford, 1976), adapted from Bio-Rad

Bradford microassay set up in a 96-well microplate. Absorbance was read at 595 nm in a microplate reader (Thermo Scientific™). A calibration curve was created using bovine serum albumin (BSA; Bio-Rad) standards.

Glutathione S–transferase (GST) activity was determined according to the procedure described by Habig et al. (1974), and optimized for a 96-well microplate. This assay uses 1-chloro-2,4-dinitrobenzene (CDNB) as substrate, and upon conjugation of the thiol group of glutathione (GSH) to the CDNB substrate, there is an increase in the absorbance. The reaction product (GS-DNB conjugate), catalyzed by GST, absorbs at 340 nm. The rate of increase in the absorption is directly proportional to the GST activity in the sample. To perform the assay, 180 µL of substrate solution were added to 20 µL of GST standard or sample in each well and the absorbance at 340 nm was recorded every minute for 6 min using a plate reader (Thermo Scientific™). GST activity was calculated using a molar extinction coefficient for CDNB (ϵ= 5.3 mM^{-1} cm^{-1}). Equine liver GST (Sigma-Aldrich) was used as a positive control to validate the assay. GST activity was calculated using the following equation: [ΔA340/min/0.0053]* [total volume/sample volume]. GST enzymatic activity in coral tissue is expressed as nmol min^{-1} mg^{-1} of protein (wet weight).

Superoxide dismutase (SOD) activity was determined spectrophotometrically by an indirect method (Therond et al., 1996) based on competition of SOD with 2-(4-iodophenyl)-3-(4-nitrophenol)-5-phenyltetrazolium chloride (I.N.T) for dismutation of superoxide anion (O-2). In this method, xanthine and xanthine oxidase were used to generate O-2 radicals which react with I.N.T quantitatively to form a red formazan dye. Absorbance was measured at 505 nm and 25 °C, 30 s after the addition of xanthine oxidase as start reagent across a 180 s incubation period (Kit Ransod SD 125, Randox). One unit of SOD is defined as the amount of enzyme that inhibits the rate of formazan dye formation by 50%. The percent inhibition of samples was calculated using the following equation: 100-[[ΔA505/min]/[ΔAblank/min]] *100. Then, a SOD standard curve is used to correlate the percent inhibition of samples with SOD activity. Coral tissue SOD activity is expressed as inhibition Units mg^{-1} of protein (wet weight).

Catalase (CAT) activity was measured spectrophotometrically, according to Beers and Sizer (1952), by measuring the rate of H_2O_2 disappearance at 240 nm (extinction coefficient, ϵ = 0, 04 mM^{-1} cm^{-1}) and 25°C across a 180 s incubation period. In this assay, total reaction volume of 300 µL was obtained with 50 mM potassium phosphate buffer (pH 7.0), 13.5 mM H_2O_2 as a substrate and initiated by the addition of the sample into well plates. Catalase from bovine liver (Sigma®) was used as a positive control for validation of the assay. Catalase activity was calculated using the following equation: [ΔA240/min/0, 04]* [total volume/sample volume]. CAT enzymatic activity in coral tissue is expressed as µmol min^{-1} mg^{-1} of protein (wet weight).

Lipid peroxidation (determination of malondialdehyde, MDA)

Lipid peroxidation was determined by the quantification of a specific end-product of the oxidative degradation process of lipids, malondialdehyde (MDA) (Kalghatgi et al., 2013). Concentrations of MDA were analyzed using a colorimetric reaction, which uses 1-methyl-2-phenylindole (MPI) as chromogen (Randox Ltd.). Condensation of one molecule of MDA with 2 molecules of MPI under acidic conditions results in the formation of a chromophore with an absorbance maximum at 586 nm. Concentrations of MDA in each tissue were calculated using a standard curve prepared with freshly prepared solutions of malondialdehyde bis [dimethyl acetal] (ACROS Organics™) and values were expressed as nmol mg^{-1} of protein (wet weight).

Molecular analysis

Gene expression profiles in *D.* aff. *meteor* were used to evaluate the physiological pathways involved in the response to exposure to PMS and quartz particles. Coral fragments were collected from each treatment at times 0, 3 and 13 days and for the control and quartz treatments also at time 27 days, snap frozen in liquid nitrogen and stored at -80°C until subsequent analysis. The sampling time point at day 3 of the experiment was performed to capture changes of gene expression reflected within a short period of exposure to the treatments. Total RNA extraction and further RNA handling until obtaining cDNA from six coral fragments of the same treatment, followed procedures described in Carreiro-Silva et al. (2014). A set of genes regarded as suitable molecular biomarkers were selected to detect changes at sub-cellular level in response to different treatments based on previous studies with cold-water corals in our laboratory (Carreiro-Silva et al., 2014; Servetto et al., 2021): genes involved in cellular stress and antioxidant reaction system (heat shock protein (HSP70), superoxide dismutase (SOD), ferritin), cell structure/integrity [α-carbonic anhydrase, receptor-type protein tyrosine phosphatase (RP Tyr-PH)] and immune responses (toll-like receptor (TLR), lysozyme, rel homology domain (RHD), ferritin). See Table S1 for details on the biological function of each of the protein-encoding genes used in this study. Specific primers amplifying 100–200 bp PCR products were designed for the genes of interest (GOI) based on the nucleotide sequences used in previous studies (see Table S1). Because the selected gene sequences have still not been published for *D.* aff. *meteor*, the identity of the sequences was confirmed by polymerase chain reaction amplification followed by sequencing of the PCR products. cDNA samples of *D.* aff. *meteor* (40 ng) were amplified in the presence of Reaction Buffer 1X; 1.5 mM $MgCl_2$; 0.2 mM dNTP mixture; 1 µM of each design primer

(sense and antisense); and 2.5 U of Taq DNA Polymerase (Invitrogen). The amplification reaction was performed using the Eppendorf MastercyclerR gradient and the following conditions: 5 min at 95°C, followed by 35 cycles of 1 min at 94°C, 1 min at 54°C and 1 min at 70°C, with a final extension of 10 min at 72°C. PCR products were directly extracted from agarose gels and their nucleic acid sequence determined. BLAST analyses were performed to verify the corresponding matching PCR products sequences to the candidate gene sequences present in GenBank database, in order to confirm their identity (Table S1). Transcript levels were determined by Real-Time PCR using the CFX Connect™ Real-Time PCR Detection System (BioRad). First cDNA strand diluted 1:200 aliquots from each sample were used in 20 µL PCR reactions in the presence of 0.5 µM of each primer and Maxima SYBR Green/ROX qPCR Master Mix (Fermentas). The thermocycling protocol was as follows: 10 min at 95°C, followed by 40 cycles of 20 s at 94°C, 45s at 54°C and 25 s at 68°C. A melting curve of PCR products (95°C – 65°C) was performed to ensure the presence of single PCR producst at the end of the qPCR reactions. For the evaluation of the expression level of each mRNA used, the comparative Ct (ΔΔCt) quantitation method was applied, using 18S and β-actin genes as suitable reference genes for their efficiencies and stable expression across all experiments. Each reaction was repeated in triplicate, and negative controls were performed without cDNA in the reaction mixture. Target mRNA genes were normalized using the combination of the expression levels with 18S and β-actin and relative abundances were calculated in relation to gene expression levels just prior to the start of the experiment (T0). The expression level of all genes was converted into relative expression level as follows:

$$\left[(\text{Efficiency GOI})^{\Delta Ct\ goi}\right] \ / \ \left[(\text{Efficiency } \beta a)^{\Delta Ct\ \beta a} \times (\text{Efficiency 18S})^{\Delta Ct\ 18S}\right]^{1/2},$$

$$\text{where } [\Delta Ct = Ct\ (T0) - Ct\ (\text{treatment})]$$

Statistical analyses

Multivariate analysis was performed using the statistical package PRIMER-E v.6 with the permutational multivariate analysis of variance (PERMANOVA) + add on (Anderson et al., 2008) to investigate the response of *D.* aff. *meteor* to treatments and through experimental times. This statistical analysis is a powerful non-parametric approach that uses a permutational technique to enable significance tests for small sample sizes to be conducted (Walters and Coen, 2006). The analyses used a resemblance matrix based on Euclidean distance and PERMANOVA was run using 9999 permutations with partial sum of squares and unrestricted permutation of raw data to produce p-values. A repeated measures PERMANOVA was used to test for treatment and experimental time effects on *D.* aff. *meteor* respiration and excretion rates and oxidative stress biomarkers. 'Treatment' and 'time' were used as fixed factors, with interaction terms, whereas corals were used as a random factor to account for repeated measures and mother colony donors. To test for differences in dissolved metal concentrations among treatments and experimental times, the analysis used 'treatment' and 'time' as fixed factors. To test for differences in total accumulated metal concentrations in corals at the end of the 27 days period, individual metal concentrations measured in coral tissues and skeletons were analysed using a one-way PERMANOVA with 'treatment' as a fixed factor. Preliminary data analysis showed that the effect of the nested factor aquaria was low ($p > 0.1$), thus, in the analysis of the data, replicate aquaria within each treatment were pooled together to increase the power of the test for sediment exposure (Underwood, 1997). Values were considered statistically significant at $p< 0.05$. No statistical tests were conducted for differences in gene expression fold changes, because of the small number of replicates and high variability. Significant main PERMANOVA tests were followed by pairwise PERMANOVA tests. Permutational P-values (PPERM) were interpreted when the number of unique permutations >100; alternatively, Monte Carlo P-values (PMC) were considered (Anderson and Robinson, 2003). Reported values in the text are mean ± standard deviation.

Results

Sediment treatments

Monitoring of the concentration of suspended PMS and quartz particles in each treatment revealed that average exposure concentrations differed from the target value of 25 mg L^{-1} (Figure S2). Suspended PMS particle concentrations were 17 ± 3 mg L^{-1}, 1 minute after particle addition, decreasing to values of 2-3 mg L^{-1} after 1 hour that remained constant during the remaining exposure time of 4 hours (Figure S2). In the quartz particles treatment, average concentrations were 24 ± 2 mg L^{-1}, 1 minute after particle addition, reaching values of 18 ± 3 mg L^{-1} after 2 hours and 15 ± 0.4 mg L^{-1} after 4 hours (Figure S2). Addition of PMS particles slightly changed the pH of aquaria by 0.2-0.6 units for the first 2-3 minutes but returned to "control" values after this short period, with no measurable changes in dissolved oxygen. Physical-chemical conditions for the experimental aquaria over the 27 days remained within the same range for all treatments (Table S2). Examination of particles under light and scanning electron microscopy showed that PMS particles had a more angular shape than quartz particles (Figure 1).

Measurements of metal content in seawater in the different experimental treatments showed increased concentration of trace elements (Co, Cu, Mn) released from the resuspension of PMS particles to the water column (Figure 2). Copper showed the highest concentration in seawater with values between 6.6 ± 1 µg L^{-1} in the

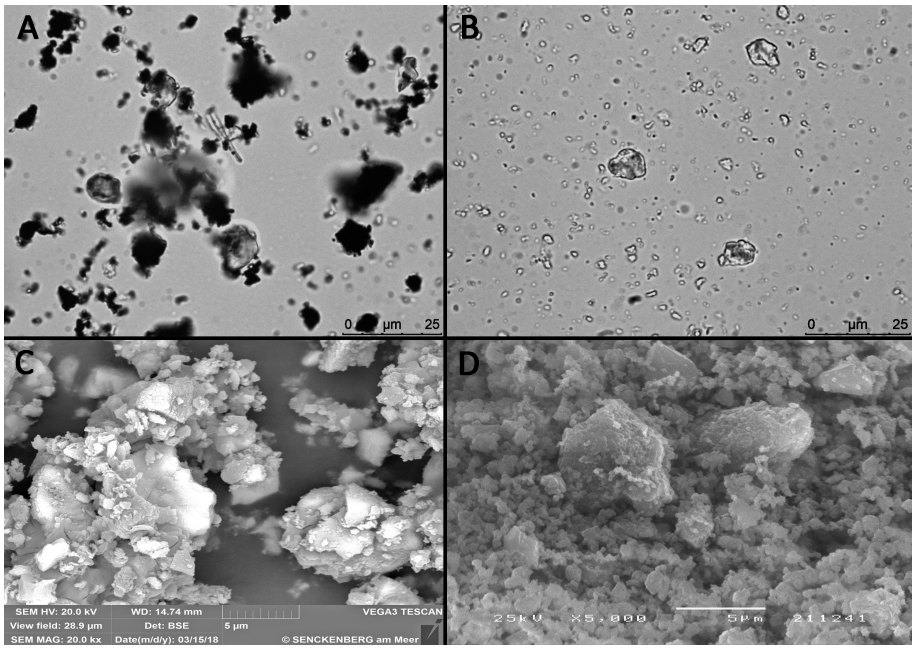

FIGURE 1
Light microscopy and scanning electron micrographs of the **(A, C)** polymetallic sulphide particles and **(B, D)** quartz particles used in the exposure experiment.

control and quartz treatments and 22 ± 8 µg L^{-1} in the PMS treatment. The concentration of Mn varied between 0.13 ± 0.05 µg L^{-1} for the control and quartz treatments and 0.26 ± 0.07 µg L^{-1} in the PMS treatment, while Co concentrations varied between 0.045 ± 0.008 µg L^{-1} in the control and quartz treatments and 0.26 ± 0.09 µg L^{-1} in the PMS treatment. The increased dissolved Co, Cu and Mn concentrations in the treatments with PMS were statistically higher than the control and quartz particle treatments (main PERMANOVA, all $P<0.05$; pairwise tests Co $t=6.36$-6.53, $p<0.05$; Cu $t=4.97$, $p<0.05$; Mn $t=3.40$-4.78, $p<0.05$, Table S3). These concentrations remained consistently higher in the PMS than in other treatments throughout the experiment, with no significant difference among sampling periods (PERMANOVA interaction term, $p_{(perm)}>0.05$, Table S3).

Tissue condition and survival

Although polyp extension behaviour of *D.* aff. *meteor* was not quantified, polyps were observed to be more fully extended in the control and quartz particles treatments than in the PMS particle treatment (Figure 3). Corals exposed to PMS particles experienced a progressive accumulation of PMS particles on *D.* aff. *meteor* fragments. Small PMS particles tended to form aggregates (Figure 1A) that appeared to coat the coral fragments covering first the coenenchyme surface with some polyps still visible during the first 3-5 days (Figure 3C) but later covering the polyps as well. Examination of coral fragments under light microscopy revealed very small PMS particles covering the polyps of coral fragments, suggesting high adherence of these particles to coral tissues and clogging of polyps (Figures 4A-C). Coral exposed to the quartz particles treatment experienced a general paling of their tissues through time of exposure in comparison with coral in the control treatment, whereas coral in the PMS treatment experienced a darkening and sloughing of the tissue through time, with visible portions of their skeletons in some fragments. Further examination of corals under scanning electron microscopy revealed undamaged tissues and polyps in the control and quartz particles treatments and what appeared as coral tissue degeneration in the PMS treatment (Figures 4D-F).

High mortality was observed in the corals exposed to PMS particles after 13 days (36%), 20 days (80%) and 25 days (95%). The experiment was terminated at time 27 days when all coral fragments were either sampled or dead. While no mortality was noted for *D.* aff. *meteor* exposed to inert particles until the end of the 27 days experiment, unexpected mortality was found for one control tank between days 8 and 13. This mortality was only found in this tank and identified as a result of a technical malfunction of the recirculating pump which decreased circulation of the incoming water leading to the observed coral mortality.

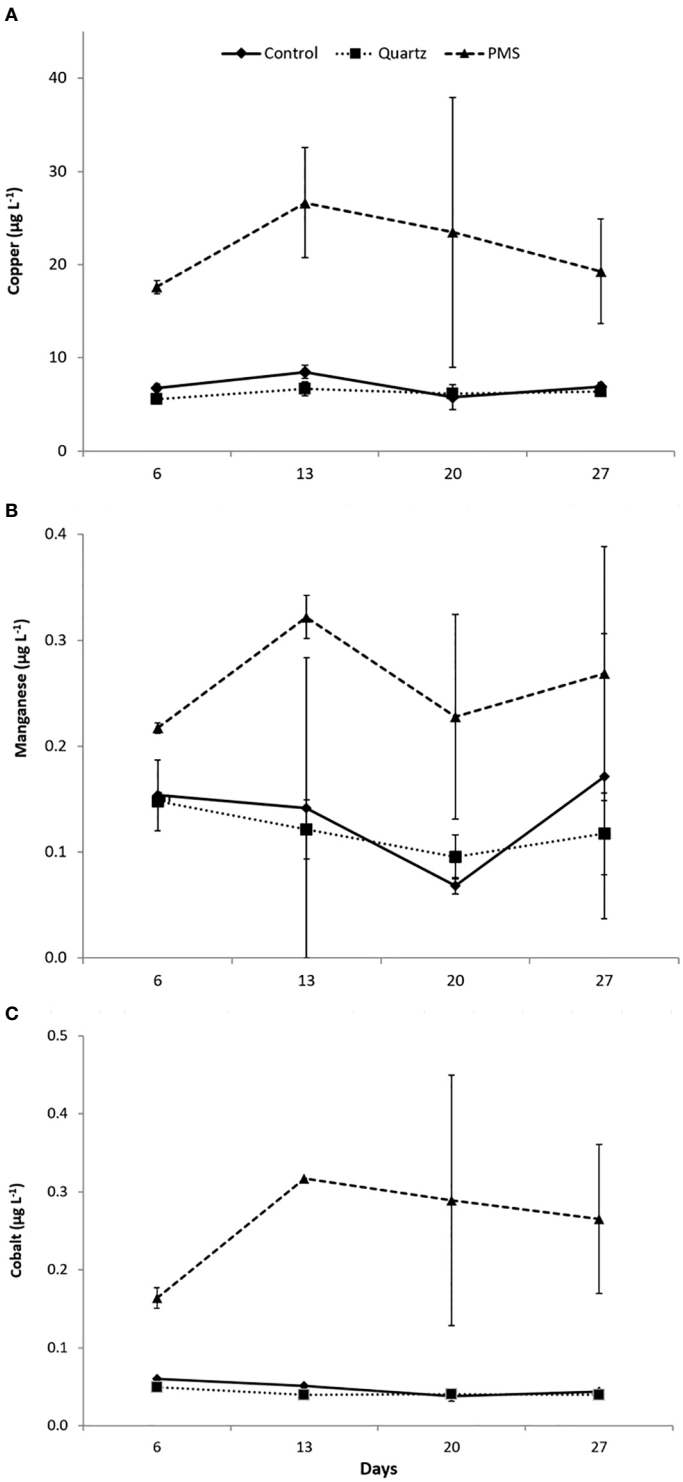

FIGURE 2
(A-C) Trace metal concentration in seawater in the treatments with polymetallic sulphide particles (PMS), with quartz particles (Quartz) and a control treatment with no sediment addition at times 6,13, 20 and 27 days of the experiment. N=2, data expressed as mean ± standard deviation.

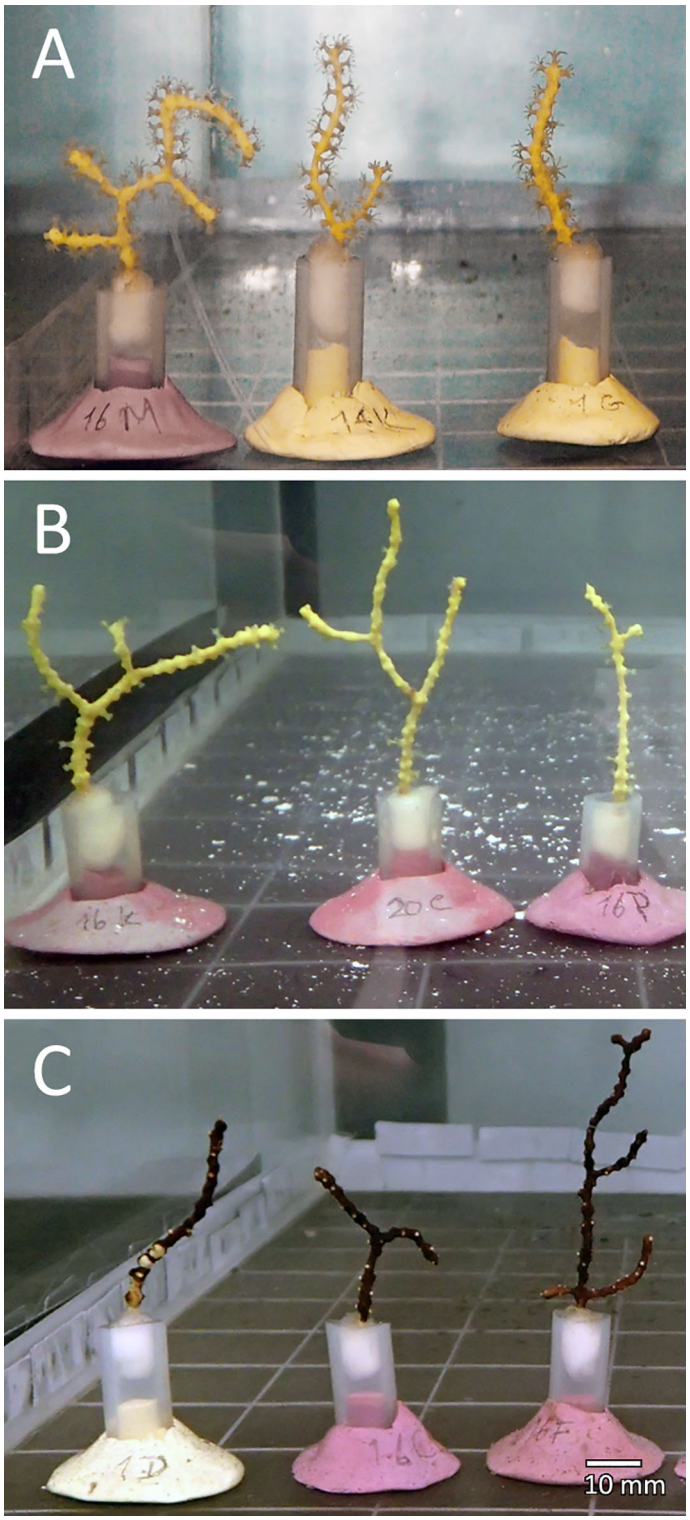

FIGURE 3
Dentomuricea aff. *meteor* fragments exposed to the different treatments **(A)** Control; **(B)** Quartz particles; and **(C)** Polymetallic sulphide particles, after 3 days of treatment exposure.

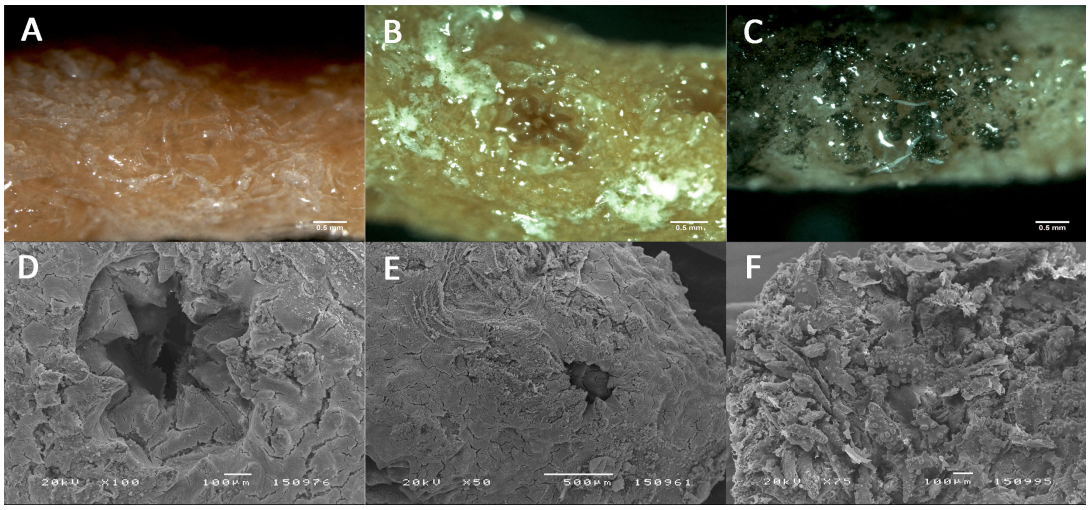

FIGURE 4
Tissue and polyps condition of *Dentomuricea* aff. *meteor* after 13 days exposure to the different treatments. **(A, D)** Control treatment; **(B, E)**; Quartz particle treatment; **(C, F)** Polymetallic sulphide treatment. Photographs A, B, C taken under the dissection microscope; photographs **(C-E)** taken under the scanning electron microscope.

Metal bioaccumulation

Similarly to what was found for the metal content in seawater in the different experimental treatments, Cu presented the highest concentrations in coral tissues exposed to PMS particles (main PERMANOVA, Pseudo-$F_{2,12}$ = 19.25, $p_{(perm)}$=0.0016, Figure 5A). Copper concentration in coral tissues after 25-27 days were 13 times higher in the PMS (274 ± 122 µg g^{-1}) than control and quartz treatments (22 ± 7 and 25 ± 8 µg g^{-1}, respectively) (pairwise tests, PMS-Control t=4.24, $p_{(mc)}$=0.0088, PMS-Quartz t=4.80, $p_{(mc)}$=0.0026). In addition, concentrations of Cu in coral skeletons (184 ± 112 µg g^{-1}) were 4 to 5 times greater than control and quartz particles treatments (55 ± 32 and 35 ± 12 µg g^{-1}, respectively) (PERMANOVA, pseudo-$F_{2,12}$ = 6.80, $p_{(perm)}$ =0.0016, pairwise tests, PMS-Control t=4.12, $p_{(mc)}$=0.028, PMS-Quartz t=4.64, $p_{(perm)}$=0.008). Concentrations of Mn in coral tissues and skeletons remained within similar levels in all treatments (range 0.7-2.2 for tissues and 0.08-0.76 µg g^{-1} for skeletons, main PERMANOVA coral tissue pseudo-$F_{2,12}$ = 0.23, $p_{(perm)}$=0.7989; coral skeleton pseudo-$F_{2,12}$ = 0.65, $p_{(perm)}$=0.5414, Figure 5B). Cobalt concentrations in coral tissues were comparable among treatments (range 0.8-1.9 µg g^{-1}, main PERMANOVA, pseudo-$F_{2,12}$ = 2.10, $p_{(perm)}$=0.1376, Figure 5C), but were significantly higher in coral skeletons of coral in the PMS treatment (0.60 ± 0.19 µg g^{-1}) when compared to the quartz treatment but not the control treatment (0.31 ± 0.09 and 0.33 ± 0.11 µg g^{-1}, respectively) (main PERMANOVA, pseudo-$F_{2,12}$ = 6.07, $p_{(perm)}$=0.02; pairwise test PMS-Quartz t=3.02, $p_{(mc)}$=0.0232, Table S3).

Coral Metabolism

Respiration and excretion rates

The permutational MANOVA revealed that responses of respiration rates to the treatments varied with experimental time (interaction term Pseudo-$F_{3,37}$ = 7.68, $p_{(perm)}$=0.002, Table S4). *D.* aff. *meteor* average respiration rates at time 0 (just prior to the start of the experiment) varied between 1.27 ± 0.31 µmol O_2 cm^2 coral surface area day^{-1} in the quartz treatment and 1.74 ± 0.89 µmol O_2 cm^{-2} coral surface area day^{-1} in the control treatment (Figure 6A), with no statistical differences between treatments (pairwise comparisons, t=0.65-1.23, $p_{(mc)}$>0.05). After 13 days of treatment exposure, respiration rates in the PMS particle treatment increased 2 times (2.98 ± 0.61 µmol O_2 cm^{-2} day^{-1}) in comparison to baseline values at time 0 (pairwise comparisons t=5.02, $p_{(perm)}$=0.009), while respiration rates in other treatments did not vary significantly between time 0 and 13 days (pairwise comparisons, t=0.27-0.40, $p_{(mc)}$>0.05). *Dentomuricea* aff. *meteor* respiration rates were 1.6 to 2 times higher in the PMS than the control and quartz particles treatments at this sampling time (pairwise comparisons PMS-Control t=3.95, $p_{(mc)}$=0.005; PMS-Quartz t=4.87, $p_{(perm)}$=0.002). No significant differences were found in *D.* aff. *meteor* respiration rates between the control and quartz particles treatments at the end of the experiment (pairwise comparison t=0.545, $p_{(mc)}$=0.603), while all *D.* aff. *meteor* used in the closed-chamber incubations had died in the PMS particle treatment by this sampling point.

Ammonium released by *D.* aff. *meteor* varied significantly between treatments depending on experimental time

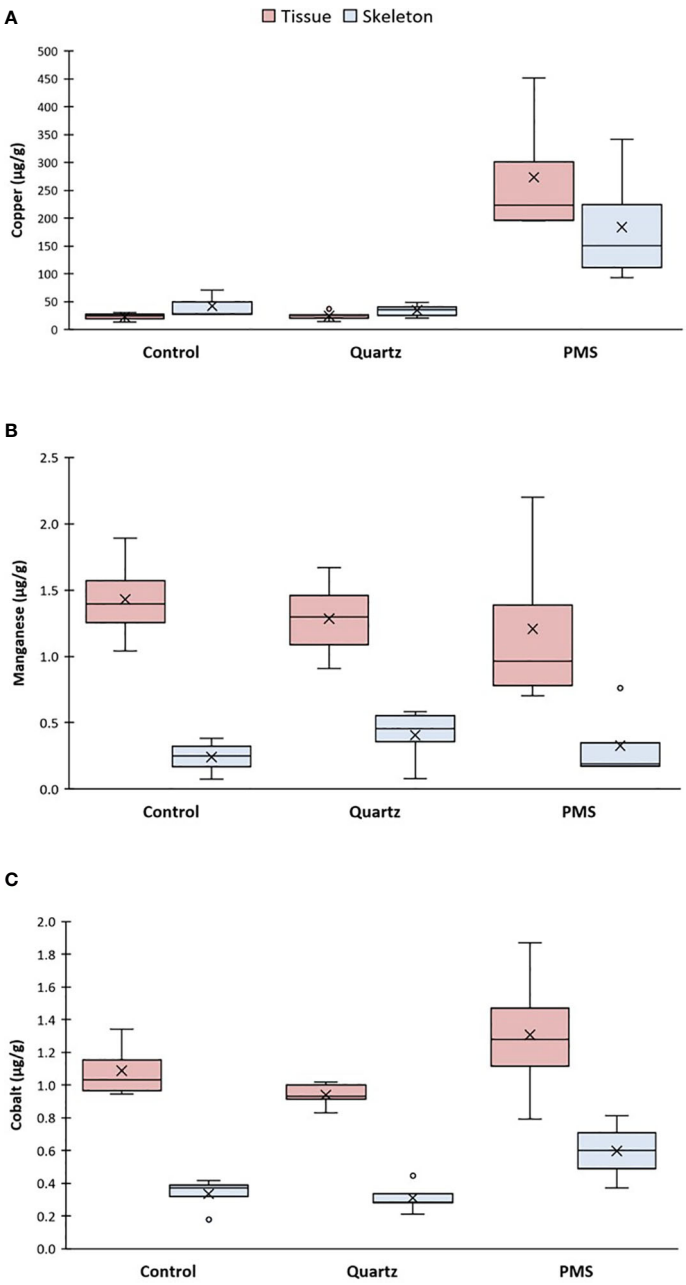

FIGURE 5
(A-C) Metal accumulation in tissue and skeleton fractions of *Dentomuricea* aff. *meteor* exposed to the treatments with polymetallic sulphide particles (PMS), with quartz particles (Quartz), and a control treatment with no sediment addition, at times 25-27 days for PMS and 27 days for control and quartz. N=4-5, data presented as μg^{-1} dry weight tissue or skeleton. The line in the box is the median, and the X is the mean. Whiskers represent the highest and lowest values and outliers are identified by a circle (○).

(PERMANOVA, interaction term Pseudo-$F_{2,38}$ = 3.10, $p_{(perm)}$= 0.0476, Table S4; Figure 6B). Ammonium excretion rates did not differ significantly between treatments at time 0, with recorded average excretion rates between 0.21 ± 0.14 and 0.36 ± 0.26 µmol cm^{-2} coral surface area day^{-1} in the quartz particles treatment and control treatment respectively (pairwise comparisons, t=0.70-1.21, p(mc)> 0.05). At time 13, ammonium excretion rates in the PMS treatment increased 2 times (0.56 ± 0.19 µmol cm^{-2} day^{-1}) in comparison to baseline values (T0) (0.27 ± 0.19 µmol cm^{-2} day^{-1}, pairwise comparison, t=2.69, $p_{(perm)}$=0.0456). Excretion rates at this time were 5 times greater in the PMS than the quartz treatment (0.11 ± 0.12 µmol cm^{-2} day^{-1})

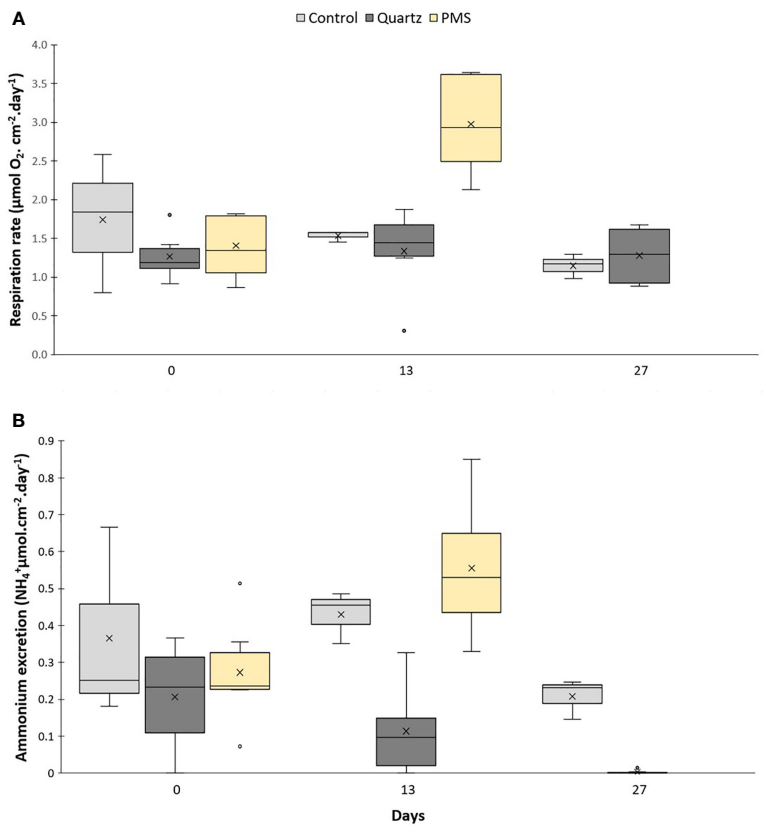

FIGURE 6
Physiological measurements on the cold-water octocoral *Dentomuricea* aff. *meteor*. **(A)** respiration and **(B)** ammonium excretion rates during the experiment (times 0, 13, 27) in treatments with polymetallic sulphide particles (PMS), with quartz particles (Quartz), and a control treatment with no sediment addition. Data normalized to coral surface area. N=3-6, no fragments in the PMS treatment at time 27 days. The line in the box is the median, and the X is the mean. Whiskers represent the highest and lowest values and outliers are identified by a circle (○).

(pairwise comparisons, t=4.83, $p_{(perm)}$=0.0027) but not significantly different in the PMS compared with the control treatment (0.43 ± 0.07 µmol cm^{-2} day^{-1}) (pairwise comparison, t=1.09, $p_{(perm)}$=0.3172). By the end of the experiment (day 27), ammonium excretion decreased in both the control and quartz treatments in comparison with day 13, with excretion rates in the latter treatment reaching significantly lower values than the control treatment (0.006 ± 0.007 and 0.21 ± 0.05 µmol cm^{-2} day^{-1}, respectively), (pairwise comparison, t=9.85, $p_{(mc)}$=0.0001). At this time, all *D.* aff. *meteor* used in the closed-chamber incubations had died in the PMS particle treatment.

Cellular stress biomarkers

The activity of the enzyme Glutathione S–transferase (GST) was not different among treatments but marginally increased between time 13 and 27 of the experiment in the quartz treatment (main PERMANOVA time factor pseudo-F=6.91, $p_{(perm)}$=0.0331; pairwise comparison t=2.55, $p_{(perm)}$=0.0513, Figures 7A). The activities of the enzymes superoxide dismutase (SOD) and catalase (CAT), and concentration of malondialdehyde (MDA) were not significantly different among treatments and sampling periods (main PERMANOVA pseudo-F=0.04-2.10, p>0.05, Table S5; Figures 7, 8). It was not possible to assess cellular response in corals exposed to PMS treatment at time 27 days due to their death.

Gene expression

During the first 13 days of the experiment, targeted genes were generally downregulated in relation to expression levels at time 0 (T0) just prior to the start of the experiment (relative fold change <1, Figure 9). However, by the end of the 27 days exposure, several genes involved in cellular stress (HSP70, ferritin), immune response (RHD, ferritin), antioxidant defense (SOD) and in cell cycle control (RP Tyr–PH) were upregulated in the quartz treatment in relation to T0 values (relative fold change >1, Figure 9). The genes encoding for

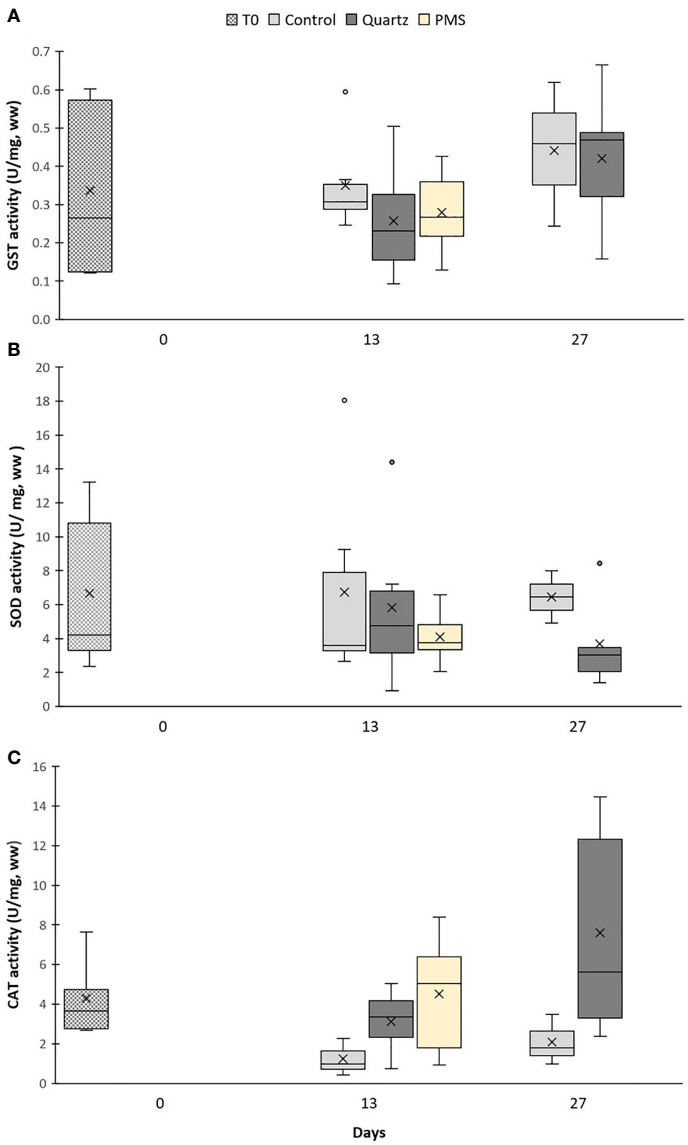

FIGURE 7
Enzyme activities of **(A)** Glutathione S–transferase (GST), **(B)** superoxide dismutase (SOD) and **(C)** catalase (CAT) in *Dentomuricea* aff. *meteor* tissues during the experiment (times 0, 13, 27) in treatments with polymetallic particles (PMS), with quartz particles (Quartz) and in the control treatments with no sediment addition. N=3-6, no fragments in the PMS treatment at T27. The line in the box is the median, and the X is the mean. Whiskers represent the highest and lowest values and outliers are identified by a circle (○).

ferritin, RP Tyr-PH and RHD were also upregulated in the control treatment by the end of the 27-days period. It was not possible to assess gene expression response in corals exposed to PMS treatment at time 27-days due to their death.

Discussion

Using a controlled aquaria experiment, we have observed how exposure to suspended polymetallic sulphide particles (PMS) from inactive chimney crushed rocks affected an important habitat-forming octocoral in the Azores, *Dentomuricea* aff. *meteor*. The two particles treatments, PMS and inert quartz particles, allowed us to explore the potential mechanical and toxicological effects of particles on corals. We attempted to mimic a dewatering sediment plume scenario that exposed corals to a PMS particle concentration of 25 mg L^{-1}. Nevertheless, due to the high density of PMS particles, a high proportion (92%), likely the larger size fraction, settled at the bottom of the aquaria, with only 2-3 mg L^{-1} of the smaller size

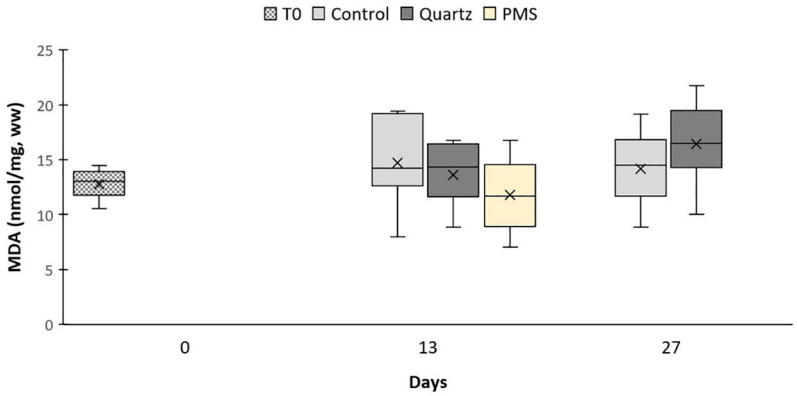

FIGURE 8
Concentrations of malondialdehyde (MDA) in *Dentomuricea* aff. *meteor* tissues during the experiment (times 0, 13, 27) in treatments with polymetallic particles (PMS), with quartz particles (Quartz) and in the control treatments with no sediment addition. N=3-6, no fragments in the PMS treatment at T27. The line in the box is the median, and the X is the mean. Whiskers represent the highest and lowest values and outliers are identified by a circle (○).

fraction remaining in suspension after 1 hour of particle addition. Quartz particles added to the experimental aquaria also partly settled at the bottom of the aquaria, but 60-70% (15-18 mg L^{-1}) remained in suspension during the exposure period.

Despite discrepancies between the target and achieved concentration of suspended particles, low suspended particles values (1.2-4 mg L^{-1}) are the most widespread concentrations projected by model simulations of the dispersal of PMS dewatering sediment plumes in Mid Atlantic Ridge around the Azores (Morato et al., 2022). Their simulations revealed that, while there are projected marked differences among sites, making generalizations of dewatering plume dispersal patterns difficult to make, the probability of having sediment plumes above 25 mg L^{-1} threshold (our initial concentration) would likely be restricted to a small area of about 0.6 km^2 around the discharge points. Instead, the dispersal of plumes with 2-3 mg L^{-1} (our achieved concentration) is predicted to reach an area from 25 to 150 km^2 (Morato et al., 2022). This suggests that our study truly simulated a scenario of particle emissions, where most of the particles settle close to the discharge point and only a small fraction travels to distant areas influencing other neighboring environments. Despite the low concentrations of PMS particles

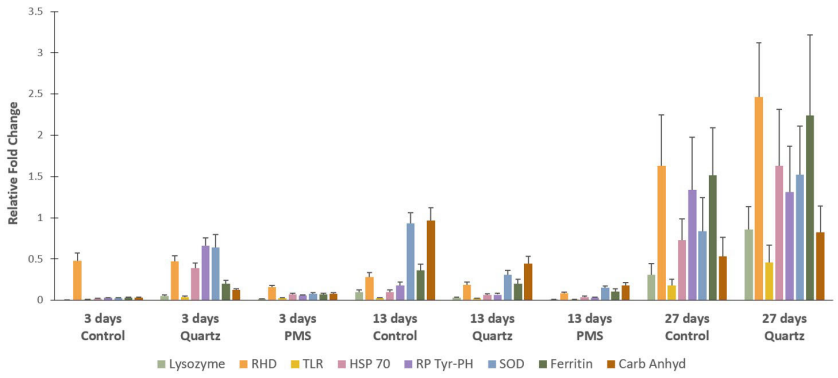

FIGURE 9
Relative gene expression of selected genes for the *Dentomuricea* aff. *meteor* during the experiment (times 3, 13, 27) in treatments with polymetallic particles (PMS), with quartz particles (Quartz) and in the control treatments with no sediment addition. Values are means of the relative gene expression normalized with the expression of two reference genes - 18S and β-actin - and relative to expression levels in T0, just prior to the start of the experiment. Expression levels (fold change) for the different target genes, Lysozyme, RHD (Rel Homology Domain), TLR (Toll-like receptor), HSP70 (heat shock protein 70), RP Tyr-PH (receptor-type protein tyrosine phosphatase), SOD (Superoxide Dismutase), Ferritin and Carb Anhy (alpha-carbonic anhydrase) are represented in different colour bars. Data expressed as mean ± standard error. Three technical replicates and n=6 for all treatments at times T3 and T13 days, n=2 for control treatment at T27, no fragments in the PMS treatment at T27.

in suspension, our results show that *D.* aff. *meteor* was very sensitive to resuspension of PMS particles, with the death of all coral fragments by the end of the 27-day exposure. Coral fragments exposed to suspended quartz particles also demonstrated physiological impairment but no coral mortality was found until the end of the experiment. The lethal and sublethal responses involved in these different results are discussed below.

Effect of particle exposure on coral behaviour and condition

The two types of particles used in the present study, PMS and quartz, differed in mineralogy, elemental composition and grain shape, which influenced the different responses of *D.* aff. *meteor* to the experimental treatments. Polymetallic sulphide particles had a more angular shape and were partly composed by toxic trace metals (mainly Cu), while quartz particles were rounder and did not contain metals. Corals exposed to PMS particles experienced a rapid accumulation of particles in their tissues, resulting in the reduction of polyp expansion behavior and feeding activity within only a few days (3-5 days) from the start of the experiment (Figure 3). This was followed by the progressive necrosis and loss of tissue, and death of all the corals fragments after 27 days in the PMS treatment. In contrast, even though some polyp retraction and tissue paling resulting from the deposition of quartz particles were also noticed in the treatment with quartz particles, polyps regularly opened in response to food and there was no coral mortality.

The differential responses of corals to different types of sediments have been reported in several studies with tropical and cold-water corals. Studies with tropical corals showed that sandy grain size fractions are rejected more effectively than nutrient-rich fine sediments (mud and silt-sized), possibly due to the greater stickiness (adhesion) of the latter (Fabricius and Wolansky (2000); Weber et al., 2006), with the accumulation of fine sediments ultimately resulting in the smothering and death of corals. The stickiness (adhesion) effect of barite has also been reported for *L. pertusa*, with particle accumulation in the dead portions of coral skeletons, whereas natural sediments were more easily removed (Larsson and Purser, 2011; Larsson et al., 2013). In the present study, the high adhesion of PMS particles to coral tissues likely hampered proper rejection of particles by *D.* aff. *meteor*, with the progressive "coating" of the coral fragments, while quartz particles were more easily rejected by the corals. Polyp retraction observed in *D.* aff. *meteor* may have conferred some protection to reduce the risk of sediment abrasion (Rogers, 1990; Erftemeijer et al., 2012), but the absence of substantial mucus production to actively reject particles, may have contributed to the rapid accumulation of PMS particles. Mucus has been shown to be important for the removal of drill cuttings in the scleractinian *L. pertusa* (Larsson and Purser, 2011; Larsson et al., 2013; Allers et al., 2013; Zetsche et al., 2016; Baussant et al., 2018; da Rocha et al., 2021) and in the alcyonacean *Primnoa resedaeformis* (Liefmann et al., 2018), reducing the risk of damage and particle accumulation on coral tissues. Thus, the different ability of corals to produce mucus could potentially lead to species-specific responses to mining impacts.

At the same time, based on SEM examinations, the sharp shape of the PMS appeared to cause degeneration or breakage of *D.* aff. *meteor* tissues (Figure 4). Injuries inflicted by sharp-edged mine tailings have also been observed in *Duva florida* and *P. resedaeformis* using histological analysis, while no damage was observed from smooth glass beads (Liefmann et al., 2018). Artic-boreal deep-water sponges were also found to be more sensitive to sharper drill cuttings (barite particles) than to natural occurring sediments (Kutti et al., 2015; Edge et al., 2016; Fang et al., 2018), with negative impacts likely resulting from a combination of the sharp characteristics and toxicity of barite particles (Edge et al., 2016).

Metal bioaccumulation

Exposure of *D.* aff. *meteor* to dissolved metals in the PMS treatment, resulting from the oxidation of sulphides in contact with seawater (Fallon et al., 2019), caused significant bioaccumulation of Cu in its tissues and skeletons (Figure 5). Trace metals can be mainly incorporated into corals by a combination of uptake of seawater-soluble metals and *via* polyp feeding (Ferrier-Pagès et al., 2005). Higher bioaccumulation of metals in tissues in comparison to skeletons, such as the ones observed here (274 ± 122 μg g^{-1} and 184 ± 112 μg g^{-1} of Cu in the tissues and skeleton, respectively) has been reported in several studies (e.g. Esslemont et al., 2000; Reichelt-Brushett and McOristb, 2003). This phenomenon has been explained by the primary incorporation of metals into tissues and subsequent transfer from the tissue to the skeleton (Harland and Brown, 1989; Ferrier-Pagès et al., 2005) and/or discrimination against metals in coral's biogenic precipitation of the skeleton (Reichelt-Brushett and McOristb, 2003).

Values of Cu recorded for corals exposed to PMS were several orders of magnitude higher than those recorded in tropical coral species in metal-polluted areas (1-63 μg.g^{-1}: Brown and Holley, 1982; Sabdono, 2009; Mohammed and Dar, 2010; Ali et al., 2011; Berry et al., 2013), and corals experimentally exposed to copper (Bielmyer et al., 2010; Chan et al., 2012; Siddiqui and Bielmyer-Fraser, 2015). Mucus production by cnidarians has been described as an important response to prevent metal uptake in corals exposed to Cu (Reichelt and Jones, 1994; Mitchelmore et al., 2003; Mitchelmore et al., 2007). The lack of substantial mucus production generally observed for the species *D.* aff. *meteor*

may explain the extensive accumulation of Cu in coral tissues and skeletons under PMS particle exposure. However, it should be noted that although care was taken to remove PMS particles attached to coral tissue, it is possible that very small particles remained attached and may have contributed to the high Cu concentrations reported in coral tissues.

Copper concentrations in *D.* aff. *meteor* under control and quartz conditions (22 ± 7 and 25 ± 8 μg g^{-1} respectively), although up to 10 times lower than those recorded in the PMS treatment, were higher than concentrations recorded as baseline values for this species in the Azores region (2.4-4.3 μg.g^{-1}, Raimundo et al., 2013). However, Raimundo et al. (2013) reported Cu concentrations for the whole individual, whereas in the present study trace metals were analyzed in tissue and skeleton, separately. These differences may also be associated with the collection site of the corals, reflecting a natural input of this element, presumably from hydrothermal origin.

Effect of particle exposure on coral metabolism

Physiological impacts of PMS particles were noted by the significant increase in respiration (a proxy of basal metabolism) and ammonium excretion rates after 13 days of coral exposure to PMS particles, in comparison with other treatments (Figure 6). Previous studies on the effects of suspended particles on corals reported differing effects on respiration rates. Increased respiration has been related to increased polyp activity or increased mucus production in shallow-water scleractinian corals and the deep-water octocoral *P. resedaeformis* (Abdel-Salam et al., 1988; Telesnicki and Goldberg, 1995; Scanes et al., 2018). Reduced respiration rates have been related to reduced polyp activity or to tissue loss in other shallow-water scleractinian and alcyonacean corals (Riegl and Branch, 1995; Riegl and Bloomer, 1995). In contrast, no significant effects of drill cuttings on respiration were reported for *L. pertusa* (Larsson et al., 2013; Baussant et al., 2018), suggesting physiological resilience of this species to drill cutting exposure.

In our study, increased respiration cannot be explained by increased polyp activity or increased energetic costs of mucus production. It could, instead, reflect physiological stress to the toxicity of Cu that bioaccumulate in coral tissues and to the mechanical injury caused by particles, as exposure to metals, such as Cu, may increase energy costs for detoxification, cellular protection and repair (Rainbow, 2002). Increased respiration rates in response to Cu toxicity have been previously recorded for the coral reef symbiont bearing foraminifer *Amphistegina gibbosa* (Marques et al., 2020) and recently for the the octocoral *Viminella flagellum* in the Azores (Martins et al., 2022). Other studies, however, showed that Cu may compromise energy production by inhibiting energy metabolism enzymes in tropical corals (Fonseca et al., 2019; Fonseca et al., 2021). Contrasting responses to Cu in these studies may reflect inter-specific variability. However, it should be noted that it was not possible to remove PMS particles encrusted in tissues of coral used in respiration incubations. Therefore, we cannot rule out the possibility that increased oxygen consumption could also resulted from increased activity of microorganisms associated with PMS particles or oxidation of redox-sensitive elements in particles.

Animals produce ammonia mainly as a byproduct of the catabolism of protein and amino acids (Baldwin, 1964). Carbon –rich lipids and carbohydrates are the main general sources of energy used by organisms, and nitrogen-rich proteins will only be used when lipids and carbohydrates (glycogen reserves) are exhausted, resulting in increased nitrogen excretion (Gabbott, 1983). Therefore, the 2-5 fold increase ammonium excretion in corals exposed to PMS particles after 13 days exposure, could signal a transition from carbohydrate and lipid reserves to the catabolism of tissue proteins (Baldwin, 1964). Ammonia excretion rate varies with the nutritional state of the individual (Baldwin, 1964) and has been reported to increase with starvation in echinoderms and molluscs (Diehl and Lawrence, 1979; Okumura et al., 2002). Although we did not measure feeding rates in the present study, coral polyps under the PMS treatment were clogged with particles (Figure 4C), preventing corals from feeding, possibly requiring the use of proteins in body tissue of *D.* aff. *meteor* for energy production. Disturbances to energy metabolism under conditions of metal exposure have been reported for coastal and deep-sea mussels (Canesi et al., 2007; Zhou et al., 2021), with organisms enhancing their energy requirements by utilizing existing carbohydrate reserves to counteract the toxicity posed by metals (Canesi et al., 2007). In the present study, the increased ammonia excretion in *D.* aff. *meteor* tissues may indicate a disturbance in energy metabolism induced by Cu toxicity.

Cellular effects to particle exposure

The potential effects of metals accumulated in coral tissues were evaluated through cellular stress biomarkers and gene expression profiles. Copper is required at trace concentrations for many cellular processes and physiological functions as cofactors of enzymes (Rainbow, 2002). However, Cu concentrations above ambient concentrations have been reported to cause physiological impairment in corals and other cnidarians (Bielmyer et al., 2010; Marangoni et al., 2017; Fonseca et al., 2019). At the cellular level, excess in Cu has been shown to cause oxidative stress through the generation of oxygen reactive species (ROS) and subsequent damages to cells (Mitchelmore et al., 2007; Schwarz et al., 2013; Siddiqui and Bielmyer-Fraser, 2015). Thus, the examination of antioxidant enzymes such as superoxide dismutase (SOD), catalase (CAT) and glutathione peroxidase (GPx) used to neutralize the harmful effects of ROS (Lushchak, 2011), provides a useful diagnosis to detect physiological effects of metals on corals (Downs et al., 2012).

Our study showed that the increase in Cu concentration in coral tissues was not followed by significant changes in anti-oxidant stress enzyme activities (GST, SOD and CAT) in the PMS particles treatment (Figure 7). In addition, gene expression of enzymes involved in cellular stress (HSP), antioxidant (SOD), and immune defense (ferritin, RHD, TLR) in corals exposed to PMS were generally downregulated in relation to expression levels just prior to the start of the experiment (T0) (Figure 9). This suggests a general physiological reaction marked by the inhibition of the cellular stress response of *D.* aff. *meteor* caused by exposure to PMS particles. This inhibitory response was rather fast during the course of the experiment, to an extent which toxic metals exposure may have caused a systemic damage to the whole organism, leading to mortality after 4 weeks.

Studies with marine invertebrates showed that while exposure to metals generally activates the enzymatic antioxidant defense system, excessive levels of ROS induced by copper toxicity can promote enzymatic inactivation when cellular defenses are unable to maintain the oxidant-antioxidant balance (Regoli and Giuliani, 2014; Zhou et al., 2021). Moreover, excessive presence of ROS may directly affect the signal transduction pathways regulating the transcriptional activity of antioxidant and immunity genes to an extent where the cellular integrity is no longer maintained (Rhee et al., 2013), and the molecular mechanisms of copper immunotoxicity seriously compromises the animal survival (Nguyen et al., 2018).

In contrast to coral response to PMS particles, corals exposed to quartz particles displayed an increasing trend, although not statistically significant, in CAT activity in relation to control levels by the end of the experimental period (Figure 7). This response was also accompanied by lipid peroxidation, as indicated by slightly higher MDA concentrations in this treatment (Figure 8). Lipid peroxidation generally indicates that levels of ROS are overwhelming the antioxidant pathways, accumulating and damaging cellular membrane lipids, thus indicating ongoing oxidative stress (Lesser, 2006). Therefore, the general loss of tissue condition (paling and thinning of tissue) observed in the quartz treatment could reflect this cellular response. The upregulation of genes involved in cellular stress (HSP70) and in immune response (Ferritin and RDH) could also reflect the worsened coral condition during exposure to quartz particles (Figure 9). Although the oxidative stress response to sedimentation exposures, or increased suspended particles, has seldom been studied, a similar response of oxidative stress (CAT increase) has recently been reported for the tropical scleractinian coral species *Porites astreoides* from South Florida coral reefs, in response to experimental exposure to sediments (Rushmore et al., 2021).

Mechanical vs. toxicological effects of polymetallic sulphide particles

The present study included two particles treatments, PMS and inert quartz particles, to distinguish potential toxicological and mechanical effects of PMS particles. Our results showed that PMS particles induced physiological changes in the energy metabolism of *D.* aff. *meteor*, while changes in the cellular stress biomarkers and gene expression profiles were more pronounced in corals exposed to quartz particles. This suggests that the mechanical effect of quartz particles, although not causing measurable changes in the physiological functions of the coral over the 4 weeks experiment, can still elicit cellular stress and immune responses, possibly as a reaction to the particle abrasive effect on coral tissues. These cellular responses together with other observed sub-lethal effects, such as loss of tissue coloration and a progressive reduction in polyp activity towards the end of the experiment, indicate an increasing decline of coral health to exposure to quartz particles that could be potentially damaging beyond the experimental period.

Although it is not clear why a rapid death of *D.* aff. *meteor* was observed upon PMS particles exposure, a probable mechanistic explanation may rely on the combined and potentially synergistic mechanical and toxicological effects of these particles. Previous studies on the lethal and sub-lethal toxicological effects of Cu added to *D.* aff. *meteor* in dissolved form (Martins et al., 2018) revealed that dissolved concentrations twice as high as to the ones recorded in the PMS treatment (60 μg. L^{-1}), did not cause death, in spite of the inflicted physiological stress. Thus, it is plausible that *D.* aff. *meteor* death in our experiment may have resulted from a combination of factors and not solely from the exposure of high Cu levels.

While metal toxicity may have contributed to the physiological changes in the energy metabolism by increasing the energy costs for detoxification and protection (Rainbow, 2002), the high adhesion of PMS particles to coral tissues also likely contributed to the reported metabolic responses. PMS particles coated the polyps and coenenchyme surface, preventing the coral from extending its polyps and feeding, which over time resulted in changes in energy metabolism and ultimately in the smothering and death of coral tissue. At the same time, the angular shape of PMS particles inflicted injuries on coral tissues further contributed to tissue degeneration and necrosis. As reported for tropical corals, tissue damage from sediment particles might leave the corals vulnerable to bacterial attack and subsequent tissue necrosis (Harvell et al., 2007).

One potential additional cause for the rapid tissue deterioration and death in the PMS particles that was not examined in the present study is the possibility that the accumulation of PMS particles at the coral tissue surface might have created a sulphur-rich micro-environment favorable to bacteria growth. The presence of bacteria was detected by scanning electron microscopy examination of coral tissues in the PMS treatment (M Carreiro-Silva, unpublished data). A similar situation has been reported for tropical coral exposed to high sediments enriched with organic matter (Weber

et al., 2012) and the cold-water coral *L. pertusa* exposed to sediments from Tisler reef (Allers et al., 2013). In both these cases, sediment coverage gradually decreased oxygen at the coral surface with release of hydrogen sulphide, presumably by sulfate-reducing microbial communities associated to sediments. Weber et al. (2012) showed how the organic matter in the sediments triggered microbial decomposition of coral tissues and mucus, with concomitant release of hydrogen sulfide that diffused to neighboring tissues leading to their damage and death. In the present case, the sulphur in the PMS particles might have directly induced bacteria growth. Hydrogen sulfide concentration can be highly toxic to corals leading to tissue damage and increased mortality (Bagarinao, 1992).

Future studies using microsensors to closely monitor changes in oxygen, pH and hydrogen sulphide at the surface of the coral following PMS particle coverage may elucidate whether the rapid death of corals under PMS exposure was microbial-mediated (Weber et al., 2012).

Management considerations

Deep-sea mining is listed as one of the major potential stressors on the marine environment (Jones et al., 2019). Contrary to other ocean-based industries such as oil and gas, that have decades of implementation, the deep-sea mining industry is only now developing protocols for good practice to reduce environmental hazards (Jones et al., 2019). However, establishing environmental management approaches for the deep-sea mining industry is challenged by the limited knowledge on the biology of deep-sea organisms, and the little information on the effects of deep-sea mining activities upon them. As such, experimental studies testing the physical and ecotoxicological effects of deep-sea mining on key benthic ecosystems are important to inform environmental planning and impact assessments aiming to avoid and minimize the impact created by the sediment plume on this type of organisms. The slow recovery capacity of deep-sea organisms to human impacts, related to their slow-growing and long-lived life histories, further emphasizes the need to avoid and minimize the impacts of mining activities on deep-sea ecosystems.

Our results show how relatively low concentrations of suspended small PMS particles can impair the physiology of cold-water octocorals, ultimately resulting in their death within a short period of time. The small size fraction of PMS particles is likely to stay in suspension for long periods of time and disperse further away from the emission point, potentially impacting fauna in the flanks and summits of close topographic features (Morato et al., 2022). The ecological consequences of these impacts may include loss of biodiversity, ecosystem functioning and the provision of goods and services by deep-sea ecosystems (Boschen et al., 2016; Le et al., 2017; Van Dover et al., 2017; Niner et al., 2018; Orcutt et al., 2020; Boschen-Rose et al., 2021).

These results highlight the need for a detailed understanding of both the mining plume dispersal and the physiological response of organisms to those plumes in the early phases of the mining project. These are key information that needs to be incorporated in the Environmental Risk Assessments and Environmental Management and Monitoring plans for the mining activities. These results also call the industry for the development of tools to monitor and minimize the creation and dispersal of particles and plume at the impact reference zones and preservation reference zones. The presented results also call the regulators of the paramount importance to implement effective area-based management tools such non-mining areas or marine protected areas (Durden et al., 2017; Jones et al., 2019; Clark et al., 2020), for the protection of cold-water coral ecosystems.

Data availability statement

The raw data supporting the conclusions of this study are available at PANGAEA (Carreiro-Silva et al., 2022: https://doi.pangaea.de/10.1594/PANGAEA.948414).

Author contributions

Conceived and designed experiment: MC-S, IM, VR, AC. Performed experiment: MC-S, VR, IM Processed the samples: MC-S, AG, IM, JR, MC, MR, RB, VR. Analyzed data: MC-S, IM, JR, MC, MR, TC, RB. All authors contributed to the writing of the paper. All authors contributed to the article and approved the submitted version.

Funding

The research leading to these results has received funding from the European Union Seventh Framework Programme (FP7/2007-2013) under the MIDAS project (grant agreement n° 603418) the European Union's Horizon 2020 programme under grant agreements No 678760 (ATLAS) and No 818123 (iAtlantic), by Fundação para a Ciência e a Tecnologia, I.P. (FCT) and Direção-Geral de Política do Mar (DGPM) project Mining2/0005/2017. We also acknowledge funds and support from the FCT through the strategic project (UIDB/05634/2020 and UIDP/05634/2020) granted to OKEANOS and through the FCT Regional Government of the Azores under the project M1.1.A/REEQ.CIENTÍFICO UI&D/2021/010. This output reflects only the authors' views and the European Union and the Regional Government of the Azores cannot be held responsible for any use that may be made of the information contained therein. AC, MCS and TM were supported by Program Stimulus of Scientific

Employment (CEECIND/00101/2021, CCCIND/03346/2020 and CCCIND/03345/2020, respectively) from the Fundação para a Ciência e Tecnologia, AC, IM and RB were funded by Projeto Investigadores Mar AZ PO Açores 2020 (ACORES 01 0145 FEDER 000140), TC was supported by FRCT fellowship (M3.1.a/F/016/2018). AG and MR were supported by the H2020 iAtlantic project (Grant Agreement No 818123). MCS was also supported by EU FP7 project MORPH (EC/ICT/2011/7/288704). TM was also supported by Program Investigador FCT (IF/01194/2013), IFCT Exploratory Project (IF/01194/2013/CP1199/CT0002) from the Fundação para a Ciência e Tecnologia (POPH and QREN) and PO2020 MapGES. (Acores-01-0145-FEDER-000056). MC and JR acknowledge the strategic project UIDB/04423/2020 granted to CIIMAR and to the JPIOceans project MiningImpact2-Mining2/0004/2017 funded by the Portuguese FCT.

Acknowledgments

We would like to thank the captain and chief scientist of the MoMARSAT 2013 cruise (https://doi.org/10.17600/13030040) for the recovery of the inactive sulfide blocks as well as the ROV *Victor6000* team. We acknowledge V. Lopes, C. Mourão and J.M.R.S. Relvas at the Geology department, Faculdade de Ciências Universidade de Lisboa (FCUL), Portugal for the preparation and granulometry analysis of the PMS particles and Sven Petersen at GEOMAR Helmholtz Centre for Ocean Research for the EDAX analyses of the grounded material. We also acknowledge Telmo Nunes at FCUL for scanning electron microscopy of quartz particles and Max Wisshak at the Senckenberg am Meer, Marine Research Department, Germany for scanning electron microscopy of polymetallic sulphide particles. We are grateful to the crew of RV Águas Vivas and Renato Bettencourt for the collection of coral colonies. We are also grateful to Noelie Reydet, Kristell de Potter and Hugo Parra for their help with the maintenance of corals in aquaria and monitoring of the experiment.

Conflict of interest

The authors declare that the research was conducted in the absence of any commercial or financial relationships that could be construed as a potential conflict of interest.

Publisher's note

Supplementary material

The Supplementary Material for this article can be found online at: https://www.frontiersin.org/articles/10.3389/fmars.2022.915650/full#supplementary-material

References

Abdel-Salam, H. A., Porter, J. W., and Hatcher, B. G. (1988). ""Physiological effects of sediment rejection on photosynthesis and respiration in three Caribbean reef corals,"," in *Proccedings of the 6th international coral reef symposium*, eds J. H. Choat, D. Barnes, M. A. Borowitzka, J. C. Coll, P. J. Davies, P. Flood, et al, Townsville (Australia), Vol. 2. , 285–292.

Addamo, A. M., Vertino, A., Stolarski, J., García-Jiménez, R., Taviani, M., and Machordom, A. (2016). Merging scleractinian genera: The overwhelming genetic similarity between solitary *Desmophyllum* and colonial *Lophelia*. *BMC Evol. Biol.* 16 (1), 108. doi: 10.1186/s12862-016-0654-8

Ali, A. A. M., Hamed, M. A., and El-Azim, H. A. (2011). Heavy metals distribution in the coral reef ecosystems of the northern red Sea. *Helgol. Mar. Res.* 65, 67–80. doi: 10.1007/s10152-010-0202-7

Allers, E., Abed, R. M., Wehrmann, L. M., Wang, T., Larsson, A. I., Purser, A., et al. (2013). Resistance of *Lophelia pertusa* to coverage by sediment and petroleum drill cuttings. *Mar. Poll. Bull.* 74, 132–140. doi: 10.1016/j.marpolbul.2013.07.016

Anderson, M. J., Gorley, R. N., and Clarke, K. R. (2008). *PERMANOVA+ for PRIMER: Guide for software and statistical methods* (PRIMER-E: Plymouth, UK.).

Anderson, M. J., and Robinson, J. (2003). Generalized discriminant analysis based on distances. *Aust. N. Z. J. Stat.* 45 (3), 301–318. doi: 10.1111/1467-842X.00285

ASA (2008). ""Modelling the dispersion of the returned water discharge plume from the solwara 1 seafloor mining project,"," in *Coffey Natural system 2008* (Papua New Guinea: Environmental Impact Statement: Solwara 1 Project, Volume B. Nautilus Minerals Niugini Limited). Available at: https://www.yumpu.com/en/document/read/12085050/appendices-5-13-nautilus-cares-nautilus-minerals.

Bagarinao, T. (1992). Sulfide as an environmental factor and toxicant: tolerance and adaptations in aquatic organisms. *Aquat. Toxicol.* 24, 21–62. doi: 10.1016/0166-445X(92)90015-F

Baldwin, E. (1964). *An introduction to comparative biochemistry. 4th edition* (Cambridge, England: Cambridge University Press).

Baussant, T., Nilsen, M., Ravagnan, E., Westerlund, S., and Ramanand, S. (2018). Effects of suspended drill cuttings on the coral *Lophelia pertusa* using pulsed and continuous exposure scenarios. *J. Toxicol. Environ. Health Part A.* 81 (10), 361–382. doi: 10.1080/15287394.2018.1444375

Beers, R. F., and Sizer, I. W. (1952). A spectrophotometric method for measuring the breakdown of hydrogen peroxide by catalase. *J. Biol. Chem.* 195, 133–140. doi: 10.1016/S0021-9258(19)50881-X

Bell, T. G., Johnson, M. T., Jickells, T. D., and Liss, P. S. (2007). Ammonia/ammonium dissociation coefficient in seawater: a significant numerical correction. *Environ. Chem.* 4, 183–258. doi: 10.1071/EN07032

Berry, K. L., Seemann, J., Dellwig, O., Struck, U., Wild, C., and Leinfelder, R. R. (2013). Sources and spatial distribution of heavy metals in scleractinian coral tissues and sediments from the bocas del toro archipelago, Panama. *Environ. Monit. Assess.* 185, 9089–9099. doi: 10.1007/s10661-013-3238-8

Bersuder, P., Amouroux, I., Belzunce-Segarra, M. J., Bolam, T., Caetano, M., Carvalho, I., et al. (2021). Concurrent sampling of transitional and coastal waters by diffusive gradient in thin-films (DGT) and spot sampling for trace metals analysis. *MethodX* 8, 101462. doi: 10.1016/j.mex.2021.101462

Bielmyer, G. K., Gillette, P., Grosell, M., Bhagooli, R., Baker, A. C., Langdon, C., et al. (2010). Effects of copper exposure on three species of scleractinian corals. *Aquat. Toxicol.* 97, 125–133. doi: 10.1016/j.aquatox.2009.12.021

Blandin, J., Sarradin, P.-M., and Cannat, M. (2013). MOMARSAT2013 cruise, RV pourquoi pas? *French Oceanographic Cruises*, available at: https://campagnes.flotteoceanographique.fr/campagnes/13030040/

Boschen-Rose, R. E., Clark, M. R., Rowden, A. A., and Gardner, J. P. (2021). Assessing the ecological risk to deep-sea megafaunal assemblages from seafloor massive sulfide mining using a functional traits sensitivity approach. *Ocean Coast. Manage.* 210, 105656. doi: 10.1016/j.ocecoaman.2021.105656

Boschen, R. E., Rowden, A. A., Clark, M. R., and Gardner, J. P. (2013). Mining of deep-sea seafloor massive sulfides: a review of the deposits, their benthic communities, impacts from mining, regulatory frameworks and management strategies. *Ocean Coast. Manage.* 84, 54–67. doi: 10.1016/j.ocecoaman.2013.07.005

Boschen, R. E., Rowden, A. A., Clark, M. R., Pallentin, A., and Gardner, J. P. A. (2016). Seafloor massive sulfide deposits support unique megafaunal assemblages: implications for seabed mining and conservation. *Mar. Environ. Res.* 115, 78–88. doi: 10.1016/j.marenvres.2016.02.005

Bradford, M. M. (1976). Rapid and sensitive method for quantification of microgram quantities of protein utilizing principle of protein-dye binding. *Anal. Biochem.* 72, 248–254. doi: 10.1016/0003-2697(76)90527-3

Braga-Henriques, A., Porteiro, F. M., Ribeiro, P. A., De Matos, V., Sampaio, Í., Ocaña, O., et al. (2013). Diversity, distribution and spatial structure of the cold-water coral fauna of the Azores (NE Atlantic). *Biogeosciences* 10, 4009–4036. doi: 10.5194/bg-10-4009-2013

Brooke, S. D., Holmes, M. W., and Young, C. M. (2009). Sediment tolerance of two different morphotyopes of the deep-sea coral *Lophelia pertusa* from the gulf of Mexico. *Mar. Ecol. Prog. Ser.* 390, 137–144. doi: 10.3354/meps08191

Brown, B., and Holley, M. C. (1982). Metal levels associated with tin dredging and smelting and their effect upon intertidal reef flats at ko phuket, Thailand. *Coral Reefs* 1, 131–137. doi: 10.1007/BF00301695

Canesi, L., Ciacci, C., Lorusso, L. C., Betti, M., Gallo, G., Pojana, G., et al. (2007). Effects of triclosan on *Mytilus galloprovincialis* hemocyte function and digestive gland enzyme activities: possible modes of action on non target organisms. *Comp. Biochem. Phys. C.* 145, 464–472. doi: 10.1016/j.cbpc.2007.02.002

Carreiro-Silva, M., Cerqueira, T., Godinho, A., Caetano, M., Santos, R. S., and Bettencourt, R. (2014). Molecular mechanisms underlying the physiological response of the cold-water coral *Desmophyllum dianthus* to ocean acidification. *Coral Reefs* 33, 465–476. doi: 10.1007/s00338-014-1129-2

Carreiro-Silva, M., Ocaña, O. V., Stanković, D., Sampaio, I., Porteiro, F., Fabri, M.-C., et al. (2017). Zoanthids associated with cold-water corals in the Azores region: hidden diversity in the deep-sea. *Front. Mar. Sci.* 4. doi: 10.3389/fmars.2017.00088

Carreiro-Silva, M., Martins, I., Raimundo, J., Caetano, M., Bettencourt, R., Cerqueira, T., et al. (2022). Results of an ex-situ experiment testing the effects of mining-generated sediment plumes on the cold-water octocoral *Dentomuricea* aff. *meteor* in the Azores. *PANGAEA*. doi: 10.1594/PANGAEA.948414

Chan, I., Tseng, L. C., Kâ, S., Chang, C. F., and Hwang, J. S. (2012). An experimental study of the response of the gorgonian coral *Subergorgia suberosa* to polluted seawater from a former coastal mining site in Taiwan. *Zool. Stud.* 51 (1), 27–37. available at: http://zoolstud.sinica.edu.tw/Journals/51.1/27.pdf

Christiansen, B., Denda, A., and Christiansen, S. (2020). Potential effects of deep seabed mining on pelagic and benthopelagic biota. *Mar. Pol.* 114, 103442. doi: 10.1016/j.marpol.2019.02.014

Clark, M. R., Bowden, D. A., Rowden, A. A., and Stewart, R. (2019). Little evidence of benthic community resilience to bottom trawling on seamounts after 15 years. *Front. Mar. Sci.* 6. doi: 10.3389/fmars.2019.00063

Clark, M. R., Durden, J. M., and Christiansen, S. (2020). Environmental impact assessments for deep-sea mining: Can we improve their future effectiveness? *Mar. Pol.* 114, 103363. doi: 10.1016/j.marpol.2018.11.026

da Rocha, I. V., Reis, E. C., da Silva, P. R., de Hollanda Cavalcanti, G., Coutinho, R., and Reynier, M. V. (2021). Deep-sea coral *Lophelia pertusa* laboratory maintenance and exposure to barite using water recirculation systems. *Toxicol. Environ. Health Sci.* 13 (1), 1–17. doi: 10.5897/JTEHS2021.0486

Diehl, W. J.III, and Lawrence, J. M. (1979). Effect of nutrition on the excretion rate of soluble nitrogenous products of *Luidia clathrata* (Say) (Echinodermata; asteroidea). *Comp. Biochem. Physiol.* 62 (4), 801–806. doi: 10.1016/0300-9629(79)90006-9

Downs, C. A., Fauth, J. E., Robinson, C. E., Curry, R., Lanzendorf, B., Halas, J. C., et al. (2005). Cellular diagnostics and coral health: declining coral health in the Florida Keys. *Mar. Poll. Bull.* 51 (5-7), 558–569. doi: 10.1016/j.marpolbul.2005.04.017

Downs, C. A., Ostrander, G. K., Rougee, L., Rongo, T., Knutson, S., Williams, D. E., et al. (2012). The use of cellular diagnostics for identifying sub-lethal stress in reef corals. *Ecotoxicology* 21 (3), 768–782. doi: 10.1007/s10646-011-0837-4

Durden, J. M., Murphy, K., Jaeckel, A., Van Dover, C. L., Christiansen, S., Gjerde, K., et al. (2017). A procedural framework for robust environmental management of deep-sea mining projects using a conceptual model. *Mar. Pol.* 84, 193–201. doi: 10.1016/j.marpol.2017.07.002

Edge, K. J., Johnston, E. L., Dafforn, K. A., Simpson, S. L., Kutti, T., and Bannister, R. J. (2016). Sub-Lethal effects of water-based drilling muds on the deep-water sponge *Geodia barretti*. *Environ. pollut.* 212, 525–534. doi: 10.1016/j.envpol.2016.02.047

Erftemeijer, P. L., Riegl, B., Hoeksema, B. W., and Todd, P. A. (2012). Environmental impacts of dredging and other sediment disturbances on corals: a review. *Mar. pollut. Bull.* 64 (9), 1737–1765. doi: 10.1016/j.marpolbul.2012.05.008

Esslemont, G., Harriot, V. J., and McConchie, D. M. (2000). Variability of trace metal concentrations within and between colonies of *Pocillopora damicornis*. *Mar. pollut. Bull.* 40 (7), 637–642. doi: 10.1016/S0025-326X(00)00068-0

Fabricius, K. E., and Wolanski, E. (2000). Rapid smothering of coral reef organisms by muddy marine snow. *Estuar. Coast. Shelf. Sci.* 50 (1), 115–120. doi: 10.1006/ecss.1999.0538

Fallon, E. K., Frische, M., Petersen, S., Brooker, R. A., and Scott, T. B. (2019). Geological, mineralogical and textural impacts on the distribution of environmentally toxic trace elements in seafloor massive sulfide occurrences. *Minerals* 9 (3), 162. doi: 10.3390/min9030162

Fang, J. K., Rooks, C. A., Krogness, C. M., Kutti, T., Hoffmann, F., and Bannister, R. J. (2018). Impact of particulate sediment, bentonite and barite (oil-drilling waste) on net fluxes of oxygen and nitrogen in Arctic-boreal sponges. *Environ. pollut.* 238, 948–958. doi: 10.1016/j.envpol.2017.11.092

FAO (2009). *International guidelines for the management of deep-sea fisheries in the high seas*. Food and Agricultural Organization of the United Nations, Rome, Italy. 73pp.

Ferrier-Pagès, C., Houlbrèque, F., Wyse, E., Richard, C., Allemand, D., and Boisson, F. (2005). Bioaccumulation of zinc in the scleractinian coral *Stylophora pistillata*. *Coral Reefs* 24 (4), 636–645. doi: 10.1007/s00338-005-0045-x

Fonseca, J. S., Marangoni, L. F. B., Marques, J. A., and Bianchini, A. (2019). Energy metabolism enzymes inhibition by the combined effects of increasing temperature and copper exposure in the coral *Mussismilia harttii*. *Chemosphere* 236, 124420. doi: 10.1016/j.chemosphere.2019.124420

Fonseca, J. S., Zebral, Y. D., and Bianchini, A. (2021). Metabolic status of the coral *Mussismilia harttii* in field conditions and the effects of copper exposure *in vitro*. *Comp. Biochem. Physiol. C. Toxicol. Pharmacol.* 240, 108924. doi: 10.1016/j.cbpc.2020.108924

Gabbott, P. A. (1983). ""Developmental and seasonal activities in marine molluscs",," in *Environmental biochemistry and physiology 2. the Mollusca*, vol. 2 . Ed. P. W. Hochachka (New York: Academic Press). doi: 10.1016/B978-0-12-751402-4.50012-1

Gomes-Pereira, J. N., Carmo, V., Catarino, D., Jakobsen, J., Alvarez, H., Aguilar, R., et al. (2017). Cold-water corals and large hydrozoans provide essential fish habitat for *Lappanella fasciata* and *Benthocometes robustus*. *Deep-Sea Res. II.: Top. Stud. Oceanogr.* 145, 33–48. doi: 10.1016/j.dsr2.2017.09.015

Gwyther, D. (2008) *Environmental impact statement, solwara 1 project. nautilus minerals niugini limited, main report Coffey natural systems, Brisbane*. Available at: https://www.yumpu.com/en/document/view/38646617/environmental-impact-statement-nautilus-cares-nautilus-minerals.

Habig, W. H., Pabst, M. J., and Jakoby, W. B. (1974). Glutathione s-transferases - first enzymatic step in mercapturic acid formation. *J. Biol. Chem.* 249, 7130–7139. doi: 10.1016/S0021-9258(19)42083-8

Harland, A. D., and Brown, B. E. (1989). Metal tolerance in the scleractinian coral *Porites lutea*. *Mar. pollut. Bull.* 20 (7), 353–357. doi: 10.1016/0025-326X(89)90159-8

Harvell, D., Jordán-Dahlgren, E., Merkel, S., Rosenberg, E., Raymundo, L., Smith, G., et al. (2007). Coral disease, environmental drivers, and the balance between coral and microbial associates. *Oceanography* 20, 172–195. doi: 10.5670/oceanog.2007.91

Hauton, C., Brown, A., Thatje, S., Mestre, N. C., Bebianno, M. J., Martins, I., et al. (2017). Identifying toxic impacts of metals potentially released during deep-sea mining–a synthesis of the challenges to quantifying risk. *Front. Mar. Sci.* 4, 368. doi: 10.3389/fmars.2017.00368

Jones, D. O., Durden, J. M., Murphy, K., Gjerde, K. M., Gebicka, A., Colaço, A., et al. (2019). Existing environmental management approaches relevant to deep-sea mining. *Mar. Policy* 103, 172–181. doi: 10.1016/j.marpol.2019.01.006

Jones, R., Ricardo, G. F., and Negri, A. P. (2015). Effects of sediments on the reproductive cycle of corals. *Mar. pollut. Bull.* 100, 13–33. doi: 10.1016/j.marpolbul.2015.08.021

Kalghatgi, S., Spina, C. S., Costello, J. C., Liesa, M., Morones-Ramirez, J. R., Slomovic, S., et al. (2013). Bactericidal antibiotics induce mitochondrial dysfunction and oxidative damage in mammalian cells. *Sci. Transl. Med.* 5 (192), 192ra85. doi: 10.1126/scitranslmed.3006055

Kutti, T., Bannister, R. J., Fosså, J. H., Krogness, C. M., Tjensvoll, I., and Søvik, G. (2015). Metabolic responses of the deep-water sponge *Geodia barretti* to suspended bottom sediment, simulated mine tailings and drill cuttings. *J. Exp. Mar. Biol. Ecol.* 473, 64–72. doi: 10.1016/j.jembe.2015.07.017

Larsson, A. I., and Purser, A. (2011). Sedimentation on the cold-water coral *Lophelia pertusa*: cleaning efficiency from natural sediments and drill cuttings. *Mar. Poll. Bull.* 62, 1159–1168. doi: 10.1016/j.marpolbul.2011.03.041

Larsson, A. I., van Oevelen, D., Purser, A., and Thomsen, L. (2013). Tolerance to long-term exposure of suspended benthic sediments and drill cuttings in the cold-water coral *Lophelia pertusa*. *Mar. Poll. Bull.* 70, 176–188. doi: 10.1016/j.marpolbul.2013.02.033

Le, J. T., Levin, L. A., and Carson, R. T. (2017). Incorporating ecosystem services into environmental management of deep-seabed mining. *Deep-Sea Res. II.: Top. Stud. Oceanogr.* 137, 486–503. doi: 10.1016/j.dsr2.2016.08.007

Lesser, M. P. (2006). Oxidative stress in marine environments: biochemistry and physiological ecology. *Annu. Rev. Physiol.* 68, 253–278. doi: 10.1146/annurev.physiol.68.040104.110001

Levin, L. A., Mengerink, K., Gjerde, K. M., Rowden, A. A., Van Dover, C. L., Clark, M. R., et al. (2016). Defining "serious harm" to the marine environment in the context of deep-seabed mining. *Mar. Policy* 74, 245–259. doi: 10.1016/j.marpol.2016.09.032

Liefmann, S., Järnegren, J., Johnsen, G., and Murray, F. (2018). Eco-physiological responses of cold-water soft corals to anthropogenic sedimentation and particle shape. *J. Exp. Mar. Biol. Ecol.* 504 (2), 61–71. doi: 10.1016/j.jembe.2018.02.009

Lushchak, V. I. (2011). Environmentally induced oxidative stress in aquatic animals. *Aquat. Toxicol.* 101, 13–30. doi: 10.1016/j.aquatox.2010.10.006

Marangoni, L. F. B., Marques, J. A., Duarte, G. A. S., Pereira, C. M., Calderon, E. N., and Castro, C. B. (2017). Copper effects on biomarkers associated with photosynthesis, oxidative status and calcification in the Brazilian coral *Mussismilia harttii* (Scleractinia, mussidae). *Mar. Environ. Res.* 130, 248–257. doi: 10.1016/j.marenvres.2017.08.002

Marques, J. A., Abrantes, D. P., Laura, F. B., Marangoni, L. F. B., and Bianchini, A. (2020). Ecotoxicological responses of a reef calcifier exposed to copper, acidification and warming: A multiple biomarker approach. *Environ. pollut.* 257, 113572. doi: 10.1016/j.envpol.2019.113572

Martins, I., Godinho, A., Goulart, J., and Carreiro-Silva, M. (2018). Assessment of Cu sub-lethal toxicity (LC50) in the cold-water gorgonian *Dentomuricea meteor* under a deep-sea mining activity scenario. *Environ. pollut.* 240, 903–907. doi: 10.1016/j.envpol.2018.05.040

Martins, I., Godinho, A., Rakka, M., and Carreiro-Silva, M. (2022). Beyond deep-sea mining sublethal effects: Delayed mortality from acute Cu exposure of the cold-water gorgonian *Viminella flagellum*. *Mar. Poll. Bull.* 183, 114051. doi: 10.1016/j.marpolbul.2022.114051

Miller, K. A., Thompson, K. F., Johnston, P., and Santillo, D. (2018). An overview of seabed mining including the current state of development, environmental impacts, and knowledge gaps. *Front. Mar. Sci.* 4 (1). doi: 10.3389/fmars.2017.00418

Mitchelmore, C. L., Verde, A. E., Ringwood, A. H., and Weis, V. M. (2003). Differential accumulation of heavy metals in the sea anemone *Anthopleura elegantissima* as a function of symbiotic state. *Aquat. Toxicol.* 64, 317–329. doi: 10.1016/j.envpol.2019.113572

Mitchelmore, C. L., Verde, E. A., and Weis, V. M. (2007). Uptake and partitioning of copper and cadmium in the coral *Pocillopora damicornis*. *Aquat. Toxicol.* 85, 48–56. doi: 10.1016/j.aquatox.2007.07.015

Mohammed, T. A. A., and Dar, M. A. (2010). Ability of corals to accumulate heavy metals, northern red Sea, Egypt. *Environ. Earth Sci.* 59, 1525–1534. doi: 10.1007/s12665-009-0138-x

Montero, N., Belzunce-Segarra, M. J., Gonzalez, J. L., Larreta, J., and Franco, J. (2012). Evaluation of diffusive gradients in thin-films (DGTs) as a monitoring tool for the assessment of the chemical status of transitional waters within the water framework directive. *Mar. Poll. Bull.* 64, 31–39. doi: 10.1016/j.marpolbul.2011.10.028

Morato, T., Dominguez-Carrió, C., Mohn, C., Ocaña, V. O., Ramos, M., Rodrigues, L., et al. (2021). Dense cold-water coral garden of *Paragorgia johnsoni* suggests the importance of the mid-Atlantic ridge for deep-sea biodiversity. *Ecol. Evol.* 11 (23), 16426–16433. doi: 10.1002/ece3.8319

Morato, T., Juliano, M., Pham, C. K., Carreiro-Silva, M., Martins, I., and Colaço, A. (2022). Modelling the dispersion of seafloor massive sulphide mining plumes in the mid Atlantic ridge around the Azores. *Front. Mar. Sci.* 9, 910940. doi: 10.3389/fmars.2022.910940

Naumann, M. S., Niggl, W., Laforsch, C., Glaser, C., and Wild, C. (2009). Coral surface area quantification - evaluation of established methods by comparison with computer tomography. *Coral Reefs* 28, 109–117. doi: 10.1007/s00338-008-0459-3

Nguyen, T. V., Alfaro, A. C., Merien, F., Lulijwa, R., and Young, T. (2018). Copper-induced immunomodulation in mussel (*Perna canaliculus*) haemocytes. *Metallomics* 10 (7), 965–978. doi: 10.1039/c8mt00092a

Niner, H. J., Ardron, J. A., Escobar, E. G., Gianni, M., Jaeckel, A., Jones, D. O., et al. (2018). Deep-sea mining with no net loss of biodiversity–an impossible aim. *Front. Mar. Sci.* 5. doi: 10.3389/fmars.2018.00053

Okumura, T., Nagasawa, T., Hayashi, I., and Sato, Y. (2002). Effects of starvation on RNA: DNA ratio, glycogen content, and c: N ratio in columellar muscle of the Japanese turban shell *Turbo (Batillus) cornutus* (Gastropoda). *Fish. Sci.* 68 (2), 306–312.2. doi: 10.1046/j.1444-2906.2002.00426.x

Orcutt, B. N., Bradley, J. A., Brazelton, W. J., Estes, E. R., Goordial, J. M., Huber, J. A., et al. (2020). Impacts of deep-sea mining on microbial ecosystem services. *Limnol. Oceanogr.* 65 (7), 1489–1510. doi: 10.1002/lno.11403

OSPAR (2010). *Background document for coral gardens, biodiversity series*. Commission. Available at: https://www.ospar.org/documents?d=7217

Petersen, S., Krätschell, A., Augustin, N., Jamieson, J., Hein, J. R., and Hannington, M. D. (2016). News from the seabed–geological characteristics and resource potential of deep-sea mineral resources. *Mar. Pol.* 70, 175–187. doi: 10.1016/j.marpol.2016.03.012

Pham, C. K., Vandeperre, F., Menezes, G., Porteiro, F., Isidro, E., and Morato, T. (2015). The importance of deep-sea vulnerable marine ecosystems for demersal fish in the Azores. *Deep-Sea Res. I.: Oceanogr. Res. Pap.* 96, 80–88. doi: 10.1016/j.dsr.2014.11.004

Raimundo, J., Vale, C., Caetano, M., Anes, B., Carreiro-Silva, M., Martins, I., et al. (2013). Element concentrations in cold-water gorgonians and black coral from Azores region. *Deep-Sea Res. II.: Top. Stud. Oceanogr.* 98, 129–136. doi: 10.1016/j.dsr2.2013.01.012

Rainbow, P. (2002). Trace metal concentrations in aquatic invertebrates: why and so what? *Environ. pollut.* 120, 497–507. doi: 10.1016/S0269-7491(02)00238-5

Rakka, M., Maier, S. R., Van Oevelen, D., Godinho, A., Bilan, M., Orejas, C., et al. (2021). Contrasting metabolic strategies of two co-occurring deep-sea octocorals. *Sci. Rep.* 11, 10633. doi: 10.1038/s41598-021-90134-5

Regoli, F., and Giuliani, M. E. (2014). Oxidative pathways of chemical toxicity and oxidative stress biomarkers in marine organisms. *Mar. Environ. Res.* 93, 106–117. doi: 10.1016/j.marenvres.2013.07.006

Reichelt-Brushett, A. J., and McOristb, G. (2003). Trace metals in the living and nonliving components of scleractinian corals. *Mar. pollut. Bull.* 46 (12), 1573–1582. doi: 10.1016/S0025-326X(03)00323-0

Reichelt, A. J., and Jones, G. B. (1994). Trace metal as tracers of dredging activity in Cleveland bay–field and laboratory studies. *Aust. J. Mar. Freshw. Res.* 45, 1237–1257. doi: 10.1071/MF9941237

Rhee, J.-S., Yu, I. T., Kim, B.-M., Jeong, C.-B., Lee, K.-W., Kim, M.-J., et al. (2013). Copper induces apoptotic cell death through reactive oxygen species-triggered oxidative stress in the intertidal copepod *Tigriopus japonicus*. *Aquat. Toxicol.* 132-133, 182–189. doi: 10.1016/J.AQUATOX.2013.02.013

Riegl, B., and Bloomer, J. P. (1995). ""Tissue damage in hard and soft corals due to experimental exposure to sedimentation"," in *Proceedings 1st European regional meeting ISKS*, vol. 20. (Vienna: Beitrage zur Palaeontologie von Oesterreich), 51–63.

Riegl, B., and Branch, G. M. (1995). Effects of sediment on the energy budgets of four scleractinian (Bourne 1900) and five alcyonacean (Lamouroux 1816) corals. *J. Exp. Mar. Biol. Ecol.* 186, 259–275. doi: 10.1016/0022-0981(94)00164-9

Roberts, J. M., Wheeler, A., Freiwald, A., and Cairns, S. (2009). *Cold-water corals: the biology and geology of deep-sea coral habitats* (Cambridge University Press: Cambridge, UK.).

Rogers, C. S. (1990). Responses of coral reefs and reef organisms to sedimentation. *Mar. Ecol. Progr. Ser.* 62 (1), 185–202. doi: 10.3354/meps062185

Rovelli, L., Carreiro-Silva, M., Attard, K. M., Rakka, M., Dominguez-Carrió, C., Bilan, M., et al. (2022). Benthic O_2 uptake by coral gardens at the condor seamount (Azores). *Mar. Ecol. Progr. Ser.* 688, 19–31. doi: 10.3354/meps14021

Rushmore, M. E., Ross, C., and Fogarty, N. D. (2021). Physiological responses to short-term sediment exposure in adults of the Caribbean coral *Montastraea cavernosa* and adults and recruits of *Porites astreoides*. *Coral Reefs* 40, 1579–1591. doi: 10.1007/s00338-021-02156-0

Sabdono, A. (2009). Heavy metal levels and their potential toxic effect on coral *Galaxea fascicularis* from Java Sea, Indonesia. *Res. J. Environ. Sci.* 3 (1), 96–102. doi: 10.3923/rjes.2009.96.102

Scanes, E., Kutti, T., Fang, J. K. H., Johnston., E. L., Ross, P. M., and Bannister, R. J. (2018). Mine waste and acute warming induce energetic stress in the deep-Sea sponge *Geodia atlantica* and coral *Primnoa resedeaformis*: Results from a mesocosm study. *Front. Mar. Sci.* 5. doi: 10.3389/fmars.2018.00129

Schwarz, J. A., Mitchelmore, C. L., Jones, R., O'Dea, A., and Seymour, S. (2013). Exposure to copper induces oxidative and stress responses and DNA damage in the coral *Montastraea franksi*. *Comp. Biochem. Phsiol. Part C.* 157, 272–279. doi: 10.1016/j.cbpc.2012.12.003

Servetto, N., de Aranzamendi, M. C., Bettencourt, R., Held, C., Abele, D., Movilla, J., et al. (2021). Molecular mechanisms underlying responses of the Antarctic coral *Malacobelemnon daytoni* to ocean acidification. *Mar. Environ. Res.* 170, 105430. doi: 10.1016/j.marenvres.2021.105430

Sharma, R. (2017). *Deep-sea mining: Resource potential, technical and environmental considerations* (Springer, Cham). doi: 10.1007/978-3-319-52557-0

Siddiqui, S., and Bielmyer-Fraser, G. K. (2015). Responses of the sea anemone, *Exaiptasia pallida*, to ocean acidification conditions and copper exposure. *Aquat. Toxicol.* 167, 228–239. doi: 10.1016/j.aquatox.2015.08.012

Smith, C. R., Tunnicliffe, V., Colaço, A., Drazen, J. C., Gollner, S., Levin, L. A., et al. (2020). Deep-sea misconceptions cause underestimation of seabed-mining impacts. *Trends Ecol. Evol.* 35 (10), 853–857. doi: 10.1016/j.tree.2020.07.002

Strachan, M. F., and Kingston, P. F. (2012). A comparative study on the effects of barite, ilmenite and bentonite on four suspension feeding bivalves. *Mar. Poll. Bull.* 64, 2029e2038. doi: 10.1016/j.marpolbul.2012.06.023

Telesnicki, G. J., and Goldberg, W. M. (1995). Effects of turbidity on the photosynthesis and respiration of two south Florida reef coral species. *Bull. Mar. Sci.* 57, 527–539.

Therond, P., Gerbaud, P., Dimon, S., Anderson, W. B., EvainBrion, D., and Raynaud, F. (1996). Antioxidant enzymes in psoriatic fibroblasts and erythrocytes. *J. Invest. Dermatol.* 106, 1325–1328. doi: 10.1111/1523-1747.ep12349055

Underwood, A. J. (1997). *Experiments in ecology: Their logical design and interpretation using analysis of variance* (Cambridge: Cambridge University Press).

Van Dover, C. L. (2014). Impacts of anthropogenic disturbances at deep-sea hydrothermal vent ecosystems: A review. *Mar. Environ. Res.* 102, 59–72. doi: 10.1016/j.marenvres.2014.03.008

VanDover,C.L.,Ardron,J.A.,Escobar,E.,Gianni,M.,Gjerde,K.M.,Jaeckel,A.,etal.(2017). Biodiversity loss from deep-sea mining. *Nat. Geosci.* 10, 464–465. doi: 10.1038/ngeo2983

Van Dover, C. L., Colaço, A., Collins, P. C., Croot, P., Metaxas, A., Murton, B. J., et al. (2020). Research is needed to inform environmental management of hydrothermally inactive and extinct polymetallic sulfide (PMS) deposits. *Mar. Pol.* 121, 104183. doi: 10.1016/j.marpol.2020.104183

Walters, K., and Coen, L. D. (2006). A comparison of statistical approaches to analyzing community convergence between natural and constructed oyster reefs. *J. Exp. Mar. Biol. Ecol.* 330 (1), 81–95. doi: 10.1016/J.JEMBE.2005.12.018

Washburn, T. W., Turner, P. J., Durden, J. M., Jones, D. O., Weaver, P., and Van Dover, C. L. (2019). Ecological risk assessment for deep-sea mining. *Ocean Coast. Manage.* 176, 24–39. doi: 10.1016/j.ocecoaman.2019.04.014

Weaver, P. P. E., and Billett, D. (2019). "Environmental impacts of nodule, crust and sulphide mining: An overview," in *Environmental issues of deep-Sea mining*, vol. pp . Ed. R. Sharma (Cham: Springer), 27–62). doi: 10.1007/978-3-030-12696-4_3

Weber, M., de Beer, D., Lott, C., Polerecky, L., Kohls, K., Abed, R. M. M., et al. (2012). Mechanisms of damage to corals exposed to sedimentation. *Proc. Natl. Acad. Sci. U.S.A.* 109, E1558–E1567. doi: 10.1073/pnas.1100715109

Weber, M., Lott, C., and Fabricius, K. E. (2006). Sedimentation stress in a scleractinian coral exposed to terrestrial and marine sediments with contrasting physical, organic and geochemical properties. *J. Exp. Mar. Biol. Ecol.* 336, 18–32. doi: 10.1016/j.jembe.2006.04.007

Wedding, L. M., Reiter, S. M., Smith, C. R., Gjerde, K. M., Kittinger, J. N., Friedlander, A. M., et al. (2015). Managing mining of the deep seabed. *Science* 349 (6244), 144–145. doi: 10.1126/science.aac6647

Zetsche, E.-M., Baussant, T., Meysman, F. J. R., and van Oevelen, D. (2016). Direct visualization of mucus production by the cold-water coral *Lophelia pertusa* with digital holographic microscopy. *PloS One* 11 (2), e0146766. doi: 10.1371/journal.pone.0146766

Zhang, H., and Davison, W. (2000). Direct *in situ* measurements of labile inorganic and organically bound metal species in synthetic solutions and natural waters using diffusive gradients in thin films. *Anal. Chem.* 72, 4447–4457. doi: 10.1021/ac0004097

Zhou, L., Li, M., Zhong, Z., Chen, H., Wang, X., Wang, M., et al. (2021). Biochemical and metabolic responses of the deep-sea mussel *Bathymodiolus platifrons* to cadmium and copper exposure. *Aquat. Toxicol.* 236, 105845. doi: 10.1016/j.aquatox.2021.105845

frontiers | Frontiers in Marine Science

TYPE Review
PUBLISHED 26 October 2022
DOI 10.3389/fmars.2022.898828

OPEN ACCESS

EDITED BY
David Billett,
Deep Seas Environmental Solutions Ltd., United Kingdom

REVIEWED BY
Jeroen Ingels,
Florida State University, United States
Daphne Cuvelier,
University of the Azores, Portugal

*CORRESPONDENCE
Teresa Radziejewska
teresa.radziejewska@usz.edu.pl

SPECIALTY SECTION
This article was submitted to Deep-Sea Environments and Ecology, a section of the journal Frontiers in Marine Science

RECEIVED 17 March 2022
ACCEPTED 28 September 2022
PUBLISHED 26 October 2022

CITATION
Radziejewska T, Błażewicz M, Włodarska-Kowalczuk M, Jóźwiak P, Pabis K and Węsławski JM (2022) Benthic biology in the Polish exploration contract area of the Mid-Atlantic Ridge: The knowns and the unknowns. A review. *Front. Mar. Sci.* 9:898828. doi: 10.3389/fmars.2022.898828

Benthic biology in the Polish exploration contract area of the Mid-Atlantic Ridge: The knowns and the unknowns. A review

Teresa Radziejewska[1]*, Magdalena Błażewicz[2], Maria Włodarska-Kowalczuk[3], Piotr Jóźwiak[2], Krzysztof Pabis[2] and Jan Marcin Węsławski[3]

[1]Institute of Marine and Environmental Sciences, University of Szczecin, Szczecin, Poland, [2]Department of Invertebrate Zoology and Hydrobiology, Faculty of Biology and Environmental Protection, University of Lodz, Łódź, Poland, [3]Institute of Oceanology, Polish Academy of Sciences, Sopot, Poland

In February 2018, the Government of Poland and the International Seabed Authority signed a 15-year contract for exploration of polymetallic sulfide deposits on a section of the Mid-Atlantic Ridge extending between the Hayes, Atlantic and Kane transform faults (32°45.378′ N, 39°57.760′ W to 26°14.411′ N, 44°18.008′ W). The contractor is obliged to collect data on the contract area environment and its ecosystem components. In this context, it is important that the contractor establishes a sound starting point which further baseline investigations can be referred to. Such a starting point involves assessment of currently held information and, most importantly, knowledge gaps on the ecosystem components in the area of exploration (and of potential future exploitation). Of major importance here is the knowledge on benthic communities, as it is the benthos that will be most affected by any human intervention in the area of interest. Based on available published evidence, we have reviewed the present state of knowledge on benthic communities in the Polish exploration contract area (PECA). In the process, we have identified important knowledge gaps that will need to be addressed during exploration surveys. These include, but are not limited to, the distribution and structure of benthic communities throughout the contract area, the spatial and temporal variability of those communities, possible differences between communities inhabiting active and inactive vent fields, connectivity issues and the recovery potential. Special consideration should be given to Lost City, a geologically and ecologically unique hydrothermal field which has been a focus of international research and an important conservation target.

KEYWORDS

benthos, Mid-Atlantic Ridge, hydrothermal vents, polymetallic sulfide exploration, International Seabed Authority

1 Introduction

The Mid-Atlantic Ridge (MAR) is a part of the global system of mid-oceanic ridges formed at the contact between crustal plates (Karson et al., 2015a). Because of the Earth's crust characteristics, the ridges are sites of considerable seismic and tectonic instability, manifested as, *inter alia*, hydrothermal activity which is particularly intense at active hydrothermal fields (Karson et al., 2015a; Karson et al., 2015b). A hydrothermal vent field is a term applied to an area supporting a cluster of vent sites, i.e. sites where heated seawater, modified into an ore-forming fluid, is ejected from the seafloor through conduits and chimneys (Weaver et al., 2021). A vent field may comprise active vent sites, inactive (or extinct) vents and sedimented slopes and plains, i.e., areas covered by soft sediments (Weaver et al., 2021). With regard to the latter, Fabri et al. (2011) distinguished between hydrothermal and pelagic sediments. A good schematic representation of a vent field and its different habitats (precipitation chimneys, basalts, soft sediments) can be found in Weaver and Billett (2019). The geological and geochemical processes associated with the hydrothermal activity induce precipitation, deposition and accumulation of minerals of commercial interest at the venting sites and in their vicinity (Hannington et al., 2011; Boschen et al., 2013; Menini and Van Dover, 2019). In view of their value for meeting the predicted global demand for minerals important in various technological applications (Petersen et al., 2016; Kawano and Furuya, 2022), deposits of polymetallic sulfides (PMS), the major mineral type of commercial interest at mid-ocean ridges, have become a focus of interest for the future deep-sea mining (Cherkashov, 2017; Van Dover et al., 2018). This entails contracts for PMS exploration in international waters with the International Seabed Authority (ISA), an institution "….mandated under the UN Convention on the Law of the Sea to organize, regulate and control all mineral-related activities in the international seabed area for the benefit of mankind as a whole." (www.isa.org.jm).

In February 2018, the Government of Poland and the ISA signed a 15-year contract for exploration of PMS deposits on a section of the MAR extending between the Hayes, Atlantic and Kane transform faults (32°45.378' N, 39°57.760' W to 26°14.411' N, 44°18.008' W) (Figure 1).

The depth range of the Polish exploration contract area (PECA), as determined from querying the GEBCO portal (www.gebco.net; accessed on 18 Aug. 2022) ranges from about 800 to about 4990 m beyond the axial rift; the mid-axial valley depth ranges from about 800 to about 5300 m, decreasing from north to south.

The PECA is known to encompass two confirmed active hydrothermal fields: the Broken Spur and Lost City (Beaulieu and Szafranski, 2019) as well as two inferred active fields (Beaulieu et al., 2013; Weaver et al., 2021). Some more detailed information on the topography, habitats and benthic fauna (primarily the macro- and megabenthos) can be encountered regarding the Broken Spur (Cruz et al., 2022) and the Lost City (see below), but the generally the area remains greatly unexplored. At the moment of writing (August 2022), the first exploration cruise organized by the Polish contractor is in progress to collect geophysical information on the PECA, including detailed bathymetry (M. Tomczak, pers. comm.).

Contract provisions[1] oblige the contractor to collect data on the contract area environment and its ecosystem as detailed by the ISA in its "Recommendations for the Guidance of Contractors for the Assessment of the possible environmental impacts arising from exploration for marine minerals in the Area" (ISA, 2019). In addition, a contractor is obliged to implement certain environmental protection measures (Van Dover et al., 2011; Van Dover et al., 2018). Such measures include area-based (AB) spatial planning whereby impact reference zones (IRZs) and preservation reference zones (PRZs) for future mining activities are defined (ISA, 2017; Jones et al., 2020). More generally, there are AB measures such as Marine Protected Areas (MPAs), e.g. an MPA encompassing the Lucky Strike and Menez Gwen hydrothermal fields in the Portuguese national jurisdiction area (Calado et al., 2011; Menini and Van Dover, 2019), and ecosystem-based conservation (e.g. Ortiz et al., 2017). There are also non-AB measures, such as evidence-based conservation (e.g. Mogensen et al., 2022), species- or multispecies-based conservation (Mace et al., 2007; Campagna et al., 2008; Vals et al., 2015) and rules-based approach (e.g. Farley, 2009). In addition, specific sites may be identified as being in need of protection (Dunn et al., 2018). Work is being currently carried out on developing a Regional Environmental Management Plan (REMP) for the MAR, to be implemented by the ISA and its contractors (Weaver et al., 2021).

Given that the resource of interest, i.e. PMS, is an inherent component of the MAR seafloor ecosystem, PMS exploration and potential exploitation will primarily affect the benthic part of the ecosystem (Gollner et al., 2017; Dunn et al., 2018). It is therefore vital for the contractor to collect information on the benthic communities in the contract area. It is also important that contractors recognize gaps in their knowledge of the biological communities they are likely to encounter during exploration, test mining and eventually the exploitation of PMS.

With this necessity in mind, we have reviewed the present state of knowledge on benthic communities in the PECA, based on information contained in publicly available sources, as no dedicated field-oriented research has been as yet undertaken by the Polish contractor. We follow a conventional size-based ecological classification of the benthos (e.g. Gage and Tyler, 1991), whereby organisms associated with the seafloor are

1 https://isa.org.jm/files/files/documents/Public%20information%20on%20contracts%20Poland.pdf.

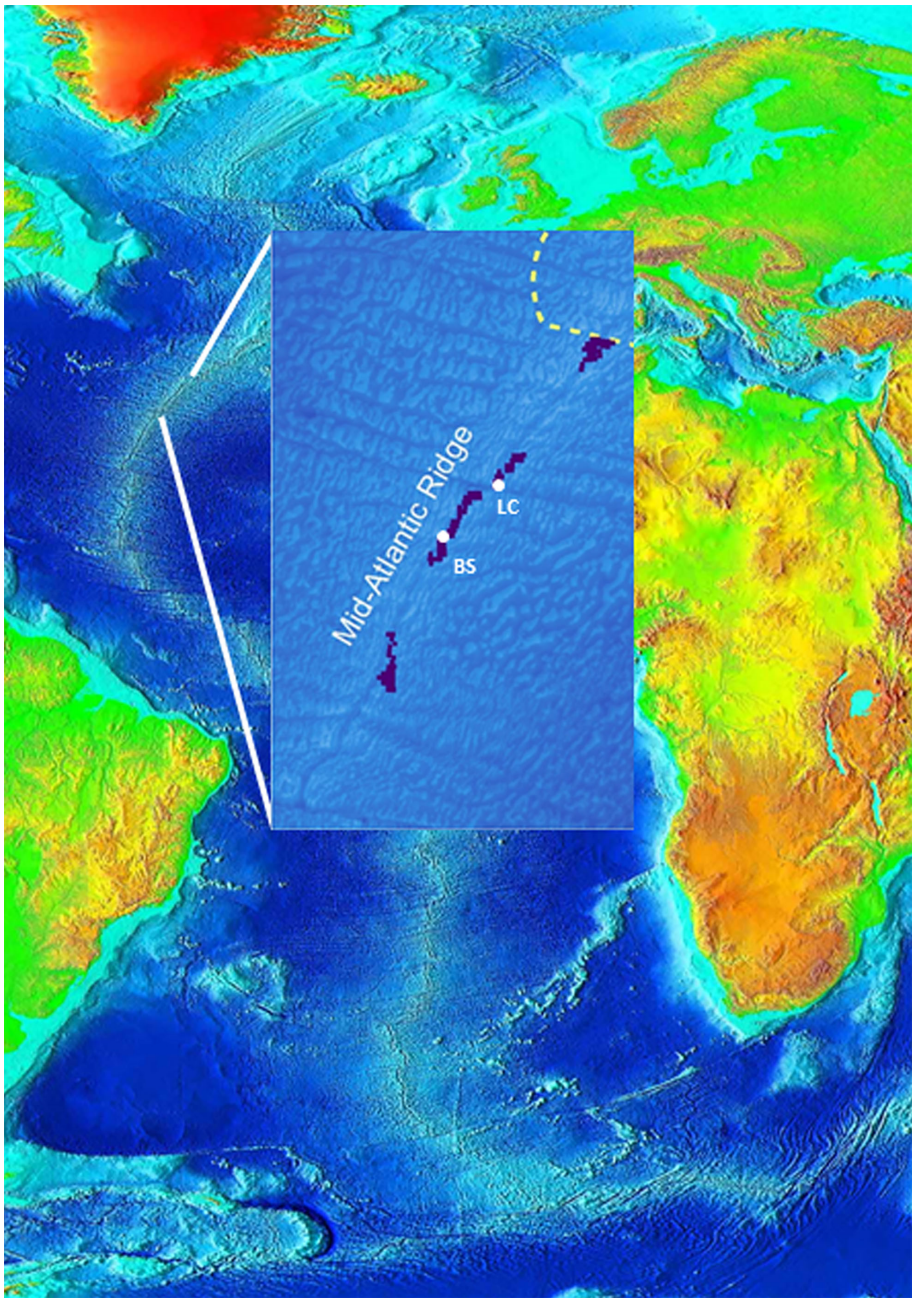

FIGURE 1
Location of the Polish contract area (PECA) on the Mid-Atlantic Ridge; LC, Lost City; BS, Broken Spur; dark squares mark exploration blocks; dotted yellow line marks the boundary of Portugal's Extended Continental Shelf (based on imagery available from NOAA, http:///www.ngdc.noaa.gov/mgg/image/2minrelief.html and ISA, https://isa.org.jm/files/files/documents/Public%20information%20on%20contracts%20Poland.pdf).

considered as representing the meio-, macro-, and megabenthos. It will be noticed, however, that the between-classes boundaries are not always sharp (or are purely pragmatic), hence some taxa are referred to in more than one category.

This paper is based on literature data mining, whereby data on benthic communities in the PECA have been sought in, and extracted from, book chapters and peer-reviewed papers stemming from information collected during research cruises to the MAR (Thaler and Amon, 2019). As can be seen from Table 1, information on the PECA benthos is limited, fragmentary and patchy. Basically, data on the PECA benthos have been collected almost exclusively at the two active

hydrothermal vent fields, the Broken Spur and the Lost City. In this context it is worth mentioning that fairly extensive data on benthic communities in the PECA, those in the Broken Spur vent field in particular, have been contributed by Russian authors investigating the MAR ecosystem, based on materials collected during cruises up to 2003 (Gebruk and Mironov, 2006) (Table 1). Boschen-Rose and Colaço (2021) looked for similarities/dissimilarities in the composition of benthic communities across the hydrothermal vent fields in studies reported up to 2020. We performed a similar analysis for the meiobenthos, not covered by Boschen-Rose and Colaço (2021) data, using the non-metric multidimensional scaling (MDS) routine of the PRIMER v. 7 software package (Clarke and Gorley, 2015). To narrow the uncertainty margin of the analysis, which might have been introduced by using taxa of various ranks, the input data matrix included taxa identified to at least the genus level only.

2 The knowns

2.1 Structural aspects of benthic communities

2.1.1 Meiobenthos

Like other ecological groupings, the MAR meiobenthos (benthic meiofauna, i.e. organisms commonly considered – in the deep sea – as falling within the 32-300 μm size range; cf. Thiel, 1975) is greatly understudied (Boschen-Rose and Colaço, 2021), including in the PECA. Most research on the hydrothermal vent meiofauna has been so far carried out in the Pacific ridge areas (e.g. Gollner et al., 2010; Zeppilli et al., 2018, and references therein). There have been few meiobenthos-focused studies in the MAR in general (Zekely et al., 2006; Flint, 2007; Ivanenko et al., 2011; Cuvelier et al., 2014; Sarrazin et al., 2015; Tchesunov, 2015; Zeppilli et al., 2015; Plum et al., 2017; Spedicato et al., 2020). However, information can be extracted by taking a broader view of MAR benthic communities, notably from the work of Galkin (2006) and Gebruk and Mironov (2006). The MAR meiobenthos has been so far reported from a number of known active hydrothermal fields (Menez Gwen, Lucky Strike, Rainbow, Lost City, Broken Spur, TAG, Snake Pit, Logatchev), two of which (Lost City and Broken Spur) are situated within the PECA. In addition to the low number of studies, the sampling effort reported has also been very low; usually researchers have had access to only 2 - 12 samples. Based on such a limited amount of material, it seems premature at the present stage to expect the researchers to provide analyses employing even basic indicators of meiobenthic diversity (rarefaction curves, abundance/diversity relationship estimates). We are at a very early stage of acquiring familiarity with the meiobenthos on the MAR in general, and in the PECA in particular. In this context, it would be highly desirable if future studies addressed habitat-related variability of meiobenthic communities. It seems quite plausible to expect differences in composition and abundances of the meiobenthos sampled from bio-ecological structures such as bivalve aggregations (as in Tchesunov, 2015), from the typical hard substrate, and from soft sediments on the flanks of the fields (Weaver et al., 2021).

Eleven major meiobenthic taxa have been reported from the PECA. The taxonomic richness in the PECA appears to be low in comparison to other areas of the MAR, but this is most likely to be the result of gross undersampling in the area rather than from any underlying biological patterns. Nematodes, ostracods and bivalves were found at the Lost City, while nematodes and siphonostomatoid, harpacticoid and cyclopoid copepods were recorded at the Broken Spur. In addition, few taxa were identified to a lower taxonomic level (family and/or genus), with the Broken Spur and Lost City featuring 13 (nematodes only) and 8 (the nematodes and copepods) such taxa, respectively (Tables 2A, B). Notably, the Lost City nematode assemblage features the genus *Oncholaimus*, which appears to be very abundant (Tchesunov, 2015; Zeppilli et al., 2018). The genus is regarded as specialising in feeding on free-living chemoautotrophic microorganisms and harbouring an epibiotic microbial community dominated by the Gammaproteobacteria, including vent symbionts (Zeppilli et al., 2018).

In addition, three species of the siphonostomatoid copepod family Dirivultidae were recorded at the Broken Spur. These copepods are regarded as endemic to hydrothermal vents worldwide and are particularly well adapted to life in the vicinity of hot venting hydrothermal fluids (Zeppilli et al., 2018).

As shown by as few as 10 quantitative MAR meiofaunal studies that have been published, meiofaunal assemblages elsewhere on the MAR are dominated by nematodes and harpacticoid copepods, but mainly nematodes. However, at one non-vent site at the TAG hydrothermal field the proportions between these two taxa were reversed (Flint, 2007). Because of the nematode dominance, most of the meiofaunal studies on the MAR focused on nematodes, as shown by the relevant lists of meiofaunal taxa. This is also the case in the PECA (cf. Tables 2A, B).

As shown in Figure 2, the similarity in faunistic composition between meiobenthic assemblages reported so far from different MAR vent fields is quite low. The Broken Spur and Lost City assemblages appear to be more similar to each other (and to the assemblage at the Rainbow) than to those from the remaining fields. The Broken Spur, Lost City and Rainbow fields are all at a similar depth, which might in part explain the apparent similarity. It has to be remembered, however, that the similarity analysis shown in Figure 2 was carried out on a limited amount of data found in a low number of published accounts.

2.1.2 Macrobenthos

Macrofaunal benthic communities (i.e. comprising organisms >300 μm; cf. Thiel, 1975) of the MAR have been

TABLE 1 A summary of data sources on the PECA benthos (environmental characteristics, sampling methodology when reported, and analyses performed.

Benthos category	PECA vent field	Reference	Environmental characteristics	Sampling methodology	Analyses performed
Meiobenthos	Broken Spur	Gebruk and Mironov (2006)	Depth 3050-3075 m; H_2S 8.5-11.0 mM kg^{-1}; CH4 0.065-0.130 mM kg^{-1}; chemosynthetic primary production 20 mg C m^{-2} d^{-1}; more than 10 smokers	Different cruises until 2003; details of sampling not reported	List of faunal taxa, including meiobenthos
	Lost City	Gebruk and Mironov (2006)	Depth 700-850 m; H_2S 0.064 mM kg^{-1}; CH_4 0.13-0.28 mM kg^{-1}; complex topography with spire-like structures 60-70 m high; hydrothermal fluid temperature 75°C	Different cruises until 2003; details of sampling not reported	List of faunal taxa, including meiobenthos
	Lost City	Tchesunov (2015)	Depth 700-800 m' bacterial mat, silt, walls of active chimney, coral wash-out	Cruises in 2003 and 2005; mussel clumps, pieces of rock and silt collected, with manipulator arm and slurp gun, from manned submersible	Taxonomic identification of nematodes
	Broken Spur	Tchesunov (2015)	Depth 3059 m; silt at chimney base	Cruises in 2003 and 2005; mussel clumps, pieces of rock and silt collected, with manipulator arm and slurp gun, from manned submersible	Taxonomic identification of nematodes
		Zeppilli et al. (2018)	Not applicable	Not applicable	A compilation of meiobenthic studies at various hydrothermal vent sites, with a particular reference to Tchesunov (2015)
Macrobenthos	Broken Spur	Tyler et al. (1995)	Hydrothermal mounds with weathered sulfide surfaces, active venting of black smokers and diffuse flow	Specimens collected with rock samples from submersible	Taxonomy: description of a new ophiuroid species
	Lost City	Kelley et al. (2005)	Depth 750-900 m; complex topography; about 60 active and inactive carbonate structures and venting hydrothermal fluids; actively venting carbonate habitats (~10- to 40°C)	Observations from manned submersible; sampling of microorganisms	Visual census and sampling macrofauna
	Lost City	Kelley et al. (2007)	Complex topography; temperature ~55-91°C; pH 10.7	Data and video imagery streamed live from robotic vehicles *via* a fiber optic cable to research vessel	Observations of geology and faunal communities
	Broken Spur	Goroslavskaya and Galkin (2011)	Active venting	Several cruises (2002-2005), sampling from manned submersibles (manipulator with 15 cm 100 um mesh size net and slurp gun)	Fauna associated with mussel beds and shrimps
Mega- and nektobenthos	Broken Spur	Copley et al. (1997)	Depth 3090 m; active venting (high and low temperature); massive sulfide deposits	Expedition BRAVEX 1994, Video surveys from manned submersible	Megafauna identification and composition, abundance estimation
	Broken Spur	Desbruyères et al. (2000)	Basaltic substratum; active venting; fluid temperature 356-364°C; H_2S 9.4 mM kg^{-1}; Fe 1.68-2.16 mM kg^{-1}; Mn 0.26 mM kg^{-1}	Several cruises; video surveys from manned submersible	Megafauna identification and composition
	Broken Spur	Gebruk et al. (2000)	Depth 3056-3060m; ambient temperature 3°C	1997 cruise, suction sampler and small net operated from manned submersible	Carbon and nitrogen stable isotopes, lipid content and elemental composition of vent shrimps
	Broken Spur	Vereshchaka et al. (2000)	Not reported	1996 cruise; sampling from manned submersibles	Isotopic composition (carbon and nitrogen) of 18 taxa and size classes
	Broken Spur	O'Mullan et al. (2001)	Not reported	Collection of specimens with manipulator arm from manned submersible	Genetic structure of hydrothermal vent mussels
	Lost City	Kelley et al. (2005)	Depth 750-900 m; complex topography; about 60 active and inactive carbonate structures and venting hydrothermal fluids; actively venting carbonate habitats (~10- to 40°C)	Observations from manned submersible; sampling of microorganisms	Visual census of megafauna

(Continued)

TABLE 1 Continued

Benthos category	PECA vent field	Reference	Environmental characteristics	Sampling methodology	Analyses performed
	Broken Spur	Galkin (2006); Gebruk and Mironov (2006)	Depth 3050-3075 m; H_2S 8.5-11.0 mM kg^{-1}; CH4 0.065-0.130 mM kg^{-1}; chemosynthetic primary production 20 mg C m^{-2} d^{-1}; more than 10 smokers	Different cruises until 2003; details of sampling not reported	Megabenthos composition, abundance and biomass
	Lost City	Galkin (2006); Gebruk and Mironov (2006)	Depth 700-850 m; H_2S 0.064 mM kg^{-1}; CH_4 0.13-0.28 mM kg^{-1}; complex topography with spire-like structures 60-70 m high; hydrothermal fluid temperature 75°C	Different cruises until 2003; details of sampling not reported	Megabenthos composition, abundance and biomass
	Lost City	Kelley et al. (2007)	Complex topography; temperature ~55-91°C; pH 10.7	Data and video imagery streamed live from robotic vehicles *via* a fiber optic cable to research vessel	Observations of geology and faunal communities
	Broken Spur	Lunina and Vereshchaka (2014)	Depth 3100 m	A series of cruises (1994-2005); baited traps and suction samplers operated from manned submersibles	Taxonomy (description of new shrimp species)
	Broken Spur	Lunina and Vereshchaka (2014)	Depth 3100 m	A series of cruises (1994-2005); baited traps and suction samplers operated from manned submersibles	Observations on alvinocaridid vent shrimps
	Broken Spur	Rybakova and Galkin (2015)	Depth 3000 m	Net, slurp gun	Compilation of data on distribution of vent mytilid bivalves and alvinocaridid shrimps

studied less extensively than the assemblages of megafaunal invertebrates (see below), resulting in a very poor general knowledge. Some detailed studies have been carried out at other localities on the MAR, notably in the Charlie-Gibbs Fracture Zone further north (Alt et al., 2013; Dilman, 2013; Shields et al., 2013; Bell et al., 2016; Alt et al., 2019) and at various hydrothermal vents [Lucky Strike, Menez Gwen, Rainbow, Snake Pit, Logatchev and Trans-Atlantic Geotraverse (TAG)] (e.g. Bellan-Santini and Thurston, 1996; Sigvaldadottir and Desbruyères, 2003; Myers and Cunha, 2004; Cunha and Wilson, 2006; Larsen et al., 2006; Bellan-Santini, 2007; Corbera et al., 2008; Riou et al., 2010; Sarrazin et al., 2015; Bebianno et al., 2018; Klunder et al., 2020).

In the PECA, macrobenthic communities have been reported to date only from the Broken Spur and Lost City hydrothermal vent fields (Tyler et al., 1995; Desbruyères et al., 2000; Kelley et al., 2005; Kelley et al., 2007; Goroslavskaya and Galkin, 2011; Rybakova and Galkin, 2015; Boschen-Rose and Colaço, 2021; Cruz et al., 2022) (see Table 3). A total of 22 species were reported from the Broken Spur (Boschen-Rose and Colaço, 2021). The fauna includes the bivalve *Bathymodiolus puteoserpentis* (alternatively reported also as the megabenthos; see below), the ampharetid polychaete *Amathys lutzi* (currently *Amphisamytha lutzi)* and the ophiuroid *Ophioctenella acies* (Rybakova and Galkin, 2015) as well as nektobenthic shrimps and polychaetes that can grow large enough to be classified as the megafauna (Desbruyères et al., 2000). A recent review (Boschen-Rose and Colaço, 2021) demonstrated a similarity between the Broken Spur fauna and benthic communities associated with other vent fields including the TAG, Snake Pit, Logatchev and Ashadze-1.

2.1.3 Mega- and nektobenthos

Owing to the limitations of physical sampling of the MAR benthos due to the rough terrain, especially in proximity to the mid-axial valley, most data on MAR benthic communities relate to larger organisms (megafauna) seen in photographic and video surveys using Remotely Operated Vehicles (ROVs) (e.g. Alt et al., 2019; Boschen-Rose and Colaço, 2021). Yet, even for the megafauna, data in the PECA are restricted to just two small hydrothermal vent areas. The few records of megafaunal species found at the Broken Spur and Lost City vents, however, allow some observations to be made using information on the same species at other locations on the MAR (e.g. Perez et al., 2012; Priede et al., 2013; Thaler and Amon, 2019; Boschen-Rose and Colaço, 2021 and references therein). Yet, the general knowledge about benthic megafauna of the PECA is still insufficient, as it lacks, *inter alia*, basic data on some components of benthic communities and is limited to the two vent fields already mentioned, the Broken Spur and Lost City (cf. Table 3).

The megafauna at the Broken Spur shows greater affinity to hydrothermal vent fields in deeper water further south than to the shallower hydrothermal sites of Menez Gwen and Lucky Strike to the north (Fabri et al., 2011). Recently, however, Cruz et al. (2022) referred to a general similarity between the Broken Spur fauna and that encountered elsewhere on the MAR. As reported by Boschen-Rose and Colaço (2021), as few as 9 benthic megafaunal

TABLE 2 Meiofaunal taxa reported from the hydrothermal vent fields in the Polish contract area (Lost City, Broken Spur) and elsewhere on MAR; A) non-nematode taxa; B) nematode taxa (data from Gebruk and Mironov, 2006; Flint, 2007; Ivanenko et al., 2011; Tchesunov, 2015; Zeppilli et al., 2015; Sarrazin et al., 2015; Zeppilli et al., 2019; Spedicato et al., 2020); +, taxon recorded; -, taxon not recorded.

A

Taxon		Lost City	Broken Spur	Other MAR fields
Gastrotricha	Gastrotricha indet.	–	–	+
Polychaeta	Polychaeta indet.	–	–	+
Halacaroidea	*Agauopsis auzendei*	–	–	+
	Bathyalacarus sp.	–	–	+
	Halacarellus alvinus	–	–	+
	Halacarus prolongatus	–	–	+
	Copidognathus nautilei	–	–	+
	C. alvinus	–	–	+
Tantulocarida	Tantulocarida indet.	–	–	+
Copepoda Siphonostomatoida	*Aphotopontius atlanteus*	–	–	+
	A. temperatus	–	–	+
	A. forcipatus	–	–	+
	Rimipontius mediospinifer	–	+	+
	Stygiopontius rimivagus	–	–	+
	S. bulgisetiger	–	–	+
	S. cladarus	–	+	+
	S. latulus	–	–	+
	S. mirus	–	–	+
	S. pectinatus	–	+	+
	S. regius	–	–	+
	S. serratus	–	–	+
	S. teres	–	–	+
	Dirivultidae indet.	–	–	+
Copepoda Harpacticoida	*Bathylaophonte azorica*	–	–	+
	Microsetella norvegica	–	+	–
	Aegisthidae indet.	–	–	+
	Ectinosomatidae indet.	–	–	+
	Miraciidae indet.	–	–	+
	Pseudotachidiidae indet.	–	–	+
	Smacigastes micheli	–	–	+
	Tegastidae indet.	–	–	+
	Tisbidae indet.	–	–	+
Copepoda Cyclopoida	*Heptnerina confusa*	–	–	+
	Oncaea sp.	–	+	–
	Cyclopinidae indet.	–	–	+
	Oithonidae indet.	–	–	+
	Lubbockiidae indet.	–	–	+
Copepoda Spinocalanoida	Spinocalanoida indet.	–	–	+
Ostracoda	*Bathyconchoecia paulula*	–	–	+
	Bairdia sp.	–	–	+
	Bythocypris sp.	–	–	+
	Krithe sp.	–	–	+
	Propontocypris sp.	–	–	+
	Poseidonamicus sp.	–	–	+

(Continued)

TABLE 2 Continued

A

Taxon		Lost City	Broken Spur	Other MAR fields
	Ostracoda indet.	+	–	+
Bivalvia	Bivalvia indet.	+	–	+

B

Taxon	Lost City	Broken Spur	Otder MAR fields
Acantholaimus	–	–	+
Acanthopharynx	–	–	+
Actinonema	+	–	–
Anoplostoma	–	–	+
Anticoma	–	–	+
Anticomidae indet	+	+	+
Amphimonhystrella	–	–	+
Aponema	–	–	+
Araeolaimus	–	–	+
Benthimermitidae indet.	–	–	+
Calomicrolaimus	–	–	+
Camacolaimus	–	–	+
Capsula	–	–	+
Cephalochaetosoma	–	–	+
Chromadorella	–	–	+
Chromadorina	–	–	+
Chromadorita	–	–	+
Cobbia	–	–	+
Cyatholaimus	–	–	+
Daptonema	+	–	+
Desmodora	+	–	+
Desmoscolex	–	–	+
Dinetia	–	–	+
Diplopeltidae indet.	–	–	+
Diplopeltoides	–	–	+
Dracogallus	–	–	+
Draconema	–	–	+
Eleutherolaimus	–	–	+
Enchelidiidae indet.	+	–	–
Enoplus	+	–	–
Enoplidae indet.	–	–	+
Epsilonema	–	–	+
Epsilonematidae indet.	–	–	+
Euchromadora	–	–	+
Eurystomina	–	–	+
Halalaimus	–	–	+
Halomonhystera	–	–	+
Halichoanalaimus	–	–	+
Leptolaimus	–	–	+
Leptolaimidae indet.	–	–	+

(Continued)

TABLE 2 Continued

B

Taxon	Lost City	Broken Spur	Otder MAR fields
Megadesmolaimus	–	–	+
Metacomesoma	–	–	+
Metacylicolaimus	+	–	–
Metachromadora	–	–	+
Metadesmolaimus	–	–	+
Metalinhomoeus	–	–	+
Metepsilonema	–	–	+
Microlaimus	–	–	+
Molgolaimus	–	–	+
Monhysteridae indet.	–	–	+
Oncholaimus	+	–	+
Oncholaimidae indet.	–	–	+
Oxystomina	–	–	+
Palinchomoeus	+	–	+
Paracanthonchus	–	–	+
Paracanthonchus olgae	+	+	+
Parapinnanema	–	–	+
Prochaetosoma ventriverruca	+	–	+
Prochromadora helenae	+	+	+
Prooncholaimus	–	–	+
Pselionema	–	–	+
Quadricoma	–	–	+
Retrotheristus	–	–	+
Rhabdocoma	–	–	+
Sabatieria	–	–	+
Sphaerolaimus	–	–	+
Synonchus	–	–	+
Syringolaimus	+	–	+
Terschellingia	–	–	+
Thalassolaimus	–	–	+
Thalassomonhystera	–	–	+
Theristus	–	–	+
Tricoma	–	–	+
Viscosia	–	–	+

taxa have been recorded so far from Broken Spur, including a cnidarian (*Maractis rimicarivora*), three molluscs: *Phymorhynchus ovatus*, *Bathymodiolus azoricus* and *B. puteoserpentis*, four decapods: *Alvinocaris markensis*, *Mirorcaris fortunata*, *Rimicaris exoculata* and *Segonzacia mesatlantica*, and an ophiuroid (*Ophioctenella acies*). In addition, the Broken Spur was also reported to be significantly impoverished in terms of megabenthic abundance, compared to other vent fields, e.g. the TAG, Snake Pit or Rainbow (Desbruyères et al., 2000). However, the apparent lower number of taxa and lower abundance of the megafauna at the Broken Spur might be due to the lower sampling intensity at this vent field.

The habitat preferences of individual megafaunal species within the Broken Spur field were briefly treated by Desbruyères et al. (2000) who reported *R. exoculata* as a species dominant on black smoker walls and *M. fortunata* aggregating at the foot of chimneys, while the two *Bathymodiolus* species and *O. acies* were distributed in the surrounding blocs within the active field area. *Mirocaris fortunata*, one of the dominants at the Lucky Strike field, is an example of "social" (aggregations > 100 ind/m^2) and epibiont-dependent shrimps (Zbinden et al., 2018), grouping in the axis of a warm (20-25°C) flow of the hydrothermal current (Shillito et al., 2006; Matabos et al., 2015). The species was observed to occur across a wide range of habitats, often in

association with beds of the mussel *Bathymodiolus azoricus*, and to graze on microorganisms or detrital remains (Gebruk and Galkin, 1997; Matabos et al., 2015). The bythograeid crab *Segonzacia mesatlantica* was variously described as a scavenger or a carnivore (predator; cf. Boschen-Rose and Colaço, 2021), but its feeding behaviors observed by Matabos et al. (2015) were far from unequivocal.

The Broken Spur vent field is of a great biogeographical importance as a boundary between the northern and the southern vent faunas on the MAR (O'Mullan et al., 2001; Dunn et al., 2018). Regarding the mytilid assemblages, the Broken Spur is also a hybridization zone between the two mussel species (*Bathymodiolus azoricus* and *B. puteoserpentis*); in other words, it has the highest proportion of mussel hybrid individuals along the MAR (Dunn et al., 2018).

The shrimp assemblages at the Broken Spur are dominated by *Rimicaris exoculata*, although shrimp swarms in the area are not as dense as those often observed at, e.g. the TAG (Rybakova and Galkin, 2015). The species' populations are reported to be stable for a relatively short time (about 15 months) (Copley et al., 1997) as well as in a long-term (decadal) perspective, as found at, e.g. the Lucky Strike (Cuvelier et al., 2011).

Four nektobenthic invertebrate species were sampled from the PECA, all representing the endemic caridean shrimps from the superfamily Bresilioidea, i.e. *Alvinocaris markensis, Rimicaris chacei, R. exoculata*, and *Mirocaris fortunata* [(= *M. keldyshi* (Komai and Segonzac, 2003)] (Mironov et al., 2002; Galkin, 2006; Gebruk and Mironov, 2006). These species are the dominant fauna in images of the seafloor. They have been reported from geologically active sites of the northern MAR, from Deyin (15.02° S) to Moytirra (45.3° N), within a wide depth range (1740–4200 m), their presence revealing clear spatial and demographical patterns (Zbinden and Cambon-Bonavita, 2020). The occurrence of the highly specialized *Rimicaris* species, whose trophic relationships are dependent on epibiotic microorganisms, is tightly associated with hydrothermal vent orifices, the optimal ambient temperatures ranging within 3.4-22.5°C (Gebruk and Galkin, 1997; Gebruk et al., 2000; Zbinden and Cambon-Bonavita, 2020). The densest swarms of *R. exoculata* (up to 3000 ind./m^2) were recorded at the Logatchev, and also at the Broken Spur (Gebruk et al., 2000). The swarms are maintained by a highly modified, eye-like organ adapted to the black-body radiation emitted by smokers (Williams and Rona, 1986; Pelli and Chamberlain, 1989; Nuckley et al., 1996), the organ enabling the shrimps to stay close to, but at a safe distance from, black-smoker orifices emitting the hot plume.

2.2 Functional aspects

Functional aspects of benthic communities on the MAR are known only partially. An interesting approach has been recently presented by Alfaro-Lucas et al. (2020) who addressed functional diversity of the Lucky Strike vent field fauna and found it enhanced at sites directly affected by hydrothermal activity and reduced at surrounding sites. An important conclusion of their study was that "Low functional richness and environmental filtering suggest that surrounding areas, with their very heterogeneous species and functional assemblages, may be especially vulnerable to environmental changes related to natural and anthropogenic impacts, including deep-sea mining". This type of reasoning, however, has not evolved into a generalization encompassing other MAR areas yet. Here we touch upon certain aspects of functioning of vent field benthos which are important as baseline information and for which there exist only limited data from the PECA.

2.2.1 Distribution

Distribution patterns of individual benthic taxa in the wider MAR, and in the PECA in particular, have not been resolved in detail, although – with regard to the MAR – there exist a number of interesting observations. For example, populations of vent-associated shrimps reveal a highly structured spatial segregation and demographic patterns (Shank et al., 1998b; Gebruk et al., 2000; Methou et al., 2022). While mature females of *R. exoculata* occur in abundance in areas close to fast flowing hydrothermal fluids, juveniles, in contrast, are found in clusters only some distance from the active vents. Mature males and females of the species form clusters clinging to rocky surfaces in localised areas, becoming prey for sea anemones occupying the space on the edges of black-smokers (Gebruk et al., 2000; Hernández-Ávila et al., 2022; Methou et al., 2022). The reasons for these spatial differences along the thermal gradient have not been fully resolved, but a similar spatial pattern is apparent in several vent invertebrate taxa, such as *Kiwa tyleri* in the Antarctic and *Calyptogena* sp. in the Pacific (Marsh et al., 2015). The proposed explanations for this segregation include habitat-thermal requirements, intraspecific and interspecific competition for space and resources or a succession effect (Shank et al., 1998a; Marsh et al., 2015). Juveniles that still hold food reserves from their larval period do not need to compete for access to the microorganism primary producers which use the hydrothermal minerals, essential for adults which are fully dependent on epibionts. It has been proposed that the eye-like organ renders *R. exoculata* a stronger competitor to *R. chacei*, a species occurring as solitary individuals or forming small aggregations of some tens to hundreds individuals in more peripheral zones at, e.g. the Snake Pit and TAG (Gebruk et al., 2000; Methou et al., 2022). *Alvinocaris markensis*, an opportunistic feeder, also stays in peripheral zones and at the foot of hyrothermal vents (Gebruk and Galkin, 1997; Lunina and Vereshchaka, 2014).

2.2.2 Abundance and biomass

Data on the benthic abundance and biomass from the PECA are generally scant, whereas overviews have been presented for

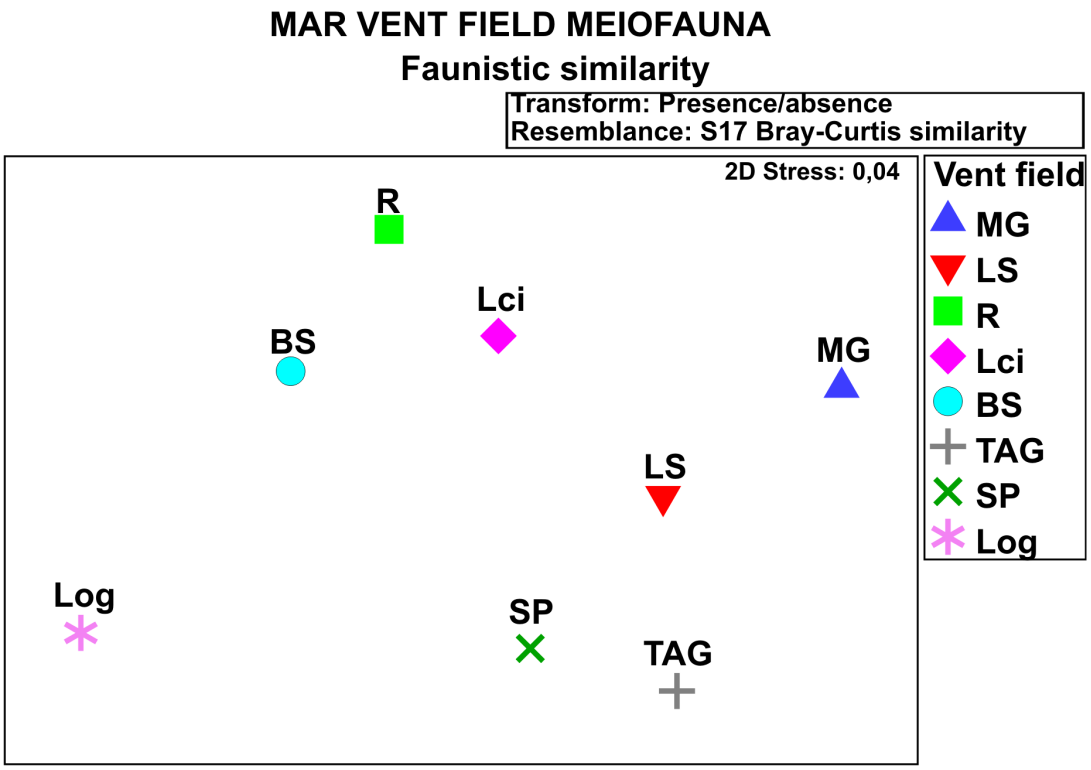

FIGURE 2
An MDS plot of similarity/dissimilarity (presence-absence transformation; group-average sorting) between the composition of meiobenthic assemblages at different MAR vent fields (presence-absence transformation; Bray-Curtis similarity); Vent field name symbols: R, Rainbow; BS, Broken Spur; Lci, Lost City; MG, Menez Gwen; LS, Lucky Strike; SP, Snake Pit; TAG, Trans-Atlantic Geotraverse; Log, Logatchev.

other areas (e.g. Galkin, 2006). Those overviews concern primarily the dominant and foundation species at hydrothermal vents, such as the bresilioid shrimps (see above). The abundance and biomass reported for *R. exoculata* at the Broken Spur were on the order of 2500-3000 ind./m^2 and up to 1-1.5 kg/m^2, respectively. Another group of foundation and dominant species is formed by mytilid bivalves a representative of which, *Bathymodiolus puteoserpentis*, forms usually dense and extensive beds, with over 70 kg/m^2 biomass at the Logatchev, but is much less abundant at the Broken Spur where it occurs in localized patches only (Galkin, 2006). The lower abundance at the Broken Spur is probably related to this vent acting as a zone of hybridization between *B. azoricus* and *B. puteoserpentis* (see above).

Van Dover (2014) described the hydrothermal vent ecosystems as dominated by holobiont taxa, i.e. organisms that host symbiotic chemoautotrophic microorganisms. These taxa often occur as the foundation species forming complex 3-dimensional habitats (Gerdes et al., 2019), e.g. mytilid and vesicomyid bivalves and polychaetes of the genus *Chaetopterus* which occur in large numbers away from active smokers. Aggregations of these taxa are used as a substratum, refugia and a habitat for epizoic microorganisms, juvenile invertebrates, and other associated organisms, including the meiobenthos (nematodes, harpacticoids, halacarids) which occasionally, e.g. at the Broken Spur, are found in abundance. There are also primary consumers (e.g. the limpets *Peltospira smaragdina* and *Lepetodrilus atlanticus* grazing on microbial biofilms) as well as secondary and tertiary consumers such as scavenging and predatory crustaceans and fishes.

The total biomass values of aggregations of *R. exoculata* or *B. puteoserpentis*, shown above, are typically very high at vents. Beyond the active hydrothermal vent area, faunal abundances and biomass are usually much lower, the megafauna being represented by solitary large anemones (e.g. *Maractis rimicarivora)* and gorgonian corals (Van Dover, 2014).

The soft sediment-covered areas away from active venting support fairly abundant meiobenthic communities compared with abundances found in other deep-sea environments. Abundances at the TAG and Snake Pit hydrothermal vent fields are 11-35 and 72-86 ind/10cm^2 respectively (Spedicato et al., 2020).

Faunal density responses appear to be a function of stress level. For example, at Middle Valley (2410 m, the Juan de Fuca hydrothermal vent field in the Pacific), very hot sediments (e.g.

TABLE 3 Non-meiofaunal taxa reported from the PECA vent fields (Lost City and Broken Spur) (data from Copley et al., 1997; Kelley et al., 2005; Gebruk and Mironov, 2006; Vereshchaka and Vinogradov, 2006; Boschen-Rose and Colaço, 2021); +, taxon recorded; -, taxon not recorded.

Taxon			Lost City	Broken Spur
Cnidaria	Hydrozoa	*Candelabrum* sp.	–	+
	Actiniaria	*Maractis rimicarivora*	–	+
	Scleractinia	*Desmophyllum pertusum*	+	–
Annelida	Polychaeta	*Amphisamytha lutzi*	–	+
		Archinome sp.	–	+
		Ophiotrocha sp.	+	–
		Branchiopolynoe aff. *seepensis*	–	+
		Prionospio sp.	–	+
Mollusca	Gastropoda	*Lirapex* sp.	+	–
		Lurifax vitreus	+	–
		Peltospira smaragdina	–	+
		Phymorchynchus carinatus	–	+
		Phymorchynchus moskalevi	–	+
		Phymorhynchus ovatus	–	+
		Phymorchynchus sp.	+	–
		Pseudorimula midatlantica	–	+
		Puncturella sp.	+	–
		Shinkailepas briandi	–	+
		Emarginula sp.	+	–
		Lepetodrilus atlanticus	–	+
	Bivalvia	*Asperarca nodulosa*	+	–
		Bathymodiolus azoricus	+	+
		Bathymodiolus puteoserpentis	–	+
		Thyasira sp.	+	–
Arthropoda	Cirripedia	*Metacerrucca inermis*	+	–
		Poecilasma aurantia	+	–
	Amphipoda	*Bouvierella* aff. *curtirama*	+	–
		Hirondella brevicaudata	–	+
		Paraphronima sp.	–	+
		Primno evansi	–	+
		Streetsia sp.	–	+
		Dulichiopsis dianae	–	+
	Decapoda	*Alvinocaris markensis*	–	+
		Chorocaris chacei	–	+
		Mirocaris fortunata	–	+
		Rimicaris exoculata	–	+
		Keldyshicaris vavilovi	–	+
		Bathynectes maravigna	+	–
		Segonzacia mesatlantica	–	+
		Munida sp.	+	–
		Munidopsis exuta	–	+
Echinodermata	Ophiuroidea	*Ophioctenella acies*	–	+
	Echinoidea	*Araeosoma fenestratum*	+	–
		Cidaris sp.	+	–

94°C at 5 cm into the sediment column) support very few macrofauna, whereas moderately warm sediments inhabited by vesicomyid bivalves may support elevated macrofaunal densities (16,500 ind./m^2) relative to those in microbial mats (6,840 ind./m^2), hot sediments (1,690 ind./m^2), and control (not heated) sediments (2,218 ind./m^2) (Bernardino et al., 2012). The only more detailed study demonstrated that, generally, the abundance and biomass of the macrofauna in the soft sediments seem to be at a level similar to that in other deep sea sites at the same depth range (Priede et al., 2013). It is worth noting that the samples analyzed by Priede et al. (2013) were all collected some distance away from the mid-axial valley. No other comparative data are as yet available either from the MAR in general or from the PECA in particular.

2.2.3 Trophic relationships

Two different trophic pathways have been reported at the Broken Spur and Lost City in the PECA, one present in the in-axis basalt-hosted systems (e.g. Broken Spur) and the other in the off-axis ultramafic-hosted systems (e.g. Lost City). Both systems are based on conversion of the hydrothermal energy into biomass of chemosynthetic bacteria, but differ in specific sources of metabolic energy utilized by primary producers: oxidation of sulfur compounds (basalt-hosted systems; McCollom and Shock, 1997) or reactions involving H_2 and CH_4 (sulfide-poor ultramafic systems; McCollom, 2007). Thermodynamic modeling indicates that metabolic reactions utilized as energy sources in the ultramafic-hosted systems can supply about twice as much chemical energy and potentially support much higher biomass than analogous systems hosted in basaltic rocks (McCollom, 2007).

There are two main types of primary consumers at the PECA hydrothermal vents studied to date; 1) those hosting endosymbionts (e.g. *Bathymodiolus* mussels) and 2) those feeding on free-living bacteria (e.g. *Rimicaris* shrimps). In addition, different types of predators, based on the type of primary consumers present, complete very simple food webs typical of hydrothermal vents (Gebruk et al., 2000; Vereshchaka et al., 2000; Colaço et al., 2002; Colaço et al., 2007). However, as observed by Matabos et al. (2015), some trophic relationships, e.g. those involving the bythograeid crab *Segonzacia mesatlantica* appear uncertain, although Boschen-Rose and Colaço (2021) – referring to studies using stable isotopes – treat the species as a predator.

2.2.4 Endemism

Endemism at hydrothermal vents can be considered from two viewpoints: one concerns vent-obligate fauna at hydrothermal vents in general, and the other – endemism at specific individual vent fields. When looked at from the first viewpoint, the vent-obligate fauna on the MAR shows a moderate degree of endemism only. The majority of such taxa are widely distributed along the MAR due to their good swimming ability, planktonic larvae and/or passive migrations (Jollivet, 1996; Teixeira et al., 2013; Hilário et al., 2015). At the present state of knowledge, only five families are considered unique for individual vent fields: the sea anemones Actinostolidae (found at TAG), the gastropods Neolepetopsidae (Lucky Strike), the Neopilinidae (Menez Gwen), and two amphipod families — Amphilochidae (Lucky Strike) and Stegocephalidae (Snake Pit). No information from the PECA in this respect is available.

Of the 61 vent-obligate taxa found at 7 sites on the MAR (Menez Gwen, Lucky Strike, Rainbow, Broken Spur, TAG, Snake Pit and Logatchev) (Mironov et al., 2002), about half (30 species or 49%) are limited in their occurrence to a single field. Most shared vent-obligatory species occurred in the Menez Gwen, Lucky Strike and Rainbow, perhaps because those three vent fields – most accessible due to their vicinity to the Azores and located at relatively shallower depths – received disproportionately large attention from researchers. Generally, a high level of endemism is observed in crustacean amphipods and alvinocarid shrimps, with four species (80%) recorded at only a single site. Incidentally, a new shrimp species, *Keldyshicaris vavilovi* was discovered in 2001 at the Broken Spur vent field (Lunina and Vereshchaka, 2014). Since it has not been so far reported from any other location, it has to be regarded as field-endemic.

A high degree of endemism (58%) was reported for the Lost City field macrofauna (Kelley et al., 2005) (see below).

Endemic taxa are also known within the macro- and meiofauna. For example, in the latter, the siphonostomatoid copepod family Dirivultidae is known exclusively from vent habitats (e.g. Gollner et al., 2010). Four known vent species of the Halacaridea (Acarina) and nine of the 13 (69.2%) species of the Dirivultidae (Copepoda) are known from only one location on the MAR.

2.3 A special case: Lost City

When discussing the available knowledge on the PECA benthos, a special consideration is due to the Lost City. It is a geologically and ecologically distinct hydrothermal field within the MAR (Kelley et al., 2005) which has become a focus of vigorous international research (e.g. Früh-Green et al., 2015). It differs from other hydrothermal fields in its age (spanning about 30,000 years, i.e. older than other MAR structures (Früh-Green et al., 2003), geological setting (serpentinite rather than basalts) and characteristics of the hydrothermal fluid (high alkalinity, lower fluid temperature) (e.g. López-Garcia et al., 2007). The unique characteristics of the Lost City (Denny et al., 2015) and its being one of the few carbonate vent fields discovered so far (Lecoeuvre et al., 2021) resulted in the field becoming an important conservation target, recognised as an Ecologically

and Biologically Significant Area (EBSA) under the Convention on Biological Diversity (CBD) (Casson et al., 2019; Johnson, 2019) and as a potential UNESCO World Heritage Site in the high seas (Freestone et al., 2016). As the Lost City does not host any mineral resources of interest, it is not likely to be targeted for mining, but the neighboring areas might be. The Lost City might therefore be affected by consequences of possible mining activities (e.g. sediment plumes, contamination) (Johnson, 2019), hence the need of a more detailed knowledge.

Most of biological research in the Lost City has concerned its microbiology (Boetius, 2005; Dulov et al., 2005), with a particular attention paid to the sub-bottom biome (e.g. Brazelton et al., 2006; Orcutt et al., 2011; Lang and Brazelton, 2020). Studies on the Lost City archaea and bacteria revealed shifts on millennial time scales (Brazelton et al., 2010), associated with preadaptation of various microbial taxa to environmental conditions. On the other hand, only a few studies have targeted benthic communities. The limited data available show the Lost City macro- and megabenthos to be very different in composition from corresponding assemblages in other fields (e.g. Fabri et al., 2011; Boschen-Rose and Colaço, 2021; cf. Table 3), most probably due to the lack of chemoautotrophic symbiont-supporting fauna (see below). The initial surveys indicated few macroorganisms, with a notable absence of large bivalves known from other vent fields. However, beds of dead mytilid bivalve shells were found in a nearby inactive field named Old Village (Lein et al., 2007). With time, as more dives were performed and a larger area was being inspected, diverse but very scattered macro- and megafaunal assemblages, including large eurybathic fish, were revealed. In 2005, Shank and Buckman[2] as well as Kelley et al. (2005) reported the presence of more than 70 "potential species" representing the macrobenthos (gastropods, bivalves, amphipods, numerous polychaetes with at least 5 new species) and meiofauna (nematodes, ostracods) as well as fish (e.g. the wreckfish *Polyprion americanus*, the cut-throat eel *Synaphobranchus kaupi).*

The biomass (wet weight) at the Lost City was apparently lower compared to a typical hydrothermal vent on the MAR. The large mobile megafauna (the fish mentioned as well as large geryonid crabs, visible around active vents) were the largest biomass components (Kelley et al., 2005).

Kelley et al. (2005) as well as Shank and Buckman[2] reported also on a sharp difference between the fauna of vent and non-vent habitats at the Lost City, whereby typical vent areas are sparsely populated, whereas non-venting habitats less than a few meters away (e.g. on the sides of inactive solidified carbonate structures, sedimented areas, and breccia cap rock just to the north of the field) are dominated by hard corals *(Desmophyllum pertusum*, known formerly as *Lophelia pertusa)*, octocorals (gorgonians), galatheid crabs, turrid gastropods, foraminifera, pteropods, urchins, asteroids, ophiuroids, and "typical" deep-sea barnacles.

It is very likely that the diverse and endemic (endemicity estimated at about 58%; Kelley et al., 2005) local macrofauna feed mainly on microbial mats, both on the surface and in the inner structures of serpentinite chimneys (Kelley et al., 2007). In contrast to other vent fields, the Lost City fauna did not show the presence of chemoautotrophic symbionts because most of the reduced energy at the Lost City comes from hydrogen, and no animals have been reported to support hydrogen oxidizers as symbionts (Boetius, 2005). However, *Bathymodiolus azoricus*, known to host methane- and sulfur-oxidizing symbionts elsewhere on the MAR was reported from the Lost City (cf. Table 3), but it is not known yet whether its survival there depends on chemosymbiosis. On the other hand, as already indicated and as can be judged from the limited data on the meiobenthic assemblages available, the meiofauna composition shows a somewhat closer affinity to the other active vent field in the PECA (Broken Spur) as well as to the Rainbow field than to the remaining hydrothermal vent fields studied (cf. Figure 2). It remains to be seen, however, to what extent the similarity is a result of the limited database rather than a manifestation of a true distributional pattern.

3 The unknowns, knowledge gaps and research needs

As can be seen from the "knowns" discussed above, the knowledge gaps with respect to the benthic communities in the PECA, like in the entire MAR (Boschen-Rose and Colaço, 2021), are considerable (see a summary, with respect to the relevant ISA guidelines and recommendations for the contractors, in Table 4).

First of all, there is poor published knowledge on the range of habitats present in the area. Detailed seabed mapping of habitats (cf. Gerdes et al., 2019) is a top priority for the effective planning of both PMS resource exploration and environmental sampling campaigns. High-resolution seabed mapping should include the identification of active and inactive hydrothermal vent fields (Van Dover, 2019; Menini and Van Dover, 2019; Jamieson and Gartman, 2020; Van Dover et al., 2020). Knowledge of extinct hydrothermal fields might be particularly important because they may be the first targets of mining activities (Van Dover et al., 2020).

In line with research needs identified recently by Amon et al. (2022), the broadening of the knowledge base on benthic communities in the PECA requires high-resolution sampling and analysis of all benthic size categories (meio-, macro-, and megabenthos as well as the nektobenthos), using both direct-access gear (e.g. cores) and visual access tools (underwater cameras). To address outstanding issues on within-PECA connectivity of benthic communities, it will be necessary to

2 https://oceanexplorer.noaa.gov/explorations/05lostcity/background/macrofauna/macrofauna.html

collect temporally and spatially resolved data on the larval abundance and larval dispersal patterns (Vrijenhoek, 2010; Hilário et al., 2015; Baco et al., 2016).

The research gaps regarding the PECA's meiobenthos are huge. As the meiobenthos is a good proxy of many natural and anthropogenic processes in the deep sea (Zeppilli et al., 2016; Zeppilli et al., 2018), there is a need to increase knowledge on the composition, abundance, and functional relationships within the meiobenthic communities and on their interactions with other benthic compartments. At hydrothermal vent sites worldwide, the meiobenthos has been found to be associated with various habitats, from inactive bare basalts (Gollner et al., 2010) and sediments (Vanreusel et al., 1997) to diffuse vent flow areas colonised by macrofaunal assemblages (Zekely et al., 2006; Sarrazin et al., 2015). When working on nematodes in the Pacific's Fiji-Lau area, Vanreusel et al. (1997) found a qualitative dissimilarity between the nematode faunas of hydrothermal vent field sediment and in the nearby abyss, with no vent-field taxa being recorded in the abyssal sediment. As no between-habitats comparisons have been conducted on the MAR and given the prevalence of sedimentary habitats there (cf. Riehl et al., 2020), it is important (also from the standpoint of connectivity) to determine how similar/dissimilar the assemblages are between the ridge itself and the surrounding deep-sea areas. In this context, it is necessary that the contractors use best practices in studying the meiofauna, such as TV-guided coring devices (Varliero et al., 2019; Haeckel and Linke, 2021), especially in and around sediment patches near rocky surfaces in the mid-axial valley, and eDNA assays. All the contractors should be tooling up if they are seriously considering mining for PMS. This includes technologies for environmental baseline studies and subsequent monitoring activities if mining is allowed to proceed.

At present, knowledge of the PECA macrobenthos is extremely limited. Current knowledge relates to data collected in other parts of the MAR, often at a great distance from the PECA, and at different depths. Knowledge on the most important and diverse macrofaunal taxa, such as polychaetes, peracarid crustaceans, bivalves and gastropods is very poor along the whole MAR, and there have been only a few quantitative assessments of the standing stock and diversity. Macrobenthos studies on mid-ocean ridges have been limited owing to the need to use the so-called contact samplers, such as dredges, epibenthic sledges, grabs and corers. However, newer technologies, such as TV-guided corers (see above) and Remotely Operated Vehicles (ROVs) are now allowing greater precision sampling in areas of difficult terrain. A particularly wide knowledge gap concerns the fauna associated with soft sediments (Bergstad et al., 2008; Gebruk et al., 2010; Shields and Blanco-Perez, 2013; Priede et al., 2013). This habitat is a very important component of the MAR region (Niedzielski et al., 2013; Denny et al., 2015; Dutkiewicz et al., 2015), most likely including the PECA. Some studies suggest that the contribution of endemic species in some groups may, even in areas located away from the hydrothermal vent ecosystems, reach several per cent (e.g. Molodtsova et al., 2008; Tabachnick and Collins, 2008; Braga-Henriques et al., 2013). Therefore, studies of the soft-bottom ecosystems located outside the actual vent fields should be amongst the priorities of future research programs in the PECA.

Taxonomic studies based on both morphological and molecular data are vital for biodiversity estimates and ecological analyses (Frutos et al., 2022; Kaiser et al., 2022), such as assessing connectivity between sites within the PECA and more widely on the MAR. Therefore, different complementary sampling techniques (e.g. epibenthic sledges and box corers), including technologies for collecting fauna that are becoming standard systems in areas of rough terrain (e.g. TV-guided box corers and ROVs) should be used to allow biodiversity inventory and taxonomic studies as well as quantitative research that links the information about the benthic biota with data about the environmental factors shaping their communities (Jóźwiak et al., 2020). Earlier studies from the MAR demonstrated that the rate at which new species are described, although increasing with time, is still very low (e.g. Tyler et al., 1995; Sigvaldadottir and Desbruyères, 2003; Myers and Cunha, 2004; Cunha and Wilson, 2006; Larsen et al., 2006; Bellan-Santini, 2007; Corbera et al., 2008; Budaeva, 2012). The identification of a wide range of different taxa in the PECA area, most of them new to science, is a particular challenge for a contractor. Developing the availability of taxonomic expertise to allow the delivery of timely environmental studies is of key importance. Although there are efforts to create relevant taxonomic clearing houses (e.g. the recent ISA's Sustainable Seabed Knowledge Initiative, www.isa.org/sski), there are difficulties in getting responses on commercial timescales without investing in local expertise by individual contractors. In many cases, contractors have mobilised national universities in supporting deep-sea mining exploration needs and future monitoring tasks.

The scale of the undescribed biodiversity is most probably huge. For example, about 50% of scavenging amphipods collected in the vicinity of the Charlie-Gibbs Fracture Zone proved to be new to science (Horton et al., 2013). The study on the polychaete fauna collected using a megacorer (a type of multiple corer) in the same MAR area (Shields and Blanco-Perez, 2013) resulted in recording 133 species in just 11 samples; almost none could be assigned to already described species. Moreover, the majority of them were singletons. It is worth mentioning that today, almost ten years after that collection was obtained, no taxonomic descriptions were published other than those of representatives of the family Polynoidae (Shields et al., 2013). The perceived high diversity, and probably also a high level of rarity, may create problems with finding appropriate taxonomic expertise and with securing a reasonable sampling effort needed to draw meaningful conclusions. Since large seafloor areas of the PECA have never been sampled, a very high number of species new to science is expected, not only amongst the most speciose and abundant taxonomic groups

such as polychaetes or molluscs (as well as other taxa undergoing development *via* planktonic larvae), but also amongst organisms with direct development, limited dispersal abilities and low abundance, such as peracarids (tanaidaceans, cumaceans and isopods). Despite their low abundance and biomass, they constitute a very important component of the deep-sea communities worldwide (Stępień et al., 2021; Jóźwiak et al., 2022). Along with polychaetes, they form a core of the marine macrobenthic assemblages at bathyal depths and deeper (McCallum et al., 2015; Brandt et al., 2018; Washburn et al., 2021). Their limited mobility (no planktonic larvae, burrowing life style) restricts dispersal, for which reasons these crustaceans are considered a good indicator of environmental conditions and potentially an ideal surrogate for assessing recovery potential of disturbed ecosystems (Jennings et al., 2018; Jakiel et al., 2018; Riehl et al., 2018; Jakiel et al., 2019). Recent molecular studies demonstrated also that the problem of endemism, cryptic diversity and connectivity along the MAR is very complex and requires further studies (Teixeira et al., 2013; Yahagi et al., 2019) which can be very important for further planning of basic taxonomic analyses but also for studies of distribution patterns and community ecology on various temporal and spatial scales. Resolving the connectivity problem is of a particular importance for contractors, as it is through connectivity that areas disturbed by mining might be recolonized and repopulated (Hilário et al., 2015).

Future studies should also include other groups of benthic animals. For example, Jones et al. (2013) showed enteropneusts (Enteropneusta), a taxon belonging to the most underestimated deep-sea organisms worldwide (Tassia et al., 2016), to be important bioturbators at MAR's bathyal depths. Since the available species lists of various benthic taxa are often scattered among various publications, including short taxonomic notes (e.g. Bellan-Santini and Thurston, 1996; Gebruk et al., 2010; Goroslavskaya and Galkin, 2011; Dilman, 2013; Shields and Blanco-Perez, 2013; Kongsrud et al., 2013), there is also a great need to incorporate the results of the current and future studies into publicly available databases.

Knowledge on environmental controls of the PECA's benthic assemblages is sorely lacking. It is necessary to find out if environmental controls such as those referred to by Boschen-Rose and Colaço (2021) and Priede et al. (2022), i.e. depth, surface primary production and POC flux, bathymetry and chimney type are likely to influence the distributions of fauna within in the PECA, Knowledge on biology and habitat requirements of individual benthic taxa is incomplete. Fauna at other locations on the MAR have shown a wide variety of associations, interactions and behaviors of individual taxa. Examples are furnished by an association between polychaetes and bivalves (Bebianno et al., 2018) in which the polychaete, *Branchipolynoe seepensis*, kleptoparasitic in and commensal with *Bathymodiolus azoricus*, plays a role in metal detoxification of the bivalve, and the association is likely an adaptation to metal concentrations at the vent sites studied (Menez Gwen and Lucky Strike) as well as by an apparently commensal association between polynoid polychaetes (*Eunoe bathydomus*) and holothurians *Deima validum* (Shields et al., 2013). These examples demonstrate a unique nature of biological interactions, particularly in the vent systems. Studies of the reproductive behaviour, physiology, and development have also been infrequent, a particular attention being paid to the vent fauna (e.g. Blake and Van Dover, 2005; Riou et al., 2010; Marticorena et al., 2020; Cruz et al., 2022; Hernández-Ávila et al., 2022). The anticipated complexity of mutual interactions as well as a high diversity of trophic and ecological groups shows also a great need for functional analyses that assess the level of niche occupancy in the communities and allow to estimate functional redundancy – a knowledge especially needed in ecosystem considered vulnerable to anthropogenic impacts. Another challenge is presented by studies on biology of individual taxa. Since such approach is often logistically difficult and requires more specialized techniques and planning, it would probably be very difficult to conduct in the near future, although the results might provide important insights into the functioning of the MAR benthic communities.

It has to be borne in mind that the general knowledge on the benthic communities on the MAR, and the PECA in particular, is based on only a relatively low number of published reports. For example, Boschen-Rose and Colaço (2021) based their analyses on 52 peer-reviewed papers (prior to exclusion of some as not meeting the predetermined criteria); Weaver et al. (2021) analysed benthic communities on information from about 110 peer-reviewed papers, whereas we searched for information on the PECA benthos in 90 available publications. Therefore, any generalisations and more comprehensive conclusions regarding the distribution patterns and factors influencing the benthic communities are very tentative and need verification by further studies based on a higher sampling effort. Moreover, methodological constraints have to be taken into consideration. For example, observations of the megafauna, usually conducted from ROVs, produce low-resolution taxonomic assessments leading to underestimation of the actual diversity (e.g. Alt et al., 2019). However, the technical advances in imaging technology (e.g. Dumke et al., 2018) and annotation software (Nuno Gomes-Pereira et al., 2016) have allowed a progress to be made in this respect. Also, methods are at present at hand with which to estimate the megafaunal biomass from underwater imagery (Benoist et al., 2019). Nevertheless, it is still very difficult to identify factors shaping spatial patterns of the megabenthos and to predict possible responses of the communities to anthropogenic impacts (Dunn et al., 2018).

Earlier research in other parts of the MAR suggests also the necessity of exploring microhabitat distribution and analysis of nutrient input that may influence the composition of nektobenthic megafaunal aggregations (Morris et al., 2012; Alt et al., 2019) as well as depth related zonation (Gebruk and

Krylova, 2013; Molodtsova et al., 2017). The role of sessile megafaunal communities must also be viewed through their importance as ecosystems engineers that may shape the overall biodiversity by increasing the habitat complexity and providing microhabitats for other invertebrates (Buhl-Mortensen et al., 2008; Alt et al., 2019).

Weaver et al. (2021) have recently published a detailed summary of knowledge on biogeography and habitat-specificity available from published accounts of the MAR fauna. With respect to geographic patterns, they commented on a very unequal coverage of different parts of the MAR, the areas north of the Azores and the vent field off the Azores having received most attention. Regarding the habitats, they distinguished hard (non-hydrothermal, hydrothermally active and hydrothermally inactive) substrata, and areas covered by soft sediment; in some areas, the sediment layer is of a considerable thickness. The non-hydrothermal substrata on the MAR were found to support cold-water corals and sponges, along with their associated fauna (macro- and meiofauna) of which little is known generally; this lack of knowledge concerns the PECA as well. More attention has been given to the fauna of hydrothermally active substrata, with some biogeographic trends detected (see below). Endemicity of the fauna supported by hydrothermally active substrata is not entirely clear. Although a number of taxa have been reported to be endemic to hydrothermal vent substrata in general (e.g. dirivultid copepods; Gollner et al., 2010) or to individual fields (see above), the absence of organisms in scientific observations may be a result of insufficient sampling effort (Weaver et al., 2021). With respect to the benthic invertebrate fauna of soft sediments along the MAR, most information can be found in accounts on the Russian Exploration Area (separated from the PECA by the French Exploration Area; cf. Figure 5.1 of Weaver et al., 2021). The trawling campaigns there revealed the presence of at least 136 megafaunal species (Molodtsova et al., 2017), including hermit crabs, ophiuroids and asteroids, bryozoans, brachiopods, ascidians and pennatulids. As remarked by Weaver et al. (2021), the distribution of macrofaunal and meiofaunal invertebrates, not captured by trawls, is very poorly known from soft sediments along the MAR and virtually no regional patterns can be discerned using the currently available data.

As highlighted by Bell et al. (2016), small scale (a distance lower than 10 km) habitat availability is amongst the most poorly understood aspects of ecological interactions in the MAR region. Recent results from the MAR demonstrated that many important interactions between benthic organisms occur at much smaller scales (Shields et al., 2013; Bebianno et al., 2018). It seems important then to understand processes occurring within a range of meters, at the microhabitat level, because large-scale zoogeographic patterns might result from smaller-scale effects. It seems that our knowledge is very strongly affected by sampling bias, or undersampling, so assessing the strength of any trend observed becomes difficult. For example, Shields and Blanco-Perez (2013) based their analysis of polychaete diversity and distribution patterns on 11 samples from as few as 4 stations widely scattered almost along the entire length of the Charlie-Gibbs Fracture Zone; the species accumulation curves they produced turned out very steep, demonstrating the magnitude of undersampling. The recent and most comprehensive analysis of literature datasets from MAR vent systems (Boschen-Rose and Colaço, 2021) was based on the presence-absence data extracted from studies employing different sampling approaches and very broadly defined environmental factors. One of the most important studies of vent meiofauna was based on no more than 10 qualitative samples per site (Tchesunov, 2015). Our whole knowledge about recovery processes in the MAR vent systems is based on just one small-scale study (macrofauna removal in eight 50 x 50 cm quadrats) at the Lucky Strike (Marticorena et al., 2021). The general paucity of quantitative data precludes modeling or multivariate analyses directly coupled with environmental factors, and allows only for some basic analyses of species distribution patterns, with no in-depth explanation of causes underlying the patterns observed. At the same time, a discussion on relationships between the whole MAR species pool and the local, vent- or habitat-specific, species pools is a challenge resulting from both 1) an almost complete lack of information on genetic connectivity and 2) the patchy distribution of sampling stations. At present it is impossible to assess the level of species rarity and/or patchiness and even calculations of basic diversity indices remain uncertain. Comprehensive studies of community ecology, diversity assessments, and post-disturbance recovery processes in the PECA or on the wider MAR are needed and will necessitate rethinking the policy and future management actions, especially in relation to Environmental Impact Assessments (EIAs) required for test mining and for the eventual exploitation of PMS. Compared to research conducted in shallow waters, the higher costs and logistic difficulties associated with deep-sea studies mean that considerable investment in time and resources is required to conduct meaningful studies that can be used to justify an EIA. Comprehensive EIAs are required to demonstrate that unique biotas are not under-appreciated or overlooked. Lack of statistically significant quantitative data poses a risk to contractors if the international community rejects any EIA and Environmental Management and Monitoring Plan. The paucity of data on the duration of larval stages as well as settlement and post settlement processes strongly affect our understanding of resilience mechanisms and recovery processes as well as the planning of conservation strategies such as those discussed by Dunn et al. (2018). Detection and understanding of patterns, and conclusions on the strength of those patterns, calls for a sound recognition of local-regional species pool relationships (Witman, 2013) and comprehensive environmental baseline data.

In this context, it is necessary to refer again to Boschen-Rose and Colaço (2021) who commented on certain biogeographic changes related to the presence and abundance of different taxa reported from various hydrothermal fields along the northern

MAR. They found a switch in the relative abundance (domination) of the macro- and megafauna as one moved along the MAR from the north to the Equator. While *Peltospira* sp. limpets and *Mirocaris* sp. shrimps dominated the northernmost sites, the dominance structure changed to the highest relative abundances of *Mirocaris fortunata* and *Bathymodiolus azoricus* just south of the Azores, *M. fortunata* domination giving way to *Rimicaris exoculata* in deeper water further south (including the Broken Spur). *B. azoricus* was first co-located with and then replaced by *B. puteoserpentis*. As already mentioned, the Broken Spur represents a hybridization zone for the two bathymodiolid species. Boschen-Rose and Colaço (2021) extracted the environmental variables which correlate best with faunal similarities they revealed between the vent fields, and found a combination of the maximum reported depth as well as the chimney type (carbonate *vs*. sulfide) to have the strongest explanatory power. Water depth is a known environmental driver of benthic faunal distributions, but it co-varies with gradients in a number of other environmental variables (e.g. temperature, pressure, food availability). Depth-related changes in faunal community, including zonation observed in the northern part of the MAR (Alt et al., 2013) are a net result of differences in physiological tolerance limits to those gradients. The effects of depth on faunal communities in the PECA are unknown. Conclusions regarding the chimney type may appear, generally, valid for the PECA macro- and megafauna (carbonate chimneys at the Lost City and sulfide chimneys at the Broken Spur). However, due to the paucity of data and biases resulting from it (e.g. a relatively detailed study of nematode assemblages at the Lost City compared to the Broken Spur; cf. Table 2 and Tchesunov, 2015; a higher meiofaunal similarity of the Lost City and Broken Spur relative to other fields; cf. Figure 2), the conclusions drawn require validation through new exploration-oriented baseline surveys.

Regarding environmental variables affecting the distribution and composition of benthic communities on the MAR, Priede et al. (2022) have recently provided a thorough analysis of these with respect to biomass of the vent field megafauna (including fish). They examined effects of net primary production, particulate organic carbon (POC) flux, depth, and substrate heterogeneity. However, their analysis draws upon data acquired primarily in the northern sector of the northern MAR (between 40 and 60° N), and the authors admit that they had limited data on the benthic fauna of the part of the MAR between 12° N and 33° N, covered by the ISA exploration contracts. The authors predict that, owing to a lower POC flux south of the Azores, compared to more northern areas and those at greater depths, the biomass in the contract areas could be at least an order of magnitude lower that at the north. Further, the authors stress a severe lack of data in the Ocean Biodiversity Information System (OBIS) south of 33° N, which restricts generalizing on biogeographic trends.

Still another aspect of mid-oceanic ridge benthos, important for any baseline assessment as well as for distinguishing between natural and anthropogenic effects (Radziejewska et al., 2022) is the temporal variability. The low sampling effort to date on the MAR section covered by the ISA exploration contracts, including the PECA, has resulted also in our poor knowledge of temporal variability in the benthos. There is some information on the temporal variability (or lack of it) in benthic invertebrate assemblages at hydrothermally-active hard substrata. For example, some taxa have been observed to have seasonal reproduction patterns (e.g. bathymodiolids; Dixon et al., 2006), whereas no such patterns have been reported for *Rimicaris exoculata* (Copley et al., 2007). Sarrazin et al. (2014) observed changes in bathymodiolid abundance between the years, whereas Audenhaege et al. (2022) provide evidence of a long-term (7 years) stability of hydrothermal vent mussel communities. Matabos et al. (2015), too, reported on stable spatial distribution patterns in the shrimp *Mirocaris fortunata* and the crab *Segonzacia mesatlantica*. Cuvelier et al. (2017) demonstrated significant multi-day periodicities in polynoid polychaetes, suggesting effects of tidal cycles. As the species mentioned have been reported from the PECA (cf. Table 3), those effects may be taking place there as well. To mention a study in the PECA, Copley et al. (1997) reported vent shrimp populations at the Broken Spur to be stable over a 15-month period. No study addressed temporal variability at the hydrothermally inactive sulfide habitat and in the soft-sediment MAR faunas (Weaver et al., 2021), except for some evidence of temporal variability seen in the large foraminifera Syringamminidae, in polychaetes and sea anemones north of the Azores (Gebruk and Krylova, 2013), related to the POC flux.

Despite the gradual increase in our understanding of the MAR ecosystems (Dunn et al., 2018; Boschen-Rose and Colaço, 2021; Weaver et al., 2021), the inferences that might be drawn from the existing knowledge suffer from problems associated with a low sampling effort or scarcity of temporal analyses. The effects of future mining can only be speculated about, since data on resilience and recovery processes are scarce or non-existent, although some experimental work has been conducted in certain MAR areas suggesting that recovery processes are slow. In particular, Marticorena et al. (2021) studied recovery patterns in 13 *Bathymodiolus azoricus* assemblages at the Lucky Strike vent field, following artificial clearance of the fauna. Taxonomic richness, but not faunal densities or community structure, was observed to recover within 2 years post-disturbance, and a shift in faunal composition towards gastropod domination was detected. In addition, mobile predators arriving in early-colonisation stages could have slowed down the recovery of abundance, particularly with respect to the major foundation species, *B. azoricus* whose larvae and juveniles were impacted by the predator pressure. Thus, the recovery processes could have been slowed down by altered biological interactions.

In addition, an appropriate future assessment of impacts produced by mining activities could benefit from molecular

TABLE 4 Knowledge gaps in view of the ISA guidelines and recommendations (ISA, 2019).

Required information	Status of knowledge in MAR	Status of knowledge in PECA
Habitat types (distribution, mapping)		
Megafauna (morphological taxonomy, abundance, biomass, species structure and diversity): A. Active hydrothermal vents		
Megafauna (morphological taxonomy, abundance, biomass, species structure and diversity): B. All other megafaunal habitats		
Megafauna (molecular studies)*		
Macrofauna (abundance, species structure, biomass and diversity)		
Metazoan meiofauna (abundance, biomass and species structure)		
Foraminiferal meiofauna (abundance, biomass and species structure)		
Temporal variability**		

No data.

Very little known; information available on some vent fields or some aspects.

Known better than other benthos groups.

*scant data for northern MAR (e.g. Shields et al., 2013); no data for PECA except for Dixon and Dixon (1996 quoted by Weaver et al., 2021).
**PECA megafaunal data in Copley et al. (1997).

studies focusing on the analysis of species composition and diversity (Klunder et al., 2020), such studies being rare in the whole MAR (cf. Table 4).

4 Conclusions

From our review of the present state of knowledge on benthic communities in the Polish exploration contract area it is evident that this knowledge is far from complete. Many knowledge gaps remain and studies are needed to investigate 1) connectivity between vent fields, 2) affinities between MAR/PECA areas and other, better studied, ridge areas, 3) symbiotic relationships, 4) distinctions between benthic communities in active and inactive PMS fields. The available data suggest that although the PECA benthos is grossly understudied, it is a diverse and abundant component of a very complex system that needs further, much more comprehensive research based on a higher sampling effort, accompanied by the analysis of various environmental factors. At the moment, we have probably managed to get a glimpse on a tip of an iceberg. Therefore, potential future research in the PECA, likely associated with exploration activities, should involve efforts aimed at broadening the benthic ecology knowledge base of PMS exploration. This knowledge will also be important as a source of data for delineation of PRZs and IRZs in the PECA and to form the basis for the Environmental Impact Statement and Environmental Management and Monitoring Plan required for an exploitation contract.

Author contributions

All authors contributed to the article and approved the submitted version.

Acknowledgments

We are grateful to Dr. Brygida Wawrzyniak-Wydrowska for the assistance with the artwork, to Mr Jakub Miluch for his help with the GEBCO data as well as to three reviewers and Editor David Billett for prompting us to delve deeper in the material and for their valuable input which helped us to improve the original submission.

Conflict of interest

The authors declare that the research was conducted in the absence of any commercial or financial relationships that could be construed as a potential conflict of interest.

Publisher's note

All claims expressed in this article are solely those of the authors and do not necessarily represent those of their affiliated organizations, or those of the publisher, the editors and the reviewers. Any product that may be evaluated in this article, or claim that may be made by its manufacturer, is not guaranteed or endorsed by the publisher.

References

Alfaro-Lucas, J. M., Pradillon, F., Zeppilli, D., Michel, L. N., Martinez-Arbizu, P., Tanaka, H., et al. (2020). High environmental stress and productivity increase functional diversity along a deep-sea hydrothermal vent gradient. *Ecology* 101, e03144. doi: 10.1002/ecy.3144

Alt, C. H. S., Kremenetskaia (Rogacheva), A., Gebruk, A. V., Gooday, A. J., and Jones, D. O. B. (2019). Bathyal benthic megafauna from the Mid-Atlantic Ridge in the region of the Charlie-Gibbs Fracture Zone based on remotely operated vehicle observations. *Deep-Sea Res. I* 145, 1–12. doi: 10.1016/j.dsr.2018.12.006

Alt, C. H. S., Rogacheva, A., Boorman, B., Hughes, J. A., Billett, D. S. M., Gooday, A. J., et al. (2013). Trawled megafaunal invertebrate assemblages from bathyal depth of the Mid-Atlantic Ridge (48°-54° N). *Deep-Sea Res. II* 98, 326–340. doi: 10.1016/j.dsr2.2013.02.003

Amon, D. J., Gollner, S., Morato, T., Smith, C. R., Chen, C., Christiansen, S., et al. (2022). Assessment of scientific gaps related to the effective environmental management of deep-seabed mining. *Mar. Pol.* 138, 105006. doi: 10.1016/j.marpol.2022.105006

Audenhaege, L., Van, Matabos, M., Brind'Amour, A., Drugmand, J., Laës-Huon, A., Sarradin, P.-M., et al. (2022). Long-term monitoring reveals unprecedented stability of a vent mussel assemblage on the Mid-Atlantic Ridge. *Prog. Oceanogr.* 204, 102791. doi: 10.1016/j.pocean.2022.102791

Baco, A. R., Etter, R. J., Ribeiro, P. A., von der Heyden, S., Beerli, P., and Kinlan, B. P. (2016). A synthesis of genetic connectivity in deep-sea fauna and implications for marine reserve design. *Molec. Ecol.* 25, 3276–3298. doi: 10.1111/mec.13689

Beaulieu, S. E., Baker, E. T., German, C. R., and Maffei, A. (2013). An authoritative global database for active submarine hydrothermal vent fields. *Geochem. Geophys. Geosys.* 14, 4892–4905. doi: 10.1002/2013GC004998

Beaulieu, S. E., and Szafranski, K. (2019) *InterRidge global database of active submarine hydrothermal vent fields, version 3.4 (2019)*. Available at: http://vents-data.interridge.org.

Bebianno, M. J., Cardoso, C., Gomes, T., Blasco, J., Santos, R. S., and Colaço, A. (2018). Metal interactions between the polychaete *Branchipolynoe seepensis* and the mussel *Bathymodiolus azoricus* from Mid-Atlantic-Ridge hydrothermal vent fields. *Mar. Env. Res.* 135, 70–81. doi: 10.1016/j.marenvres.2018.01.017

Bell, J. B., Alt, C. H. S., and Jones, D. O. B. (2016). Benthic megafauna on steep slopes at the northern Mid-Atlantic Ridge. *Mar. Ecol.* 37, 1290–1302. doi: 10.1111/maec.12319

Bellan-Santini, D. (2007). New amphipods of hydrothermal vent environments on the Mid-Atlantic Ridge, Azores Triple Junction zone. *J. Nat. Hist.* 41, 567–596. doi: 10.1080/00222930701262537

Bellan-Santini, D., and Thurston, M. H. (1996). Amphipoda of the hydrothermal vents along the Mid-Atlantic Ridge. *J. Nat. Hist.* 30, 685–702. doi: 10.1080/00222939600770381

Benoist, N. M. A., Bett, B. J., Morris, K. J., and Ruhl, H. A. (2019). A generalised volumetric method to estimate the biomass of photographically surveyed benthic megafauna. *Prog. Oceanog.* 178, 102188. doi: 10.1016/j.pocean.2019.102188

Bergstad, O. A., Falkenhaug, T., Astthorsson, O. S., Byrkjedal, I., Gebruk, A. V., Piatkowski, U., et al. (2008). Towards improved understanding of the diversity and abundance patterns of the mid-ocean ridge macro- and megafauna. *Deep-Sea Res. II* 55, 1–5. doi: 10.1016/j.dsr2.2007.10.001

Bernardino, A. F., Levin, L. A., Thurber, A. R., and Smith, C. R. (2012). Comparative composition, diversity and trophic ecology of sediment macrofauna at vents, seeps and organic falls. *PloS One* 7, e33515. doi: 10.1371/journal.pone.0033515

Blake, E. A., and Van Dover, C. L. (2005). The reproductive biology of *Amathys lutzi*, an ampharetid polychaete from hydrothermal vents on the Mid-Atlantic Ridge. *Inv. Biol.* 124, 254–264. doi: 10.1111/j.1744-7410.2005.00022.x

Boetius, A. (2005). Lost City life. *Science* 307, 1420–1421. doi: 10.1126/science.1109849

Boschen-Rose, R. E., and Colaço, A. (2021). Northern Mid-Atlantic Ridge hydrothermal habitats: A systematic review of knowledge status for environmental management. *Front. Mar. Sci.* 8. doi: 10.3389/fmars.2021.657358

Boschen, R. E., Rowden, A. A., Clark, M. R., and Gardner, J. P. A. (2013). Mining of deep-sea seafloor massive sulfides: A review of the deposits, their benthic communities, impacts from mining, regulatory frameworks and management strategies. *Ocean Coast. Manage.* 84, 54e67. doi: 10.1016/j.ocecoaman.2013.07.005

Braga-Henriques, A., Porteiro, F. M., Ribeiro, P. A., de Matos, V., Sampaio, I., Ocaña, O., et al. (2013). Diversity, distribution and spatial structure of the cold-water coral fauna of the Azores (NE Atlantic). *Biogeosci.* 10, 4009–4036. doi: 10.5194/bg-10-4009-2013

Brandt, A., Frutos, I., Bober, S., Brix, S., Brenke, N., Guggolz, T., et al. (2018). Composition of abyssal macrofauna along the Vema Fracture Zone and the hadal Puerto Rico Trench, northern tropical Atlantic. *Deep-Sea Res. Part II Top. Stud. Oceanogr.* 148, 35–44. doi: 10.1016/J.DSR2.2017.07.014

Brazelton, W. J., Ludwig, K. A., Sogin, M. L., Andreishcheva, E. N., Kelley, D. S., Shen, C.-C., et al. (2010). Archaea and bacteria with surprising microdiversity show shifts in dominance over 1,000-year time scales in hydrothermal chimneys. *PNAS* 107 (4), 1612–1617. doi: 10.1073/pnas.0905369107

Brazelton, W. J., Schrenk, M. O., Kelley, D. S., and Baros, J. A. (2006). Methane- and sulfur-metabolizing microbial communities dominate the Lost City hydrothermal field ecosystem. *Appl. Env. Microbiol.* 72, 6257–6270. doi: 10.1128/AEM.00574-06

Budaeva, N. (2012). *Leptoecia midatlantica*, a new species of the deep-sea quill-worms (Polychaeta: Onuphidae: Hyalinoeciinae) from the Mid-Atlantic Ridge. *Zootaxa* 3176, 45–60. doi: 10.11646/zootaxa.3176.1.2

Buhl-Mortensen, P., Buhl-Mortensen, L., Gebruk, A. V., and Krylova, E. M. (2008). Occurrence of deep-water corals on the Mid-Atlantic Ridge based on MAR-ECO data. *Deep Sea Res. II Top. Stud. Oceanogr.* 55, 142–152. doi: 10.1016/j.dsr2.2007.09.018

Calado, H., Ng, K., Lopes, C., and Paramio, L. (2011). Introducing a legal management instrument for offshore marine protected areas in the Azores – the Azores Marine Park. *Env. Sci. Pol.* 14, 1175–1187. doi: 10.1007/978-3-030-87982-2_11

Campagna, C., Sanderson, E. W., Coppolillo, P. B., Falabella, V., Piola, A. R., Strindberg, S., et al. (2008). A species approach to marine ecosystem conservation. *Aquat. Conserv. Mar. Freshw. Ecosyst.* 17, S122–S147. doi: 10.1002/aqc.918

Casson, L., Losada, S., Tsenikli, S., Santillo, D., Currie, D., Sharma, G., et al. (2019). *In deep water: The emerging threat of deep sea mining* (Greenpeace International). Available at: https://issuu.com/greenpeaceinternational/docs/indeep-water-201.

Cherkashov, G. (2017). "Seafloor massive sulfide deposits: Distribution and prospecting," in *Deep-Sea mining. resource potential, technical and environmental considerations*. Ed. R. Sharma (Cham: Springer), 143–187. doi: 10.1007/978-3-319-52557-0_4

Clarke, K. R., and Gorley, R. N. (2015). *PRIMER v7: User Manual/Tutorial* (PRIMER-E Plymouth).

Colaço, A., Dehairs, F., and Desbruyères, D. (2002). Nutritional relations of deep-sea hydrothermal fields at the Mid-Atlantic Ridge: A stable isotope approach. *Deep Sea Res. I* 49, 395–412. doi: 10.1016/S0967-0637(01)00060-7

Colaço, A., Desbruyères, D., and Guezennec, J. (2007). Polar lipid fatty acids as indicators of trophic associations in a deep-sea vent system community. *Mar. Ecol.* 28, 15–24. doi: 10.1111/j.1439-0485.2006.00123.x

Copley, J. T. P., Jorgensen, P. B. K., and Sohn, R. A. (2007). Assessment of decadal-scale ecological change at a deep mid-Atlantic hydrothermal vent and reproductive time-series in the shrimp *Rimicaris exoculata*. *J. Mar. Biol. Ass. UK* 87, 859–867. doi: 10.1017/S0025315407056512

Copley, J. T. P., Tyler, P. A., Murton, B. J., and Van Dover, C. L. (1997). Spatial and interannual variation in the faunal distribution at Broken Spur vent field (29°N, Mid-Atlantic Ridge). *Mar. Biol.* 129, 723–733. doi: 10.1007/s002270050215

Corbera, J., Segonzac, M., and Cunha, M. R. (2008). A new deep-sea genus of Nannastacidae (Crustacea, Cumacea) from the Lucky Strike hydrothermal vent field (Azores Triple Junction, Mid-Atlantic Ridge). *Mar. Biol. Res.* 4, 180–192. doi: 10.1080/17451000801898576

Cruz, M., Le Bris, N., and Colaço, A. (2022). Reproductive traits of the vent crab *Segonzacia mesatlantica* (Guinot, 1989) from the Mid-Atlantic Ridge. *Front. Mar. Sci.* 9. doi: 10.3389/fmars.2022.900990

Cunha, M. R., and Wilson, G. D. F. (2006). The North Atlantic genus *Heteromesus* (Crustacea: Isopoda: Asellota: Ischnomesidae). *Zootaxa* 1192, 3–76. doi: 10.11646/zootaxa.1192.1

Cuvelier, D., Beesau, J., Ivanenko, V. N., Zeppilli, D., Sarradin, P. M., and Sarrazin, J. (2014). First insights into macro- and meiofaunal colonisation patterns on paired wood/slate substrata at Atlantic deep-sea hydrothermal vents. *Deep Sea Res. I* 87, 70–81. doi: 10.1016/j.dsr.2014.02.008

Cuvelier, D., Legendre, P., Laës-Huon, A., Sarradin, P. M., and Sarrazin, J. (2017). Biological and environmental rhythms in (dark) deep-sea hydrothermal ecosystems. *Biogeosci.* 14, 2955–2977. doi: 10.5194/bg-14-2955-2017

Cuvelier, D., Sarrazin, J., Colaço, A., Copley, J., Glover, A., Tyler, P., et al. (2011). Community dynamics over 14 years at the Eiffel Tower hydrothermal edifice on the Mid-Atlantic Ridge. *Limnol. Oceanog.* 56, 1624–1640. doi: 10.4319/lo.2011.56.5.1624

Denny, A. R., Kelley, D. S., and Früh-Green, G. L. (2015). Geologic evolution of the Lost City hydrothermal field. *Geochem. Geophys. Geosyst.* 17, 375–394. doi: 10.1002/2015GC005869

Desbruyères, D., Almeida, A., Biscoito, M., Comtet, T., Khripounoff, A., Le Bris, N., et al. (2000). A review of the distribution of hydrothermal vent communities along the northern Mid-Atlantic Ridge: Dispersal vs. environmental controls. *Hydrobiologia* 440, 201–216. doi: 10.1023/A:1004175211848

Dilman, A. B. (2013). Asteroid fauna of the northern Mid-Atlantic Ridge: additional records. *Mar. Biol. Res.* 9, 563–586. doi: 10.1080/17451000.2012.749993

Dixon, D. R., Lowe, D. M., Miller, P. I., Villemin, G. R., Colaço, A., Serrao-Santos, R., et al. (2006). Evidence of seasonal reproduction in the Atlantic vent mussel *Bathymodiolus azoricus*, and an apparent link with the timing of photosynthetic primary production. *J. Mar. Biol. Ass. UK* 86, 1363–1371. doi: 10.1017/S0025315406014391

Dulov, L. E., Lein, A. Y., Dubinina, G. A., and Pimenov, N. V. (2005). Microbial processes at the Lost City vent field, Mid-Atlantic Ridge. *Microbiology* 74, 97–103. doi: 10.1007/s11021-005-0035-6

Dumke, I., Purser, A., Marcon, Y., Nornes, S. M., Johnsen, G., Ludvigsen, M., et al. (2018). Underwater hyperspectral imaging as an *in situ* taxonomic tool for deep-sea megafauna. *Sci. Rep.* 8, 12860. doi: 10.1038/s41598-018-31261-4

Dunn, D. C., Van Dover, C. L., Etter, R. J., Smith, C. R., Levin, L. A., Morato, T., et al. (2018). A strategy for the conservation of biodiversity on mid-ocean ridges from deep-sea mining. *Sci. Adv.* 4, eaar4313. doi: 10.1126/sciadv.aar4313

Dutkiewicz, A., Müller, R. D., O'Callaghan, S., and Jónasson, H. (2015). Census of seafloor sediments in the world's ocean. *Geology* 43, 795–798. doi: 10.1130/G36883.1

Fabri, M. C., Bargain, A., Briand, P., Gebruk, A., Fouquet, Y., Morineaux, M., et al. (2011). The hydrothermal vent community of a new deep-sea field, Ashadze-1, 12°58'N on the Mid-Atlantic Ridge. *J. Mar. Biol. Ass. U. K.* 91, 1–13. doi: 10.1017/S0025315410000731

Farley, J. (2010). Conservation through the economics lens. *Env. Manag* 45, 26–38. doi: 10.1007/s00267-008-9232-1

Flint, H. C. (2007). *Diversity of meiofauna at deep-sea hydrothermal vents and cold seeps with particular reference to nematodes* (Southampton: National Oceanography Centre).

Freestone, D., Laffoley, D., Douvere, F., and Badman, T. (2016). *World heritage in the high seas: An idea whose time has come* (IUCN). Available at: https://unesdoc.unesco.org/ark:/48223/pf0000245467.

Früh-Green, G., Kelley, D. S., Bernasconi, S., Karson, J. A., Ludwig, K. A., Butterfield, D. A., et al. (2003). 30,000 years of hydrothermal activity at the Lost City vent field. *Science* 301, 495–498. doi: 10.1126/science.1085582

Früh-Green, G. L., Orcutt, B. N., and Green, S. (2015). *Expedition 357 scientific prospectus: Atlantis massif serpentinization and life* International Ocean Discovery Program. doi: 10.14379/iodp.sp.327.2015

Frutos, I., Kaiser, S., Pułaski, Ł., Studzian, M., and Błażewicz, M. (2022). Challenges and advances in the taxonomy of deep-sea peracarida: From traditional to modern methods. *Front. Mar. Sci.* 9. doi: 10.3389/fmars.2022.799191

Gage, J. D., and Tyler, P. A. (1991). *Deep-Sea biology. A natural history of organisms at the deep-sea floor* (Cambridge: Cambridge University Press) 9, 504.

Galkin, S. V. (2006). "Prostranstvennaya struktura gidrotermalnykh soobshchestv sredinno-atlanticheskogo khrebta," in *Ekosistemy atlanticheskikh gidroterm [Ecosystems of the Atlantic hydrothermal vents]*. Eds. M. E. Vinogradov and A. L. Vereshchaka (Moskva: Nauka), 163–202.

Gebruk, A. V., Budaeva, N. E., and King, N. J. (2010). Bathyal benthic fauna of the Mid-Atlantic Ridge between the Azores and the Reykjanes Ridge. *J. Mar. Biol. Ass. U. K.* 90, 1–14. doi: 10.1017/S0025315409991111

Gebruk, A. V., and Galkin, S. V. (1997). Ecology and biogeography of the hydrothermal vent fauna of the Mid-Atlantic Ridge. *Adv. Mar. Biol.* 32, 93–144. doi: 10.1016/s0065-2881(08)60016-4

Gebruk, A. V., and Krylova, E. M. (2013). Megafauna of the Charlie-Gibbs Fracture Zone (northern Mid-Atlantic Ridge) based on video observations. *J. Mar. Biol. Ass. U. K.* 93, 1143–1150. doi: 10.1017/S0025315412001890

Gebruk, A. V., and Mironov, A. N. (2006). "Biogeografiya gidroterm sredinno-atlanticheskogo khrebta," in *Ekosistemy atlanticheskikh gidroterm [Ecosystems of the Atlantic hydrothermal vents]*. Eds. M. E. Vinogradov and A. L. Vereshchaka (Moskva: Nauka), 119–162.

Gebruk, A. V., Southward, E. C., Kennedy, H., and Southward, A. J. (2000). Food sources, behaviour, and distribution of hydrothermal vent shrimps at the Mid-Atlantic Ridge. *J. Mar. Biol. Ass. U. K.* 80, 485–499. doi: 10.1017/S0025315400002186

Gerdes, K., Martinez Arbizu, P., Schwarz-Schampera, U., Schwentner, M., and Kihara, T. C. (2019). Detailed mapping of hydrothermal vent fauna: A 3D reconstruction approach based on video imagery. *Front. Mar. Sci.* 6. doi: 10.3389/fmars.2019.00096

Gollner, S., Kaiser, S., Menzel, L., Jones, D. O. B., Brown, A., Mestre, N. C., et al. (2017). Resilience of benthic deep-sea fauna to mining activities. *Mar. Environ. Res.* 129, 76–101. doi: 10.1016/j.marenvres.2017.04.010

Gollner, S., Riemer, B., Martínez Arbizu, P., Le Bris, N., and Bright, M. (2010). Diversity of meiofauna from the 9°50'N East Pacific Rise across a gradient of hydrothermal fluid emissions. *PloS One* 5, e12321. doi: 10.1371/journal.pone.0012321

Goroslavskaya, E. I., and Galkin, S. V. (2011). Benthic fauna associated with mussel beds and shrimp swarms at hydrothermal fields on the Mid-Atlantic Ridge. *Oceanology* 51, 69–79. doi: 10.1134/S0001437011010048

Haeckel, M., and Linke, P. (2021). RV SONNE fahrtbericht /Cruise report SO268. assessing the impacts of nodule mining on the deep-sea environment. NoduleMonitoring. Manzanillo (Mexico) – Vancouver (Canada). 17.02. – 27.05.2019. *GEOMAR Rep N. Ser.* 059. doi: 10.3289/GEOMAR_REP_NS_59_2021

Hannington, M., Jamieson, J., Monecke, T., Petersen, S., and Beaulieu, S. (2011). The abundance of seafloor massive sulfide deposits. *Geology* 39, 1155–1158. doi: 10.1130/G32468.1

Hernández-Ávila, I., Cambon-Bonavita, M.-A., Sarrazin, J., and Pradillon, F. (2022). Population structure and reproduction of the alvinocaridid shrimp *Rimicaris exoculata* on the Mid-Atlantic Ridge: Variations between habitats and vent fields. *Deep-Sea Res. I* 186, 103827. doi: 10.1016/j.dsr.2022.103827

Hilário, A., Metaxas, A., Gaudron, S. M., Howell, K. L., Mercier, A., Mestre, N. C., et al. (2015). Estimating dispersal distance in the deep sea: Challenges and applications to marine reserves. *Front. Mar. Sci.* 2. doi: 10.3389/fmars.2015.00006

Horton, T., Thurston, M. H., and Duffy, G. A. (2013). Community composition of scavenging amphipods at bathyal depths on the Mid-Atlantic Ridge. *Deep Sea Res. II Top. Stud. Oceanogr.* 98, 352–359. doi: 10.1016/j.dsr2.2013.01.032

ISA (2019). *Recommendations for the guidance of contractors for the assessment of the possible environmental impacts arising from exploration for marine minerals in the area.*

ISA (2017). ISBA/25/LTC/6. International Seabed Authority, Kingston. "Report of ISA workshop on the design of impact reference zones and preservation reference zones," in (Report of ISA Workshop on the Design of "Impact Reference Zones" and "Preservation Reference Zones" in Deep- Sea Mining Contract Areas. ISA Technical Study), 41. Available at: https://isa.org.jm/files/files/documents/TechnicalStudy21-ebk_0.pdf.

Ivanenko, V. N., Corgosinho, P. H. C., Ferrari, F., Sarradin, P.-M., and Sarrazin, J. (2011). Microhabitat distribution of *Smacigastes micheli* (Copepoda: Harpacticoida: Tegastidae) from deep-sea hydrothermal vents at the Mid-Atlantic Ridge, 37° N (Lucky Strike), with a morphological description of its nauplius. *Mar. Ecol.* 33, 246–256. doi: 10.1111/j.1439-0485.2011.00484.x

Jakiel, A., Palero, F., and Błażewicz, M. (2019). Deep ocean seascape and Pseudotanaidae (Crustacea: Tanaidacea) diversity at the Clarion-Clipperton Fracture Zone. *Sci. Rep.* 9, 17305. doi: 10.1038/s41598-019-51434

Jakiel, A., Stępień, A., and Błażewicz, M. (2018). A tip of the iceberg – Pseudotanaidae (Tanaidacea) diversity in the North Atlantic. *Mar. Biodiv.* 48, 859–895. doi: 10.1007/s12526-018-0881-x

Jamieson, J. W., and Gartman, A. (2020). Defining active, inactive, and extinct seafloor massive sulfide deposits. *Mar. Pol.* 117, 103926. doi: 10.1016/j.marpol.2020.103926

Jennings, R. M., Brix, S., Bober, S., Svavarsson, J., and Driskell, A. (2018). More diverse than expected: distributional patterns of *Oecidiobranchus* Hessler, 1970 (Isopoda, Asellota) on the Greenland-Iceland-Faeroe Ridge based on molecular markers. *Mar. Biodiv.* 48, 845–957. doi: 10.1007/s12526-018-0857-x

Johnson, D. E. (2019). Protecting the Lost City hydrothermal vent system: All is not lost, or is it? *Mar. Pol.* 107, 103593. doi: 10.1016/j.marpol.2019.103593

Jollivet, D. (1996). Specific and genetic diversity at deep-sea hydrothermal vents: an overview. *Biodivers. Conserv.* 5, 1619–1653. doi: 10.1007/BF00052119

Jones, D. O. B., Alt, C. H. S., Priede, I. G., Reid, W. D. K., Wigham, B. D., Billett, D. S. M., et al. (2013). Deep-sea surface-dwelling enteropneusts from the Mid-Atlantic Ridge: Their ecology, distribution and mode of life. *Deep Sea Res. II Top. Stud. Oceanogr.* 98, 374–387. doi: 10.1016/j.dsr2.2013.05.009

Jones, D. O. B., Ardron, J. A., Colaço, A., and Durden, J. M. (2020). Environmental considerations for impact and preservation reference zones for deep-sea polymetallic nodule mining. *Mar. Pol.* 118, 103312. doi: 10.1016/j.marpol.2018.10.025

Jóźwiak, P., Pabis, K., Brandt, A., and Blazewicz, M. (2020). Epibenthic sled versus giant box corer – comparison of sampling gears for tanaidacean species richness assessment in the abyssal benthic ecosystem. *Prog. Oceanog.* 181, 102255. doi: 10.1016/j.pocean.2019.102255

Jóźwiak, P., Pabis, K., Sobczyk, R., and Serigstad, B. (2022). A paradise for rare species: Tanaidacean fauna of the West African continental margin. *Front. Mar. Sci.* 9. doi: 10.3389/fmars.2022.779134

Kaiser, S., Błażewicz, M., Kocot, K. M., Leduc, D., Riehl, T., and Rouse, G. W. (2022). Editorial: Recent and emerging innovations in deep-sea taxonomy to enhance biodiversity assessment and conservation. *Front. Mar. Sci.* 9. doi: 10.3389/fmars.2022.989245

Karson, J. A., Kelley, D. S., Fornari, D. J., Perfit, M. R., and Shank, T. M. (2015a). "Diversity in seafloor spreading," in *Discovering the deep. a photographic atlas of the seafloor and ocean crust*. Eds. J. A. Karson, D. S. Kelley, D. J. Fornari, M. R. Perfit and T. M. Shank (Cambridge: Cambridge University Press), 56–86.

Karson, J. A., Kelley, D. S., Fornari, D. J., Perfit, M. R., and Shank, T. M. (2015b). "Hydrothermal vents," in *Discovering the deep. a photographic atlas of the seafloor and ocean crust*. Eds. J. A. Karson, D. S. Kelley, D. J. Fornari, M. R. Perfit and T. M. Shank (Cambridge: Cambridge University Press), 87–120.

Kawano, S., and Furuya, H. (2022). "Mining and processing of seafloor massive sulfides: Experiences and challenges," in *Perspectives on deep-sea mining. sustainability, technology, environmental policy and management*. Ed. R. Sharma (Cham: Springer), 167–198. doi: 10.1007/978-3-030-87982-2_7

Kelley, D. S., Früh-Green, G. L., Karson, J. A., and Ludwig, K. A. (2007). The Lost City hydrothermal field revisited. *Oceanography* 20, 90–99. doi: 10.5670/oceanog.2007.09

Kelley, D. S., Karson, J. A., Früh-Green, G. L., Yoerger, D. R., Shank, T. M., Butterfield, D. A., et al. (2005). A serpentinite-hosted ecosystem: The Lost City hydrothermal field. *Science* 307, 1428–1433. doi: 10.1126/science.1102556

Klunder, L., Stigter, H., de, Lavaleye, M. S. S., van Bleijswijk, J. D. L., van der Veer, H. W., Reichart, G. J., et al. (2020). A molecular approach to explore the background benthic fauna around a hydrothermal vent and their larvae: Implications for future mining of deep-sea SMS deposits. *Front. Mar. Sci.* 7. doi: 10.3389/fmars.2020.00134

Kongsrud, J. A., Budaeva, N., Barnich, R., Oug, E., and Bakken, T. (2013). Benthic polychaetes from the northern Mid-Atlantic Ridge between the Azores and

the Reykjanes Ridge. *Mar. Biol. Res.* 9, 516–546. doi: 10.1080/17451000.2012.749997

Lang, S. Q., and Brazelton, W. J. (2020). Habitability of the marine serpentinite subsurface: A case study of the Lost City hydrothermal field. *Phil. Trans. R. Soc.* A378, 20180429. doi: 10.1098/rsta.2018.0429

Larsen, K., Błażewicz-Paszkowycz, M., and Cunha, M. R. (2006). Tanaidacean (Crustacea: Peracarida) fauna from chemically reduced habitats – the Lucky Strike hydrothermal vent system, Mid-Atlantic Ridge. *Zootaxa* 1187, 1–36. doi: 10.11646/zootaxa.1187.1.1

Lecoeuvre, A., Ménez, B., Cannat, M., Chavagnac, V., and Gérard, E. (2021). Microbial ecology of the newly discovered serpentinite-hosted Old City hydrothermal field (Southwest Indian Ridge). *ISME J.* 15, 818–832. doi: 10.1038/s41396-020-00816-7

Lein, A., Galkin, S. V., Maslennikov, V. V., Bogdanov,, Yu, A., Bogdanova,, et al. (2007). A new type of carbonate rocks on the ocean floor (Mid-Atlantic Ridge, 30° 07′ N). *Dokl. Earth Sci.* 412, 136–140. doi: 10.1134/S1028334X0701031X

López-Garcia, P., Vereshchaka, A., and Moreira, D. (2007). Eukaryotic diversity associated with carbonates and fluid-seawater interface in Lost City hydrothermal field. *Envir. Microbiol.* 9, 546–554. doi: 10.1111/j.1462-2920.2006.01158.x

Lunina, A. A., and Vereshchaka, A. L. (2014). Distribution of hydrothermal alvinocaridid shrimps: Effect of geomorphology and specialization to extreme biotopes. *PloS One* 9, e92802. doi: 10.1371/journal.pone.0092802

Mace, G. M., Possingham, H. P., and Leader-Williams, N. (2007). "Prioritizing choices in conservation," in *Key topics in conservation biology*. Eds. D. M. Macdonald and K. Service (Oxford: Blackwell Publications), 17–34.

Marsh, L., Copley, J. T., Tyler, P. A., and Thatje, S. (2015). In hot and cold water: Differential life-history traits are key to success in contrasting thermal deep-sea environments. *J. Anim. Ecol.* 84, 898–913. doi: 10.1111/1365-2656.12337

Marticorena, J., Matabos, M., Ramirez-Llodra, E., Cathalot, C., Laes-Huon, A., Leroux, R., et al. (2021). Recovery of hydrothermal vent communities in response to an induced disturbance at the Lucky Strike vent field (Mid-Atlantic Ridge). *Mar. Environ. Res.* 168, 105316. doi: 10.1016/j.marenvres.2021.105316

Marticorena, J., Matabos, M., Sarrazin., J., and Ramirez-Llodra, E. (2020). Contrasting reproductive biology of two hydrothermal gastropods from the Mid-Atlantic Ridge: implications for resilience of vent communities. *Mar. Biol.* 167, 1–19. doi: 10.1007/s00227-020-03721-x

Matabos, M., Cuvelier, D., Brouard, J., Shillito, B., Ravaux, J., Zbinden, M., et al. (2015). Behavioural study of two hydrothermal crustacean decapods: *Mirocaris fortunata* and *Segonzacia mesatlantica*, from the Lucky Strike vent field (Mid-Atlantic Ridge). *Deep Sea Res. II* 121, 146–158. doi: 10.1016/j.dsr2.2015.04.008

McCallum, A. W., Woolley, S., Błażewicz-Paszkowycz, M., Browne, J., Gerken, S., Kloser, R., et al. (2015). Productivity enhances benthic species richness along an oligotrophic Indian Ocean continental margin. *Glob. Ecol. Biogeogr* 24, 462–471. doi: 10.1111/geb.12255

McCollom, T. M. (2007). Geochemical constraints on sources of metabolic energy for chemolithoautotrophy in ultramafic-hosted deep-sea hydrothermal systems. *Astrobiology* 7, 933–950. doi: 10.1089/ast.2006.0119

McCollom, T. M., and Shock, E. L. (1997). Geochemical constraints on chemolithoautotrophic metabolism by microorganisms in seafloor hydrothermal systems. *Geochim Cosmochim. Acta* 61, 4375–4391. doi: 10.1016/S0016-7037(97)00241-X

Menini, E., and Van Dover, C. L. (2019). An atlas of protected hydrothermal vents. *Mar. Pol.* 108, 103654. doi: 10.1016/j.marpol.2019.103654

Methou, P., Hernández-Ávila, I., Cathalot, C., Cambon-Bonavita, M., and Pradillon, F. (2022). Population structure and environmental niches of *Rimicaris* shrimps from the Mid-Atlantic Ridge. *Mar. Ecol. Prog. Ser.* 684, 1–20. doi: 10.3354/meps13986

Mironov, A. N., Gebruk, A. V., and Moskalev, L. I. (2002). "Geografiya gidrotermalnykh soobshchestv i obligatnykh gidrotermalnykh taksonov [Biogeography of hydrothermal vent communities and obligate hydrothermal taxa]," in *Biologiya gidrotermalnykh sistem [Biology of hydrothermal systems]*. Ed. A. V. Gebruk (Moscow: KMK Scientific Press), 410–455.

Mogensen, L. M. W., Mei, Z., Hao, Y., Harrison, X. A., Wang, D., and Turvey, S. T. (2022). Precautionary principle or evidence-based conservation? Assessing the information content of threat data for the Yangtze finless porpoise. *Front. Mar. Sci.* 8. doi: 10.3389/fmars.2021.791484

Molodtsova, T. N., Galkin, S. V., Kobylianksy, S. G., Simakova, U. V., Vedenin, A. A., Dobretsova, I. G., et al. (2017). First data on benthic and fish communities from the Mid-Atlantic Ridge, 16°40′-17°14′N. *Deep Sea Res. II Top. Stud. Oceanogr.* 137, 69–77. doi: 10.1016/j.dsr2.2016.10.006

Molodtsova, T., Sanamyan, N. P., and Keller, N. B. (2008). Anthozoa from the northern Mid-Atlantic Ridge and Charlie-Gibbs Fracture Zone. *Mar. Biol. Res.* 4, 112–130. doi: 10.1080/17451000701821744

Morris, K. J., Tyler, P. A., Murton, B., and Rogers, A. D. (2012). Lower bathyal and abyssal distribution of coral in the axial volcanic ridge of the Mid-Atlantic Ridge at 45°N. *Deep-Sea Res. I* 62, 32–39. doi: 10.1016/j.dsr.2011.11.009

Myers, A. A., and Cunha, M. R. (2004). New and little known corophiidean amphipods from the 'Lucky Strike' hydrothermal vent, Mid-Atlantic Ridge. *J. Mar. Biol. Ass. U. K.* 84, 1019–1025. doi: 10.1017/S0025315404010343h

Niedzielski, T., Høines, A., Shields, M. A., Linley, T. D., and Priede, I. G. (2013). A multi-scale investigation into seafloor topography of the northern Mid-Atlantic Ridge based on geographic information system analysis. *Deep Sea Res. II Top. Stud. Oceanogr.* 98, 231–243. doi: 10.1016/j.dsr2.2013.10.006

Nuckley, D. J., Jinks, R. N., Battelle, B. A., Herzog, E. D., Kass, L., Renninger, G. H., et al. (1996). Retinal anatomy of a new species of bresiliid shrimp from a hydrothermal vent field on the Mid-Atlantic Ridge. *Biol. Bull.* 190, 98–110. doi: 10.2307/1542679

Nuno Gomes-Pereira, J., Auger, V., Beisiegel, K., Benjamin, R., Bergmann, M., Bowden, D., et al. (2016). Current and future trends in marine image annotation software. *Prog. Oceanog.* 149, 106–129. doi: 10.1016/j.pocean.2016.07.005

O'Mullan, G. D., Maas, P. A. Y., Lutz, R. A., and Vrijenhoek, R. C. (2001). A hybrid zone between hydrothermal vent mussels (Bivalvia: Mytilidae) from the Mid-Atlantic Ridge. *Molec. Ecol.* 10, 2819–2831. doi: 10.1046/j.0962-1083.2001.01401.x

Orcutt, B. N., Sylvan, J. B., Knab, N. J., and Edwards, K. J. (2011). Microbial ecology of the dark ocean above, at, and below the seafloor. *Microbiol. Molec. Biol. Rev.* 75, 361–422. doi: 10.1128/MMBR.00039-10

Ortiz, M., Hermosillo Nuñez, B., Gonzalez, J., Rodgriguez-Zaragoza, F., Gómez, J., and Jordan, F. (2017). Quantifying keystone species complexes: Ecosystem-based conservation management in the King George Island (Antarctic Peninsula). *Ecol. Ind.* 81, 453–460. doi: 10.1016/j.ecolind.2017.06.016

Pelli, D. G., and Chamberlain, S. C. (1989). The visibility of 350°C black-body radiation by the shrimp *Rimicaris exoculata* and man. *Nature* 337, 460–461. doi: 10.1038/337460a0

Perez, J. A. A., dos Santos Alves, E., Clark, M. R., Bergstad, O. A., Gebruk, A., Azevedo Cardoso, I., et al. (2012). Patterns of life on the Southern Mid-Atlantic Ridge: Compiling what is known and addressing future research. *Oceanography* 25, 16–31. doi: 10.5670/oceanog.2012.102

Petersen, S., Krätschell, A., Augustin, N., Jamieson, J., Hein, J. R., and Hannington, M. D. (2016). News from the seabed – geological characteristics and resource potential of deep-sea mineral resources. *Mar. Pol.* 70, 175–187. doi: 10.1016/j.marpol.2016.03.012

Plum, C., Pradillon, F., Fujiwara, Y., and Sarrazin, J. (2017). Copepod colonization of organic and inorganic substrata at a deep-sea hydrothermal vent site on the Mid-Atlantic Ridge. *Deep-Sea Res. II* 137, 335–348. doi: 10.1016/j.dsr2.2016.06.008

Priede, I. G., Bergstad, O. A., Miller, P. I., Vecchione, M., Gebruk, A., Falkenhaug, T., et al. (2013). Does presence of a mid-ocean ridge enhance biomass and biodiversity? *PloS One* 8, e61550. doi: 10.1371/journal.pone.0061550

Priede, I. G., Muller-Karger, F. E., Niedzielski, T., Gebruk, A. V., Jones, D. O. B., and Colaço, A. (2022). Drivers of biomass and biodiversity of non-chemosynthetic benthic fauna of the Mid-Atlantic Ridge in the North Atlantic. *Front. Mar. Sci.* 9. doi: 10.3389/fmars.2022.866654

Radziejewska, T., Mianowicz, K., and Abramowski, T. (2022). "Natural variability versus anthropogenic impacts on deep-sea ecosystems of importance for deep-sea mining," in *Perspectives on deep-sea mining. sustainability, technology, environmental policy and management*. Ed. R. Sharma (Cham: Springer), 281–311. doi: 10.1007/978-3-030-87982-2_11

Riehl, T., Lins, L., and Brandt, A. (2018). The effects of depth, distance, and the Mid-Atlantic Ridge on genetic differentiation of abyssal and hadal isopods (Macrostylidae). *Deep Sea Res. II Top. Stud. Oceanogr.* 148, 74–90. doi: 10.1016/j.dsr2.2017.10.005

Riehl, T., Wölfl, A.-C., Augustin, N., Devey, C. W., and Brandt, A. (2020). Discovery of widely available abyssal rock patches reveals overlooked habitat type and prompts rethinking deep-sea biodiversity. *Proc. Nat. Acad. Sci. U.S.A.* 117, 15450–15459. doi: 10.1073/pnas.1920706117

Riou, V., Duperron, S., Dehairs, H. F., Bouillon, S., Martin, I., Colaço, A., et al. (2010). Variation in physiological indicators in *Bathymodiolus azoricus* (Bivalvia: Mytilidae) at the Menez Gwen Mid-Atlantic Ridge deep-sea hydrothermal vent site within a year. *Mar. Environ. Res.* 70, 264–271. doi: 10.1016/j.marenvres.2010.05.008

Rybakova, E., and Galkin, S. (2015). Hydrothermal assemblages associated with different foundation species on the East Pacific Rise and Mid-Atlantic Ridge, with a special focus on mytilids. *Mar. Ecol.* 36, 45–61. doi: 10.1111/maec.12262

Sarrazin, J., Cuvelier, D., Peton, L., Legendre, P., and Sarradin, P. M. (2014). High-resolution dynamics of a deep-sea hydrothermal vent mussel assemblage monitored by the EMSO-Azores MoMAR observatory. *Deep-Sea Res. I* 90, 62–75. doi: 10.1016/j.dsr.2014.04.004

Sarrazin, J., Legendre, P., De Busserolles, F., Fabri, M. C., Guilini, K., Ivanenko, V. N., et al. (2015). Biodiversity patterns, environmental drivers and indicator species on a high-temperature hydrothermal edifice, Mid-Atlantic Ridge. *Deep-Sea Res. II Top. Stud. Oceanogr.* 121, 177–192. doi: 10.1016/j.dsr2.2015.04.013

Shank, T. M., Fornari, D. J., Von Damm, K. L., Lilley, M. D., Haymon, R. M., and Lutz, R. A. (1998a). Temporal and spatial patterns of biological community development at nascent deep-sea hydrothermal vents (9°50'N, East Pacific Rise). *Deep-Sea Res. II Top. Stud. Oceanogr.* 45, 465–515. doi: 10.1016/S0967-0645(97)00089-1

Shank, T. M., Lutz, R. A., and Vrijenhoek, R. C. (1998b). Molecular systematics of shrimp (Decapoda: Bresiliidae) from deep-sea hydrothermal vents, I: Enigmatic "small orange" shrimp from the Mid-Atlantic Ridge are juvenile *Rimicaris exoculata*. *Molec. Mar. Biol. Biotechnol.* 7, 88–96.

Shields, M. A., and Blanco-Perez, R. (2013). Polychaete abundance, biomass and diversity patterns at the Mid-Atlantic Ridge, North Atlantic Ocean. *Deep Sea Res. II* 98, 315–325. doi: 10.1016/j.dsr2.2013.04.010

Shields, M. A., Glover, A. G., and Wiklund, H. (2013). Polynoid polychaetes of the Mid-Atlantic Ridge and a new holothurian association. *Mar. Biol. Res.* 9, 547–553. doi: 10.1080/17451000.2012.749992

Shillito, B., Le Bris, N., Hourdez, S., Ravaux, J., Cottin, D., Caprais, J. C., et al. (2006). Temperature resistance studies on the deep-sea vent shrimp *Mirocaris fortunata*. *J. Exp. Biol.* 209, 945–955. doi: 10.1242/jeb.02102

Sigvaldadottir, E., and Desbruyères, D. (2003). Two new species of Spionidae (Annelida: Polychaeta) from Mid-Atlantic Ridge hydrothermal vents. *Cah. Biol. Mar.* 44, 219–225.

Spedicato, A., Sánchez, N., Pastor, L., Menot, L., and Zeppilli, D. (2020). Meiofauna community in soft sediments at TAG and Snake Pit hydrothermal vent fields. *Front. Mar. Sci.* 7. doi: 10.3389/fmars.2020.00200

Stępień, A., Pabis, K., Sobczyk, R., and Serigstad, B. (2021). High species richness and extremely low abundance of cumacean communities along the shelf and slope of the Gulf of Guinea (West Africa). *Front. Mar. Sci.* 8. doi: 10.3389/fmars.2021.703547

Tabachnick, K., and Collins, A. G. (2008). Glass sponges (Porifera, Hexactinellida) of the northern Mid-Atlantic Ridge. *Mar. Biol. Res.* 4, 25–47. doi: 10.1080/17451000701847848

Tassia, M. G., Cannon, J. T., Konikoff, C. E., Shenkar, N., Halanych, K. M., and Swalla, B. J. (2016). The global diversity of Hemichordata. *PloS One* 11 (10), e0162564. doi: 10.1371/journal.pone.0162564

Tchesunov, A. V. (2015). Free-living nematode species (Nematoda) dwelling in hydrothermal sites of the North Mid-Atlantic Ridge. *Helgol. Mar. Res.* 69, 343–384. doi: 10.1007/s10152-015-0443-6

Teixeira, S., Olu, K., Decker, C., Cunha, R. L., Fuchs, S., Hourdez, S., et al. (2013). High connectivity across the fragmented chemosynthetic ecosystems of the deep Atlantic equatorial belt: Efficient dispersal mechanisms or questionable endemism? *Molec. Ecol.* 22, 4663–4680. doi: 10.1111/mec.12419

Thaler, A. D., and Amon, D. (2019). 262 voyages beneath the sea: A global assessment of macro- and megafaunal biodiversity and research effort at deep-sea hydrothermal vents. *PeerJ* 7, e7397. doi: 10.7717/peerj.7397

Thiel, H. (1975). The size structure of the deep-sea benthos. *Int. Rev. Ges. Hydrobiol.* 60, 575–606.

Tyler, P. A., Paterson, G. J. L., Sibuet, M., and Guille, A. F. (1995). A new genus of ophiuroid (Echinodermata: Ophiuroidea) from hydrothermal mounds along the Mid-Atlantic Ridge. *J. Mar. Biol. Ass. U. K.* 75, 977–986. doi: 10.1017/S0025315400038303

Vals, A., Coll, M., and Christensen, V. (2015). Keystone species: Toward an operational concept for marine biodiversity conservation. *Ecol. Monogr.* 85, 29–47. doi: 10.1890/14-0306.1

Van Dover, C. L. (2014). Impacts of anthropogenic disturbances at deep-sea hydrothermal vent ecosystems: A review. *Mar. Environ. Res.* 102, 59–72. doi: 10.1016/j.marenvres.2014.03.008

Van Dover, C. L. (2019). Inactive sulfide ecosystems in the deep sea: A review. *Front. Mar. Sci.* 6. doi: 10.3389/fmars.2019.00461

Van Dover, C. L., Arnaud-Haond, S., Gianni, M., Helmreich, S., Huber, J. A., Jaeckel, A. L., et al. (2018). Scientific rationale and international obligations for protection of active hydrothermal vent ecosystems from deep-sea mining. *Mar. Pol.* 90, 20–28. doi: 10.1016/j.marpol.2018.01.020

Van Dover, C. L., Colaço, A., Collins, P. C., Croot, P., Metaxas, A., Murton, B. J., et al. (2020). Research is needed to inform environmental management of hydrothermally inactive and extinct polymetallic sulfide (PMS) deposits. *Mar. Pol.* 121, 104183. doi: 10.1016/j.marpol.2020.104183

Van Dover, C. L., Smith, C. R., Ardron, J., Arnaud, S., Beaudoin, Y., Bezaury, J., et al. (2011). Environmental management of deep-sea chemosynthetic ecosystems: Justification of and consideration for a spatially-based approach. *ISA Tech. Study 9 Kingston Jamaica: Int. Seabed Authority*.

Vanreusel, A., Bossche, I., van den,, and Thiermann, F. (1997). Free-living marine nematodes from hydrothermal sediments: Similarities with communities from diverse reduced habitats. *Mar. Ecol. Prog. Ser.* 157, 207–219. doi: 10.3354/meps157207

Varliero, G., Blenhold, C., Schmid, F., Boetius, A., and Molari, M. (2019). Microbial diversity and connectivity in deep-sea sediments of the South Atlantic polar front. *Front. Microbiol.* 10. doi: 10.3389/fmicb.2019.00665

Vereshchaka, A. L., and Vinogradov, M. E. (2006). "Struktura bentopelagicheskoy komponenty gidrotermalnykh soobschchestv," in *Ekosistemy atlanticheskikh gidroterm [Ecosystems of the Atlantic hydrothermal vents]*. Eds. M. E. Vinogradov and A. L. Vereshchaka (Moskva: Nauka), 275–290.

Vereshchaka, A., Vinogradov, G., Lein, A. Y., Dalton, S., and Dehairs, F. (2000). Carbon and nitrogen isotopic composition of the fauna from the Broken Spur hydrothermal vent field. *Mar. Biol.* 136, 11–17. doi: 10.1007/s002270050002

Vrijenhoek, R. C. (2010). Genetic diversity and connectivity of deep-sea hydrothermal vent metapopulations. *Mol. Ecol.* 19, 4391–4411. doi: 10.1111/j.1365-294X.2010.04789.x

Washburn, T. W., Menot, L., Bonifácio, P., Pape, E., Błażewicz, M., Bribiesca-Contreras, G., et al. (2021). Patterns of macrofaunal biodiversity across the Clarion-Clipperton Zone: An area targeted for seabed mining. *Front. Mar. Sci.* 8. doi: 10.3389/fmars.2021.626571

Weaver, P. P. E., and Billett, D. (2019). "Environmental impacts of nodule, sulphide and crust mining: An overview," in *Environmental issues of deep-sea mining*. Ed. R. Sharma (Cham: Springer), 27–62. doi: 10.1007/978-3-030-12696-4_3

Weaver, P. P. E., Boschen-Rose, R. E., Dale, A. C., Jones, D., Billett, D. S. M., Colaço, A., et al. (2021). Regional environmental assessment of the northern Mid-Atlantic Ridge. *ISA Tech. Study 28 Int. Seabed Authority Kingston Jamaica: Int. Seabed Authority*.

Williams, A. B., and Rona, P. A. (1986). Two new caridean shrimps (Bresiliidae) from a hydrothermal field on the Mid-Atlantic Ridge. *J. Crust. Biol.* 6, 446–462. doi: 10.2307/1548184

Witman, J. D. (2013). Are regional effects on local diversity more important in marine than in terrestrial communities? *Oikos* 122, 300–305. doi: 10.2307/41937670

Yahagi, T., Fukumori, H., Warén, A., and Kano, Y. (2019). Population connectivity of hydrothermal-vent limpets along the northern Mid-Atlantic Ridge (Gastropoda: Neritimorpha: Phenacolepadidae). *J. Mar. Biol. Ass. U.K.* 99, 179–185. doi: 10.1017/S0025315417001898

Zbinden, M., and Cambon-Bonavita, M. A. (2020). *Rimicaris exoculata*: Biology and ecology of a shrimp from deep-sea hydrothermal vents associated with ectosymbiotic bacteria. *Mar. Ecol. Prog. Ser.* 652, 187–222. doi: 10.3354/meps13467

Zbinden, M., Gallet, A., Szafranski, K. M., Machon, J., Ravaux, J., Léger, N., et al. (2018). Blow your nose, shrimp! Unexpectedly dense bacterial communities occur on the antennae and antennules of hydrothermal vent shrimp. *Front. Mar. Sci.* 5. doi: 10.3389/fmars.2018.00357

Zekely, J., Van Dover, C. L., Nemeschkal, H. L., and Bright, M. (2006). Hydrothermal vent meiobenthos associated with mytilid mussel aggregations from the Mid-Atlantic Ridge and the East Pacific Rise. *Deep Sea Res. I* 53, 1363–1378. doi: 10.1016/j.dsr.2006.05.010

Zeppilli, D., Bellec, L., Cambon-Bonavita, M.-A., Decraemer, W., Fontaneto, D., Fuchs, S., et al. (2019). Ecology and trophic role of *Oncholaimus dyvae* sp. nov. (Nematoda: Oncholaimidae) from the Lucky Strike hydrothermal vent field (Mid-Atlantic Ridge). *BMC Zool* 4, 6. doi: 10.1186/s40850-019-0044-yx

Zeppilli, D., Leduc, D., Fontanier, C., Fontaneto, D., Fuchs, S., Gooday, A. J., et al. (2018). Characteristics of meiofauna in extreme marine ecosystems: A review. *Mar. Biodiv.* 48, 35–71. doi: 10.1007/s12526-017-0815-z

Zeppilli, D., Pusceddu, A., Trincardi, F., and Danovaro, R. (2016). Seafloor heterogeneity influences the biodiversity–ecosystem functioning relationships in the deep sea. *Sci. Rep.* 6, 26352. doi: 10.1038/srep26352

Zeppilli, D., Vanreusel, A., Pradillon, F., Fuchs, S., Mandon, P., James, T., et al. (2015). Rapid colonisation by nematodes on organic and inorganic substrata deployed at the deep-sea Lucky Strike hydrothermal vent field (Mid-Atlantic Ridge). *Mar. Biodiv.* 45, 489–504. doi: 10.1007/s12526-015-0348-2

Frontiers in Marine Science

Explores ocean-based solutions for emerging global challenges

The third most-cited marine and freshwater biology journal, advancing our understanding of marine systems and addressing global challenges including overfishing, pollution, and climate change.

Discover the latest Research Topics

See more →

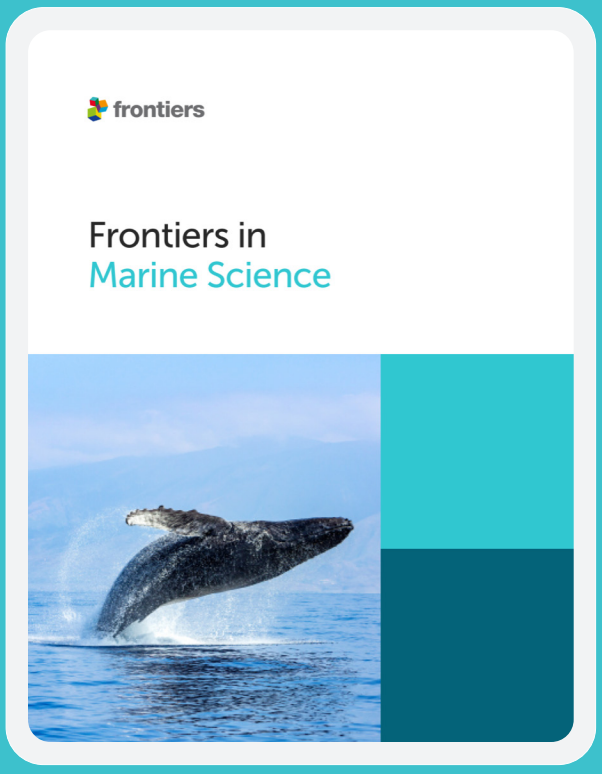

Frontiers

Avenue du Tribunal-Fédéral 34
1005 Lausanne, Switzerland
frontiersin.org

Contact us

+41 (0)21 510 17 00
frontiersin.org/about/contact